Third Edition

PRINCIPLES OF SOIL DYNAMICS

BRAJA M. DAS • ZHE LUO

Principles of Soil Dynamics

THIRD EDITION

Braja M. Das

Dean Emeritus, California State University, Sacramento

Zhe Luo

Assistant Professor, University of Akron, Ohio

CENGAGE Learning™

Australia • Brazil • Japan • Korea • Mexico • Singapore • Spain • United Kingdom • United States

Copyright 2017 Cengage Learning. All Rights Reserved. May not be copied, scanned, or duplicated, in whole or in part. Due to electronic rights, some third party content may be suppressed from the eBook and/or eChapter(s). Editorial review has deemed that any suppressed content does not materially affect the overall learning experience. Cengage Learning reserves the right to remove additional content at any time if subsequent rights restrictions require it.

This is an electronic version of the print textbook. Due to electronic rights restrictions, some third party content may be suppressed. Editorial review has deemed that any suppressed content does not materially affect the overall learning experience. The publisher reserves the right to remove content from this title at any time if subsequent rights restrictions require it. For valuable information on pricing, previous editions, changes to current editions, and alternate formats, please visit www.cengage.com/highered to search by ISBN#, author, title, or keyword for materials in your areas of interest.

Important Notice: Media content referenced within the product description or the product text may not be available in the eBook version.

Copyright 2017 Cengage Learning. All Rights Reserved. May not be copied, scanned, or duplicated, in whole or in part. Due to electronic rights, some third party content may be suppressed from the eBook and/or eChapter(s). Editorial review has deemed that any suppressed content does not materially affect the overall learning experience. Cengage Learning reserves the right to remove additional content at any time if subsequent rights restrictions require it.

CENGAGE Learning®

***Principles of Soil Dynamics*, Third Edition**
Braja M. Das and Zhe Luo

Product Director, Global Engineering: Timothy L. Anderson

Senior Content Developer: Mona Zeftel

Associate Media Content Developer: Ashley Kaupert

Product Assistant: Alexander Sham

Marketing Manager: Kristin Stine

Director, Higher Education Production: Sharon L. Smith

Content Project Manager: D. Jean Buttrom

Production Service: RPK Editorial Services, Inc.

Copyeditor: Shelly Gerger-Knechtl

Proofreader: Martha McMaster

Indexer: Braja M. Das

Compositor: SPi-Global

Senior Art Director: Michelle Kunkler

Cover and Internal Designer: Harasymczuk Design

Cover Image: Everything/Shutterstock.com

Intellectual Property Analyst: Christine Myaskovsky
Project Manager: Sarah Shainwald

Text and Image Permissions Researcher: Kristiina Paul

Manufacturing Planner: Doug Wilke

© 2017, 2011 Cengage Learning®

WCN: 02-200-202

ALL RIGHTS RESERVED. No part of this work covered by the copyright herein may be reproduced or distributed in any form or by any means, except as permitted by U.S. copyright law, without the prior written permission of the copyright owner.

For product information and technology assistance, contact us at **Cengage Learning Customer & Sales Support, 1-800-354-9706**.

For permission to use material from this text or product, submit all requests online at **www.cengage.com/permissions**. Further permissions questions can be emailed to **permissionrequest@cengage.com**.

Library of Congress Control Number: 2015956451

ISBN: 978-1-305-38943-4

Cengage Learning
20 Channel Center Street
Boston, MA 02210
USA

Cengage Learning is a leading provider of customized learning solutions with employees residing in nearly 40 different countries and sales in more than 125 countries around the world. Find your local representative at **www.cengage.com**.

Cengage Learning products are represented in Canada by Nelson Education Ltd.

To learn more about Cengage Learning Solutions, visit **www.cengage.com/engineering**.

Purchase any of our products at your local college store or at our preferred online store **www.cengagebrain.com**.

Unless otherwise noted, all items © Cengage Learning.

Printed in the United States of America

Print Number: 01 Print Year: 2015

Copyright 2017 Cengage Learning. All Rights Reserved. May not be copied, scanned, or duplicated, in whole or in part. Due to electronic rights, some third party content may be suppressed from the eBook and/or eChapter(s). Editorial review has deemed that any suppressed content does not materially affect the overall learning experience. Cengage Learning reserves the right to remove additional content at any time if subsequent rights restrictions require it.

To Elizabeth Madison

Copyright 2017 Cengage Learning. All Rights Reserved. May not be copied, scanned, or duplicated, in whole or in part. Due to electronic rights, some third party content may be suppressed from the eBook and/or eChapter(s). Editorial review has deemed that any suppressed content does not materially affect the overall learning experience. Cengage Learning reserves the right to remove additional content at any time if subsequent rights restrictions require it.

CONTENTS

Copyright 2017 Cengage Learning. All Rights Reserved. May not be copied, scanned, or duplicated, in whole or in part. Due to electronic rights, some third party content may be suppressed from the eBook and/or eChapter(s). Editorial review has deemed that any suppressed content does not materially affect the overall learning experience. Cengage Learning reserves the right to remove additional content at any time if subsequent rights restrictions require it.

Copyright 2017 Cengage Learning. All Rights Reserved. May not be copied, scanned, or duplicated, in whole or in part. Due to electronic rights, some third party content may be suppressed from the eBook and/or eChapter(s). Editorial review has deemed that any suppressed content does not materially affect the overall learning experience. Cengage Learning reserves the right to remove additional content at any time if subsequent rights restrictions require it.

Copyright 2017 Cengage Learning. All Rights Reserved. May not be copied, scanned, or duplicated, in whole or in part. Due to electronic rights, some third party content may be suppressed from the eBook and/or eChapter(s). Editorial review has deemed that any suppressed content does not materially affect the overall learning experience. Cengage Learning reserves the right to remove additional content at any time if subsequent rights restrictions require it.

Copyright 2017 Cengage Learning. All Rights Reserved. May not be copied, scanned, or duplicated, in whole or in part. Due to electronic rights, some third party content may be suppressed from the eBook and/or eChapter(s). Editorial review has deemed that any suppressed content does not materially affect the overall learning experience. Cengage Learning reserves the right to remove additional content at any time if subsequent rights restrictions require it.

8 LATERAL EARTH PRESSURE ON RETAINING WALLS 343

9 COMPRESSIBILITY OF SOILS UNDER DYNAMIC LOADS 404

Copyright 2017 Cengage Learning. All Rights Reserved. May not be copied, scanned, or duplicated, in whole or in part. Due to electronic rights, some third party content may be suppressed from the eBook and/or eChapter(s). Editorial review has deemed that any suppressed content does not materially affect the overall learning experience. Cengage Learning reserves the right to remove additional content at any time if subsequent rights restrictions require it.

Copyright 2017 Cengage Learning. All Rights Reserved. May not be copied, scanned, or duplicated, in whole or in part. Due to electronic rights, some third party content may be suppressed from the eBook and/or eChapter(s). Editorial review has deemed that any suppressed content does not materially affect the overall learning experience. Cengage Learning reserves the right to remove additional content at any time if subsequent rights restrictions require it.

Copyright 2017 Cengage Learning. All Rights Reserved. May not be copied, scanned, or duplicated, in whole or in part. Due to electronic rights, some third party content may be suppressed from the eBook and/or eChapter(s). Editorial review has deemed that any suppressed content does not materially affect the overall learning experience. Cengage Learning reserves the right to remove additional content at any time if subsequent rights restrictions require it.

PREFACE

During the past four to five decades, considerable progress has been made in the area of soil dynamics. Soil dynamics courses have been added or expanded for graduate-level study in many universities. The knowledge gained from the intensive research conducted all over the world has gradually filtered into the actual planning, design, and construction process of various types of earth-supported and earth-retaining structures. Based on the findings of those research initiatives, this text is prepared for an introductory course in soil dynamics. While writing a textbook, all authors are tempted to include research of advanced studies to some degree. However, because the text is intended for an introductory course, it stresses the fundamental principles without becoming cluttered with too many details and alternatives. The text is divided into twelve chapters and an appendix. SI units are used throughout the text.

New to this Edition

Following are some of the revisions/additions to this edition.

- In Chapter 1, "Introduction," a brief discussion on air blast loading has been added.
- In Chapter 2 on "Fundamentals of Vibration" the discussion of vibration of a mass-spring system with two degrees of freedom (Section 2.10) has been revised for clarity. The application of the analysis of the theory related to two-degree freedom system to the vibration of a drop hammer foundation has been presented in an example problem.
- Chapter 3 on "Waves in Elastic Medium" has a section on viscoelastic waves in a bar (Section 3.16).
- Chapter 4 on "Properties of Dynamically Loaded Soils" now has discussions on bender element test for determination of shear wave velocity, recently developed quasi-fixed base and free top type resonant column device (Werden et al., 2013), correlations for shear wave velocity with standard penetration number, correlations for shear modulus and damping ratio with cyclic shear strain for gravelly soils (Rollins et al., 1998), correlations for shear modulus and damping ratio of clayey soils which includes the effects of soil plasticity and overconsolidation ratio (Hardin and Black, 1968; Hardin, 1978; Vucetic and Dobry, 1991), and spectral analysis of surface wave (SASW) to obtain the shear wave velocity profile at a test site.
- A detailed discussion on the improved methods for estimation of the dynamic spring constant and dashpot coefficient (Dobry and Gazetas, 1986) has been added to Chapter 5 on "Foundation Vibration."

Copyright 2017 Cengage Learning. All Rights Reserved. May not be copied, scanned, or duplicated, in whole or in part. Due to electronic rights, some third party content may be suppressed from the eBook and/or eChapter(s). Editorial review has deemed that any suppressed content does not materially affect the overall learning experience. Cengage Learning reserves the right to remove additional content at any time if subsequent rights restrictions require it.

- In Chapter 6 on "Dynamic Bearing Capacity of Shallow Foundations," the section on seismic bearing capacity (Section 6.6) has been expanded to include a more detailed discussion of the solution of Richards et al. (1993). Also included in this section are the solutions of Budhu and al-Karni (1993) and Choudhury and Subba Rao (2005).
- Chapter 7 on "Earthquake and Ground Vibration" has now a more detailed discussion on the moment magnitude scale of earthquakes and its relationship to the Richter scale.
- In Chapter 8 on "Lateral Earth Pressure on Retaining Walls," the section on active earth pressure theory (Section 8.11) has been expanded to include the analysis of Shukla et al. (2009). The summary of the study of Soubra (2000) on the passive earthquake coefficient has been included.
- A new section on simplified procedures for determining soil liquefaction using in situ index has been added to Chapter 10 on "Liquefaction of Soil."
- New example problems and end-of-chapter problems have been added.

This text was originally published as *Fundamentals of Soil Dynamics* with a 1983 copyright by Elsevier Science Publishing Company, New York. The first edition of *Principles of Soil Dynamics* was published by PWS-Kent Publishing Company, Boston, with a 1993 copyright, and the second edition was published by Cengage Learning, Stamford, Connecticut, with a 2011 copyright. The co-author of this third edition is Dr. Zhe Luo of the University of Akron, Ohio.

INSTRUCTOR RESOURCE MATERIAL

To access instructor resources, including a secure, downloadable Instructor's Solution Manual and Lecture Note PowerPoint Slides, please visit our Instructor Resource Center at http://sso.cengage/com.

ACKNOWLEDGMENTS

Thanks are due to:

- Professors Megan Hart, University of Missouri at Kansas City; Vijay K. Puri, Civil, and Environmental Engineering at Southern Illinois University; and Khaled Sobhan, Civil, Environmental, and Geomatics Engineering at Florida Atlantic University, and other individuals for their review and helpful suggestions.
- Janice Das, for her encouragement and help in preparing the revised manuscript and the Instructor's Solution Manual.
- Lin Li of Kent State University for the initial typing of the Instructor's Solution Manual.

Copyright 2017 Cengage Learning. All Rights Reserved. May not be copied, scanned, or duplicated, in whole or in part. Due to electronic rights, some third party content may be suppressed from the eBook and/or eChapter(s). Editorial review has deemed that any suppressed content does not materially affect the overall learning experience. Cengage Learning reserves the right to remove additional content at any time if subsequent rights restrictions require it.

- Professor C. Hsien Juang of Clemson University for providing the data for developing the liquefaction plots.
- Dr. Chih-Shen Ku of I-Shou University, Taiwan, for providing photographs of the Chi-Chi earthquake in 1999.
- Dr. W. Allen Marr, Founder and Chief Executive Officer of of Geocomp Corporation, for providing photographs of bender element and resonant column assembly.
- Finnegan Mwape and Kaveh Zehtab, Geocomp Corporation, for their helpful suggestions.
- The staff at Cengage Learning—namely: Timothy L. Anderson, Product Director; Hilda M. Gowans, former Senior Development Editor; Mona Zeftel, Senior Content Developer, and Alexander Sham, Product Assistant.
- Rose P. Kernan, RPK Editorial Services, for shaping the style and overseeing the production of this edition.

The senior author, Braja M. Das, would like to express a special thank-you to his wife, Janice, who has been the primary source of inspiration over the past 35 years in preparing this and other text and reference books. The co-author, Zhe Luo, would like to thank his parents, Lijuan and Yongxin, for their love and support. He also expresses his sincere gratitude and respect to Professor Das for the advice, inspiration, and encouragement through the course of this work.

Braja M. Das
Zhe Luo

Copyright 2017 Cengage Learning. All Rights Reserved. May not be copied, scanned, or duplicated, in whole or in part. Due to electronic rights, some third party content may be suppressed from the eBook and/or eChapter(s). Editorial review has deemed that any suppressed content does not materially affect the overall learning experience. Cengage Learning reserves the right to remove additional content at any time if subsequent rights restrictions require it.

Copyright 2017 Cengage Learning. All Rights Reserved. May not be copied, scanned, or duplicated, in whole or in part. Due to electronic rights, some third party content may be suppressed from the eBook and/or Chapter(s). Editorial review has deemed that any suppressed content does not materially affect the overall learning experience. Cengage Learning reserves the right to remove additional content at any time if subsequent rights restrictions require it.

Introduction

1

1.1 GENERAL INFORMATION

Soil mechanics is the branch of civil engineering that deals with the engineering properties and behavior of soil under stress. Since the publication of the book *Erdbaumechanik aur Bodenphysikalischer Grundlage* by Karl Terzaghi (1925), theoretical and experimental studies in the area of soil mechanics have progressed at a very rapid pace. Most of these studies have been devoted to the determination of soil behavior under static load conditions, in a broader sense, although the term load includes both static and dynamic loads. Dynamic loads are imposed on soils and geotechnical structures by several sources, such as earthquakes, bomb blasts, operation of machinery, construction operations, mining, traffic, wind, and wave actions. It is well known that the stress-strain properties of a soil and its behavior depend upon several factors and can be different in many ways under dynamic loading conditions as compared to the case of static loading. Soil dynamics is the branch of soil mechanics that deals with the behavior of soil under dynamic load, including the analysis of the stability of earth-supported and earth-retaining structures.

During the last 50 years, several factors, such as damage due to liquefaction of soil during earthquakes, stringent safety requirements for nuclear power plants, industrial advancements (for example, design of foundations for power generation equipment and other machinery), design and construction of offshore structures, and defense requirements, have resulted in a rapid growth in the area of soil dynamics.

1.2 NATURE AND TYPE OF DYNAMIC LOADING ON SOILS

The type of dynamic loading in soil or the foundation of a structure depends on the nature of the source producing it. Dynamic loads vary in their magnitude, direction, or position with time. More than one type of variation of forces may

Copyright 2017 Cengage Learning. All Rights Reserved. May not be copied, scanned, or duplicated, in whole or in part. Due to electronic rights, some third party content may be suppressed from the eBook and/or eChapter(s).
Editorial review has deemed that any suppressed content does not materially affect the overall learning experience. Cengage Learning reserves the right to remove additional content at any time if subsequent rights restrictions require it.

coexist. Periodic load is a special type of load that varies in magnitude with time and repeats itself at regular intervals—for example, operation of a reciprocating or a rotary machine. Nonperiodic loads are those loads that do not show any periodicity—for example, wind loading on a building. Deterministic loads are those loads that can be specified as definite functions of time, irrespective of whether the time variation is regular or irregular, for example, the harmonic load imposed by unbalanced rotating machinery. Nondeterministic loads are those loads that can not be described as definite functions of time because of their inherent uncertainty in their magnitude and form of variation with time—for example, earthquake loads (Humar 2001). Cyclic loads are those loads which exhibit a degree of regularity both in its magnitude and frequency. Static loads are those loads that build up gradually over time, or with negligible dynamic effects. They are also known as monotonic loads. Stress reversals, rate effects, and dynamic effects are the important factors that distinguish cyclic loads from static loads (Reilly and Brown 1991).

The operation of a reciprocating or a rotary machine typically produces a dynamic load pattern, as shown in Figure 1.1a. This dynamic load is more or less sinusoidal in nature and may be idealized, as shown in Figure 1.1b.

The impact of a hammer on a foundation produces a transient loading condition in soil, as shown in Figure 1.2a. The load typically increases with time up to a maximum value at time $t = t_1$ and drops to zero after that. The case shown in Figure 1.2a is a single-pulse load. A typical loading pattern (vertical acceleration) due to a pile-driving operation is shown in Figure 1.2b.

Dynamic loading associated with an earthquake is random in nature. A load that varies in a highly irregular fashion with time is sometimes referred to as a random load. Figure 1.3 shows the accelerogram of the El Centro, California, earthquake of May 18, 1940 (north-south component).

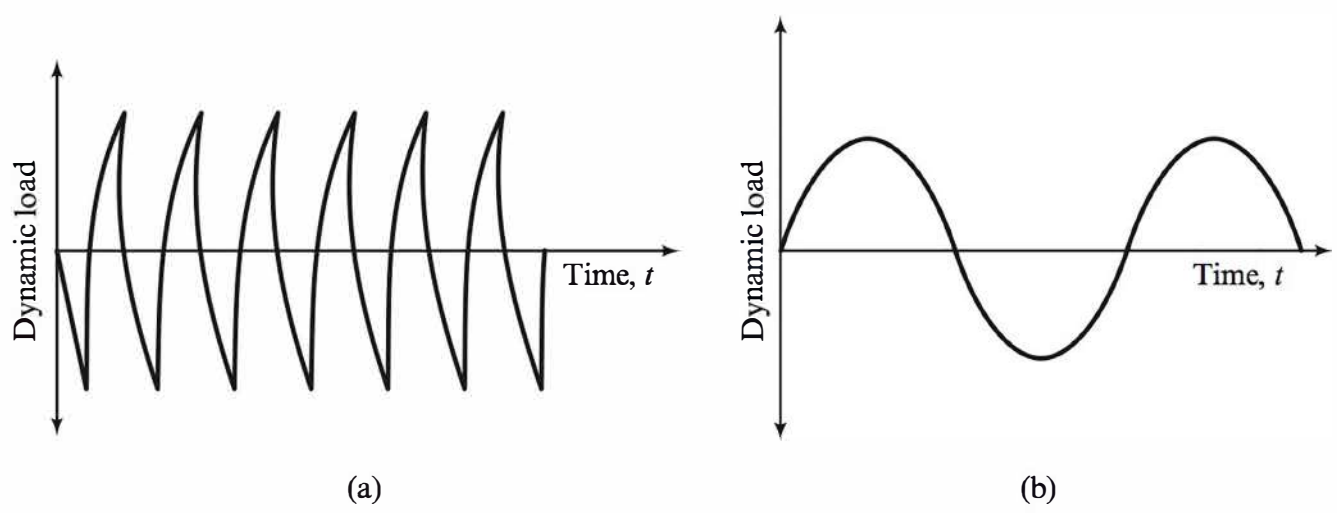

Figure 1.1 (a) Typical load versus record for a low-speed rotary machine; (b) Sinusoidal idealization for (a)

Copyright 2017 Cengage Learning. All Rights Reserved. May not be copied, scanned, or duplicated, in whole or in part. Due to electronic rights, some third party content may be suppressed from the eBook and/or eChapter(s). Editorial review has deemed that any suppressed content does not materially affect the overall learning experience. Cengage Learning reserves the right to remove additional content at any time if subsequent rights restrictions require it.

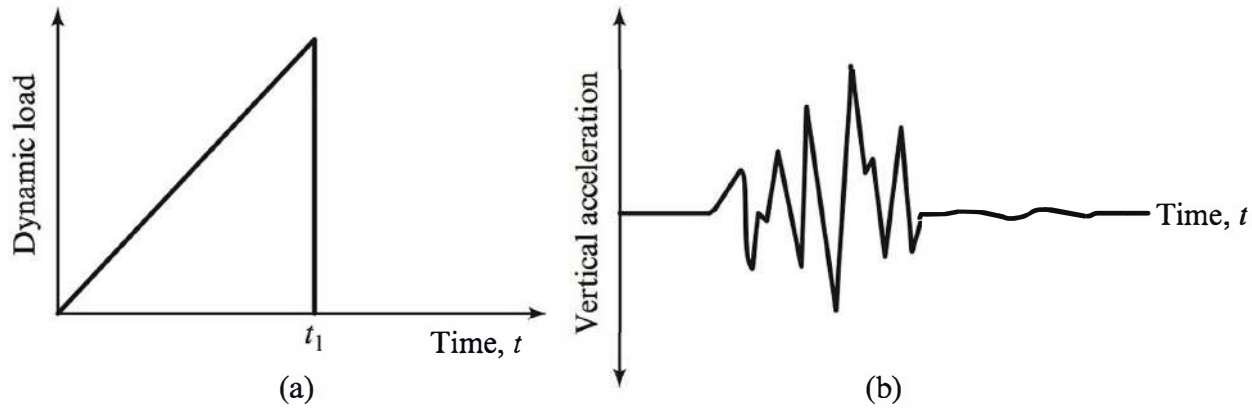

Figure 1.2 Typical loading diagrams: (a) transient loading due to single impact of a hammer; (b) vertical component of ground acceleration due to pile driving

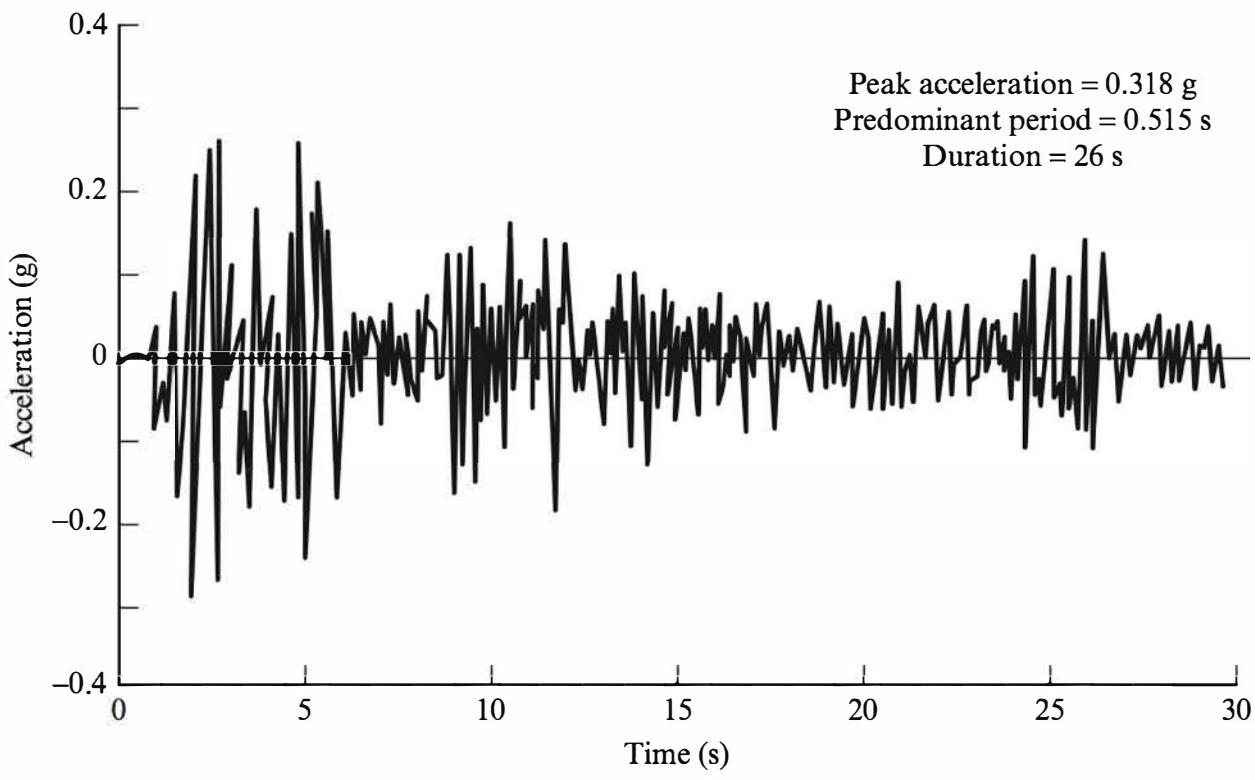

Figure 1.3 Accelerogram of the El Centro, California, earthquake of May 18, 1940 (N-S component)

For consideration of land-based structures, earthquakes are the important source of dynamic loading on soils. This is due to the damage-causing potential of strong motion earthquakes and the fact that they represent an unpredictable and uncontrolled phenomenon in nature. The ground motion due to an earthquake may lead to permanent settlement and tilting of footings and, thus, the structures supported by them. Soils may liquify, leading to buildings sinking and lighter structures such as septic tanks floating up (Prakash, 1981). The damage caused by an earthquake depends on the energy released at its source, as discussed in Chapter 7.

Copyright 2017 Cengage Learning. All Rights Reserved. May not be copied, scanned, or duplicated, in whole or in part. Due to electronic rights, some third party content may be suppressed from the eBook and/or eChapter(s). Editorial review has deemed that any suppressed content does not materially affect the overall learning experience. Cengage Learning reserves the right to remove additional content at any time if subsequent rights restrictions require it.

For offshore structures, the dynamic load due to storm waves generally represents the significant load. However, in some situations the most severe loading conditions may occur due to the combined action of storm waves and earthquakes loading. In some cases the offshore structure must be analyzed for the waves and earthquake load acting independently of each other (Puri and Das, 1989; Puri, 1990).

The loadings represented in Figures 1.1, 1.2 and 1.3 are rather simplified presentations of the actual loading conditions. For example, it is well known that earthquakes cause random motion in every direction. Also, pure dynamic loads do not occur in nature and are always a combination of static and dynamic loads. For example, in the case of a well-designed foundation supporting a machine, the dynamic load due to machine operation is a small fraction of the static weight of the foundation (Barkan, 1962). The loading conditions may be represented schematically by Figure 1.4. Thus in a real situation the loading conditions are complex. Most experimental studies have been conducted using simplified loading conditions.

The displacement of the surface of the earth's crust due to a nuclear or similar type explosion is caused by cratering and is also due to the *air blast loading*. Immediately below the center of the explosion, a crater is formed due to the conversion of thermonuclear energy into mechanical energy. The center of the explosion is called *ground zero*. At larger distances from ground zero, displacement of the ground is caused by high air pressure initiated by the explosion. The nature of variation with distance of the high air pressure caused by a nuclear explosion is shown in Figure 1.5. The front of the air pressure moves radially outwards like a ring load with a near vertical front with a peak value of p_0 and decays in an exponential manner. The pressure front moves with a velocity V as shown in Figure 1.5. Under certain conditions, the overpressure becomes negative after some time when the blast pressure reaches some point on the ground surface at seismic velocities. Knowledge of stress wave propagation (Chapter 3) through the ground is important for the design of underground protective structures (e.g., US Air Force Special Weapons Center, 1962; Anderson, 1960; Borde, 1964; Heierli, 1962; Hendron and Auld, 1967; Newmark, 1964; Wilson and Sibley, 1962).

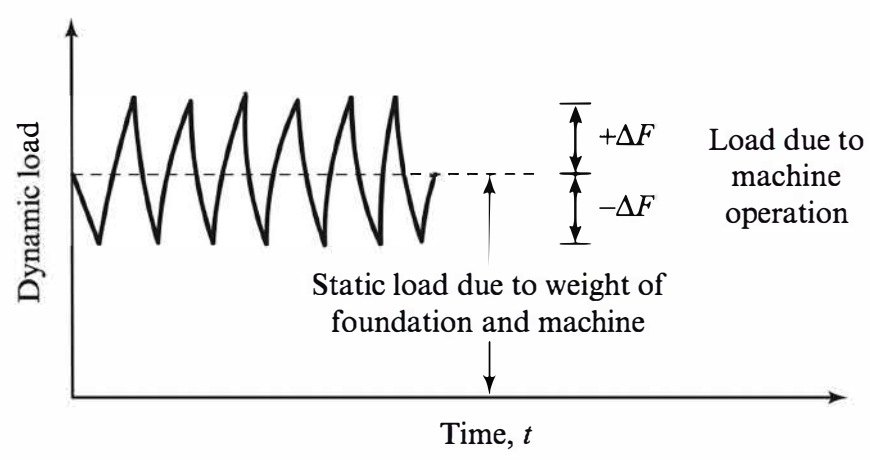

Figure 1.4 Schematic diagram showing loading on the soil below the foundation during machine operation

Copyright 2017 Cengage Learning. All Rights Reserved. May not be copied, scanned, or duplicated, in whole or in part. Due to electronic rights, some third party content may be suppressed from the eBook and/or eChapter(s). Editorial review has deemed that any suppressed content does not materially affect the overall learning experience. Cengage Learning reserves the right to remove additional content at any time if subsequent rights restrictions require it.

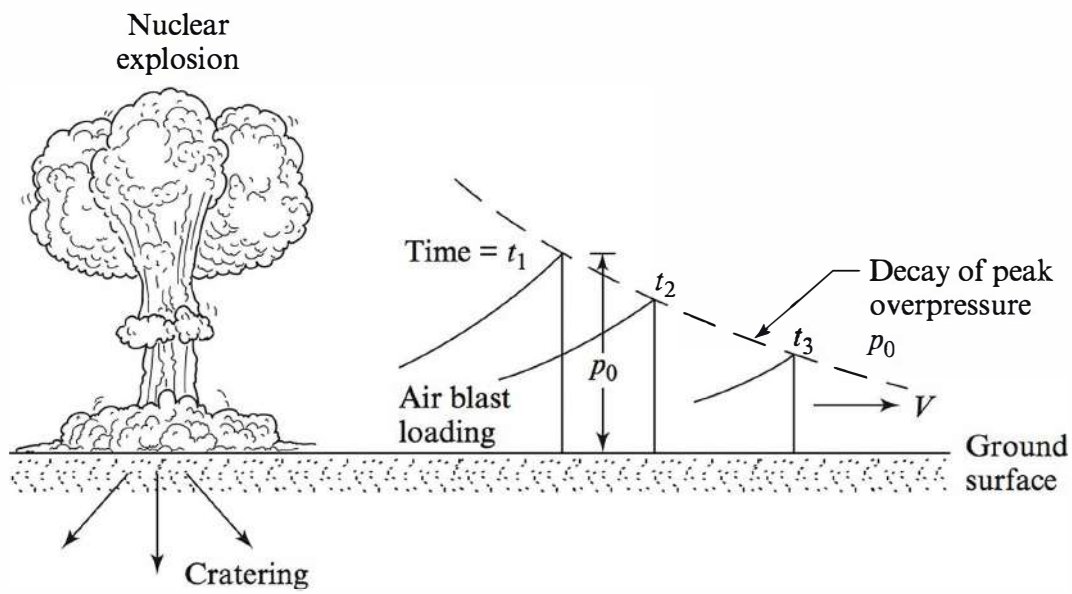

Figure 1.5 Air blast loading

1.3 IMPORTANCE OF SOIL DYNAMICS

The problems related to the dynamic loading of soils and earth structures frequently encountered by a geotechnical engineer include, but are not limited to the following:

1. Earthquake, ground vibration, and wave propagation through soils
2. Dynamic stress, deformation, and strength properties of soils
3. Dynamic earth pressure problem
4. Dynamic bearing capacity problems and design of shallow foundations
5. Problems related to soil liquefaction
6. Design of foundations for machinery and vibrating equipment
7. Design of embedded foundations and piles under dynamic loads
8. Stability of embankments under earthquake loading.

In order to arrive at rational analyses and design procedures for these problems, one must have an insight into the behavior of soil under both static and dynamic loading conditions. For example, in designing a foundation to resist dynamic loading imposed by the operation of machinery or an external source, the engineer has to arrive at a special solution dictated by the local soil conditions and environmental factors. The foundation must be designed to satisfy the criteria for static loading and, in addition, must be safe for resisting the dynamic load. When designing for dynamic loading conditions, the geotechnical engineer requires answers to questions such as the following:

1. How should failure be defined and what should be the failure criteria?
2. What is the relationship between applied loads and the significant parameters used in defining the failure criteria?

Copyright 2017 Cengage Learning. All Rights Reserved. May not be copied, scanned, or duplicated, in whole or in part. Due to electronic rights, some third party content may be suppressed from the eBook and/or eChapter(s). Editorial review has deemed that any suppressed content does not materially affect the overall learning experience. Cengage Learning reserves the right to remove additional content at any time if subsequent rights restrictions require it.

3. How can the significant parameters be identified and evaluated?
4. What will be an acceptable factor of safety, and will the factor of safety as used for static design condition be enough to ensure satisfactory performance or will some additional conditions need to be satisfied?

The problems relating to the vibration of soil and earth-supported and earth-retaining structures have received increased attention of geotechnical engineers in recent years, and significant advances have been made in this direction. New theoretical procedures have been developed for computing the response of foundations, analysis of liquefaction potential of soils, and design of retaining walls and embankments. Improved field and laboratory methods for determining dynamic behavior of soils and field measurements to evaluate the performance of prototypes deserve a special mention. In this text an attempt has been made to present the information available on some of the important problems in the field of soil dynamics. Gaps in the existing literature, if any, have also been pointed out. The importance of soil dynamics lies in providing safe, acceptable, and time-tested solutions to the problem of dynamic loading in soil, in spite of the fact that the information in some areas may be lacking and the actual loading condition may not be predictable, as in the case of the earthquake phenomenon.

From the above, it can be seen that soil dynamics is an interdisciplinary area and in addition to traditional soil mechanics, requires a knowledge of theory of vibrations, principles of wave propagation, soil behavior under dynamic/cyclic conditions, numerical methods such as finite element methods, etc., in finding appropriate solutions for problems of practical interest.

References

Anderson, F. E. (1960). "Blast Phenomena from a Nuclear Burst," *Transactions*, ASCE, Vol. 125, No. 1, pp. 667–672.

Barkan, D. D. (1962). *Dynamics of Bases and Foundations*. McGraw-Hill Book Company, New York.

Borde, H. L. (1964). "A Review of Nuclear Explosion Phenomena Pertinent to Protective Construction," *R-425-PR*, The Rand Corporation, Santa Monica, California.

Heierli, W. (1962). "Inelastic Wave Propagation in Soil Columns," *Journal of the Soil Mechanics and Foundations Division*, ASCE, Vol. 88, No. SM6, pp. 33–63.

Hendron, A. J., and Auld, H. E. (1967). "The Effect of the Soil Properties on the Attenuation of Air-Blast Induced Ground Motions," *Proceedings*, International Symposium on Wave Propagation and Dynamic Properties of Earth Material, University of New Mexico Press, pp. 29–47.

Humar, J. L. (2001). *Dynamics of Structures*. Balkema, Tokyo.

Newmark, N. M. (1964). "The Basis of Current Criteria for the Design of Underground Protective Construction," Opening Address—Session I, *Proceedings*, Symposium on Soil-Structure Interaction, University of Arizona, Tucson, pp. 1–24.

Prakash, S. (1981). *Soil Dynamics*. McGraw-Hill Book Company, New York.

Puri, V. K. (1990). "Dynamics Loading of Marine Soils," *Proceedings*, 9th International Conference on Offshore Mechanics in Arctic Engineering, ASME, Vol. 1, pp. 421–426.

Copyright 2017 Cengage Learning. All Rights Reserved. May not be copied, scanned, or duplicated, in whole or in part. Due to electronic rights, some third party content may be suppressed from the eBook and/or eChapter(s). Editorial review has deemed that any suppressed content does not materially affect the overall learning experience. Cengage Learning reserves the right to remove additional content at any time if subsequent rights restrictions require it.

Puri, V. K., and Das, B. M. (1989). "Some Considerations in the Design of Offshore Structures: Role of Soil Dynamics," *Proceedings, Oceans* '89, Vol. 5, Seattle, Washington, pp. 1544–1551.

Reilly, M. P., and Brown, S. F. (1991). *Cyclic Loading of Soils: From Theory to Design*, Blackie and Son Ltd, London.

Terzaghi, K. (1925). *Erdbaumechanik auf Bodenphysikalischer Grundlage*, Deuticke, Vienna.

US Air Force Special Weapons Center (1962). "Principles in Practices for Design of Hardened Structures," Air Force Design Manual, *Technical Documentary Report No. AFSMCTDR-62-138*, Kirtland Air Force Base, New Mexico.

Wilson, S. D., and Sibley, E. A. (1962). "Ground Displacement from Air-Blast Loading," *Journal of the Soil Mechanics and Foundations Division*, ASCE, Vol. 88, No. SM6, pp. 1–31.

Copyright 2017 Cengage Learning. All Rights Reserved. May not be copied, scanned, or duplicated, in whole or in part. Due to electronic rights, some third party content may be suppressed from the eBook and/or Chapter(s). Editorial review has deemed that any suppressed content does not materially affect the overall learning experience. Cengage Learning reserves the right to remove additional content at any time if subsequent rights restrictions require it.

Fundamentals of Vibration

2

2.1 INTRODUCTION

Satisfactory design of foundations for vibrating equipments is mostly based on displacement considerations. Displacement due to vibratory loading can be classified under two major divisions:

1. Cyclic displacement due to the elastic response of the soil-foundation system to the vibrating loading
2. Permanent displacement due to compaction of soil below the foundation

In order to estimate the displacement due to the first loading condition listed above, it is essential to know the nature of the unbalanced forces (usually supplied by the manufacturer of the machine) in a foundation such as shown in Figure 2.1.

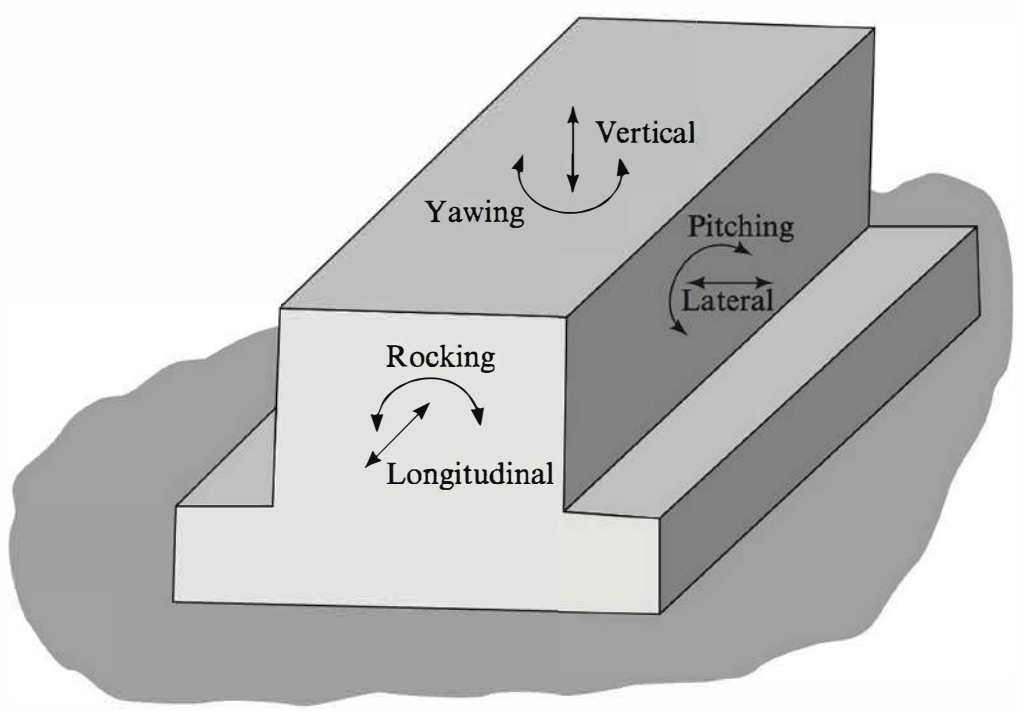

Figure 2.1 Six modes of vibration for foundation

Copyright 2017 Cengage Learning. All Rights Reserved. May not be copied, scanned, or duplicated, in whole or in part. Due to electronic rights, some third party content may be suppressed from the eBook and/or eChapter(s). Editorial review has deemed that any suppressed content does not materially affect the overall learning experience. Cengage Learning reserves the right to remove additional content at any time if subsequent rights restrictions require it.

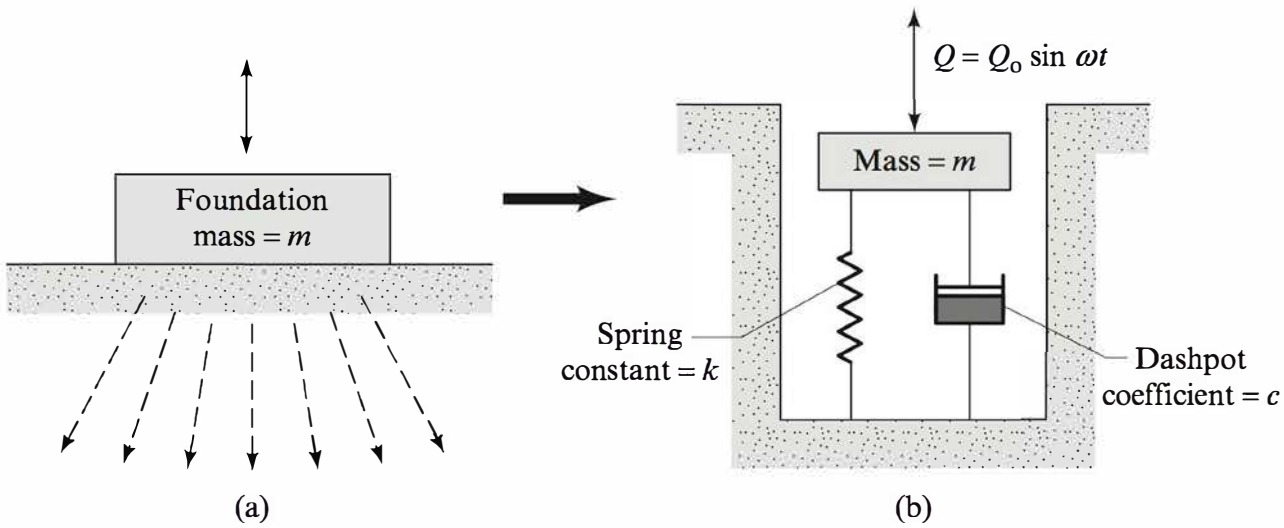

Figure 2.2 A lumped parameter vibrating system

Note that a foundation can vibrate in any or all six possible modes. For ease of analysis, each mode is considered separately and design is carried out by considering the displacement due to each mode separately. Approximate mathematical models for computing the displacement of foundations under dynamic loads can be developed by treating soil as a viscoelastic material. This can be explained with the aid of Figure 2.2a, which shows a foundation subjected to a vibratory loading in the vertical direction. The parameters for the vibration of the foundation can be evaluated by treating the soil as equivalent to a spring and a dashpot which supports the foundation as shown in Figure 2.2b. This is usually referred to as a lumped parameter vibrating system.

In order to solve the vibration problems of lumped parameter systems, one needs to know the fundamentals of structural dynamics. Therefore, a brief review of the mathematical solutions of simple vibration problems is presented. More detailed discussion regarding other approaches to solving foundation vibration problems and evaluation of basic parameters such as the spring constant and damping coefficient are presented in Chapter 5.

2.2 FUNDAMENTALS OF VIBRATION

Following are some fundamental definitions that are essential in the development of the theories of vibration.

Free Vibration: Vibration of a system under the action of forces inherent in the system itself and in the absence of externally applied forces.

The response of a system is called free vibration when it is disturbed and then left free to vibrate about some mean position.

Forced Vibration: Vibration of a system caused by an external force.

Copyright 2017 Cengage Learning. All Rights Reserved. May not be copied, scanned, or duplicated, in whole or in part. Due to electronic rights, some third party content may be suppressed from the eBook and/or eChapter(s). Editorial review has deemed that any suppressed content does not materially affect the overall learning experience. Cengage Learning reserves the right to remove additional content at any time if subsequent rights restrictions require it.

Vibrations that result from regular (rotating or pulsating machinery) and irregular (chemical process plant) exciting agencies are also called as forced vibrations.

Degree of Freedom: The number of independent coordinates required to describe the solution of a vibrating system.

For example, the position of the mass m in Figure 2.3a can be described by a single coordinate z, so it is a *single degree of freedom system*. In Figure 2.3b, two coordinates (z_1 and z_2) are necessary to describe the motion of the system; hence this system has *two* degrees of freedom. Similarly, in Figure 2.3c, two coordinates (z and θ) are necessary, and the number of degrees of freedom is two. A rigid body has total six degrees of freedom: three rotational and three translational.

To understand the mathematical models that will be frequently used in analysis of machine foundations, a thorough understanding of physics as well as mathematics of a single degree of freedom system is required and is explained in the following sections. Once the mathematics as well as physics of a single degree of freedom system is clear, it is easy to extend this to multi-degree of freedom systems as well as modal analysis of complicated physical systems. In addition, the concept of *response spectrum*, often used by structural engineers, is also based on a single degree of freedom system. A proper selection of vibration measuring instruments, design of vibration isolation as well as force isolation also require a good understanding of concepts such as natural frequency, damping ratio, etc., that can be easily understood from one degree of freedoms systems.

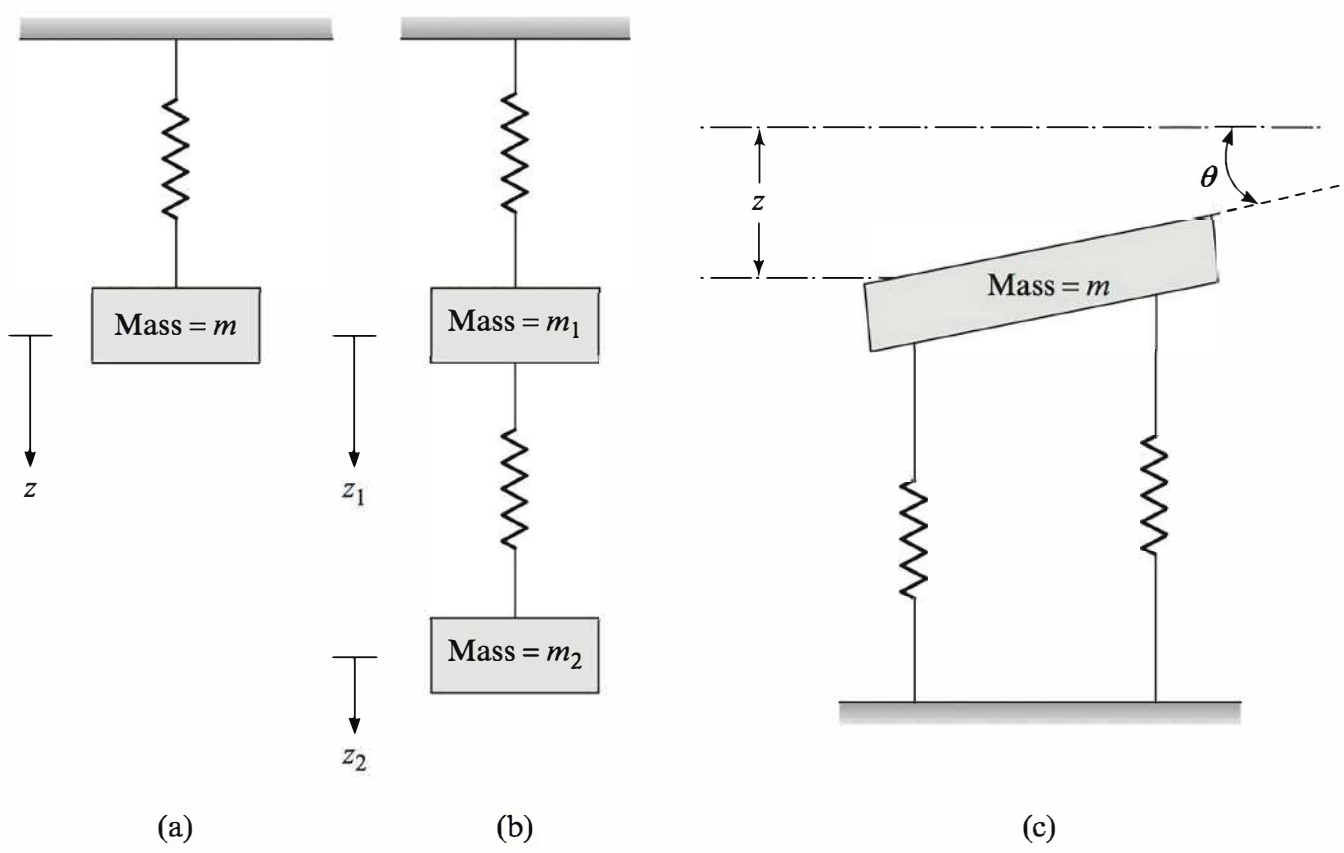

Figure 2.3 Degree of freedom for vibrating system

Copyright 2017 Cengage Learning. All Rights Reserved. May not be copied, scanned, or duplicated, in whole or in part. Due to electronic rights, some third party content may be suppressed from the eBook and/or eChapter(s). Editorial review has deemed that any suppressed content does not materially affect the overall learning experience. Cengage Learning reserves the right to remove additional content at any time if subsequent rights restrictions require it.

System with Single Degree of Freedom

2.3 FREE VIBRATION OF A SPRING-MASS SYSTEM

Figure 2.4 shows a foundation resting on a spring. Let the spring represent the elastic properties of the soil. The load W represents the weight of the foundation plus that which comes from the machinery supported by the foundation.

If the area of the foundation is equal to A, the intensity of load transmitted to the subgrade can be given by

$$q = \frac{W}{A} \tag{2.1}$$

Due to the load W, a static deflection z_s will develop. By definition,

$$k = \frac{W}{z_s} \tag{2.2}$$

where k = spring constant for the elastic support.

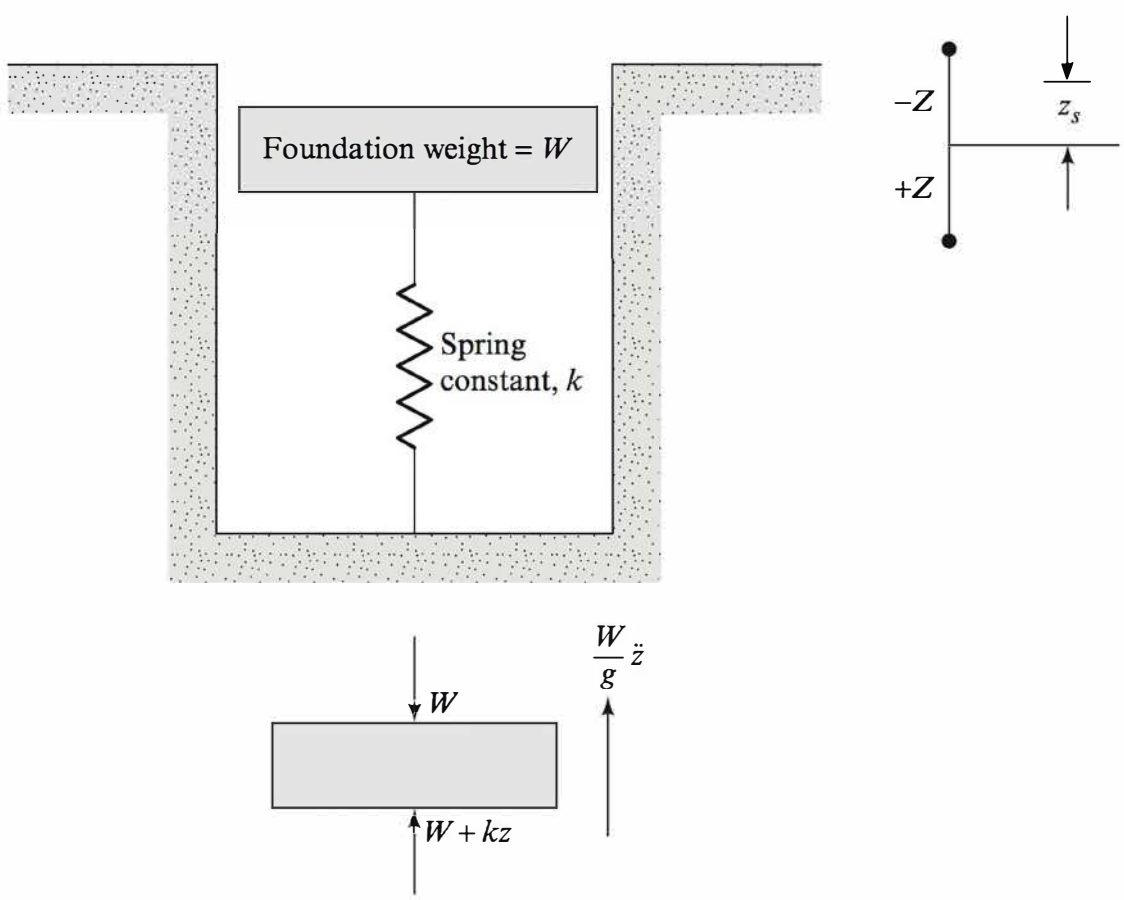

Figure 2.4 Free vibration of a mass-spring system

Copyright 2017 Cengage Learning. All Rights Reserved. May not be copied, scanned, or duplicated, in whole or in part. Due to electronic rights, some third party content may be suppressed from the eBook and/or eChapter(s). Editorial review has deemed that any suppressed content does not materially affect the overall learning experience. Cengage Learning reserves the right to remove additional content at any time if subsequent rights restrictions require it.

The coefficient of subgrade reaction k_s can be given by

$$k_s = \frac{q}{z_s} \tag{2.3}$$

If the foundation is disturbed from its static equilibrium position, the system will vibrate. The equation of motion of the foundation when it has been disturbed through a distance z can be written from Newton's second law of motion as

$$\left(\frac{W}{g}\right)\ddot{z} + kz = 0$$

or

$$\ddot{z} + \left(\frac{k}{m}\right)z = 0 \tag{2.4}$$

where g = acceleration due to gravity
$\ddot{z} = d^2z/dt^2$
t = time
m = mass = W/g

In order to solve Eq. (2.4), let

$$z = A_1 \cos \omega_n t + A_2 \sin \omega_n t \tag{2.5}$$

where A_1 and A_2 = constants
ω_n = undamped natural circular frequency

Substitution of Eq. (2.5) into Eq. (2.4) yields

$$-\omega_n^2(A_1 \cos \omega_n t + A_2 \sin \omega_n t) + \left(\frac{k}{m}\right)(A_1 \cos \omega_n t + A_2 \sin \omega_n t) = 0$$

or

$$\omega_n = \sqrt{\frac{k}{m}} \tag{2.6}$$

The unit of ω_n is in radians per second (rad/s). Hence,

$$z = A_1 \cos\left(\sqrt{\frac{k}{m}}t\right) + A_2 \sin\left(\sqrt{\frac{k}{m}}t\right) \tag{2.7}$$

In order to determine the values of A_1 and A_2, one must substitute the proper boundary conditions. At time $t = 0$, let

Displacement $z = z_0$

Copyright 2017 Cengage Learning. All Rights Reserved. May not be copied, scanned, or duplicated, in whole or in part. Due to electronic rights, some third party content may be suppressed from the eBook and/or eChapter(s). Editorial review has deemed that any suppressed content does not materially affect the overall learning experience. Cengage Learning reserves the right to remove additional content at any time if subsequent rights restrictions require it.

and

$$\text{Velocity} = \frac{dz}{dt} = \dot{z} = v_0$$

Substituting the first boundary condition in Eq. (2.7),

$$z_0 = A_1 \tag{2.8}$$

Again, from Eq. (2.7)

$$\dot{z} = -A_1\sqrt{\frac{k}{m}}\sin\left(\sqrt{\frac{k}{m}}t\right) + A_2\sqrt{\frac{k}{m}}\cos\left(\sqrt{\frac{k}{m}}t\right) \tag{2.9}$$

Substituting the second boundary condition in Eq. (2.9)

$$\dot{z} = v_0 = A_2\sqrt{\frac{k}{m}}$$

or

$$A_2 = \frac{v_0}{\sqrt{k/m}} \tag{2.10}$$

Combination of Eqs. (2.7), (2.8), and (2.10) gives

$$z = z_0\cos\left(\sqrt{\frac{k}{m}}t\right) + \frac{v_0}{\sqrt{k/m}}\sin\left(\sqrt{\frac{k}{m}}t\right) \tag{2.11}$$

Now let

$$z_0 = Z\cos\alpha \tag{2.12}$$

and

$$\frac{v_0}{\sqrt{k/m}} = Z\sin\alpha \tag{2.13}$$

Substitution of Eqs. (2.12) and (2.13) into Eq. (2.11) yields

$$\boxed{z = Z\cos(\omega_n t - \alpha)} \tag{2.14}$$

where

$$\boxed{\alpha = \tan^{-1}\left(\frac{v_0}{z_0\sqrt{k/m}}\right)} \tag{2.15}$$

Copyright 2017 Cengage Learning. All Rights Reserved. May not be copied, scanned, or duplicated, in whole or in part. Due to electronic rights, some third party content may be suppressed from the eBook and/or eChapter(s). Editorial review has deemed that any suppressed content does not materially affect the overall learning experience. Cengage Learning reserves the right to remove additional content at any time if subsequent rights restrictions require it.

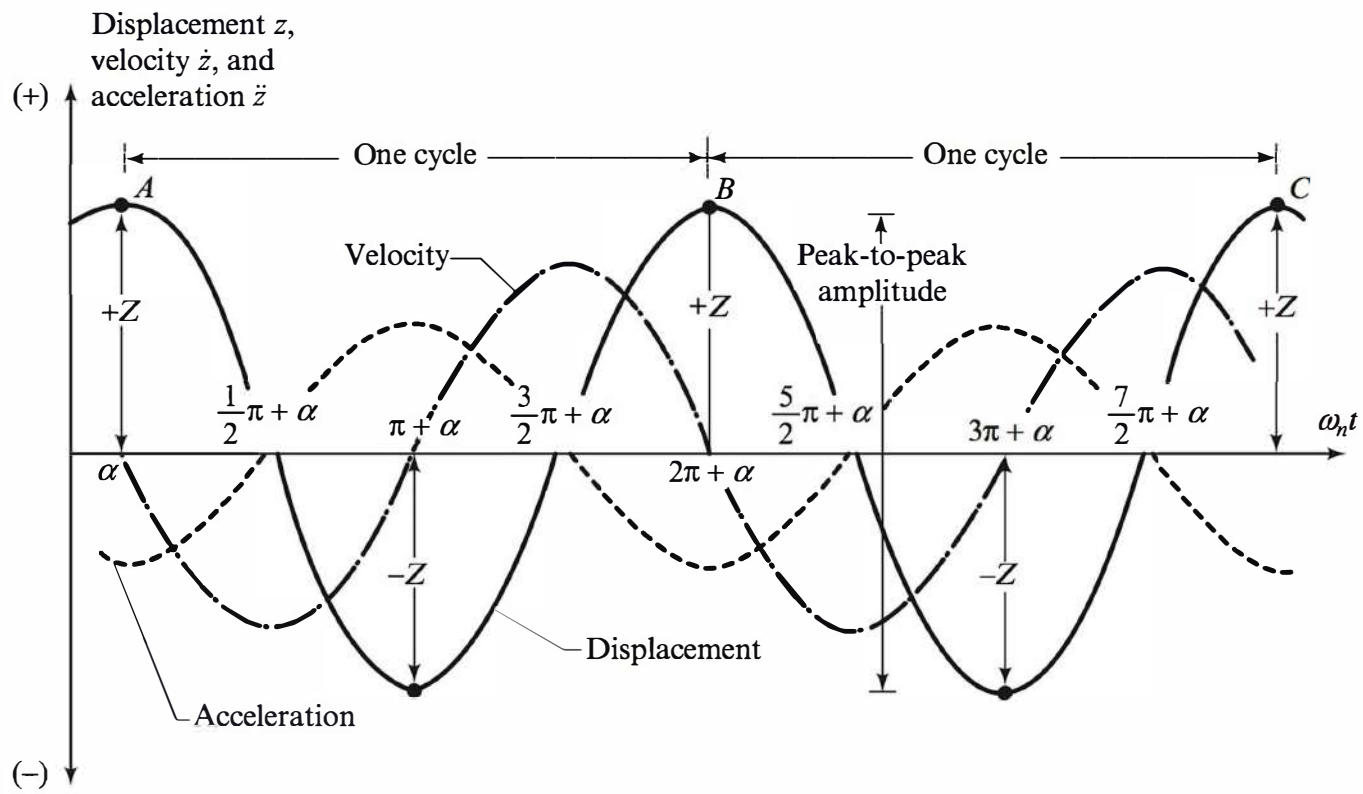

Figure 2.5 Plot of displacement, velocity, and acceleration for the free vibration of a mass-spring system

(Note: Velocity leads displacement by $\pi/2$ rad: acceleration leads velocity by $\pi/2$ rad.)

$$\boxed{Z = \sqrt{z_0^2 + \left(\frac{v_0}{\sqrt{k/m}}\right)^2} = \sqrt{z_0^2 + \left(\frac{m}{k}\right)v_0^2}} \tag{2.16}$$

The relation for the displacement of the foundation given by Eq. (2.14) can be represented graphically as shown in Figure 2.5.

At time

$$t = 0, \qquad z = Z\cos(-\alpha) \qquad = Z\cos\alpha$$

$$t = \frac{\alpha}{\omega_n}, \qquad z = Z\cos\left(\omega_n \frac{\alpha}{\omega_n} - \alpha\right) \qquad = Z$$

$$t = \frac{\frac{1}{2}\pi + \alpha}{\omega_n}, \qquad z = Z\cos\left(\omega_n \frac{\frac{1}{2}\pi + \alpha}{\omega_n} - \alpha\right) = 0$$

$$t = \frac{\pi + \alpha}{\omega_n}, \qquad z = Z\cos\left(\omega_n \frac{\pi + \alpha}{\alpha_n} - \alpha\right) \qquad = -Z$$

Copyright 2017 Cengage Learning. All Rights Reserved. May not be copied, scanned, or duplicated, in whole or in part. Due to electronic rights, some third party content may be suppressed from the eBook and/or eChapter(s). Editorial review has deemed that any suppressed content does not materially affect the overall learning experience. Cengage Learning reserves the right to remove additional content at any time if subsequent rights restrictions require it.

$$t = \frac{\frac{3}{2}\pi + \alpha}{\omega_n}, \quad z = Z\cos\left(\omega_n \frac{\frac{3}{2}\pi + \alpha}{\omega_n} - \alpha\right) = 0$$

$$t = \frac{2\pi + \alpha}{\omega_n}, \quad z = Z\cos\left(\omega_n \frac{2\pi + \alpha}{\omega_n} - \alpha\right) = Z$$

From Figure 2.5, it can be seen that the nature of displacement of the foundation is sinusoidal. The magnitude of maximum displacement is equal to Z. This is usually referred to as the single amplitude. The peak-to-peak displacement amplitude is equal to $2Z$, which is sometimes referred to as the double amplitude. The time required for the motion to repeat itself is called the period of the vibration. Note that in Figure 2.5 the motion is repeating itself at points A, B, and C. The period T of this motion can therefore be given by

$$\boxed{T = \frac{2\pi}{\omega_n}} \tag{2.17}$$

The frequency of oscillation f is defined as the number of cycles in unit time, or

$$\boxed{f = \frac{1}{T} = \frac{\omega_n}{2\pi}} \tag{2.18}$$

It has been shown in Eq. (2.6) that, for this system, $\omega_n = \sqrt{k/m}$. Thus,

$$\boxed{f = f_n = \left(\frac{1}{2\pi}\right)\sqrt{\frac{k}{m}}} \tag{2.19}$$

The term f_n is generally referred to as the undamped natural frequency. Since $k = W/z_s$, and $m = W/g$, Eq. (2.19) can also be expressed as

$$f_n = \left(\frac{1}{2\pi}\right)\sqrt{\frac{g}{z_s}} \tag{2.20}$$

Table 2.1 gives values of f_n for various values of z_s

The variation of the velocity and acceleration of the motion with time can also be represented graphically. From Eq.(2.14), the expressions for the velocity and the acceleration can be obtained as

$$\dot{z} = -(Z\omega_n)\sin(\omega_n t - \alpha) = Z\omega_n \cos\left(\omega_n t - \alpha + \frac{1}{2}\pi\right) \tag{2.21}$$

and

$$\ddot{z} = -Z\omega_n^2 \cos(\omega_n t - \alpha) = Z\omega_n^2 \cos(\omega_n t - \alpha + \pi) \tag{2.22}$$

Copyright 2017 Cengage Learning. All Rights Reserved. May not be copied, scanned, or duplicated, in whole or in part. Due to electronic rights, some third party content may be suppressed from the eBook and/or eChapter(s). Editorial review has deemed that any suppressed content does not materially affect the overall learning experience. Cengage Learning reserves the right to remove additional content at any time if subsequent rights restrictions require it.

Table 2.1 Undamped natural frequencies

z_s (mm)	Undamped natural frequency (Hz)
0.02	111
0.05	71
0.10	50
0.20	35
0.50	22
1.0	16
2	11
5	7
10	5

The variation of the velocity and acceleration of the foundations is also shown in Figure 2.5.

EXAMPLE 2.1

A mass is supported by a spring. The static deflection of the spring due to the mass is 0.381mm. Find the natural frequency vibration.

SOLUTION:

From Eq. (2.20),

$$f_n = \left(\frac{1}{2\pi}\right)\sqrt{\frac{g}{z_s}}$$

$$g = 9.81 \text{ m/s}^2,\ z_s = 0.381 \text{ mm} = 0.000381 \text{ m}.$$

So,

$$f_n = \left(\frac{1}{2\pi}\right)\sqrt{\frac{9.81}{0.000381}} = \mathbf{25.54\ Hz}$$

Copyright 2017 Cengage Learning. All Rights Reserved. May not be copied, scanned, or duplicated, in whole or in part. Due to electronic rights, some third party content may be suppressed from the eBook and/or eChapter(s). Editorial review has deemed that any suppressed content does not materially affect the overall learning experience. Cengage Learning reserves the right to remove additional content at any time if subsequent rights restrictions require it.

EXAMPLE 2.2

For a machine foundation, given weight of the foundation $= 45$ kN and spring constant $= 10^4$ kN/m, determine

a. natural frequency of vibration, and
b. period of oscillation

SOLUTION:

a. $f_n = \frac{1}{2\pi}\sqrt{\frac{k}{m}} = \frac{1}{2\pi}\sqrt{\frac{10^4}{(45/9.81)}} = \mathbf{7.43\ Hz}$

b. From Eq. (2.18),

$$T = \frac{1}{f_n} = \frac{1}{7.43} = \mathbf{0.135\ s}$$

2.4 FORCED VIBRATION OF A SPRING-MASS SYSTEM

Figure 2.6 shows a foundation that has been idealized to a simple spring-mass system. Weight W is equal to the weight of the foundation itself and that supported by it; the spring constant is k. This foundation is being subjected to an alternating force $Q = Q_0 \sin(\omega t + \beta)$. This type of problem is generally encountered with foundations supporting reciprocating engines, and so on.

The equation of motion for this problem can be given by

$$m\ddot{z} + kz = Q_0 \sin(\omega t + \beta) \tag{2.23}$$

Let $z = A_1 \sin(\omega t + \beta)$ be a particular solution to Eq. (2.23) ($A_1 = \text{const}$). Substitution of this into Eq. (2.23) gives

$$-\omega^2 m A_1 \sin(\omega t + \beta) + kA_1 \sin(\omega t + \beta) = Q_0 \sin(\omega t + \beta)$$

$$A_1 = \frac{Q_0/m}{(k/m) - \omega^2} \tag{2.24}$$

Hence the particular solution to Eq. (2.23) is of the form

$$\boxed{z = A_1 \sin(\omega t + \beta) = \frac{Q_0/m}{(k/m) - \omega^2}\sin(\omega t + \beta)} \tag{2.25}$$

The complementary solution of Eq. (2.23) must satisfy

$$m\dot{z} + kz = 0$$

Copyright 2017 Cengage Learning. All Rights Reserved. May not be copied, scanned, or duplicated, in whole or in part. Due to electronic rights, some third party content may be suppressed from the eBook and/or eChapter(s). Editorial review has deemed that any suppressed content does not materially affect the overall learning experience. Cengage Learning reserves the right to remove additional content at any time if subsequent rights restrictions require it.

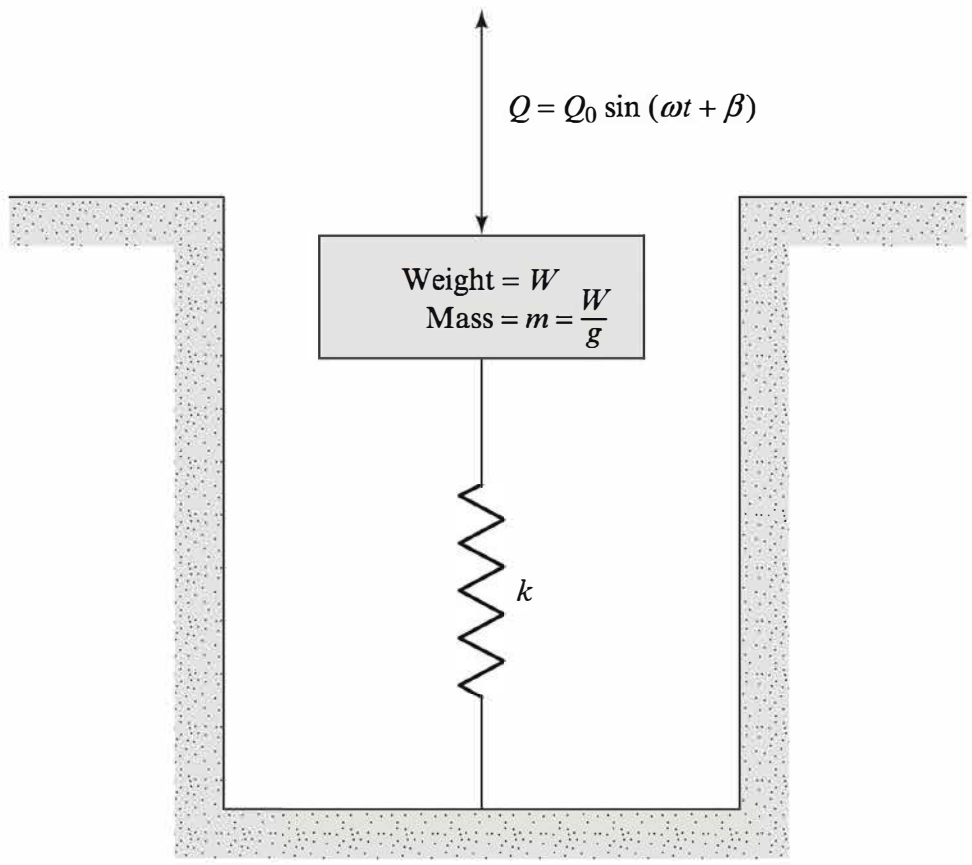

Figure 2.6 Forced vibration of mass-spring system title

As shown in the preceding section, the solution to this equation may be given as

$$z = A_2 \cos \omega_n t + A_3 \sin \omega_n t \tag{2.26}$$

where $\omega_n = \sqrt{\frac{k}{m}}$

$A_2, A_3 = \text{const}$

Hence, the general solution of Eq. (2.23) is obtained by adding Eqs. (2.25) and (2.26), or

$$z = A_1 \sin(\omega t + \beta) + A_2 \cos \omega_n t + A_3 \sin \omega_n t \tag{2.27}$$

Now, let the boundary conditions be as follows:

At time $t = 0$,

$$z = z_0 = 0 \tag{2.28}$$

$$\frac{dz}{dt} = \text{velocity} = v_0 = 0 \tag{2.29}$$

From Eqs. (2.27) and (2.28),

$$A_1 \sin \beta + A_2 = 0$$

or

$$A_2 = -A_1 \sin \beta \tag{2.30}$$

Copyright 2017 Cengage Learning. All Rights Reserved. May not be copied, scanned, or duplicated, in whole or in part. Due to electronic rights, some third party content may be suppressed from the eBook and/or eChapter(s). Editorial review has deemed that any suppressed content does not materially affect the overall learning experience. Cengage Learning reserves the right to remove additional content at any time if subsequent rights restrictions require it.

Again, from Eq. (2.27),

$$\frac{dz}{dt} = A_1\,\omega\cos(\omega t + \beta) - A_2\,\omega_n \sin\omega_n t + A_3\,\omega_n \cos\omega_n t$$

Substituting the boundary condition given by Eq. (2.29) in the preceding equation gives

$$A_1\,\omega\cos\beta + A_3\,\omega_n = 0$$

or

$$A_3 = -\left(\frac{A_1\,\omega}{\omega_n}\right)\cos\beta \tag{2.31}$$

Combining Eqs. (2.27), (2.30), and (2.31),

$$z = A_1\left[\sin(\omega t + \beta) - \cos(\omega t)\sin\beta - \left(\frac{\omega}{\omega_n}\right)\sin(\omega_n t)\cos\beta\right] \tag{2.32}$$

For a real system, the last two terms inside the brackets in Eq. (2.32) will vanish due to damping, leaving the only term for steady-state solution.

If the forcing function is in phase with the vibratory system (*i.e.*, $\beta = 0$), then

$$z = A_1\left(\sin\omega t - \left(\frac{\omega}{\omega_n}\right)\sin\omega_n t\right)$$

$$= \frac{Q_0/m}{(k/m) - \omega^2}\left(\sin\omega t - \frac{\omega}{\omega_n}\sin\omega_n t\right)$$

or

$$\boxed{z = \frac{Q_0/k}{1-(\omega^2/\omega_n^2)}\left(\sin\omega t - \frac{\omega}{\omega_n}\sin\omega_n t\right)} \tag{2.33}$$

However, $Q_0/k = z_s =$ static deflection. If one lets $1/(1-\omega^2/\omega_n^2)$ be equal to M [equal to the magnification factor or $A_1/(Q_0/k)$], Eq. (2.33) reads as

$$z = z_s M\left[\sin\omega t - \left(\frac{\omega}{\omega_n}\right)\sin\omega_n t\right] \tag{2.34}$$

The nature of variation of the magnification factor M with ω/ω_n is shown in Figure 2.7a. Note that the magnification factor goes to infinity when $\omega/\omega_n = 1$. This is called the *resonance condition.* For the resonance condition, the right-hand side of Eq. (2.34) yields 0/0.

Copyright 2017 Cengage Learning. All Rights Reserved. May not be copied, scanned, or duplicated, in whole or in part. Due to electronic rights, some third party content may be suppressed from the eBook and/or eChapter(s). Editorial review has deemed that any suppressed content does not materially affect the overall learning experience. Cengage Learning reserves the right to remove additional content at any time if subsequent rights restrictions require it.

Thus, applying *L'Hopital's rule*,

$$\lim_{\omega \to \omega_n}(z) = z_s\left[\frac{(d/d\omega)\left[\sin\omega t - (\omega/\omega_n)\sin\omega_n t\right]}{(d/d\omega)(1-\omega^2/\omega_n^2)}\right]$$

or

$$z = \frac{1}{2}z_s(\sin\omega_n t - \omega_n t\cos\omega_n t) \tag{2.35}$$

The velocity at resonance condition can be obtained from Eq. (2.35) as

$$\begin{aligned}\dot{z} &= \frac{1}{2}z_s(\omega_n\cos\omega_n t - \omega_n\cos\omega_n t + \omega_n^2 t\sin\omega_n t)\\ &= \frac{1}{2}(z_s\omega_n^2 t)\sin\omega_n t\end{aligned} \tag{2.36}$$

Since the velocity is equal to zero at the point where the displacement is at maximum, for maximum displacement

$$\dot{z} = 0 = \frac{1}{2}(z_s\omega_n^2 t)\sin\omega_n t$$

or

$$\sin\omega_n t = 0, \text{ i.e., } \omega_n t = n\pi \tag{2.37}$$

where n is an integer.

For the condition given by Eq. (2.37), the displacement equation (2.35) yields

$$|z_{\max}|_{\text{res}} = \frac{1}{2}n\pi z_s \tag{2.38}$$

where $z_{\max}$ = maximum displacement.

It may be noted that when n tends to ∞, $|z_{\max}|$ is also infinite, which points out the danger to the foundation. The nature of variation of z/z_s versus time for the *resonance condition* is shown in Figure 2.7b.

Maximum Force on Foundation Subgrade

The maximum and minimum force on the foundation subgrade will occur at the time when the amplitude is maximum, i.e., when velocity is equal to zero. This can be derived from displacement Eq. (2.33):

$$z = \frac{Q_0}{k}\frac{1}{(1-\omega^2/\omega_n^2)}\left(\sin\omega t - \frac{\omega}{\omega_n}\sin\omega_n t\right)$$

Copyright 2017 Cengage Learning. All Rights Reserved. May not be copied, scanned, or duplicated, in whole or in part. Due to electronic rights, some third party content may be suppressed from the eBook and/or eChapter(s). Editorial review has deemed that any suppressed content does not materially affect the overall learning experience. Cengage Learning reserves the right to remove additional content at any time if subsequent rights restrictions require it.

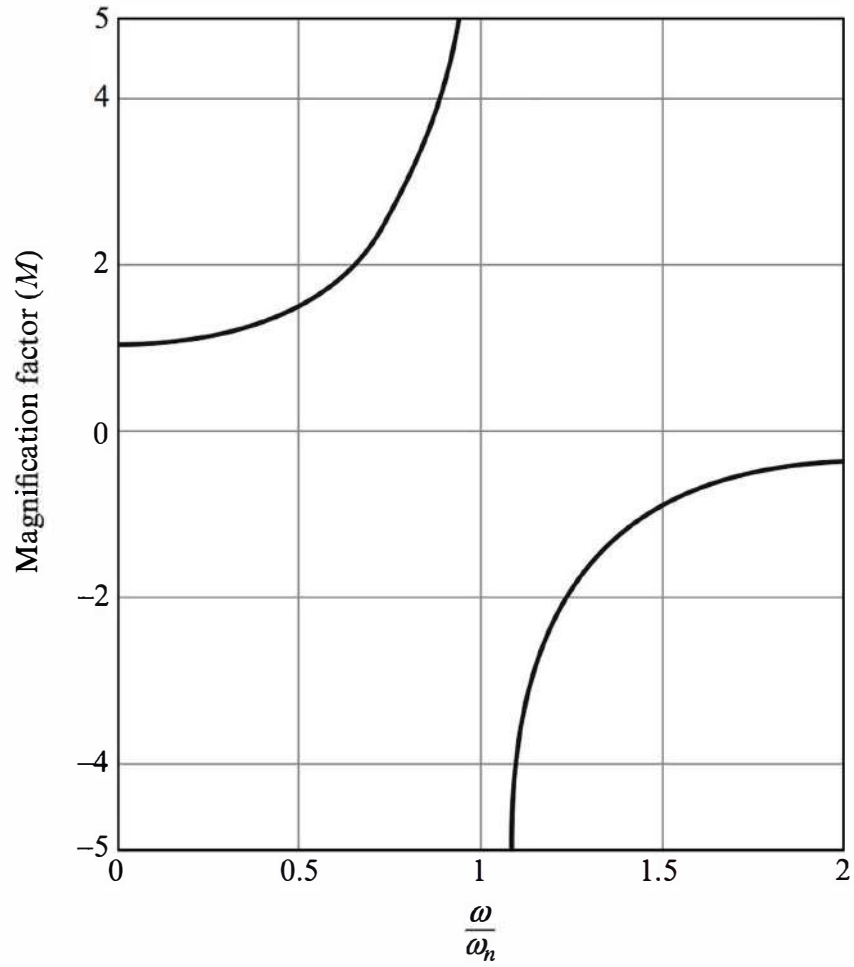

(a)

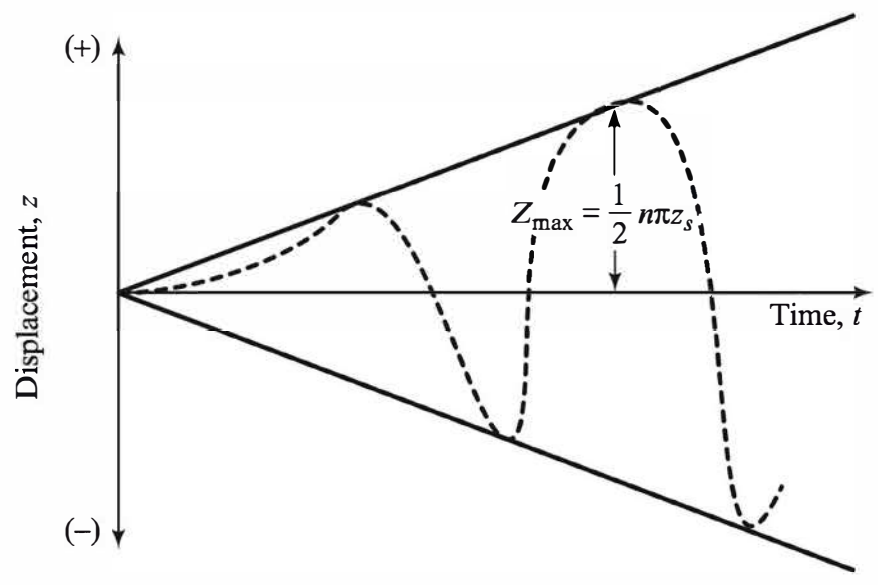

(b)

Figure 2.7 Forced vibration of a mass-spring system: (a) variation of magnification factor with ω/ω_n; (b) vibration of displacement with time at resonance ($\omega = \omega_n$)

Thus, the velocity at any time is

$$\dot{z} = \frac{Q}{k}\frac{1}{\left(1-\omega^2/\omega_n^2\right)}(\omega\cos\omega t - \omega\cos\omega_n t)$$

Copyright 2017 Cengage Learning. All Rights Reserved. May not be copied, scanned, or duplicated, in whole or in part. Due to electronic rights, some third party content may be suppressed from the eBook and/or eChapter(s). Editorial review has deemed that any suppressed content does not materially affect the overall learning experience. Cengage Learning reserves the right to remove additional content at any time if subsequent rights restrictions require it.

For maximum deflection, $\dot{z} = 0$, or

$$\omega \cos \omega t - \omega \cos \omega_n t = 0$$

Since ω is not equal to zero,

$$\cos \omega t - \cos \omega_n t = 2 \sin\left(\frac{\omega_n - \omega}{2}\right) t \sin\left(\frac{\omega_n + \omega}{2}\right) t = 0$$

thus,

$$\frac{1}{2}(\omega_n - \omega)t = n\pi; \quad t = \frac{2n\pi}{\omega_n - \omega} \tag{2.39}$$

or

$$\frac{1}{2}(\omega_n + \omega)t = m\pi; \quad t = \frac{2m\pi}{\omega_n + \omega} \tag{2.40}$$

where m and $n = 1, 2, 3, \ldots$.

Equation (2.39) is not relevant (beating phenomenon). Substituting Eq. (2.40) into Eq. (2.33) and simplifying it further,

$$z = z_{\max} = \frac{Q_0}{k} \frac{1}{(1 - \omega/\omega_n)} \sin\left(\frac{2\pi m\omega}{\omega_n + \omega}\right) \tag{2.41}$$

In order to determine the maximum dynamic force, the maximum value of $z_{\max}$ given in Eq. (2.41) is required:

$$z_{\max(\max)} = \frac{(Q_0/k)}{1 - \omega/\omega_n} \tag{2.42}$$

Hence,

$$\boxed{F_{\text{dynam}(\max)} = k[z_{\max(\max)}] = \frac{k(Q_0/k)}{1 - \omega/\omega_n} = \frac{Q_0}{1 - \omega/\omega_n}} \tag{2.43}$$

Hence, the total force on the subgrade will vary between the limits

$$W - \frac{Q_0}{1 - \omega/\omega_n} \text{ and } W + \frac{Q_0}{1 - \omega/\omega_n}$$

Copyright 2017 Cengage Learning. All Rights Reserved. May not be copied, scanned, or duplicated, in whole or in part. Due to electronic rights, some third party content may be suppressed from the eBook and/or eChapter(s). Editorial review has deemed that any suppressed content does not materially affect the overall learning experience. Cengage Learning reserves the right to remove additional content at any time if subsequent rights restrictions require it.

EXAMPLE 2.3

A machine foundation can be idealized as a mass-spring system. This foundation can be subjected to a force that can be given as Q (kN) $= 35.6 \sin \omega t$.
Given

$$f = 13.33 \text{ Hz}$$

$$\text{Weight of the machine + foundation} = 178 \text{ kN}$$

$$\text{Spring constant} = 70{,}000 \text{ kN/m}$$

Determine the maximum and minimum force transmitted to the subgrade.

SOLUTION:

$$\text{Natural angular frequency} = \omega_n = \sqrt{\frac{k}{m}} = \sqrt{\frac{70000 \times 10^3}{178 \times 10^3/9.81}}$$

$$= 62.11 \text{ rad/s}$$

$$F_{\text{dynam}} = \frac{Q_0}{1 - \omega/\omega_n}$$

But

$$\omega = 2\pi f = 2\pi \times 13.33 = 83.75 \text{ rad/s}$$

Thus

$$|F_{\text{dynam}}| = \frac{35.6}{1 - (83.75/62.11)} = 102.18 \text{ kN}$$

Maximum force on the subgrade $= 178 + 102.18 =$ **280.18 kN**
Minimum force on the subgrade $= 178 - 102.18 =$ **75.82 kN**

2.5 FREE VIBRATION WITH VISCOUS DAMPING

In the case of undamped free vibration as explained in Section 2.3, vibration would continue once the system has been set in motion. However, in practical cases, all vibrations undergo a gradual decrease of amplitude with time. This characteristic of vibration is referred to as damping. Figure 2.2b shows a foundation supported by a spring and a dashpot. The dashpot represents the damping characteristic of the soil. The dashpot coefficient is equal to c. For free vibration of the foundation (i.e., the force $Q = Q_0 \sin \omega t$ on the foundation is zero), the differential equation of motion can be given by

$$m\ddot{z} + c\dot{z} + kz = 0 \tag{2.44}$$

Let $z = Ae^{rt}$ be a solution to Eq. (2.44), where A is a constant. Substitution of this into Eq. (2.44) yields

$$mAr^2e^{rt} + cAre^{rt} + kAe^{rt} = 0$$

Copyright 2017 Cengage Learning. All Rights Reserved. May not be copied, scanned, or duplicated, in whole or in part. Due to electronic rights, some third party content may be suppressed from the eBook and/or eChapter(s). Editorial review has deemed that any suppressed content does not materially affect the overall learning experience. Cengage Learning reserves the right to remove additional content at any time if subsequent rights restrictions require it.

or

$$r^2 + \left(\frac{c}{m}\right)r + \frac{k}{m} = 0 \tag{2.45}$$

The solutions to Eq. (2.45) can be given as

$$r = -\frac{c}{2m} \pm \sqrt{\frac{c^2}{4m^2} - \frac{k}{m}} \tag{2.46}$$

There are three general conditions that may be developed from Eq. (2.46):

1. If $c/2m > \sqrt{k/m}$, both roots of Eq. (2.45) are real and negative. This is referred to as an *overdamped* case.
2. If $c/2m = \sqrt{k/m}$, $r = -c/2m$. This is called the *critical damping* case. Thus, for this case,

$$\boxed{c = c_c = 2\sqrt{km}} \tag{2.47a}$$

3. If $c/2m < \sqrt{k/m}$, the roots of Eq. (2.45) are complex:

$$r = -\frac{c}{2m} \pm i\sqrt{\frac{k}{m} - \frac{c^2}{4m^2}}$$

This is referred to as a case of *underdamping*.

It is possible now to define a damping ratio D, which can be expressed as

$$\boxed{D = \frac{c}{c_c} = \frac{c}{2\sqrt{km}}} \tag{2.47b}$$

Using the damping ratio, Eq. (2.46) can be rewritten as

$$r = -\frac{c}{2m} \pm \sqrt{\frac{c}{4m^2} - \frac{k}{m}} = \omega_n\left(-D \pm \sqrt{D^2 - 1}\right) \tag{2.48}$$

where $\omega_n = \sqrt{k/m}$

For the *overdamped condition* ($D > 1$),

$$r = \omega_n\left(-D \pm \sqrt{D^2 - 1}\right)$$

For this condition, the equation for displacement (i.e., $z = Ae^{rt}$) may be written as

$$Z = A_1 \exp\left[\omega_n t\left(-D + \sqrt{D^2 - 1}\right)\right] + A_2 \exp\left[\omega_n t\left(-D - \sqrt{D^2 - 1}\right)\right] \tag{2.49}$$

Copyright 2017 Cengage Learning. All Rights Reserved. May not be copied, scanned, or duplicated, in whole or in part. Due to electronic rights, some third party content may be suppressed from the eBook and/or eChapter(s). Editorial review has deemed that any suppressed content does not materially affect the overall learning experience. Cengage Learning reserves the right to remove additional content at any time if subsequent rights restrictions require it.

where A_1 and A_2 are two constants. Now, let

$$A_1 = \frac{1}{2}(A_3 + A_4) \tag{2.50}$$

and

$$A_2 = \frac{1}{2}(A_3 - A_4) \tag{2.51}$$

Substitution of Eqs. (2.50) and (2.51) into Eq. (2.49) and rearrangement gives

$$z = e^{-D\omega_n t}\left\{\frac{1}{2}A_3\left[\exp\left(\omega_n\sqrt{D^2-1}\,t\right)+\exp\left(-\omega_n\sqrt{D^2-1}\,t\right)\right]\right.$$
$$\left.+\frac{1}{2}A_4\left[\exp\left(\omega_n\sqrt{D^2-1}\,t\right)+\exp\left(-\omega_n\sqrt{D^2-1}\,t\right)\right]\right.$$

or

$$z = e^{-D\omega_n t}\left[A_3\cosh\left(\omega_n\sqrt{D^2-1}\,t\right)+A_4\sinh\left(\omega_n\sqrt{D^2-1}\,t\right)\right] \tag{2.52}$$

Equation (2.52) shows that the system which is overdamped will not oscillate at all. The variation of z with time will take the form shown in Figure 2.8a.

The constants A_3 and A_4 in Eq. (2.52) can be evaluated by knowing the initial conditions. Let, at time $t = 0$, displacement $= z = z_0$ and velocity $= dz/dt = v_0$. From Eq. (2.52) and the first boundary condition,

$$z = z_0 = A_3 \tag{2.53}$$

Again, from Eq. (2.52) and the second boundary condition,

$$\frac{dz}{dt} = v_0 = \left(\omega_n\sqrt{D^2-1}\,A_4\right) - D\,\omega_n A_3$$

or

$$A_4 = \frac{v_0 + D\omega_n A_3}{\omega_n\sqrt{D^2-1}} = \frac{v_0 + D\omega_n z_0}{\omega_n\sqrt{D^2-1}} \tag{2.54}$$

Substituting Eqs. (2.53) and (2.54) into Eq. (2.52)

$$\boxed{z = e^{-D\omega_n t}\left[z_0\cosh\left(\omega_n\sqrt{D^2-1}\,t\right)+\frac{v_0 + D\omega_n z_0}{\omega_n\sqrt{D^2-1}}\sinh\left(\sqrt{D^2-1}\,t\right)\right]} \tag{2.55}$$

For a *critically damped condition* ($D = 1$), from Eq. (2.48),

$$r = -\omega_n \tag{2.56}$$

Copyright 2017 Cengage Learning. All Rights Reserved. May not be copied, scanned, or duplicated, in whole or in part. Due to electronic rights, some third party content may be suppressed from the eBook and/or eChapter(s). Editorial review has deemed that any suppressed content does not materially affect the overall learning experience. Cengage Learning reserves the right to remove additional content at any time if subsequent rights restrictions require it.

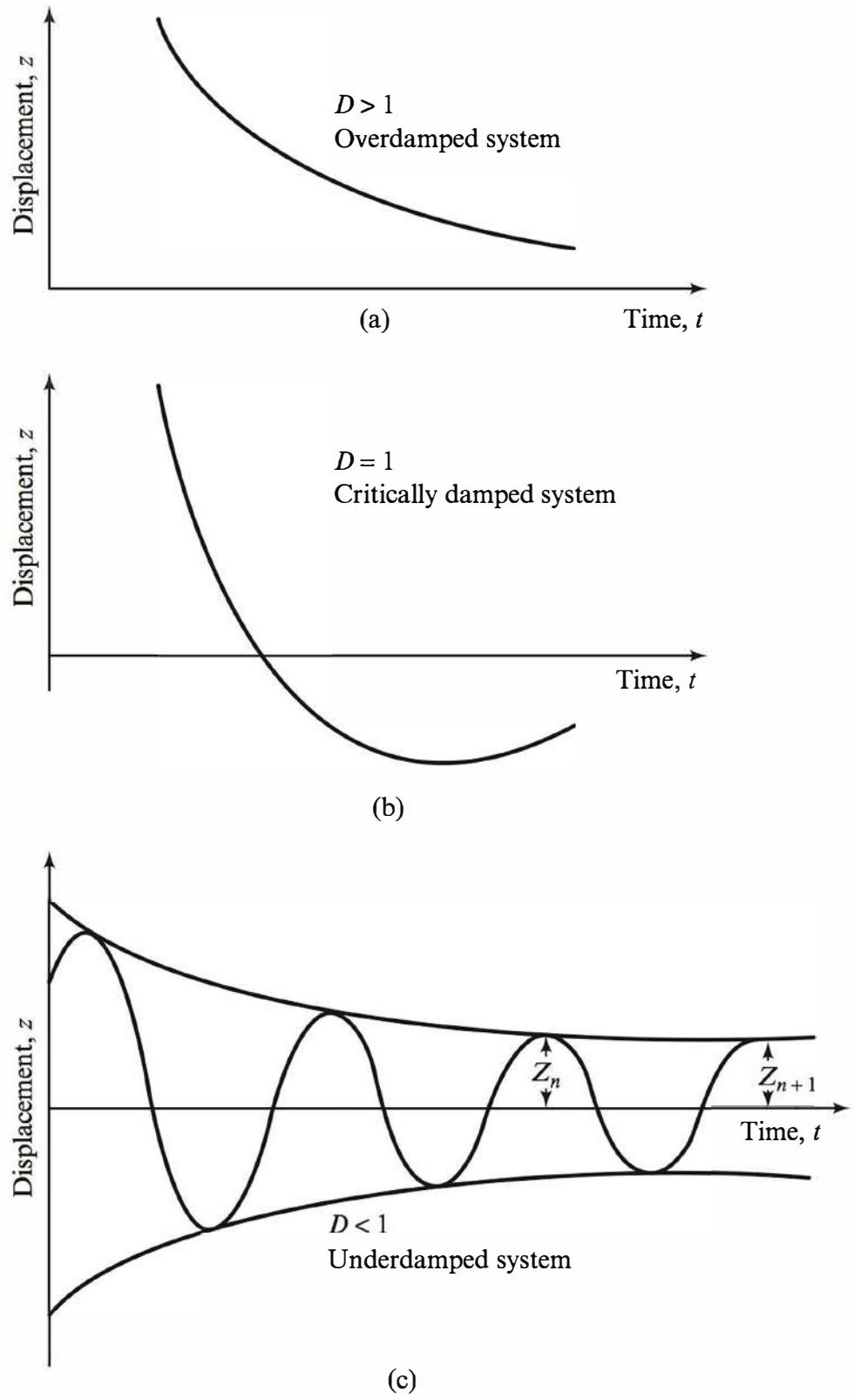

Figure 2.8 Free vibration of a mass-spring-dashpot system: (a) overdamped case; (b) critically damped case; (c) underdamped case

Given this condition, the equation for displacement ($z = Ae^{rt}$) may be written as

$$z = (A_5 + A_6 t)e^{-\omega_n t} \tag{2.57}$$

where A_5 and A_6 are two constants. This is similar to the case of the overdamped system except for the fact that the sign of z changes only once. This is shown in Figure 2.8b.

Copyright 2017 Cengage Learning. All Rights Reserved. May not be copied, scanned, or duplicated, in whole or in part. Due to electronic rights, some third party content may be suppressed from the eBook and/or eChapter(s). Editorial review has deemed that any suppressed content does not materially affect the overall learning experience. Cengage Learning reserves the right to remove additional content at any time if subsequent rights restrictions require it.

The values of A_5 and A_6 in Eq. (2.57) can be determined by using the initial conditions of vibration. Let, at time $t = 0$,

$$z = z_0, \qquad \frac{dz}{dt} = v_0$$

From the first of the preceding two conditions and Eq. (2.57),

$$z = z_0 = A_5 \tag{2.58}$$

Similarly, from the second condition and Eq. (2.57)

$$\frac{dz}{dt} = v_0 = -\omega_n A_5 + A_6 = -\omega_n z_0 + A_6$$

or

$$A_6 = v_0 + \omega_n z_0 \tag{2.59}$$

A combination of Eqs. (2.57) – (2.59) yields

$$\boxed{z = [z_0 + (v_0 + \omega_n z_0)t]e^{-\omega_n t}} \tag{2.60}$$

Finally, for the underdamped condition ($D < 1$),

$$r = \omega_n\left(-D \pm i\sqrt{1 - D^2}\right)$$

Thus, the general form of the equation for the displacement ($z = Ae^{rt}$) can be expressed as

$$z = e^{-D\omega_n t}\left[A_7 \exp\left(i\omega_n\sqrt{1 - D^2}\, t\right) + A_8 \exp\left(-i\omega_n\sqrt{1 - D^2}\, t\right)\right] \tag{2.61}$$

where A_7 and A_8 are two constants.

Equation (2.61) can be simplified to the form

$$z = e^{-D\omega_n t}\left[A_9 \cos\left(\omega_n\sqrt{1 - D^2}\, t\right) + A_{10} \sin\left(\omega_n\sqrt{1 - D^2}\, t\right)\right] \tag{2.62}$$

where A_9 and A_{10} are two constants.

The values of the constants A_9 and A_{10} in Eq. (2.62) can be determined by using the following initial conditions of vibration. Let, at time $t = 0$,

$$z = z_0 \qquad \text{and} \qquad \frac{dt}{dz} = v_0$$

The final equation with theses boundary conditions will be of the form

$$z = e^{-D\omega_n t}\left[z_0 \cos\left(\omega_n\sqrt{1 - D^2}\, t\right) + \frac{v_0 + D\omega_n z_0}{\omega_n\sqrt{1 - D^2}} \cdot \sin\left(\omega_n\sqrt{1 - D^2}\, t\right)\right] \tag{2.63}$$

Copyright 2017 Cengage Learning. All Rights Reserved. May not be copied, scanned, or duplicated, in whole or in part. Due to electronic rights, some third party content may be suppressed from the eBook and/or eChapter(s). Editorial review has deemed that any suppressed content does not materially affect the overall learning experience. Cengage Learning reserves the right to remove additional content at any time if subsequent rights restrictions require it.

Equation (2.63) can further be simplified as

$$z = Z\cos(\omega_d t - \alpha) \tag{2.64}$$

where

$$Z = e^{-D\omega_n t}\sqrt{z_0^2 + \left(\frac{v_0 + D\omega_n z_0}{\omega_n\sqrt{1-D^2}}\right)^2} \tag{2.65}$$

$$\alpha = \tan^{-1}\left(\frac{v_0 + D\omega_n z_0}{\omega_n z_0\sqrt{1-D^2}}\right) \tag{2.66}$$

$$\boxed{\omega_d = \text{damped natural circular frequency} = \omega_n\sqrt{1-D^2}} \tag{2.67}$$

The effect of damping is to decrease gradually the amplitude of vibration with time. In order to evaluate the magnitude of decrease of the amplitude of vibration with time, let Z_n and Z_{n+1} be the two successive positive or negative maximum values of displacement at times t_n and t_{n+1} from the start of the vibration as shown in Figure 2.8c. From Eq. (2.65),

$$\frac{Z_{n+1}}{Z_n} = \frac{\exp(-D\omega_n t_{n+1})}{\exp(-D\omega_n t_n)} = \exp\left[-D\omega_n\left(t_{n+1} - t_n\right)\right] \tag{2.68}$$

However, $t_{n+1} - t_n$ is the period of vibration T,

$$\boxed{T = \frac{2\pi}{\omega_d} = \frac{2\pi}{\omega_n\sqrt{1-D^2}}} \tag{2.69}$$

Thus, combining Eqs. (2.68) and (2.69),

$$\delta = \ln\left(\frac{Z_n}{Z_{n+1}}\right) = \frac{2\pi D}{\sqrt{1-D^2}} \tag{2.70}$$

The term δ is called the *logarithmic decrement*.
If the damping ratio D is small, Eq. (2.70) can be approximated as

$$\boxed{\delta = \ln\left(\frac{Z_n}{Z_{n+1}}\right) = 2\pi D} \tag{2.71}$$

EXAMPLE 2.4

For a machine foundation, given weight = 60 kN,
spring constant = 11,000 kN/m, and c = 200 kN-s/m, determine

a. whether the system is overdamped, underdamped, or critically damped,
b. the logarithmic decrement, and
c. the ratio of two successive amplitudes.

Copyright 2017 Cengage Learning. All Rights Reserved. May not be copied, scanned, or duplicated, in whole or in part. Due to electronic rights, some third party content may be suppressed from the eBook and/or eChapter(s). Editorial review has deemed that any suppressed content does not materially affect the overall learning experience. Cengage Learning reserves the right to remove additional content at any time if subsequent rights restrictions require it.

SOLUTION:

a. From Eq. (2.47a),

$$c_c = 2\sqrt{km} = 2\sqrt{11{,}000\left(\frac{60}{9.81}\right)} = 518.76 \text{ kN.s/m}$$

$$\frac{c}{c_c} = D = \frac{200}{518.76} = 0.386 < 1$$

Hence, the system is **underdamped**.

b. From Eq. (2.70),

$$\delta = \frac{2\pi D}{\sqrt{1-D^2}} = \frac{2\pi(0.386)}{\sqrt{1-(0.386)^2}} = \mathbf{2.63}$$

c. Again, from Eq. (2.70),

$$\frac{Z_n}{Z_{n+1}} = e^{\delta} = e^{2.63} = \mathbf{13.87}$$

EXAMPLE 2.5

For Example 2.4, determine the damped natural frequency.

SOLUTION:

From Eq. (2.67),

$$f_d = \sqrt{1-D^2}\, f_n$$

where f_d = damped natural frequency.

$$f_n = \frac{1}{2\pi}\sqrt{\frac{k}{m}} = \frac{1}{2\pi}\sqrt{\frac{11{,}000 \times 9.81}{60}} = 6.75 \text{ Hz}$$

Thus,

$$f_d = \left(\sqrt{1-(0.386)^2}\right)(6.75) = \mathbf{6.23\ Hz}$$

Copyright 2017 Cengage Learning. All Rights Reserved. May not be copied, scanned, or duplicated, in whole or in part. Due to electronic rights, some third party content may be suppressed from the eBook and/or eChapter(s). Editorial review has deemed that any suppressed content does not materially affect the overall learning experience. Cengage Learning reserves the right to remove additional content at any time if subsequent rights restrictions require it.

2.6 STEADY-STATE FORCED VIBRATION WITH VISCOUS DAMPING

Figure 2.2b shows the case of a foundation resting on a soil that can be approximated to an equivalent spring and dashpot. This foundation is being subjected to a sinusoidally varying force $Q = Q_0 \sin \omega t$. The differential equation of motion for this system can be given be

$$m\ddot{z} + kz + c\dot{z} = Q_0 \sin \omega t \tag{2.72}$$

The transient part of the vibration is damped out quickly; so, considering the particular solution for Eq. (2.72) for the steady-state motion, let

$$z = A_1 \sin \omega t + A_2 \cos \omega t \tag{2.73}$$

where A_1 and A_2 are two constants.

Substituting Eq. (2.73) into Eq. (2.72),

$$m(-A_1\omega^2 \sin \omega t - A_2\omega^2 \cos \omega t) + k(A_1 \sin \omega t + A_2 \cos \omega t) + c(A_1\omega \cos \omega t - A_2\omega \sin \omega t) = Q_0 \sin \omega t \tag{2.74}$$

Collecting *sine* and *cosine* functions in Eq. (2.74) separately,

$$(-mA_1\omega^2 + kA_1 - cA_2\omega)\sin \omega t = Q_0 \sin \omega t \tag{2.75a}$$

$$(-mA_2\omega^2 + A_2k + cA_1\omega)\cos \omega t = 0 \tag{2.75b}$$

From Eq. (2.75a),

$$A_1\left(\frac{k}{m} - \omega^2\right) - A_2\left(\frac{c}{m}\omega\right) = \frac{Q_0}{m} \tag{2.76}$$

And from Eq. (2.75b),

$$A_1\left(\frac{c}{m}\omega\right) + A_2\left(\frac{k}{m} - \omega^2\right) = 0 \tag{2.77}$$

Solution of Eqs. (2.76) and (2.77) will give the following relations for the constants A_1 and A_2:

$$A_1 = \frac{(k - m\omega^2)Q_0}{\left(k - m\omega^2\right)^2 + c^2\omega^2} \tag{2.78}$$

Copyright 2017 Cengage Learning. All Rights Reserved. May not be copied, scanned, or duplicated, in whole or in part. Due to electronic rights, some third party content may be suppressed from the eBook and/or eChapter(s). Editorial review has deemed that any suppressed content does not materially affect the overall learning experience. Cengage Learning reserves the right to remove additional content at any time if subsequent rights restrictions require it.

and

$$A_2 = \frac{-c\omega Q_0}{\left(k - m\omega^2\right)^2 + c^2\omega^2} \tag{2.79}$$

By substituting Eqs. (2.78) and (2.79) into Eq. (2.73) and simplifying, one can obtain

$$\boxed{z = Z\cos(\omega t + \alpha)} \tag{2.80}$$

where

$$\alpha = \tan^{-1}\left(-\frac{A_1}{A_2}\right) = \tan^{-1}\left(\frac{k - m\omega^2}{c\omega}\right) = \tan^{-1}\left[\frac{1 - \left(\omega^2/\omega_n^2\right)}{2D\left(\omega/\omega_n\right)}\right] \tag{2.81}$$

and

$$\boxed{Z = \sqrt{A_1^2 + A_2^2} = \frac{\left(Q_0/k\right)}{\sqrt{\left[1 - \left(\omega^2/\omega_n^2\right)\right]^2 + 4D^2\left(\omega^2/\omega_n^2\right)}}} \tag{2.82}$$

where $\omega_n = \sqrt{k/m}$ is the undamped natural frequency and D is the damping ratio.

Equation (2.82) can be plotted in a nondimensional form as $Z/(Q_0/k)$ against ω/ω_n. This is shown in Figure 2.9. In this figure, note that the maximum values of $Z/(Q_0/k)$ do not occur at $\omega = \omega_n$, as occurs in the case of forced vibration of a spring-mass system (Section 2.4). Mathematically, this can be shown as follows: From Eq. (2.82),

$$\frac{Z}{\left(Q_0/k\right)} = \frac{1}{\sqrt{\left[1 - \left(\omega^2/\omega_n^2\right)\right]^2 + 4D^2\left(\omega^2/\omega_n^2\right)}} \tag{2.83}$$

For maximum value of $Z/(Q_0/k)$,

$$\frac{\partial\left[Z/\left(Q_0/k\right)\right]}{\partial\left(\omega/\omega_n\right)} = 0 \tag{2.84}$$

From Eqs. (2.83) and (2.84),

$$\frac{\omega}{\omega_n}\left(1 - \frac{\omega^2}{\omega_n^2}\right) - 2D^2\left(\frac{\omega}{\omega_n}\right) = 0$$

or

$$\omega = \omega_n\sqrt{1 - 2D^2} \tag{2.85}$$

Copyright 2017 Cengage Learning. All Rights Reserved. May not be copied, scanned, or duplicated, in whole or in part. Due to electronic rights, some third party content may be suppressed from the eBook and/or eChapter(s). Editorial review has deemed that any suppressed content does not materially affect the overall learning experience. Cengage Learning reserves the right to remove additional content at any time if subsequent rights restrictions require it.

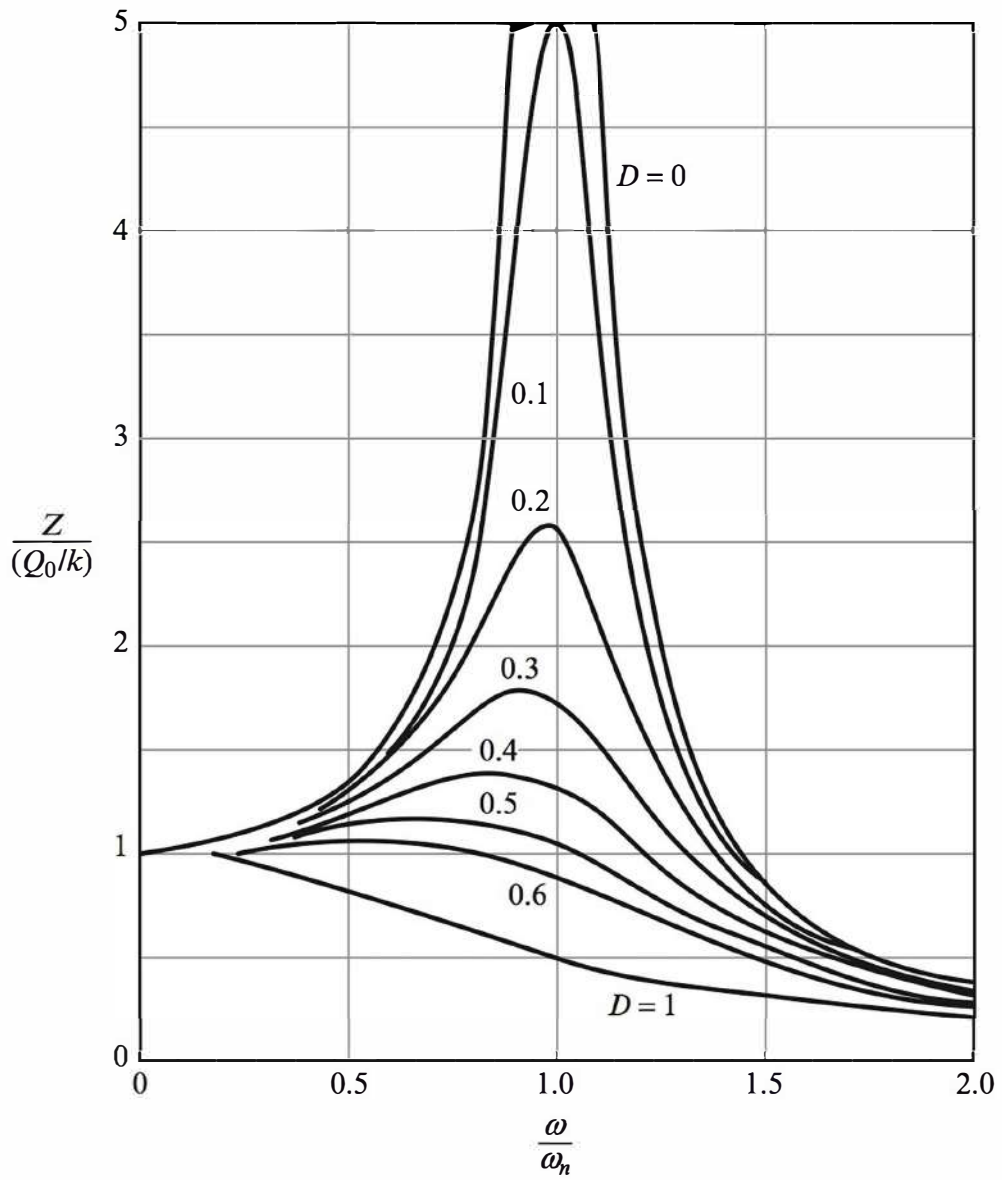

Figure 2.9 Plot of $Z/(Q_0/k)$ against ω/ω_n

Hence,

$$f_m = f_n\sqrt{1-2D^2} \tag{2.86}$$

where f_m is the frequency at maximum amplitude (*the resonant frequency for vibration with damping*), and f_n is the natural frequency $= (1/2\pi)\sqrt{k/m}$. Hence, the amplitude of vibration at resonance can be obtained by substituting Eq. (2.85) into Eq. (2.82):

$$\boxed{\begin{aligned} Z_{\text{res}} &= \frac{Q_0}{k}\frac{1}{\sqrt{\left[1-\left(1-2D^2\right)\right]^2+4D^2\left(1-2D^2\right)}} \\ &= \frac{Q_0}{k}\frac{1}{2D\sqrt{1-D^2}} \end{aligned}} \tag{2.87}$$

Copyright 2017 Cengage Learning. All Rights Reserved. May not be copied, scanned, or duplicated, in whole or in part. Due to electronic rights, some third party content may be suppressed from the eBook and/or eChapter(s). Editorial review has deemed that any suppressed content does not materially affect the overall learning experience. Cengage Learning reserves the right to remove additional content at any time if subsequent rights restrictions require it.

Maximum Dynamic Force Transmitted to the Subgrade

For vibrating foundations, it is sometimes necessary to determine the dynamic force transmitted to the foundation. This can be given by summing the spring force and the damping force caused by relative motion between mass and dashpot; that is,

$$F_{\text{dynam}} = k\,z + c\,\dot{z} \tag{2.88a}$$

From Eq. (2.80),

$$z = Z\cos(\omega t + \alpha)$$

therefore,

$$\dot{z} = -\omega Z \sin\left(\omega t + \alpha\right)$$

and

$$F_{\text{dynam}} = kZ\cos(\omega t + \alpha) - c\omega Z \sin(\omega + \alpha) \tag{2.88b}$$

If one lets

$$kZ = A\cos\phi \quad \text{and} \quad c\omega Z = A\sin\phi,$$

Then Eq. (2.88) can be written as

$$F_{\text{dynam}} = A\cos(\omega t + \phi + \alpha) \tag{2.89}$$

where

$$A = \sqrt{\left(A\cos\phi\right)^2 + \left(A\sin\phi\right)^2} = Z\sqrt{k^2 + (c\omega)^2} \tag{2.90}$$

Hence, the *magnitude of maximum dynamic force* will be equal to $Z\sqrt{k^2 + (c\omega)^2}$.

EXAMPLE 2.6

A machine and its foundation weigh 140 kN. The spring constant and the damping ratio of the soil supporting the soil may be taken as 12×10^4 kN/m and 0.2, respectively. Forced vibration of the foundation is caused by a force that can be expressed as

$$Q(\text{kN}) = Q_0 \sin\omega t$$
$$Q_0 = 46\text{ kN}, \omega = 157\text{ rad/s}$$

Determine

a. the undamped natural frequency of the foundation,
b. amplitude of motion, and
c. maximum dynamic force transmitted to the subgrade.

Copyright 2017 Cengage Learning. All Rights Reserved. May not be copied, scanned, or duplicated, in whole or in part. Due to electronic rights, some third party content may be suppressed from the eBook and/or eChapter(s). Editorial review has deemed that any suppressed content does not materially affect the overall learning experience. Cengage Learning reserves the right to remove additional content at any time if subsequent rights restrictions require it.

SOLUTION:

a. $f_n = \frac{1}{2\pi}\sqrt{\frac{k}{m}} = \frac{1}{2}\sqrt{\frac{12\times10^4}{140/9.81}} = \mathbf{14.59\ Hz}$

b. From Eq. (2.82),

$$Z = \frac{Q_0/k}{\sqrt{\left(1-\omega^2/\omega_n^2\right)^2 + 4D^2\left(\omega^2/\omega_n^2\right)}}$$

$$\omega_n = 2\pi f_n = 2\pi(14.59) = 91.67 \text{ rad/s}$$

$$Z = \frac{46/(12\times10^4)}{\sqrt{\left[1-(157/91.67)^2\right]^2 + 4(0.2)^2\times(157/91.67)^2}}$$

$$= \frac{3.833\times10^{-4}}{\sqrt{3.737+0.469}} = 0.000187 \text{ m} = \mathbf{0.187\ mm}$$

c. From Eq. (2.90), the dynamic force transmitted to the subgrade

$$A = Z\sqrt{k^2 + (c\omega)^2}$$

From Eq. (2.47b),

$$c = 2D\sqrt{km} = 2(0.2)\sqrt{\left(12\times10^4\right)\left(\frac{140}{9.81}\right)} = 523.46 \text{ kN.s/m}$$

Thus, the maximum dynamic force transmitted to the subgrade is

$$F_{\text{dynam}} = 0.000187\sqrt{(12\times10^4)^2 + (523.46\times157)^2} = \mathbf{27.20\ kN}$$

2.7 ROTATING-MASS-TYPE EXCITATION

In many cases of foundation equipment, vertical vibration of foundation is produced by counter-rotating masses as shown in Figure 2.10a. Since horizontal forces on the foundation at any instant cancel, the net vibrating force on the foundation can be determined to be equal to $2m_e e\omega^2 \sin\omega t$ (where m_e = mass of each counter-rotating element, e = eccentricity, and ω = angular frequency of the masses). In such cases, the equation of motion with viscous damping [Eq. (2.72)] can be modified to the form

$$m\ddot{z} + kz + c\dot{z} = Q_0 \sin\omega t \tag{2.91}$$

Copyright 2017 Cengage Learning. All Rights Reserved. May not be copied, scanned, or duplicated, in whole or in part. Due to electronic rights, some third party content may be suppressed from the eBook and/or eChapter(s). Editorial review has deemed that any suppressed content does not materially affect the overall learning experience. Cengage Learning reserves the right to remove additional content at any time if subsequent rights restrictions require it.

$$Q_0 = 2m_e e\omega^2 = U\omega^2 \tag{2.92}$$

$$U = 2m_e e \tag{2.93}$$

and m is the mass of the foundation, including $2m_e$.

Equations (2.91)-(2.93) can be similarly solved by the procedure presented in Section 2.6.

The solution for displacement may be given as

$$\boxed{z = Z\cos(\omega t + \alpha)} \tag{2.94}$$

where

$$\boxed{Z = \frac{(U/m)(\omega/\omega_n)^2}{\sqrt{(1-\omega^2/\omega_n^2)^2 + 4D^2(\omega^2/\omega_n^2)}}} \tag{2.95}$$

$$\alpha = \tan^{-1}\left[\frac{1-(\omega^2/\omega_n^2)}{2D(\omega/\omega_n)}\right] \tag{2.96}$$

In Section 2.6a, a nondimensional plot for the amplitude of vibration was given in Figure 2.9 [i.e., $Z(Q_0/k)$ versus ω/ω_n]. This was for a vibration produced by a sinusoidal forcing function ($Q_0 = \text{const}$). For a rotating-mass type of excitation, a similar type of non-dimensional plot for the amplitude of vibration can also be prepared. This is shown in Figure 2.10b, which is a plot of $Z/(U/m)$ versus ω/ω_n. Also proceeding in the same manner [as in Eq. (2.86) for the case where $Q = \text{const}$], the angular resonant frequency for rotating-mass-type excitation can be obtained as

$$\omega = \frac{\omega_n}{\sqrt{1-2D^2}} \tag{2.97}$$

or

$$\boxed{f_m = \text{damped resonant frequency} = \frac{f_n}{\sqrt{1-2D^2}}} \tag{2.98}$$

The amplitude at damped resonant frequency can be given [similar to Eq. (2.87)] as

$$Z_{\text{res}} = \frac{U/m}{2D\sqrt{1-D^2}} \tag{2.99}$$

Copyright 2017 Cengage Learning. All Rights Reserved. May not be copied, scanned, or duplicated, in whole or in part. Due to electronic rights, some third party content may be suppressed from the eBook and/or eChapter(s). Editorial review has deemed that any suppressed content does not materially affect the overall learning experience. Cengage Learning reserves the right to remove additional content at any time if subsequent rights restrictions require it.

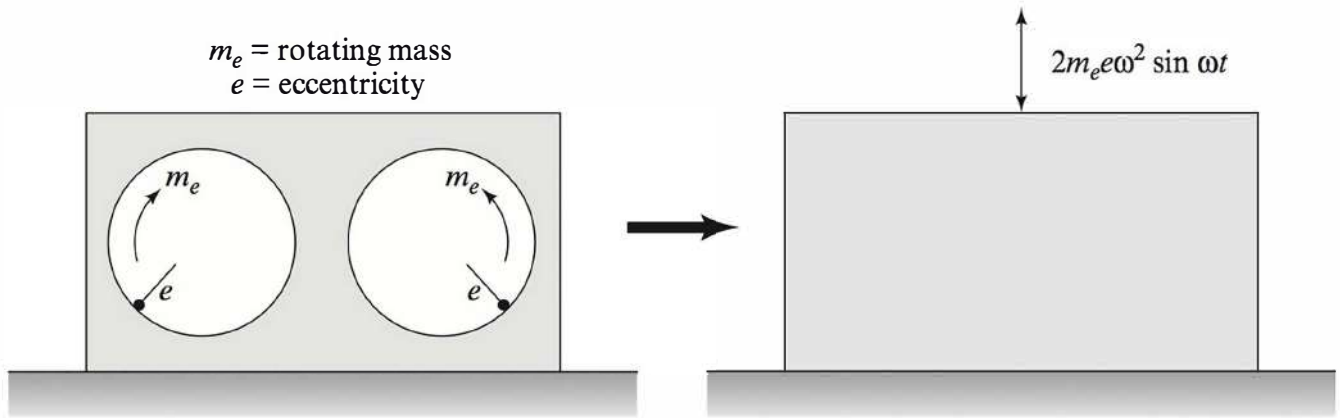

(a)

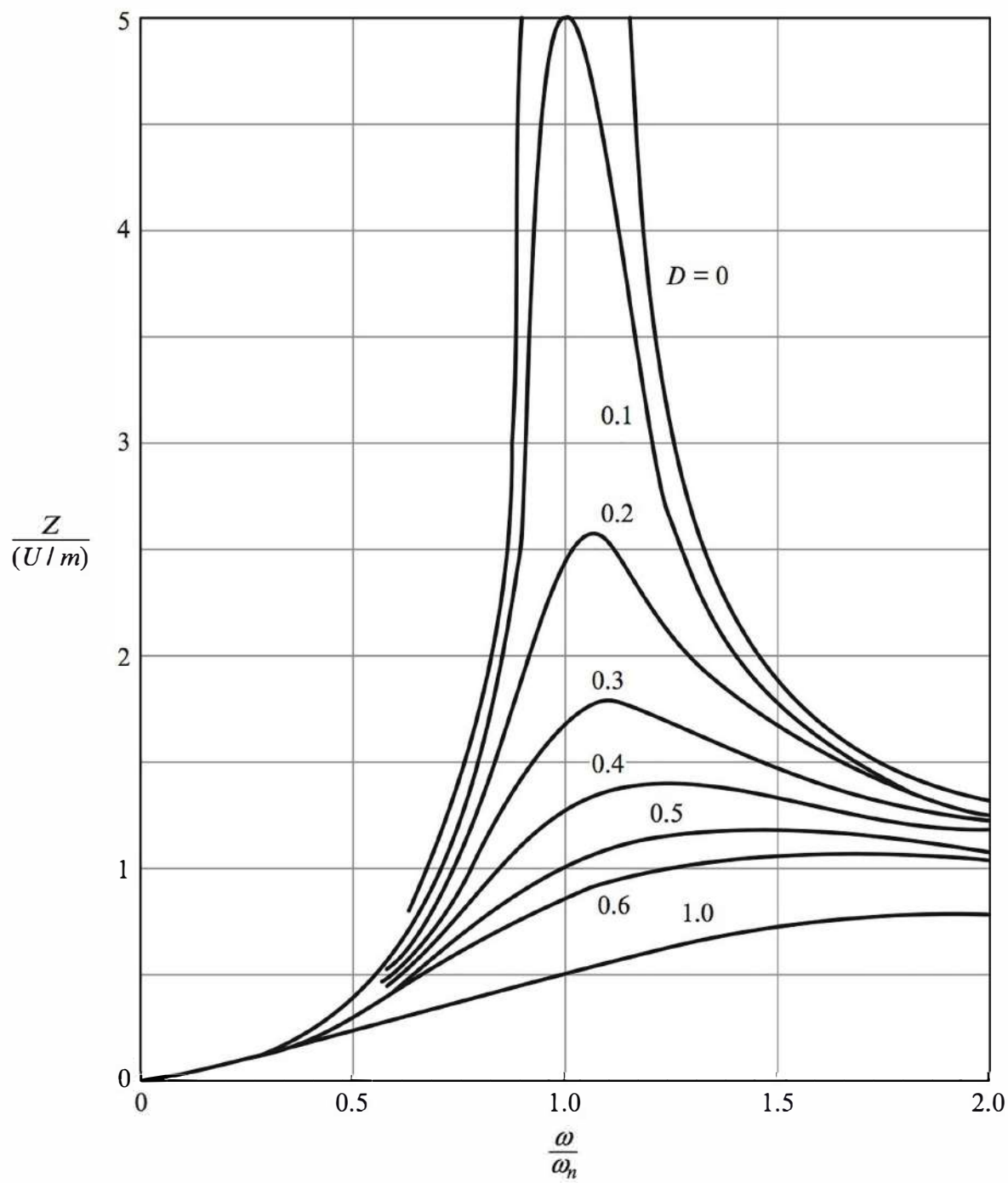

(b)

Figure 2.10 (a) Rotating mass-type excitation; (b) plot of $Z/(U/m)$ against ω/ω_n

Copyright 2017 Cengage Learning. All Rights Reserved. May not be copied, scanned, or duplicated, in whole or in part. Due to electronic rights, some third party content may be suppressed from the eBook and/or eChapter(s). Editorial review has deemed that any suppressed content does not materially affect the overall learning experience. Cengage Learning reserves the right to remove additional content at any time if subsequent rights restrictions require it.

EXAMPLE 2.7

A machine and its foundation weigh 100 kN. Given:

$$\text{Spring constant of the soil} = 10 \times 10^4 \text{ kN/m}$$
$$\text{Damping ratio} = 0.18$$

Forced vibration of the foundation is caused by rotating-mass-type of excitation. Given:

$$m_e = 2.5 \text{ kg}$$
$$e = 0.075 \text{ m}$$
$$\omega = 150 \text{ rad/s}$$

Determine:

a. Undamped natural frequency of the foundation
b. Amplitude of motion
c. Amplitude of damped resonant frequency

SOLUTION:

a. $$f_n = \frac{1}{2\pi}\sqrt{\frac{k}{m}} = \frac{1}{2\pi}\sqrt{\frac{10 \times 10^4}{\left(\frac{100}{9.81}\right)}} = \mathbf{15.76\ cps}$$

b. From Eq. (2.92)

$$Q_0 = 2m_e\, e\, \omega^2 = (2)(2.5)(0.075)(150)^2 = 8438 \text{ N} \approx 8.44 \text{ kN}$$

From Eq. (2.95)

$$Z = \frac{\left(\frac{U}{m}\right)\left(\frac{\omega}{\omega_n}\right)^2}{\sqrt{\left(1-\frac{\omega^2}{\omega_n^2}\right)^2 + 4D^2\left(\frac{\omega^2}{\omega_n^2}\right)}}$$

$$U = 2m_e e = (2)(2.5)(0.075) = 0.375$$

$$m = \frac{100 \times 1000}{9.81} \approx 10{,}194 \text{ kg}$$

$$\omega_n = 2\pi f_n = (2)(\pi)(15.76) = 99.02 \text{ rad/s}$$

$$Z = \frac{\left(\frac{0.375}{10{,}194}\right)\left(\frac{150}{99.02}\right)^2}{\sqrt{\left[1-\left(\frac{150}{99.02}\right)^2\right]^2 + (4)(0.18)(0.18)^2\left(\frac{150}{99.02}\right)^2}}$$

$$= 0.0000428 \text{ m} = \mathbf{0.0428\ mm}$$

Copyright 2017 Cengage Learning. All Rights Reserved. May not be copied, scanned, or duplicated, in whole or in part. Due to electronic rights, some third party content may be suppressed from the eBook and/or eChapter(s). Editorial review has deemed that any suppressed content does not materially affect the overall learning experience. Cengage Learning reserves the right to remove additional content at any time if subsequent rights restrictions require it.

c. From Eq. (2.99)

$$Z = \frac{\dfrac{U}{m}}{2D\sqrt{1-D^2}} = \frac{\dfrac{0.375}{10{,}194}}{(2)(0.18)\sqrt{1-(0.18)^2}} = 0.000104 = \mathbf{0.104\ mm}$$

2.8 DETERMINATION OF DAMPING RATIO

The damping ratio D can be determined from free and forced vibration tests on a system. In a free vibration test, the system is displaced from its equilibrium position, after which the amplitudes of displacement are recorded with time. Now, from Eq. (2.70)

$$\delta = \ln\left(\frac{Z_n}{Z_{n+1}}\right) = \frac{2\pi D}{\sqrt{1-D^2}}$$

If D is small, then

$$\delta = \ln\left(\frac{Z_n}{Z_{n+1}}\right) = 2\pi D \tag{2.100}$$

It can also be shown that

$$n\delta = \ln\frac{Z_0}{Z_n} = 2\pi n D \tag{2.101}$$

where Z_n = the peak amplitude of the nth cycle.
Thus,

$$\boxed{D = \frac{1}{2\pi n}\ln\frac{Z_0}{Z_n}} \tag{2.102}$$

In a forced vibration test, the following procedure can be used to determine the damping ratio.

1. Vibrate the system with a constant force type of excitation and obtain a plot of amplitude (Z) with frequency (f), as shown in Figure 2.11.
2. Determine Z_{res} from Figure 2.11.
3. Calculate $0.707Z_{res}$. Obtain the frequencies f_1 and f_2 that correspond to $0.707Z_{res}$.
4. From Eq. (2.87)

$$Z_{res} = \left(\frac{Q_0}{k}\right)\left(\frac{1}{2D\sqrt{1-D^2}}\right)$$

Copyright 2017 Cengage Learning. All Rights Reserved. May not be copied, scanned, or duplicated, in whole or in part. Due to electronic rights, some third party content may be suppressed from the eBook and/or eChapter(s). Editorial review has deemed that any suppressed content does not materially affect the overall learning experience. Cengage Learning reserves the right to remove additional content at any time if subsequent rights restrictions require it.

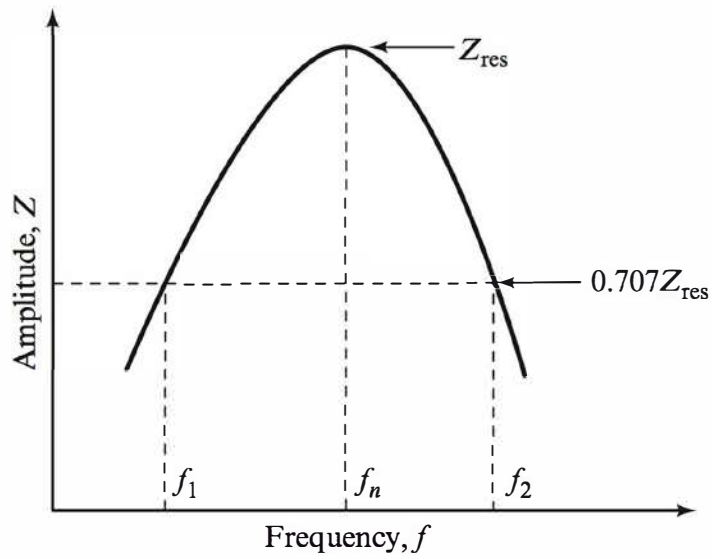

Figure 2.11 Bandwidth method of determination of damping ratio from forced vibration test

However, if D is small,

$$Z_{res} = \left(\frac{Q_0}{k}\right)\left(\frac{1}{2D}\right) \tag{2.103}$$

Again, from Eq. (2.83)

$$Z = 0.707\ Z_{res} = \frac{Q_0/k}{\sqrt{\left[1-\left(f/f_n\right)^2\right]^2 + 4D\left(f/f_n\right)^2}} \tag{2.104}$$

Combining Eqs. (2.103) and (2.104),

$$\frac{0.707}{2D} = \frac{1}{\sqrt{\left[1-\left(f/f_n\right)^2\right]^2 + 4D^2\left(f/f_n\right)^2}}$$

$$\left(\frac{f}{f_n}\right)^2 - 2\left(\frac{f}{f_n}\right)^2\left(1-2D^2\right) + \left(1-8D^2\right) = 0$$

$$\left(\frac{f}{f_n}\right)_{1,2}^2 = \left(1-2D^2\right) \pm 2D\sqrt{1+D^2}$$

$$\left(\frac{f_2}{f_n}\right)^2 - \left(\frac{f_1}{f_n}\right)^2 = 4D\sqrt{1+D^2} \approx 4D \tag{2.105}$$

However,

$$\left(\frac{f_2}{f_n}\right)^2 - \left(\frac{f_1}{f_n}\right)^2 = \left(\frac{f_2 - f_1}{f_n}\right)\left(\frac{f_2 + f_1}{f_n}\right)$$

Copyright 2017 Cengage Learning. All Rights Reserved. May not be copied, scanned, or duplicated, in whole or in part. Due to electronic rights, some third party content may be suppressed from the eBook and/or eChapter(s). Editorial review has deemed that any suppressed content does not materially affect the overall learning experience. Cengage Learning reserves the right to remove additional content at any time if subsequent rights restrictions require it.

But

$$\frac{f_1 + f_1}{f_n} \approx 2$$

So

$$\left(\frac{f_2}{f_n}\right)^2 - \left(\frac{f_1}{f_n}\right)^2 \approx 2\left(\frac{f_2 - f_1}{f_n}\right) \tag{2.106}$$

Now, combining Eqs. (2.105) and (2.106)

$$4D = 2\left(\frac{f_2 - f_1}{f_n}\right)$$

or

$$\boxed{D = \frac{1}{2}\left(\frac{f_2 - f_1}{f_n}\right)} \tag{2.107}$$

Knowing the resonant frequency to be approximately equal to f_n, the magnitude of D can be calculated. This is referred to as the bandwidth method.

2.9 VIBRATION-MEASURING INSTRUMENT

Based on the theories of vibration presented in the preceding sections, it is now possible to study the principles of a vibration-measuring instrument, as shown in Figure 2.12. The instrument consists of a spring-mass-dashpot system. It is mounted on a vibrating base. The relative motion of the mass m with respect to the vibrating base is monitored.

Let the motion of the base be given as

$$z' = Z' \sin \omega t \tag{2.108}$$

Neglecting the transients let the absolute motion of the mass be given as

$$z'' = Z'' \sin \omega t \tag{2.109}$$

So, the equation of motion for the mass can be written as

$$m\ddot{z}'' + k(z'' - z') + c(\dot{z}'' - \dot{z}') = 0$$

By letting $z'' - z' = z$ and $\dot{z}'' - \dot{z}' = \dot{z}$, the equation of motion can be rewritten as:

$$m\ddot{z} + kz + c\dot{z} = m\omega^2 Z' \sin \omega t \tag{2.110}$$

Copyright 2017 Cengage Learning. All Rights Reserved. May not be copied, scanned, or duplicated, in whole or in part. Due to electronic rights, some third party content may be suppressed from the eBook and/or eChapter(s). Editorial review has deemed that any suppressed content does not materially affect the overall learning experience. Cengage Learning reserves the right to remove additional content at any time if subsequent rights restrictions require it.

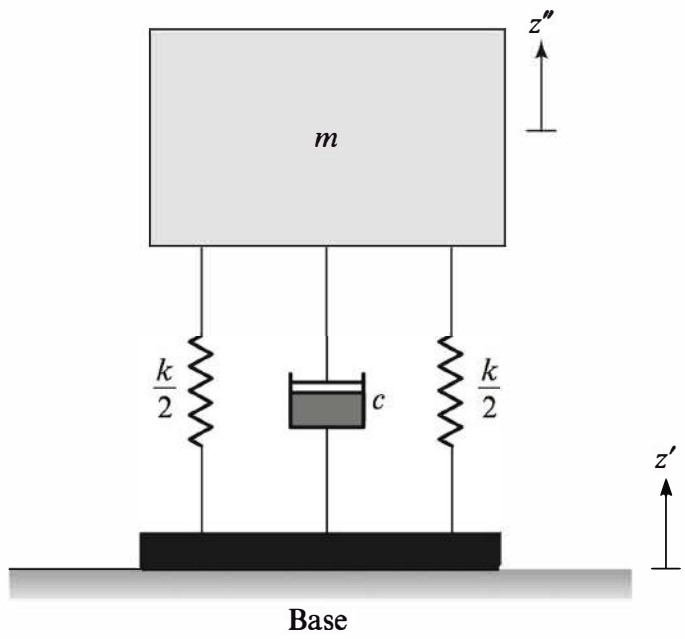

Figure 2.12 Principles of vibration-measuring instrument

The solution to the Eq. (2.110) can be given as [similar to Eqs. (2.80), (2.81), and (2.82)]

$$z = Z\cos(\omega t + \alpha) \tag{2.111}$$

where

$$Z = \frac{m\omega^2 Z'}{\sqrt{\left(k - m\omega^2\right)^2 + \left(c\omega\right)^2}} \tag{2.112}$$

$$\alpha = \tan^{-1}\left(\frac{k - m\omega^2}{c\omega}\right) \tag{2.113}$$

Again, from Eq. (2.112),

$$\frac{Z}{Z'} = \frac{\left(\omega/\omega_n\right)^2}{\sqrt{\left[1 - \left(\omega/\omega_n\right)^2\right]^2 + 4D^2\left(\omega/\omega_n\right)^2}} \tag{2.114}$$

If the natural frequency of the instrument ω_n is small and ω/ω_n is large, then for practically all values of D, the magnitude of Z/Z' is about 1. Hence the instrument works as a *velocity pickup*.

Also, from Eq. (2.114) one can write that

$$\frac{Z}{\omega^2 Z'} = \frac{1}{\omega_n^2\sqrt{\left[1 - \left(\omega/\omega_n\right)^2\right]^2 + 4D^2\left(\omega/\omega_n\right)^2}} \tag{2.115}$$

Copyright 2017 Cengage Learning. All Rights Reserved. May not be copied, scanned, or duplicated, in whole or in part. Due to electronic rights, some third party content may be suppressed from the eBook and/or eChapter(s). Editorial review has deemed that any suppressed content does not materially affect the overall learning experience. Cengage Learning reserves the right to remove additional content at any time if subsequent rights restrictions require it.

If $D = 0.69$ and ω/ω_n is varied from zero to 0.4 (Prakash, 1981), then Eq. (2.115) will result in

$$\frac{Z}{\omega^2 Z'} \approx \frac{1}{\omega_n^2} = \text{const}$$

So

$$Z \propto \omega^2 Z'$$

However, $\omega^2 Z'$ is the absolute acceleration of the vibrating base. For this condition, the instrument works as an acceleration pickup. Note that, for this case, the natural frequency of the instrument and, thus, ω_n are large, and hence the ratio ω/ω_n is small.

System with Two Degrees of Freedom

2.10 VIBRATION OF A MASS-SPRING SYSTEM

A mass-spring system with two degrees of freedom is shown in Figure 2.13. If the masses m_1 and m_2 are displaced from their static equilibrium positions, the system will start to vibrate. The equations of motion of the two masses can be given as

$$m_1\ddot{z}_1 + k_1 z_1 + k_2(z_1 - z_2) = 0 \tag{2.116}$$

$$m_2\ddot{z}_2 + k_3 z_2 + k_2(z_2 - z_1) = 0 \tag{2.117}$$

where m_1 and m_2 are the masses of the two bodies, k_1, k_2, and k_3 are the spring constants, and z_1 and z_2 are the displacements of masses m_1 and m_2, respectively. Now, let

$$z_1 = A\sin(\omega t + \alpha) \tag{2.118}$$

and

$$z_2 = B\sin(\omega t + \alpha) \tag{2.119}$$

where A, B, and α are arbitrary constants.

Substitution of Eqs. (2.118) and (2.119) into Eqs. (2.116) and (2.117), respectively, yields

$$(k_1 + k_2 - m_1\omega^2)A - k_2 B = 0 \tag{2.120}$$

and

$$-k_2 A + (k_2 + k_3 - m_2\omega^2)B = 0 \tag{2.121}$$

Copyright 2017 Cengage Learning. All Rights Reserved. May not be copied, scanned, or duplicated, in whole or in part. Due to electronic rights, some third party content may be suppressed from the eBook and/or eChapter(s). Editorial review has deemed that any suppressed content does not materially affect the overall learning experience. Cengage Learning reserves the right to remove additional content at any time if subsequent rights restrictions require it.

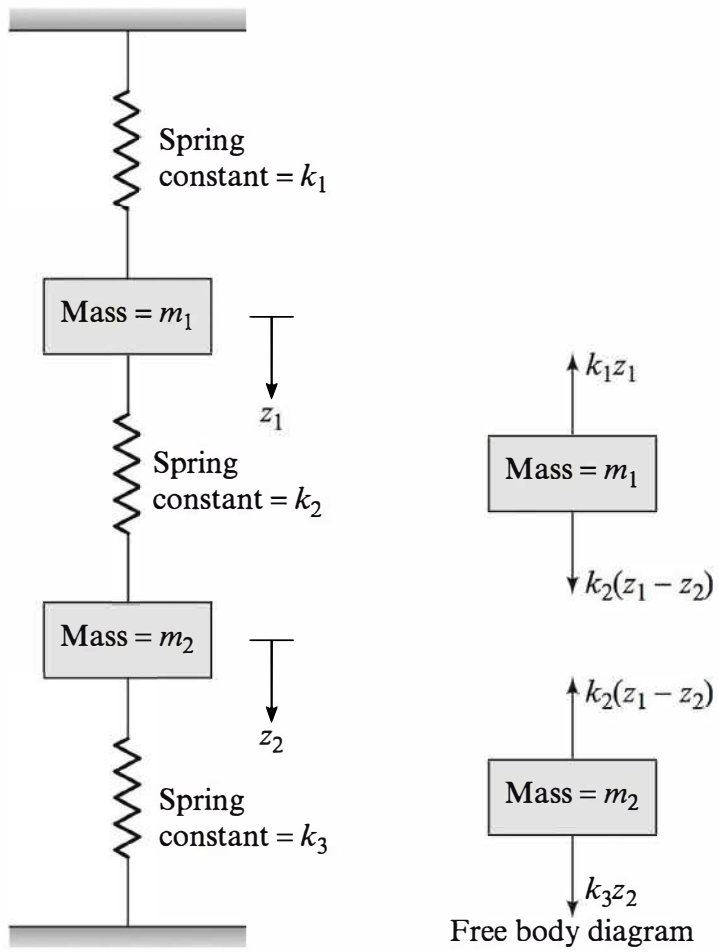

Figure 2.13 A mass-spring system with two degrees of freedom

For nontrivial solutions of ω in Eqs. (2.120) and (2.121)

$$\begin{vmatrix} (k_1 + k_2 - m_1\omega^2) & -k_2 \\ -k_2 & (k_2 + k_3 - m_2\omega^2) \end{vmatrix} = 0$$

or

$$\omega^4 - \left(\frac{k_1 + k_2}{m_1} + \frac{k_2 + k_3}{m_2}\right)\omega^2 + \frac{k_1k_2 + k_2k_3 + k_3k_1}{m_1m_2} = 0 \tag{2.122}$$

The roots of the above equation are

$$\omega^2 = \frac{1}{2}\left\{\left(\frac{k_1 + k_2}{m_1} + \frac{k_2 + k_3}{m_2}\right) \mp \left[\left(\frac{k_1 + k_2}{m_1} - \frac{k_2 + k_3}{m_2}\right)^2 + 4\frac{k_2^2}{m_1m_2}\right]^{1/2}\right\} \tag{2.123}$$

Copyright 2017 Cengage Learning. All Rights Reserved. May not be copied, scanned, or duplicated, in whole or in part. Due to electronic rights, some third party content may be suppressed from the eBook and/or eChapter(s). Editorial review has deemed that any suppressed content does not materially affect the overall learning experience. Cengage Learning reserves the right to remove additional content at any time if subsequent rights restrictions require it.

or

$$\begin{matrix}\omega_1\\ \omega_2\end{matrix} = \frac{1}{\sqrt{2}}\left\{\left(\frac{k_1+k_2}{m_1}+\frac{k_2+k_3}{m_2}\right)\right.$$
$$\left.\mp\left[\left(\frac{k_1+k_2}{m_1}-\frac{k_2+k_3}{m_2}\right)^2+4\frac{k_2^2}{m_1m_2}\right]^{1/2}\right\}^{1/2} \tag{2.124}$$

In the above equation, ω_1 and ω_2 are the natural frequencies of the system. ω_1 is the first mode and ω_2 is the second. The general equation of motion of the two masses can now be written as

$$z_1 = A_1 \sin\left(\omega_1 t + \alpha_1\right) + A_2 \sin\left(\omega_2 t + \alpha_2\right) \tag{2.125}$$

and

$$z_2 = B_1 \sin\left(\omega_1 t + \alpha_1\right) + B_2 \sin\left(\omega_2 t + \alpha_2\right) \tag{2.126}$$

The ratios of A_1/B_1 and A_2/B_2 can also be determined from Eqs. (2.120) and (2.121) as

$$\frac{A_1}{B_1} = \frac{k_2}{k_1+k_2-m_1\omega_1^2} = \frac{k_2+k_3-m_2\omega_1^2}{k_2} \tag{2.127}$$

and

$$\frac{A_2}{B_2} = \frac{k_2}{k_1+k_2-m_1\omega_2^2} = \frac{k_2+k_3-m_2\omega_2^2}{k_2} \tag{2.128}$$

EXAMPLE 2.8

Refer to Figure 2.13. At time $t = 0$, let the mass m_1 be displaced through a vertical distance of 5 mm and released. Determine the displacement equations of m_1 and m_2 with time. Assume $m_1 = m_2 = m$ and $k_1 = k_2 = k_3 = k$.

SOLUTION:

From Eq. (2.124), the natural frequencies ω_1 and ω_2 can be obtained as

$$\begin{matrix}\omega_1\\ \omega_2\end{matrix} = \frac{1}{\sqrt{2}}\left\{\left(\frac{2k}{m}+\frac{2k}{m}\right)\mp\left[\left(\frac{2k}{m}-\frac{2k}{m}\right)^2+\frac{4k^2}{m^2}\right]^{1/2}\right\}^{1/2} = \frac{1}{\sqrt{2}}\left(\frac{4k}{m}\mp\frac{2k}{m}\right)^{1/2}$$

or

$$\omega_1 = \sqrt{k/m} \qquad \text{and} \qquad \omega_2 = \sqrt{3k/m}$$

Copyright 2017 Cengage Learning. All Rights Reserved. May not be copied, scanned, or duplicated, in whole or in part. Due to electronic rights, some third party content may be suppressed from the eBook and/or eChapter(s). Editorial review has deemed that any suppressed content does not materially affect the overall learning experience. Cengage Learning reserves the right to remove additional content at any time if subsequent rights restrictions require it.

Again, from Eq. (2.127)

$$A_1/B_1 = k/[2k - m_1(k/m)] = 1 \qquad \text{or} \qquad A_1 = B_1$$

Similarly, using Eq. (2.128)

$$A_2/B_2 = -1 \qquad \text{or} \qquad A_2 = -B_2$$

Thus, the general equations of motion for the two masses [Eqs. (2.125) and (2.126)] are,

$$z_1 = A_1 \sin\left(\sqrt{k/m}\, t + \alpha_1\right) + A_2 \sin\left(\sqrt{3k/m}\, t + \alpha_2\right) \tag{a}$$

and

$$z_2 = A_1 \sin\left(\sqrt{k/m}\, t + \alpha_1\right) - A_2 \sin\left(\sqrt{3k/m}\, t + \alpha_2\right) \tag{b}$$

Based on the initial condition at time $t = 0$, (1) $z_1 = 5$ mm, $z_2 = 0$; and (2) $\dot{z}_1 = 0$, $\dot{z}_2 = 0$. From Eq. (a)

$$5 = A_1 \sin\alpha_1 + A_2 \sin\alpha_2 \tag{c}$$

From Eq. (b)

$$0 = A_1 \sin\alpha_1 - A_2 \sin\alpha_2 \tag{d}$$

Combining Eqs. (c) and (d)

$$A_1 = 2.5/\sin\alpha_1 \tag{e}$$

and

$$A_2 = 2.5/\sin\alpha_2 \tag{f}$$

From Eq. (a) and the second initial condition (i.e., $\dot{z}_1 = 0$ at time $t = 0$),

$$\dot{z}_1 = 0 = A_1\omega_1 \cos\alpha_1 + A_2\omega_2 \cos\alpha_2 \tag{g}$$

Similarly, from Eq. (b) and the second initial condition ($\dot{z}_2 = 0$ at time $t = 0$),

$$\dot{z}_2 = 0 = A_1\omega_1 \cos\alpha_1 - A_2\omega_2 \cos\alpha_2 \tag{h}$$

Combining Eqs. (g) and (h),

$$2A_1\omega_1 \cos\alpha_1 = 0 \qquad \text{and} \qquad 2A_2\omega_2 \cos\alpha_2 = 0$$

or

$$\alpha_1 = \alpha_2 = \tfrac{1}{2}\pi \tag{i}$$

Substituting Eq. (i) into Eqs. (e) and (f),

$$A_1 = A_2 = 2.5 \text{ mm}$$

Copyright 2017 Cengage Learning. All Rights Reserved. May not be copied, scanned, or duplicated, in whole or in part. Due to electronic rights, some third party content may be suppressed from the eBook and/or eChapter(s). Editorial review has deemed that any suppressed content does not materially affect the overall learning experience. Cengage Learning reserves the right to remove additional content at any time if subsequent rights restrictions require it.

With $A_1 = A_2 = 2.5$ mm, Eqs. (a) and (b) can be rewritten as

$$z_1(\text{mm}) = 2.5\cos\left(\sqrt{k/m}\,t\right) + 2.5\cos\left(\sqrt{3k/m}\,t\right)$$
$$z_2(\text{mm}) = 2.5\cos\left(\sqrt{k/m}\,t\right) - 2.5\cos\left(\sqrt{3k/m}\,t\right)$$

EXAMPLE 2.9

Consider a drop hammer foundation (Figure 2.14a). This hammer foundation can be approximated as a mass–spring system as shown in Figure 2.14b. Determine the amplitude of displacement for the anvil and the foundation. Given

Weight of the anvil and the frame $= W_1 = 578$ kN lb
Weight of the foundation $= W_2 = 890$ kN
The spring constant for the pad between the foundation and the anvil $= k_2 = 2.19 \times 10^6$ kN/m
The spring constant for the soil supporting the foundation $= k_3 = 0.32 \times 10^6$ kN/m
Weight of the hammer $= W_h = 35.6$ kN
Velocity of the hammer before impact $= 3.05$m/s

SOLUTION:

At the impact of the hammer, the initial conditions are as follows:

$$z_1 = 0 \quad \dot{z}_1 = v_0$$
$$z_2 = 0 \quad \dot{z}_2 = 0$$

According to the theory of conservation of momentum,

$$m_h v_{h(\text{before})} = m_h v_{h(\text{after})} + m_1 v_0 \tag{a}$$

where

m_h = mass of the hammer
m_1 = mass of the anvil and frame
$v_{h(\text{before})}$ = velocity of the hammer before impact
$v_{h(\text{after})}$ = velocity of the hammer after impact
v_0 = velocity of the anvil and frame

Copyright 2017 Cengage Learning. All Rights Reserved. May not be copied, scanned, or duplicated, in whole or in part. Due to electronic rights, some third party content may be suppressed from the eBook and/or eChapter(s). Editorial review has deemed that any suppressed content does not materially affect the overall learning experience. Cengage Learning reserves the right to remove additional content at any time if subsequent rights restrictions require it.

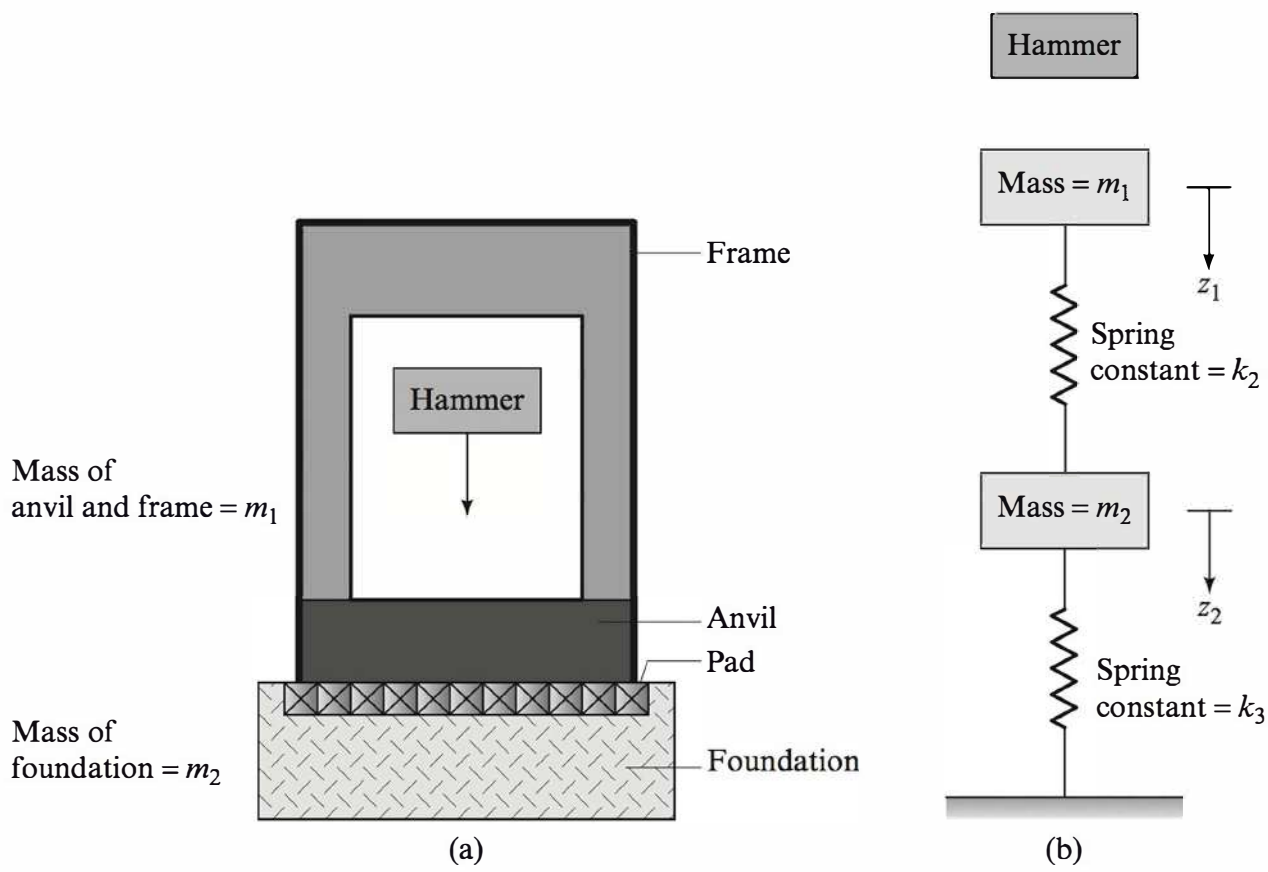

Figure 2.14 (a) Drop hammer foundation; (b) approximation to a mass-spring system

Also,

$$n = \frac{v_0 - v_{\text{h(after)}}}{v_{\text{h(before)}}} \tag{b}$$

where n is the coefficient of restitution. The value of n may vary between 0.2 and 0.5. For this problem, let $n = 0.4$. Combining Eqs. (a) and (b),

$$v_0 = \frac{1+n}{1+m_1/m_{\text{h}}} v_{\text{h(before)}} \tag{c}$$

or

$$v_0 = \frac{1+0.4}{1+\left(\dfrac{578}{35.6}\right)}(3.05) = 0.247 \text{ m/s}$$

Comparing the system given in Figure 2.14b with that given in Figure 2.13, it can be seen that they are equivalent if k_1 in Figure 2.13 is equal to zero. The initial boundary conditions for the motion will be as follows: At time $t = 0$,

$$z_1 = 0, \qquad z_2 = 0$$

Copyright 2017 Cengage Learning. All Rights Reserved. May not be copied, scanned, or duplicated, in whole or in part. Due to electronic rights, some third party content may be suppressed from the eBook and/or eChapter(s). Editorial review has deemed that any suppressed content does not materially affect the overall learning experience. Cengage Learning reserves the right to remove additional content at any time if subsequent rights restrictions require it.

Using the initial boundary conditions and Eqs. (2.125)–(2.128) with $k_1 = 0$, the following equations for displacement can be obtained.

$$z_1 = P_1\left[\left(\frac{k_2}{m_1} - \omega_2^2\right)\frac{\sin\omega_1 t}{\omega_1} - \left(\frac{k_2}{m_1} - \omega_1^2\right)\frac{\sin\omega_2 t}{\omega_2}\right] \tag{d}$$

and

$$z_2 = P_2\left(\frac{\sin\omega_1 t}{\omega_1} - \frac{\sin\omega_2 t}{\omega_2}\right) \tag{e}$$

where

$$P_1 = \frac{v_0}{\left(\omega_1^2 - \omega_2^2\right)} \tag{f}$$

$$P_2 = \frac{\left(k_2/m_1 - \omega_2^2\right)\left(k_2/m_1 - \omega_1^2\right)}{\left(k_2/m_1\right)\left(\omega_1^2 - \omega_2^2\right)} v_0 \tag{g}$$

The values ω_1 and ω_2 can be calculated by using Eq. (2.124). Note that, in that equation, $\omega_1 < \omega_2$. According to Barkan (1962, p. 207), it will be sufficient for these types of problems to approximate Eqs. (d) and (e) as follows:

$$z_1 = P_1\left(\frac{k_2}{m_1} - \omega_2^2\right)\left(\sin\omega_1 t/\omega_1\right) \tag{h}$$

and

$$z_2 = P_2\left(\sin\omega_1 t/\omega_1\right) \tag{i}$$

Calculation of ω_1 *and* ω_2 [Eq. (2.124)]

$$\begin{aligned}
\begin{matrix}\omega_1\\ \omega_2\end{matrix} &= \frac{1}{\sqrt{2}}\left\{\left(\frac{0 + 2.19\times10^6}{(578)/9.81} + \frac{2.19\times10^6 + 0.32\times10^6}{(890)/9.81}\right)\right.\\
&\quad \mp\left[\left(\frac{0 + 2.19\times10^6}{(578)/9.81} - \frac{2.19\times10^6 + 0.32\times10^6}{(890)/9.81}\right)^2\right.\\
&\quad \left.\left. + \frac{4(2.19\times10^6)^2}{(578\times890)/(9.81\times9.81)}\right]^{1/2}\right\}^{1/2}\\
&= \left(1/\sqrt{2}\right)\left[64.84\times10^3 \mp (89.49\times10^6 + 3589\times10^6)^{1/2}\right]^{1/2}\\
&= \left(1/\sqrt{2}\right)\left(64.84\times10^3 \mp 60.65\times10^3\right)^{1/2}
\end{aligned}$$

Copyright 2017 Cengage Learning. All Rights Reserved. May not be copied, scanned, or duplicated, in whole or in part. Due to electronic rights, some third party content may be suppressed from the eBook and/or eChapter(s). Editorial review has deemed that any suppressed content does not materially affect the overall learning experience. Cengage Learning reserves the right to remove additional content at any time if subsequent rights restrictions require it.

or

$$\omega_1 = 45.78 \text{ rad/sec}, \qquad \omega_2 = 250.53 \text{ rad/sec}$$

Calculation of Maximum Displacement of Anvil
From Eq. (h)

$$\text{maximum displacement} = \left[P_1\left(k_2/m_1 - \omega_2^2\right)\right]/\omega_1$$

$$P_1 = \frac{v_0}{\omega_1^2 - \omega_2^2} = \frac{0.247}{(45.78)^2 - (250.53)^2} = -\frac{0.247}{60669.5}$$

Therefore,

$$\text{maximum displacement} = -\frac{0.247}{60669.5}\left[\frac{\dfrac{2.19\times10^6}{(578)/9.81} - (250.53)^2}{45.78}\right]$$

$$= 0.00228 \text{ m} \approx \mathbf{2.28\ mm}$$

Maximum Displacement of Foundation
From Eq. (i)

$$\text{maximum displacement of foundation}$$

$$= \frac{\left(k_2/m_1 - \omega_2^2\right)\left(k_2/m_1 - \omega_1^2\right)v_0}{\left(k_2/m_1\right)\left(\omega_1^2 - \omega_2^2\right)\omega_1}$$

$$= \frac{\left[\dfrac{2.19\times10^6}{(578)/9.81} - (45.78)^2\right]\left[\dfrac{2.19\times10^6}{(578)/9.81} - (250.53)^2\right](0.247)}{\dfrac{2.19\times10^6}{(578)/9.81}\left[(45.78)^2 - (250.53)^2\right]45.78}$$

$$= 0.00215 \text{ m} \approx \mathbf{2.15\ mm}$$

2.11 COUPLED TRANSLATION AND ROTATION OF A MASS-SPRING SYSTEM (FREE VIBRATION)

Figure 2.15 shows a mass-spring system that will undergo translation and rotation. The equations of motion of the mass m can be given as

$$m\ddot{z} + k_1(z - l_1\theta) + k_2(z + l_2\theta) = 0 \tag{2.129}$$

$$mr^2\ddot{\theta} - l_1k_1(z - l_1\theta) + l_2k_2(z + l_2\theta) = 0 \tag{2.130}$$

Copyright 2017 Cengage Learning. All Rights Reserved. May not be copied, scanned, or duplicated, in whole or in part. Due to electronic rights, some third party content may be suppressed from the eBook and/or eChapter(s). Editorial review has deemed that any suppressed content does not materially affect the overall learning experience. Cengage Learning reserves the right to remove additional content at any time if subsequent rights restrictions require it.

where θ = angle of rotation of the mass m

$\ddot{\theta} = \dfrac{d^2\theta}{dt^2}$

r = radius of gyration of the body about the center of gravity (Note: $mr^2 = J$ = mass moment of inertia about the center of gravity)

k_1, k_2 = spring constants

z = distance of translation of the center of gravity of the body

Now, let

$$k_1 + k_2 = k_z \tag{2.131}$$

and

$$l_1^2 k_1 + l_2^2 k_2 = k_\theta \tag{2.132}$$

So, the equations of motion can be written as

$$m\ddot{z} + k_z z + (l_2 k_2 - l_1 k_2)\theta = 0 \tag{2.133}$$

$$mr^2\ddot{\theta} + k_\theta \theta + (l_2 k_2 - l_1 k_1) z = 0 \tag{2.134}$$

If $l_1 k_1 = l_2 k_2$, Eq. (2.133) is independent of θ and Eq. (2.134) is independent of z. This means that the two motions (i.e., translation and rotation) can exist independently of each one another (uncoupled motion); that is,

$$m\ddot{z} + k_z z = 0 \tag{2.135}$$

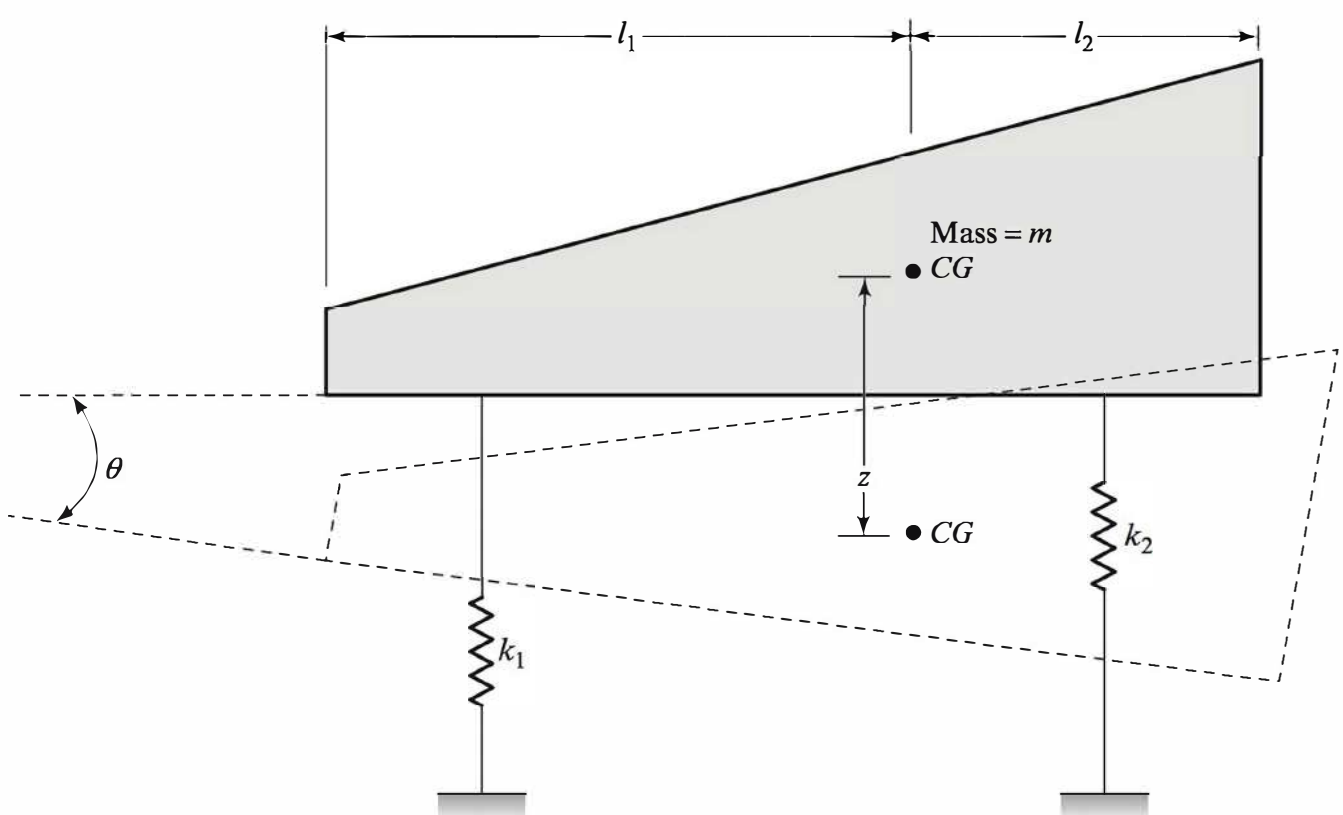

Figure 2.15 Coupled translation and rotation of a mass-spring system

Copyright 2017 Cengage Learning. All Rights Reserved. May not be copied, scanned, or duplicated, in whole or in part. Due to electronic rights, some third party content may be suppressed from the eBook and/or eChapter(s). Editorial review has deemed that any suppressed content does not materially affect the overall learning experience. Cengage Learning reserves the right to remove additional content at any time if subsequent rights restrictions require it.

and

$$mr^2\ddot{\theta} + k_\theta\theta = 0 \tag{2.136}$$

The natural circular frequency ω_{nz} of translation can be obtained by

$$\omega_{nz} = \sqrt{\frac{k_z}{m}} \tag{2.137}$$

Similarly, the natural circular frequency of rotation $\omega_{n\theta}$ can be given by

$$\omega_{n\theta} = \sqrt{\frac{k_\theta}{mr^2}} \tag{2.138}$$

However, if l_1k_1 is not equal to l_2k_2, the equations of motion (coupled motion) can be solved as follows: Let

$$\frac{k_z}{m} = E_1 \tag{2.139}$$

$$\frac{l_2k_2 - l_1k_2}{m} = E_2 \tag{2.140}$$

$$\frac{k_\theta}{m} = E_3 \tag{2.141}$$

Combining Eqs. (2.133), (2.134), (2.139)–(2.141),

$$\ddot{z} + E_1z + E_2\theta = 0 \tag{2.142}$$

$$\ddot{\theta} + \left(\frac{E_3}{r^2}\right)\theta + \left(\frac{E_2}{r^2}\right)z = 0 \tag{2.143}$$

For solution of these equations, let

$$z = Z\cos\omega_n t \tag{2.144}$$

and

$$\theta = \Theta\cos\omega_n t \tag{2.145}$$

Substitution of Eqs. (2.144) and (2.145) into Eqs. (2.142) and (2.143) results in

$$(E_1 - \omega_n^2)Z + E_2\Theta = 0 \tag{2.146}$$

and

$$\left(\frac{E_3}{r^2} - \omega_n^2\right)\Theta + \left(\frac{E_2}{r^2}\right)Z = 0 \tag{2.147}$$

Copyright 2017 Cengage Learning. All Rights Reserved. May not be copied, scanned, or duplicated, in whole or in part. Due to electronic rights, some third party content may be suppressed from the eBook and/or eChapter(s). Editorial review has deemed that any suppressed content does not materially affect the overall learning experience. Cengage Learning reserves the right to remove additional content at any time if subsequent rights restrictions require it.

For nontrivial solutions of Eqs. (2.146) and (2.147),

$$\begin{vmatrix} E_1 - \omega_n^2 & E_2 \\ \dfrac{E_2}{r^2} & \dfrac{E_3}{r^2} - \omega_n^2 \end{vmatrix} = 0 \tag{2.148}$$

or

$$\omega_n^4 - \left(\frac{E_3}{r^2} + E_1\right)\omega_n^2 + \left(\frac{E_1E_3 - E_2^2}{r^2}\right) = 0 \tag{2.149}$$

The natural frequencies ω_{n_1}, ω_{n_2} of system can be determined from Eq. (2.149) as

$$\begin{matrix}\omega_{n_1} \\ \omega_{n_2}\end{matrix} = \frac{1}{\sqrt{2}}\left\{\left(\frac{E_3}{r^2} + E_1\right) \mp \left[\left(\frac{E_3}{r^2} - E_1\right)^2 + 4\frac{E_2^2}{r^2}\right]^{1/2}\right\}^{1/2} \tag{2.150}$$

Hence, the general equations of motion can be given as

$$z = Z_1 \cos\omega_{n_1} t + Z_2 \cos\omega_{n_2} t \tag{2.151}$$

and

$$\theta = \Theta_1 \cos\omega_{n_1} t + \Theta_2 \cos\omega_{n_2} t \tag{2.152}$$

The amplitude ratios can also be obtained from Eqs. (2.146) and (2.147) as

$$\frac{Z_1}{\Theta_1} = -\frac{E_2}{E_1 - \cos\omega_{n_1}^2} = \frac{-(E_3/r^2 - \omega_{n_1}^2)}{E_2/r^2} \tag{2.153}$$

and

$$\frac{Z_2}{\Theta_2} = -\frac{E_2}{E_1 - \cos\omega_{n_2}^2} = \frac{-(E_3/r^2 - \omega_{n_2}^2)}{E_2/r^2} \tag{2.154}$$

PROBLEMS

2.1 Define the following terms:

- **a.** Spring constant
- **b.** Coefficient of subgrade reaction
- **c.** Undamped natural circular frequency
- **d.** Undamped natural frequency
- **e.** Period
- **f.** Resonance
- **g.** Critical damping coefficient

Copyright 2017 Cengage Learning. All Rights Reserved. May not be copied, scanned, or duplicated, in whole or in part. Due to electronic rights, some third party content may be suppressed from the eBook and/or eChapter(s). Editorial review has deemed that any suppressed content does not materially affect the overall learning experience. Cengage Learning reserves the right to remove additional content at any time if subsequent rights restrictions require it.

h. Damping ratio
i. Damped natural frequency

2.2 A machine foundation can be idealized to a mass-spring system, as shown in Figure 2.4.
Given

Weight of machine + foundation = 400 kN
Spring constant = 100,000 kN/m

Determine the natural frequency of undamped free vibration of this foundation and the natural period.

2.3 Refer to Problem 2.2, What would be the static deflection z_s of this foundation?

2.4 Refer to Example 2.3. For this foundation let at time $t = 0$, $z = z_0 = 0$. $\dot{z} = v_0 = 0$.

a. Determine the natural period T of the foundation.
b. Plot the dynamic force on the subgrade of the foundation due to the forced part of the response for time $t = 0$ to $t = 2T$.
c. Plot the dynamic force on the subgrade of the foundation due to the free part of the response for $t = 0$ to $2T$.
d. Plot the total dynamic force on the subgrade [that is, the algebraic sum of (b) and (c)]. Hint: Refer to Eq. (2.33)

$$\text{Force due to forced part} = k\left(\frac{Q_0/k}{1-\omega^2/\omega_n^2}\right)\sin\omega t$$

$$\text{Force due to free part} = k\left(\frac{Q_0/k}{1-\omega^2/\omega_n^2}\right)\left(-\frac{\omega}{\omega_n}\sin\omega_n t\right)$$

2.5 A foundation of mass m is supported by two springs attached in series. (See Figure P2.5). Determine the natural frequency of the undamped free vibration.

2.6 A foundation of mass m is supported by two springs attached in parallel (Figure P2.6). Determine the natural frequency of the undamped free vibration.

2.7 For the system shown in Figure P2.7, calculate the natural frequency and period given $k_1 = 100$ N/mm, $k_2 = 200$ N/mm, $k_3 = 150$ N/mm, $k_4 = 100$ N/mm, $k_5 = 150$ N/mm, and $m = 100$ kg.

2.8 Refer to Problem 2.7. If a sinusoidally varying force $Q = 50\sin\omega t$ (N) is applied to the mass as shown, what would be the amplitude of vibration given $\omega = 47$ rad/s?

2.9 A body weighs 135 N. A *spring* and a *dashpot* are attached to the body in the manner shown in Figure 2.2b. The spring constant is 2600 N/m.

Copyright 2017 Cengage Learning. All Rights Reserved. May not be copied, scanned, or duplicated, in whole or in part. Due to electronic rights, some third party content may be suppressed from the eBook and/or eChapter(s). Editorial review has deemed that any suppressed content does not materially affect the overall learning experience. Cengage Learning reserves the right to remove additional content at any time if subsequent rights restrictions require it.

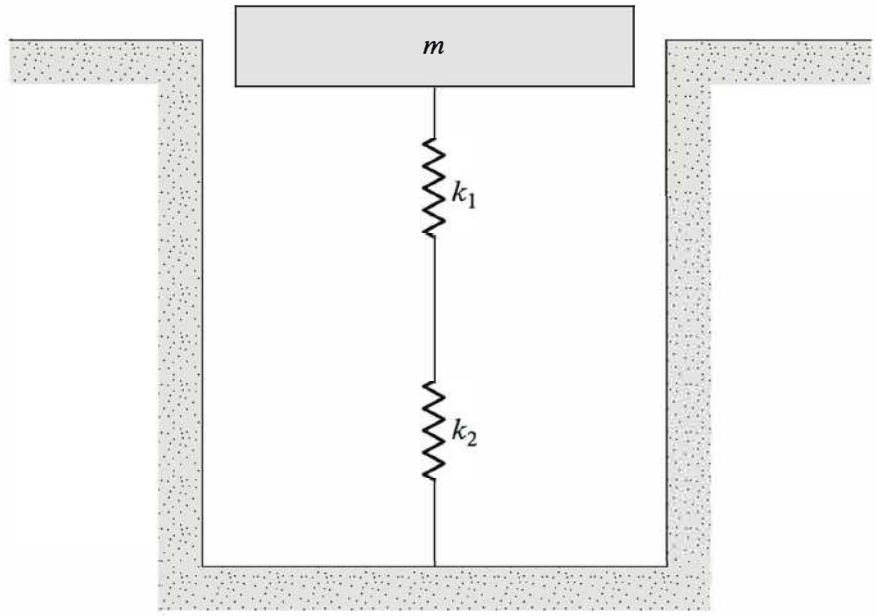

Figure P2.5

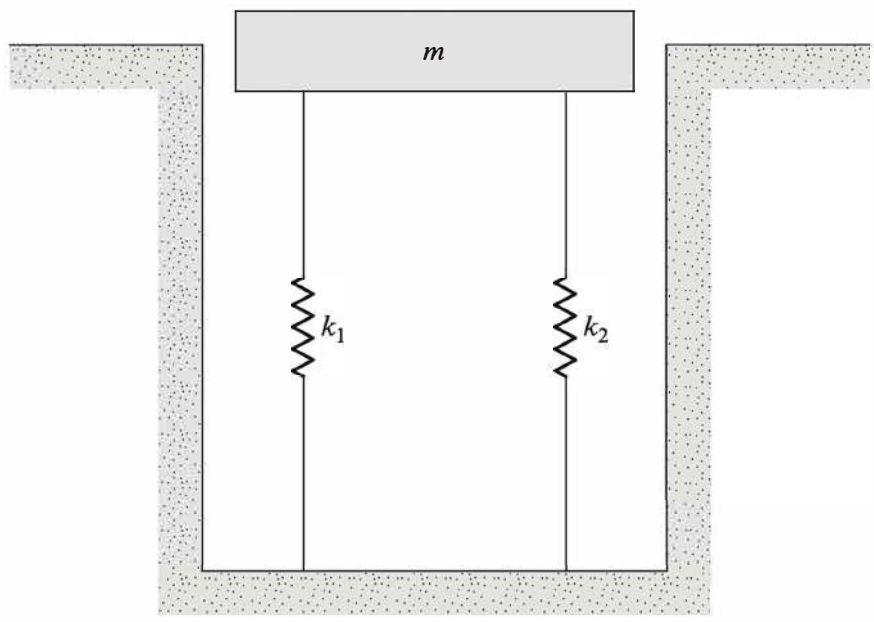

Figure P2.6

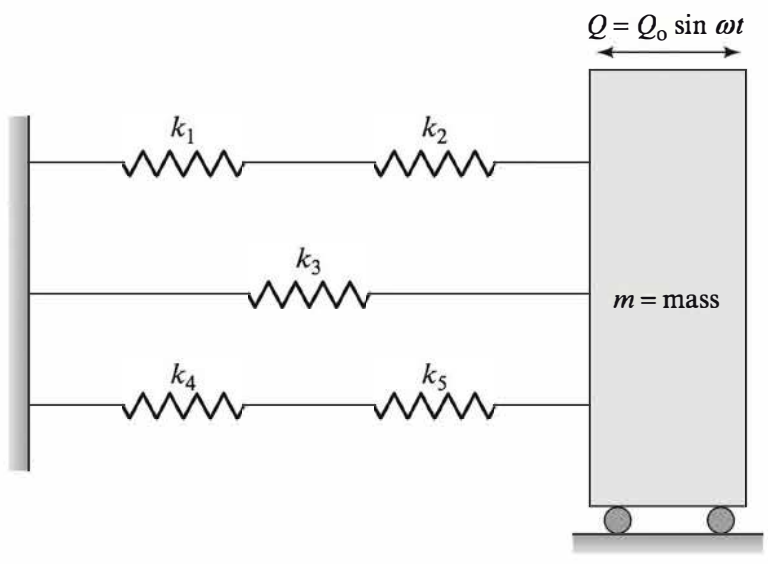

Figure P2.7

Copyright 2017 Cengage Learning. All Rights Reserved. May not be copied, scanned, or duplicated, in whole or in part. Due to electronic rights, some third party content may be suppressed from the eBook and/or eChapter(s). Editorial review has deemed that any suppressed content does not materially affect the overall learning experience. Cengage Learning reserves the right to remove additional content at any time if subsequent rights restrictions require it.

The dashpot has a resistance of 0.7 N at a velocity of 60 mm/s. Determine the following for free vibration:

a. Damped natural frequency of the system
b. Damping ratio
c. Ratio of successive amplitudes of the body (Z_n/Z_{n+1})
d. Amplitude of the body 5 cycles after it is disturbed, assuming that at time $t = 0$, $z = 25$ mm.

2.10 A machine foundation can be identified as a mass-spring system. This is subjected to a forced vibration. The vibrating force is expressed as
$Q = Q_0 \sin \omega t$
$Q_0 = 6.7$ kN, $\omega = 3100$ rad/min

Given

Weight of machine + foundation = 290 kN
Spring constant = 875 kN/m

Determine the maximum and minimum force transmitted to the subgrade.

2.11 Repeat Problem 2.10 if
$Q_0 = 200$ kN, $\omega = 6000$ rad/min

Weight of machine + foundation = 400 kN
Spring constant = 120,000 kN/m

2.12 A foundation weighs 800 kN. The foundation and the soil can be approximated as a mass-spring-dashpot system as shown in Figure 2.2b. Given
Spring constant = 200,000 kN/m
Dashpot coefficient = 2340 kN·s/m
Determine the following:

a. Critical damping coefficient c_c.
b. Damping ratio
c. Logarithmic decrement
d. Damped natural frequency

2.13 The foundation given in Problem 2.12 is subjected to a vertical force $Q = Q_0 \sin \omega t$ in which
$Q_0 = 25$ kN, $\omega = 100$ rad/s
Determine

a. the amplitude of the vertical vibration of the foundation, and
b. the maximum dynamic force transmitted to the subgrade.

References

Barkan, D. D. (1962). *Dynamics of Bases and Foundations*, McGraw-Hill, New York.
Prakash, S. (1981). *Soil Dynamics*. McGraw-Hill Book Company, New York.

Copyright 2017 Cengage Learning. All Rights Reserved. May not be copied, scanned, or duplicated, in whole or in part. Due to electronic rights, some third party content may be suppressed from the eBook and/or eChapter(s). Editorial review has deemed that any suppressed content does not materially affect the overall learning experience. Cengage Learning reserves the right to remove additional content at any time if subsequent rights restrictions require it.

Waves in Elastic Medium

3

3.1 INTRODUCTION

If a stress is suddenly applied to a body, the part of the body closest to the source of disturbance will be affected first. The deformation of the body due to the load will gradually spread throughout the body via *stress waves*. The nature of propagation of stress waves in an elastic medium is the subject of discussion in this chapter. Stress wave propagation is of extreme importance in geotechnical engineering, since it allows determination of soil properties such as modulus of elasticity, shear wave velocity, shear modulus, interpretation of test results of geophysical investigation, numerical formulation of ground response analysis; and also helps in the development of the design parameters for earthquake-resistant structures. The problem of stress wave propagation can be divided into three major categories:

Elastic stress waves in a bar
Stress waves in an infinite elastic medium
Stress waves in an elastic half-space

However, before the relationships for the stress waves can be developed, it is essential to have some knowledge of the fundamental definitions of stress, strain, and other related parameters that are generally encountered in an elastic medium. These definitions are given in Sections 3.2 and 3.3.

3.2 STRESS AND STRAIN

Notations for Stress

Figure 3.1 shows an element in an elastic medium whose sides measure dx, dy and dz. The normal stresses acting on the plane normal to the x, y, and z axes are σ_x, σ_y and σ_z, respectively. The shear stresses are τ_{xy}, τ_{yx}, τ_{yz}, τ_{zy}, τ_{xz}, and τ_{zx}. The notations for the shear stresses are as follows.

Copyright 2017 Cengage Learning. All Rights Reserved. May not be copied, scanned, or duplicated, in whole or in part. Due to electronic rights, some third party content may be suppressed from the eBook and/or eChapter(s).
Editorial review has deemed that any suppressed content does not materially affect the overall learning experience. Cengage Learning reserves the right to remove additional content at any time if subsequent rights restrictions require it.

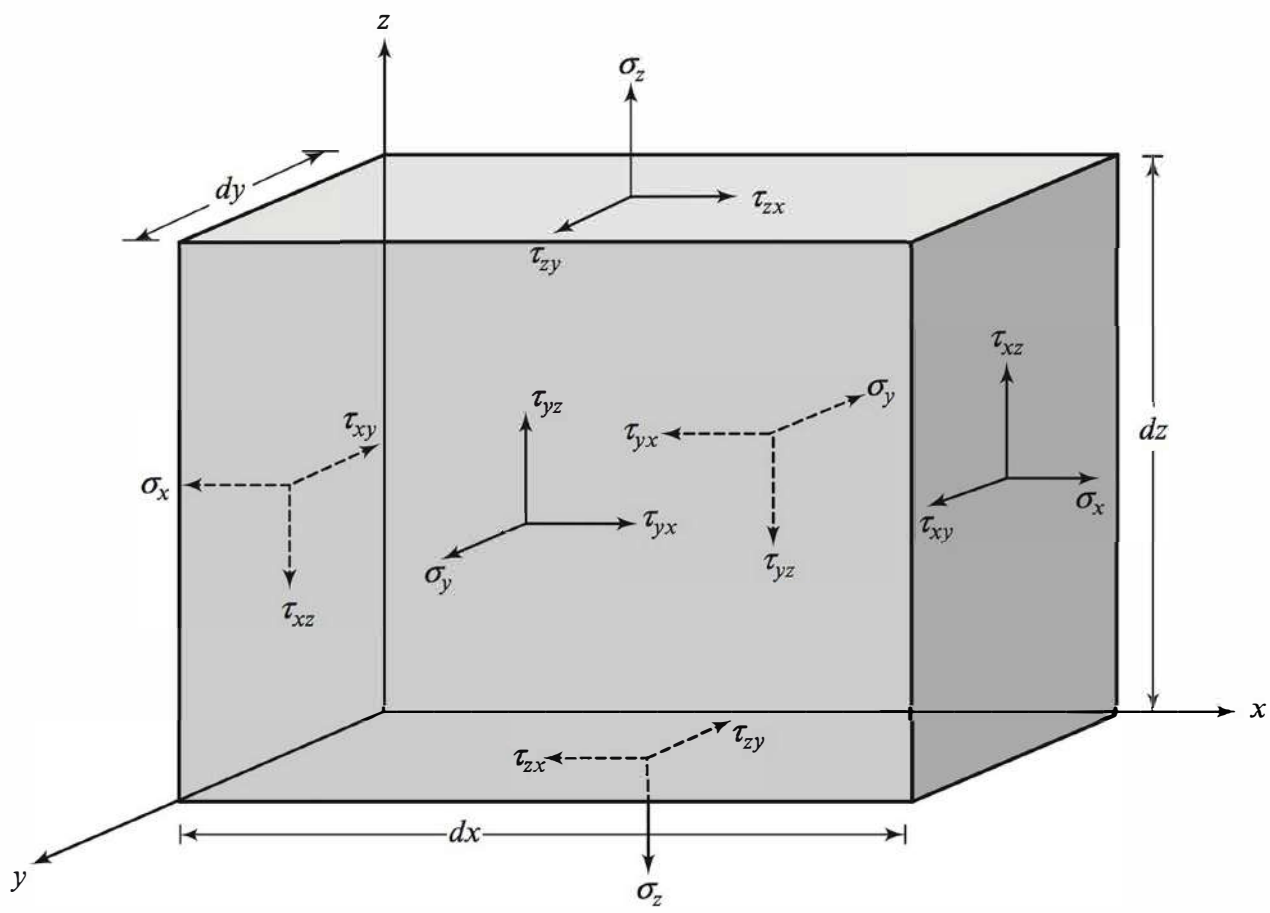

Figure 3.1 Notations for normal and shear stresses

If τ_{ij} is a shear stress, it means that it is acting on a plane normal to the i axis, and its direction is parallel to the j axis. For equilibrium purposes, by taking moments, it may be seen that

$$\tau_{xy} = \tau_{yx} \tag{3.1}$$

$$\tau_{xz} = \tau_{zx} \tag{3.2}$$

$$\tau_{yz} = \tau_{zy} \tag{3.3}$$

Strain

Due to a given stress condition, let the displacements in the x, y, and z directions (Figure 3.1) be, respectively, u, υ and w. Then the equations for strains and rotations of elastic and isotropic materials in terms of displacements are as follows:

$$\varepsilon_x = \frac{\partial u}{\partial x} \tag{3.4}$$

$$\varepsilon_y = \frac{\partial \upsilon}{\partial y} \tag{3.5}$$

$$\varepsilon_z = \frac{\partial w}{\partial z} \tag{3.6}$$

Copyright 2017 Cengage Learning. All Rights Reserved. May not be copied, scanned, or duplicated, in whole or in part. Due to electronic rights, some third party content may be suppressed from the eBook and/or eChapter(s). Editorial review has deemed that any suppressed content does not materially affect the overall learning experience. Cengage Learning reserves the right to remove additional content at any time if subsequent rights restrictions require it.

$$\gamma'_{xy} = \frac{\partial \upsilon}{\partial x} + \frac{\partial u}{\partial y} \tag{3.7}$$

$$\gamma'_{yz} = \frac{\partial w}{\partial y} + \frac{\partial \upsilon}{\partial z} \tag{3.8}$$

$$\gamma'_{zx} = \frac{\partial u}{\partial z} + \frac{\partial w}{\partial x} \tag{3.9}$$

$$\bar{\omega}_x = \frac{1}{2}\left(\frac{\partial w}{\partial y} - \frac{\partial \upsilon}{\partial z}\right) \tag{3.10}$$

$$\bar{\omega}_y = \frac{1}{2}\left(\frac{\partial u}{\partial z} - \frac{\partial w}{\partial x}\right) \tag{3.11}$$

$$\bar{\omega}_z = \frac{1}{2}\left(\frac{\partial \upsilon}{\partial x} - \frac{\partial u}{\partial y}\right) \tag{3.12}$$

where

$\varepsilon_x, \varepsilon_y$ and ε_z = normal strains in the direction of x, y and z, respectively

γ'_{xy} = sheering strain between the planes xz and yz

γ'_{yz} = shearing strain between the planes yx and zx

γ'_{zx} = shearing strain between the planes zy and xy

$\bar{\omega}_x, \bar{\omega}_y$ and $\bar{\omega}_z$ = the components of rotation about the x, y, and z axes.

These derivations are given in most of the textbooks on the theory of elasticity (e.g., Timoshenko and Goodier, 1970). The interested reader may consult these books as the derivations not covered here in detail.

3.3 HOOKE'S LAW

For an elastic, isotropic material, the normal strains and normal stresses can be related by the following equations:

$$\varepsilon_x = \frac{1}{E}\left[\sigma_x - \mu(\sigma_y + \sigma_z)\right] \tag{3.13}$$

$$\varepsilon_y = \frac{1}{E}\left[\sigma_y - \mu(\sigma_x + \sigma_z)\right] \tag{3.14}$$

$$\varepsilon_z = \frac{1}{E}\left[\sigma_z - \mu(\sigma_x + \sigma_y)\right] \tag{3.15}$$

where ε_x, ε_y and ε_z are the respective normal strains in the directions of x, y, and z, E is *Young's modulus*, and μ is *Poisson's ratio*.

Copyright 2017 Cengage Learning. All Rights Reserved. May not be copied, scanned, or duplicated, in whole or in part. Due to electronic rights, some third party content may be suppressed from the eBook and/or eChapter(s). Editorial review has deemed that any suppressed content does not materially affect the overall learning experience. Cengage Learning reserves the right to remove additional content at any time if subsequent rights restrictions require it.

The shear stresses and the shear strains can be related by the following equations:

$$\tau_{xy} = G\gamma'_{xy} \tag{3.16}$$

$$\tau_{yz} = G\gamma'_{yz} \tag{3.17}$$

$$\tau_{zx} = G\gamma'_{zx} \tag{3.18}$$

where the *shear modulus* (G) is

$$G = \frac{E}{2(1+\mu)} \tag{3.19}$$

and γ'_{xy}, γ'_{yz} , and γ'_{zx} are the shear strains.

Equations (3.13) – (3.15) can be solved to express normal stresses in terms of normal strains as

$$\sigma_x = \lambda\bar{\varepsilon} + 2G\varepsilon_x \tag{3.20}$$

$$\sigma_y = \lambda\bar{\varepsilon} + 2G\varepsilon_y \tag{3.21}$$

$$\sigma_z = \lambda\bar{\varepsilon} + 2G\varepsilon_z \tag{3.22}$$

where

$$\lambda = \frac{\mu E}{(1+\mu)(1-2\mu)} \tag{3.23}$$

$$\bar{\varepsilon} = \varepsilon_x + \varepsilon_y + \varepsilon_z \tag{3.24}$$

λ is known as the Lame's constant and can easily estimated by a relatively easy measurement of E and μ of any material and thus can be used for describing the velocity of waves through the material.

From Eqs (3.19) and (3.23), it is easy to see that

$$\mu = \frac{\lambda}{2(\lambda+G)} \tag{3.25}$$

Elastic Stress Waves in a Bar

3.4 LONGITUDINAL ELASTIC WAVES IN A BAR

Figure 3.2 shows a rod, of which the cross-sectional area is equal to A. Let the Young's modulus and the unit weight of the material that constitutes the rod be equal to E and γ, respectively. Now, let the stress along section $a-a$ of the rod increase by σ. The stress increase along the section $b-b$ can then be given by $\sigma + (\partial\sigma/\partial x)\Delta x$. Based on Newton's second law,

Copyright 2017 Cengage Learning. All Rights Reserved. May not be copied, scanned, or duplicated, in whole or in part. Due to electronic rights, some third party content may be suppressed from the eBook and/or eChapter(s). Editorial review has deemed that any suppressed content does not materially affect the overall learning experience. Cengage Learning reserves the right to remove additional content at any time if subsequent rights restrictions require it.

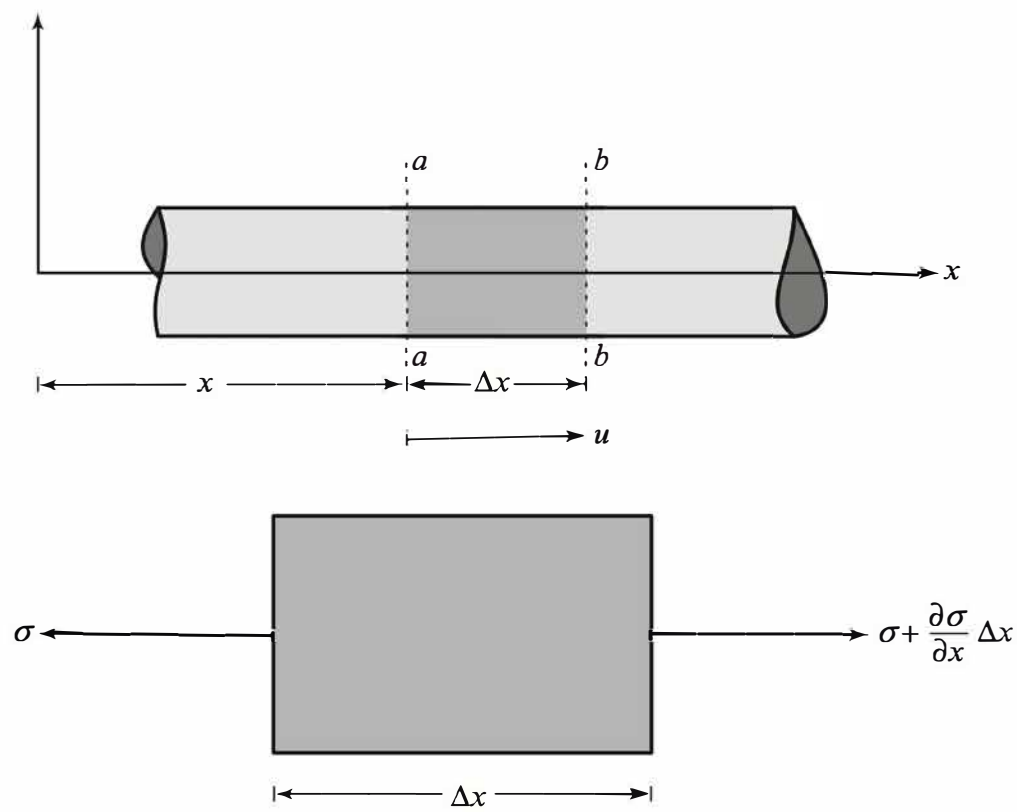

Figure 3.2 Longitudinal elastic waves in a bar

$$\sum \text{force} = (\text{mass})\,(\text{acceleration})$$

Thus, summing the forces in the x direction,

$$-\sigma A + \left(\sigma + \frac{\partial \sigma}{\partial x}\Delta x\right)A = \frac{A\gamma(\Delta x)}{g}\frac{\partial^2 u}{\partial t^2} \tag{3.26}$$

where $A\gamma(\Delta x)$ = weight of the rod of length Δx, g is the acceleration due to gravity, u is displacement in the x direction, and t is time.

Equation (3.26) is based on the assumptions that (1) the stress is uniform over the entire cross-sectional area and (2) the cross section remains plane during the motion. Simplification of Eq. (3.26) gives

$$\frac{\partial \sigma}{\partial x} = \rho\left(\frac{\partial^2 u}{\partial t^2}\right) \tag{3.27}$$

where $\rho = \gamma/g$ is the density of the material of the bar. However,

$$\sigma = (\text{strain})\,(\text{Young's modulus}) = \left(\frac{\partial u}{\partial x}\right)E \tag{3.28}$$

Substitution of Eq. (3.28) into (3.27) yields

$$\frac{\partial^2 u}{\partial t^2} = \left(\frac{E}{\rho}\right)\left(\frac{\partial^2 u}{\partial x^2}\right)$$

Copyright 2017 Cengage Learning. All Rights Reserved. May not be copied, scanned, or duplicated, in whole or in part. Due to electronic rights, some third party content may be suppressed from the eBook and/or eChapter(s). Editorial review has deemed that any suppressed content does not materially affect the overall learning experience. Cengage Learning reserves the right to remove additional content at any time if subsequent rights restrictions require it.

or

$$\boxed{\frac{\partial^2 u}{\partial t^2} = v_c^2 \frac{\partial^2 u}{\partial x^2}} \tag{3.29}$$

where

$$\boxed{v_c = \sqrt{\frac{E}{\rho}}} \tag{3.30}$$

The term v_c is the velocity of the *longitudinal* stress wave propagation. This fact can be demonstrated as follows. The solution to Eq. (3.29) can be written in the form

$$u = F(v_c t + x) + G(v_c t - x) \tag{3.31}$$

where $F(v_c t + x)$ and $G(v_c t - x)$ represent some functions of $(v_c t + x)$ and $(v_c t - x)$, respectively. At a given time t, let the function $F(v_c t + x)$ be represented by block 1 in Figure 3.3, and

$$u_t = F(v_c t + x)$$

At time $t + \Delta t$, the function will be represented by block 2 in Figure 3.3. Thus,

$$u_t + \Delta t = F[v_c(t + \Delta t) + (x - \Delta x)] \tag{3.32}$$

If the block moves unchanged in shaped from position 1 to position 2,

$$u_t = u_{t+\Delta t}$$

or

$$F(v_c t + x) = F[v_c(t + \Delta t) + (x - \Delta x)]$$

or

$$v_c \, \Delta t = \Delta x \tag{3.33}$$

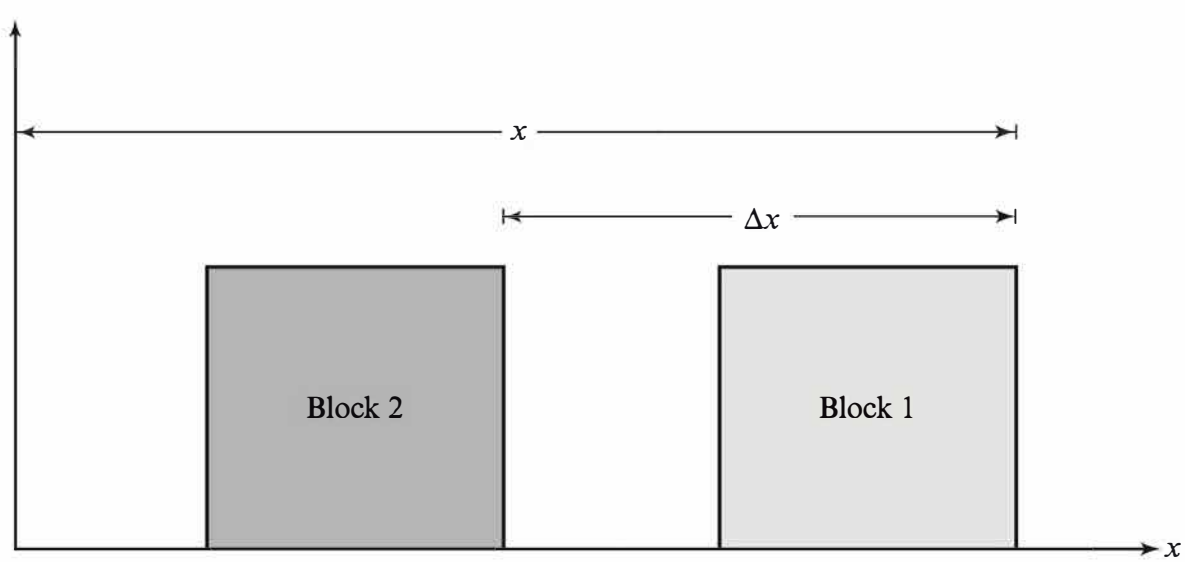

Figure 3.3 Motion of longitudinal elastic wave in a bar

Copyright 2017 Cengage Learning. All Rights Reserved. May not be copied, scanned, or duplicated, in whole or in part. Due to electronic rights, some third party content may be suppressed from the eBook and/or eChapter(s). Editorial review has deemed that any suppressed content does not materially affect the overall learning experience. Cengage Learning reserves the right to remove additional content at any time if subsequent rights restrictions require it.

Thus the velocity of the longitudinal stress wave propagation is equal to $\Delta x/\Delta t = \upsilon_c$. In a similar manner, it can be shown that the function $G(\upsilon_c t - x)$ represents a wave traveling in the positive direction of x.

If the bar described above is confined, so that no lateral expansion is possible, then the above equation can be modified as

$$\boxed{\frac{\partial^2 u}{\partial t^2} = \upsilon_c'^2 \frac{\partial^2 u}{\partial x^2}} \tag{3.34}$$

where

$$\boxed{\upsilon_c' = \sqrt{\frac{M}{\rho}}} \tag{3.35}$$

$$M = \text{constrained modulus} = \frac{E(1-\mu)}{(1-2\mu)(1+\mu)}; \mu = \text{Poisson's ratio}$$

3.5 VELOCITY OF PARTICLES IN THE STRESSED ZONE

It is important for readers to appreciate the difference between the velocity of the longitudinal wave propagation (υ_c) and the velocity of the particles in the stressed zone. In order to distinguish them, consider a compressive stress pulse of intensity σ_x and duration t' (Figure 3.4a) applied to the end of a rod (shown in Figure 3.4b). When this stress pulse is applied initially, a small zone of the rod will undergo compression. With time this compression will be transmitted to successive zones. During a time interval Δt the stress will travel through a distance

$$\Delta x = \upsilon_c \, \Delta t$$

At any time $t > t'$, a segment of the rod of length $\bar{x}$ will constitute the compressed zone. Note that

$$\bar{x} = \upsilon_c \, t'$$

The elastic shortening of the rod then is

$$u = \left(\frac{\sigma_x}{E}\right)(\bar{x}) = \left(\frac{\sigma_x}{E}\right)(\upsilon_c t')$$

Note that u is the displacement of the end of the rod. Now, the velocity of the end of the rod and, thus, the particle velocity is

$$\dot{u} = \frac{u}{t'} = \frac{\sigma_x \upsilon_c}{E}$$

Also, it is important to note the following:

1. Particle velocity $\dot{u}$ is a function of the intensity of stress σ_x. The higher the amplitude of the intensity of stress, the higher the particle velocity for the same medium is.

Copyright 2017 Cengage Learning. All Rights Reserved. May not be copied, scanned, or duplicated, in whole or in part. Due to electronic rights, some third party content may be suppressed from the eBook and/or eChapter(s). Editorial review has deemed that any suppressed content does not materially affect the overall learning experience. Cengage Learning reserves the right to remove additional content at any time if subsequent rights restrictions require it.

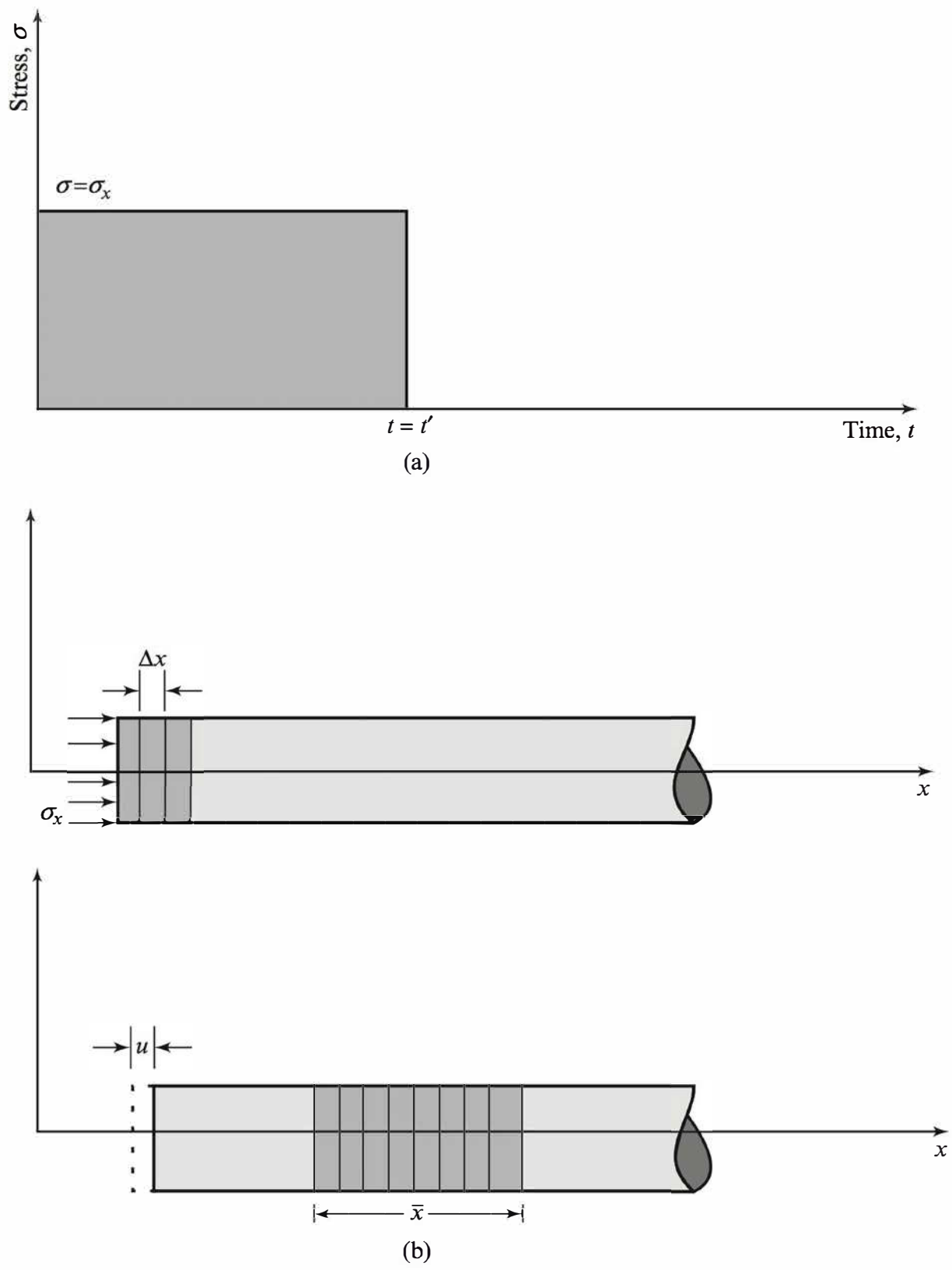

Figure 3.4 Velocity of wave propagation and velocity of particles

2. However, the longitudinal wave propagation velocity is a function of material property only. It is independent of the amplitude of stress applied.
3. The wave propagation velocity and the particle velocity are in the same direction when a compressive stress is applied. However, when a tensile stress is applied, the wave propagation and the particle velocity are in opposite directions.

The above concepts are used in non-destructive testing apparatus such as pile integrity testing (PIT).

Copyright 2017 Cengage Learning. All Rights Reserved. May not be copied, scanned, or duplicated, in whole or in part. Due to electronic rights, some third party content may be suppressed from the eBook and/or eChapter(s). Editorial review has deemed that any suppressed content does not materially affect the overall learning experience. Cengage Learning reserves the right to remove additional content at any time if subsequent rights restrictions require it.

The vibration measuring instruments pick the particle vibration velocity and not the wave propagation velocity. Usually, in geophysical methods, described later in Chapter 4, the peaks in particle vibration velocities are detected, and the wave propagation velocities are interpreted.

3.6 REFLECTIONS OF ELASTIC STRESS WAVES AT THE END OF A BAR

Bars must terminate at some point. One needs to consider the case of what happens when one of these disturbances, $F(v_c t + x)$ or $G(v_c t - x)$ [Eq. (3.31)], meets the end of the bar.

Figure 3.5a shows a compression wave moving along a bar in the positive x direction. Additionally, a tension wave of the same length is moving along the negative direction of x. When the two waves meets each other (at section $a-a$), the compression and tension cancel each other, resulting in zero stress; however, the particle velocity is doubled (Figure 3.5b). This is because the particle velocity for a compression wave is in the direction of the motion, and in the tension wave, the particle velocity is opposed to the direction of motion. After the two waves pass each other, the stress and the particle velocity again return to zero at section $a-a$ (Figure 3.5c). The section $a-a$ corresponds to having the stress condition that a free end of a bar would have. Figure 3.5d shows the portion of the rod located to the left of section $a-a$, and the section can be considered as a free end. By observation it can be seen that, at the free end of a bar, a *compression wave* is *reflected back as a tension wave* having the same magnitude and shape. In a similar manner, a tension wave is reflected back as a compression wave at the free end of a bar.

Figure 3.6a shows a bar in which two identical compression waves are traveling in opposite directions. When the two waves cross each other at section $a-a$, the magnitude of the stress will be doubled. However, the particle velocity $\dot{u}$ will be equal to zero (Figure 3.6b). After the two waves pass each other, the stress and the particle velocity return to zero at section $a-a$ (Figure 3.6c). Section $a-a$ remains stationary and behaves as a fixed end of a rod. By observation it can be seen (Figure 3.6d) that a compression wave is reflected back as a compression wave of the same magnitude and shape, but the stress is doubled at the fixed end. In a similar manner, a tension wave is reflected back as a tension wave at the fixed end of a bar.

3.7 TORSIONAL WAVES IN A BAR

Figure 3.7 shows a rod to which a torque T is applied at a distance x, and the end at x will be rotated through an angle θ. The torque at the section located at a distance $x + \Delta x$ can be given by $T + (\partial T/\partial x)\Delta x$ and the corresponding rotation by $\theta + (\partial\theta/\partial x)\Delta x$. Applying Newton's second law of motion,

Copyright 2017 Cengage Learning. All Rights Reserved. May not be copied, scanned, or duplicated, in whole or in part. Due to electronic rights, some third party content may be suppressed from the eBook and/or eChapter(s). Editorial review has deemed that any suppressed content does not materially affect the overall learning experience. Cengage Learning reserves the right to remove additional content at any time if subsequent rights restrictions require it.

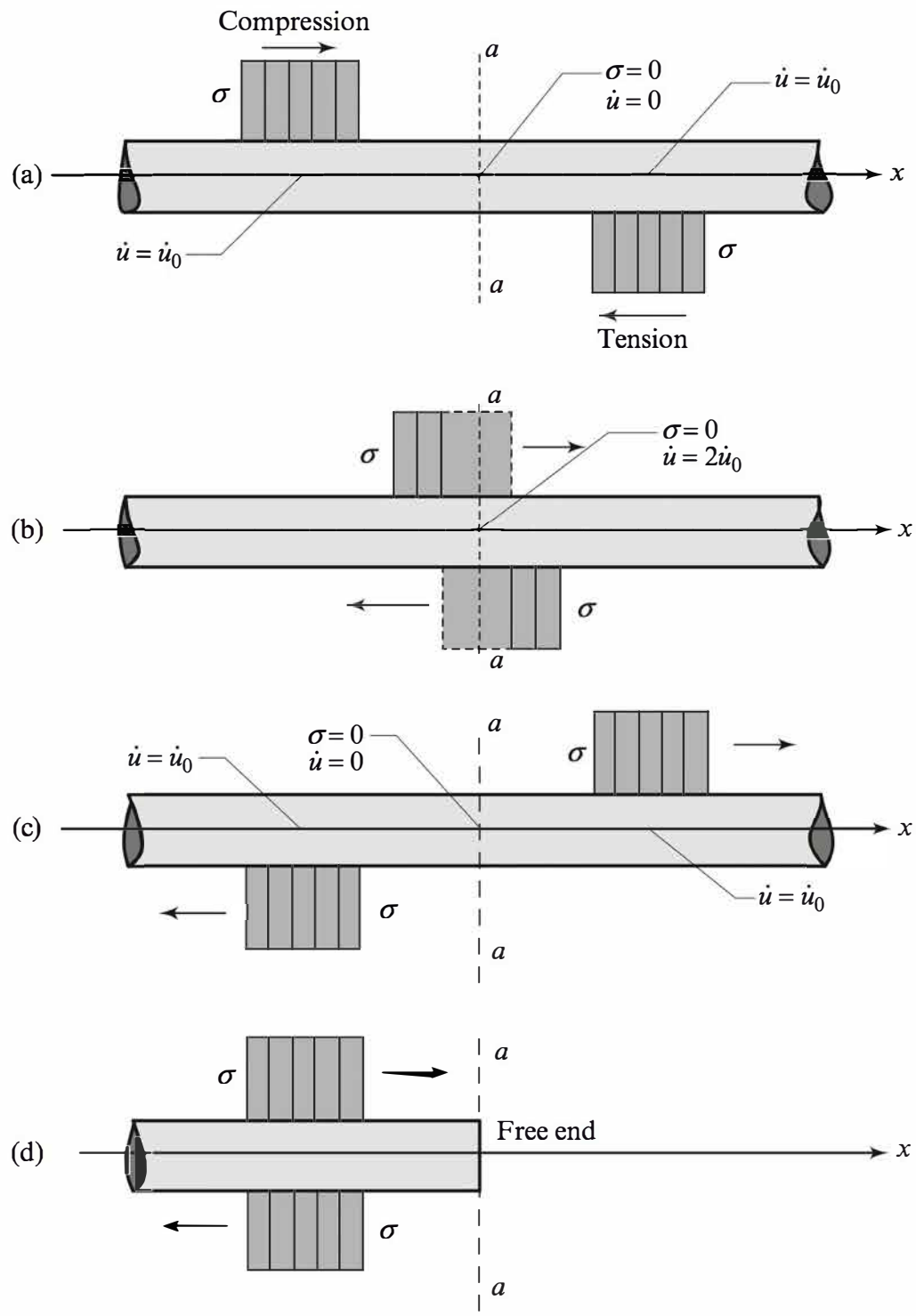

Figure 3.5 Reflection of stress waves at a free end of a bar

$$-T + \left(T + \frac{\partial T}{\partial x}\Delta x\right) = \rho J \Delta x \frac{\partial^2 \theta}{\partial t^2} \tag{3.36}$$

where J is the polar moment of inertia of the cross section of the bar. However, torque T can be expressed by the relation

$$T = JG\frac{\partial \theta}{\partial x} \tag{3.37}$$

Copyright 2017 Cengage Learning. All Rights Reserved. May not be copied, scanned, or duplicated, in whole or in part. Due to electronic rights, some third party content may be suppressed from the eBook and/or eChapter(s). Editorial review has deemed that any suppressed content does not materially affect the overall learning experience. Cengage Learning reserves the right to remove additional content at any time if subsequent rights restrictions require it.

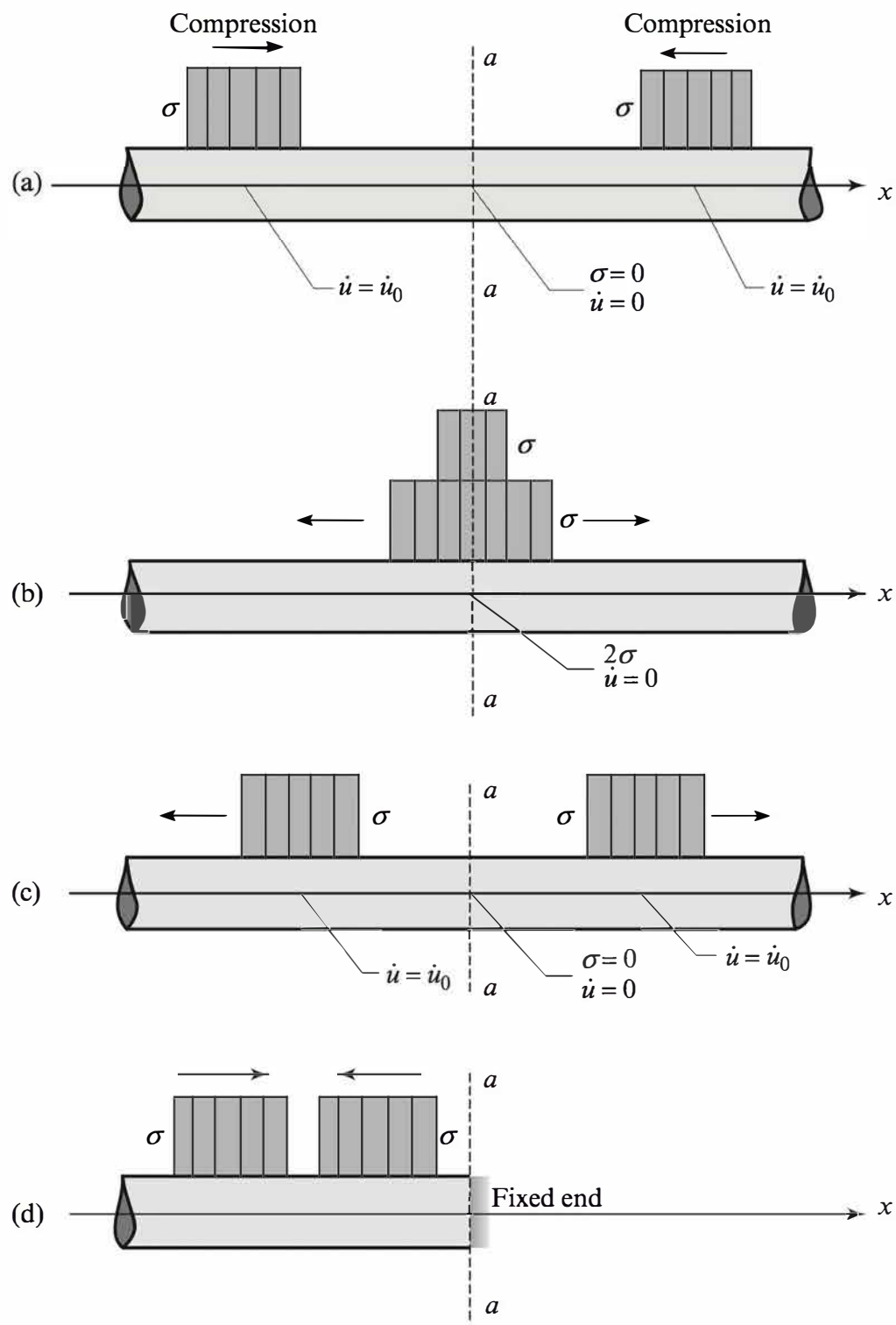

Figure 3.6 Reflection of stress waves at a fixed end of a bar

Substitution of Eq. (3.37) into Eq. (3.36) results in

$$\frac{\partial^2 \theta}{\partial t^2} = \frac{G}{\rho}\frac{\partial^2 \theta}{\partial x^2} \tag{3.38}$$

or

$$\frac{\partial^2 \theta}{\partial t^2} = v_s^2 \frac{\partial^2 \theta}{\partial x^2} \tag{3.39}$$

Copyright 2017 Cengage Learning. All Rights Reserved. May not be copied, scanned, or duplicated, in whole or in part. Due to electronic rights, some third party content may be suppressed from the eBook and/or eChapter(s). Editorial review has deemed that any suppressed content does not materially affect the overall learning experience. Cengage Learning reserves the right to remove additional content at any time if subsequent rights restrictions require it.

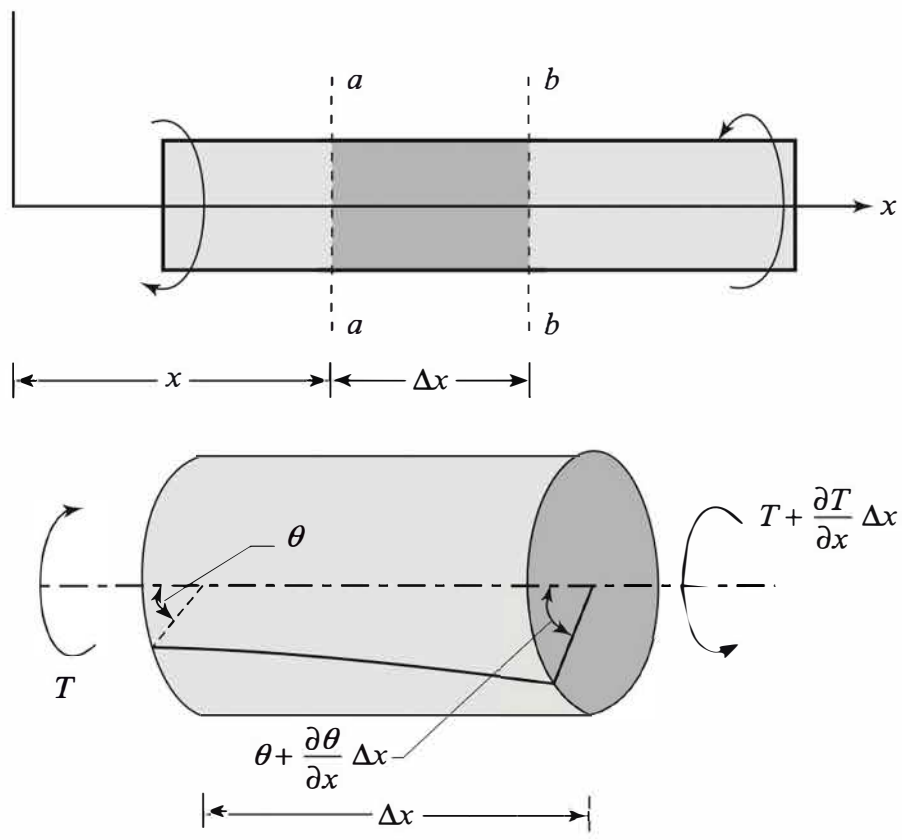

Figure 3.7 Torsional waves in a bar

where

$$\boxed{v_s = \sqrt{\frac{G}{\rho}}} \tag{3.40}$$

is the velocity of torsional waves.

Note that Eqs. (3.39) and (3.29) are of similar form.

3.8 LONGITUDINAL VIBRATION OF SHORT BARS

The solution to the wave equations for short bars vibrating in a natural mode can be written in the general form as

$$u(x,t) = U(x)(A_1 \sin \omega_n t + A_2 \cos \omega_n t) \tag{3.41}$$

where A_1 and A_2 are constants, ω_n is the natural circular frequency of vibration, and $U(x)$ is the amplitude of displacement along the length of the rod and is independent of time.

For longitudinal vibration of uniform bars, if Eq. (3.41) is substituted into Eq. (3.29), it yields

$$\frac{\partial^2 u(x,t)}{\partial x^2} - \frac{\rho}{E}\frac{\partial^2 u(x,t)}{\partial t^2} = 0$$

Copyright 2017 Cengage Learning. All Rights Reserved. May not be copied, scanned, or duplicated, in whole or in part. Due to electronic rights, some third party content may be suppressed from the eBook and/or eChapter(s). Editorial review has deemed that any suppressed content does not materially affect the overall learning experience. Cengage Learning reserves the right to remove additional content at any time if subsequent rights restrictions require it.

or

$$\frac{\partial^2 U(x)}{\partial x^2} + \frac{\rho}{E}(\omega_n^2)\,U(x) = 0 \tag{3.42}$$

The solution to Eq. (3.42) may be expressed in the form

$$U(x) = B_1 \sin\left(\frac{\omega_n x}{v_c}\right) + B_2 \cos\left(\frac{\omega_n x}{v_c}\right) \tag{3.43}$$

where B_1 and B_2 are constants. These constants may be determined by the end condition to which a rod may be subjected.

A. End Condition: Free–Free

For the free–free condition, the stress and thus the strain at the ends are zero. So at $x = 0$, $dU(x)/dx = 0$; and at $x = L$, $dU(x)/dx = 0$, where L is the length of the bar. Differentiating Eq. (3.43) with respect to x.

$$\frac{dU(x)}{dx} = \frac{B_1\omega_n}{v_c}\cos\left(\frac{\omega_n x}{v_c}\right) - \frac{B_2\omega_n}{v_c}\sin\left(\frac{\omega_n x}{v_c}\right) \tag{3.44}$$

Substitution of the first boundary condition into Eq. (3.44) results in

$$0 = \frac{B_1\omega_n}{v_c}; \quad \text{i.e.}, B_1 = 0 \tag{3.45}$$

Again, from the second boundary condition and Eq. (3.44),

$$0 = -\left(\frac{B_2\omega_n}{v_c}\right)\sin\left(\frac{\omega_n L}{v_c}\right)$$

Since B_2 is not equal to zero,

$$\frac{\omega_n L}{v_c} = n\pi \tag{3.46}$$

or

$$\boxed{\omega_n = \frac{n\pi v_c}{L}} \tag{3.47}$$

where $n = 1, 2, 3, \ldots$; thus,

$$\boxed{v_c = \frac{\omega_n L}{n\pi}} \tag{3.48}$$

The equation for the amplitude of displacement for this case can be given by combining Eqs. (3.43), (3.45), and (3.48), or

$$U(x) = B_2 \cos\left(\frac{n\pi x}{L}\right) \tag{3.49}$$

Copyright 2017 Cengage Learning. All Rights Reserved. May not be copied, scanned, or duplicated, in whole or in part. Due to electronic rights, some third party content may be suppressed from the eBook and/or eChapter(s). Editorial review has deemed that any suppressed content does not materially affect the overall learning experience. Cengage Learning reserves the right to remove additional content at any time if subsequent rights restrictions require it.

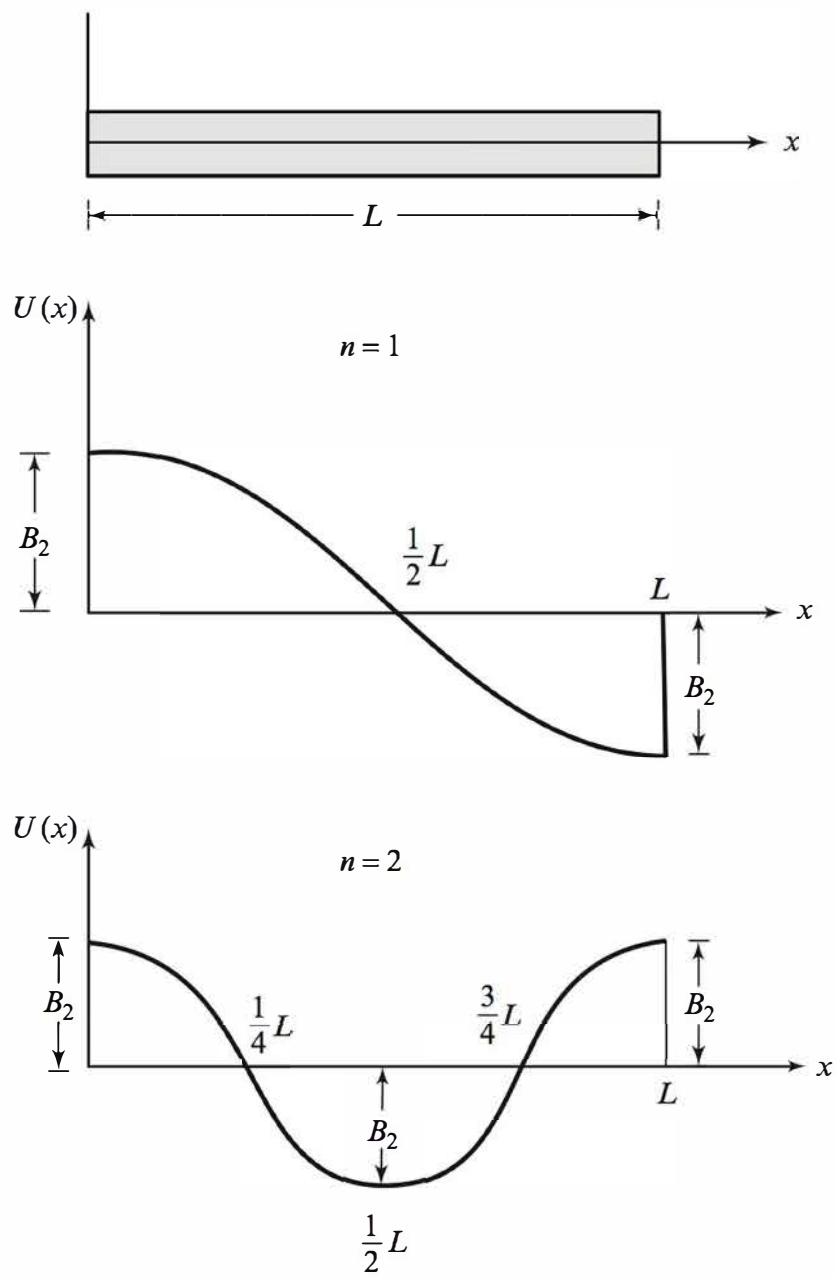

Figure 3.8 Longitudinal vibration of a short bar: free–free end condition

The variation of the nature of $U(x)$ for the first two harmonics (i.e., $n = 1$ and 2) is shown in Figure 3.8. The equation for $u(x, t)$ for all modes of vibration can also be given by combining Eqs. (3.49) and (3.41).

B. End Condition: Fixed–Fixed

For a fixed–fixed end condition, at $x = 0$, $U(x) = 0$ (i.e., displacement is zero); and at $x = L$, $U(x) = 0$

Substituting the first boundary condition into Eq. (3.43) results in

$$0 = B_2 \tag{3.50}$$

Again, combining the second boundary condition and Eq. (3.43),

$$0 = B_1 \sin\left(\frac{\omega_n L}{v_c}\right)$$

Copyright 2017 Cengage Learning. All Rights Reserved. May not be copied, scanned, or duplicated, in whole or in part. Due to electronic rights, some third party content may be suppressed from the eBook and/or eChapter(s). Editorial review has deemed that any suppressed content does not materially affect the overall learning experience. Cengage Learning reserves the right to remove additional content at any time if subsequent rights restrictions require it.

Since $B_1 \neq 0$,

$$\left(\frac{\omega_n L}{v_c}\right) = n\pi \tag{3.51}$$

where $n = 1, 2, 3, \ldots$; or

$$\boxed{\omega_n = \frac{n\pi v_c}{L}} \tag{3.52}$$

or

$$\boxed{v_c = \frac{\omega_n L}{n\pi}} \tag{3.53}$$

The displacement amplitude equation can now be given be combining Eqs. (3.43), (3.50), and (3.52) as

$$U(x) = B_1 \sin\left(\frac{n\pi x}{L}\right) \tag{3.54}$$

Figure 3.9 shows the variation of $U(x)$ for the first two harmonics $(n = 1 \text{ and } 2)$

C. End Condition: Fixed–Free

The boundary conditions for the fixed–free case can be given as follows:

$$\text{At } x = 0 \text{ (fixed end)}, \qquad U(x) = 0$$

$$\text{At } x = L \text{ (free end)}, \qquad \frac{dU(x)}{dx} = 0$$

From the first boundary condition and Eq. (3.43),

$$U(x) = 0 = B_2 \tag{3.55}$$

Again, from the second boundary condition and Eq. (3.43)

$$\frac{dU(x)}{dx} = 0 = \frac{B_1\omega_n}{v_c}\cos\left(\frac{\omega_n L}{v_c}\right) \tag{3.56}$$

or

$$\frac{\omega_n L}{v_c} = \frac{1}{2}(2n-1)\pi$$

where $n = 1, 2, 3, \ldots$; so

$$\boxed{\omega_n = \frac{1}{2}(2n-1)\pi\left(\frac{v_c}{L}\right)} \tag{3.57}$$

Copyright 2017 Cengage Learning. All Rights Reserved. May not be copied, scanned, or duplicated, in whole or in part. Due to electronic rights, some third party content may be suppressed from the eBook and/or eChapter(s). Editorial review has deemed that any suppressed content does not materially affect the overall learning experience. Cengage Learning reserves the right to remove additional content at any time if subsequent rights restrictions require it.

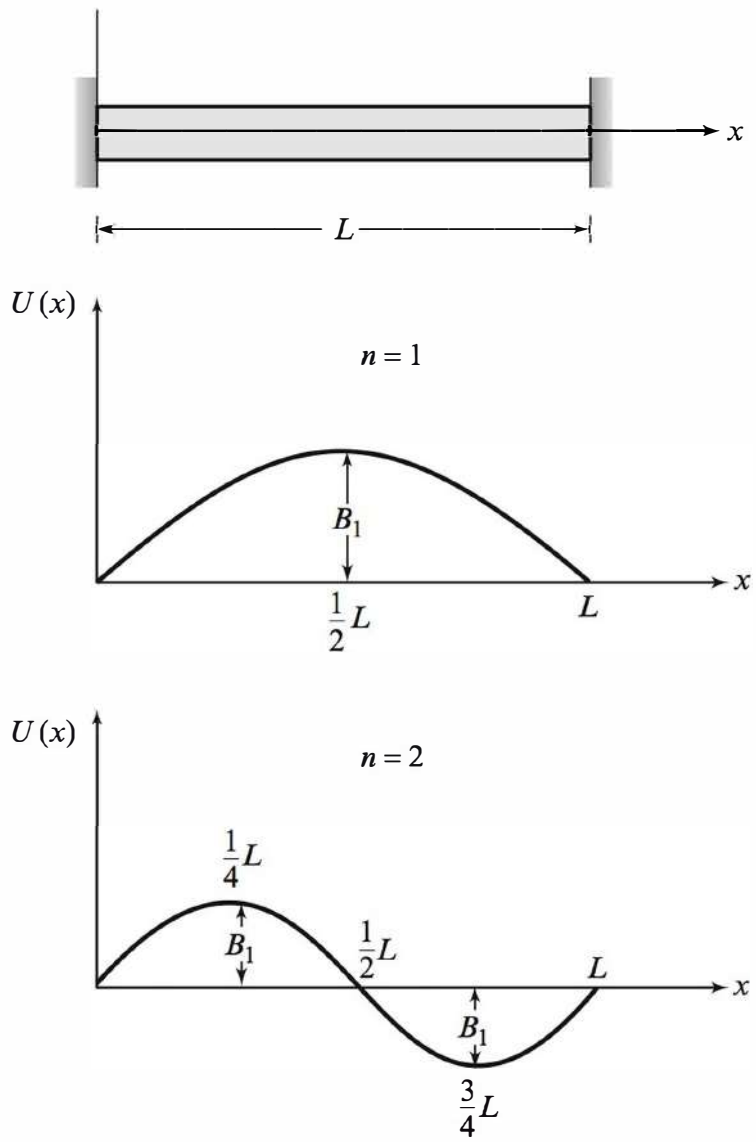

Figure 3.9 Longitudinal vibration of a short bar: fixed–fixed end condition

The displacement amplitude equation can now be written by combining Eqs. (3.43), (3.55), and (3.57) as

$$U(x) = B_1 \sin\left[\frac{\frac{1}{2}(2n-1)\pi x}{L}\right] \tag{3.58}$$

Figure 3.10 shows the variation of $U(x)$ for the first two harmonics

3.9 TORSIONAL VIBRATION OF SHORT BARS

The torsional vibration of short bars can be treated in a manner similar to the longitudinal vibration given in Section 3.8 by writing the equation for natural modes of vibration as

$$\theta(x,t) = \Theta(x)(A_1 \sin\omega_n t + A_2 \cos\omega_n t) \tag{3.59}$$

Copyright 2017 Cengage Learning. All Rights Reserved. May not be copied, scanned, or duplicated, in whole or in part. Due to electronic rights, some third party content may be suppressed from the eBook and/or eChapter(s). Editorial review has deemed that any suppressed content does not materially affect the overall learning experience. Cengage Learning reserves the right to remove additional content at any time if subsequent rights restrictions require it.

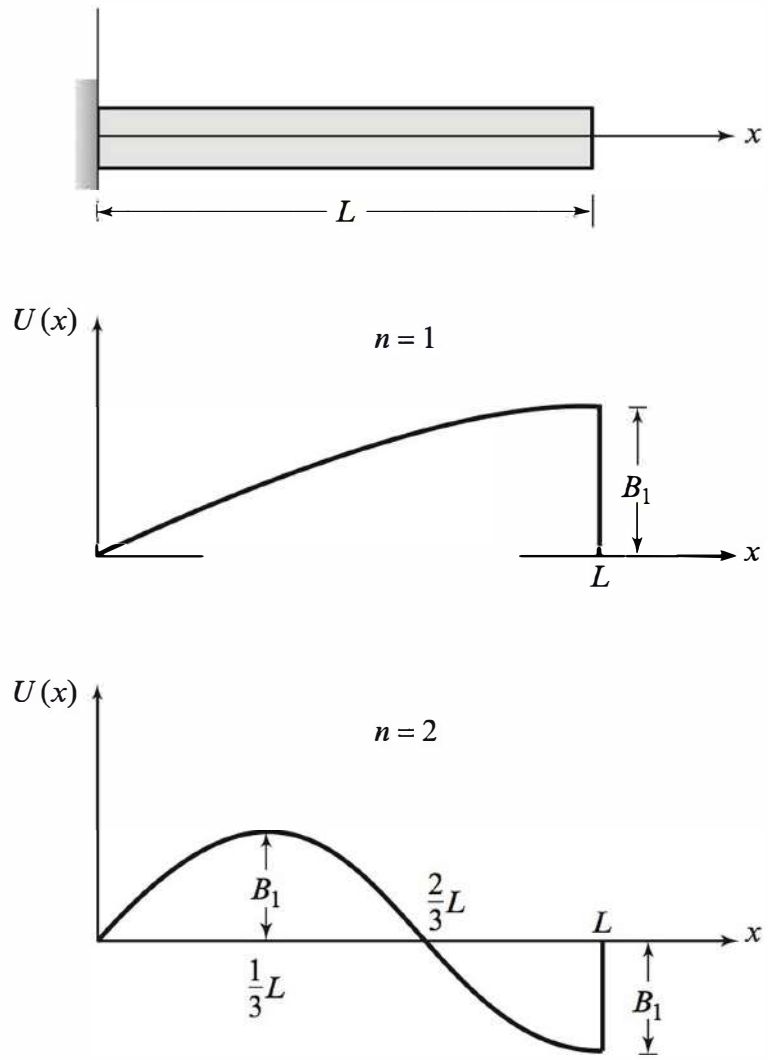

Figure 3.10 Longitudinal vibration of a short bar fixed–free end condition

where $\Theta =$ amplitude of angular distortion and A_1 and A_2 are constants. Solution of Eqs. (3.39) and (3.59) results in

$$\omega_n = \frac{n\pi v_s}{L} \tag{3.60}$$

for the free–free end and fixed–fixed end conditions; and

$$\omega_n = \frac{\frac{1}{2}(2n-1)\pi v_s}{L} \tag{3.61}$$

for the fixed–free end condition, where L is the length of the bar and $n = 1, 2, 3, \ldots$.

Copyright 2017 Cengage Learning. All Rights Reserved. May not be copied, scanned, or duplicated, in whole or in part. Due to electronic rights, some third party content may be suppressed from the eBook and/or eChapter(s). Editorial review has deemed that any suppressed content does not materially affect the overall learning experience. Cengage Learning reserves the right to remove additional content at any time if subsequent rights restrictions require it.

Stress Waves in an Infinite Elastic Medium

3.10 EQUATION OF MOTION IN AN ELASTIC MEDIUM

Figure 3.11 shows the stresses acting on an element of elastic medium with sides measuring dx, dy and dz. For obtaining the differential equations of motion, one needs to sum the forces in the x, y, and z directions. Along the x direction,

$$\left[\left(\sigma_x + \frac{\partial \sigma_x}{\partial x} dx\right) - \sigma_x\right](dy)(dz) + \left[\left(\tau_{zx} + \frac{\partial \tau_{zx}}{\partial z} dz\right) - \tau_{zx}\right](dx)(dy)$$
$$+ \left[\left(\tau_{yx} + \frac{\partial \tau_{yx}}{\partial y} dy\right) - \tau_{yx}\right](dx)(dz) = \rho(dx)(dy)(dz)\frac{\partial^2 u}{\partial t^2}$$

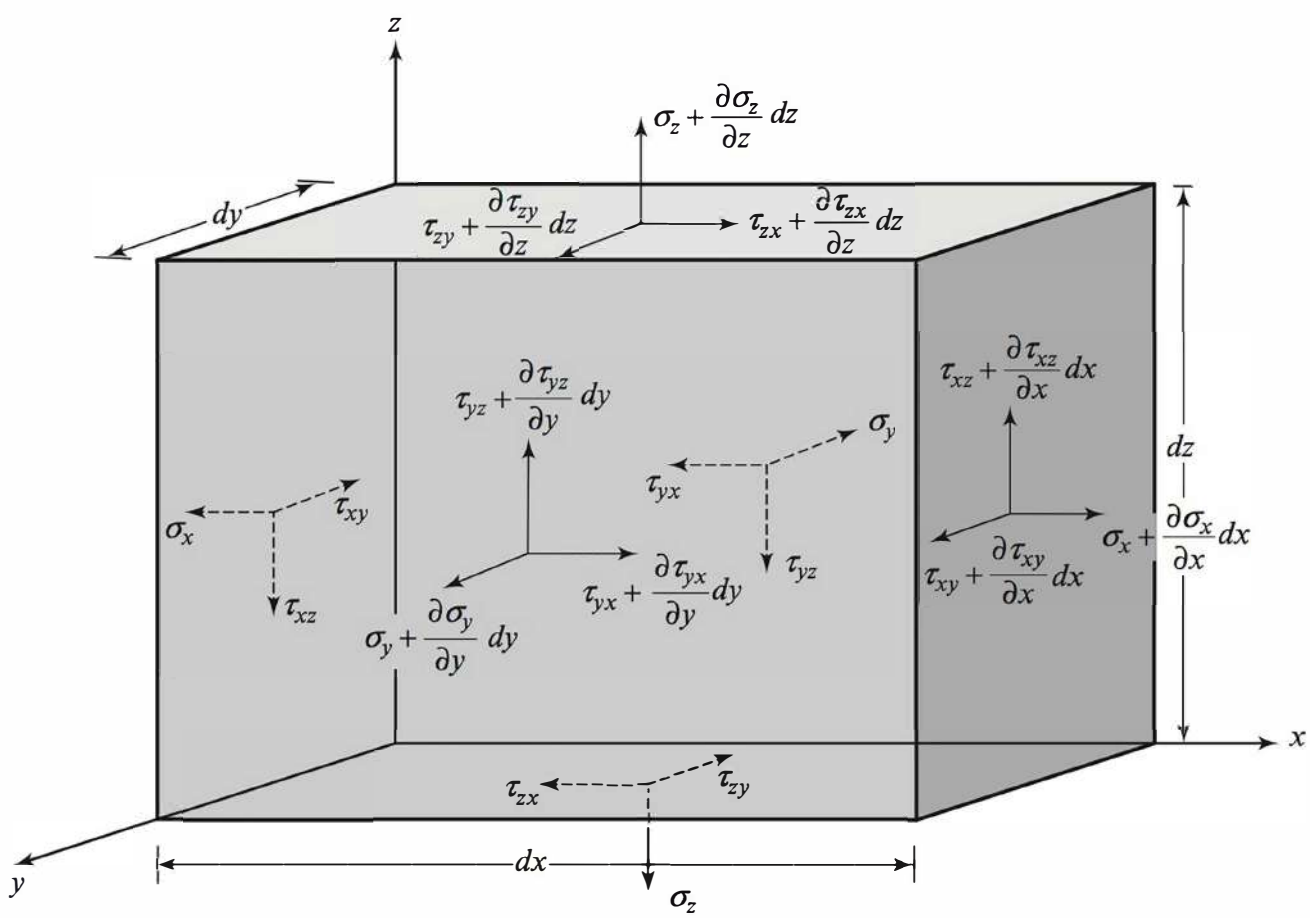

Figure 3.11 Derivation of the equation of motion in an elastic medium

Copyright 2017 Cengage Learning. All Rights Reserved. May not be copied, scanned, or duplicated, in whole or in part. Due to electronic rights, some third party content may be suppressed from the eBook and/or eChapter(s). Editorial review has deemed that any suppressed content does not materially affect the overall learning experience. Cengage Learning reserves the right to remove additional content at any time if subsequent rights restrictions require it.

where ρ is the density of the medium and u is the displacement component along the x direction. Alternatively,

$$\frac{\partial \sigma_x}{\partial x} + \frac{\partial \tau_{yx}}{\partial y} + \frac{\partial \tau_{zx}}{\partial z} = \rho \frac{\partial^2 u}{\partial t^2} \tag{3.62}$$

Similarly, summing forces on the element in the y and z directions

$$\frac{\partial \sigma_y}{\partial y} + \frac{\partial \tau_{xy}}{\partial x} + \frac{\partial \tau_{zy}}{\partial z} = \rho \frac{\partial^2 \upsilon}{\partial t^2} \tag{3.63}$$

and

$$\frac{\partial \sigma_z}{\partial z} + \frac{\partial \tau_{xz}}{\partial x} + \frac{\partial \tau_{yz}}{\partial y} = \rho \frac{\partial^2 w}{\partial t^2} \tag{3.64}$$

where υ and w are the components of displacement in the y and z directions, respectively.

3.11 EQUATIONS FOR STRESS WAVES

A. Compression Waves

Equations (3.62)–(3.64) give the equations of motion in terms of stresses. Now, considering Eq. (3.62) and noting that $\tau_{xy} = \tau_{yx}$ and $\tau_{xz} = \tau_{zx}$,

$$\rho \frac{\partial^2 u}{\partial t^2} = \frac{\partial \sigma_x}{\partial x} + \frac{\partial \tau_{xy}}{\partial y} + \frac{\partial \tau_{xz}}{\partial z}$$

Substitution of Eqs. (3.16), (3.18), and (3.20) into the preceding equation yields

$$\rho \frac{\partial^2 u}{\partial t^2} = \frac{\partial}{\partial x}(\lambda \bar{\varepsilon} + 2G\varepsilon_x) + \frac{\partial}{\partial y}(G\gamma'_{xy}) + \frac{\partial}{\partial z}(G\gamma'_{xz})$$

Again, substitution of Eqs. (3.7) and (3.9) into the last expression will yield

$$\rho \frac{\partial^2 u}{\partial t^2} = \frac{\partial}{\partial x}(\lambda \bar{\varepsilon} + 2G\varepsilon_x) + G\frac{\partial}{\partial y}\left(\frac{\partial \upsilon}{\partial x} + \frac{\partial u}{\partial y}\right) + G\frac{\partial}{\partial z}\left(\frac{\partial u}{\partial z} + \frac{\partial w}{\partial x}\right)$$

or

$$\rho \frac{\partial^2 u}{\partial t^2} = \lambda \frac{\partial \bar{\varepsilon}}{\partial x} + G\left(\frac{\partial^2 u}{\partial x^2} + \frac{\partial^2 \upsilon}{\partial x \partial y} + \frac{\partial^2 w}{\partial x \partial z} + \frac{\partial^2 u}{\partial x^2} + \frac{\partial^2 u}{\partial y^2} + \frac{\partial^2 u}{\partial z^2}\right) \tag{3.65}$$

But

$$\frac{\partial^2 u}{\partial x^2} + \frac{\partial^2 \upsilon}{\partial x \partial y} + \frac{\partial^2 w}{\partial x \partial z} = \frac{\partial \bar{\varepsilon}}{\partial x} \tag{3.66}$$

Copyright 2017 Cengage Learning. All Rights Reserved. May not be copied, scanned, or duplicated, in whole or in part. Due to electronic rights, some third party content may be suppressed from the eBook and/or eChapter(s). Editorial review has deemed that any suppressed content does not materially affect the overall learning experience. Cengage Learning reserves the right to remove additional content at any time if subsequent rights restrictions require it.

So

$$\rho \frac{\partial^2 u}{\partial t^2} = (\lambda + G)\frac{\partial \bar{\varepsilon}}{\partial x} + G\nabla^2 u \tag{3.67}$$

where

$$\nabla^2 = \frac{\partial^2}{\partial x^2} + \frac{\partial^2}{\partial y^2} + \frac{\partial^2}{\partial z^2} \tag{3.68}$$

Similarly, by proper substitution in Eqs. (3.63) and (3.64), the following relations can be obtained:

$$\rho \frac{\partial^2 v}{\partial t^2} = (\lambda + G)\frac{\partial \bar{\varepsilon}}{\partial y} + G\nabla^2 v \tag{3.69}$$

and

$$\rho \frac{\partial^2 w}{\partial t^2} = (\lambda + G)\frac{\partial \bar{\varepsilon}}{\partial z} + G\nabla^2 w \tag{3.70}$$

Now, differentiating Eqs. (3.67), (3.69), and (3.70) with respect to x, y, and z, respectively, and adding

$$\rho \frac{\partial^2}{\partial t^2}\left(\frac{\partial u}{\partial x} + \frac{\partial v}{\partial y} + \frac{\partial w}{\partial z}\right) = (\lambda + G)\left(\frac{\partial^2 \bar{\varepsilon}}{\partial x^2} + \frac{\partial^2 \bar{\varepsilon}}{\partial y^2} + \frac{\partial^2 \bar{\varepsilon}}{\partial z^2}\right) + G\nabla^2\left(\frac{\partial u}{\partial x} + \frac{\partial v}{\partial y} + \frac{\partial w}{\partial z}\right)$$

or

$$\rho \frac{\partial^2 \bar{\varepsilon}}{\partial t^2} = (\lambda + G)(\nabla^2 \bar{\varepsilon}) + G(\nabla^2 \bar{\varepsilon}) = (\lambda + 2G)\nabla^2 \bar{\varepsilon} \tag{3.71}$$

Therefore,

$$\boxed{\frac{\partial^2 \bar{\varepsilon}}{\partial t^2} = \frac{\lambda + 2G}{\rho}\nabla^2 \bar{\varepsilon} = v_p^2 \nabla^2 \bar{\varepsilon}} \tag{3.72}$$

where

$$\boxed{v_p = \sqrt{\frac{\lambda + 2G}{\rho}}} \tag{3.73}$$

Equation (3.73) is in the same form as the wave equation given in Eq. (3.29). Also note that $\bar{\varepsilon}$ is the volumetric strain and v_p is the *velocity of the dilatational waves.* This is also referred to as the *primary wave*, *P-wave*, or *compression wave*. Also another fact that needs to be pointed out here is that the expression for v_c was

Copyright 2017 Cengage Learning. All Rights Reserved. May not be copied, scanned, or duplicated, in whole or in part. Due to electronic rights, some third party content may be suppressed from the eBook and/or eChapter(s). Editorial review has deemed that any suppressed content does not materially affect the overall learning experience. Cengage Learning reserves the right to remove additional content at any time if subsequent rights restrictions require it.

given as $v_c = \sqrt{E/\rho}$. Comparing the expressions for v_c and v_p, one can see that the velocity of compression waves is faster than v_c.

B. Distortional Waves or Shear Waves

Differentiating Eq. (3.69) with respect to z and Eq. (3.70) with respect to y,

$$\rho \frac{\partial^2}{\partial t^2}\left(\frac{\partial v}{\partial z}\right) = (\lambda + G)\frac{\partial^2 \bar{\varepsilon}}{(\partial y)(\partial z)} + G\nabla^2 \frac{\partial v}{\partial z} \tag{3.74}$$

and

$$\rho \frac{\partial^2}{\partial t^2}\left(\frac{\partial w}{\partial y}\right) = (\lambda + G)\frac{\partial^2 \bar{\varepsilon}}{(\partial y)(\partial z)} + G\nabla^2 \frac{\partial w}{\partial y} \tag{3.75}$$

Subtracting Eq. (3.74) from (3.75) yields

$$\rho \frac{\partial}{\partial t^2}\left(\frac{\partial w}{\partial y} - \frac{\partial v}{\partial z}\right) = G\nabla^2\left(\frac{\partial w}{\partial y} - \frac{\partial v}{\partial z}\right)$$

However, $\partial w/\partial y - \partial v/\partial z = 2\bar{\omega}_x$ [Eq. (3.10)]; thus,

$$\rho \frac{\partial^2 \bar{\omega}_x}{\partial t^2} = G\nabla^2 \bar{\omega}_x \tag{3.76}$$

or

$$\boxed{\frac{\partial^2 \bar{\omega}_x}{\partial t^2} = \frac{G}{\rho}\nabla^2 \bar{\omega}_x = v_s^2 \nabla^2 \bar{\omega}_x} \tag{3.77}$$

where $v_s = \sqrt{G/\rho}$.

Equation (3.77) represents the equation for distortional waves and the *velocity* of propagation is v_s.This is also referred to as the *shear wave*, or *S-wave*. Comparison of the shear wave velocity given above with that in a rod [Eq. (3.40)] shows that they are the same. Using the process of similar manipulation, one can also obtain two more equations similar to Eq. (3.77):

$$\boxed{\frac{\partial^2 \bar{\omega}_y}{\partial t^2} = v_s^2 \nabla^2 \bar{\omega}_y} \tag{3.78}$$

and

$$\boxed{\frac{\partial^2 \bar{\omega}_z}{\partial t^2} = v_s^2 \nabla^2 \bar{\omega}_z} \tag{3.79}$$

Copyright 2017 Cengage Learning. All Rights Reserved. May not be copied, scanned, or duplicated, in whole or in part. Due to electronic rights, some third party content may be suppressed from the eBook and/or eChapter(s). Editorial review has deemed that any suppressed content does not materially affect the overall learning experience. Cengage Learning reserves the right to remove additional content at any time if subsequent rights restrictions require it.

3.12 GENERAL COMMENTS

Based on the derivations for the velocities of comparison waves and shear waves as derived in the preceding section, the following general observations can be made.

1. There are two types of stress waves that can propagate through an infinite elastic medium; however, they travel at different velocities.
2. From Eq. (3.73),

$$v_p = \sqrt{\frac{\lambda + 2G}{\rho}}$$

However,

$$\lambda = \frac{\mu E}{(1+\mu)(1-\mu)}$$

and

$$G = \frac{E}{2(1+\mu)}$$

Substitution of the preceding two relationships into the expression of v_p yields

$$v_p = \sqrt{\frac{E(1-\mu)}{\rho(1+\mu)(1-2\mu)}} \tag{3.80}$$

Similarly,

$$v_s = \sqrt{\frac{G}{\rho}} = \sqrt{\frac{E}{2(1+\mu)\rho}} \tag{3.81}$$

Combining Eqs. (3.80) and (3.81),

$$\frac{v_p}{v_s} = \sqrt{\frac{2(1-\mu)}{(1-2\mu)}} \tag{3.82}$$

Figure 3.12 shows a plot of v_p/v_s versus μ based on Eq. (3.82). It can be seen from the plot that for all values of μ, v_p/v_s are greater than 1.

3. Table 3.1 gives some typical values of v_p and v_s encountered through various types of soils and rocks. Techniques for field determination of the velocities of compression waves and shear waves traveling through various soil media are described in Chapter 4.
4. The more rigid the materials, the higher the shear and compressional wave velocities.
5. If μ is 0.5, the velocity of compressional wave becomes unbounded.

Copyright 2017 Cengage Learning. All Rights Reserved. May not be copied, scanned, or duplicated, in whole or in part. Due to electronic rights, some third party content may be suppressed from the eBook and/or eChapter(s). Editorial review has deemed that any suppressed content does not materially affect the overall learning experience. Cengage Learning reserves the right to remove additional content at any time if subsequent rights restrictions require it.

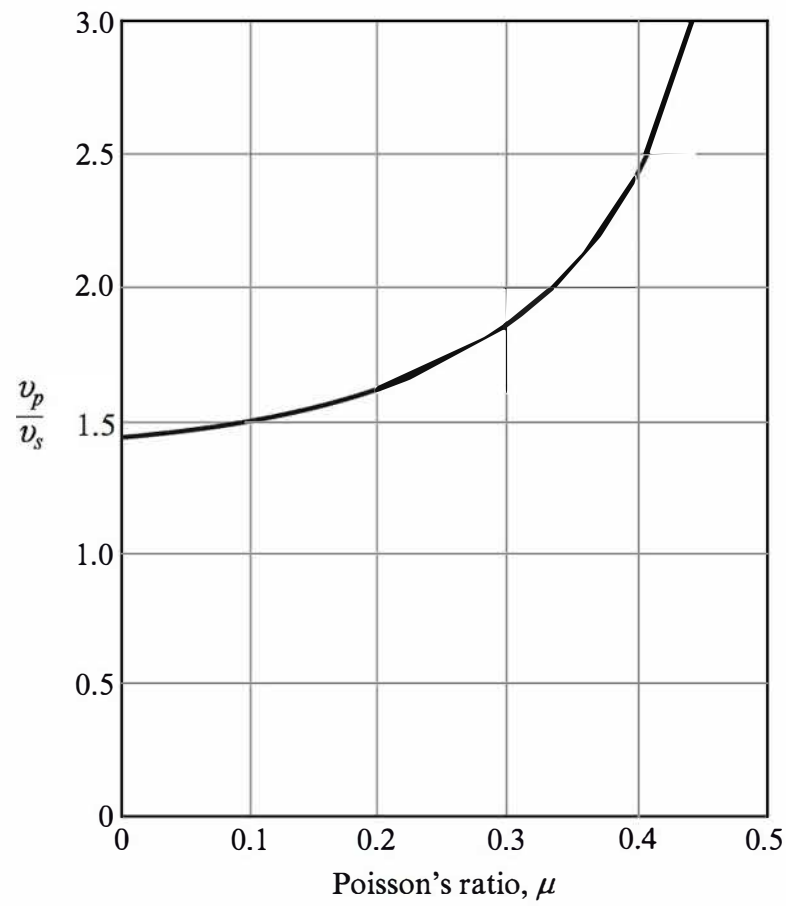

Figure 3.12 Variation of v_p/v_s with μ [Eq. (3.82)]

Wave propagation through saturated soils involves the soil skeleton and water in the void spaces. A comprehensive theoretical study of this problem is given by Biot (1956). This study shows that there are two compressive waves and one shear wave through the saturated medium. Some investigators have referred to the two compressive waves as the fluid wave (transmitted through the fluid) and the frame wave (transmitted through the soil structure), although there is coupled motion of the fluid and the frame waves. As far as the shear wave is concerned, the pore water has no rigidity to shear. Hence, the shear wave in the soil is dependent only on the properties of the soil skeleton.

Figure 3.13 shows the theoretical variation of the *compressive frame wave* velocities in dry and saturated sands, based on Biot's theory, using the values of the constants representative for a quartz sand (Hardin and Richart, 1963). Along with

Table 3.1 Typical values of v_p and v_s

Soil type	Compressive wave velocity, v_p (m/s)	Shear wave velocity, v_s (m/s)
Fine sand	300	90 – 150
Dense sand	460	230
Gravel	762	180 – 215
Moist clay	1220 – 1370	150
Granite	3960 – 5490	2130 – 3350
Sandstone	1370 – 3960	610 – 2130

Copyright 2017 Cengage Learning. All Rights Reserved. May not be copied, scanned, or duplicated, in whole or in part. Due to electronic rights, some third party content may be suppressed from the eBook and/or eChapter(s). Editorial review has deemed that any suppressed content does not materially affect the overall learning experience. Cengage Learning reserves the right to remove additional content at any time if subsequent rights restrictions require it.

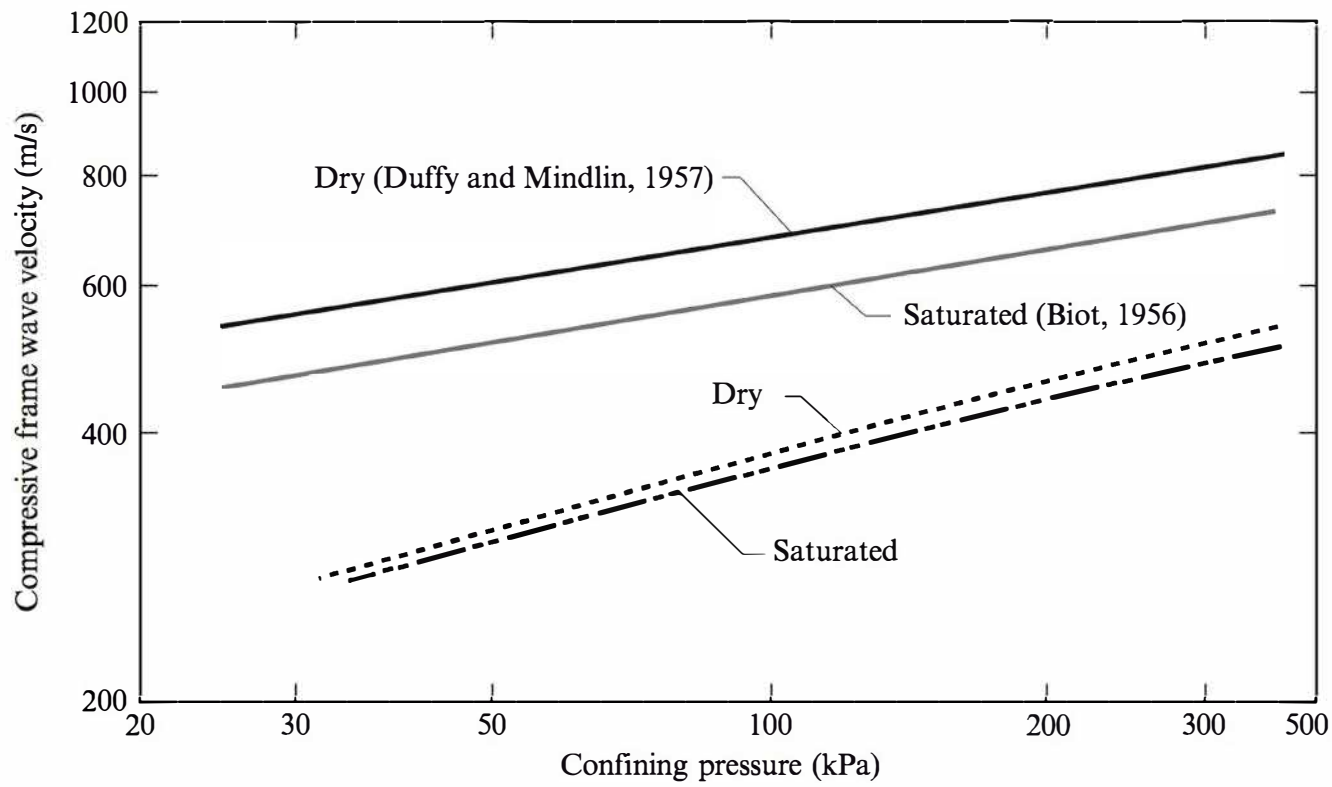

Figure 3.13 Comparison of experimental and theoretical results for compressive frame wave velocities in dry and saturated Ottawa sand (after Hardin and Richart, 1963)

Source: Hardin, B. O., and Richard, F. E., Jr. (1963). "Elastic Wave Velocity in Granular Soils," *Journal of the Soil Mechanics and Foundations Division,* ASCE, Vol. 89, No. SM1, pp. 33–65. With permission from ASCE.

that, for comparison purposes, are shown the experimental *longitudinal wave* velocities [v_c from Eq. (3.30)] for dry and saturated Ottawa sands. For a given confining pressure, the difference of wave velocities between dry and saturated specimens is negligible and may be accounted for by the difference in the unit weight of the soil.

The velocity of compression waves (v_w) through water can be expressed as

$$v_w = \sqrt{\frac{B_w}{\rho_w}} \tag{3.83}$$

where B_w is the bulk modulus of water and ρ_w is the density of water. Usually the value of v_w is of the order of 1463 m/s.

Figure 3.14 shows the variation of the experimental shear wave velocity for dry, drained, and saturated Ottawa sand. It may be noted that for a given confining pressure, the range of variation of v_s is very small.

The velocity equations lead to the following generalizations: (i) for the same material, shear waves will always travel slower than compression waves (ii) the more rigid the material, the higher the shear and compression wave velocities and (iii) shear waves cannot propagate through liquids as the shear modulus of liquids is zero. As a rough approximation, compression or primary wave velocity is about 60% more than shear wave velocity in soils.

Copyright 2017 Cengage Learning. All Rights Reserved. May not be copied, scanned, or duplicated, in whole or in part. Due to electronic rights, some third party content may be suppressed from the eBook and/or eChapter(s). Editorial review has deemed that any suppressed content does not materially affect the overall learning experience. Cengage Learning reserves the right to remove additional content at any time if subsequent rights restrictions require it.

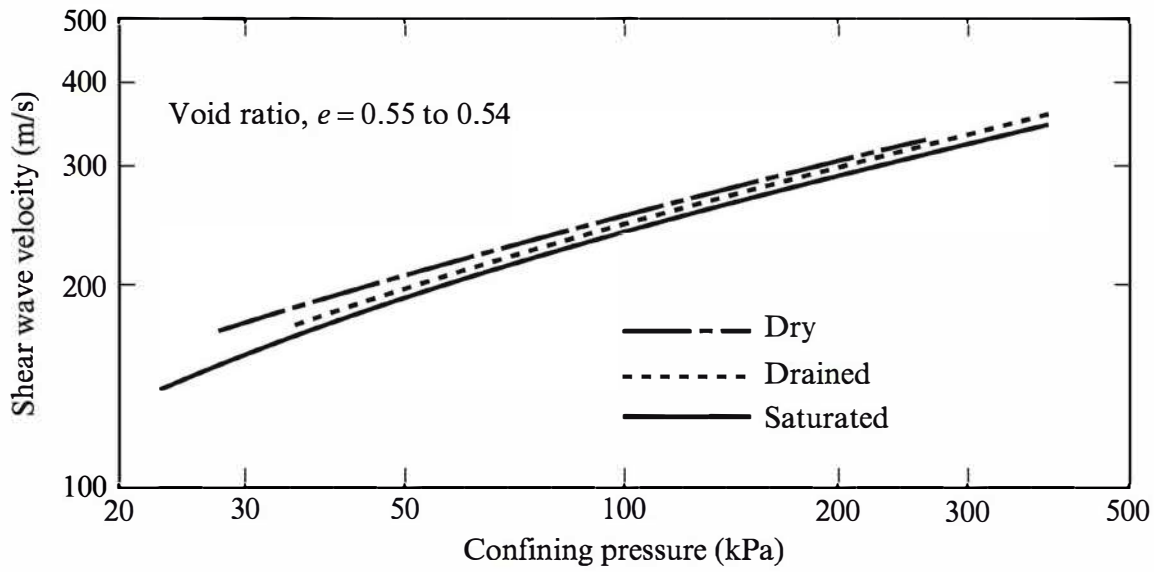

Figure 3.14 Variation of shear wave velocity with confining pressure for Ottawa sand (after Hardin and Richart, 1963)

Source: Hardin, B. O., and Richard, F. E., Jr. (1963). "Elastic Wave Velocity in Granular Soils," *Journal of the Soil Mechanics and Foundations Division,* ASCE, Vol. 89, No. SM1, pp. 33–65. With permission from ASCE.

Stress Waves in Elastic Half-Space

3.13 RAYLEIGH WAVES

Equations derived in Section 3.11 are for stress waves in the body of an infinite, elastic, and isotropic medium. Another type of wave, called a *Rayleigh wave*, also exists near the boundary of an elastic half-space. This type of wave was first investigated by Lord Rayleigh (1885). In order to study this, consider a plane wave through an elastic medium with a plane boundary as shown in Figure 3.15. Note that the plane $x - y$ is the boundary of the elastic half-space and z is positive downward. Let u and w represent the displacements in the directions x and z, respectively, and be independent of y. Therefore,

$$u = \frac{\partial \phi}{\partial x} + \frac{\partial \psi}{\partial z} \tag{3.84}$$

and

$$w = \frac{\partial \phi}{\partial z} - \frac{\partial \psi}{\partial x} \tag{3.85}$$

where ϕ and ψ are two potential functions. The dilation $\bar{\varepsilon}$ can be defined as

$$\begin{aligned} \bar{\varepsilon} &= \varepsilon_x + \varepsilon_y + \varepsilon_z = \frac{\partial u}{\partial x} + \frac{\partial v}{\partial y} + \frac{\partial w}{\partial z} \\ &= \left(\frac{\partial^2 \phi}{\partial x^2} + \frac{\partial^2 \psi}{\partial x \partial z}\right) + (0) + \left(\frac{\partial^2 \phi}{\partial z^2} - \frac{\partial^2 \psi}{\partial x \partial z}\right) = \frac{\partial^2 \phi}{\partial x^2} + \frac{\partial^2 \phi}{\partial z^2} = \nabla^2 \phi \end{aligned} \tag{3.86}$$

Copyright 2017 Cengage Learning. All Rights Reserved. May not be copied, scanned, or duplicated, in whole or in part. Due to electronic rights, some third party content may be suppressed from the eBook and/or eChapter(s). Editorial review has deemed that any suppressed content does not materially affect the overall learning experience. Cengage Learning reserves the right to remove additional content at any time if subsequent rights restrictions require it.

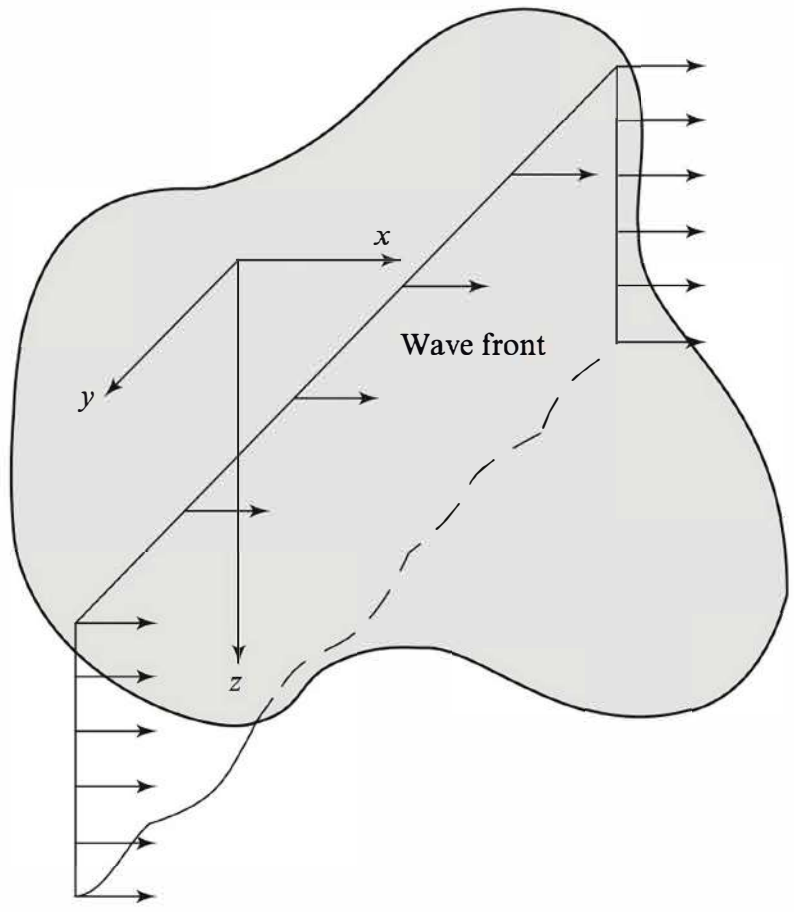

Figure 3.15 Plane wave through an elastic medium with a plane boundary

Similarly, the rotation in the $x-z$ plane can be given by

$$2\bar{\omega}_y = \frac{\partial u}{\partial z} - \frac{\partial w}{\partial x} = \frac{\partial^2 \psi}{\partial x^2} + \frac{\partial^2 \psi}{\partial z^2} = \nabla^2 \psi \tag{3.87}$$

Substituting Eqs. (3.84) and (3.86) into Eq. (3.67) yields

$$\rho \frac{\partial^2}{\partial t^2}\left(\frac{\partial \phi}{\partial x} + \frac{\partial \psi}{\partial z}\right) = (\lambda + G)\frac{\partial}{\partial x}(\nabla^2 \phi) + G\nabla^2\left(\frac{\partial \phi}{\partial x} + \frac{\partial \psi}{\partial z}\right)$$

or

$$\rho \frac{\partial}{\partial x}\left(\frac{\partial^2 \phi}{\partial t^2}\right) + \rho \frac{\partial}{\partial z}\left(\frac{\partial^2 \psi}{\partial t^2}\right) = (\lambda + 2G)\frac{\partial}{\partial x}(\nabla^2 \phi) + G\frac{\partial}{\partial z}(\nabla^2 \psi) \tag{3.88}$$

In a similar manner, substituting Eqs. (3.85) and (3.86) into Eqs. (3.70), we get

$$\rho \frac{\partial}{\partial z}\left(\frac{\partial^2 \phi}{\partial t^2}\right) - \rho \frac{\partial}{\partial x}\left(\frac{\partial^2 \psi}{\partial t^2}\right) = (\lambda + 2G)\frac{\partial}{\partial z}(\nabla^2 \phi) - G\frac{\partial}{\partial z}(\nabla^2 \psi) \tag{3.89}$$

Equations (3.88) and (3.89) will be satisfied if

(1) $$\rho(\partial^2 \phi / \partial t^2) = (\lambda + 2G)\nabla^2 \phi$$

Copyright 2017 Cengage Learning. All Rights Reserved. May not be copied, scanned, or duplicated, in whole or in part. Due to electronic rights, some third party content may be suppressed from the eBook and/or eChapter(s). Editorial review has deemed that any suppressed content does not materially affect the overall learning experience. Cengage Learning reserves the right to remove additional content at any time if subsequent rights restrictions require it.

or

$$\frac{\partial^2 \phi}{\partial t^2} = \left(\frac{\lambda + 2G}{\rho}\right)\nabla^2\phi = \upsilon_p^2 \nabla^2 \phi \tag{3.90}$$

and (2)

$$\rho(\partial^2 \psi / \partial t^2) = G\nabla^2 \psi$$

$$\frac{\partial^2 \psi}{\partial t^2} = \left(\frac{G}{\rho}\right)\nabla^2\psi = \upsilon_s^2 \nabla^2 \psi \tag{3.91}$$

Now, consider a sinusoidal wave traveling in the positive x direction. Let the solution of ϕ and ψ be expressed as

$$\phi = F(z)\exp[i(\omega t - fx)] \tag{3.92}$$

and

$$\psi = G(z)\exp[i(\omega t - fx)] \tag{3.93}$$

where $F(z)$ and $G(z)$ are functions of depth

$$f = \frac{2\pi}{\text{wavelength}} \tag{3.94}$$

$$i = \sqrt{-1} \tag{3.95}$$

Substituting Eq. (3.92) into Eq. (3.90), we get

$$\left(\frac{\partial^2}{\partial t^2}\right)\{F(z)\exp[i(\omega t - fx)]\} = \upsilon_p^2 \nabla^2 \{F(z)\exp[i(\omega t - fx)]\}$$

or

$$-\omega^2 F(z) = \upsilon_p^2[F''(z) - f^2 F(z)] \tag{3.96}$$

Similarly, substituting Eq. (3.93) into Eq. (3.91) results in

$$-\omega^2 G(z) = \upsilon_s^2[G''(z) - f^2 G(z)] \tag{3.97}$$

where

$$F''(z) = \frac{\partial^2 F(z)}{\partial z^2} \tag{3.98}$$

$$G''(z) = \frac{\partial^2 G(z)}{\partial z^2} \tag{3.99}$$

Copyright 2017 Cengage Learning. All Rights Reserved. May not be copied, scanned, or duplicated, in whole or in part. Due to electronic rights, some third party content may be suppressed from the eBook and/or eChapter(s). Editorial review has deemed that any suppressed content does not materially affect the overall learning experience. Cengage Learning reserves the right to remove additional content at any time if subsequent rights restrictions require it.

Equations (3.96) and (3.97) can be rearranged to the form

$$F''(z) - q^2 F(z) = 0 \tag{3.100}$$

and

$$G''(z) - s^2 G(z) = 0 \tag{3.101}$$

where

$$q^2 = f^2 - \frac{\omega^2}{v_p^2} \tag{3.102}$$

$$s^2 = f^2 - \frac{\omega^2}{v_s^2} \tag{3.103}$$

Solutions to Eqs. (3.100) and (3.101) can be given as

$$F(z) = A_1 e^{-qz} + A_2 e^{qz} \tag{3.104}$$

and

$$G(z) = B_1 e^{-sz} + B_2 e^{sz} \tag{3.105}$$

where A_1, A_2, B_1, and B_2 are constants.

From Eqs. (3.104) and (3.105), it can be seen that A_2 and B_2 must equal zero; otherwise $F(z)$ and $G(z)$ will approach infinity with depth, which is not the type of wave that is considered here. With A_2 and B_2 equal zero,

$$F(z) = A_1 e^{-qz} \tag{3.106}$$

$$G(z) = B_1 e^{-sz} \tag{3.107}$$

Combining Eqs. (3.92) and (3.106) and Eqs. (3.93) and (3.107),

$$\phi = (A_1 e^{-qz})[e^{i(\omega t - fx)}] \tag{3.108}$$

or

$$\psi = (B_1 e^{-sz})[e^{i(\omega t - fx)}] \tag{3.109}$$

The boundary conditions for the two preceding equations are at $z = 0$, $\sigma_z = 0$, $\tau_{zx} = 0$, and $\tau_{zy} = 0$. From Eq. (3.22),

$$\sigma_{z(z=0)} = \lambda\bar{\varepsilon} + 2G\varepsilon_z = \lambda\bar{\varepsilon} + 2G\left(\frac{\partial w}{\partial z}\right) = 0 \tag{3.110}$$

Combining Eqs. (3.85), (3.86), and (3.108)–(3.110), one obtains

$$A_1[(\lambda + 2G)q^2 - \lambda f^2] - 2iB_1 Gfs = 0 \tag{3.111}$$

Copyright 2017 Cengage Learning. All Rights Reserved. May not be copied, scanned, or duplicated, in whole or in part. Due to electronic rights, some third party content may be suppressed from the eBook and/or eChapter(s). Editorial review has deemed that any suppressed content does not materially affect the overall learning experience. Cengage Learning reserves the right to remove additional content at any time if subsequent rights restrictions require it.

or

$$\frac{A_1}{B_1} = \frac{2iGfs}{(\lambda + 2G)q^2 - \lambda f^2} \tag{3.112}$$

Similarly,

$$\tau_{zx(z=0)} = G\gamma_{zx} = G\left(\frac{\partial w}{\partial x} + \frac{\partial u}{\partial z}\right) = 0 \tag{3.113}$$

Again, combining Eqs. (3.84), (3.85), (3.108), (3.109), and (3.113),

$$2iA_1 fq + (s^2 + f^2)\, B_1 = 0$$

or

$$\frac{A_1}{B_1} = -\frac{(s^2 + f^2)}{2ifq} \tag{3.114}$$

Equating the right-hand sides of Eqs. (3.112) and (3.114),

$$\frac{2iGfs}{(\lambda + 2G)q^2 - \lambda f^2} = \frac{(s^2 + f^2)}{2ifq}$$

$$4Gf^2 sq = (s^2 + f^2)\,[(\lambda + 2G)q^2 - \lambda f^2]$$

or

$$16G^2 f^4 s^2 q^2 = (s^2 + f^2)^2\,[\lambda + 2G]q^2 - \lambda f^2]^2 \tag{3.115}$$

Substituting for q and s and then dividing both sides of Eq. (3.115) by $G^2 f^8$, we get

$$16\left(1 - \frac{\omega^2}{v_p^2 f^2}\right)\left(1 - \frac{\omega^2}{v_s^2 f^2}\right) = \left[2 - \left(\frac{\lambda + 2G}{G}\right)\frac{\omega^2}{v_p^2 f^2}\right]^2 \left(2 - \frac{\omega^2}{v_s^2 f^2}\right)^2 \tag{3.116}$$

From Eq. (3.94)

$$\text{Wavelength} = \frac{2\pi}{f} \tag{3.117}$$

However,

$$\text{Wavelength} = \frac{\text{velocity of wave}}{(\omega/2\pi)} = \frac{v_r}{(\omega/2\pi)} \tag{3.118}$$

where v_r is the *Rayleigh* wave velocity. Thus, from Eqs. (3.117) and (3.118), $2\pi/f = 2\pi v_r/\omega$, or

$$f = \frac{\omega}{v_r} \tag{3.119}$$

Copyright 2017 Cengage Learning. All Rights Reserved. May not be copied, scanned, or duplicated, in whole or in part. Due to electronic rights, some third party content may be suppressed from the eBook and/or eChapter(s). Editorial review has deemed that any suppressed content does not materially affect the overall learning experience. Cengage Learning reserves the right to remove additional content at any time if subsequent rights restrictions require it.

So,

$$\frac{\omega^2}{v_p^2 f^2} = \frac{\omega^2}{v_p^2(\omega^2/v_r^2)} = \frac{v_r^2}{v_p^2} = \alpha^2 V^2 \tag{3.120}$$

Similarly,

$$\frac{\omega^2}{v_s^2 f^2} = \frac{\omega^2}{v_s^2(\omega^2/v_r^2)} = \frac{v_r^2}{v_s^2} = V^2 \tag{3.121}$$

where

$$\alpha^2 = \frac{v_s^2}{v_p^2} \tag{3.122}$$

However, $v_p^2 = (\lambda + 2G)/\rho$ and $v_s^2 = G/\rho$. Thus

$$\alpha^2 = \frac{v_s^2}{v_p^2} = \frac{G}{\lambda + 2G} \tag{3.123}$$

Table 3.2 Values of V [Eq. (3.126)]

μ	$V = v_r/v_s$
0.25	0.919
0.29	0.926
0.33	0.933
0.4	0.943
0.5	0.955

The term α^2 can also be expressed in terms of Poisson's ratio. From the relations given in Eq. (3.25),

$$\lambda = \frac{2\mu G}{1 - 2\mu} \tag{3.124}$$

Substitution of this relation in Eq. (3.123) yields

$$\alpha^2 = \frac{G}{[2\mu G/(1-2\mu)] + 2G} = \frac{(1-2\mu)G}{2\mu G + 2G - 4\mu G} = \frac{(1-2\mu)}{(2-2\mu)} \tag{3.125}$$

Again, substituting Eqs. (3.120), (3.121), and (3.123) into Eq. (3.116),

$$16(1 - \alpha^2 V^2)(1 - V^2) = (2 - V^2)(2 - V^2)^2$$

Copyright 2017 Cengage Learning. All Rights Reserved. May not be copied, scanned, or duplicated, in whole or in part. Due to electronic rights, some third party content may be suppressed from the eBook and/or eChapter(s). Editorial review has deemed that any suppressed content does not materially affect the overall learning experience. Cengage Learning reserves the right to remove additional content at any time if subsequent rights restrictions require it.

or

$$\boxed{V^6 - 8V^4 - (16\alpha^2 - 24)V^2 - 16(1-\alpha^2) = 0} \tag{3.126}$$

Equation (3.126) is a cubic equation in V^2. For a given value of Poisson's ratio, the proper value of V^2 can be found and, hence, so can the value of v_r in terms of v_p or v_s. An example of this is shown in Example 3.1. Table 3.2 gives some values of $v_r/v_s\,(=V)$ for various values of Poisson's ratio.

3.14 DISPLACEMENT OF RAYLEIGH WAVES

From Eqs. (3.84) and (3.85),

$$u = \frac{\partial\phi}{\partial x} + \frac{\partial\psi}{\partial z} \tag{3.84}$$

and

$$w = \frac{\partial\phi}{\partial z} - \frac{\partial\psi}{\partial x} \tag{3.85}$$

Substituting the relations developed for ϕ and ψ [Eqs. (3.108), (3.109)] in these equations, one obtains

$$u = -(if\ A_1 e^{-qz} + B_1 s e^{-sz})[e^{i(\omega t - fx)}] \tag{3.127}$$

$$w = -(A_1 q e^{-qz} - B_1 i f e^{-sz})[e^{i(\omega t - fx)}] \tag{3.128}$$

However, from Eq. (3.114), $B_1 = -2iA_1 fq/(s^2 + f^2)$. Substituting this relation in Eqs. (3.127) and (3.128) gives

$$u = A_1 fi\left(-e^{-qz} + \frac{2qs}{s^2 + f^2}e^{-sz}\right)[e^{i(\omega t - fx)}] \tag{3.129}$$

and

$$w = A_1 q\left(-e^{-qz} + \frac{2f^2}{s^2 + f^2}e^{-sz}\right)[e^{i(\omega t - fx)}] \tag{3.130}$$

From the preceding two equations, it is obvious that the rate of attenuation of the displacement along the x direction with depth z will depend on the factor U, where

$$\boxed{U = -e^{-qz} + \frac{2qs}{s^2 + f^2}e^{-sz} = -e^{-(q/f)(fz)} + \left[\frac{2(q/f)(s/f)}{(s^2/f^2) + 1}\right]e^{-(s/f)(fz)}} \tag{3.131}$$

Copyright 2017 Cengage Learning. All Rights Reserved. May not be copied, scanned, or duplicated, in whole or in part. Due to electronic rights, some third party content may be suppressed from the eBook and/or eChapter(s). Editorial review has deemed that any suppressed content does not materially affect the overall learning experience. Cengage Learning reserves the right to remove additional content at any time if subsequent rights restrictions require it.

Similarly, the rate of attenuation of the displacement along the z direction with depth will depend on factor W, where

$$\boxed{W = -e^{-qz} + \frac{2f^2}{s^2 + f^2} e^{-sz} = -e^{-(q/f)(fz)} + \frac{2}{\left(s^2/f^2\right)+1} e^{-(s/f)(fz)}} \tag{3.132}$$

However,

$$q^2 = f^2 - \frac{\omega^2}{v_p^2} \tag{3.102}$$

or

$$\frac{q^2}{f^2} = 1 - \frac{\omega^2}{f^2 v_p^2} = 1 - \frac{v_r^2}{v_p^2} = 1 - \alpha^2 V^2 \tag{3.133}$$

Also,

$$s^2 = f^2 - \frac{\omega^2}{v_s^2} \tag{3.103}$$

$$\frac{s^2}{f^2} = 1 - \frac{\omega^2}{f^2 v_s^2} = 1 - \frac{v_r^2}{v_s^2} = 1 - V^2 \tag{3.134}$$

If the Poisson's ratio is known, one can determine the value of V from Eq. (3.126). Substituting the previously determined values of V in Eqs. (3.133) and (3.134), q/f and s/f can be determined; hence, U and W are determinable as functions of z and f. From Example 3.1, it can be seen that for $\mu = 0.25$, $V = 0.9194$. Thus,

$$\frac{q^2}{f^2} = 1 - \alpha^2 V^2 = 1 - \left(\frac{1-2\mu}{2-2\mu}\right) V^2 = 1 - \left(\frac{1-0.5}{2-0.5}\right)(0.9194)^2 = 0.7182$$

or

$$\frac{q}{f} = 0.8475$$

$$\frac{s^2}{f^2} = 1 - V^2 = 1 - (0.9194)^2 = 0.1547$$

or

$$\frac{s}{f} = 0.3933$$

Copyright 2017 Cengage Learning. All Rights Reserved. May not be copied, scanned, or duplicated, in whole or in part. Due to electronic rights, some third party content may be suppressed from the eBook and/or eChapter(s). Editorial review has deemed that any suppressed content does not materially affect the overall learning experience. Cengage Learning reserves the right to remove additional content at any time if subsequent rights restrictions require it.

Substituting these values of q/f and s/f into Eqs. (3.131) and (3.132),

$$U_{(\mu=0.25)} = -\exp(-0.8475fz) + 0.5773\exp(-0.3933fz) \tag{3.135}$$

$$W_{(\mu=0.25)} = -\exp(-0.8475fz) + 1.7321\exp(-0.3933fz) \tag{3.136}$$

Based on Eqs. (3.135) and (3.136), the following observations can be made:

1. The magnitude of U decreases rapidly with increasing value of fz. At $fz = 1.21$, U becomes equal to zero; so, at $z = 1.21/f$, there is no motion parallel to the surface. It has been shown in Eq. (3.94) that $f = 2\pi/(z)$. Thus, at $z = 1.21/f = 1.21(\text{wave length})/2\pi = 0.1926(\text{wave length})$, the value of U is zero. At greater depths, U becomes finite; however, it is of the opposite sign, so the vibration takes place in opposite phase.
2. The magnitude of W first increases with fz, reaches a maximum value at $z = 0.076(\text{wave length})$ (i.e., $fz = 0.4775$), and then decreases with depth.

Figure 3.16 shows a nondimensional plot of the variation of amplitude of vertical and horizontal components of Rayleigh waves with depth for $\mu = 0.25$. Equations (3.135) and (3.136) show that the path of a particle in the medium is an *ellipse* with its *major axis normal to the surface*.

3.15 ATTENUATION OF THE AMPLITUDE OF ELASTIC WAVES WITH DISTANCE

If an impulse of short duration is created at the surface of an elastic half-space, the body waves travel into the medium with hemispherical wave fronts, as shown in Figure 3.17. The *Rayleigh waves* will propagate radially outward along a *cylindrical wave front*. At some distance from the point of disturbance, the displacement of the ground will be of the nature shown in Figure 3.18. Since P-waves are the fastest, they will arrive first, followed by S-waves and then the Rayleigh waves. As may be seen from Figure 3.18, the ground displacement due to the Rayleigh wave arrival is much greater than that for P- and S-waves. The amplitude of disturbance gradually decreases with distance.

Referring to Figure 3.18a and b, it can be seen that the particle motion due to Rayleigh waves starting at ① can be combined to give the lines of the surface particle motion as shown in Figure 3.18c. The part of the motion is a *retrograde ellipse*.

When *body waves* spread out along a hemispherical wave front, the energy is distributed over an area that increases with the square of the radius:

$$E' \propto \frac{1}{r^2} \tag{3.137}$$

Copyright 2017 Cengage Learning. All Rights Reserved. May not be copied, scanned, or duplicated, in whole or in part. Due to electronic rights, some third party content may be suppressed from the eBook and/or eChapter(s). Editorial review has deemed that any suppressed content does not materially affect the overall learning experience. Cengage Learning reserves the right to remove additional content at any time if subsequent rights restrictions require it.

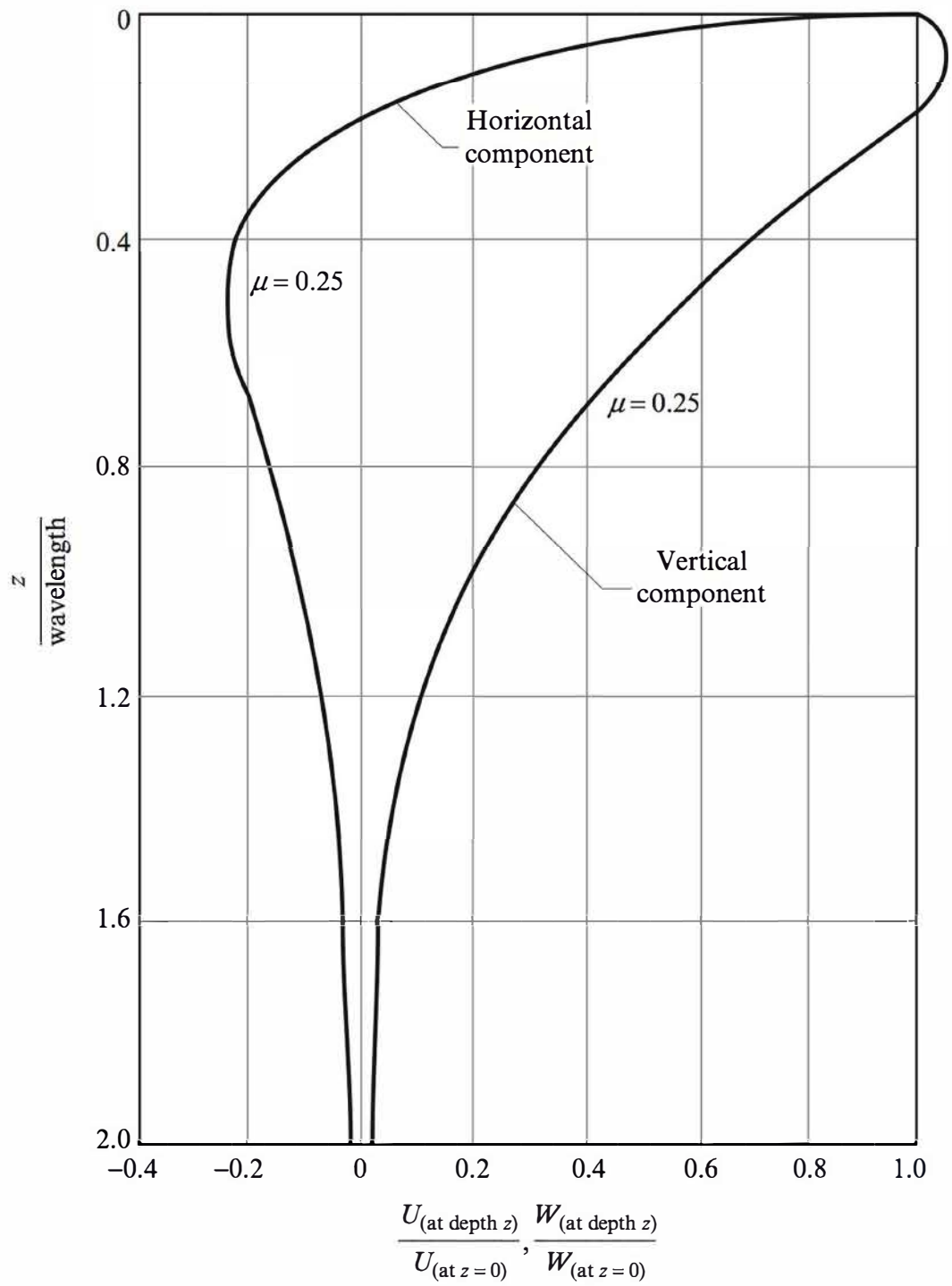

Figure 3.16 Variation of the amplitude of vibration of the horizontal and vertical components of Rayleigh waves with depth ($\mu = 0.25$)

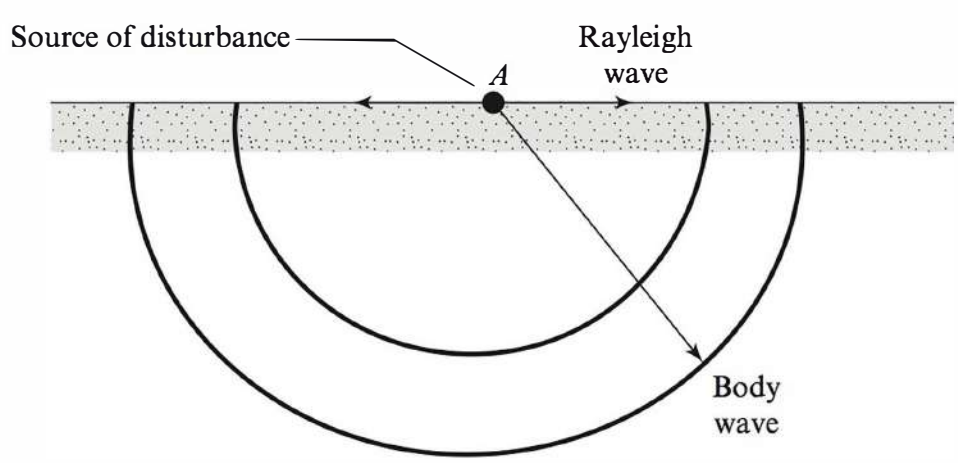

Figure 3.17 Propagation of body waves and Rayleigh waves

Copyright 2017 Cengage Learning. All Rights Reserved. May not be copied, scanned, or duplicated, in whole or in part. Due to electronic rights, some third party content may be suppressed from the eBook and/or eChapter(s). Editorial review has deemed that any suppressed content does not materially affect the overall learning experience. Cengage Learning reserves the right to remove additional content at any time if subsequent rights restrictions require it.

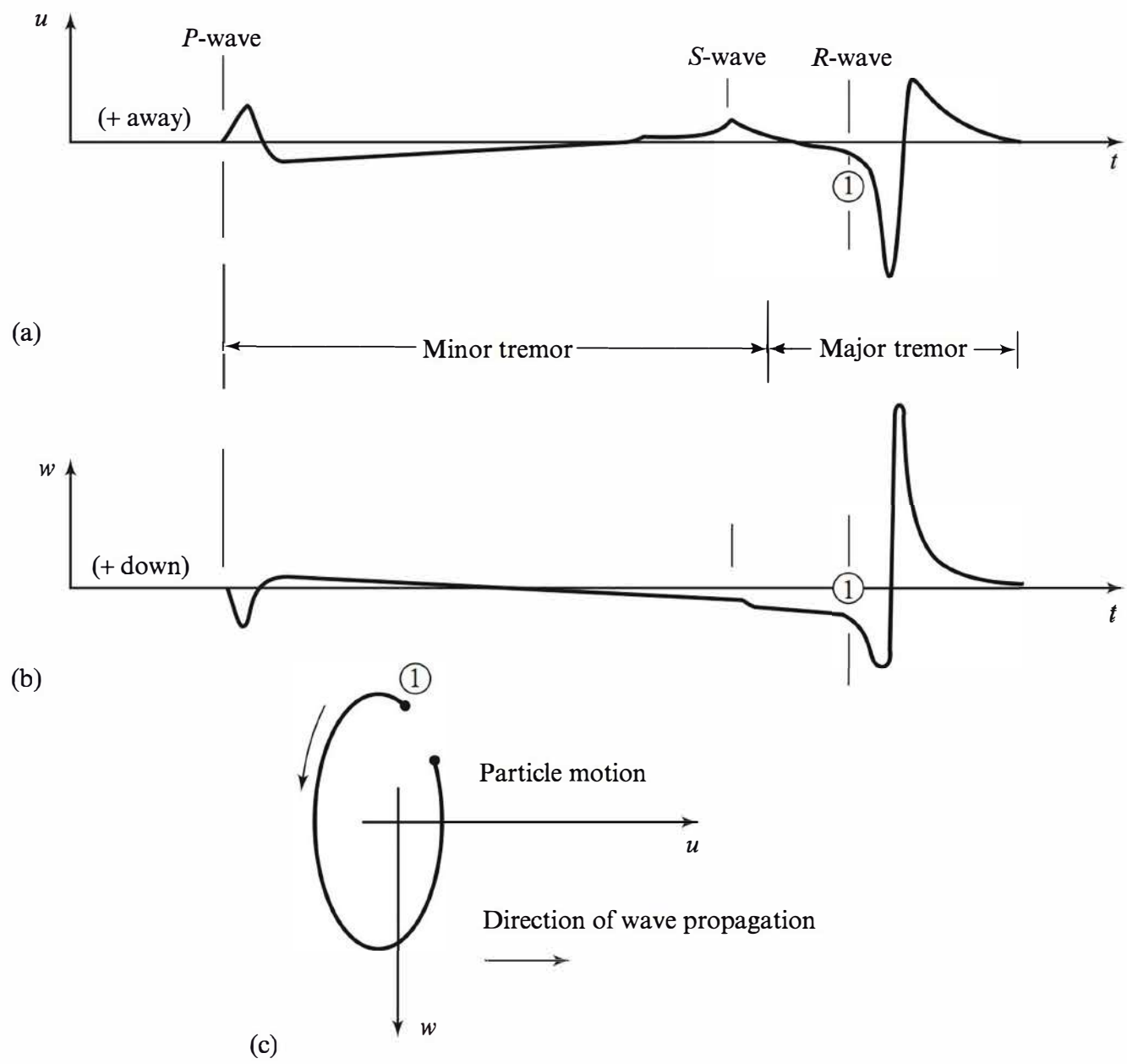

Figure 3.18 Wave systems from surface point source in ideal medium (after Richart, Hall, and Woods, 1970)

Source: RICHART & HALL, VIBRATIONS OF SOILS & FOUNDATIONS, 1st,©1970. Printed and Electronically reproduced by permission of Pearson Education, Inc., NEW YORK, NEW YORK.

where E' is the energy per unit area and r is the radius. However, the amplitude is proportional to the square root of the energy per unit area:

$$\text{Amplitude} \propto \sqrt{E'} \propto \sqrt{\frac{1}{r^2}}$$

or

$$\text{Amplitude} \propto \frac{1}{r} \tag{3.138}$$

Along the surface of the half-space only, the amplitude of the body waves is proportional to $1/r^2$.

Copyright 2017 Cengage Learning. All Rights Reserved. May not be copied, scanned, or duplicated, in whole or in part. Due to electronic rights, some third party content may be suppressed from the eBook and/or eChapter(s). Editorial review has deemed that any suppressed content does not materially affect the overall learning experience. Cengage Learning reserves the right to remove additional content at any time if subsequent rights restrictions require it.

Similarly, the amplitude of the Rayleigh waves, which spread out in a *cylindrical* wave front, is proportional to $1/\sqrt{r}$. Thus the attention of the amplitude of the *Rayleigh* waves is *slower* than that for the body waves.

The loss of the amplitude of waves due to spreading out is called *geometrical damping*. In addition to the above damping, there is another type of loss—that from *absorption* in real earth material. This is called *material damping*. Thus, accounting for both types of damping, the vertical amplitude of Rayleigh waves can be given by the relation

$$\bar{w}_n = \bar{w}_1 \sqrt{\frac{r_1}{r_n}} \exp[-\beta(r_n - r_1)] \tag{3.139}$$

where $\bar{w}_n$ and $\bar{w}_1$ are vertical amplitudes at distance r_n and r_1, and β is the absorption coefficient.

Equation (3.139) is given by Bornitz (1931). (See also Hall and Richart, 1963.) The magnitude of β depends on the type of soil.

EXAMPLE 3.1

Given $\mu = 0.25$, determine the value of the Rayleigh wave velocity in terms of v_s.

SOLUTION:

From Eq. (3.126),

$$V^6 - 8V^4 - (16\alpha^2 - 24)V^2 - 16(1 - \alpha^2) = 0$$

For $\mu = 0.25$,

$$\alpha^2 = \frac{1 - 2\mu}{2 - 2\mu} = \frac{1 - 0.5}{2 - 0.5} = \frac{1}{3}$$

$$V^6 - 8V^4 - \left(\tfrac{16}{3} - 24\right) V^2 - 16\left(1 - \tfrac{1}{3}\right) = 0$$

$$3V^6 - 24V^4 + 56V^2 - 32 = 0$$

$$(V^2 - 4)(3V^4 - 12V^2 + 8) = 0$$

Therefore,

$$V^2 = 4, \quad 2 + \frac{2}{\sqrt{3}}, \quad 2 - \frac{2}{\sqrt{3}}$$

If $V^2 = 4$,

$$\frac{s^2}{f^2} = 1 - V^2 = 1 - 4 = -3$$

Copyright 2017 Cengage Learning. All Rights Reserved. May not be copied, scanned, or duplicated, in whole or in part. Due to electronic rights, some third party content may be suppressed from the eBook and/or eChapter(s). Editorial review has deemed that any suppressed content does not materially affect the overall learning experience. Cengage Learning reserves the right to remove additional content at any time if subsequent rights restrictions require it.

and s/f is imaginary. This is also the case for $V^2 = 2 + 2/\sqrt{3}$.

Keeping Eqs. (3.129), (3.131), and (3.130), (3.132) in mind, one can see that when q/f and s/f are imaginary, it does not yield the type of wave that is being discussed here. Thus,

$$V^2 = 2 - \frac{2}{\sqrt{3}} \qquad V = \frac{v_r}{v_s} = 0.9194$$

or

$$v_r = \mathbf{0.9194}\, v_s$$

3.16 VISCOELASTIC WAVES IN A BAR

In Section 3.4, the propagation of longitudinal elastic waves in a bar was discussed. In some cases, soil behavior exhibits viscoelastic characteristics. In many instances, the Voigt model as shown in Figure 3.19 has been used to represent soil behavior. According to the Voigt model, which is a spring-dashpot system,

$$\sigma = E\varepsilon + \eta \frac{d\varepsilon}{dt} \tag{3.140}$$

where E = elastic modulus of the spring

η = dashpot coefficient

ε = strain

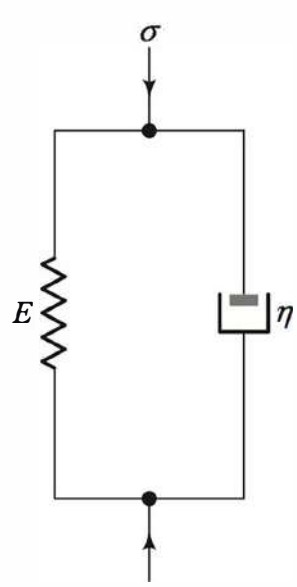

Figure 3.19 Voigt model

Copyright 2017 Cengage Learning. All Rights Reserved. May not be copied, scanned, or duplicated, in whole or in part. Due to electronic rights, some third party content may be suppressed from the eBook and/or eChapter(s). Editorial review has deemed that any suppressed content does not materially affect the overall learning experience. Cengage Learning reserves the right to remove additional content at any time if subsequent rights restrictions require it.

From Eq. (3.27) we have

$$\frac{\partial \sigma}{\partial x} = \rho\left(\frac{\partial^2 u}{\partial t^2}\right) \tag{3.27}$$

Again, from Eq. (3.140)

$$\sigma = E\left(\frac{\partial u}{\partial x}\right) + \eta \frac{\partial u}{\partial x \partial t} \tag{3.141}$$

Combining Eqs. (3.27) and (3.141)

$$E\frac{\partial^2 u}{\partial x^2} + \eta \frac{\partial^2 u}{\partial x^2 \partial t} = \rho \frac{\partial^2 u}{\partial t^2} \tag{3.142}$$

Let the input at one end of the bar (i.e., $x = 0$) be given as

$$u(0, t) = \cos \omega t \tag{3.143}$$

Equations (3.142) and (3.143) can be solved to give

$$u = \exp[Az\cos(ut - Bz] \tag{3.144}$$

where

$$A^2 = \frac{\rho\omega^2}{2E(1 + t_r^2\omega^2)}\left[(1 + t_t^2\omega^2)^{0.5} - 1\right] \tag{3.145}$$

and

$$B^2 = \frac{\rho\omega^2}{2E(1 + t_r^2\omega^2)}\left[(1 + t_r^2\omega^2)^{0.5} + 1\right] \tag{3.146}$$

where

$$t_r = \text{relaxation time} = \frac{\eta}{E} \tag{3.147}$$

The velocity of wave propagation can be given as

$$v_0 = \frac{\omega}{B} \tag{3.148}$$

Combining Eqs. (3.146) and (3.148), we obtain

$$v_0 = \left(\frac{2E}{\rho}\right)^{0.5}\left[\frac{1 + t_r^2\omega^2}{(1 + t_r^2\omega^2)^{0.5} + 1}\right]^{0.5} \tag{3.149}$$

When $t_r^2\omega^2$ becomes very small, $v_0 \approx (E/\rho)^{0.5}$, which is the velocity in elastic material [see Eq. (3.30)].

Copyright 2017 Cengage Learning. All Rights Reserved. May not be copied, scanned, or duplicated, in whole or in part. Due to electronic rights, some third party content may be suppressed from the eBook and/or eChapter(s). Editorial review has deemed that any suppressed content does not materially affect the overall learning experience. Cengage Learning reserves the right to remove additional content at any time if subsequent rights restrictions require it.

References

Biot, M. A. (1956). "Theory of Propagation of Elastic Waves in a Fluid-Saturated Solid," *Journal of the Acoustical Society of America*. Vol. 28, No. 2, pp. 168–178.

Bornitz, G. (1931). *Über die Ausbreitung der von Großkolbenmaschinen erzeugten Bodenschwingungen in die Tiefe*, J. Springer, Berlin.

Duffy, J., and Mindlin, R. D. (1957). "Stress-Strain Relations of a Granular Medium," *Transaction*, ASME, Vol. 24, pp. 585–593.

Hall, J· R., Jr., and Richart, F. E., Jr. (1963). "Dissipation of Elastic Wave Energy in Granular Soils," *Journal of the Soil Mechanics and Foundations Division*, ASCE, Vol. 89, No. SM6, PP. 27–56.

Hardin, B. O., and Richart, F. E., Jr. (1963). "Elastic Wave Velocities in Granular Soils," *Journal of the Soil Mechanics and Foundations Division*, ASCE, Vol. 89, No. SM1, pp. 33–65.

Rayleigh, L. (1885). "On Waves Propagated Along the Plane Surface of Elastic Solid," *Proceedings*, London Mathematical Society, Vol. 17, pp. 4–11.

Richart, F. E., Jr., Hall, J. R., Jr., and Woods, R. D. (1970). *Vibrations of Soils and Foundations*, Prentice Hall, Englewood Cliffs, New Jersey.

Timoshenko, S. P., and Goodier, J· N. (1970). *Theory of Elasticity*, 3rd Edition, McGraw-Hill, New York.

Copyright 2017 Cengage Learning. All Rights Reserved. May not be copied, scanned, or duplicated, in whole or in part. Due to electronic rights, some third party content may be suppressed from the eBook and/or eChapter(s). Editorial review has deemed that any suppressed content does not materially affect the overall learning experience. Cengage Learning reserves the right to remove additional content at any time if subsequent rights restrictions require it.

Properties of Dynamically Loaded Soils

4

4.1 INTRODUCTION

It is a well-known fact that earthquake damage is strongly influenced by the dynamic properties of local soil deposits. In addition, many problems in civil engineering practice require the knowledge of the properties of soils subjected to dynamic loading. These problems include the dynamic bearing capacity of foundations, response of machine foundations subjected to cyclic loading, soil-structure interaction during the propagation of stress waves generated due to an earthquake, and earthquake resistance of dams and embankments.

A variety of laboratory tests as well as field techniques are available, each having its own limitations as well as advantages. Some of these tests are specifically developed for measuring properties of dynamically loaded soils whereas some are modified versions of tests used in the domain of traditional soil mechanics. Some of these methods are suitable for small strain range whereas some are suitable for large strain range. The range of strain of interest usually dictates the type of equipment/method to be used which in turn depends on the problem to be analyzed at hand. Some of these equipments are very specialized, expensive, and require special training to use and interpret the results. It is worth noting that soil behavior over a wide range of strains is nonlinear and, on unloading, follows a different stress-strain path forming a hysteresis loop.

This chapter is devoted primarily to describing various laboratory and field test procedures available to measure as well as estimate the soil properties using empirical correlations subjected to dynamic loading. This chapter is divided into three major parts:

a. Laboratory tests and results
b. Field tests and measurements
c. Empirical correlations for the shear modulus and damping ratio obtained from field and laboratory tests. These are the two most important parameters needed for most design work.

Copyright 2017 Cengage Learning. All Rights Reserved. May not be copied, scanned, or duplicated, in whole or in part. Due to electronic rights, some third party content may be suppressed from the eBook and/or eChapter(s).
Editorial review has deemed that any suppressed content does not materially affect the overall learning experience. Cengage Learning reserves the right to remove additional content at any time if subsequent rights restrictions require it.

Laboratory Tests and Results

4.2 SHEAR STRENGTH OF SOILS UNDER RAPID LOADING CONDITIONS

Saturated Clay

In most common soil test programs, the undrained shear strength of saturated cohesive soils is determined by conducting *unconsolidated-undrained triaxial tests*. The soil specimen for this type of test is initially subjected to a confining pressure σ_3 in a triaxial test chamber, as shown in Figure 4.1a. After that an axial stress $\Delta\sigma$ is applied to the specimen (Figure 4.1b). The axial stress $\Delta\sigma$ is gradually increased from zero to higher values at a constant rate of compressive strain. The strain rate $\dot{\varepsilon}$ is maintained at about 0.5% or less. The general nature of $\Delta\sigma$ versus axial strain ε diagram thus obtained is shown in Figure 4.1c. The *total* major and minor principal stresses at failure can now be given as:

$$\text{Major principal stress (total)} = \sigma_{1(f)} = \sigma_3 + \Delta\sigma_{\max}$$

$$\text{Minor principal stress (total)} = \sigma_3$$

The *total stress Mohr's circle* at failure is shown in Figure 4.1d. It can be shown (see Das, 1990) that for a given saturated clayey soil, the magnitude of $\Delta\sigma_{\max}$ is practically independent of the confining pressure σ_3, as shown in Figure 4.1e. The total stress Mohr's envelope for this case is parallel to the normal stress axis and is referred to as the $\phi = 0$ *condition* (where ϕ = angle of shearing resistance of the soil). The undrained shear strength c_u is expressed as

$$c_u = \frac{\Delta\sigma_{\max}}{2} = \frac{\sigma_{1(f)} - \sigma_3}{2} \tag{4.1}$$

The undrained shear strength obtained by conducting tests at such low-axial strain rates is representative of the *static loading condition*, or $c_u = c_{u(\text{static})}$. Experimental results have shown that the magnitude of $\Delta\sigma_{\max} = \sigma_{1(f)} - \sigma_3$ gradually increases with the increase of axial strain rate $\dot{\varepsilon}$. This conclusion can be seen from the laboratory test results on Buckshot clay (Figure 4.2). From Figure 4.2, it can be observed that $c_u = \Delta\sigma_{\max}/2 = (\sigma_{1(f)} - \sigma_3)/2$ obtained between strain rates of 50% to 425% are not too different and can be approximated to be a single value (Carroll, 1963). This value can be referred to as the *dynamic undrained shear strength*, or

$$c_u = c_{u(\text{dynamic})}$$

Carroll suggested that for most practical cases, one can assume that

$$\boxed{\frac{c_{u(\text{dynamic})}}{c_{u(\text{static})}} \approx 1.5} \tag{4.2}$$

Copyright 2017 Cengage Learning. All Rights Reserved. May not be copied, scanned, or duplicated, in whole or in part. Due to electronic rights, some third party content may be suppressed from the eBook and/or eChapter(s). Editorial review has deemed that any suppressed content does not materially affect the overall learning experience. Cengage Learning reserves the right to remove additional content at any time if subsequent rights restrictions require it.

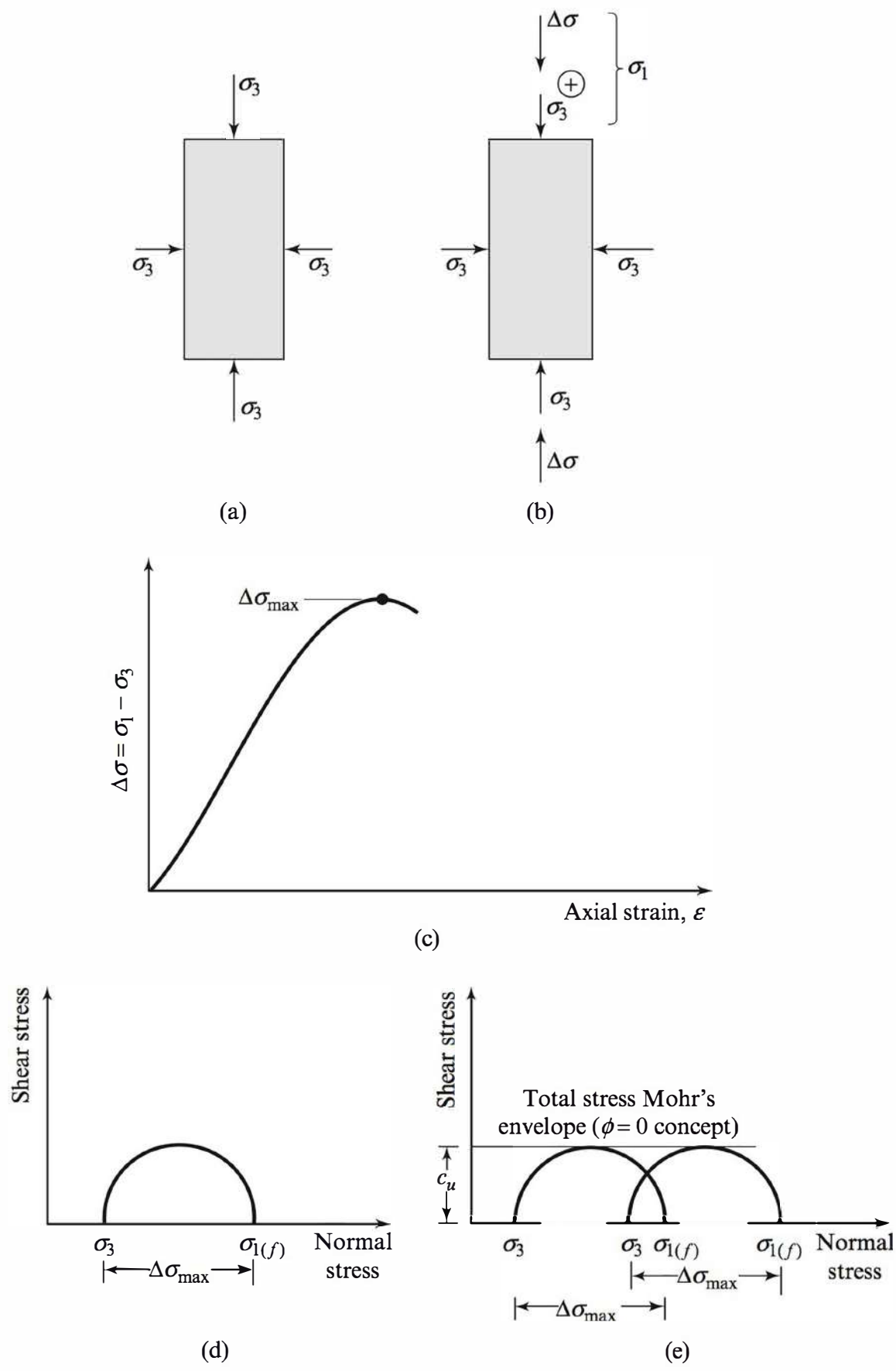

Figure 4.1 Unconsolidated undrained triaxial tests

Sand

Several vacuum triaxial test results on different dry sands (that is, standard Ottawa sand, Fort Peck sand, and Camp Cooke sand) were reported by Whitman and Healy (1963). These tests were conducted with various effective confining

Copyright 2017 Cengage Learning. All Rights Reserved. May not be copied, scanned, or duplicated, in whole or in part. Due to electronic rights, some third party content may be suppressed from the eBook and/or eChapter(s). Editorial review has deemed that any suppressed content does not materially affect the overall learning experience. Cengage Learning reserves the right to remove additional content at any time if subsequent rights restrictions require it.

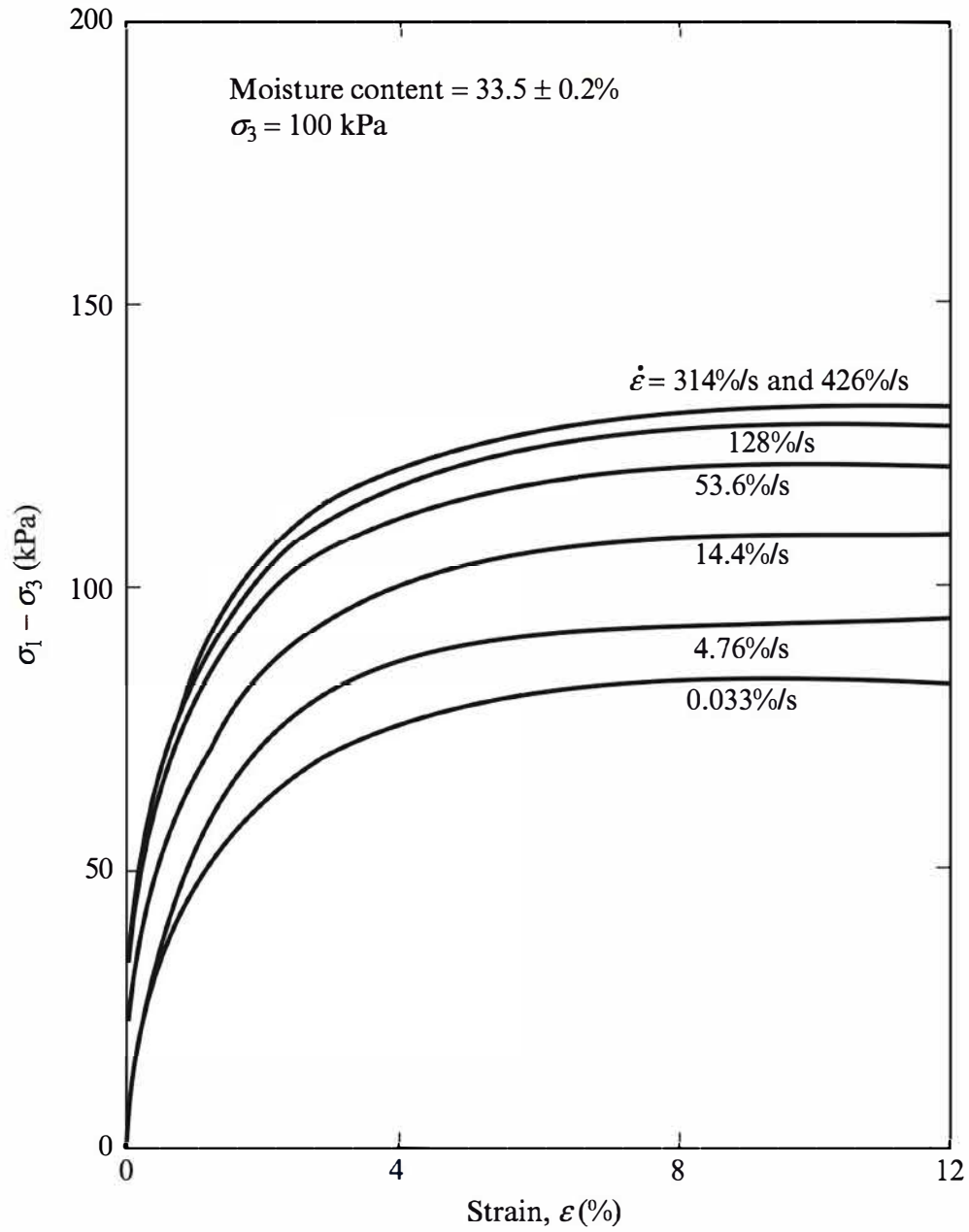

Figure 4.2 Unconsolidated-undrained triaxial test results on Buckshot clay (after Carroll, 1963)

Source: Carroll, W.F. (1963). "Dynamic Bearing Capacity of Soils. Vertical Displacements of Spread Footings on Clay: Statics and Impulsive Loadings." *Technical Report No. 3–599,* U.S. Army Corps of Engineers, Waterways Experiment Station, Vicksburg, Mississippi.

pressures ($\bar{\sigma}_3$) and axial strain rates. The *compressive strength* $\Delta\sigma_{max}$ determined from these tests can be given as

$$\Delta\sigma_{max} = \bar{\sigma}_{1(f)} - \bar{\sigma}_3 \tag{4.3}$$

where $\bar{\sigma}_3$ = effective minor principle stress

$\bar{\sigma}_{1(f)}$ = effective major principal stress at failure

An example of the effect of axial strain rate on dry Ottawa sand is shown in Figure 4.3. It can be seen that for a given $\bar{\sigma}_3$ the magnitude of $\Delta\sigma_{max}$ decreases initially with the increase of the strain rate to a minimum value and increases thereafter. From fundamentals of soil mechanics it is known that

Copyright 2017 Cengage Learning. All Rights Reserved. May not be copied, scanned, or duplicated, in whole or in part. Due to electronic rights, some third party content may be suppressed from the eBook and/or eChapter(s). Editorial review has deemed that any suppressed content does not materially affect the overall learning experience. Cengage Learning reserves the right to remove additional content at any time if subsequent rights restrictions require it.

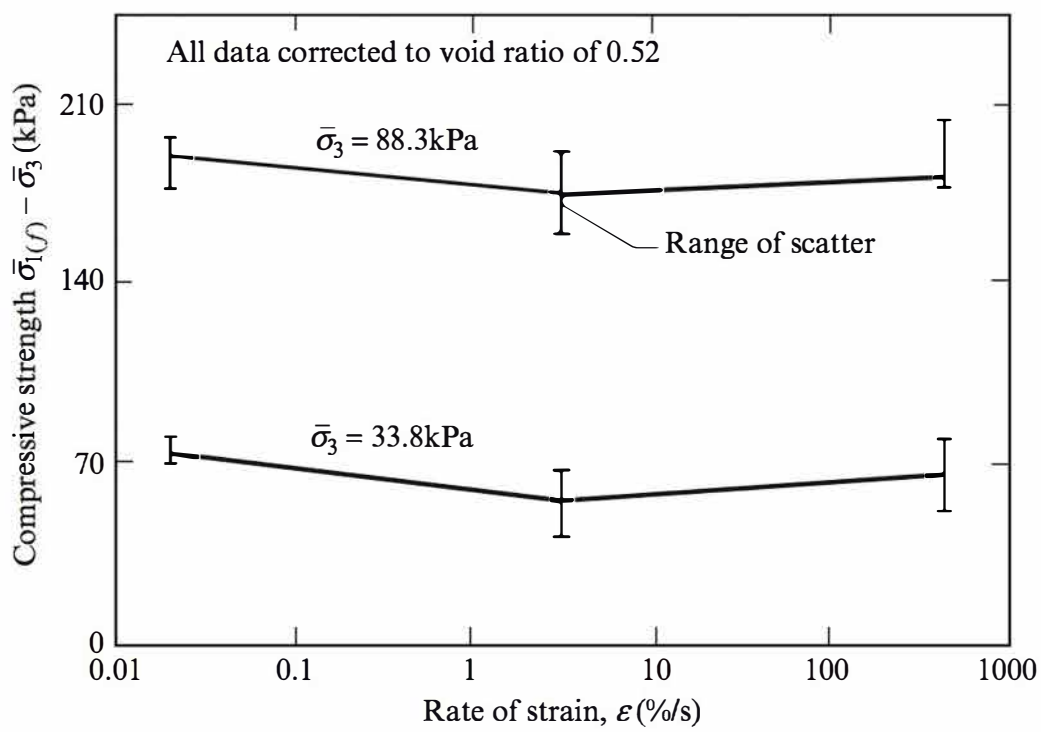

Figure 4.3 Strain-rate effect for dry Ottawa sand (after Whitman and Healy, 1963)

Source: Whitman, R.V., and Healy, K.A. (1963). "Shear Strength of Sands During Rapid Loadings," *Transactions,* ASCE, Vol. 128, Part 1, pp. 1553–1594. With permission from ASCE.

$$\phi = \sin^{-1}\left(\frac{\bar{\sigma}_{1(f)} - \bar{\sigma}_3}{\bar{\sigma}_{1(f)} + \bar{\sigma}_3}\right) \tag{4.4}$$

where ϕ = drained soil friction angle

Based on Figure 4.3 and Eq. (4.4) it is obvious that the initial increase of the strain rate results in a decrease of the soil friction angle. The minimum dynamic friction angle may be given as (Vesic, 1973)

$$\phi_{\text{dynamic}} \approx \phi - 2^\circ \tag{4.5}$$

(obtained from static tests—
that is, small strain rate of loading)

4.3 STRENGTH AND DEFORMATION CHARACTERISTICS OF SOILS UNDER TRANSIENT LOAD

In many circumstances it may be necessary to know the strength and deformation characteristics of soils under *transient loading*. A typical example of transient loading is that occurring due to a blast. Figure 4.4 shows the nature of an idealized load versus time variation for such a case. In this figure, Q_p is the peak load, t_L is the time of loading, and t_D is the time of decay.

Copyright 2017 Cengage Learning. All Rights Reserved. May not be copied, scanned, or duplicated, in whole or in part. Due to electronic rights, some third party content may be suppressed from the eBook and/or eChapter(s). Editorial review has deemed that any suppressed content does not materially affect the overall learning experience. Cengage Learning reserves the right to remove additional content at any time if subsequent rights restrictions require it.

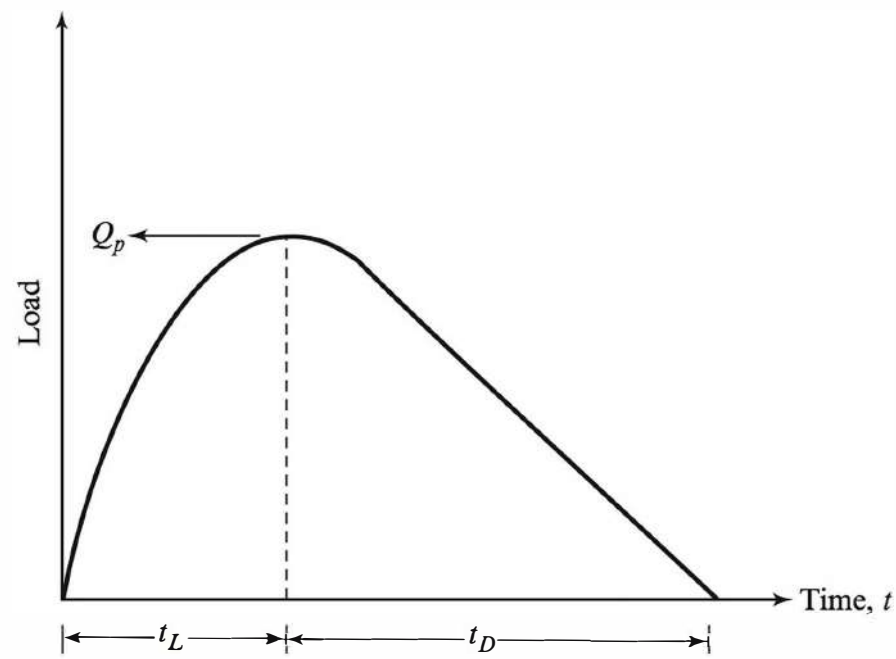

Figure 4.4 Transient load

Casagrande and Shannon (1949) conducted some early investigations to study the stress-deformation and strength characteristics of Manchester sand and Cambridge clay soils. Undrained tests were conducted in three specially devised apparatuses—one falling-beam apparatus and two pendulum-loading apparatuses. In these specially devised pieces of equipments, the loading pattern on soil specimens was similar to that shown in Figure 4.4. Figure 4.5a shows the variation of stress and strain with time for an unconfined Cambridge clay specimen with $t_L = 0.02$ s. Similarly, Figure 4.5b compares the nature of variation of strain versus stress for static and transient ($t_L = 0.02$ s) loading conditions on unconfined Cambridge clay specimens. The unconfined compressive strength determined in this manner with varying times of loading is shown in Figure 4.6. Based on Figures 4.5b and 4.6, the following conclusions may be drawn.

1. $\dfrac{q_{u(\text{transient})}}{q_{u(\text{static})}} \approx 1.5 \text{ to } 2$

   where q_u = unconfined compression strength. This is consistent with the findings of Carroll (1963) discussed in Section 4.2.

2. The modulus of deformation E as defined in Figure 4.7 is about two times as great for transient loading as compared to that for static loading.

The nature of the stress-versus-strain plot for confined compression tests on Manchester sand conducted by Casagrande and Shannon (1949) is as shown in Figure 4.8. From this study it was concluded that

1. $\dfrac{[\bar{\sigma}_{1(f)} - \bar{\sigma}_3]_{\text{transient}}}{[\bar{\sigma}_{1(f)} - \bar{\sigma}_3]_{\text{static}}} \approx 1.1$ and

2. The modulus of deformation as defined by Figure 4.7 is approximately the same for transient and static loading conditions.

Copyright 2017 Cengage Learning. All Rights Reserved. May not be copied, scanned, or duplicated, in whole or in part. Due to electronic rights, some third party content may be suppressed from the eBook and/or eChapter(s). Editorial review has deemed that any suppressed content does not materially affect the overall learning experience. Cengage Learning reserves the right to remove additional content at any time if subsequent rights restrictions require it.

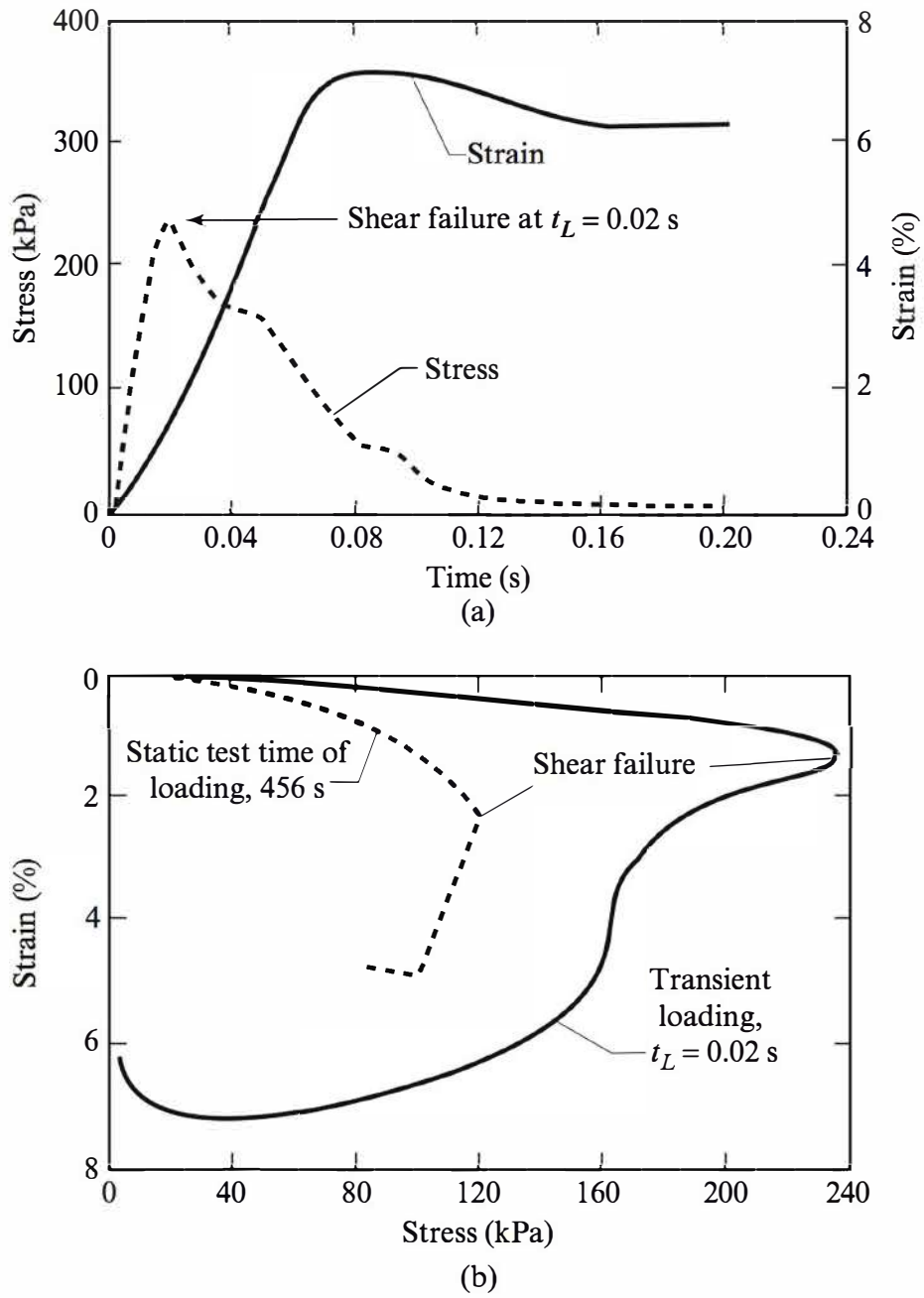

Figure 4.5 Unconfined compressive strength of Cambridge clay for varying time of loading (after Casagrande and Shannon, 1949)

Source: Casagrande, A., and Shannon, W.L. (1949). "Strength of Soils Under Dynamic Loads," *Transactions*, ASCE, Vol. 114, pp. 755–772. With permission from ASCE.

4.4 TRAVEL-TIME TEST FOR DETERMINATION OF LONGITUDINAL AND SHEAR WAVE VELOCITIES (υ_c AND υ_s)

Using electronic equipment, the time t_c requirement for travel of elastic waves through a soil specimen of length L can be measured in the laboratory. For *longitudinal wave*

$$\upsilon_c = \frac{L}{t_c} \tag{4.6}$$

Copyright 2017 Cengage Learning. All Rights Reserved. May not be copied, scanned, or duplicated, in whole or in part. Due to electronic rights, some third party content may be suppressed from the eBook and/or eChapter(s). Editorial review has deemed that any suppressed content does not materially affect the overall learning experience. Cengage Learning reserves the right to remove additional content at any time if subsequent rights restrictions require it.

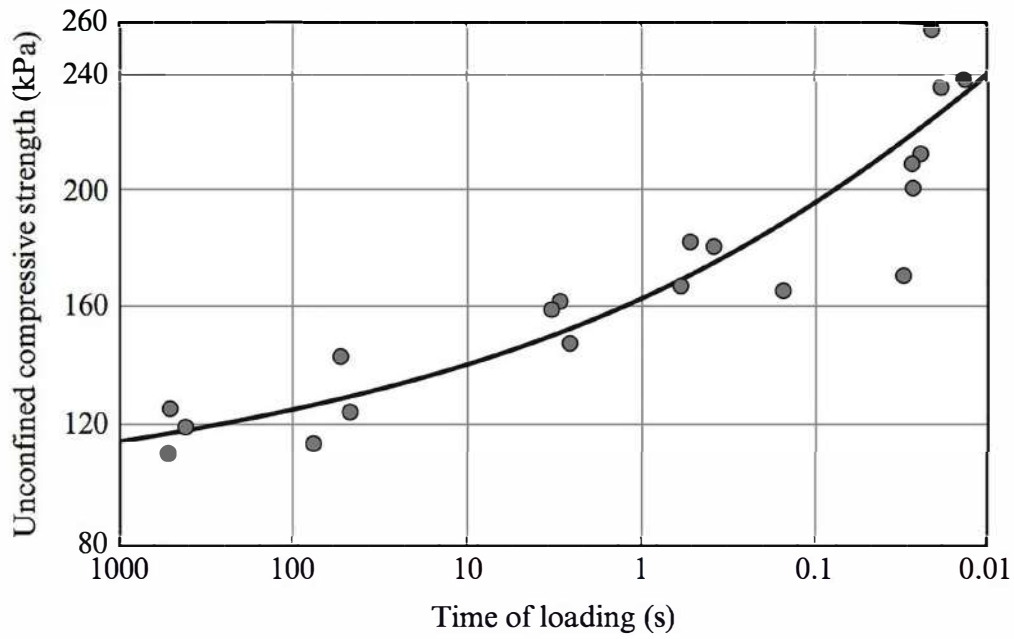

Figure 4.6 Unconfined compressive strength of Cambridge clay for varying time of loading (after Casagrande and Shannon, 1949)

Source: Casagrande, A., and Shannon, W.L. (1949). "Strength of Soils Under Dynamic Loads," *Transactions*, ASCE, Vol. 114, pp. 755–772. With permission from ASCE.

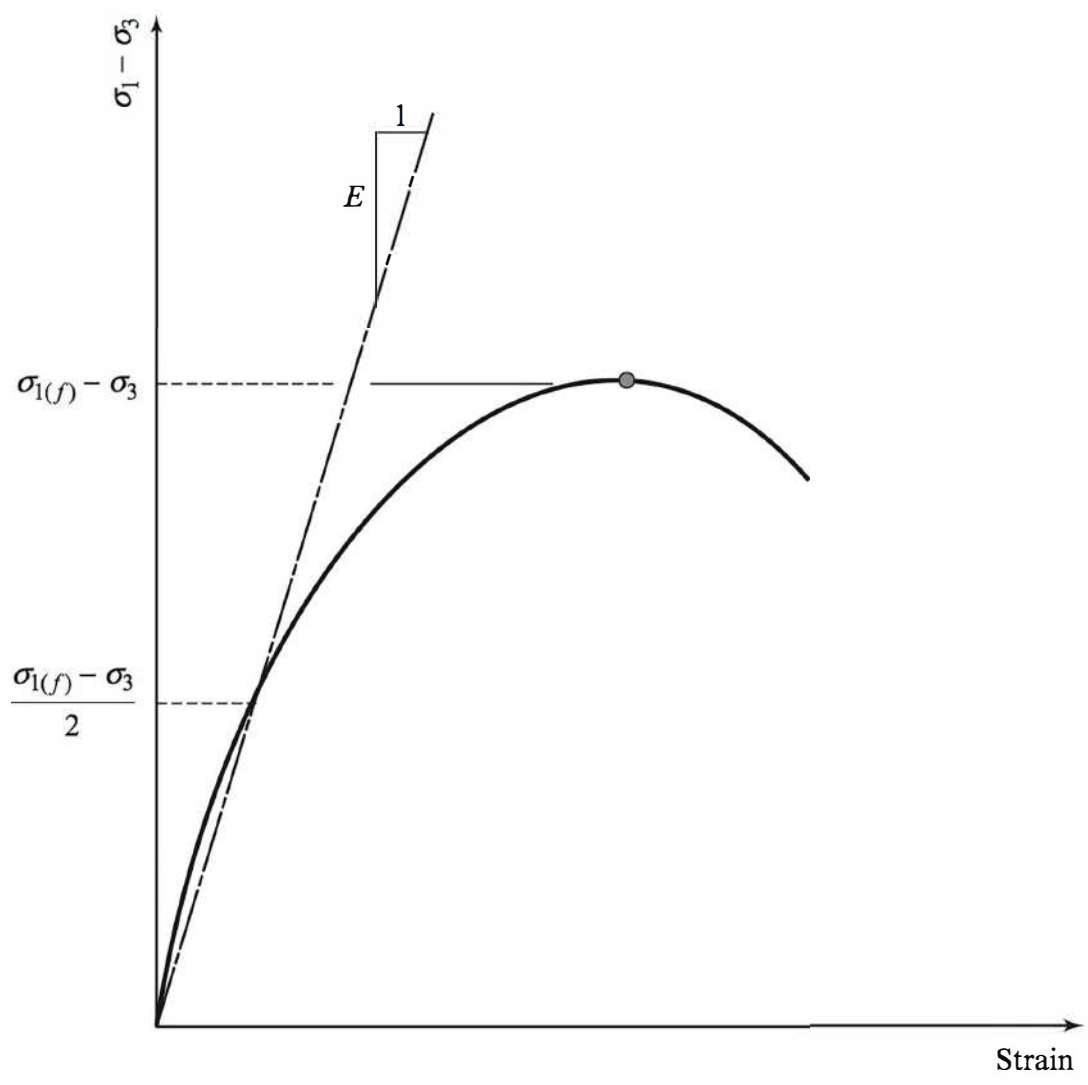

Figure 4.7 Definition of modulus of deformation, E

Copyright 2017 Cengage Learning. All Rights Reserved. May not be copied, scanned, or duplicated, in whole or in part. Due to electronic rights, some third party content may be suppressed from the eBook and/or eChapter(s). Editorial review has deemed that any suppressed content does not materially affect the overall learning experience. Cengage Learning reserves the right to remove additional content at any time if subsequent rights restrictions require it.

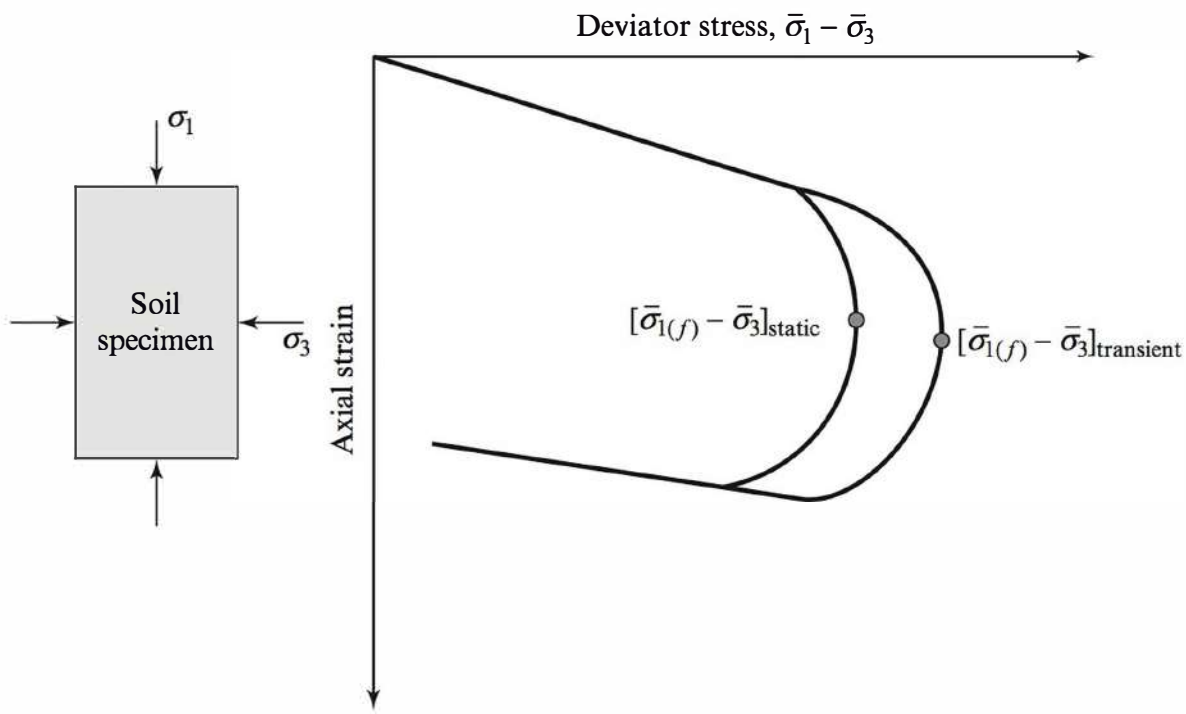

Figure 4.8 Confined-compression test on sand—stress-versus-strain behavior under static and transient loading

The modulus of elasticity E can then be calculated from Eq. (3.30) as

$$\upsilon_c = \sqrt{\frac{E}{\rho}}$$

or

$$E = \rho \upsilon_c^2 = \rho \frac{L^2}{t_c^2} \tag{4.7}$$

If the soil specimen is *confined laterally*, then the travel time will give the value of υ'_c as shown in Eq. (3.35). Thus $\upsilon_c = L/t'_c$, and

$$M = \rho \frac{L^2}{t_c'^2} \tag{4.8}$$

where t'_c = time of travel of longitudinal waves in a laterally confined specimen

M = constrained modulus

Similarly, if the travel time t_s for *torsional waves* through a soil of length L is determined, the velocity υ_s can be given as $\upsilon_s = L/t_c$, and

$$G = \rho \upsilon_s^2 = \rho \frac{L^2}{t_s^2} \tag{4.9}$$

Whitman and Lawrence (1963) have provided limited test results for υ'_c in 20–30 Ottawa sand. The schematic diagram of the apparatus used for measuring υ'_c is shown in Figure 4.9a. The soil specimen was confined in 76.2 mm diameter Shelby tube (Figure 4.9b). Vertical load was applied by an aluminum piston. In this system, a pulse was sent from one piezo-electric crystal and received

Copyright 2017 Cengage Learning. All Rights Reserved. May not be copied, scanned, or duplicated, in whole or in part. Due to electronic rights, some third party content may be suppressed from the eBook and/or eChapter(s). Editorial review has deemed that any suppressed content does not materially affect the overall learning experience. Cengage Learning reserves the right to remove additional content at any time if subsequent rights restrictions require it.

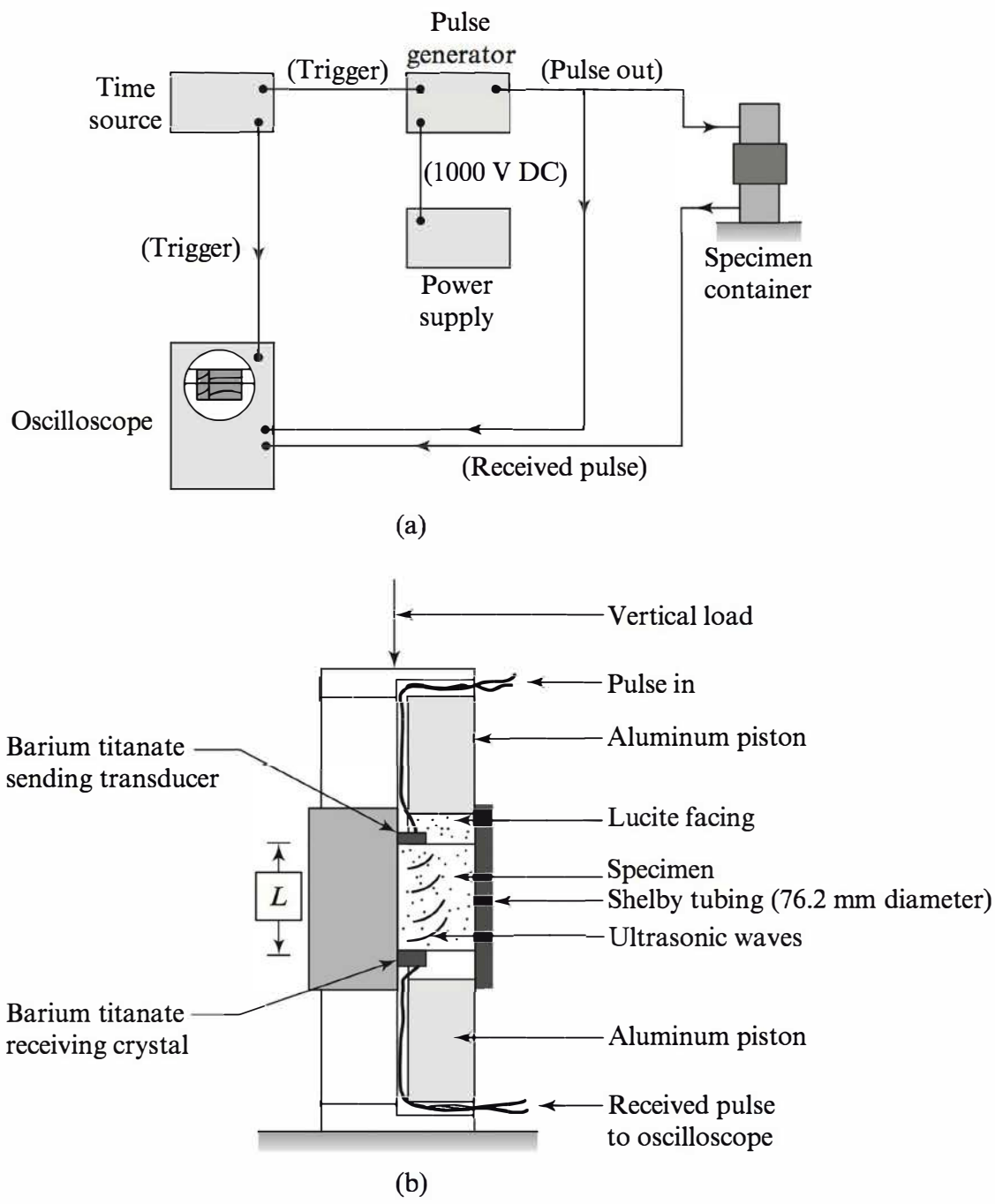

Figure 4.9 Travel-time method: (a) schematic diagram of the laboratory setup for measuring v'_c; (b) details of the soil specimen and container for the laboratory setup (after Whitman and Lawrence, 1963)

Source: Whitman, R.V., and Lawrence, F.V. (1963). "Discussion on Elastic Wave Velocities on Granular Soils," *Journal of the Soil Mechanics and Foundations Division*, ASCE, Vol. 89, No. SM5, pp. 112–118. With permission from ASCE.

by a second one at the opposite end. The received signal was displayed on an oscilloscope, which allowed measurement of t'_c. It was found that the velocity v'_c increases with the increase of axial pressure.

4.5 BENDER ELEMENT TEST FOR DETERMINATION OF SHEAR WAVE VELOCITY (v_s)

The bender element test is now commonly used in the laboratory to evaluate the small-strain shear modulus (G_{max}) by measurement of the shear wave velocity

Copyright 2017 Cengage Learning. All Rights Reserved. May not be copied, scanned, or duplicated, in whole or in part. Due to electronic rights, some third party content may be suppressed from the eBook and/or eChapter(s). Editorial review has deemed that any suppressed content does not materially affect the overall learning experience. Cengage Learning reserves the right to remove additional content at any time if subsequent rights restrictions require it.

(v_s) propagation in a soil specimen. The bender element is a thin transducer that consists of two piezoelectric plates rigidly bonded to a center shim of brass or stainless steel plate. The bender element can be implemented in most common laboratory soil research equipment including unconfined compression, oedometer, direct shear, triaxial, resonant column, centrifuges, and so forth. Two in-line bender elements as a pair are usually installed at both ends of a soil specimen, acting as transmitter and receiver, respectively. Figure 4.10a shows a pair of bender elements implemented in a triaxial cell, and Figure 4.10b shows a soil specimen with a pair of bender elements.

Various waveforms such as sinusoidal and square waves can be used as an excitation signal. The bender element can convert between electrical voltage and mechanical excitation/bending motion. The wave form of the input voltage yields a bending motion in the transmitter element, which produces a shear wave propagating through the specimen. When the receiver element at the other end of specimen is bent by the arrival of shear wave, an electrical signal is generated in a wave form. The transmitted and received wave forms can be captured and displayed by a digital oscilloscope to determine the shear wave travel time (t_s). The shear wave velocity is calculated as

$$v_s = \frac{L}{t_s}$$

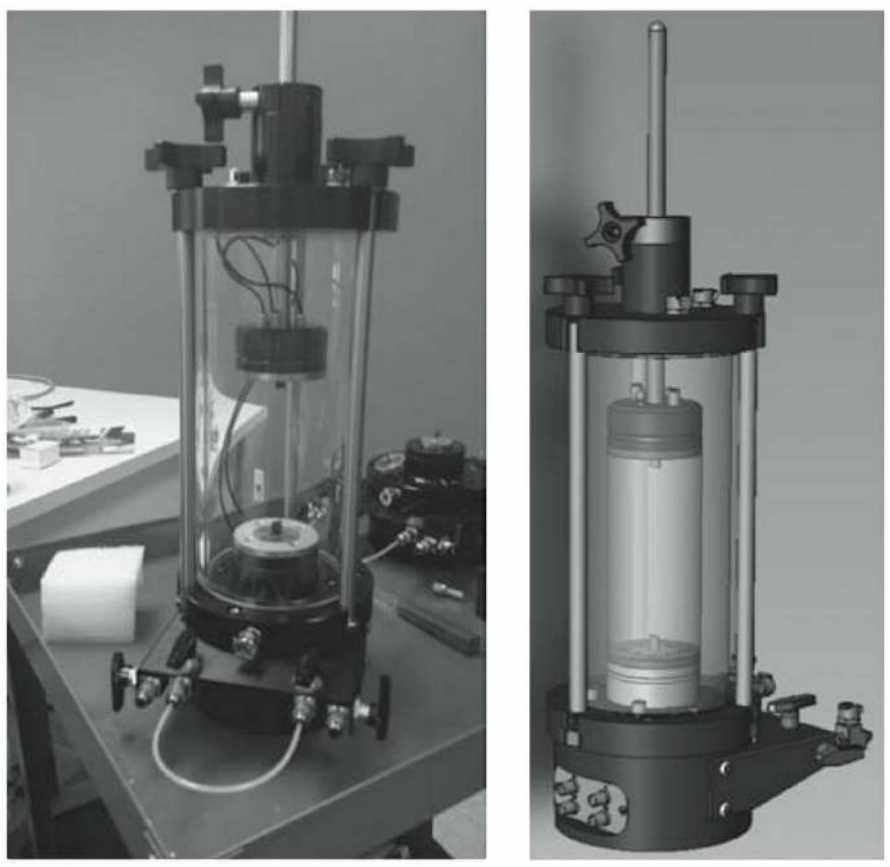

(a) (b)

Figure 4.10 Test with bender element: (a) a pair of bender elements installed in a triaxial cell; (b) soil specimen with the pair of bender elements (Courtesy of Geocomp Corporation, Acton, Massachusetts)

Source: Courtesy of Geocomp Corporation, Acton, Massachusetts

Copyright 2017 Cengage Learning. All Rights Reserved. May not be copied, scanned, or duplicated, in whole or in part. Due to electronic rights, some third party content may be suppressed from the eBook and/or eChapter(s). Editorial review has deemed that any suppressed content does not materially affect the overall learning experience. Cengage Learning reserves the right to remove additional content at any time if subsequent rights restrictions require it.

where L is the travel distance and can be determined as the distance between the two tips of the two bender elements (Dyvik and Madshus, 1985). The small-strain shear modulus can be determined from elastic wave theory [similar to Eq. (4.9)]:

$$G = G_{\max} = \rho v_s^2 = \rho\left(\frac{L}{t_s}\right)^2$$

where ρ is the mass density of soil. The $G_{\max}$ measured by bender element can generally have good agreement with that obtained from the resonant column test (Section 4.6). The advantages of bender element are: (a) the test procedure of bender element is simple and efficient; (b) the bender element test is nondestructive; and (c) the number of specimens required is minimal.

4.6 RESONANT COLUMN TEST

The resonant column test essentially consists of a soil column that is excited to vibrate in one of its natural modes. Once the frequency at *resonance* is known, the wave velocity can easily be determined. The soil column in the resonant column device can be excited longitudinally or torsionally, yielding velocities of v_c or v_s, respectively. The resonant column technique was first applied to testing of soils in Japan by Ishimato and Iida (1937) and Iida (1938, 1940). Since then it has been extensively used in many countries, with several modifications using different end conditions to constrain the specimen. One of the earlier types of resonant column devices in the United States was used by Wilson and Dietrich (1960) for testing clay specimens.

Hardin and Richart (1963) reported the use of two types of resonant column devices—one for longitudinal vibration and the other for torsional vibration. The specimen were free at each end (*free–free end condition*). A schematic diagram of the laboratory experimental setup is shown in Figure 4.11. The power supply and amplifier No. 1 were used to amplify the sinusoidal output signal of the oscillator, which had a frequency range of 5 Hz to 600,000 Hz. The amplified signals were fed into the driver, producing the desired vibrations. Figure 4.12a shows the schematic diagram of the driver for torsional oscillation. Similarly, the schematic diagram of the driver for longitudinal vibration is shown in Figure 4.12b. These devices will give results for *low-amplitude vibration conditions*. With *free–free end conditions*, for longitudinal vibrations at resonance

$$v_c = \frac{\omega_n L}{n\pi} \tag{3.53}$$

For $n = 1$ (that is, normal mode of vibration),

$$v_c = \frac{\omega_n L}{\pi} = \frac{2\pi f_n L}{\pi} = 2 f_n L$$

Copyright 2017 Cengage Learning. All Rights Reserved. May not be copied, scanned, or duplicated, in whole or in part. Due to electronic rights, some third party content may be suppressed from the eBook and/or Chapter(s). Editorial review has deemed that any suppressed content does not materially affect the overall learning experience. Cengage Learning reserves the right to remove additional content at any time if subsequent rights restrictions require it.

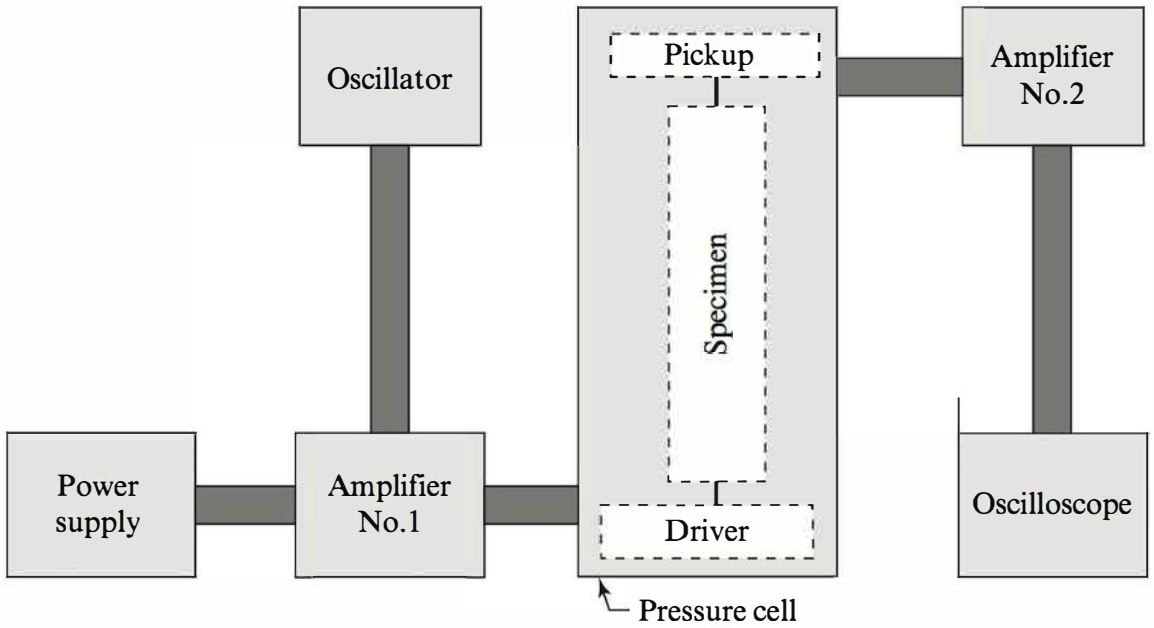

Figure 4.11 Schematic diagram of experimental setup for resonant column test of Hardin and Richart—free–free end condition

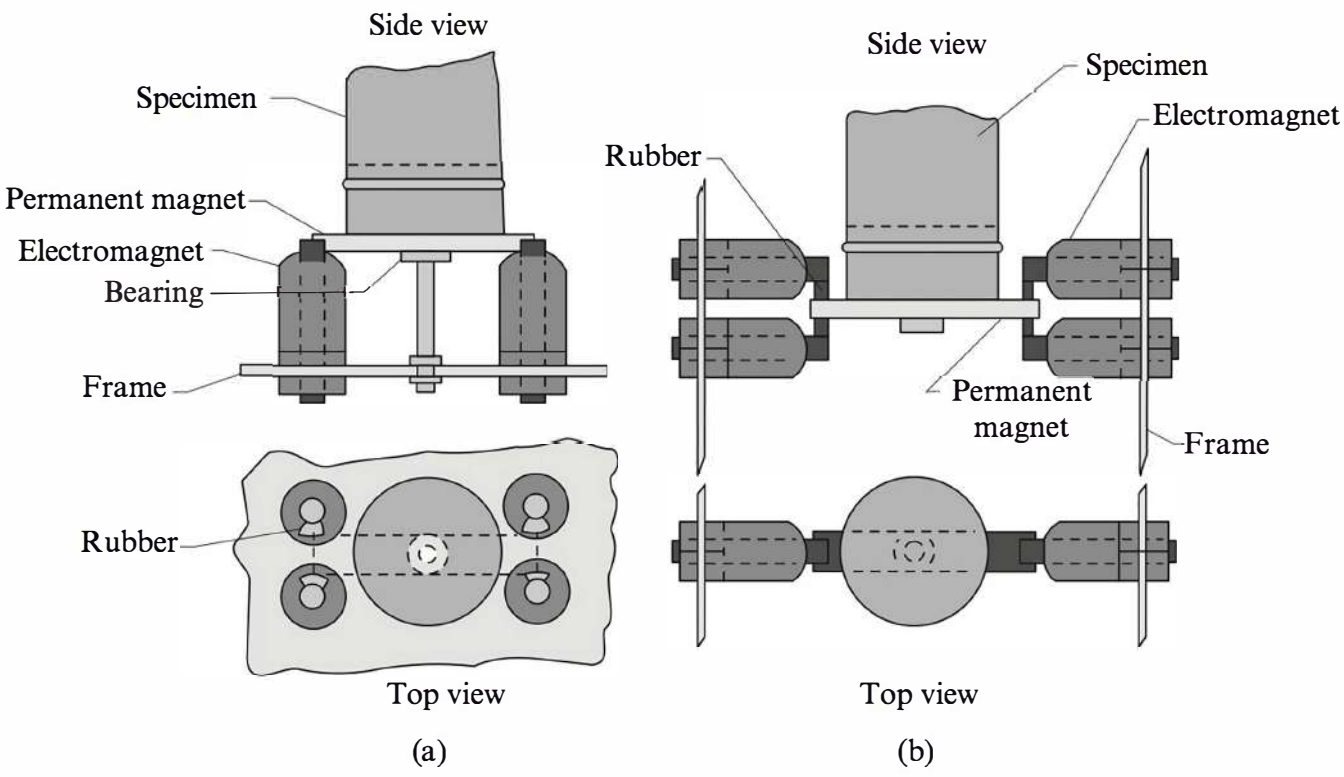

Figure 4.12 Drawings for steady-system vibration drivers in the resonant column devices with free–free end conditions: (a) for torsional vibration; (b) for longitudinal vibration (after Hardin and Richart, 1963)

Source: Hardin, B. O., and Richard, F. E., Jr. (1963). "Elastic Wave Velocity in Granular Soils," *Journal of the Soil Mechanics and Foundations Division*, ASCE, Vol. 89, No. SM1, pp. 33–65. With permission from ASCE.

or

$$v_c = \sqrt{\frac{E}{\rho}} = 2 f_n L$$

Copyright 2017 Cengage Learning. All Rights Reserved. May not be copied, scanned, or duplicated, in whole or in part. Due to electronic rights, some third party content may be suppressed from the eBook and/or eChapter(s). Editorial review has deemed that any suppressed content does not materially affect the overall learning experience. Cengage Learning reserves the right to remove additional content at any time if subsequent rights restrictions require it.

or

$$\boxed{E = 4 f_n^2 \rho L^2} \tag{4.10}$$

Similarly, for torsional vibration, at resonance (with $n = 1$)

$$v_s = 2 f_n L$$

or

$$v_s = \sqrt{\frac{G}{\rho}} = 2 f_n L$$

or

$$\boxed{G = 4 f_n^2 \rho L^2} \tag{4.11}$$

Once the magnitudes of E and G are known, the value of the Poisson's ratio can be obtained as

$$\mu = \frac{E}{2G} - 1 \tag{4.12}$$

Hall and Richart (1963) also used two other types of resonant column devices (one for longitudinal vibration and the other for torsional vibration). The end conditions for these two types of devices were *fixed–free*–fixed at the bottom and free at the top of the specimen. The general layouts of the laboratory setup for this equipment were almost the same as shown in Figure 4.11, except for the fact that the driver and the pickup were located at the top of the specimen. This is shown in Figure 4.13. Since the driver and the pickup were located close together, a correction circuit was introduced to correct the inductive coupling between the driver and the pickup. The driver and pickup were attached to a common frame. The differences in construction and arrangement of the driver and the pickup produce either longitudinal or torsional vibration of the specimen.

A. Derivation of Expressions for v_c and E for Use in the Fixed–Free–Type Resonant Column Test

An equation for the circular natural frequency for the longitudinal vibration of short rods with *fixed–free end conditions* was derived in Eq. (3.57) as

$$\omega_n = \frac{(2n-1)\pi}{2} \frac{v_c}{L}$$

However, in a fixed–free type resonant column test, the driving mechanism and also the motion-monitoring device have to be attached to the top of the specimen (Figure 4.14), in effect changing the boundary conditions assumed in deriving Eq. (3.57). So a modified equation for the circular natural frequency needs to be derived. This can be done as follows.

Copyright 2017 Cengage Learning. All Rights Reserved. May not be copied, scanned, or duplicated, in whole or in part. Due to electronic rights, some third party content may be suppressed from the eBook and/or eChapter(s). Editorial review has deemed that any suppressed content does not materially affect the overall learning experience. Cengage Learning reserves the right to remove additional content at any time if subsequent rights restrictions require it.

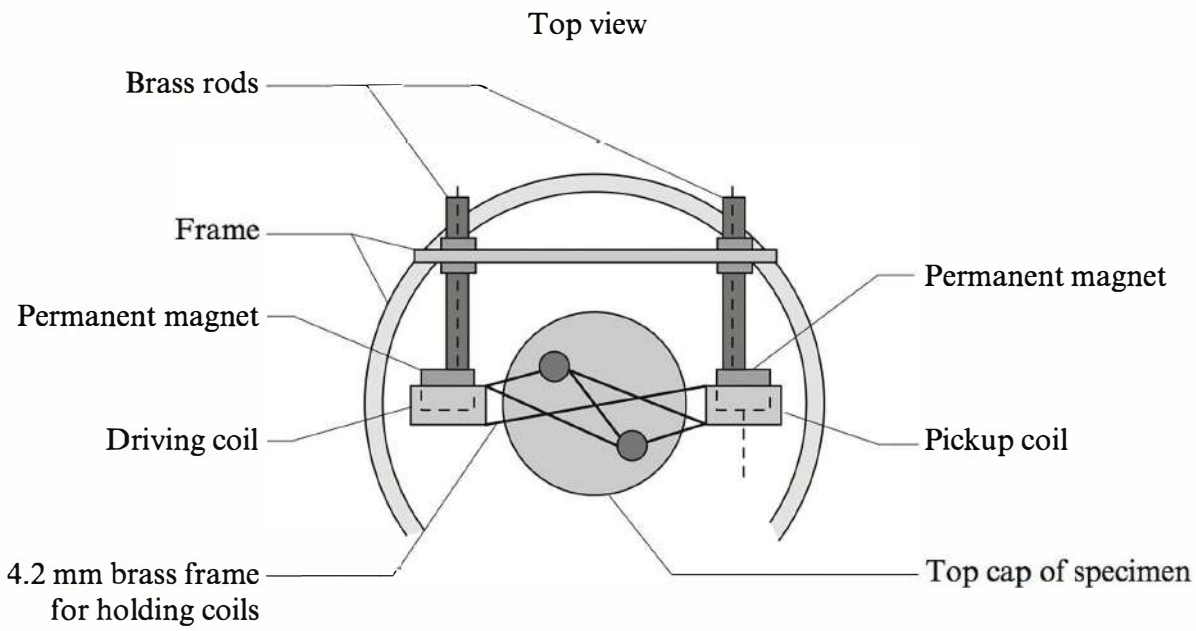

(a)

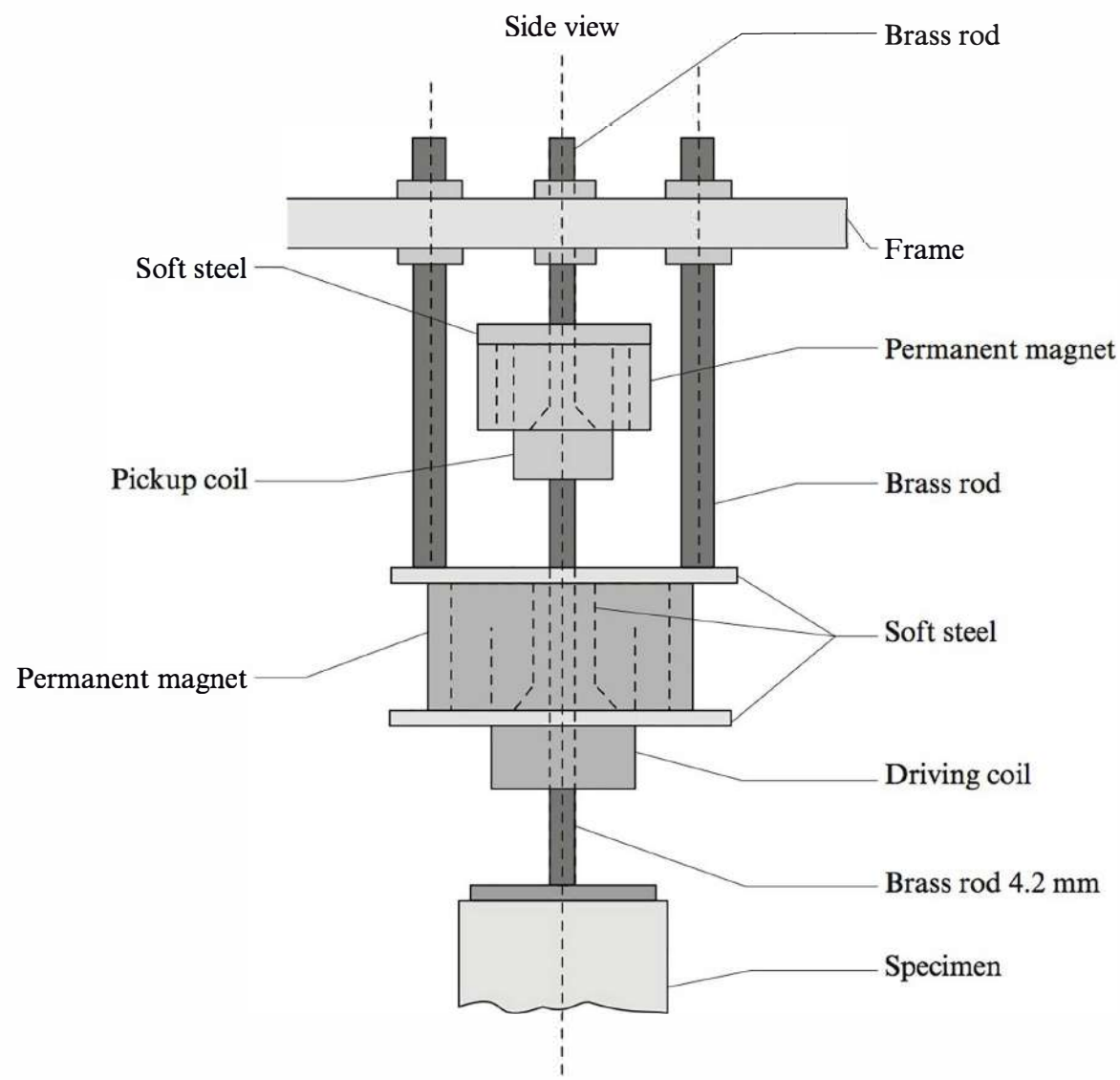

(b)

Figure 4.13 Driving and measuring components for a fixed–free resonant column device (after Hall and Richart, 1963)

Source: Hall, J.R., Jr., and Richard, F.E., Jr. (1963). "Dissipation on Elastic Wave Energy in Granular Soils," *Journal of the Soil Mechanics and Foundations Division*, ASCE, Vol. 89, No. SM6, pp. 27–56. With permission from ASCE.

Copyright 2017 Cengage Learning. All Rights Reserved. May not be copied, scanned, or duplicated, in whole or in part. Due to electronic rights, some third party content may be suppressed from the eBook and/or eChapter(s). Editorial review has deemed that any suppressed content does not materially affect the overall learning experience. Cengage Learning reserves the right to remove additional content at any time if subsequent rights restrictions require it.

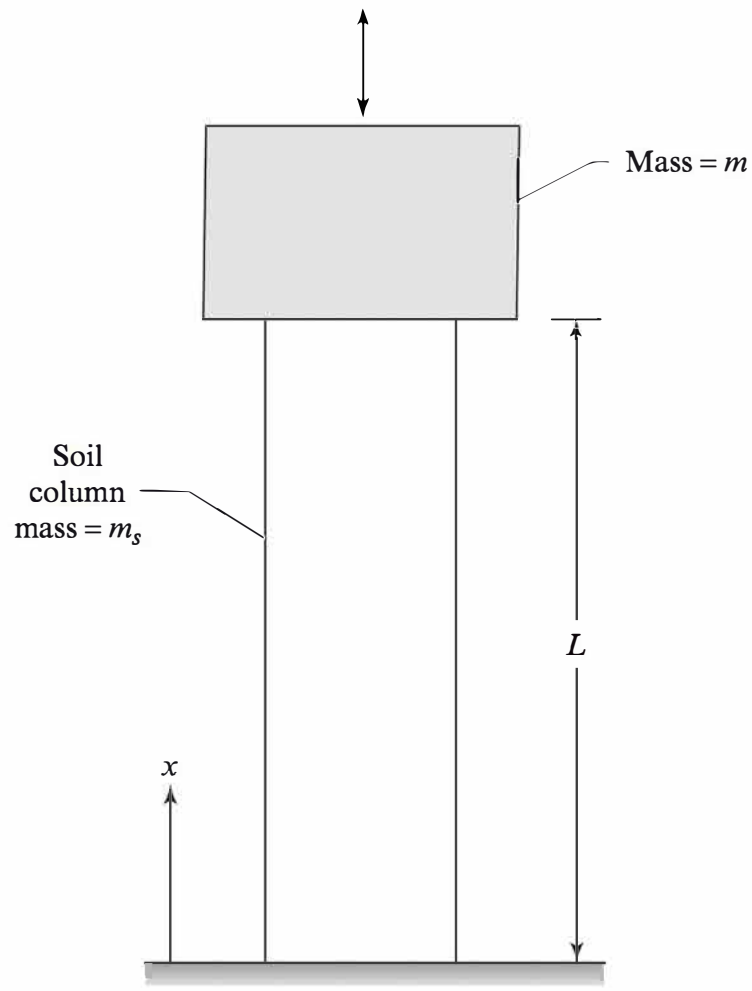

Figure 4.14 Derivation of Eq. (4.20)

Let the mass of the attachments placed on the specimen be equal to m. For the vibration of the soil column in a natural mode,

$$u(x,t) = U(x)(A_1 \sin \omega_n t + A_2 \cos \omega_n t) \tag{3.41}$$

and

$$U(x) = B_1 \sin\left(\frac{\omega_n x}{v_c}\right) + B_2 \cos\left(\frac{\omega_n x}{v_c}\right) \tag{3.43}$$

At $x = 0$, $U(x) = 0$. So B_2 in Eq. (3.43) is zero. Thus

$$U(x) = B_1 \sin\left(\frac{\omega_n x}{v_c}\right) \tag{4.13}$$

At $x = L$, the inertia force of mass m is acting on the soil column, and this can be expressed as

$$F = -m\frac{\partial^2 u}{\partial t^2} \tag{4.14}$$

where F = inertia force. Also, the strain

$$\frac{\partial u}{\partial x} = \frac{F}{AE} \tag{4.15}$$

Copyright 2017 Cengage Learning. All Rights Reserved. May not be copied, scanned, or duplicated, in whole or in part. Due to electronic rights, some third party content may be suppressed from the eBook and/or eChapter(s). Editorial review has deemed that any suppressed content does not materially affect the overall learning experience. Cengage Learning reserves the right to remove additional content at any time if subsequent rights restrictions require it.

where A = cross-sectional area of specimen

E = modulus of elasticity.

Combining Eqs. (3.41), (4.13), and (4.15) we get

$$\frac{F}{AE} = \frac{\partial u}{\partial x} = \left(\frac{\partial U}{\partial x}\right)(A_1 \sin \omega_n t + A_2 \cos \omega_n t)$$

$$= \frac{\partial}{\partial x}\left[B_1 \sin\left(\frac{\omega_n x}{v_c}\right)\right](A_1 \sin \omega_n t + A_2 \cos \omega_n t) \tag{4.16}$$

$$= \left(\frac{B_1 \omega_n}{v_c}\right)\left[\cos\left(\frac{\omega_n x}{v_c}\right)\right](A_1 \sin \omega_n t + A_2 \cos \omega_n t)$$

Again, combining Eqs. (3.41), (4.13), and (4.14),

$$F = -m\frac{\partial^2 u}{\partial t^2} = -m\left[B_1 \sin\left(\frac{\omega_n x}{v_c}\right)\right]\left(\frac{\partial^2}{\partial t^2}\right)(A_1 \sin \omega_n t + A_2 \cos \omega_n t)$$

$$= m\,\omega_n^2 B_1 \sin\left(\frac{\omega_n x}{v_c}\right)(A_1 \sin \omega_n t + A_2 \cos \omega_n t) \tag{4.17}$$

Now, from Eqs. (4.16) and (4.17),

$$\frac{AE}{v_c}\cos\left(\frac{\omega_n x}{v_c}\right) = m\,\omega_n \sin\left(\frac{\omega_n x}{v_c}\right) \tag{4.18}$$

At $x = L$

$$AE = m\omega_n v_c \tan\left(\frac{\omega_n L}{v_c}\right) \tag{4.19}$$

However, $v_c = \sqrt{E/\rho}$; or $E = v_c^2 \rho$. Substitution of this in Eq. (4.19) gives

$$A\,v_c^2\,\rho = m\,\omega_n\,v_c \tan\left(\frac{\omega_n L}{v_c}\right)$$

$$\frac{A\rho}{m} = \frac{\omega_n}{v_c}\tan\left(\frac{\omega_n L}{v_c}\right)$$

$$\frac{AL\rho}{m} = \frac{\omega_n L}{v_c}\tan\left(\frac{\omega_n L}{v_c}\right)$$

or

$$\boxed{\frac{AL\gamma}{W} = \alpha \tan \alpha} \tag{4.20}$$

where $\gamma = \rho g$ = unit weight of soil

$W = mg$ = weight of the attachments on top of the specimen

Copyright 2017 Cengage Learning. All Rights Reserved. May not be copied, scanned, or duplicated, in whole or in part. Due to electronic rights, some third party content may be suppressed from the eBook and/or eChapter(s). Editorial review has deemed that any suppressed content does not materially affect the overall learning experience. Cengage Learning reserves the right to remove additional content at any time if subsequent rights restrictions require it.

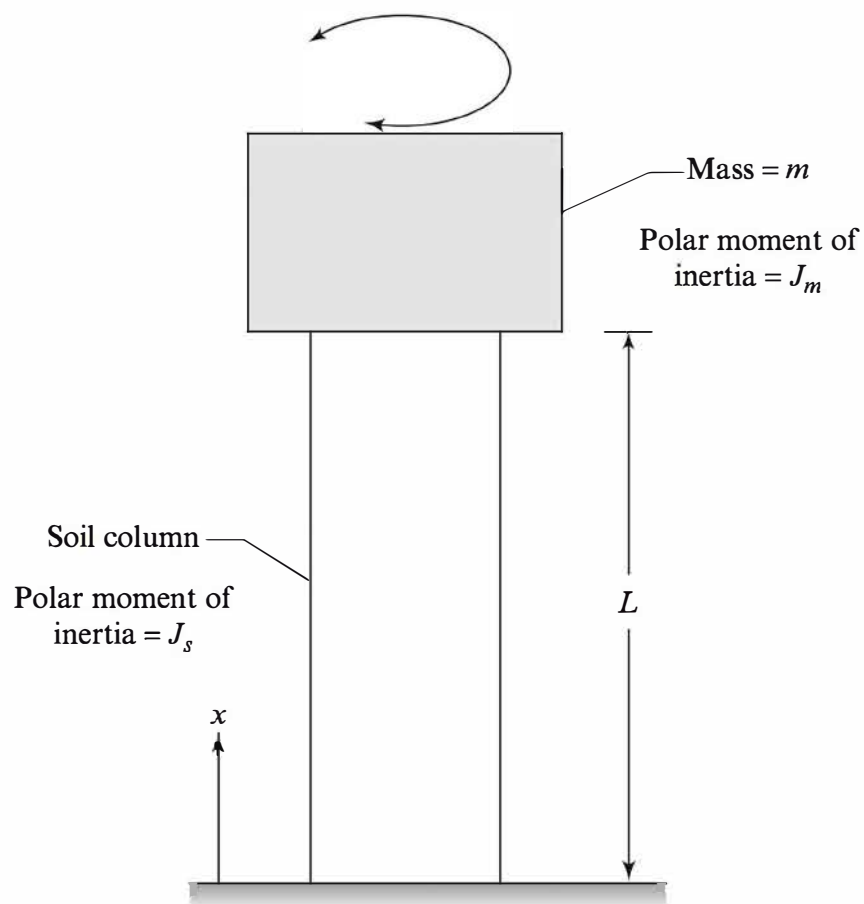

Figure 4.15 Derivation of Eq. (4.23)

where J_s = mass polar moment of inertia of the soil specimen and J_m = mass polar moment of inertia of the attachments with mass m.

Thus

$$v_s = \frac{\omega_n L}{\alpha} = \frac{2\pi f_n L}{\alpha} \tag{4.24}$$

and

$$\boxed{G = \rho v_s^2 = 39.48\left(\frac{f_n^2 L^2}{\alpha^2}\right)\rho} \tag{4.25}$$

C. Recent Developments in Resonant Column Test Equipment

Figure 4.16 shows a recently developed fully automated resonant column assembly with a *quasi-fixed base and free top* (Werden et al., 2013). Unlike the fixed-free end condition shown in Figure 4.15, Figure 4.17 shows a schematic diagram for the *quasi-fixed base and free-top* condition. This type of resonant column device has a torque transducer attached between the specimen's bottom plate and the fixed base. The actual torque transmitted through the specimen can be directly measured by the torque transducer.

Copyright 2017 Cengage Learning. All Rights Reserved. May not be copied, scanned, or duplicated, in whole or in part. Due to electronic rights, some third party content may be suppressed from the eBook and/or eChapter(s). Editorial review has deemed that any suppressed content does not materially affect the overall learning experience. Cengage Learning reserves the right to remove additional content at any time if subsequent rights restrictions require it.

Figure 4.16 Photograph of a fully automated resonant column assembly (Courtesy of Geocomp Corporation, Acton, Massachusetts).

Source: Courtesy of Geocomp Corporation, Acton, Massachusetts

D. Typical Laboratory Test Results from Resonant Column Tests

Most of the laboratory test results obtained from resonant column tests are for *low amplitudes* of vibration. Low amplitudes of vibration mean strain amplitudes of the order of 10^{-4} or less.

Typical values of v_c and v_s with low amplitudes of vibration for No. 20–30 Ottawa sand compacted at a void ratio of about 0.55 are shown in Figures 3.13 and 3.14. These were conducted using the free–free and fixed–free types of resonant column device developed by Hardin and Richart (1963) and Hall and Richart (1963). Based on the results given in Figures 3.13 and 3.14, the following general conclusions can be drawn:

1. The values of v_c and v_s in soils increase with the increase of the effective average confining pressure $\bar{\sigma}_0$.

Copyright 2017 Cengage Learning. All Rights Reserved. May not be copied, scanned, or duplicated, in whole or in part. Due to electronic rights, some third party content may be suppressed from the eBook and/or eChapter(s). Editorial review has deemed that any suppressed content does not materially affect the overall learning experience. Cengage Learning reserves the right to remove additional content at any time if subsequent rights restrictions require it.

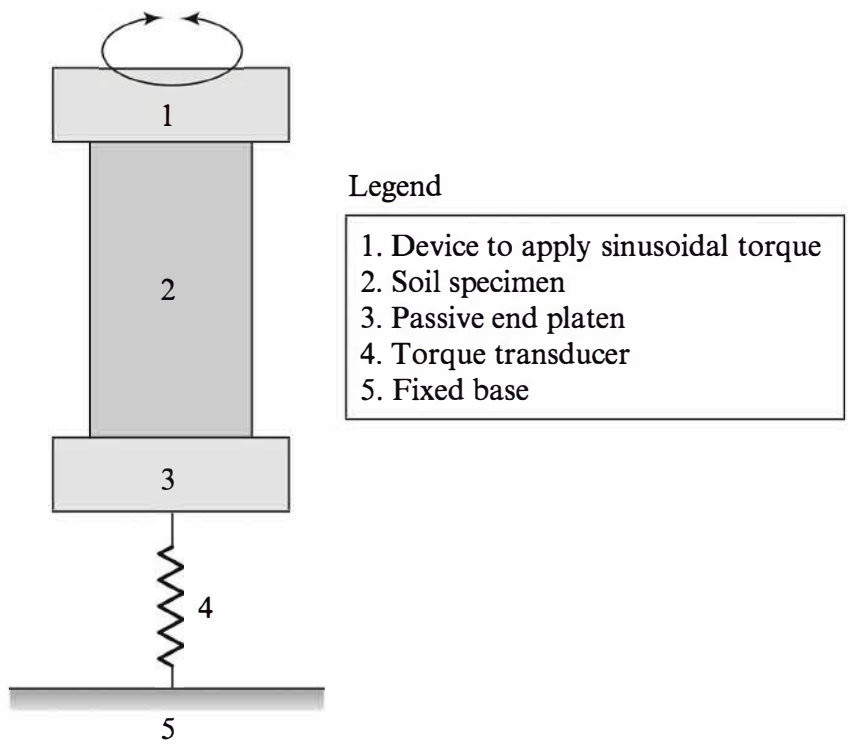

Figure 4.17 Schematic diagram showing quasi-fixed base and free-top condition for the soil specimen

2. The values of v_c and v_s for saturated soils are slightly lower than those for dry soils. This can be accounted for by the increase of the unit weight of soil due to the presence of water in the void spaces.

Hardin and Richart (1963) also reported the results of several resonant column tests conducted in dry Ottawa sand. The shear wave velocities determined from these tests are shown in Figure 4.18. The peak-to-peak shear strain amplitude for these tests was 10^{-3} rad. From Figure 4.18, it may be seen that the values of v_s are independent of the gradation, grain-size distribution, and also the relative density of compaction. However, v_s is dependent on the void ratio and the effective confining pressure.

E. Shear Modulus for Large Strain Amplitudes

For solid cylindrical specimens torsionally excited by resonant column devices, the shear strain varies from *zero at the center to a maximum at the periphery*, and it is difficult to evaluate a representative strain. For that reason, hollow cylindrical soil specimens in a resonant column device (Drnevich, Hall, and Richart, 1966, 1967) may be used to determine the shear modulus and damping at large strain amplitudes. Figure 4.19 shows a schematic diagram of this type of apparatus, in which the average shearing strain in the soil specimen is not greatly different from the maximum to the minimum. The variation of the shear modulus of dense C–190 Ottawa sand with the shear strain amplitude γ' is shown in Figure 4.20. Note that the value of G decreases with γ', but it decreases more

Copyright 2017 Cengage Learning. All Rights Reserved. May not be copied, scanned, or duplicated, in whole or in part. Due to electronic rights, some third party content may be suppressed from the eBook and/or eChapter(s). Editorial review has deemed that any suppressed content does not materially affect the overall learning experience. Cengage Learning reserves the right to remove additional content at any time if subsequent rights restrictions require it.

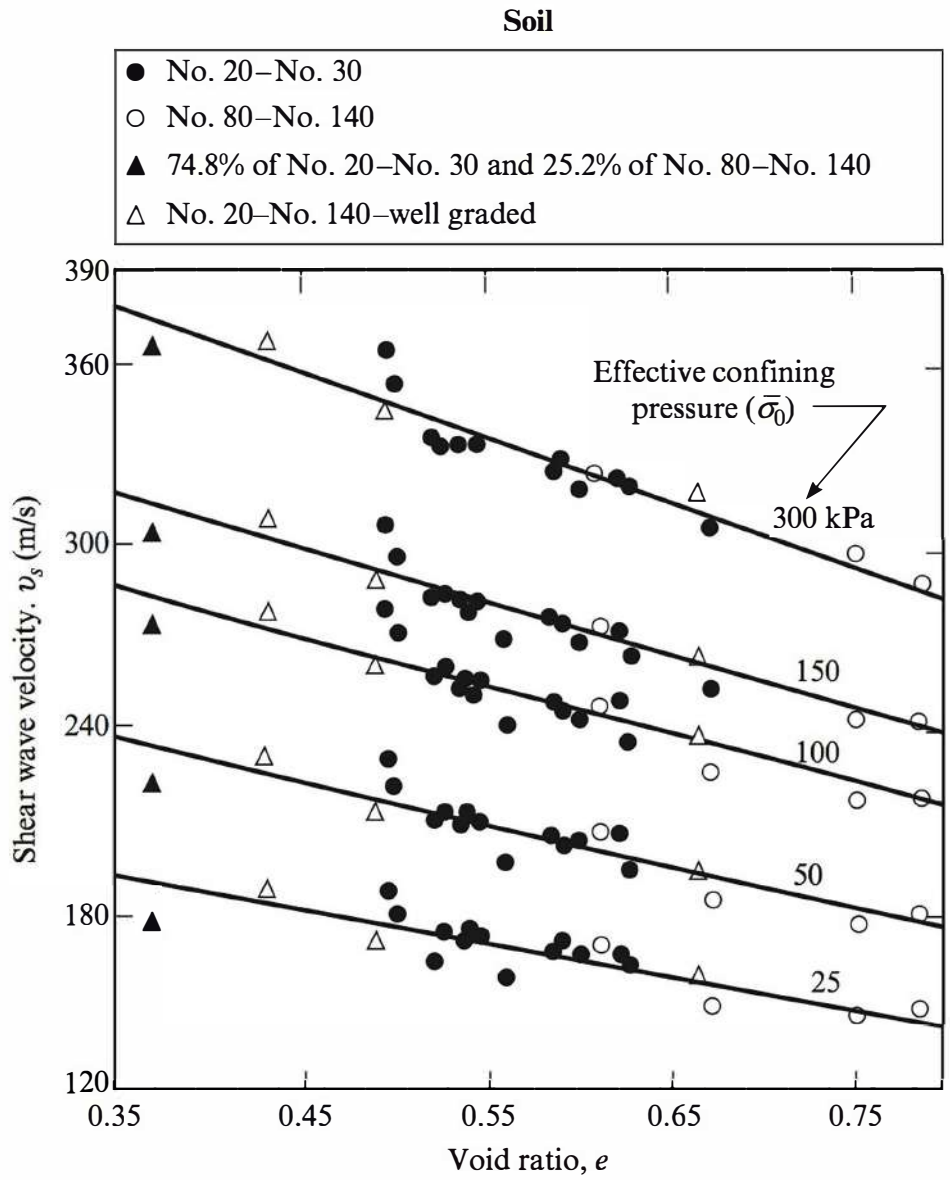

Figure 4.18 Variation of shear wave velocity with effective confining pressure $\bar{\sigma}_0$ for round-grained dry Ottawa sand (after Hardin and Richart, 1963)

Source: Hardin, B. O., and Richard, F. E., Jr. (1963). "Elastic Wave Velocity in Granular Soils," *Journal of the Soil Mechanics and Foundations Division*, ASCE, Vol. 89, No. SM1, pp. 33–65. With permission from ASCE.

rapidly for $\gamma' > 10^{-4}$. This is true for all soils. The reason for this can be explained by the use of Figure 4.21, which is shear-stress-versus-strain diagram for a soil. The stress-strain relationships of soils are curvilinear. The shear modulus that is experimentally determined is the secant modulus obtained by joining the extreme points on the hysteresis loop. Note that when the amplitude of strain is small (that is, $\gamma' = \gamma'_1$; Figure 4.21), the value of G is larger compared to that for the larger strain level (that is, $\gamma' = \gamma'_2$).

F. Effect on Prestraining on the Shear Modulus of Soils

The effect of shear modulus of soils due to prestraining was reported by Drnevich, Hall, and Richart (1967). These tests were conducted using C–190 Ottawa sand specimens. The specimens were first vibrated at a large amplitude for a certain number of cycles under a constant effective confining pressure ($\bar{\sigma}_0$).

Copyright 2017 Cengage Learning. All Rights Reserved. May not be copied, scanned, or duplicated, in whole or in part. Due to electronic rights, some third party content may be suppressed from the eBook and/or eChapter(s). Editorial review has deemed that any suppressed content does not materially affect the overall learning experience. Cengage Learning reserves the right to remove additional content at any time if subsequent rights restrictions require it.

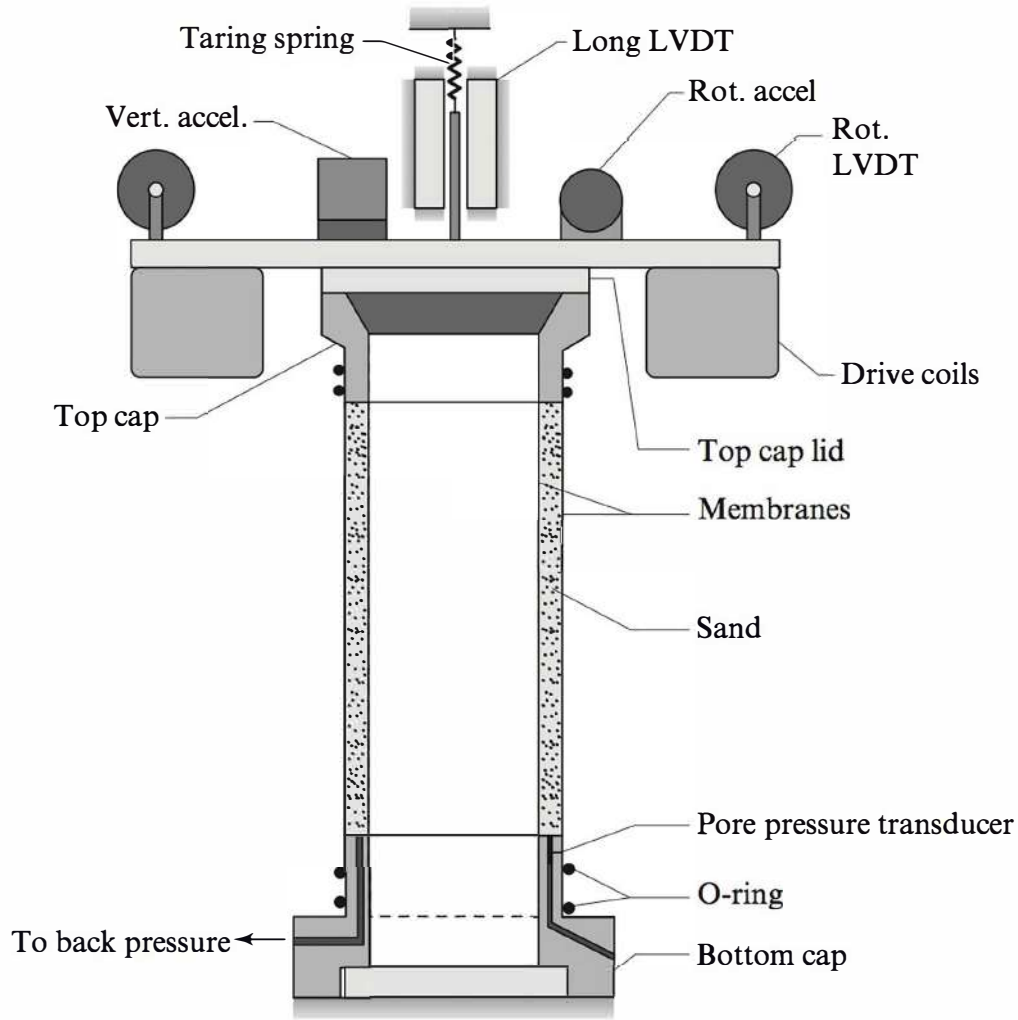

Figure 4.19 Schematic diagram of hollow-specimen resonant column device (after Drnevich, 1972).

Source: Drnevich, V.P. (1972). "Undrained Cyclic Shear of Saturated Sand," *Journal of the Soil Mechanics and Foundations Division*, ASCE, Vol. 98, No. SM8, pp. 807–825. With permission from ASCE.

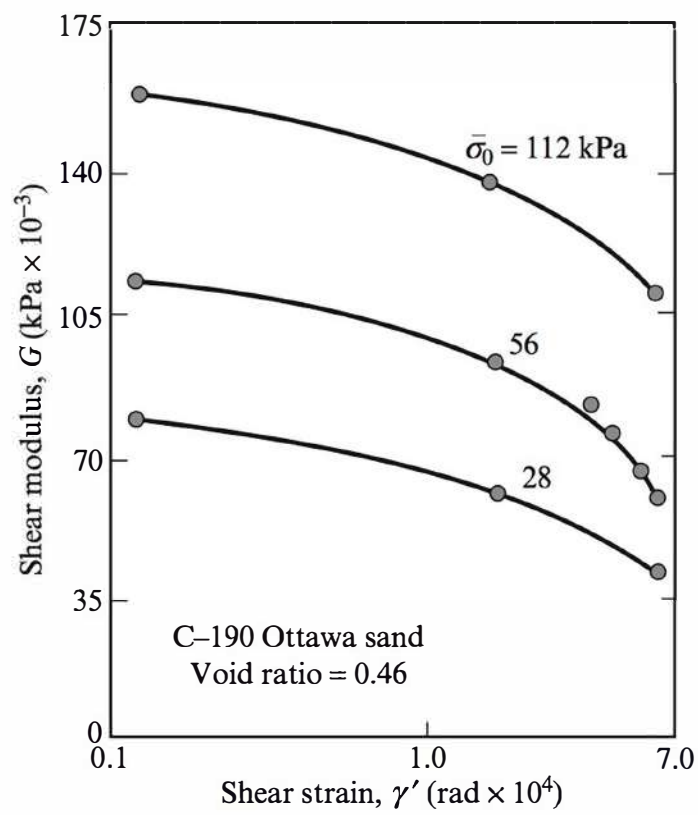

Figure 4.20 Effect of strain amplitude on shear modulus of sand (after Drnevich, Hall, and Richart, 1967)

Source: Drnevich, V.P., Hail, J.R., Jr., and Richart, F.E. Jr. (1967). "Effects of the Amplitude of Vibration on the Shear Modulus of Sand," *Proceedings, International Symposium on Wave Propagation and Dynamic Properties of Earth Materials*, University of New Mexico Press, pp. 189–199.

Copyright 2017 Cengage Learning. All Rights Reserved. May not be copied, scanned, or duplicated, in whole or in part. Due to electronic rights, some third party content may be suppressed from the eBook and/or eChapter(s). Editorial review has deemed that any suppressed content does not materially affect the overall learning experience. Cengage Learning reserves the right to remove additional content at any time if subsequent rights restrictions require it.

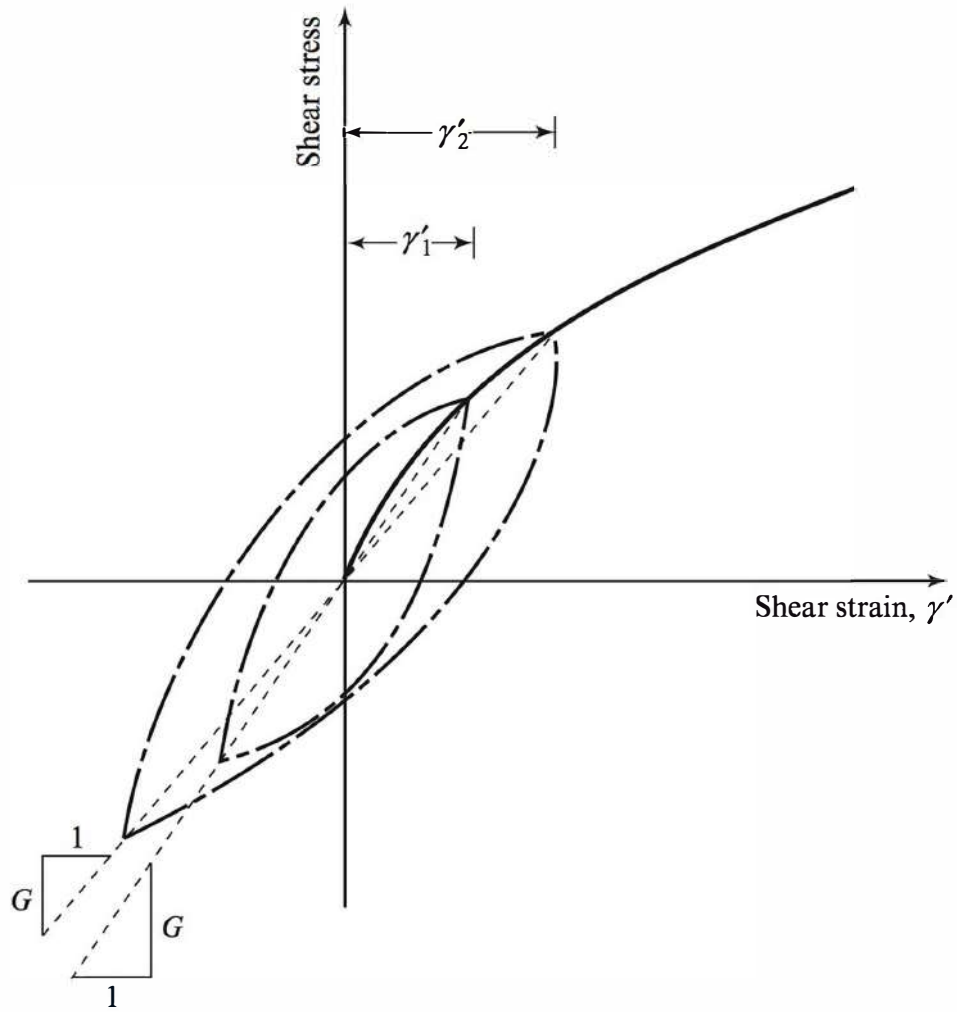

Figure 4.21 Nature of variation of shear stress versus shear strain

After that the shear modulii were determined by torsionally vibrating the specimens at small amplitudes (shearing strain $< 10^{-5}$). Figure 4.22 shows the results of six series of this type of test for dense sand (void ratio = 0.46). In general, the value of G increases with increase of prestrain cycles.

G. Determination of Internal Damping

In Section 3.15, a distinction was made between *internal damping* and *material damping*. The internal damping of a soil specimen can be determined by resonant column tests.

In Chapter 2, the derivation of the expression for the logarithmic decrement was given as

$$\delta = \ln \frac{X_n}{X_{n+1}} = \frac{2\pi D}{1 - D^2} \tag{2.70}$$

where δ = logarithmic decrement
D = damping ratio.

The preceding equation is for the case of free vibration of a mass-spring-dashpot system. The damping ratio is given by the expression

Copyright 2017 Cengage Learning. All Rights Reserved. May not be copied, scanned, or duplicated, in whole or in part. Due to electronic rights, some third party content may be suppressed from the eBook and/or eChapter(s). Editorial review has deemed that any suppressed content does not materially affect the overall learning experience. Cengage Learning reserves the right to remove additional content at any time if subsequent rights restrictions require it.

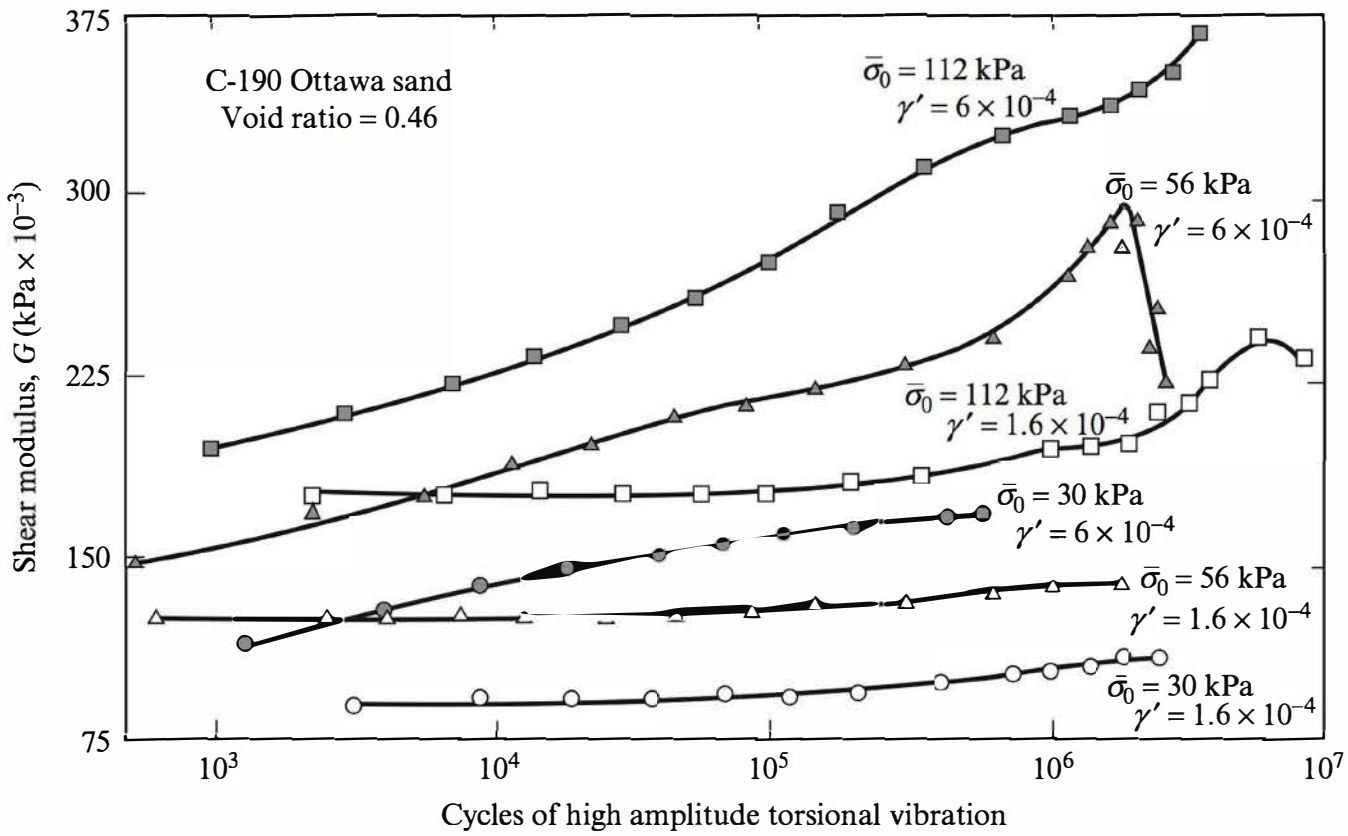

Figure 4.22 Effect of number of cycle of high-amplitude vibration on shear modulus determined at low amplitude (after Drnevich, Hall, and Richart, 1967)

Source: Drnevich, V.P., Hail, J.R., Jr., and Richart, F.E. Jr. (1967). "Effects of the Amplitude of Vibration on the Shear Modulus of Sand," *Proceedings, International Symposium on Wave Propagation and Dynamic Properties of Earth Materials*, University of New Mexico Press, pp. 189–199.

$$D = \frac{c}{c_{cr}} = \frac{c}{2\sqrt{km_s}} \tag{1.47b}$$

where m_s = mass of the soil specimen (in this case).

For soils, the value of D is small and Eq. (2.70) can be approximated as

$$\boxed{\delta = \ln \frac{X_n}{X_{n+1}} = 2\pi D} \tag{4.26}$$

Now, combining Eqs. (1.47b) and (4.26)

$$\delta = \frac{\pi c}{\sqrt{km_s}} \tag{4.27}$$

The logarithmic decrement of a soil specimen (and hence the damping ratio D) can easily be measured by using a fixed–free type resonant column device.

The soil specimen is first set into steady-state forced vibration. The driving power is then shut off, and the decay of the amplitude of vibration is plotted against the corresponding number of cycles. This plots as a straight line on a semilogarithmic graph paper, as shown in Figure 4.23. The logarithmic decrement can then be evaluated as

$$\delta_{\text{uncorrected}} = \left(\frac{1}{n}\right)\left(\ln \frac{X_0}{X_n}\right) \tag{4.28}$$

Copyright 2017 Cengage Learning. All Rights Reserved. May not be copied, scanned, or duplicated, in whole or in part. Due to electronic rights, some third party content may be suppressed from the eBook and/or eChapter(s). Editorial review has deemed that any suppressed content does not materially affect the overall learning experience. Cengage Learning reserves the right to remove additional content at any time if subsequent rights restrictions require it.

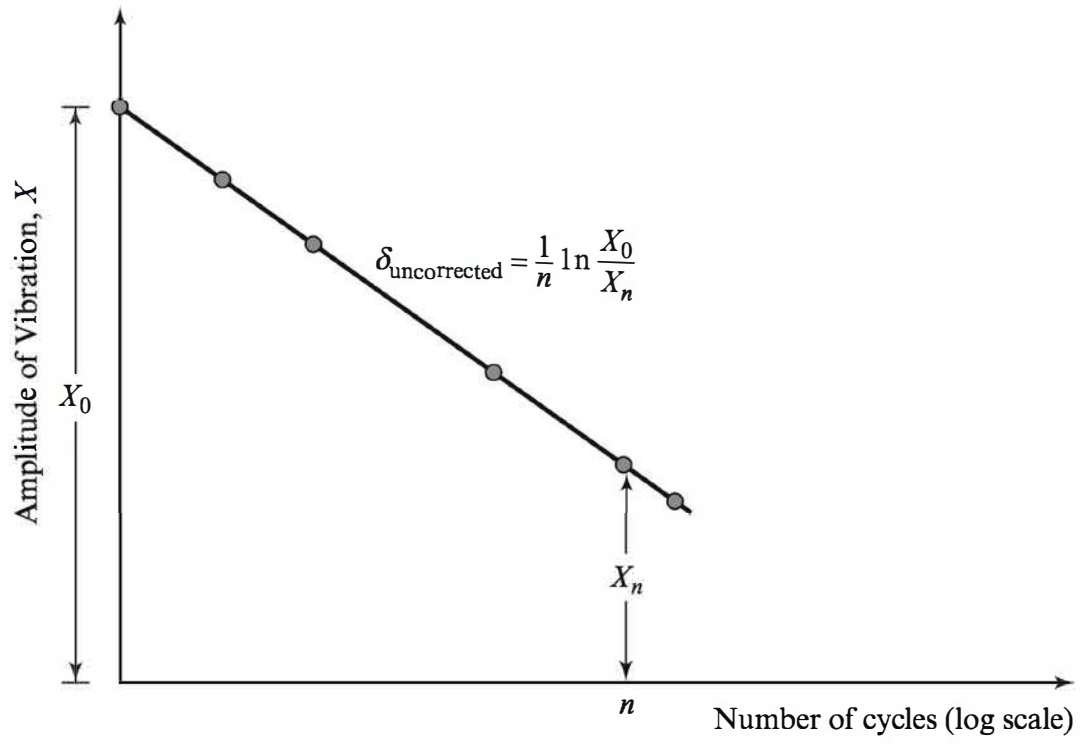

Figure 4.23 Plot of the amplitude of vibration against the corresponding number of cycles for determination of logarithmic decrement

However, in a fixed–free type of resonant column device, the driving and the motion–monitoring equipment is placed on the top of the specimen. Hence, for determination of the true logarithmic decrement of the soil specimen, a correction to Eq. (4.28) is necessary. This has been discussed by Hall and Richart (1963). Consider the case of longitudinal vibration of a soil column, as shown in Figure 4.24, in which m = mass of the attachments on the top of the soil specimen and m_s = mass of the soil specimen. With the addition of mass m, Eq. (4.27) can be modified as

$$\delta_{\text{uncorrected}} = \frac{\pi c}{\sqrt{k(m_s + m)}} \tag{4.29}$$

From Eqs. (4.27) and (4.29),

$$\frac{\delta}{\delta_{\text{uncorrected}}} = \sqrt{\frac{m_s + m}{m_s}} = \sqrt{1 + \frac{m}{m_s}} \tag{4.30}$$

In order to use Eq. (4.30), it will be required to convert the mass m_s into an equivalent concentrated mass. The equivalent concentrated mass can be shown to be equal to $0.405m_s$. Thus, replacing m_s in Equation (4.30) by $0.405m_s$,

$$\delta = \delta_{\text{uncorrected}} \sqrt{1 + \frac{m}{0.405m_s}} \tag{4.31}$$

A similar correction may be used for specimens subjected to torsional vibration, which will be of the form

Copyright 2017 Cengage Learning. All Rights Reserved. May not be copied, scanned, or duplicated, in whole or in part. Due to electronic rights, some third party content may be suppressed from the eBook and/or eChapter(s). Editorial review has deemed that any suppressed content does not materially affect the overall learning experience. Cengage Learning reserves the right to remove additional content at any time if subsequent rights restrictions require it.

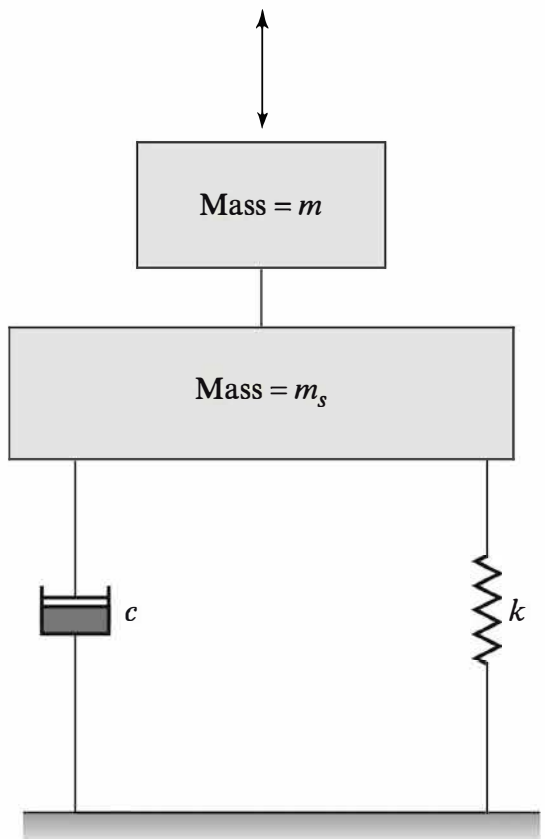

Figure 4.24 Fixed–free soil column

$$\delta = \delta_{\text{uncorrected}} \sqrt{1 + \frac{J_m}{0.405 J_s}}$$

Hardin (1965) suggested a relation for δ of *dry sand* in low amplitude torsional vibration as

$$\delta = 9\pi(\gamma')^{0.2}(\bar{\sigma}_0)^{-0.5} \tag{4.32}$$

Equation (4.32) is valid for $\gamma' = 10^{-6}$ to 10^{-4} and $\bar{\sigma}_0 = 24$ kPa to 144 kPa.

4.7 CYCLIC SIMPLE SHEAR TEST

A cyclic simple shear test is a convenient method for determining the shear modulus and damping ratio of soils. It is also a convenient device for studying the liquefaction parameters of saturated cohesionless soils (Chapter 10). In cyclic simple shear tests a soil specimen, usually 20–30 mm high with a side length (or diameter) of 60–80 mm, is subjected to a vertical effective stress $\bar{\sigma}_v$ and a cyclic shear stress τ, as shown in Figure 4.25. The horizontal load necessary to deform the specimen is measured by a load cell, and the shear deformation of the specimen is measured by a linear variable differential transformer.

Copyright 2017 Cengage Learning. All Rights Reserved. May not be copied, scanned, or duplicated, in whole or in part. Due to electronic rights, some third party content may be suppressed from the eBook and/or eChapter(s). Editorial review has deemed that any suppressed content does not materially affect the overall learning experience. Cengage Learning reserves the right to remove additional content at any time if subsequent rights restrictions require it.

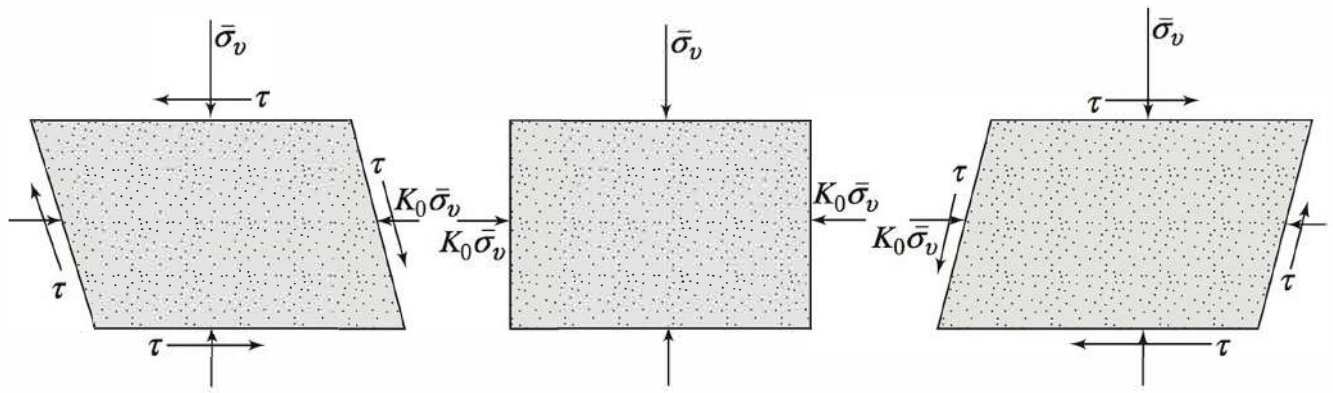

Figure 4.25 Cyclic simple shear test

The shear modulus of a soil in the cyclic simple shear test can be determined as

$$G = \frac{\text{amplitude of cyclic shear stress, } \tau}{\text{amplitude of cyclic shear strain, } \gamma'} \tag{4.33}$$

The damping ratio at a given shear strain amplitude can be obtained from the hysteretic stress-strain properties. Referring to Figure 4.26 (also see Figure 4.21), the damping ratio can be given as

$$D = \frac{1}{2\pi} \frac{\text{area of the hysteresis loop}}{\text{area of traingle } OAB \text{ and } OA'B'} \tag{4.34}$$

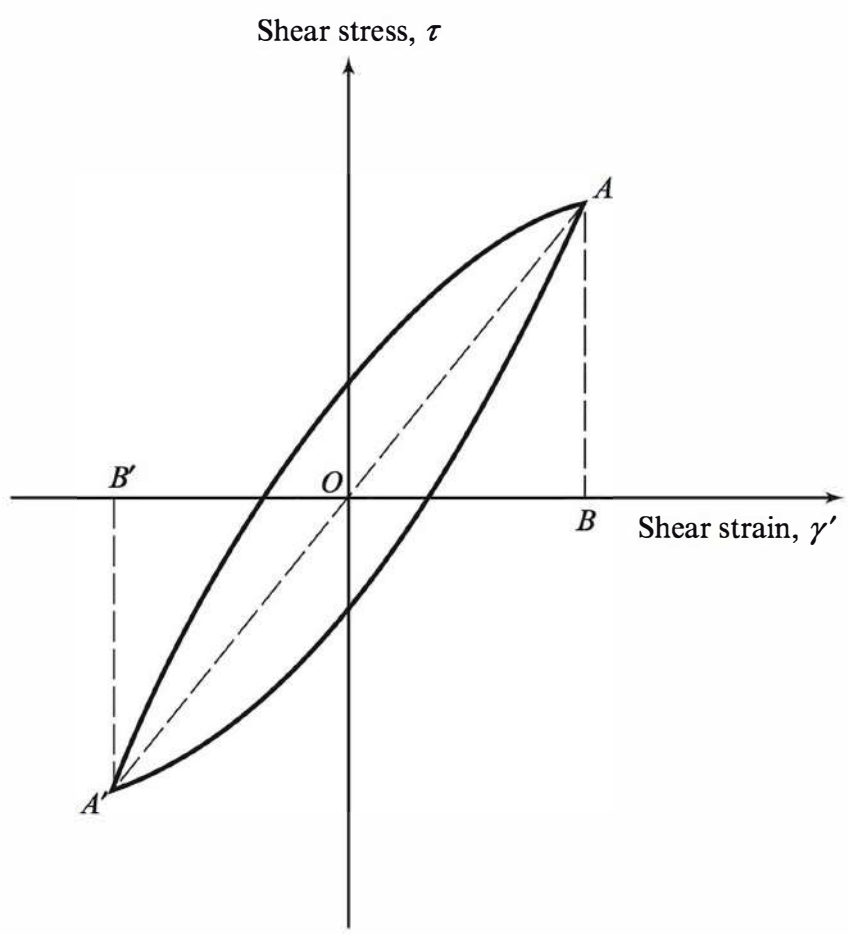

Figure 4.26 Determination of damping ratio from hysteresis loop [Eq. (4.34)]

Copyright 2017 Cengage Learning. All Rights Reserved. May not be copied, scanned, or duplicated, in whole or in part. Due to electronic rights, some third party content may be suppressed from the eBook and/or eChapter(s). Editorial review has deemed that any suppressed content does not materially affect the overall learning experience. Cengage Learning reserves the right to remove additional content at any time if subsequent rights restrictions require it.

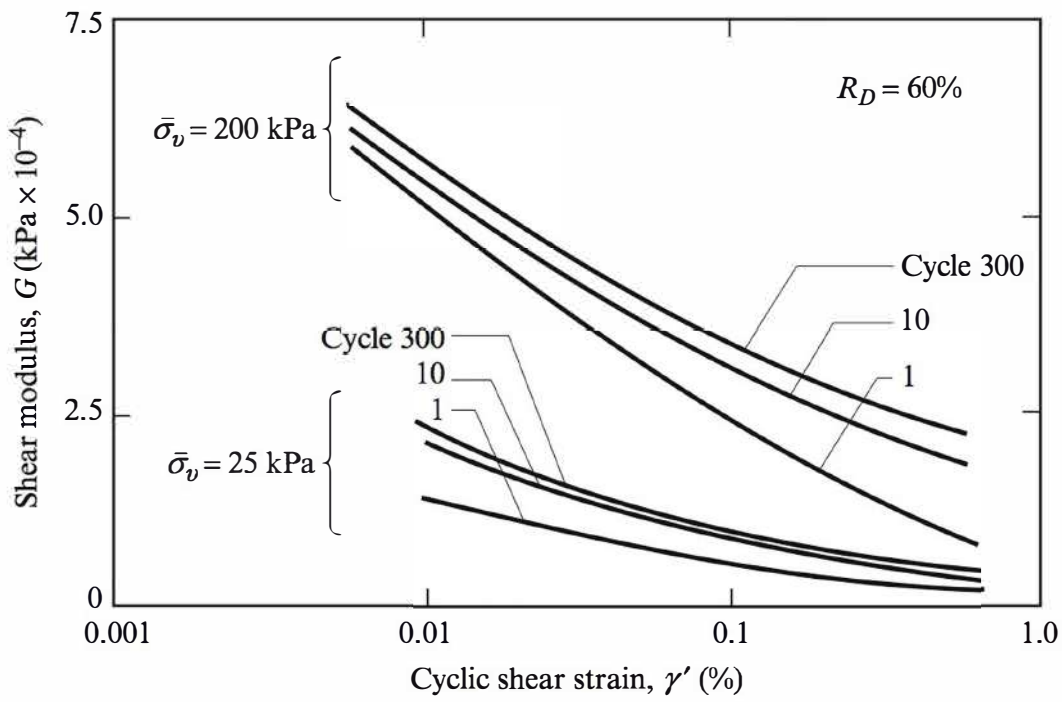

Figure 4.27 Shear modulus–shear strain relationship for medium dense sand (after Silver and Seed, 1971)

Source: Silver, M.L., and Seed, H.B. (1971). "Deformation Characteristics of Sands Under Cyclic Loading," *Journal of the Soil Mechanics and Foundation Division*, ASCE, Vol. 94, No. SM8, pp. 1081–1098. With permission from ASCE.

Figure 4.27 shows a plot of shear modulus G with cyclic shear strain γ' for two values of $\bar{\sigma}_v$ (Silver and Seed, 1971) obtained from cyclic simple shear tests on a medium dense sand (relative density, $R_D = 60\%$). From the results of this study, the following can be stated:

1. For a given value of γ' and $\bar{\sigma}_v$, the shear modulus increases with the number of cycles of shear stress application. Most of the increase in G takes place in the first ten cycles, after which the rate of increase is relatively small.
2. For a given value of $\bar{\sigma}_v$ and number of cycles of stress application, the magnitude of G decreases with the amplitude of shear strain γ'. (*Note:* Similar results are shown in Figure 4.20.)
3. For a given value of γ' and number of cycles, the magnitude of G increases with the increases of $\bar{\sigma}_v$.

The nature of the shear-stress-versus-shear-strain behavior of a dense sand under cyclic loading is shown in Figure 4.28. Using the hysteresis loops of this type and Eq. (4.34), the damping ratios obtained from a cyclic simple shear test for a medium dense sand are shown in Figure 4.29. Note the following:

1. For a given value of $\bar{\sigma}_v$ and amplitude of shear strain γ', the damping ratio decreases with the number of cycles. Since, in most seismic events, the number of significant cycles is likely to be less than 20 (Chapter 7), the values determined at 5 cycles are likely to provide reasonable values for all practical purposes.
2. For a given number of cycles and $\bar{\sigma}_v$, the magnitude of D decreases with the decrease of γ'.

Copyright 2017 Cengage Learning. All Rights Reserved. May not be copied, scanned, or duplicated, in whole or in part. Due to electronic rights, some third party content may be suppressed from the eBook and/or eChapter(s). Editorial review has deemed that any suppressed content does not materially affect the overall learning experience. Cengage Learning reserves the right to remove additional content at any time if subsequent rights restrictions require it.

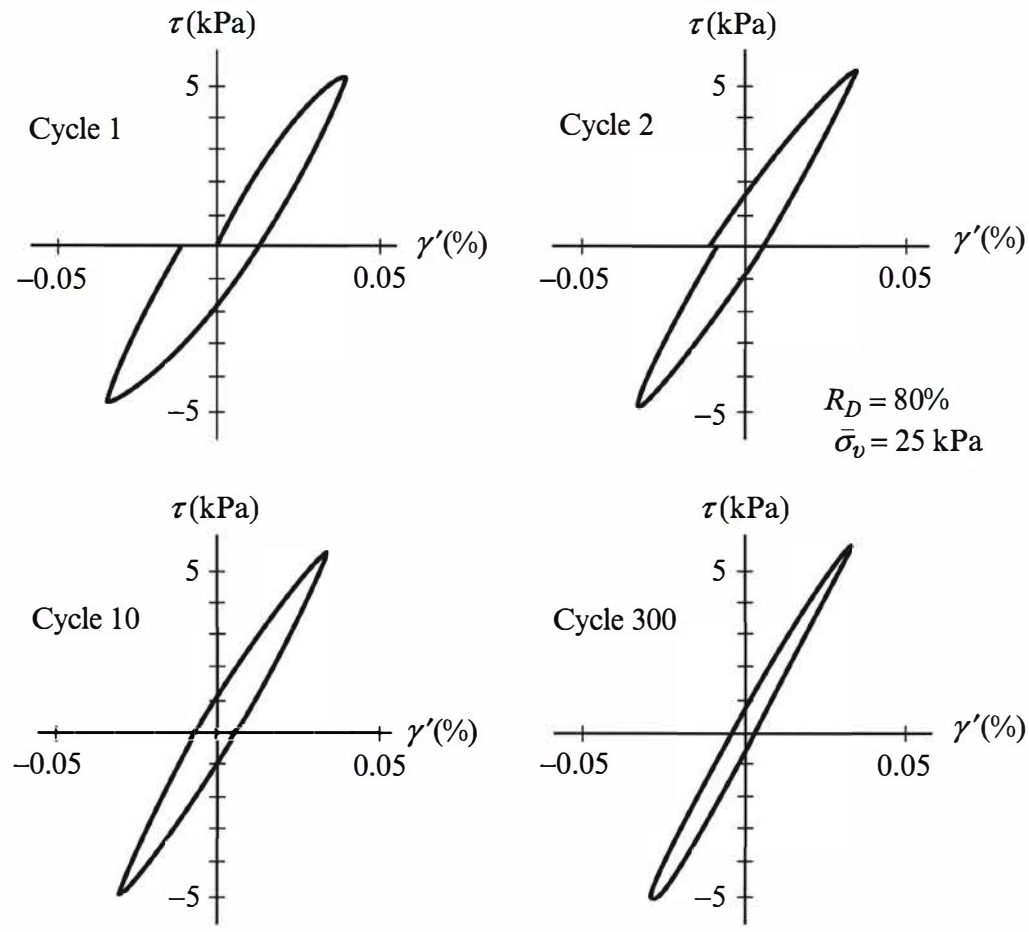

Figure 4.28 Stress-strain behavior of dense sand under cyclic shear (after Silver and Seed, 1971)

Source: Silver, M.L., and Seed, H.B. (1971). "Deformation Characteristics of Sands Under Cyclic Loading," *Journal of the Soil Mechanics and Foundation Division*, ASCE, Vol. 94, No. SM8, pp. 1081–1098. With permission from ASCE.

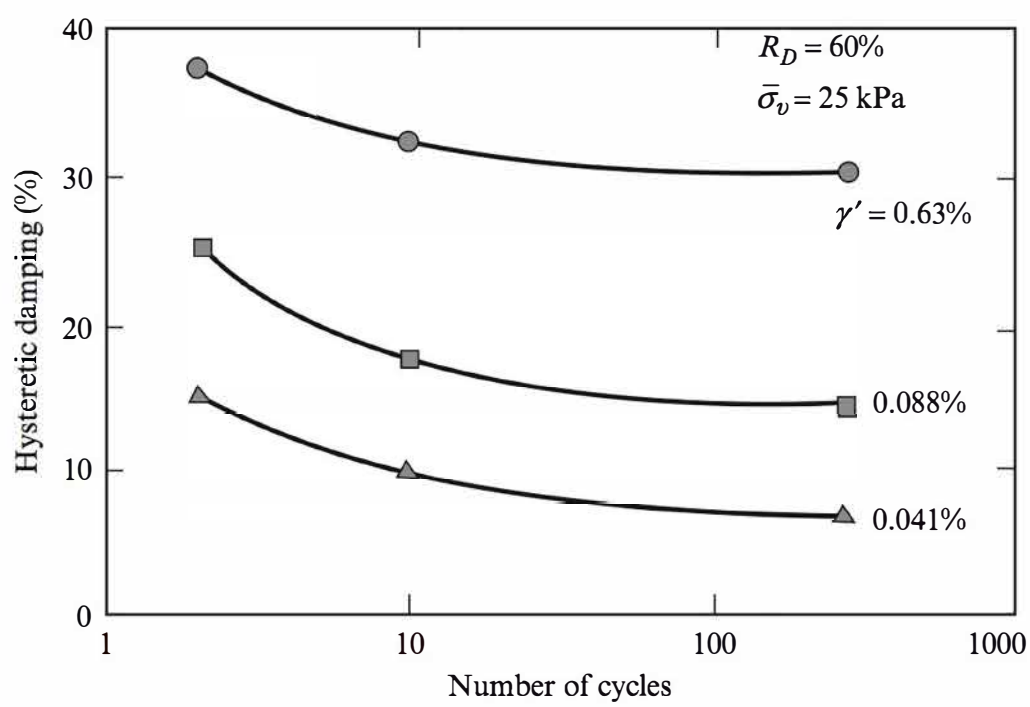

Figure 4.29 Effect of number of stress cycles on hysteretic damping for medium dense sand (after Silver and Seed, 1971)

Source: Silver, M.L., and Seed, H.B. (1971). "Deformation Characteristics of Sands Under Cyclic Loading," *Journal of the Soil Mechanics and Foundation Division*, ASCE, Vol. 94, No. SM8, pp. 1081–1098. With permission from ASCE.

Copyright 2017 Cengage Learning. All Rights Reserved. May not be copied, scanned, or duplicated, in whole or in part. Due to electronic rights, some third party content may be suppressed from the eBook and/or eChapter(s). Editorial review has deemed that any suppressed content does not materially affect the overall learning experience. Cengage Learning reserves the right to remove additional content at any time if subsequent rights restrictions require it.

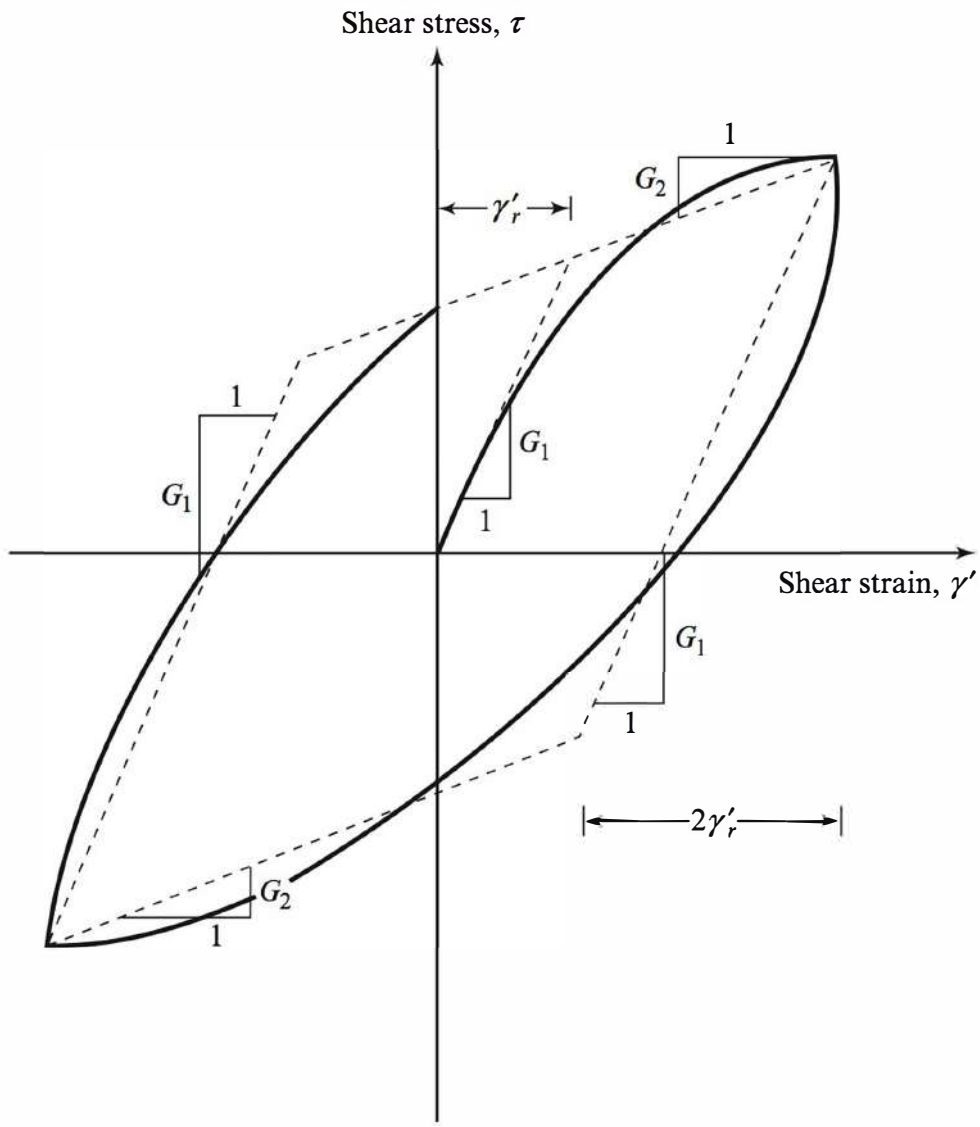

Figure 4.30 Bilinear idealization of shear-stress-versus-shear-strain plots

Other parameters remaining the same (that is, R_D, number of cycles, and amplitude of shear strain), a vertical stress increase will decrease the damping ratio. In many seismic analysis studies, it is convenient to represent the nonlinear shear-stress-versus-shear-strain relationship in the form of a bilinear model (also see Figure 7.10), as shown in Figure 4.30 (Thiers and Seed, 1968). In this figure G_1 is shear modulus up to a limiting strain of γ'_r and G_2 is the modulus for strain beyond γ'_r.

Advantages of the Cyclic Simple Shear Test

There are several advantages in conducting cyclic simple shear tests. They are more representative of the field conditions, since the specimens can be consolidated in K_0 state. Solid soil specimens used in resonant column tests can provide good results up to a shear strain amplitude of about $10^{-3}\%$. Similarly, the hollow samples used in resonant column studies provide results within a strain amplitude range of $10^{-3}\%$ to about 1%. However, cyclic simple shear tests can be conducted for a wider range of strain amplitude (that is, $10^{-2}\%$ to about 5%. This range is the general range of strain encountered in the ground motion during seismic activities.

The pore water pressure developed during the vibration of saturated soil specimens by a resonant column device is not usually measured. However, in cyclic

Copyright 2017 Cengage Learning. All Rights Reserved. May not be copied, scanned, or duplicated, in whole or in part. Due to electronic rights, some third party content may be suppressed from the eBook and/or eChapter(s). Editorial review has deemed that any suppressed content does not materially affect the overall learning experience. Cengage Learning reserves the right to remove additional content at any time if subsequent rights restrictions require it.

simple shear tests, the pore water pressure can be measured at the boundary (see Section 10.10 and Figure 10.20).

4.8 CYCLIC TORSIONAL SIMPLE SHEAR TEST

Another technique used to study the behavior of soils subjected to cyclic loading involves a torsional simple shear device. The torsional simple shear device accommodates a "doughnut-like" specimen, as shown in Figure 4.31 (Ishibashi and Sherif, 1974). The specimen has outside and inside radii of $r_1 = 50.8$ mm and $r_2 = 25.4$ mm. The outside and inside heights of the specimen are $h_1 = 25.4$ mm and $h_2 = 12.7$ mm. The soil is initially subjected to a vertical effective stress $\bar{\sigma}_v$, an outside and inside horizontal effective stress of $\bar{\sigma}_h$, and a cyclic shear stress of τ (Figure 4.32). When a shear stress τ is applied, line AB moves to the position of $A'B'$ (Figure 4.32). So, the shearing strain is

$$\gamma'_A = \frac{r_1\theta}{h_1} \text{ and } \gamma'_B = \frac{r_2\theta}{h_2}$$

For uniform shear strain throughout the sample,

$$\gamma'_A = \gamma'_B$$

or

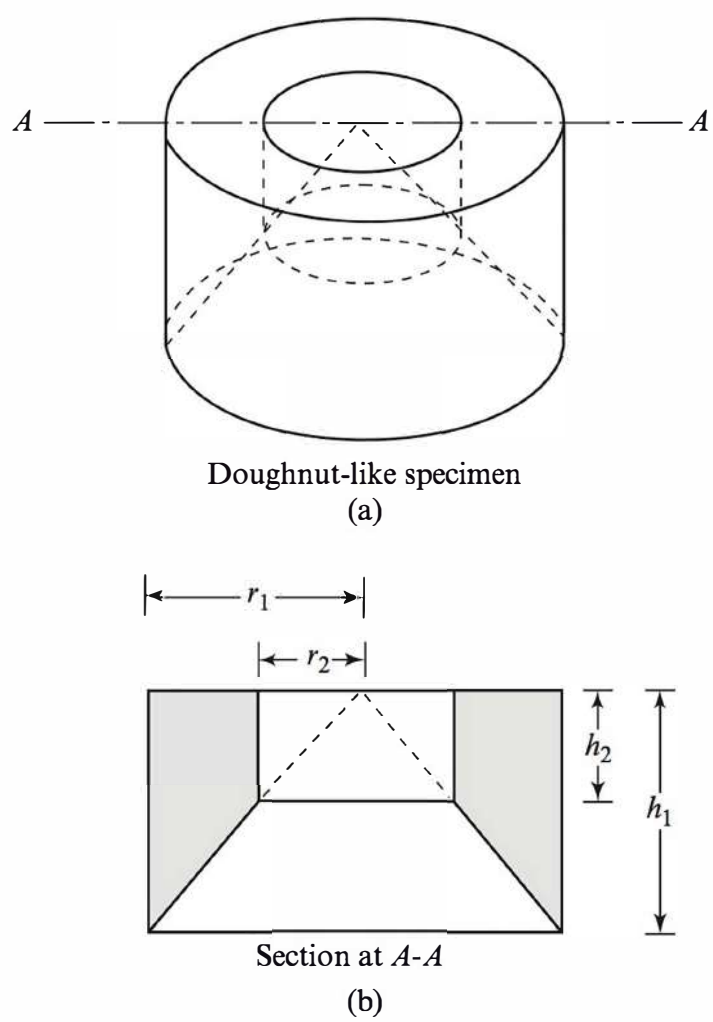

Figure 4.31 Soil specimen for torsional simple shear test

Copyright 2017 Cengage Learning. All Rights Reserved. May not be copied, scanned, or duplicated, in whole or in part. Due to electronic rights, some third party content may be suppressed from the eBook and/or eChapter(s). Editorial review has deemed that any suppressed content does not materially affect the overall learning experience. Cengage Learning reserves the right to remove additional content at any time if subsequent rights restrictions require it.

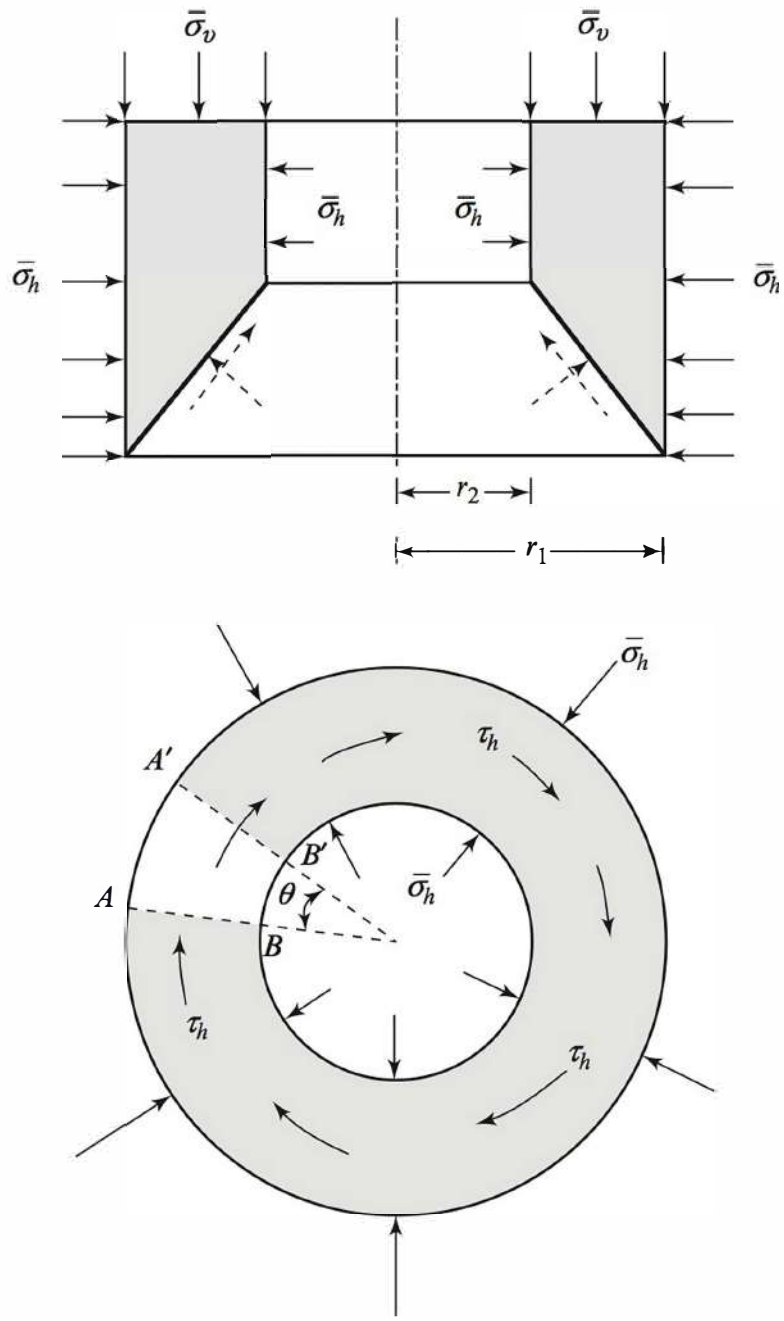

Figure 4.32 Applied stresses on a torsional simple shear test specimen

$$\frac{r_1\theta}{h_1} = \frac{r_2\theta}{h_2}$$

So

$$\boxed{\frac{r_1}{r_2} = \frac{h_1}{h_2}} \tag{4.35}$$

The following can be calculated after application of the horizontal shear stress on the specimen.

Major effective principal stress:

$$\bar{\sigma}_1 = \frac{\bar{\sigma}_v + \bar{\sigma}_h}{2} + \sqrt{\tau_h^2 + \left(\frac{\bar{\sigma}_v - \bar{\sigma}_h}{2}\right)^2} \tag{4.36a}$$

Copyright 2017 Cengage Learning. All Rights Reserved. May not be copied, scanned, or duplicated, in whole or in part. Due to electronic rights, some third party content may be suppressed from the eBook and/or eChapter(s). Editorial review has deemed that any suppressed content does not materially affect the overall learning experience. Cengage Learning reserves the right to remove additional content at any time if subsequent rights restrictions require it.

Intermediate effective principle stress:

$$\bar{\sigma}_2 = \bar{\sigma}_h \tag{4.36b}$$

Minor principal effective stress:

$$\bar{\sigma}_3 = \frac{\bar{\sigma}_v + \bar{\sigma}_h}{2} - \sqrt{\tau_h^2 + \left(\frac{\bar{\sigma}_v - \bar{\sigma}_h}{2}\right)^2} \tag{4.36c}$$

With proper design [Eq. (4.35)], a cyclic torsional shear device can apply near uniform shear strain on the specimen. It can apply shear strains up to about 1%. It also eliminates any sidewall frictional stresses that are encountered in cyclic simple shear tests.

The shear modulus of a specimen tested can be determined as

$$G = \frac{\text{amplitude of shear stress, } \tau}{\text{amplitude of shear strain, } \gamma'}$$

The damping ratio corresponding to a given shear strain amplitude can be determined by using Figure 4.21 and Eq. (4.34).

Liquefaction studies on saturated granular soils can also be conducted by this device along with pore water pressure measurement.

4.9 CYCLIC TRIAXIAL TEST

Cyclic triaxial tests can be performed to determine the modulus of elasticity E and the damping ratio D of soils. In these tests, in most cases, the soil specimen is subjected to a confining pressure $\sigma_0 = \sigma_3$. After that, an axial cyclic stress $\Delta\sigma_d$ is applied to the specimen, as shown in Figure 4.33. The tests conducted for the evaluation of the modulus of elasticity and damping ratio are *strain-controlled* tests. A servo-system is used to apply cycles of controlled deformation.

Figure 4.34 shows the nature of a hysteresis loop obtained from a dynamic triaxial test. From this,

$$E = \frac{\Delta\sigma_d}{\varepsilon}$$

Once the magnitude of E is determined, the value of shear modulus can be calculated by assuming a representative value of Poisson's ration, or

$$G = \frac{E}{2(1+\mu)}$$

Again referring to Figure 4.34, the damping ratio can be calculated as

$$D = \frac{1}{2\pi} \frac{\text{area of the hysteresis loop}}{\text{area of triangle } OAB \text{ and } OA'B'}$$

Copyright 2017 Cengage Learning. All Rights Reserved. May not be copied, scanned, or duplicated, in whole or in part. Due to electronic rights, some third party content may be suppressed from the eBook and/or eChapter(s). Editorial review has deemed that any suppressed content does not materially affect the overall learning experience. Cengage Learning reserves the right to remove additional content at any time if subsequent rights restrictions require it.

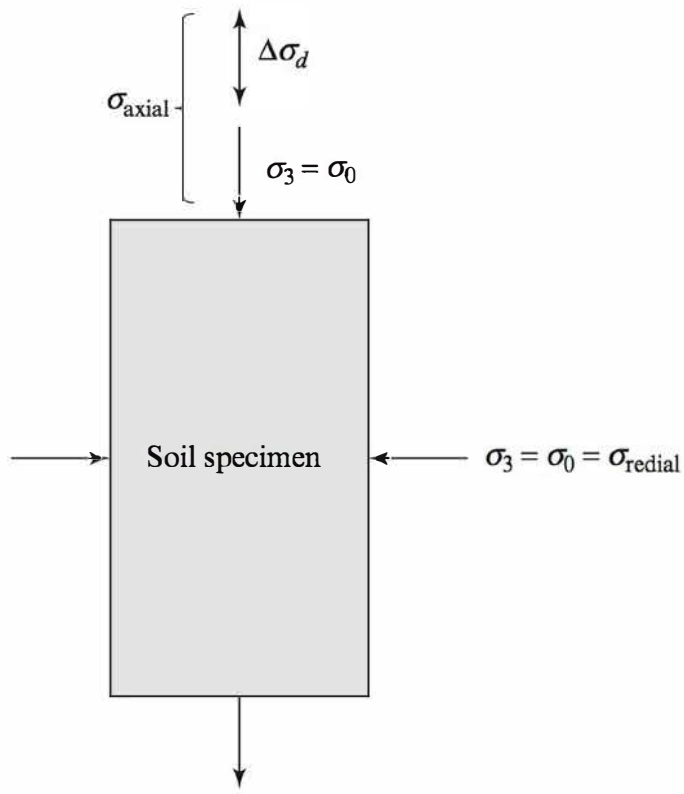

Figure 4.33 Cyclic triaxial test

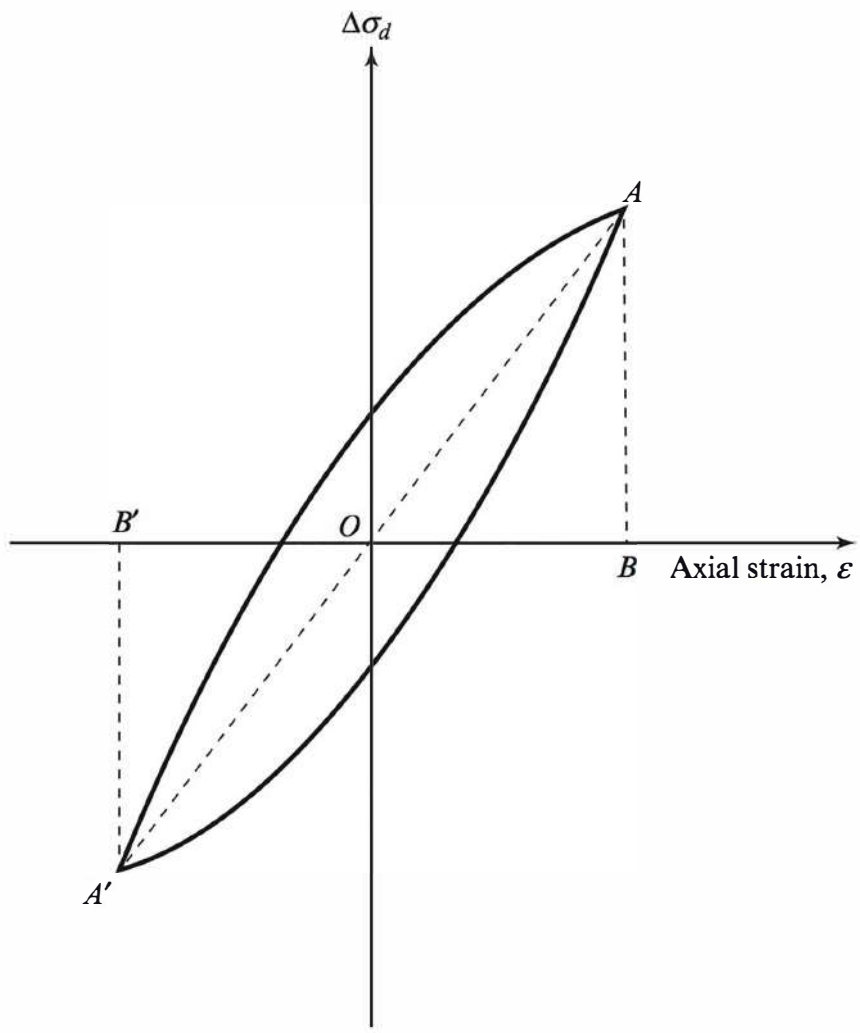

Figure 4.34 Determination of damping ratio from cyclic triaxial test

Copyright 2017 Cengage Learning. All Rights Reserved. May not be copied, scanned, or duplicated, in whole or in part. Due to electronic rights, some third party content may be suppressed from the eBook and/or eChapter(s). Editorial review has deemed that any suppressed content does not materially affect the overall learning experience. Cengage Learning reserves the right to remove additional content at any time if subsequent rights restrictions require it.

Stress-controlled dynamic triaxial tests are used for liquefaction studies on saturated granular soils (see Chapter 10).

A more elaborate type of dynamic test device has also been used by several investigators to study the cyclic stress-strain history and shear characteristics of soils. Matsui, Ohara, and Ito (1980) used a dynamic triaxial system that could generate sinusoidally varying axial and radial stresses.

A. Cyclic Strength of Clay

During earthquakes, the soil underlying building foundations and in structures such as earth embankments, is subjected to a series of vibratory stress applications. These vibratory stresses may induce large deformation in soil and thus failure. In order to evaluate the strength of clay under earthquake loading conditions, Seed and Chan (1966) conducted a number of dynamic triaxial tests.

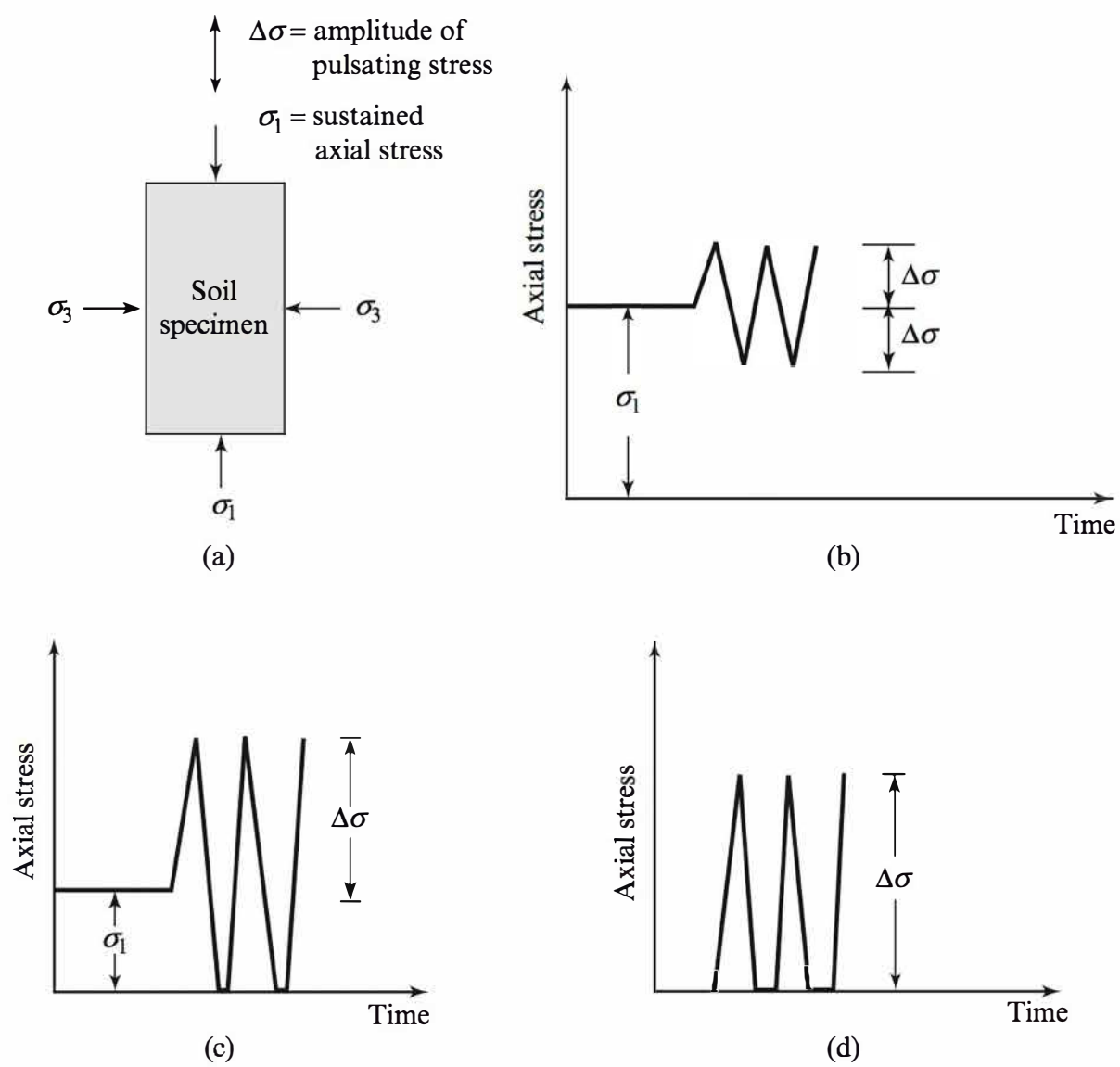

Figure 4.35 Stress conditions on a soil specimen

[*Note*: (b) One-directional loading with symmetrical stress pulses; (c) and (d) one-directional loading with nonsymmetrical stress pulses]

Copyright 2017 Cengage Learning. All Rights Reserved. May not be copied, scanned, or duplicated, in whole or in part. Due to electronic rights, some third party content may be suppressed from the eBook and/or eChapter(s). Editorial review has deemed that any suppressed content does not materially affect the overall learning experience. Cengage Learning reserves the right to remove additional content at any time if subsequent rights restrictions require it.

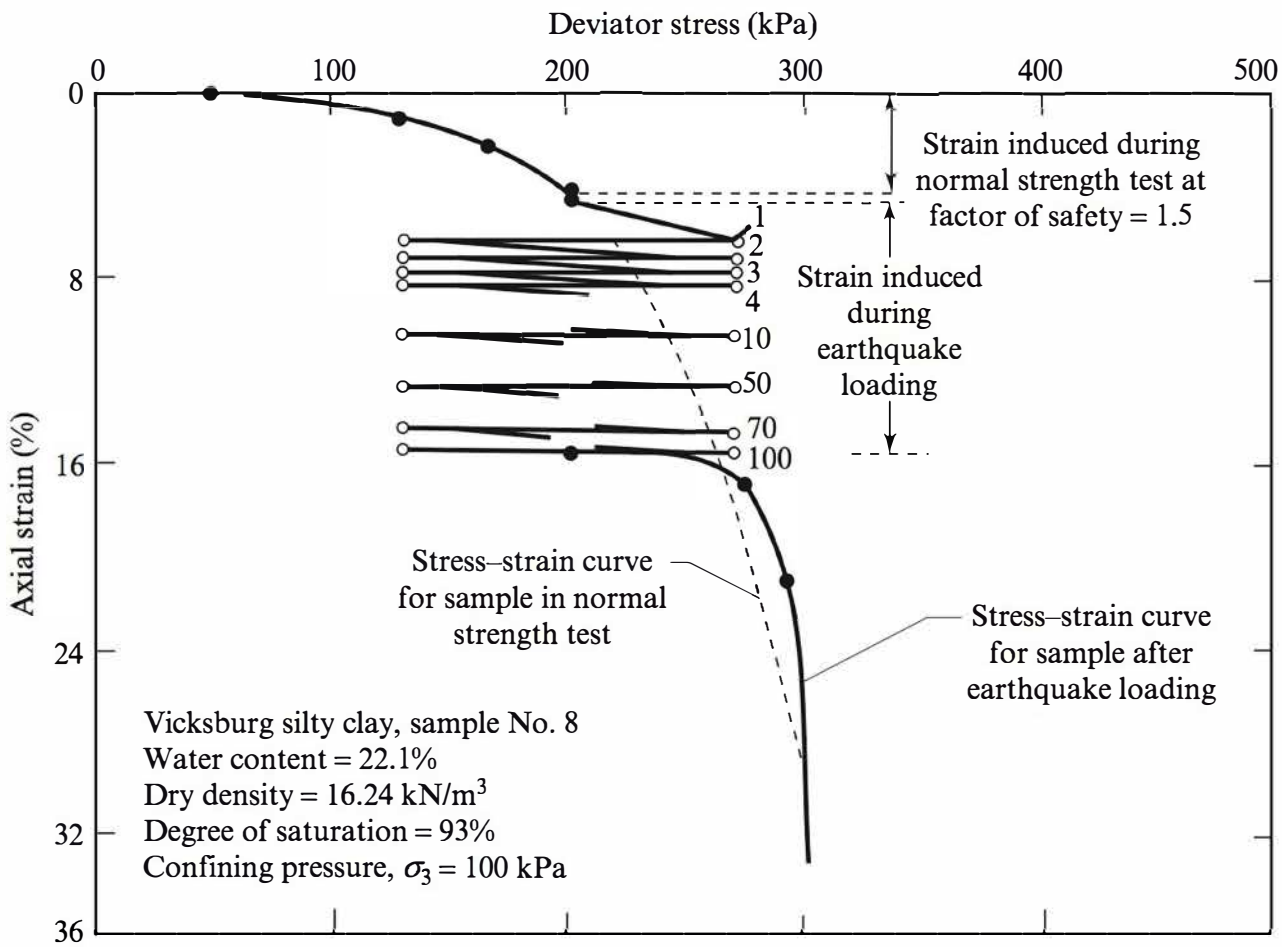

Figure 4.36 Stress-versus-strain relationship for Vicksburg silty clay under sustained and axial pulsating stress (after Seed and Chan, 1966)

Source: Seed, H.B., and Chan, C.K. (1966). "Clay Strength Under Earthquake Loading Conditions," *Journal of the Soil Mechanics and Foundation Division*, ASCE, Vol. 92, No. SM2, pp. 53–78. With permission from ASCE.

Figure 4.35 shows the nature of some of the stress conditions imposed on the soil specimens during those tests. The results of this study are very instructive and are described in some detail in this section.

Figure 4.36 shows the results of a laboratory test on a specimen of Vicksburg silty clay subjected to sustained and pulsating stresses. The specimen with a degree of saturation of 93% was initially subjected to a confining pressure of $\sigma_3 = 100$ kPa and then to a conventional axial loading in undrained conditions up to 66% of its static strength. This implies that the *sustained stress* $\sigma_1 - \sigma_3$ was equal to $0.66\,[\sigma_{1(f)} - \sigma_3]$, which corresponds to a factor of safety of 1.5. At this time the axial deformation of the specimen was about 5%. After that, 100 transient stress pulses were applied to the specimen. (*Note*: Loading type is similar to that shown in Figure 4.35b). These stress pulses induced an additional axial strain of about 11%, although the static strength was never exceeded.

Figure 4.37 shows the nature of soil deformation on three soil specimens of San Francisco Bay mud subjected to pulsating stress levels to 100%, 80%, and 60% of normal strength (that is, static strength). For these tests, *no sustained stress* was applied. (*Note*: Loading type is similar to that shown in Figure 4.35d.) It is worth noting that, for each level of pulsating stress, the specimen ultimately failed.

Copyright 2017 Cengage Learning. All Rights Reserved. May not be copied, scanned, or duplicated, in whole or in part. Due to electronic rights, some third party content may be suppressed from the eBook and/or eChapter(s). Editorial review has deemed that any suppressed content does not materially affect the overall learning experience. Cengage Learning reserves the right to remove additional content at any time if subsequent rights restrictions require it.

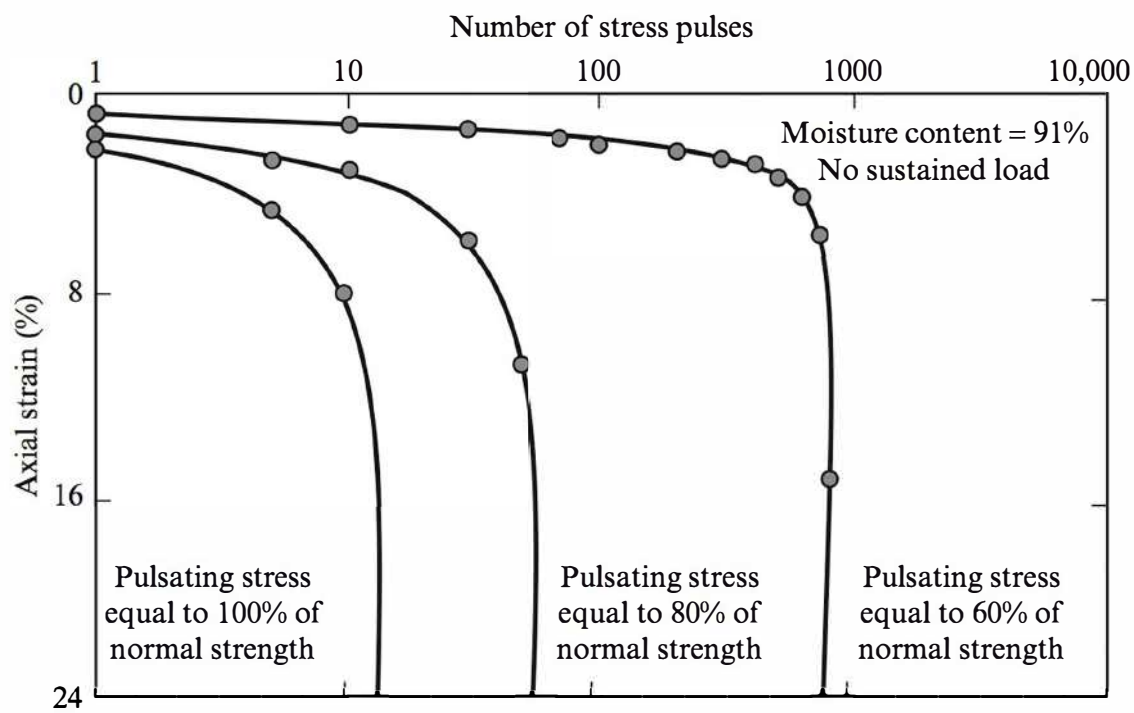

Figure 4.37 Deformation of San Francisco Bay mud specimens subjected to pulsating stress (after Seed and Chan, 1966)

Source: Seed, H.B., and Chan, C.K. (1966). "Clay Strength Under Earthquake Loading Conditions," Journal of the Soil Mechanics and Foundation Division, ASCE, Vol. 92, No. SM2, pp. 53–78. With permission from ASCE.

Figure 4.38 is a plot of the pulsating stress level (as a percent of normal strength) versus sustained stress level (as a percent of normal strength) causing failure of San Francisco Bay mud at various numbers of transient stress pulses. As the number of stress pulses are increasing at the same pulsating stress level, the sustained stress level inducing failure is decreasing. The interested readers should refer to the original paper by Seed and Chan (1966). Similar plots could be developed for various soils to help in the design procedure of various structures.

4.10 SUMMARY OF CYCLIC TESTS

In the preceding sections, various types of laboratory test methods were presented, from which the fundamental soil properties such as the shear modulus, modulus of elasticity, and damping ratio are determined. These parameters are used in the design and evaluation of the behavior of earthen, earth-supported, and earth-retaining structures. As was discussed in the preceding sections, the magnitudes of G and D are functions of the shear strain amplitude γ'. Hence, while selecting the values of G and D for a certain design work, it is essential to know the following:

a. Type of test from which the parameters can be obtained
b. Magnitude of the shear–strain amplitude at which these parameters needs to be measured

Copyright 2017 Cengage Learning. All Rights Reserved. May not be copied, scanned, or duplicated, in whole or in part. Due to electronic rights, some third party content may be suppressed from the eBook and/or eChapter(s). Editorial review has deemed that any suppressed content does not materially affect the overall learning experience. Cengage Learning reserves the right to remove additional content at any time if subsequent rights restrictions require it.

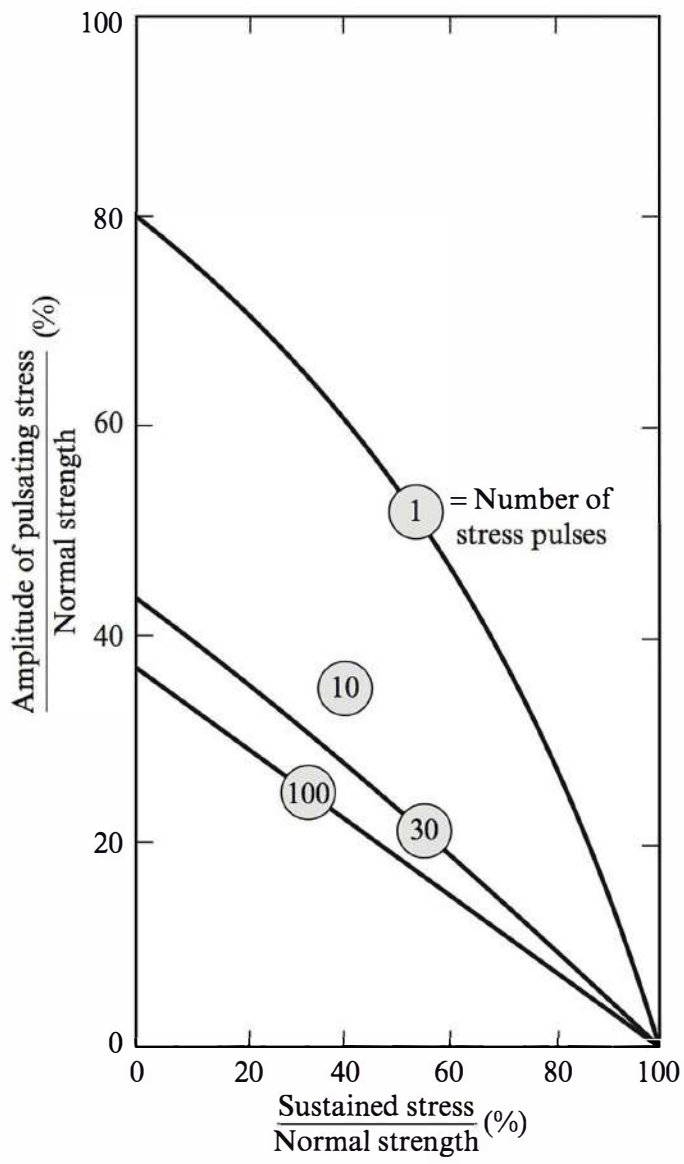

Figure 4.38 Combinations of sustained and pulsating stress intensities causing failure—San Francisco Bay mud (after Seed and Chan, 1966)

Source: Seed, H.B., and Chan, C.K. (1966). "Clay Strength Under Earthquake Loading Conditions," Journal of the Soil Mechanics and Foundation Division, ASCE, Vol. 92, No. SM2, pp. 53–78. With permission from ASCE.

For example, strong ground motion and nuclear explosion can develop large strain amplitudes whereas some sensitive equipment such as electron microscopes may be very sensitive to small strain amplitudes.

Figure 4.39 provides is a useful reference table for geotechnical engineers, as it gives the amplitude of shear–strain levels, type of applicable dynamic tests, and the area of applicability of these test results. Despite the fact that laboratory testing is not ideal, it will continue to be important because soil conditions can be better controlled in the laboratory. Parametric studies necessary for understanding the soil behaviour of soils under dynamic loading conditions must be performed in the laboratory conditions. Table 4.2 provides a comparison of the relative qualities (what property can be measured and what is the degree of quality of the measured property) of various laboratory techniques for measuring dynamic soil properties. Similarly, Table 4.3 gives a summary of the different engineering parameters that can be measured in different dynamic or cyclic laboratory tests.

Copyright 2017 Cengage Learning. All Rights Reserved. May not be copied, scanned, or duplicated, in whole or in part. Due to electronic rights, some third party content may be suppressed from the eBook and/or eChapter(s). Editorial review has deemed that any suppressed content does not materially affect the overall learning experience. Cengage Learning reserves the right to remove additional content at any time if subsequent rights restrictions require it.

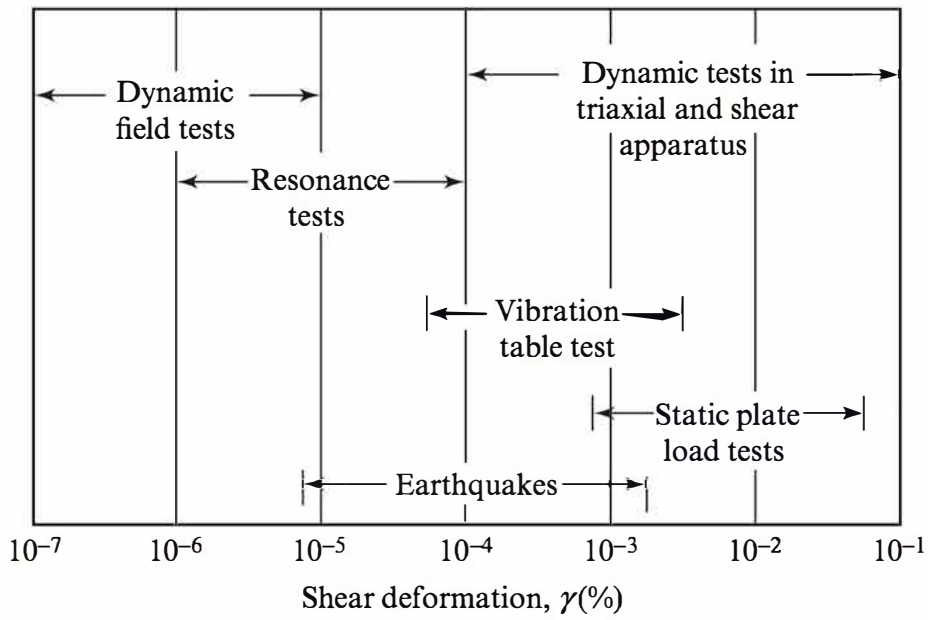

Figure 4.39 Range and applicability of dynamic laboratory tests

Table 4.2 Relative Quality of Laboratory Techniques for Measuring Dynamic Soil Properties[a]

	Relative Quality of Test Results				
	Shear modulus	**Young's modulus**	**Material damping**	**Effect of number of cycles**	**Attenuation**
Resonant column	Good	Good	Good	Good	-
with application	-	-	-	-	Fair
Ultrasonic pulse	Fair	Fair	-	-	Poor
Cyclic triaxial	-	Good	Good	Good	-
Cyclic simple shear	Good	-	Good	Good	-
Cyclic torsional shear	Good	-	Good	Good	-

[a]After Silver (1981)

Source: Silver, M.L. (1981). "Load deformation and Strength Behavior of Soild under Dynamic Loading," *State-of-the-Art Paper, Proceedings, International Conference on Recent Advances in geotechnical Earthquake Engineering and Soil Dynamics* (Ed. Shamsher Prakash), Vol. 3, pp. 873–896.

Field Test Measurements

4.11 REFLECTION AND REFRACTION OF ELASTIC BODY WAVES—FUNDAMENTAL CONCEPTS

When an elastic stress wave impinges on the boundary of two layers, the wave is reflected and refracted. As has already been discussed in Chapter 3, there are two types of body waves—that is, compression waves (or *P*–waves) and shear waves (or *S*–waves). In the case of *P*–waves, the direction of the movements of

Copyright 2017 Cengage Learning. All Rights Reserved. May not be copied, scanned, or duplicated, in whole or in part. Due to electronic rights, some third party content may be suppressed from the eBook and/or Chapter(s). Editorial review has deemed that any suppressed content does not materially affect the overall learning experience. Cengage Learning reserves the right to remove additional content at any time if subsequent rights restrictions require it.

Table 4.3 Parameters Measured in Dynamic or Cyclic Laboratory Tests[a]

	Resonant column	Cyclic triaxial	Cyclic simple shear	Torsional shear
Load	**Resonant frequency**	**Axial force**	**Horizontal force**	**Torque**
Deformation				
Axial	Vertical displacement	Vertical displacement	Vertical displacement	Vertical displacement
Shear	Acceleration	Not measured	Horizontal displacement	Rotation
Lateral	Not usually measured	Not usually measured	Often controlled	Not usually measured
Volumetric	None for undrained tests			
	Volume of fluid moving into or out of the sample for drained tests			
Pore water pressure	Not usually measured	Measured at boundary	Measured at boundary	Measured at boundary

[a]After Silver (1981)

Source: Silver, M.L. (1981). "Load deformation and Strength Behavior of Soild under Dynamic Loading," *State-of-the-Art Paper, Proceedings, International Conference on Recent Advances in geotechnical Earthquake Engineering and Soil Dynamics* (Ed. Shamsher Prakash), Vol. 3, pp. 873–896.

the particles coincides with the direction of propagation. This is shown by the arrows in Figure 4.40a. The shear waves can be separated into two components:

a. *SV-waves*, in which the motion of the particles is in the plane of propagation as shown by the arrows in Figure 4.40b
b. *SH-waves*, in which the motion of the particles is perpendicular to the plane of propagation, as shown by a dark dot in Figure 4.40c

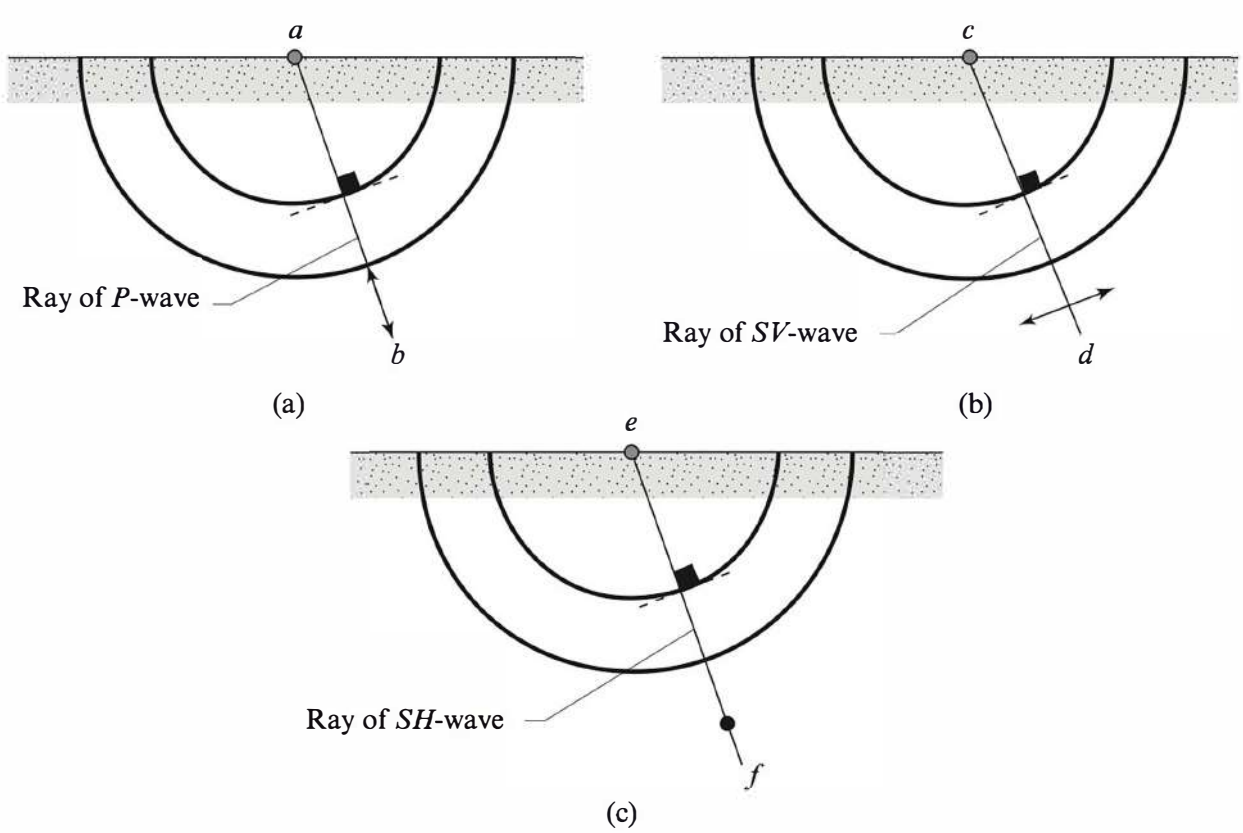

Figure 4.40 (a) *P*-wave; (b) *SV*-wave; and (c) *SH*-wave

Copyright 2017 Cengage Learning. All Rights Reserved. May not be copied, scanned, or duplicated, in whole or in part. Due to electronic rights, some third party content may be suppressed from the eBook and/or eChapter(s). Editorial review has deemed that any suppressed content does not materially affect the overall learning experience. Cengage Learning reserves the right to remove additional content at any time if subsequent rights restrictions require it.

If a P-wave impinges on the boundary between two layers, as shown in Figure 4.41a, there will be two reflected waves and two refracted waves. The reflected waves consist of (1) a P-wave shown as P_1 in layer 1 and (2) an SV-wave shown as SV_1 in layer 1.

The refracted waves will consist of (1) a P-wave, shown as P_2 in layer 2, and (2) an SV-wave, shown as SV_2 in layer 2. Referring to the angles in Figure 4.41a, it can be shown that

$$\alpha_1 = \alpha_2 \tag{4.37}$$

and

$$\boxed{\frac{\sin\alpha_1}{v_{p_1}} = \frac{\sin\alpha_2}{v_{p_1}} = \frac{\sin\beta_2}{v_{s_1}} = \frac{\sin\alpha_3}{v_{p_2}} = \frac{\sin\beta_3}{v_{s_2}}} \tag{4.38}$$

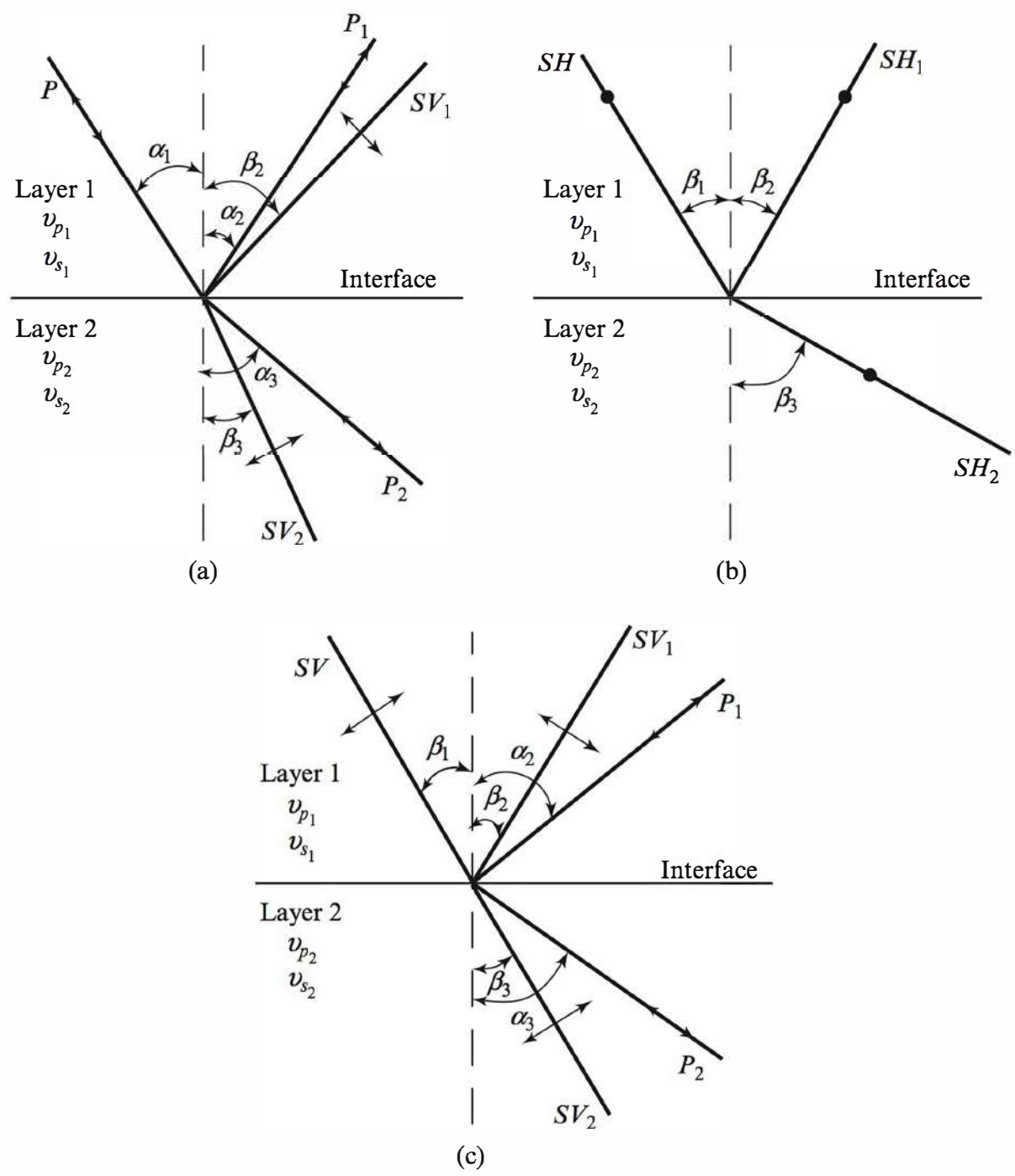

Figure 4.41 Reflection and refraction for (a) an incident P-ray; (b) an incident SH-ray; and (c) an incident SV-ray

Copyright 2017 Cengage Learning. All Rights Reserved. May not be copied, scanned, or duplicated, in whole or in part. Due to electronic rights, some third party content may be suppressed from the eBook and/or eChapter(s). Editorial review has deemed that any suppressed content does not materially affect the overall learning experience. Cengage Learning reserves the right to remove additional content at any time if subsequent rights restrictions require it.

where

v_{p_1} and v_{p_2} = the velocities of the P-wave front in layers 1 and 2, respectively
v_{s_1} and v_{s_2} = the velocities of the S-wave front in layers 1 and 2, respectively

If an SH-wave impinges the boundary between two layers, as shown in Figure 4.41b, there will be one reflected SH-wave (shown as SH_1) and one refracted SH-wave (shown as SH_2). For this case

$$\beta_1 = \beta_2 \tag{4.39}$$

and

$$\boxed{\frac{\sin\beta_1}{v_{s_1}} = \frac{\sin\beta_2}{v_{s_1}} = \frac{\sin\beta_3}{v_{s_2}}} \tag{4.40}$$

Finally, if an SV-wave impinges the boundary between two layers, as shown in Figure 4.41c, there will be two reflected waves and two refracted waves. The reflected waves are (1) a P-wave, shown as P_1 in layer 1 and (2) an SV-wave, shown as SV_1 in layer 1. The refracted waves are (a) a P-wave, shown as P_2 in layer 2, and (b) an SV-wave, shown as SV_2 in layer 2. For this case, $\beta_1 = \beta_2$:

$$\boxed{\frac{\sin\beta_1}{v_{s_1}} = \frac{\sin\alpha_2}{v_{p_1}} = \frac{\sin\beta_2}{v_{s_1}} = \frac{\sin\beta_3}{v_{s_2}} = \frac{\sin\alpha_3}{v_{p_2}}} \tag{4.41}$$

The mathematical derivations of these facts will not be shown here. For further details the reader is referred to Kolsky (1963, pp. 24–38).

4.12 SEISMIC REFRACTION SURVEY (HORIZONTAL LAYERING)

Seismic refraction surveys are sometimes used to determine the wave propagation velocities through various soil layers in the field and to obtain thicknesses of each layer. Consider the case where there are two layers of soil, as shown in Figure 4.42a. Let the velocities of P-waves in layers 1 and 2 be v_{p_1} and v_{p_2}, respectively, and let $v_{p_1} < v_{p_2}$. A is a source of impulsive energy. If seismic waves are generated at A, the energy from the point will travel in hemispherical wave fronts. Consider the case of P-waves, since they are the fastest. If a detecting device is placed at point B, which is located at a *small* distance x from A, the P-wave that travels through the upper medium will reach it first before any other wave. The travel time for this first arrival may be given as

$$t = \frac{x}{v_{p_1}} \tag{4.42}$$

where $\overline{AB} = x$.

Copyright 2017 Cengage Learning. All Rights Reserved. May not be copied, scanned, or duplicated, in whole or in part. Due to electronic rights, some third party content may be suppressed from the eBook and/or eChapter(s). Editorial review has deemed that any suppressed content does not materially affect the overall learning experience. Cengage Learning reserves the right to remove additional content at any time if subsequent rights restrictions require it.

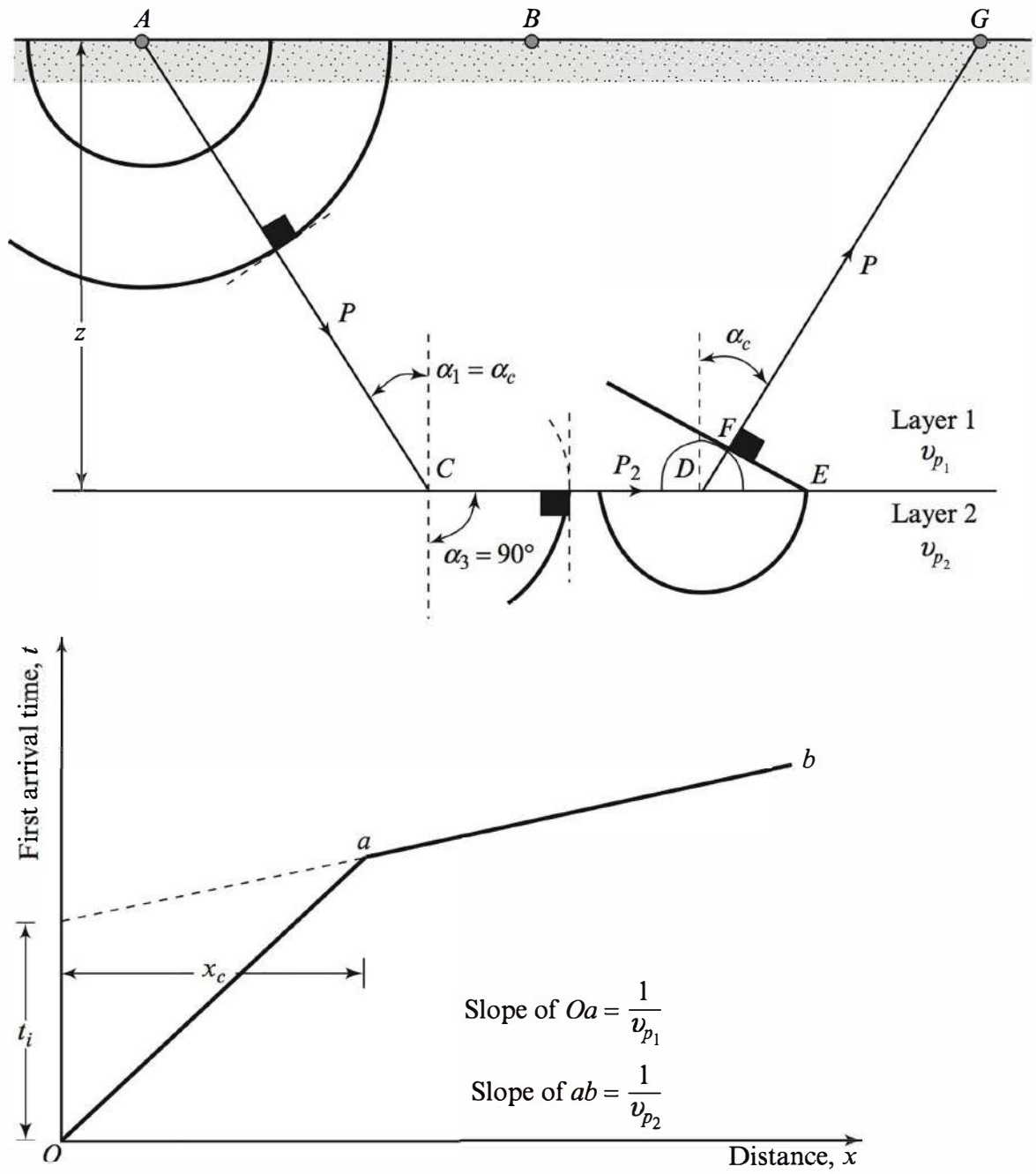

Figure 4.42 Seismic refraction survey—horizontal layering

Again, consider the first arrival time of a P-wave at a point G, which is located at a greater distance from A. In order to understand this, one considers a spherical P-wave front that originates at A striking the interface of the two layers. At some point C, the refracted P-wave front in the lower medium will be such that the tangent to the sphere will be perpendicular to the interface. In that case, the refracted P-ray (shown as P_2 in Figure 4.42a) will be parallel to the boundary and will travel with a velocity v_{p_2}. Note that because $v_{p_1} < v_{p_2}$, this wave front will travel faster than those described previously. From Eq. (4.38)

$$\frac{\sin \alpha_1}{v_{p_1}} = \frac{\sin \alpha_3}{v_{p_2}}$$

Copyright 2017 Cengage Learning. All Rights Reserved. May not be copied, scanned, or duplicated, in whole or in part. Due to electronic rights, some third party content may be suppressed from the eBook and/or eChapter(s). Editorial review has deemed that any suppressed content does not materially affect the overall learning experience. Cengage Learning reserves the right to remove additional content at any time if subsequent rights restrictions require it.

Since $\alpha_3 = 90°$, $\sin \alpha_3 = 1$, and

$$\alpha_1 = \sin^{-1}\left(\frac{v_{p_1}}{v_{p_2}}\right) = \alpha_c \tag{4.43}$$

where α_c = critical angle of incidence.

The wave front just described traveling with a velocity v_{p_2} will create vibrating stresses at the interface, and this will generate wave fronts that will spread out into the upper medium. These *P*-waves will spread with a velocity of v_{p_1}. The spherical wave front traveling downward from *D* in layer 2 will have a radius equal to *DE* after a time Δt. At the same time Δt, the spherical wave front traveling upward from point *D* will have a radius equal to *DF*. The resultant wave front in the upper layer will follow a line *EF*. It can be seen from the diagram that

$$\frac{v_{p_1}\Delta t}{v_{p_2}\Delta t} = \frac{DF}{DE} = \sin i_c \tag{4.44}$$

So ray *DFG* will make an angle i_c with the vertical. It can be mathematically shown that for x greater than a *critical value* x_c, the *P*-wave that travels the path *ACDG* will be the *first to arrive* at point *G*. Let the time of travel for the *P*-wave along the path *ACDG* be equal to t. Thus, $t = t_{AC} + t_{CD} + t_{DG}$, or

$$t = \left(\frac{z}{\cos i_c}\right)\left(\frac{1}{v_{p_1}}\right) + \frac{x - 2z\tan i_c}{v_{p_2}} + \left(\frac{z}{\cos i_c}\right)\left(\frac{1}{v_{p_1}}\right)$$

$$= \frac{x}{v_{p_2}} - \frac{2z\sin i_c}{v_{p_2}\cos i_c} + \frac{2z}{v_{p_1}\cos i_c}$$

where $x = \overline{AG}$. But $v_{p_2} = v_{p_1}/\sin i_c$ [from Eq. (4.44)]; thus

$$t = \frac{x}{v_{p_2}} - \frac{2z\sin^2 i_c}{v_{p_1}\cos i_c} + \frac{2z}{v_{p_1}\cos i_c} = \frac{x}{v_{p_2}} + \frac{2z}{v_{p_1}}\left(\frac{1-\sin^2 i_c}{\cos i_c}\right)$$

$$= \frac{x}{v_{p_2}} + \frac{2z}{v_{p_1}}\cos i_c \tag{4.45}$$

Since $\sin i_c = v_{p_1}/v_{p_2}$

$$\cos i_c = \sqrt{1-\sin^2 i_c} = \sqrt{1-\left(\frac{v_{p_1}}{v_{p_2}}\right)^2} \tag{4.46}$$

Substituting Eq. (4.46) into Eq. (4.45), one obtains

$$\boxed{t = \frac{x}{v_{p_2}} + \frac{2z\sqrt{v_{p_2}^2 - v_{p_1}^2}}{(v_{p_1})(v_{p_2})}} \tag{4.47}$$

Copyright 2017 Cengage Learning. All Rights Reserved. May not be copied, scanned, or duplicated, in whole or in part. Due to electronic rights, some third party content may be suppressed from the eBook and/or eChapter(s). Editorial review has deemed that any suppressed content does not materially affect the overall learning experience. Cengage Learning reserves the right to remove additional content at any time if subsequent rights restrictions require it.

If detecting instruments are placed at various distances from the source of disturbance to obtain first arrival times and the results are plotted in graphical form, the graph will be like that shown in Figure 4.42b. The line *Oa* represents the data that follow Eq.(4.42). The slope of this line will give $1/v_{p_1}$. The line *ab* represents the data that follow Eq. (4.47). The slope of this line is $1/v_{p_2}$. Thus the velocities of v_{p_1} and v_{p_2} can now be obtained.

If line *ab* is projected back to $x = 0$, one obtains

$$t = t_i = \frac{2z\sqrt{v_{p_2}^2 - v_{p_1}^2}}{(v_{p_1})(v_{p_2})}$$

or

$$\boxed{z = \frac{(t_i)(v_{p_1})(v_{p_2})}{2\sqrt{v_{p_2}^2 - v_{p_1}^2}} = \frac{t_i v_{p_1}}{2\cos i_c}} \tag{4.48}$$

where t_i is the intercept time. Hence, the thickness of layer 1 can be easily obtained.

The *critical distance* x_c (Figure 4.42b) beyond which the wave refracted at the interface arrives at the detector before the direct wave can be obtained by equating the right-hand sides of Eqs. (4.42) and (4.47):

$$\frac{x_c}{v_{p_1}} = \frac{x_c}{v_{p_2}} + \frac{2z\sqrt{v_{p_2}^2 - v_{p_1}^2}}{v_{p_1} v_{p_2}}$$

or

$$x_c = 2z\frac{\sqrt{v_{p_2}^2 - v_{p_1}^2}}{v_{p_1} v_{p_2}}\frac{v_{p_1} v_{p_2}}{v_{p_2} - v_{p_1}} = 2z\sqrt{\frac{v_{p_2} + v_{p_1}}{v_{p_2} - v_{p_1}}} \tag{4.49}$$

The depth of the first layer can be calculated from Eq. (4.49) as

$$\boxed{z = \frac{x_c}{2}\sqrt{\frac{v_{p_2} - v_{p_1}}{v_{p_2} + v_{p_1}}}} \tag{4.50}$$

A. Refraction Survey in a Three-Layered Soil Medium

Figure 4.43 considers the case of a refraction survey through a three-layered soil medium. Let v_{p_1}, v_{p_2} and v_{p_3} be the *P*-wave velocities in layers 1, 2, and 3, respectively, as shown in Figure 4.43a ($v_{p_1} < v_{p_2} < v_{p_3}$). If *A* in Figure 4.43a is a source of disturbance, the *P*-wave traveling through layer 1 will arrive first at *B*, which is located a small distance away from *A*. The travel time for this can be given by Eq. (4.42) as $t = x/v_{p_1}$. At a greater distance x, the first arrival will correspond to the wave taking the path *ACDE*. The travel time for this case be given by Eq. (4.47) as

Copyright 2017 Cengage Learning. All Rights Reserved. May not be copied, scanned, or duplicated, in whole or in part. Due to electronic rights, some third party content may be suppressed from the eBook and/or eChapter(s). Editorial review has deemed that any suppressed content does not materially affect the overall learning experience. Cengage Learning reserves the right to remove additional content at any time if subsequent rights restrictions require it.

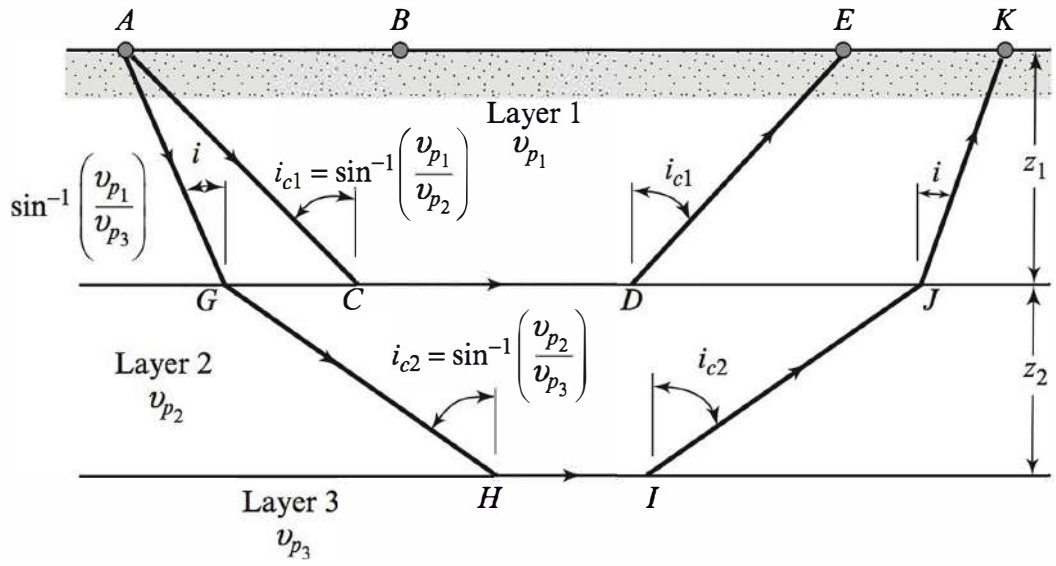

(a)

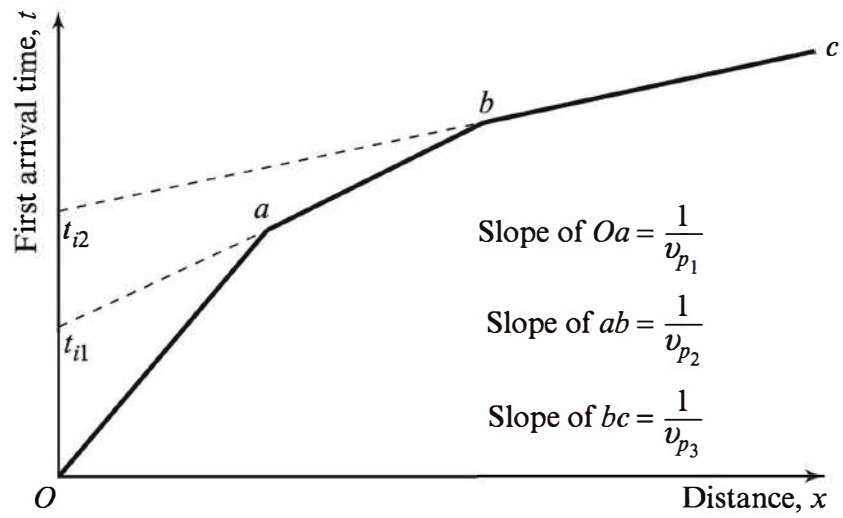

(b)

Figure 4.43 Refraction survey in a three-layer soil

$$t = \frac{x}{v_{p_2}} + \frac{2z_1\sqrt{v_{p_2}^2 - v_{p_1}^2}}{(v_{p_1})(v_{p_2})}$$

where z_1 = thickness of top layer.

At a still larger distance, the first arrival will correspond to the path $AGHIJK$. Note that the refracted ray H-I will travel with a velocity of v_{p_3}. The angle i_{c2} is the critical angle for layer 3.

$$i_{c2} = \sin^{-1}\left(\frac{v_{p_2}}{v_{p_3}}\right) \tag{4.51}$$

For this path ($AGHIJK$) the total travel time can be derived as

$$\boxed{t = \frac{x}{v_{p_3}} + \frac{2z_1\sqrt{v_{p_3}^2 - v_{p_1}^2}}{(v_{p_3})(v_{p_1})} + \frac{2z_2\sqrt{v_{p_3}^2 - v_{p_2}^2}}{(v_{p_3})(v_{p_2})}} \tag{4.52}$$

Copyright 2017 Cengage Learning. All Rights Reserved. May not be copied, scanned, or duplicated, in whole or in part. Due to electronic rights, some third party content may be suppressed from the eBook and/or eChapter(s). Editorial review has deemed that any suppressed content does not materially affect the overall learning experience. Cengage Learning reserves the right to remove additional content at any time if subsequent rights restrictions require it.

where z_2 = thickness of layer 2.

So, if detecting instruments are placed at various distances from the source of disturbance to obtain first arrival times, they can be plotted in a t-versus-x graph. This graph will appear as shown in Figure 4.43b. The line Oa corresponds to Eq. (4.42), ab corresponds to Eq. (4.47), and bc corresponds to Eq. (4.52). The slopes of Oa, ab, and bc will be $1/v_{p_1}$, $1/v_{p_2}$ and $1/v_{p_3}$, respectively. The thickness of the first layer z_1 can be determined from the intercept time t_{i1} in a similar manner, as shown in Eq. (4.48), or

$$z_1 = \frac{(t_{i1})(v_{p_1})(v_{p_2})}{2\sqrt{v_{p_2}^2 - v_{p_1}^2}}$$

The thickness of the second layer can be obtained from Eq. (4.52). Referring to Figure 4.43b, the expression for the intercept time t_{i2} can be evaluated by substituting $x = 0$ into Eq. (4.52):

$$t = t_{i2} = \frac{2z_1\sqrt{v_{p_3}^2 - v_{p_1}^2}}{(v_{p_3})(v_{p_1})} + \frac{2z_2\sqrt{v_{p_3}^2 - v_{p_2}^2}}{(v_{p_3})(v_{p_2})}$$

or

$$\boxed{z_2 = \frac{1}{2}\left[t_{i2} - \frac{2z_1\sqrt{v_{p_3}^2 - v_{p_1}^2}}{(v_{p_3})(v_{p_1})}\right]\frac{(v_{p_3})(v_{p_2})}{\sqrt{v_{p_3}^2 - v_{p_2}^2}}} \tag{4.53}$$

B. Refraction Survey for Multilayer Soil

In general, if there are n layers, the first arrival time at various distances from the source of disturbance will plot as shown in Figure 4.44. There will be n segments in the t-versus-x plot. The slope of the nth segment will give the value $1/v_{p_n}$ $(n = 1, 2, \ldots)$. More details on advanced test methods (detecting inclination of the bedrock is briefly described later) and interpretation could be found in several geophysics books.

The value of P-wave velocity in a natural deposit of soil will depend on several factors, such as confining pressure, moisture content, and void ratio. Some typical values of v_p are given in Table 3.1. It is worth noting that P-wave velocity through saturated soils will be approximately 1500 m/sec. However, P-wave velocity value could reach the order of few kilometers per second in case of rocks.

Copyright 2017 Cengage Learning. All Rights Reserved. May not be copied, scanned, or duplicated, in whole or in part. Due to electronic rights, some third party content may be suppressed from the eBook and/or eChapter(s). Editorial review has deemed that any suppressed content does not materially affect the overall learning experience. Cengage Learning reserves the right to remove additional content at any time if subsequent rights restrictions require it.

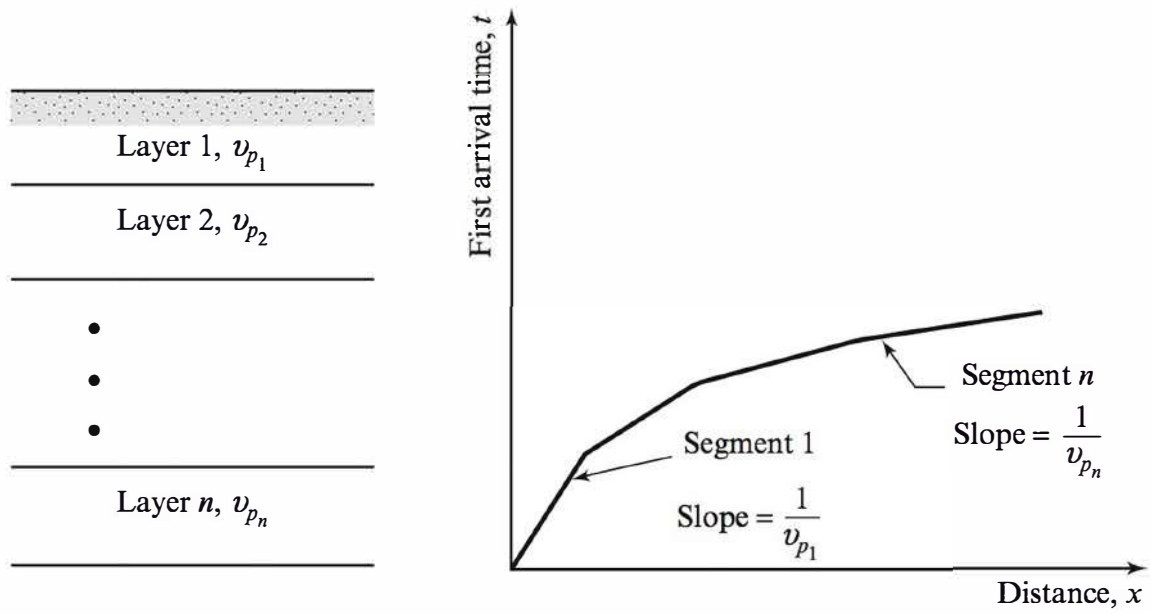

Figure 4.44 Refraction survey for multilayer soil

EXAMPLE 4.1

Following are the results of a refraction survey (horizontal layering of soil). Determine the P-wave velocities of the soil layers and their thicknesses.

Distance (m)	Time of first arrival (ms)
2.5	5.5
5.0	11.1
7.5	16.1
15.0	24.0
25.0	30.8
35.0	38.2
45.0	46.1
55.0	51.3
60.0	52.8

SOLUTION

The time-distance plot is given in Figure 4.45. From the plot,

$$v_{p_1} = \frac{5}{10.6 \times 10^{-3}} = \mathbf{472\ m/s}$$

$$v_{p_2} = \frac{10}{7.2 \times 10^{-3}} = \mathbf{1389\ m/s}$$

$$v_{p_3} = \frac{10}{3 \times 10^{-3}} = \mathbf{3333\ m/s}$$

Copyright 2017 Cengage Learning. All Rights Reserved. May not be copied, scanned, or duplicated, in whole or in part. Due to electronic rights, some third party content may be suppressed from the eBook and/or eChapter(s). Editorial review has deemed that any suppressed content does not materially affect the overall learning experience. Cengage Learning reserves the right to remove additional content at any time if subsequent rights restrictions require it.

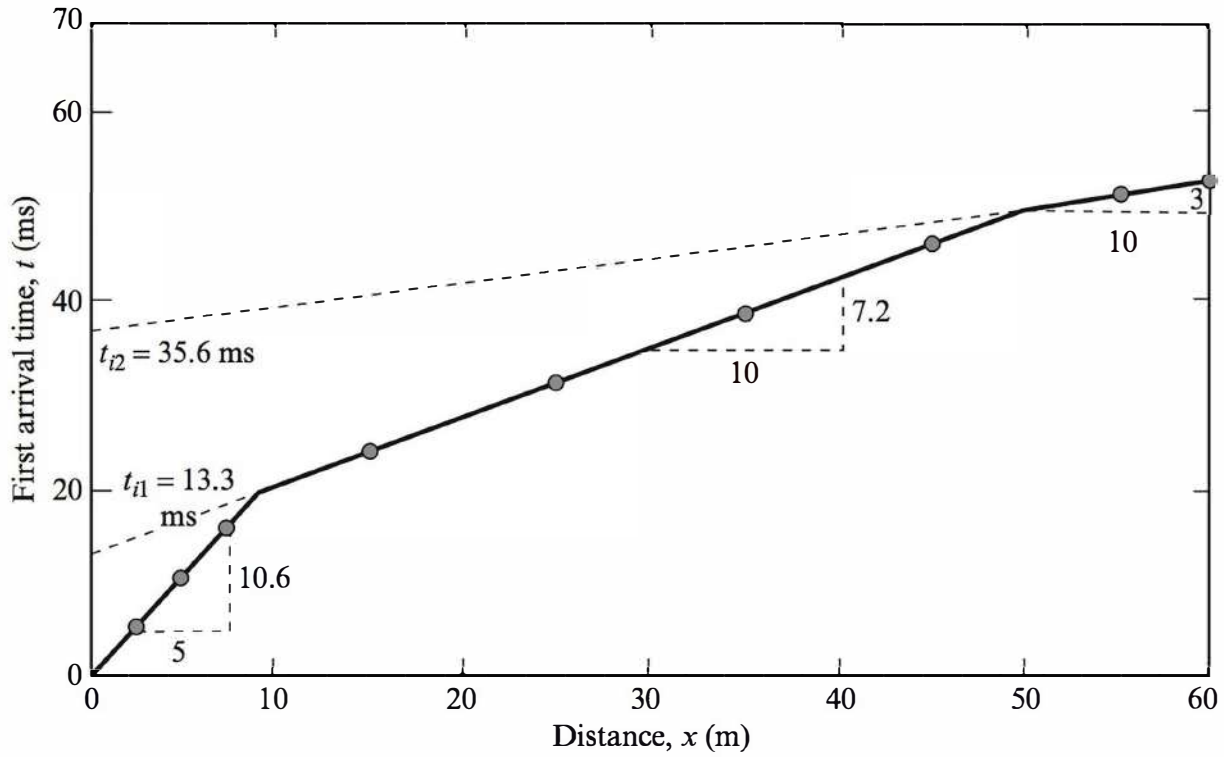

Figure 4.45

$$t_{i1} = 13.3 \times 10^{-3} \text{ s}; \; t_{i2} = 35.6 \times 10^{-3} \text{ s}.$$

From Eq. (4.48)

$$z_1 = \frac{(t_{i1})(v_{p_1})(v_{p_2})}{2\sqrt{v_{p_2}^2 - v_{p_1}^2}} = \frac{(13.3 \times 10^{-3})(472)(1389)}{2\sqrt{(1389)^2 - (472)^2}}$$
$$= \mathbf{3.39\ m}$$

From Eq. (4.53)

$$z_2 = \frac{1}{2}\left[t_{i2} - \frac{2z_1\sqrt{v_{p_3}^2 - v_{p_1}^2}}{(v_{p_3})(v_{p_1})}\right]\frac{(v_{p_3})(v_{p_2})}{\sqrt{v_{p_3}^2 - v_{p_2}^2}}$$
$$= \frac{1}{2}\left[35.6 \times 10^{-3} - \frac{(2)(3.39)\sqrt{(3333)^2 - (472)^2}}{(3333)(472)}\right]$$
$$\times \frac{(3333)(1389)}{\sqrt{(3333)^2 - (1389)^2}}$$
$$= \frac{1}{2}(0.02138)(1528) = \mathbf{16.33\ m}$$

Copyright 2017 Cengage Learning. All Rights Reserved. May not be copied, scanned, or duplicated, in whole or in part. Due to electronic rights, some third party content may be suppressed from the eBook and/or eChapter(s). Editorial review has deemed that any suppressed content does not materially affect the overall learning experience. Cengage Learning reserves the right to remove additional content at any time if subsequent rights restrictions require it.

4.13 REFRACTION SURVEY IN SOILS WITH INCLINED LAYERING

Figure 4.46a shows two soil layers. The interface of soil layers 1 and 2 is inclined at an angle β with respect to the horizontal. Let the P-wave velocities in layers 1 and 2 be v_{p_1} and v_{p_2}, respectively ($v_{p_1} < v_{p_2}$).

If a disturbance is created at A and a detector is placed at B, which is small distance away from A, the detector will first receive the P-wave traveling through layer 1. The time for its arrival may be given by

$$t_d = \frac{x}{v_{p_1}}$$

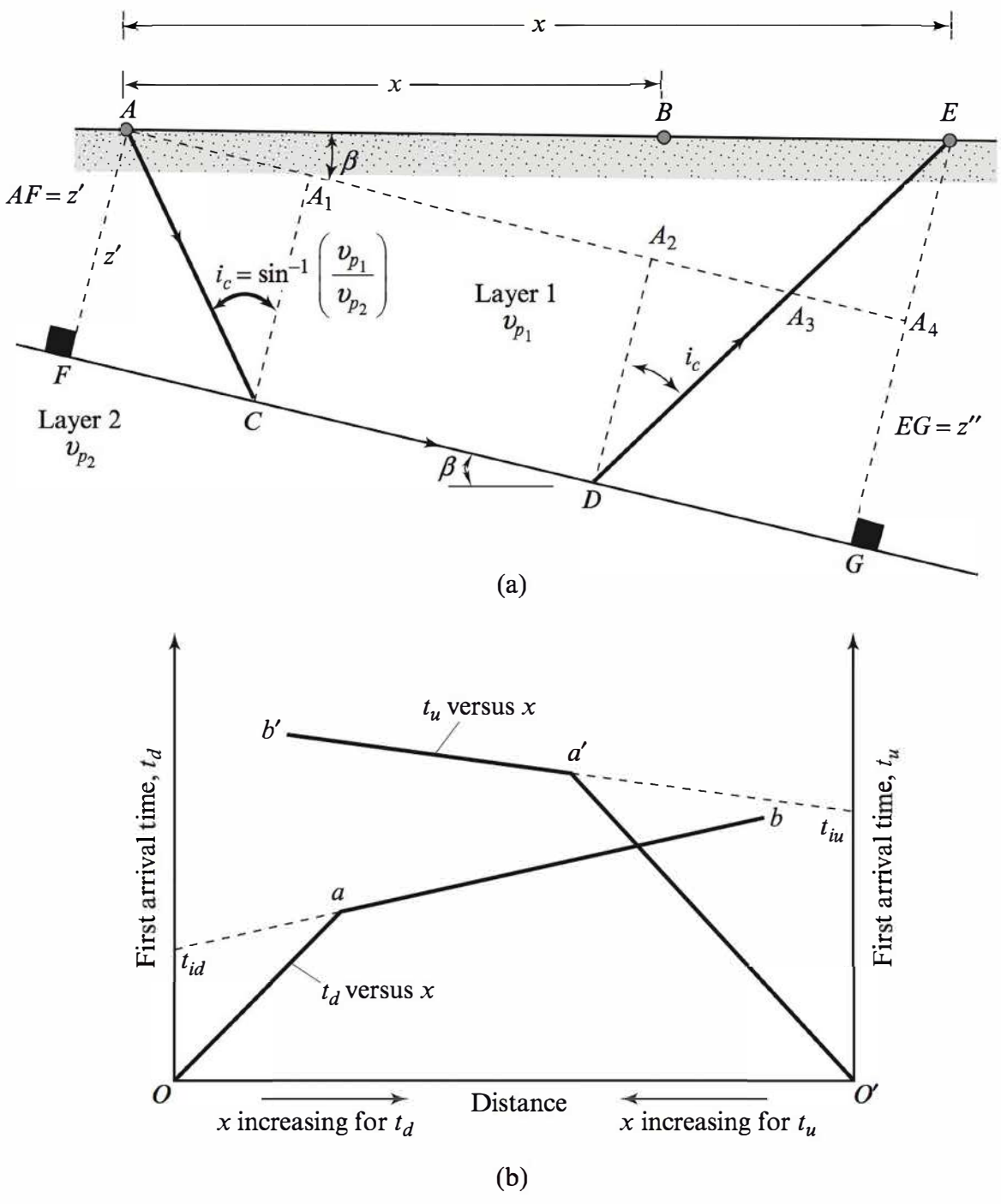

Figure 4.46 Refraction survey in soils with inclined layering

Copyright 2017 Cengage Learning. All Rights Reserved. May not be copied, scanned, or duplicated, in whole or in part. Due to electronic rights, some third party content may be suppressed from the eBook and/or eChapter(s). Editorial review has deemed that any suppressed content does not materially affect the overall learning experience. Cengage Learning reserves the right to remove additional content at any time if subsequent rights restrictions require it.

However, at a larger distance the first arrival will be for the P-wave following the path $ACDE$—which consists of three parts. The time taken can be written as

$$t_d = t_{AC} + t_{CD} + t_{DE} \tag{4.54}$$

Referring to Figure 4.46a,

$$t_{AC} = \frac{z'}{v_{p_1} \cos i_c} \tag{4.55}$$

$$\begin{aligned} t_{CD} &= \frac{CD}{v_{p_2}} = \frac{AA_4 - AA_1 - A_2A_3 - A_3A_4}{v_{p_2}} \\ &= \frac{x\cos\beta - z'\tan i_c - z'\tan i_c - x\sin\beta\tan i_c}{v_{p_2}} \end{aligned} \tag{4.56}$$

$$t_{DE} = \frac{DA_3 + A_3E}{v_{p_1}} = \frac{\dfrac{z'}{\cos i_c} + \dfrac{x\sin\beta}{\cos i_c}}{v_{p_1}} \tag{4.57}$$

Substitution of Eqs. (4.55), (4.46), and (4.57) into Eq. (4.54) and simplification yields

$$t_d = \frac{2z'\cos i_c}{v_{p_1}} + \frac{x}{v_{p_1}} \sin(i_c + \beta) \tag{4.58}$$

Now, if the source of disturbance is E and the detector is placed at A, the first arrival time along the refracted ray path may be given by

$$t_u = \frac{2z''\cos i_c}{v_{p_1}} + \frac{x}{v_{p_1}} \sin(i_c - \beta) \tag{4.59}$$

In the actual survey, one can have a source of disturbance such as A and observe the first arrival time at several points to the right of A and have a source of disturbance such as E and observe the first arrival time at several points to the left of E. These results can be plotted in a graphical form, as shown in Figure 4.46b (time-versus-x plot). From Figure 4.46b note that the slopes of Oa and $O'a'$ are both $1/v_{p_1}$. The slope of the branch ab will be $[\sin(i_c + \beta)]/v_{p_1}$, as can be seen from Eq. (4.58). Similarly, the slope of the branch of $a'b'$ will be $[\sin(i_c - \beta)]/v_{p_1}$ [see Eq. (4.59)]. Let

$$m_d = \frac{\sin(i_c + \beta)}{v_{p_1}} \tag{4.60}$$

and

$$m_u = \frac{\sin(i_c - \beta)}{v_{p_1}} \tag{4.61}$$

Copyright 2017 Cengage Learning. All Rights Reserved. May not be copied, scanned, or duplicated, in whole or in part. Due to electronic rights, some third party content may be suppressed from the eBook and/or eChapter(s). Editorial review has deemed that any suppressed content does not materially affect the overall learning experience. Cengage Learning reserves the right to remove additional content at any time if subsequent rights restrictions require it.

From Eq. (4.60),

$$i_c = \sin^{-1}(m_d v_{p_1}) - \beta \tag{4.62}$$

Again, from Eq. (4.61)

$$i_c = \sin^{-1}(m_u v_{p_1}) + \beta \tag{4.63}$$

Solving the two preceding equations,

$$\boxed{i_c = \tfrac{1}{2}[\sin^{-1}(v_{p_1} m_d) + \sin^{-1}(v_{p_1} m_u)]} \tag{4.64}$$

and

$$\boxed{\beta = \tfrac{1}{2}[\sin^{-1}(v_{p_1} m_d) - \sin^{-1}(v_{p_1} m_u)]} \tag{4.65}$$

Once i_c is determined, the value of v_{p_2} can be obtained as

$$\boxed{v_{p_2} = \frac{v_{p_1}}{\sin i_c}} \tag{4.66}$$

Again referring to Figure 4.46b, if the ab and $a'b'$ branches are projected back, they will intercept the time axes at t_{id} and t_{iu}, respectively. From Eqs. (4.58) and (4.59), it can be seen that

$$t_{id} = \frac{2z' \cos i_c}{v_{p_1}}$$

or

$$\boxed{z' = \frac{(t_{id}) v_{p_1}}{2 \cos i_c}} \tag{4.67}$$

and

$$t_{iu} = \frac{2z'' \cos i_c}{v_{p_1}}$$

or

$$\boxed{z'' = \frac{(t_{iu}) v_{p_1}}{2 \cos i_c}} \tag{4.68}$$

Since i_c and v_{p_1} are known and t_{id} and t_{iu} can be determined from a graph, one can obtain the values of z' and z''.

Copyright 2017 Cengage Learning. All Rights Reserved. May not be copied, scanned, or duplicated, in whole or in part. Due to electronic rights, some third party content may be suppressed from the eBook and/or eChapter(s). Editorial review has deemed that any suppressed content does not materially affect the overall learning experience. Cengage Learning reserves the right to remove additional content at any time if subsequent rights restrictions require it.

EXAMPLE 4.2

Referring to Figure 4.46a, the results of a refraction survey are as follows. The distance between A and E is 60 m.

Point of disturbance A		Point of disturbance E	
Distance from A (m)	Time of first arrival (ms)	Distance from E (m)	Time of first arrival (ms)
5	12.1	5	11.5
10	25.2	10	22.8
15	35.3	15	34.5
20	48.0	20	44.8
30	60.2	30	69.1
40	68.5	40	78.1
50	76.8	50	82.8
60	85.1	60	87.7

Determine

a. v_{p_1} and v_{p_2},
b. z' and z'', and
c. β

SOLUTION

The time-distance records have been plotted in Figure 4.47.

a. From branch Oa,

$$v_{p_1} = \frac{10}{25 \times 10^{-3}} = 400 \text{ m/s}$$

From branch $O'a'$

$$v_{p_1} = \frac{10}{22 \times 10^{-3}} = 454 \text{ m/s}$$

The average value of v_{p_1} is **427 m/s**.

From the slope of branch ab,

$$m_d = \frac{8.8 \times 10^{-3}}{10} = 0.88 \times 10^{-3}$$

Again, from the slope of branch $a'b'$,

$$m_u = \frac{5 \times 10^{-3}}{10} = 0.5 \times 10^{-3}$$

Copyright 2017 Cengage Learning. All Rights Reserved. May not be copied, scanned, or duplicated, in whole or in part. Due to electronic rights, some third party content may be suppressed from the eBook and/or eChapter(s). Editorial review has deemed that any suppressed content does not materially affect the overall learning experience. Cengage Learning reserves the right to remove additional content at any time if subsequent rights restrictions require it.

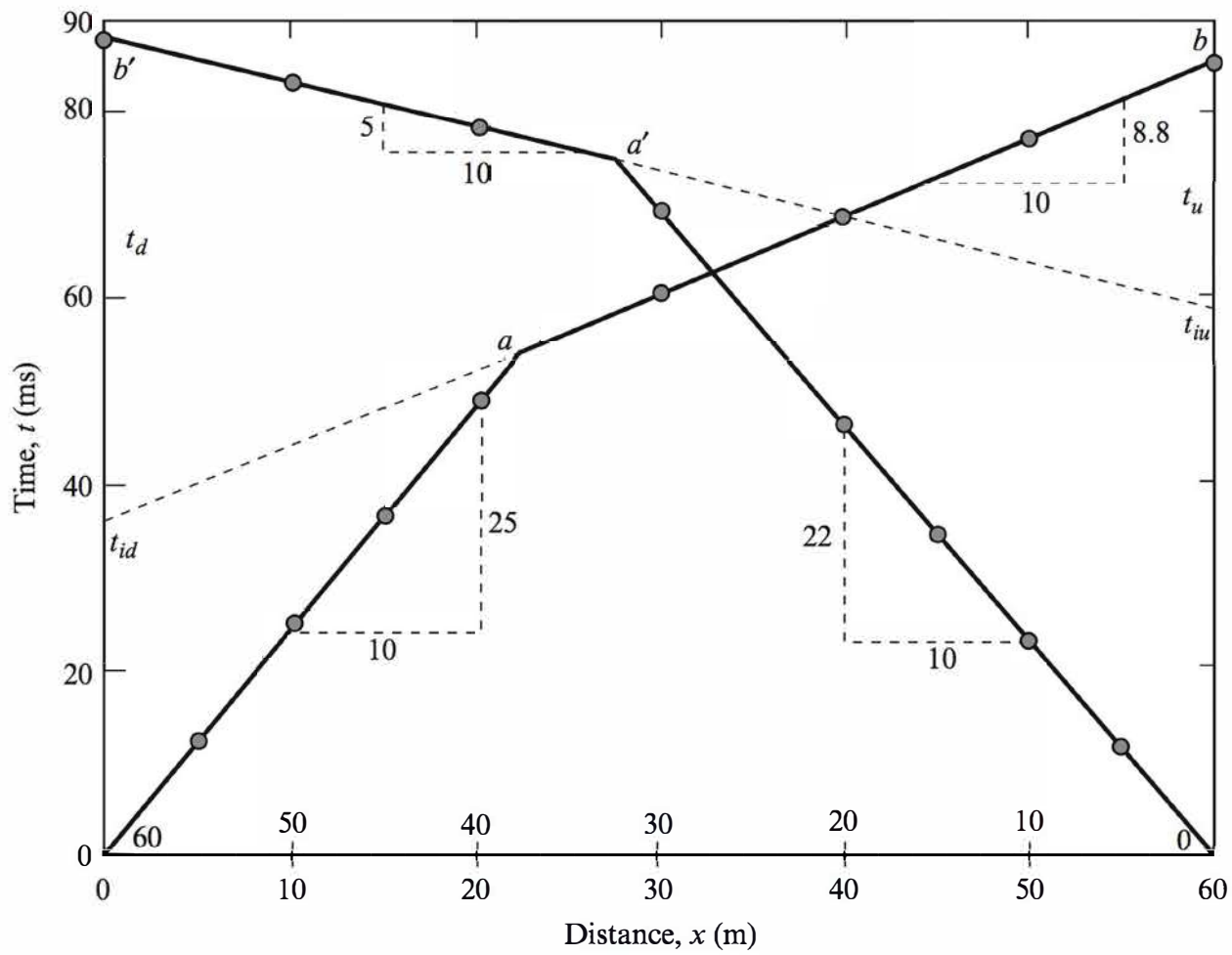

Figure 4.47

From Eq. (4.64),

$$i_c = \tfrac{1}{2}[\sin^{-1}(v_{p_1} m_d) + \sin^{-1}(v_{p_1} m_u)]$$

$$\sin^{-1}(v_{p_1} m_d) = \sin^{-1}[(427)(0.88 \times 10^{-3})] = 22.07°$$

$$\sin^{-1}(v_{p_1} m_u) = \sin^{-1}[(427)(0.5 \times 10^{-3})] = 12.33°$$

Hence

$$i_c = \tfrac{1}{2}(22.07° + 12.33°) = 17.2°$$

Using Eq. (4.66)

$$v_{p_2} = \frac{v_{p_1}}{\sin i_c} = \frac{427}{\sin(17.2)} = \mathbf{1444\ m/s}$$

b. From Eq. (4.67)

$$z' = \frac{(t_{id})(v_{p_1})}{2\cos i_c}$$

$t_{id} = 35.9 \times 10^{-3}$ s (from Figure 4.47). So

$$z' = \frac{(35.9 \times 10^{-3})(427)}{2\cos(17.2)} = \mathbf{8.03\ m}$$

Copyright 2017 Cengage Learning. All Rights Reserved. May not be copied, scanned, or duplicated, in whole or in part. Due to electronic rights, some third party content may be suppressed from the eBook and/or eChapter(s). Editorial review has deemed that any suppressed content does not materially affect the overall learning experience. Cengage Learning reserves the right to remove additional content at any time if subsequent rights restrictions require it.

Again, from Eq. (4.68),

$$z'' = \frac{(t_{iu})(v_{p_1})}{2\cos i_c}$$

From Figure 4.47, $t_{iu} = 59.8 \times 10^{-3}$ s.

$$z'' = \frac{(59.8 \times 10^{-3})(427)}{2\cos(17.2)} = \mathbf{13.37\ m}$$

c. From Eq. (4.65),

$$\beta = \tfrac{1}{2}[\sin^{-1}(v_{p_1} m_d) - \sin^{-1}(v_{p_1} m_u)] = \tfrac{1}{2}(22.07° - 12.33°) = \mathbf{4.87°}$$

4.14 REFLECTION SURVEY IN SOIL (HORIZONTAL LAYERING)

Reflection surveys can also be conducted to obtain information about the soil layers. Figure 4.48a shows a two-layered soil system. A is the point of disturbance. If a recorder is placed at C at a distance x away from A, the travel time for the reflected P-wave can be given as

$$t = \frac{AB + BC}{v_{p_1}} = \frac{2}{v_{p_1}}\sqrt{z^2 + \left(\frac{x}{2}\right)^2} \tag{4.69}$$

where t = total travel time for the ray path ABC.

From Eq. (4.69), the thickness of layer 1 can be obtained as

$$\boxed{z = \tfrac{1}{2}\sqrt{(v_{p_1} t)^2 - x^2}} \tag{4.70}$$

If the travel times t for the reflected P-waves at various distances x are obtained, they can be plotted in a graphical form, as shown in Figure 4.48b. Note that the time-distance curve obtained form Eq. (4.69) will be a hyperbola. The line Oa shown in Figure 4.48b is the time-distance plot for the direct P-waves traveling through layer 1 (compare line Oa in Figure 4.48b to the line Oa in Figure 4.42b). The slope of this line will give $1/v_{p_1}$.

If the time-distance curve obtained from the reflection data is extended back, it will intersect the time axis at t_0. From Eq. (4.69) it can be seen that at $x = 0$,

$$t_0 = \frac{2z}{v_{p_1}}$$

Copyright 2017 Cengage Learning. All Rights Reserved. May not be copied, scanned, or duplicated, in whole or in part. Due to electronic rights, some third party content may be suppressed from the eBook and/or eChapter(s). Editorial review has deemed that any suppressed content does not materially affect the overall learning experience. Cengage Learning reserves the right to remove additional content at any time if subsequent rights restrictions require it.

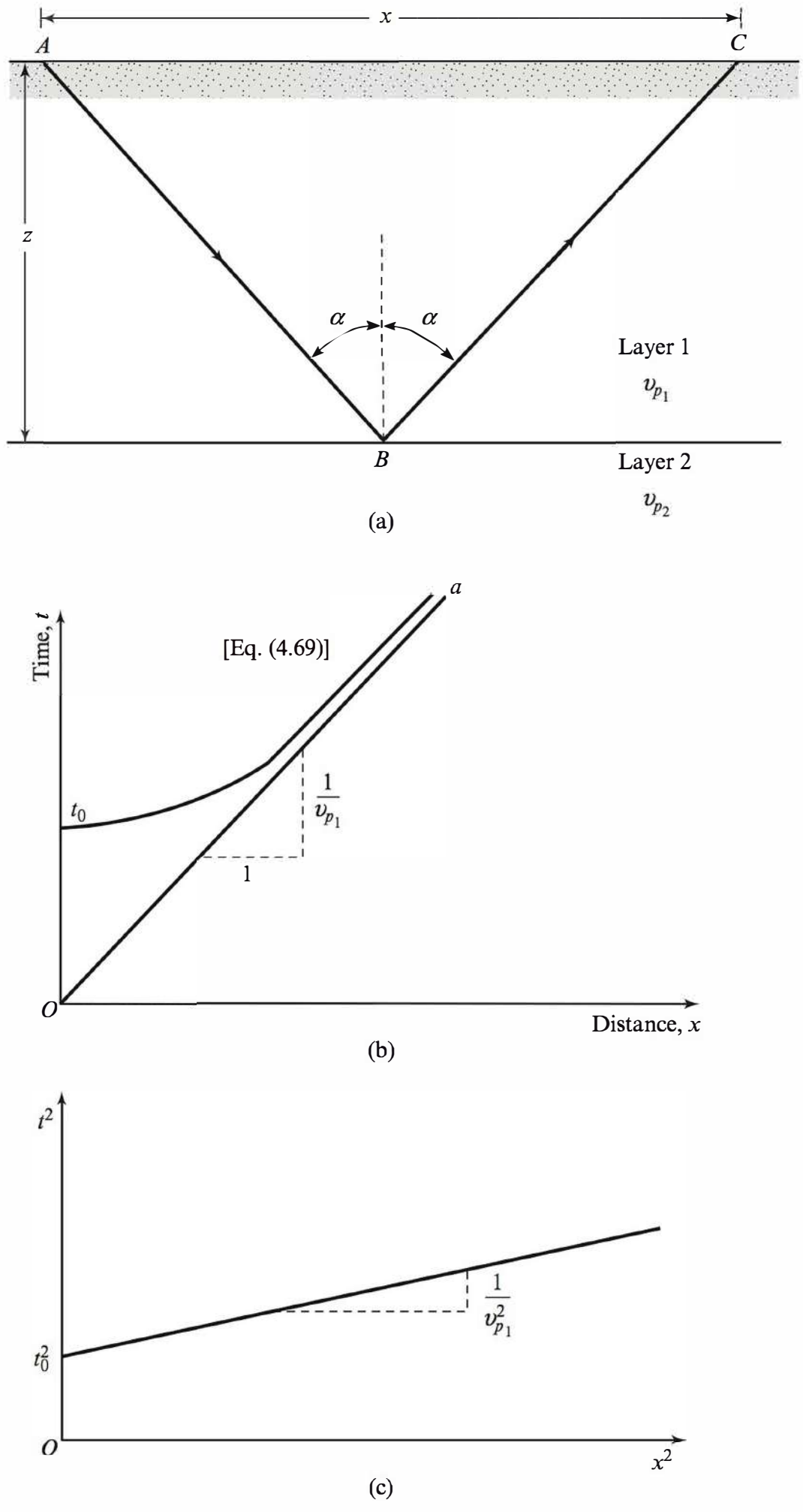

Figure 4.48 Reflection survey in soil—horizontal layering

Copyright 2017 Cengage Learning. All Rights Reserved. May not be copied, scanned, or duplicated, in whole or in part. Due to electronic rights, some third party content may be suppressed from the eBook and/or eChapter(s). Editorial review has deemed that any suppressed content does not materially affect the overall learning experience. Cengage Learning reserves the right to remove additional content at any time if subsequent rights restrictions require it.

or

$$\boxed{z = \frac{t_0 v_{p_1}}{2}} \tag{4.71}$$

With v_{p_1} and t_0 known, the thickness of the top layer z can be calculated.

Another convenient way to interpret the reflection survey record is to plot a graph of t^2 versus x^2. From Eq. (4.69),

$$t^2 = \frac{4}{v_{p_1}^2}\left[z^2 + \left(\frac{x}{2}\right)^2\right] = \frac{1}{v_{p_1}^2}(4z^2 + x^2) \tag{4.72}$$

This relation indicates that the plot of t^2 versus x^2 will be a straight line, as shown in Figure 4.48c. The slope of this line give $1/v_{p_1}^2$ and the intercept on the t^2 axis will be equal to t_0^2. Substituting $t = t_0$ and $x = 0$ into Eq. (4.72),

$$t_0^2 = \frac{4z^2}{v_{p_1}^2}$$

or

$$\boxed{z^2 = \frac{t_0^2 v_{p_1}^2}{4}} \tag{4.73}$$

With t_0^2 and $v_{p_1}^2$ known, the thickness of the top layer can now be calculated.

EXAMPLE 4.3

The results of a reflection survey on a relatively flat area (shale underlain by granite) are given here. Determine the velocity of P-waves in the shale.

Distance from point of disturbance (m)	Time for first reflection (s)
30	1.000
90	1.002
150	1.003
210	1.007
270	1.011
330	1.017
390	1.023

Copyright 2017 Cengage Learning. All Rights Reserved. May not be copied, scanned, or duplicated, in whole or in part. Due to electronic rights, some third party content may be suppressed from the eBook and/or eChapter(s). Editorial review has deemed that any suppressed content does not materially affect the overall learning experience. Cengage Learning reserves the right to remove additional content at any time if subsequent rights restrictions require it.

SOLUTION

Using the time-distance records, the following table can be prepared.

x (m)	x^2 (m^2)	t (s)	t^2 (s^2)
30	900	1.000	1.000
90	8,100	1.002	1.004
150	22,500	1.003	1.006
210	44,100	1.007	1.014
270	72,900	1.011	1.022
330	108,900	1.017	1.034
390	152,100	1.023	1.046

A plot of t^2 versus x^2 is shown in Figure 4.49. From the plot,

$$v_{p_1} = \sqrt{\frac{(\Delta x)^2}{(\Delta t)^2}} = \sqrt{\frac{79200}{0.023}} = \mathbf{1816.6\ m/s}$$

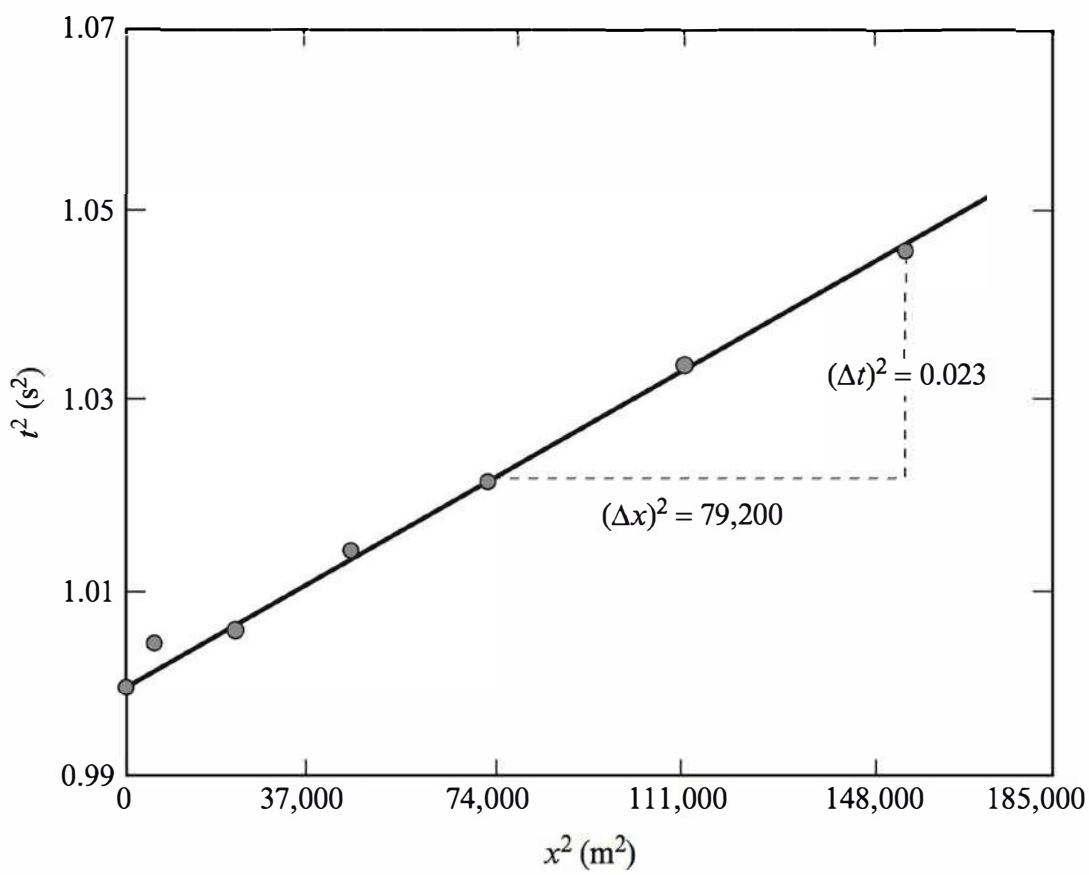

Figure 4.49

Copyright 2017 Cengage Learning. All Rights Reserved. May not be copied, scanned, or duplicated, in whole or in part. Due to electronic rights, some third party content may be suppressed from the eBook and/or eChapter(s). Editorial review has deemed that any suppressed content does not materially affect the overall learning experience. Cengage Learning reserves the right to remove additional content at any time if subsequent rights restrictions require it.

4.15 REFLECTION SURVEY IN SOIL (INCLINED LAYERING)

Figure 4.50 considers the case of a reflection survey where the reflecting boundary is inclined at an angle β with respect to the horizontal. A is the point for the source of disturbance. The reflected P-ray reaching point C will take the path ABC. Referring to Figure 4.50,

$$AB + BC = A'B + BC = A'C$$

But

$$(A'C)^2 = (A'A_2)^2 + (A_2C)^2 \tag{4.74}$$

$$A'A_2 = AA' \cos\beta = 2z' \cos\beta \tag{4.75}$$

$$A_2C = A_2A + AC = 2z' \sin\beta + x_C \tag{4.76}$$

Substituting Eqs. (4.75) and (4.76) into Eq. (4.74),

$$A'C = \sqrt{(2z'\cos\beta)^2 + (2z'\sin\beta + x_C)^2}$$
$$= \sqrt{4z'^2 + x_C^2 + 4z'x_C \sin\beta}$$

Thus, the travel time for the reflected P-wave along the path ABC will be

$$t_C = \frac{A'C}{v_{p_1}}$$

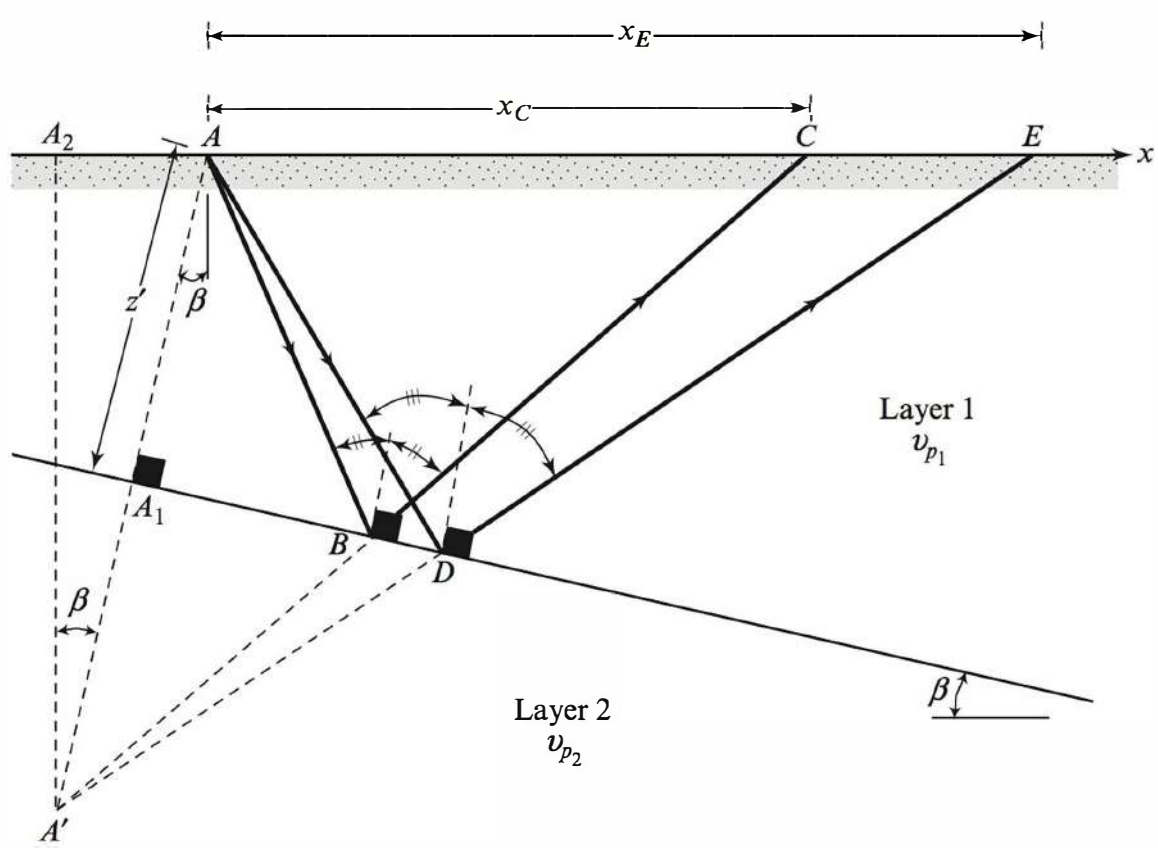

Figure 4.50 Reflection survey in soil—inclined layering

Copyright 2017 Cengage Learning. All Rights Reserved. May not be copied, scanned, or duplicated, in whole or in part. Due to electronic rights, some third party content may be suppressed from the eBook and/or eChapter(s). Editorial review has deemed that any suppressed content does not materially affect the overall learning experience. Cengage Learning reserves the right to remove additional content at any time if subsequent rights restrictions require it.

So

$$t_C = \frac{1}{v_{p_1}}\sqrt{4z'^2 + x_C^2 + 4z'x_C \sin\beta} \tag{4.77}$$

In a similar manner, the time of arrival for the reflected P-waves received at point E can be given as

$$t_E = \frac{1}{v_{p_1}}\sqrt{4z'^2 + x_E^2 + 4z'x_E \sin\beta} \tag{4.78}$$

Combining Eqs. (4.77) and (4.78),

$$\sin\beta = \frac{v_{p_1}^2(t_E^2 - t_C^2)}{4z'(x_E - x_C)} - \frac{x_E + x_C}{4z'} \tag{4.79}$$

Now, let $\bar{t} = (t_E + t_C)/2$ and $\Delta t = t_E - t_C$

Substitution of the preceding relations in Eq. (4.79) gives

$$\sin\beta = \frac{v_{p_1}^2\bar{t}(\Delta t)}{2z'(x_E - x_C)} - \frac{x_E + x_C}{4z'} \tag{4.80}$$

If x_C is equal to zero, Eq. (4.80) will transform to

$$\sin\beta = \frac{v_{p_1}^2\bar{t}(\Delta t)}{2z'x_E} - \frac{x_E}{4z'} \tag{4.81}$$

If $x_C = 0$ and $\beta = 0$ (that is, the reflecting layer is horizontal) then, from Eq. (4.81),

$$\Delta t = \frac{x_E^2}{2v_{p_1}^2\bar{t}} \tag{4.82}$$

If $x_C = 0$ and $\Delta t > x_E^2/2v_{p_1}^2\bar{t}$, the reflecting layer is sloping down in the direction of positive x, as shown in Figure 4.50. If $x_C = 0$ and $\Delta t < x_E^2/2v_{p_1}^2\bar{t}$, the reflecting layer is sloping down in the direction of negative x (that is, opposite to that shown in Figure 4.50).

In actual practice, that point of disturbance A (Figure 4.51) is generally placed midway between the two detectors, so $x_E = -x_C = x$. So, from Eq. (4.80)

$$\sin\beta = \frac{v_{p_1}^2\bar{t}(\Delta t)}{4z'x} \tag{4.83}$$

Copyright 2017 Cengage Learning. All Rights Reserved. May not be copied, scanned, or duplicated, in whole or in part. Due to electronic rights, some third party content may be suppressed from the eBook and/or eChapter(s). Editorial review has deemed that any suppressed content does not materially affect the overall learning experience. Cengage Learning reserves the right to remove additional content at any time if subsequent rights restrictions require it.

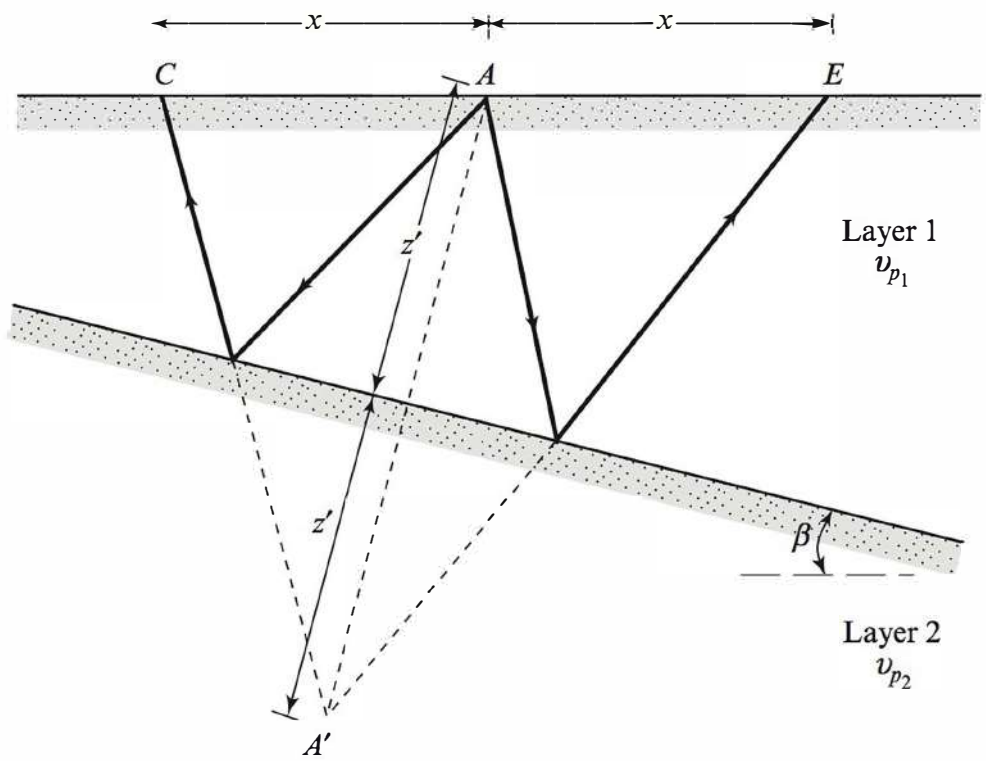

Figure 4.51

Referring to Figure 4.51, $AA' = 2z' = (A'C + A'E)/2$. So

$$\frac{2z'}{v_{p_1}} = \frac{1}{2}\left(\frac{A'C}{v_{p_1}} + \frac{A'E}{v_{p_1}}\right) = \frac{1}{2}(t_C + t_E) = \bar{t} \tag{4.84}$$

Combining Eqs. (4.83) and (4.84),

$$\sin\beta = \frac{v_{p_1}(\Delta t)}{2x} \tag{4.85}$$

EXAMPLE 4.4

Refer to Figure 4.51. Given: $x = 85.5$ m, $t_C = 0.026$ s, and $t_E = 0.038$ s. Determine β and z'. The value of v_{p_1} i.e., the velocity of the primary wave through the top layer has been previously determined to be 410 m/s.

SOLUTION

$$t = \frac{t_C + t_E}{2} = \frac{0.026 + 0.038}{2} = 0.032 \text{ s}$$

$$\Delta t = t_E - t_C = 0.038 - 0.026 = 0.012 \text{ s}$$

Copyright 2017 Cengage Learning. All Rights Reserved. May not be copied, scanned, or duplicated, in whole or in part. Due to electronic rights, some third party content may be suppressed from the eBook and/or eChapter(s). Editorial review has deemed that any suppressed content does not materially affect the overall learning experience. Cengage Learning reserves the right to remove additional content at any time if subsequent rights restrictions require it.

From Eq. (4.85)

$$\beta = \sin^{-1}\left[\frac{v_{p_1}(\Delta t)}{2x}\right] = \sin^{-1}\left[\frac{(410)(0.012)}{(2)(85.5)}\right] = \mathbf{1.65°}$$

From Eq. (4.84)

$$\frac{2z'}{v_{p_1}} = \bar{t}$$

or

$$z' = \frac{\bar{t}\,v_{p_1}}{2} = \frac{(0.032)(410)}{2} = \mathbf{6.56\ m}$$

4.16 SUBSOIL EXPLORATION BY STEADY-STATE VIBRATION

In steady-state vibration, a circular plate placed on the ground surface is vibrated vertically by a sinusoidal loading (Figure 4.52a). This vibration will send out *Rayleigh waves* (Section 3.13), and the vertical motion of the ground surface will predominantly be due to these waves. This can be picked up by motion transducers. The velocity of the *Rayleigh waves* can be given as

$$v_r = fL \tag{4.86}$$

where f = frequency of vibration of the plate and L = wavelength.

If the wavelength L can be measured, the velocity of Rayleigh waves can easily be calculated. The wavelength is generally determined by the number of waves occurring at a given distance x. For a given frequency f_1 the wavelength can be given as

$$L_1 = \frac{x}{n_1} \tag{4.87}$$

where n_1 = number of waves at a distance x for frequency f_1 (as shown in Figure 4.52b).

It was shown in Chapter 3 that the Rayleigh wave velocity is approximately equal to the shear wave velocity. So

$$v_r \approx v_s \tag{4.88}$$

It was also discussed in Chapter 3 that, for all practical purposes, the Rayleigh wave travels through the soil within a depth of one wavelength. Hence for a given

Copyright 2017 Cengage Learning. All Rights Reserved. May not be copied, scanned, or duplicated, in whole or in part. Due to electronic rights, some third party content may be suppressed from the eBook and/or eChapter(s). Editorial review has deemed that any suppressed content does not materially affect the overall learning experience. Cengage Learning reserves the right to remove additional content at any time if subsequent rights restrictions require it.

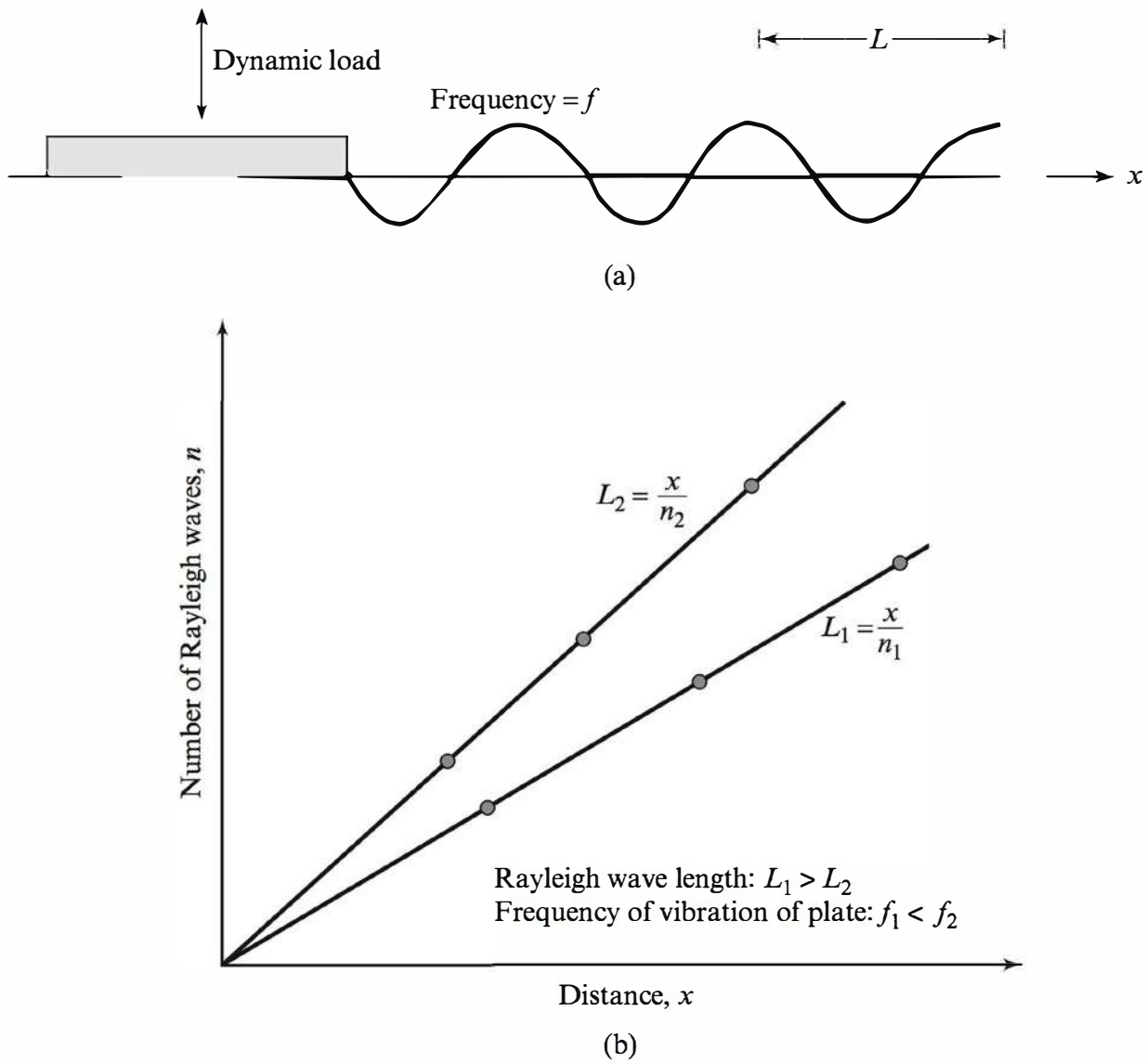

Figure 4.52 Subsoil exploration by steady-state vibration

frequency f, if the wavelength L is known, the value of v_s determined by the preceding technique will represent the soil conditions at an average depth of $L/2$. Thus for a *large value of f*, the value of v_s is representative of soil conditions at a *smaller depth*; and, for a *small value of f*, the value of v_s obtained is representative of the soil conditions at a *larger depth*. Figure 4.53 shows the results of wave propagation on a stratified pavement system obtained using this technique.

4.17 SPECTRAL ANALYSIS OF SURFACE WAVE (SASW)

The Spectral Analysis of Surface Wave (SASW) method is a nonintrusive technique developed from the steady-state vibration. The fundamentals of SASW method involve the generation, measurement, and analysis of Rayleigh waves at the test site. The shear wave velocity (v_s) profile of the test site can be derived from the measured Rayleigh wave velocity.

Figure 4.52 shows a traditional configuration of equipment adopted in SASW testing with a two-channel recording system. The surface waves are

Copyright 2017 Cengage Learning. All Rights Reserved. May not be copied, scanned, or duplicated, in whole or in part. Due to electronic rights, some third party content may be suppressed from the eBook and/or eChapter(s). Editorial review has deemed that any suppressed content does not materially affect the overall learning experience. Cengage Learning reserves the right to remove additional content at any time if subsequent rights restrictions require it.

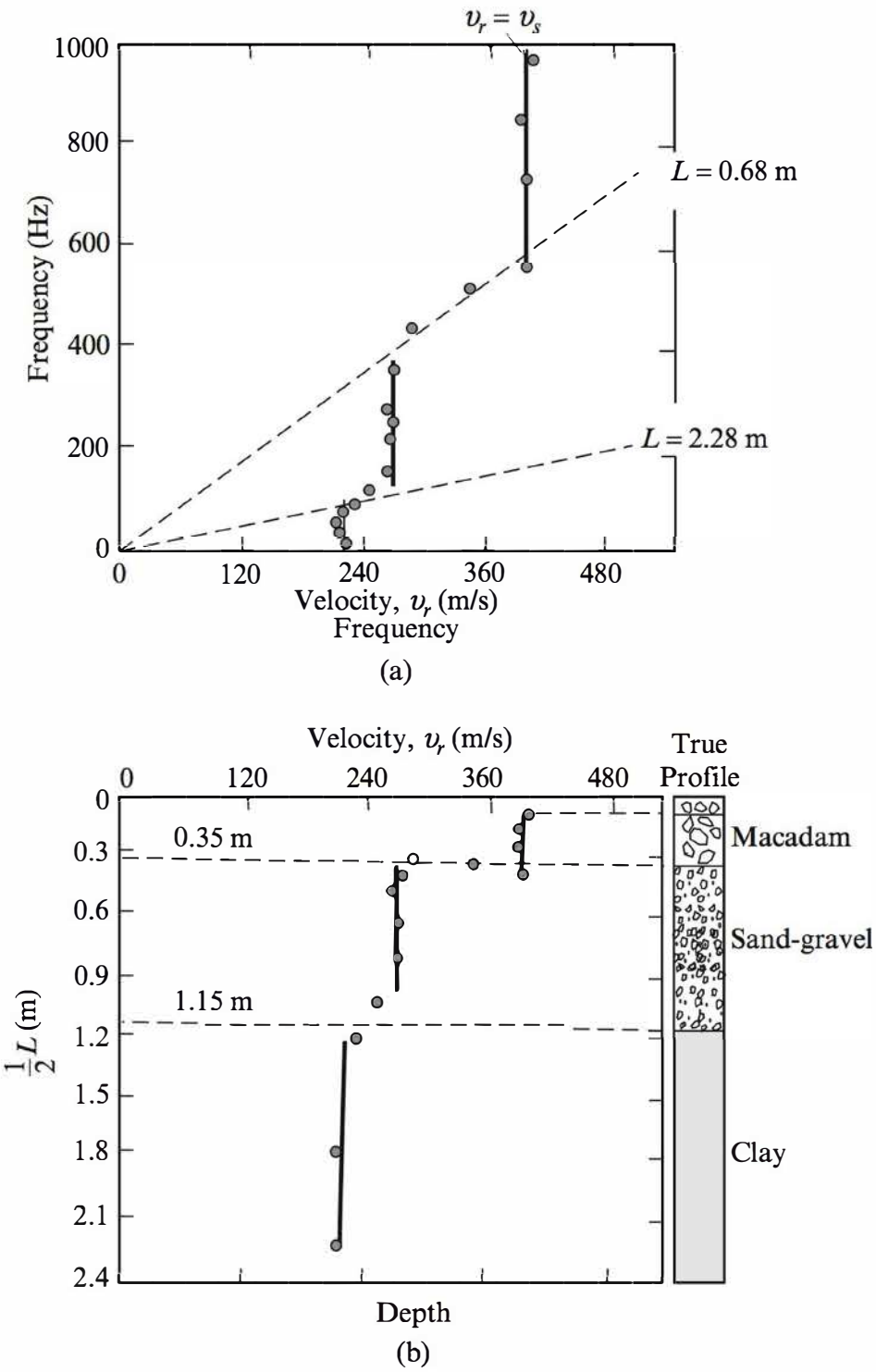

Figure 4.53 v_r as a function of frequency and depth determined by the steady-state vibration technique (after Heukelom and Foster 1960)

Source: Heukelom, W., and Foster, C.R. (1960). "Dynamic Testing of Pavements," *Journal of the Soil Mechanics and Foundations Division*, ASCE, Vol. 86, No. SM1, Part 1, pp. 1–28. With permission from ASCE.

generated by a dynamic vertical load (such as by hammer or bulldozer) to the ground surface. All the equipment in SASW test is deployed on the ground surface, and thus no boreholes are required. The time delay between the two receivers is a function of wave frequency (f) and is determined as

$$t(f) = \frac{\phi(f)}{2\pi f} \tag{4.89}$$

Copyright 2017 Cengage Learning. All Rights Reserved. May not be copied, scanned, or duplicated, in whole or in part. Due to electronic rights, some third party content may be suppressed from the eBook and/or eChapter(s). Editorial review has deemed that any suppressed content does not materially affect the overall learning experience. Cengage Learning reserves the right to remove additional content at any time if subsequent rights restrictions require it.

where $\phi(f)$ = phase angle for a given frequency in radians. The surface wave phase velocity (v_r) and the surface wave length (L) are calculated as

$$v_r = \frac{d_2}{t(f)} \tag{4.90}$$

$$L = \frac{v_r}{f} \tag{4.91}$$

where d_2 = distance between receivers. The v_r and L are calculated for each frequency at various receiver spacing d_2, and the resulting $v_r - L$ relationship is the experimental dispersion curve (for example, see Figure 4.55). A dispersion curve is the correlation between the surface wave velocity and the wavelength (or the equivalent frequency).

The dispersion curves are then used to determine the shear wave velocity (v_s) profile. The v_s profile of the test site can be determined by iteratively fitting the experiment dispersion curve with a theoretical dispersion curve, the latter is derived from an assumed v_s profile. In this iterative procedure, the values of shear wave velocity and the thicknesses of each soil layer in the assumed v_s profile are updated by trial and error until a satisfactory theoretical dispersion curve that fits the experiment dispersion curve is obtained (for example, see Figure 4.55). The corresponding v_s profile for the best-fit theoretical dispersion curve is determined to be the v_s profile for this test site. Figure 4.56 shows the shear wave velocity profile for the best-fit theoretical dispersion curve shown in Figure 4.55.

The SASW method is typically used to obtain shear wave velocity profiles for earthquake site response, liquefaction analysis, soil compaction control, pavement evaluation, mapping subsurface stratigraphy, etc. The shear wave velocity profiles at greater depth require a high-energy and low-frequency wave source, while profiles with shallower depth need a low-energy and high-frequency wave source.

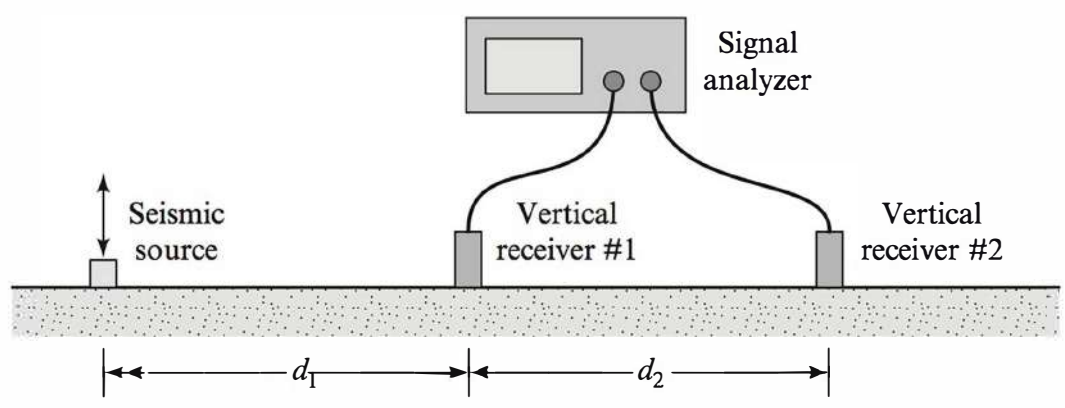

Figure 4.54 Standard configuration of equipment in SASW testing with a two-channel recording system

Copyright 2017 Cengage Learning. All Rights Reserved. May not be copied, scanned, or duplicated, in whole or in part. Due to electronic rights, some third party content may be suppressed from the eBook and/or eChapter(s). Editorial review has deemed that any suppressed content does not materially affect the overall learning experience. Cengage Learning reserves the right to remove additional content at any time if subsequent rights restrictions require it.

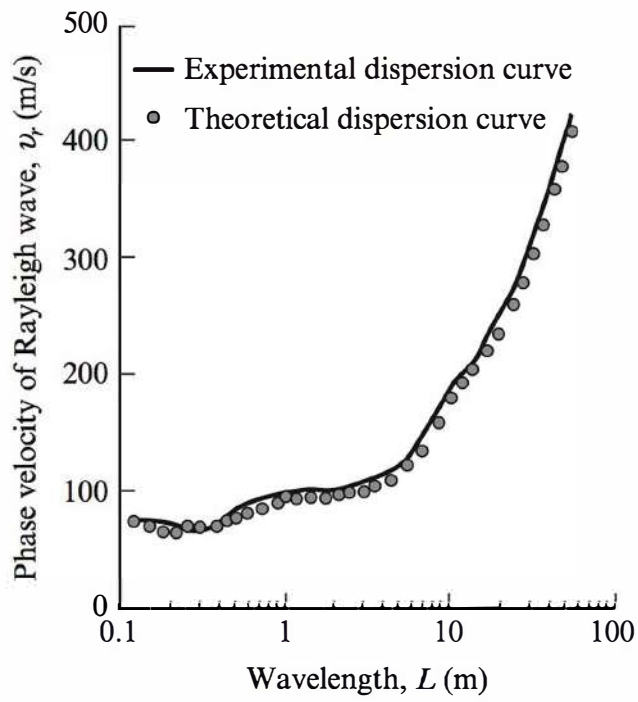

Figure 4.55 Comparison between experimental and theoretical dispersion curves (adapted from Stokoe et al., 1994)

Source: Based on Stokoe, K.H. II, Wright, S.G., Bay, J.A., and Roesset, J.M. (1994). "Characterization of Geotechnical Sites by SASW Method." *Technical Review: Geophysical Characterization of Sites, ISSMFE Technical Committee* 10, edited by R.D. Woods, Oxford, New Delhi, pp. 11–25.

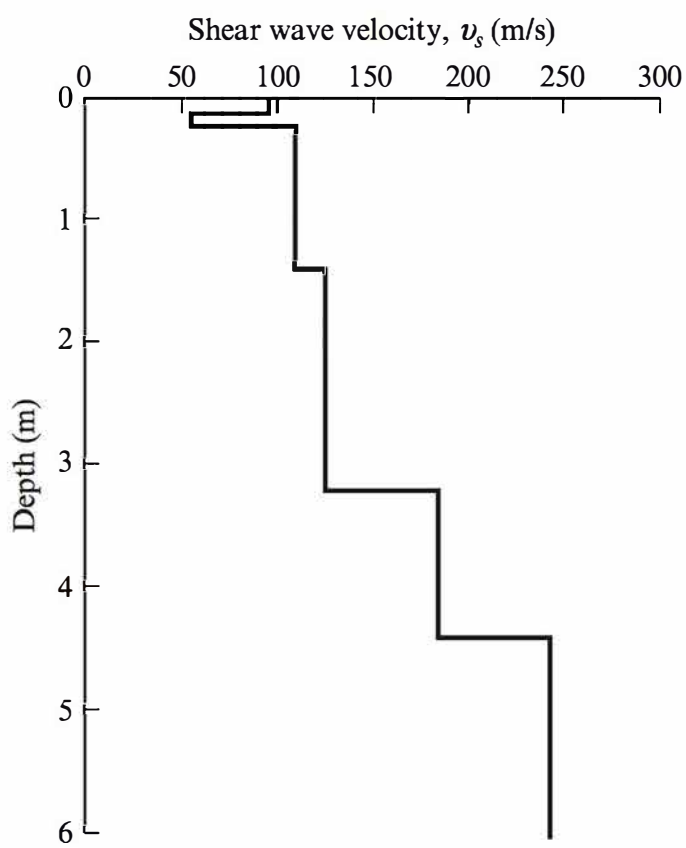

Figure 4.56 Shear wave velocity profile determined from SASW (adapted from Stokoe et al., 1994)

Source: Based on Stokoe, K.H. II, Wright, S.G., Bay, J.A., and Roesset, J.M. (1994). "Characterization of Geotechnical Sites by SASW Method." *Technical Review: Geophysical Characterization of Sites, ISSMFE Technical Committee* 10, edited by R.D. Woods, Oxford, New Delhi, pp. 11–25.

Copyright 2017 Cengage Learning. All Rights Reserved. May not be copied, scanned, or duplicated, in whole or in part. Due to electronic rights, some third party content may be suppressed from the eBook and/or eChapter(s). Editorial review has deemed that any suppressed content does not materially affect the overall learning experience. Cengage Learning reserves the right to remove additional content at any time if subsequent rights restrictions require it.

4.18 SOIL EXPLORATION BY "SHOOTING UP THE HOLE," "SHOOTING DOWN THE HOLE," AND "CROSS-HOLE SHOOTING"

Shooting Up the Hole

In the technique of shooting up the hole, a hole is drilled into the ground and a detector is placed at the ground surface. Charges are exploded at various depths in the hole and the direct travel time of body waves (P or S) along the boundary of the hole is measured. Thus the values of v_p and v_s of various soil layers can be easily obtained. There is a definite advantage in this technique, since it determines the *shear wave velocities of various soil layers*. The refraction and reflection techniques give only the P-wave velocity. However, below the groundwater table, the compression waves will travel through water. The first arrival for points below the water table will usually be for this type, and the wave velocity will generally be higher than the compression wave velocity in soils. On the other hand, shear waves cannot travel through water, and the shear wave velocity measure above or below the water table will be the same.

Shooting Down the Hole

Shear wave velocity determination of various soil layers by shooting down the hole has been described by Schwarz and Musser (1972), Beeston and McEvilly (1977), and Larkin and Taylor (1979). Figure 4.57 shows a schematic diagram for the down-hole method of seismic waves testing as presented by Larkin and Taylor, which relies on measuring the time interval for SH-waves to travel between the ground surface and the subsurface points. A bidirectional impulsive source for the propagation of SH-waves is placed on the surface adjacent to a borehole. A horizontal sensitive transducer is located at a depth in the borehole. The depth of the transducer in varied throughout the length of the borehole. The shear wave velocity can then be obtained as

$$\boxed{v_s = \frac{\Delta z}{\Delta t}} \tag{4.92}$$

where z = depth below the ground surface
t = time of travel of the shear wave from the surface impulsive source to the transducer

During the process of field investigation, Larkin and Taylor (1979) determined that the shear strains at depths of 3 m and 50 m were about 1×10^{-6} and 0.3×10^{-6}, respectively. In order to compare the field and laboratory values of v_s, some undisturbed samples from various depths were collected. The shear wave

Copyright 2017 Cengage Learning. All Rights Reserved. May not be copied, scanned, or duplicated, in whole or in part. Due to electronic rights, some third party content may be suppressed from the eBook and/or eChapter(s). Editorial review has deemed that any suppressed content does not materially affect the overall learning experience. Cengage Learning reserves the right to remove additional content at any time if subsequent rights restrictions require it.

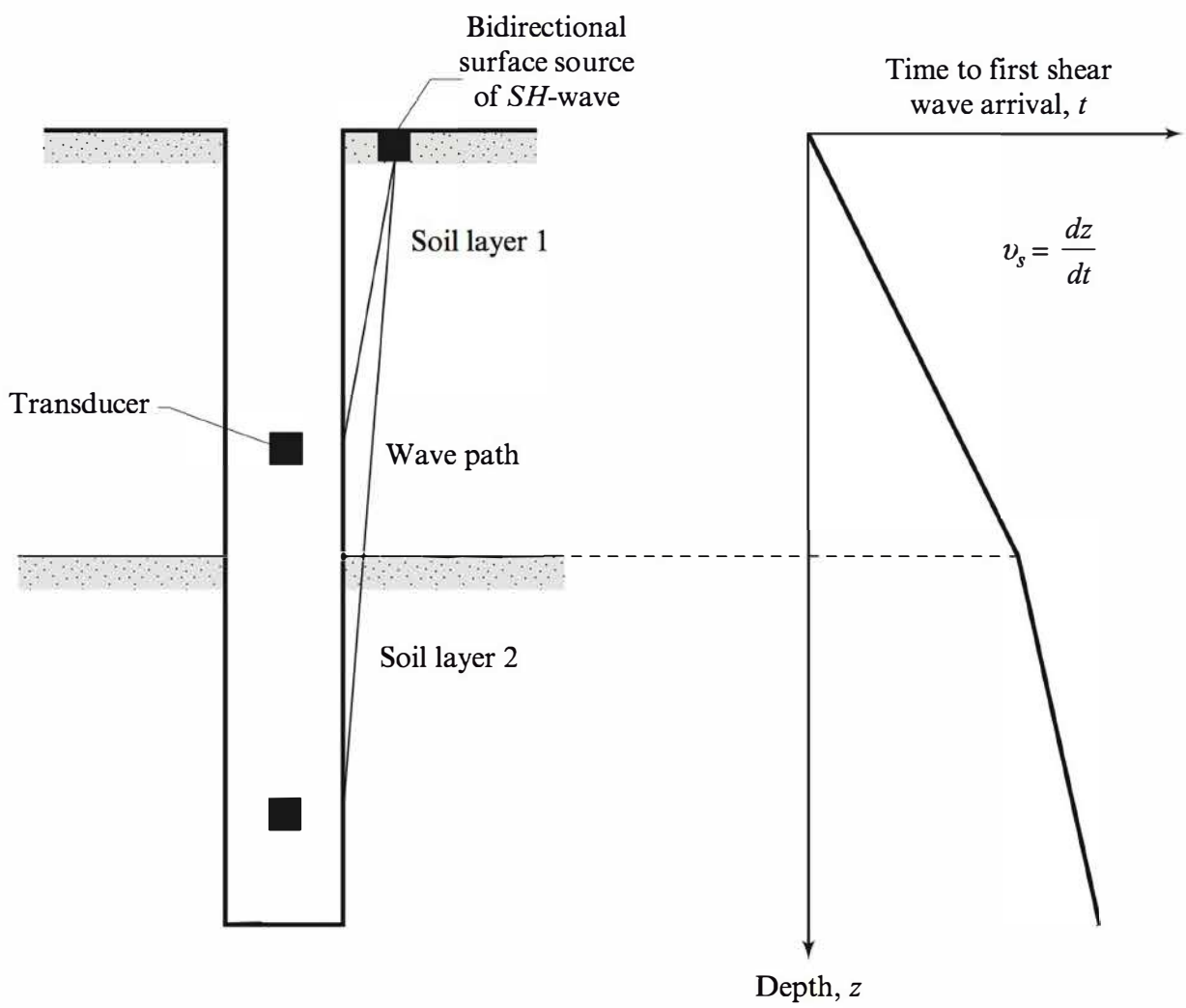

Figure 4.57 The down-hole method of seismic wave testing

velocity of various specimens at a shear strain level of 1×10^{-6} was determined. A comparison of the laboratory and field test results showed that, for similar soils, the value of $v_{s(\text{lab})}$ is considerably lower than that obtained in the field. For *the range of soil tested*,

$$v_{s(\text{lab})} \approx 0.25\, v_{s(\text{field})} + 83$$

where $v_{s(\text{lab})}$ and $v_{s(\text{field})}$ are in meters per second.

Larkin and Taylor also defined a quantity called the sample disturbance factor S_D:

$$S_D = \left[\frac{v_{s(\text{field})}}{v_{s(\text{lab})}}\right]^2 = \frac{G_{\text{field}}}{G_{\text{lab}}} \tag{4.93}$$

The average value of S_D in Larkin and Taylor's investigation varied from about 1 for $v_{s(\text{field})} = 140$ m/s to about 4 for $v_{s(\text{field})} = 400$ m/s. This shows that small disturbances in the sampling could introduce large errors in the evaluation of representative shear moduli of soils.

Copyright 2017 Cengage Learning. All Rights Reserved. May not be copied, scanned, or duplicated, in whole or in part. Due to electronic rights, some third party content may be suppressed from the eBook and/or eChapter(s). Editorial review has deemed that any suppressed content does not materially affect the overall learning experience. Cengage Learning reserves the right to remove additional content at any time if subsequent rights restrictions require it.

Cross-Hole Shooting

The seismic cross-hole survey is considered by many engineers to be the most reliable method of determining the dynamic shear modulus of soil. The technique of cross-hole shooting relies on the measurement of SV-wave velocity. In this procedure of seismic surveying, two vertical boreholes at a given distance apart are advanced into the ground (Figure 4.58). Shear waves are generated by a vertical impact at the bottom of one borehole. The arrival of the body wave is recorded by a vertically sensitive transducer placed at the bottom of another borehole at the same depth. Thus

$$v_s = \frac{L}{t} \tag{4.94}$$

where t = travel time for the shear wave
L = length between the two boreholes.

The smallest possible borehole diameter should be used as small uncased boreholes are more stable than larger diameter holes. Even if casing is required, a small diameter borehole will cause less soil disturbance. Usually aluminium or PVC casing is used instead of steel casing. Void spaces around the casing must be filled with weak cement slurry grout. Spacing between the boreholes can be 2

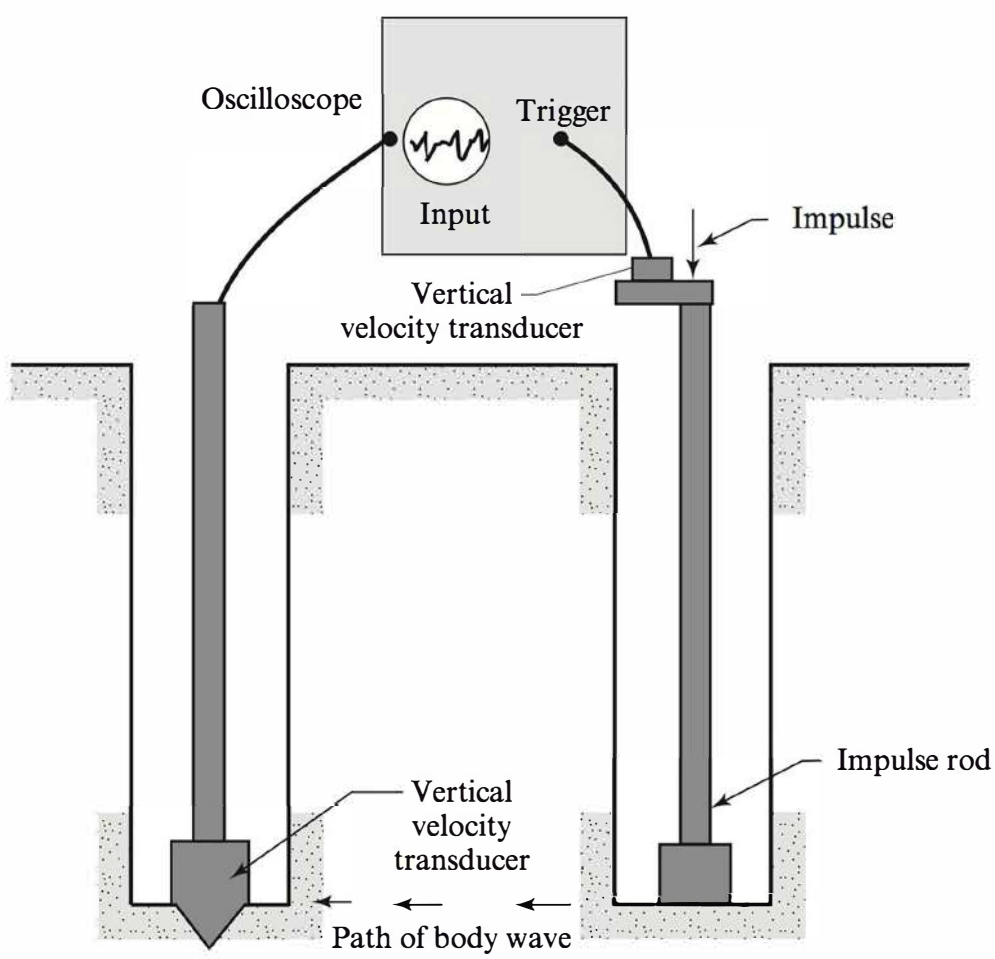

Figure 4.58 Schematic diagram of cross-hole seismic survey technique

Copyright 2017 Cengage Learning. All Rights Reserved. May not be copied, scanned, or duplicated, in whole or in part. Due to electronic rights, some third party content may be suppressed from the eBook and/or eChapter(s). Editorial review has deemed that any suppressed content does not materially affect the overall learning experience. Cengage Learning reserves the right to remove additional content at any time if subsequent rights restrictions require it.

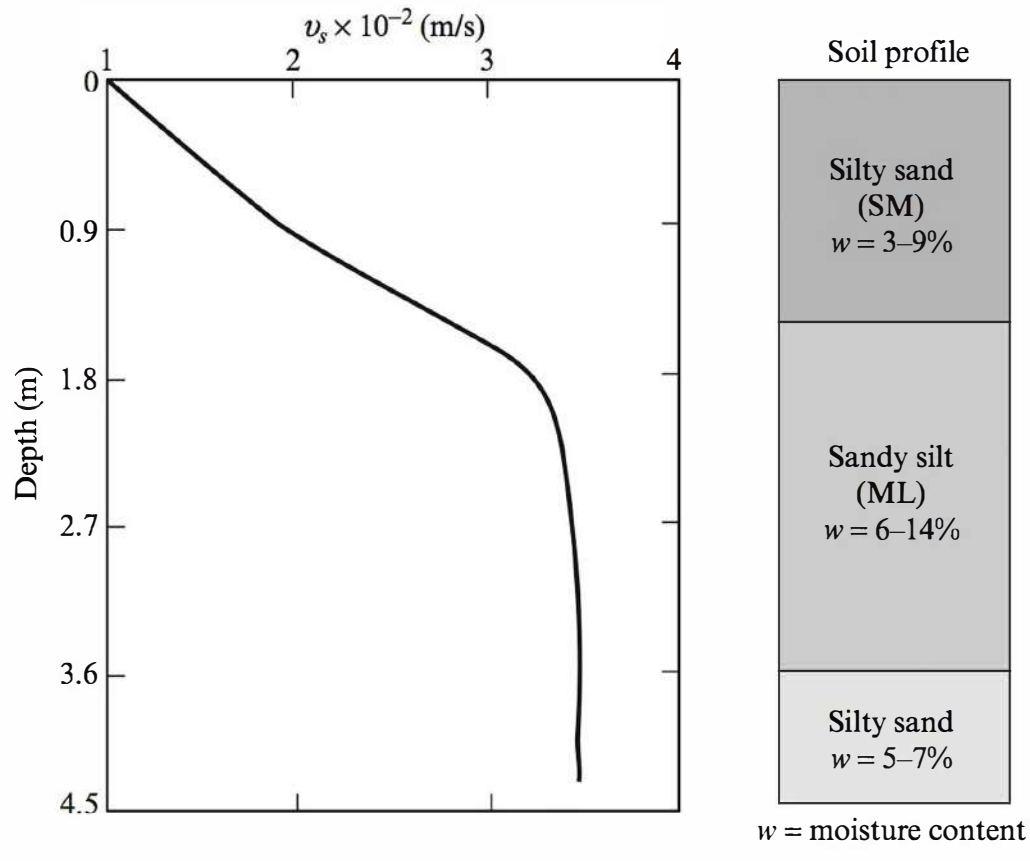

Figure 4.59 Shear wave velocity versus depth from cross-hole seismic survey (redrawn after Stokoe and Woods. 1972)
Source: Based on Stokoe, K.H. II, Wright, S.G., Bay, J.A., and Roesset, J.M. (1994). "Characterization of Geotechnical Sites by SASW Method." *Technical Review: Geophysical Characterization of Sites, ISSMFE Technical Committee* 10, edited by R.D. Woods, Oxford, New Delhi, pp. 11–25.

to 3 meters. The borehole spacing at the surface can be used as L, and for deeper boreholes (say more than 10 m in depth), inclinometers must be used to calculate L accurately as a small error in L can lead to large differences in estimated shear wave velocity. Figure 4.59 shows the plot of the shear wave velocity against depth for a test site obtained from the cross-hole shooting technique of seismic surveying.

4.19 CORRELATIONS FOR SHEAR WAVE VELOCITY, v_s

Several correlations between the shear wave velocity v_s and field standard penetration number N have been presented in the past. A few of these correlations are given in Table 4.4. Significant differences exist among the published relations that may be due to differences in geology along with the measurement of N and v_s.

4.20 CYCLIC PLATE LOAD TEST

The cyclic field plate load test is similar to the plate bearing test conducted in the field for evaluation of the allowable bearing capacity of soil for foundation design purposes. The plates used for tests in the field are usually made of steel and are 25 mm thick and 150 mm to 762 mm in diameter.

Copyright 2017 Cengage Learning. All Rights Reserved. May not be copied, scanned, or duplicated, in whole or in part. Due to electronic rights, some third party content may be suppressed from the eBook and/or eChapter(s). Editorial review has deemed that any suppressed content does not materially affect the overall learning experience. Cengage Learning reserves the right to remove additional content at any time if subsequent rights restrictions require it.

Table 4.4 Some Correlations between v_s (m/s) and N.

Source	Correlation
Imai (1977)	All soils: $v_s = 91N^{0.377}$
	Sand: $v_s = 80.6N^{0.331}$
	Clay: $v_s = 80.2N^{0.292}$
Ohta and Goto (1978)	All soils: $v_s = 85.35N^{0.348}$
Seed and Idriss (1981)	All soils: $v_s = 61.4N^{0.5}$
Sykora and Stokoe (1983)	Sand: $v_s = 100.5N^{0.29}$
Okamoto et al. (1989)	Sand $v_s = 125N^{0.3}$
Pitilakis et al. (1999)	Sand: $v_s = 145N^{0.178}$
	Clay: $v_s = 132N^{0.271}$
Kiku et al. (2001)	All soils: $v_s = 68.3N^{0.292}$
Jafari et al. (2002)	Sand: $v_s = 22N^{0.77}$
	Clay: $v_s = 27N^{0.73}$
Hasancebi and Ulusay (2006)	All soils: $v_s = 99N^{0.309}$
	Sand: $v_s = 90.82N^{0.319}$
	Clay: $v_s = 97.89N^{0.269}$
Dikman (2009)	All soils: $v_s = 58N^{0.39}$
	Sand: $v_s = 73N^{0.33}$
	Silt: $v_s = 60N^{0.36}$
	Clay $v_s = 44N^{0.48}$

To conduct a test, a hole is excavated to the desired depth. The plate is placed at the center of the hole, and load is applied to the plate in steps—about one-fourth to one-fifth of estimated ultimate load—by a jack. Each step load is kept constant until the settlement becomes negligible. The final settlement is recorded by dial gauges. Then the load is removed and the plate is allowed to rebound. At the end of the rebounding period, the settlement of the plate is recorded. Following that, the load on the plate is increases to reach a magnitude of the next proposed stage of loading. The process of settlement recording is then repeated.

Figure 4.60 shows the nature of the plot of q versus settlement (s) obtained from a cyclic plate load test. Note that

$$q = \frac{\text{load on the plate}, Q}{\text{area of the plate}, A}$$

Based on field test results, the magnitude of the spring constant k [See Chapter 2, Eq. (2.3)] and the shear modulus G of the soil can be calculated in the following

Copyright 2017 Cengage Learning. All Rights Reserved. May not be copied, scanned, or duplicated, in whole or in part. Due to electronic rights, some third party content may be suppressed from the eBook and/or eChapter(s). Editorial review has deemed that any suppressed content does not materially affect the overall learning experience. Cengage Learning reserves the right to remove additional content at any time if subsequent rights restrictions require it.

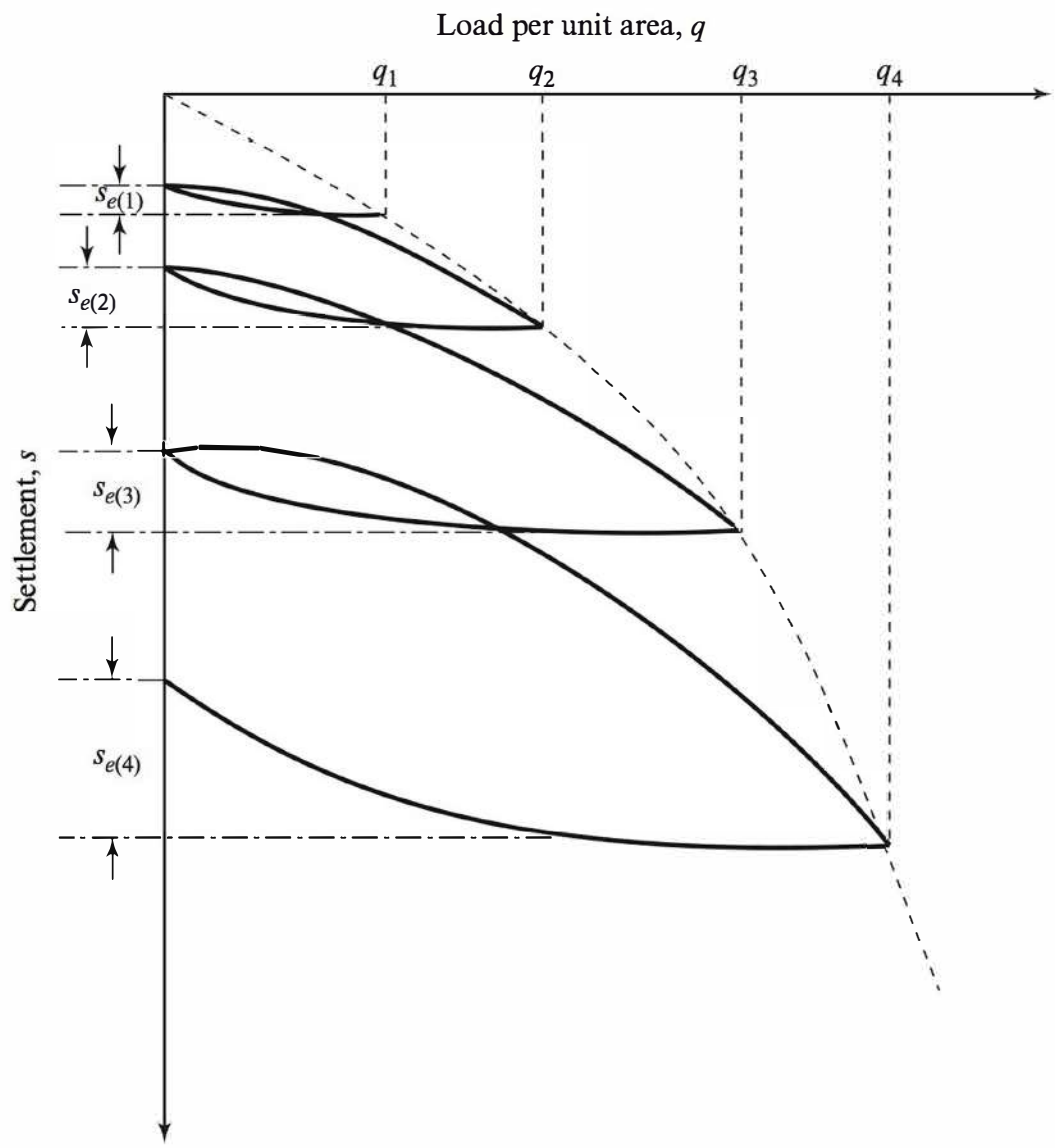

Figure 4.60 Nature of load settlement diagram for a cyclic plate load test

manner. It is worth noting that in order to accurately reflect the nonlinear response of the soil, it would be necessary to establish the similar strains between the small scale footing and prototype footing. A number of cycles of loading of the plate may be needed to replicate the elastic condition in the soil under footing.

Spring Constant *k*

1. Referring to Figure 4.60, calculate the elastic settlement $[s_{e(1)}, s_{e(2)}, \ldots]$ for each loading stage.
2. Plot a graph of q versus s_e, as shown in Figure 4.61.
3. Calculate the spring constant of the plate as

$$\boxed{k_{\text{plate}} = \frac{qA}{s_e}} \tag{4.95}$$

Copyright 2017 Cengage Learning. All Rights Reserved. May not be copied, scanned, or duplicated, in whole or in part. Due to electronic rights, some third party content may be suppressed from the eBook and/or eChapter(s). Editorial review has deemed that any suppressed content does not materially affect the overall learning experience. Cengage Learning reserves the right to remove additional content at any time if subsequent rights restrictions require it.

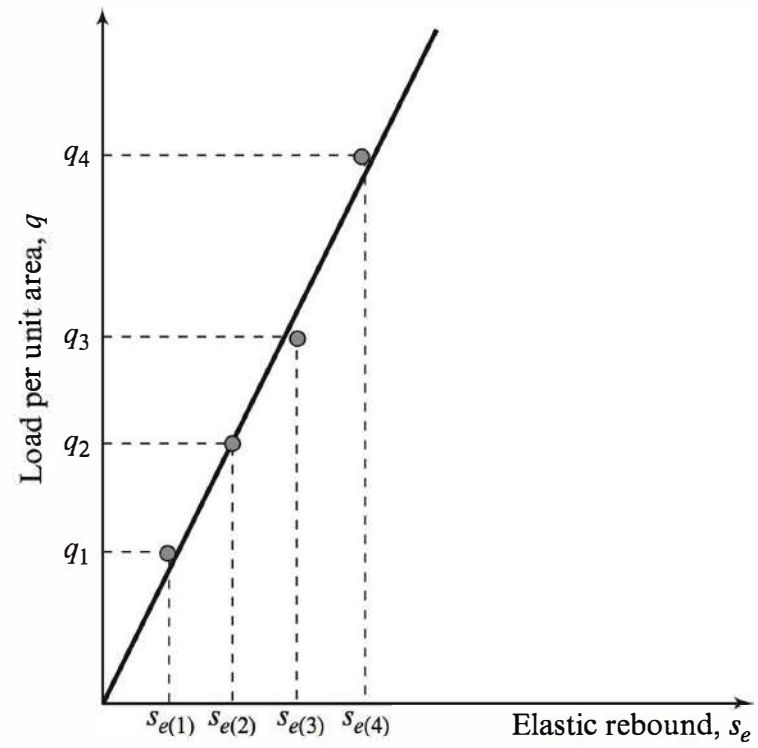

Figure 4.61

4. The spring constant for vertical loading for a proposed foundation can then be extrapolated as follows (Terzaghi, 1955).

Cohesive soil:

$$k_{\text{foundation}} = k_{\text{plate}}\left(\frac{\text{foundation width}}{\text{plate width}}\right) \tag{4.96}$$

Cohesionless soil:

$$k_{\text{foundation}} = k_{\text{plate}}\left(\frac{\text{foundation width} + \text{plate width}}{2 \times \text{plate width}}\right)^2 \tag{4.97}$$

Shear Modulus, *G*

It can be shown theoretically (Barkan, 1962) that

$$C_z = \frac{q}{s_e} = 1.13\frac{E}{1-\mu^2}\frac{1}{\sqrt{A}} \tag{4.98}$$

where C_z = subgrade modulus
E = modulus of elasticity
μ = Poisson's ratio
A = area of the plate

Copyright 2017 Cengage Learning. All Rights Reserved. May not be copied, scanned, or duplicated, in whole or in part. Due to electronic rights, some third party content may be suppressed from the eBook and/or Chapter(s). Editorial review has deemed that any suppressed content does not materially affect the overall learning experience. Cengage Learning reserves the right to remove additional content at any time if subsequent rights restrictions require it.

However,

$$G = \frac{E}{2(1+\mu)}$$

So

$$C_z = \frac{2.26G(1+\mu)}{1-\mu^2}\frac{1}{\sqrt{A}}$$

or

$$\boxed{G = \frac{(1-\mu)C_z\sqrt{A}}{2.26}} \tag{4.99}$$

The magnitude of C_z can be obtained from the plot of q versus s_e (Figure 4.61). With the known value of A and a representative value of μ, the shear modulus can be calculated from Eq. (4.99). In nonhomogenous soils, it may be desirable to conduct the test at different depths or one may use different plate sizes to reflect the change in soil stiffness with depth. Again, it should be noted that this test suffers from the same limitations as reported in traditional geotechnical engineering practice for the design of foundations.

EXAMPLE 4.5

The plot of q versus s (settlement) obtained from a cyclic plate load test is shown in Figure 4.62. The area of the plate used for the test was 0.3 m^2. Calculate

a. k_{plate}, and
b. shear modulus G (assume $\mu = 0.35$).

SOLUTION

a. From Figure 4.62, the following can be determined.

Load per unit area, q (kPa)	Elastic settlement, s_e (mm).
75	0.53
150	1.10
225	1.50
300	2.10

Copyright 2017 Cengage Learning. All Rights Reserved. May not be copied, scanned, or duplicated, in whole or in part. Due to electronic rights, some third party content may be suppressed from the eBook and/or eChapter(s). Editorial review has deemed that any suppressed content does not materially affect the overall learning experience. Cengage Learning reserves the right to remove additional content at any time if subsequent rights restrictions require it.

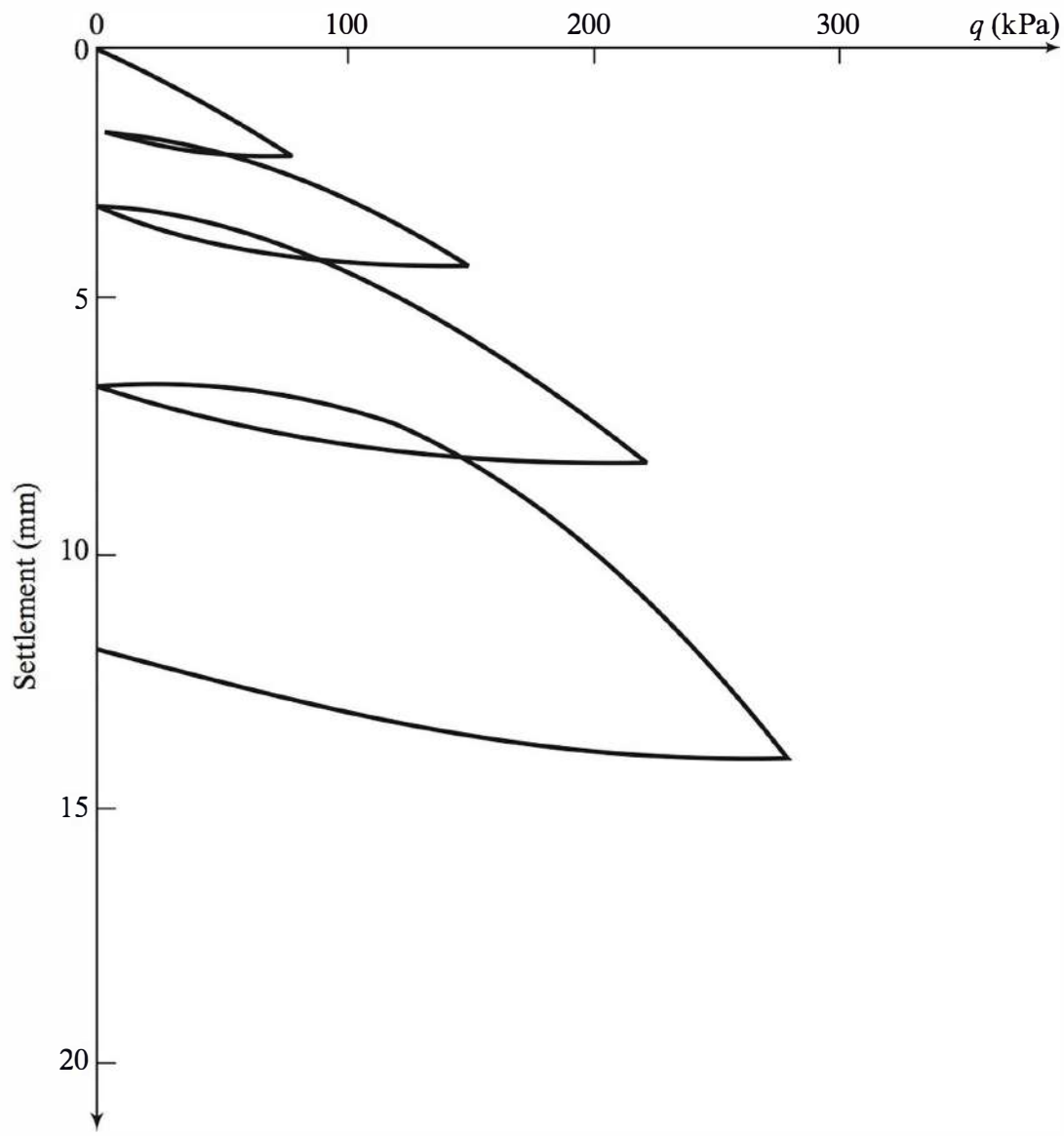

Figure 4.62

Figure 4.63 shows a plot of q versus s_e. From the average plot,

$$C_z = \frac{q}{s_e} = \frac{300}{0.0021} = 142.86 \text{ MN/m}^3$$

From Eq. (4.95)

$$k_{\text{plate}} = \frac{qA}{s_e} = (142.86)(0.3) = \mathbf{42.86\ MN/m.}$$

b. From Eq. (4.99)

$$G = \frac{(1-\mu)C_z\sqrt{A}}{2.26} = \frac{(1-0.35)(142.86)(\sqrt{0.3})}{2.26}$$
$$\approx \mathbf{22.5\ MPa}$$

This method can be extremely useful in sandy soils, provided it is being preceded by a boring program. But this test may not give good results if a weak stratum lies below the significant depth of test plate but within the

Copyright 2017 Cengage Learning. All Rights Reserved. May not be copied, scanned, or duplicated, in whole or in part. Due to electronic rights, some third party content may be suppressed from the eBook and/or eChapter(s). Editorial review has deemed that any suppressed content does not materially affect the overall learning experience. Cengage Learning reserves the right to remove additional content at any time if subsequent rights restrictions require it.

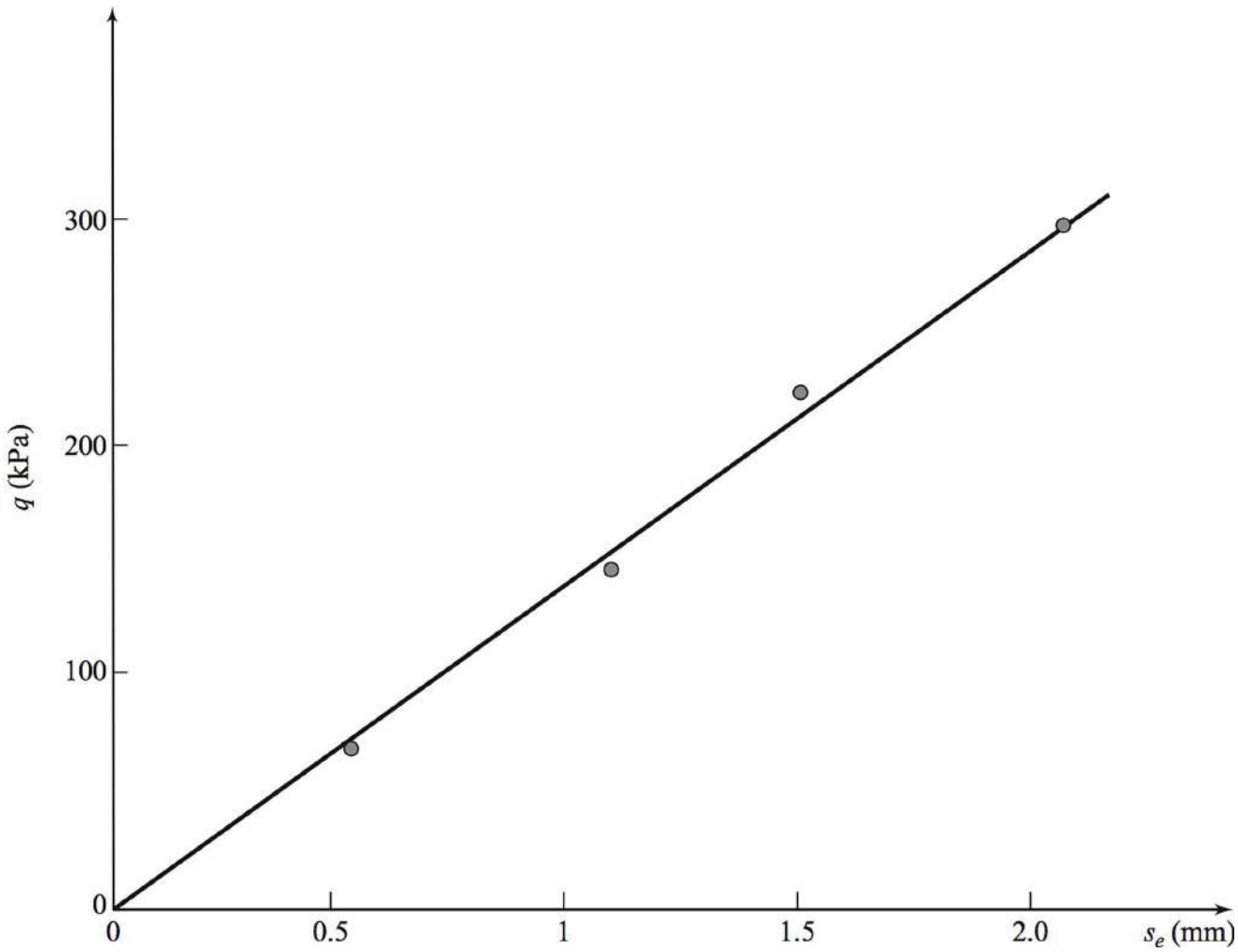

Figure 4.63

significant depth of the foundation. The procedure is costly, particularly if the ground water level is near the foundation and ground water lowering becomes necessary.

Correlations for Shear Modulus and Damping Ratio

4.21 TEST PROCEDURES FOR MEASUREMENT OF MODULI AND DAMPING CHARACTERISTICS

For design of machine foundations subjected to vibration, calculation of ground response during an earthquake, analysis of the stability of slopes during an earthquake, and other dynamic analysis of soil, it is required that the shear modulus and the damping ratio of the soil be known. The shear modulus G and the damping ratio D of soils are dependent on several factors, such as type of soil, confining pressure, level of dynamic strain, degree of saturation, frequency, and number of cycles of dynamic load application, magnitude of dynamic stress, and dynamic prestrain (Hardin and Black, 1968).

Copyright 2017 Cengage Learning. All Rights Reserved. May not be copied, scanned, or duplicated, in whole or in part. Due to electronic rights, some third party content may be suppressed from the eBook and/or eChapter(s). Editorial review has deemed that any suppressed content does not materially affect the overall learning experience. Cengage Learning reserves the right to remove additional content at any time if subsequent rights restrictions require it.

From the preceding discussions in this chapter, it is obvious that a wide variety of procedures, including laboratory and field tests, can be used to obtain the shear moduli and damping characteristics of soils. A summary of those test conditions, range of applicability, and the parameters obtained are given in Table 4.5. Based on these studies several correlations for estimation of G and D have evolved during the last 30 to 40 years. Some of these correlations are summarized in the following sections.

In general, the shear-stress-versus-shear strain relationship for soils will be of the nature as shown in Figure 4.64. The following can be seen from this figure:

1. The shear modulus G decreases with the increased level of shear strain.
2. At a very low strain level, the magnitude of the shear modulus is maximum (that is, $G = G_{max}$).
3. The shear stress-versus-shear-strain relationship shown in Figure 4.64 can be approximated as (Hardin and Drnevich, 1972)

$$\boxed{\tau = \frac{\gamma'}{1/G_{max} + \gamma'/\tau_{max}}} \tag{4.100}$$

where τ = shear stress and γ' = shear strain.

Table 4.5 Test Procedures for Measuring Moduli and Damping Characteristics

General procedure	Test condition	Approximate strain range	Properties determined
Determination of hysteretic stress-strain relationships	Triaxial compression	10^{-2} to 5%	Modulus; damping
	Simple shear	10^{-2} to 5%	Modulus; damping
	Torsional shear	10^{-2} to 5%	Modulus; damping
Forced vibration	Longitudinal vibrations	10^{-4} to 10^{-2} %	Modulus; damping
	Torsional vibrations	10^{-4} to 10^{-2} %	Modulus; damping
	Shear vibrations—lab	10^{-4} to 10^{-2} %	Modulus; damping
	Shear vibration—field	10^{-4} to 10^{-2} %	Modulus
Free vibration tests	Longitudinal vibrations	10^{-3} to 1%	Modulus; damping
	Torsional vibrations	10^{-3} to 1%	Modulus; damping
	Shear vibration—lab	10^{-3} to 1%	Modulus; damping
	Shear vibration—field	10^{-3} to 1%	Modulus
Field wave velocity measurements	Comparison waves	$\approx 5 \times 10^{-4}$ %	Modulus
	Shear waves	$\approx 5 \times 10^{-4}$ %	Modulus
	Rayleigh waves	$\approx 5 \times 10^{-4}$ %	Modulus
Field seismic response	Measurement of motions at different levels in deposit		Modulus; damping

After Seed and Idriss, 1970

Source: Seed, H.B., and Idriss, I.M. (1970). "Soil Moduli and Damping Factors for Dynamic Response Analysis," *Report No. EERC 70–10*, Earthquake Engineering Research Center, University of Calofornia, Berkley. Reprinted by permission of the PEER Center, UC Berkeley.

Copyright 2017 Cengage Learning. All Rights Reserved. May not be copied, scanned, or duplicated, in whole or in part. Due to electronic rights, some third party content may be suppressed from the eBook and/or eChapter(s). Editorial review has deemed that any suppressed content does not materially affect the overall learning experience. Cengage Learning reserves the right to remove additional content at any time if subsequent rights restrictions require it.

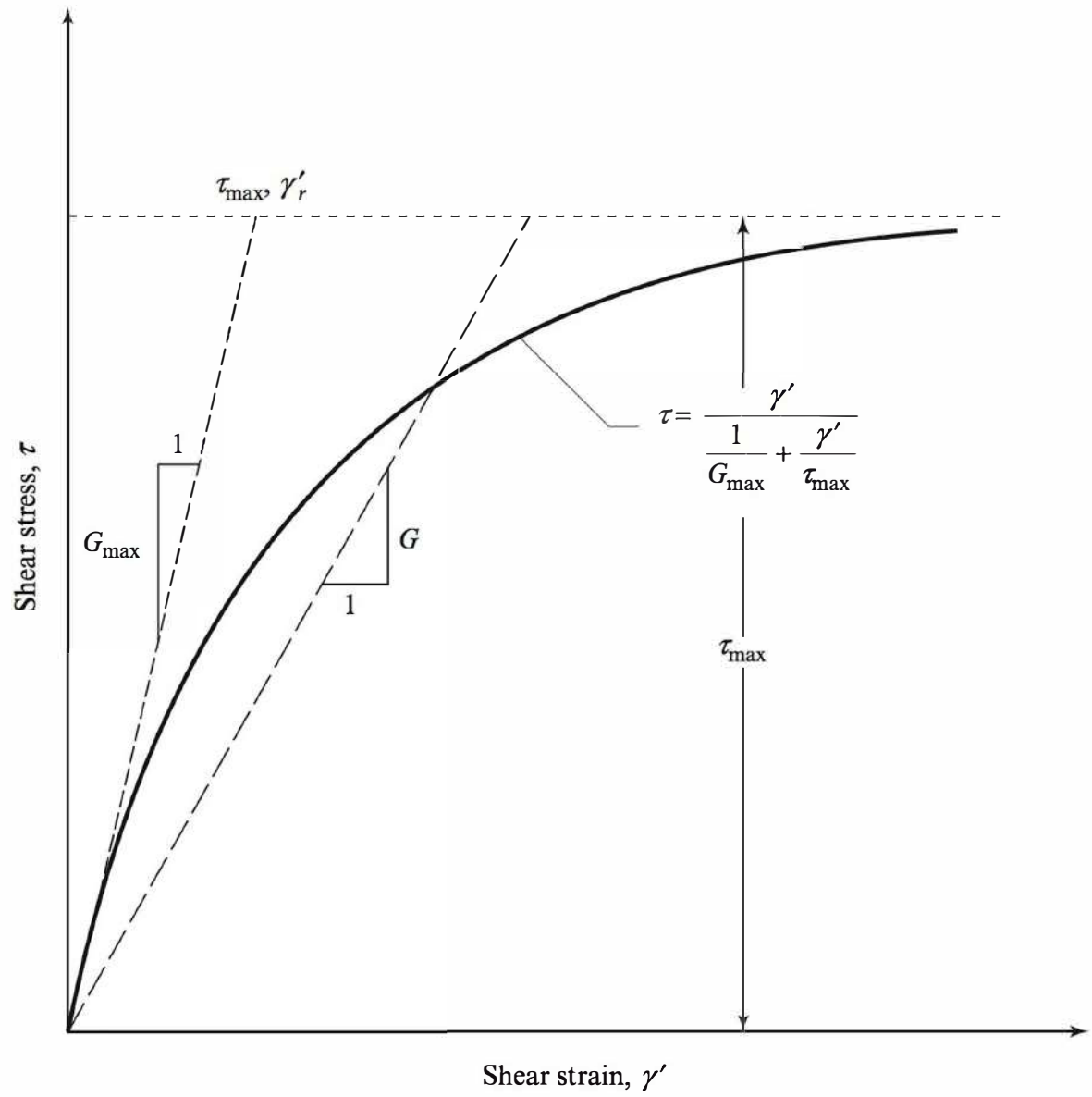

Figure 4.64 Nature of variation of shear modulus with strain

4.22 SHEAR MODULUS AND DAMPING RATIO IN SAND

Hardin and Richart (1963) reported the results of several resonant column tests conducted in dry Ottawa sand. The shear wave velocities v_s determined from some of these tests are shown in Figure 4.18. The peak-to-peak shear strain amplitude for these tests was 10^{-3} rad. From Figure 4.18 it may be seen that the values of v_s are independent of the gradation, grain-size distribution, and also the relative density of compaction. However, v_s is dependent on the void ratio e and the effective confining $\bar{\sigma}_0$ and can be expressed by the following empirical relations:

$$v_s = (19.7 - 9.06\,e)\,\bar{\sigma}_0^{1/4} \quad \text{for } \bar{\sigma}_0 \geq 95.8 \text{ kPa} \tag{4.101}$$

and

$$v_s = (11.36 - 5.35\,e)\,\bar{\sigma}_0^{0.3} \quad \text{for } \bar{\sigma}_0 < 95.8 \text{ kPa} \tag{4.102}$$

Copyright 2017 Cengage Learning. All Rights Reserved. May not be copied, scanned, or duplicated, in whole or in part. Due to electronic rights, some third party content may be suppressed from the eBook and/or eChapter(s). Editorial review has deemed that any suppressed content does not materially affect the overall learning experience. Cengage Learning reserves the right to remove additional content at any time if subsequent rights restrictions require it.

In Eqs. (4.101) and (4.102), the units of v_s and $\bar{\sigma}_0$ are meters per second and Newtons per square meter (Pa), respectively.

Several experimental results for shear wave velocity in extremely *angular crushed quartz sands* were also reported by Hardin and Richart (1963). Based on these results, the value of v_s for *angular sands* can be expressed by the empirical relation

$$\underset{\substack{\uparrow \\ (\text{m/s})}}{v_s} = (18.43 - 6.2e)\underset{\substack{\uparrow \\ (\text{N/m}^2)}}{\bar{\sigma}_0^{1/4}} \tag{4.103}$$

Based on the shear wave velocity relations presented here, the shear modulus of sands for *low amplitudes of vibration* can be given by the following relations (Hardin and Black, 1968):

$$\boxed{G_{\max} = \frac{6908(2.17 - e)^2}{1 + e}\bar{\sigma}_0^{1/2} \quad \text{(round-grained)}} \tag{4.104}$$

and

$$\boxed{G_{\max} = \frac{3230(2.97 - e)^2}{1 + e}\bar{\sigma}_0^{1/2} \quad \text{(angular-grained)}} \tag{4.105}$$

where $G_{\max}$ and $\bar{\sigma}_0$ are in kPa.

For a soil specimen subjected to a stress condition such that $\bar{\sigma}_1 \neq \bar{\sigma}_2 \neq \bar{\sigma}_3$ (where $\bar{\sigma}_1, \bar{\sigma}_2$ and $\bar{\sigma}_3$ are the major, intermediate, and minor effective principal stresses, respectively), the average effective confining pressure is

$$\bar{\sigma}_0 = \tfrac{1}{3}(\bar{\sigma}_1 + \bar{\sigma}_2 + \bar{\sigma}_3) = \text{effective octahedral stress}$$

This value of $\bar{\sigma}_0$ can be used in Eqs. (4.101) – (4.105).

For field conditions at any given depth,

$$\bar{\sigma}_1 = \text{effective vertical stress} = \bar{\sigma}_v$$
$$\bar{\sigma}_2 = \bar{\sigma}_3 = K_0\bar{\sigma}_v$$

where K_0 = at-rest earth pressure coefficient $\approx 1 - \sin\phi$ (where ϕ = drained friction angle).

So

$$\begin{aligned}\bar{\sigma}_0 &= \tfrac{1}{3}[\bar{\sigma}_v + 2\bar{\sigma}_v(1 - \sin\phi)] \\ &= \frac{\bar{\sigma}_v}{3}(3 - 2\sin\phi)\end{aligned} \tag{4.106}$$

Copyright 2017 Cengage Learning. All Rights Reserved. May not be copied, scanned, or duplicated, in whole or in part. Due to electronic rights, some third party content may be suppressed from the eBook and/or eChapter(s). Editorial review has deemed that any suppressed content does not materially affect the overall learning experience. Cengage Learning reserves the right to remove additional content at any time if subsequent rights restrictions require it.

Several investigators (e.g., Weissman and Hart, 1961; Richart, Hall, and Lysmer (1962); Drnevich, Hall, and Richart, 1966; Silver and Seed, 1969; Hardin and Drnevich, 1972; Seed and Idriss, 1970; Shibata and Soelarno, 1975; and Iwasaki, Tatsuoka, and Takagi, 1976), have reported the results of shear modulus and damping ratio measurements using various types of test techniques. From these test results, it appears that the shear modulus at a given strain level can be expressed as (Seed and Idriss, 1970)

$$\boxed{G = 218.82\, K_2(\bar{\sigma}_0)^{0.5}} \tag{4.107}$$

where G and $\bar{\sigma}_0$ are in kPa.

For low strain amplitudes ($\gamma' \leq 10^{-4}$ %), the preceding equation will be

$$\boxed{G_{max} = 218.82\, K_{2(max)}(\bar{\sigma}_0)^{0.5}} \tag{4.108}$$

The magnitudes of $K_{2(max)}$ vary from about 30 for loose sands to about 75 for dense sands. Seed and Idriss (1970) recommended the following values of $K_{2(max)}$.

Relative density, R_D (%)	$K_{2(max)}$
30	34
40	40
45	43
60	52
75	61
90	70

Hence,

$$\frac{G}{G_{max}} = \frac{K_2}{K_{2(max)}} F' \tag{4.109}$$

Figure 4.65 shows the variation of F' with shear strain γ'(%) obtained from several studies. These values fall in a rather narrow band and, for all practical purposes, the average plot can be used for design and estimation purposes. Thus Eqs. (4.104), (4.105), (4.107), (4.108), and (4.109) can be combined to estimate the shear modulus at any required shear strain level.

Studies by Hardin and Drnevich (1972) and Seed and Idriss (1970) show that the damping ratios for sands are affected by factors such as (a) grain-size characteristics, (b) degree of saturation, (c) void ratio, (d) earth pressure coefficient at rest (K_0), (e) angle of internal friction (ϕ), (f) number of stress cycles (N'), (g) level of strain, and (h) effective confining pressure. The last two factors, however, have the major effect on the magnitude of the damping ratio. Figure 4.66 shows a compilation of past studies (Seed et al. 1986) to determine D. For most practical cases the average plot of the variation of D versus γ' can be used for most calculation purposes.

Copyright 2017 Cengage Learning. All Rights Reserved. May not be copied, scanned, or duplicated, in whole or in part. Due to electronic rights, some third party content may be suppressed from the eBook and/or eChapter(s). Editorial review has deemed that any suppressed content does not materially affect the overall learning experience. Cengage Learning reserves the right to remove additional content at any time if subsequent rights restrictions require it.

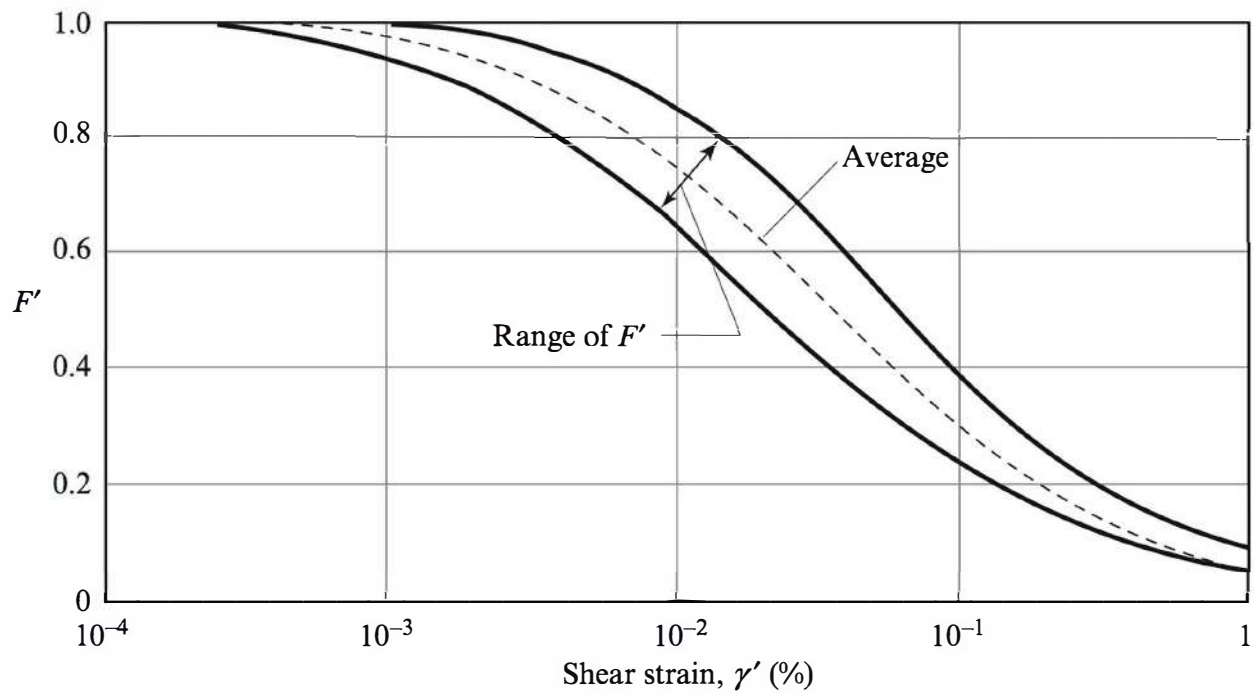

Figure 4.65 Variation of F' with shear strain for sands (after Seed et al., 1986)

Source: SourceSeed, H.B., Wong, R.T., Idriss, I.M., and Tokimatsu, K. (1986). "Moduli and Damping Factors for Dynamic Analyses of Cohesionless Soils," *Journal of Geotechnical Engineering*, ASCE, Vol. 112, No. GT11, pp. 1016–1032. With permission from ASCE.

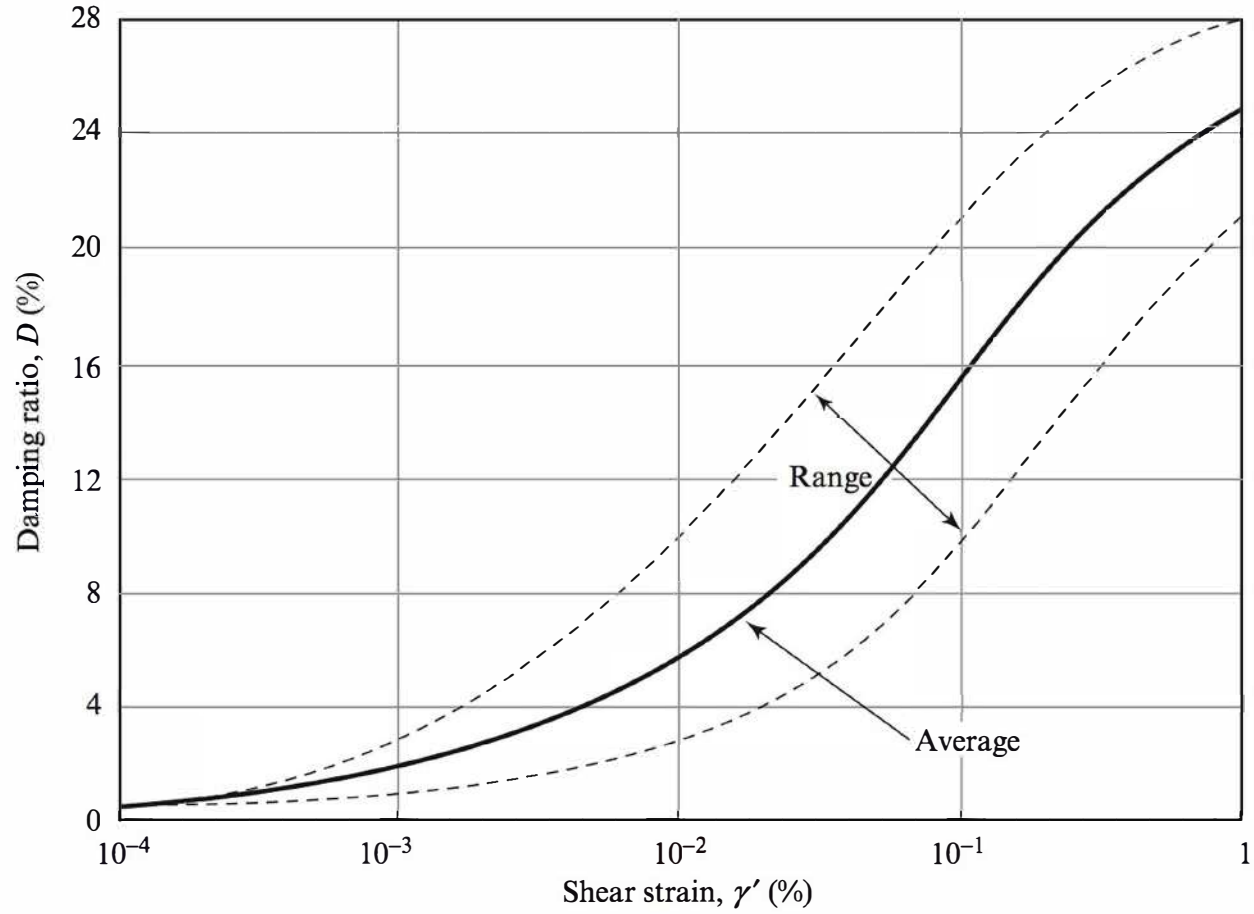

Figure 4.66 Damping ratios for sands (after Seed et al.,1986)

Source: Seed, H.B., Wong, R.T., Idriss, I.M., and Tokimatsu, K. (1986). "Moduli and Damping Factors for Dynamic Analyses of Cohesionless Soils," *Journal of Geotechnical Engineering*, ASCE, Vol. 112, No. GT11, pp. 1016–1032. With permission from ASCE.

Copyright 2017 Cengage Learning. All Rights Reserved. May not be copied, scanned, or duplicated, in whole or in part. Due to electronic rights, some third party content may be suppressed from the eBook and/or eChapter(s). Editorial review has deemed that any suppressed content does not materially affect the overall learning experience. Cengage Learning reserves the right to remove additional content at any time if subsequent rights restrictions require it.

Based on tests on dry sands using a torsional simple shear device, Sherif, Ishibashi, and Gaddah (1977) proposed the following relationship for damping ratio.

$$D = \frac{50 - 0.087\,\bar{\sigma}_0}{38}(73.3F - 53.3)(\gamma')^{0.3}(1.01 - 0.046\log N) \qquad (4.110)$$

where D = damping ratio (%)
$\bar{\sigma}_0$ = effective confining pressure (kPa)
γ' = shear strain (%)
F = sphericity factor of the soil grains
N' = number of cycles of strain application

The sphericity factor is defined as

$$F = \frac{1}{\psi^2 C_g} \qquad (4.111)$$

where

$$C_g = \frac{D_{30}^2}{(D_{10})(D_{60})} \qquad (4.112)$$

D_{10}, D_{30}, D_{60} = diameters, respectively, through which 10%, 30%, and 60% of the soil will pass

$$\psi = \frac{S'}{S}$$

where S' and S are, respectively, the surface area of a sphere of the same volume as the soil particle and the actual surface area of the soil.

EXAMPLE 4.6

The groundwater table in a normally consolidated sand layer is located at a depth of 3 m below the ground surface. The unit weight of sand above the groundwater table is 15.5 kN/m³. Below the groundwater table, the saturated unit weight of sand is 18.5 kN/m³. Assuming that the void ratio and effective angle of friction of sand below the groundwater table are 0.6 and 36°, respectively, determine the damping ratio and the shear modulus of this sand at a depth of 7.5 m below the ground surface if the strain is expected to be about 0.12%.

SOLUTION

From Eq. (4.106)

$$\bar{\sigma}_0 = \frac{\bar{\sigma}_v}{3}(3 - 2\sin\phi)$$

$$\bar{\sigma}_v = 3(15.5) + 4.5(18.5 - 9.81) = 85.61\text{ kPa}$$

$$\bar{\sigma}_0 = \frac{85.61}{3}[3 - (2)(\sin 36)] = 52.06\text{ kPa}$$

Copyright 2017 Cengage Learning. All Rights Reserved. May not be copied, scanned, or duplicated, in whole or in part. Due to electronic rights, some third party content may be suppressed from the eBook and/or eChapter(s). Editorial review has deemed that any suppressed content does not materially affect the overall learning experience. Cengage Learning reserves the right to remove additional content at any time if subsequent rights restrictions require it.

When ϕ is equal to 36°, R_D is about 40 to 50%. Assuming $R_D \approx 45\%$, $K_{2(\max)} \approx 43$. So, from Eq. (4.108)

$$G_{\max} = 218.82\, K_{2(\max)}(\bar{\sigma}_0)^{0.5}$$

or

$$\begin{aligned} G_{\max} &= (218.82)(43)(52.06)^{0.5} \\ &= 67{,}890 \text{ kPa} \approx 67.9 \text{ MPa} \end{aligned}$$

Referring to Figure 4.65, for $\gamma' = 0.12\%$, the value of F' is about 0.28. So

$$G = F'G_{\max} = (0.28)(67.9) \approx \mathbf{19\ MPa}$$

Referring to the average curve in Figure 4.66, for $\gamma' = 0.12\%$

$$\boldsymbol{D \approx 17\%}$$

4.23 CORRELATION OF G_{max} OF SAND WITH STANDARD PENETRATION RESISTANCE

The standard penetration test is used in soil-exploration programs in the United States and other countries. In granular soils the standard penetration numbers (N in blows/0.3 m) are widely used for the design of foundation. The standard penetration number can be correlated (Seed et al., 1986) in the following form to predict the maximum shear modulus:

$$\boxed{\begin{array}{ccc} G_{\max} & \approx 5652.5 N_{60}^{0.34} & (\bar{\sigma}_0)^{0.4} \\ \uparrow & & \uparrow \\ \text{(kPa)} & & \text{(kPa)} \end{array}} \tag{4.113}$$

where $\bar{\sigma}_0$ = effective confining pressure (kPa)

N_{60} = N-value measured in SPT delivering 60% of the theoretical free-fall energy to the drill rod

Equation (4.113) is very useful in predicting the variation of the maximum shear modulus with depth for a granular soil deposit.

4.24 SHEAR MODULUS AND DAMPING RATIO FOR GRAVELS

Seed et al. (1986) provided the experimental results of several well-graded gravels. An example of such a study on well-graded Oroville material is shown in Figure 4.67. Based on several studies of this type, Seed et al. concluded that Eqs. (4.108)

Copyright 2017 Cengage Learning. All Rights Reserved. May not be copied, scanned, or duplicated, in whole or in part. Due to electronic rights, some third party content may be suppressed from the eBook and/or eChapter(s). Editorial review has deemed that any suppressed content does not materially affect the overall learning experience. Cengage Learning reserves the right to remove additional content at any time if subsequent rights restrictions require it.

and (4.109) can also be used to predict the variation of shear modulus with shear strain. However, the magnitude of $K_{2(\max)}$ for gravels ranges between 80 to 180 (as compared to a range of 30 to 75 for sand). Thus,

$$\boxed{\begin{array}{ll} G = G_{\max}F' = 218.82F'K_{2(\max)}(\bar{\sigma}_0)^{0.5} & \\ \uparrow & \uparrow \\ \text{(kPa)} & \text{(kPa)} \end{array}} \tag{4.114}$$

The variation of F' with the level of shear strain is shown in Figure 4.68.

The equivalent damping ratio of gravelly soils determined in the laboratory from the hysteresis loops at the fifth cycle of each strain amplitude is shown in Figure 4.69. It can be seen that, for a given value of γ', the equivalent damping ratio increases with the increase of the relative density R_D of the gravel. Seed et al. (1986) also observed that

a. there is not significant effect of gradation on the equivalent damping ratios of gravelly soil, and

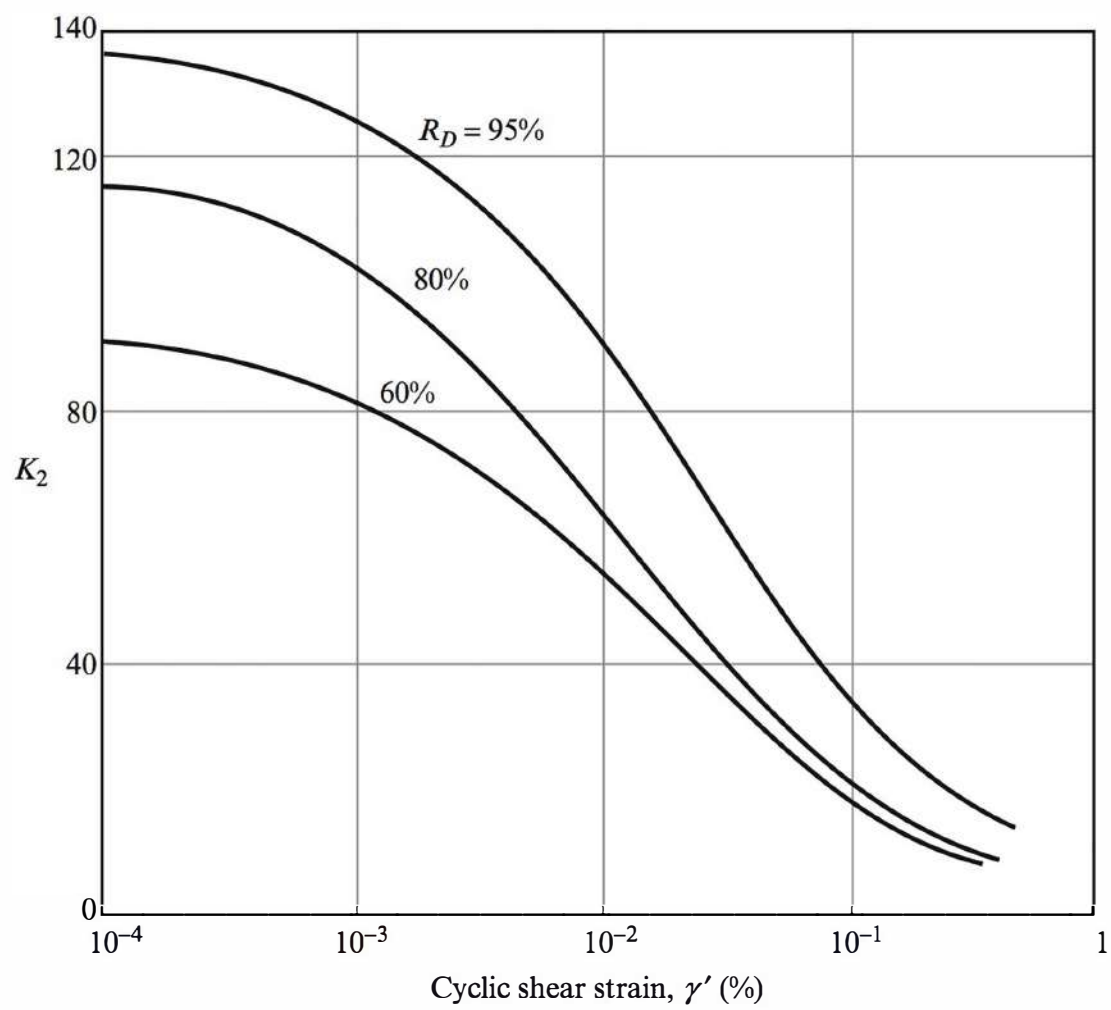

Figure 4.67 Shear moduli of well-graded Oroville material (after Seed et al., 1986)

Source: Seed, H.B., Wong, R.T., Idriss, I.M., and Tokimatsu, K. (1986). "Moduli and Damping Factors for Dynamic Analyses of Cohesionless Soils," *Journal of Geotechnical Engineering*, ASCE, Vol. 112, No. GT11, pp. 1016–1032. With permission from ASCE.

Copyright 2017 Cengage Learning. All Rights Reserved. May not be copied, scanned, or duplicated, in whole or in part. Due to electronic rights, some third party content may be suppressed from the eBook and/or eChapter(s). Editorial review has deemed that any suppressed content does not materially affect the overall learning experience. Cengage Learning reserves the right to remove additional content at any time if subsequent rights restrictions require it.

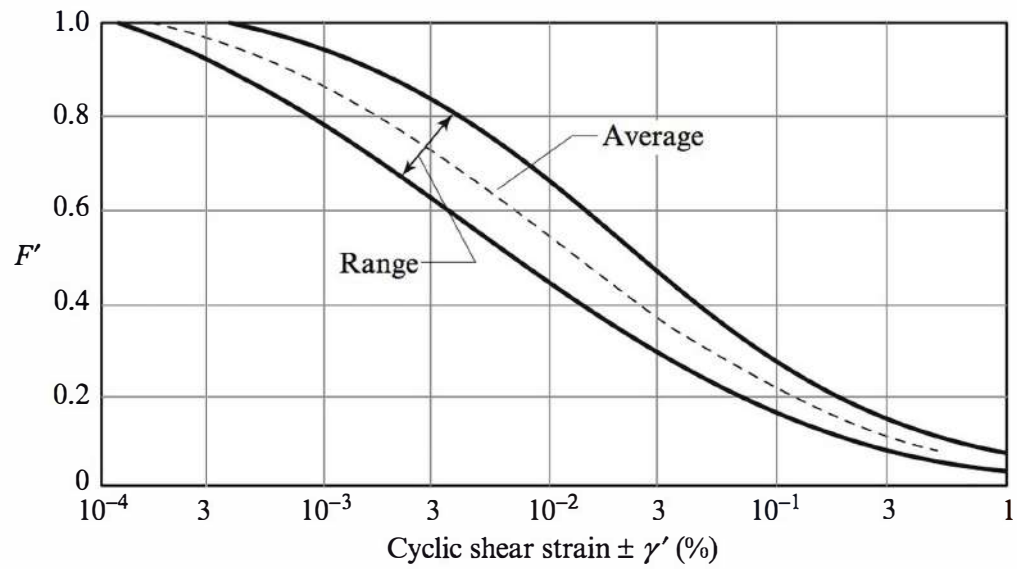

Figure 4.68 Variation of F' with shear strain for gravelly soils (after Seed et al., 1986)

Source: Seed, H.B., Wong, R.T., Idriss, I.M., and Tokimatsu, K. (1986). "Moduli and Damping Factors for Dynamic Analyses of Cohesionless Soils," *Journal of Geotechnical Engineering*, ASCE, Vol. 112, No. GT11, pp. 1016–1032. With permission from ASCE.

b. the damping ratio is not significantly affected by the number of cycles at very small strain amplitudes. However, it decreases to approximately three-fourths of its original value after 60 cycles at any axial strain amplitude of ± 0.2%.

Seed et al. showed that the range and the average plot of the damping ratio D with strain amplitude γ' for gravelly soils is approximately the same as that for sands (Figure 4.66).

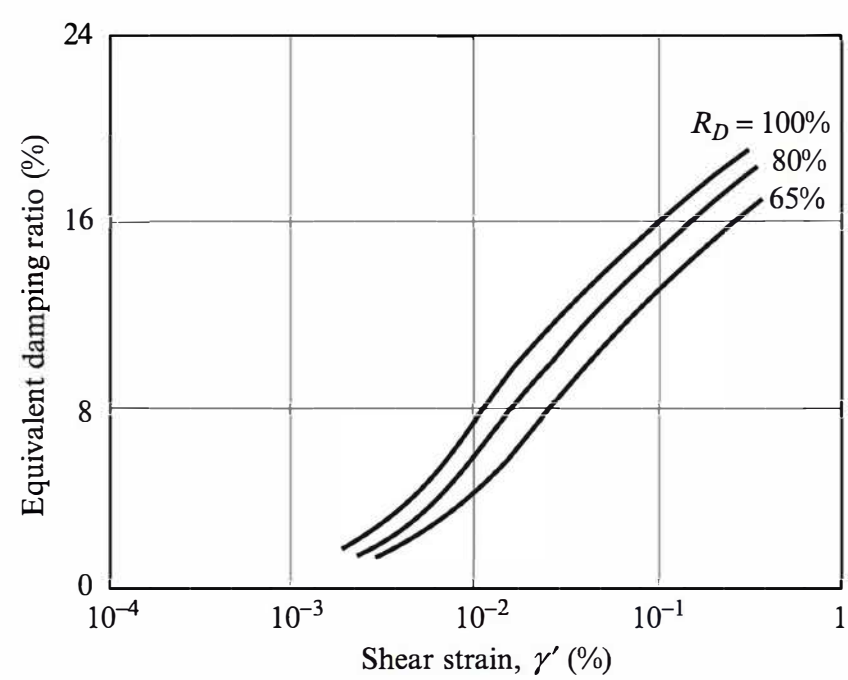

Figure 4.69 Effect of relative density on damping ratio of gravelly soils (after Seeds et al., 1986)

Source: Seed, H.B., Wong, R.T., Idriss, I.M., and Tokimatsu, K. (1986). "Moduli and Damping Factors for Dynamic Analyses of Cohesionless Soils," *Journal of Geotechnical Engineering*, ASCE, Vol. 112, No. GT11, pp. 1016–1032. With permission from ASCE.

Copyright 2017 Cengage Learning. All Rights Reserved. May not be copied, scanned, or duplicated, in whole or in part. Due to electronic rights, some third party content may be suppressed from the eBook and/or eChapter(s). Editorial review has deemed that any suppressed content does not materially affect the overall learning experience. Cengage Learning reserves the right to remove additional content at any time if subsequent rights restrictions require it.

Rollins et al. (1998) analyzed the results of several investigators between 1986 and 1998 which were obtained from cyclic triaxial tests and large diameter cyclic torsional simple shear tests. Based on this analysis it was suggested that the relationships for the best fit curves can be given as

$$\frac{G}{G_{max}} = \frac{1}{[1.2 + 16\gamma'(1 + 10^{-20\gamma'})]} \tag{4.115}$$

and

$$D(\%) = 0.8 + 18\left(1 + 0.15\gamma'^{-0.9}\right)^{-0.75} \tag{4.116}$$

where γ' = cyclic shear strain (%)

The variations of G/G_{max} and D based on Eqs. (4.115) and (4.116), along with the standard deviation bounds, are given in Figures 4.70 and 4.71, respectively.

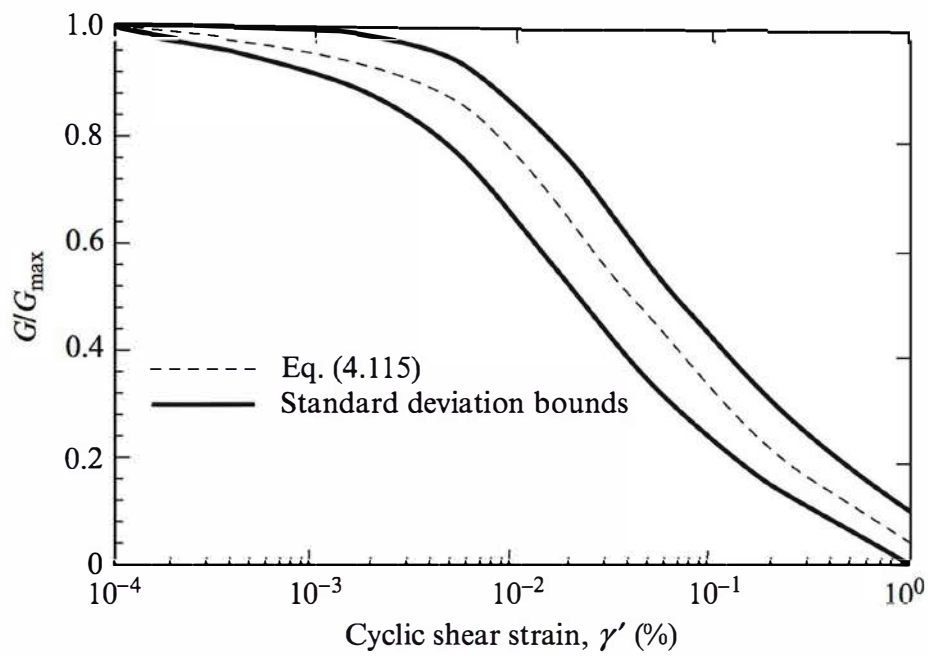

Figure 4.70 Variation of G/G_{max} with γ' for gravel—Eq. (4.115)

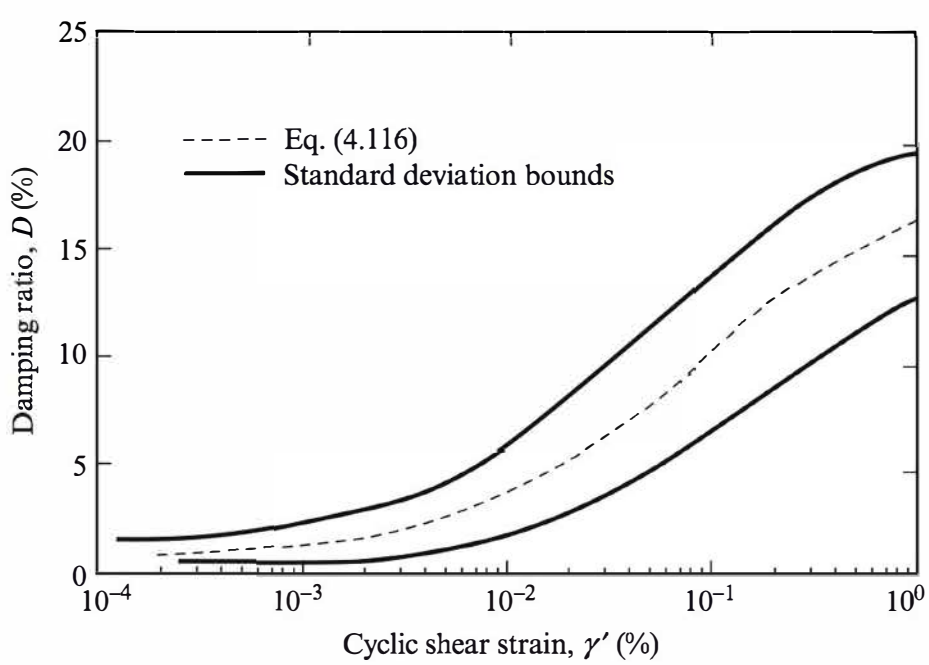

Figure 4.71 Variation of damping ratio with γ' for gravel—Eq. (4.116)

Copyright 2017 Cengage Learning. All Rights Reserved. May not be copied, scanned, or duplicated, in whole or in part. Due to electronic rights, some third party content may be suppressed from the eBook and/or eChapter(s). Editorial review has deemed that any suppressed content does not materially affect the overall learning experience. Cengage Learning reserves the right to remove additional content at any time if subsequent rights restrictions require it.

EXAMPLE 4.7

Consider a gravel deposit. At a certain depth below the ground surface, given:

Vertical effective stress, $\bar{\sigma}'_v = 76$ kPa
Friction angle, $\phi = 38°$
Relative density, $R_D = 80\%$

Estimate the shear modulus and damping ratio at a cyclic shear strain level of 10^{-2} %. Use Eqs. (4.115) and (4.116).

SOLUTION

From Eq. (4.106)

$$\bar{\sigma}_0 = \frac{\bar{\sigma}_v}{3}(3 - 2\sin\phi) = \left(\frac{76}{3}\right)(3 - 2\sin 38°) = 44.81\,\text{kN/m}^2$$

From Eq. (4.114)

$$G_{\max} = 218.82 K_{2(\max)}(\bar{\sigma}_0)^{0.5}$$

From Figure 4.67 for $\gamma' \approx 10^{-4}$ %, the value of $K_2 \approx 116$. Hence,

$$G_{\max} = (218.82)(116)(44.81)^{0.5} = 169{,}915\text{ kPa} \approx 169.92\text{ MPa}$$

From Eq. (4.115)

$$\frac{G}{G_{\max}} = \frac{1}{[1.2 + 16\gamma'(1 + 10^{-20\gamma'})]} = \frac{1}{[1.2 + (16)(0.01)(1 + 10^{-20\times 0.01})]} \approx 0.685$$

Hence,

$$G = (169.92)(0.685) = \mathbf{116.4\ MPa}$$

From Eq. (4.116)

$$D(\%) = 0.8 + 18(1 + 0.15\gamma'^{-0.9})^{-0.75} = 0.8 + 18[1 + (0.15)(0.01)^{-0.9}]^{-0.75} = \mathbf{3.89\%}$$

Copyright 2017 Cengage Learning. All Rights Reserved. May not be copied, scanned, or duplicated, in whole or in part. Due to electronic rights, some third party content may be suppressed from the eBook and/or eChapter(s). Editorial review has deemed that any suppressed content does not materially affect the overall learning experience. Cengage Learning reserves the right to remove additional content at any time if subsequent rights restrictions require it.

4.25 SHEAR MODULUS AND DAMPING RATIO FOR CLAYS

Hardin and Black (1968) and Hardin (1978) proposed the following empirical relationship for the shear modulus of clays at low amplitudes of strain, which includes the effects of soil plasticity and the overconsolidation ratio (OCR). Or

$$\boxed{G_{\max} = 625 \frac{\mathrm{OCR}^K}{0.3 + 0.7e^2} \sqrt{p_a \bar{\sigma}_0}} \tag{4.117}$$

where e = void ratio
p_a = atmospheric pressure expressed in the same units ($\approx$ 100 kPa) as $G_{\max}$
$K = f$(plasticity index, PI)

Following are the recommended values of K for use in the preceding equation.

Plasticity index, PI (%)	K
0	0
20	0.18
40	0.30
60	0.41
80	0.48
$\geq$100	0.5

For field conditions

$$\bar{\sigma}_0 = \tfrac{1}{3}(\bar{\sigma}_v + 2K_0\bar{\sigma}_v) \tag{4.118}$$

where $\bar{\sigma}_v$ = effective vertical stress
K_0 = at-rest earth pressure coefficient

For normally consolidated clays (Booker and Ireland, 1965)

$$K_0 = 0.4 + 0.007\,(\mathrm{PI}) \quad (\text{for } 0 \leq \mathrm{PI} \leq 40\%) \tag{4.119}$$

and

$$K_0 = 0.68 + 0.001\,(\mathrm{PI} - 40) \quad (\text{for } 40\% \leq \mathrm{PI} \leq 80\%) \tag{4.120}$$

For over consolidated soils, K_0 can be approximated as (Mayne and Kulhawy, 1982)

$$K_0 = (1 - \sin\phi)\,\mathrm{OCR}^{\sin\phi} \tag{4.121}$$

Copyright 2017 Cengage Learning. All Rights Reserved. May not be copied, scanned, or duplicated, in whole or in part. Due to electronic rights, some third party content may be suppressed from the eBook and/or eChapter(s). Editorial review has deemed that any suppressed content does not materially affect the overall learning experience. Cengage Learning reserves the right to remove additional content at any time if subsequent rights restrictions require it.

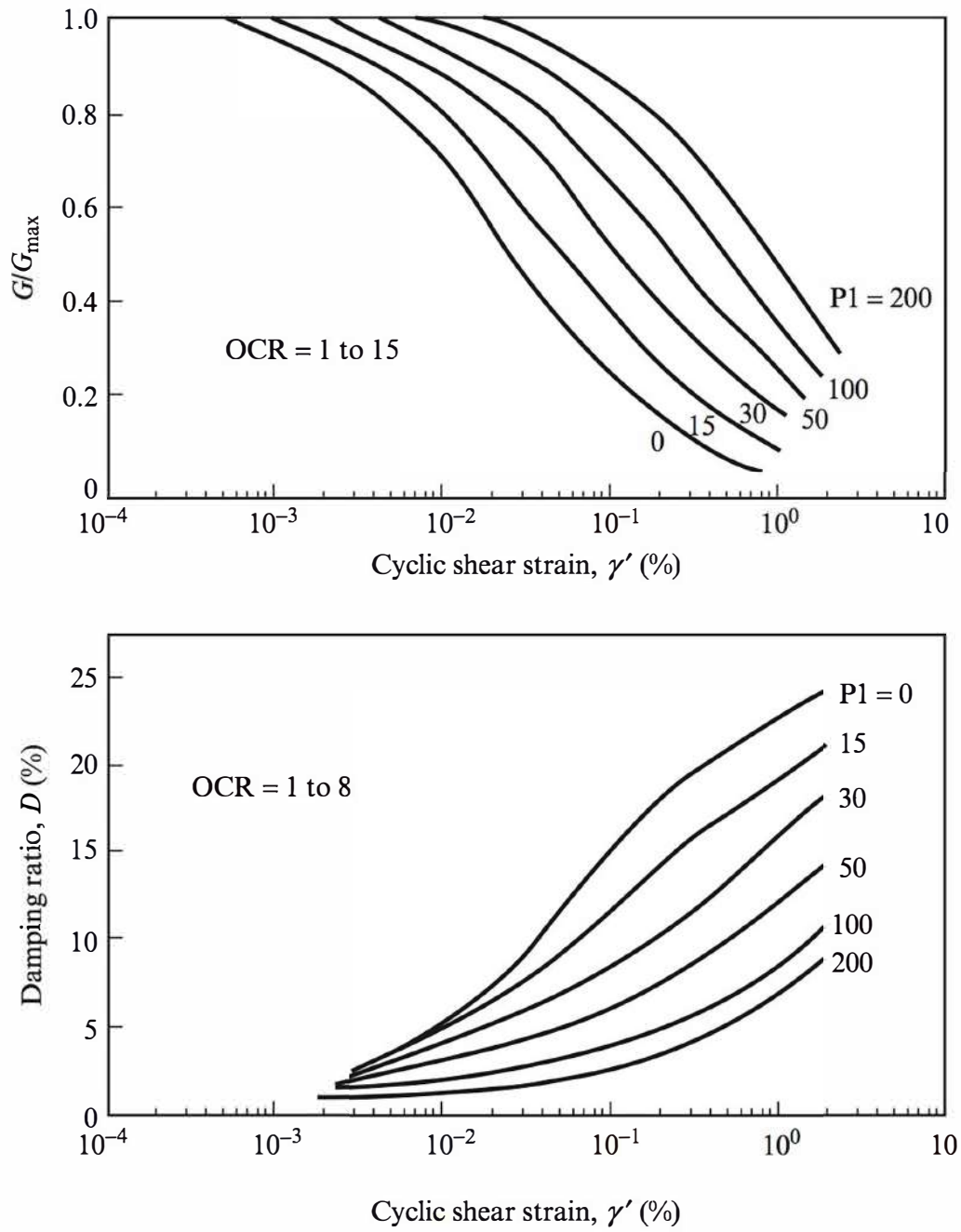

Figure 4.72 Test results of Vucetic and Dobry (1991) – Variation of G/G_{max} and D

Vucetic and Dobry (1991) used a large database and provided the variation of G/G_{max} and D at various cyclic shear strain levels which are functions of PI and OCR. These variations are shown in Figure 4.72.

Correlation of Seed and Idriss

Seed and Idriss (1970) collected the experimental results for shear modulus and damping ratio from various sources for saturated cohesive soils. Based on these results the variation of G/c_u (where c_u =undrained cohesion) with shear strain is shown in Figure 4.73. Also, Figure 4.74 shows the upper limit, average, and lower limit for the damping ratio at various strain levels.

Copyright 2017 Cengage Learning. All Rights Reserved. May not be copied, scanned, or duplicated, in whole or in part. Due to electronic rights, some third party content may be suppressed from the eBook and/or eChapter(s). Editorial review has deemed that any suppressed content does not materially affect the overall learning experience. Cengage Learning reserves the right to remove additional content at any time if subsequent rights restrictions require it.

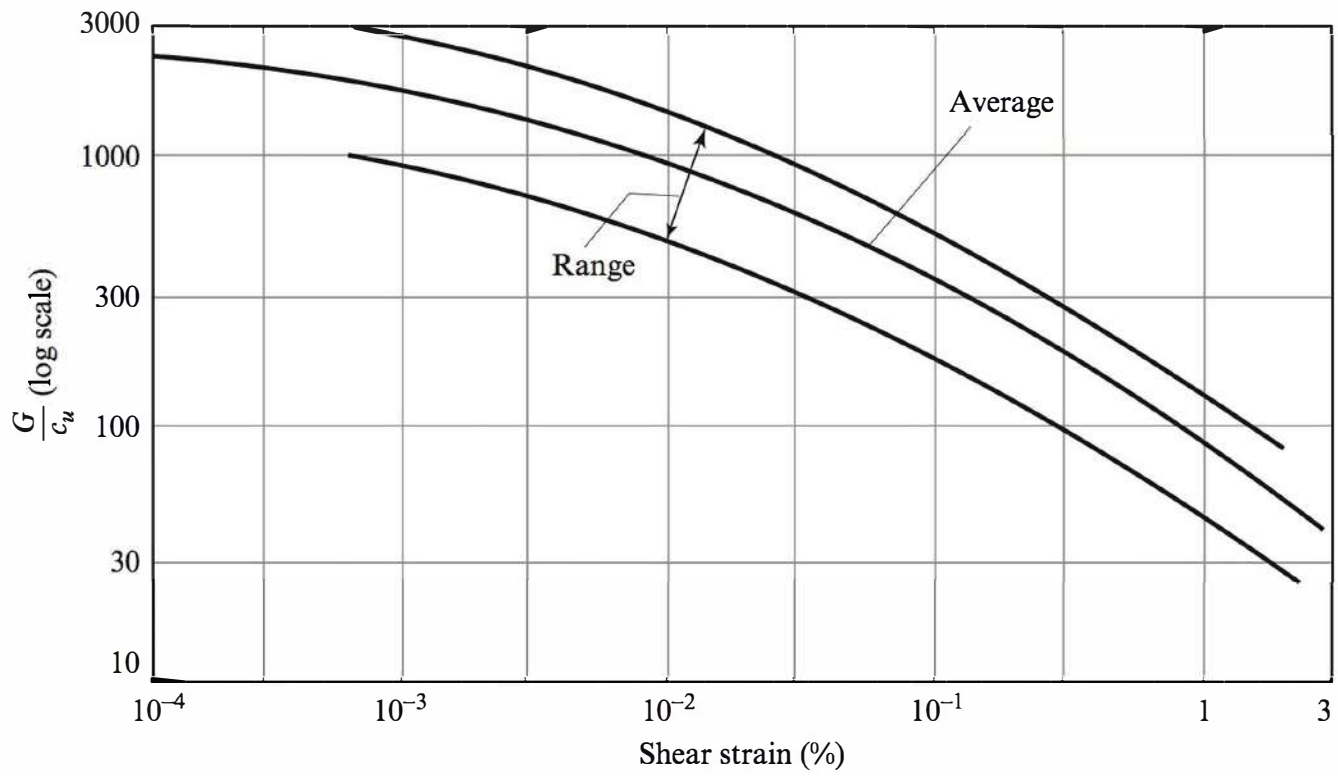

Figure 4.73 In situ shear modulus for saturated clays (after Seed and Idriss, 1970)

Source: Seed, H.B., and Idriss, I.M. (1970). "Soil Moduli and Damping Factors for Dynamic Response Analysis," *Report No. EERC 70–10*, Earthquake Engineering Research Center, University of Calofornia, Berkley. Reprinted by permission of the PEER Center, UC Berkeley.

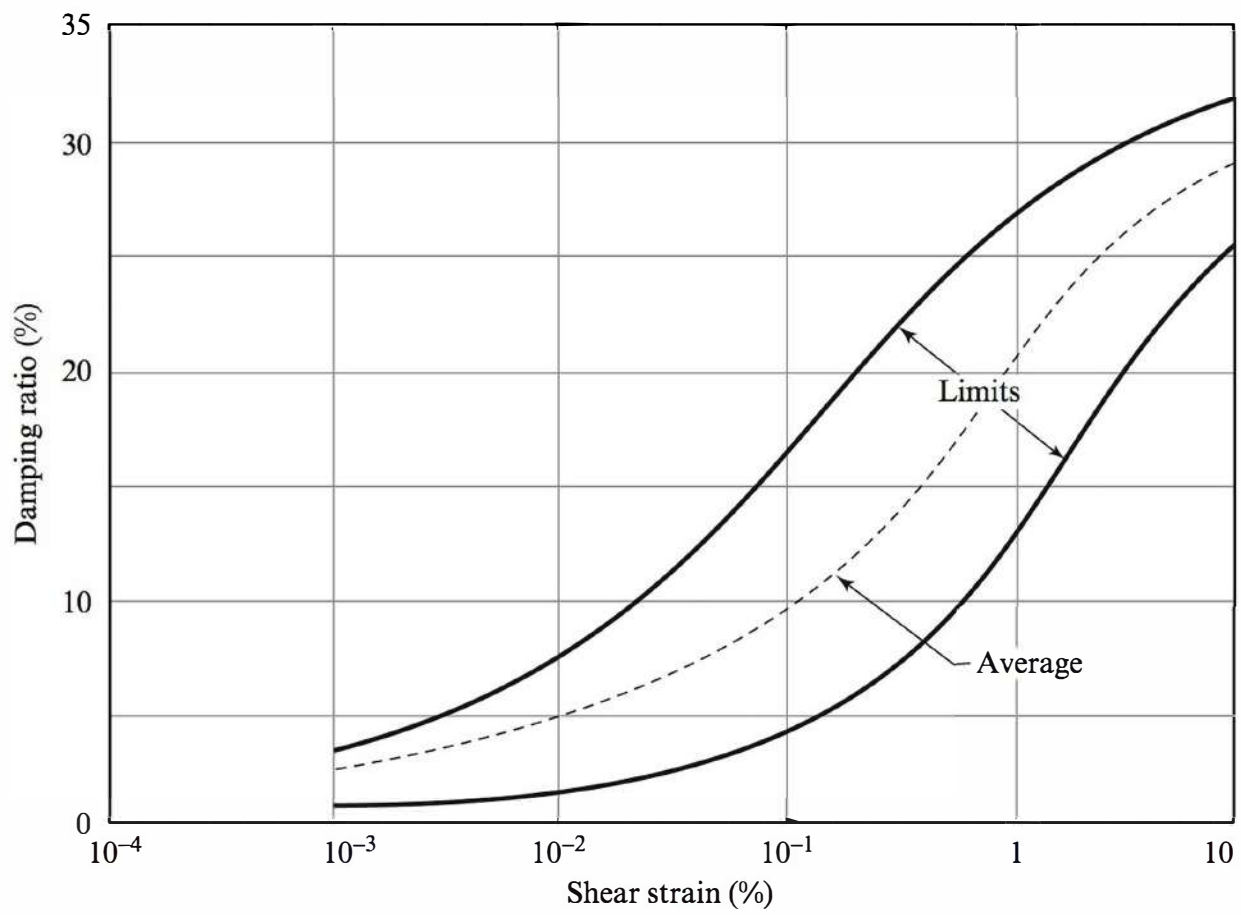

Figure 4.74 Damping ratio for saturated clays (after Seed and Idriss, 1970)

Source: Seed, H.B., and Idriss, I.M. (1970). "Soil Moduli and Damping Factors for Dynamic Response Analysis," *Report No. EERC 70–10*, Earthquake Engineering Research Center, University of Calofornia, Berkley. Reprinted by permission of the PEER Center, UC Berkeley.

Copyright 2017 Cengage Learning. All Rights Reserved. May not be copied, scanned, or duplicated, in whole or in part. Due to electronic rights, some third party content may be suppressed from the eBook and/or eChapter(s). Editorial review has deemed that any suppressed content does not materially affect the overall learning experience. Cengage Learning reserves the right to remove additional content at any time if subsequent rights restrictions require it.

EXAMPLE 4.8

A soil profile is shown in Figure 4.75a. Calculate and plot the variation of shear modulus with depth (for low amplitude of vibration).

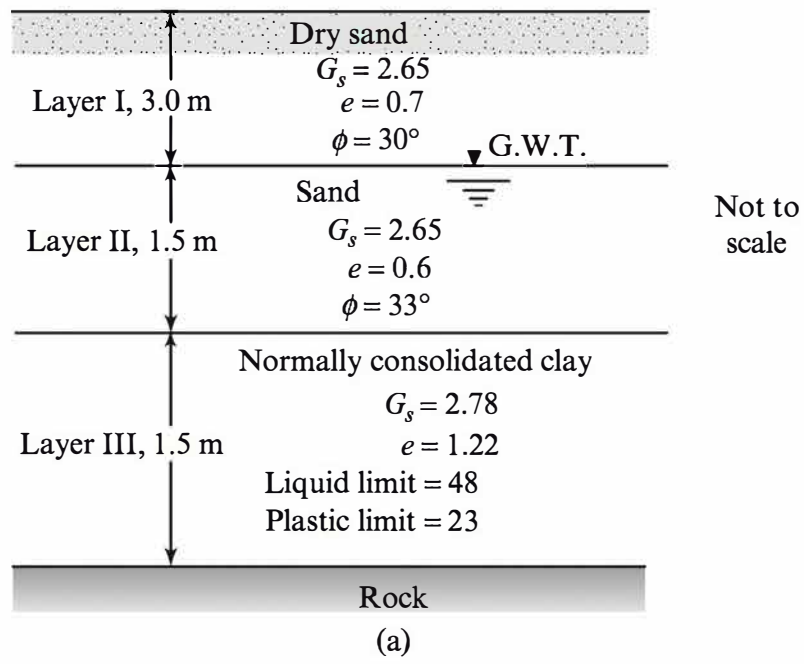

Figure 4.75a

SOLUTION

At any depth z

$$\bar{\sigma}_0 = \tfrac{1}{3}(\bar{\sigma}_1 + \bar{\sigma}_2 + \bar{\sigma}_3); \quad \bar{\sigma}_2 = \bar{\sigma}_3 = K_0\bar{\sigma}$$

where K_0 is the coefficient of earth pressure at rest and $\bar{\sigma}_1$ is the vertical effective pressure. For sands,

$$K_0 = 1 - \sin\phi = 1 - \sin 30° = 0.5$$

In layer II,

$$K_0 = 1 - \sin\phi = 1 - \sin 33° = 0.455$$

For normally consolidated clays,

$$K_0 = 0.4 + 0.007(\text{PI}) \quad \text{for } 0 \le \text{PI} \le 40\%$$
$$= 0.4 + 0.007(48 - 23) = 0.575$$

Copyright 2017 Cengage Learning. All Rights Reserved. May not be copied, scanned, or duplicated, in whole or in part. Due to electronic rights, some third party content may be suppressed from the eBook and/or eChapter(s). Editorial review has deemed that any suppressed content does not materially affect the overall learning experience. Cengage Learning reserves the right to remove additional content at any time if subsequent rights restrictions require it.

Calculation of Effective Unit Weights

$z = 0 - 3.0$ m

$$\gamma_{\text{dry}} = \gamma_{\text{eff}} = \frac{G_s \gamma_w}{1+e} = \frac{(2.65)(9.81)}{1+0.7} = 15.29 \text{ kN/m}^3$$

$z = 3.0 - 4.5$ m

$$\gamma_{\text{eff}} = \gamma_{\text{sat}} - \gamma_w = \frac{(G_s + e)\gamma_w}{1+e} - \gamma_w = \left(\frac{G_s - 1}{1+e}\right)\gamma_w$$

$$= \frac{(2.65-1)(9.81)}{1+0.6} = 10.12 \text{ kN/m}^3$$

$z = 4.5 - 6.0$ m:

$$\gamma_{\text{eff}} = \frac{(G_s - 1)\gamma_w}{1+e} \frac{(2.78-1)(9.81)}{1+1.22} = 7.87 \text{ kN/m}^3$$

The following table can now be prepared.

Depth z (m)	$\bar{\sigma}_1$ (kPa)	$\bar{\sigma}_2 = \bar{\sigma}_3 = K_0\bar{\sigma}_1$ (kPa)	$\bar{\sigma}_0$ (kPa)	e	$G = G_{max}$ (MPa)
0	0	0	0	0.7	**0**
1.5	$15.29 \times 1.5 = 22.94$	11.47	15.29	0.7	**34.34**[a]
3.0 (in layer I)	$15.29 \times 3 = 45.87$	22.94	30.58	0.7	**48.56**[a]
3.0 (in layer II)	45.87	20.87	29.20	0.6	**57.51**[a]
4.5 (in layer II)	$45.87 + 10.12 \times 1.5 = 61.05$	27.78	38.87	0.6	**66.35**[a]
4.5 (in layer III)	61.05	35.10	43.75	1.22	**30.81**[b]
6.0	$61.05 + 7.87 \times 1.5 = 72.86$	41.89	52.21	1.22	**33.65**[b]

[a]Eq. (4.104)

[b]Eq. (4.117). Note OCR = 1

Copyright 2017 Cengage Learning. All Rights Reserved. May not be copied, scanned, or duplicated, in whole or in part. Due to electronic rights, some third party content may be suppressed from the eBook and/or eChapter(s). Editorial review has deemed that any suppressed content does not materially affect the overall learning experience. Cengage Learning reserves the right to remove additional content at any time if subsequent rights restrictions require it.

The variation of $G = G_{max}$ with depth is plotted in Figure 4.69b.

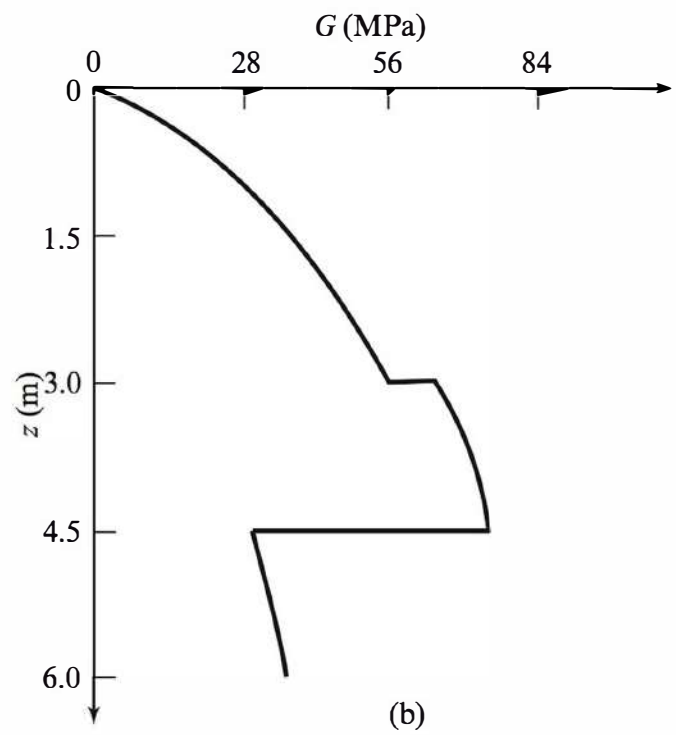

Figure 4.75b

EXAMPLE 4.9

At a given depth in a saturated clay layer, given:

Vertical effective stress, $\bar{\sigma}_v = 30$ kPa
Soil friction angle, $\phi = 28°$
Liquid limit = 47
Plastic limit = 27
Void ratio, $e = 0.92$
Overconsolidation ratio = 2

Estimate the shear modulus and damping ratio at a cyclic shear strain of 0.01%. Use Eq. (4.117) and Figure 4.72.

SOLUTION

From Eq. (4.121)

$$K_0 = (1 - \sin\phi)\mathrm{OCR}^{\sin\phi} = (1 - \sin 28)(2)^{\sin 28} = 0.734$$

$$\bar{\sigma}_0 = \frac{1}{3}\left(\bar{\sigma}_v + 2K_0\bar{\sigma}_v\right) = \frac{\bar{\sigma}_v}{3}\left(1 + 2K_0\right) = \frac{30}{3}(1 + 2 \times 0.734) = 24.68 \text{ kPa}$$

Copyright 2017 Cengage Learning. All Rights Reserved. May not be copied, scanned, or duplicated, in whole or in part. Due to electronic rights, some third party content may be suppressed from the eBook and/or eChapter(s). Editorial review has deemed that any suppressed content does not materially affect the overall learning experience. Cengage Learning reserves the right to remove additional content at any time if subsequent rights restrictions require it.

From Eq. (4.117)

$$G_{\max} = 625\frac{\mathrm{OCR}^K}{0.3+0.7e^2}\sqrt{p_a\bar{\sigma}_0}$$

Plasticity index $= 47 - 27 = 20$. Hence $K = 0.18$. Thus

$$G_{\max} = (625)\frac{(2)^{0.18}}{0.3+(0.7)(0.92)^2}\sqrt{(100)(24.68)} = 39{,}412 \text{ kPa} \approx 39.4 \text{ MPa}$$

From Figure 4.72, for $\gamma' = 0.01\%$

$$\frac{G}{G_{\max}} = 0.84$$

Or

$$G = (0.84)(39.4) \approx \mathbf{33.1\ MPa}$$

Again, from Figure 4.72 for $\gamma' = 0.01\%$ and PI $= 20$

$$\boldsymbol{D \approx 4\%}$$

4.26 SHEAR MODULUS AND DAMPING RATIO FOR LIGHTLY CEMENTED SAND

Lightly cemented sand deposits are encountered in many parts of the world. The cementing material in the sand deposits is primarily calcium carbonate. More recently, the results of several research projects relating to the properties of lightly cemented sands have been published. From these studies it appears that the behavior of lightly cemented sands can be duplicated in the laboratory by mixing sand and Portland cement in required properties. The maximum sheer modulus can be expressed as (Saxena, Avramidis, and Reddy, 1988)

$$G_{\max(CS)} = G_{\max(S)} + \Delta G_{\max(C)} \tag{4.122}$$

where $G_{\max(CS)}$ = maximum shear modulus of lightly cemented sand
$G_{\max(S)}$ = maximum shear modulus of sand alone
$\Delta G_{\max(C)}$ = increase of maximum shear modulus due to cementation effect

According to Saxena, Avramidis, and Reddy, the magnitudes of $G_{\max(S)}$ and $\Delta G_{\max(C)}$ can be obtained from the following empirical relationships.

$$\boxed{\begin{array}{ccc} G_{\max(S)} = \dfrac{428.2}{0.3+0.7e^2}(p_a)^{0.426}(\bar{\sigma}_0)^{0.574} & & \\ \uparrow & \uparrow & \uparrow \\ \text{(kPa)} & \text{(kPa)} & \text{(kPa)} \end{array}} \tag{4.123}$$

Copyright 2017 Cengage Learning. All Rights Reserved. May not be copied, scanned, or duplicated, in whole or in part. Due to electronic rights, some third party content may be suppressed from the eBook and/or eChapter(s). Editorial review has deemed that any suppressed content does not materially affect the overall learning experience. Cengage Learning reserves the right to remove additional content at any time if subsequent rights restrictions require it.

where p_a = atmospheric pressure in the same units as $G_{\max(S)}$

$$\frac{\Delta G_{\max(C)}}{p_a} = \frac{172}{(e-0.5168)}(CC)^{0.88}\left(\frac{\bar{\sigma}_0}{p_a}\right)^{0.515e-0.13CC+0.285} \quad (4.124)$$

(for $CC < 2\%$)

$$\frac{\Delta G_{\max(C)}}{p_a} = \frac{773}{e}(CC)^{1.2}\left(\frac{\bar{\sigma}_0}{p_a}\right)^{0.698e-0.04CC-0.2} \quad (4.125)$$

(for $2\% \leq CC \leq 8\%$)

where CC = cement content (in percent) and e = void ratio.
When using Eqs. (4.124) and (4.125), the units of $G_{\max(S)}$, p_a, and $\bar{\sigma}_0$ need to be consistent.

The damping ratio at low strain amplitudes ($\gamma' \leq 10^{-3}$ %) can be expressed as (Saxena, Avramidis, and Reddy, 1988)

$$D_{CS} = D_S + \Delta D_C \quad (4.126)$$

where D_{CS} = damping ratio of cemented sand (%)
D_S = damping ratio of sand alone (%)
ΔD_C = increase in the damping ratio due to cementation effect

$$\boxed{D_S = 0.94\left(\frac{\bar{\sigma}_0}{p_a}\right)^{-0.38}} \quad (4.127)$$

$$\boxed{\Delta D_C = 0.49(CC)^{1.07}\left(\frac{\bar{\sigma}_0}{p_a}\right)^{-0.36}} \quad (4.128)$$

where CC = cement content (in percent). The units of p_a and $\bar{\sigma}_0$ need to be consistent.

EXAMPLE 4.10

If a lightly cemented sand specimen is subjected to an effective confining pressure of 98 kPa, estimate the value of $G_{\max(CS)}$, given $e = 0.7$ and $CC = 3\%$.

SOLUTION

From Eq. (4.123),

$$G_{\max(S)} = \frac{428.2}{0.3+0.7e^2}(p_a)^{0.426}(\bar{\sigma}_0)^{0.574}$$

Copyright 2017 Cengage Learning. All Rights Reserved. May not be copied, scanned, or duplicated, in whole or in part. Due to electronic rights, some third party content may be suppressed from the eBook and/or eChapter(s). Editorial review has deemed that any suppressed content does not materially affect the overall learning experience. Cengage Learning reserves the right to remove additional content at any time if subsequent rights restrictions require it.

Given $e = 0.7$, $p_a = 100$ kPa, and $\bar{\sigma}_0 = 98$ kPa,

$$G_{\max(S)} = \frac{428.2}{0.3 + (0.7)(0.7)^2}(100)^{0.426}(98)^{0.574}$$
$$= 65{,}805 \text{ kPa} = 0.066 \text{ GPa}$$

From Eq. (4.125),

$$\frac{\Delta G_{\max(C)}}{p_a} = \frac{773}{e}(CC)^{1.2}\left(\frac{\bar{\sigma}_0}{p_a}\right)^{0.698e - 0.04CC - 0.2}$$

or

$$\frac{\Delta G_{\max(C)}}{100} = \frac{773}{0.7}(3)^{1.2}\left(\frac{98}{100}\right)^{0.698(0.7) - 0.04(3) - 0.2}$$
$$= (1104.3)(3.737)(0.997) = 4114.39$$
$$\Delta G_{\max(C)} = 411{,}439 \text{ kPa} = 0.411 \text{ GPa}$$

So

$$G_{\max(CS)} = G_{\max(S)} + \Delta G_{\max(C)}$$
$$= 0.066 + 0.411 = 0.477 \text{ GPa} = \mathbf{477\ MPa}$$

PROBLEMS

4.1 A uniformly graded dry sand specimen was tested in a resonant column device. The shear wave velocity v_s determined by torsional vibration of the specimen was 231.65 m/s. The longitudinal wave velocity determined by using a similar specimen was 387.40 m/s. Determine each of the following.

a. Poisson's ratio

b. Modulus of elasticity (E) and shear modulus (G) if the void ratio and the specific gravity of soil solids of the specimen were 0.5 and 2.65, respectively.

4.2 A clayey soil specimen was tested in a resonant column device (torsional vibration; free–free end condition) for determination of shear modulus. Given: length of specimen = 90 mm, diameter of specimen = 35.6 mm, mass of specimen = 170 g, frequency at normal mode of vibration ($n = 1$) = 790 Hz. Determine the shear modulus of the specimen in kPa.

4.3 The Poisson's ratio for the clay specimen described in Problem 4.2 is 0.52. If a similar specimen is vibrated longitudinally in a resonant

Copyright 2017 Cengage Learning. All Rights Reserved. May not be copied, scanned, or duplicated, in whole or in part. Due to electronic rights, some third party content may be suppressed from the eBook and/or eChapter(s). Editorial review has deemed that any suppressed content does not materially affect the overall learning experience. Cengage Learning reserves the right to remove additional content at any time if subsequent rights restrictions require it.

column device (free–free end condition), what would be its frequency at normal mode of vibration ($n = 1$)?

4.4 The results of a refraction survey in terms of time of first arrival (in milliseconds) and distance in meters is given below in tabular form. Assuming that the soil layers are perfectly horizontal, determine the *P*-wave velocities of the underlying soil layers and the thickness of the top layer.

Distance (m)	Time of first arrival (ms)
7.5	49.08
15.0	81.96
23.0	122.8
30.5	148.2
45.5	174.2
61.0	202.8
76.0	228.6
91.5	256.7

4.5 Repeat Problem 4.4 for the following.
Comment regarding the material encountered in the second layer.

Distance (m)	Time of first arrival (ms)	Distance (m)	Time of first arrival (ms)
10	19.23	100	125.82
20	38.40	150	138.72
30	57.71	200	152.61
40	76.90	250	166.81
60	115.40	300	178.31
80	120.71		

4.6 Repeat Problem 4.4 with the following results. Also determine the thickness of the second layer of soil encountered.

Distance (m)	Time of first arrival (ms)	Distance (m)	Time of first arrival (ms)
10	41.66	60	119.21
15	62.51	70	128.11
20	83.37	80	136.22
30	91.82	90	141.00
40	101.22	100	143.81
50	110.16	120	152.00

Copyright 2017 Cengage Learning. All Rights Reserved. May not be copied, scanned, or duplicated, in whole or in part. Due to electronic rights, some third party content may be suppressed from the eBook and/or eChapter(s). Editorial review has deemed that any suppressed content does not materially affect the overall learning experience. Cengage Learning reserves the right to remove additional content at any time if subsequent rights restrictions require it.

4.7 The results of a reflection survey are given here. Determine the velocity of P-waves in the top layer and its thickness.

Distance from shot point (m)	Time for first arrival of reflected wave (ms)
10	32.5
20	39.05
30	48.02
40	58.3
60	80.78
100	128.55

4.8 Refer to Figure 4.46 for the results of the following refraction survey:

Distance from point of disturbance, A (m)	Time of first arrival (ms)	Distance from point of disturbance, E (m)	Time of first arrival (ms)
0	0	0	0
6.0	20	6.0	20
12.0	40	12.0	40.1
18.0	60	18.0	59.8
24.5	78.2	24.5	79.7
36.5	92.8	36.5	121.0
61.0	122.2	61.0	167.2
85.5	149.8	85.5	175.1
Point E 110.0	177.9	Point A 110.0	180.2

Determine:
a. the P-wave velocities in the two layers,
b. z' and z'', and
c. the angle β.

4.9 For a reflection survey refer to Figure 4.51, in which A is the shot point. Distance $AC = AE = 180$ m. The times for arrival of the first reflected wave at points C and E are 45.0 ms and 64.1 ms, respectively. If the P-wave velocity in layer 1 is 280 m/s, determined β and z'.

4.10 The results of a subsoil exploration by steady-state vibration technique are given here (Section 4.16):

Copyright 2017 Cengage Learning. All Rights Reserved. May not be copied, scanned, or duplicated, in whole or in part. Due to electronic rights, some third party content may be suppressed from the eBook and/or eChapter(s). Editorial review has deemed that any suppressed content does not materially affect the overall learning experience. Cengage Learning reserves the right to remove additional content at any time if subsequent rights restrictions require it.

Distance from the plate vibrated x (m)	Number of waves per second	Frequency of vibration of the plate (Hz)
10	41.00	900
10	18.00	400
10	9.00	200
10	4.55	100
10	2.65	90
10	2.30	75
10	1.77	60
10	1.47	50

Make necessary calculations and plot the variation of the wave velocity with depth.

4.11 Figure P4.11 shows a soil profile with the standard penetration resistance (N) values with depth. Using the relationships given by Imai (1977; see Table 4.4), estimate the variation of the shear wave velocity (v_s) with depth.

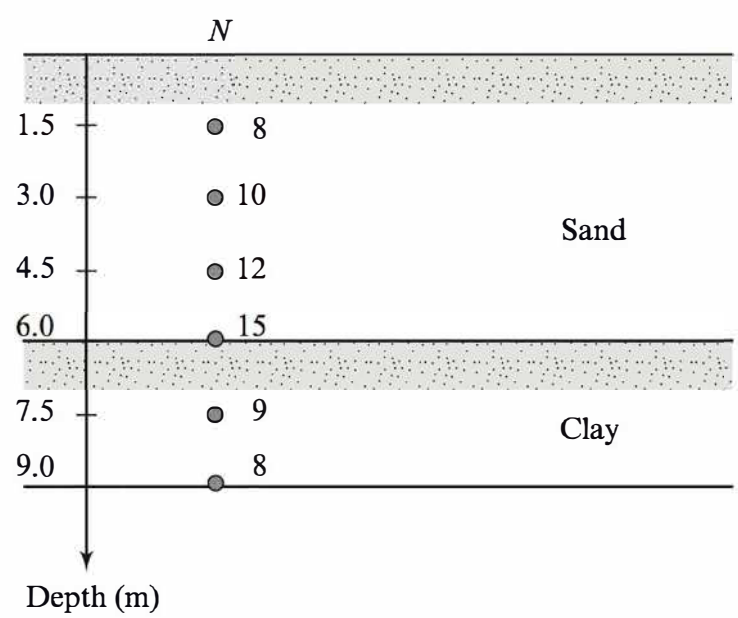

Figure P4.11

4.12 An angular-grained sand has maximum and minimum void ratios of 1.1 and 0.55, respectively. Using Eq. (4.105), determine and plot the variation of maximum shear modulus G_{max} versus relative density ($R_D = 0 - 100\%$) for mean confining pressures of 50, 100, 150, 200 and 300 kPa.

4.13 A 20-m-thick sand layer in the field is underlain by rock. The groundwater table is located at a depth of 5 m measured from the ground surface.

Copyright 2017 Cengage Learning. All Rights Reserved. May not be copied, scanned, or duplicated, in whole or in part. Due to electronic rights, some third party content may be suppressed from the eBook and/or eChapter(s). Editorial review has deemed that any suppressed content does not materially affect the overall learning experience. Cengage Learning reserves the right to remove additional content at any time if subsequent rights restrictions require it.

Determine the maximum shear modulus of this sand at a depth of 10 m below the ground surface. Given: void ratio = 0.6, specific gravity of soil solids = 2.68, angle of friction of sand = 36°. Assume the sand to be round-grained. Use Eq. (4.104)

4.14 For a deposit of sand, at a certain depth in the field the effective vertical pressure is 120 kPa. The void ratio and the relative density are 0.72 and 30° respectively. Determine the shear modulus and damping ratio for a shear strain levels of 5×10^{-2} %. Use eqs. (4.105) and (47.109)

4.15 A remolded clay specimen was consolidated by a hydrostatic pressure of 205 kPa. The specimen was then allowed to swell under a hydrostatic pressure of 105 kPa. The void ratio at the end of swelling was 0.8. If this clay is subjected to a torsional vibration in a resonant column test, what would be its maximum shear modulus (G_{max})? These liquid and plastic limits of the clay are 58 and 28, respectively.

4.16 Refer to the overconsolidated soil specimen in Problem 4.15. Estimate the shear modulus and damping ratio of the specimen at a cyclic shear strain of 0.01%.

4.17 Refer to Figure P4.17. Given:

$$H_1 = 2 \text{ m} \qquad G_{s(1)} = 2.68$$
$$H_2 = 8 \text{ m} \qquad G_{s(2)} = 2.65$$
$$H_3 = 3 \text{ m} \qquad \phi_1 = 35°$$
$$e_1 = 0.6 \qquad \phi_2 = 30°$$
$$e_2 = 0.7 \qquad \text{PI of clay} = 32$$

Estimate and plot the variation of the maximum shear modulus (G_{max}) with depth for the soil profile

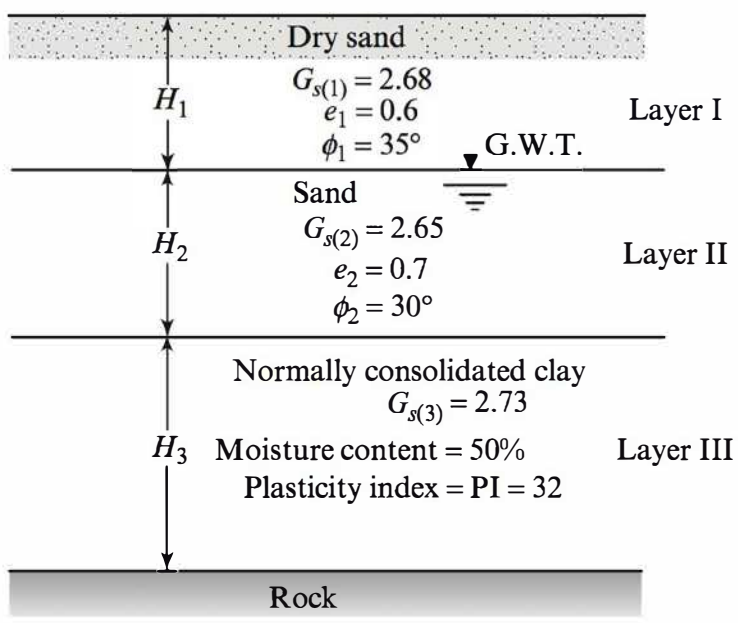

Figure P4.17

Copyright 2017 Cengage Learning. All Rights Reserved. May not be copied, scanned, or duplicated, in whole or in part. Due to electronic rights, some third party content may be suppressed from the eBook and/or eChapter(s). Editorial review has deemed that any suppressed content does not materially affect the overall learning experience. Cengage Learning reserves the right to remove additional content at any time if subsequent rights restrictions require it.

4.18 Repeat Problem 4.17 given

$$H_1 = H_2 = H_3 = 6\text{ m} \qquad G_{s(1)} = G_{s(2)} = 2.66$$
$$e_1 = 0.88 \qquad \phi_1 = 28°$$
$$e_2 = 0.68 \qquad \phi_2 = 32°$$
$$\text{PI of clay} = 20$$

4.19 The unit weight of a sand deposit is 16.98 kN/m^3 at a relative density of 60%. Assume that, for this sand

$$\phi = 30 + 0.15R_D$$

where ϕ is the drained friction angle and R_D is the relative density (in percent). At a depth of 6.09 m below the ground surface, estimate its shear modulus and damping ratio at a shear strain level of 0.01%. Use the equations proposed by Seed and Idriss (1970).

4.20 The results of a standard unconsolidated undrained triaxial test on a undisturbed saturated clay specimen are as follows:

Confining pressure = 70 kPa

Total axial stress at failure = 166.6 kPa

Using the method proposed by Seed and Idriss (1970), determine and plot the variation of shear modulus and damping ratio with shear strain (strain range 10^{-3} % to 1%).

4.21 For Example 4.10, determine the damping ratio of the cemented sand.

References

Barkan, D. D. (1962), *Dynamics of Bases and Foundations,* McGraw-Hill Book Company, New York.

Beeston, H. E., and McEvilly, T. V. (1977). "Shear Wave Velocities from Down Hole Measurements," *Journal of the International Association for Earthquake Engineering*, Vol. 5, No. 2, pp. 181–190.

Booker, E. W., and Ireland, H. O. (1965). "Earth Pressure at Rest Related to Stress History," *Canadian Geotechnical Journal*, Vol. 2, No. 1, pp. 1–15.

Carroll, W. F. (1963), "Dynamic Bearing Capacity of Soils. Vertical Displacements of Spread Footing on Clay: Static and Impulsive Loadings," *Technical Report No. 3-599*, Report 5, U.S. Army Corps of Engineers, Waterways Experiment Station, Vicksburg, Mississippi.

Casagrande, A., and Shannon, W. L. (1949). "Strength of Soils under Dynamic Loads," *Transactions*, ASCE, Vol. 114, pp. 755–772.

Das, B. M. (1990). *Principles of Geotechnical Engineering*, 2nd ed., PWS-KENT, Boston.

Copyright 2017 Cengage Learning. All Rights Reserved. May not be copied, scanned, or duplicated, in whole or in part. Due to electronic rights, some third party content may be suppressed from the eBook and/or eChapter(s). Editorial review has deemed that any suppressed content does not materially affect the overall learning experience. Cengage Learning reserves the right to remove additional content at any time if subsequent rights restrictions require it.

Dikmen, Ü. (2009). Statistical Correlations of Shear Wave Velocity and Penetration Resistance for Soils," *Journal of Geophysics and Engineering*, Vol. 6, No. 1, pp. 61–72.

Drnevich, V. P. (1972). "Undrained Cyclic Shear of Saturated Sand," *Journal of the Soil Mechanics and Foundations Division*, ASCE, Vol. 98, No. SM8, pp. 807–825.

Drnevich, V. P., Hall, J. R., Jr., and Richart F. E., Jr. (1966). "Large Amplitude Vibration Effects on the Shear Modulus of Sand," University of Michigan Report to Waterways Experiment Station, Corps of Engineers, US Army Contact DA-22-079-Eng-340, October 1966.

Drnevich, V. P., Hall, J.R., Jr., and Richart, F. E., Jr. (1967). "Effects of Amplitude of Vibration on the Shear Modulus of Sand," *Proceedings*, International Symposium on Wave Propagation and Dynamic Properties of Earth Materials, Ed. G. E. Triandafilidis, University of New Mexico Press, Albuquerque, New Mexico, pp. 189–199.

Dyvik, R., and Madshus, C. (1985). "Lab Measurements of G_{max} Using Bender Elements," *Proceedings*, Advances in the Art of Testing Soils under Cyclic Conditions, ASCE Annual Convention, Detroit, Michigan, pp. 186–196.

Hall, J. R., Jr., and Richart, F. E., Jr. (1963). "Dissipation of Elastic Wave Energy in Granular Soils," *Journal of the Soil Mechanics and Foundations Division*, ASCE, Vol. 89, No. SM6, pp. 27–56.

Hardin, B. O. (1978). "The Nature of Stress-Strain Behavior for Soils," *Proceedings*, Specialty Conference on Earthquake Engineering and Soil Dynamics, ASCE, Pasadena, California, Vol. 1, pp. 3–90.

Hardin, B. O. (1965). "The Nature of Damping of Sands," *Journal of the Soil Mechanics and Foundations Division*, ASCE, Vol. 91, No. SM1, pp. 63–97.

Hardin, B. O., and Black, W. L. (1968). "Vibration Modulus of Normally Consolidated Clay," *Journal of the Soil Mechanics and Foundations Division*, ASCE, Vol. 94, No. SM2, pp. 353–369.

Hardin, B. O., and Drnevich, V. P. (1972). "Shear Modulus and Damping in Soils: Design Equations and Curves," *Journal of Soil Mechanics and Foundations Division*, ASCE, Vol. 98, No. SM7, pp. 667–692.

Hardin, B. O., and Richart, F. E., Jr. (1963). "Elastic Wave Velocities in Granular Soils," *Journal of the Soil Mechanics and Foundations Division*, ASCE, Vol. 89, No. SM1, pp. 33–65.

Hasancebi, N., and Ulusay, R. (2007). "Empirical Correlations between Shear Wave Velocity and Penetration Resistance for Ground Shaking Assessments," *Bulletin of Engineering Geology and the Environment*," Vol. 66, No. 2, pp. 203–213.

Heukelom, W., and Foster, C. R. (1960). "Dynamic Testing of Pavements," *Journal of the Soil Mechanics and Foundation Division,* ASCE, Vol. 86, No. SM1, Part 1, pp. 1–28.

Iida, K. (1938). "The Velocity of Elastic Waves in Sand," *Bulletin of the Earthquake Research Institute*, Tokyo Imperial University, Vol. 16, pp. 131–144.

Iida, K. (1940). "On the Elastic Properties of Soil Particularly in Relation to Its Water Contents," *Bulletin of the Earthquake Research Institute*, Tokyo Imperial University, Vol. 18, pp. 675–690.

Imai, T. (1977). "P- and S-Wave Velocities of the Ground in Japan," *Proceedings*, 9th International Conference on Soil Mechanics and Foundation Engineering, Tokyo, Japan, Vol. 2, pp. 257–260.

Ishibashi, I., and Sherif, M. A. (1974). "Soil Liquefaction by Torsional Simple Shear Device," *Journal of the Geotechnical Engineering Division*, ASCE, Vol. 100, No. GT8, pp. 871–888.

Ishimato, M,. and Iida, K. (1937). "Determination of Elastic Constants of Soils by Means of Vibration Methods," *Bulletin of the Earthquake Research Institute*, Tokyo Imperial University, Vol. 15, p. 67.

Iwasaki, T., Tatsuoka, F., and Takagi, Y. (1976). "Dynamic Shear Deformation Properties of Sand for Wide Strain Range," *Report of the Civil Engineering Institute, No. 1085*, Ministry of Construction, Tokyo, Japan.

Copyright 2017 Cengage Learning. All Rights Reserved. May not be copied, scanned, or duplicated, in whole or in part. Due to electronic rights, some third party content may be suppressed from the eBook and/or eChapter(s). Editorial review has deemed that any suppressed content does not materially affect the overall learning experience. Cengage Learning reserves the right to remove additional content at any time if subsequent rights restrictions require it.

Jafari, M. K., Shafiee, A., and Razmkhah, A. (2002). "Dynamic Properties of the Fine Grained Soils in South of Tehran," *Journal of Seismology and Earthquake Engineering*, Vol. 4, No. 1, pp. 25–35.

Kiku, H., Yoshida, N., Yasuda, S., Irisawa, T., Nakazawa, H., Shimizu, Y., Ansal, A., and Erkan, A. (2001). "In-situ Penetration Tests and Soil Profiling in Adapazari, Turkey," *Proceedings*, 15th International Conference on Soil Mechanics and Geotechnical Engineering, TC4 Satellite Conference on "Lessons Learned from Recent Strong Earthquakes," Istanbul, Turkey, pp. 259–269.

Kolsky, H. (1963). *Stress Waves in Solids*, Dover Publications, Inc., New York.

Larkin, T. J·, and Taylor, P. W. (1979). "Comparison of Down Hole and Laboratory Shear Wave Velocities," *Canadian Geotechnical Journal*, Vol. 16, No. 1, pp. 152–162.

Matsui, T., Ohara, H., and Ito, T. (1980). "Cyclic Stress-Strain History and Shear Characteristics of Clay," *Journal of the Geotechnical Engineering Division*, ASCE, Vol. 106, No. GT10, pp. 1101–1120.

Mayne, P. W. and Kulhawy, F.H. (1982). " K_0 -OCR Relationships in Soil," *Journal of the Geotechnical Engineering Division*, ASCE, Vol. 108, No, 6, pp. 851–872.

Ohta, Y., and Goto, N. (1978). "Empirical Shear Wave Velocity Equations in Terms of Characteristic Soil Indexes," *Earthquake Engineering and Structural Dynamics*, Vol. 6, pp. 167–187.

Okamoto, T., Kokusho, T., Yoshida, Y., and Kusuonoki, K. (1989). "Comparison of Surface Versus Subsurface Wave Source for P-S Logging in Sand Layer," *Proceedings*, 44th Annual Conference, Japan Society of Civil Engineers, Vol. 3, pp. 996–997 (in Japanese).

Pitilakis, K., Raptakis, D., Lontzetidis, K. T., Vassilikou, T., and Jongmans, D. (1999). "Geotechnical and Geophysical Description of Euro-Seistests Using Field and Laboratory Tests, and Moderate Strong Ground Motions," *Journal of Earthquake Engineering*, Vol. 3, pp. 381–409.

Richart, F. E., Jr., Hall, J. R. Jr., and Lysmer, J· (1962). "Study of the Propagation and Dissipation of 'Elastic' Wave Energy in Granular Soils," University of Florida Report to Waterways Experiment Station, Corps of Engineers, US Army Contract DA-22-070-Eng-314.

Rollins, K. M., Evans, M. D., Diehl, N. B., and Daily, W. D., III (1998). "Shear Modulus and Damping Relationships for Gravels," *Journal of Geotechnical and Geoenvironmental Engineering*, ASCE, Vol. 124, No. 5, pp. 396–405.

Saxena, S. K., Avramidis, A. S., and Reddy, K. R. (1988). "Dynamic Moduli and Damping Ratios for Cemented Sands at Low Strains," Canadian Geotechnical Journal, Vol. 25, No.2, pp. 353–368.

Schwarz, S. D., and Musser, J· M., Jr. (1972). "Various Techniques for Making In Situ Shear Wave Velocity Measurements: A Description and Evaluation," *Proceedings*, International Conference on Microzonation for Safer Construction, Research and Application, Seattle, Washington, Vol. 2, pp. 593–608.

Seed, H. B., and Chan, C.K (1966). "Clay Strength under Earthquake Loading Conditions," *Journal of the Soil Mechanics and Foundations Division*, ASCE, Vol. 92, No. SM2, pp. 53–78.

Seed, H.B., and Idriss, I. M. (1970). "Soil Moduli and Damping Factors for Dynamic Response Analysis," *Report No. EERC 75-29*, Earthquake Engineering Research Center, University of California, Berkeley, California.

Seed, H. B., and Idriss, I. M. (1981). "Evaluation of Liquefaction Potential of Sand Deposits Based on Observations and Performance in Previous Earthquakes," Preprint No. 81–544, *In Situ Testing to Evaluate Liquefaction Susceptibility*, Session No. 24, ASCE Annual Conference, St. Louis, Missouri.

Seed, H. B., Wong, R. T., Idriss, I. M., and Tokimatsu, K. (1986). "Moduli and Damping Factors for Dynamic Analyses of Cohesive Soils," *Journal of Geotechnical Engineering*, ASCE, Vol. 112, No. GT11, pp. 1016–1032.

Sherif, M. A., Ishibashi, I., and Gaddah, A. H. (1972). "Damping Ratio for Dry Sands," *Journal of the Geotechnical Engineering Divison*, ASCE, Vol. 103, No. GT7, pp. 743–756.

Copyright 2017 Cengage Learning. All Rights Reserved. May not be copied, scanned, or duplicated, in whole or in part. Due to electronic rights, some third party content may be suppressed from the eBook and/or eChapter(s). Editorial review has deemed that any suppressed content does not materially affect the overall learning experience. Cengage Learning reserves the right to remove additional content at any time if subsequent rights restrictions require it.

Shibata, T., and Soelarno, D. S. (1975). "Stress-Strain Characteristic of Sands under Cyclic Loading," *Proceedings of the Japanese Society of Civil Engineers*, No. 239, pp. 57–65 (in Japanese).

Silver, M. L. (1981), "Load Deformation and Strength Behavior of Soils under Loading," State-of-the-Art-Paper, *Proceedings*, 2nd International Conference on Recent Advances in Geotechnical Earthquake Engineering and Soil Dynamics, St. Louis, Missouri, Vol. 3, pp. 873–896.

Silver, M. L., and Seed, H. B.(1969). "The Behavior of Sands under Seismic Loading Conditions," *Report No. EERC 69-16*, Earthquake Engineering Research Center, University of California, Berkeley, California.

Silver, M. L., and Seed, H. B (1971). "Deformation Characteristics of Sands under Cyclic Loading," *Journal of the Soil Mechanics and Foundations Division*, ASCE, Vol. 94, No. SM8, pp. 1081–1098.

Stokoe, K. H. II, Wright, S. G., Bay, J. A., and Roesset, J. M. (1994). "Characterization of Geotechnical Sites by SASW Method," *Technical Review: Geophysical Characterization of Sites, ISSMFE Technical Committee 10*, edited by R. D. Woods, Oxford, New Delhi, pp. 11–25

Stokoe, K. H. II, and Woods, R. D. (1972), "*In Situ* Shear Wave Velocity by Cross-Hole Method," *Journal of Soil Mechanics and Foundations Division*, ASCE, Vol. 98, No. SM5, pp. 443–460.

Sykora, D. E., and Stokoe, K. H. (1983). "Correlations of In-Situ Measurements in Sands of Shear Wave Velocity," *Soil Dynamics and Earthquake Engineering*, Vol. 20, pp. 125–136.

Terzaghi, K. (1955). "Evaluation of Coefficients of Subgrade Reaction," *Geotechnique*, Vol. 5, No. 4, pp. 297–326.

Thiers, G, R., and Seed, H. B. (1968). "Cyclic Stress-Strain Characteristics of Clay," *Journal of the Soil Mechanics and Foundations Division*, ASCE, Vol. 94, No. SM6, pp. 555–569.

Vesic, A. S. (1973). "Analysis of Ultimate Loads of Shallow Foundations," *Journal of the Soil Mechanics and Foundations Division*, ASCE, Vol. 99, No. SM1, pp. 45–73.

Vucetic, M., and Dobry, R. (1991). "Effect of Soil Plasticity on Cyclic Response," Journal of Geotechnical Engineering, ASCE, Vol. 117, No. 1, pp. 89–107.

Weissman, G. F., and Hart, R. R. (1961). "The Damping Capacity of Some Granular Soils," *ASTM Special Technical Publication No. 305*, Symposium on Soil Dynamics, pp. 45–54.

Werden, S. K., Drnevich, V. P., Hall, J. R. Jr., Hankour, C., Conlee, C. T., and Marr, W. A. (2013). "New Approach to Resonant Column Testing," *Geotechnical Testing Journal*, Vol. 36, No. 2, pp. 1–9.

Whitman, R. V. and Healy, K. A. (1963). "Shear Strength of Sands During Rapid Loadings," *Transactions*, ASCE, Vol. 128, Part 1, pp. 1553–1594.

Whitman, R. V. and Lawrence, F. V. (1963). "Discussion on Elastic Wave Velocities in Granular Soils," *Journal of the Soil Mechanics and Foundations Division*, ASCE, Vol. 89, No. SM5, pp. 112–118.

Wilson, S. D. and Dietrich, R. J. (1960). "Effect of Consolidation Pressure on Elastic and Strength Properties of Clay," *Proceedings*, Research Conference on Shear Strength of Cohesive Soils, ASCE, Boulder, Colorado, pp. 419–435.

Copyright 2017 Cengage Learning. All Rights Reserved. May not be copied, scanned, or duplicated, in whole or in part. Due to electronic rights, some third party content may be suppressed from the eBook and/or eChapter(s). Editorial review has deemed that any suppressed content does not materially affect the overall learning experience. Cengage Learning reserves the right to remove additional content at any time if subsequent rights restrictions require it.

Foundation Vibration

5

5.1 INTRODUCTION

In Chapter 2 (Figure 2.1), it was briefly mentioned that foundations supporting vibrating equipment do experience rigid body displacements. The cyclic displacement of a foundation can have six possible modes. They are

1. translation in the vertical direction;
2. translation in the longitudinal direction;
3. translation in the lateral direction;
4. rotation about the vertical axis (that is, yawing);
5. rotation about the longitudinal axis (that is, rocking); and
6. rotation about the lateral axis (that is, pitching).

In this chapter, the fundamentals of the vibration of foundations, in various modes, supported on an elastic medium will be developed. The elastic medium that supports the foundation will be considered to be homogeneous and isotropic. In general, the behavior of soils departs considerably from that of an elastic material; only at low strain levels may it be considered as a reasonable approximation to an elastic material. Hence, the theories developed here should be considered as applicable only to the cases where foundations undergo low amplitudes of vibration.

5.2 VERTICAL VIBRATION OF CIRCULAR FOUNDATIONS RESTING ON ELASTIC HALF-SPACE—HISTORICAL DEVELOPMENT

In 1904, Lamb studied the problem of vibration of a single vibrating force acting at a point on the surface of an elastic half-space. This study included cases in which the oscillating force R acts in the vertical direction and in the horizontal direction, as shown in Figure 5.1a and b. This is generally referred to as the *dynamic Boussinesq problem*.

Copyright 2017 Cengage Learning. All Rights Reserved. May not be copied, scanned, or duplicated, in whole or in part. Due to electronic rights, some third party content may be suppressed from the eBook and/or eChapter(s).
Editorial review has deemed that any suppressed content does not materially affect the overall learning experience. Cengage Learning reserves the right to remove additional content at any time if subsequent rights restrictions require it.

In 1936, Reissner analyzed the problem of vibration of a *uniformly loaded flexible circular area* resting on an elastic half-space. The solution was obtained by integration of Lamb's solution for a point load. Based on Reissner's work, the vertical displacement at the *center* of the flexible loaded area (Figure 5.2a) can be given by

$$z = \frac{Q_0 e^{i\omega t}}{G r_0}\left(f_1 + i f_2\right) \tag{5.1}$$

where
Q_0 = amplitude of the exciting force acting on the foundation
z = periodic displacement at the center of the loaded area
ω = circular frequency of the applied load
r_0 = radius of the loaded area
G = shear modulus of the soil
Q = exciting force, which has an amplitude of Q_0
f_1, f_2 = Reissner's displacement functions

The displacement functions f_1 and f_2 are related to the Poisson's ratio of the medium and the frequency of the exciting force.

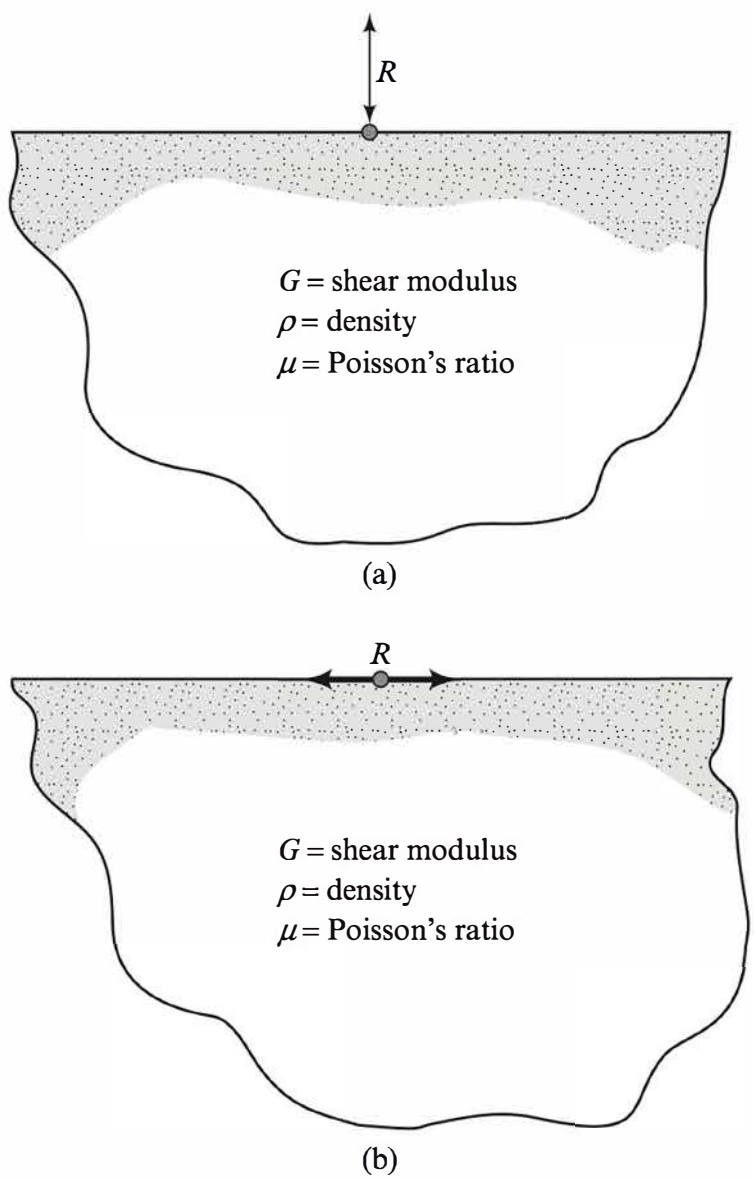

Figure 5.1 Vibrating force on the surface of an elastic half-space

Copyright 2017 Cengage Learning. All Rights Reserved. May not be copied, scanned, or duplicated, in whole or in part. Due to electronic rights, some third party content may be suppressed from the eBook and/or eChapter(s). Editorial review has deemed that any suppressed content does not materially affect the overall learning experience. Cengage Learning reserves the right to remove additional content at any time if subsequent rights restrictions require it.

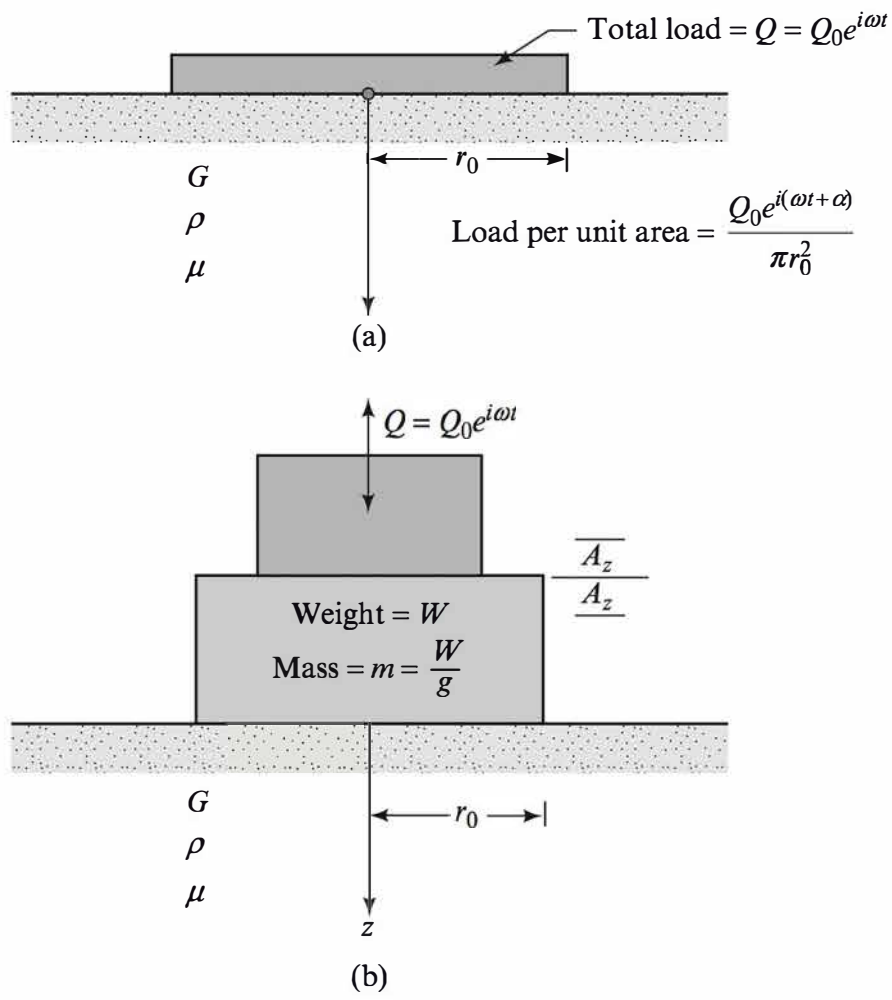

Figure 5.2 (a) Vibration of a uniformly loaded circular flexible area; (b) flexible circular foundation subjected to forced vibration

Now, consider a flexible circular foundation of weight W (mass $= m = W/g$) resting on an elastic half-space and subjected to an exciting force of magnitude of $Q_0\, e^{i(\omega t+\alpha)}$, as shown in Figure 5.2b. (*Note*: α is the phase difference between the exciting force and the displacement of the foundation.)

Using the displacement relation given in Eq. (5.1) and solving the equation of equilibrium of force, Reissner obtained the following relationships:

$$A_z = \frac{Q_0}{G r_0} Z \tag{5.2}$$

where A_z = the amplitude of the vibration

Z = dimensionless amplitude

$$= \sqrt{\frac{f_1^2 + f_2^2}{\left(1 - b a_0^2 f_1\right)^2 + \left(b a_0^2 f_2\right)^2}} \tag{5.3}$$

b = dimensionless mass ratio

$$= \frac{m}{\rho r_0^3} = \left(\frac{W}{g}\right)\left[\frac{1}{(\gamma/g) r_0^3}\right] = \frac{W}{\gamma r_0^3} \tag{5.4}$$

Copyright 2017 Cengage Learning. All Rights Reserved. May not be copied, scanned, or duplicated, in whole or in part. Due to electronic rights, some third party content may be suppressed from the eBook and/or eChapter(s). Editorial review has deemed that any suppressed content does not materially affect the overall learning experience. Cengage Learning reserves the right to remove additional content at any time if subsequent rights restrictions require it.

ρ = density of the elastic material
γ = unit weight of the elastic material
(for this problem, it is soil)

$$a_0 = \text{dimensionless frequency} = \omega r_0 \sqrt{\frac{\rho}{G}} = \frac{\omega r_0}{\upsilon_s} \tag{5.5}$$

υ_s = velocity of shear waves in the elastic material on which the foundation is resting

The classical work of Reissner was further extended by Quinlan (1953) and Sung (1953). As mentioned before, Reissner's work related only to the case of flexible circular foundations where the soil reaction is uniform over the entire area (Figure 5.3a). Both Quinlan and Sung considered the cases of rigid circular foundations, the contact pressure of which is shown in Figure 5.3b, flexible foundations (Figure 5.3a), and the types of foundations for which the contact pressure distribution is parabolic, as shown in Figure 5.3c. The distribution of contact pressure q for all three cases may be expressed as follows.

For flexible circular foundations (Figure 5.3a):

$$q = \frac{Q_0\, e^{i(\omega t + \alpha)}}{\pi r_0^2} \text{ (for } r \le r_0) \tag{5.6}$$

For rigid circular foundations (Figure 5.3b):

$$q = \frac{Q_0\, e^{i(\omega t + \alpha)}}{2\pi r_0 \sqrt{r_0^2 - r^2}} \text{ (for } r \le r_0) \tag{5.7}$$

For foundations with parabolic contact pressure distribution (Figure 5.3c):

$$q = \frac{2\left(r_0^2 - r^2\right) Q_0\, e^{i(\omega t + \alpha)}}{\pi r_0^4} \text{ (for } r \le r_0) \tag{5.8}$$

where q = contact pressure at a distance r measured from the center of the foundation

Quinlan derived the equations only for the *rigid circular* foundation; however, Sung presented the solutions for all the three class described. For all cases, the amplitude of motion can be expressed in a similar form to Eqs. (5.2), (5.3), (5.4), and (5.5). However, the displacement functions f_1 and f_2 will change, depending on the contact pressure distribution.

Copyright 2017 Cengage Learning. All Rights Reserved. May not be copied, scanned, or duplicated, in whole or in part. Due to electronic rights, some third party content may be suppressed from the eBook and/or eChapter(s). Editorial review has deemed that any suppressed content does not materially affect the overall learning experience. Cengage Learning reserves the right to remove additional content at any time if subsequent rights restrictions require it.

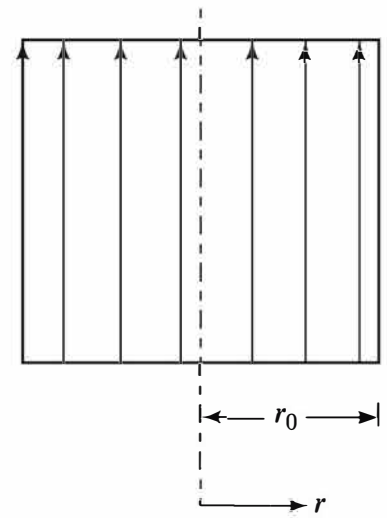

Uniform pressure distribution

(a)

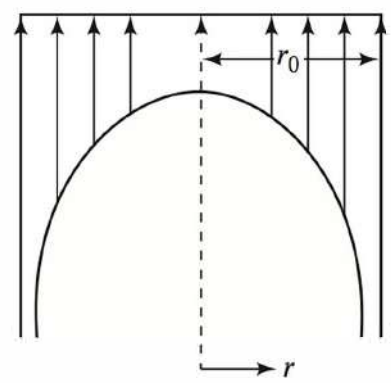

Pressure distribution under rigid foundation

(b)

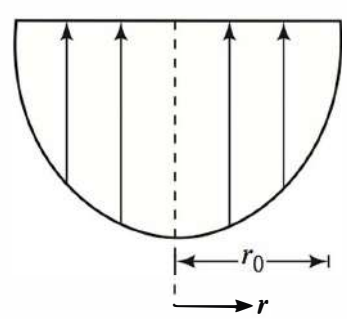

Parabolic pressure distribution

(c)

Figure 5.3 Contact pressure distribution under a circular foundation of radius r_0

Foundations, on some occasions, may be subjected to a *frequency-dependent excitation*, in contrast to the *constant-force* type of excitation just discussed. Figure 5.4 shows a foundation excited by two rotating masses. The amplitude of the exciting force can be given as

$$Q = 2m_e\, e\omega^2 = m_1 e\omega^2 \tag{5.9}$$

where m_1 = total of the rotating masses
ω = circular frequency of the rotating masses

Copyright 2017 Cengage Learning. All Rights Reserved. May not be copied, scanned, or duplicated, in whole or in part. Due to electronic rights, some third party content may be suppressed from the eBook and/or eChapter(s). Editorial review has deemed that any suppressed content does not materially affect the overall learning experience. Cengage Learning reserves the right to remove additional content at any time if subsequent rights restrictions require it.

For this condition, the amplitude of vibration A_z may be given by the relation

$$A_z = \frac{m_1 e \omega^2}{G r_0} \sqrt{\frac{f_1^2 + f_2^2}{\left(1 - b a_0^2 f_1\right)^2 + \left(b a_0^2 f_2\right)^2}} \tag{5.10}$$

From Eq. (5.5)

$$a_0 = \omega r_0 \sqrt{\frac{\rho}{G}}$$

or

$$\omega^2 = \frac{a_0^2 G}{\rho r_0^2} \tag{5.11}$$

Substituting Eq. (5.11) into (5.10), one obtains

$$A_z = \frac{m_1 e a_0^2}{\rho r_0^3} \sqrt{\frac{f_1^2 + f_2^2}{\left(1 - b a_0^2 f_1\right)^2 + \left(b a_0^2 f_2\right)^2}} = \frac{m_1 e}{\rho r_0^3} Z' \tag{5.12}$$

where $Z' =$ <u>dimensionless amplitude</u>

$$= a_0^2 \sqrt{\frac{f_1^2 + f_2^2}{\left(1 - b a_0^2 f_1\right)^2 + \left(b a_0^2 f_2\right)^2}} \tag{5.13}$$

Figures 5.5 and 5.6 show the plots of the variation of the dimensionless amplitude with a_0 (Richart, 1962) for *rigid circular* foundations (for $\mu =$ Poisson's ratio $= 0.25$ and $b = 5, 10, 20,$ and 40).

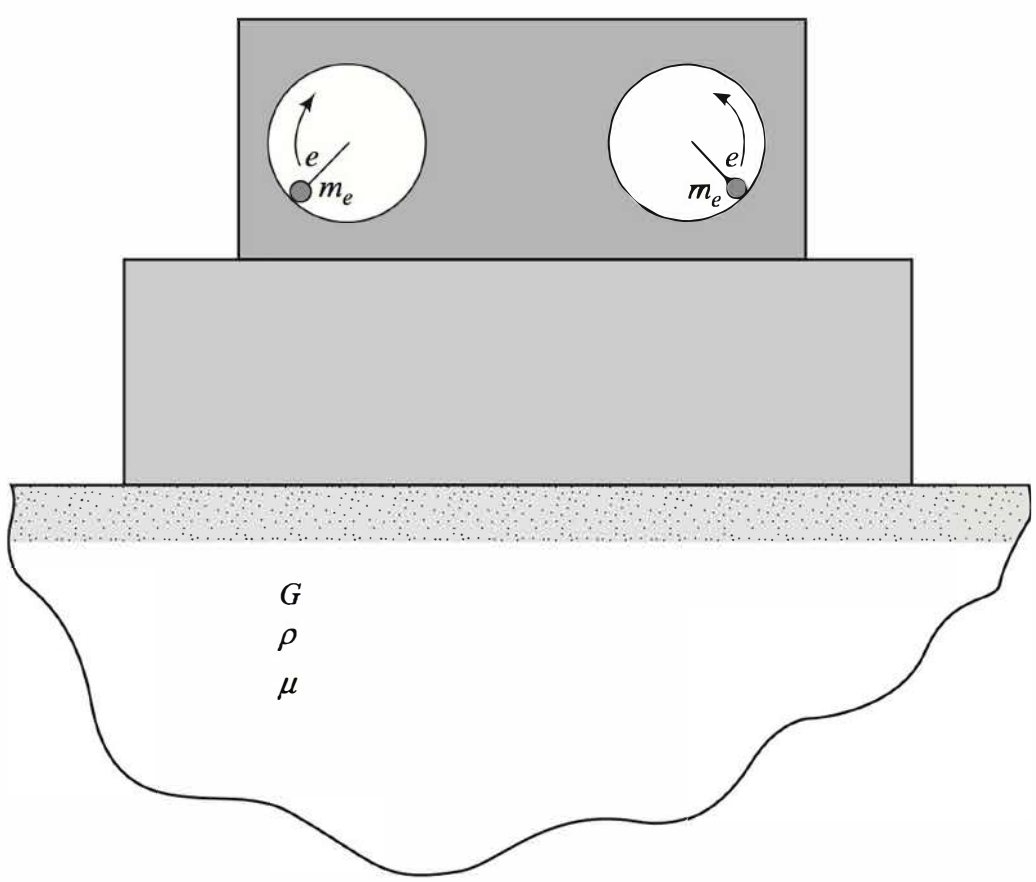

Figure 5.4 Foundation vibration by a frequency-dependent exciting force

Copyright 2017 Cengage Learning. All Rights Reserved. May not be copied, scanned, or duplicated, in whole or in part. Due to electronic rights, some third party content may be suppressed from the eBook and/or eChapter(s). Editorial review has deemed that any suppressed content does not materially affect the overall learning experience. Cengage Learning reserves the right to remove additional content at any time if subsequent rights restrictions require it.

Effect of Contact Pressure Distribution and Poisson's Ratio

The effect of the contact pressure distribution on the nature of variation of the nondimensional amplitude Z' with a_0 is shown in Figure 5.7 (for $b = 5$ and $\mu = 0.25$). As can be seen, for a given value of a_0, the magnitude of the amplitude is highest for the case of parabolic pressure distribution and lowest for rigid bases.

For a given type of pressure distribution and mass ratio (b), the magnitude of Z' also greatly depends on the assumption of the Poisson's ratio μ. This is shown in Figure 5.8.

Variation of Displacement Functions f_1 and f_2

As mentioned before, the displacement functions are related to the dimensionless frequency a_0 and Poisson's ratio μ. In Sung's original study, it was assumed

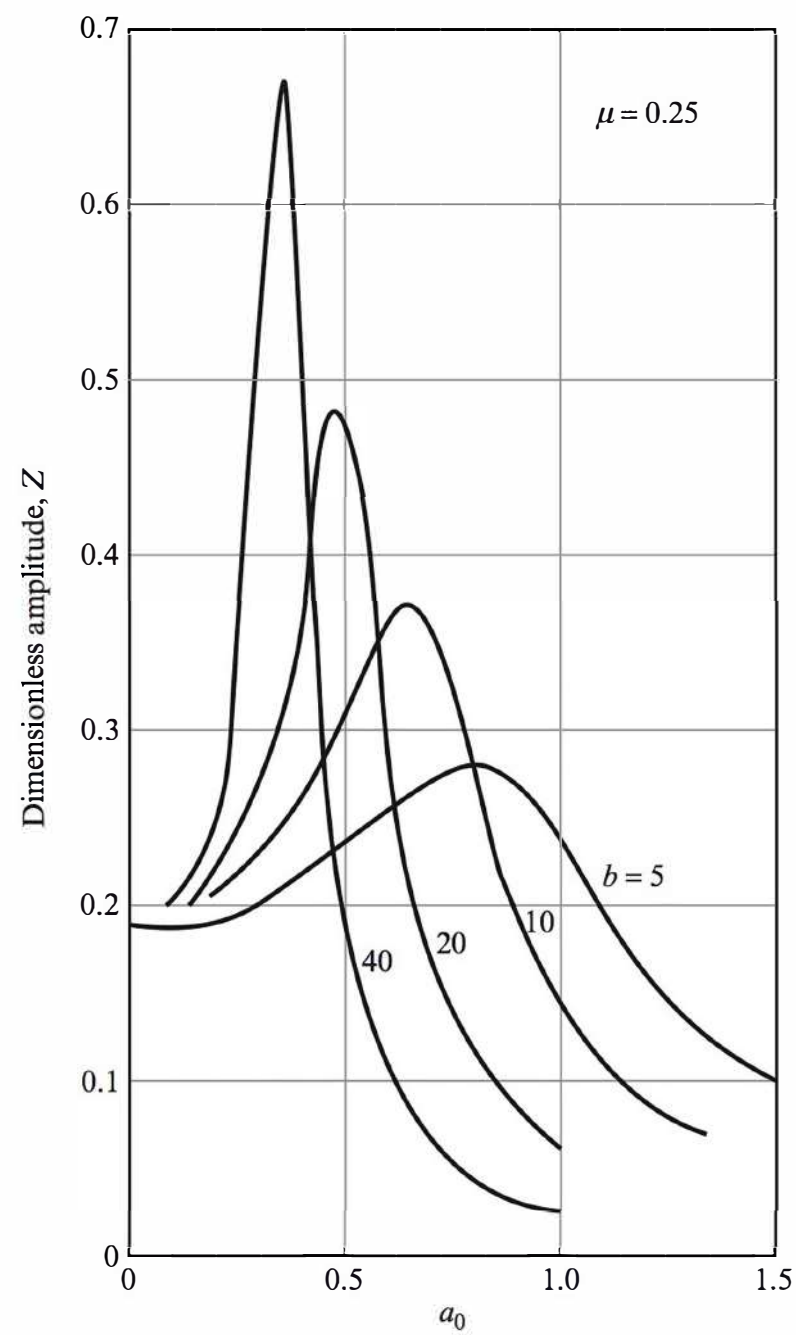

Figure 5.5 Plot of Z versus a_0 for rigid circular foundation (from Richart, 1962)

Source: Richart, F.E., Jr. (1962). "Foundation Vibrations," *Transactions,* ASCE, Vol. 27, Part 1, pp. 863–898. With permission from ASCE.

Copyright 2017 Cengage Learning. All Rights Reserved. May not be copied, scanned, or duplicated, in whole or in part. Due to electronic rights, some third party content may be suppressed from the eBook and/or eChapter(s). Editorial review has deemed that any suppressed content does not materially affect the overall learning experience. Cengage Learning reserves the right to remove additional content at any time if subsequent rights restrictions require it.

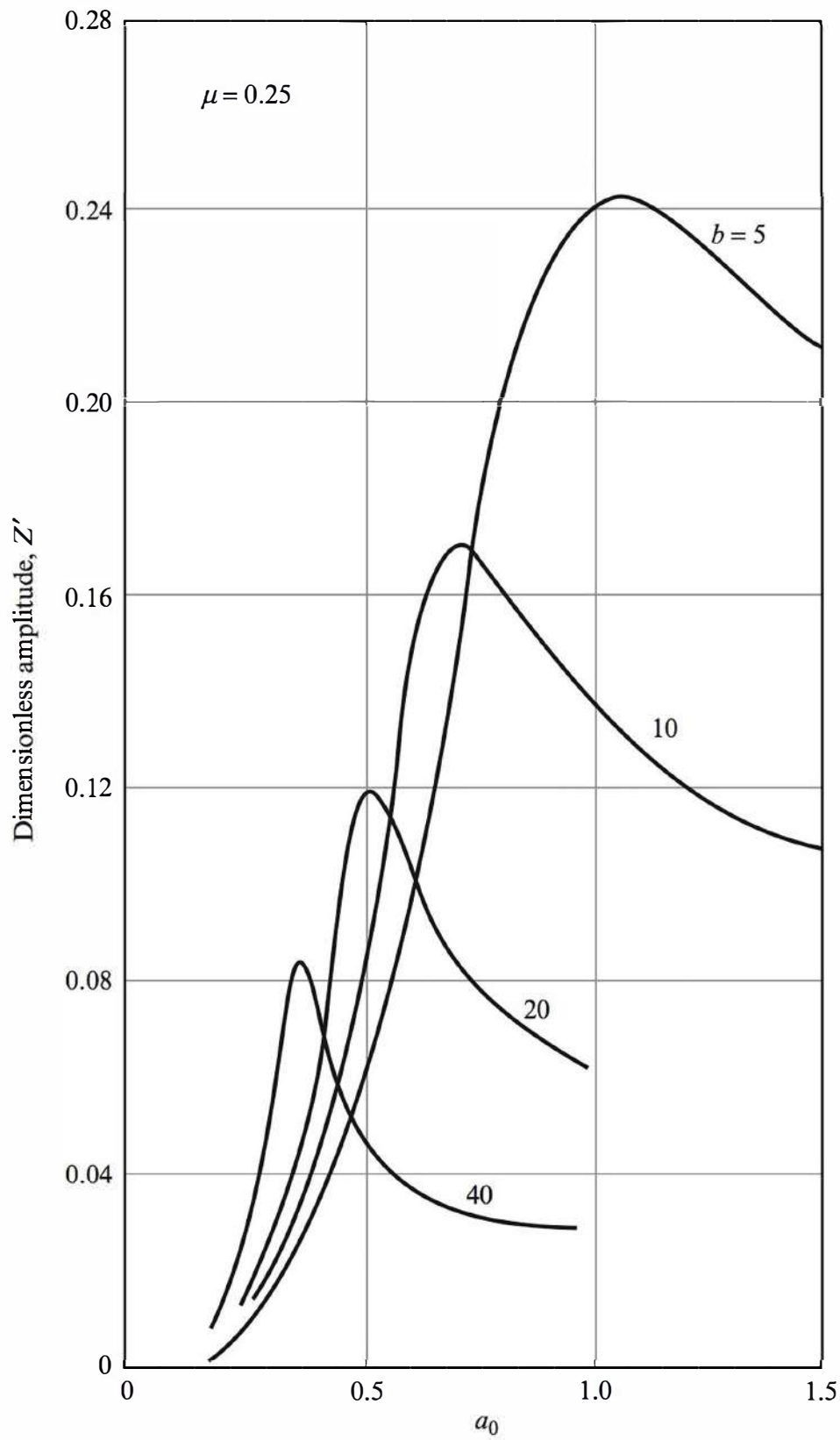

Figure 5.6 Variation of Z' with a_0 for rigid circular foundation (redrawn from Richart, 1962)

Source: Richart, F.E., Jr. (1962). "Foundation Vibrations," *Transactions,* ASCE, Vol. 27, Part 1, pp. 863-898. With permission from ASCE.

that the contact pressure distribution remains the same throughout the range of frequency considered; however, for dynamic loading conditions, the rigid-base pressure distribution does not produce uniform displacement under the foundation. For that reason, Bycroft (1956) determined the weighted average of the displacements under a foundation. The variation of the displacement functions determined by the study is shown in Figure 5.9.

Copyright 2017 Cengage Learning. All Rights Reserved. May not be copied, scanned, or duplicated, in whole or in part. Due to electronic rights, some third party content may be suppressed from the eBook and/or eChapter(s). Editorial review has deemed that any suppressed content does not materially affect the overall learning experience. Cengage Learning reserves the right to remove additional content at any time if subsequent rights restrictions require it.

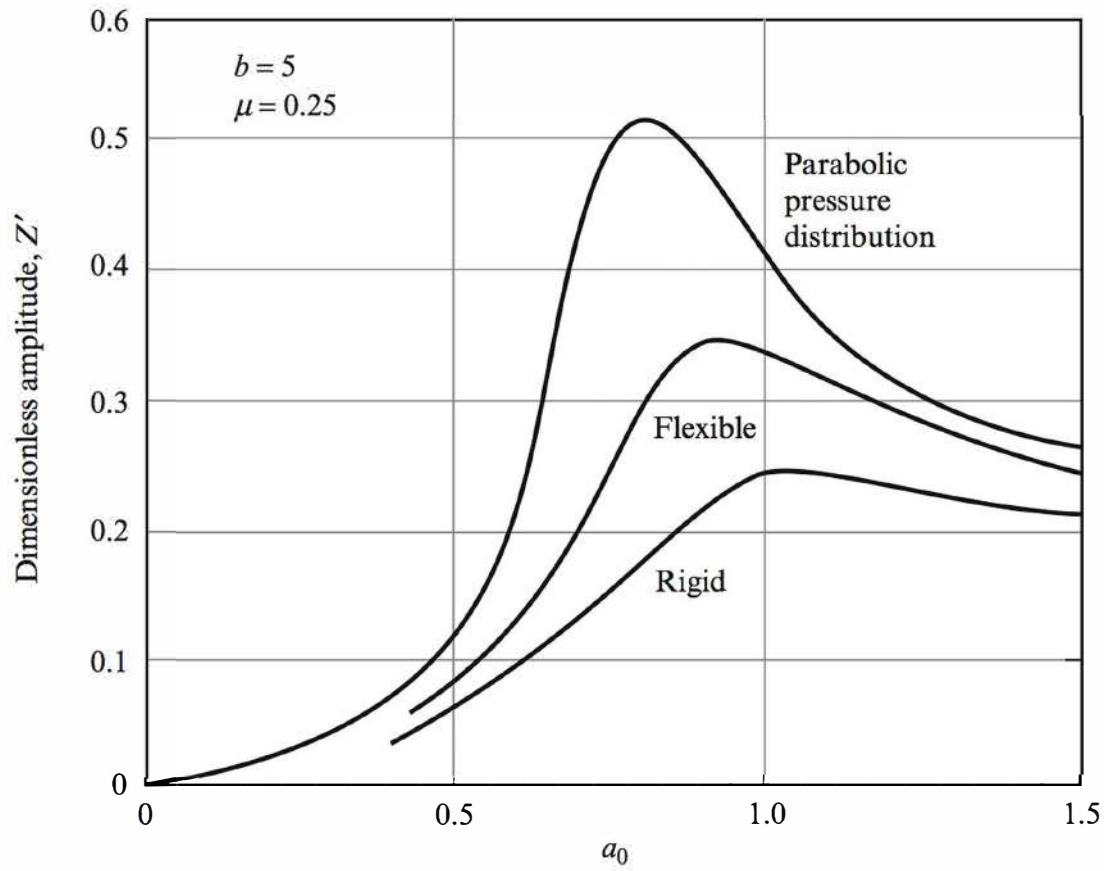

Figure 5.7 Effect of contact pressure distribution on the variation of Z' with a_0 (redrawn from Richart and Whitman, 1967)

Source: Richart, F.E., Jr., and Whitman, R.V. (1967). "Comparison of Footing Foundation Tests with Theory," *Journal of the Soil Mechanics and Foundations,* ASCE, Vol. 93, No. SM6, pp. 143–167. With permission from ASCE.

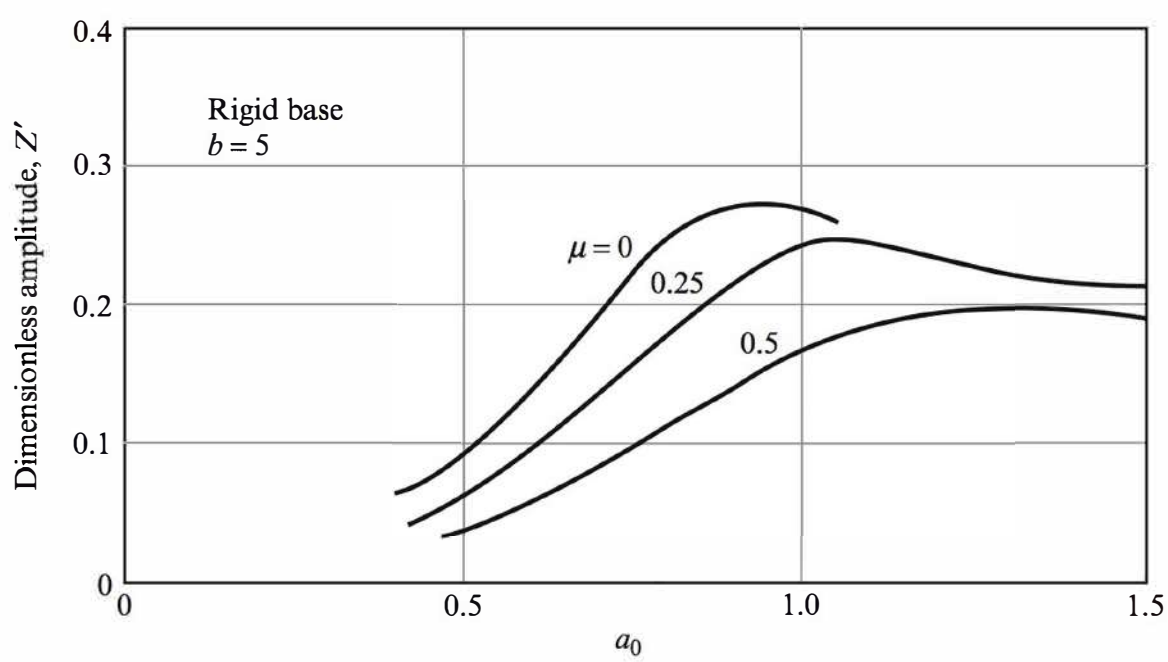

Figure 5.8 Effect of Poisson's ratio on the variation of Z' with a_0 (redrawn from Richart and Whitman, 1967)

Source: Richart, F.E., Jr., and Whitman, R.V. (1967). "Comparison of Footing Foundation Tests with Theory," *Journal of the Soil Mechanics and Foundations,* ASCE, Vol. 93, No. SM6, pp. 143–167. With permission from ASCE.

Copyright 2017 Cengage Learning. All Rights Reserved. May not be copied, scanned, or duplicated, in whole or in part. Due to electronic rights, some third party content may be suppressed from the eBook and/or eChapter(s). Editorial review has deemed that any suppressed content does not materially affect the overall learning experience. Cengage Learning reserves the right to remove additional content at any time if subsequent rights restrictions require it.

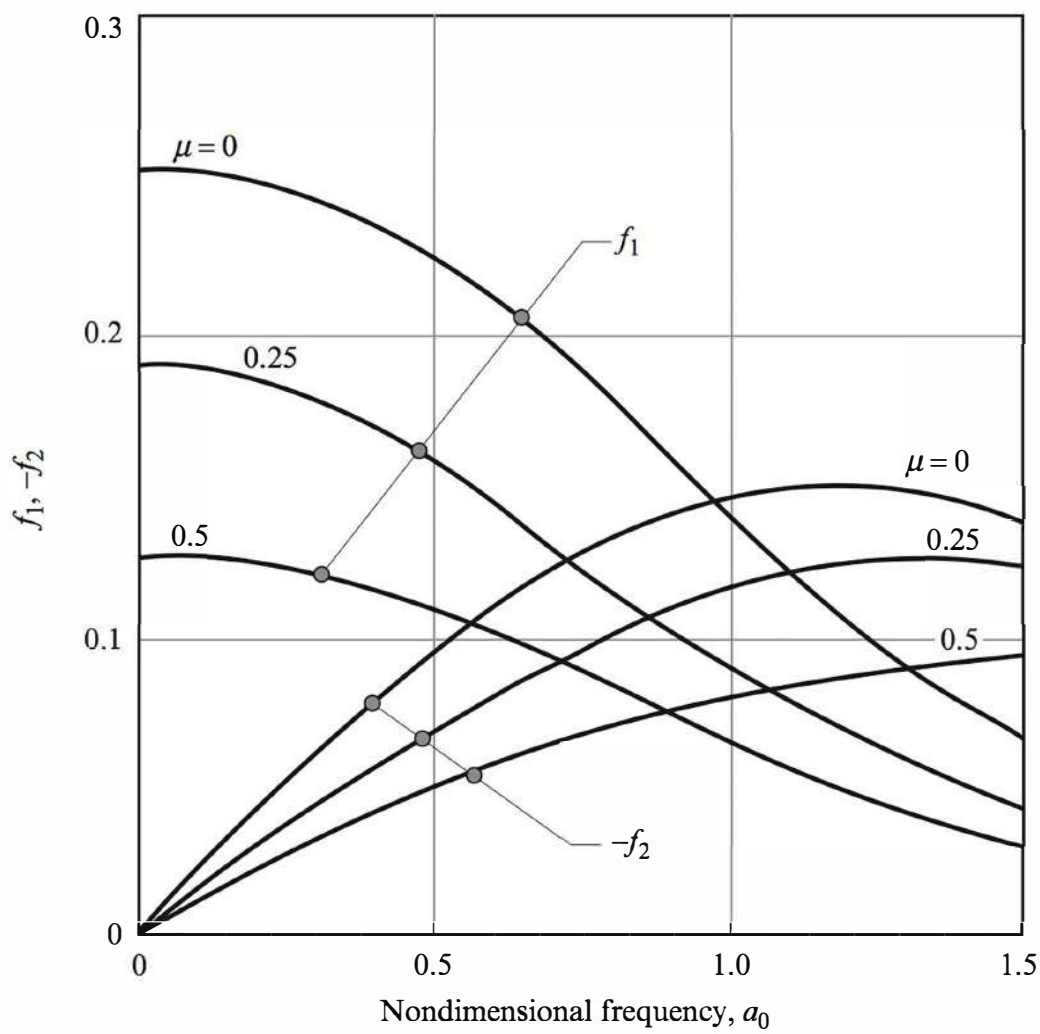

Figure 5.9 Variation of the displacement functions with a_0 and μ

5.3 ANALOG SOLUTIONS FOR VERTICAL VIBRATION OF FOUNDATIONS

Hsieh's Analog

Hsieh (1962) attempted to modify the original solution of Reissner in order to develop an equation similar to that for damped vibrations of single-degree free system [Eq. (2.72)]. Hsieh's analog can be explained with reference to Figure 5.10. Consider a rigid circular weightless disc on the surface of an elastic halfspace. The disc is subjected to a vertical vibration by a force

$$P = P_0 e^{i\omega t} \tag{5.14}$$

The vertical displacement of the disk can be given by Eq. (5.1) as

$$z = \frac{P_0 e^{i\omega t}}{G r_0}(f_1 + i f_2)$$

Now,

$$\frac{dz}{dt} = \frac{P_0 \omega e^{i\omega t}}{G r_0}(i f_1 - f_2) \tag{5.15}$$

Copyright 2017 Cengage Learning. All Rights Reserved. May not be copied, scanned, or duplicated, in whole or in part. Due to electronic rights, some third party content may be suppressed from the eBook and/or eChapter(s). Editorial review has deemed that any suppressed content does not materially affect the overall learning experience. Cengage Learning reserves the right to remove additional content at any time if subsequent rights restrictions require it.

or

$$f_1\omega z - f_2\frac{dz}{dt} = \frac{P_0\omega}{Gr_0}(f_1^2 + f_2^2)e^{i\omega t}$$

Since $P = P_0e^{i\omega t}$, the preceding relationship can be written as

$$f_1\omega z - f_2\frac{dz}{dt} = \frac{P\omega}{G\,r_0}(f_1^2 + f_2^2)$$

or

$$P = \underbrace{\left[(Gr_0)\left(\frac{f_1}{f_1^2 + f_2^2}\right)\right]}_{k_z} z + \underbrace{\left[\left(\frac{G\,r_0}{\omega}\right)\left(\frac{-f_2}{f_1^2 + f_2^2}\right)\right]}_{c_z}\frac{dz}{dt}$$

So

$$P = k_z z + c_z\dot{z} \tag{5.16}$$

Now consider a rigid circular foundation having a mass m and radius r_0 placed on the surface of the elastic half-space (Figure 5.10b). The foundation undergoes vibration by a periodic force

$$Q = Q_0e^{i\omega t} \tag{5.17}$$

For dynamic equilibrium

$$m\ddot{z} = Q - P \tag{5.18}$$

Combining Equations (5.16), (5.17), and (5.18)

$$\boxed{m\ddot{z} + c_z\dot{z} + k_z z = Q_0e^{i\omega t}} \tag{5.19}$$

The preceding relationship is an equivalent mass-spring-dashpot model similar to Eq. (2.72). However, the spring constant k_z and the dashpot coefficient c_z are frequency dependent.

Lysmer's Analog

A simplified model was also proposed by Lysmer and Richart (1966), in which the expressions for k_z and c_z were frequency independent. Lysmer and Richart (1966) redefined the displacement functions in the form

$$F = \frac{f}{\left(\frac{1-\mu}{4}\right)} = \frac{f_1 + if_2}{\left(\frac{1-\mu}{4}\right)} = F_1 + iF_2 \tag{5.20}$$

The functions F_1 and F_2 are practically independent of Poisson's ratio, as shown in Figure 5.11.

Copyright 2017 Cengage Learning. All Rights Reserved. May not be copied, scanned, or duplicated, in whole or in part. Due to electronic rights, some third party content may be suppressed from the eBook and/or eChapter(s). Editorial review has deemed that any suppressed content does not materially affect the overall learning experience. Cengage Learning reserves the right to remove additional content at any time if subsequent rights restrictions require it.

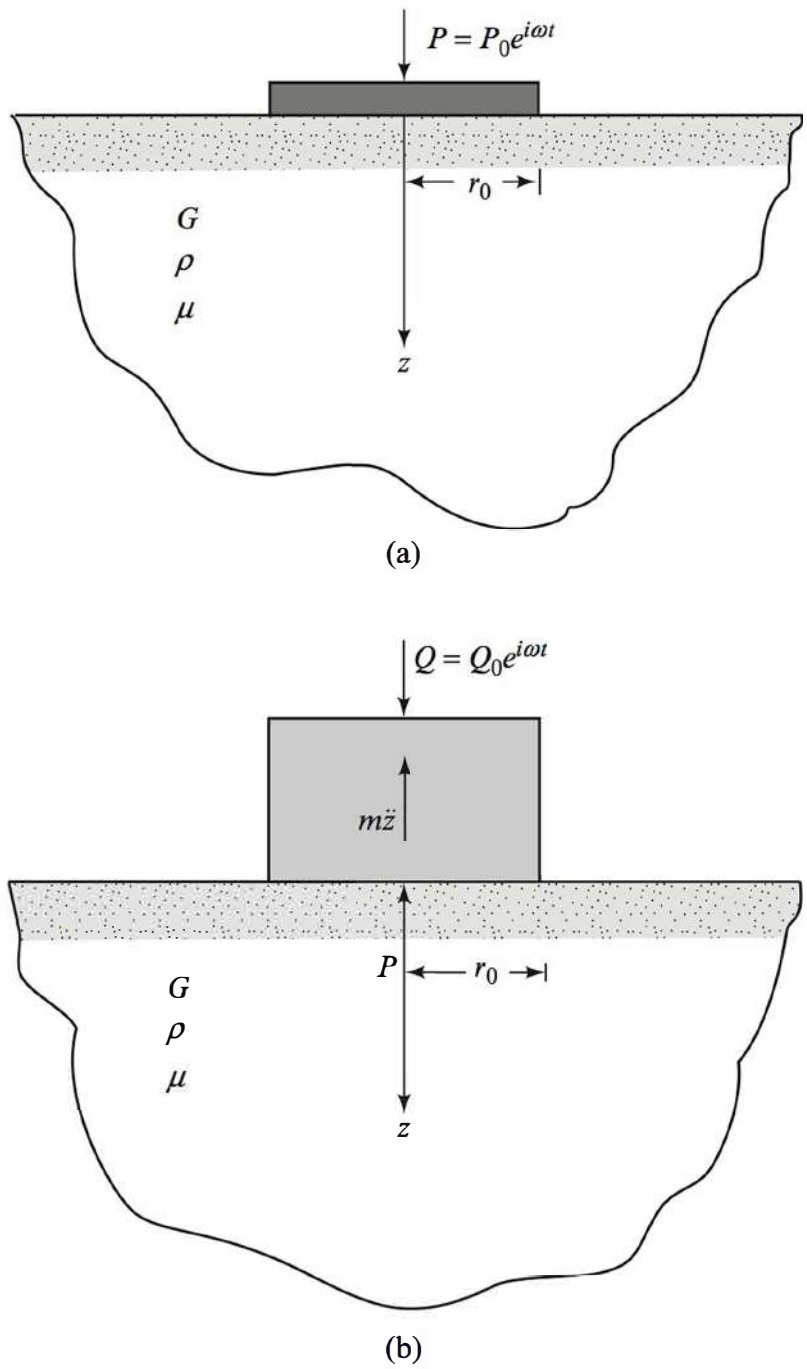

Figure 5.10 Hsieh's analog

The term *mass ratio* [Eq. (5.4)] was also modified as

$$B_z = \left(\frac{1-\mu}{4}\right)b = \left(\frac{1-\mu}{4}\right)\left(\frac{m}{\rho r_0^3}\right) \tag{5.21}$$

where B_z = modified mass ratio.

In this analysis, it was proposed that satisfactory results can be obtained within the range of practical interest by expressing the rigid circular foundation vibration in the form

$$\boxed{m\ddot{z} + c_z\dot{z} + k_z z = Q_0 e^{i\omega t}} \tag{5.22}$$

Copyright 2017 Cengage Learning. All Rights Reserved. May not be copied, scanned, or duplicated, in whole or in part. Due to electronic rights, some third party content may be suppressed from the eBook and/or eChapter(s). Editorial review has deemed that any suppressed content does not materially affect the overall learning experience. Cengage Learning reserves the right to remove additional content at any time if subsequent rights restrictions require it.

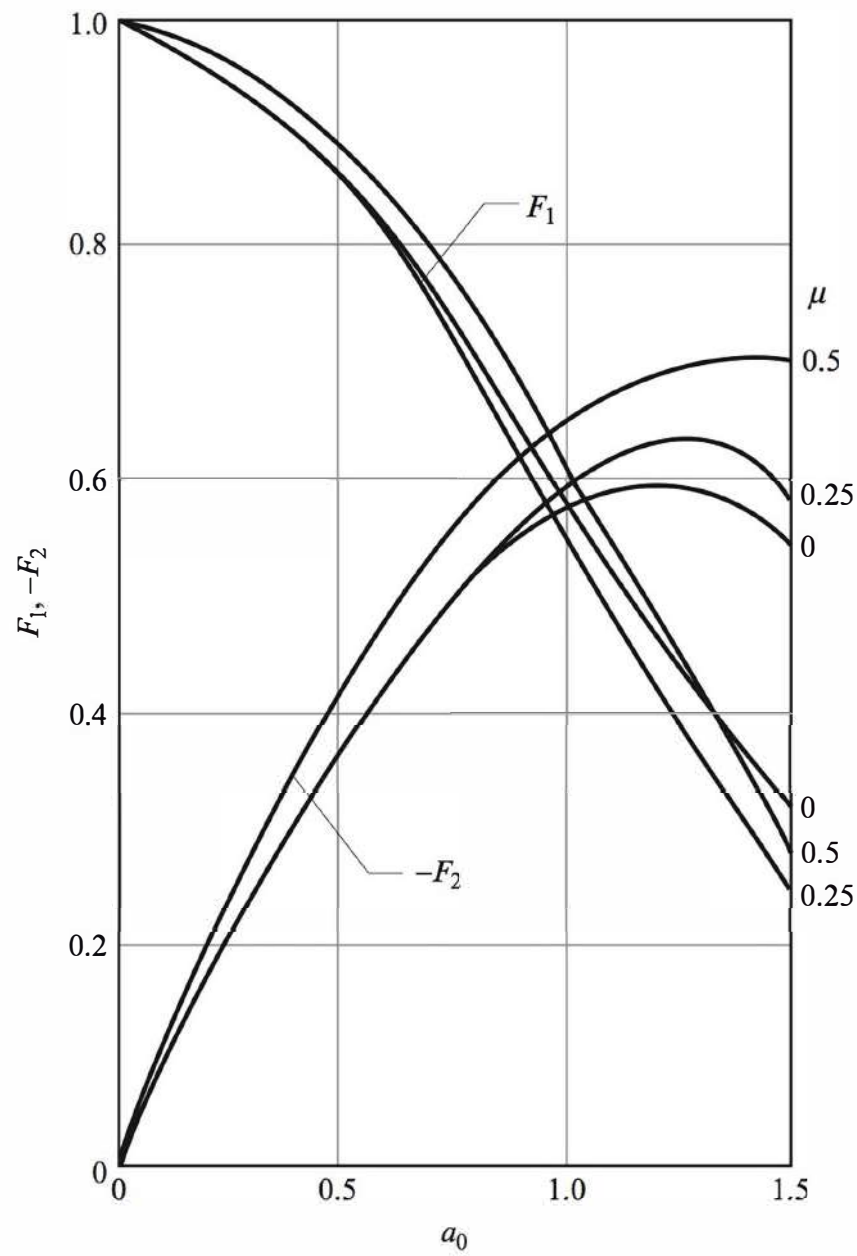

Figure 5.11 Plot of F_1 and $-F_2$ against a_0 for rigid circular foundation subjected to vertical vibration (from Lysmer and Richart, 1966)

Source: Lysmer, J., and Richart, F.E., Jr. (1966). "Dynamic Response to Footings to Vertical Loading," *Journal of the Soil Mechanics and Foundations Division,* ASCE, Vol. 92, No. SM1, pp. 65–91. With permission from ASCE.

where

$$\boxed{\begin{aligned} k_z &= \text{static spring constant for rigid circular foundation} \\ &= \frac{4Gr_0}{1-\mu} \end{aligned}} \tag{5.23}$$

$$\boxed{c_z = \frac{3.4r_0^2}{1-\mu}\sqrt{G\rho}} \tag{5.24}$$

In Eqs. (5.23) and (5.24) the relationships for k_z and c_z are frequency independent. Equations (5.22), (5.23), and (5.24) are referred to as *Lysmer's analog.*

Copyright 2017 Cengage Learning. All Rights Reserved. May not be copied, scanned, or duplicated, in whole or in part. Due to electronic rights, some third party content may be suppressed from the eBook and/or eChapter(s). Editorial review has deemed that any suppressed content does not materially affect the overall learning experience. Cengage Learning reserves the right to remove additional content at any time if subsequent rights restrictions require it.

5.4 CALCULATION PROCEDURE FOR FOUNDATION RESPONSE—VERTICAL VIBRATION

Once the equation of motion of a rigid circular foundation is expressed in the form given in Equation (5.22), it is easy to obtain the resonant frequency and amplitude of vibration based on the mathematical expressions presented in Chapter 2. The general procedure is outlined next.

A. Resonant Frequency

1. *Calculation of natural frequency*. From Eqs. (2.6) and (2.18),

$$f_n = \frac{1}{2\pi}\sqrt{\frac{k_z}{m}} = \frac{1}{2\pi}\sqrt{\left(\frac{4Gr_0}{1-\mu}\right)\frac{1}{m}} \tag{5.25}$$

2. *Calculation of damping ratio D_z*. From Eq. (2.47a),

$$\begin{aligned} c_{cz} &= 2\sqrt{k_z m} = 2\sqrt{\left(\frac{4Gr_0}{1-\mu}\right)(m)} \\ &= 8\sqrt{\left(\frac{Gr_0}{1-\mu}\right)\left(\frac{B_z\rho r_0^3}{1-\mu}\right)} = \frac{8r_0^2}{1-\mu}\sqrt{GB_z\rho} \end{aligned} \tag{5.26}$$

From Eq. (2.47b)

$$D_z = \frac{c}{c_{cz}} = \frac{\dfrac{3.4r_0^2}{1-\mu}\sqrt{G\rho}}{\dfrac{8r_0^2}{1-\mu}\sqrt{GB_z\rho}} = \frac{0.425}{\sqrt{B_z}} \tag{5.27}$$

3. *Calculation of the resonance frequency* (that is, frequency at maximum displacement). From Eq. (2.86), *for constant force-type excitation*,

$$\boxed{f_m = f_n\sqrt{1-2D_z^2} = \left[\frac{1}{2\pi}\sqrt{\left(\frac{4Gr_0}{1-\mu}\right)\frac{1}{m}}\right]\sqrt{1-2\left(\frac{0.425}{\sqrt{B_z}}\right)^2}} \tag{5.28}$$

It has also been shown by Lysmer that, for $B_z \geq 0.3$, the following approximate relationship can be established:

$$\boxed{f_m = \left(\frac{1}{2\pi}\right)\left(\sqrt{\frac{G}{\rho}}\right)\left(\frac{1}{r_0}\right)\sqrt{\frac{B_z-0.36}{B_z}}} \tag{5.29}$$

Copyright 2017 Cengage Learning. All Rights Reserved. May not be copied, scanned, or duplicated, in whole or in part. Due to electronic rights, some third party content may be suppressed from the eBook and/or eChapter(s). Editorial review has deemed that any suppressed content does not materially affect the overall learning experience. Cengage Learning reserves the right to remove additional content at any time if subsequent rights restrictions require it.

For *rotating mass-type excitation* [Eq. (2.98)]

$$f_m = \frac{f_n}{\sqrt{1-2D_z^2}} = \frac{\dfrac{1}{2\pi}\sqrt{\left(\dfrac{4Gr_0}{1-\mu}\right)\left(\dfrac{1}{m}\right)}}{\sqrt{1-2\left(\dfrac{0.425}{\sqrt{B_z}}\right)^2}} \tag{5.30}$$

Lysmer's corresponding approximate relationship for f_m is as follows:

$$\boxed{f_m = \left(\frac{1}{2\pi}\right)\left(\sqrt{\frac{G}{\rho}}\right)\left(\frac{1}{r_0}\right)\sqrt{\frac{0.9}{B_z - 0.45}}} \tag{5.31}$$

B. Amplitude of Vibration at Resonance

The amplitude of vibration A_z at resonance for *constant force-type excitation* can be determined from Eq. (2.87) as

$$A_{z(\text{resonance})} = \left(\frac{Q_0}{k_z}\right)\left(\frac{1}{2D_z\sqrt{1-D_z^2}}\right) \tag{5.32}$$

where $$k_z = \frac{4Gr_0}{1-\mu}$$

and

$$D_z = \frac{0.425}{\sqrt{B_z}}$$

Substitution of the relationships for k_z and D_z in Eq. (5.32) yields

$$\boxed{A_{z(\text{resonance})} = \frac{Q_0(1-\mu)}{4Gr_0}\frac{B_z}{0.85\sqrt{B_z - 0.18}}} \tag{5.33}$$

The amplitude of vibration for *rotating mass-type vertical excitation* can be given as [see Eq. (2.99)]

$$A_{z(\text{resonance})} = \frac{U}{m}\frac{1}{2D_z\sqrt{1-D_z^2}}$$

where $U = m_1 e$ (m_1 = total rotating mass causing excitation), or

$$\boxed{A_{z(\text{resonance})} = \frac{m_1 e}{m}\frac{B_z}{0.85\sqrt{B_z - 0.18}}} \tag{5.34}$$

Copyright 2017 Cengage Learning. All Rights Reserved. May not be copied, scanned, or duplicated, in whole or in part. Due to electronic rights, some third party content may be suppressed from the eBook and/or eChapter(s). Editorial review has deemed that any suppressed content does not materially affect the overall learning experience. Cengage Learning reserves the right to remove additional content at any time if subsequent rights restrictions require it.

C. Amplitude of Vibration at Frequencies Other Than Resonance

For *constant force-type excitation*, Eq. (2.82) can be used for estimation of the amplitude of vibration, or

$$A_z = \frac{\dfrac{Q_0}{k_z}}{\sqrt{\left[1-(\omega^2/\omega_n^2)\right]^2 + 4D_z^2(\omega^2/\omega_n^2)}} \tag{5.35}$$

The relationships for k_z and D_z are given by Eqs. (5.23) and (5.27) and

$$\omega_n = \sqrt{\frac{k_z}{m}} \tag{5.36}$$

Figure 5.12 shows the plot of $A_z/(Q_0/k_z)$ versus (ω/ω_n). So, with known values of D_z and (ω/ω_n), one can determine the value of $A_z/(Q_0/k_z)$ and, from that, A_z can be obtained.

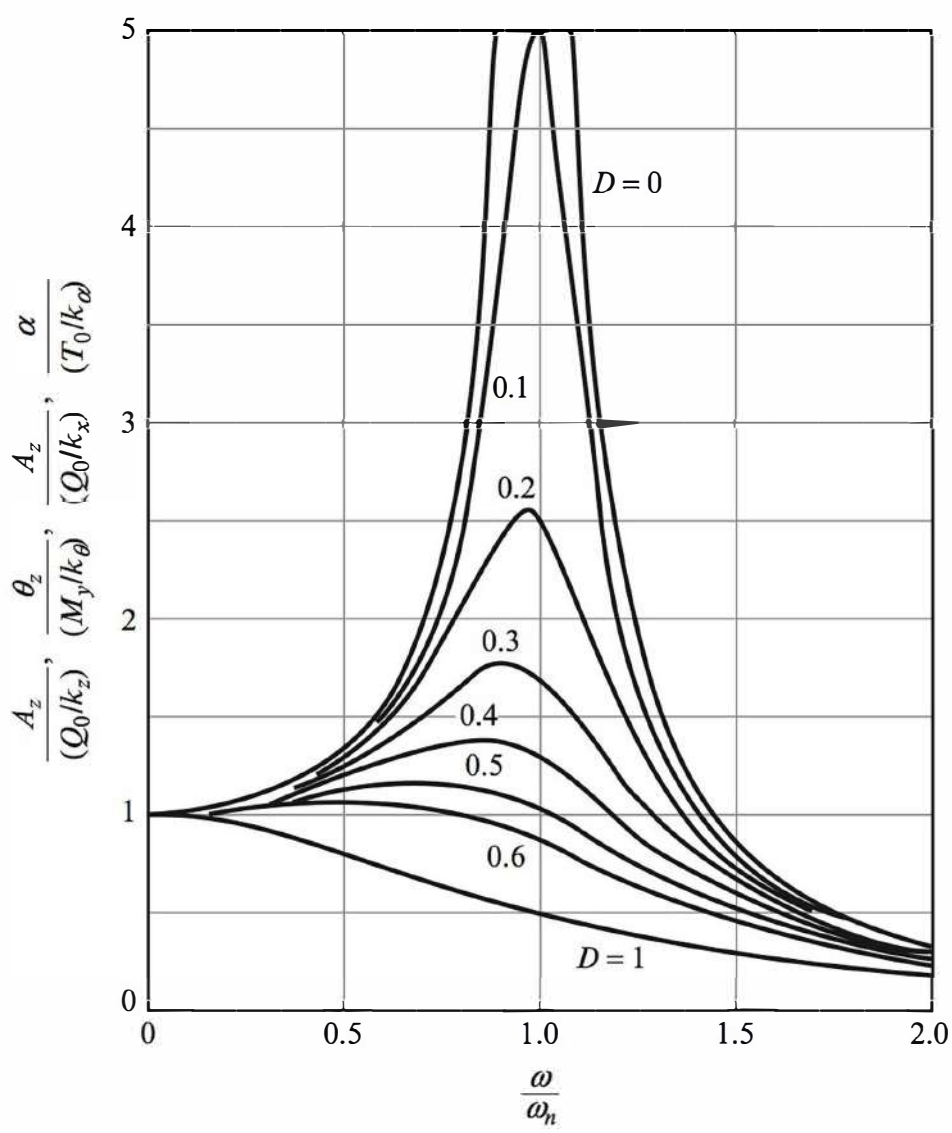

Figure 5.12 Plot of $A_z/(Q_0/k_z)$, $\theta/(M_y/k_\theta)$, $A_x/(Q_0/k_x)$, and $\alpha/(T_0/k_\alpha)$ against (ω/ω_n) for constant force-type vibrator (*Note:* $D = D_z$ for vertical vibration, $D = D_\theta$ for rocking, $D = D_x$ for sliding; $D = D_\alpha$ for torsional vibration.)

Copyright 2017 Cengage Learning. All Rights Reserved. May not be copied, scanned, or duplicated, in whole or in part. Due to electronic rights, some third party content may be suppressed from the eBook and/or eChapter(s). Editorial review has deemed that any suppressed content does not materially affect the overall learning experience. Cengage Learning reserves the right to remove additional content at any time if subsequent rights restrictions require it.

In a similar manner, for *rotating mass-type excitation*, Eq. (2.95) can be used to determine the amplitude of vibration, or

$$A_z = \frac{(m_1 e/m)(\omega/\omega_n)^2}{\sqrt{\left[1-(\omega^2/\omega_n^2)\right]^2 + 4D_z^2(\omega^2/\omega_n^2)}} \tag{5.37}$$

Figure 5.13 shows a plot of $A_z/(m_1 e/m)$ versus ω/ω_n, from which the magnitude of A_z can also be determined.

The procedure just described relates to a rigid circular foundation having a radius of r_0. If a foundation is rectangular in shape with length L and width B, it is conventional to obtain an equivalent radius, which can then be used in the

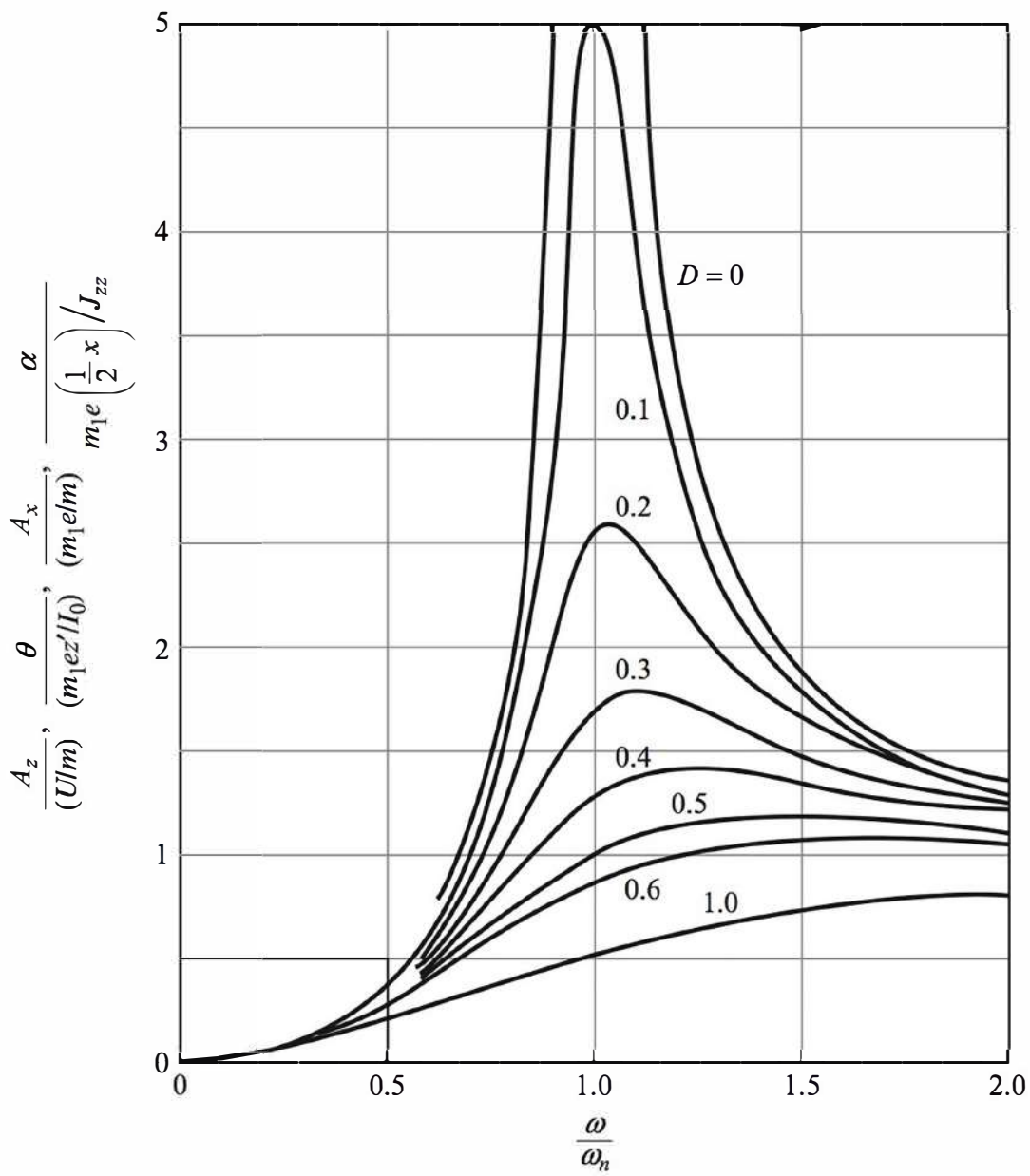

Figure 5.13 Plot of $A_z/(U/m), \theta/(m_1 ez'/I_0), A_x/(m_1 e/m), \alpha\Big/\left[m_1 e\left(\frac{1}{2}x\right)\Big/J_{zz}\right]$ against (ω/ω_n) for rotating mass-type excitation (*Note:* $D = D_z$ for vertical vibration, $D = D_\theta$ for rocking, $D = D_x$ for sliding; $D = D_\alpha$ for torsional vibration.)

Copyright 2017 Cengage Learning. All Rights Reserved. May not be copied, scanned, or duplicated, in whole or in part. Due to electronic rights, some third party content may be suppressed from the eBook and/or eChapter(s). Editorial review has deemed that any suppressed content does not materially affect the overall learning experience. Cengage Learning reserves the right to remove additional content at any time if subsequent rights restrictions require it.

preceding relationships. This can be done by equating the area of the given foundation to the area of an equivalent circle. Thus

$$\pi r_0^2 = BL$$

or

$$r_0 = \sqrt{\frac{BL}{\pi}} \tag{5.38}$$

where r_0 = radius of the equivalent circle

The procedure for transforming areas of any shape to an equivalent circle of the same area gives good results in the evaluation of foundation response. Dobry and Gazetas (1986) demonstrated that any shape can be transformed to an equivalent circle and demonstrated the validity of this method through comparison with experimental results.

It is obviously impossible to eliminate vibration near a foundation. However, an attempt can be made to reduce the vibration problem as much as possible. Richart (1962) compiled guidelines for allowable vertical vibration amplitude for a particular frequency of vibration, and this is given in Figure 5.14. The data presented in Figure 5.14 refer to the maximum allowable amplitudes of vibration. These can be converted to maximum allowable accelerations by

$$\text{Maximum acceleration} = (\text{maximum displacement})\omega^2$$

For example, in Figure 5.14, the limiting amplitude of displacement at an operating frequency of 2000 cpm is about 0.127 mm. So the maximum operating acceleration for a frequency of 2000 cpm is

$$(0.127 \text{ mm})\left[\frac{(2\pi)(2000)}{60}\right]^2 = 5570 \text{ mm/s}^2$$

In the design of machine foundations, the following general rules may be kept in mind to avoid possible resonance conditions:

1. The resonant frequency of foundation-soil system should be less than half the operating frequency for high-speed machines (that is, operating frequency ≥ 1000 cpm). For this case, during starting or stopping the machine will briefly vibrate at resonant frequency.
2. For low-speed machines (speed less than about 350-400 cpm), the resonant frequency of the foundation-soil system should be at least two times the operating frequency.
3. In all types of foundations, the increase of weight will decrease the resonant frequency.
4. An increase of r_0 will increase the resonant frequency of the foundation.
5. An increase of shear modulus of soil (for example, by grouting) will increase the resonant frequency of the foundation.

Copyright 2017 Cengage Learning. All Rights Reserved. May not be copied, scanned, or duplicated, in whole or in part. Due to electronic rights, some third party content may be suppressed from the eBook and/or eChapter(s). Editorial review has deemed that any suppressed content does not materially affect the overall learning experience. Cengage Learning reserves the right to remove additional content at any time if subsequent rights restrictions require it.

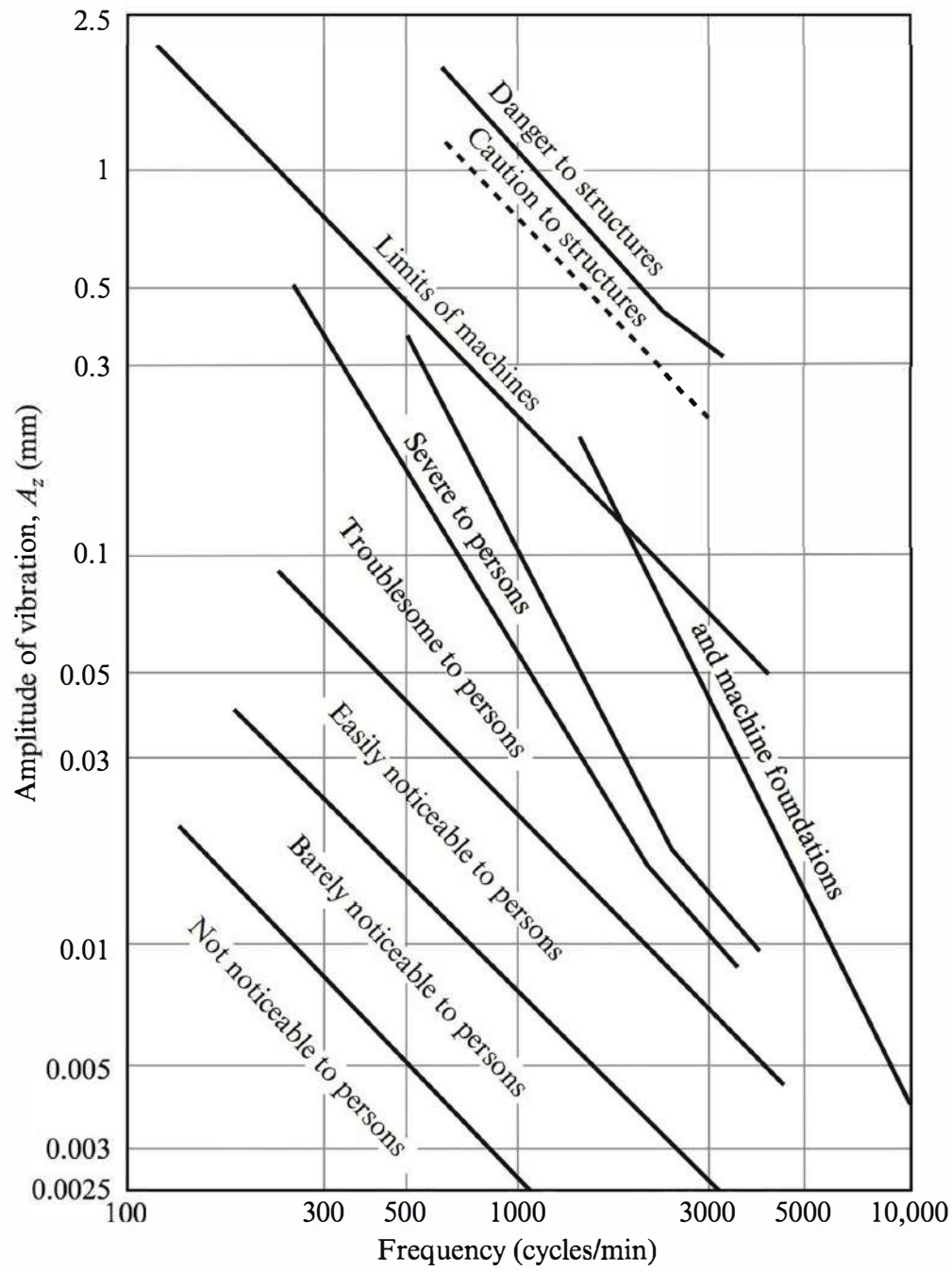

Figure 5.14 Allowable vertical vibration amplitudes (from Richart, 1962)

Source: Richart, F.E., Jr. (1962). "Foundation Vibrations," *Transactions,* ASCE, Vol. 27, Part 1, pp. 863–898. With permission from ASCE.

EXAMPLE 5.1

A foundation is subjected to a constant force-type vertical vibration. Given the total weight of the machinery and foundation block, $W = 680$ kN; unit weight of soil, $\gamma = 18.5$ kN/m³; $\mu = 0.4$; $G = 20700$ kPa; the amplitude of the vibrating force, $Q_0 = 7$ kN; the operating frequency, $f = 180$ cpm; and that the foundation is 6 m long and 2 m wide:

a. Determine the resonant frequency. Check if

$$\frac{f_{\text{resonance}}}{f_{\text{operating}}} > 2$$

b. Determine the amplitude of vibration at resonance.

Copyright 2017 Cengage Learning. All Rights Reserved. May not be copied, scanned, or duplicated, in whole or in part. Due to electronic rights, some third party content may be suppressed from the eBook and/or eChapter(s). Editorial review has deemed that any suppressed content does not materially affect the overall learning experience. Cengage Learning reserves the right to remove additional content at any time if subsequent rights restrictions require it.

SOLUTION:

a. This is a rectangular foundation, so the equivalent radius [Eq. (5.38)] is

$$r_0 = \sqrt{\frac{BL}{\pi}} = \sqrt{\frac{(2)(6)}{\pi}} = 1.954 \text{ m}$$

The mass ratio [Eq. (5.21)]

$$B_z = \left(\frac{1-\mu}{4}\right)\left(\frac{m}{\rho r_0^3}\right) = \left(\frac{1-\mu}{4}\right)\left(\frac{W}{\gamma r_0^3}\right)$$

$$= \left(\frac{1-0.4}{4}\right)\left[\frac{680}{18.5 \times 1.954^3}\right]$$

$$= 0.739$$

From Eq. (5.29), the resonant frequency is

$$f_m = \left(\frac{1}{2\pi}\right)\left(\sqrt{\frac{G}{\rho}}\right)\left(\frac{1}{r_0}\right)\sqrt{\frac{B_z - 0.36}{B_z}}$$

$$= \left(\frac{1}{2\pi}\right)\left[\sqrt{\frac{20700}{18.5/9.81}}\right]\left(\frac{1}{1.954}\right)\sqrt{\frac{0.739-0.36}{0.739}}$$

$$= \mathbf{6.11\ Hz \approx 366.6\ cpm}$$

Hence,

$$\frac{f_{\text{resonance}}}{f_{\text{operating}}} = \frac{366.6}{180} = 2.04 > 2$$

b. From Eq. (5.33)

$$A_{z(\text{resonance})} = \frac{Q_0(1-\mu)}{4Gr_0}\frac{B_z}{0.85\sqrt{B_z - 0.18}}$$

$$= \left[\frac{(7)(0.6)}{(4)(20,700)(1.954)}\right]\left[\frac{0.739}{(0.85)\sqrt{0.739-0.18}}\right]$$

$$= 0.00003 \text{ m} = \mathbf{0.03\ mm}$$

EXAMPLE 5.2

Figure 5.15a shows a single-cylinder reciprocating engine. The data for the engine are as follows: operating speed = 1500 cpm; connecting rod (r_2) = 0.3 m; crank (r_1) = 75 mm; total reciprocating weight = 54 N; total engine weight = 14 kN. Figure 5.15b shows the dimensions of the concrete foundation for the engine. The properties of the soil are as follows: $\gamma = 18.5$ kN/m^3; $G = 18,000$ kPa; and $\mu = 0.5$. Calculate:

a. primary and secondary unbalanced forces at operating frequency (refer to Appendix A);

Copyright 2017 Cengage Learning. All Rights Reserved. May not be copied, scanned, or duplicated, in whole or in part. Due to electronic rights, some third party content may be suppressed from the eBook and/or eChapter(s). Editorial review has deemed that any suppressed content does not materially affect the overall learning experience. Cengage Learning reserves the right to remove additional content at any time if subsequent rights restrictions require it.

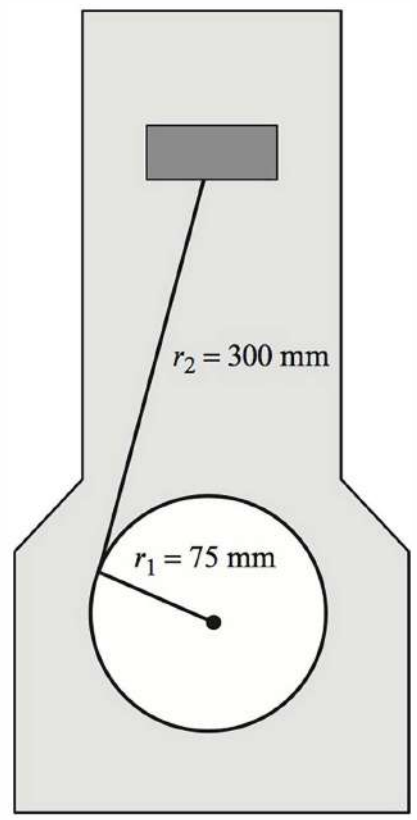

(a)

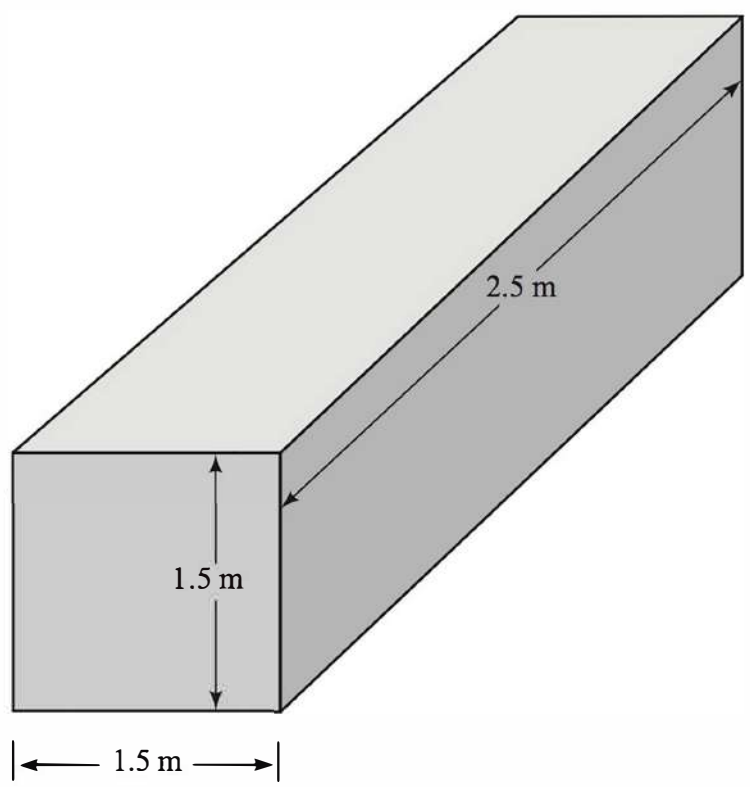

(b)

Figure 5.15

b. the resonance frequency; and
c. the vertical vibration amplitude at resonance.

Copyright 2017 Cengage Learning. All Rights Reserved. May not be copied, scanned, or duplicated, in whole or in part. Due to electronic rights, some third party content may be suppressed from the eBook and/or eChapter(s). Editorial review has deemed that any suppressed content does not materially affect the overall learning experience. Cengage Learning reserves the right to remove additional content at any time if subsequent rights restrictions require it.

SOLUTION:

a. The equations for obtaining the maximum *primary* and *secondary* unbalanced forces for a single cylinder reciprocating engine are given in Appendix A. From Eqs. (A.9) and (A.10)

Primary unbalanced force $= m_{rec} r_1 \omega^2$

$$= \frac{54}{(1000)(9.81)}\left(\frac{75}{1000}\right)\left(\frac{2\pi \times 1500}{60}\right)^2$$

$$= \mathbf{10.19\ kN}$$

Secondary unbalanced force $= \dfrac{m_{rec} r_1^2 \omega^2}{r_2}$

$$\frac{r_1}{r_2} = \frac{0.075}{0.3} = 0.25$$

So

$$\text{Secondary force} = (\text{primary force})\left(\frac{r_1}{r_2}\right) = (10.19)(0.25)$$

$$= \mathbf{2.55\ kN}$$

b. From Eq. (5.38),

$$r_0 = \sqrt{\frac{BL}{\pi}} = \sqrt{\frac{(1.5)(2.5)}{\pi}} = 1.093\ \text{m}$$

The mass ratio is

$$B_z = \left(\frac{1-\mu}{4}\right)\left(\frac{W}{\gamma r_0^3}\right)$$

Total weight is W =weight of foundation + engine. Assume the unit weight of concrete is 23.58 kN/m³. So

$$W = (1.5 \times 2.5 \times 1.5)(23.58) + 14 = 146.64\ \text{kN}$$

$$B_z = \left(\frac{1-0.5}{4}\right)\left[\frac{146.64}{(18.5)(1.093)^3}\right] = 0.759$$

The resonant frequency [Eq. (5.31)] is

$$f_m = \left(\frac{1}{2\pi}\right)\left(\sqrt{\frac{G}{\rho}}\right)\left(\frac{1}{r_0}\right)\sqrt{\frac{0.9}{B_z - 0.45}}$$

$$= \left(\frac{1}{2\pi}\right)\left[\sqrt{\frac{(18{,}000)(9.81)}{18.5}}\right]\left(\frac{1}{1.093}\right)\sqrt{\frac{0.9}{0.759 - 0.45}}$$

$$= \mathbf{24.28\ Hz \approx 1457\ cpm}$$

Copyright 2017 Cengage Learning. All Rights Reserved. May not be copied, scanned, or duplicated, in whole or in part. Due to electronic rights, some third party content may be suppressed from the eBook and/or eChapter(s). Editorial review has deemed that any suppressed content does not materially affect the overall learning experience. Cengage Learning reserves the right to remove additional content at any time if subsequent rights restrictions require it.

c. From Eq. (5.34),

$$A_{z(\text{resonance})} = \frac{m_1 e}{m} \frac{B_z}{0.85\sqrt{B_z} - 0.18}$$

At 1500 cpm, the total unbalanced force = primary force + secondary force

$$= 10.19 + 2.55 = 12.74 \text{ kN}.$$

$$Q_{0(1457\text{ cpm})} = Q_{0(1500\text{ cpm})}\left(\frac{1457}{1500}\right)^2 = (12.74)\left(\frac{1457}{1500}\right)^2$$

$$= 12.02 \text{ kN}$$

$$Q_{0(1457\text{ cpm})} = m_1 e\omega^2 = 12.02 \text{ kN}$$

Therefore,

$$m_1 e = \frac{12.02}{\omega^2}; \omega = \frac{2\pi(1457)}{60} = 152.58 \text{ rad/s}; m_1 e = \frac{12.02}{(152.58)^2}$$

Hence

$$A_{z(\text{resonance})} = \left[\frac{12.02/(152.58)^2}{146.64/9.81}\right]\left(\frac{0.759}{0.85\sqrt{0.759 - 0.18}}\right)$$

$$= 0.0000405 \text{ m} = \mathbf{0.0405\ mm}$$

5.5 ROCKING VIBRATION OF FOUNDATIONS

Theoretical solutions for foundations subjected to rocking vibration have been presented by Arnold, Bycroft, and Wartburton (1955) and Bycroft (1956). For *rigid circular foundations* (Figure 5.16), the contact pressure can be described by the equation

$$q = \frac{3M_y r\cos\alpha}{2\pi r_0^3\sqrt{r_0^2 - r^2}} e^{i\omega t}$$

where q = pressure at any point defined by point a on the plan
M_y = the exciting moment about the y axis = $M_y e^{i\omega t}$

Hall (1967) developed a mass-spring-dashpot model for rigid circular foundations in the same manner as Lysmer and Richart (1966) developed for vertical vibration. According to Hall, the equation of motion for a rocking vibration can be given as

$$\boxed{I_0\ddot{\theta} + c_\theta\dot{\theta} + k_\theta\theta = M_y e^{i\omega t}} \tag{5.39}$$

where θ = rotation of the vertical axis of the foundation at any time t
I_0 = mass moment of inertia about the y axis (through its base)

$$= \frac{W_0}{g}\left(\frac{r_0^2}{4} + \frac{h^2}{3}\right) \tag{5.40}$$

Copyright 2017 Cengage Learning. All Rights Reserved. May not be copied, scanned, or duplicated, in whole or in part. Due to electronic rights, some third party content may be suppressed from the eBook and/or eChapter(s). Editorial review has deemed that any suppressed content does not materially affect the overall learning experience. Cengage Learning reserves the right to remove additional content at any time if subsequent rights restrictions require it.

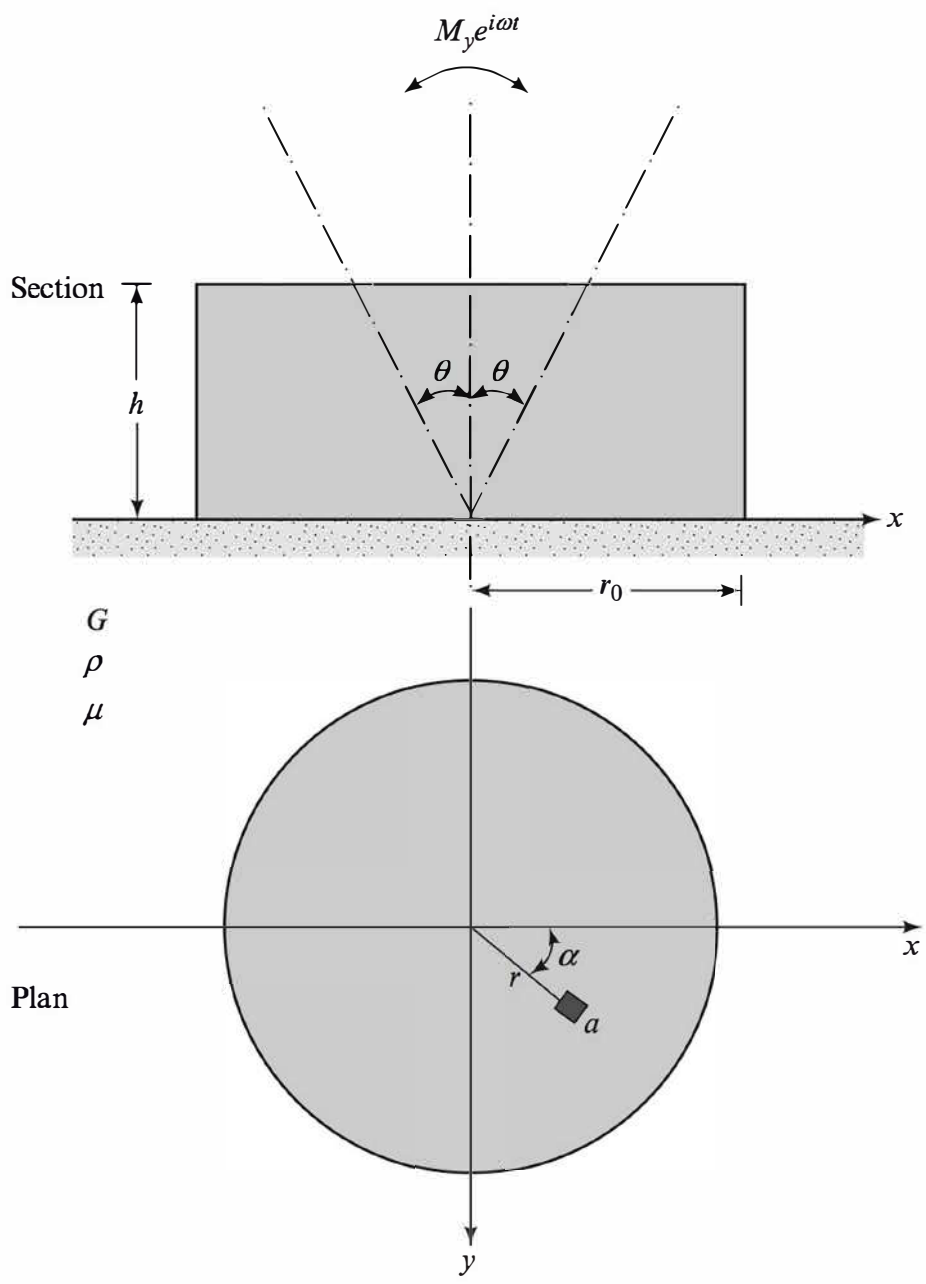

Figure 5.16 Rocking vibration of rigid circular foundation

where W_0 = weight of the foundation
g = acceleration due to gravity
h = height of the foundation

$$\boxed{k_\theta = \text{static spring constant} = \frac{8Gr_0^3}{3(1-\mu)}} \tag{5.41}$$

$$\boxed{c_\theta = \text{dashpot coefficient} = \frac{0.8r_0^4\sqrt{G}}{(1-\mu)(1+B_\theta)}} \tag{5.42}$$

where

$$\boxed{B_\theta = \text{inertia ratio} = \frac{3(1-\mu)}{8}\frac{I_0}{\rho r_0^5}} \tag{5.43}$$

The calculation procedure for foundation response using Eq. (5.39) is as follows.

Copyright 2017 Cengage Learning. All Rights Reserved. May not be copied, scanned, or duplicated, in whole or in part. Due to electronic rights, some third party content may be suppressed from the eBook and/or eChapter(s). Editorial review has deemed that any suppressed content does not materially affect the overall learning experience. Cengage Learning reserves the right to remove additional content at any time if subsequent rights restrictions require it.

A. Resonant Frequency

1. Calculate the natural frequency:

$$f_n = \frac{1}{2\pi}\sqrt{\frac{k_\theta}{I_0}} \tag{5.44}$$

2. Calculate the damping ratio D_θ:

$$c_{c\theta} = 2\sqrt{k_\theta I_0}$$
$$D_\theta = \frac{c_\theta}{c_{c\theta}} = \frac{0.15}{\sqrt{B_\theta}(1+B_\theta)} \tag{5.45}$$

3. Calculate the resonant frequency:

$$f_m = f_n\sqrt{1-2D_\theta^2} \quad \text{(for constant force excitation)}$$
$$f_m = \frac{f_n}{\sqrt{1-2D_\theta^2}} \quad \text{(for rotating mass-type excitation)}$$

B. Amplitude of Vibration at Resonance

$$\boxed{\theta_{\text{resonance}} = \frac{M_y}{k_\theta}\frac{1}{2D_\theta\sqrt{1-D_\theta^2}}} \quad \text{(for constant force excitation)} \tag{5.46}$$

$$\boxed{\theta_{\text{resonance}} = \frac{m_1 e z'}{I_0}\frac{1}{2D_\theta\sqrt{1-D_\theta^2}}} \quad \text{(for rotating mass-type excitation; see Figure 5.17)} \tag{5.47}$$

where m_1 = total rotating mass causing excitation
e = eccentricity of each mass

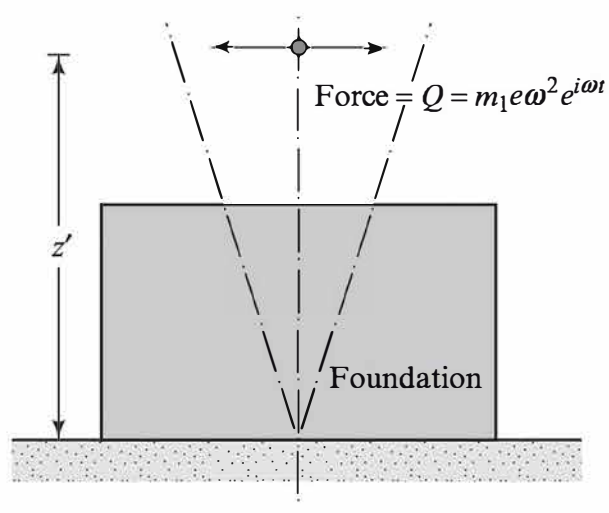

Figure 5.17 Rotating mass-type excitation

Copyright 2017 Cengage Learning. All Rights Reserved. May not be copied, scanned, or duplicated, in whole or in part. Due to electronic rights, some third party content may be suppressed from the eBook and/or eChapter(s). Editorial review has deemed that any suppressed content does not materially affect the overall learning experience. Cengage Learning reserves the right to remove additional content at any time if subsequent rights restrictions require it.

C. Amplitude of Vibration at Frequencies Other Than Resonance

For constant force-type excitation [Eq. (2.82)]:

$$\theta = \frac{M_y/k_\theta}{\sqrt{\left[1-\left(\omega^2/\omega_n^2\right)\right]^2 + 4D_\theta^2\left(\omega^2/\omega_n^2\right)}} \tag{5.48}$$

A plot of $\theta/(M_y/k_\theta)$ versus ω/ω_n is given in Figure 5.12.

For *rotating mass-type excitation* [Eq. (2.95)]:

$$\theta = \frac{\left(m_1 ez'/I_0\right)\left(\omega^2/\omega_n^2\right)}{\sqrt{\left[1-\left(\omega^2/\omega_n^2\right)\right]^2 + 4D_\theta^2\left(\omega^2/\omega_n^2\right)}} \tag{5.49}$$

Figure 5.13 shows a plot of $\theta/(m_1 ez'/I_0)$ versus ω/ω_n.

In the case of rectangular foundation, the preceding relationships can be used by determining the equivalent radius as

$$r_0 = \sqrt[4]{\frac{BL^3}{3\pi}} \tag{5.50}$$

The definitions of B and L are shown in Figure 5.18.

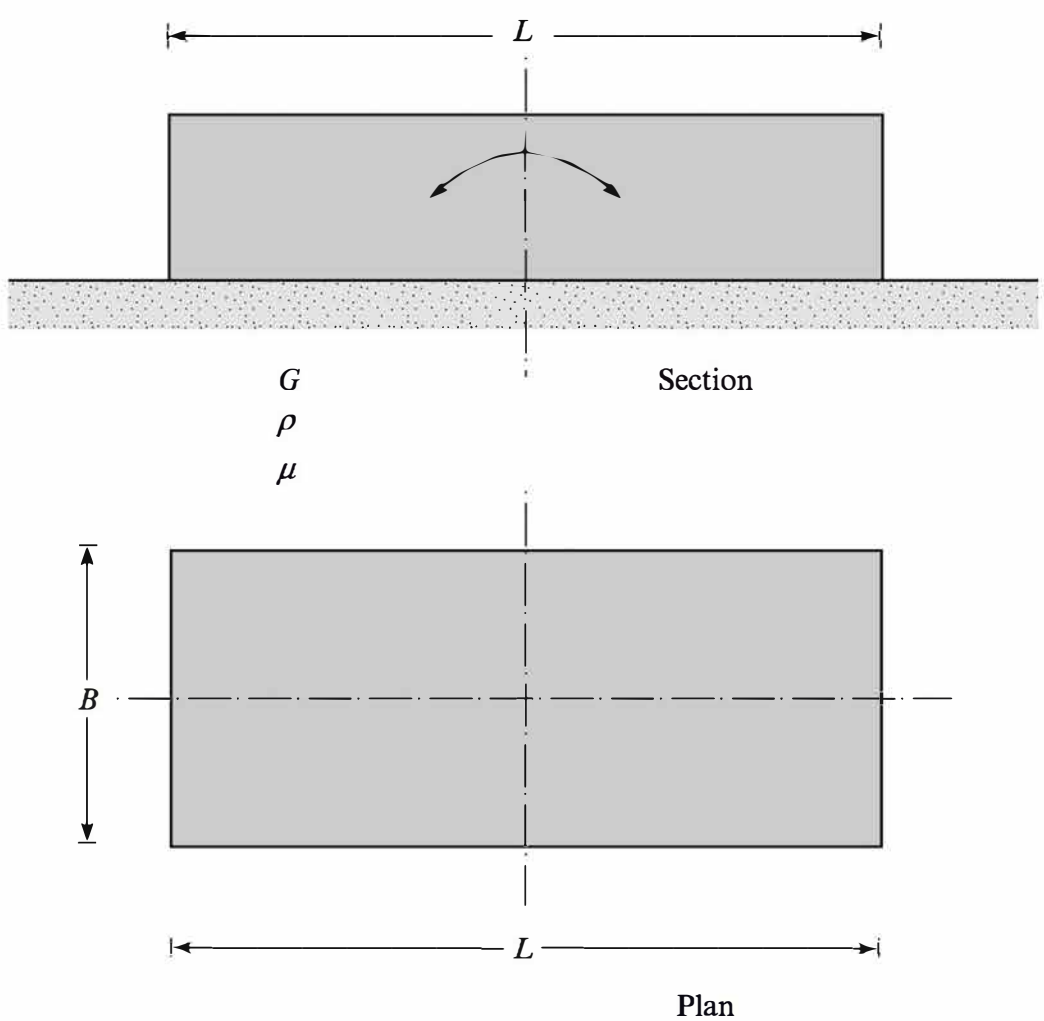

Figure 5.18 Equivalent radius of rectangular rigid foundation—rocking motion

Copyright 2017 Cengage Learning. All Rights Reserved. May not be copied, scanned, or duplicated, in whole or in part. Due to electronic rights, some third party content may be suppressed from the eBook and/or eChapter(s). Editorial review has deemed that any suppressed content does not materially affect the overall learning experience. Cengage Learning reserves the right to remove additional content at any time if subsequent rights restrictions require it.

EXAMPLE 5.3

A horizontal piston-type compressor is shown in Figure 5.19. The operating frequency is 600 cpm. The amplitude of the horizontal unbalanced force of the compressor is 30 kN, and it creates a rocking motion of the foundation about point O (see Figure 5.19b). The mass moment of inertia of the compressor assembly about the axis $b'Ob'$ is 16×10^5 kg-m^2 (see Figure 5.19c). Determine

a. the resonant frequency, and
b. the amplitude of rocking vibration at resonance.

SOLUTION:

Moment of inertia of the foundation block and the compressor assembly about b′Ob′:

$$I_0 = \left(\frac{W_{\text{foundation block}}}{3g}\right)\left[\left(\frac{L}{2}\right)^2 + h^2\right] + 16 \times 10^5 \text{ kg-m}^2$$

Assume the unit weight of concrete is 23.58 kN/m^3.

$$W_{\text{foundation block}} = (8 \times 6 \times 3)(23.58) = 3395.52 \text{ kN}$$
$$= 3395.52 \times 10^3 \text{ N}$$

$$I_0 = \frac{3395.52 \times 10^3}{(3)(9.81)}(3^2 + 3^2) + 16 \times 10^5$$
$$= 36.768 \times 10^5 \text{ kg-m}^2$$

Calculation of equivalent radius of the foundation: From Eq. (5.50), the equivalent radius is

$$r_0 = \sqrt[4]{\frac{BL^3}{3\pi}} = \sqrt[4]{\frac{8 \times 6^3}{3\pi}} = 3.67 \text{ m}$$

a. Determination of resonant frequency:

$$k_\theta = \frac{8Gr_0^3}{3(1-\mu)} = \frac{(8)(18{,}000)(3.67)^3}{(3)(1-0.35)} = 3650279 \text{ kN-m/rad}$$

$$f_n = \frac{1}{2\pi}\sqrt{\frac{k_\theta}{I_0}} = \frac{1}{2\pi}\sqrt{\frac{3650279 \times 10^3 \text{ N-m/rad}}{36.768 \times 10^5}} = 5.01 \text{ Hz}$$
$$\approx 300 \text{ cpm}$$

$$B_\theta = \frac{3(1-\mu)}{8}\frac{I_0}{\rho r_0^5} = \frac{3(1-0.35)\,36.768 \times 10^5}{(8)(1800)(3.67)^5} = 0.748$$

$$D_\theta = \frac{0.15}{\sqrt{B_\theta}(1+B_\theta)} = \frac{0.15}{\sqrt{0.748}\,(1+0.748)} = 0.099$$

$$f_m = \frac{f_n}{\sqrt{1-2D_\theta^2}} = \frac{300}{\sqrt{1-2D_\theta^2}} = \frac{300}{\sqrt{1-2(0.099)^2}} = \mathbf{303\ cpm}$$

Copyright 2017 Cengage Learning. All Rights Reserved. May not be copied, scanned, or duplicated, in whole or in part. Due to electronic rights, some third party content may be suppressed from the eBook and/or eChapter(s). Editorial review has deemed that any suppressed content does not materially affect the overall learning experience. Cengage Learning reserves the right to remove additional content at any time if subsequent rights restrictions require it.

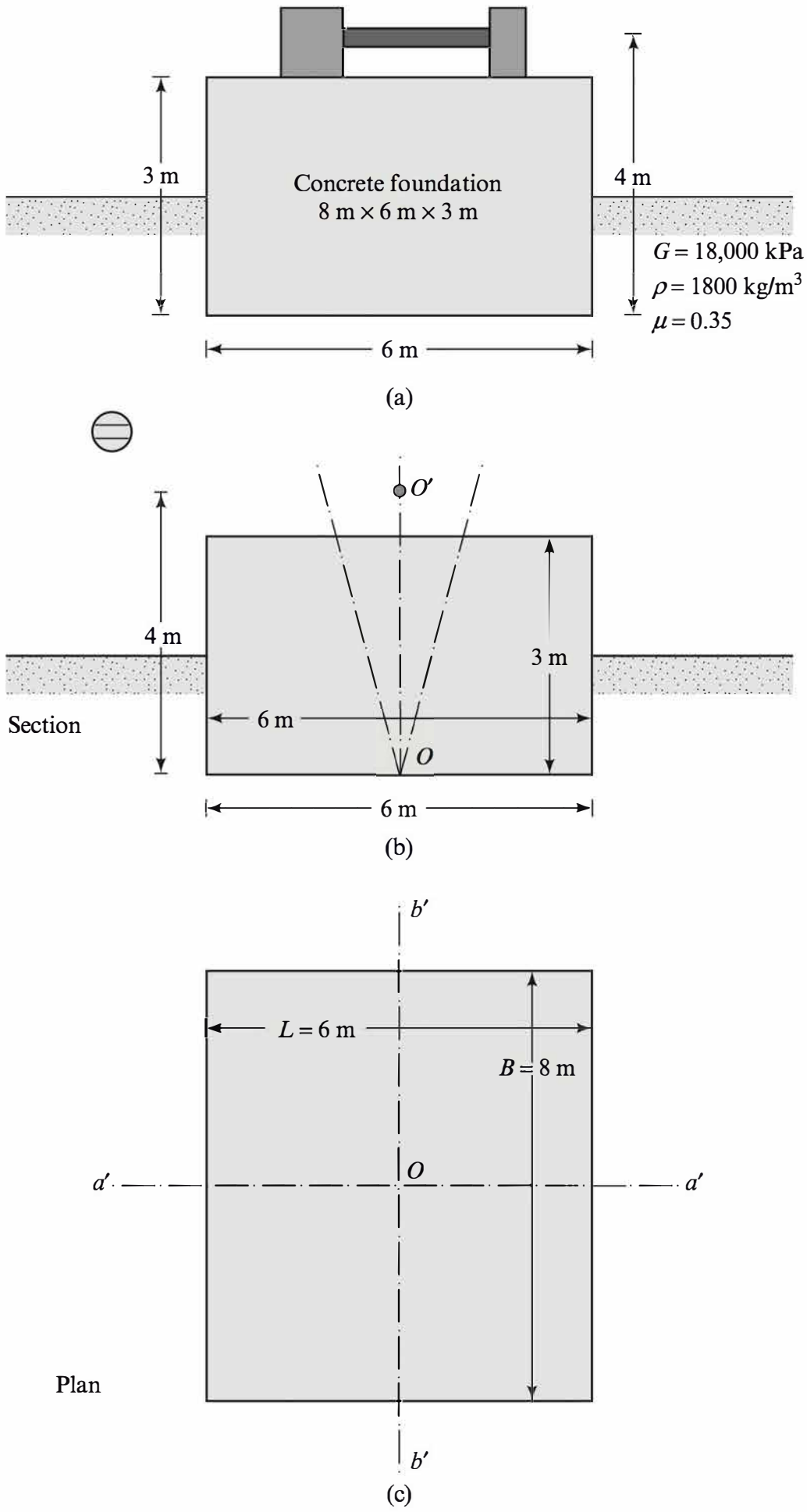

Figure 5.19

Copyright 2017 Cengage Learning. All Rights Reserved. May not be copied, scanned, or duplicated, in whole or in part. Due to electronic rights, some third party content may be suppressed from the eBook and/or eChapter(s). Editorial review has deemed that any suppressed content does not materially affect the overall learning experience. Cengage Learning reserves the right to remove additional content at any time if subsequent rights restrictions require it.

b. Calculation of amplitude of vibration at resonance:

$$M_{y(\text{operating frequency})} = \text{unbalanced force} \times 4$$
$$= 30 \times 4 = 120 \text{ kN-m}$$

$$M_{y(\text{at resonance})} = 120\left(\frac{f_n}{f_{\text{operation}}}\right)^2$$
$$= 120\left(\frac{303}{600}\right)^2 = 30.6 \text{ kN-m}$$

$$(m_1 e\omega^2)z' = M_y$$

$$\omega_{\text{resonance}} = \frac{(2\pi)(303)}{60} = 31.73 \text{ rad/s}$$

$$m_1 ez' = \frac{M_y}{\omega^2} = \frac{30.6 \times 10^3 \text{ N-m}}{(31.73)^3} = 0.0304 \times 10^3$$

From Eq. (5.47)

$$\theta_{\text{resonance}} = \frac{m_1 ez'}{I_0} \frac{1}{2D_\theta\sqrt{1 - D_\theta^2}}$$
$$= \left(\frac{0.0304 \times 10^3}{36.768 \times 10^5}\right)\left[\frac{1}{(2)(0.099)\sqrt{1-(0.099)^2}}\right]$$
$$= 4.2 \times 10^{-5} \text{ rad}$$

5.6 SLIDING VIBRATION OF FOUNDATIONS

Arnold, Bycroft, and Wartburton (1955) have provided theoretical solutions for sliding vibration of a *rigid circular* foundation (Figure 5.20) acted on by a force $Q = Q_0\, e^{i\omega t}$. Hall (1967) developed the mass-spring-dashpot analog for this type of vibration. According to this analog, the equation of motion of the foundation can be given in the form

$$\boxed{m\ddot{x} + c_x\dot{x} + k_x x = Q_0 e^{i\omega t}} \tag{5.51}$$

where m = mass of the foundation

$$\boxed{\begin{aligned} k_x &= \text{static spring constant for sliding} \\ &= \frac{32(1-\mu)Gr_0}{7-8\mu} \end{aligned}} \tag{5.52}$$

Copyright 2017 Cengage Learning. All Rights Reserved. May not be copied, scanned, or duplicated, in whole or in part. Due to electronic rights, some third party content may be suppressed from the eBook and/or eChapter(s). Editorial review has deemed that any suppressed content does not materially affect the overall learning experience. Cengage Learning reserves the right to remove additional content at any time if subsequent rights restrictions require it.

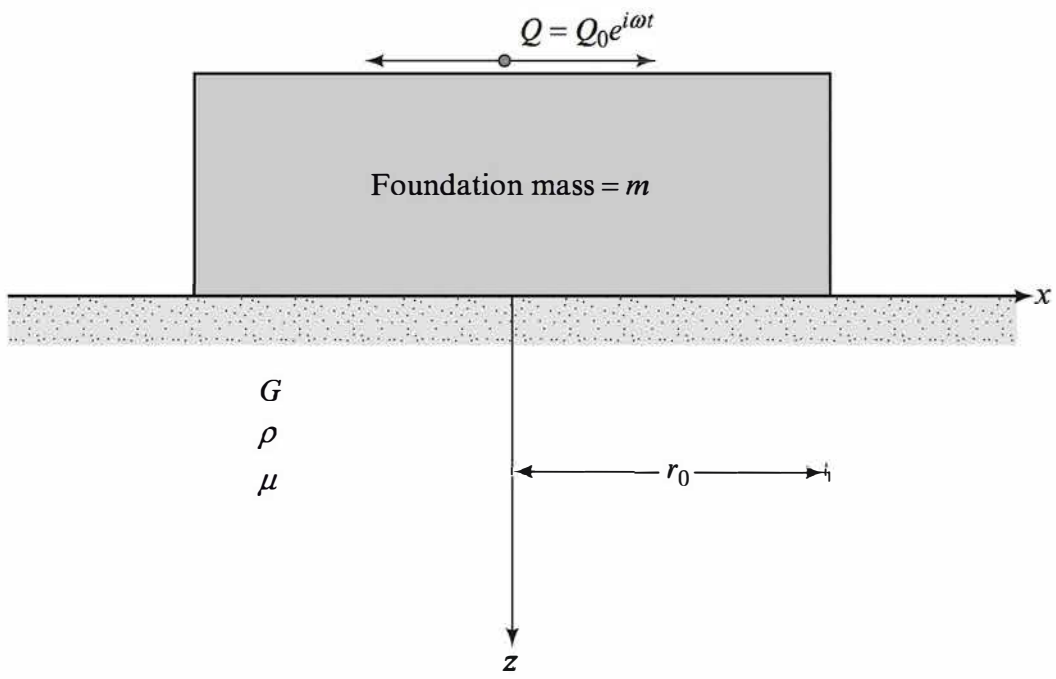

Figure 5.20 Sliding vibration of rigid circular foundation

$$\boxed{\begin{aligned} c_x &= \text{dashpot coefficient for sliding} \\ &= \frac{18.4(1-\mu)}{7-8\mu} r_0^2 \sqrt{\rho G} \end{aligned}} \tag{5.53}$$

Based on Eqs. (5.51), (5.52), and (5.53), the natural frequency of the foundation for sliding can be calculated as

$$f_n = \frac{1}{2\pi}\sqrt{\frac{k_x}{m}} = \frac{1}{2\pi}\sqrt{\frac{32(1-\mu)Gr_0}{(7-8\mu)m}} \tag{5.54}$$

The critical damping and damping ratio in sliding can be evaluated as

$$\begin{aligned} c_{cx} &= \text{critical damping in sliding} \\ &= 2\sqrt{k_x m} = 2\sqrt{\frac{32(1-\mu)\, Gr_0 m}{(7-8\mu)}} \end{aligned} \tag{5.55}$$

$$\begin{aligned} D_x &= \text{damping ratio in sliding} \\ &= \frac{c_x}{c_{cx}} = \frac{0.288}{\sqrt{B_x}} \end{aligned} \tag{5.56}$$

where the dimensionless mass ratio

$$\boxed{B_x = \frac{7-8\mu}{32(1-\mu)} \frac{m}{\rho r_0^3}} \tag{5.57}$$

For rectangular foundation, the preceding relationships can be used by obtaining the equivalent radius r_0, or

Copyright 2017 Cengage Learning. All Rights Reserved. May not be copied, scanned, or duplicated, in whole or in part. Due to electronic rights, some third party content may be suppressed from the eBook and/or eChapter(s). Editorial review has deemed that any suppressed content does not materially affect the overall learning experience. Cengage Learning reserves the right to remove additional content at any time if subsequent rights restrictions require it.

$$r_0 = \sqrt{\frac{BL}{\pi}}$$

where B and L are the length and width of the foundation, respectively.

Calculation Procedure for Foundation Response Using Eq. (5.51)

Resonant Frequency

1. Calculate the natural frequency f_n using Eq. (5.54)
2. Calculate the damping ratio D_x using Eq. (5.56). [Note: B_x can be obtained from Eq. (5.57).]
3. For constant force excitation (that is, Q_0 = constant), calculate

$$f_m = f_n\sqrt{1-2D_x^2}$$

4. For rotating mass-type excitation, calculate

$$f_m = \frac{f_n}{\sqrt{1-2D_x^2}}$$

Amplitude of Vibration at Resonance

1. For constant force excitation, amplitude of vibration at resonance is

$$\boxed{A_{x(\text{resonance})} = \frac{Q_0}{k_x}\frac{1}{2D_x\sqrt{1-D_x^2}}} \tag{5.58}$$

where $A_{x(\text{resonance})}$ = amplitude of vibration at resonance.

2. For rotating mass-type excitation,

$$\boxed{A_{x(\text{resonance})} = \frac{m_1 e}{m}\frac{1}{2D_x\sqrt{1-D_x^2}}} \tag{5.59}$$

where m_1 = total rotating mass causing excitation
e = eccentricity of each rotating mass

Amplitude of Vibration at Frequency Other Than Resonance

1. For constant force-type excitation,

$$\boxed{A_x = \frac{Q_0/k_x}{\sqrt{\left[1-\left(\omega^2/\omega_n^2\right)\right]^2 + 4D_x^2\left(\omega^2/\omega_n^2\right)}}} \tag{5.60}$$

Figure 5.12 can also be used to determine $A_x/(Q_0/k_x)$ for given values of ω/ω_n and D_x.

Copyright 2017 Cengage Learning. All Rights Reserved. May not be copied, scanned, or duplicated, in whole or in part. Due to electronic rights, some third party content may be suppressed from the eBook and/or eChapter(s). Editorial review has deemed that any suppressed content does not materially affect the overall learning experience. Cengage Learning reserves the right to remove additional content at any time if subsequent rights restrictions require it.

2. For rotating mass-type excitation,

$$\boxed{A_x = \frac{(m_1 e/m)(\omega/\omega_n)^2}{\sqrt{\left[1-(\omega^2/\omega_n^2)\right]^2 + 4D_x^2(\omega^2/\omega_n^2)}}} \tag{5.61}$$

Figure 5.13 provides a plot of $A_x/(m_1 e/m)$ versus ω/ω_n for various values of D_x.

5.7 TORSIONAL VIBRATION OF FOUNDATIONS

Figure 5.21a shows a circular foundation of radius r_0 subjected to a torque $T = T_0\theta^{i\omega t}$ about an axis z-z. Reissner (1937) solved the vibration problem of this type by considering a linear distribution of shear stress $\tau_{z\theta}$ (shear stress zero at center and maximum at the periphery of the foundation), as shown in Figure 5.21b. This represents the case of a *flexible* foundation. In 1944 Reissner and Sagoli solved the same problem for the case of a rigid foundation, considering a *linear variation of displacement from the center to the periphery* of the foundation. For this case, the shear stress can be given by (Figure 5.21c)

$$\tau_{z\theta} = \frac{3}{4\pi}\frac{Tr}{r_0^3\sqrt{r_0^2 - r^2}} \quad \text{for } 0 < r < r_0 \tag{5.62}$$

Similar to the cases of vertical, rocking, and sliding modes of vibration, the equation for the torsional vibration of a *rigid circular* foundation can be written as

$$\boxed{J_{zz}\ddot{\alpha} + c_\alpha\dot{\alpha} + k_\alpha\alpha = T_0 e^{i\omega t}} \tag{5.63}$$

where J_{zz} = mass moment of inertia of the foundation about the axis z-z

c_α = dashpot coefficient for torsional vibration

k_α = static spring constant for torsional vibration $= \frac{16}{3}Gr_0^3$ (5.64)

α = rotation of the foundation at any time due to the application of a torque $T = T_0\theta^{i\omega t}$

The damping ratio D_α for this mode of vibration has been determined as (Richart, Hall, and Wood, 1970)

$$D_\alpha = \frac{0.5}{1 + 2B_\alpha} \tag{5.65}$$

where

B_α = the dimensionless mass ratio for torsion at vibration

$$= \frac{J_{zz}}{\rho r_0^5} \tag{5.66}$$

Copyright 2017 Cengage Learning. All Rights Reserved. May not be copied, scanned, or duplicated, in whole or in part. Due to electronic rights, some third party content may be suppressed from the eBook and/or eChapter(s). Editorial review has deemed that any suppressed content does not materially affect the overall learning experience. Cengage Learning reserves the right to remove additional content at any time if subsequent rights restrictions require it.

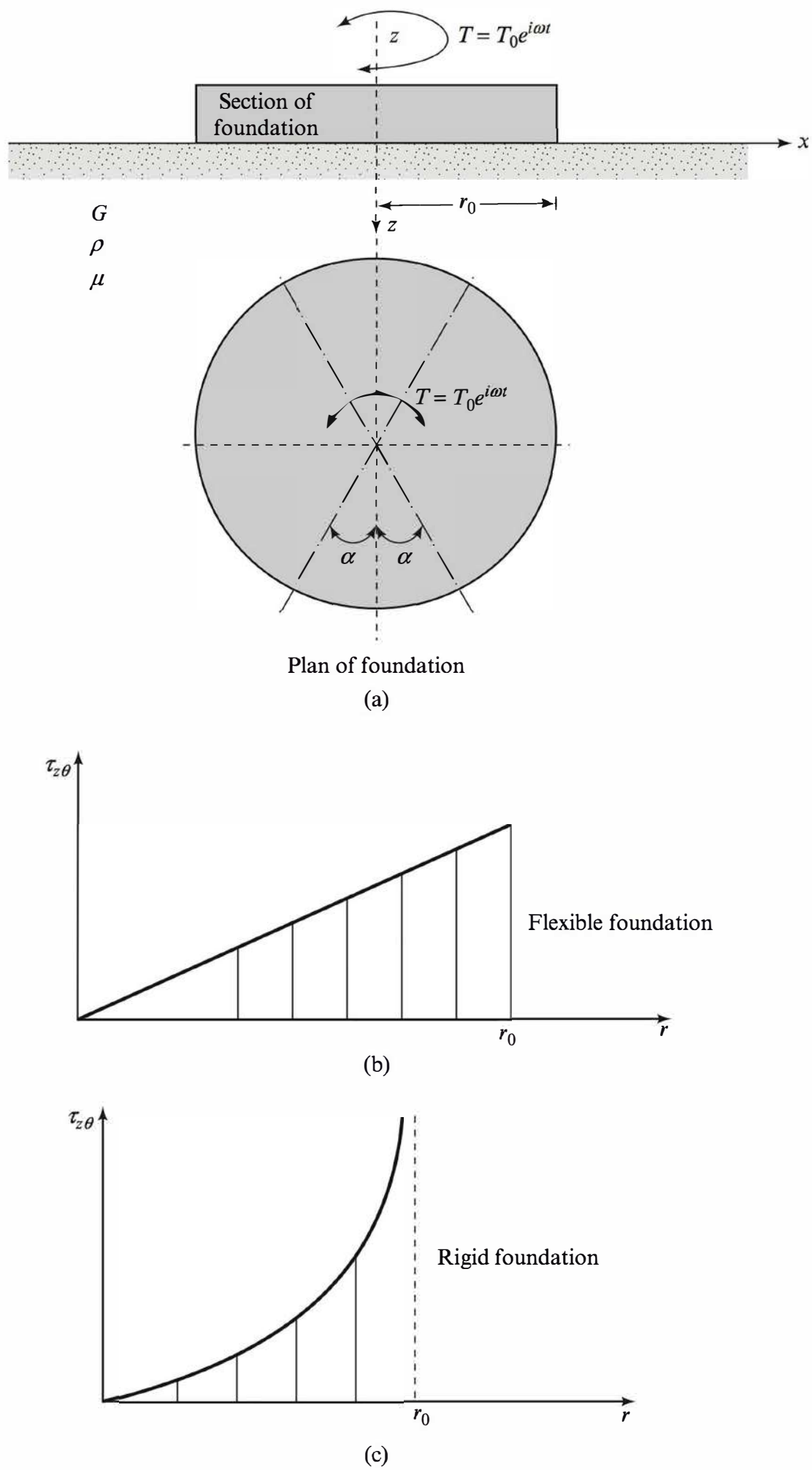

Figure 5.21 Torsional vibration of rigid circular foundation

Copyright 2017 Cengage Learning. All Rights Reserved. May not be copied, scanned, or duplicated, in whole or in part. Due to electronic rights, some third party content may be suppressed from the eBook and/or eChapter(s). Editorial review has deemed that any suppressed content does not materially affect the overall learning experience. Cengage Learning reserves the right to remove additional content at any time if subsequent rights restrictions require it.

Calculation Procedure for Foundation Response Using Eq. (5.63)

Resonant Frequency

1. Calculate the natural frequency of the foundation as

$$f_n = \frac{1}{2\pi}\sqrt{\frac{k_\alpha}{J_{zz}}} \tag{5.67}$$

2. Calculate B_α using Eq. (5.66) and then D_α using Eq. (5.65).
3. For constant force excitation (that is, T_0 = constant)

$$f_m = f_n\sqrt{1-2D_\alpha^2}$$

For rotating mass-type excitation

$$f_m = \frac{f_n}{\sqrt{1-2D_\alpha^2}}$$

Amplitude of Vibration at Resonance: For constant force excitation, the amplitude of vibration at resonance is

$$\boxed{\alpha_{\text{resonance}} = \frac{T_0}{k_\alpha}\frac{1}{2D_\alpha\sqrt{1-D_\alpha^2}}} \tag{5.68}$$

For rotating mass-type excitation

$$\boxed{\alpha_{\text{resonance}} = \frac{m_1 e\left(\frac{x}{2}\right)}{J_{zz}}\frac{1}{2D_\alpha\sqrt{1-D_\alpha^2}}} \tag{5.69}$$

Where m_1 = total rotating mass causing the excitation
e = eccentricity of each rotating mass

For the definition of x in Eq, (5.69), see, Figure 5.22.

Amplitude of Vibration at Frequency Other Than Resonance: For constant force excitation, calculate ω/ω_n and then refer to Figure 5.12 to obtain $\alpha/(T_0/k_\alpha)$. For rotating mass-type excitation, calculate ω/ω_n and then refer to Figure 5.13 to obtain $\alpha/[m_1 e(x/2)/J_{zz}]$.

For a rectangular foundation with dimensions $B \times L$, the equivalent radius may be given by

$$r_0 = \sqrt[4]{\frac{BL\left(B^2+L^2\right)}{6\pi}} \tag{5.70}$$

The torsional vibration of foundations is uncoupled motion and hence can be treated independently of any vertical motion. Also, Poisson's ratio does not influence the torsional vibration of foundations.

Copyright 2017 Cengage Learning. All Rights Reserved. May not be copied, scanned, or duplicated, in whole or in part. Due to electronic rights, some third party content may be suppressed from the eBook and/or eChapter(s). Editorial review has deemed that any suppressed content does not materially affect the overall learning experience. Cengage Learning reserves the right to remove additional content at any time if subsequent rights restrictions require it.

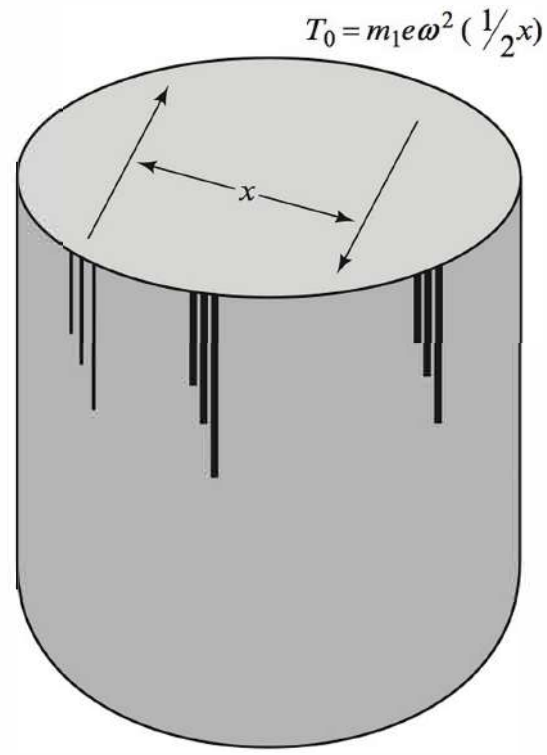

Figure 5.22

EXAMPLE 5.4

A radar antenna foundation is shown in Figure 5.23. For torsional vibration of the foundation, given

$$T_0 = 250 \text{ kN-m (due to inertia)}$$
$$T_0 = 83 \text{ kN-m (due to wind)}$$

Mass moment of inertia of the tower about the axis z-$z = 13 \times 10^6 \text{ kg} \cdot \text{m}^2$, and the unit weight of concrete used in the foundation $= 24 \text{ kN/m}^3$. Calculate

a. the resonant frequency for torsional mode of vibration; and
b. angular deflection at resonance.

SOLUTION:

a.

$$\begin{aligned} J_{zz} &= J_{zz(\text{tower})} + J_{zz(\text{foundation})} \\ &= 13 \times 10^6 + \frac{1}{2}\left[\pi r_0^2 h\left(\frac{24 \times 1000}{9.81}\right)\right] r_0^2 \\ &= 13 \times 10^6 + \frac{1}{2}\left[\pi (7.6)^2 (2.5)\left(\frac{24 \times 1000}{9.81}\right)\right](7.6)^2 \\ &= 13 \times 10^6 + 32.05 \times 10^6 = 45.05 \times 10^6 \text{ kg-m}^2 \end{aligned}$$

From Eq. (5.66)

Copyright 2017 Cengage Learning. All Rights Reserved. May not be copied, scanned, or duplicated, in whole or in part. Due to electronic rights, some third party content may be suppressed from the eBook and/or eChapter(s). Editorial review has deemed that any suppressed content does not materially affect the overall learning experience. Cengage Learning reserves the right to remove additional content at any time if subsequent rights restrictions require it.

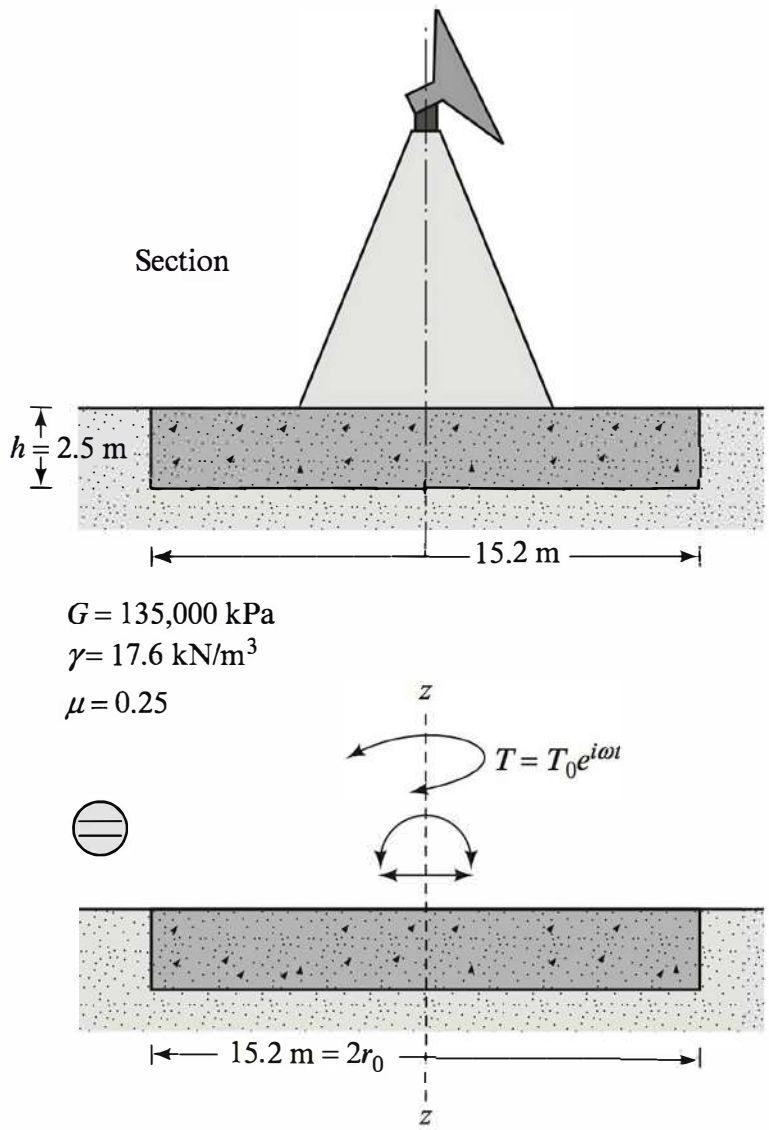

Figure 5.23

$$B_\alpha = \frac{J_{zz}}{\rho r_0^5} = \frac{45.05 \times 10^6}{(17.6 \times 10^3/9.81)(7.6)^5} = 0.99$$

Again from Eq. (5.65),

$$D_\alpha = \frac{0.5}{1+2B_\alpha} = \frac{0.5}{1+(2)(0.99)} = 0.168$$

Also, k_α [Eq. (5.64)] is

$$k_\alpha = \frac{16}{3} G r_0^3 = \left(\frac{16}{3}\right) \times 135 \times 10^6 \times (7.6)^3 = 3.16 \times 10^{11} \text{ N-m}$$

$$f_n = \frac{1}{2\pi}\sqrt{\frac{k_\alpha}{J_{zz}}} = \frac{1}{2\pi}\sqrt{\frac{3.16 \times 10^{11}}{45.05 \times 10^6}}$$

$$= 13.33 \text{ Hz}$$

Thus, the damped natural frequency

$$f_m = f_n\sqrt{1-2D_\alpha^2} = (13.33)\sqrt{1-(2)(0.168)^2}$$

$$= \mathbf{12.92\ Hz}$$

Copyright 2017 Cengage Learning. All Rights Reserved. May not be copied, scanned, or duplicated, in whole or in part. Due to electronic rights, some third party content may be suppressed from the eBook and/or eChapter(s). Editorial review has deemed that any suppressed content does not materially affect the overall learning experience. Cengage Learning reserves the right to remove additional content at any time if subsequent rights restrictions require it.

b. *Angular deflection at resonant frequency:*
If the torque due to wind (T_0) is to be treated as a static torque, then

$$\frac{T_0}{\alpha_{\text{static}}} = k_\alpha$$

or

$$\alpha_{\text{static}} = \frac{T_0}{k_\alpha}$$

So

$$\alpha_{\text{static}} = \frac{3}{16Gr_0^3} T_{0(\text{static})} = \left[\frac{83 \times 10^3}{3.16 \times 10^{11}}\right]$$
$$= 0.0263 \times 10^{-5} \text{ rad}$$

Using Eq. (5.68), for the torque due to inertia

$$\alpha_{\text{resonance}} = \frac{T_0}{k_\alpha} \frac{1}{2D_\alpha \sqrt{1 - D_\alpha^2}}$$

$$= \left[\frac{250 \times 10^3}{3.16 \times 10^{11}}\right]\left[\frac{1}{(2)(0.168)\sqrt{1-(0.168)^2}}\right]$$
$$= 0.24 \times 10^{-5} \text{ rad}$$

At resonance, the total angular deflection is

$$\alpha = \alpha_{\text{inertia}} + \alpha_{\text{static}} = (0.24 + 0.0263) \times 10^{-5} = \mathbf{0.2663 \times 10^{-5}\ rad}$$

5.8 COMPARISON OF FOOTING VIBRATION TESTS WITH THEORY

Richart and Whitman (1967) conducted a comprehensive study to evaluate the applicability of the preceding theoretical findings to actual field problems. Ninety-four large-scale field test results for large footings 1.52 m to 4.88 m in diameter subjected to *vertical vibration* were reported by Fry (1963). Of these 94 test results, 55 were conducted at the US Army Waterways Experiment Station, Vicksburg, Mississippi. The remaining 39 were conducted at Eglin Field, Florida. The classification of the soils for the Vicksburg site and Eglin site were CL and SP, respectively (Unified soil classification system). For these tests, the *vertical dynamic force* on footings was generated by rotating mass vibrators.

Figure 5.24 shows a comparison of the theoretical amplitudes of vibration A_z as determined from elastic half-space theory with the experimental results obtained for two bases at the Vicksburg site. The nondimensional mass ratios b [Eq. (5.4)] of these two bases were 5.2 and 3.8. For the base with $b = 5.2$, the experimental results fall between the theoretical curves, with $\mu = 0.5$ and $\mu = 0.25$. However, for the base with $b = 3.8$, the experimental curve is nearly identical to

Copyright 2017 Cengage Learning. All Rights Reserved. May not be copied, scanned, or duplicated, in whole or in part. Due to electronic rights, some third party content may be suppressed from the eBook and/or eChapter(s). Editorial review has deemed that any suppressed content does not materially affect the overall learning experience. Cengage Learning reserves the right to remove additional content at any time if subsequent rights restrictions require it.

the theoretical curve with $\mu = 0.5$. Figure 5.25 shows a comparison of the theory and experimental values reported by Fry in a nondimensional plot of $A_z m / m_1 e$ at resonance versus b. Similarly, a comparison of these test results with theory in a nondimensional plot of a_0 [Eq. (5.5)] at resonance versus b is shown in Figure 5.26.

From these two plots it may be seen that the results of the Vicksburg site follow the general trends indicated by the theoretical curve obtained from the elastic half-space theory for a *rigid base*. A considerable scatter, however, exists for the tests conducted at Eglin Field. This may be due to the clean fine sand found at that site, for which the shear modulus will change with depth. The fundamental assumption of the theoretical derivation of a homogeneous, elastic, isotropic body is very much different than the actual field conditions.

Figure 5.27 shows a summary of all vertical vibration tests, which is plot of $A_{z(\text{computed})}/A_{z(\text{measured})}$ versus $A_z\omega^2/g$ (that is, nondimensional acceleration, g, equals acceleration due to gravity). When the nondimensional acceleration reaches 1, the footing probably leaves the ground on the upswing and acts as a hammer. In any case, in actual design problems, a machine foundation is not subjected to an acceleration greater than $0.3g$. However, for dynamic

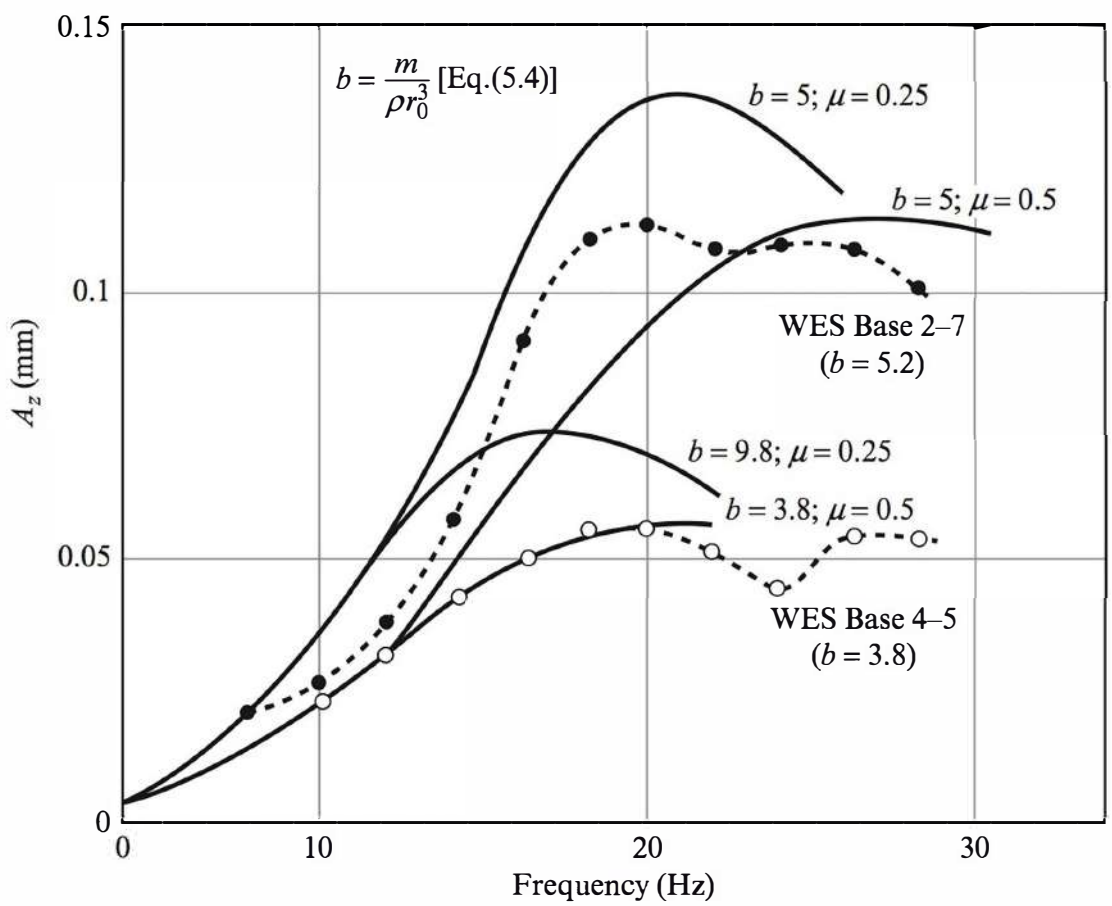

Figure 5.24 Vertical vibration of foundation—comparison of test results with theory (from Richart and Whitman, 1967)

Source: Richart, F.E., Jr., and Whitman, R.V. (1967). "Comparison of Footing Foundation Tests with Theory," *Journal of the Soil Mechanics and Foundations,* ASCE, Vol. 93, No. SM6, pp. 143–167. With permission from ASCE.

Copyright 2017 Cengage Learning. All Rights Reserved. May not be copied, scanned, or duplicated, in whole or in part. Due to electronic rights, some third party content may be suppressed from the eBook and/or eChapter(s). Editorial review has deemed that any suppressed content does not materially affect the overall learning experience. Cengage Learning reserves the right to remove additional content at any time if subsequent rights restrictions require it.

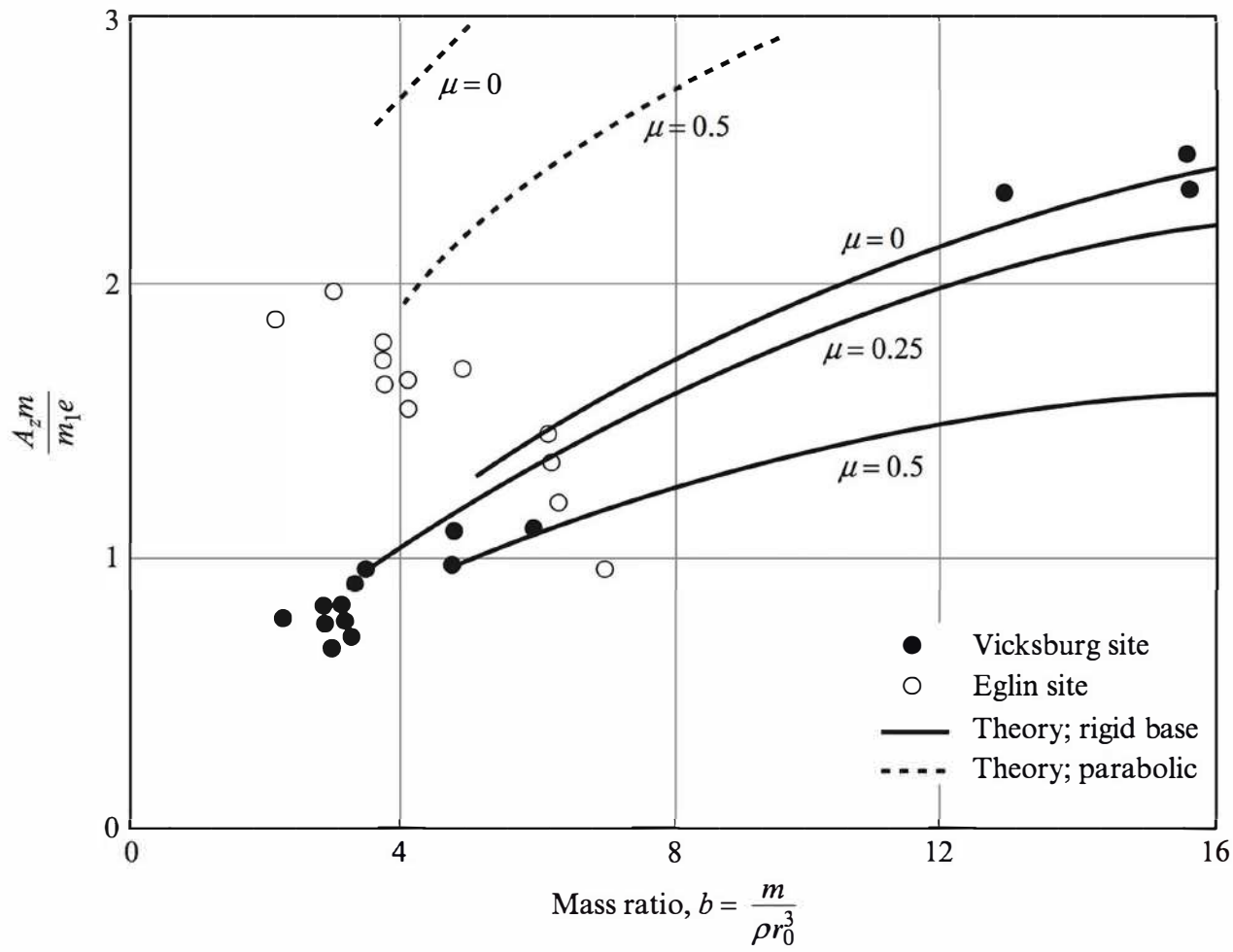

Figure 5.25 Motion at resonance for vertical excitation—comparison between theory and experiment (from Richart and Whitman, 1967)

Source: Richart, F.E., Jr., and Whitman, R.V. (1967). "Comparison of Footing Foundation Tests with Theory," *Journal of the Soil Mechanics and Foundations,* ASCE, Vol. 93, No. SM6, pp. 143–167. With permission from ASCE.

problems of this nature, the general agreement between theory and experiment is fairly good.

Several large-scale field test were conducted by the US Army Waterways Experiment Station (Fry, 1963) in which footings were subjected to torsional vibration. Mechanical vibrators were set to produce pure torque on a horizontal plane. Figure 5.28 shows a plot of the dimensionless amplitude $\alpha J_{zz}/[m_1 e(x/2)]$ versus B_α(α =amplitude of torsional motion and m_1 = sum of the rotating masses; for definition of x, see the insert in Figure 5.28) for some of these tests that correspond to the lowest settings of the eccentric masses on the vibrator. The theoretical curve based on the elastic half-space theory is also plotted in this figure for comparison purposes. It can be seen that, for low amplitudes of vibration, the agreement between theory and field test results is good.

The limiting torsional motion in most practical cases is about 2.5×10^{-3} mm. So the half-space theory generally serves well for most practical design considerations. Comparisons between the elastic half-space theory and experimental results for footing vibration tests in rocking and sliding modes were also presented by Richart and Whitman (1967). The agreement seemed fairly good.

Copyright 2017 Cengage Learning. All Rights Reserved. May not be copied, scanned, or duplicated, in whole or in part. Due to electronic rights, some third party content may be suppressed from the eBook and/or eChapter(s). Editorial review has deemed that any suppressed content does not materially affect the overall learning experience. Cengage Learning reserves the right to remove additional content at any time if subsequent rights restrictions require it.

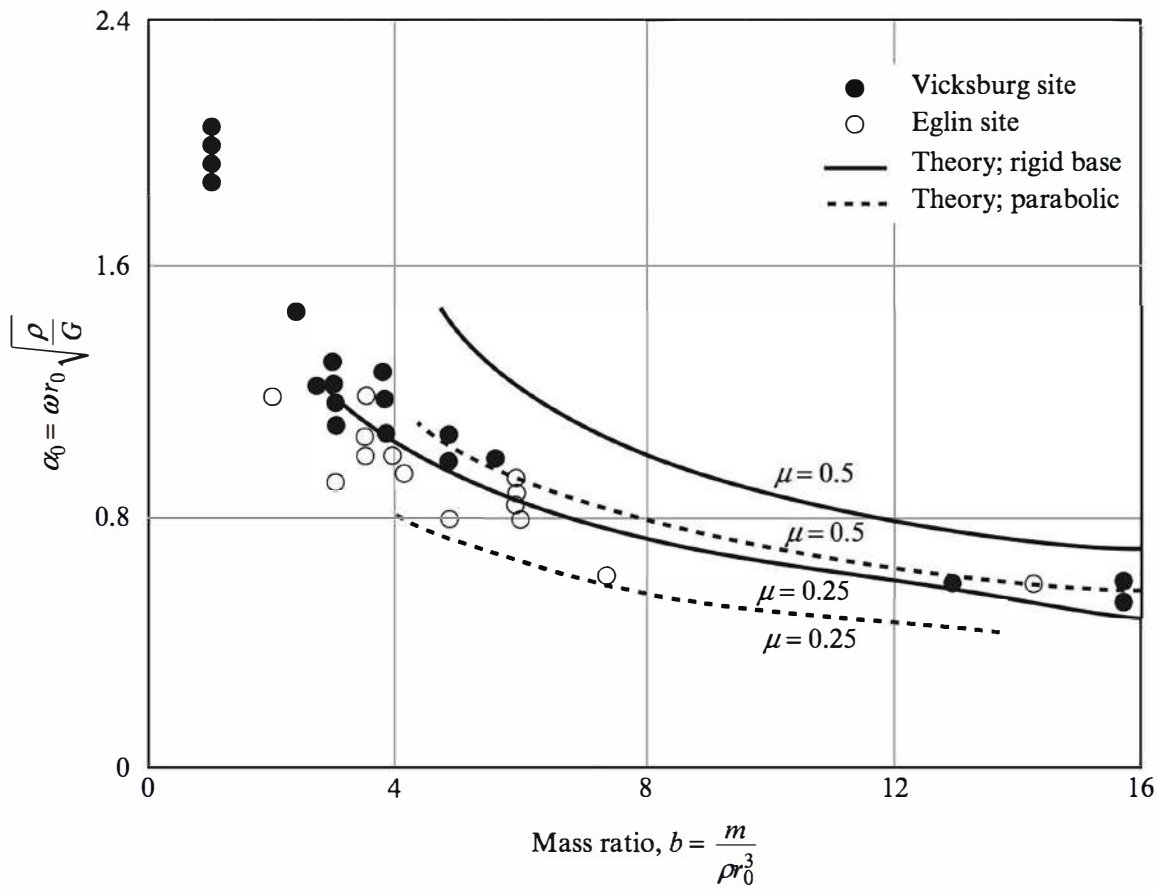

Figure 5.26 Plot of a_0 at resonance versus b—comparison of theory with field test results (from Richart and Whitman, 1967)

Source: Richart, F.E., Jr., and Whitman, R.V. (1967). "Comparison of Footing Foundation Tests with Theory," *Journal of the Soil Mechanics and Foundations,* ASCE, Vol. 93, No. SM6, pp. 143–167. With permission from ASCE.

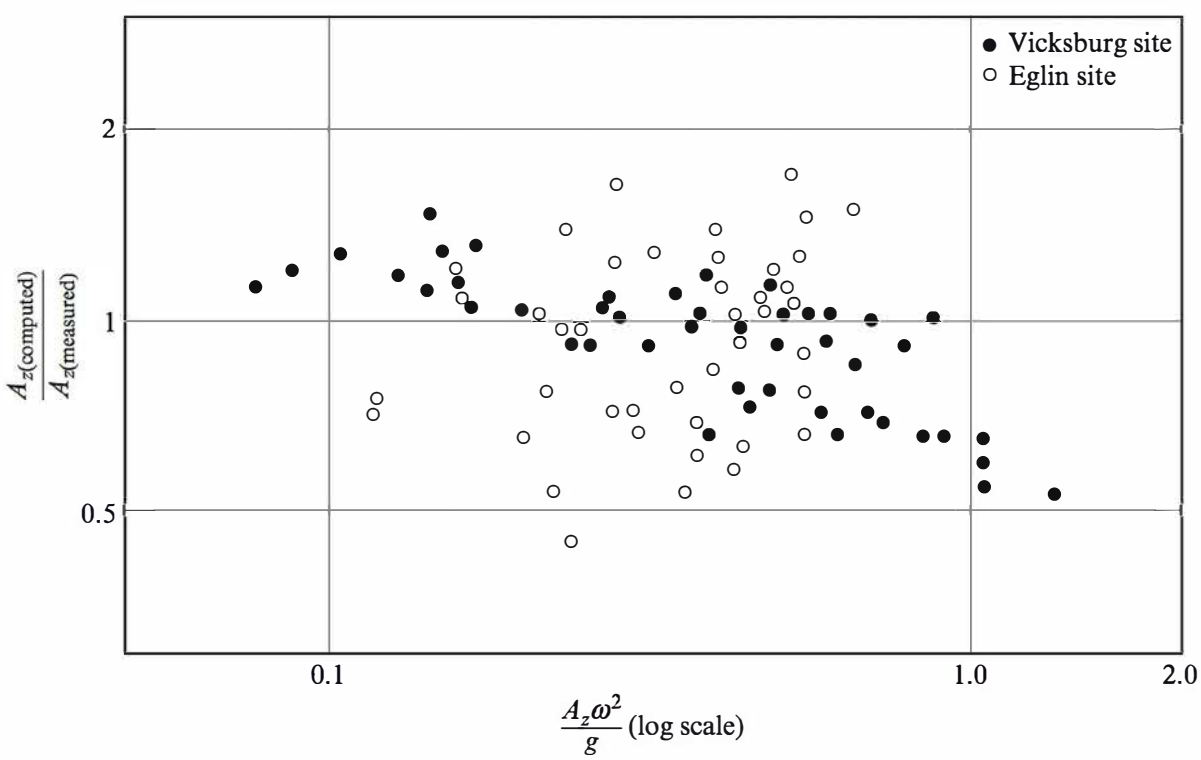

Figure 5.27 Summary of vertical vibration tests (from Richart and Whitman, 1967)

Source: Richart, F.E., Jr., and Whitman, R.V. (1967). "Comparison of Footing Foundation Tests with Theory," *Journal of the Soil Mechanics and Foundations,* ASCE, Vol. 93, No. SM6, pp. 143–167. With permission from ASCE.

Copyright 2017 Cengage Learning. All Rights Reserved. May not be copied, scanned, or duplicated, in whole or in part. Due to electronic rights, some third party content may be suppressed from the eBook and/or eChapter(s). Editorial review has deemed that any suppressed content does not materially affect the overall learning experience. Cengage Learning reserves the right to remove additional content at any time if subsequent rights restrictions require it.

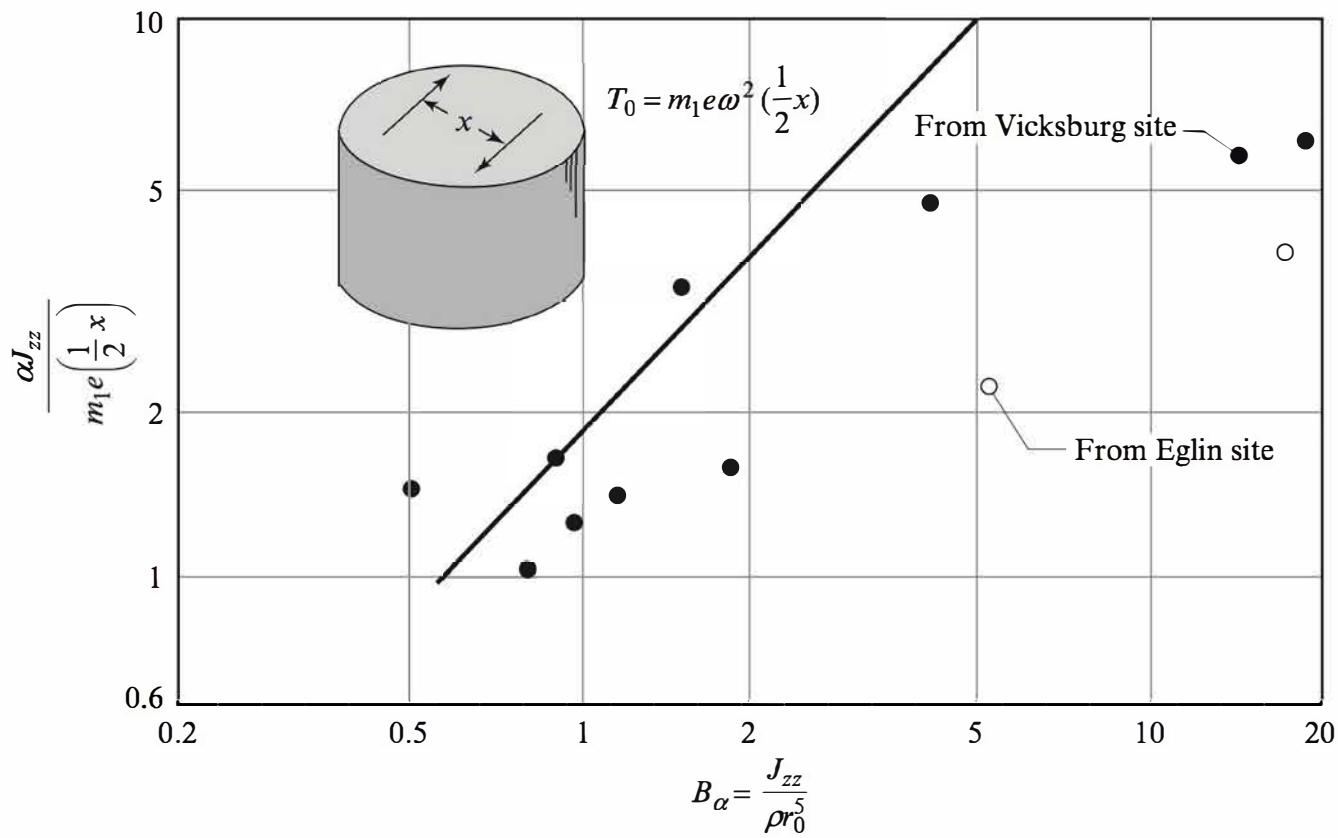

Figure 5.28 Comparison of amplitudes for torsional vibration (redrawn from Richart and Whitman, 1967)

Source: Richart, F.E., Jr., and Whitman, R.V. (1967). "Comparison of Footing Foundation Tests with Theory," *Journal of the Soil Mechanics and Foundations,* ASCE, Vol. 93, No. SM6, pp. 143–167. With permission from ASCE.

5.9 COMMENTS ON THE MASS-SPRING-DASHPOT ANALOG USED FOR SOLVING FOUNDATION VIBRATION PROBLEMS

The equations for the mass-spring-dashpot analog for various modes of vibration of *rigid circular* foundations developed in the preceding sections may be summarized as follows:

For vertical vibration,

$$m\ddot{z} + c_z\dot{z} + k_z z = Q_0 e^{i\omega t} \tag{5.22}$$

For rocking vibration,

$$I_0\ddot{\theta} + c_\theta\dot{\theta} + k_\theta\theta = M_y e^{i\omega t} \tag{5.39}$$

For sliding vibration,

$$m\ddot{x} + c_x\dot{x} + k_x x = Q_0 e^{i\omega t} \tag{5.51}$$

For torsional vibration

$$J_{zz}\ddot{\alpha} + c_\alpha\dot{\alpha} + k_\alpha\alpha = T_0\, o^{i\omega t} \tag{5.63}$$

Copyright 2017 Cengage Learning. All Rights Reserved. May not be copied, scanned, or duplicated, in whole or in part. Due to electronic rights, some third party content may be suppressed from the eBook and/or eChapter(s). Editorial review has deemed that any suppressed content does not materially affect the overall learning experience. Cengage Learning reserves the right to remove additional content at any time if subsequent rights restrictions require it.

The mathematical approach for solution of the preceding equations is similar for determination of the natural frequency, resonant frequency, critical damping, damping ratio, and the amplitudes of vibration at various frequencies. The agreement of these solutions with field conditions will depend on proper choice of the parameters (that is, m, I_0, J_{zz}, c_z, c_θ, c_x, c_α, k_z, k_θ, k_x, and k_α. In this section, we will make a critical evaluation of these parameters.

Choice of Mass and Mass Moments of Inertia

The mass terms m used in Eqs. (5.22) and (5.51) are actually the sum of

1. mass of structure foundation block m_f, and
2. mass of all the machinery mounted on the block m_m.

During the vibration of foundations, there is a mass of soil under the foundation that vibrates along with the foundation. Thus, it would be reasonable to consider the term m in Eqs. (5.22) and (5.51) to be the sum of

$$m = m_f + m_m + m_s \tag{5.71}$$

where m_s = effective mass of soil vibrating with foundation.

In a similar manner, the mass moment of inertia terms I_0 and J_{zz} included in Eqs (5.39) and (5.63) include the contributions of the mass of the foundation and that of the machine mounted on the block. It appears reasonable also to add the contribution of the effective mass of the vibrating soil (m_s), that is, the effective soil mass moment of inertia. Thus

$$I_0 = I_{0(\text{foundation})} + I_{0(\text{machine})} + I_{0(\text{effective soil mass})} \tag{5.72}$$

and

$$J_{zz} = J_{zz(\text{foundation})} + J_{zz(\text{machine})} + J_{zz(\text{effective soil mass})} \tag{5.73}$$

Theoretically, calculated values of m_s, $I_{0(\text{effective soil mass})}$, and $J_{zz(\text{effective soil mass})}$ are given by Hsieh (1962). They are as follows:

1. Values of m_s for vertical vibration:

Poisson's ratio, μ	m_s
0.00	$0.5\rho r_0^3$
0.25	$0.5\rho r_0^3$
0.50	$2.0\rho r_0^3$

2. Values of m_s for horizontal vibration:

Poisson's ratio, μ	m_s
0.0	$0.2\rho r_0^3$
0.25	$0.2\rho r_0^3$
0.50	$0.1\rho r_0^3$

Copyright 2017 Cengage Learning. All Rights Reserved. May not be copied, scanned, or duplicated, in whole or in part. Due to electronic rights, some third party content may be suppressed from the eBook and/or eChapter(s). Editorial review has deemed that any suppressed content does not materially affect the overall learning experience. Cengage Learning reserves the right to remove additional content at any time if subsequent rights restrictions require it.

3. Values of $I_{0(\text{effective soil mass})}$ for rocking vibration: Poisson's ratio $\mu = 0$; $I_{0(\text{effective soil mass})} = 0.4\rho r_0^5$
4. Values of $J_{zz(\text{effective soil mass})}$ for torsional vibration:

Poisson's ratio, μ	m_s
0.00	$0.3\rho r_0^5$
0.25	$0.3\rho r_0^5$
0.50	$0.3\rho r_0^5$

In most cases, for design purposes the contribution of the effective soil mass is neglected. This will, in general, lead to answers that are within 30% accuracy.

Choice of Spring Constants

In Eqs. (5.23), (5.41), (5.52), and (5.64), the spring constants defined were for the cases of *rigid circular* foundations. In examples where rigid rectangular foundations were encountered, the equivalent radii r_0 were first determined. These values of r_0 were then used to determine the value of the spring constants. However, more exact solutions for spring constants for rectangular foundations derived from the theory of elasticity can be used. These are given in Table 5.1 along with those for circular foundations. Dobry and Gazetas (1986) have developed more realistic values of spring constants and demonstrated their use through a design exercise.

Table 5.1 Values of Spring Constants for Rigid Foundations (after Whitman and Richart, 1967)

Motion	Spring constant	Reference
	Circular foundations	
Vertical	$k_z = \dfrac{4Gr_0}{1-\mu}$	Timoshenko and Goodier (1951)
Horizontal (sliding)	$k_x = \dfrac{32(1-\mu)Gr_0^3}{7-8\mu}$	Bycroft (1956)
Rocking	$k_\theta = \dfrac{8Gr_0^3}{3(1-\mu)}$	Borowicka (1943)
Torsion	$k_\alpha = \dfrac{16}{3}Gr_0^3$	Reissner and Sagoci (1944)
	Rectangular foundations	
Vertical[a]	$k_z = \dfrac{G}{1-\mu}F_z\sqrt{BL}$	Barkan (1962)

Copyright 2017 Cengage Learning. All Rights Reserved. May not be copied, scanned, or duplicated, in whole or in part. Due to electronic rights, some third party content may be suppressed from the eBook and/or eChapter(s). Editorial review has deemed that any suppressed content does not materially affect the overall learning experience. Cengage Learning reserves the right to remove additional content at any time if subsequent rights restrictions require it.

Horizontal[a] (sliding)	$k_x = 2(1+\mu)\,GF_x\sqrt{BL}$	Barkan (1962)
Rocking[b]	$k_\theta = \dfrac{G}{1-\mu}F_\theta BL^2$	Gorbunov-Possadov and Serebrajanyi(1961)

[a] B = width of foundation; L = length of foundation.
[b] For definition of B and L, refer to Figure 5.18. Refer to Figure 5.29 for values of F_z, F_x, and F_θ.

Source: Whitman, R.V., and Richart, F.E., Jr. (1967). "Design Procedures for Dynamically Loaded Foundations," *Journal of the Soil Mechanics and Foundations Division,* ASCE, Vol. 93, No. SM6, pp. 169–193. With permission from ASCE.

Another fact that needs to be kept in mind is that the foundation blocks are never placed at the surface. If the bottom of the foundation block is placed at a depth z measured from the ground surface, the spring constants will be higher than that calculated by theory. This fact is demonstrated in Figure 5.30 for the case

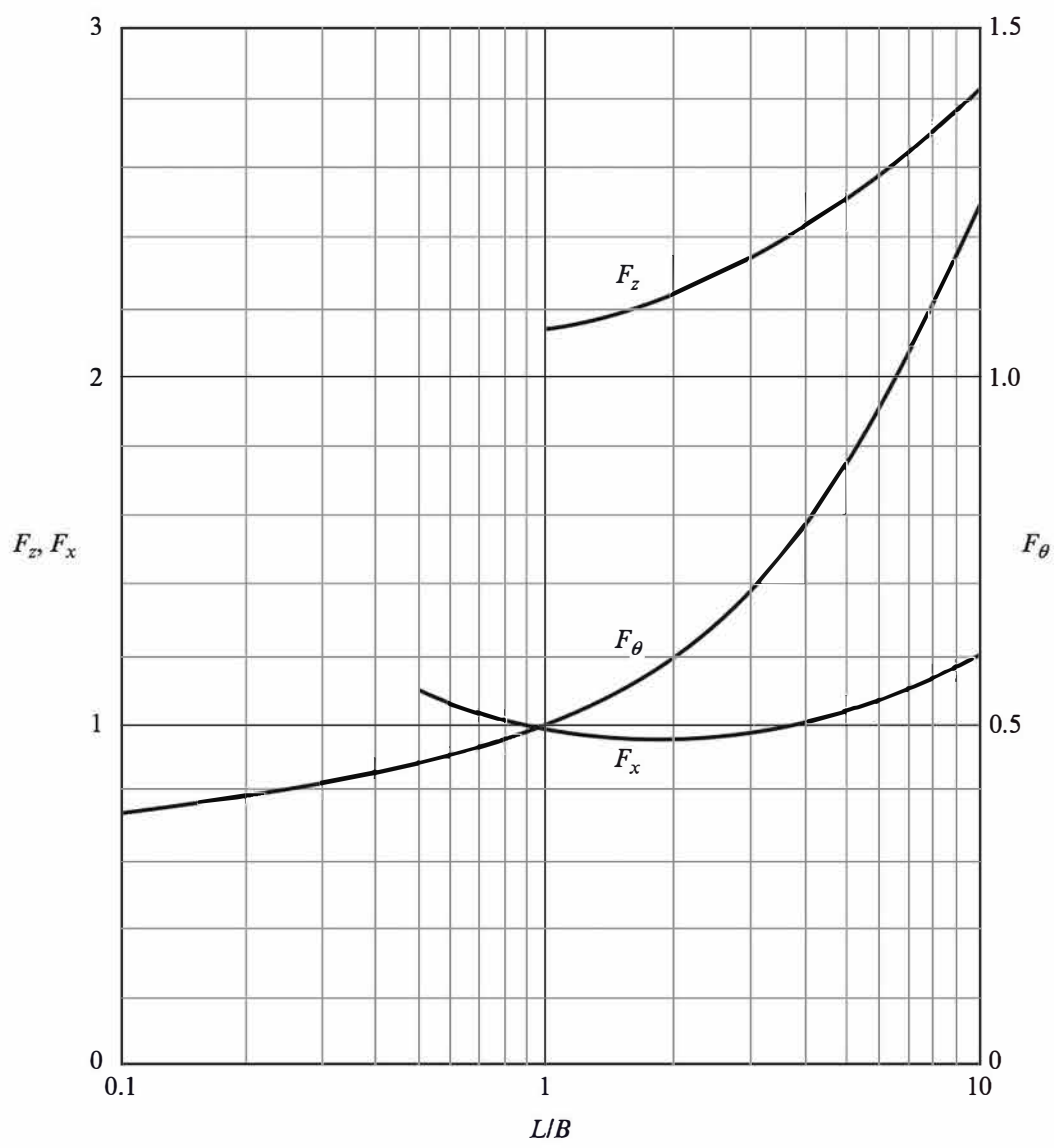

Figure 5.29 Plot of F_z, F_x and F_θ against L/B (from Whitman and Richart, 1967)

Source: Whitman, R.V., and Richart, F.E., Jr. (1967). "Design Procedures for Dynamically Loaded Foundations," *Journal of the Soil Mechanics and Foundations Division,* ASCE, Vol. 93, No. SM6, pp. 169–193. With permission from ASCE.

Copyright 2017 Cengage Learning. All Rights Reserved. May not be copied, scanned, or duplicated, in whole or in part. Due to electronic rights, some third party content may be suppressed from the eBook and/or eChapter(s). Editorial review has deemed that any suppressed content does not materially affect the overall learning experience. Cengage Learning reserves the right to remove additional content at any time if subsequent rights restrictions require it.

of vertical motion of rigid foundations. This could possibly due to the frictional resistance of the sides of the foundations. The behavior of embedded foundations subjected to various types of vibration is presented in Sections 5.12 through 5.15.

Choice of Poisson's Ratio

Whitman and Richart (1967) recommended the following values of Poisson's ratio for different types of soils:

Sand (dry, moist, partially saturated) $\mu = 0.35$ to 0.4

Clay (saturated) $\mu = 0.5$

A good value for most partially saturated soils is about 0.4

Choice of Damping Ratio

In soils there are two types of damping, geometric damping (also known as radiation damping) and internal damping (also known as material damping or hysteretic damping). The radiation damping (defined as loss of energy over one wave length) depends on parameters such as Poisson's ratio, mass of the foundation, equivalent radius, and the density of the soil. The relations for the damping ratio given in Eqs. (5.27), (5.45), (5.56), and (5.65) are for radiation damping only.

The internal damping D_i varies over a wide range, depending on the type of soil and the strains generated in the soil. Generally the values of D_i are the range of 0.01 to 0.1. Thus an average value of D_i would be a good estimate to be used in foundation design (Whitman and Richart, 1967). The damping ratio can then be approximated as

$$\boxed{D = D_{\text{radiation}} + 0.05} \tag{5.74}$$

For vertical and sliding motions, the contribution of internal damping can be somewhat neglected. However, for torsional and rocking modes of vibration, the contribution of the internal damping may be too large to be ignored.

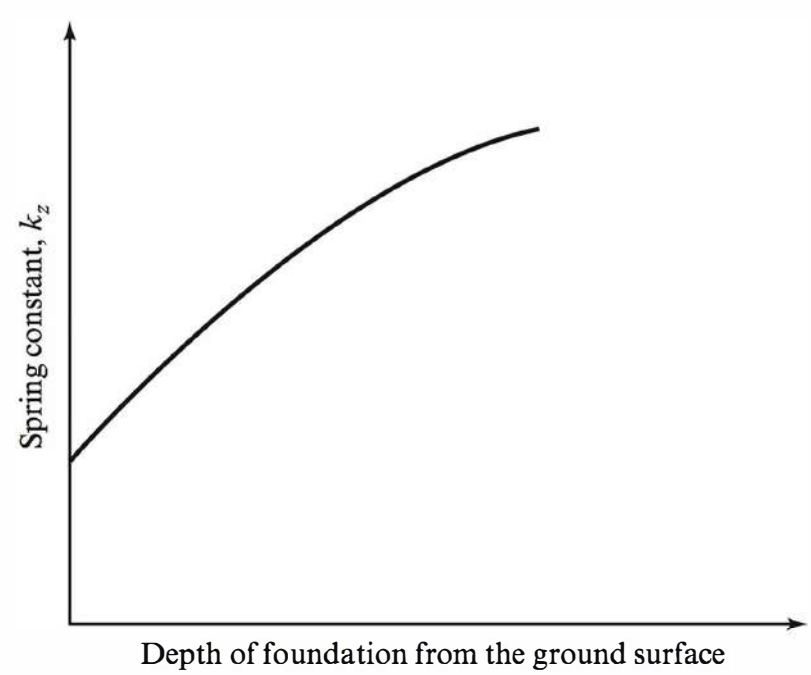

Figure 5.30 Nature of variation of k_z with the depth of the foundation

Copyright 2017 Cengage Learning. All Rights Reserved. May not be copied, scanned, or duplicated, in whole or in part. Due to electronic rights, some third party content may be suppressed from the eBook and/or eChapter(s). Editorial review has deemed that any suppressed content does not materially affect the overall learning experience. Cengage Learning reserves the right to remove additional content at any time if subsequent rights restrictions require it.

5.10 IMPROVED METHODS FOR ESTIMATION OF DYNAMIC SPRING CONSTANT AND DASHPOT COEFFICIENT

In Sections 5.4 – 5.7, we have used an equivalent radius (r_0) for dynamically excited rectangular foundations to determine the resonant frequency and the amplitude of vibration. The quality of solutions with that type of assumption deteriorates as the length-to-width ratio (L/B) of the foundation increases. To that extent, Dobry and Gazetas (1986) have provided improved solutions to estimate the spring constant and dashpot coefficient for evaluation of the dynamic response of an arbitrarily-shaped foundation, which is the subject of discussion in this section.

Figure 5.31a shows the plan of an arbitrarily-shaped foundation. The circumscribed rectangular area has a length of $2L'$ and a width of $2B'$. The area of the foundation is A. Note carefully the directions of the x and y axes. The z axis is directed downward from the centroid of the foundation O. Figures 5.31b and 5.31c show the dimensions $2L'$ and $2B'$ for a rectangular and a circular

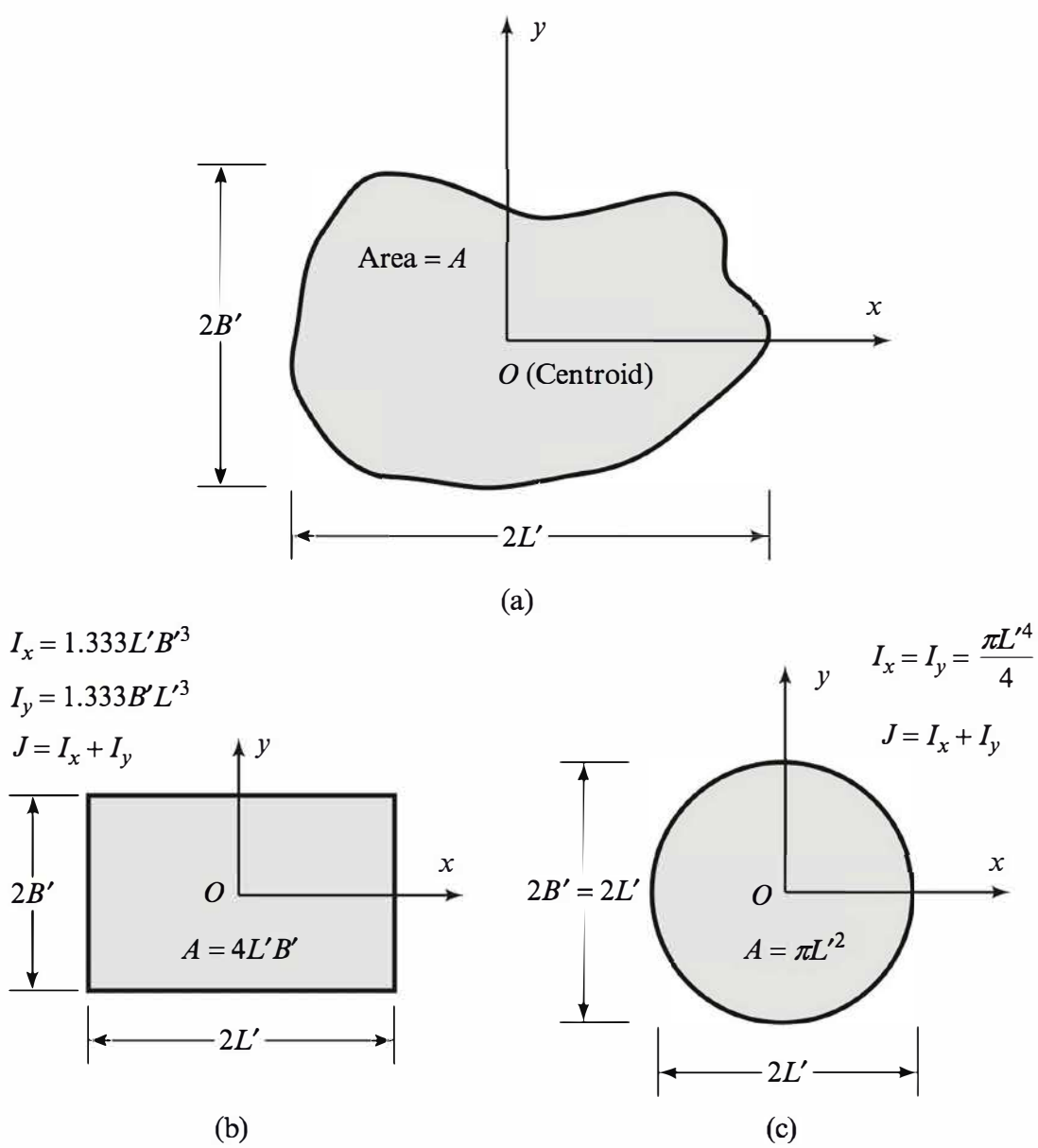

Figure 5.31 Plan of: (*a*) arbitrarily shaped foundation; (*b*) rectangular shaped foundation; (c) circular shaped foundation.

Copyright 2017 Cengage Learning. All Rights Reserved. May not be copied, scanned, or duplicated, in whole or in part. Due to electronic rights, some third party content may be suppressed from the eBook and/or eChapter(s). Editorial review has deemed that any suppressed content does not materially affect the overall learning experience. Cengage Learning reserves the right to remove additional content at any time if subsequent rights restrictions require it.

foundation. The dynamic spring constant $k_{(d)}$ and dashpot coefficient $c_{(d)}$ for a given mode of vibration can be expressed as, in general,

$$k_{(d)} = Sk\alpha - \omega cD \tag{5.75}$$

$$c_{(d)} = c + \frac{2Sk}{\omega} D \tag{5.76}$$

where k = static spring stiffness

c = static radiation dashpot coefficient with zero material damping

D = damping ratio

α, S = dimensionless coefficients

Following are the relationships of parameters given in Eqs. (5.75) and (5.76) for various modes of vibration of foundations:

a. ***Vertical Vibration***

Table 5.2 gives the relationships for $k = k_z$, $S = S_z$, and $c = c_z$. For the variation of $\alpha = \alpha_z$, refer to Figure 5.32.

Table 5.2 Variation of k_s, S_z and c_s

Parameter	Relationship
	General Shape
k_z	$\frac{2L'G}{1-\mu}$
S_z	$0.8\left(\text{for } \frac{A}{4L'^2} < 0.02\right)$
	$0.73 + 1.54\left(\frac{A}{4L'^2}\right)^{0.75} \quad \left(\text{for } \frac{A}{4L'^2} > 0.02\right)$
	Circle
$S_z\, k_z$	$\frac{4GB'}{1-\mu}$
c_z	See Figure 5.33. At high frequency, $\frac{3.4}{\pi(1-\mu)}\rho\sqrt{\frac{G}{\rho}}$

Hence, from Eqs. (5.75) and (5.76),

$$k_{z(d)} = S_z k_z \alpha_z - \omega c_z D \tag{5.77}$$

Copyright 2017 Cengage Learning. All Rights Reserved. May not be copied, scanned, or duplicated, in whole or in part. Due to electronic rights, some third party content may be suppressed from the eBook and/or eChapter(s). Editorial review has deemed that any suppressed content does not materially affect the overall learning experience. Cengage Learning reserves the right to remove additional content at any time if subsequent rights restrictions require it.

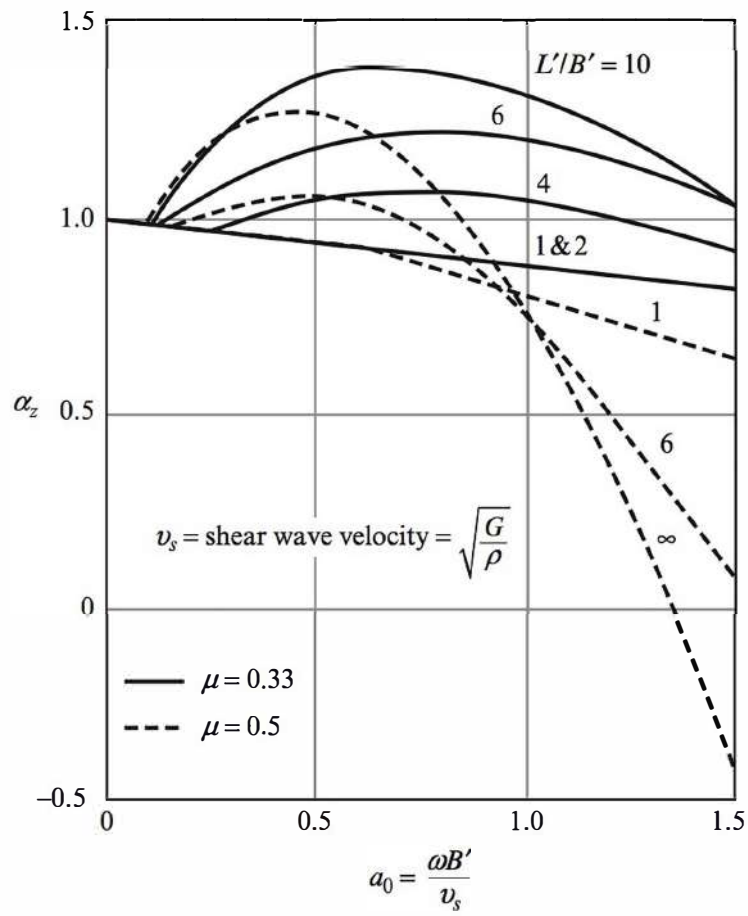

Figure 5.32 Variation of α_z with $a_0 = \dfrac{\omega B'}{v_s}$ (adapted from Dobry and Gazetas, 1986)

Source: Based on Dobry, R., and Gazetas, G. (1986). "Dynamic Response of Arbitrarily Shaped Foundations," *Journal of the Geotechnical Engineering Division,* ASCE, Vol. 112, No. GT2, pp. 109–135.

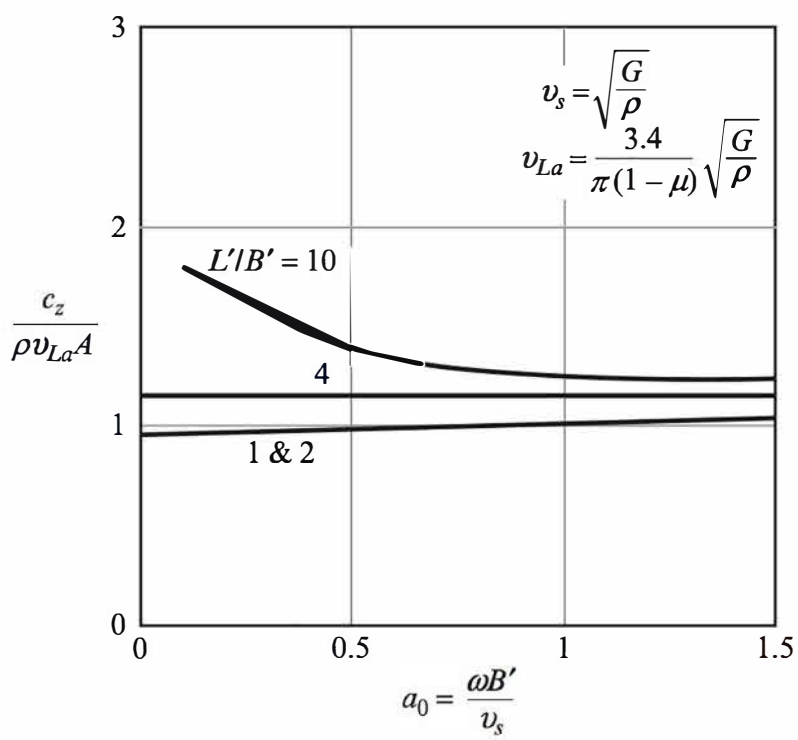

Figure 5.33 Variation of $\dfrac{c_z}{\rho v_{La} A}$ with $a_0 = \dfrac{\omega B'}{v_s}$ (adapted from Dobry and Gazetas, 1986)

Source: Based on Dobry, R., and Gazetas, G. (1986). "Dynamic Response of Arbitrarily Shaped Foundations," *Journal of the Geotechnical Engineering Division,* ASCE, Vol. 112, No. GT2, pp. 109–135.

Copyright 2017 Cengage Learning. All Rights Reserved. May not be copied, scanned, or duplicated, in whole or in part. Due to electronic rights, some third party content may be suppressed from the eBook and/or eChapter(s). Editorial review has deemed that any suppressed content does not materially affect the overall learning experience. Cengage Learning reserves the right to remove additional content at any time if subsequent rights restrictions require it.

and

$$c_{z(d)} = c_z + \frac{2S_z k_z}{\omega} D \tag{5.78}$$

The values of $k_{z(d)}$ and $c_{z(d)}$ can now be substituted in Eq.(5.22) in place of k_z and c_z, respectively, and solved for the desired parameters.

EXAMPLE 5.5

Refer to Example 5.1. For the foundation, calculate $k_{z(d)}$ and $c_{z(d)}$. Use $D \approx 0.05$

SOLUTION:

For the foundation, $2L' = 6$ m, so $L' = 3$

$2B' = 2$ m, so $B' = 1$

$A = (2L')(2B') = (6)(2) = 12 \text{ m}^2$

Calculation of $c_{z(d)}$.:

$$\omega = 2\pi f = (2)(\pi)\left(\frac{180}{60}\right) = 18.85 \text{ rad/s}$$

$$a_0 = \frac{\omega B'}{v_s} = \frac{\omega B'}{\sqrt{\frac{G}{\rho}}} = \frac{(18.85)(1)}{\sqrt{\frac{20{,}700}{\frac{18.5}{9.81}}}} \approx 0.18$$

From Figure 5.33, for $a_0 = 0.18$ and $L'/B' = 3$, the value of $c_z/(\rho v_{La} A)$ is about 1.1.

$$v_{La} = \frac{3.4}{\pi(1-\mu)}\sqrt{\frac{G}{\rho}} = \frac{3.4}{\pi(1-0.4)}\sqrt{\frac{20{,}700}{\left(\frac{18.5}{9.81}\right)}} = 188.98 \text{ m/s}$$

Hence,

$$c_z = (1.1)\rho v_{La} A = (1.1)\left(\frac{18.5}{9.81}\right)(188.98)(12) = 4704.3 \text{ kN}\cdot\text{s/m}$$

$$k_z = \frac{2L'G}{1-\mu} = \frac{(2)(3)(20{,}700 \text{ kPa})}{1-0.4} = 207{,}000 \text{ kN/m}$$

$$\frac{A}{4L'^2} = \frac{12}{(4)(3)^2} = 0.333\ (> 0.02)$$

Copyright 2017 Cengage Learning. All Rights Reserved. May not be copied, scanned, or duplicated, in whole or in part. Due to electronic rights, some third party content may be suppressed from the eBook and/or eChapter(s). Editorial review has deemed that any suppressed content does not materially affect the overall learning experience. Cengage Learning reserves the right to remove additional content at any time if subsequent rights restrictions require it.

Hence,

$$S_z = 0.73 + 1.54\left(\frac{A}{4L'^2}\right)^{0.75} = 0.73 + 1.54(0.333)^{0.75} = 1.405$$

$$c_{z(d)} = c_z + \frac{2S_z k_z}{\omega} D = 4704.3 + \frac{(2)(1.405)(207{,}000)(0.05)}{18.85} \approx \mathbf{6247\ kN \cdot s/m}$$

Calculation of $k_{z(d)}$:

$$k_{z(d)} = S_z k_z \alpha_z - \omega c_z D$$

From Figure 5.32, for $a_0 = 0.18$, $L'/B' = 3$ and $\mu = 0.4$, the value of α_z is about 1. So,

$$k_{z(d)} = (1.405)(207{,}000)(1) - (18.85)(4704.3)(0.05) = \mathbf{286{,}481\ kN/m}$$

Note: In Example 5.1, we used k_z [not $k_{z(d)}$] and c_z [not $c_{z(d)}$] in Eq. (5.22) with

$$k_z = \frac{4Gr_0}{1-\mu} = \frac{(4)(20{,}700)(1.954)}{1-0.4} = 269{,}652\ \text{kN/m}$$

$$c_z = \frac{3.4r_0^2}{1-\mu}\sqrt{G\rho} = \frac{(3.4)(1.954)^2}{1-0.4}\sqrt{(20{,}700)\left(\frac{18.5}{9.82}\right)} = 4274.8\ \text{kN} \cdot \text{s/m}$$

b. ***Rocking Vibration***

Table 5.3 gives the relationships for $k = k_\theta$, $S = S_\theta$, and $c = c_\theta$. For the variation of $\alpha = \alpha_\theta$, refer to Figure 5.34.

Table 5.3 Variation of k_θ, S_θ, and c_θ

Parameter	Relationship
General shape—rocking about *x* axis	
$k_\theta = k_{\theta x}$	$\frac{G}{1-\mu} I_x^{0.75}$
$S_\theta = S_{\theta x}$	$\frac{2.54}{\left(\frac{B'}{L'}\right)^{0.25}}\left(\text{for } \frac{B'}{L'} < 0.4\right);\quad 3.2\left(\text{for } \frac{B'}{L'} > 0.4\right)$
Circle—rocking about *x* axis	
$S_{\theta x} k_{\theta x}$	$\frac{8GB'^3}{3(1-\mu)}$
$c_\theta = c_{\theta x}$	See Figure 5.35. At high frequency, $c_{\theta x} = \frac{3.4}{\pi(1-\mu)}\rho\sqrt{\frac{G}{\rho}} I_x$

(*Continued*)

Copyright 2017 Cengage Learning. All Rights Reserved. May not be copied, scanned, or duplicated, in whole or in part. Due to electronic rights, some third party content may be suppressed from the eBook and/or eChapter(s). Editorial review has deemed that any suppressed content does not materially affect the overall learning experience. Cengage Learning reserves the right to remove additional content at any time if subsequent rights restrictions require it.

General shape—rocking about y axis	
$k_\theta = k_{\theta y}$	$\frac{G}{1-\mu}(I_y)^{0.75}$
$S_\theta = S_{\theta y}$	3.2
Circle—rocking about y axis	
$S_{\theta y} k_{\theta y}$	$\frac{8GB'^3}{3(1-\mu)}$
$c_\theta = c_{\theta y}$	See Figure 5.35. At high frequency, $c_{\theta y} = \frac{3.4}{\pi(1-\mu)}\rho\sqrt{\frac{G}{\rho}}I_y$

It is important to recognize that, for rectangular foundations (Figure 5.31b), $I_x = 1.333L'B'^3$ and $I_y = 1.333B'L'^3$. When the circumscribed dimensions (Figure 5.31a) are not completely filled in, it is necessary to compute I_x and I_y. Hence, from Eqs. (5.75) and (5.76),

$$k_{\theta x(d)} = S_{\theta x} k_{\theta x} \alpha_{\theta x} - \omega c_{\theta x} D \tag{5.79}$$

$$c_{\theta x(d)} = c_{\theta x} + \frac{2S_{\theta x} k_{\theta x}}{\omega} D \tag{5.80}$$

and

$$k_{\theta y(d)} = S_{\theta y} k_{\theta y} \alpha_{\theta y} - \omega c_{\theta y} D \tag{5.81}$$

$$c_{\theta y(d)} = c_{\theta y} + \frac{2S_{\theta y} k_{\theta y}}{\omega} D \tag{5.82}$$

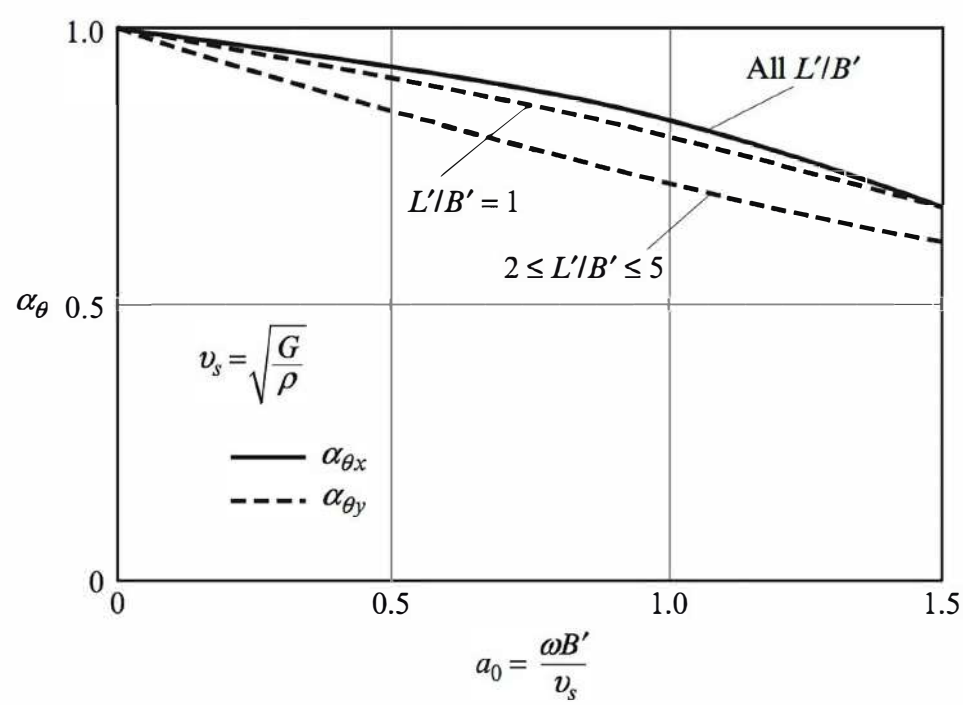

Figure 5.34 Variation of $\alpha_{\theta x}$ and $\alpha_{\theta y}$ with $a_0 = \frac{\omega B'}{v_s}$ (adapted from Dobry and Gazetas, 1986)

Source: Based on Dobry, R., and Gazetas, G. (1986). "Dynamic Response of Arbitrarily Shaped Foundations," *Journal of the Geotechnical Engineering Division,* ASCE, Vol. 112, No. GT2, pp. 109–135.

Copyright 2017 Cengage Learning. All Rights Reserved. May not be copied, scanned, or duplicated, in whole or in part. Due to electronic rights, some third party content may be suppressed from the eBook and/or eChapter(s). Editorial review has deemed that any suppressed content does not materially affect the overall learning experience. Cengage Learning reserves the right to remove additional content at any time if subsequent rights restrictions require it.

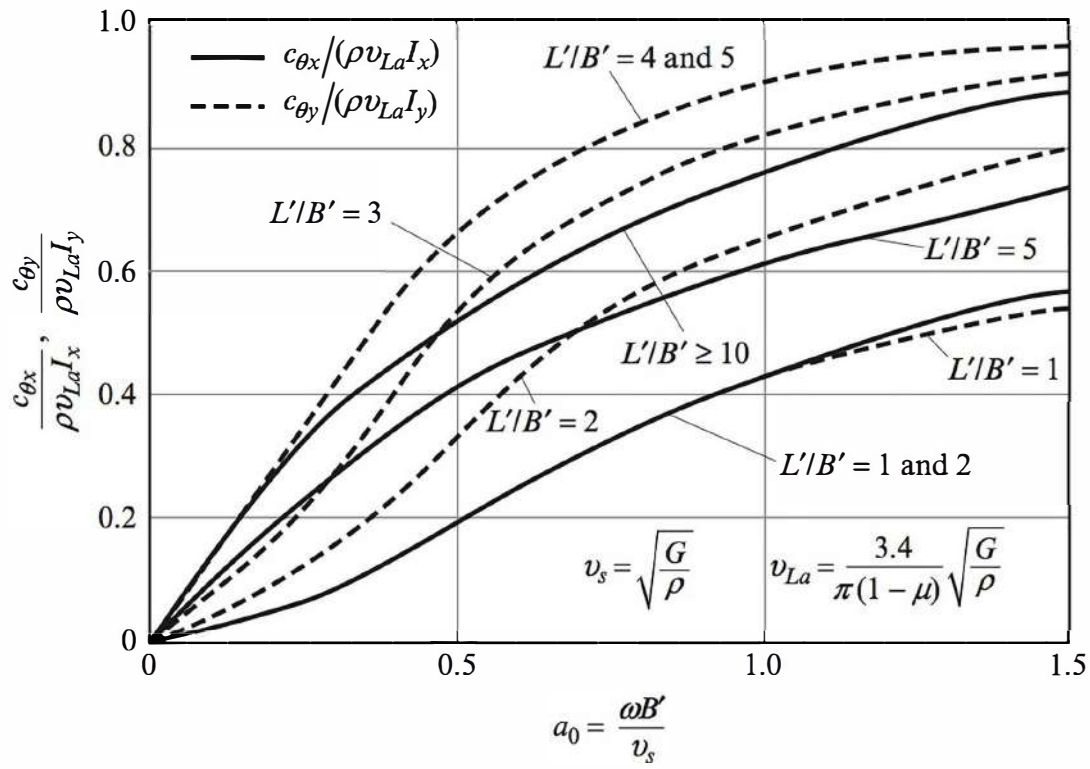

Figure 5.35 Variation of $\dfrac{c_{\theta x}}{\rho \upsilon_{La} I_x}$ and $\dfrac{c_{\theta y}}{\rho \upsilon_{La} I_y}$ with $a_0 = \dfrac{\omega B'}{\upsilon_s}$ (adapted from Dobry and Gazetas, 1986)

Source: Based on Dobry, R., and Gazetas, G. (1986). "Dynamic Response of Arbitrarily Shaped Foundations," *Journal of the Geotechnical Engineering Division,* ASCE, Vol. 112, No. GT2, pp. 109–135.

EXAMPLE 5.6

Refer to Example 5.3. Estimate the value of $k_{\theta(d)}$ and $c_{\theta(d)}$ for the mode of vibration shown. Use $D = 0.05$.

SOLUTION:

Refer to Figure 5.19. For this case, $L' = 4$ m and $B' = 3$ m. With reference to directions of the x and y axes shown in Figure 5.30 and the mode of vibration shown in Figure 5.19, the foundation is rocking about the x axis.

Calculation of $c_{\theta x(d)}$:

$$\omega = 2\pi f = 2\pi\left(\frac{600}{60}\right) = 62.83 \text{ rad/s}$$

$$\gamma = \frac{1800 \times 9.81}{1000} = 17.66 \text{ kN/m}^3$$

$$a_0 = \frac{\omega B'}{\upsilon_s} = \frac{\omega B'}{\sqrt{\dfrac{G}{\rho}}} = \frac{(62.83)(3)}{\sqrt{\dfrac{18{,}000}{\left(\dfrac{17.66}{9.81}\right)}}} = 1.885$$

Copyright 2017 Cengage Learning. All Rights Reserved. May not be copied, scanned, or duplicated, in whole or in part. Due to electronic rights, some third party content may be suppressed from the eBook and/or eChapter(s). Editorial review has deemed that any suppressed content does not materially affect the overall learning experience. Cengage Learning reserves the right to remove additional content at any time if subsequent rights restrictions require it.

From Figure 5.35, for $a_0 = 0.1885$ and $L'/B' = 4/3 = 1.33$, the value of $c_{\theta x}/(\rho v_{La} I_x) \approx 0.5$

$$v_{La} = \frac{3.4}{\pi(1-\mu)}\sqrt{\frac{G}{\rho}} = \left[\frac{3.4}{\pi(1-0.35)}\right]\sqrt{\frac{18{,}000}{\left(\frac{17.66}{9.81}\right)}} = 166.49 \text{ m/s}$$

So,

$$c_{\theta x} = (0.5)\left(\frac{17.66}{9.81}\right)(166.49)(143.96) = 21{,}564.6 \text{ kN}\cdot\text{s/m}$$

$$k_{\theta x} = \frac{G}{1-\mu} I_x^{0.75}$$

$$I_x = 1.333L'B'^3 = (1.333)(4)(3)^3 = 143.96 \text{ m}^4;\ S_{\theta x} = 3.2$$

$$k_{\theta x} = \frac{18{,}000}{1-0.35}(143.96)^{0.75} = 1{,}150{,}908 \text{ kN}\cdot\text{m/rad}$$

From Eq. (5.80),

$$c_{\theta x(d)} = c_{\theta x} + \frac{(2)(3.2)(1{,}150{,}908)k_{\theta x}}{\omega} D$$

$$= 21{,}564.6 + \frac{(2)(3.2)(1{,}150{,}908)(0.05)}{62.83} = \mathbf{27{,}426.3\ kN\cdot s/rad}$$

Calculation of $k_{\theta x(d)}$: From Eq. (5.79),

$$k_{\theta x(d)} = S_{\theta x} k_{\theta x} \alpha_{\theta x} - \omega\, c_{\theta x}\, D$$

From Figure 5.34 by extrapolation (for $a_0 = 1.885$), $\alpha_{\theta x} \approx 0.7$.

$$k_{\theta x(d)} = (3.2)(1{,}150{,}908)(0.7) - (62.83)(21{,}564.6)(0.05) = \mathbf{2{,}510{,}289\ kN\cdot m/rad}$$

c. *Sliding Vibration*

Table 5.4 gives the relationships for $k = k_s$, $S = S_s$, and $c = c_s$. For the variation of $\alpha = \alpha_{sy}$, refer to Figure 5.36. Also note that $\alpha = \alpha_{sx} = 1$.

Table 5.4 Variation of k_s, S_s, and c_s

Parameter	Relationship
General shape—sliding parallel to *y* axis	
$k_s = k_{sy}$	$\frac{2L'G}{2-\mu}$
$S_s = S_{sy}$	$2.24 \quad \left(\text{for } \frac{A}{4L'^2} < 0.4\right)$

Copyright 2017 Cengage Learning. All Rights Reserved. May not be copied, scanned, or duplicated, in whole or in part. Due to electronic rights, some third party content may be suppressed from the eBook and/or eChapter(s). Editorial review has deemed that any suppressed content does not materially affect the overall learning experience. Cengage Learning reserves the right to remove additional content at any time if subsequent rights restrictions require it.

	$4.5\left(\frac{A}{4L'^2}\right)^{0.38}$ $\left(\text{for } \frac{A}{4L'^2} > 0.16\right)$
Circle—sliding parallel to *y* axis	
$S_{sy}k_{sy}$	$\frac{8GB'}{2-\mu}$
$c_s = c_{sy}$	See Figure 5.37. At high frequency, $c_{sy} = \rho\sqrt{\frac{G}{\rho}}A$
General shape—sliding parallel to *x* axis	
$S_{sx}k_{sx}$	$S_{sy}k_{sy} - \frac{0.21L'G}{0.75-\mu}\left(1-\frac{B'}{L'}\right)$
Circle—sliding parallel to *y* axis	
$S_{sx}k_{sx}$	$\frac{8GB'}{2-\mu}$
$c_s = c_{sx}$	For $\frac{L'}{B'} < 3$, see Figure 5.38 For $\frac{L'}{B'} > 3$, $c_{sx} = \rho\sqrt{\frac{G}{\rho}}A$

Hence, from Eqs. (5.75) and (5.76),

$$k_{sy(d)} = S_{sy}k_{sy}\alpha_{sy} - \omega c_{sy} D \tag{5.83}$$

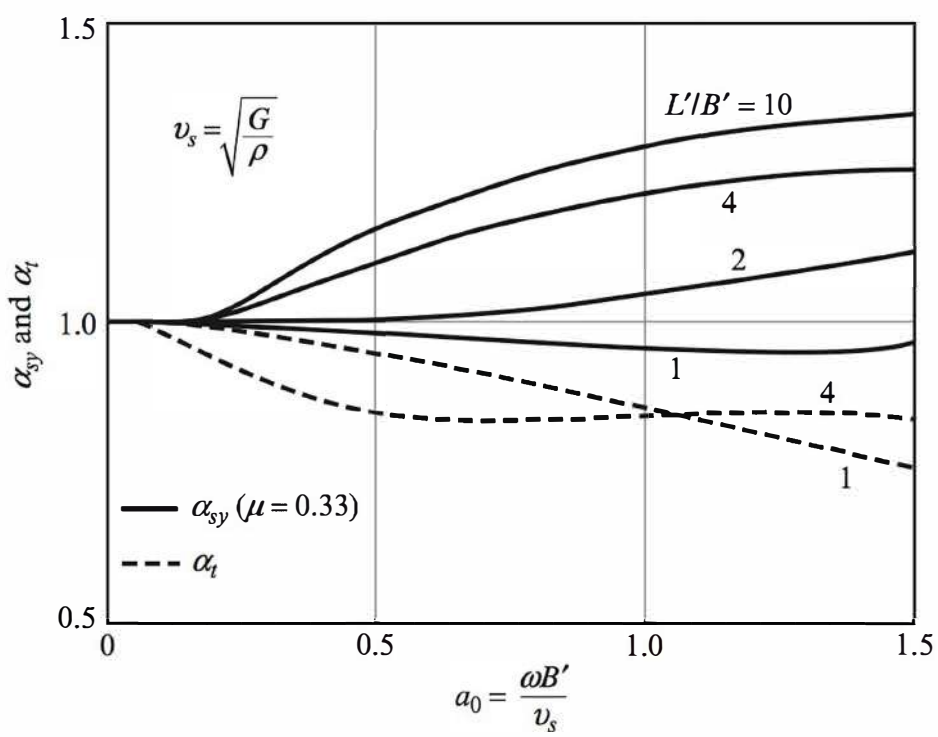

Figure 5.36 Variation of α_{sy} and α_t, with $a_0 = \frac{\omega B'}{v_s}$ (adapted from Dobry and Gazetas, 1986)

Source: Based on Dobry, R., and Gazetas, G. (1986). "Dynamic Response of Arbitrarily Shaped Foundations," *Journal of the Geotechnical Engineering Division,* ASCE, Vol. 112, No. GT2, pp. 109–135.

Copyright 2017 Cengage Learning. All Rights Reserved. May not be copied, scanned, or duplicated, in whole or in part. Due to electronic rights, some third party content may be suppressed from the eBook and/or eChapter(s). Editorial review has deemed that any suppressed content does not materially affect the overall learning experience. Cengage Learning reserves the right to remove additional content at any time if subsequent rights restrictions require it.

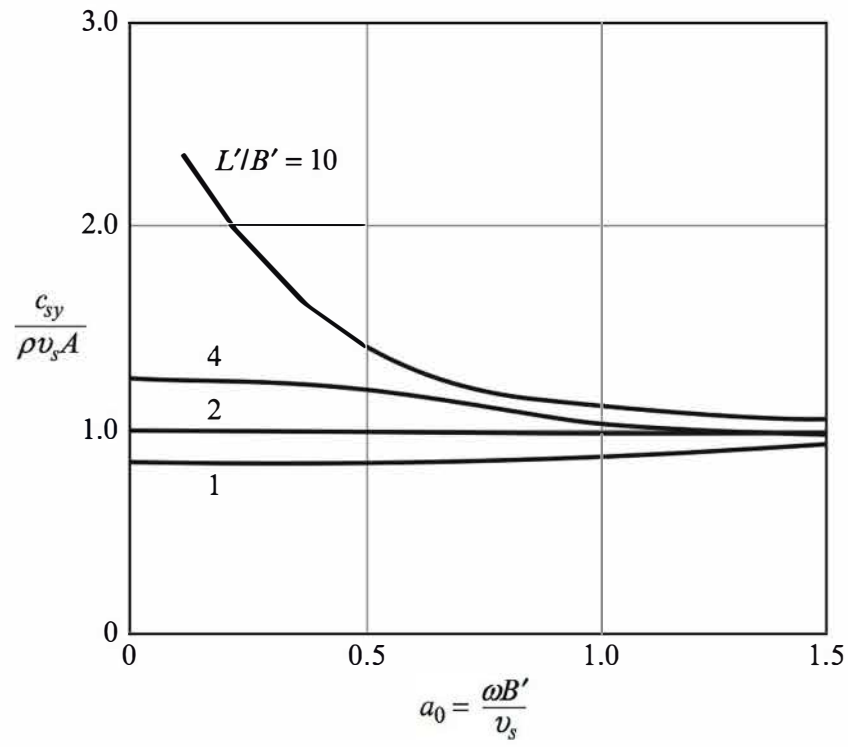

Figure 5.37 Variation of $\frac{c_{sy}}{\rho v_s A}$ with $a_0 = \frac{\omega B'}{v_s}$ (adapted from Dobry and Gazetas, 1986)

Source: Based on Dobry, R., and Gazetas, G. (1986). "Dynamic Response of Arbitrarily Shaped Foundations," *Journal of the Geotechnical Engineering Division,* ASCE, Vol. 112, No. GT2, pp. 109–135.

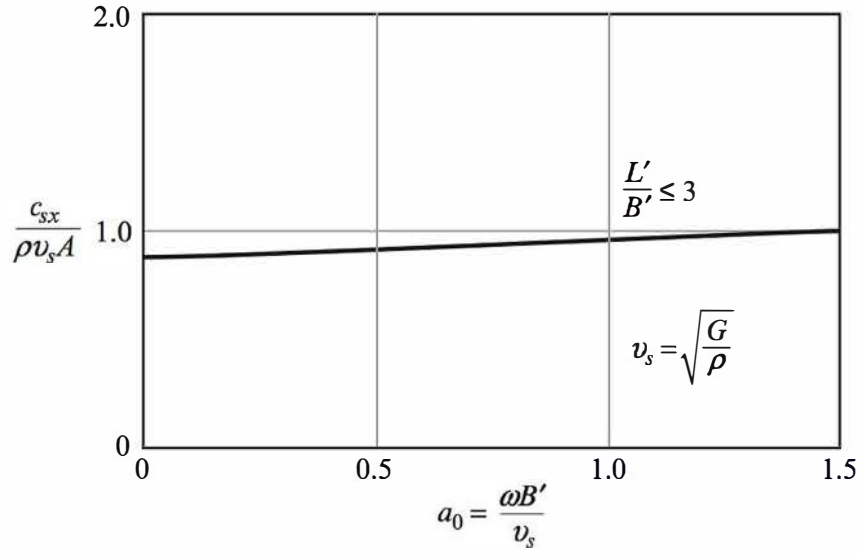

Figure 5.38 Variation of $\frac{c_{sx}}{\rho v_s A}$ with $a_0 = \frac{\omega B'}{v_s}$ for $\frac{L'}{B'} \leq 3$ (adapted from Dobry and Gazetas, 1986)

Source: Based on Dobry, R., and Gazetas, G. (1986). "Dynamic Response of Arbitrarily Shaped Foundations," *Journal of the Geotechnical Engineering Division,* ASCE, Vol. 112, No. GT2, pp. 109–135.

$$c_{sy(d)} = c_{sy} + \frac{2S_{sy}k_{sy}}{\omega} D \tag{5.84}$$

$$k_{sx(d)} = S_{sx}k_{sx} - \omega c_{sx} D \tag{5.85}$$

(*Note*: $\alpha_{sx} = 1$.)

$$c_{sx(d)} = c_{sx} + \frac{2S_{sx}k_{sx}}{\omega} D \tag{5.86}$$

Copyright 2017 Cengage Learning. All Rights Reserved. May not be copied, scanned, or duplicated, in whole or in part. Due to electronic rights, some third party content may be suppressed from the eBook and/or eChapter(s). Editorial review has deemed that any suppressed content does not materially affect the overall learning experience. Cengage Learning reserves the right to remove additional content at any time if subsequent rights restrictions require it.

EXAMPLE 5.7

Consider a foundation rectangular in plan measuring 8 m × 4 m. Given for the soil supporting the foundation,

$$G = 18{,}000 \text{ kPa}$$
$$\gamma = 18 \text{ kN/m}^3$$
$$\mu = 0.333$$

The foundation is subjected to sliding vibration parallel to the y axis (see Figure 5.31 for the direction of the axes). The frequency of vibration is 400 cpm. Estimate the values of $c_{sy(d)}$ and $k_{sy(d)}$. Use $D = 0.04$.

SOLUTION:

Calculation of $c_{sy(d)}$:

$$\omega = 2\pi f = 2\pi\left(\frac{400}{60}\right) = 41.89 \text{ rad/s}$$

$B' = 4/2 = 2$ m; $L' = 8/2 = 4$ m

$$a_0 = \frac{\omega B'}{v_s} = \frac{\omega B'}{\sqrt{\dfrac{G}{\rho}}} = \frac{(41.89)(2)}{\sqrt{\dfrac{18{,}000}{\left(\dfrac{18}{9.81}\right)}}} = 0.846$$

From Figure 5.37, for $L'/B' = 4/2 = 2$ and $a_0 = 0.84$, the value of $c_{sy}/(\rho\, v_s A) \approx 1$. So,

$$c_{sy} = \rho v_s A = \left(\frac{18}{9.81}\right)\sqrt{\frac{18{,}000}{\left(\dfrac{18}{9.81}\right)}}(8 \times 4) = 5815.5 \text{ kN} \cdot \text{s/m}$$

$$k_{sy} = \frac{2L'G}{2-\mu} = \frac{(2)(4)(18{,}000)}{2-0.333} = 86{,}382.7 \text{ kN/m}$$

$$\frac{A}{4L'^2} = \frac{(2)(4)}{(4)(4)^2} = 0.125$$

So, $S_{sy} = 2.24$. From Eq. (5.84),

$$c_{sy(d)} = c_{sy} + \frac{2S_{sy}k_{sy}}{\omega}D = 5815.5 + \frac{(2)(2.24)(86{,}382.7)}{41.89}(0.04)$$
$$= \mathbf{6185 \text{ kN} \cdot \text{s/m}}$$

Calculation of $k_{sy(d)}$: From Eq. (5.83),

$$k_{sy(d)} = S_{sy}k_{sy}\alpha_{sy} - \omega\, c_{sy}\, D$$

Copyright 2017 Cengage Learning. All Rights Reserved. May not be copied, scanned, or duplicated, in whole or in part. Due to electronic rights, some third party content may be suppressed from the eBook and/or eChapter(s). Editorial review has deemed that any suppressed content does not materially affect the overall learning experience. Cengage Learning reserves the right to remove additional content at any time if subsequent rights restrictions require it.

For $L'/B' = 4/2 = 2$ and $a_0 = 0.846$, the value of $\alpha_{sy} \approx 1.04$ (Figure 5.36).

$$k_{sy(d)} = (2.24)(86{,}382.7)(1.04) - (41.89)(5815.5)(0.04) = \mathbf{191{,}493\ kN/m}$$

d. *Torsional Vibration*

Table 5.5 gives the relationships for $k = k_t$, $S = S_t$ and $c = c_t$. For the variation of $\alpha = \alpha_t$, refer to Figure 5.36.

Table 5.5 Variation of k_t, S_t and c_t

Parameter	Relationship
General shape	
k_t	$G(J)^{0.75}$
S_t	$3.8 + 10.7\left(1 - \frac{B'}{L'}\right)^{10}$
Circle	
$S_t k_t$	$\frac{16GB'^3}{3}$
c_t	See Figure 5.39. At high frequency, $c_t = \rho\sqrt{\frac{G}{\rho}}J$ $(J = I_x + I_y)$

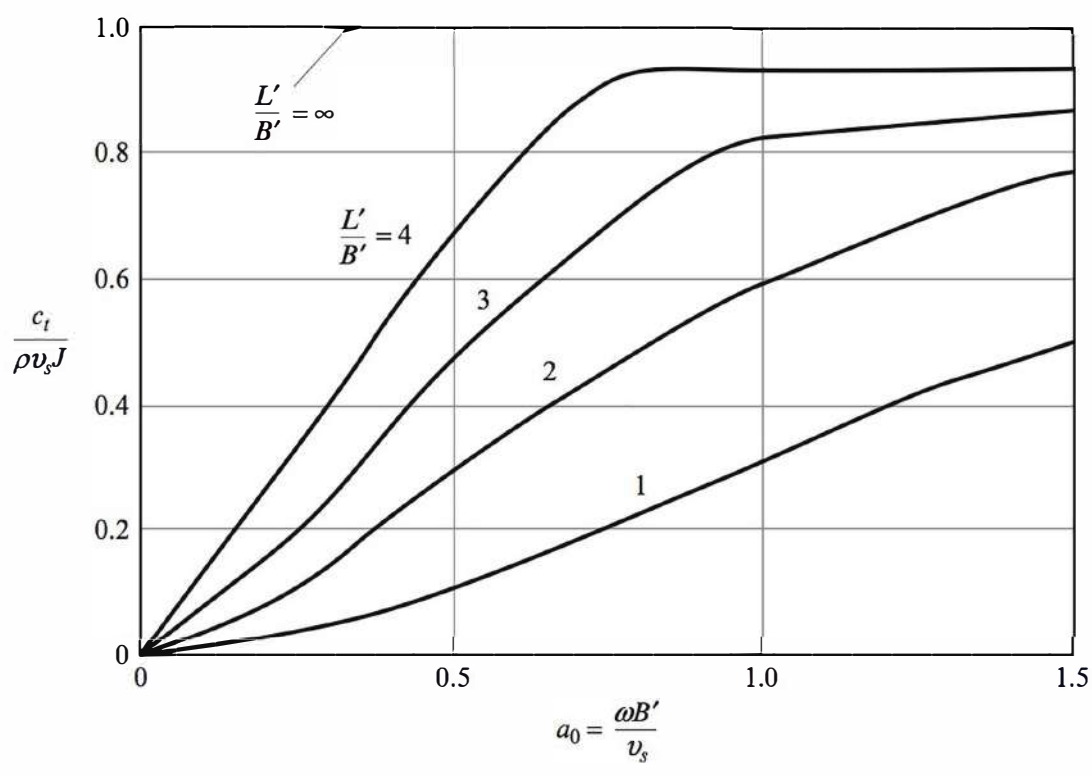

Figure 5.39 Variation of $\frac{c_t}{\rho v_s J}$ with $a_0 = \frac{\omega B'}{v_s}$ (adapted from Dobry and Gazetas, 1986)

Source: Based on Dobry, R., and Gazetas, G. (1986). "Dynamic Response of Arbitrarily Shaped Foundations," *Journal of the Geotechnical Engineering Division,* ASCE, Vol. 112, No. GT2, pp. 109–135.

Copyright 2017 Cengage Learning. All Rights Reserved. May not be copied, scanned, or duplicated, in whole or in part. Due to electronic rights, some third party content may be suppressed from the eBook and/or eChapter(s). Editorial review has deemed that any suppressed content does not materially affect the overall learning experience. Cengage Learning reserves the right to remove additional content at any time if subsequent rights restrictions require it.

Hence, from Eqs. (5.75) and (5.76),

$$k_{t(d)} = S_t k_t \alpha_t - \omega c_t D \tag{5.87}$$

and

$$c_{t(d)} = c_t + \frac{2S_t k_t}{\omega} D \tag{5.88}$$

5.11 COUPLED ROCKING AND SLIDING VIBRATION OF RIGID CIRCULAR FOUNDATIONS

In several cases of machine foundations, the rocking and sliding vibrations are coupled. This is because the center of gravity of the foundation and vibrators are not coincident with the center of sliding resistance, as can be seen from Figure 5.40a. This is a case of vibration of a foundation with two degrees of freedom. The derivation given next for the coupled motion for rocking and sliding is based on the analysis of Richart and Whitman (1967). From Figure 5.40, it can be seen that the nature of foundation motion shown in Figure 5.40a is equal to sum of the sliding motion shown in Figure 5.40b and the rocking motion shown in Figure 5.40c. Note that

$$x_b = x_g - h'\theta \tag{5.89}$$

For the sliding motion,

$$m\ddot{x}_g = P \tag{5.90}$$

where P = horizontal resistance to sliding

$$= -c_x \frac{dx_b}{dt} - k_x x_b \tag{5.91}$$

Substitution of Eq. (5.89) into (5.91) yields

$$\begin{aligned} P &= -c_x \frac{d}{dt}(x_g - h'\theta) - k_x(x_g - h'\theta) \\ &= -c_x \dot{x}_g + c_x h'\dot{\theta} - k_x x_g + k_x h'\theta \end{aligned} \tag{5.92}$$

Now, combining Eqs. (5.90) and (5.92)

$$\boxed{m\ddot{x}_g + c_x \dot{x}_g + k_x x_g - c_x h'\theta - k_x h'\theta = 0} \tag{5.93}$$

For rocking motion about the center of gravity,

$$I_g \ddot{\theta} = M + M_r - h'P \tag{5.94}$$

where I_g = mass moment of inertia about the horizontal axis passing through the center of gravity (at right angles to the cross section shown)

Copyright 2017 Cengage Learning. All Rights Reserved. May not be copied, scanned, or duplicated, in whole or in part. Due to electronic rights, some third party content may be suppressed from the eBook and/or eChapter(s). Editorial review has deemed that any suppressed content does not materially affect the overall learning experience. Cengage Learning reserves the right to remove additional content at any time if subsequent rights restrictions require it.

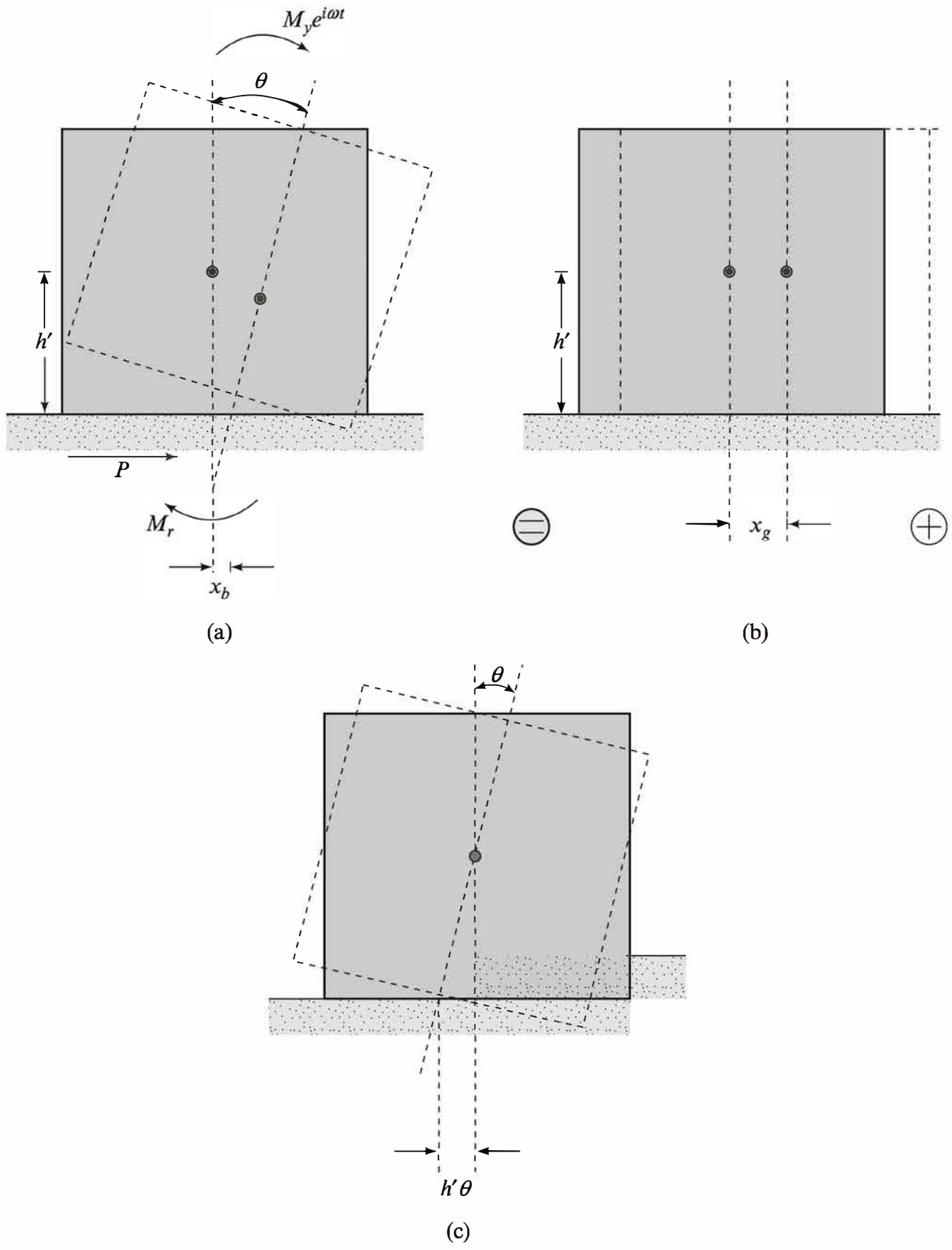

Figure 5.40 Coupled rocking and sliding vibration

$$M_r = \text{the soil resistance to rotational motion}$$

But

$$M_r = -c_\theta \dot{\theta} - k_\theta \theta \tag{5.95}$$

Substitution of Eqs. (5.92) and (5.95) into Eq. (5.94) gives

Copyright 2017 Cengage Learning. All Rights Reserved. May not be copied, scanned, or duplicated, in whole or in part. Due to electronic rights, some third party content may be suppressed from the eBook and/or eChapter(s). Editorial review has deemed that any suppressed content does not materially affect the overall learning experience. Cengage Learning reserves the right to remove additional content at any time if subsequent rights restrictions require it.

$$I_g\ddot{\theta} = M - (c_\theta\dot{\theta} + k_\theta\theta) - h'(-c_x\dot{x}_g + c_x h'\dot{\theta} - k_x x_g + k_x h'\theta)$$

or

$$I_g\ddot{\theta} + (c_\theta + c_x h'^2)\dot{\theta} + (k_\theta + k_x h'^2)\theta - h'(c_x\dot{x}_g + k_x x_g) = M = M_y e^{i\omega t} \tag{5.96}$$

For a foundation resting on an elastic half-space, the spring and dashpot coefficients are frequency dependent. They need to be calculated first for a given frequency before Eqs. (5.93) and (5.96) can be solved. However, if they are assumed to be frequency independent, as in the case of analog solutions, Eqs. (5.93) and (5.96) can be easily solved. For that case, for determination of the damped natural frequency, one can make M in Eq. (5.96) equal zero. So

$$I_g\ddot{\theta} + (c_\theta + c_x h'^2)\dot{\theta} + (k_\theta + k_x h'^2)\theta - h'(c_x\dot{x}_g + k_x x_g) = 0 \tag{5.97}$$

For solving Eqs. (5.93) and (5.97), let

$$x_g = A_1 e^{i\omega_m t} \tag{5.98}$$

and

$$\theta = A_2 e^{i\omega_m t} \tag{5.99}$$

where ω_m = damped natural frequency.

Substituting Eqs. (5.98) and (5.99) into Eqs. (5.93) and (5.97) and rearranging, one obtains (Prakash and Puri, 1981, 1988)

$$\boxed{\begin{aligned}&\left[\omega_m^4 - \omega_m^2\left(\frac{\omega_{n\theta}^2 + \omega_{nx}^2}{\delta} - \frac{4D_\theta D_x\,\omega_{n\theta}\omega_{nx}}{\delta}\right) + \frac{\omega_{n\theta}^2\omega_{nx}^2}{\delta}\right]^2 \\ &\quad + 4\left[\frac{D_x\omega_{nx}\omega_m}{\delta}\left(\omega_{n\theta}^2 - \omega_m^2\right) + \frac{D_\theta\omega_{n\theta}\omega_m}{\delta}\left(\omega_{nx}^2 - \omega_m^2\right)\right] = 0\end{aligned}} \tag{5.100}$$

where D_x = damping ratio for sliding vibration [Eq. (5.56)]
D_θ = damping ratio for rocking vibration [Eq. (5.45)]

$$\delta = \frac{I_g}{I_0} \tag{5.101}$$

[Note: The term I_0 was defined in Eq. (5.40).]

$$\omega_{nx} = \sqrt{\frac{32(1-\mu)Gr_0}{(7-8\mu)m}} \tag{5.102}$$

$\uparrow$

[from Eq. (5.54)]

Copyright 2017 Cengage Learning. All Rights Reserved. May not be copied, scanned, or duplicated, in whole or in part. Due to electronic rights, some third party content may be suppressed from the eBook and/or eChapter(s). Editorial review has deemed that any suppressed content does not materially affect the overall learning experience. Cengage Learning reserves the right to remove additional content at any time if subsequent rights restrictions require it.

and

$$\omega_{n\theta} = \sqrt{\frac{8Gr_0^3}{3(1-\mu)I_0}} \tag{5.103}$$

↑

[from Eqs. (5.41) and (5.44)]

Equation (5.100) can then be solved to obtain two values of ω_m.

The damped amplitudes of rocking and sliding vibrations can be obtained as

$$\boxed{A_x = \left(\frac{M_y}{I_g}\right)\frac{\left[(\omega_{nx}^2)^2 + (2D_x\omega_{nx})^2\right]^{1/2}}{\Delta(\omega^2)}} \tag{5.104}$$

and

$$\boxed{A_\theta = \left(\frac{M_y}{I_g}\right)\frac{\left[(\omega_{nx}^2 - \omega^2)^2 + (2D_x\omega_{nx}\omega)^2\right]^{1/2}}{\Delta(\omega^2)}} \tag{5.105}$$

where

$$\Delta(\omega^2) = \left\{\left[\omega^4 - \omega^2\left(\frac{\omega_{n\theta}^2 + \omega_{nx}^2}{\delta} - \frac{4D_\theta D_x\omega_{n\theta}\omega_{nx}}{\delta}\right) + \frac{\omega_{n\theta}^2\omega_{nx}^2}{\delta}\right]^2 + 4\left[\frac{D_x\omega_{nx}\omega}{\delta}(\omega_{n\theta}^2 - \omega^2) + \frac{D_\theta\omega_{n\theta}\omega}{\delta}(\omega_{nx}^2 - \omega^2)\right]^2\right\}^{1/2} \tag{5.106}$$

Vibration of Embedded Foundations

In the theories for the vibration of foundations in various modes, as developed in Sections 5.2 through 5.10, it was assumed that the foundation rests on the ground surface. In reality, however, all foundations are constructed below the ground surface. For an embedded foundation, soil resistance is mobilized at its base and also along its sides. A limited number of theories have so far been developed for the dynamic response of embedded block foundations. The findings from these studies are summarized in the following four sections.

5.12 VERTICAL VIBRATION OF RIGID CYLINDRICAL FOUNDATIONS

The dynamic response of vertically vibrating rigid cylindrical foundations (Figure 5.41) has been studied by Novak and Beredugo (1972). The foundation shown in Figure 5.41 has a radius of r_0. The shear modulus and the density of

Copyright 2017 Cengage Learning. All Rights Reserved. May not be copied, scanned, or duplicated, in whole or in part. Due to electronic rights, some third party content may be suppressed from the eBook and/or eChapter(s). Editorial review has deemed that any suppressed content does not materially affect the overall learning experience. Cengage Learning reserves the right to remove additional content at any time if subsequent rights restrictions require it.

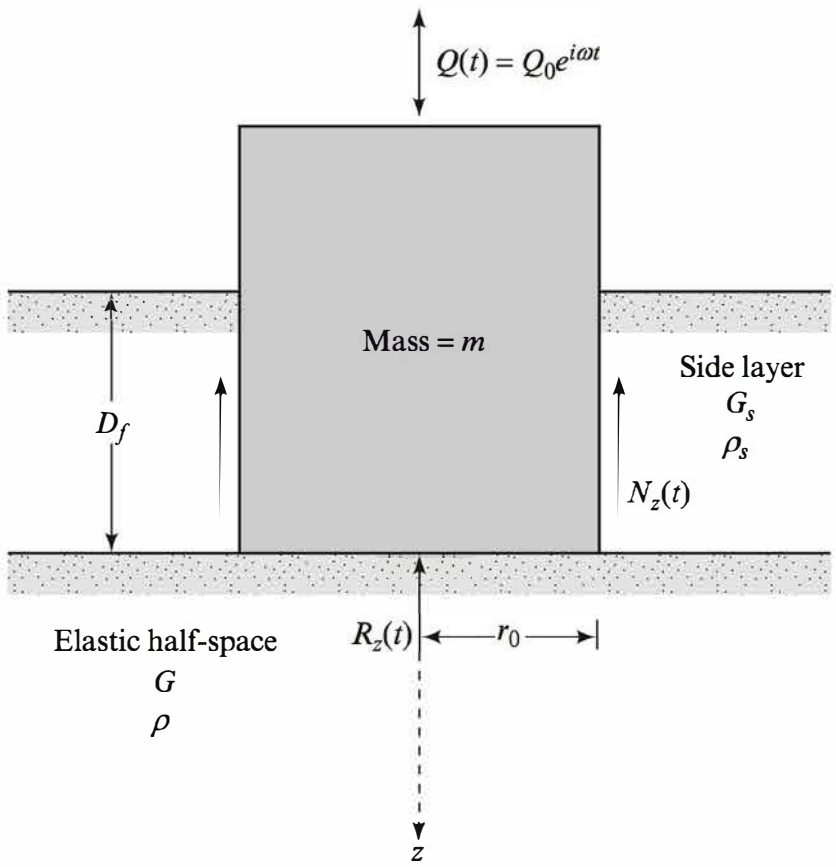

Figure 5.41 Embedded rigid cylindrical foundation—vertical vibration

the side layer of soil are G_s and ρ_s, respectively. Similarly, the shear modulus and the density of the soil beneath the foundation are, respectively, G and ρ. If the foundation is subjected to a vertical exciting force, the equation of motion may be written in the form

$$m\ddot{z}(t) = Q(t) - R_z(t) - N_z(t) \tag{5.107}$$

The dynamic reaction $R_z(t)$ is considered to be independent of the depth of embedment. Using the elastic half-space solution, the dynamic reaction can be expressed as

$$R_z(t) = Gr_0(C_1 + iC_2)z(t) \tag{5.108}$$

where

$$C_1 = \frac{-f_1'}{f_1'^2 + f_2'^2} \tag{5.109}$$

and

$$C_2 = \frac{f_2'}{f_1'^2 + f_2'^2} \tag{5.110}$$

f_1', f_2' = functions of nondimensional frequency a_0 [Eq. (5.5)], Poisson's ratio, and stress distribution at the base

Copyright 2017 Cengage Learning. All Rights Reserved. May not be copied, scanned, or duplicated, in whole or in part. Due to electronic rights, some third party content may be suppressed from the eBook and/or eChapter(s). Editorial review has deemed that any suppressed content does not materially affect the overall learning experience. Cengage Learning reserves the right to remove additional content at any time if subsequent rights restrictions require it.

The dynamic soil reaction on the sides can be obtained as

$$N_z(t) = \int_0^{D_f} s(z,t)dz \tag{5.111}$$

where s is the dynamic reaction per unit depth of embedment.

If s is considered to be independent of depth (Baranov, 1967), then $s = s(t)$, or

$$s(t) = G_s(S_1 + iS_2)z(t) \tag{5.112}$$

where

$$S_1 = 2\pi a_0 \frac{J_1(a_0)J_0(a_0) + Y_1(a_0)Y_0(a_0)}{J_0^2(a_0) + Y_0^2(a_0)} \tag{5.113a}$$

and

$$S_2 = \frac{4}{J_0^2(a_0) + Y_0^2(a_0)}. \tag{5.113b}$$

$J_0(a_0), J_1(a_0)$ = Bessel functions of the first kind of order 0 and 1, respectively

$Y_0(a_0), Y_1(a_0)$ = Bessel functions of the second kind of order 0 and 1, respectively

So

$$N_z(t) = \int_0^{D_f} G_s(S_1 + iS_2)z(t)dz = G_s D_f (S_1 + iS_2)z(t) \tag{5.114}$$

Now, combining Eqs. (5.107), (5.108), and (5.114)

$$\begin{aligned} m\ddot{z}(t) + Gr_0[C_1 + iC_2 + \frac{G_s}{G}\frac{D_f}{r_0}(S_1 + iS_2)]z(t) \\ = Q(t) = Q_0 e^{i\omega t} = Q_0(\cos\omega t + i\sin\omega t) \end{aligned} \tag{5.115}$$

The steady-state response is

$$z(t) = z e^{i\omega t} \tag{5.116}$$

In the preceding two equations, Q_0 and z are, respectively, the real force amplitudes and real response. The relationships for the spring constant and the damping coefficient can thus be derived as

$$k_z = Gr_0\left(C_1 + \frac{G_s}{G}\frac{D_f}{r_0}S_1\right) \tag{5.117}$$

$$c_z = \frac{Gr_0}{\omega}\left(C_2 + \frac{G_s}{G}\frac{D_f}{r_0}S_2\right) \tag{5.118}$$

Copyright 2017 Cengage Learning. All Rights Reserved. May not be copied, scanned, or duplicated, in whole or in part. Due to electronic rights, some third party content may be suppressed from the eBook and/or eChapter(s). Editorial review has deemed that any suppressed content does not materially affect the overall learning experience. Cengage Learning reserves the right to remove additional content at any time if subsequent rights restrictions require it.

Note that k_z and c_z, as expressed by the two preceding relationships, are frequency dependent. However, without losing much accuracy, one can assume that

$$C_1 = \bar{C}_1 = \text{constant}$$
$$S_1 = \bar{S}_1 = \text{constant}$$
$$C_2 = a_0\bar{C}_2 (\text{where } \bar{C}_2 \text{ is a constant})$$
$$S_2 = a_0\bar{S}_2 (\text{where } \bar{S}_2 \text{ is a constant})$$

When the preceding assumptions are substituted into Eqs. (5.117) and (5.118), one obtains the frequency-independent k_z and c_z as follows:

$$\boxed{k_z = Gr_0\left(\bar{C}_1 + \frac{G_s}{G}\frac{D_f}{r_0}\bar{S}_1\right)} \tag{5.119}$$

$$\boxed{c_z = r_0^2\sqrt{\rho G}\left(\bar{C}_2 + \bar{S}_2\frac{D_f}{r_0}\sqrt{\frac{G_s\rho_s}{G\rho}}\right)} \tag{5.120}$$

Hence, the damping ratio can be given as

$$\boxed{D_z = \left(\frac{1}{2\sqrt{b}}\right)\frac{\left(\bar{C}_2 + \bar{S}_2\frac{D_f}{r_0}\sqrt{\frac{G_s\rho_s}{G\rho}}\right)}{\sqrt{\bar{C}_1 + \frac{G_s}{G}\frac{D_f}{r_0}\bar{S}_1}}} \tag{5.121}$$

where $b = \text{mass ratio} = \dfrac{m}{\rho r_0^3}$ [Eq. (5.4)]

The values of $\bar{C}_1, \bar{C}_2, \bar{S}_1$, and $\bar{S}_2$ (Novak and Beredugo, 1972) are given in Table 5.6.

Table 5.6 Values of $\bar{C}_1, \bar{C}_2, \bar{S}_1$, and $\bar{S}_2$

Poisson's ratio, μ	$\bar{C}_1^a$	$\bar{C}_2^a$	$\bar{S}_1^b$	$\bar{S}_2^b$
0.0	3.9	3.5	2.7	6.7
0.25	5.2	5.0	2.7	6.7
0.5	7.5	6.8	2.7	6.7

[a] Validity range: $0 \le a_0 \le 1.5$
[b] Validity range: $0 \le a_0 \le 2$

Once the spring constant, dashpot coefficient, and the damping ratio are determined, the foundation response (natural frequency, amplitude of vibration at resonance and at frequencies other than the resonance) can be calculated using the formulae given below.

Copyright 2017 Cengage Learning. All Rights Reserved. May not be copied, scanned, or duplicated, in whole or in part. Due to electronic rights, some third party content may be suppressed from the eBook and/or eChapter(s). Editorial review has deemed that any suppressed content does not materially affect the overall learning experience. Cengage Learning reserves the right to remove additional content at any time if subsequent rights restrictions require it.

Undamped natural frequency:

$$\omega_n = \sqrt{\frac{k_z}{m}}$$

$$f_n = \frac{1}{2\pi}\sqrt{\frac{k_z}{m}}$$

Amplitude of vibration at resonance:

$$A_z = \frac{Q_0}{k_z}\frac{1}{2D_z\sqrt{1-D_z^2}} \quad \text{(for constant force excitation)}$$

$$A_z = \frac{m_1 e}{m}\frac{1}{2D_z\sqrt{1-D_z^2}} \quad \text{(for rotating mass excitation)}$$

Amplitude of vibration at frequency other than resonance:

$$A_z = \frac{Q_0/k_z}{\sqrt{\left[1-\left(\omega^2/\omega_n^2\right)\right]^2 + 4D_z^2\left(\omega^2/\omega_n^2\right)}} \quad \text{(for constant force excitation)}$$

$$A_z = \frac{\left(m_1 e/m\right)\left(\omega/\omega_n\right)^2}{\sqrt{\left[1-\left(\omega^2/\omega_n^2\right)\right]^2 + 4D_z^2\left(\omega^2/\omega_n^2\right)}} \quad \text{(for rotating mass excitation)}$$

The natural frequency of the foundation-soil system increases and its amplitude of vibration decreases, if depth of embedment is taken into account.

5.13 SLIDING VIBRATION OF RIGID CYLINDRICAL FOUNDATIONS

Figure 5.42 shows an embedded rigid cylindrical foundation subjected to sliding vibration. The response of this type of system was analyzed by Beredugo and Novak (1972). The frequency-independent spring constant and dashpot coefficient suggested by them are as follows:

$$k_x = Gr_0\left(\bar{C}_{x1} + \frac{G_s}{G}\frac{D_f}{r_0}\bar{S}_{x1}\right) \tag{5.122}$$

$$c_x = r_0^2\sqrt{\rho G}\left(\bar{C}_{x2} + \bar{S}_{x2}\frac{D_f}{r_0}\sqrt{\frac{G_s\rho_s}{G\rho}}\right) \tag{5.123}$$

Copyright 2017 Cengage Learning. All Rights Reserved. May not be copied, scanned, or duplicated, in whole or in part. Due to electronic rights, some third party content may be suppressed from the eBook and/or eChapter(s). Editorial review has deemed that any suppressed content does not materially affect the overall learning experience. Cengage Learning reserves the right to remove additional content at any time if subsequent rights restrictions require it.

The variation of $\bar{C}_{x1}, \bar{C}_{x2}, \bar{S}_{x1}$, and $\bar{S}_{x2}$ as evaluated by Beredugo and Novak are as follows:

Poisson's ratio μ	Parameter	
0	$\bar{C}_{x1} = 4.3$	$\bar{C}_{x2} = 2.70$
0.5	$\bar{C}_{x1} = 5.1$	$\bar{C}_{x2} = 3.15$
0	$\bar{S}_{x1} = 3.6$	$\bar{S}_{x2} = 8.20$
0.25	$\bar{S}_{x1} = 4.0$	$\bar{S}_{x2} = 9.10$
0.4	$\bar{S}_{x1} = 4.1$	$\bar{S}_{x2} = 10.6$

The undamped frequency of vibration for this case can be given as

$$\omega_n = \sqrt{\frac{k_x}{m}}$$

and

$$f_n = \frac{1}{2\pi}\sqrt{\frac{k_x}{m}}$$

The damping ratio can be calculated as

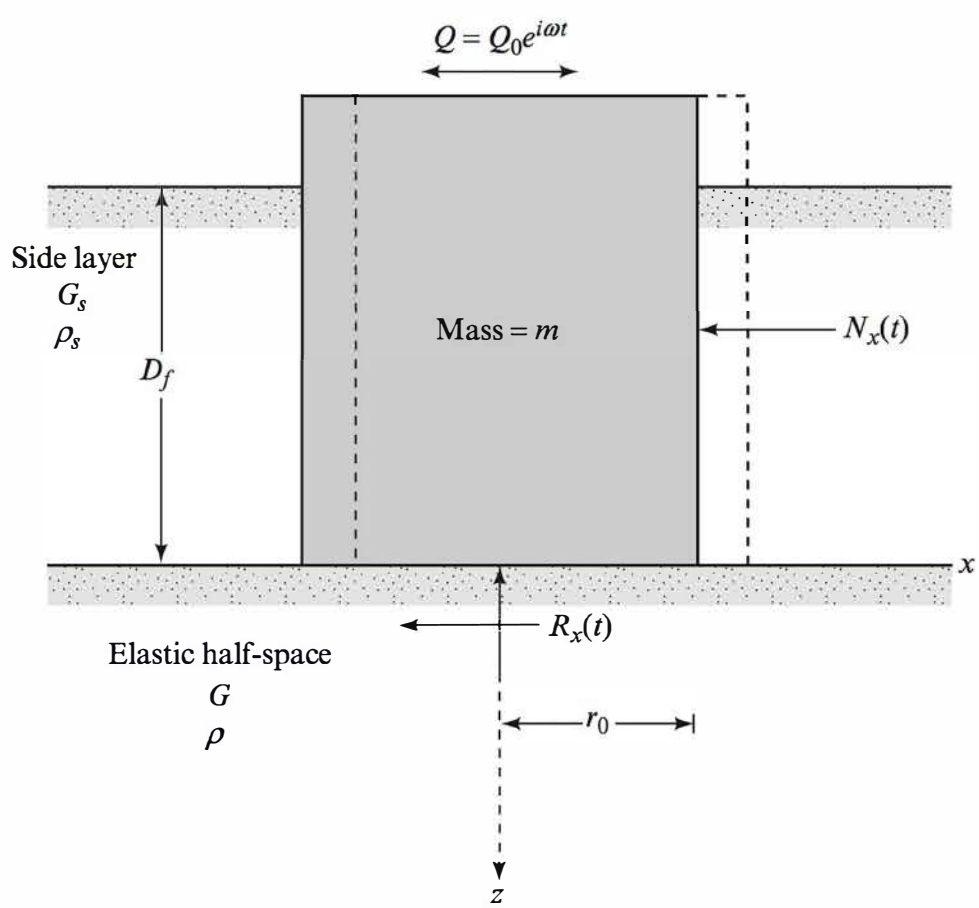

Figure 5.42 Embedded rigid cylindrical foundation—horizontal vibration

Copyright 2017 Cengage Learning. All Rights Reserved. May not be copied, scanned, or duplicated, in whole or in part. Due to electronic rights, some third party content may be suppressed from the eBook and/or eChapter(s). Editorial review has deemed that any suppressed content does not materially affect the overall learning experience. Cengage Learning reserves the right to remove additional content at any time if subsequent rights restrictions require it.

$$D_x = \frac{c_x}{2\sqrt{k_x m}}$$

Once ω_n and D_x are calculated, the amplitudes of vibration can be estimated using Eqs. (5.58), (5.59), (5.60), and (5.61).

5.14 ROCKING VIBRATION OF RIGID CYLINDRICAL FOUNDATIONS

Beredugo and Novak (1972) analyzed the problem of rocking vibration of rigid cylindrical foundations, as shown in Figure 5.43. Based on their analysis, the frequency-independent spring constant and dashpot coefficient can be given as

$$k_\theta = G r_0^3 \left[\bar{C}_{\theta 1} + \frac{G_s}{G} \frac{D_f}{r_0} \left(\bar{S}_{\theta 1} + \frac{D_f^2}{3 r_0^2} \bar{S}_{x1} \right) \right] \tag{5.124}$$

and

$$c_\theta = r_0^4 \sqrt{\rho G} \left[\bar{C}_{\theta 2} + \frac{G_s}{G} \frac{D_f}{r_0} \left(\bar{S}_{\theta 2} + \frac{D_f^2}{3 r_0^2} \bar{S}_{x2} \right) \right] \tag{5.125}$$

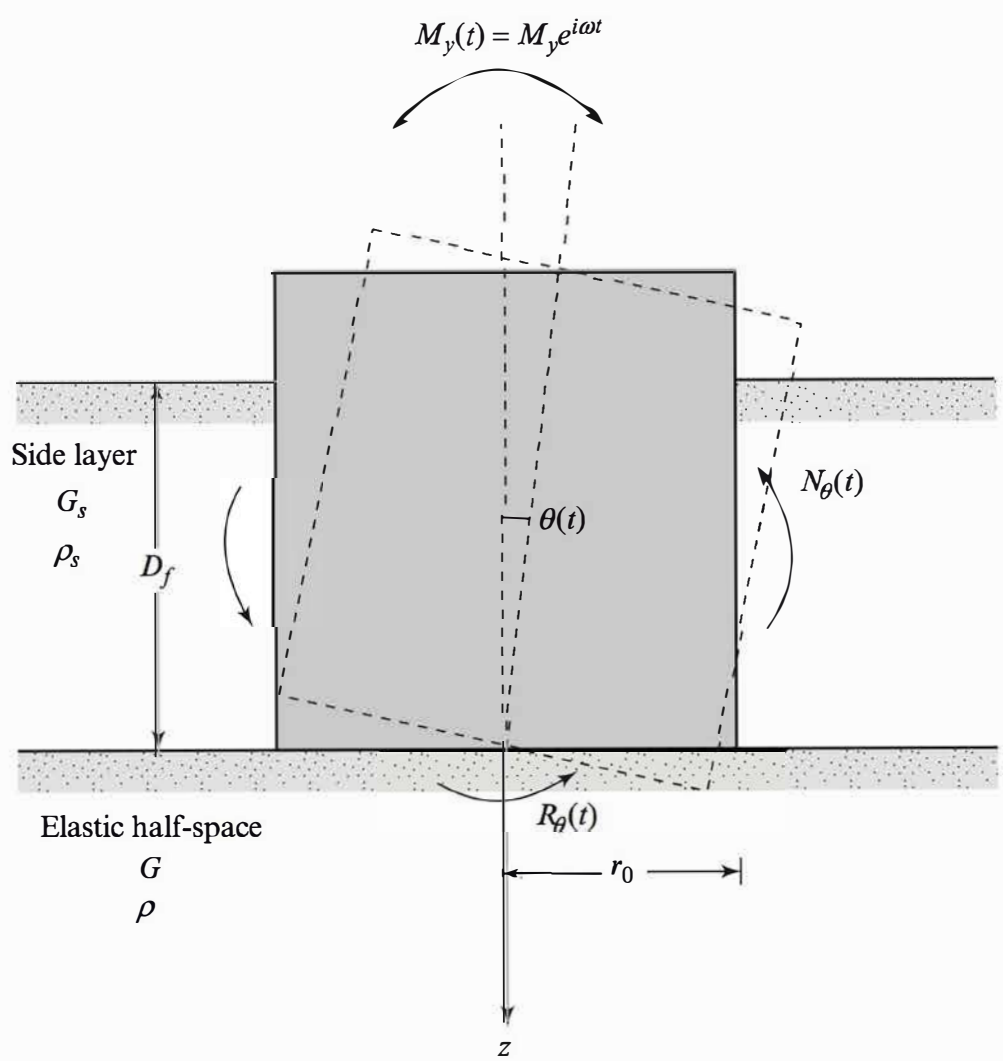

Figure 5.43 Embedded rigid cylindrical foundation—rocking vibration

Copyright 2017 Cengage Learning. All Rights Reserved. May not be copied, scanned, or duplicated, in whole or in part. Due to electronic rights, some third party content may be suppressed from the eBook and/or eChapter(s). Editorial review has deemed that any suppressed content does not materially affect the overall learning experience. Cengage Learning reserves the right to remove additional content at any time if subsequent rights restrictions require it.

For this problem, the undamped natural frequency is

$$\omega_n = \sqrt{\frac{k_\theta}{I_0}}$$

For the definition of I_0, see Eq. (5.40). The damping ratio is

$$D_\theta = \frac{c_\theta}{2\sqrt{k_\theta I_0}}$$

The amplitudes of vibration can be calculated using Eqs. (5.46), (5.47), (5.48), and (5.49).

The variation of $\bar{S}_{x1}$, and $\bar{S}_{x2}$ was given in the preceding section. For $\mu = 0$,

$$\bar{C}_{\theta 1} = 2.5 \quad \bar{C}_{\theta 2} = 0.43$$

and, for any value of μ,

$$\bar{S}_{\theta 1} = 2.5 \quad \bar{S}_{\theta 2} = 1.8$$

5.15 TORSIONAL VIBRATION OF RIGID CYLINDRICAL FOUNDATIONS

Figure 5.44 shows a rigid cylindrical foundation subjected to a torsional vibration. Novak and Sachs (1973) evaluated the frequency-independent spring constant and dashpot coefficient, and they are as follows:

$$k_\alpha = G r_0^3 \left(\bar{C}_{\alpha 1} + \frac{G_s}{G} \frac{D_f}{r_0} \bar{S}_{\alpha 1} \right) \tag{5.126a}$$

and

$$c_\alpha = r_0^4 \sqrt{\rho G} \left(\bar{C}_{\alpha 2} + \bar{S}_{\alpha 2} \frac{D_f}{r_0} \sqrt{\frac{G_s \rho_s}{G \rho}} \right) \tag{5.126b}$$

The values of the parameters $\bar{C}_{\alpha 1}, \bar{C}_{\alpha 2}, \bar{S}_{\alpha 1}$ and $\bar{S}_{\alpha 2}$ are

$$\left.\begin{aligned} \bar{C}_{\alpha 1} &= 4.3 \\ \bar{C}_{\alpha 2} &= 0.7 \end{aligned}\right\} \quad \text{for } 0 \le a_0 \le 2.0$$

$$\left.\begin{aligned} \bar{S}_{\alpha 1} &= 12.4 \\ \bar{S}_{\alpha 2} &= 2.0 \end{aligned}\right\} \quad \text{for } 0 \le a_0 \le 0.2$$

$$\left.\begin{aligned} \bar{S}_{\alpha 1} &= 10.2 \\ \bar{S}_{\alpha 2} &= 5.4 \end{aligned}\right\} \quad \text{for } 0.2 \le a_0 \le 2.0$$

Once the magnitudes of k_α and c_α are calculated, the undamped natural circular frequency can be obtained as

Copyright 2017 Cengage Learning. All Rights Reserved. May not be copied, scanned, or duplicated, in whole or in part. Due to electronic rights, some third party content may be suppressed from the eBook and/or eChapter(s). Editorial review has deemed that any suppressed content does not materially affect the overall learning experience. Cengage Learning reserves the right to remove additional content at any time if subsequent rights restrictions require it.

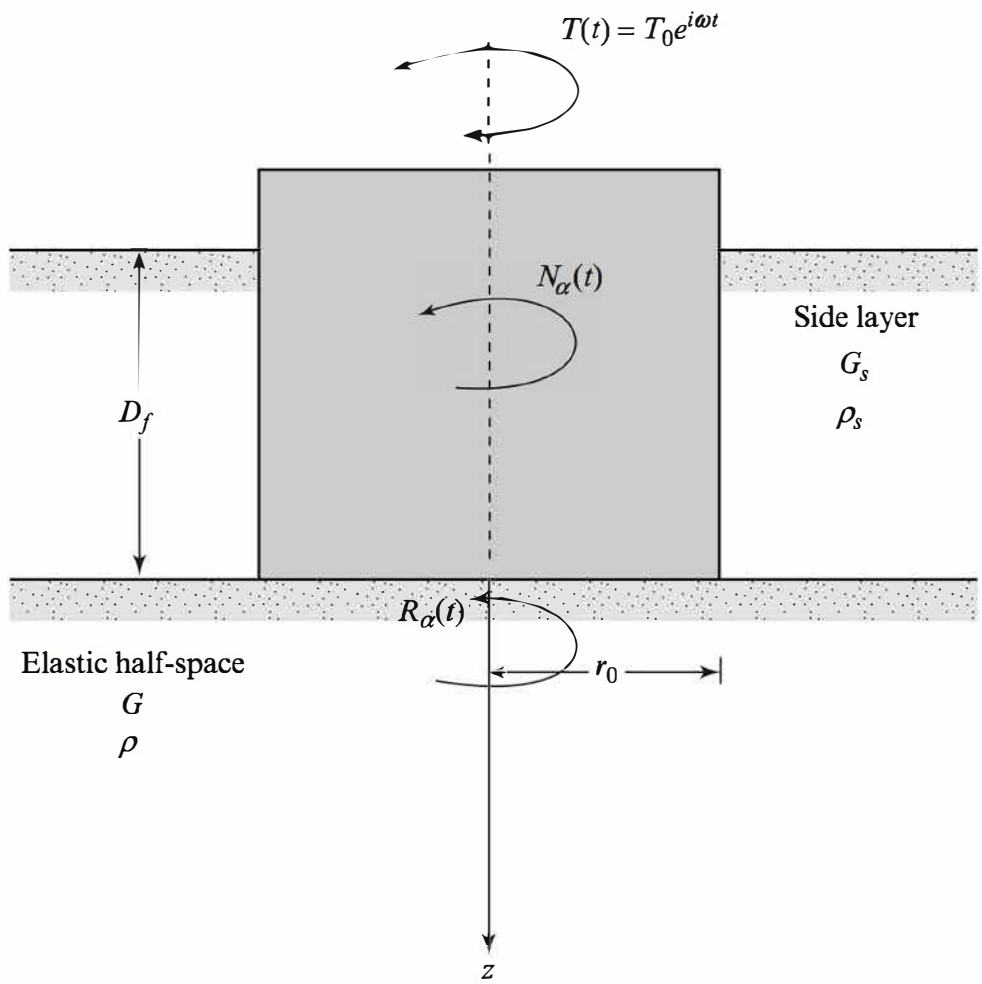

Figure 5.44 Embedded rigid cylindrical foundation—torsional vibration

$$\omega_n = \sqrt{\frac{k_\alpha}{J_{zz}}}$$

where J_{zz} = mass moment of inertia of the foundation about the z axis [see Eq.(5.63)]

The damping ratio is

$$D_\alpha = \left(\frac{1}{2\sqrt{B_\alpha}}\right)\frac{\left(\bar{C}_{\alpha 2} + \bar{S}_{\alpha 2}\dfrac{D_f}{r_0}\sqrt{\dfrac{G_s\rho_s}{G\rho}}\right)}{\sqrt{\bar{C}_{\alpha 1} + \dfrac{G_s}{G}\dfrac{D_f}{r_0}\bar{S}_{\alpha 1}}} \tag{5.127}$$

where B_α = mass ratio = $\dfrac{J_{zz}}{\rho r_0^5}$ [see Eq.(5.66)]

The amplitudes of vibration can be calculated using Eqs. (5.68) and (5.69) and Figures 5.12 and 5.13.

Copyright 2017 Cengage Learning. All Rights Reserved. May not be copied, scanned, or duplicated, in whole or in part. Due to electronic rights, some third party content may be suppressed from the eBook and/or eChapter(s). Editorial review has deemed that any suppressed content does not materially affect the overall learning experience. Cengage Learning reserves the right to remove additional content at any time if subsequent rights restrictions require it.

Effect of Layering

In general, soils are layered in nature and shear modulus increases with depth. Several researchers attempted to develop approximate analytical, as well as numerical, solutions to calculate the vibration response of foundations on the surface of an incompressible soil layer for which shear modulus increases linearly with depth. The effect of layer thickness and depth of embedment have also been reported in the literature. It is generally concluded that omission of layering in theoretical solutions leads to underestimation of vibration amplitudes. Parametric studies are also reported by considering soil as a two layer system, the bottom layer being an elastic half-space. The presence of rigid layer below the elastic layer produces a stiffening effect and increases the natural frequency.

Vibration Screening

In Section 5.4, the allowable vertical vibration amplitudes for machine foundation were considered. It is sometimes possible that, for some rugged vibratory equipment, the intensity of vibration may not be objectionable for the equipment itself. However, the vibration may not be within a tolerable limit for sensitive equipment nearby. Under these circumstances it is desirable to control the vibration energy reaching the sensitive zone. This is referred to as *vibration screening*. It needs to be kept in mind that most of the vibratory energy affecting structures nearby is carried by *Rayleigh (surface)* waves traveling from the source of vibration. Effective screening of vibration may be achieved by proper *interception, scattering*, and *diffraction* of surface waves using barriers such as trenches, sheet pile walls, and piles.

5.16 ACTIVE AND PASSIVE ISOLATION: DEFINITIONS

While studying the problem of vibration screening, it is convenient to group the screening problems into two major categories.

Active Isolation: Active isolation involves screening at the source of vibration, as shown in Figure 5.45, in which a circular trench of radius R and depth H surrounds the foundation that is the source of disturbance.

Passive Isolation: The passive isolation process involves providing a barrier at a point remote from the source of disturbance but near a site where vibration has to be reduced. An example of this is shown in Figure 5.46, in which an open trench of length L and depth H is used near a sensitive instrument foundation to protect if from damage.

5.17 ACTIVE ISOLATION BY USE OF OPEN TRENCHES

Woods (1968) reported the results of a field investigation for active isolation using open trenches. The field tests were conducted at a site with a deep stratum of silty sand. The experimental study consisted of applying vertical vibrations

Copyright 2017 Cengage Learning. All Rights Reserved. May not be copied, scanned, or duplicated, in whole or in part. Due to electronic rights, some third party content may be suppressed from the eBook and/or eChapter(s). Editorial review has deemed that any suppressed content does not materially affect the overall learning experience. Cengage Learning reserves the right to remove additional content at any time if subsequent rights restrictions require it.

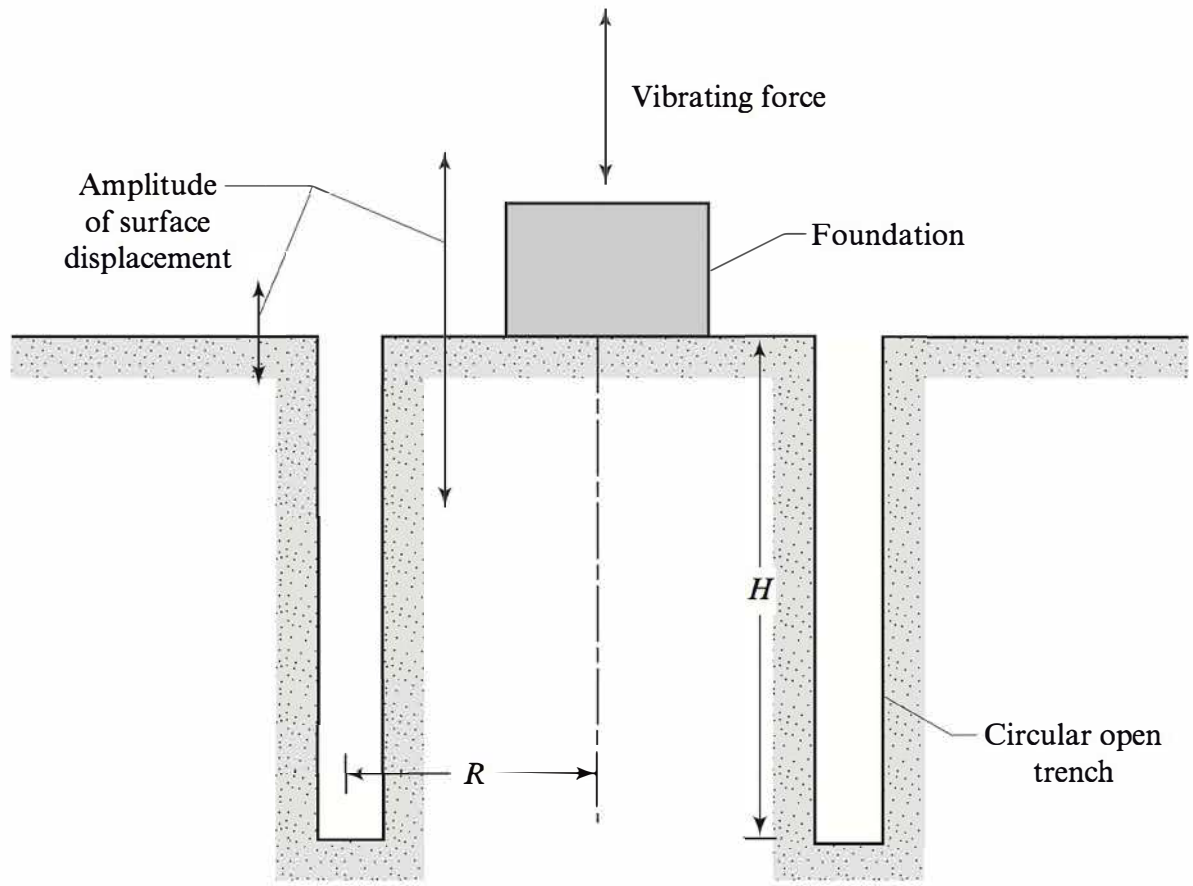

Figure 5.45 Schematic diagram of vibration isolation using a circular trench surrounding the source of vibration for active isolation

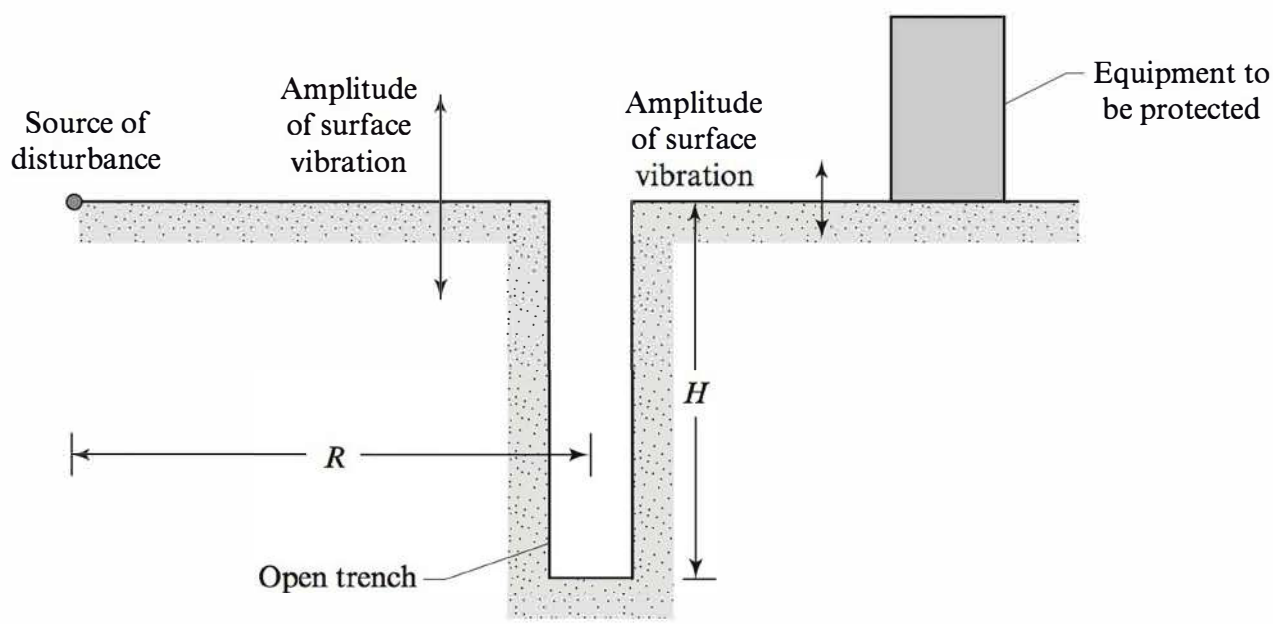

Figure 5.46 Passive isolation by using an open trench

by a small vibrator (80.1 N maximum force) resting on a circular pad. Trenches were constructed around the circular pad to screen the surface displacement due to the surface waves. Vertical velocity transducers were used for measurement of surface displacement around the trench over a 7.62 m diameter area. Other conditions remaining the same, measurements for the surface displacement due to the vibration of the circular pad were also taken without the trenches surrounding the pad. Some results of this investigation are shown in Figure 5.47 in the

Copyright 2017 Cengage Learning. All Rights Reserved. May not be copied, scanned, or duplicated, in whole or in part. Due to electronic rights, some third party content may be suppressed from the eBook and/or eChapter(s). Editorial review has deemed that any suppressed content does not materially affect the overall learning experience. Cengage Learning reserves the right to remove additional content at any time if subsequent rights restrictions require it.

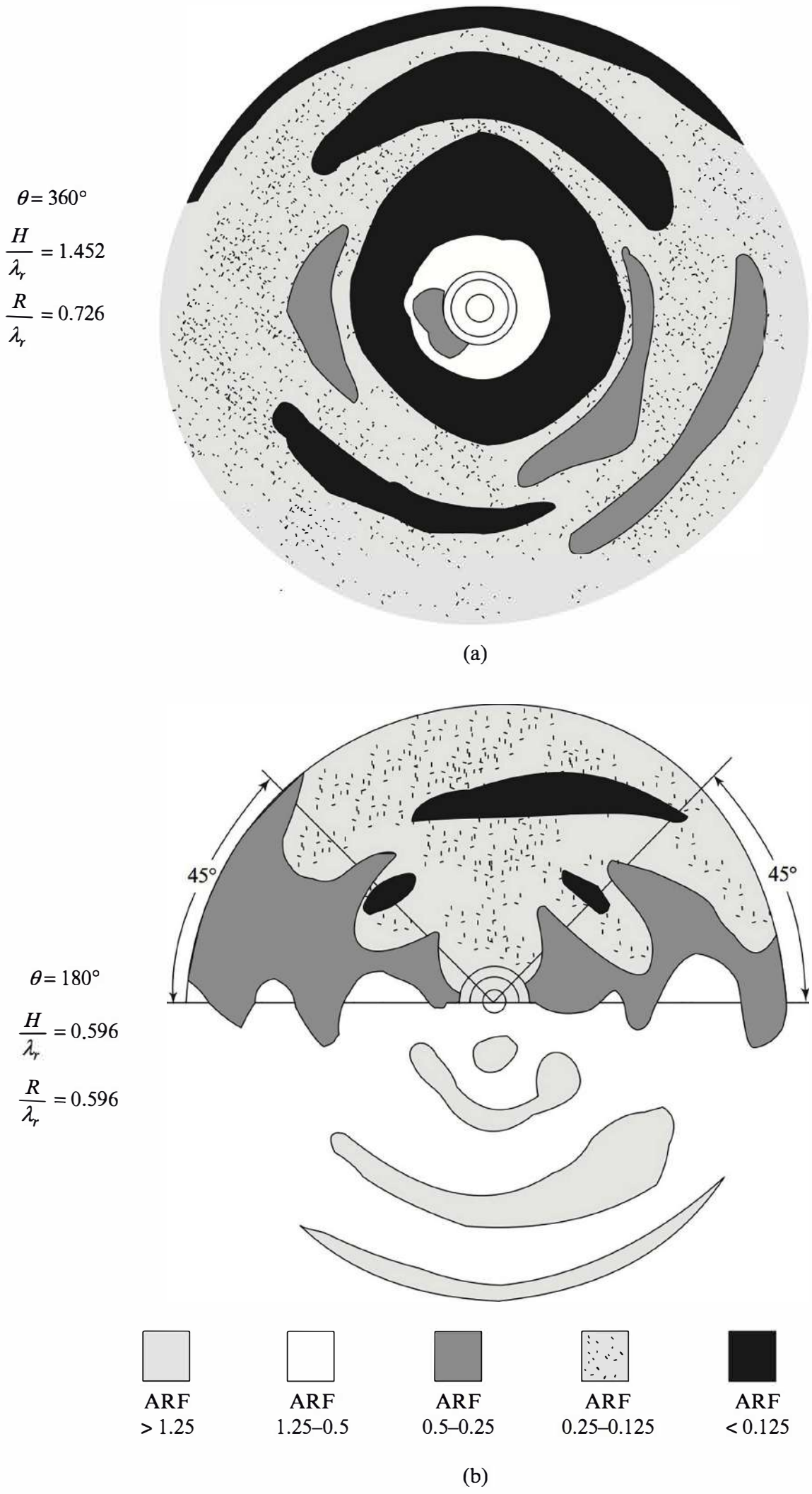

Figure 5.47 Amplitude-reduction-factor contour diagrams (from Woods, 1968)

Source: Woods, R.D. (1968). "Screening of Surface Waves in Soils," *Journal of the Soil Mechanics and Foundations Division,* ASCE, Vol. 94, No. SM4, pp. 951–979. With permission from ASCE.

Copyright 2017 Cengage Learning. All Rights Reserved. May not be copied, scanned, or duplicated, in whole or in part. Due to electronic rights, some third party content may be suppressed from the eBook and/or eChapter(s). Editorial review has deemed that any suppressed content does not materially affect the overall learning experience. Cengage Learning reserves the right to remove additional content at any time if subsequent rights restrictions require it.

form of *amplitude-reduction-factor* contour diagrams. The amplitude-reduction factor (ARF) is defined as

$$\text{ARF} = \frac{\text{vertical amplitude of vibration with trench}}{\text{vertical amplitude of vibration without trench}} \tag{5.128}$$

Also note that in Figure 5.47, θ is the angular length of the trench (in degrees) and λ_r is the length of Rayleigh waves. The value of λ_r for a given frequency of vibration at a given site can be determined in a manner similar to that described in Section 4.15.

The tests of Woods (1968) were conducted for $R/\lambda_r = 0.222$ to 0.910 and $H/\lambda_r = 0.222$ to 1.82. For satisfactory isolation, Woods defined the ARF to be less than or equal to 0.25. The conclusions of this study can be summarized as follows:

1. For $\theta = 360°$, a minimum value of $H/\lambda_r = 0.6$ is required to achieve ARFs less than or equal to 0.25.
2. For $360° > \theta > 90°$, the screened zone may be defined as an area outside the trench bounded on the sides by radial lines from the center of the source through points 45° from the ends of the trench. To obtain ARFs less than or equal to 0.25 in the screened zone, a minimum value of $H/\lambda_r = 0.6$ is required.
3. For $\theta \leq 90°$, effective screen of vibration by trenches cannot be obtained.

5.18 PASSIVE ISOLATION BY USE OF OPEN TRENCHES

Woods (1968) also investigated the case of passive isolation in the field using open trenches. The plan view of the field site layout used for screening at a distance is shown in Figure 5.48. The layout consisted of two vibrator exciter footings (used one at a time for the tests), a trench barrier, and 75 pickup benches. For these tests, it was assumed that the zone screened by the trench will be symmetrical about the 0° line. The variables used to study the passive isolation tests were:

- Distance from the source of vibration to the center of the open trench, R
- Length of the trench, L
- Width of the trench, W, and
- Depth of the trench, H.

In this investigation, the value of R/λ_r was varied from 2.22 to 9.10. For satisfactory isolation, it was defined that ARF's [Eq. (5.128)] should be less than or equal to 0.25 in a semicircular zone of radius $L/2$ behind the trench.

Figure 5.49 shows the ARF contour diagram for one of these tests. The conclusions of this study may be summarized as follows:

1. For a satisfactory passive isolation (for $R = 2\lambda_r$ to about $7\lambda_r$), the minimum trench depth H should be about $1.2\lambda_r$ to $1.5\lambda_r$. This means that, in general, H/λ_r should be about 1.33.

Copyright 2017 Cengage Learning. All Rights Reserved. May not be copied, scanned, or duplicated, in whole or in part. Due to electronic rights, some third party content may be suppressed from the eBook and/or eChapter(s). Editorial review has deemed that any suppressed content does not materially affect the overall learning experience. Cengage Learning reserves the right to remove additional content at any time if subsequent rights restrictions require it.

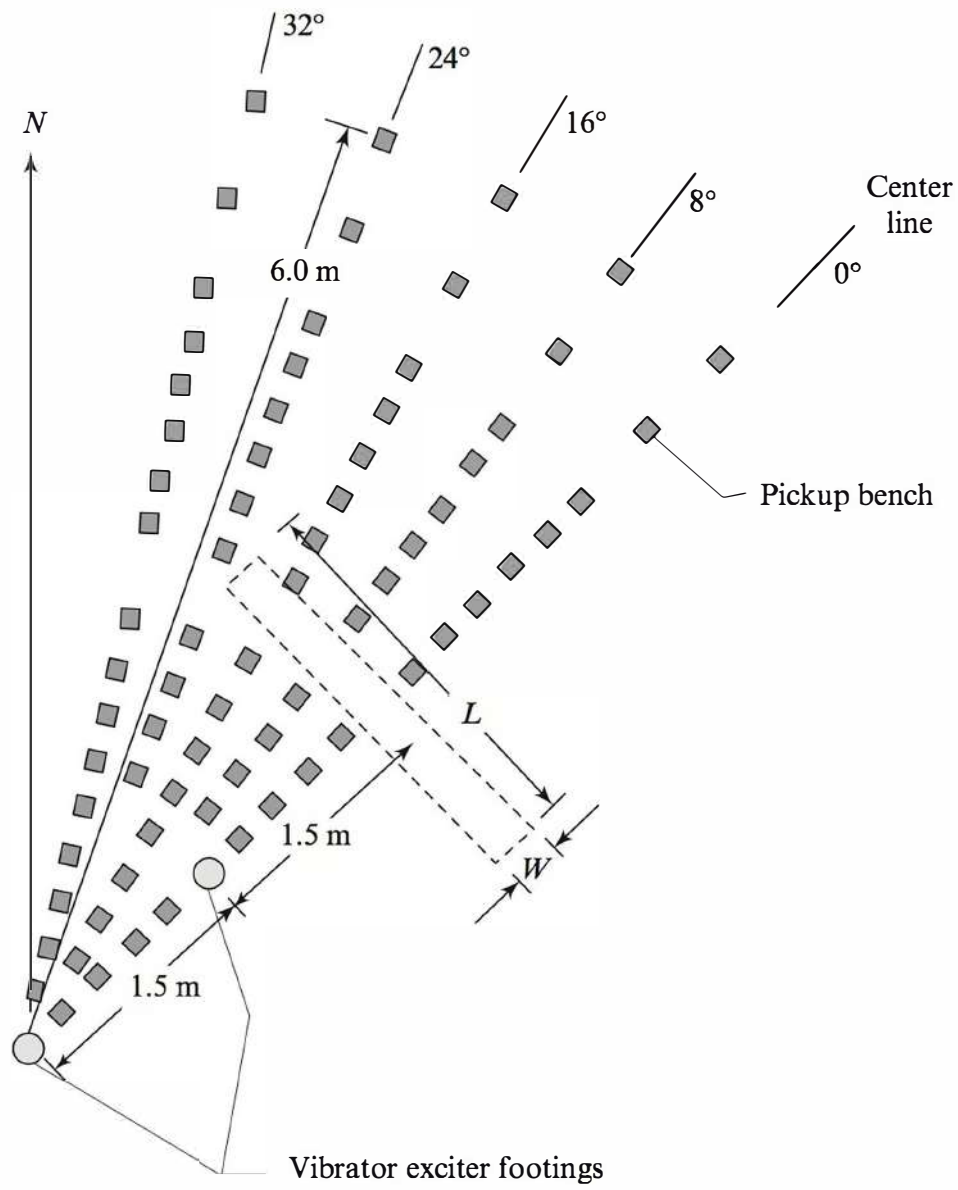

Figure 5.48 Plan view of the field site layout for passive isolation by use of open trench (from Woods, 1968)

Source: Woods, R.D. (1968). "Screening of Surface Waves in Soils," *Journal of the Soil Mechanics and Foundations Division,* ASCE, Vol. 94, No. SM4, pp. 951–979. With permission from ASCE.

2. The trench width W has practically no influence on the effectiveness of screening.
3. To maintain the same degree of isolation, the least area of the trench in the vertical direction (that is $LH = A_T$) should be as follows:

$$A_T = 2.5\,\lambda_r^2 \text{ at } R = 2\lambda_r$$

and

$$A_T = 6.0\,\lambda_r^2 \text{ at } R = 7\lambda_r$$

5.19 PASSIVE ISOLATION BY USE OF PILES

There are several situations where Rayleigh waves that emanate from manufactured sources may be in the range of 40 to 50 m. For these types of problems, a trench depth of 1.33 times 60 to 75 m is needed for effective passive isolation. Open

Copyright 2017 Cengage Learning. All Rights Reserved. May not be copied, scanned, or duplicated, in whole or in part. Due to electronic rights, some third party content may be suppressed from the eBook and/or eChapter(s). Editorial review has deemed that any suppressed content does not materially affect the overall learning experience. Cengage Learning reserves the right to remove additional content at any time if subsequent rights restrictions require it.

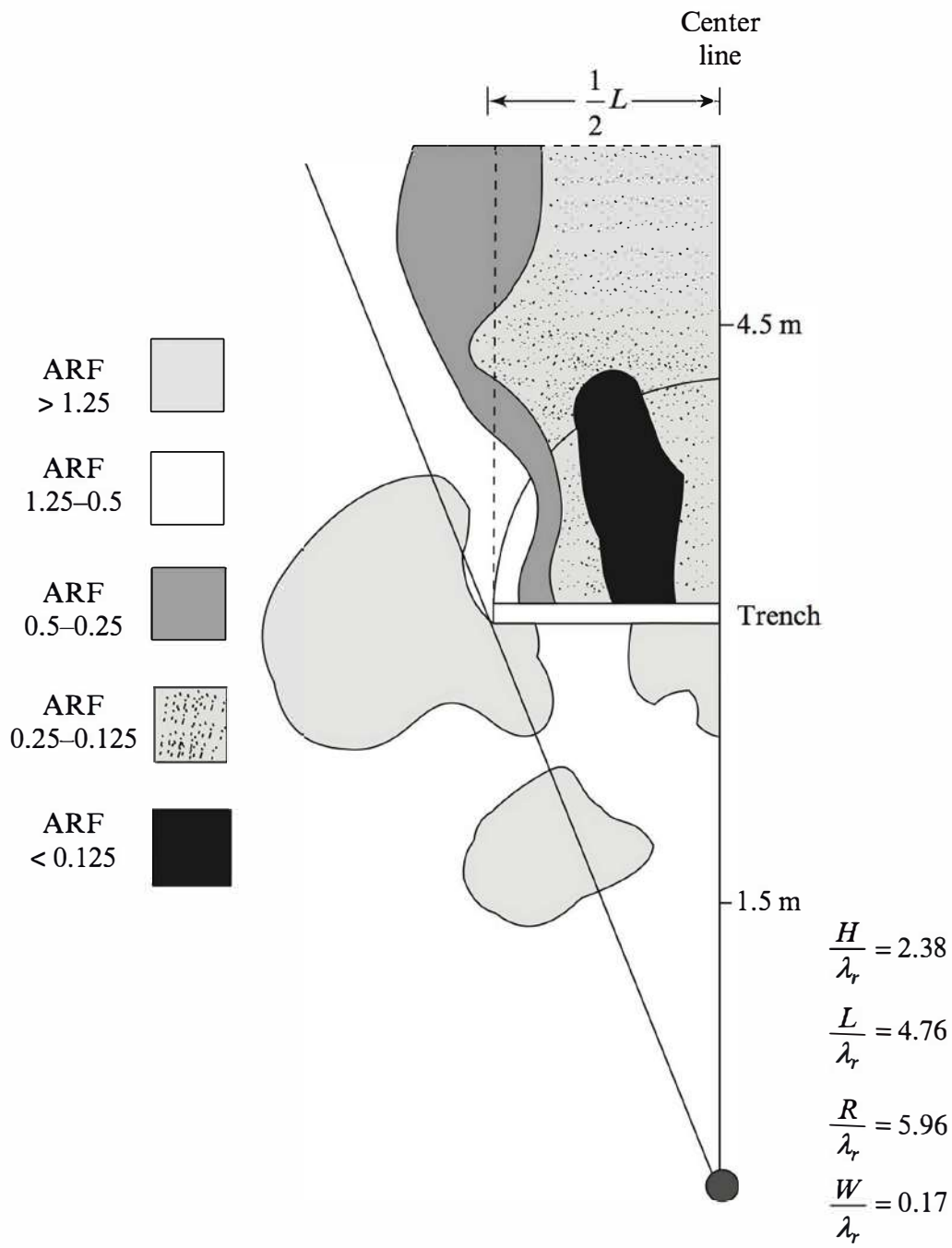

Figure 5.49 Amplitude-reduction-factor contour diagram for passive isolation (from Woods, 1968)

Source: Woods, R.D. (1968). "Screening of Surface Waves in Soils," *Journal of the Soil Mechanics and Foundations Division,* ASCE, Vol. 94, No. SM4, pp. 951–979. With permission from ASCE.

trenches or bentonite-slurry-filled trenches deep enough to be effective are not practical. At the same time, solidification of bentonite slurry will also pose a problem. For this reason, possible use of rows of piles as an energy barrier was studied by Woods, Barnett, and Sagesser (1974) and Liao and Sangrey (1978). Woods, Barnett, and Sagesser used the principle of holography and observed vibrations in a model half-space in order to develop the criteria for *void cylindrical obstacles* for passive isolation (Figure 5.50). The model half-space was prepared in a fine sand medium in a box. In Figure 5.50, the diameter of the cylindrical obstacle is D, and the net space for the energy to penetrate between two consecutive void obstacles is equal to S_n. The numerical evaluation of the barrier effectiveness was made by obtaining the average ARFs from several lines beyond the barrier in a section ±15°

Copyright 2017 Cengage Learning. All Rights Reserved. May not be copied, scanned, or duplicated, in whole or in part. Due to electronic rights, some third party content may be suppressed from the eBook and/or eChapter(s). Editorial review has deemed that any suppressed content does not materially affect the overall learning experience. Cengage Learning reserves the right to remove additional content at any time if subsequent rights restrictions require it.

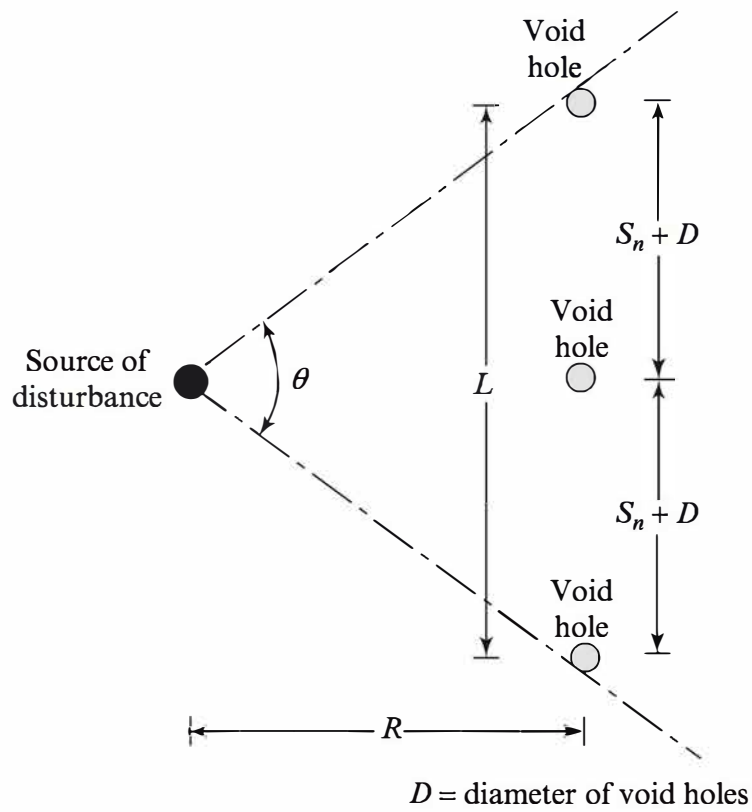

Figure 5.50 Void cylindrical obstacles for passive isolation

on both sides of an axis through the source of disturbance and perpendicular to the barrier. For all tests, H/λ_r and L/λ_r were kept at 1.4 and 2.5, respectively. These values of H/λ_r, and L/λ_r are similar to those suggested in Section 5.18 for open trenches. A nondimensional plot of the *isolation effectiveness* developed from these tests is given in Figure 5.51. The isolation effectiveness is defined as

$$\text{Effectiveness} = 1 - \text{ARF} \tag{5.128}$$

Based on these test results, Woods, Barnett, and Sagesser (1974) suggested that a row of void cylindrical holes may act as an isolation barrier if

$$\frac{D}{\lambda_r} \geq \frac{1}{6} \tag{5.129}$$

and

$$\frac{S_n}{\lambda_r} < \frac{1}{4} \tag{5.130}$$

Liao and Sangrey (1978) used an acoustic model employing sound waves in a fluid medium to evaluate the possibility of the use of rows of piles as passive isolation barriers. Model piles for the tests were made from aluminum, steel, styrofoam, and polystyrene plastic. Based on their study, Liao and Sangrey determined that Eqs. (5.129) and (5.130) suggested by Woods, Barnett, and Sagesser are generally valid. They also determined that $S_n = 0.4\lambda_r$ may be the upper limit for a barrier to have some effectiveness. However, the degree of effectiveness of the barrier will depend on whether the piles are soft or hard compared to the

Copyright 2017 Cengage Learning. All Rights Reserved. May not be copied, scanned, or duplicated, in whole or in part. Due to electronic rights, some third party content may be suppressed from the eBook and/or eChapter(s). Editorial review has deemed that any suppressed content does not materially affect the overall learning experience. Cengage Learning reserves the right to remove additional content at any time if subsequent rights restrictions require it.

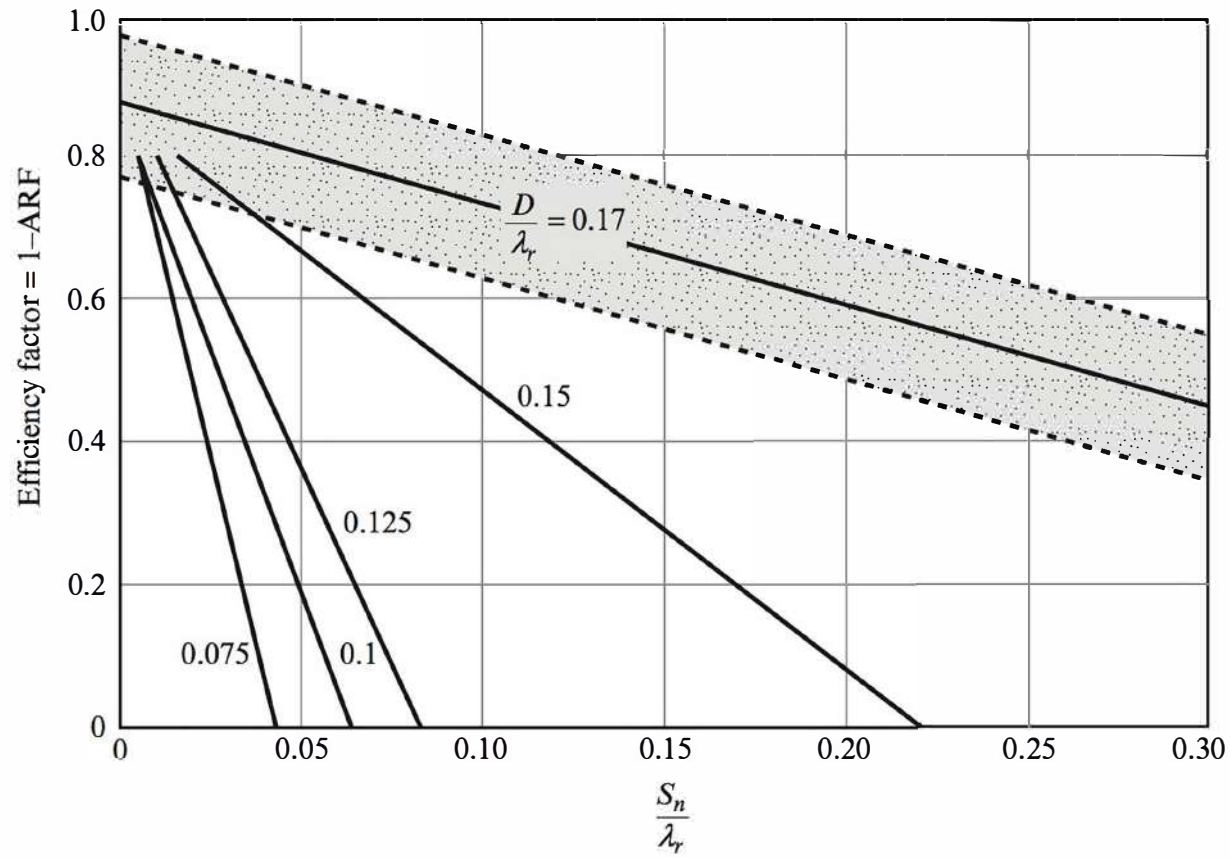

Figure 5.51 Isolation effectiveness as a function of hole diameter and spacing (redrawn from Woods, Barnett, and Sagesser, 1974)

Source: Woods, R.D. (1968). "Screening of Surface Waves in Soils," *Journal of the Soil Mechanics and Foundations Division,* ASCE, Vol. 94, No. SM4, pp. 951–979. With permission from ASCE.

soil in which they are embedded. The degree of softness or hardness may be determined by the term *impedance ratio* (IR), defined as

$$\text{IR} = \frac{\rho_P v_{r(P)}}{\rho_S v_{r(S)}} \tag{5.131}$$

where ρ_P and ρ_S = the densities of the pile material and soil, respectively
$v_{r(P)}$ and $v_{r(S)}$ = the velocities of Rayleigh waves in the pile material and soil, respectively

The piles are considered *soft* if IR is less than 1 and hard if IR is greater than 1. Soft piles are more efficient as isolation barriers compared to hard piles.
Figure 5.52 gives a general range of the Rayleigh wave impedance ($=\rho v_r$) for various soils and pile materials. For a more detailed discussion, the reader is referred to the original paper of Liao and Sangrey.

PROBLEMS

5.1 A concrete foundation is 2.5 m in diameter. The foundation is supporting a machine. The total weight of the machine and the foundation is 270 kN. The machine imparts a vertical vibrating force $Q = Q_0 \sin \omega t$. Given: Q_0 = 27 kN (not frequency dependent). The operating frequency is 150 cpm.

Copyright 2017 Cengage Learning. All Rights Reserved. May not be copied, scanned, or duplicated, in whole or in part. Due to electronic rights, some third party content may be suppressed from the eBook and/or eChapter(s). Editorial review has deemed that any suppressed content does not materially affect the overall learning experience. Cengage Learning reserves the right to remove additional content at any time if subsequent rights restrictions require it.

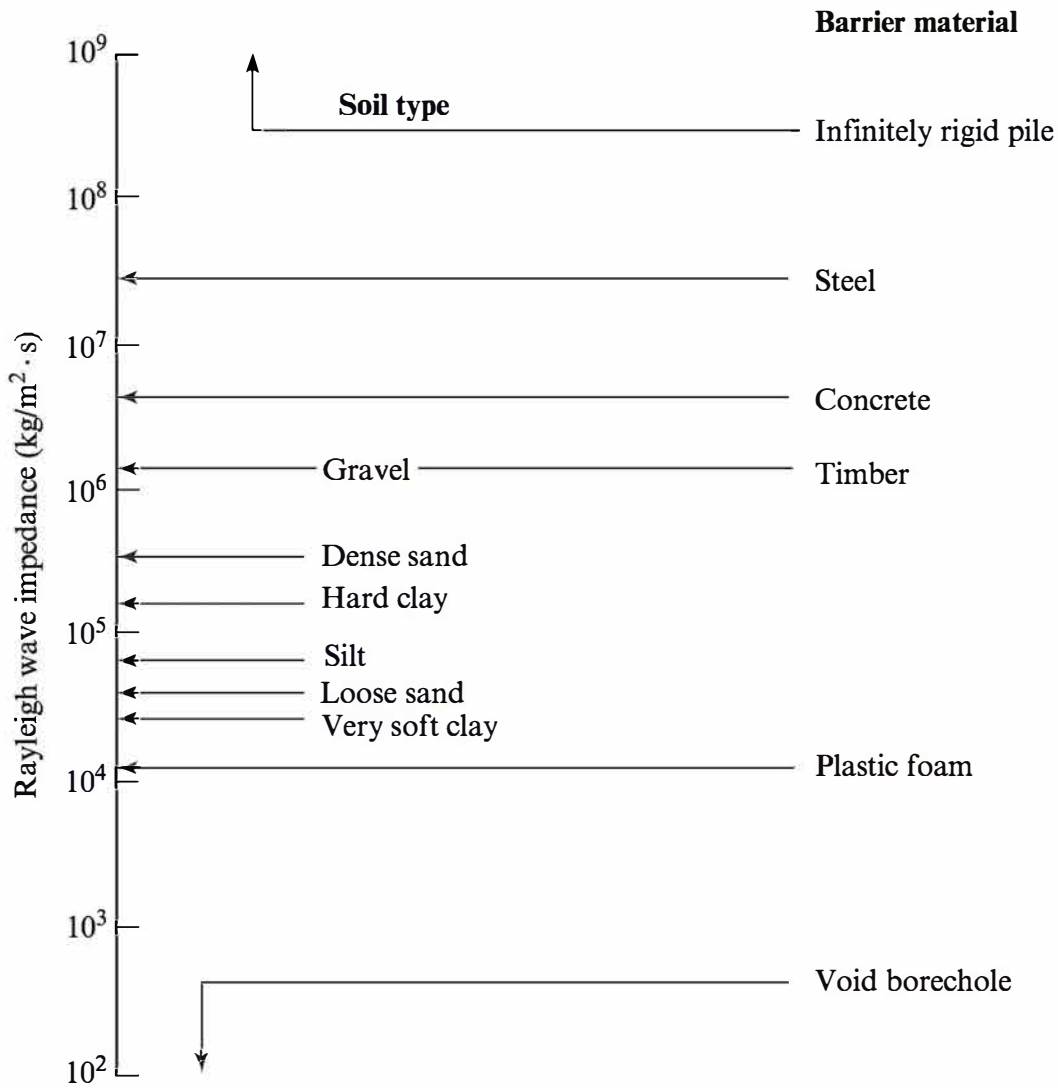

Figure 5.52 Estimated values of Rayleigh wave impedance for various soils and pile materials (from Liao and Sangrey, 1978)

Source: Liao, S., and Sangrey, D.A. (1978). "Use of Piles as Isolation Barriers," *Journal of the Geotechnical Engineering Division,* ASCE, Vol. 104, No. GT9, pp. 1139–1152. With permission from ASCE.

For the soil supporting the foundation, unit weight = 19.5 kN/m³, shear modulus = 45000 kPa, and Poisson' ratio = 0.3. Determine:

a. resonant frequency;
b. the amplitude of vertical vibration at resonant frequency; and
c. the amplitude of vertical vibration at the operating frequency.

Use the procedure described in Section 5.4

5.2 Redo Problem 5.1 assuming the foundation is 2.5 m × 2 m in plan. Assume the total weight of the foundation and the machine is the same as in Problem 5.1. Use the procedure described in Section 5.4

5.3 A concrete foundation (unit weight = 23.58 kN/m³) supporting a machine is 3.5 m × 2.5 m in plan and is subjected to a sinusoidal vibrating force (vertical) having an amplitude of 10 kN (not frequency dependent). The operating frequency is 2000 cpm. The weight of the machine and foundation is 400 kN. The soil properties are unit weight = 18 kN/m³, shear modulus = 38,000 kPa, and Poisson' ratio = 0.25. Determine

Copyright 2017 Cengage Learning. All Rights Reserved. May not be copied, scanned, or duplicated, in whole or in part. Due to electronic rights, some third party content may be suppressed from the eBook and/or eChapter(s). Editorial review has deemed that any suppressed content does not materially affect the overall learning experience. Cengage Learning reserves the right to remove additional content at any time if subsequent rights restrictions require it.

a. the resonant frequency of the foundation, and
b. the amplitude of vertical vibration at operating frequency.

Use the procedure described in Section 5.4

5.4 Consider the case of a single-cylinder reciprocating engine (Figure 5.15a). For the engine, operating speed = 1000 cpm, crank (r_1) = 90 mm, connecting rod (r_2) = 350 mm, weight of the engine = 20 kN and reciprocating weight = 65 N. The engine is supported by a concrete foundation block of 3 m × 2 m × 1.5 m ($L \times B \times H$). The unit weight of concrete is 23.58 kN/m^3. The properties of the soil supporting the foundation are unit weight = 19 kN/m^3, G = 24,000 kPa, and $\mu = 0.25$. Calculate
a. the resonant frequency, and
b. the amplitude of vertical vibration at resonance.

Use the procedure described in Section 5.4

5.5 Refer to Problem 5.4. What will be the amplitude of vibration at operating frequency?

5.6 Solve Problem 5.2, parts (b) and (c) by assuming that the Poisson's ratio is $\mu = 0.25$.

5.7 The concrete foundation (unit weight = 23.58 kN/m^3) of a machine has the following dimensions (refer to Figure 5.18): L = 3 m, B = 4 m, height of the foundation = 1.5 m. The foundation is subjected to a sinusoidal horizontal force from the machine having an amplitude of 10 kN at a height of 2 m measured from the base of the foundation. The soil supporting the foundation is sandy clay. Given G = 30,000 kPa, $\mu = 0$, and ρ = 1700 kg/m^3. Determine
a. the resonant frequency for the rocking mode of vibration of the foundation, and
b. the amplitude of rocking vibration at resonance.

Use the procedure described in Section 5.8

(*Note*: The amplitude of horizontal force is not frequency dependent. Neglect the moment of inertia of the machine.)

5.8 Solve Problem 5.7 assuming that the horizontal force is frequency dependent. The amplitude of the force at an operating speed of 800 cpm is 20 kN.

5.9 Refer to Problem 5.7. Determine
a. the resonant frequency for the sliding mode of vibration, and
b. amplitude for the sliding mode of vibration at resonance.

Assume the weight of the machinery on the foundation to be 100 kN. Use $\mu = 0.2$, and the procedure out lined in Section 5.6.

Copyright 2017 Cengage Learning. All Rights Reserved. May not be copied, scanned, or duplicated, in whole or in part. Due to electronic rights, some third party content may be suppressed from the eBook and/or eChapter(s). Editorial review has deemed that any suppressed content does not materially affect the overall learning experience. Cengage Learning reserves the right to remove additional content at any time if subsequent rights restrictions require it.

5.10 Repeat Problem 5.9 assuming that the horizontal force is frequency dependent. The amplitude of the horizontal force at an operating frequency of 800 cpm is 40 kN. The weight of the machinery of the foundation is 100 kN.

5.11 A concrete foundation (unit weight = 23.5 kN/m^3) supporting a machine has the following dimensions: length = 5 m, width = 4 m, height = 2 m. The machine imparts a torque T on the foundation such that $T = T_0 e^{i\omega t}$. Given $T_0 = 3000$ N · m. The mass moment of inertia of the machine about the vertical axis passing through the center of gravity of the foundation is 75×10^3 kg-m^2. The soil has the following properties: $\mu = 0.25$, unit weight = 18 kN/m^3, and $G = 28{,}000$ kPa. Determine

a. the resonant frequency for the torsional mode of vibration, and
b. angular deflection at resonance.

5.12 Refer to Figure 5.41 for the vertical foundation of a rigid cylindrical concrete foundation. Given the following:

Foundation radius = 1.3 m; height = 1.5 m
depth of embedment, D_f = 1 m;
unit weight of concrete = 24 kN/m^3

Vibrating machine Weight = 100 kN ; amplitude of vibrating force = 10 kN (not frequency dependent); operating speed = 600 cpm

Soil G_s = 22 Mpa; G = 20.5 MPa; μ = 0.25 unit weight, γ_s = 18.5 kN/m^3 (for side layer); unit weight, γ = 19.5 kN/m^3 (below the base)

Determine:

a. damped natural frequency;
b. amplitude of vertical vibration at resonance; and
c. amplitude of vibration at operating speed.

5.13 Solve Problem 5.12 with the following changes:

Concrete foundation

length = 2 m
width = 1.5 m
height = 1.5 m
depth of embedment, D_f = 1.2 m
unit weight of concrete = 24 kN/m^3

Copyright 2017 Cengage Learning. All Rights Reserved. May not be copied, scanned, or duplicated, in whole or in part. Due to electronic rights, some third party content may be suppressed from the eBook and/or Chapter(s). Editorial review has deemed that any suppressed content does not materially affect the overall learning experience. Cengage Learning reserves the right to remove additional content at any time if subsequent rights restrictions require it.

Vibrating machine

weight = 90 kN

frequency-dependent amplitude of vibrating force = 9 kN

at an operating speed of 500 cpm

5.14 Refer to Figure 5.42 for the sliding vibration of a rigid cylindrical foundation. Given the following:

Concrete foundation radius = 3m; height = 4 m;
depth of embedment, D_f = 2.5 m; unit weight of concrete = 24 kN/m^3

Vibrating machine weight = 100 kN; frequency-dependent unbalanced force at an operating frequency of 600 cpm = 40 kN

Soil G_s = 16,000 kPa; G = 18,000 kPa, $\mu = 0$; unit weight, γ_s = 17.8 kN/m^3 (for side layer); unit weight, γ = 18.8 kN/m^3 (below the base)

Determine

a. the damped natural frequency;
b. the amplitude of horizontal vibration at resonance; and
c. the amplitude of horizontal vibration at operating speed.

References

Arnold, R. N., Bycroft, G. N., and Warburton, G. B. (1955). "Forced Vibrations of a Body on an Infinite Elastic Solid," *Journal of Applied Mechanics*, ASME, Vol. 77, pp. 391–401.

Baranov, V. A. (1967). "On the Calculation of Excited Vibrations of an Embedded Foundation," (in Russian), *Vopr. Dyn. Prochn.*, Vol. 14, pp. 195–209

Barkan, D. D. (1962) *Dynamic Bases and Foundations*, McGraw-Hill Book Company, New York.

Beredugo, Y. O., and Novak, M. (1972). "Coupled Horizontal and Rocking Vibration of Embedded Footing," *Canadian Geotechnical Journal*, Vol. 9, No. 4, pp. 477–497.

Borowicka, H. (1943). "Uber Ausmittig Belastere Starre Platten auf Elastischisotropem Undergrund," *Ingenieur-Archiv, Berlin*, Vol. 1, pp. 1–8.

Bycroft, G. N. (1956). "Forced Vibrations of a Rigid Circular Plate on a Semi-Infinite Elastic Space and on an Elastic Stratum," *Philosophical Transactions of the Royal Society, London, Ser*. A., Vol. 248, pp. 327–368.

Dobry, R., and Gazetas, G. (1986). "Dynamic Response of Arbitrarily Shaped Foundations," *Journal of the Geotechnical Engineering Division*, ASCE, Vol. 112, No. GT2, pp. 109–135.

Fry, Z. B. (1963). "Report 1: Development and Evaluation of Soil Bearing Capacity, Foundation of Structures, Field Vibratory Test Data," *Technical Report No. 3–362*, US Army Engineers Waterways Experiment Station, Vicksburg, Mississippi.

Gorbunov-Possadov, M. I., and Serebrajanyi, R. V. (1961). "Design of Structures upon Elastic Foundations," *Proceedings, 5th International Conference on Soil Mechanics and Foundation Engineering*, Vol. 1, pp. 643–648.

Hall, J. R. Jr. (1967). "Coupled Rocking and Sliding Oscillations of Rigid Circular Footings," *Proceedings*, International Symposium on Wave Propagation and Dynamic Properties of Earth Materials, Albuquerque, New Mexico, pp. 139–148.

Copyright 2017 Cengage Learning. All Rights Reserved. May not be copied, scanned, or duplicated, in whole or in part. Due to electronic rights, some third party content may be suppressed from the eBook and/or eChapter(s). Editorial review has deemed that any suppressed content does not materially affect the overall learning experience. Cengage Learning reserves the right to remove additional content at any time if subsequent rights restrictions require it.

Hsieh, T. K. (1962), "Foundation Vibrations," *Proceedings,* Institute of Civil Engineers, London, Vol. 22, pp. 211–226.

Lamb, H. (1904). "On the Propagation of Tremors over the Surface of an Elastic Solid," *Philosophical Transactions of the Royal Society*, London, Ser. A., Vol. 203, pp. 1–42.

Liao, S., and Sangrey, D. A. (1978). "Use of Piles an Isolation Barriers," *Journal of the Geotechnical Engineering Division*, ASCE, Vol. 104, No. GT9, pp. 1139–1152.

Lysmer, J., and Richart, F. E., Jr. (1966). "Dynamic Response to Footings to Vertical Loading," *Journal of the Soil Mechanics and Foundations Division*, ASCE, Vol. 92, No. SM1, pp. 65–91. With permission from ASCE.

Novak, M., and Beredugo, Y. O. (1972). "Vertical Vibration of Embedded Footings," *Journal of the Soil Mechanics and Foundations Division*, ASCE, Vol. 98, No. SM12, pp. 1291–1310.

Novak, M., and Sachs, K. (1973). "Torsional and Coupled Vibrations of Embedded Footings," *International Journal of Earthquake Engineering and Structural Dynamics*, Vol. 2, No. 1, pp. 11–33.

Prakash, S., and Puri, V. K. (1981). "Observed and Predicted Response of a Machine Foundation," *Proceedings*, 10th International Conference on Soil Mechanics and Foundation Engineering, Strockholm, Vol. 3, pp. 269–272.

Prakash, S., and Puri, V. K. (1988). *Foundations for Machines: Analysis and Design*, John Wiley and Sons, New York.

Quinlan, P. M. (1953). "The Elastic Theory of Soil Dynamics," Symposium on Dynamic Testing of Soils, *Special Technical Publication 156*, ASTM, pp. 3–34.

Reissner, E. (1936). "Stationare, axialsymmetrische durch eine Schuttelnde Masseerregte Schwingungen eines homogenen elastischen halbraumes," *Ingenieur-Archiv*., Vol. 7, No. 6. pp. 381–396.

Reissner, E. (1937). "Freie and erzwungene Torsionschwingungen des elastischen halbraumes," *Ingenieur-Archiv*., Vol. 8, No. 4, pp. 229–245.

Reissner, E., and Sagochi, H. F. (1944). "Forced Torsional Oscillations of an Elastic Half Space," *Journal of Applied Physics*, Vol. 15, pp. 652–662.

Richart, F. E., Jr. (1962). "Foundation Vibrations," *Transactions*, ASCE, Vol. 127, Part 1, pp. 863–898. With permission from ASCE.

Richart, F. E., Jr., Hall, J. R., and Woods, R. D. (1970). *Vibration of Soils and Foundations*, Prentice-Hall, Inc., Englewood Cliffs, New Jersey.

Richart. F. E., Jr., and Whitman, R. V. (1967). "Comparison of Footing Foundation Tests with Theory," *Journal of the Soil Mechanics and Foundations,* ASCE, Vol. 93, No. SM6, pp. 143–167. With permission from ASCE.

Sung, T. Y. (1953). "Vibration in Semi-Infinite Solids Due to Periodic Surface Loadings," Symposium on Dynamic Testing of Soils, *Special Technical Publication No. 156,* ASTM, pp. 35–54.

Timoshenko, S. P., and Goodier, J. H. (1951). *Theory of Elasticity*. McGraw-Hill Book Company, New York.

Whitman, R. V., and Richart, F. E., Jr. (1967). "Design Procedures for Dynamically Loaded Foundations," *Journal of the Soil Mechanics and Foundations Division*, ASCE, Vol. 93, No. SM6. pp. 169–193.

Woods, R. D. (1968). "Screening of Surface Waves in Soils," *Journal of the Soil Mechanics and Foundations Division*, ASCE, Vol. 94, No. SM4, pp. 951–979.

Woods, R. D., Barnett, N. E., and Sagesser, R. (1974). "Holography – A New Tool for Soil Dynamics," *Journal of Geotechnical Engineering Division*, ASCE, Vol. 100, No. GT11, pp. 1231–1247.

Copyright 2017 Cengage Learning. All Rights Reserved. May not be copied, scanned, or duplicated, in whole or in part. Due to electronic rights, some third party content may be suppressed from the eBook and/or eChapter(s). Editorial review has deemed that any suppressed content does not materially affect the overall learning experience. Cengage Learning reserves the right to remove additional content at any time if subsequent rights restrictions require it.

Dynamic Bearing Capacity of Shallow Foundations

6

6.1 INTRODUCTION

The static bearing capacity of shallow foundations has been extensively studied and reported in literature. However, foundations can be subjected to single pulse dynamic loads, which may be in vertical or horizontal directions. The dynamic loads due to nuclear blasts are mainly vertical. Horizontal dynamic loads on foundations are due mostly to earthquakes. These types of loading may induce large permanent deformation in foundations. Isolated column footings, strip footings, mat footings, and even pile foundations all may fail during seismic events. Such failures are generally attributed to liquefaction (a condition where the mean effective stress in a saturated soil reduces to zero, as explained in Chapter 10). However, a number of failures have occurred where field conditions indicate there was only partial saturation or a dense soil, and therefore liquefaction alone is a very unlikely explanation. Rather, the reason for the seismic settlements of these foundations seems to be that the bearing capacity was reduced (Richards, Elms, and Budhu, 1993).

Though a large amount of information on the dynamic bearing capacity of foundations is available in literature, it is mostly based on theoretical procedures and not supported by field data. Hence, most of such published studies are yet to enter the design offices. Most of the important works on this topic now available in the literature are summarized in this chapter.

However, one must keep in mind that, during the analysis of the time-dependent motion of a foundation subjected to dynamic loading or estimating the bearing capacity under dynamic conditions, several factors need to be considered. Most important of these factors are

a. nature of variation of the magnitude of the loading pulse;
b. duration of the pulse; and
c. strain-rate response of the soil during deformation.

Copyright 2017 Cengage Learning. All Rights Reserved. May not be copied, scanned, or duplicated, in whole or in part. Due to electronic rights, some third party content may be suppressed from the eBook and/or eChapter(s). Editorial review has deemed that any suppressed content does not materially affect the overall learning experience. Cengage Learning reserves the right to remove additional content at any time if subsequent rights restrictions require it.

Ultimate Dynamic Bearing Capacity

6.2 BEARING CAPACITY IN SAND

The static ultimate bearing capacity of shallow foundations subjected to vertical loading (Figure 6.1) can be given by the equation

$$q_u = cN_cS_cd_c + qN_qS_qd_q + \frac{1}{2}\gamma BN_\gamma S_\gamma d_\gamma \tag{6.1}$$

where q_u = ultimate load per unit area of the foundation
γ = effective unit weight of soil
$q = \gamma D_f$
D_f = depth of foundation
B = width of foundation
c = cohesion of soil
N_c, N_q, N_γ = bearing capacity factors which are only functions of the soil friction angle ϕ
S_c, S_q, S_γ = shape factors
d_c, d_q, d_γ = depth factors

In sand, with $c = 0$, Eq. (6.1) becomes

$$q_u = qN_qS_qd_q + \frac{1}{2}\gamma BN_\gamma S_\gamma d_\gamma \tag{6.2}$$

The values of N_q (Reissner, 1924), N_c (Prandtl, 1921), and N_γ (Caquot and Kerisel, 1953; Vesic, 1973) can be represented by the following equations:

$$N_q = e^{\pi \tan\phi} \tan^2\left(45 + \frac{\phi}{2}\right) \tag{6.3}$$

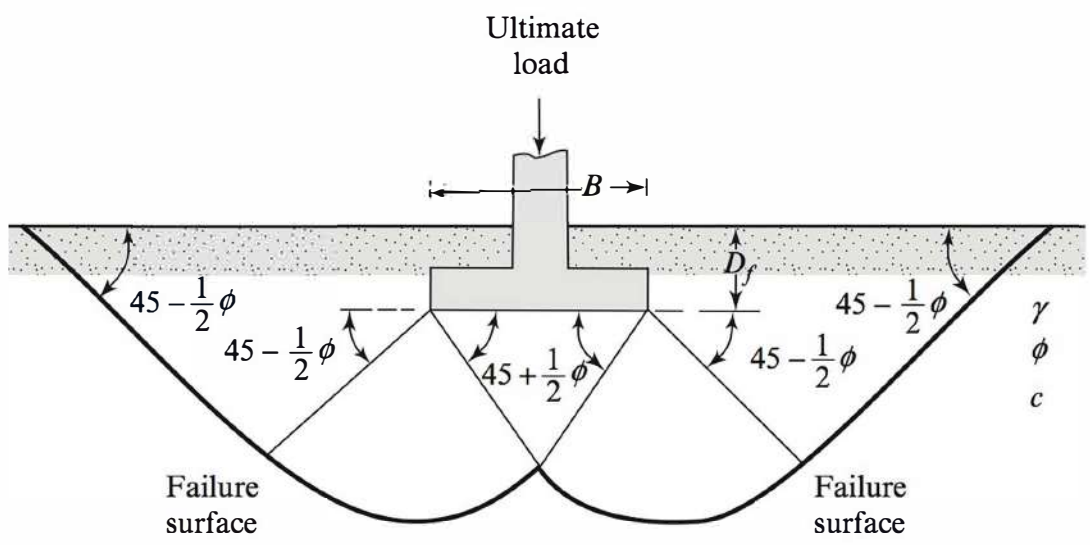

Figure 6.1 Static ultimate bearing capacity of continuous shallow foundations

Copyright 2017 Cengage Learning. All Rights Reserved. May not be copied, scanned, or duplicated, in whole or in part. Due to electronic rights, some third party content may be suppressed from the eBook and/or eChapter(s). Editorial review has deemed that any suppressed content does not materially affect the overall learning experience. Cengage Learning reserves the right to remove additional content at any time if subsequent rights restrictions require it.

$$N_c = (N_q - 1)\cot\phi \tag{6.4}$$

$$N_\gamma = 2(N_q + 1)\tan\phi \tag{6.5}$$

where ϕ is the angle of friction of soil. The values of N_c, N_q, and N_γ for various soil friction angles are given in Table 6.1.

Table 6.1 Values[a] of Bearing Capacity Factors, N_c, N_q and N_γ

ϕ (deg)	N_c	N_q	N_γ	ϕ (deg)	N_c	N_q	N_γ
0	5.14	1.00	0.00	26	22.25	11.85	12.54
				27	23.94	13.20	14.47
1	5.38	1.09	0.07	28	25.80	14.72	16.72
2	5.63	1.20	0.15	29	27.86	16.44	19.34
3	5.90	1.31	0.24	30	30.14	18.40	22.40
4	6.19	1.43	0.34				
5	6.49	1.57	0.45	31	32.67	20.63	25.99
				32	35.49	23.18	30.22
6	6.81	1.72	0.57	33	38.64	26.09	35.19
7	7.16	1.88	0.71	34	42.16	29.44	41.06
8	7.53	2.06	0.86	35	46.12	33.30	48.03
9	7.92	2.25	1.03				
10	8.35	2.47	1.22	36	50.59	37.75	56.31
				37	55.63	42.92	66.19
11	8.80	2.71	1.44	38	61.35	48.93	78.03
12	9.28	2.97	1.69	39	67.87	55.96	92.25
13	9.81	3.26	1.97	40	75.31	64.20	109.41
14	10.37	3.59	2.29				
15	10.98	3.94	2.65	41	83.86	73.90	130.22
				42	93.71	85.38	155.55
16	11.63	4.34	3.06	43	105.11	99.02	186.54
17	12.34	4.77	3.53	44	118.37	115.31	224.64
18	13.10	5.26	4.07	45	133.88	134.88	271.76
19	13.93	5.80	4.68				
20	14.83	6.40	5.39	46	152.10	158.51	330.35
				47	173.64	187.21	403.67
21	15.82	7.07	6.20	48	199.26	222.31	496.01
22	16.88	7.82	7.13	49	229.93	265.51	613.16
23	18.05	8.66	8.20	50	266.89	319.07	762.89
24	19.32	9.60	9.44				
25	20.72	10.66	10.88				

Copyright 2017 Cengage Learning. All Rights Reserved. May not be copied, scanned, or duplicated, in whole or in part. Due to electronic rights, some third party content may be suppressed from the eBook and/or eChapter(s). Editorial review has deemed that any suppressed content does not materially affect the overall learning experience. Cengage Learning reserves the right to remove additional content at any time if subsequent rights restrictions require it.

The shape and depth factors have been proposed by DeBeer (1970) and Brinch Hanson (1970):

Shape Factors

$$S_c = 1 + \left(\frac{B}{L}\right)\left(\frac{N_q}{N_c}\right) \tag{6.6}$$

$$S_q = 1 + \left(\frac{B}{L}\right)\tan\phi \tag{6.7}$$

$$S_\gamma = 1 - 0.4\left(\frac{B}{L}\right) \tag{6.8}$$

where L = length of the rectangular foundation

Depth Factors

$$\text{For} \quad \frac{D_f}{B} \le 1, \qquad d_c = 1 + 0.4\left(\frac{D_f}{B}\right) \tag{6.9}$$

$$\text{For} \quad \frac{D_f}{B} > 1, \qquad d_c = 1 + 0.4\underbrace{\tan^{-1}\left(\frac{D_f}{B}\right)}_{\text{radian}} \tag{6.10}$$

$$\text{For} \quad \frac{D_f}{B} \le 1, \qquad d_q = 1 + 2\tan\phi(1-\sin\phi)^2\left(\frac{D_f}{B}\right) \tag{6.11}$$

$$\text{For} \quad \frac{D_f}{B} > 1, \qquad d_q = 1 + 2\tan\phi(1-\sin\phi)^2\underbrace{\tan^{-1}\left(\frac{D_f}{B}\right)}_{\text{radian}} \tag{6.12}$$

$$d_\gamma = 1 \tag{6.13}$$

In Eqs. (6.6)–(6.12), B and L are the width and length of rectangular foundations, respectively. For circular foundations, B is the diameter, and $B = L$.

The preceding equations for static ultimate bearing capacity evaluation are valid for dense sands where the failure surface in the soil extends to the ground surface as shown in Figure 6.1. This is what is referred to as the case of general shear failure. For shallow foundations (i.e., $D_f/B \le 1$), if the relative density of granular soils R_D is less than about 70%, *local or punching shear failure* may occur. Hence, for static ultimate bearing capacity calculation, if $0 \le R_D \le 0.67$, the values of ϕ in Eqs. (6.3)–(6.13) should be replaced by the modified friction angle (vesic, 1973)

$$\phi' = \tan^{-1}[(0.67 + R_D - 0.75R_D^2)\tan\phi] \tag{6.14}$$

The facts just described relate to the static bearing capacity of shallow foundations. However, when load is applied rapidly to a foundation to cause failure, the ultimate bearing capacity changes somewhat. This fact has been shown

Copyright 2017 Cengage Learning. All Rights Reserved. May not be copied, scanned, or duplicated, in whole or in part. Due to electronic rights, some third party content may be suppressed from the eBook and/or eChapter(s). Editorial review has deemed that any suppressed content does not materially affect the overall learning experience. Cengage Learning reserves the right to remove additional content at any time if subsequent rights restrictions require it.

experimentally by Vesic, Banks, and Woodward (1965), who conducted several laboratory model tests with a 101.6 mm diameter rigid rough model footing placed on the surface of a dense river sand (i.e., $D_f = 0$), both dry and saturated. The rate of loading to cause failure was varied in a range of 2.54×10^{-4} mm/s to over 254 mm/s. Hence, the rate was in the range of static (2.54×10^{-4} mm/s) to impact (254 mm/s) loading conditions. All but the four most rapid tests in submerged sand [loading velocity, (14.63–20.07 mm/s)] showed peak failure loads as obtained in the case of general shear failure of soil.

The four most rapid tests in submerged sand gave the load-displacement plots as obtained in the case of punching shear failure, where the failure planes do not extend to the ground surface.

For surface foundations ($D_f = 0$) in sand, $q = 0$ and $d_\gamma = 1$. So

$$q_u = \frac{1}{2}\gamma B N_\gamma S_\gamma \tag{6.15}$$

or

$$\frac{q_u}{(1/2)\gamma B} = N_\gamma S_\gamma \tag{6.16}$$

The variation of $q_u/(1/2)\gamma B$ with load velocity for the tests of Vesic, Banks, and Woodward (1965) is shown in Figure 6.2. It may be seen that, for any given

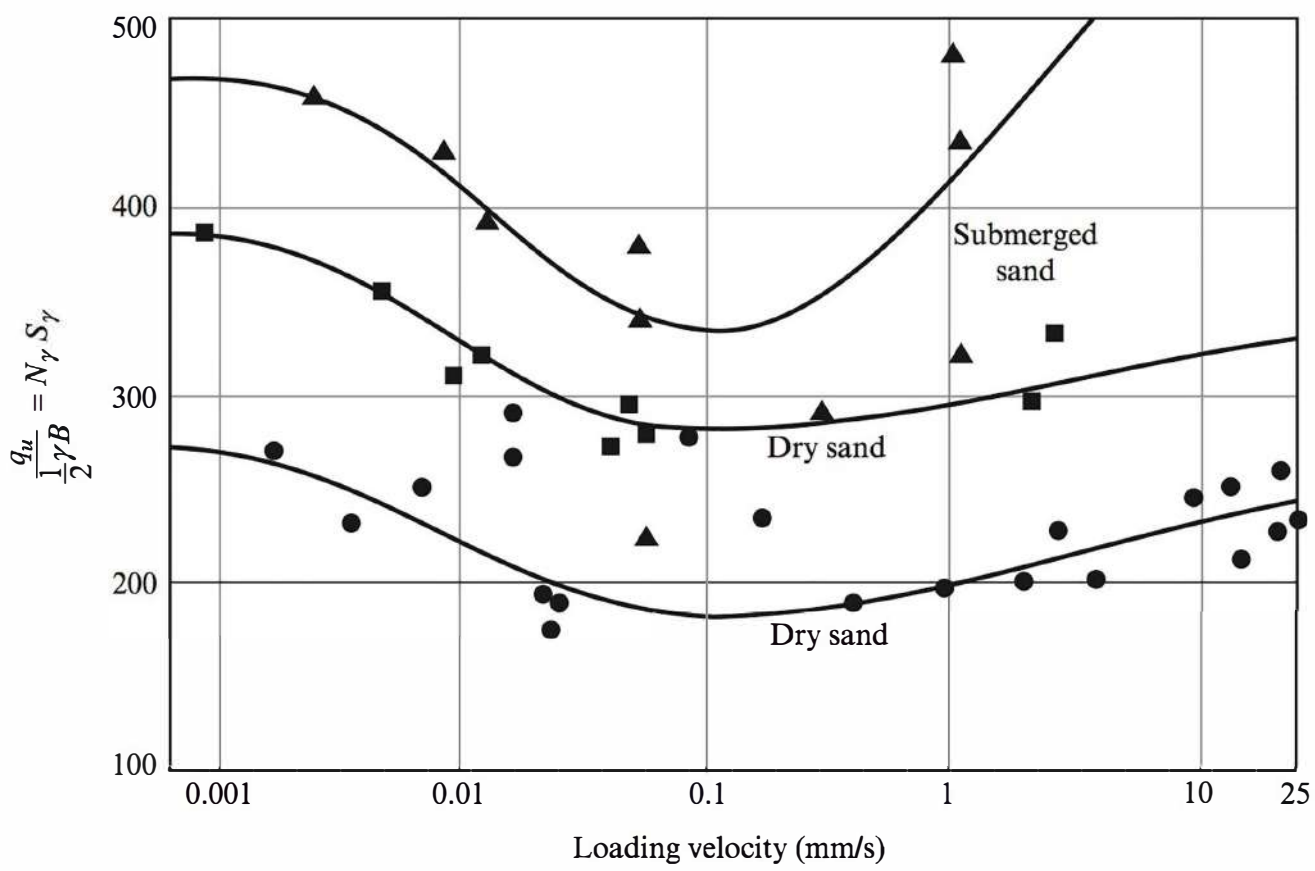

Figure 6.2 Plot of bearing capacity factor versus loading velocity (adapted from Vesic, Banks, and Woodward, 1965)

Source: Based on Vesic, A.S., Banks, D.C., and Woodard, J.M. (1965). "An Experimental Study of Dynamic Bearing Capacity of Footings on Sand," *Proceedings, 6th International Conference on Soil Mechanics and Foundation Engineering,* Montreal, Canada, Vol. II, pp. 209–213.

Copyright 2017 Cengage Learning. All Rights Reserved. May not be copied, scanned, or duplicated, in whole or in part. Due to electronic rights, some third party content may be suppressed from the eBook and/or eChapter(s). Editorial review has deemed that any suppressed content does not materially affect the overall learning experience. Cengage Learning reserves the right to remove additional content at any time if subsequent rights restrictions require it.

series of tests, the value of $q_u/(1/2)\gamma B$ gradually decreases with the loading velocity to a minimum value and then continues to increase.

This, in effect, corresponds to a decrease in the angle of friction of soil by about 2° when the loading velocity reached a value of about 50.8×10^{-3} mm/s. Such effects of strain rate in reducing the angle of friction of sand has also been observed by Whitman and Healy (1962), as described in Chapter 4.

Based on the experimental results available, the following general conclusions regarding the ultimate dynamic bearing capacity of shallow foundations in sand can be drawn:

1. For a foundation resting on sand and subjected to an acceleration level of $a_{max} \leq 13g$, it is possible for general shear type of failure to occur in soil (Heller, 1964).
2. For a foundation on sand subjected to an acceleration level of $a_{max} > 13g$, the nature of soil failure is by punching (Heller, 1964).
3. The difference in the nature of failure in soil is due to the inertial restraint of the soil involved in failure during the dynamic loading. The restraint has almost a similar effect as the overburden pressure as observed during the dynamic loading which causes the punching shear type failure in soil.
4. The minimum value of the ultimate dynamic bearing capacity of shallow foundations on dense sands obtained between static to impact loading range can be estimated by using a friction angle ϕ_{dy}, such that (Vesic, 1973)

$$\phi_{dy} = \phi - 2^\circ \tag{6.17}$$

   The value of ϕ_{dy} can be substituted in place of ϕ in Eqs. (6.2)–(6.13). However, if the soil strength parameters with proper strain rate are known from laboratory testing, they should be used instead of the approximate equation [Eq. (6.17)].
5. The increase of the ultimate bearing capacity at high loading rates as seen in Figure 6.2 is due to the fact that the soil particles in the failure zone do not always follow the path of least resistance. This results in a higher shear strength of soil, which leads to a higher bearing capacity.
6. In the case of foundations resting on loose submerged sands, transient liquefaction effects (Chapter 10) may exist (Vesic, 1973). This may results in unreliable prediction of ultimate bearing capacity.
7. The rapid increase of the ultimate bearing capacity in dense saturated sand at fast loading rates is due to the development of negative pore water pressure in the soil.

EXAMPLE 6.1

A square foundation with dimensions $B \times B$ has to be constructed on a dense sand. Its depth is $D_f = 1$ m. The unit weight and the static angle of friction of the soil can be assigned representative values of 18 kN/m³ and 39°, respectively.

Copyright 2017 Cengage Learning. All Rights Reserved. May not be copied, scanned, or duplicated, in whole or in part. Due to electronic rights, some third party content may be suppressed from the eBook and/or eChapter(s). Editorial review has deemed that any suppressed content does not materially affect the overall learning experience. Cengage Learning reserves the right to remove additional content at any time if subsequent rights restrictions require it.

The foundation may occasionally be subjected to a maximum dynamic load of 1800 kN increasing at a moderate rate. Determine the size of the foundation using a safety factor of 3.

SOLUTION:

Given that $\phi = 39°$ in the absence of any other experimental data, for minimum ultimate dynamic bearing capacity

$$\phi_{dy} = \phi - 2° = 39 - 2 = 37°$$

From Eq. (6.2)

$$q_u = qN_qS_qd_q + \frac{1}{2}\gamma BN_\gamma S_\gamma d_\gamma$$

$$q = \gamma D_f = (18)(1) = 18 \text{ kPa}$$

For $\phi_{dy} = 37°$, $N_q = 42.92$ and $N_\gamma = 66.19$.

$$S_q = 1 + \left(\frac{B}{L}\right)\tan\phi = 1 + \tan 37° = 1.754$$

$$S_\gamma = 1 - 0.4\left(\frac{B}{L}\right) = 1 - 0.4 = 0.6$$

$$d_q = 1 + 2\tan\phi(1 - \sin\phi)^2\left(\frac{D_f}{B}\right)$$

$$= 1 + 2\tan 37(1 - \sin 37)^2\left(\frac{1}{B}\right) = 1 + \frac{0.239}{B}$$

$$d_\gamma = 1$$

Thus

$$q_u = (18)(42.92)(1.754)\left(1 + \frac{0.239}{B}\right) + \frac{1}{2}(18)(B)(66.19)(0.6)(1)$$
$$= 1355 + \frac{323.9}{B} + 357.4B \qquad \text{(a)}$$

Given

$$q_u = \frac{1800 \times 3}{B^2} \text{ kPa} \qquad \text{(b)}$$

Combining Eq. (a) and (b),

$$\frac{5400}{B^2} = 1355 + \frac{323.9}{B} + 357.4B \qquad \text{(c)}$$

Copyright 2017 Cengage Learning. All Rights Reserved. May not be copied, scanned, or duplicated, in whole or in part. Due to electronic rights, some third party content may be suppressed from the eBook and/or eChapter(s). Editorial review has deemed that any suppressed content does not materially affect the overall learning experience. Cengage Learning reserves the right to remove additional content at any time if subsequent rights restrictions require it.

Following is a table to determine the value of B by trial and error. Clearly, $B \approx$ **1.6 m**.

B (m)	$5400/B^2$ (kPa)	$1355 + 323.9/B + 357.4B$ (kPa)
2.0	1350	2331.75
1.5	2400	2107.00
1.6	2109	2133.00

6.3 BEARING CAPACITY IN CLAY

For foundations resting on saturated clays ($\phi = 0$ and $c = c_u$, i.e., undrained condition), Eq. (6.1) transforms to the form

$$q_u = c_u N_c S_c d_c + q N_q S_q d_q \tag{6.18}$$

(*Note*: $N_\gamma = 0$ for $\phi = 0$ in Table 6.1)

$$N_c = 5.14 \tag{6.19}$$

and

$$N_q = 1 \tag{6.20}$$

From Eq. (6.6)

$$S_c = 1 + \left(\frac{B}{L}\right)\left(\frac{N_q}{N_c}\right)$$

For $\phi = 0$,

$$S_c = 1 + \left(\frac{B}{L}\right)\left(\frac{1}{5.14}\right) = 1 + 0.1946\left(\frac{B}{L}\right) \tag{6.21}$$

From Eq. (6.7),

$$S_q = 1 + \left(\frac{B}{L}\right)\tan\phi$$

with $\phi = 0$,

$$S_q = 1 \tag{6.22}$$

From Eqs. (6.9) and (6.10),

$$d_c = 1 + 0.4\left(\frac{D_f}{B}\right) \text{ for } \frac{D_f}{B} \le 1 \tag{6.23}$$

$$d_c = 1 + 0.4\tan^{-1}\left(\frac{D_f}{B}\right) \text{ for } \frac{D_f}{B} > 1 \tag{6.24}$$

Copyright 2017 Cengage Learning. All Rights Reserved. May not be copied, scanned, or duplicated, in whole or in part. Due to electronic rights, some third party content may be suppressed from the eBook and/or eChapter(s). Editorial review has deemed that any suppressed content does not materially affect the overall learning experience. Cengage Learning reserves the right to remove additional content at any time if subsequent rights restrictions require it.

Also, from Eqs. (6.11) and (6.12), with $\phi = 0$,

$$d_q = 1 \tag{6.25}$$

Substituting Eqs. (6.19)–(6.25) into Eq. (6.18),

$$\boxed{q_u = 5.14c_u\left[1 + 0.1946\left(\frac{B}{L}\right)\right]\left[1 + 0.4\left(\frac{D_f}{B}\right)\right] + q \quad \text{for } \frac{D_f}{B} \le 1} \tag{6.26}$$

and

$$\boxed{q_u = 5.14c_u\left[1 + 0.1946\left(\frac{B}{L}\right)\right]\left[1 + 0.4\tan^{-1}\left(\frac{D_f}{B}\right)\right] + q \quad \text{for } \frac{D_f}{B} > 1} \tag{6.27}$$

The ultimate bearing capacity of foundations resting on saturated clay soils can be estimated by using Eqs. (6.26) and (6.27), provided the strain-rate effect due to dynamic loading is taken into consideration in determination of the undrained cohesion. Unlike the case in sand, the undrained cohesion of saturated clays increases with the increase of the strain rate. This fact has been discussed in Chapter 4 in relation to the unconsolidated-undrained triaxial tests on *Buckshot* clay. Based on those results, Carroll (1963) suggested that $c_{u(\text{dyn})}/c_{u(\text{stat})}$ may be approximated to be about 1.5.

For a given foundation, the strain rate $\dot{\varepsilon}$ can be approximated as (Figure 6.3)

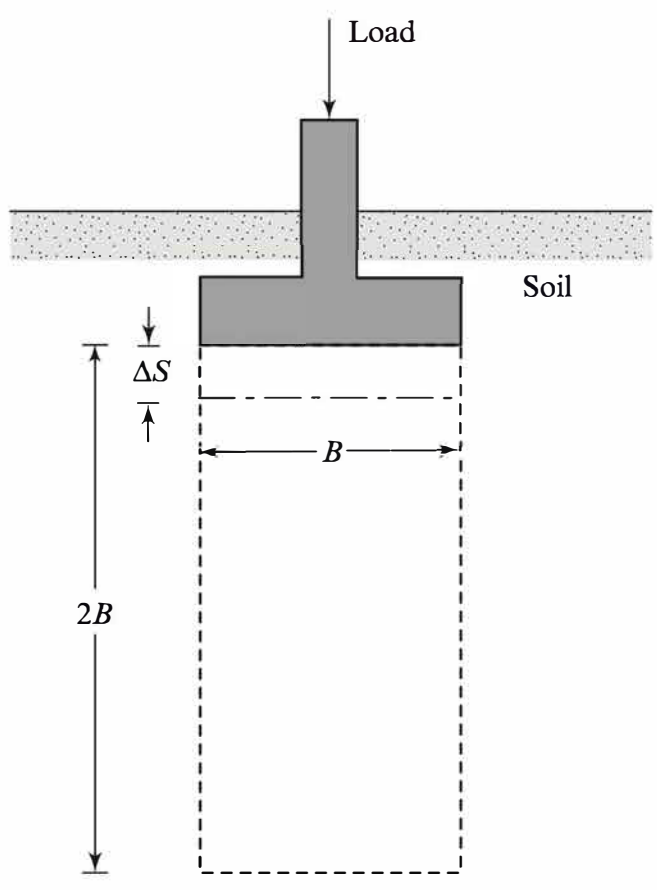

Figure 6.3 Definition of strain rate under a foundation

Copyright 2017 Cengage Learning. All Rights Reserved. May not be copied, scanned, or duplicated, in whole or in part. Due to electronic rights, some third party content may be suppressed from the eBook and/or eChapter(s). Editorial review has deemed that any suppressed content does not materially affect the overall learning experience. Cengage Learning reserves the right to remove additional content at any time if subsequent rights restrictions require it.

$$\dot{\varepsilon} = \left(\frac{1}{\Delta t}\right)\left(\frac{(1/2)\,\Delta S}{B}\right) \tag{6.28}$$

where B is the width of the foundation.

6.4 BEHAVIOR OF FOUNDATIONS UNDER TRANSIENT LOADS

Triandafilidis (1965) has presented a solution for dynamic response of continuous foundation supported by saturated cohesive soil ($\phi = 0$ condition) and subjected to a transient load. The rigid plastic analysis for the bearing capacity in cohesive soils presented by Triandafilidis (1965) has been extended for determination of the bearing capacity of continuous foundations resting on a c-ϕ soil and subjected to a transient horizontal load by Prakash and Chummar (1967). Both these two works considered a rotational mode of failure. However, it is possible that a foundation may fail by vertically punching into the soil mass due to the application of a vertical transient load. Wallace (1961) has presented a procedure for the estimation of the vertical displacement of a continuous foundation with the assumption that the soil behaves as a *rigid plastic material*. In this analysis, the failure surface in the soil mass is assumed to be of similar type as suggested by Terzaghi (1943) for the evaluation of static bearing capacity of strip foundations. Interested readers may refer to these articles.

6.5 EXPERIMENTAL OBSERVATION OF LOAD-SETTLEMENT RELATIONSHIP FOR VERTICAL TRANSIENT LOADING

A limited number of laboratory tests for observation of load-settlement relationships of foundations under transient loading are available. (Cunny and Sloan, 1961; Shenkman and McKee, 1961; Jackson and Hadala, 1964; Carroll, 1963). The experimental evaluations of these tests are presented in this section.

Load-settlement observations of *square* model foundations resting on sand and clay and subjected to transient loads have been presented by Cunny and Sloan (1961). The model foundations were of varying sizes from 114.3−228.6 mm squares and were placed on the surface of the compacted soil layers. The transient loads to which the foundations were subjected were of the nature shown in Figure 6.4. The nature of the settlement of foundations with time during the application of the dynamic load is also shown in the same figure. In general, during *rise time* (t_r) of the dynamic load, the settlement of a foundation

Copyright 2017 Cengage Learning. All Rights Reserved. May not be copied, scanned, or duplicated, in whole or in part. Due to electronic rights, some third party content may be suppressed from the eBook and/or eChapter(s). Editorial review has deemed that any suppressed content does not materially affect the overall learning experience. Cengage Learning reserves the right to remove additional content at any time if subsequent rights restrictions require it.

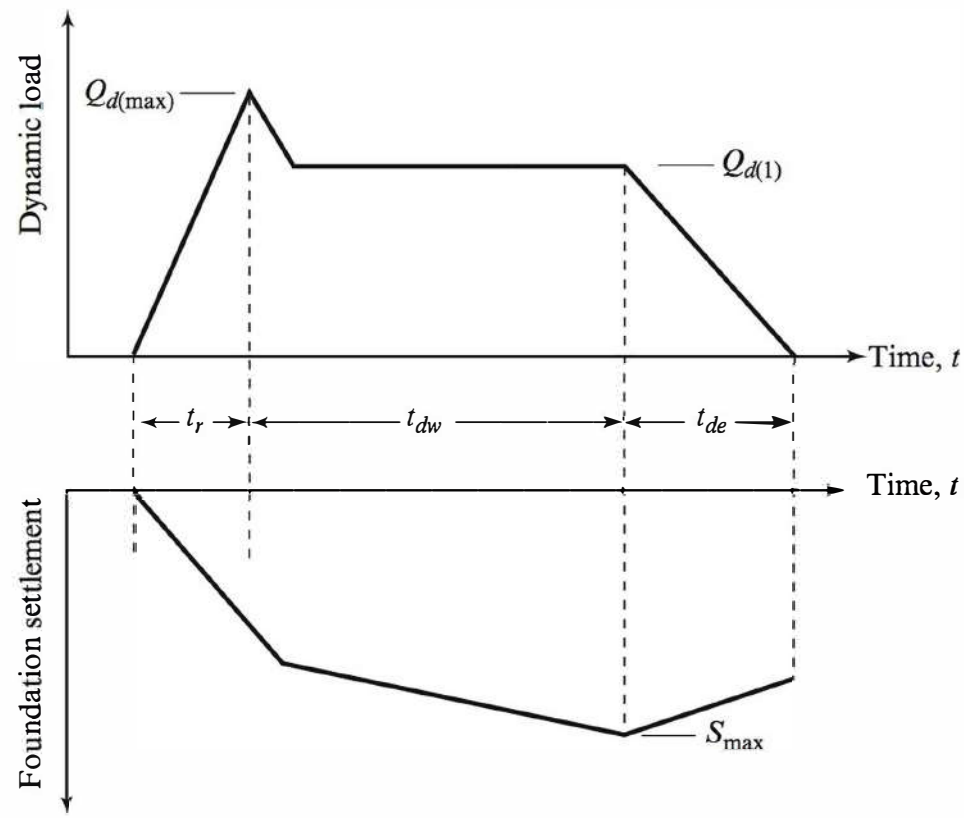

Figure 6.4 Nature of dynamic load applied to laboratory model foundations

increases rapidly. Once the peak load [$Q_{d(\max)}$] is reached, the rate of settlement with time decreases. However, the total settlement of a foundation continues to increase during the dwell time of the load (t_{dw}) and reaches a maximum value ($S_{\max}$) at the end of the dwell time. During the *decay period* of the load (t_{de}), the foundation rebounds to some degree.

The results of the model foundation tests on sand obtained by Cunny and Sloan are given in Table 6.2. Also, the results of model tests for square surface foundations on clay as reported by Cunny and Sloan are shown in Table 6.3. Based on these results, a few general observations may be made:

1. The settlement of foundations under transient loading is generally uniform. This can be seen by observing the settlement at three corners of the model foundations—both in sand and clay.
2. Foundations under dynamic loading may fail by punching type of failure in soil, although general shear failure may be observed for the same footings tested under static conditions.
3. In Table 6.2, the 228 mm foundation failed at a load of 11.52 kN under static loading conditions. The total settlement after the failure load application was 66.55 mm. However, under dynamic loading conditions, when $Q_{d(1)}/Q_u$ was equal to 1.25 (Test 4), the settlement of the footing was about 10.16 mm. Similarly, in Table 6.3, the static failure load Q_u of the 114.3 mm foundation was 10.94 kN with a settlement of 50.8 mm. The same foundation under dynamic loading with $Q_{d(1)}/Q_u = 1.17$ (Test 2) showed a total settlement of about 17.78 mm.

Copyright 2017 Cengage Learning. All Rights Reserved. May not be copied, scanned, or duplicated, in whole or in part. Due to electronic rights, some third party content may be suppressed from the eBook and/or eChapter(s). Editorial review has deemed that any suppressed content does not materially affect the overall learning experience. Cengage Learning reserves the right to remove additional content at any time if subsequent rights restrictions require it.

Table 6.2 Load-Settlement Relationship of Square Foundations on Sand Due to Transient Loading[a]

Test No.	Size of footing (mm)	Q_u (kN)[b]	$Q_{d(max)}$ (kN)	$Q_{d(1)}$ (kN)	$\frac{Q_{d(1)}}{Q_u}$ %	t_r (ms)	t_{dw} (ms)	t_{de} (ms)	$S_{max(mm)}$[c] Pot.1	Pot.2	Pot.3
1	152 × 152	3.43	3.56	3.56	104	18	122	110	7.11	1.27	2.79
2	203 × 203	8.09	13.97	12.46	154	8	420	255	—	—	—
3	203 × 203	8.09	10.12	9.67	120	90	280	290	21.08	23.62	24.13
4	228 × 228	11.52	15.57	14.46	125	11	0	350	10.16	10.67	10.16

[a] Compiled from Cunny and Sloan (1961): Compacted dry unit weight of sand = 16.26 kN/m³; relative density of compaction of sand = 96%; triaxial angle of friction of sand = 32°.
[b] Ultimate failure load tested under static conditions.
[c] Settlement of foundations measured at three corners of each foundation by linear potentiometer.

Source: Based on Cunny, R. W., and Sloan, R. C. (1961). "Dynamic Loading Machine and Results of Preliminary Small-Scale Footing Tests," *Special Technical Publication No. 305,* American Society for Testing and Materials, pp. 65–67.

Table 6.3 Load-Settlement Relationship of Square Foundations on Clay Due to Transient Loading[a]

Test No.	Size of footing (mm)	Q_u (kN)[b]	$Q_{d(max)}$ (kN)	$Q_{d(1)}$ (kN)	$\frac{Q_{d(1)}}{Q_u}$ %	t_r (ms)	t_{dw} (ms)	t_{de} (ms)	$S_{max(mm)}$[c] Pot.1	Pot.2	Pot.3
1	114 × 114	10.94	12.68	10.12	93	9	170	350	12.70	12.70	12.19
2	114 × 114	10.94	13.79	12.54	117	9	0	380	16.76	18.29	17.78
3	114 × 114	10.94	15.39	13.21	121	10	0	365	43.18	42.67	43.18
4	127 × 127	13.52	15.92	13.12	97	9	0	360	14.73	13.97	13.97

[a] Compiled from Cunny and Sloan (1961): Compacted moist unit weight = 14.79-1547 kN/m³; moisture content = 22.5 ± 1.7%; c = 115 kPa; ϕ = 4°(undrained test).
[b] Ultimate failure load tested under static loading conditions.
[c] Settlement of foundations measured at three corners of each foundation by linear potentiometer.

Source: Based on Cunny, R. W., and Sloan, R. C. (1961). "Dynamic Loading Machine and Results of Preliminary Small-Scale Footing Tests," *Special Technical Publication No. 305,* American Society for Testing and Materials, pp. 65–67.

These facts show that, for a limiting settlement condition, a foundation can support a higher load under dynamic loading conditions than those observed from static tests.

Dynamic Load versus Settlement Prediction in Clayey Soils

Jackson and Hadala (1964) reported several laboratory model tests on 114.3−203.2 mm square foundations resting on highly saturated, compacted, plastic Buckshot clay. The tests were similar in nature to those described previously in this section. Based on these results, Jackson and Hadala have shown that there is a unique nondimensional relation between $Q_{d(\max)}/B^2c_u$ and $S_{\max}/B$ (c_u

Copyright 2017 Cengage Learning. All Rights Reserved. May not be copied, scanned, or duplicated, in whole or in part. Due to electronic rights, some third party content may be suppressed from the eBook and/or eChapter(s). Editorial review has deemed that any suppressed content does not materially affect the overall learning experience. Cengage Learning reserves the right to remove additional content at any time if subsequent rights restrictions require it.

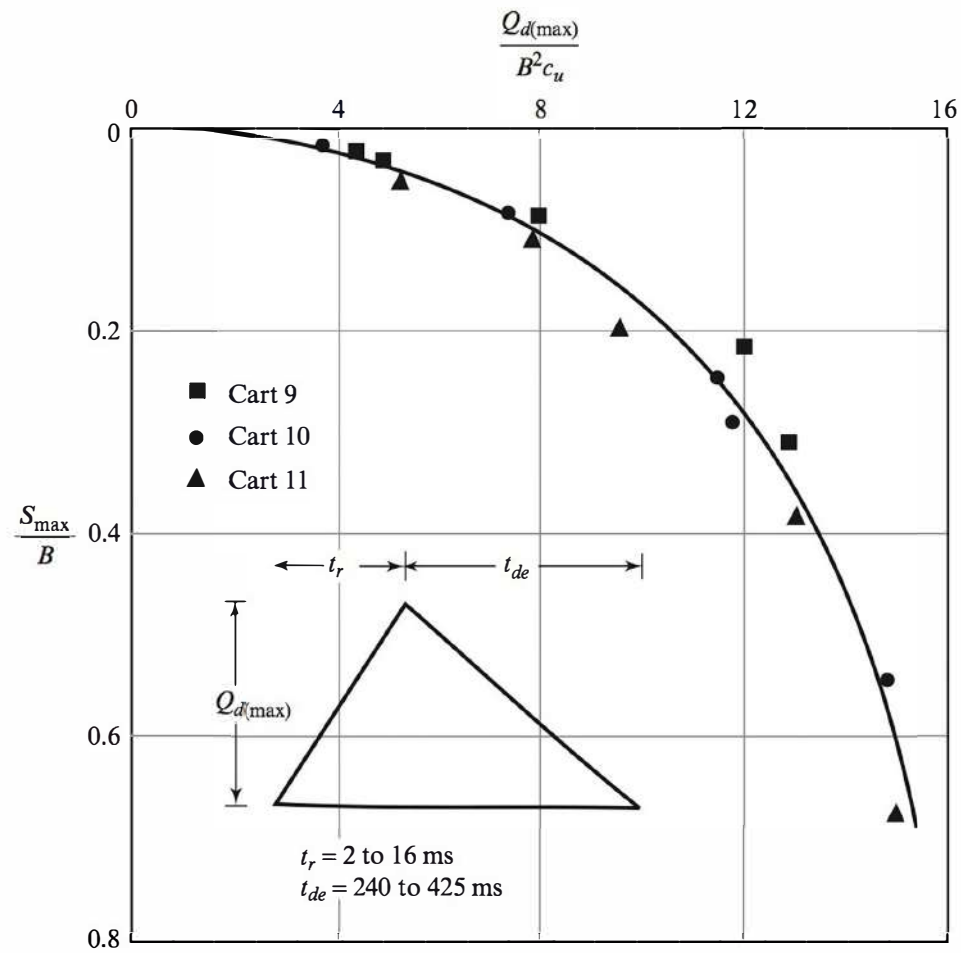

Figure 6.5 Nondimensional relationship of $Q_{d(\max)}/B^2c_u$ and $S_{(\max)}/B$ for model foundation tests in Buckshot clay (compiled from Jackson and Hadala, 1964)

Source: Based on Jackson, J. G., Jr., and Hadala, P. F. (1964). "Dynamic Bearing Capacity of Soils. Report 3: The application of Similitude of Small-Scale Footings Tests," U.S. Army Corps of Engineers, Waterways Experiment Station, Vicksburg, Mississippi.

is undrained shear strength). This is shown in Figure 6.5. Note that the tests on which Figure 6.5 are based have $t_{dw} = 0$. However, for dynamic loads with $t_{dw} > 0$, the results would not be too different.

The preceding finding is of great practical importance in estimation of the dynamic load-settlement relationships of foundations. Jackson and Hadala have recommended the following procedure for that purpose.

1. Determine the static load Q versus settlement S relationship for a foundation from plate bearing tests in the field.
2. Determine the unconfined compression strength of the soil q_{uc} in the laboratory.

$$q_{uc} = 2c_u$$

3. Plot a graph of Q/B^2c_u versus S_{stat}/B. (See Figure 6.6, curve *a*.)

$$\frac{Q_{d(\max)}}{B^2c_u}$$

4. For any given value of S_{stat}/B, multiply Q/B^2c_u by the strain rate factor ($\approx$1.5) and plot it in the same graph. The resulting graph of S_{stat}/B versus $1.5Q/B^2c_u$ will be the predicted relationship between $Q_{d(\max)}/B^2c_u$ and $S_{\max}/B$. (See Figure 6.6, curve *b*.)

Copyright 2017 Cengage Learning. All Rights Reserved. May not be copied, scanned, or duplicated, in whole or in part. Due to electronic rights, some third party content may be suppressed from the eBook and/or eChapter(s). Editorial review has deemed that any suppressed content does not materially affect the overall learning experience. Cengage Learning reserves the right to remove additional content at any time if subsequent rights restrictions require it.

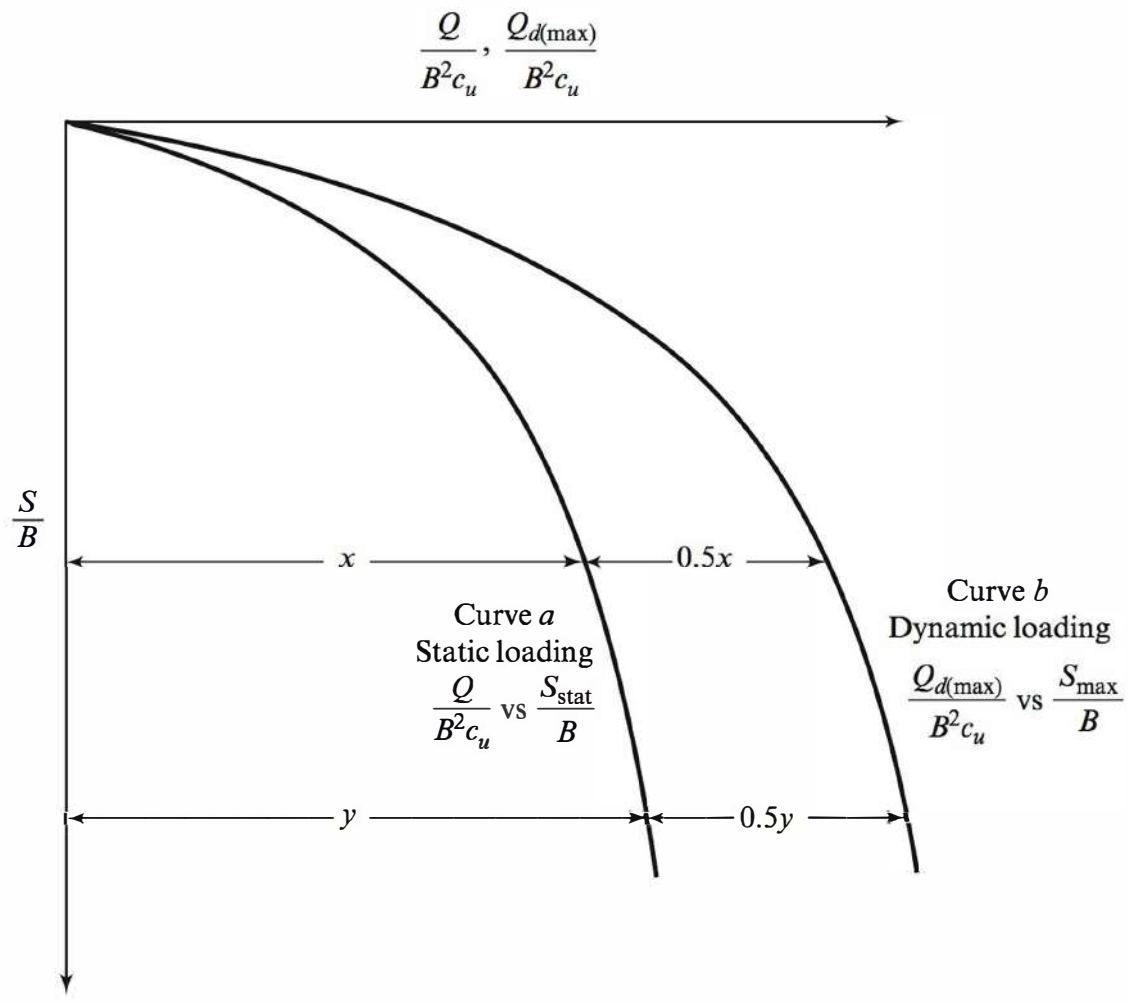

Figure 6.6 Prediction of dynamic load-settlement relationship for foundations on clay

EXAMPLE 6.2

The estimated static plate load-bearing test results of a foundation resting on stiff clay and 1.5 m in diameter are given below.

Q (kN)	Settlement (mm)	Q (kN)	Settlement (mm)
0	0	27.0	41.9
4.5	6.4	36.0	73.7
9.0	12.2	40.5	94.0
18.0	27.9	45.0	172.7

The unconfined compression strength of this clay was 160 kPa.

a. Plot a graph of estimated $S_{\max}/B$ versus $Q_{d(\max)}/B^2c_u$ assuming a strain-rate factor of 1.5.
b. Determine the magnitude of the maximum dynamic load $Q_{d(\max)}$ that produces a maximum settlement $S_{\max}$ of 0.15 m.

SOLUTION:

Given $B = 1.5\text{ m} = 1500\text{ mm}$. and $c_u = \frac{1}{2}(160) = 80\text{ kPa}$, the following table can be prepared.

Copyright 2017 Cengage Learning. All Rights Reserved. May not be copied, scanned, or duplicated, in whole or in part. Due to electronic rights, some third party content may be suppressed from the eBook and/or eChapter(s). Editorial review has deemed that any suppressed content does not materially affect the overall learning experience. Cengage Learning reserves the right to remove additional content at any time if subsequent rights restrictions require it.

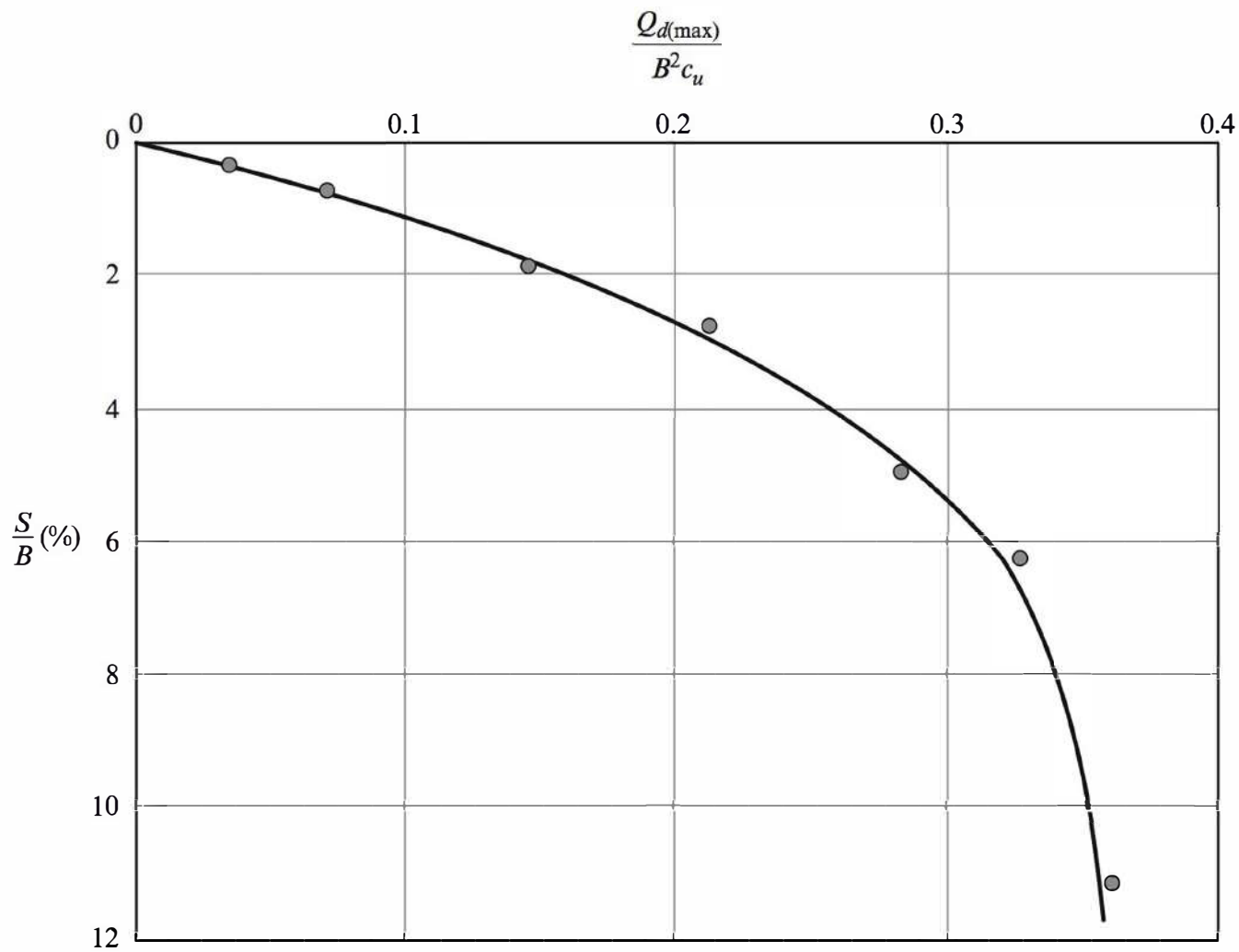

Figure 6.7

Q (kN) (1)	S_{stat} (mm) (2)	$\frac{S}{B}$ (%) (3)	$\frac{Q}{B^2 c_u}$ (4)	$\frac{1.5\,Q}{B^2 c_u}$ (5)
0	0	0	0	0
4.5	6.4	0.4267	0.025	0.037
9.0	12.2	0.8133	0.050	0.075
18.0	27.9	1.8600	0.100	0.150
27.0	41.9	2.7930	0.150	0.225
36.0	73.7	4.9130	0.200	0.300
40.5	94.0	6.2670	0.225	0.337
45.0	172.7	11.5130	0.250	0.375

Assuming S/B (Col.3) to be equal to S_{max}/B and $1.5\,Q/B^2c_u$ to be equal to $Q_{d(\max)}/B^2c_u$, a graph can be plotted (Figure 6.7).

For $S_{max} = 0.15$ m, $\frac{S_{max}}{B} = \frac{0.15}{1.5} \times 100 = 10\%$

Copyright 2017 Cengage Learning. All Rights Reserved. May not be copied, scanned, or duplicated, in whole or in part. Due to electronic rights, some third party content may be suppressed from the eBook and/or eChapter(s). Editorial review has deemed that any suppressed content does not materially affect the overall learning experience. Cengage Learning reserves the right to remove additional content at any time if subsequent rights restrictions require it.

From Figure 6.7, the value of $Q_{d(\max)}/B^2c_u$ corresponding to $S_{\max}/B = 10\%$ is about 0.348. Hence

$$Q_{d(\max)} = (0.348)(1.5^2)(80) = \mathbf{62.64\ kN}$$

6.6 SEISMIC BEARING CAPACITY

6.6.1 Solution of Richards et al. (1993)

In some instances, as stated before, shallow foundations may fail during seismic events. Published studies relating to the bearing capacity of shallow foundations in such instances are rare. In 1993, Richards et al. developed a seismic bearing capacity theory that shall be detailed in this section.

Figure 6.8 shows a failure surface in soil assumed for the subsequent analysis, under static conditions. Similarly, Figure 6.9 shows the assumed failure under earthquake conditions. Note that, in the two figures,

$$\alpha_A, \alpha_{AE} = \text{inclination angles for active pressure conditions}$$

and

$$\alpha_P, \alpha_{PE} = \text{inclination angles for passive pressure conditions}$$

According to this theory, the ultimate bearing capacities for *continuous foundations* in granular soil are

$$q_u = cN_c + qN_q + \frac{1}{2}\gamma BN_\gamma \qquad \text{(Static conditions)} \tag{6.29}$$

and

$$q_{uE} = cN_{cE} + qN_{qE} + \frac{1}{2}\gamma BN_{\gamma E} \quad \text{(Earthquake conditions)} \tag{6.30}$$

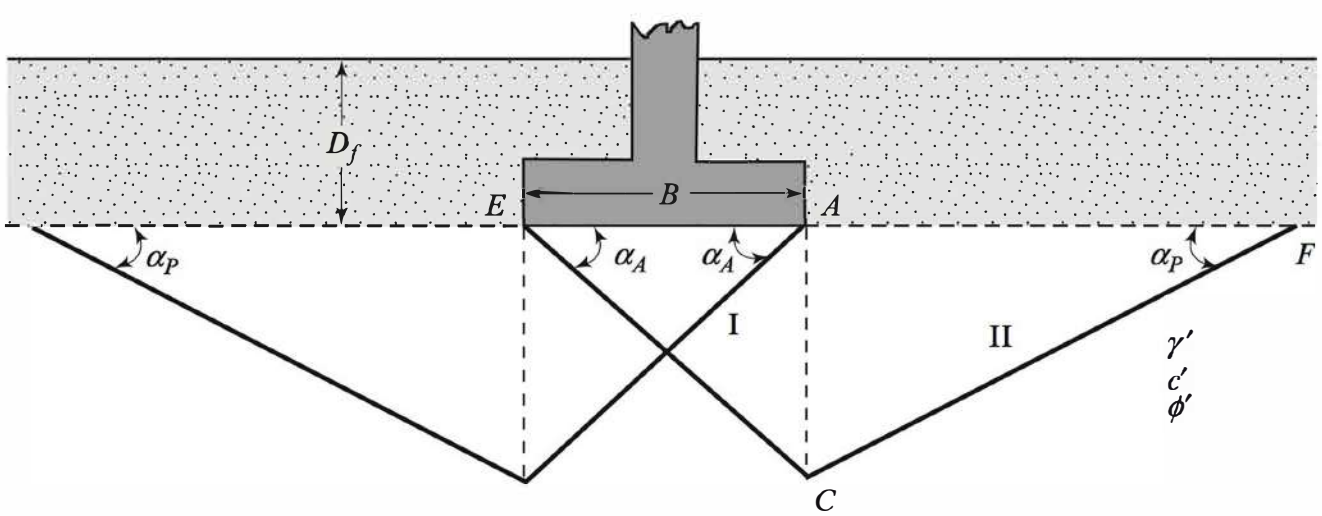

Figure 6.8 Assumed failure surface in soil for static bearing capacity analysis

Copyright 2017 Cengage Learning. All Rights Reserved. May not be copied, scanned, or duplicated, in whole or in part. Due to electronic rights, some third party content may be suppressed from the eBook and/or eChapter(s). Editorial review has deemed that any suppressed content does not materially affect the overall learning experience. Cengage Learning reserves the right to remove additional content at any time if subsequent rights restrictions require it.

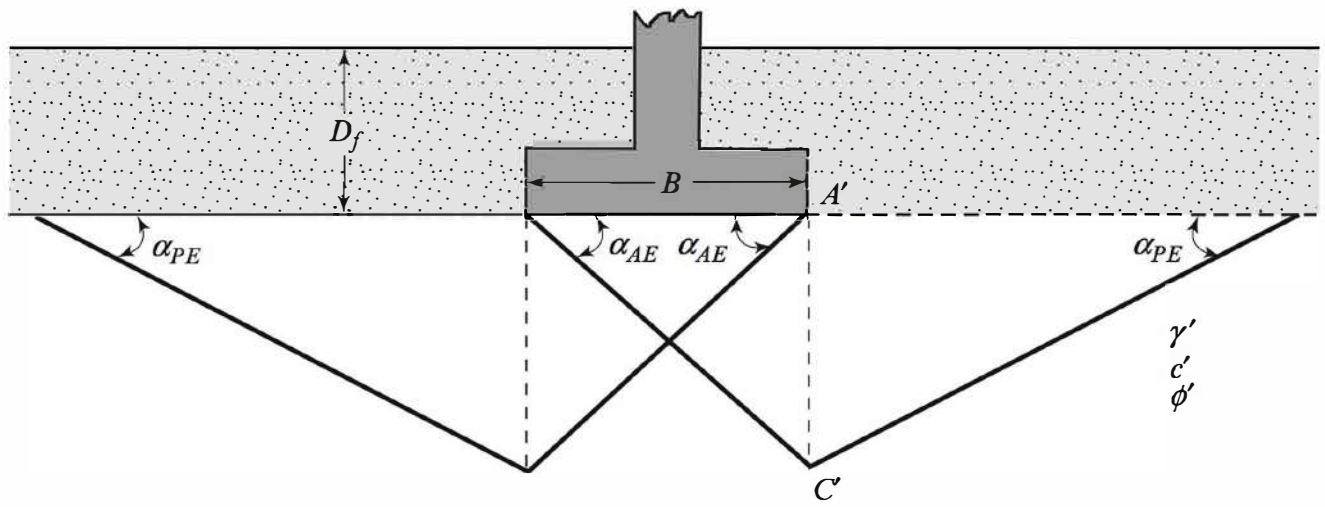

Figure 6.9 Assumed failure surface in soil for seismic bearing capacity analysis

where $N_c, N_q, N_\gamma, N_{cE}, N_{qE}, N_{\gamma E}$ = bearing capacity factors

$$q = \gamma D_f$$

Note that

$$N_c, N_q \text{ and } N_\gamma = f(\phi')$$

and

$$N_{cE}, N_{qE} \text{ and } N_{\gamma E} = f(\phi', \tan\theta)$$

where
$$\tan\theta = \frac{k_h}{1 - k_v} \tag{6.31}$$

k_h = horizontal coefficient of acceleration due to an earthquake
k_v = vertical coefficient of acceleration due to an earthquake

The variation of N_c, N_q, and N_γ can be determined by considering AC as a vertical soil retaining wall with a horizontal backfill (Figure 6.8) and Coulomb's earth pressure. The wall AC is subjected to an active thrust from Zone I (i.e., AEC) and a passive thrust from Zone II (i.e., ACF).

If $c = 0$, $\gamma = 0$, $q \neq 0$, then from Eq. (6.29),

$$q_u = qN_q \tag{6.32}$$

where
$$N_q = \frac{K_P}{K_A} \tag{6.33}$$

K_P = Coulomb's passive earth pressure coefficient
K_A = Coulomb's active earth pressure coefficient

Copyright 2017 Cengage Learning. All Rights Reserved. May not be copied, scanned, or duplicated, in whole or in part. Due to electronic rights, some third party content may be suppressed from the eBook and/or eChapter(s). Editorial review has deemed that any suppressed content does not materially affect the overall learning experience. Cengage Learning reserves the right to remove additional content at any time if subsequent rights restrictions require it.

Similarly, if $q = 0$, $c = 0$, and $\gamma \neq 0$, then from Eq. (6.29),

$$q_u = \frac{1}{2}\gamma B N_\gamma \tag{6.34}$$

where

$$N_\gamma = \tan\alpha_A\left(\frac{K_P}{K_A} - 1\right) \tag{6.35}$$

The relationships for K_A, K_P, α_A, and α_P can be given as follow:

$$K_A = \frac{\cos^2\phi}{\cos\delta\left\{1 + \sqrt{\dfrac{\sin(\phi+\delta)\sin\phi}{\cos\delta}}\right\}^2} \tag{6.36}$$

$$K_P = \frac{\cos^2\phi}{\cos\delta\left\{1 - \sqrt{\dfrac{\sin(\phi-\delta)\sin\phi}{\cos\delta}}\right\}^2} \tag{6.37}$$

$$\alpha_A = \phi + \tan^{-1}\left\{\frac{[\tan\phi(\tan\phi + \cot\phi)(1 + \tan\delta\cot\phi]^{1/2} - \tan\phi}{1 + \tan\delta(\tan\phi + \cot\phi)}\right\} \tag{6.38}$$

$$\alpha_P = -\phi + \tan^{-1}\left\{\frac{[\tan\phi(\tan\phi + \cot\phi)(1 + \tan\delta\cot\phi]^{1/2} + \tan\phi}{1 + \tan\delta(\tan\phi + \cot\phi)}\right\} \tag{6.39}$$

where δ = soil-wall friction angle
It has been recommended to use $\delta = \phi/2$ in calculation of N_q and N_γ.

If $q = 0$ and $\gamma = 0$, then From Eq. (6.29),

$$q_u = cN_c \tag{6.40}$$

where

$$N_c = (N_q - 1)\cot\phi \tag{6.41}$$

The variations of N_q, N_γ, and N_c as determined from Eqs. (6.33), (6.35), and (6.41) are given in Table 6.4 and Figure 6.10.

Table 6.4 Bearing capacity factors – N_c, N_q, and N_γ

ϕ (deg)	N_c	N_q	N_γ
0	6.0	1.0	0
10	7.77	2.37	1.38
20	13.46	5.90	6.06
30	26.86	16.51	23.76
40	69.16	59.03	111.9

Copyright 2017 Cengage Learning. All Rights Reserved. May not be copied, scanned, or duplicated, in whole or in part. Due to electronic rights, some third party content may be suppressed from the eBook and/or eChapter(s). Editorial review has deemed that any suppressed content does not materially affect the overall learning experience. Cengage Learning reserves the right to remove additional content at any time if subsequent rights restrictions require it.

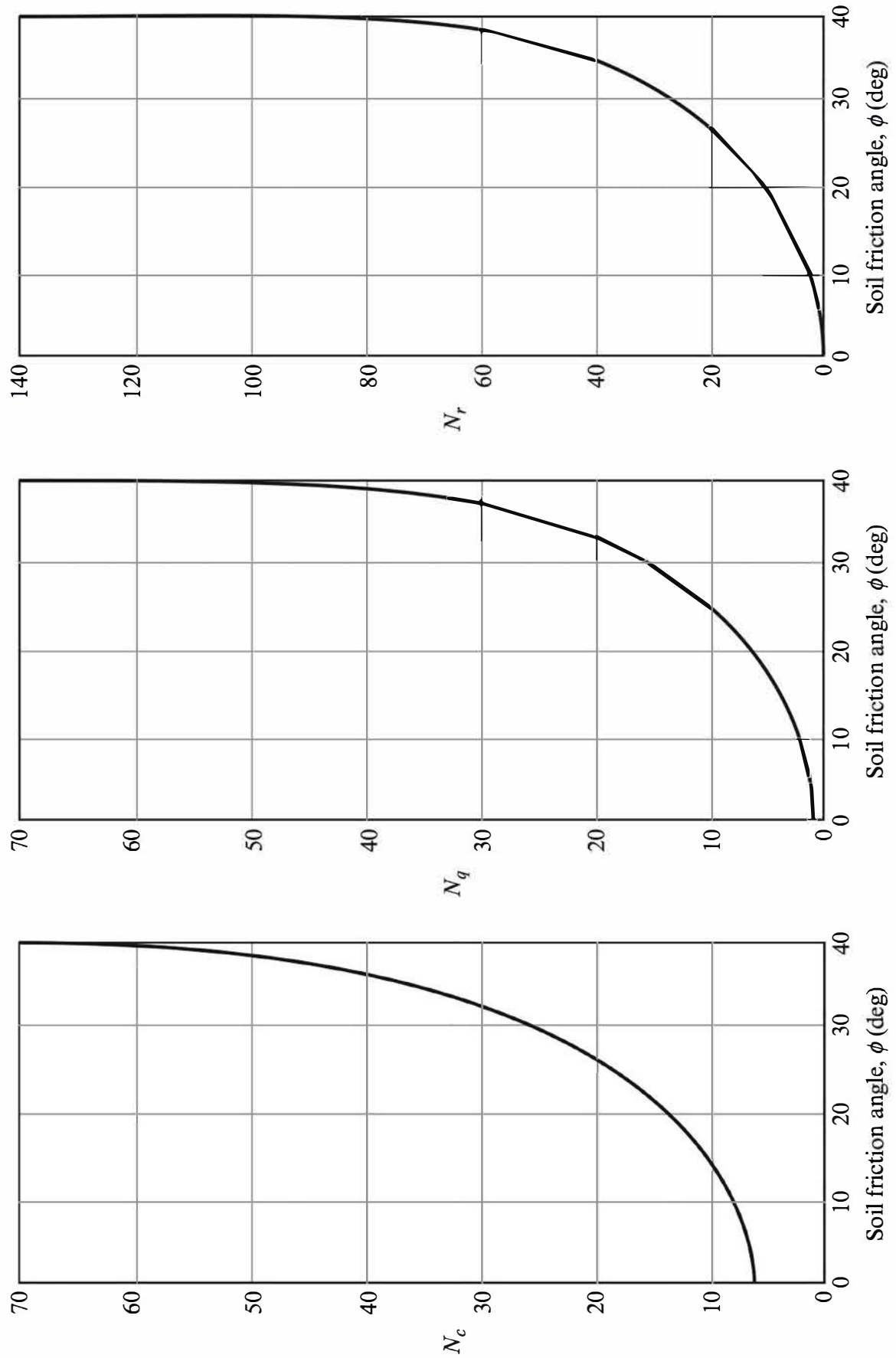

Figure 6.10 Variation of N_c, N_q, and N_γ based on failure surface assumed in Figure 6.8

Copyright 2017 Cengage Learning. All Rights Reserved. May not be copied, scanned, or duplicated, in whole or in part. Due to electronic rights, some third party content may be suppressed from the eBook and/or eChapter(s). Editorial review has deemed that any suppressed content does not materially affect the overall learning experience. Cengage Learning reserves the right to remove additional content at any time if subsequent rights restrictions require it.

The variation of N_{cE}, N_{qE}, and $N_{\gamma E}$ can be evaluated in a similar manner described above to evaluate of N_c, N_q, and N_γ. For this we can consider $A'C'$ (Figure 6.9) as a vertical soil retaining wall with a horizontal backfill and extend the Coulomb failure mechanism to the dynamic earthquake situation. With that, we obtain

$$N_q = \frac{K_{PE}}{K_{AE}} \tag{6.42}$$

$$N_\gamma = \tan\alpha_{AE}\left(\frac{K_{PE}}{K_{AE}} - 1\right) \tag{6.43}$$

where

$$K_{AE} = \frac{\cos^2(\phi-\theta)}{\cos\theta\cos(\delta+\theta)\left\{1+\sqrt{\dfrac{\sin(\phi+\delta)\sin(\phi-\theta)}{\cos(\delta+\theta)}}\right\}^2} \tag{6.44}$$

$$K_{PE} = \frac{\cos^2(\phi-\theta)}{\cos\theta\cos(\delta+\theta)\left\{1-\sqrt{\dfrac{\sin(\phi+\delta)\sin(\phi-\theta)}{\cos(\delta+\theta)}}\right\}^2} \tag{6.45}$$

$$\alpha_{AE} = a + \tan^{-1}\left\{\frac{\sqrt{(1+\tan^2 a)[1+\tan(\delta+\theta)\cot a]} - \tan a}{1+\tan(\delta+\theta)(\tan a + \cot a)}\right\} \tag{6.46}$$

$$\alpha_{PE} = -a + \tan^{-1}\left\{\frac{\sqrt{(1+\tan^2 a)[1+\tan(\delta-\theta)\cot a]} + \tan a}{1+\tan(\delta+\theta)(\tan a + \cot a)}\right\} \tag{6.47}$$

$$a = \phi - \theta \tag{6.48}$$

The bearing capacity factor N_{cE} can be obtained from a similar relationship as in Eq. (6.41), or

$$N_{cE} = (N_{qE} - 1)\cot\phi \tag{6.49}$$

Figure 6.11 gives the variation of N_{cE}/N_c, N_{qE}/N_q, and $N_{\gamma E}/N_\gamma$ with $\tan\theta = k_h/(1-k_v)$. It should be noted that N_{cE}, N_{qE}, and $N_{\gamma E}$ have been calculated with $\delta = \phi/2$.

Under static conditions, bearing capacity failure can lead to a substantial sudden downward movement of the foundation. However, bearing capacity-related settlement in an earthquake is important, and it takes place when the ratio $\tan\theta = k_h/(1-k_v)$ reaches the critical value $(k_h/1-k_v)^*$. If $k_v = 0$, then $(k_h/1-k_v)^*$ becomes equal to k_h^*.

Copyright 2017 Cengage Learning. All Rights Reserved. May not be copied, scanned, or duplicated, in whole or in part. Due to electronic rights, some third party content may be suppressed from the eBook and/or eChapter(s). Editorial review has deemed that any suppressed content does not materially affect the overall learning experience. Cengage Learning reserves the right to remove additional content at any time if subsequent rights restrictions require it.

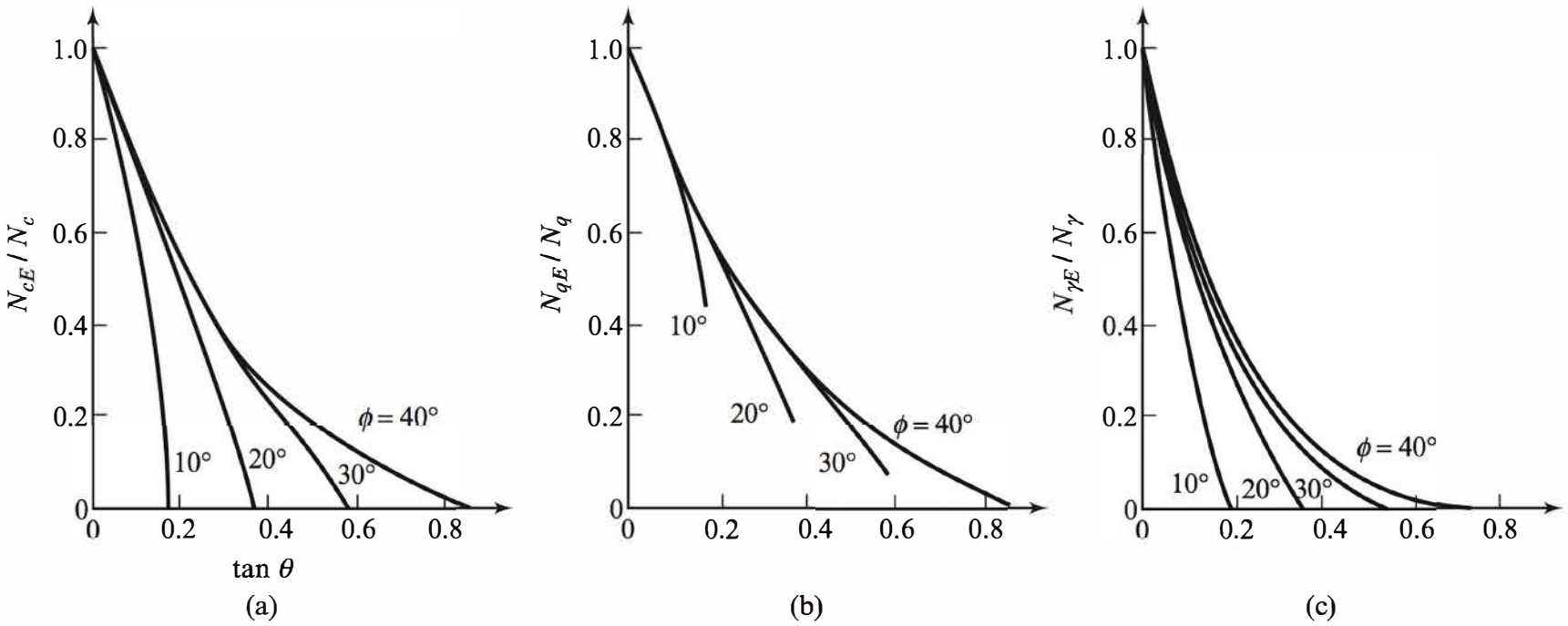

Figure 6.11 Variation of N_{cE}/N_c, N_{qE}/N_q, $N_{\gamma E}/N_\gamma$ with $\tan\theta$

Figure 6.12 shows the variation of k_h^* (for $k_v = 0$) with the factor of safety (FS) applied to the ultimate static bearing capacity [Eq. 6.29], with ϕ', and D_f/B (for $\phi' = 30°$ and 40°).

The settlement of a strip foundation due to an earthquake using a sliding block approach can be estimated (Richards, Elms and Budhu, 1993) as

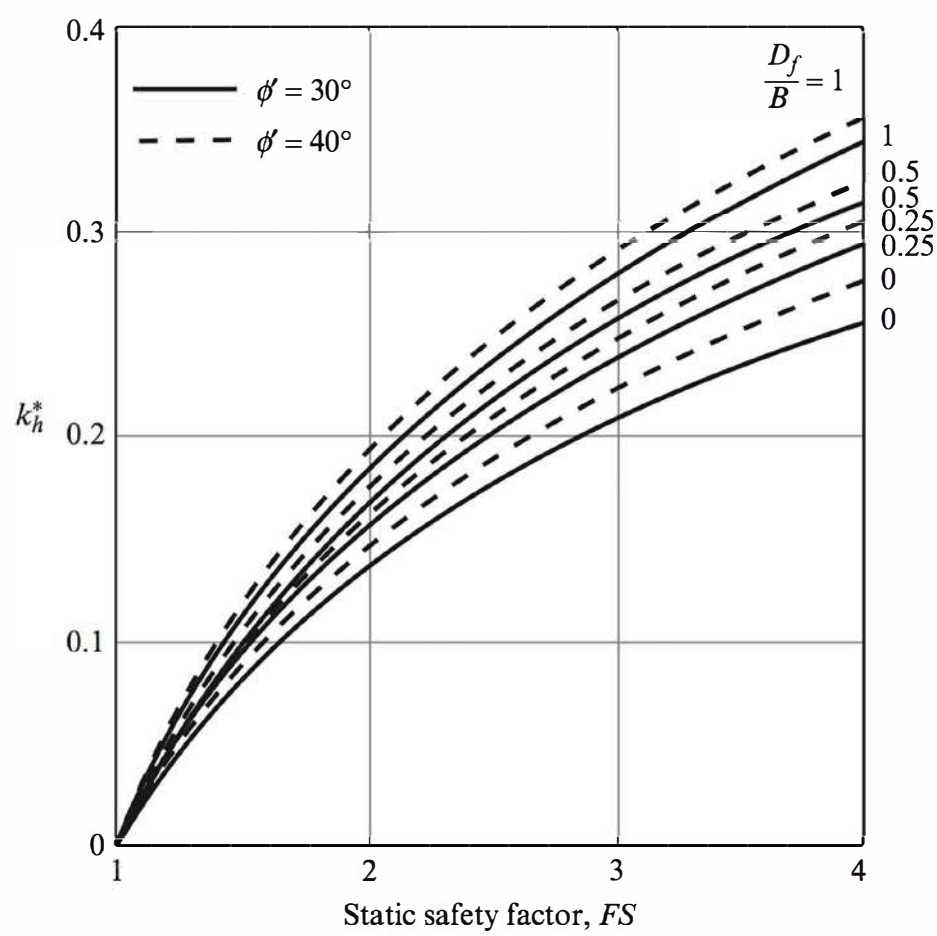

Figure 6.12 Critical acceleration k_h^* for $k_v = 0$ for granular soil ($c = 0$)

Copyright 2017 Cengage Learning. All Rights Reserved. May not be copied, scanned, or duplicated, in whole or in part. Due to electronic rights, some third party content may be suppressed from the eBook and/or eChapter(s). Editorial review has deemed that any suppressed content does not materially affect the overall learning experience. Cengage Learning reserves the right to remove additional content at any time if subsequent rights restrictions require it.

$$S_{Eq}(\text{m}) = 0.174\frac{V^2}{Ag}\left[\frac{k_h^*}{A}\right]^{-4}\tan\alpha_{AE} \tag{6.50}$$

where V = peak velocity for the design earthquake (m/sec)
A = acceleration coefficient for the design earthquake
g = acceleration due to gravity (9.81 m/sec^2)

The values of k_h^* and α_{AE} can be obtained from Figure 6.12 and Table 6.5, respectively. This approach can be used to design a foundation based on limiting seismic settlements.

Table 6.5 Variation of α_{AE} with k_h^* and soil friction angle ϕ' (Compiled from Richards, Elms, and Budhu, 1993)

	$\tan\alpha_{AE}$				
k_h^*	$\phi' = 20°$	$\phi' = 25°$	$\phi' = 30°$	$\phi' = 35°$	$\phi' = 40°$
0.05	1.10	1.24	1.39	1.57	1.75
0.10	0.97	1.13	1.26	1.44	1.63
0.15	0.82	1.00	1.15	1.32	1.48
0.20	0.71	0.87	1.02	1.18	1.35
0.25	0.56	0.74	0.92	1.06	1.23
0.30		0.61	0.77	0.94	1.10
0.35		0.47	0.66	0.84	0.98
0.40		0.32	0.55	0.73	0.88
0.45			0.42	0.63	0.79
0.50			0.27	0.50	0.68
0.55				0.44	0.60
0.60				0.32	0.50

Source: Based on Richards, R., Jr., Elms, D. G., and Budhu, M. (1993). "Seismic Bearing Capacity of and Settlements of Foundations," *Journal of Geotechnical Engineering Division,* ASCE, Vol. 119, No. 4, pp. 662–674.

EXAMPLE 6.3

A strip foundation is to be constructed on a sandy soil with $B = 1.2$ m, $D_f = 0.9$ m, $\gamma = 17.6$ kN/m^3, and $\phi = 30°$.

a. Determine the gross ultimate bearing capacity q_{uE}. Assume that $k_v = 0$ and $k_h = 0.176$.
b. If the design earthquake parameters are $V = 0.4$ m/s and $A = 0.32$, determine the seismic settlement of the foundation. Use $FS = 3$ to obtain the static allowable bearing capacity.

SOLUTION:

a. From Figure 6.10, for $\phi = 30°$, $N_q = 16.51$, and $N_\gamma = 23.76$ Also,

$$\tan\theta = \frac{k_h}{1-k_v} = \frac{0.176}{1-0} = 0.176$$

Copyright 2017 Cengage Learning. All Rights Reserved. May not be copied, scanned, or duplicated, in whole or in part. Due to electronic rights, some third party content may be suppressed from the eBook and/or eChapter(s). Editorial review has deemed that any suppressed content does not materially affect the overall learning experience. Cengage Learning reserves the right to remove additional content at any time if subsequent rights restrictions require it.

For $\tan\theta = 0.176$, Figure 6.11

$$\frac{N_{\gamma E}}{N_\gamma} = 0.4 \qquad \text{and} \qquad \frac{N_{qE}}{N_q} = 0.63$$

Thus,

$$N_{\gamma E} = (0.4)(23.76) = 9.5$$

$$N_{qE} = (0.63)(16.51) = 10.4$$

and

$$\begin{aligned} q_{uE} &= qN_{qE} + \frac{1}{2}\gamma B N_{\gamma E} \\ &= (17.6 \times 0.9)(10.4) + \left(\frac{1}{2}\right)(17.6)(1.2)(9.5) \\ &= \mathbf{265.06\ kPa} \end{aligned}$$

b. For the foundation,

$$\frac{D_f}{B} = \frac{0.9}{1.2} = 0.75$$

From Figure 6.12, for $\phi = 30°$, $FS = 3$, and $D_f/B = 0.75$, the value of $k_h^* \approx 0.26$. Also, from Table 6.5, for $k_h^* = 0.26$, the value of $\tan\alpha_{AE} \approx 0.92$.

From Eq. (6.50), we have

$$S_{\text{Eq}}(\text{m}) = 0.174\frac{V^2}{Ag}\left[\frac{k_h^*}{A}\right]^{-4}\tan\alpha_{AE}$$

with $V = 0.4$ m/s,

it follows that

$$\begin{aligned} S_{\text{Eq}} &= 0.174\left[\frac{0.26}{0.32}\right]^{-4}(0.92)\frac{(0.4)^2}{(0.32)(9.81)} \\ &= 0.0187\ \text{m} = \mathbf{18.7\ mm} \end{aligned}$$

6.6.2 Solution of Budhu and al-Karni (1993)

Budhu and al-Karni (1993) used the failure surface in soil as shown in Figure 6.13 to determine the ultimate bearing capacity of a shallow foundation q_{uE}. Note that, in this figure, $\widehat{AB}$ and $\widehat{EF}$ are arcs of logarithmic spirals. According to this solution,

$$q_{uE} = cN_cS_cd_ce_c + qN_qS_qd_qe_q + \frac{1}{2}\gamma BN_\gamma S_\gamma d_\gamma e_\gamma \tag{6.51}$$

Copyright 2017 Cengage Learning. All Rights Reserved. May not be copied, scanned, or duplicated, in whole or in part. Due to electronic rights, some third party content may be suppressed from the eBook and/or eChapter(s). Editorial review has deemed that any suppressed content does not materially affect the overall learning experience. Cengage Learning reserves the right to remove additional content at any time if subsequent rights restrictions require it.

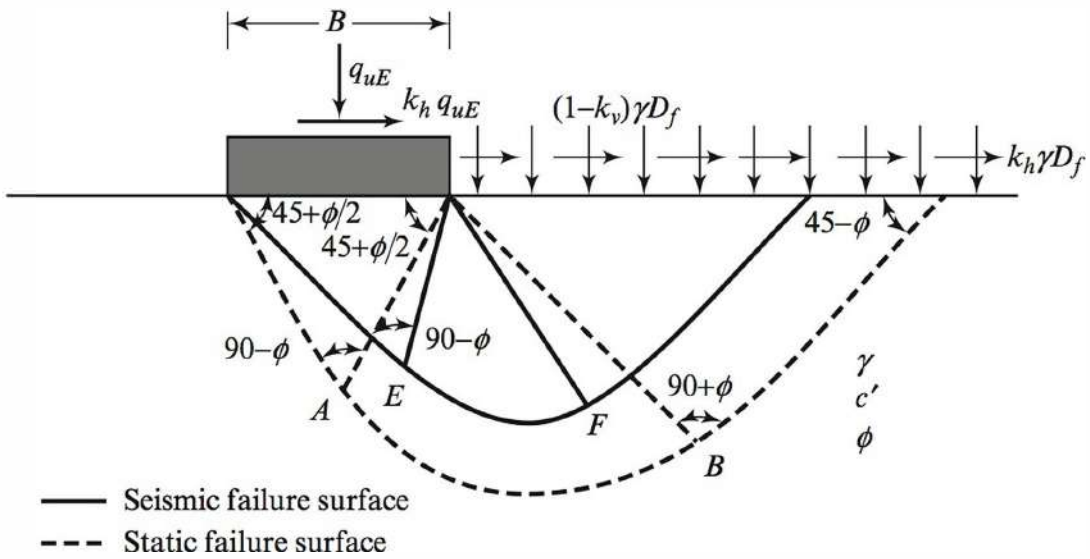

Figure 6.13. Failure surface under a strip foundation as assumed by Budhu and al-Karni (1993)

Source: Based on Budhu, M., and al-Karni, A. A. (1993). "Seismic Bearing Capacity of Soils," *Geotechnique,* Vol. 43, No. 1, pp. 181–187.

where c = cohesion

N_c, N_q, N_γ = static bearing capacity factors (see Table 6.1)

S_c, S_q, S_γ = static shape factors [see Eqs. (6.6) – (6.8)]

d_c, d_q, d_γ = static depth factors [see Eqs. (6.9) – (6.13)]

e_c, e_q, e_γ = seismic factors

The relationships for the seismic factors can be given as follows:

$$e_c = \exp(-4.3k_h^{1+D}) \tag{6.52}$$

$$e_q = (1-k_v)\exp\left[-\left(\frac{5.3k_h^{1.2}}{1-k_v}\right)\right] \tag{6.53}$$

$$e_\gamma = \left(1+\frac{2}{3}k_v\right)\exp\left[-\left(\frac{9k_h^{1.2}}{1-k_v}\right)\right] \tag{6.54}$$

where k_h and k_v = horizontal and vertical acceleration coefficients respectively

$$D = \frac{c}{\gamma H} \tag{6.55}$$

$$H = \frac{0.5B}{\cos\left(\frac{\pi}{4}+\frac{\phi}{2}\right)}\exp\left(\frac{\pi}{2}\tan\phi\right) + D_f \tag{6.56}$$

Copyright 2017 Cengage Learning. All Rights Reserved. May not be copied, scanned, or duplicated, in whole or in part. Due to electronic rights, some third party content may be suppressed from the eBook and/or eChapter(s). Editorial review has deemed that any suppressed content does not materially affect the overall learning experience. Cengage Learning reserves the right to remove additional content at any time if subsequent rights restrictions require it.

EXAMPLE 6.4

Consider a foundation measuring $1\,\text{m} \times 1.5\,\text{m}$ supported by a soil with $\gamma = 18\,\text{kN/m}^3$, $c = 36\,\text{kN/m}^2$, $\phi = 27°$. Given $D_f = 1\,\text{m}$. Assume $k_v = 0.25$ and $k_h = 0$ and estimate the ultimate bearing capacity q_{uE}. Use Eq. (6.51).

SOLUTION:

Eq. (6.51):

$$q_{uE} = cN_cS_cd_ce_c + qN_qS_qd_qe_q + \frac{1}{2}\gamma BN_\gamma S_\gamma d_\gamma e_\gamma$$

$c = 36\,\text{kN/m}^2$; $\phi = 27°$ (Table 6.1)

$N_c = 23.94$; $N_q = 13.2$; $N_\gamma = 14.47$.

From Eqs. (6.6) – (6.8),

$$S_c = 1 + \left(\frac{B}{L}\right)\left(\frac{N_q}{N_c}\right) = 1 + \left(\frac{1}{1.5}\right)\left(\frac{13.2}{23.94}\right) = 1.368$$

$$S_q = 1 + \left(\frac{B}{L}\right)\tan\phi = 1 + \left(\frac{1}{1.5}\right)\tan 27 = 1.34$$

$$S_\gamma = 1 - 0.4\left(\frac{B}{L}\right) = 1 - 0.4\left(\frac{1}{1.5}\right) = 0.733$$

From Eqs. (6.9), (6.11), and (6.13),

$$d_c = 1 + 0.4\left(\frac{D_f}{B}\right) = 1 + 0.4\left(\frac{1}{1}\right) = 1.4$$

$$d_q = 1 + 2\tan\phi(1 - \sin\phi)^2\left(\frac{D_f}{B}\right) = 1 + 2\tan 27(1 - \sin 27)^2\left(\frac{1}{1}\right) = 1.304$$

$$d_\gamma = 1$$

From Eqs. (6.52)–(6.56),

$$H = \frac{0.5B}{\cos\left(\frac{\pi}{4} + \frac{\phi}{2}\right)}\exp\left(\frac{\pi}{2}\tan\phi\right) + D_f$$

$$= \frac{(0.5)(1)}{\cos(45 + 13.5)}\exp\left(\frac{\pi}{2} \times \tan 27\right) + 1 = 3.13\,\text{m}$$

$$D = \frac{c}{\gamma H} = \frac{36}{(18)(3.13)} = 0.639$$

$$e_c = \exp(-4.3k_h^{1+D}) = \exp\left[(-4.3)(0.25)^{1+0.639}\right] = 0.642$$

Copyright 2017 Cengage Learning. All Rights Reserved. May not be copied, scanned, or duplicated, in whole or in part. Due to electronic rights, some third party content may be suppressed from the eBook and/or eChapter(s). Editorial review has deemed that any suppressed content does not materially affect the overall learning experience. Cengage Learning reserves the right to remove additional content at any time if subsequent rights restrictions require it.

$$e_q = (1-k_v)\exp\left[-\left(\frac{5.3k_h^{1.2}}{1-k_v}\right)\right] = (1-0)\exp\left[-\left(\frac{5.3\times 0.25^{1.2}}{1-0}\right)\right] = 0.366$$

$$e_\gamma = \left(1+\frac{2}{3}k_v\right)\exp\left[-\left(\frac{9k_h^{1.2}}{1-k_v}\right)\right] = (1+0)\exp\left[-\left(\frac{9\times 0.25^{1.2}}{1-0}\right)\right] = 0.182$$

Hence,

$$q_{uE} = (36)(23.94)(1.368)(1.4)(0.642) + (18\times 1)(13.2)(1.34)(1.304)(0.366) + \left(\frac{1}{2}\right)(18)(1)(14.47)(0.733)(1)(0.182)$$

$$= \mathbf{1229\ kPa}$$

6.6.3 Solution by Choudhury and Subba Rao (2005)

Choudhury and Subba Rao (2005) assumed a similar failure surface in soil as shown in Figure 6.13 and limit equilibrium method by pseudo-static approach and expressed the ultimate bearing capacity q_{uE} for a strip foundation as

$$q_{uE} = cN_{cE} + qN_{qE} + \frac{1}{2}\gamma BN_{\gamma E} \tag{6.57}$$

The variation of N_{cE}, N_{qE}, and $N_{\gamma E}$ with k_h and ϕ with $k_v = 0$ is shown in Figure 6.14. The depth and shape factors can be incorporated into Eq. (6.57) to estimate q_{uE} for rectangular foundations, or

$$q_{uE} = cN_{cE}S_c d_c + qN_{qE}S_q d_q + \frac{1}{2}\gamma BN_\gamma S_\gamma d_\gamma \tag{6.58}$$

where S_c, S_q, S_γ = static shape factors [see Eqs. (6.6) – (6.8)]
d_c, d_q, d_γ = static depth factors [see Eqs. (6.9) – (6.13)]

EXAMPLE 6.5

Solve Example 6.4 using Eq. (6.58).

SOLUTION:

Given $\phi = 27°$ and $k_h = 0.25$. Thus, from Figure 6.14, $N_{cE} \approx 8$, $N_{qE} \approx 5$, and $N_{\gamma E} \approx 3$. From Example 6.4, $S_c = 1.368$, $S_q = 1.34$, $S_\gamma = 0.733$, $d_c = 1.4$, $d_q = 1.304$, and $d_\gamma = 1$.

Copyright 2017 Cengage Learning. All Rights Reserved. May not be copied, scanned, or duplicated, in whole or in part. Due to electronic rights, some third party content may be suppressed from the eBook and/or eChapter(s). Editorial review has deemed that any suppressed content does not materially affect the overall learning experience. Cengage Learning reserves the right to remove additional content at any time if subsequent rights restrictions require it.

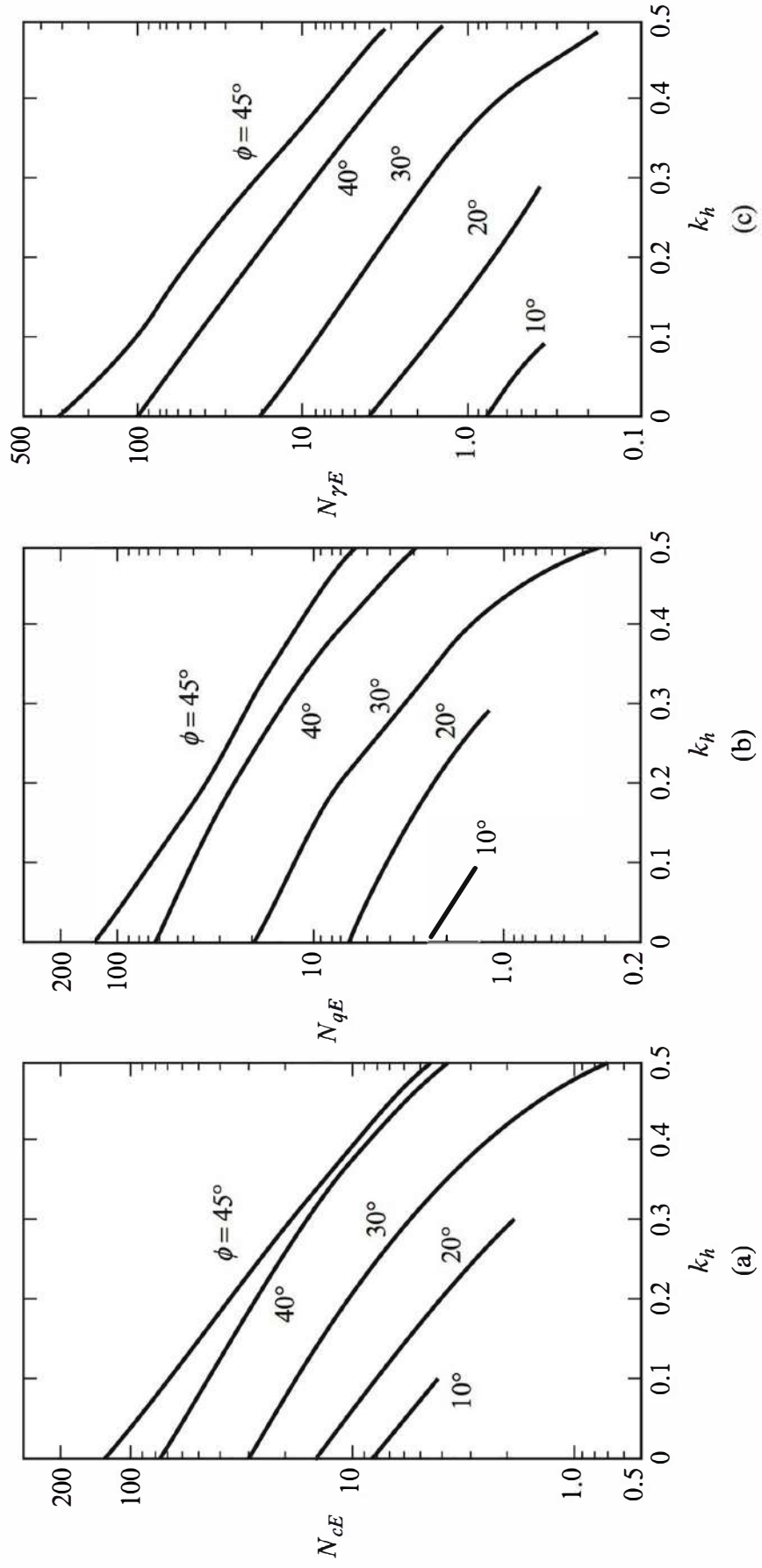

Figure 6.14 Variation of N_{cE}, N_{qE}, and $N_{\gamma E}$ with k_h and ϕ [Eq. (6.57)]. Note $k_v = 0$

Copyright 2017 Cengage Learning. All Rights Reserved. May not be copied, scanned, or duplicated, in whole or in part. Due to electronic rights, some third party content may be suppressed from the eBook and/or eChapter(s). Editorial review has deemed that any suppressed content does not materially affect the overall learning experience. Cengage Learning reserves the right to remove additional content at any time if subsequent rights restrictions require it.

Hence,

$$q_{uE} = cN_{cE}S_c d_c + qN_{qE}S_q d_q + \frac{1}{2}\gamma B N_\gamma S_\gamma d_\gamma$$
$$= (36)(8)(1.368)(1.4) + (18 \times 1)(5)(1.34)(1.304)$$
$$+ \frac{1}{2}(18)(1)(3)(0.733)(1)$$
$$= \mathbf{728.62\ kPa}$$

Note: The ultimate bearing capacity of 728.62 is approximately 60% of what was estimated in Example 6.4. The difference is due to the contribution of cohesion. If c would have been zero, q_{uE} in Examples 6.4 and 6.5 would have been about 169 kN/m² and 177 kN/m², respectively. The results of field tests are not yet available to verify the results.

6.7 SEISMIC BEARING CAPACITY OF A FOUNDATION AT THE EDGE OF A GRANULAR SOIL SLOPE

Figure 6.15 shows a strip surface foundation ($B/L = 0$, $D_f/B = 0$) at the edge of a granular slope. The foundation is subjected to a loading inclined at an angle α to the vertical. Let the foundation be subjected to seismic loading with a horizontal coefficient of acceleration, k_h. Based on their analysis of method of slices, Huang and Kang (2008) expressed the ultimate inclined load per unit area as

$$q_{uE} = \frac{1}{2\cos\alpha} B N_\gamma F_{\gamma i} F_{\gamma\beta} F_{\gamma e} \quad (k_v = 0) \tag{6.59}$$

where

N_γ = bearing capacity factor (Table 6.1)

$F_{\gamma i}$ = load inclination factor

$F_{\gamma\beta}$ = slope inclination factor

$F_{\gamma e}$ = correction factor for the inertia force induced by seismic loading

The relationships for $F_{\gamma i}$, $F_{\gamma\beta}$, and $F_{\gamma e}$ are as follow:

$$F_{\gamma i} = \left[1 - \left(\frac{\alpha^\circ}{\phi^\circ}\right)\right]^{(0.1\phi - 1.21)} \tag{6.60}$$

$$F_{\gamma\beta} = [1 - (1.062 - 0.014\phi)\tan\phi]^{\left(\frac{\beta^\circ}{10^\circ}\right)} \tag{6.61}$$

and

$$F_{\gamma e} = 1 - [(2.57 - 0.043\phi)e^{1.45\tan\beta}]^{k_h} \tag{6.62}$$

In Eqs. (6.60) through (6.62), ϕ is in degrees.

Copyright 2017 Cengage Learning. All Rights Reserved. May not be copied, scanned, or duplicated, in whole or in part. Due to electronic rights, some third party content may be suppressed from the eBook and/or eChapter(s). Editorial review has deemed that any suppressed content does not materially affect the overall learning experience. Cengage Learning reserves the right to remove additional content at any time if subsequent rights restrictions require it.

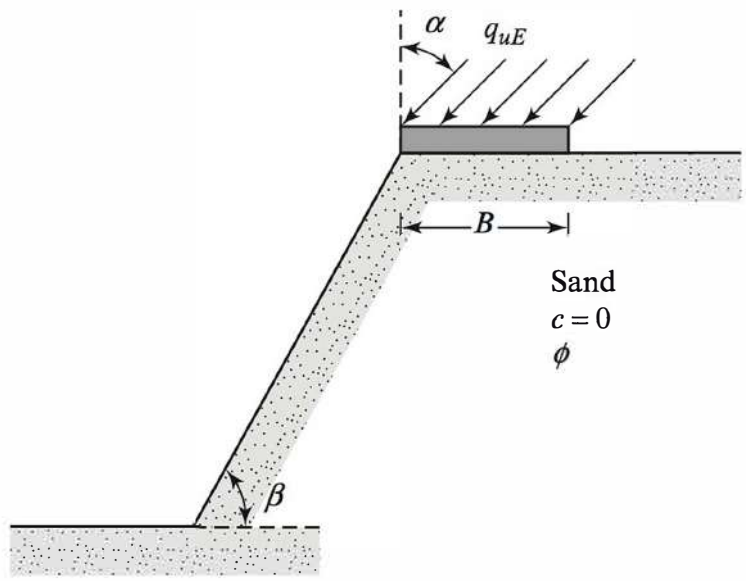

Figure 6.15 Strip foundation at the edge of a granular slope subjected to seismic loading

EXAMPLE 6.6

Consider a strip surface foundation on a granular soil slope subjected to a seismic loading, as shown in Figure 6.15. Given: $B = 1.5$ m, $\gamma = 17.5$ kN/m^3, $\phi = 35°$, $c = 0$, $\beta = 30°$, $\alpha = 10°$, and $k_h = 0.2$. Calculate the ultimate inclined load per unit area, q_{uE}.

SOLUTION

From Eq. (6.59),

$$q_{uE} = \frac{1}{2\cos\alpha} B N_\gamma F_{\gamma i} F_{\gamma\beta} F_{\gamma e}$$

For $\phi = 35°$, $N_\gamma = 48.03$ (Table 6.1). Thus,

$$F_{\gamma i} = \left[1 - \left(\frac{\alpha°}{\phi°}\right)\right]^{(0.1\phi - 1.21)} = \left[1 - \left(\frac{10}{35}\right)\right]^{[(0.1\times 35) - 1.21]} = 0.463$$

$$F_{\gamma\beta} = [1 - (1.062 - 0.014\phi)\tan\phi]^{\left(\frac{\beta°}{10°}\right)}$$

$$= [1 - (1.062 - 0.014\times 35)\tan 35]^{\left(\frac{30}{10}\right)} = 0.215$$

$$F_{\gamma e} = 1 - [(2.57 - 0.043\phi)e^{1.45\tan\beta}]k_h$$

$$= 1 - [(2.57 - 0.043\times 35)e^{1.45\tan 30}](0.2) = 0.508$$

So

$$q_{uE} = \frac{1}{2\cos 10}(17.5)(1.5)(48.03)(0.463)(0.215)(0.508) = \mathbf{32.37\ kPa}$$

Copyright 2017 Cengage Learning. All Rights Reserved. May not be copied, scanned, or duplicated, in whole or in part. Due to electronic rights, some third party content may be suppressed from the eBook and/or eChapter(s). Editorial review has deemed that any suppressed content does not materially affect the overall learning experience. Cengage Learning reserves the right to remove additional content at any time if subsequent rights restrictions require it.

PROBLEMS

6.1 A 0.9 m square shallow foundation is supported by a dense sand. The relative density of compaction, unit weight, and angle of friction (static) of this sand are 75%, 19.2 kN/m^3, and 38°, respectively. Given the depth of the foundation to be 0.9 m, estimate the minimum ultimate bearing capacity of this foundation that might be obtained if the vertical loading velocity on this foundation were varied from static to impact range.

6.2 Redo Problem 6.1 with the depth of the foundation as 1.40 m.

6.3 Redo Problem 6.1 with the following:

$$\text{Foundation width} = 1.6 \text{ m}$$
$$\text{Foundation depth} = 0.75 \text{ m}$$
$$\text{Angle of friction of sand} = 35°$$
$$\text{Unit weight of compacted soil} = 17.4 \text{ kN/m}^3$$
$$\text{Relative density of the compaction of sand} = 80\%$$

6.4 A rectangular foundation has a length L of 2.5 m. It is supported by a medium dense sand with a unit weight of 17 kN/m^3. The sand has an angle of friction of 36°. The foundation may be subjected to a dynamic load of 735 kN increasing at a moderate rate. Using a factor of safety equal to 2, determine the width of the foundation. Use $D_f = 0.8$ m.

6.5 A foundation 2.25 m square is supported by saturated clay. The unit weight of this clay is 18.6 kN/m^3. The depth of the foundation is 1.2 m. Determine the ultimate bearing capacity of this foundation assuming that the load will be applied very rapidly. Given the following for the clay [laboratory unconsolidated-undrained triaxial (static) test results]:

$$\text{Undrained cohesion, } c_u = 90 \text{ kPa}$$
$$\text{Strain-rate factor} = 1.4$$

6.6 Redo Problem 6.5 with the following changes:

$$\text{Foundation width} = 1.5 \text{ m}$$
$$\text{Foundation length} = 2.6 \text{ m}$$
$$\text{Foundation depth} = 1.75 \text{ m}$$

6.7 A clay deposit has an undrained cohesion (static test) of 90 kPa. A static field plate load test was conducted with a plate having a diameter of 0.5 m. When the load per unit area q was 200 kPa, the settlement was 20 mm.

Copyright 2017 Cengage Learning. All Rights Reserved. May not be copied, scanned, or duplicated, in whole or in part. Due to electronic rights, some third party content may be suppressed from the eBook and/or eChapter(s). Editorial review has deemed that any suppressed content does not materially affect the overall learning experience. Cengage Learning reserves the right to remove additional content at any time if subsequent rights restrictions require it.

a. Assume that, for a given value of q, settlement is proportional to the width of the foundation. Estimate the settlement of a prototype circular foundation in the same clay with a diameter of 3 m (static loading).

b. The strain-rate factor of the clay is 1.4. If a vertical transient load pulse were applied to the foundation as given in part (a), what would be the maximum transient load (in kN) that will produce the same maximum settlement (S_{max}) as calculated in part (a)?

6.8 Consider a shallow strip foundation with $B = 1.2$ m, $D_f = 1$ m. The foundation is supported by a soil with $c = 25$ kPa, $\phi = 20°$, and $\gamma = 17.2$ kN/m^2. Estimate the ultimate seismic bearing capacity if $k_h = 0.2$ and $k_v = 0$. Use Eq. (6.30) and the theory of Richards et al. (1993).

6.9 Repeat Problem 6.8 using Eq. (6.51).

6.10 Repeat Problem 6.8 using Eq. (6.58).

6.11 For a granular soil deposit, assume γ to be 16.5 kN/m^3, $c = 0$, and $\phi = 37°$. Estimate the seismic ultimate bearing capacity (q_{uE}) for a continuous foundation with the following: $B = 1.5$ m, $D_f = 1.0$ m, $k_h = 0.2$, and $k_v = 0$. Use Eq. (6.30) and the analysis of Richards et al. (1993).

6.12 Refer to Problem 6.11. If the design earthquake parameters are $V = 0.35$ m/s and $A = 0.3$, determine the seismic settlement of the foundation. Assume $FS = 4$ for obtaining static allowable bearing capacity.

References

Brinch Hansen, J. (1970). "A Revised and Extended Formula for Bearing Capacity," *Bulletin No. 28*, Danish Geotechnical Institute, Copenhagen, Denmark.

Budhu, M., and al-Karni, A.A. (1993). "Seismic Bearing Capacity of Soils," *Geotechnique*, Vol. 43, No. 1, pp. 181–187.

Carroll, W. F. (1963). "Dynamic Bearing Capacity of Soils. Vertical Displacements of Spread Footings on Clay: Static and Impulsive Loadings," *Technical Report No. 3-599*, Report 5, US Army Corps of Engineers, Waterways Experiment Station, Vicksburg, Mississippi.

Caquot, A., and Kerisel, J. (1953). "Sur le Terme de Surface Dans le Calcul des Foundations en Milieu Pulverulent," *Proceedings*, 3rd International Conference on Soil Mechanics and Foundation Engineering, Zurich, Switzerland, Vol. I, pp. 336–337.

Choudhury, D., and Subba Rao, K.S. (2005). "Seismic Bearing Capacity of Shallow Strip Footings," *Geotechnical and Geological Engineering*, Vol. 23, No. 4, pp. 403–418.

Cunny, R. W., and Sloan, R. C. (1961). "Dynamic Loading Machine and Results of Preliminary Small-Scale Foundation Tests," *Special Technical Publication No. 305*, American Society for Testing and Materials, pp. 65–67.

DeBeer, E. E. (1970). "Experimental Determination of the Shape Factors and the Bearing Capacity Factors of Sand," *Geotechnique*, Vol. 20, No. 4, pp. 387–411.

Copyright 2017 Cengage Learning. All Rights Reserved. May not be copied, scanned, or duplicated, in whole or in part. Due to electronic rights, some third party content may be suppressed from the eBook and/or eChapter(s). Editorial review has deemed that any suppressed content does not materially affect the overall learning experience. Cengage Learning reserves the right to remove additional content at any time if subsequent rights restrictions require it.

Heller, L. W. (1964). "Failure Modes of Impact-Loaded Footings on Dense Sand," *Technical Report R – 281*, U.S. Naval Civil Engineering Laboratory, Port Hueneme, California.

Huang, C. C., and Kang, W. W. (2008). "Seismic Bearing Capacity of a Rigid Footing Adjacent to a Cohesionless Slope," *Soils and Foundations*, Vol. 48, No. 5, pp. 641–651.

Jackson, J. G., Jr., and Hadala, P. F. (1964). "Dynamic Bearing Capacity of Soils. Report 3: The application of Similitude of Small-Scale Footings Tests," US Army Corps of Engineers, Waterways Experiment Station, Vicksburg, Mississippi.

Prakash, S., and Chummar, A. V. (1967). "Response of Footings to Lateral Loads," *Proceedings*, International Symposium on Wave Propagation and Dynamic Properties of Earth Materials, Ed., G. E. Triandafilidis, University of New Mexico, Albuquerque, New Mexico, pp. 679–691.

Prandtl, L. (1921). "Über die Eindringungsfestigkeit (Härte) plastischer Baustoffe und die Festigkeit von Schneiden," *Zeitschrift für angewandte Mathematik und Mechanik*, Vol. 1, No. 1, pp. 15–20.

Reissner, H. (1924). "Zum Erddrukproblem," *Proceedings*, First International Conference on Applied Mechanis, Delft, The Netherlands, pp. 294–311.

Richards, R., Jr., Elms, D. G., and Budhu, M. (1993). "Seismic Bearing Capacity of and Settlements of Foundations," *Journal of Geotechnical Engineering Division*, ASCE, Vol. 119, No. 4, pp. 662–674.

Shenkman, S., and Mckee, K. E. (1961). "Bearing Capacity of Dynamically Loaded Footings," *Special Technical Publication No. 305*, American Society for Testing and Materials, pp. 78–90.

Terzaghi, K. (1943). *Theoretical Soil Mechanics*, Wiley, New York.

Triandafilidis, G. E. (1965). "The Dynamic Response of Continuous Footings Supported on Cohesive Soils," *Proceedings*, 6th International Conference on Soil Mechanics and Foundation Engineering, Montreal, Canada, Vol. II, pp. 205–208.

Vesic, A. S. (1973). "Analysis of Ultimate Loads of Shallow Foundations," *Journal of the Soil Mechanics and Foundations Division*, ASCE, Vol. 99, No. SM1, pp. 45–73.

Vesic, A. S., Banks, D. C., and Woodard, J. M. (1965). "An Experiment Study of Dynamic Bearing Capacity of Footings of Sand," *Proceedings*, 6th International Conference on Soil Mechanics and Foundation Engineering, Montreal, Canada, Vol. II, pp. 209–213.

Wallace, W. F. (1961). "Displacements of Long Footings by Dynamic Loads," *Journal of the Soil Mechanics and Foundation Division*, ASCE, Vol. 87, No. SM5, pp. 45–68.

Whitman, R. V., and Healy, K. A. (1962). "Shear Strength of Sands During Rapid Loadings," *Journal of the Soil Mechanics and Foundations Division*, ASCE, Vol. 88, No. SM2, pp. 99–132.

Copyright 2017 Cengage Learning. All Rights Reserved. May not be copied, scanned, or duplicated, in whole or in part. Due to electronic rights, some third party content may be suppressed from the eBook and/or eChapter(s). Editorial review has deemed that any suppressed content does not materially affect the overall learning experience. Cengage Learning reserves the right to remove additional content at any time if subsequent rights restrictions require it.

Earthquake and Ground Vibration

7

7.1 INTRODUCTION

The study of earthquakes is important for scientific, social, and economic reasons. Earthquakes attest to the fact that dynamic forces are operating within the earth. Stress builds up through time, storing strain energy, and earthquakes represent the release of this stored strain energy.

The ground vibrations due to earthquakes have resulted in several major structural damages in the past. In the North American continent, earthquakes are believed to originate from the rupture of faults. The ground vibration resulting from an earthquake is due to the upward transmission of the stress waves from rock to the softer soil layers(s). In recent times, several major studies have been performed to study the nature of occurrence of earthquakes and the associated amount of energy released. Also, modern techniques have been developed to analyze and estimate the physical properties of soils under earthquake conditions and to predict the ground motion. These developments are the subjects of discussion in this chapter.

7.2 DEFINITION OF SOME EARTHQUAKE-RELATED TERMS

Focus (or hypocenter): The focus of an earthquake is a point below the ground surface where the rupture of a fault first occurs (point F in Figure 7.1a).

Focal Depth: The vertical distance from the ground surface to the focus (EF in Figure 7.1a). The maximum focal depth of all earthquakes recorded so far does not exceed 700 km, because they are confined to the rigid lithosphere, which can undergo brittle fracture.

Copyright 2017 Cengage Learning. All Rights Reserved. May not be copied, scanned, or duplicated, in whole or in part. Due to electronic rights, some third party content may be suppressed from the eBook and/or eChapter(s).
Editorial review has deemed that any suppressed content does not materially affect the overall learning experience. Cengage Learning reserves the right to remove additional content at any time if subsequent rights restrictions require it.

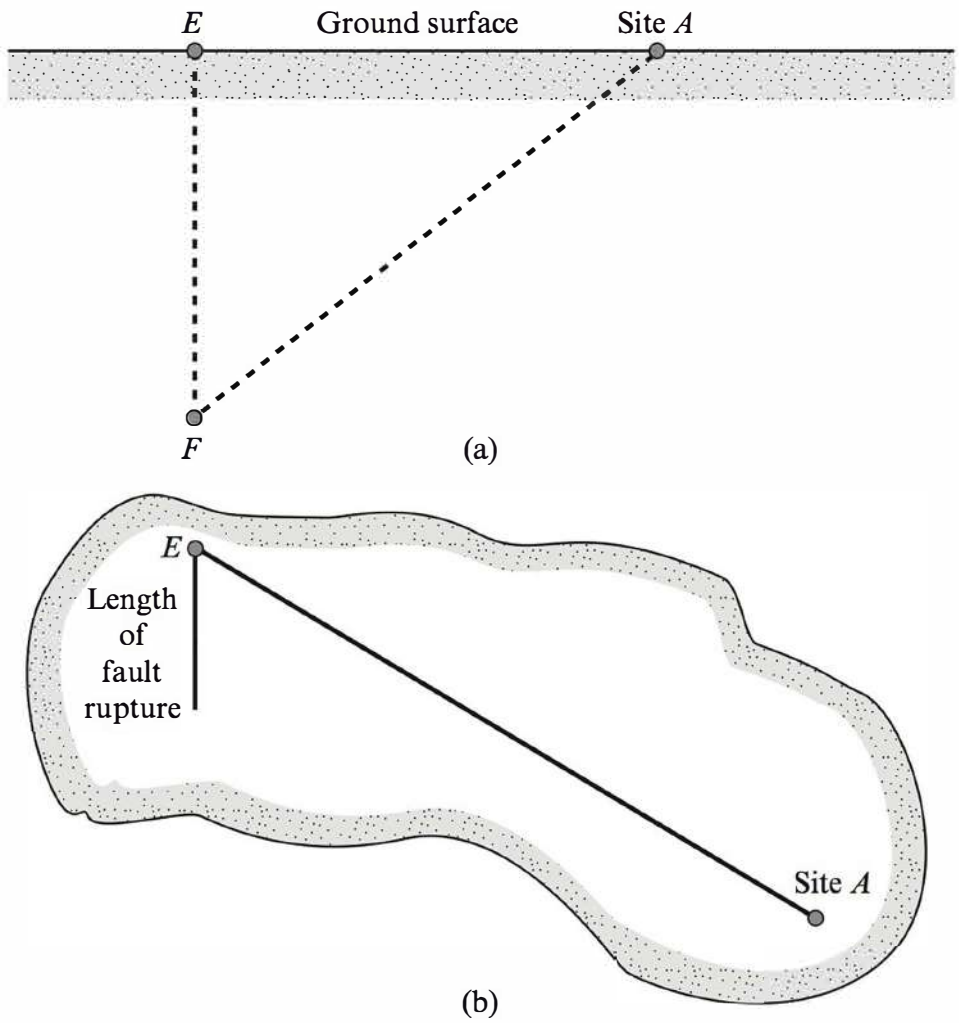

Figure 7.1 Definition of focus and epicenter: (a) section; (b) plan

Focal depths are normally related the type of plate boundary from which earthquakes originate. Based on focal depth, earthquakes may be divided into the following three categories:

1. *Deep-focus earthquakes*: These have focal depths of 300–700 km. They constitute about 3% of all earthquakes recorded around the world and are mostly located in the Circum-Pacific belt.
2. *Intermediate-focus earthquakes*: These have focal depths of 70–300 km.
3. *Shallow-focus earthquakes*: The focal depth for these is less than 70 km. About 75% of all the earthquakes around the world belong to this category. The California earthquakes have focal depths of about 10–15 km.

Epicenter: The point vertically above the focus located on the ground surface (point *E* in Figure 7.1).

Epicentric Distance: The horizontal distance between the epicenter and the given site (line *EA* in Figure 7.1).

Hypocentric Distance: The distance between a given site and the focus (line *FA* in Figure 7.1a).

Effective Distance to Causative Fault: The distance from a fault to a given site for calculation of ground motion (Figure 7.2).

Copyright 2017 Cengage Learning. All Rights Reserved. May not be copied, scanned, or duplicated, in whole or in part. Due to electronic rights, some third party content may be suppressed from the eBook and/or eChapter(s). Editorial review has deemed that any suppressed content does not materially affect the overall learning experience. Cengage Learning reserves the right to remove additional content at any time if subsequent rights restrictions require it.

This distance is commonly presumed to be the epicentric distance. This type of assumption, under circumstances, may lead to gross errors. It can be explained with reference to Figure 7.2, which shows the plans of two cases of fault rupture. In Figure 7.2a, the length of the fault rupture L is small as compared to the epicentric distance EA. In this case, the effective distance could be taken to be equal to the epicentric distance. However, a better estimate of the effective distance is BA (B is the midpoint of the ruptured fault). Figure 7.2b shows the case where the length of the fault rupture is large. In such circumstances, the length AC is the effective distance, which is the perpendicular distance from the site to the line of fault rupture in the plan.

Intensity: An arbitrary scale developed to measure the destructiveness of an earthquake at the surface. It is qualitative and is based on the damage caused by the earthquake. The same earthquake may have different intensities at two different locations depending on soil conditions, ground water location, and type of construction at that particular location. It is worth noting that there are several intensity scales available in the literature, and the Modified Mercalli Scale (reported in Roman numerals) is presently in use in the United States for that purpose, divided into 12 degrees of intensity. An abridged version of the Modified Mercalli Scale is given in Table 7.1.

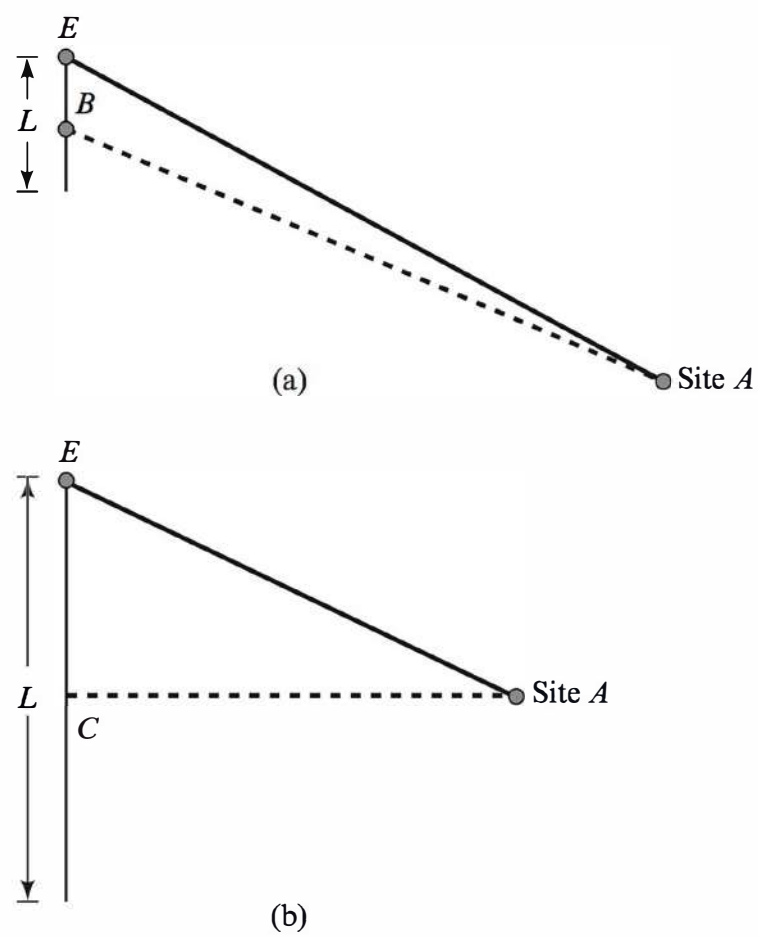

Figure 7.2 Effective distance from a site to the causative faults (*Note*: L is the length of the fault rupture.)

Copyright 2017 Cengage Learning. All Rights Reserved. May not be copied, scanned, or duplicated, in whole or in part. Due to electronic rights, some third party content may be suppressed from the eBook and/or eChapter(s). Editorial review has deemed that any suppressed content does not materially affect the overall learning experience. Cengage Learning reserves the right to remove additional content at any time if subsequent rights restrictions require it.

Table 7.1 Abridged Modified Mercalli Intensity Scale[a]

Intensity	Description
I	Detected only by sensitive instruments
II	Felt by a few persons at rest, especially on upper floors; delicate suspended objects may swing
III	Felt noticeably indoors, but not always recognized as a quake; standing autos rock slightly, vibration like passing trucks
IV	Felt indoors by many, outdoors by a few; at night some awaken; dishes, windows, doors disturbed; motor cars rock noticeably
V	Felt by most people; some breakage of dishes, windows, and plaster; disturbance of tall objects
VI	Felt by all; many are frightened and run outdoors; falling plaster and chimneys; damage small
VII	Everybody runs outdoors; damage to building varies, depending on quality of construction; noticed by drivers of autos
VIII	Panel walls thrown out of frames; fall of walls, monuments, chimneys; sand and mud ejected; drivers of autos disturbed
IX	Buildings shifted off foundations, cracked, thrown out of plumb; ground cracked; underground pipes broken
X	Most masonry and frame structures destroyed; ground cracked; rails bent; landslides
XI	New structures remain standing; bridges destroyed; fissures in ground; pipes broken; landslides; rails bent
XII	Damage total; waves seen on ground surface; lines of sight and level distorted; objects thrown up into air.

[a]After Wiegel, R. W. (1970).

Source: Based on Wiegel, *Earthquake Engineering,* 1st, 1970, Pearson Education, Inc., Upper Saddle River, New Jersey.

7.3 EARTHQUAKE MAGNITUDE

Magnitude is a measure of the size of an earthquake, based on the amplitude of elastic waves it generates, at known distances from the epicenter, using seismographs. The magnitude scale presently in use was first developed by C. F. Richter. The historical developments of the magnitude scale have been summarized by Richter himself (1958).

Richter's earthquake magnitude is defined by the equation

$$\log_{10} E = 11.4 + 1.5M \tag{7.1}$$

where E is the energy released (in ergs) and M is magnitude. Bath (1966) slightly modified the constant given in Eq. (7.1) and presented it in the form

$$\log_{10} E = 12.24 + 1.44M \tag{7.2}$$

Copyright 2017 Cengage Learning. All Rights Reserved. May not be copied, scanned, or duplicated, in whole or in part. Due to electronic rights, some third party content may be suppressed from the eBook and/or eChapter(s). Editorial review has deemed that any suppressed content does not materially affect the overall learning experience. Cengage Learning reserves the right to remove additional content at any time if subsequent rights restrictions require it.

Table 7.2 Comparison of Richter Scale Magnitude with the Modified Mercalli Scale

Richter scale Magnitude, M	Maximum intensity, Modified Mercalli Scale
1	–
2	I, II
3	III
4	IV
5	VI, VII
6	VIII
7	IX, X
8	XI

From Eq. (7.2), it can be seen that the increase of M by one unit will generally correspond to about a 30-fold increase of the energy released (E) due to the earthquake. A comparison of the magnitude M of an earthquake with the *maximum intensity* of the Modified Mercalli Scale is given in Table 7.2. Table 7.3 gives a list of some of the past major earthquakes around the world with their magnitudes.

As mentioned previously, the main cause of earthquakes is the rupture of faults. In general the greater the length of the fault rupture, the greater the magnitude of an earthquake. Several relations for the magnitude of the earthquake and the length of fault rupture have been presented by various investigators (Tocher, 1958; Bonilla, 1967; Housner, 1969). Tocher (1958), based on observations of some earthquakes in the area of California and Nevada, suggested the relationship

$$\log L = 1.02\,M - 5.77 \tag{7.3}$$

where L is the length of fault rupture (kilometers).

Table 7.3 Some Past Major Earthquakes

Name	Epicenter Location	Date	Magnitude
Alaska	61.1° N, 147.5° W	March 27, 1964	8.4
Chile (South America)	38° S, 73.5 W	May 22, 1960	8.4
Colombia (South America)	1° N, 82°W	January 31, 1906	8.6
Peru (South America)	9.2° S, 78.8° W	May 31, 1970	7.8
San Francisco, California	38° N, 123° W	April 18, 1906	8.3
Kern County, California	35° N, 119° W	July 21, 1952	7.7
Dixie Valley, Nevada	39.8°N, 118.1° W	December 16, 1954	6.8
Hebgen Lake, Montana	44.8° N, 111.1°W	August 17, 1959	7.1

Copyright 2017 Cengage Learning. All Rights Reserved. May not be copied, scanned, or duplicated, in whole or in part. Due to electronic rights, some third party content may be suppressed from the eBook and/or eChapter(s). Editorial review has deemed that any suppressed content does not materially affect the overall learning experience. Cengage Learning reserves the right to remove additional content at any time if subsequent rights restrictions require it.

Based on Eq. (7.3), it can be seen that for an earthquake of magnitude 6, the length of fault rupture is about 2.3 km. However, when the magnitude is increased to 8, the length of fault rupture associated is about 250 km.

The Richter scale is based on the P-wave amplitude (in mm) measured by a Wood-Anderson seismograph at a distance of 100 km from the epicenter of the earthquake. The magnitude $M = 0$ is defined as the maximum amplitude of 0.001 mm (at a distance of 100 km). It accurately reflects the amount of seismic energy released by an earthquake up to about $M = 6.5$. For $M > 6.5$, the scale seems to "saturate" for a variety of reasons (Kanamori, 1983). In the literature, the Richter scale magnitude is also referred to as *local magnitude* (M_L).

In order to solve the so-called saturation problem for $M > 6.5$, a surface-wave magnitude scale (M_S) was developed (Gutenberg, 1945) to measure the peak wave amplitude of surface waves (Rayleigh and Love waves) that have periods of 20 s at distant location. The surface wave magnitude (M_S) works well for $M_S \approx 8$.

The most recent scale for measuring earthquakes is the *moment magnitude scale*, M_W (Kanamori, 1977; Hanks and Kanamori, 1979), which can be defined as

$$M_W = \frac{2}{3}\log_{10} M_O - 10.7 \tag{7.4}$$

where M_O = seismic moment of an earthquake (dyne · cm)

The seismic moment is expressed as,

$$M_O = \mu A D \tag{7.5}$$

where D = average displacement over the entire fault surface
A = area of rupture
μ = average shear rigidity of the faulted rock

The average value of μ is generally assumed to be about $3.0 - 3.5 \times 10^{11}$ dyne/cm^2.

Table 7.4 provides a comparison between M_L and M_W for some past earthquakes in the United States. In Section 10.18, M_W has been used to evaluate soil liquefaction potential.

The Chi-Chi earthquake which occurred on September 21, 1999, in Nantou County, Taiwan, had a surface wave magnitude (M_S) of 7.3 and the moment magnitude (M_W) of 7.6 to 7.7. Figures 7.3, 7.4, and 7.5 show some damage due to the earthquake.

Copyright 2017 Cengage Learning. All Rights Reserved. May not be copied, scanned, or duplicated, in whole or in part. Due to electronic rights, some third party content may be suppressed from the eBook and/or eChapter(s). Editorial review has deemed that any suppressed content does not materially affect the overall learning experience. Cengage Learning reserves the right to remove additional content at any time if subsequent rights restrictions require it.

Table 7.4 Comparison between M_L and M_W for Some Past Earthquakes in the United States

Earthquake	M_L	M_W
[a] Southern California		
• Long Beach Earthquake (March 11, 1933)	6.3	6.2
• Imperial Valley Earthquake (May 19, 1940)	6.4	7.0
• Santa Barbara Coastal Area Earthquake (July 1, 1941)	5.9	6.0
• Fish Creek Mountains Earthquake (October 21, 1942)	6.5	6.6
• Kern County Earthquake (March 15, 1946)	6.3	6.0
• Manix Earthquake (April 10, 1947)	6.2	6.5
• Desert Hot Spring Earthquake (December 4, 1948)	6.5	6.0
• [b] New Madrid, Missouri (1812)	8.7	8.1
• [b] San Francisco, California (1906)	8.3	7.7
• [b] Prince William, Alaska (1964)	8.4	9.2
• [b] Northridge, California (1994)	6.4	6.0

[a] Hanks and Kanamori (1979)

[b] Arkansas Earthquake Center (1998)

Source: Based on data from Akansas Earthquake Center (1998). "The Moment Magnitude Scale," http://quake.ealr.edu/public/moment.htm. AND Hanks, T. C., and Kanamori, H. (1979). "A Moment Magnitude Scale," *Journal of Geophysical Research,* Vol. 85, No. B5, pp. 2348–2358.

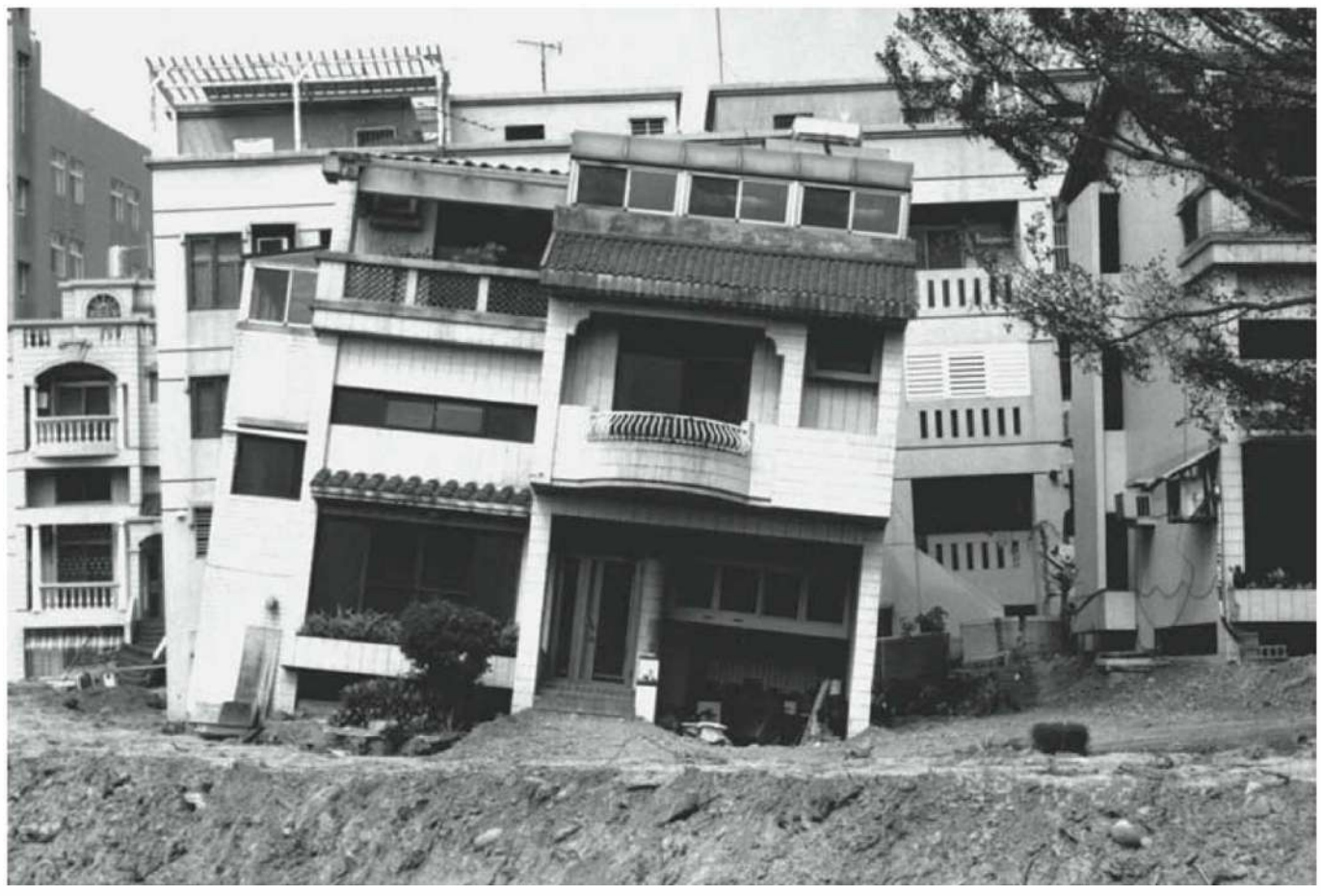

Figure 7.3 House tilted due to liquefaction from Chi-Chi earthquake, Taiwan (Courtesy of Dr. Chih-Sheng Ku, I-Shou University, Taiwan)

Source: Courtesy of Dr. Chih-Sheng Ku, I-Shou University, Taiwan

Copyright 2017 Cengage Learning. All Rights Reserved. May not be copied, scanned, or duplicated, in whole or in part. Due to electronic rights, some third party content may be suppressed from the eBook and/or eChapter(s). Editorial review has deemed that any suppressed content does not materially affect the overall learning experience. Cengage Learning reserves the right to remove additional content at any time if subsequent rights restrictions require it.

Figure 7.4 Sand boil observed in reclaimed land from Chi-Chi earthquake, Taiwan (Courtesy of Dr. Chih-Sheng Ku, I-Shou University, Taiwan)
Source: Courtesy of Dr. Chih-Sheng Ku, I-Shou University, Taiwan

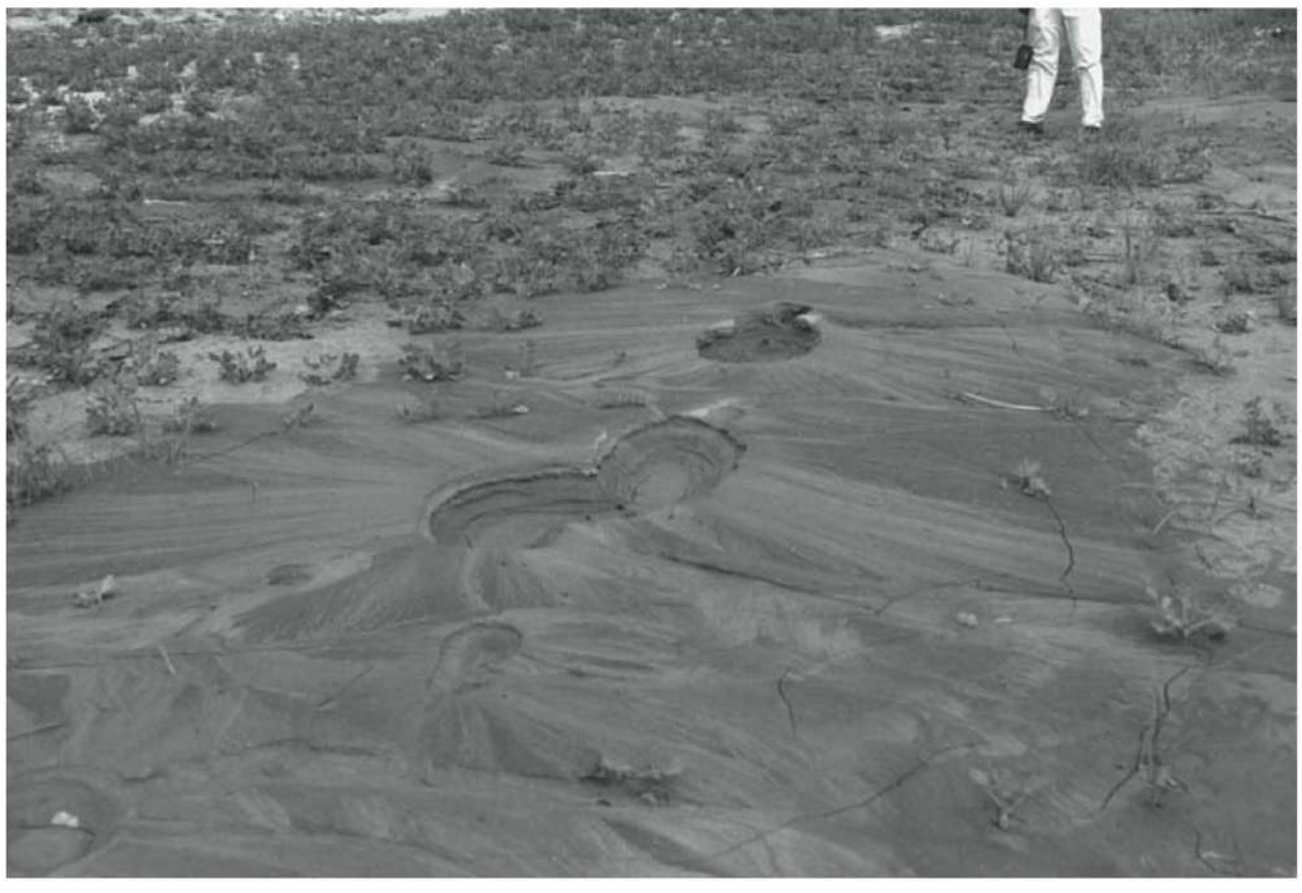

Figure 7.5 Sand boils in the peanut field from Chi-Chi earthquake, Taiwan (Courtesy of Dr. Chih-Sheng Ku, I-Shou University, Taiwan) *Source:* Courtesy of
Source: Courtesy of Dr. Chih-Sheng Ku, I-Shou University, Taiwan

Copyright 2017 Cengage Learning. All Rights Reserved. May not be copied, scanned, or duplicated, in whole or in part. Due to electronic rights, some third party content may be suppressed from the eBook and/or eChapter(s). Editorial review has deemed that any suppressed content does not materially affect the overall learning experience. Cengage Learning reserves the right to remove additional content at any time if subsequent rights restrictions require it.

7.4 CHARACTERISTICS OF ROCK MOTION DURING AN EARTHQUAKE

The ground motion near the surface of a soil deposit is mostly attributed to the upward propagation of shear waves from the underlying rock or "rocklike" layers. The term rocklike implies that the shear wave velocity in the material is similar to that associated with soft rocks. The typical range of shear wave velocities in hard rocks such as granite is about 3050–3660 m/s. Shear wave velocities associated with soft rocks can be in the low range of 762–915 m/s. However, the rocklike material may not exhibit the characteristics associated with hard base rocks (Seed, Idriss, and Kiefer, 1969). Hence, for arriving at a solution of the nature of ground motion at or near the ground surface, one needs to know some aspects of the earthquake-induced motion in the rock or rocklike materials. The most important of these are

- duration of the earthquake;
- predominant period of acceleration; and
- maximum amplitude of motion.

Each of these factors has been well summarized by Seed, Idriss, and Kiefer.

Duration of an Earthquake

Duration of an earthquake is related to the magnitude, but not in a perfectly strict sense. In general, it can be assumed that the duration of an earthquake will be somewhat similar to that of the fault rupture. The rate of propagation of fault rupture has been estimated by Housner (1965) to be about 3.2 km/s. Based on this, Housner has estimated the following variation of the duration of fault rupture with the magnitude of an earthquake.

Magnitude of earthquake (Richter scale)	Duration of fault rupture (s)
5	5
6	15
7	25–30

It may be noted that the approximate duration of fault rupture can be estimated from Eq. (7.3). Once the length of rupture L for a given magnitude of earthquake is estimated, the duration can be given by L/(velocity of rupture).

Predominant Period of Rock Acceleration

Gutenberg and Richter (1956) have given an estimate of the predominant periods of *acceleration* developed in rock for California earthquakes. Similar results for earthquakes of magnitude $M > 7$ have been reported by Figueroa (1960).

Copyright 2017 Cengage Learning. All Rights Reserved. May not be copied, scanned, or duplicated, in whole or in part. Due to electronic rights, some third party content may be suppressed from the eBook and/or Chapter(s). Editorial review has deemed that any suppressed content does not materially affect the overall learning experience. Cengage Learning reserves the right to remove additional content at any time if subsequent rights restrictions require it.

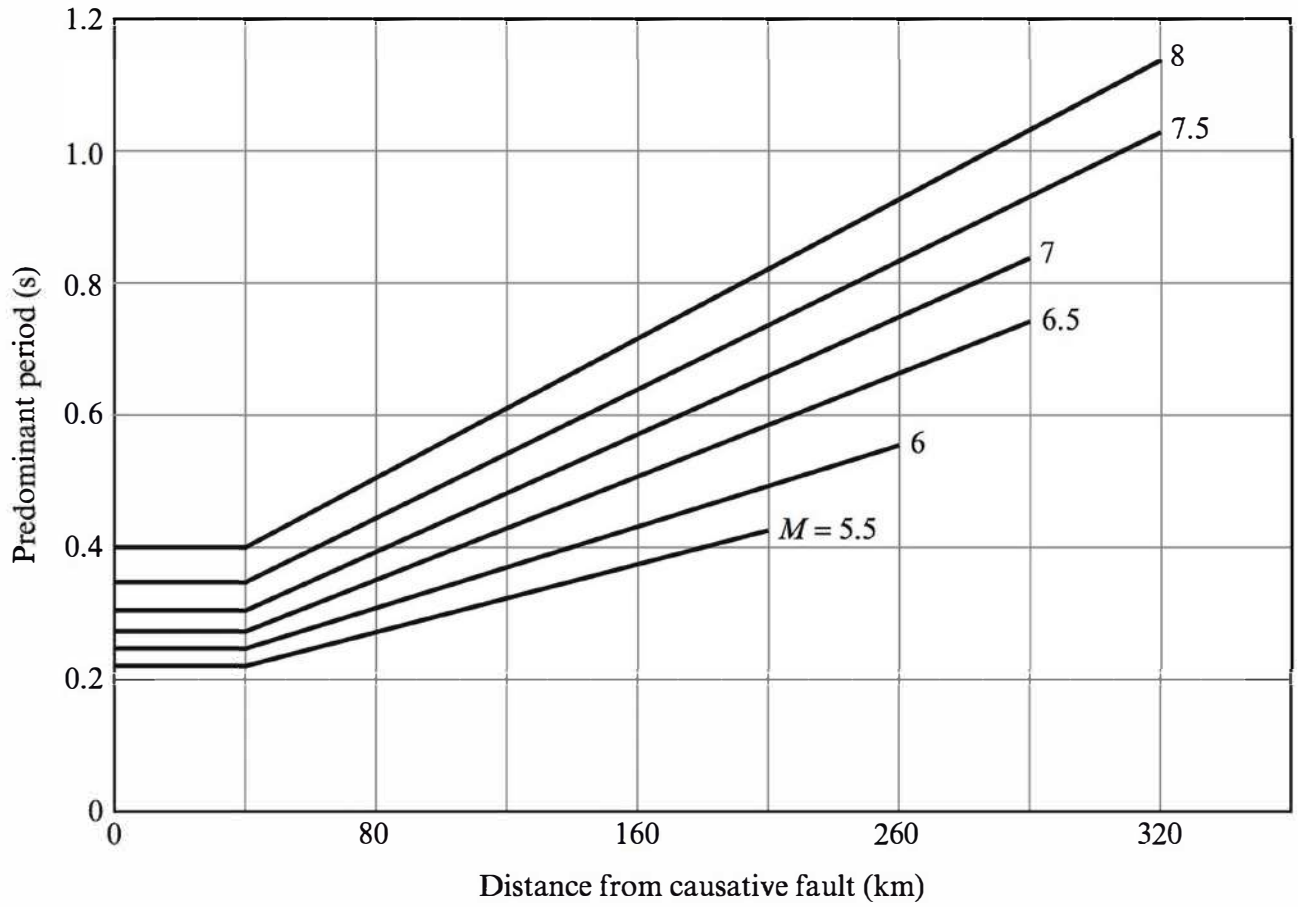

Figure 7.6 Predominant period for maximum rock acceleration (from Seed, Idriss, and Kiefer, 1969)

Source: Seed, H.B., Idriss, I.M., and Kiefer, F.W. (1969). "Characteristics of Rock Motions During Earthquakes," *Journal of the Soil Management and Foundations Division,* ASCE, Vol. 95, No. SM5, pp. 1199–1218. With permission from ASCE.

Using these results, Seed, Idriss, and Kiefer (1969) developed a chart for the *average predominant periods of acceleration* for various earthquakes magnitudes. This is shown in Figure 7.6. Note that in this figure the predominant periods are plotted against the distance from the causative fault (Figure 7.2).

Maximum Amplitude of Acceleration

The maximum amplitude of acceleration in rock in the epicentric region for shallow earthquakes (focal depth about 16 km) can be approximated as (Gutenberg and Richter, 1956)

$$\log a_0 = -2.1 + 0.81M - 0.027M^2 \tag{7.6}$$

where a_0 is the maximum amplitude of acceleration.

At any other point away from the epicenter, the magnitude of the maximum amplitude of acceleration decreases. Relations for the attenuation factor of maximum acceleration have been given by Gutenberg and Richter (1956), Banioff (1962), Esteva and Rosenblueth (1963), Kanai (1966), and Blume (1965). Based on these studies, Seed, Idriss, and Kiefer (1969) have given the average values of maximum acceleration for various magnitudes of earthquakes and distances from the causative faults. These are given in Figure 7.7.

Copyright 2017 Cengage Learning. All Rights Reserved. May not be copied, scanned, or duplicated, in whole or in part. Due to electronic rights, some third party content may be suppressed from the eBook and/or eChapter(s). Editorial review has deemed that any suppressed content does not materially affect the overall learning experience. Cengage Learning reserves the right to remove additional content at any time if subsequent rights restrictions require it.

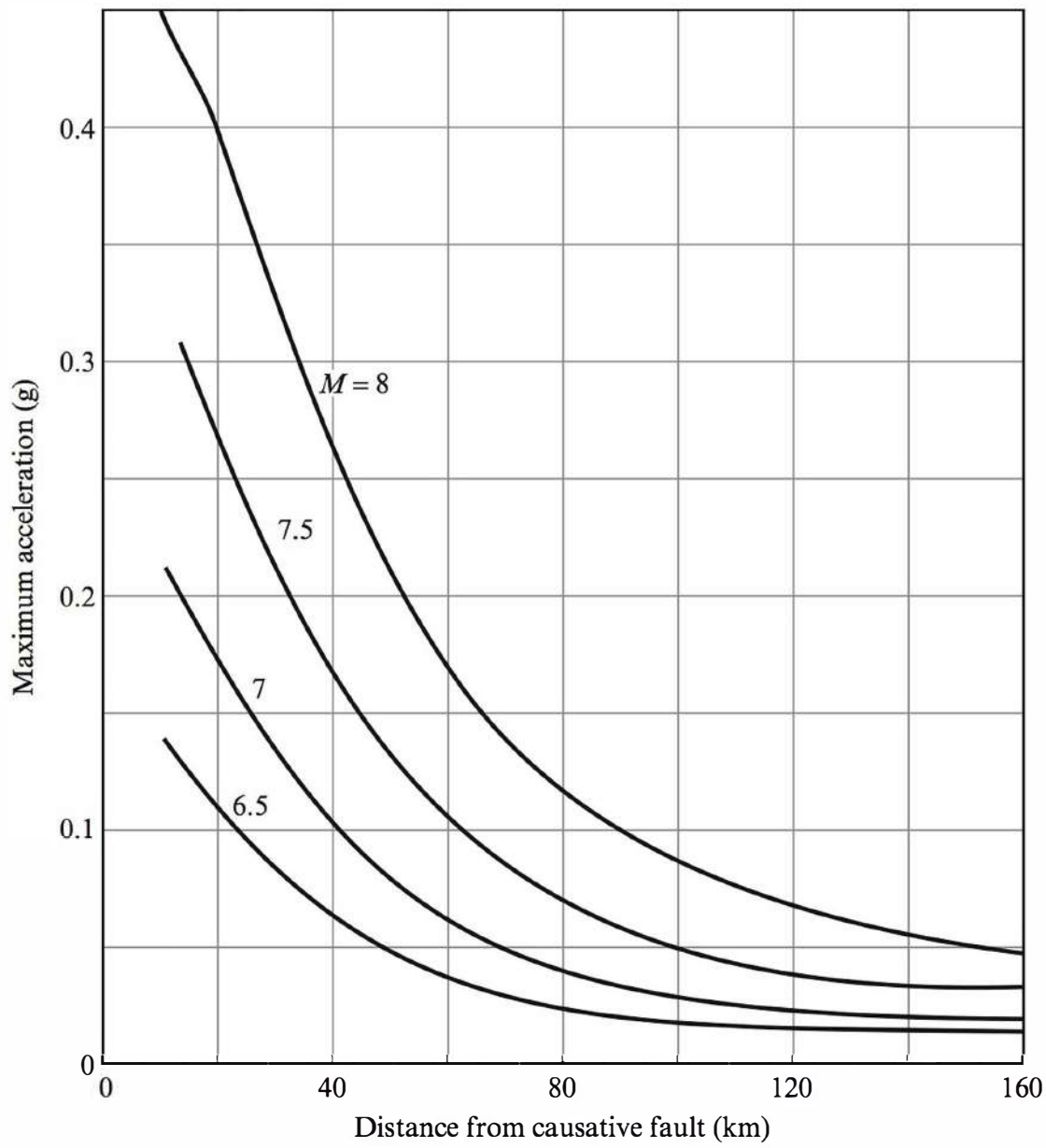

Figure 7.7 Variation of maximum acceleration with earthquake magnitude and distance from causative fault (from Seed, Idriss, and Kiefer, 1969)

Source: Seed, H.B., Idriss, I.M., and Kiefer, F.W. (1969). "Characteristics of Rock Motions During Earthquakes," *Journal of the Soil Management and Foundations Division,* ASCE, Vol. 95, No. SM5, pp. 1199–1218. With permission from ASCE.

7.5 VIBRATION OF HORIZONTAL SOIL LAYERS WITH LINEARLY ELASTIC PROPERTIES

As stated before, the vibration of the soil layers due to an earthquake is due to the upward propagation of shear waves from the underlying rock or rock-like layer. The response of a horizontal soil layer with linearly elastic properties, developed by Idriss and Seed (1968), is presented in this section.

Homogeneous Soil Layer

Figure 7.8 shows a horizontal soil layer of thickness H underlain by a rock or rocklike material. Let the underlying rock layer be subjected to a seismic motion

Copyright 2017 Cengage Learning. All Rights Reserved. May not be copied, scanned, or duplicated, in whole or in part. Due to electronic rights, some third party content may be suppressed from the eBook and/or eChapter(s). Editorial review has deemed that any suppressed content does not materially affect the overall learning experience. Cengage Learning reserves the right to remove additional content at any time if subsequent rights restrictions require it.

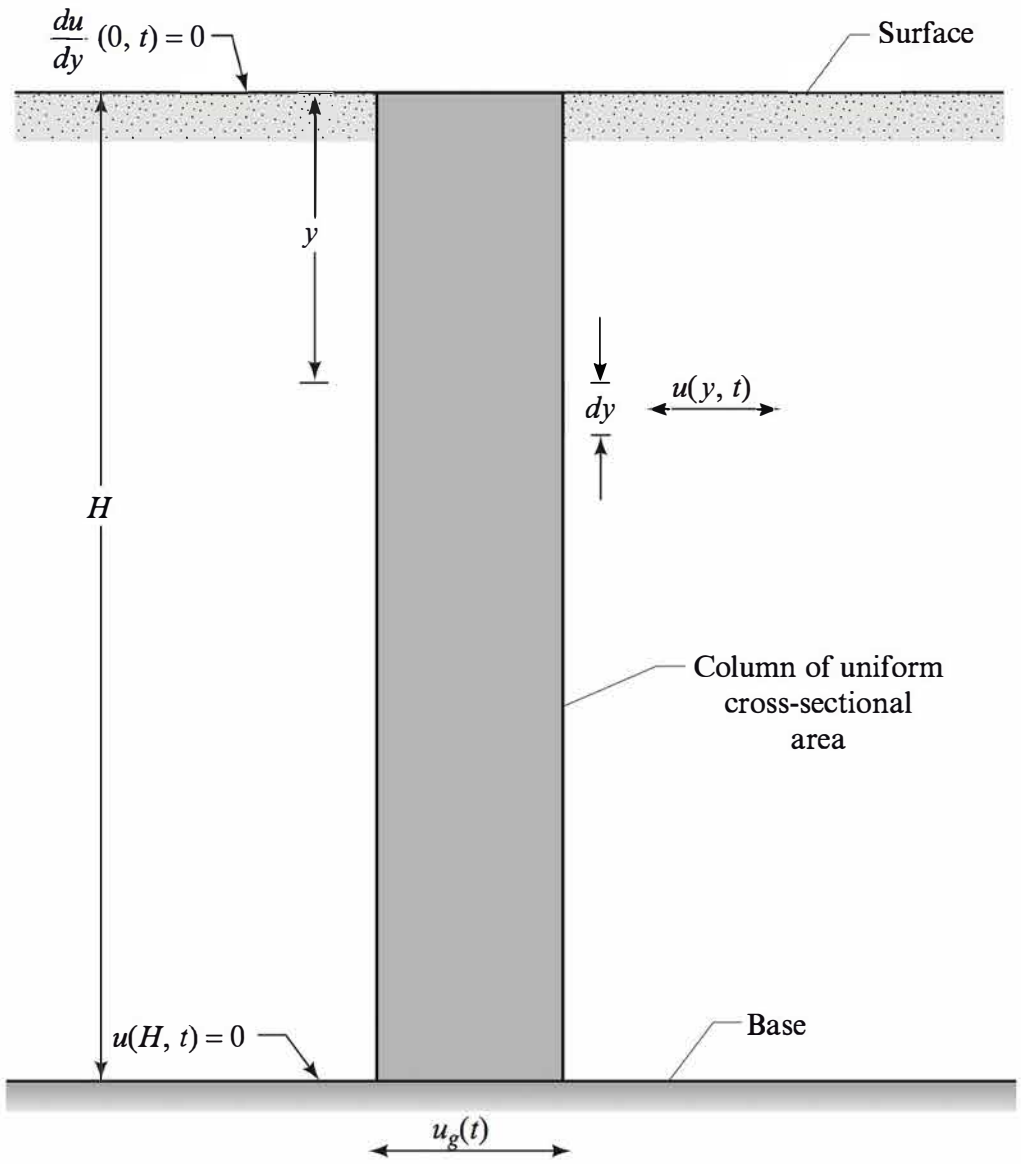

Figure 7.8 Cross section and boundary conditions of a semi-infinite soil layer subjected to a horizontal seismic motion at its base

u_g that is a function of time t. Considering a soil column of unit cross-sectional area, the equation of motion can be written as

$$\rho(y)\frac{\partial^2 u}{\partial t^2} + c(y)\frac{\partial u}{\partial t} - \frac{\partial}{\partial y}\left[G(y)\frac{\partial u}{\partial y}\right] = -\rho(y)\frac{\partial^2 u_g}{\partial t^2} \tag{7.7}$$

where u = relative displacement at depth y and time t
$G(y)$ = shear modulus at depth y
$c(y)$ = viscous damping coefficient at depth y
$\rho(y)$ = density of soil at depth y

The shear modulus can be given by the equation (see the discussion in Chapter 4)

$$G(y) = Ay^B \tag{7.8}$$

where A and B are constant depending on the nature of the soil.

Copyright 2017 Cengage Learning. All Rights Reserved. May not be copied, scanned, or duplicated, in whole or in part. Due to electronic rights, some third party content may be suppressed from the eBook and/or eChapter(s). Editorial review has deemed that any suppressed content does not materially affect the overall learning experience. Cengage Learning reserves the right to remove additional content at any time if subsequent rights restrictions require it.

Substituting Eq. (7.8) into Eq. (7.7), we obtain

$$\rho \frac{\partial^2 u}{\partial t^2} + c\frac{\partial u}{\partial t} - \frac{\partial}{\partial y}\left[Ay^B \frac{\partial u}{\partial y}\right] = -\rho \frac{\partial^2 u_g}{\partial t^2} \tag{7.9}$$

For the case of $B \neq 0$ (but < 0.5), using the method of separation of variables, the solution to Eq. (7.9) can be given in the form

$$u(y,t) = \sum_{n=1}^{n=\infty} Y_n(y) X_n(t) \tag{7.10}$$

where

$$Y_n(y) = \left(\frac{1}{2}\beta_n\right)^b \Gamma(1-b)\left(\frac{y}{H}\right)^{b/\theta} J_{-b}\left[\beta_n\left(\frac{y}{H}\right)^{1/\theta}\right] \tag{7.11}$$

and

$$\ddot{X}_n + 2D_n\omega_n\dot{X}_n + \omega_n^2 X_n = -R_n\ddot{u}_g \tag{7.12}$$

J_{-b} is the Bessel function of first kind of order $-b$, β_n represents the roots of $J_{-b}(\beta_n) = 0, n = 1, 2, 3\ldots$, and the circular natural frequency of nth mode of vibration is

$$\omega_n = \frac{\beta_n\sqrt{A/\rho}}{\theta H^{1/\theta}} \tag{7.13}$$

The damping ratio in the nth mode is

$$D_n = \frac{\frac{1}{2}c}{\rho\omega_n} \tag{7.14}$$

and Γ is the gamma function,

$$R_n = \left[\left(\frac{1}{2}\beta_n\right)^{1+b} \Gamma(1-b) J_{1-b}(\beta_n)\right]^{-1} \tag{7.15}$$

The terms b and θ are related as follows:

$$B\theta - \theta + 2b = 0 \tag{7.16}$$

and

$$B\theta - 2\theta + 2 = 0 \tag{7.17}$$

For detailed derivations, see Idriss and Seed (1967).

For obtaining the relative displacement at a depth y, the general procedure is as follows:

1. Determine the system shape $Y_n(y)$ during the nth mode of vibration [Eq. (7.11)].
2. Determine $X_n(t)$ from Eq. (7.12). This can be done by direct numerical step-by-step procedure (Berg and Housner, 1961; Wilson and Clough, 1962) or the iterative procedure as proposed by Newmark (1962).

Copyright 2017 Cengage Learning. All Rights Reserved. May not be copied, scanned, or duplicated, in whole or in part. Due to electronic rights, some third party content may be suppressed from the eBook and/or eChapter(s). Editorial review has deemed that any suppressed content does not materially affect the overall learning experience. Cengage Learning reserves the right to remove additional content at any time if subsequent rights restrictions require it.

3. Determine $u(y, t)$ from Eq. (7.10).
4. The relative velocity $[\dot{u}(y, t)]$, relative acceleration $[\ddot{u}(y, t)]$, and strain $\partial u/\partial y$ can be obtained by differentiation of Eq. (7.10).
5. The values of total acceleration, velocity, and displacement can be obtained as

$$\text{Total acceleration} = \ddot{u} + \ddot{u}_g$$
$$\text{Total velocity} = \dot{u} + \dot{u}_g$$
$$\text{Total displacement} = u + u_g$$

The values of $\dot{u}_g$ and u_g can be obtained by integration of the acceleration record $[\ddot{u}_g(t)]$.

Special Cases

Cohesionless Soils: In the case of cohesionless soils, the shear modulus [Eq. (7.8)] can be approximated as

$$G(y) = Ay^{1/2} \text{ or } G(y) = Ay^{1/3}$$

Assuming the latter to be representative (i.e., $B = 1/3$), Eqs. (7.16) and (7.17) can be solved, yielding

$$b = 0.4 \text{ and } \theta = 1.2$$

Hence, Eqs. (7.11)–(7.13) take the following form:

$$Y_n(y) = \left(\tfrac{1}{2}\beta_n\right)^{0.4} \Gamma(0.6)\left(\frac{y}{H}\right)^{1/3} J_{-0.4}\left[\beta_n\left(\frac{y}{H}\right)^{5/6}\right] \tag{7.18}$$

$$\ddot{X}_n + 2D_n\omega_n\dot{X}_n + \omega_n^2 X_n = -\ddot{u}_g\left[\left(\frac{\beta_n}{2}\right)^{1.4} \Gamma(0.6) J_{0.6}(\beta_n)\right]^{-1} \tag{7.19}$$

and

$$\omega_n = \frac{\beta_n\sqrt{A/\rho}}{1.2H^{5/6}} \tag{7.20}$$

(*Note:* $\beta_1 = 1.7510$, $\beta_2 = 4.8785$, $\beta_3 = 8.0166$, $\beta_4 = 11.1570\ldots$.)

Cohesive Soils: In cohesive soils, the shear modulus may be considered to be approximately constant with depth; so, in Eq. (7.8), $B = 0$ and

$$G(y) = A \tag{7.21}$$

Copyright 2017 Cengage Learning. All Rights Reserved. May not be copied, scanned, or duplicated, in whole or in part. Due to electronic rights, some third party content may be suppressed from the eBook and/or eChapter(s). Editorial review has deemed that any suppressed content does not materially affect the overall learning experience. Cengage Learning reserves the right to remove additional content at any time if subsequent rights restrictions require it.

With this assumption, Eqs. (7.11)–(7.13) are simplified as

$$Y_n(y) = \cos\left[\frac{1}{2}(2n-1)\left(\frac{y}{H}\right)\right] \tag{7.22}$$

$$\ddot{X}_n + 2D_n\omega_n\dot{X}_n + \omega_n^2 X_n = (-1)^n\left[\frac{4}{(2n-1)\pi}\right]\ddot{u}_g \tag{7.23}$$

and

$$\omega_n = \left[\frac{(2n-1)\pi}{2H}\right]\sqrt{\frac{G}{\rho}} \tag{7.24}$$

Computer programs for determination of acceleration, velocity, and displacement of soil profiles for these two special cases can be found in Idriss and Seed (1967, Appendix C).

An example of a solution for cohesionless (granular) soil is given in Figure 7.9. Figure 7.10 shows the variation of shear modulus, maximum shear strain, and maximum shear stress with depth for the same soil layer shown in Figure 7.9. For this example,

$$H = 30 \text{ m}$$

$$\text{Total unit weight of soil} = \gamma = 19.65 \text{ kN/m}^3$$

$$\text{Effective unit weight of soil} = \gamma' = 9.43 \text{ kN/m}^3$$

$$\text{Shear modulus of soil} = 4.79 \times 10^3\, y^{1/3}\text{kPa}$$

$$D = 0.2(\text{for all modes}, n = 1, 2, \ldots \infty)$$

For a discussion on the damping coefficient of soil under earthquake conditions, see Chapter 4.

Layered Soils

If a soil profile consists of several layers of varying properties that are linearly elastic, a lumped mass type of approach can be taken (Idriss and Seed, 1968). These lumped masses ($m_1, m_2, \ldots, m_N$) are shown in Figure 7.11. Note

$$m_1 = \frac{\gamma_1 h_1}{g} \tag{7.25}$$

where m_1 is a lumped mass placed at the top of soil layer 1, γ_1 is the unit weight of soil in layer 1, h_1 is the half thickness of soil layer 1, and

$$m_i = \frac{\gamma_{i-1}h_{i-1} + \gamma_i h_i}{g}, i = 2, 3, \ldots, N \tag{7.26}$$

These masses are connected by springs which resist lateral deformation. The spring constant can be given by

Copyright 2017 Cengage Learning. All Rights Reserved. May not be copied, scanned, or duplicated, in whole or in part. Due to electronic rights, some third party content may be suppressed from the eBook and/or eChapter(s). Editorial review has deemed that any suppressed content does not materially affect the overall learning experience. Cengage Learning reserves the right to remove additional content at any time if subsequent rights restrictions require it.

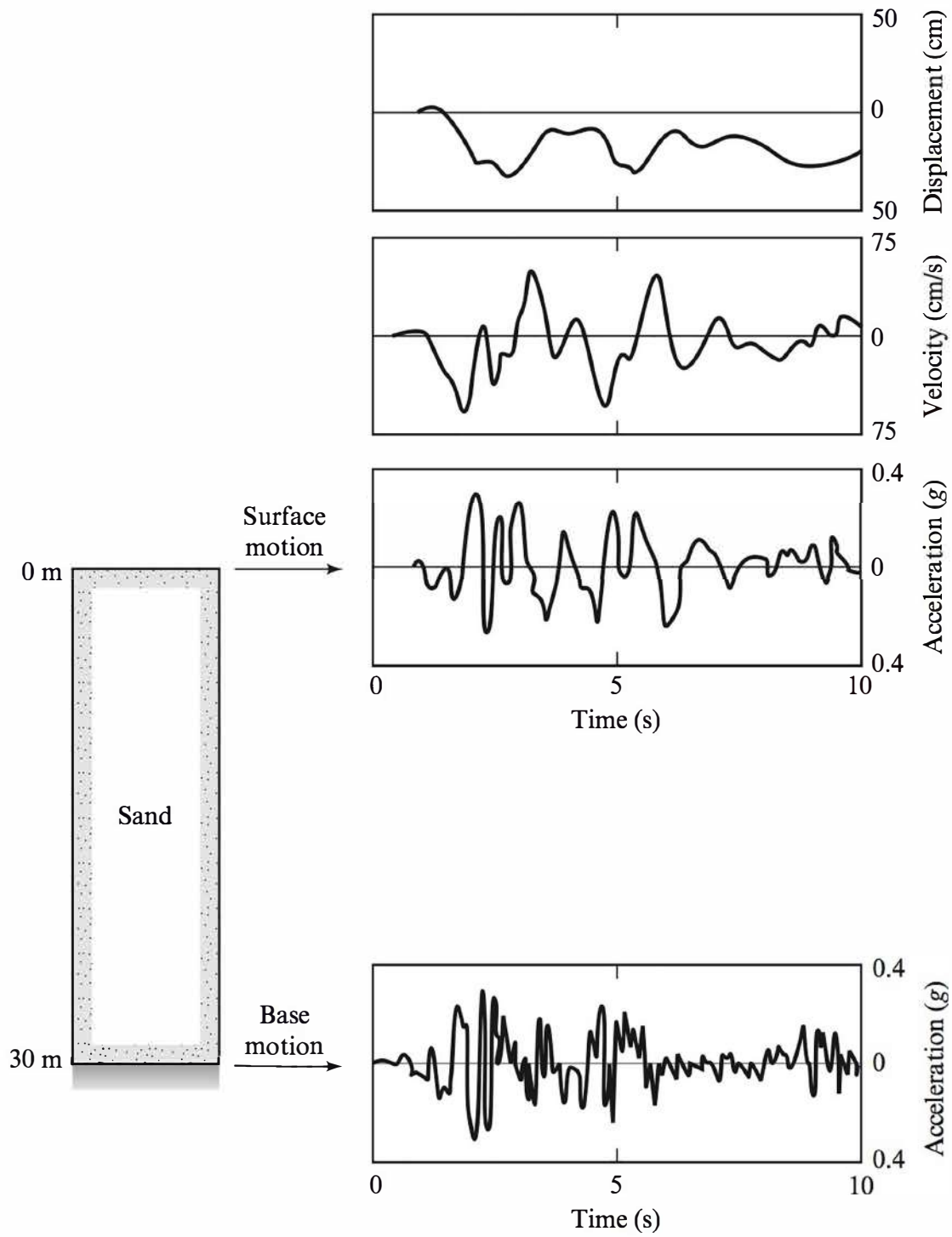

Figure 7.9 Surface response of layer with modulus proportional to cube root of depth (from Idriss and Seed, 1968)

Source: Idriss, I.M. and Seed, H.B. (1968). "Seismic Response of Horizontal Soil Layers," *Journal of the Soil Mechanics and Foundations Division,* ASCE, Vol. 94, No. SM4, pp. 1003–1031. With permission from ASCE.

$$k_i = \frac{G_i}{2h_i}, i = 1, 2, \ldots, N \tag{7.27}$$

where k_i is the spring constant of the spring connecting the masses m_i and m_{i+1}, and G_i is the shear modulus of layer i.

The equation of motion of the system can be given by the expression

$$[M]\{\ddot{u}\} + [C]\{\dot{u}\} + [K]\{u\} = \{R(t)\} \tag{7.28}$$

Copyright 2017 Cengage Learning. All Rights Reserved. May not be copied, scanned, or duplicated, in whole or in part. Due to electronic rights, some third party content may be suppressed from the eBook and/or eChapter(s). Editorial review has deemed that any suppressed content does not materially affect the overall learning experience. Cengage Learning reserves the right to remove additional content at any time if subsequent rights restrictions require it.

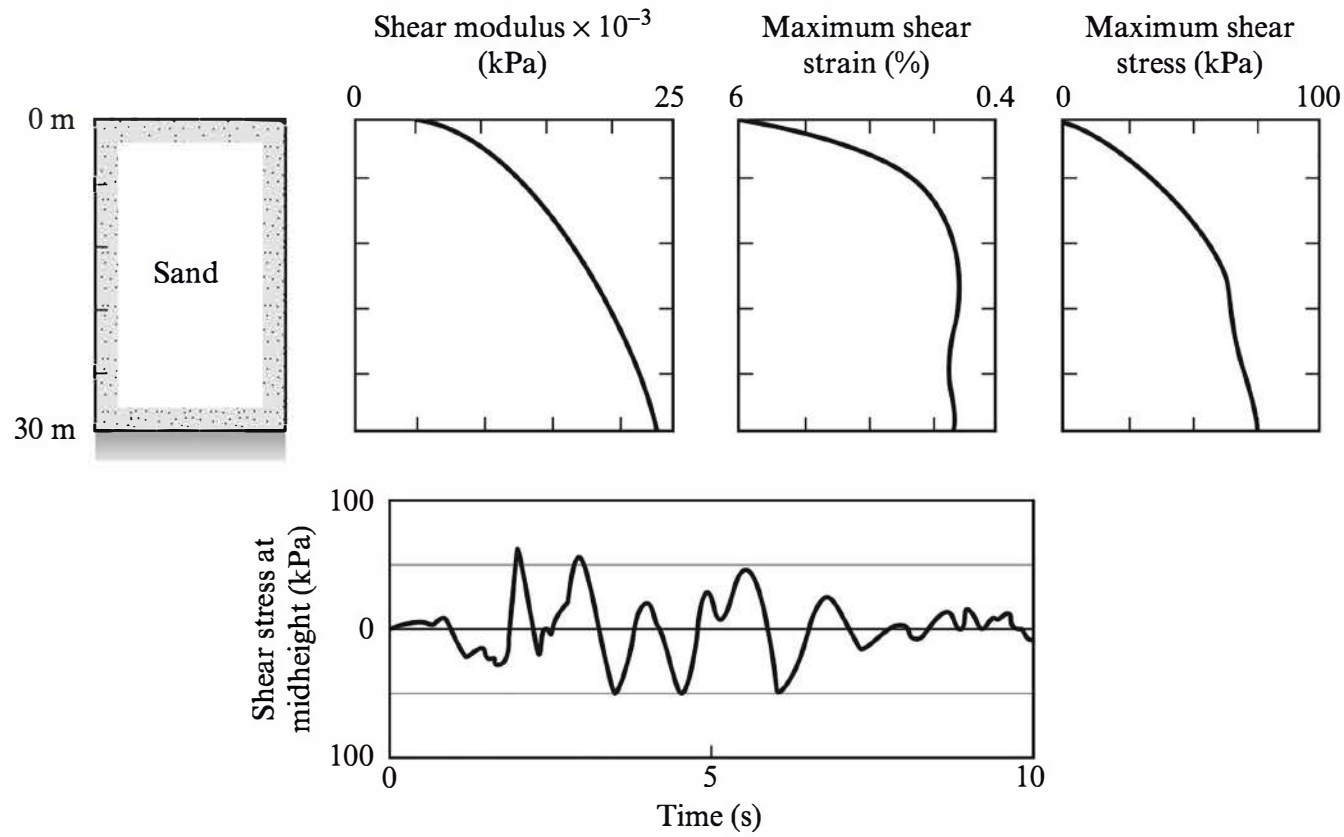

Figure 7.10 Stress and strain developed within the layer of soil shown in Figure 7.6 (from Idriss and Seed, 1968)

Source: Idriss, I.M. and Seed, H.B. (1968). "Seismic Response of Horizontal Soil Layers," *Journal of the Soil Mechanics and Foundations Division,* ASCE, Vol. 94, No. SM4, pp. 1003–1031. With permission from ASCE.

where $[M]$ is a matrix for mass, $[C]$ is a matrix for viscous damping, $[K]$ is the stiffness matrix, and $\{u\}$, $\{\dot{u}\}$, and $\{\ddot{u}\}$ are relative displacement, relative velocity, and relative acceleration vectors, respectively. The matrices $[M]$, $[C]$, and $[K]$ are of the order N (the number of layers considered). The matrix $[M]$ is a diagonal matrix such that

$$\text{diag}[M] = (m_1, m_2, m_3, \ldots, m_N) \tag{7.29}$$

The matrix $[K]$ is tridiagonal and symmetric and

$$\begin{aligned} K_{11} &= k_1 \\ K_{ij} &= k_{i-1} + k_i && \text{for } i = j \\ K_{ij} &= -k_i && \text{for } i = j-1 \\ K_{ij} &= -k_j && \text{for } i = j+1 \end{aligned}$$

All other K_{ij} are equal to zero.

The load vector $\{R(t)\}$ is

$$\{R(t)\} = -\,\text{col}\,(m_1, m_2, \ldots, m_N)\,\ddot{u}_g \tag{7.30}$$

A computer program for solution of Eq. (7.28) is given in Idriss and Seed (1967, Appendix C). The general outline of the solution is as follows:

1. The number of layers of soil (N) and the mass and stiffness matrices are first obtained.

Copyright 2017 Cengage Learning. All Rights Reserved. May not be copied, scanned, or duplicated, in whole or in part. Due to electronic rights, some third party content may be suppressed from the eBook and/or eChapter(s). Editorial review has deemed that any suppressed content does not materially affect the overall learning experience. Cengage Learning reserves the right to remove additional content at any time if subsequent rights restrictions require it.

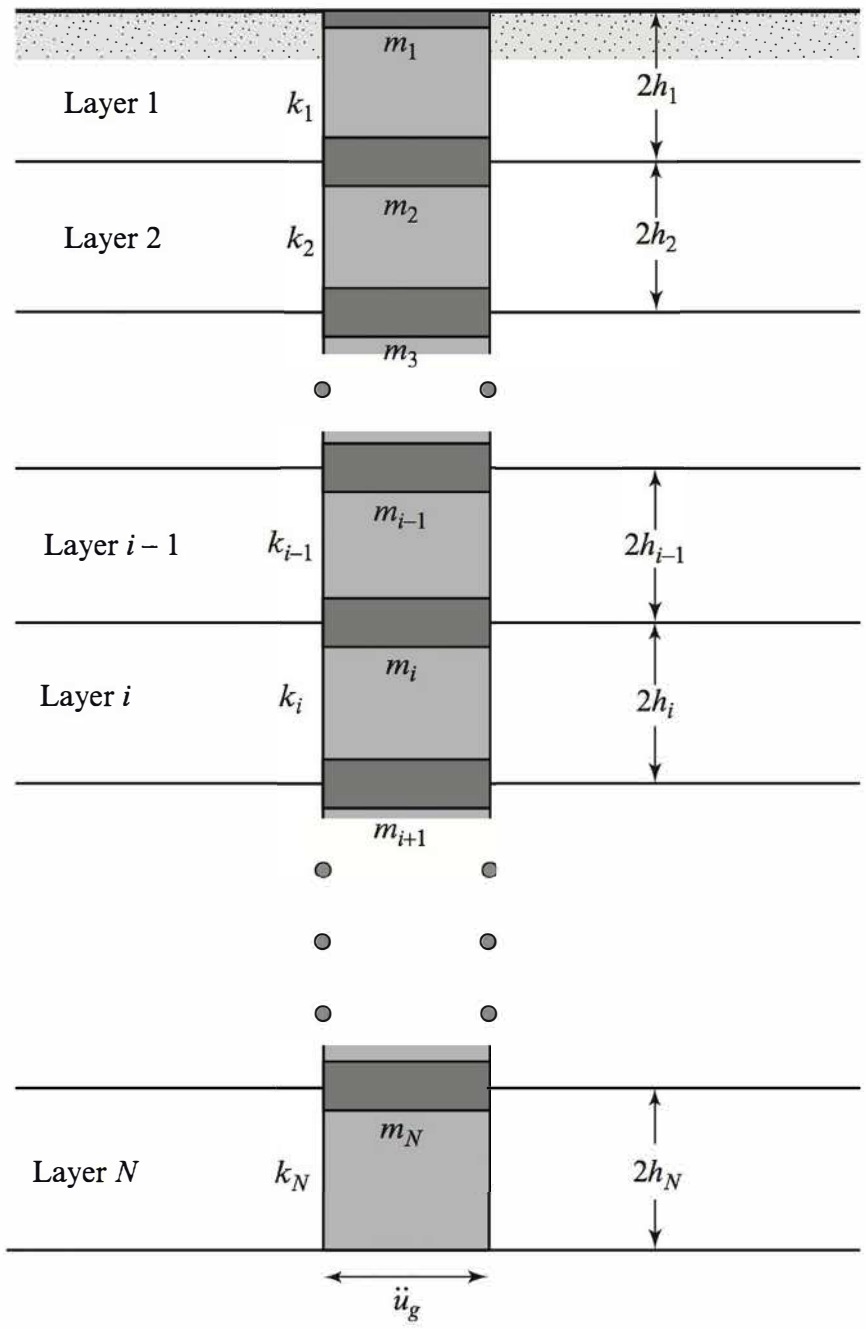

Figure 7.11 Lumped mass idealization of horizontal soil layers

2. The mode shapes and frequencies are obtained from the characteristic value problem as

$$[K]\{\phi^n\} = \omega_n^2[M]\{\phi^n\} \tag{7.31}$$

where ϕ_i^n is the mode shape at the ith level during the nth mode of vibration and ω_n is the circular frequency at the nth mode of vibration.

3. Equation (7.28) is then reduced to a set of uncoupled normal equations. The normal equations are solved for the response of each mode at each instant of time. The relative displacements at level i can then be expressed as

$$u_i(t) = \sum_{n=1}^{N} \phi_i^n X_n(t) \tag{7.32}$$

Copyright 2017 Cengage Learning. All Rights Reserved. May not be copied, scanned, or duplicated, in whole or in part. Due to electronic rights, some third party content may be suppressed from the eBook and/or eChapter(s). Editorial review has deemed that any suppressed content does not materially affect the overall learning experience. Cengage Learning reserves the right to remove additional content at any time if subsequent rights restrictions require it.

where $X_n(t)$ is the normal coordinate for the nth mode and $u_i(t)$ is the relative displacements at the ith level at time t.

4. The relative velocity $[\dot{u}_i(t)]$ and the relative acceleration $[\ddot{u}_i(t)]$ can be obtained by differentiation of Eq. (7.32), or

$$\dot{u}_i(t) = \sum_{n=1}^{N} \phi_i^n \dot{X}_n(t) \tag{7.33}$$

$$\ddot{u}_i(t) = \sum_{n=1}^{N} \phi_i^n \ddot{X}_n(t) \tag{7.34}$$

5. The total acceleration, velocity, and displacement at level i and time t can be given as follows:

$$\begin{aligned} \text{Total acceleration} &= \ddot{u}_i(t) + \ddot{u}_g \\ \text{Total velocity} &= \dot{u}_i(t) + \dot{u}_g \\ \text{Total displacement} &= u_i(t) + u_g \end{aligned}$$

6. The shear strain between level i and $i+1$ can be expressed as

$$[u_i(t) - u_{i+1}(t)]/2h_i \tag{7.35}$$

7. The shear stress between level i and $i+1$ can now be obtained as

$$\tau_i(t) = (\text{shear strain})G \tag{7.36}$$

Degree of Accuracy and Stability of the Analysis

The degree of accuracy of the lumped mass solution depends on the number of layers of soils used in an analysis. (*Note*: The value of the shear modulus for each layer is assumed to be constant.) In order to select a reasonable number of layers N with a tolerable degree of accuracy, Idriss and Seed (1968) prepared the graph shown in Figure 7.12, where ERS means the percentage of error in the lumped mass representation.

The use of this figure can be explained as follows:

Let the height, shear modulus, and unit weight of the ith layer of soil be H_i, G_i, and γ_i respectively. The fundamental frequency of this layer can be obtained from Eq. (7.24) as

$$\begin{aligned} \omega_{n(i)} &= \left[\frac{(2n-1)\pi}{2H_i}\right]\sqrt{\frac{G_i}{\rho_i}} \\ &= \left(\frac{\pi}{2H_i}\right)\sqrt{\frac{G_i}{\rho_i}} \quad \text{for } n = 1 \end{aligned}$$

Copyright 2017 Cengage Learning. All Rights Reserved. May not be copied, scanned, or duplicated, in whole or in part. Due to electronic rights, some third party content may be suppressed from the eBook and/or eChapter(s). Editorial review has deemed that any suppressed content does not materially affect the overall learning experience. Cengage Learning reserves the right to remove additional content at any time if subsequent rights restrictions require it.

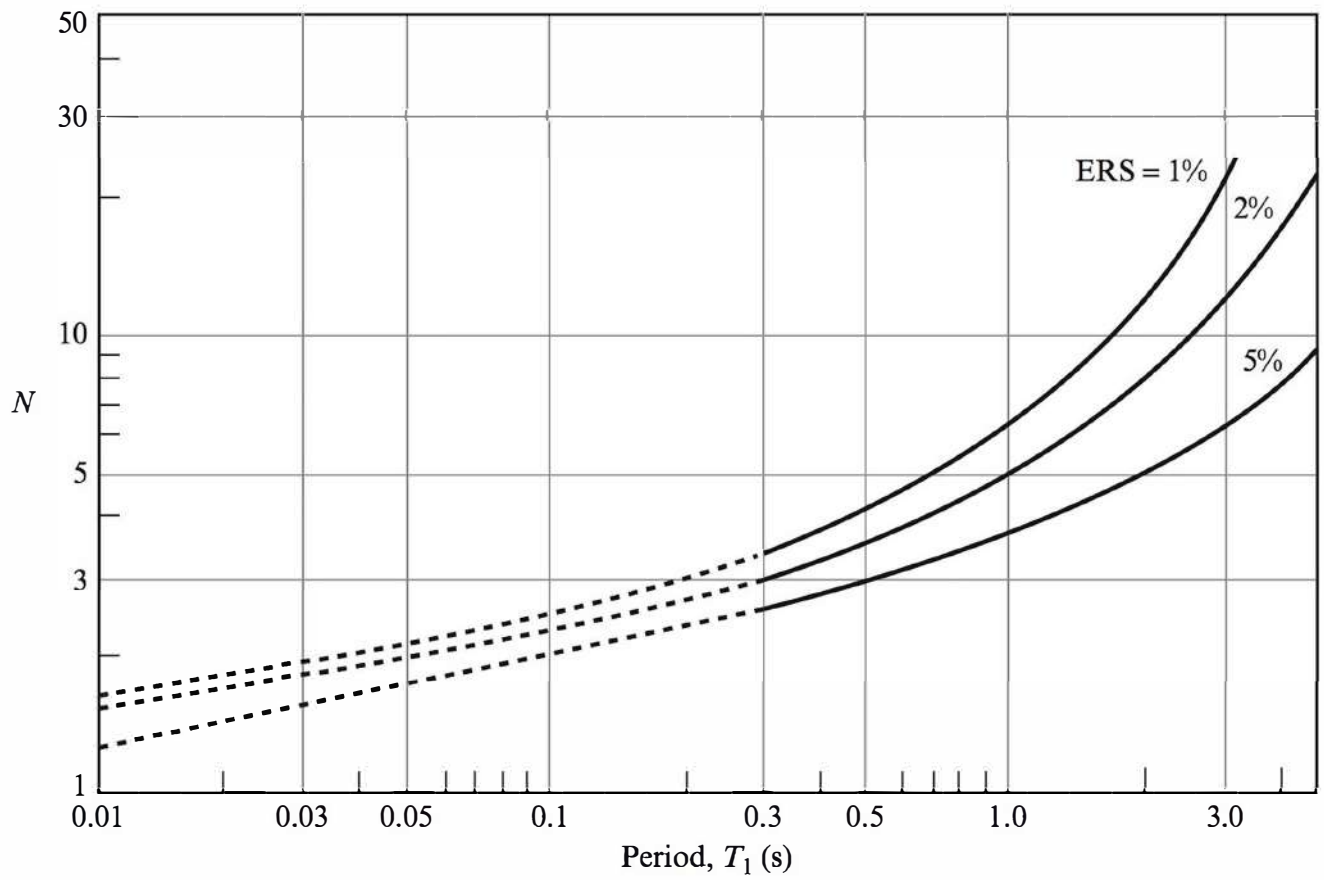

Figure 7.12 Plot of N versus T_1 for equal values of ERS (from Idriss and Seed, 1968)

Source: Idriss, I.M. and Seed, H.B. (1968). "Seismic Response of Horizontal Soil Layers," *Journal of the Soil Mechanics and Foundations Division,* ASCE, Vol. 94, No. SM4, pp. 1003–1031. With permission from ASCE.

Hence, the fundamental period can be given by

$$T_{1(i)} = \frac{2\pi}{\omega_{1(i)}} = \frac{4H_i}{\sqrt{G_i g/\gamma_i}} \tag{7.37}$$

where g is acceleration due to gravity.

Using the value of this, $T_{1(i)}$ and a given value of ERS, the value of N_i can be obtained from Figure 7.12; this is the number of layers into which the ith layer has to be divided for the analysis of the ground vibration. Since this needs to be done for each layer of soil,

$$N = \sum N_i \tag{7.38}$$

For the stability of the lumped mass solution, Idriss and Seed (1978) have suggested the following condition.

For the step-by-step solution (Berg and Housner, 1961; Wilson and Clough, 1962):

$$T_{NN} \geq 2\Delta t \tag{7.39}$$

For Newmark's iterative solution (1962)

$$T_{NN} \geq 5\Delta t \tag{7.40}$$

Copyright 2017 Cengage Learning. All Rights Reserved. May not be copied, scanned, or duplicated, in whole or in part. Due to electronic rights, some third party content may be suppressed from the eBook and/or eChapter(s). Editorial review has deemed that any suppressed content does not materially affect the overall learning experience. Cengage Learning reserves the right to remove additional content at any time if subsequent rights restrictions require it.

where Δt is the time interval used for integrating the normal equations and T_{NN} is the lowest period included in the analysis. Note that this corresponds to the highest mode of vibration.

General Remarks for Ground Vibration Analysis

First of all, it should be kept in mind that soil deposits, in general, tend to amplify the underlying rock motion to some degree.

Secondly, for appropriate analysis of ground motion due to an earthquake, it is necessary that an earthquake acceleration–time record be available at the level of the *bedrock* or *bedrock-like material* for a given site. The design accelerogram can be obtained by selecting an actual motion, which has been recorded in the past, of a somewhat similar magnitude and fault distance as the design conditions. This accelerogram is then modified by taking into account the differences between the recorded and design conditions. This modification can be better explained by the following example.

Let the design earthquake be of magnitude 7 and the site be located at a distance of 80 km. Hence, its predominant period at *bedrock* or *bedrock-like material* is 0.4 s (Figure 7.6) and the maximum acceleration is of the order of 0.04g (Figure 7.7). The estimated duration of this earthquake is about 30 s (equal to the duration of the fault break; Section 7.7). Also, let the recorded earthquake have a predominant period of 0.45 s, maximum acceleration of 0.05g, and a duration of 40 s. The recorded earthquake may now be modified by reducing the ordinates (i.e., magnitudes of acceleration) by 0.04/0.05 = 4/5 and by compressing the time scale by 0.40/0.45 = 8/9. This results in a maximum acceleration of 0.04g with a predominant period of 0.4 s and a duration of 35.5 s. The first 30 s of this accelerogram can now be taken for the analysis of ground motion.

Appropriate parts of an accelerogram could be repeated to obtain the desired period of predicted significant motion.

EXAMPLE 7.1

In a soil deposit, a clay layer has a thickness of 16 m. The unit weight and the shear modulus of the clay soil deposit are 17.8 kN/m^3 and 24,000 kPa, respectively. Determine the number of layers into which this should be divided so that the ERS in the lumped mass solution does not exceed 5%.

SOLUTION:

Given that $H_i = 16$ m and $G_i = 24{,}000$ kPa. From Eq. (7.37),

$$T_{1(i)} = \frac{4H_i}{\sqrt{G_i g/\gamma_i}} = \frac{(4)(16)}{\sqrt{(24{,}000 \times 9.81)/17.8}} = 0.566 \text{ s}$$

Copyright 2017 Cengage Learning. All Rights Reserved. May not be copied, scanned, or duplicated, in whole or in part. Due to electronic rights, some third party content may be suppressed from the eBook and/or eChapter(s). Editorial review has deemed that any suppressed content does not materially affect the overall learning experience. Cengage Learning reserves the right to remove additional content at any time if subsequent rights restrictions require it.

From Figure 7.12, with $T_{1(i)} = 0.556$ s and ERS = 5%, the value of N_i is equal to **3**. Thus, this clay layer should be subdivided into at least 3 layers with thickness of **5.33 m each**.

7.6 OTHER STUDIES FOR VIBRATION OF SOIL LAYERS DUE TO EARTHQUAKES

In the preceding section, for the evaluation of the ground vibration, it was assumed that

1. the soil layer(s) possess linearly elastic properties, and
2. the soil layer(s) are horizontal.

Under strong ground-shaking conditions, the stress-strain relationships may be of the nature shown in Figure 7.13a and not linearly elastic. This type of stress-strain relationship can be approximated to a bilinear system as shown in Figure 7.13b, and the analysis of ground vibration can then be carried out.

The lumped mass type of solution using bilinear stress-strain relationships of horizontally layered soils (Figure 7.14) have been presented by Parmelee et al. (1964) and Idriss and Seed (1967, 1968), whose works may be examined for further details.

Studies of the vibration of soils with sloping boundaries have also been made by Idriss, Dezfulian, and Seed (1969) and Dezfulian and Seed (1970). This involves a finite element method of analysis. For a computer program of such an analysis, refer to Idriss, Dezfulian, and Seed.

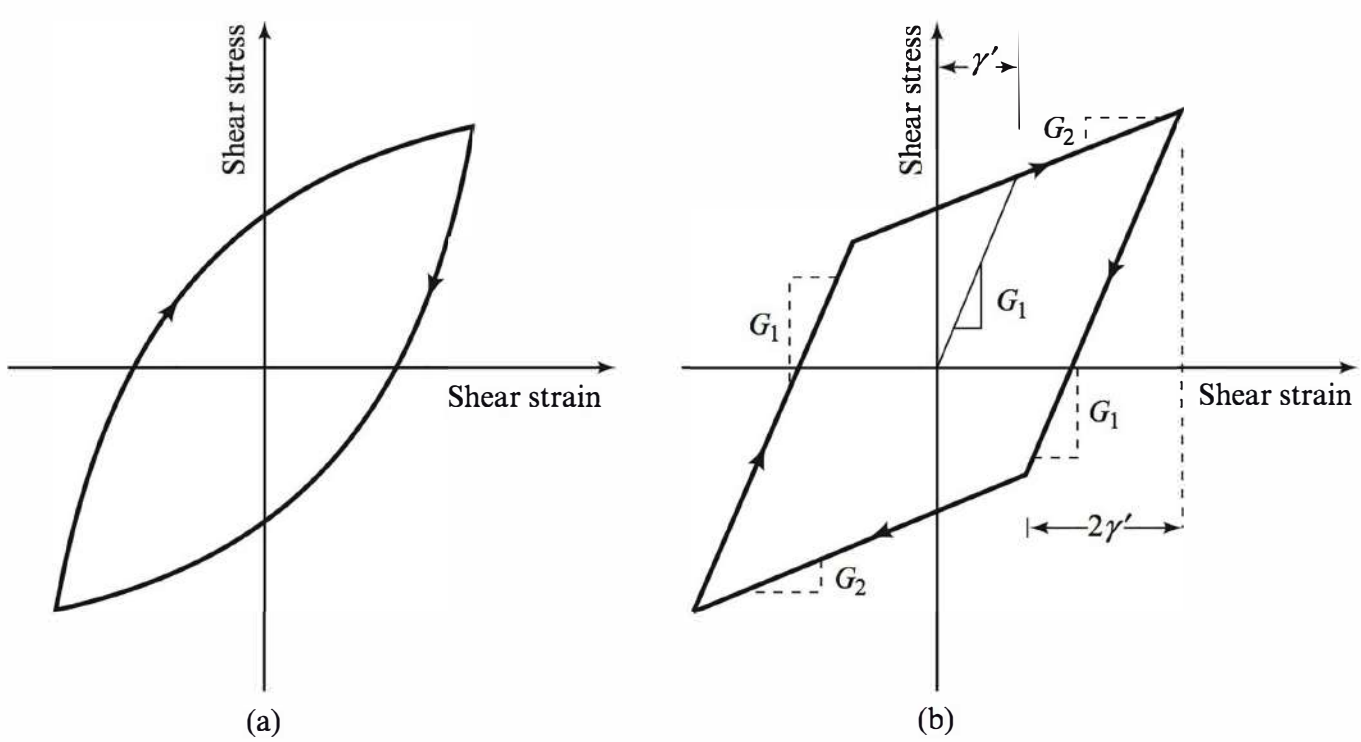

Figure 7.13 Shear stress-strain characteristics of soil: (a) stress-strain curve; (b) bilinear idealization

Copyright 2017 Cengage Learning. All Rights Reserved. May not be copied, scanned, or duplicated, in whole or in part. Due to electronic rights, some third party content may be suppressed from the eBook and/or eChapter(s). Editorial review has deemed that any suppressed content does not materially affect the overall learning experience. Cengage Learning reserves the right to remove additional content at any time if subsequent rights restrictions require it.

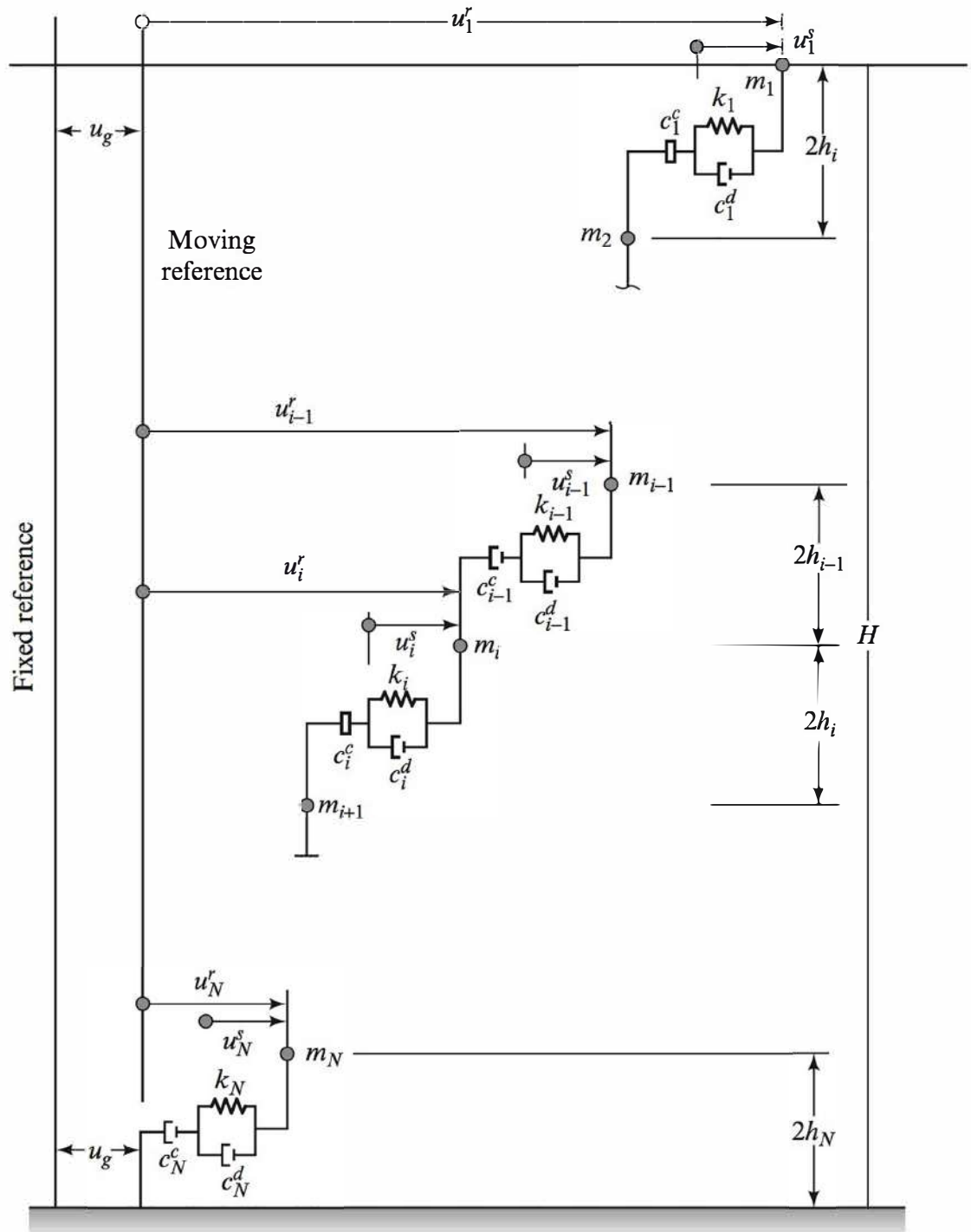

Figure 7.14 Lumped parameter solution of a semi-infinite layer: bilinear solution (from Idriss and Seed, 1968)

Source: Idriss, I.M. and Seed, H.B. (1968). "Seismic Response of Horizontal Soil Layers," *Journal of the Soil Mechanics and Foundations Division,* ASCE, Vol. 94, No. SM4, pp. 1003–1031. With permission from ASCE.

7.7 EQUIVALENT NUMBER OF SIGNIFICANT UNIFORM STRESS CYCLES FOR EARTHQUAKES

In the study of soil liquefaction of granular soils (Chapter 10), it becomes necessary to determine the equivalent number of significant uniform stress cycles for an earthquake that has *irregular stress-time history*. This is explained with the aid of Figure 7.15. Figure 7.15a shows the irregular pattern of shear stress on a soil

Copyright 2017 Cengage Learning. All Rights Reserved. May not be copied, scanned, or duplicated, in whole or in part. Due to electronic rights, some third party content may be suppressed from the eBook and/or eChapter(s). Editorial review has deemed that any suppressed content does not materially affect the overall learning experience. Cengage Learning reserves the right to remove additional content at any time if subsequent rights restrictions require it.

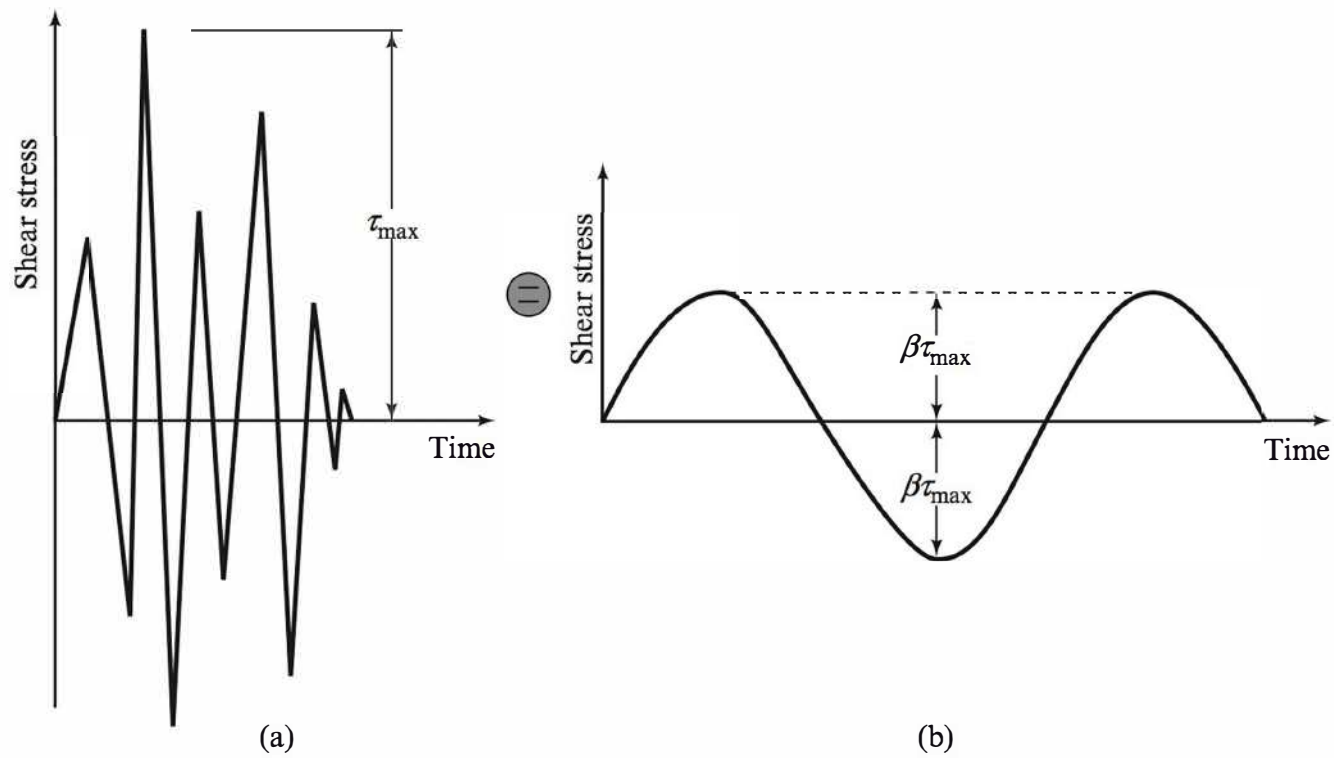

Figure 7.15 Equivalent uniform stress cycles: (a) irregular stress-time history; (b) equivalent uniform stress–time history

deposit with time for an earthquake. The maximum shear stress induced is τ_{max}. This irregular stress-time history may be *equivalent* to uniformly intense N number of cyclic shear stresses of maximum magnitude equal to $\beta\tau_{max}$ (Figure 7.15b). The term equivalent means that the effect of the stress history shown in Figure 7.15a on a given soil deposit should be the same as the uniform stress cycles as shown in Figure 7.15b. From the point of view of soil liquefaction, this fact has been studied by Lee and Chan (1972), Seed et al. (1975), Seed (1976, 1979), and Valera and Donovan (1977).

The basic procedure involved in developing the equivalent stress cycles is fairly simple and has been described by Seed et al. (1975). This is done by using the results of the soil liquefaction study by simple shear tests obtained by DeAlba, Chan, and Seed (1975). Figure 7.16 shows a plot of τ/τ_{max} against the equivalent number of uniform cyclic stresses N at a maximum stress magnitude of $0.65\,\tau_{max}$. This means, for example, that *one cycle* of shear stress of maximum magnitude of τ_{max} is equivalent to three cycles of shear stress of maximum magnitude $0.65\,\tau_{max}$. Similarly, one cycle of shear stress with maximum magnitude of $0.75\,\tau_{max}$ is equivalent to 1.4 cycles of shear stress with a maximum magnitude of $0.65\,\tau_{max}$. Figure 7.16 can be used to evaluate the values of N for various earthquakes for a maximum magnitude of uniform cyclic shear stress level equaling $0.65\,\tau_{max}$.(*Note*: $\beta = 0.65$.) This can be most effectively explained by a numerical example. While doing this, one must recognize that, within the top 6–7 m of a given soil deposit, the cyclic shear stress–time history of an earthquake is similar in form to the acceleration–time history at the ground surface.

Copyright 2017 Cengage Learning. All Rights Reserved. May not be copied, scanned, or duplicated, in whole or in part. Due to electronic rights, some third party content may be suppressed from the eBook and/or eChapter(s). Editorial review has deemed that any suppressed content does not materially affect the overall learning experience. Cengage Learning reserves the right to remove additional content at any time if subsequent rights restrictions require it.

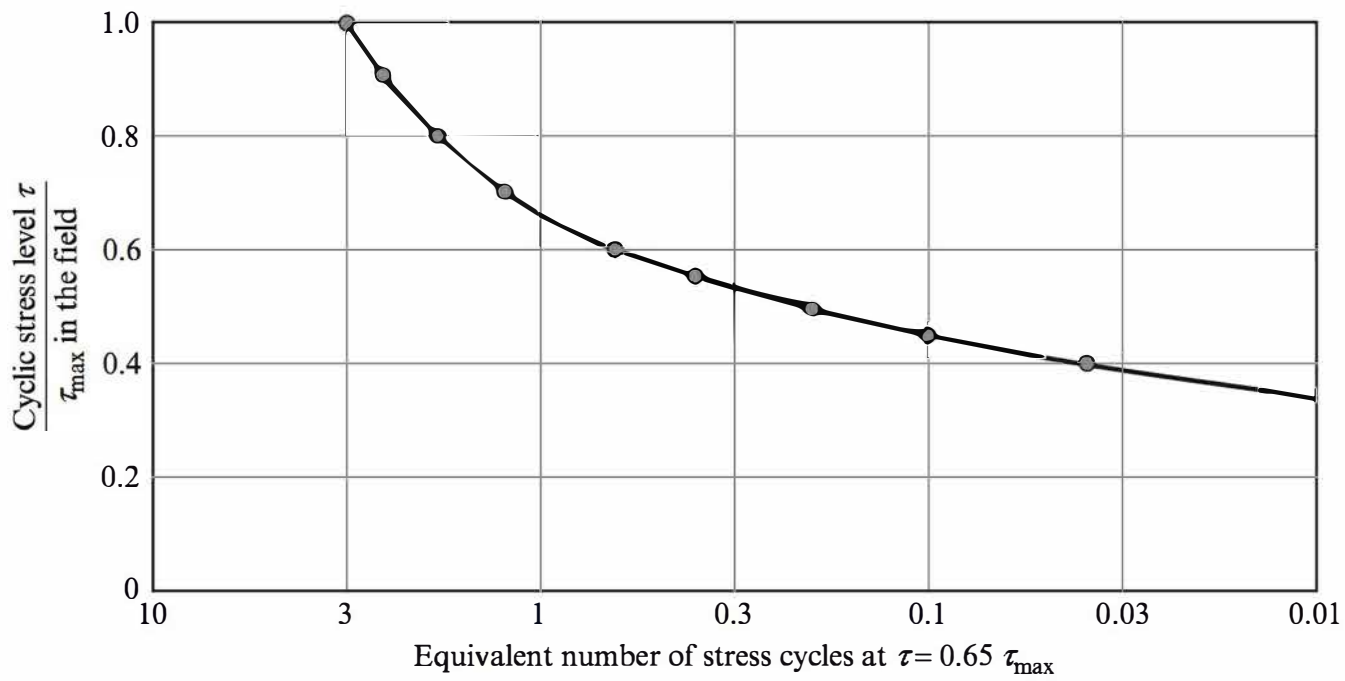

Figure 7.16 Plot of τ/τ_{max} versus N at $\tau = 0.65\,\tau_{max}$ (from Seed at al 1975)

Source: Seed, H.B., Idriss, I.M. Makdidi, F. and Banerjee, N. (1975). "Representation of Irregular Stress-Time Histories by EquivalentUniform Stress Series of Liquefaction Analyses," *Report No. EERC* 75–29. Earthquake Engineering Research Center, University of California, Berkley. Reprinted by permission of the PEER Center, UC Berkeley.

The acceleration–time history for the San Jose earthquake (1955) is shown in Figure 7.17. Note that the maximum acceleration in this case is 0.106 g. Hence, τ_{max} is proportional to 0.106 g. In order to determine N, one needs to prepare Table 7.5. This can be done in the following manner.

1. Looking at Figure 7.17, determine the number of stress cycles at various stress levels such as $\tau_{max}, 0.95\,\tau_{max}, 0.9\,\tau_{max}$ ..., above the horizontal axis (col. 2) and below the horizontal axis (col. 5).

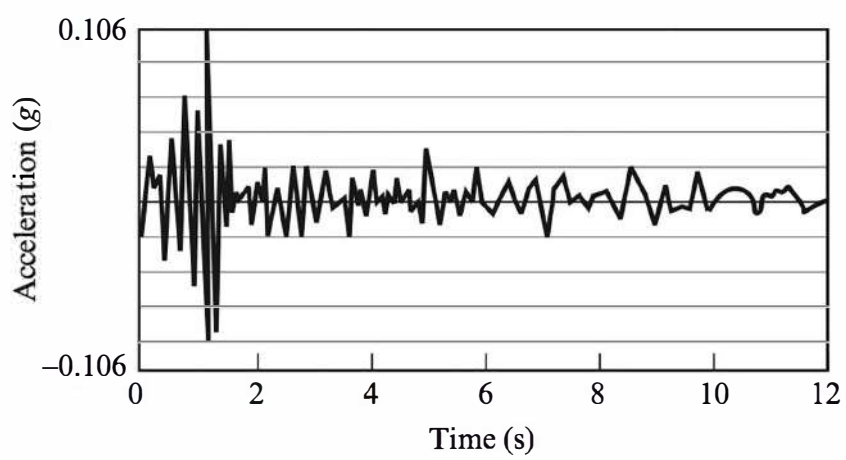

Figure 7.17 San Jose earthquake record, 1955 (from Seed et al., 1975)

Source: Seed, H.B., Idriss, I.M. Makdidi, F. and Banerjee, N. (1975). "Representation of Irregular Stress-Time Histories by EquivalentUniform Stress Series of Liquefaction Analyses," *Report No. EERC* 75–29. Earthquake Engineering Research Center, University of California, Berkley. Reprinted by permission of the PEER Center, UC Berkeley.

Copyright 2017 Cengage Learning. All Rights Reserved. May not be copied, scanned, or duplicated, in whole or in part. Due to electronic rights, some third party content may be suppressed from the eBook and/or eChapter(s). Editorial review has deemed that any suppressed content does not materially affect the overall learning experience. Cengage Learning reserves the right to remove additional content at any time if subsequent rights restrictions require it.

Table 7.5 Example of Determination of Equivalent Uniform Cyclic Stress Series from Figure 7.14[a]

	Above horizontal axis			Below horizontal axis		
Stress level (τ_{max})	No. of stress cycles	Conversion factor	Equivalent no. of cycles at 0.65 τ_{max}	No. of stress cylces	Conversion factor	Equivalent no. of cycles at 0.65 τ_{max}
(1)	(2)	(3)	(4)	(5)	(6)	(7)
1.00	1	3.00	3.00			
0.95						
0.90	–	–	–			
0.85	–	–	–	1	2.05	2.05
0.80	–	–	–	1	1.70	1.70
0.75	–	–	–			
0.70	–	–	–			
0.65	–	–	–			
0.60	1	0.70	0.70			
0.55	1	0.40	0.40	1	0.40	0.40
0.50						
0.45						
0.40	1	0.04	0.04	1	0.04	0.04
0.35	2	0.02	0.04	1	0.02	0.02
		Total	4.2		Total	4.2
Average number of cycles of $0.65\,\tau_{max} \approx 4.2$						

[a]Seed et al. (1975)

Source: Seed, H.B., Idriss, I.M. Makdidi, F. and Banerjee, N. (1975). "Representation of Irregular Stress-Time Histories by EquivalentUniform Stress Series of Liquefaction Analyses," *Report No. EERC* 75–29. Earthquake Engineering Research Center, University of California, Berkley. Reprinted by permission of the PEER Center, UC Berkeley.

2. Determine the conversion factors from Figure 7.16 (cols. 3 and 6).
3. Determine the equivalent number of uniform cycles at a maximum stress level of 0.65 τ_{max} (cols. 4 and 7).

$$\text{col. } 2 \times \text{col. } 3 = \text{col. } 4$$

and

$$\text{col. } 5 \times \text{col. } 6 = \text{col. } 7$$

4. Determine the total number of equivalent stress cycles at 0.65 τ_{max} above and below the horizontal axis.

5. $$N = \frac{1}{2}(\text{equivalent no. of cycles above the horizontal} + \text{equivalent no. of cycles below the horizontal})$$

Copyright 2017 Cengage Learning. All Rights Reserved. May not be copied, scanned, or duplicated, in whole or in part. Due to electronic rights, some third party content may be suppressed from the eBook and/or eChapter(s). Editorial review has deemed that any suppressed content does not materially affect the overall learning experience. Cengage Learning reserves the right to remove additional content at any time if subsequent rights restrictions require it.

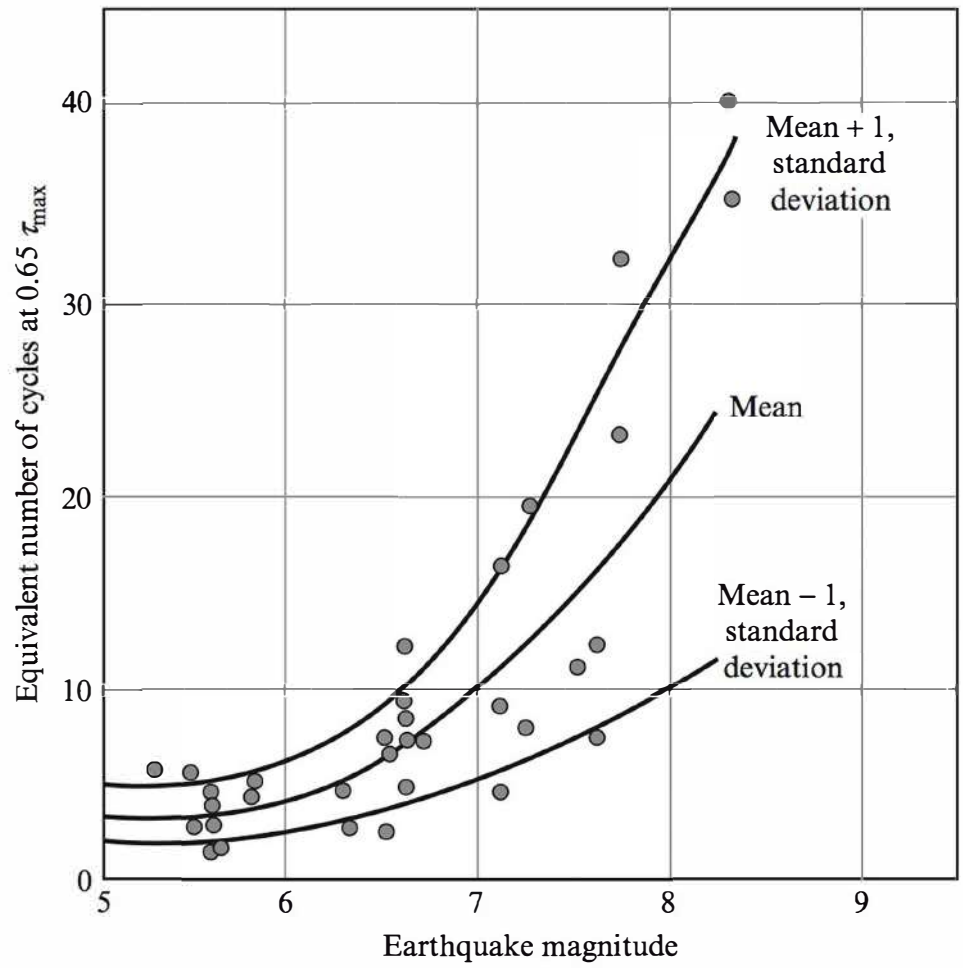

Figure 7.18 Equivalent numbers of uniform stress cycles based on strong component of ground motion (from Seed et al. 1975)

Source: Seed, H.B., Idriss, I.M. Makdidi, F. and Banerjee, N. (1975). "Representation of Irregular Stress-Time Histories by EquivalentUniform Stress Series of Liquefaction Analyses," *Report No. EERC* 75–29. Earthquake Engineering Research Center, University of California, Berkley. Reprinted by permission of the PEER Center, UC Berkeley.

Equivalent numbers of uniform stress cycles (at a maximum level of 0.65 τ_{max}) for several earthquakes with magnitudes of 5.3−7.7 analyzed in the preceding manner are shown in Figure 7.18. These are for the strongest component of the ground motion recorded. The mean and the mean ±1 standard deviation (i.e., 16, 50, and 84 percentile) are also shown. This helps the designer to choose the proper value of the equivalent uniform stress cycles, depending on the degree of conservation required.

Using a similar procedure, Lee and Chan (1972) have given the variation of N with the earthquake magnitude for maximum uniform cyclic stress levels of 0.65 τ_{max}, 0.75 τ_{max}, and 0.85 τ_{max}. A cumulative damage approach has also been described by Valera and Donovan (1977) for determination of N. This approach is based on Miner's law and involves the natural period of the soil deposit and the duration of earthquake shaking.

Copyright 2017 Cengage Learning. All Rights Reserved. May not be copied, scanned, or duplicated, in whole or in part. Due to electronic rights, some third party content may be suppressed from the eBook and/or eChapter(s). Editorial review has deemed that any suppressed content does not materially affect the overall learning experience. Cengage Learning reserves the right to remove additional content at any time if subsequent rights restrictions require it.

References

Arkansas Earthquake Center (1998). "The Moment Magnitude Scale," http://quake.ualr.edu/public/moment.htm.

Banioff, H. (1962). Unpublished report to A. R. Golze, Chief Engineer, Department of Water Resources, Sacramento, California, by Department of Water Resources Consulting Board for Earthquake Analysis.

Båth, M. (1966). "Earthquake Seismology," *Earth Science Reviews*, Vol. 1, p. 69.

Berg, G. V., and Housner, G. W. (1961). "Integrated Velocity and Displacement of Strong Earthquakes Ground Motion," *Bulletin*, Seismological Society of America, Vol. 51, No. 2, pp. 175–189.

Blume, J. A. (1965). "Earthquake Ground Motion and Engineering Procedures for Important Installations Near Active Faults," *Proceedings*, 3rd World Conference on Earthquake Engineering, New Zealand, Vol. 3.

Bonilla, M. G. (1967). "Historic Surface Faulting in Continental United States and Adjacent Parts of Mexico," Interagency Report, US Department of the Interior, Geological Survey.

DeAlba, P., Chan, C., and Seed, H. B. (1975). "Determination of Soil Liquefaction Characteristics by Large-Scale Laboratory Tests," Earthquake Engineering Research Center, *Report EERC* 75-14, University of California, Berkeley.

Dezfulian, H., and Seed, H. B. (1970). "Seismic Response of Soil Deposits Underlain by Sloping Rock Boundaries," *Journal of the Soil Mechanics and Foundations Division*, ASCE, Vol. 96, No. SM6, pp. 1893–1916.

Esteva, L., and Rosenblueth, E. (1963). "Espectros de Temblores a Distancias Moderadas y Grandes," *Proceedings*, Chilean Conference on Seismology and Earthquake Engineering, Vol. 1, University of Chile.

Figueroa, J. J. (1960). "Some Considerations About the Effect of Mexican Earthquakes," *Proceedings*, 2nd World Conference on Earthquake Engineering, Japan, Vol. III.

Gutenberg, B, and Richter, C.F. (1956), "Earthquake Magnitude, Intensity, Energy and Acceleration," *Bulletin*, Sesismological Society of America, Vol. 46, No. 2, pp. 105–146.

Gutenberg, B, (1945). "Amplitude of Surface Waves and Magnitude of Shallow Earthquakes," *Bulletin*, Seismological Society of America, Vol. 35, pp. 57–69.

Gutenberg, G. W. (1965). "Intensity of Earthquakes Ground Shaking Near the Causative Fault," *Proceedings*, 3rd World Conference on Earthquake Engineering, New Zealand, Vol. I.

Hanks, T. C., and Kanamori, H. (1979). "A Moment Magnitude Scale," *Journal of Geophysical Research*, Vol. 85, No. B5, pp. 2348–2358.

Housner, G. W. (1969). "Engineering Estimate of Ground Shaking and Maximum Earthquake Magnitude," *Proceedings*, 4th World Conference on Earthquake Engineering, Santiago, Chile.

Housner, G. W. (1970). "Design Spectrum" in *Earthquake Engineering*, ed., R. W. Wiegel, Prentice-Hall, Englewood Cliffs, New Jersey, pp. 97–106.

Idriss, I. M., Dezfulian, H., and Seed, H. B. (1969). "Computer Programs for Evaluating the Seismic Response of Soil Deposits with Nonlinear Characteristics Using Equivalent Linear Procedures," *Research Repor*t, Earthquake Engineering Research Center, College of Engineering, University of California, Berkeley.

Idriss, I. M., and Seed, H. B. (1967). "Response of Horizontal Soil Layers During Earthquakes," *Research Report*, Soil Mechanics and Bituminous Materials Laboratory, University of California, Berkeley.

Idriss, I. M., and Seed, H. B. (1968). "Seismic Response of Horizontal Soil Layers." *Journal of the Soil Mechanics and Foundations Division*, ASCE, Vol. 94, No. SM4, pp. 1003–1031.

Copyright 2017 Cengage Learning. All Rights Reserved. May not be copied, scanned, or duplicated, in whole or in part. Due to electronic rights, some third party content may be suppressed from the eBook and/or eChapter(s). Editorial review has deemed that any suppressed content does not materially affect the overall learning experience. Cengage Learning reserves the right to remove additional content at any time if subsequent rights restrictions require it.

Kanai, K. (1966). "Improved Empirical Formula for the Characteristics of Strong Earthquakes Motions," *Proceedings*, Japan Earthquake Engineering Symposium, Tokyo, pp. 1–4.

Kanamori, H. (1977). "The Energy Release in Great Earthquakes," *Journal of Geophysical Research*, Vol. 82, pp. 2981–2987.

Kanamori, H. (1983). "Magnitude Scale and Quantification of Earthquakes," *Technophysics*, Elsevier, Amsterdam, Vol. 93, pp 185–199.

Lee, K. L., and Chan, K. (1972). "Number of Equivalent Significant Cycles in Strong Motion Earthquakes," *Proceedings*, International Conference on Microzonation, Seattle, Washington, Vol. 2, pp. 609–627.

Newmark, N. M. (1962). "A Method of Computations for Structural Dynamics," *Transactions*, ASCE, Vol. 127, Part I, pp. 1406–1435.

Parmelee, R., Penzien, J., Scheffey, C. F., Seed, H. B., and Thiers, G. R. (1964). "Seismic Effects on Structures Supported on Piles Extending Through Deep Sensitive Clays," *Report No.* 64–2, Institute of Engineering Research, University of California, Berkeley.

Richter, C. F. (1958). *Elementary Seismology*, W. H. Freeman, San Francisco, California.

Seed, H. B. (1976). "Evaluation of Soil Liquefaction Effects on Level Ground During Earthquakes," *Preprint No.* 2752, ASCE National Convention, Sept. 27-Oct. 1, pp. 1–104.

Seed, H. B. (1979). "Soil Liquefaction and Cyclic Mobility Evaluation for Level Ground During Earthquakes," *Journal of the Geotechnical Engineering Division*, ASCE, Vol. 105, No. GT2, pp. 102–155.

Seed, H. B., Idriss, I, M., and Kiefer, F. W. (1969). "Characteristics of Rock Motion During Earthquakes," *Journal of the Soil Mechanics and Foundations Division*, ASCE, Vol. 95, No. SM5, pp. 1199–1218.

Seed, H. B., Idriss, I. M., Makdisi, F., and Banerjee, N. (1975). "Representation of Irregular Stress – Time Histories by Equivalent Uniform Stress Series in Liquefaction Analysis," *Report No. EERC* 75-29, Earthquake Engineering Research Center, University of California, Berkeley.

Tocher, D. (1958). "Earthquake Energy and Ground Breakage," *Bulletin*, Seismological Society of America, Vol. 48, No.2, pp. 147–153.

Valera, J. E. and Donovan, N. C. (1977). "Soil Liquefaction Procedures – A Review," *Journal of the Geotechnical Engineering Division*, ASCE, Vol. 103, No. GT6, pp. 607–625.

Wiegel, R. W. (ed.)(1970). *Earthquake Engineering*, Prentice-Hall, Englewood Cliffs, New Jersey.

Wilson, E. L., and Clough, R. W. (1962). "Dynamic Response by Step-by-step Matrix Analysis," *Proceedings*, Symposium on the Use of Computers in Civil Engineering, Lisbon, Portugal.

Copyright 2017 Cengage Learning. All Rights Reserved. May not be copied, scanned, or duplicated, in whole or in part. Due to electronic rights, some third party content may be suppressed from the eBook and/or eChapter(s). Editorial review has deemed that any suppressed content does not materially affect the overall learning experience. Cengage Learning reserves the right to remove additional content at any time if subsequent rights restrictions require it.

Lateral Earth Pressure on Retaining Walls

8

8.1 INTRODUCTION

Excessive dynamic lateral earth pressure on retaining structures resulting from earthquakes has caused major damage in the past. The increase of lateral earth pressure during earthquakes induces sliding and/or tilting to the retaining structures. The majority of case histories of failures reported in the literature until now concern waterfront structures such as quay walls and bridge abutments. Some of the examples of failures and lateral movements of quay walls due to earthquakes are given in Table 8.1. Seed and Whitman (1970) have suggested that some of these failures may have been due to several reasons, such as

1. increase of lateral earth pressure behind the wall,
2. reduction of water pressure at the front of the wall, and
3. liquefaction of the backfill material (see Chapter 10)

Nazarian and Hadjan (1979) have given a comprehensive review of the dynamic lateral earth pressure studies advanced so far. Based on this study, the theories can be divided into three broad categories, such as

1. fully plastic (static or pseudostatic) solution,
2. solutions based on elastic wave theory, and
3. solutions based on elastoplastic and nonlinear theory.

Because of the complex soil-structure interaction (mode of wall movement) during earthquakes, the lateral earth pressure theory based on the fully plastic solution (also known as pseudostatic method), which is widely used by most of the design engineers, is detailed in this chapter. In most of the codes of practice, for the soils that do not lose shear strength during shaking, an increase (about 33%) in bearing capacity and passive earth pressure is generally recommended.

8.2 MONONOBE-OKABE ACTIVE EARTH PRESSURE THEORY

In 1776, Coulomb derived an equation for active earth pressure on a retaining wall due to a dry cohesionless backfill (Figure 8.1), which is of the form

Copyright 2017 Cengage Learning. All Rights Reserved. May not be copied, scanned, or duplicated, in whole or in part. Due to electronic rights, some third party content may be suppressed from the eBook and/or eChapter(s).
Editorial review has deemed that any suppressed content does not materially affect the overall learning experience. Cengage Learning reserves the right to remove additional content at any time if subsequent rights restrictions require it.

$$P_A = \frac{1}{2}\gamma H^2 K_A \tag{8.1}$$

Table 8.1 Failures and Movements of Quay Walls[a]

Earthquake	Date	M[e]	Harbor	Distance from Epicenter	Damage	Approximate Movement
Kitaizu	25 November 1930	7.1	Shimizu	48 km	Failure of gravity walls[b]	7.93 m
Shizuoka	11 July 1935		Shimizu		Retaining wall collapse[b]	4.88 m
Tonankai	7 December 1944	8.2	Shimizu	175 km	Sliding of retaining wall[b]	
			Nagoya	128 km	Outward movement of bulkhead with relieving platform[b]	3.05–3.96 m
			Yokkaichi	144 km	Outward movement of pile-supported deck[b]	3.66 m
Nankai	21 December 1946	8.1	Nagoya	200–304 km	Outward movement of bulkhead with relieving platform[b]	3.96 m
			Osaka	200–304 km	Failure of retaining wall above relieving platform[b]	4.27 m
			Yokkaichi	200–304 km	Outward movement of pile-supported deck[b]	3.66 m
			Uno		Outward movement of gravity wall[b]	0.61 m
Tokachioki	4 March 1952	7.8	Kushiro	144 km	Outward movement of gravity wall[b]	5.49 m
Chile	22 May 1960	8.4	Puerto Montt	112 km	Complete over-turning of gravity walls[c]	>4.57 m
					Outward movement of anchored bulkheads[c]	0.60–0.9 m
Niigata	16 June 1964	7.5	Niigata	51.2 km	Tilting of gravity wall[d]	3.05 m
					Outward movement of anchored bulkheads[d]	0.30–2.1 m

[a] After Seed and Whitman (1970)
[b] Reported by Amano, Azuma, and Ishii (1956)
[c] Reported by Duke and Leeds (1963)
[d] Reported by Hayashi, Kubo, and Nakase (1966)
[e] Magnitude

Source: Seed, H.B., and Whitman, R.V. (1970). "Design of Earth Retaining Structures for Dynamic Loads," *Proceedings, Specialty Conference on Lateral Stresses in the Ground and Design of Earth Retaining Structures*, ASCE, pp. 103–147. With permission from ASCE.

Copyright 2017 Cengage Learning. All Rights Reserved. May not be copied, scanned, or duplicated, in whole or in part. Due to electronic rights, some third party content may be suppressed from the eBook and/or eChapter(s). Editorial review has deemed that any suppressed content does not materially affect the overall learning experience. Cengage Learning reserves the right to remove additional content at any time if subsequent rights restrictions require it.

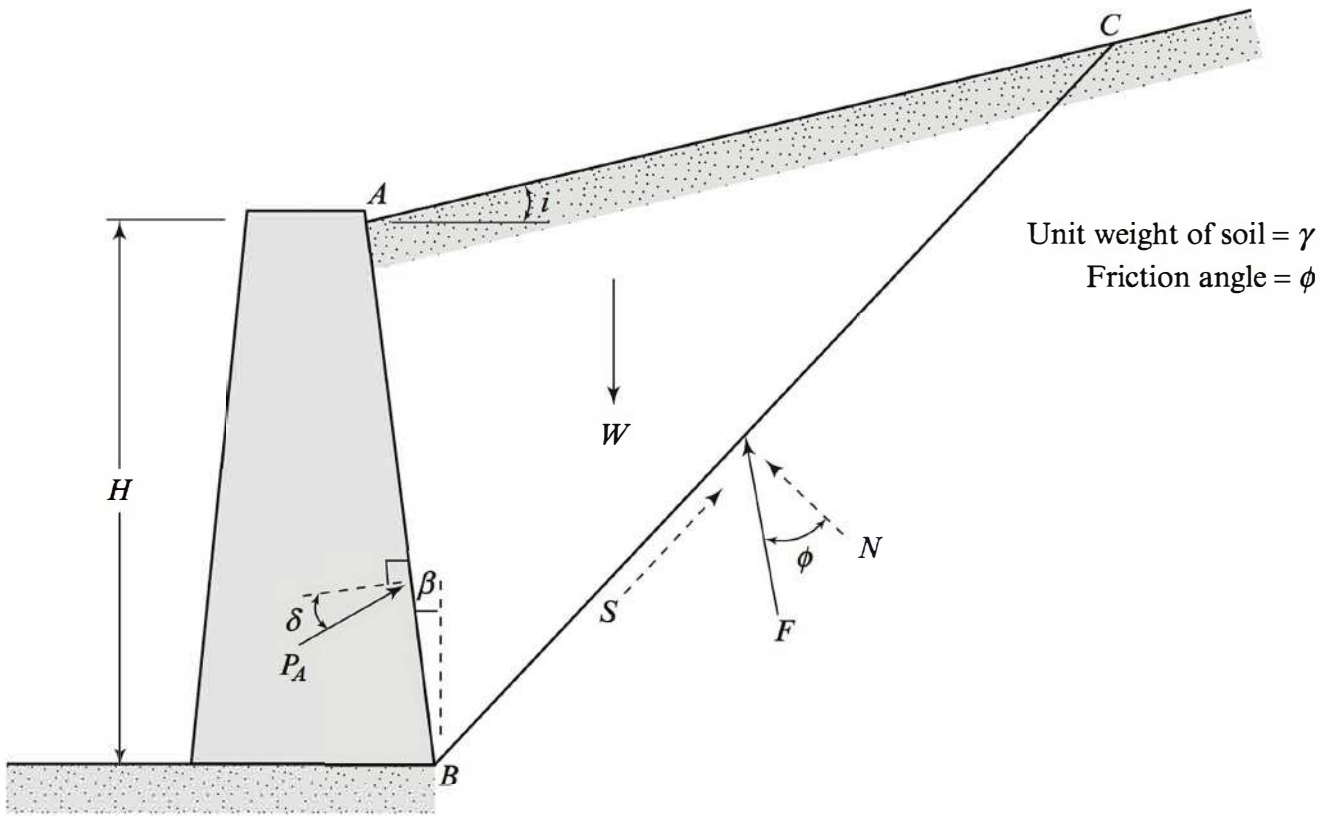

Figure 8.1 Coulomb's active earth pressure (*Note: BC* is the failure plane; W = weight of the wedge ABC; S and N = shear and normal forces on the plane BC; F = resultant of S and N)

where P_A = active force per unit length of the wall

γ = unit weight of soil

H = height of the retaining wall

K_A = active earth pressure coefficient

$$= \frac{\cos^2(\phi - \beta)}{\cos^2\beta\cos(\delta + \beta)\left[1 + \left\{\dfrac{\sin(\delta + \phi)\sin(\phi - i)}{\cos(\delta + \beta)\cos(\beta - i)}\right\}^{1/2}\right]^2} \tag{8.2}$$

where ϕ = soil friction angle

δ = angle of friction between the wall and the soil

β = slope of the back of the wall with respect to the vertical

i = slope of the backfill with respect to the horizontal

The values of K_A for $\beta = 0°, i = 0°$ and various values of ϕ and δ are given in Table 8.2.

In the actual design of retaining walls, the value of the wall friction δ is assumed to be between $\phi/2$ and $\frac{2}{3}\phi$. The active earth pressure coefficients for various values of ϕ, i, and β, with $\delta = \frac{2}{3}\phi$ and $\delta = \dfrac{\phi}{2}$, are given in Tables 8.3 and 8.4, respectively. This is a very useful table for design considerations.

Copyright 2017 Cengage Learning. All Rights Reserved. May not be copied, scanned, or duplicated, in whole or in part. Due to electronic rights, some third party content may be suppressed from the eBook and/or eChapter(s). Editorial review has deemed that any suppressed content does not materially affect the overall learning experience. Cengage Learning reserves the right to remove additional content at any time if subsequent rights restrictions require it.

Table 8.2 Values of K_A [Eq. (8.2)] for $\beta = 0°$ and $i = 0°$

	δ (deg)					
ϕ (deg)	0	5	10	15	20	25
28	0.3610	0.3448	0.3330	0.3251	0.3203	0.3186
30	0.3333	0.3189	0.3085	0.3014	0.2973	0.2956
32	0.3073	0.2945	0.2853	0.2791	0.2755	0.2745
34	0.2827	0.2714	0.2633	0.2579	0.2549	0.2542
36	0.2596	0.2497	0.2426	0.2379	0.2354	0.2350
38	0.2379	0.2292	0.2230	0.2190	0.2169	0.2167
40	0.2174	0.2098	0.2045	0.2011	0.1994	0.1995
42	0.1982	0.1916	0.1870	0.1841	0.1828	0.1831

Coulomb's active earth pressure equation can be modified to take into account the vertical and horizontal coefficients of acceleration induced by an earthquake. This is generally referred to as the *Mononobe-Okabe analysis* (Mononobe, 1929; Okabe, 1926). The Mononobe-Okabe solution is based on the following assumptions:

1. The failure in soil takes place along a plane such as BC shown in Figure 8.2.
2. The movement of the wall is sufficient to produce minimum active pressure.
3. The shear strength of the dry cohesionless soil can be given by the equation

$$s = \sigma' \tan\phi \tag{8.3}$$

   where σ' is the effective stress and s is shear strength.
4. At failure, full shear strength along the failure plane (plane BC, Figure 8.2) is mobilized.
5. The soil behind the retaining wall behaves as a rigid body.

Figure 8.2 shows the forces considered in the Mononobe-Okabe solution. Line AB is the back face of the retaining wall and ABC is the soil wedge which will fail. The forces on the failure wedge per unit length of the wall are

a. weight of wedge W;
b. active force P_{AE};
c. resultant of shear and normal forces along the failure plane F; and
d. k_hW and k_vW, the inertia forces in the horizontal and vertical directions, respectively, where,

$$k_h = \frac{\text{horiz. component of earthquake accel.}}{g}$$

$$k_v = \frac{\text{vert. component of earthquake accel.}}{g}$$

and g is acceleration due to gravity.

Copyright 2017 Cengage Learning. All Rights Reserved. May not be copied, scanned, or duplicated, in whole or in part. Due to electronic rights, some third party content may be suppressed from the eBook and/or eChapter(s). Editorial review has deemed that any suppressed content does not materially affect the overall learning experience. Cengage Learning reserves the right to remove additional content at any time if subsequent rights restrictions require it.

Table 8.3 Values of K_A [Eq. (8.2)] (*Note:* $\delta = \frac{2}{3}\phi$)

		β (deg)					
i (deg)	ϕ (deg)	0	5	10	15	20	25
0	28	0.3213	0.3588	0.4007	0.4481	0.5026	0.5662
	29	0.3091	0.3467	0.3886	0.4362	0.4908	0.5547
	30	0.2973	0.3349	0.3769	0.4245	0.4794	0.5435
	31	0.2860	0.3235	0.3655	0.4133	0.4682	0.5326
	32	0.2750	0.3125	0.3545	0.4023	0.4574	0.5220
	33	0.2645	0.3019	0.3439	0.3917	0.4469	0.5117
	34	0.2543	0.2916	0.3335	0.3813	0.4367	0.5017
	35	0.2444	0.2816	0.3235	0.3713	0.4267	0.4919
	36	0.2349	0.2719	0.3137	0.3615	0.4170	0.4824
	37	0.2257	0.2626	0.3042	0.3520	0.4075	0.4732
	38	0.2168	0.2535	0.2950	0.3427	0.3983	0.4641
	39	0.2082	0.2447	0.2861	0.3337	0.3894	0.4553
	40	0.1998	0.2361	0.2774	0.3249	0.3806	0.4468
	41	0.1918	0.2278	0.2689	0.3164	0.3721	0.4384
	42	0.1840	0.2197	0.2606	0.3080	0.3637	0.4302
5	28	0.3431	0.3845	0.4311	0.4843	0.5461	0.6190
	29	0.3295	0.3709	0.4175	0.4707	0.5325	0.6056
	30	0.3165	0.3578	0.4043	0.4575	0.5194	0.5926
	31	0.3039	0.3451	0.3916	0.4447	0.5067	0.5800
	32	0.2919	0.3329	0.3792	0.4324	0.4943	0.5677
	33	0.2803	0.3211	0.3673	0.4204	0.4823	0.5558
	34	0.2691	0.3097	0.3558	0.4088	0.4707	0.5443
	35	0.2583	0.2987	0.3446	0.3975	0.4594	0.5330
	36	0.2479	0.2881	0.3338	0.3866	0.4484	0.5221
	37	0.2379	0.2778	0.3233	0.3759	0.4377	0.5115
	38	0.2282	0.2679	0.3131	0.3656	0.4273	0.5012
	39	0.2188	0.2582	0.3033	0.3556	0.4172	0.4911
	40	0.2098	0.2489	0.2937	0.3458	0.4074	0.4813
	41	0.2011	0.2398	0.2844	0.3363	0.3978	0.4718
	42	0.1927	0.2311	0.2753	0.3271	0.3884	0.4625
10	28	0.3702	0.4164	0.4686	0.5287	0.5992	0.6834
	29	0.3548	0.4007	0.4528	0.5128	0.5831	0.6672
	30	0.3400	0.3857	0.4376	0.4974	0.5676	0.6516
	31	0.3259	0.3713	0.4230	0.4826	0.5526	0.6365
	32	0.3123	0.3575	0.4089	0.4683	0.5382	0.6219
	33	0.2993	0.3442	0.3953	0.4545	0.5242	0.6078
	34	0.2868	0.3314	0.3822	0.4412	0.5107	0.5942

(*Continued*)

Copyright 2017 Cengage Learning. All Rights Reserved. May not be copied, scanned, or duplicated, in whole or in part. Due to electronic rights, some third party content may be suppressed from the eBook and/or eChapter(s). Editorial review has deemed that any suppressed content does not materially affect the overall learning experience. Cengage Learning reserves the right to remove additional content at any time if subsequent rights restrictions require it.

Table 8.3 (*Continued*)

		β (deg)					
i (deg)	ϕ (deg)	0	5	10	15	20	25
	35	0.2748	0.3190	0.3696	0.4283	0.4976	0.5810
	36	0.2633	0.3072	0.3574	0.4158	0.4849	0.5682
	37	0.2522	0.2957	0.3456	0.4037	0.4726	0.5558
	38	0.2415	0.2846	0.3342	0.3920	0.4607	0.5437
	39	0.2313	0.2740	0.3231	0.3807	0.4491	0.5321
	40	0.2214	0.2636	0.3125	0.3697	0.4379	0.5207
	41	0.2119	0.2537	0.3021	0.3590	0.4270	0.5097
	42	0.2027	0.2441	0.2921	0.3487	0.4164	0.4990
15	28	0.4065	0.4585	0.5179	0.5868	0.6685	0.7670
	29	0.3881	0.4397	0.4987	0.5672	0.6483	0.7463
	30	0.3707	0.4219	0.4804	0.5484	0.6291	0.7265
	31	0.3541	0.4049	0.4629	0.5305	0.6106	0.7076
	32	0.3384	0.3887	0.4462	0.5133	0.5930	0.6895
	33	0.3234	0.3732	0.4303	0.4969	0.5761	0.6721
	34	0.3091	0.3583	0.4150	0.4811	0.5598	0.6554
	35	0.2954	0.3442	0.4003	0.4659	0.5442	0.6393
	36	0.2823	0.3306	0.3862	0.4513	0.5291	0.6238
	37	0.2698	0.3175	0.3726	0.4373	0.5146	0.6089
	38	0.2578	0.3050	0.3595	0.4237	0.5006	0.5945
	39	0.2463	0.2929	0.3470	0.4106	0.4871	0.5805
	40	0.2353	0.2813	0.3348	0.3980	0.4740	0.5671
	41	0.2247	0.2702	0.3231	0.3858	0.4613	0.5541
	42	0.2146	0.2594	0.3118	0.3740	0.4491	0.5415
20	28	0.4602	0.5205	0.5900	0.6714	0.7689	0.8880
	29	0.4364	0.4958	0.5642	0.6445	0.7406	0.8581
	30	0.4142	0.4728	0.5403	0.6195	0.7144	0.8303
	31	0.3935	0.4513	0.5179	0.5961	0.6898	0.8043
	32	0.3742	0.4311	0.4968	0.5741	0.6666	0.7799
	33	0.3559	0.4121	0.4769	0.5532	0.6448	0.7569
	34	0.3388	0.3941	0.4581	0.5335	0.6241	0.7351
	35	0.3225	0.3771	0.4402	0.5148	0.6044	0.7144
	36	0.3071	0.3609	0.4233	0.4969	0.5856	0.6947
	37	0.2925	0.3455	0.4071	0.4799	0.5677	0.6759
	38	0.2787	0.3308	0.3916	0.4636	0.5506	0.6579
	39	0.2654	0.3168	0.3768	0.4480	0.5342	0.6407
	40	0.2529	0.3034	0.3626	0.4331	0.5185	0.6242
	41	0.2408	0.2906	0.3490	0.4187	0.5033	0.6083
	42	0.2294	0.2784	0.3360	0.4049	0.4888	0.5930

Copyright 2017 Cengage Learning. All Rights Reserved. May not be copied, scanned, or duplicated, in whole or in part. Due to electronic rights, some third party content may be suppressed from the eBook and/or eChapter(s). Editorial review has deemed that any suppressed content does not materially affect the overall learning experience. Cengage Learning reserves the right to remove additional content at any time if subsequent rights restrictions require it.

Table 8.4 Values of K_A [Eq. (8.2)] (*Note:* $\delta = \phi/2$)

		β (deg)					
i (deg)	ϕ (deg)	0	5	10	15	20	25
0	28	0.3264	0.3629	0.4034	0.4490	0.5011	0.5616
	29	0.3137	0.3502	0.3907	0.4363	0.4886	0.5492
	30	0.3014	0.3379	0.3784	0.4241	0.4764	0.5371
	31	0.2896	0.3260	0.3665	0.4121	0.4645	0.5253
	32	0.2782	0.3145	0.3549	0.4005	0.4529	0.5137
	33	0.2671	0.3033	0.3436	0.3892	0.4415	0.5025
	34	0.2564	0.2925	0.3327	0.3782	0.4305	0.4915
	35	0.2461	0.2820	0.3221	0.3675	0.4197	0.4807
	36	0.2362	0.2718	0.3118	0.3571	0.4092	0.4702
	37	0.2265	0.2620	0.3017	0.3469	0.3990	0.4599
	38	0.2172	0.2524	0.2920	0.3370	0.3890	0.4498
	39	0.2081	0.2431	0.2825	0.3273	0.3792	0.4400
	40	0.1994	0.2341	0.2732	0.3179	0.3696	0.4304
	41	0.1909	0.2253	0.2642	0.3087	0.3602	0.4209
	42	0.1828	0.2168	0.2554	0.2997	0.3511	0.4117
5	28	0.3477	0.3879	0.4327	0.4837	0.5425	0.6115
	29	0.3337	0.3737	0.4185	0.4694	0.5282	0.5972
	30	0.3202	0.3601	0.4048	0.4556	0.5144	0.5833
	31	0.3072	0.3470	0.3915	0.4422	0.5009	0.5698
	32	0.2946	0.3342	0.3787	0.4292	0.4878	0.5566
	33	0.2825	0.3219	0.3662	0.4166	0.4750	0.5437
	34	0.2709	0.3101	0.3541	0.4043	0.4626	0.5312
	35	0.2596	0.2986	0.3424	0.3924	0.4505	0.5190
	36	0.2488	0.2874	0.3310	0.3808	0.4387	0.5070
	37	0.2383	0.2767	0.3199	0.3695	0.4272	0.4954
	38	0.2282	0.2662	0.3092	0.3585	0.4160	0.4840
	39	0.2185	0.2561	0.2988	0.3478	0.4050	0.4729
	40	0.2090	0.2463	0.2887	0.3374	0.3944	0.4620
	41	0.1999	0.2368	0.2788	0.3273	0.3840	0.4514
	42	0.1911	0.2276	0.2693	0.3174	0.3738	0.4410
10	28	0.3743	0.4187	0.4688	0.5261	0.5928	0.6719
	29	0.3584	0.4026	0.4525	0.5096	0.5761	0.6549
	30	0.3432	0.3872	0.4368	0.4936	0.5599	0.6385
	31	0.3286	0.3723	0.4217	0.4782	0.5442	0.6225
	32	0.3145	0.3580	0.4071	0.4633	0.5290	0.6071
	33	0.3011	0.3442	0.3930	0.4489	0.5143	0.5920
	34	0.2881	0.3309	0.3793	0.4350	0.5000	0.5775

(*Continued*)

Copyright 2017 Cengage Learning. All Rights Reserved. May not be copied, scanned, or duplicated, in whole or in part. Due to electronic rights, some third party content may be suppressed from the eBook and/or eChapter(s). Editorial review has deemed that any suppressed content does not materially affect the overall learning experience. Cengage Learning reserves the right to remove additional content at any time if subsequent rights restrictions require it.

Table 8.4 (*Continued*)

		β (deg)					
i (deg)	ϕ (deg)	0	5	10	15	20	25
	35	0.2757	0.3181	0.3662	0.4215	0.4862	0.5633
	36	0.2637	0.3058	0.3534	0.4084	0.4727	0.5495
	37	0.2522	0.2938	0.3411	0.3957	0.4597	0.5361
	38	0.2412	0.2823	0.3292	0.3833	0.4470	0.5230
	39	0.2305	0.2712	0.3176	0.3714	0.4346	0.5103
	40	0.2202	0.2604	0.3064	0.3597	0.4226	0.4979
	41	0.2103	0.2500	0.2956	0.3484	0.4109	0.4858
	42	0.2007	0.2400	0.2850	0.3375	0.3995	0.4740
15	28	0.4095	0.4594	0.5159	0.5812	0.6579	0.7498
	29	0.3908	0.4402	0.4964	0.5611	0.6373	0.7284
	30	0.3730	0.4220	0.4777	0.5419	0.6175	0.7080
	31	0.3560	0.4046	0.4598	0.5235	0.5985	0.6884
	32	0.3398	0.3880	0.4427	0.5059	0.5803	0.6695
	33	0.3244	0.3721	0.4262	0.4889	0.5627	0.6513
	34	0.3097	0.3568	0.4105	0.4726	0.5458	0.6338
	35	0.2956	0.3422	0.3953	0.4569	0.5295	0.6168
	36	0.2821	0.3282	0.3807	0.4417	0.5138	0.6004
	37	0.2692	0.3147	0.3667	0.4271	0.4985	0.5846
	38	0.2569	0.3017	0.3531	0.4130	0.4838	0.5692
	39	0.2450	0.2893	0.3401	0.3993	0.4695	0.5543
	40	0.2336	0.2773	0.3275	0.3861	0.4557	0.5399
	41	0.2227	0.2657	0.3153	0.3733	0.4423	0.5258
	42	0.2122	0.2546	0.3035	0.3609	0.4293	0.5122
20	28	0.4614	0.5188	0.5844	0.6608	0.7514	0.8613
	29	0.4374	0.4940	0.5586	0.6339	0.7232	0.8313
	30	0.4150	0.4708	0.5345	0.6087	0.6968	0.8034
	31	0.3941	0.4491	0.5119	0.5851	0.6720	0.7772
	32	0.3744	0.4286	0.4906	0.5628	0.6486	0.7524
	33	0.3559	0.4093	0.4704	0.5417	0.6264	0.7289
	34	0.3384	0.3910	0.4513	0.5216	0.6052	0.7066
	35	0.3218	0.3736	0.4331	0.5025	0.5851	0.6853
	36	0.3061	0.3571	0.4157	0.4842	0.5658	0.6649
	37	0.2911	0.3413	0.3991	0.4668	0.5474	0.6453
	38	0.2769	0.3263	0.3833	0.4500	0.5297	0.6266
	39	0.2633	0.3120	0.3681	0.4340	0.5127	0.6085
	40	0.2504	0.2982	0.3535	0.4185	0.4963	0.5912
	41	0.2381	0.2851	0.3395	0.4037	0.4805	0.5744
	42	0.2263	0.2725	0.3261	0.3894	0.4653	0.5582

Copyright 2017 Cengage Learning. All Rights Reserved. May not be copied, scanned, or duplicated, in whole or in part. Due to electronic rights, some third party content may be suppressed from the eBook and/or eChapter(s). Editorial review has deemed that any suppressed content does not materially affect the overall learning experience. Cengage Learning reserves the right to remove additional content at any time if subsequent rights restrictions require it.

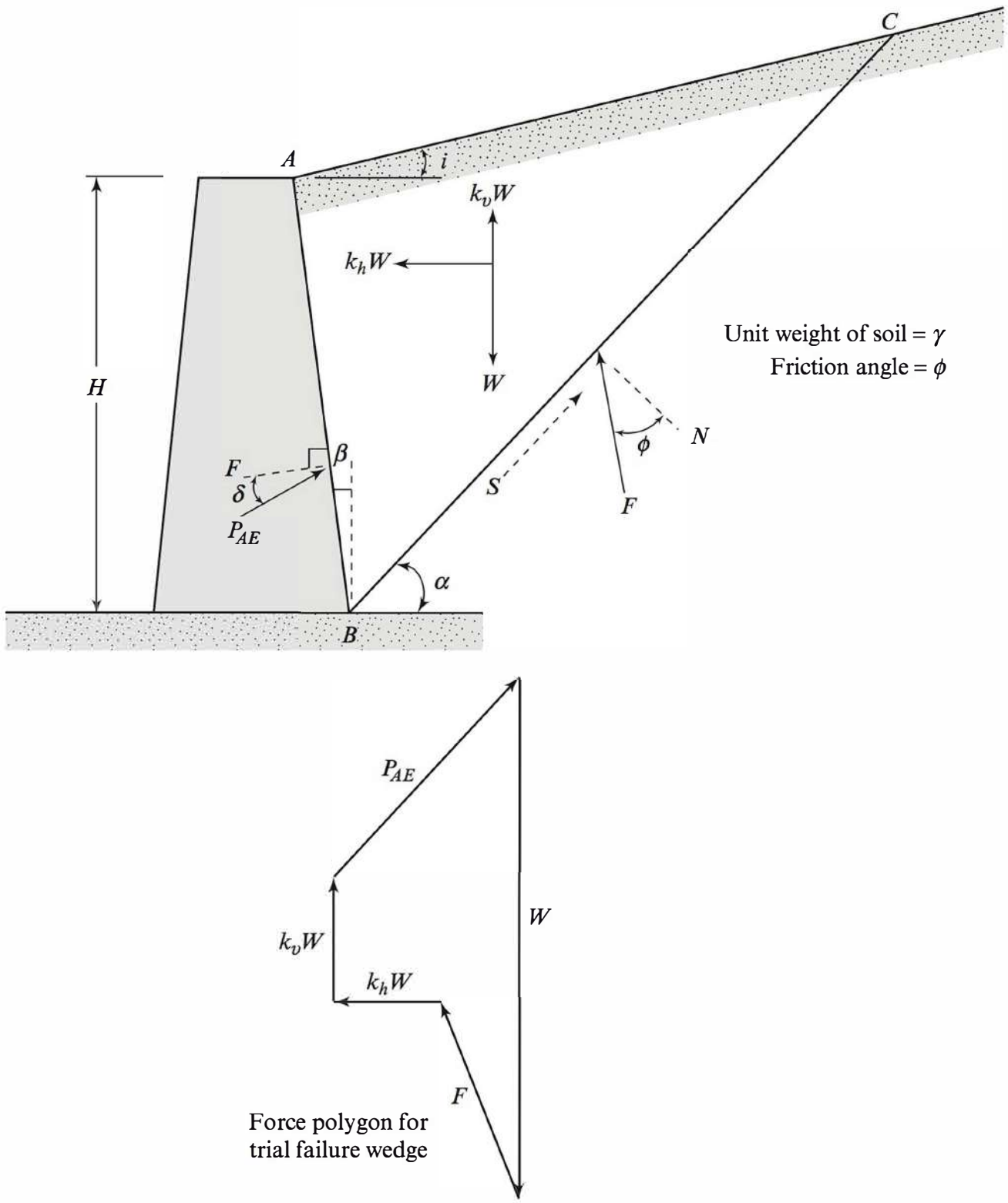

Figure 8.2 Derivation of Mononobe–Okabe equation

The active force determined by the wedge analysis described here may be expressed as

$$P_{AE} = \frac{1}{2}\gamma H^2(1-k_v)K_{AE} \tag{8.4}$$

where K_{AE} is the active earth pressure coefficient with earthquake effect:

$$K_{AE} = \frac{\cos^2(\phi-\theta-\beta)}{\cos\theta\cos^2\beta\cos(\delta+\beta+\theta)\left[1+\sqrt{\dfrac{\sin(\phi+\delta)\sin(\phi-\theta-i)}{\cos(\delta+\beta+\theta)\cos(i-\beta)}}\right]^2} \tag{8.5}$$

Copyright 2017 Cengage Learning. All Rights Reserved. May not be copied, scanned, or duplicated, in whole or in part. Due to electronic rights, some third party content may be suppressed from the eBook and/or eChapter(s). Editorial review has deemed that any suppressed content does not materially affect the overall learning experience. Cengage Learning reserves the right to remove additional content at any time if subsequent rights restrictions require it.

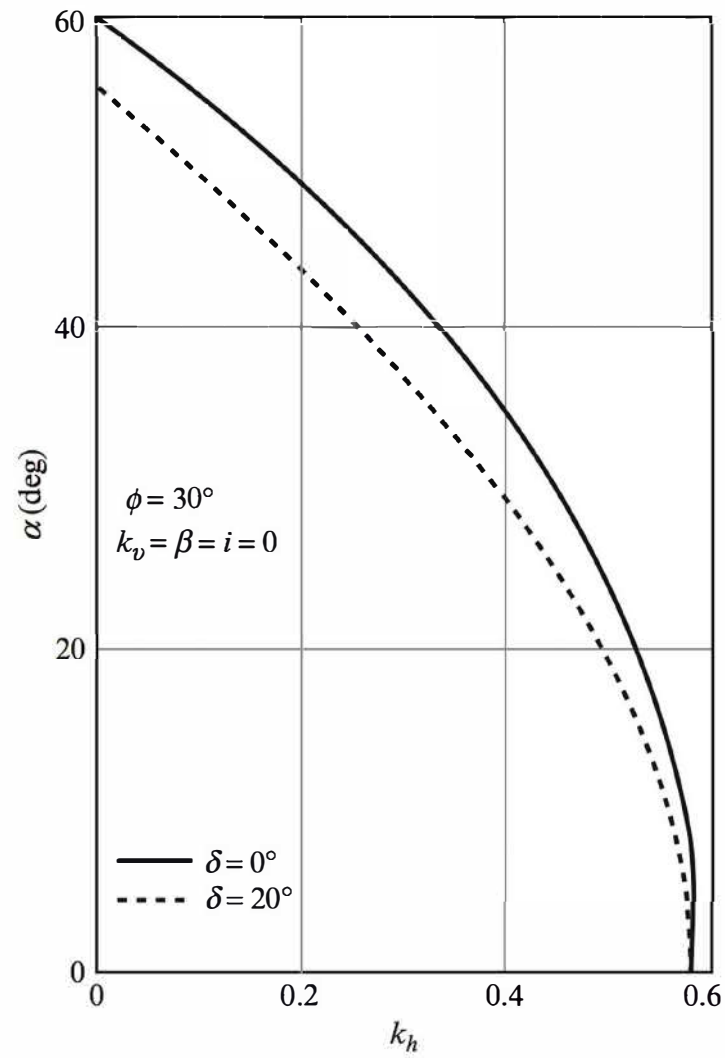

Figure 8.3 Inclination of the failure plane with the horizontal (from Davies, Richards, and Chen, 1986)

Source: Davies, T.G., Richards, R., and Chen, K.H. (1986). "Passive Pressure during Seismic Loading," *Journal of Geotechnical Engineering*, ASCE, Vol. 112, No. GT4, pp. 479–484. With permission from ASCE.

$$\theta = \tan^{-1}\left(\frac{k_h}{1-k_v}\right) \tag{8.6}$$

Equation (8.4) is generally referred to as the *Mononobe-Okabe active earth pressure equation.* For the active force condition (P_{AE}), the angle α that the soil wedge ABC located behind the retaining wall (Figure 8.2) makes with the horizontal (for $k_v = 0°, \beta = 0°, i = 0°, \phi = 30°$, and $\delta = 0°$ and 20°) is shown in Figure 8.3.

Tables 8.5 through 8.8 give the values of K_{AE} [Eq. (8.5)] for various values of ϕ, δ, i, and k_h with $k_v = 0$ and $\beta = 0°, 5°, 10°$, and 15°.

Table 8.5 Values of K_{AE} [Eq. (8.5)] with $k_v = 0$ and $\beta = 0°$

			ϕ (deg)				
k_h	δ (deg)	i (deg)	28	30	35	40	45
0.1	0	0	0.427	0.397	0.328	0.268	0.217
0.2			0.508	0.473	0.396	0.382	0.270

Copyright 2017 Cengage Learning. All Rights Reserved. May not be copied, scanned, or duplicated, in whole or in part. Due to electronic rights, some third party content may be suppressed from the eBook and/or eChapter(s). Editorial review has deemed that any suppressed content does not materially affect the overall learning experience. Cengage Learning reserves the right to remove additional content at any time if subsequent rights restrictions require it.

Table 8.5 (*Continued*)

			ϕ (deg)				
k_h	δ (deg)	i (deg)	28	30	35	40	45
0.3			0.611	0.569	0.478	0.400	0.334
0.4			0.753	0.697	0.581	0.488	0.409
0.5			1.005	0.890	0.716	0.596	0.500
0.1	0	5	0.457	0.423	0.347	0.282	0.227
0.2			0.554	0.514	0.424	0.349	0.285
0.3			0.554	0.514	0.424	0.349	0.285
0.4			0.942	0.825	0.653	0.535	0.442
0.5			-	-	0.855	0.673	0.551
0.1	0	10	0.497	0.457	0.371	0.299	0.238
0.2			0.623	0.570	0.461	0.375	0.303
0.3			0.856	0.748	0.585	0.472	0.383
0.4			-	-	0.780	0.604	0.486
0.5			-	-	-	0.809	0.624
0.1	$\phi/2$	0	0.396	0.368	0.306	0.253	0.207
0.2			0.485	0.452	0.380	0.319	0.267
0.3			0.604	0.563	0.474	0.402	0.340
0.4			0.778	0.718	0.599	0.508	0.433
0.5			1.115	0.972	0.774	0.648	0.552
0.1	$\phi/2$	5	0.428	0.396	0.326	0.268	0.218
0.2			0.537	0.497	0.412	0.342	0.283
0.3			0.699	0.640	0.526	0.438	0.367
0.4			1.025	0.881	0.690	0.568	0.475
0.5			-	-	0.962	0.752	0.620
0.1	$\phi/2$	10	0.472	0.433	0.352	0.285	0.230
0.2			0.616	0.562	0.454	0.371	0.303
0.3			0.908	0.780	0.602	0.487	0.400
0.4			-	-	0.857	0.656	0.531
0.5			-	-	-	0.944	0.722
0.1	$(2/3)\,\phi$	0	0.393	0.366	0.306	0.256	0.212
0.2			0.486	0.454	0.384	0.326	0.276
0.3			0.612	0.572	0.486	0.416	0.357
0.4			0.801	0.740	0.622	0.533	0.462
0.5			1.177	1.023	0.819	0.693	0.600
0.1	$(2/3)\,\phi$	5	0.427	0.395	0.327	0.271	0.224
0.2			0.541	0.501	0.418	0.350	0.294

(*Continued*)

Copyright 2017 Cengage Learning. All Rights Reserved. May not be copied, scanned, or duplicated, in whole or in part. Due to electronic rights, some third party content may be suppressed from the eBook and/or eChapter(s). Editorial review has deemed that any suppressed content does not materially affect the overall learning experience. Cengage Learning reserves the right to remove additional content at any time if subsequent rights restrictions require it.

Table 8.5 (*Continued*)

			ϕ (deg)				
k_h	δ (deg)	i (deg)	28	30	35	40	45
0.3			0.714	0.655	0.541	0.455	0.386
0.4			1.073	0.921	0.722	0.600	0.509
0.5			-	-	1.034	0.812	0.679
0.1	$(2/3)\phi$	10	0.472	0.434	0.354	0.290	0.237
0.2			0.625	0.570	0.463	0.381	0.317
0.3			0.942	0.807	0.624	0.509	0.423
0.4			-	-	0.909	0.699	0.573
0.5			-	-	-	1.037	0.800

Table 8.6 Values of K_{AE} [Eq. (8.5)] with $k_v = 0$ and $\beta = 5°$

			ϕ (deg)				
k_h	δ (deg)	i (deg)	28	30	35	40	45
0.1	0	0	0.462	0.432	0.363	0.303	0.250
0.2			0.543	0.509	0.432	0.365	0.306
0.3			0.647	0.606	0.516	0.439	0.372
0.4			0.792	0.736	0.622	0.530	0.451
0.5			1.054	0.936	0.762	0.642	0.546
0.1	0	5	0.496	0.462	0.386	0.320	0.263
0.2			0.594	0.554	0.465	0.389	0.324
0.3			0.733	0.678	0.566	0.475	0.398
0.4			0.996	0.875	0.702	0.583	0.489
0.5			—	—	0.914	0.728	0.604
0.1	0	10	0.540	0.500	0.413	0.339	0.277
0.2			0.669	0.616	0.507	0.419	0.345
0.3			0.912	0.801	0.635	0.521	0.430
0.4			—	—	0.842	0.660	0.540
0.5			—	—	—	0.879	0.687
0.1	$\phi/2$	0	0.434	0.407	0.344	0.291	0.245
0.2			0.526	0.494	0.423	0.362	0.329
0.3			0.651	0.610	0.523	0.451	0.389
0.4			0.836	0.775	0.657	0.566	0.541
0.5			1.202	1.050	0.847	0.719	0.623
0.1	$\phi/2$	5	0.472	0.440	0.369	0.309	0.258
0.2			0.585	0.546	0.460	0.389	0.330

Copyright 2017 Cengage Learning. All Rights Reserved. May not be copied, scanned, or duplicated, in whole or in part. Due to electronic rights, some third party content may be suppressed from the eBook and/or eChapter(s). Editorial review has deemed that any suppressed content does not materially affect the overall learning experience. Cengage Learning reserves the right to remove additional content at any time if subsequent rights restrictions require it.

Table 8.6 (*Continued*)

			ϕ (deg)				
k_h	δ (deg)	i (deg)	28	30	35	40	45
0.3			0.756	0.698	0.583	0.494	0.421
0.4			1.111	0.959	0.761	0.636	0.542
0.5			—	—	1.063	0.841	0.705
0.1	$\phi/2$	10	0.521	0.482	0.399	0.331	0.274
0.2			0.674	0.619	0.509	0.424	0.355
0.3			0.990	0.855	0.670	0.551	0.462
0.4			—	—	0.952	0.739	0.609
0.5			—	—	—	1.067	0.827
0.1	$(\frac{2}{3})\phi$	0	0.433	0.407	0.347	0.296	0.253
0.2			0.530	0.499	0.431	0.373	0.323
0.3			0.664	0.624	0.540	0.471	0.413
0.4			0.868	0.806	0.689	0.601	0.531
0.5			1.284	1.119	0.907	0.781	0.689
0.1	$(\frac{2}{3})\phi$	5	0.472	0.441	0.373	0.316	0.267
0.2			0.593	0.554	0.471	0.403	0.346
0.3			0.779	0.719	0.605	0.519	0.449
0.4			1.175	1.012	0.805	0.681	0.589
0.5			—	—	1.159	0.923	0.787
0.1	$(\frac{2}{3})\phi$	10	0.524	0.486	0.405	0.339	0.284
0.2			0.688	0.632	0.523	0.440	0.373
0.3			1.036	0.892	0.701	0.583	0.495
0.4			—	—	1.024	0.800	0.668
0.5			—	—	—	1.195	0.936

Table 8.7 Values of K_{AE} [Eq. (8.5)] with $k_v = 0$ and $\beta = 10°$

			ϕ (deg)				
k_h	δ (deg)	i (deg)	28	30	35	40	45
0.1	0	0	0.500	0.470	0.402	0.342	0.288
0.2			0.582	0.549	0.473	0.406	0.346
0.3			0.688	0.648	0.559	0.483	0.415
0.4			0.838	0.782	0.669	0.577	0.498
0.5			1.115	0.993	0.816	0.695	0.599
0.1	0	5	0.539	0.505	0.428	0.362	0.303
0.2			0.639	0.599	0.510	0.434	0.368

(*Continued*)

Copyright 2017 Cengage Learning. All Rights Reserved. May not be copied, scanned, or duplicated, in whole or in part. Due to electronic rights, some third party content may be suppressed from the eBook and/or eChapter(s). Editorial review has deemed that any suppressed content does not materially affect the overall learning experience. Cengage Learning reserves the right to remove additional content at any time if subsequent rights restrictions require it.

Table 8.7 (*Continued*)

			ϕ (deg)				
k_h	δ (deg)	i (deg)	28	30	35	40	45
0.3			0.782	0.728	0.615	0.524	0.446
0.4			1.060	0.935	0.758	0.638	0.543
0.5			—	—	0.984	0.793	0.665
0.1	0	10	0.588	0.548	0.460	0.385	0.320
0.2			0.721	0.668	0.558	0.469	0.393
0.3			0.979	0.863	0.693	0.577	0.484
0.4			—	—	0.914	0.725	0.601
0.5			—	—	—	0.962	0.760
0.1	$\phi/2$	0	0.477	0.450	0.388	0.334	0.287
0.2			0.573	0.542	0.471	0.410	0.412
0.3			0.705	0.665	0.579	0.507	0.446
0.4			0.904	0.843	0.724	0.634	0.700
0.5			1.311	1.147	0.935	0.805	0.709
0.1	$\phi/2$	5	0.520	0.488	0.417	0.357	0.304
0.2			0.641	0.601	0.515	0.444	0.383
0.3			0.825	0.765	0.649	0.559	0.485
0.4			1.216	1.053	0.845	0.717	0.621
0.5			—	—	1.188	0.950	0.808
0.1	$\phi/2$	10	0.577	0.538	0.454	0.384	0.324
0.2			0.742	0.685	0.573	0.486	0.414
0.3			1.089	0.944	0.750	0.628	0.535
0.4			—	—	1.068	0.840	0.704
0.5			—	—	—	1.221	0.958
0.1	$\left(\frac{2}{3}\right)\phi$	0	0.479	0.452	0.394	0.343	0.299
0.2			0.581	0.551	0.484	0.427	0.378
0.3			0.724	0.685	0.603	0.536	0.479
0.4			0.948	0.885	0.768	0.682	0.614
0.5			1.419	1.239	1.017	0.889	0.800
0.1	$\left(\frac{2}{3}\right)\phi$	5	0.524	0.493	0.425	0.367	0.318
0.2			0.653	0.614	0.531	0.464	0.406
0.3			0.856	0.796	0.680	0.594	0.524
0.4			1.302	1.124	0.906	0.779	0.687
0.5			—	—	1.319	1.064	0.923
0.1	$\left(\frac{2}{3}\right)\phi$	10	0.584	0.545	0.463	0.396	0.340
0.2			0.762	0.705	0.594	0.510	0.441
0.3			1.151	0.995	0.794	0.672	0.582
0.4			—	—	1.167	0.924	0.786
0.5			—	—	—	1.400	1.112

Copyright 2017 Cengage Learning. All Rights Reserved. May not be copied, scanned, or duplicated, in whole or in part. Due to electronic rights, some third party content may be suppressed from the eBook and/or eChapter(s). Editorial review has deemed that any suppressed content does not materially affect the overall learning experience. Cengage Learning reserves the right to remove additional content at any time if subsequent rights restrictions require it.

Table 8.8 Values of K_{AE} [Eq. (8.5)] with $k_v = 0$ and $\beta = 15°$

			ϕ (deg)				
k_h	δ (deg)	i (deg)	28	30	35	40	45
0.1	0	0	0.543	0.514	0.446	0.385	0.329
0.2			0.626	0.594	0.519	0.451	0.391
0.3			0.735	0.696	0.608	0.532	0.464
0.4			0.892	0.836	0.723	0.631	0.552
0.5			1.190	1.061	0.879	0.756	0.659
0.1	0	5	0.587	0.554	0.477	0.409	0.348
0.2			0.691	0.651	0.562	0.485	0.417
0.3			0.841	0.785	0.672	0.579	0.500
0.4			1.139	1.007	0.824	0.701	0.604
0.5			—	—	1.069	0.868	0.736
0.1	0	10	0.643	0.603	0.514	0.437	0.369
0.2			0.783	0.729	0.617	0.525	0.447
0.3			1.059	0.937	0.761	0.641	0.545
0.4			—	—	1.000	0.802	0.672
0.5				—	—	1.062	0.846
0.1	$\phi/2$	0	0.526	0.499	0.438	0.384	0.336
0.2			0.627	0.596	0.527	0.467	0.526
0.3			0.769	0.729	0.644	0.573	0.512
0.4			0.987	0.925	0.805	0.714	0.963
0.5			1.450	1.270	1.044	0.911	0.814
0.1	$\phi/2$	5	0.576	0.544	0.473	0.412	0.358
0.2			0.705	0.665	0.580	0.508	0.446
0.3			0.906	0.845	0.727	0.636	0.561
0.4			1.349	1.169	0.948	0.815	0.717
0.5			—	—	1.348	1.088	0.938
0.1	$\phi/2$	10	0.642	0.602	0.517	0.445	0.384
0.2			0.822	0.763	0.648	0.559	0.485
0.3			1.211	1.053	0.847	0.719	0.623
0.4			—	—	1.214	0.965	0.820
0.5			—	—	—	1.420	1.125
0.1	$\left(\frac{2}{3}\right)\phi$	0	0.530	0.505	0.447	0.397	0.353
0.2			0.640	0.611	0.545	0.490	0.442
0.3			0.796	0.758	0.677	0.613	0.559
0.4			1.046	0.983	0.866	0.782	0.718

(Continued)

Copyright 2017 Cengage Learning. All Rights Reserved. May not be copied, scanned, or duplicated, in whole or in part. Due to electronic rights, some third party content may be suppressed from the eBook and/or eChapter(s). Editorial review has deemed that any suppressed content does not materially affect the overall learning experience. Cengage Learning reserves the right to remove additional content at any time if subsequent rights restrictions require it.

Table 8.8 (*Continued*)

k_h	δ (deg)	i (deg)	ϕ (deg) 28	30	35	40	45
0.5			1.597	1.395	1.157	1.029	0.944
0.1	$(\frac{2}{3})\phi$	5	0.583	0.553	0.485	0.427	0.378
0.2			0.724	0.685	0.603	0.536	0.479
0.3			0.949	0.887	0.771	0.684	0.616
0.4			1.465	1.266	1.033	0.902	0.811
0.5			—	—	1.531	1.250	1.105
0.1	$(\frac{2}{3})\phi$	10	0.654	0.615	0.532	0.464	0.406
0.2			0.851	0.792	0.679	0.593	0.523
0.3			1.296	1.123	0.908	0.781	0.689
0.4			—	—	1.351	1.083	0.938
0.5			—	—	—	1.681	1.353

8.3 SOME COMMENTS ON THE ACTIVE FORCE EQUATION

Considering the active force relation given by Eqs. (8.4)–(8.6), the term $\sin(\phi - \theta - i)$ in Eq. (8.5) has some important implications.

First, if $\phi - \theta - i < 0$ (i.e., negative), no real solution of K_{AE} is possible. Physically it implies that an *equilibrium condition will not exist*. Hence, for stability, the limiting slope of the backfill may be given by

$$i \leq \phi - \theta \tag{8.7}$$

For no earthquake condition, $\theta = 0$; for stability, Eq. (8.7) gives the familiar relation

$$i \leq \phi \tag{8.8}$$

Secondly, for horizontal backfill, $i = 0$; for stability,

$$\theta \leq \phi \tag{8.9}$$

Since $\theta = \tan^{-1}[k_h/(1 - k_v)]$, for stability, combining Eqs. (8.6) and (8.9) results in

$$k_h \leq (1 - k_v)\tan\phi \tag{8.10}$$

Hence, the critical value of the horizontal acceleration can be defined as

$$k_{h(\mathrm{cr})} = (1 - k_v)\tan\phi \tag{8.11}$$

where $k_{h(\mathrm{cr})}$ = critical value of horizontal acceleration (Figure 8.4).

Copyright 2017 Cengage Learning. All Rights Reserved. May not be copied, scanned, or duplicated, in whole or in part. Due to electronic rights, some third party content may be suppressed from the eBook and/or eChapter(s). Editorial review has deemed that any suppressed content does not materially affect the overall learning experience. Cengage Learning reserves the right to remove additional content at any time if subsequent rights restrictions require it.

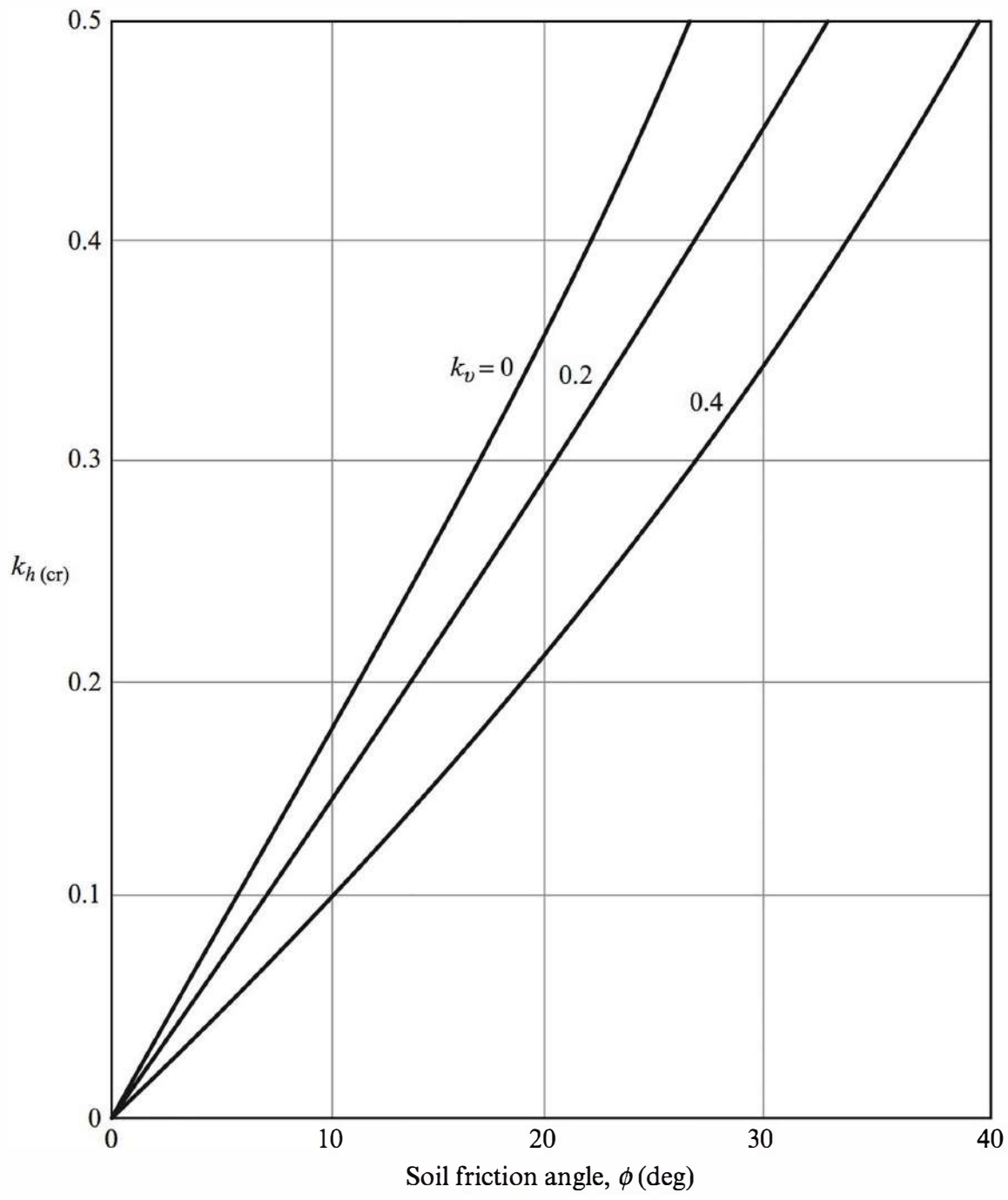

Figure 8.4 Critical values of horizontal acceleration (Eq. 8.11)

8.4 PROCEDURE FOR OBTAINING P_{AE} USING STANDARD CHARTS OF K_A

Since the values of K_A are available in most standard handbooks and textbooks, Arango (1969) developed a simple procedure for obtaining the values of K_{AE} from the standard charts of K_A. This procedure has been described by Seed and Whitman (1970). Referring to Eqs. (8.1) and (8.2),

$$P_A = \frac{1}{2}\gamma H^2 K_A = \frac{1}{2}\gamma H^2 A_c (\cos^2 \beta)^{-1} \tag{8.12}$$

Copyright 2017 Cengage Learning. All Rights Reserved. May not be copied, scanned, or duplicated, in whole or in part. Due to electronic rights, some third party content may be suppressed from the eBook and/or eChapter(s). Editorial review has deemed that any suppressed content does not materially affect the overall learning experience. Cengage Learning reserves the right to remove additional content at any time if subsequent rights restrictions require it.

where

$$A_c = K_A \cos^2 \beta$$
$$= \frac{\cos^2(\phi - \beta)}{\cos(\delta + \beta)\left[1 + \left\{\frac{\sin(\delta + \phi)\sin(\phi - i)}{\cos(\delta + \beta)\cos(\beta - i)}\right\}^{1/2}\right]^2} \tag{8.13}$$

In a similar manner, from Eq. (8.4)

$$P_{AE} = \frac{1}{2}\gamma H^2(1 - k_v)K_{AE}$$
$$= \frac{1}{2}\gamma H^2(1 - k_v)(\cos\theta \cos^2 \beta)^{-1}(A_m) \tag{8.14}$$

where

$$A_m = K_{AE} \cos\theta \cos^2 \beta$$
$$= \frac{\cos^2(\phi - \beta - \theta)}{\cos(\delta + \beta + \theta)\left[1 + \left\{\frac{\sin(\phi + \delta)\sin(\phi - i - \theta)}{\cos(\delta + \beta + \theta)\cos(\beta - i)}\right\}^{1/2}\right]^2} \tag{8.15}$$

Now let

$$i' = i + \theta \tag{8.16}$$

and

$$\beta' = \beta + \theta \tag{8.17}$$

Substitution of Eqs. (8.16) and (8.17) into Eq. (8.15) yields

$$A_m = \frac{\cos^2(\phi - \beta')}{\cos(\delta + \beta')\left[1 + \left\{\frac{\sin(\phi + \delta)\sin(\phi - i')}{\cos(\delta + \beta')\cos(\beta' - i')}\right\}^{1/2}\right]^2} \tag{8.18}$$

The preceding equation is similar to Eq. (8.13) except for the fact that i' and β' are used in place of i and β. Thus, it can be said that

$$A_m = A_c(i', \beta') = K_A(i', \beta')\cos^2 \beta'$$

The active earth pressure P_{AE} can now be expressed as

$$P_{AE} = \frac{1}{2}\gamma H^2(1 - k_v)\left(\frac{\cos^2 \beta'}{\cos\theta \cos^2 \beta}\right)K_A(i', \beta')$$
$$= P_A(i', \beta')(1 - k_v)(\overset{*}{p}) \tag{8.19}$$

where

$$\overset{*}{p} = \left(\frac{\cos^2 \beta'}{\cos\theta \cos^2 \beta}\right) \tag{8.20}$$

Copyright 2017 Cengage Learning. All Rights Reserved. May not be copied, scanned, or duplicated, in whole or in part. Due to electronic rights, some third party content may be suppressed from the eBook and/or eChapter(s). Editorial review has deemed that any suppressed content does not materially affect the overall learning experience. Cengage Learning reserves the right to remove additional content at any time if subsequent rights restrictions require it.

In order to calculate P_{AE} by using Eq. (8.19), one needs to follow these steps:

1. Calculate i' [Eq. (8.16)].
2. Calculate β' [Eq. (8.17)].
3. With known values of ϕ, δ, i', and β', calculate K_A (from Tables 8.2, Table 8.3, or other available charts).
4. Calculate P_A as equal to $\frac{1}{2}\gamma H^2 K_A$ (K_A from Step 3).
5. Calculate $(1 - k_v)$.
6. Calculate $\overset{*}{p}$ [Eq. (8.20)].
7. Calculate

$$P_{AE} = P_A(i', \beta')(1 - k_v)(\overset{*}{p})$$

For convenience, some typical values of $\overset{*}{p}$ are plotted in Figure 8.5.

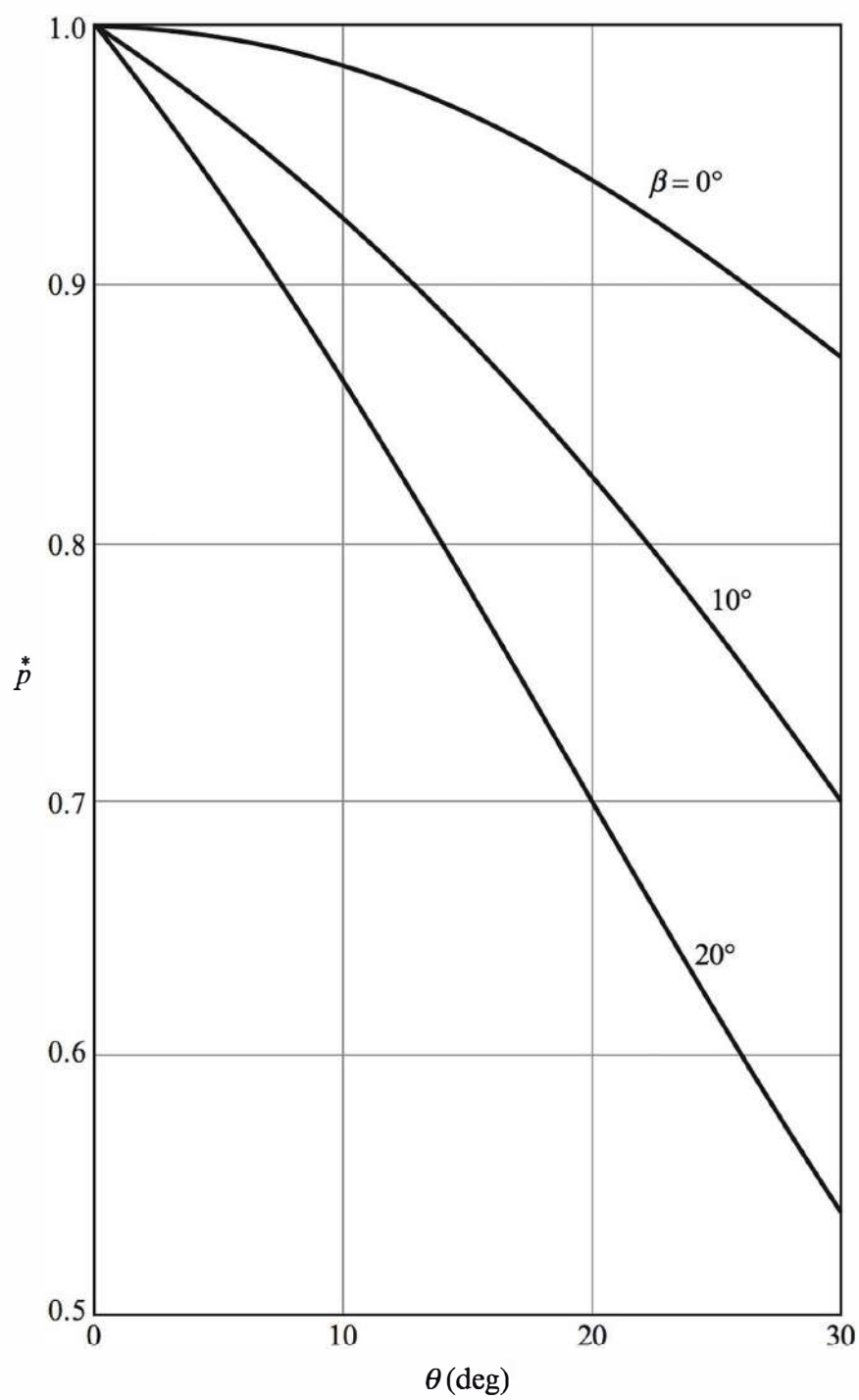

Figure 8.5 Variation of $\overset{*}{p}$ and θ

Copyright 2017 Cengage Learning. All Rights Reserved. May not be copied, scanned, or duplicated, in whole or in part. Due to electronic rights, some third party content may be suppressed from the eBook and/or eChapter(s). Editorial review has deemed that any suppressed content does not materially affect the overall learning experience. Cengage Learning reserves the right to remove additional content at any time if subsequent rights restrictions require it.

EXAMPLE 8.1

Refer to Figure 8.2. If $\beta = 0°$, $i = 0°$, $\phi = 36°$, $\delta = 18°$, $H = 4.5$ m, $\gamma = 17.6$ kN/m^3, $k_v = 0.2$, and $k_h = 0.3$, determine the active force per unit length of the wall.

SOLUTION:

$$\theta = \tan^{-1}\left(\frac{k_h}{1-k_v}\right) = \tan^{-1}\left(\frac{0.3}{1-0.2}\right) = 20.56°$$

$$i' = i + \theta = 0 + 20.56° = 20.56°$$

$$\beta' = \beta + \theta = 0 + 20.56° = 20.56°$$

$$K_A(i', \beta') = \frac{\cos^2(\phi - \beta')}{\cos^2\beta'\cos(\delta+\beta')\left[1+\left\{\frac{\sin(\delta+\phi)\sin(\phi-i')}{\cos(\delta+\beta')\cos(\beta'-i')}\right\}^{1/2}\right]^2}$$

$$= \frac{\cos^2(15.44)}{(\cos^2 20.56)(\cos 38.56)\left[1+\left\{\frac{(\sin 54)(\sin 15.44)}{(\cos 38.56)(\cos 0)}\right\}^{1/2}\right]^2}$$

$$= 0.583$$

$$P_A(i', \beta') = \frac{1}{2}\gamma H^2 K_A(i', \beta')$$

$$= \frac{1}{2}(17.6)(4.5)^2(0.583) = 103.89 \text{ kN/m}$$

$$\overset{*}{p} = \left(\frac{\cos^2\beta'}{\cos\theta\cos^2\beta}\right) = \frac{\cos^2 20.56}{(\cos 20.56)(\cos 0)}$$

$$= 0.9363$$

Hence, from Eq. (8.19),

$$P_{AE} = P_A(i', \beta')(1 - k_v)(\overset{*}{p}) = (103.89)(1-0.2)(0.9363) = \mathbf{77.81\ kN/m.}$$

8.5 EFFECT OF VARIOUS PARAMETERS ON THE VALUE OF THE ACTIVE EARTH PRESSURE COEFFICIENT

Parameters such as the angle of wall friction, angle of friction of soil, and slope of the backfill influence the magnitude of the active earth pressure coefficient K_{AE} to varying degrees. The effect of each of these factors is considered briefly.

Copyright 2017 Cengage Learning. All Rights Reserved. May not be copied, scanned, or duplicated, in whole or in part. Due to electronic rights, some third party content may be suppressed from the eBook and/or eChapter(s). Editorial review has deemed that any suppressed content does not materially affect the overall learning experience. Cengage Learning reserves the right to remove additional content at any time if subsequent rights restrictions require it.

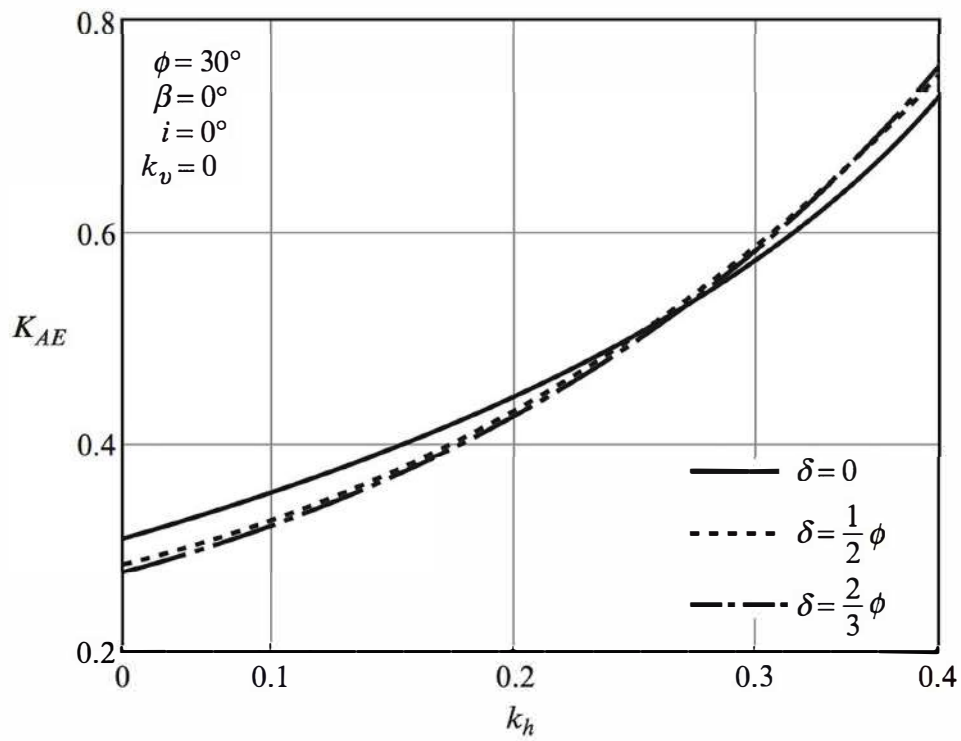

Figure 8.6 Influence of wall friction, δ, on K_{AE}

A. Effect of Wall Friction Angle δ

Figure 8.6 shows the variation of the active earth pressure coefficient K_{AE} with k_h for $\phi = 30°$ with $\delta = 0°, \phi/2$, and $\frac{2}{3}\phi$ ($k_v = 0$, $\beta = 0°$, and $i = 0°$), It can be seen from the plot that, for $0 \le \delta \le \frac{2}{3}\phi$, the effect of wall friction on the active earth pressure coefficient is rather small.

B. Effect of Soil Friction Angle ϕ

Figure 8.7 shows the plot of $K_{AE}\cos\delta$ (that is, the horizontal component of the active earth pressure coefficient) for a vertical retaining wall with horizontal backfill ($\beta = 0°$ and $i = 0°$). In this plot, it has been assumed that $\delta = \frac{1}{2}\phi$. From the plot, it may be seen that, for $k_v = 0$ and $\delta = \frac{1}{2}\phi$, $K_{AE(\phi = 30°)}$ is about 35% higher than $K_{AE(\phi = 40°)}$. Hence, a small error in the assumption of the soil friction angle could lead to a large error in the estimation of P_{AE}.

C. Effect of Slope of the Backfill i

Figure 8.8 shows the variation of the value of $K_{AE}\cos\delta$ with i for a wall with $\beta = 0, \delta = \frac{2}{3}\phi, \phi = 30°$, and $k_v = 0$. Note that the value of $K_{AE}\cos\delta$ sharply increases with the increase of the slope of the backfill.

8.6 GRAPHICAL CONSTRUCTION FOR DETERMINATION OF ACTIVE FORCE, P_{AE}

Culmann (1875) developed a graphical method for determination of the active force P_A [Eq. (8.1)] developed behind a retaining wall. A modified form of Culmann's graphical construction for determination of the active force P_{AE} per unit length of

Copyright 2017 Cengage Learning. All Rights Reserved. May not be copied, scanned, or duplicated, in whole or in part. Due to electronic rights, some third party content may be suppressed from the eBook and/or eChapter(s). Editorial review has deemed that any suppressed content does not materially affect the overall learning experience. Cengage Learning reserves the right to remove additional content at any time if subsequent rights restrictions require it.

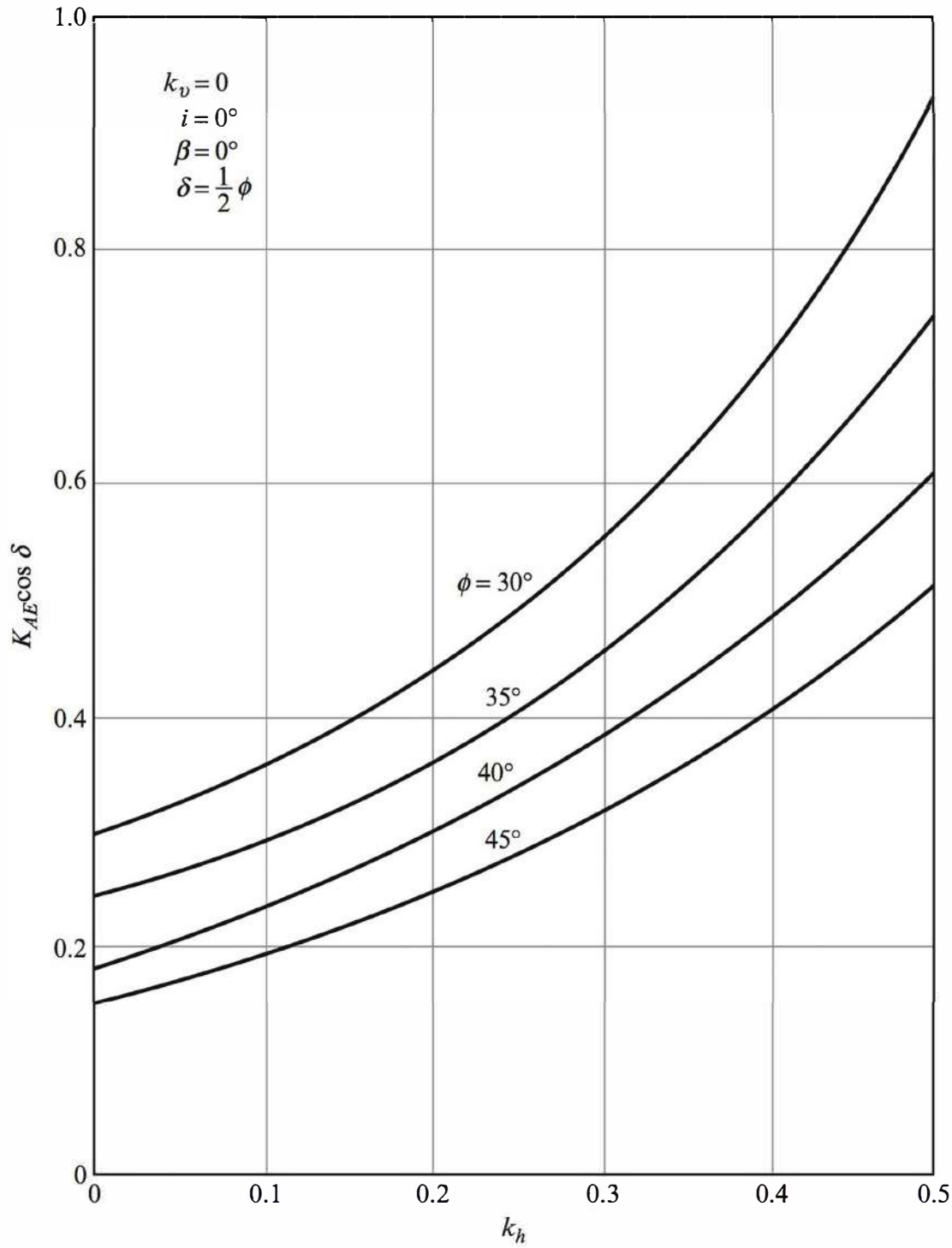

Figure 8.7 Effect of soil friction angle, ϕ, on $K_{AE}\cos\delta$

a retaining wall has been proposed by Kapila (1962). In order to understand this, consider the force polygon for the wedge ABC shown in Figure 8.2. For convenience, this has been replotted in Figure 8.9a. The force polygon can be reduced to a force triangle with forces P_{AE}, F, and $W\sqrt{(1-k_v)^2 + k_h^2}$ (Figure 8.9b). Note that in Figure 8.9a, b, α is the angle that the failure wedge makes with the horizontal.

The idea behind this graphical construction is to determine the *maximum* value of P_{AE} by considering several trial wedges. With references to Figure 8.9c, following are steps for the graphical construction:

1. Draw line BE, which makes an angle $\phi - \theta$ with horizontal.
2. Draw a line BD, which makes an angle $90° - \beta - \delta - \theta$ with the line BE.
3. Draw $BC_1, BC_2, BC_3, \ldots$, which are the trial failure surface.
4. Determine k_h and k_v and then $\sqrt{(1-k_v)^2 + k_h^2}$

Copyright 2017 Cengage Learning. All Rights Reserved. May not be copied, scanned, or duplicated, in whole or in part. Due to electronic rights, some third party content may be suppressed from the eBook and/or eChapter(s). Editorial review has deemed that any suppressed content does not materially affect the overall learning experience. Cengage Learning reserves the right to remove additional content at any time if subsequent rights restrictions require it.

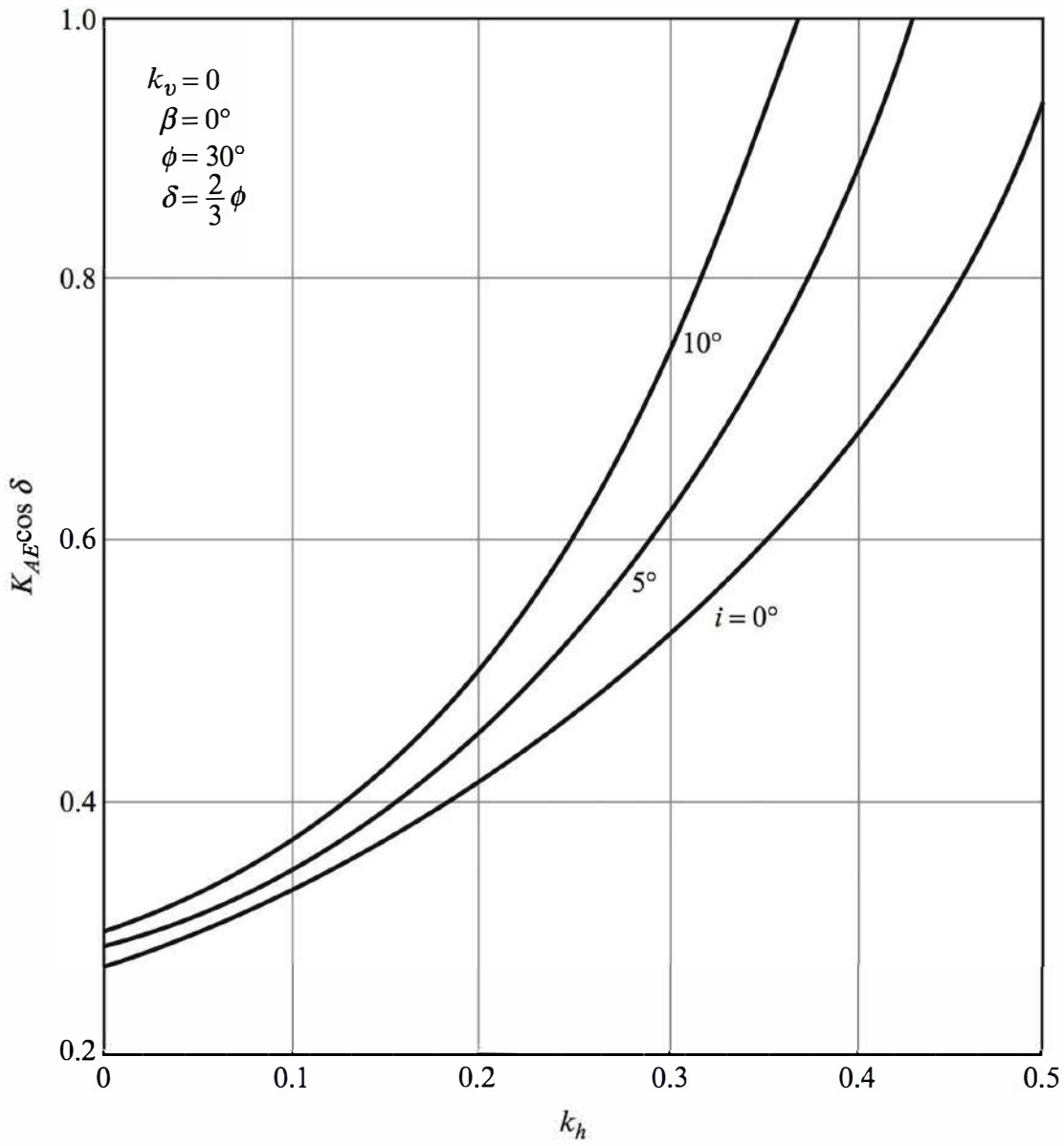

Figure 8.8 Effect of backfill inclination, i, on $K_{AE}\cos\delta$

5. Determine the weights $W_1, W_2, W_3, \ldots$ of trial failure wedges ABC_1, ABC_2, $ABC_3, \ldots$, respectively (per unit length at right angle to the cross section shown).

   Note

$$W_1 = (\text{area of } ABC_1) \times \gamma \times 1$$
$$W_2 = (\text{area of } ABC_2) \times \gamma \times 1$$
$$\vdots$$

6. Determine $W_1', W_2', W_3' \ldots$, as

$$W_1' = \sqrt{(1-k_v)^2 + k_h^2}\, W_1$$
$$W_2' = W_2' = \sqrt{(1-k_v)^2 + k_h^2}\, W_2$$
$$\vdots$$

7. Adopt a load scale.

Copyright 2017 Cengage Learning. All Rights Reserved. May not be copied, scanned, or duplicated, in whole or in part. Due to electronic rights, some third party content may be suppressed from the eBook and/or eChapter(s). Editorial review has deemed that any suppressed content does not materially affect the overall learning experience. Cengage Learning reserves the right to remove additional content at any time if subsequent rights restrictions require it.

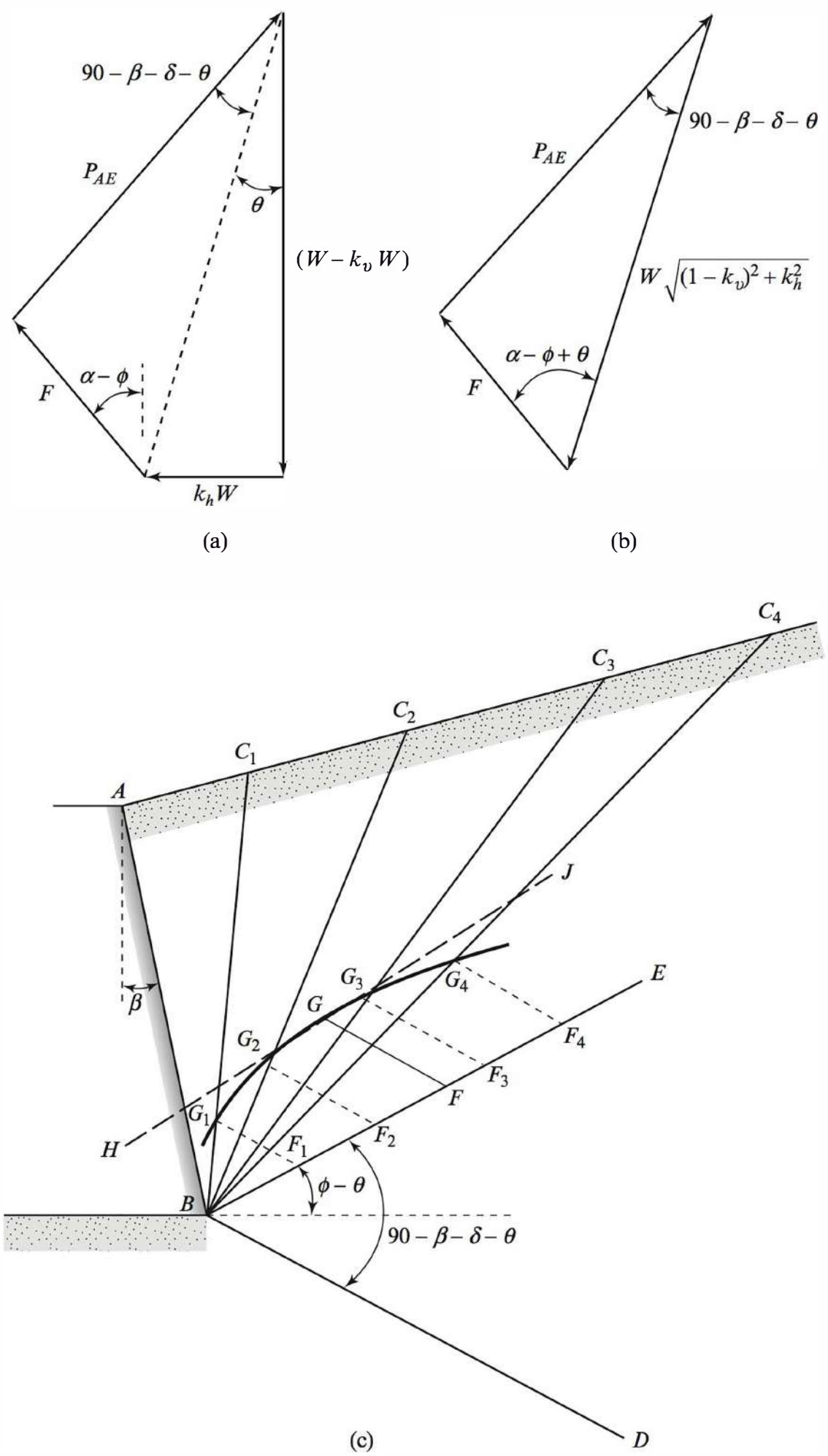

Figure 8.9 Modified Culmann constructing

Copyright 2017 Cengage Learning. All Rights Reserved. May not be copied, scanned, or duplicated, in whole or in part. Due to electronic rights, some third party content may be suppressed from the eBook and/or eChapter(s). Editorial review has deemed that any suppressed content does not materially affect the overall learning experience. Cengage Learning reserves the right to remove additional content at any time if subsequent rights restrictions require it.

8. Using the load scale adopted in step 7, draw $BF_1 = W_1'$, $BF_2 = W_2'$, $BF_3 = W_3'$, ... on the line BE.
9. Draw F_1G_1, F_2G_2, F_3G_3, ..., parallel to line BD. Note that BF_1G_1 is the force triangle for the trial wedge ABC_1 smaller to that shown in Figure 8.9b. Similarly, BF_2G_2, BF_3G_3, ..., are the force triangles for the trial wedges ABC_2, ABC_3, ..., respectively.
10. Join the points $G_1, G_2, G_3, \ldots$, by a smooth curve.
11. Draw a line HJ parallel to line BE. Let G be point of tangency.
12. Draw line GF parallel to BD.
13. Determine active force P_{AE} as $GF \times$ (load scale).

8.7 LABORATORY MODEL TEST RESULTS FOR ACTIVE EARTH PRESSURE COEFFICIENT, K_{AE}

In the early stages of the development of the Mononobe-Okabe solution [Eq. (8.4)], several small-scale laboratory model test results relating to the determination of the magnitude of lateral force on a rigid wall with dry granular backfill, and thus K_{AE}, have been reported in the literature (e.g., Mononobe and Matsuo, 1929; Jacobsen, 1939). More recently, Sherif, Ishibashi, and Lee (1982), Sherif and Fang (1984), and Ishibashi and Fang (1987) have published results of lateral earth pressure measurement behind a heavily instrumented rigid retaining wall. For all the preceding tests, the height of the retaining wall was 1 m. The retaining wall was resting on a shaking table with a granular backfill. A sinusoidal input motion with a 3.5 Hz frequency and maximum acceleration up to 0.5 g was applied to the shaking table during the experiments. The results of these tests are very instructive and will be summarized here.

The nature of distribution of active earth pressure and thus the magnitude of the active force on a retaining wall is very much dependent on the nature of yielding of the wall itself. Figure 8.10 shows the three possible modes of wall yielding for the development of an active state:

a. Rotation about the bottom (Figure 8.10a)
b. Translation (Figure 8.10b)
c. Rotation about the top (Figure 8.10c)

Model test results relating to each of the three modes of wall yielding are described next.

A. Rotation about the Bottom

Ishibashi and Fang (1987) measured the dynamic active earth pressure distribution behind the model rigid retaining wall of 1 m height ($\beta = 0°$) described in the first paragraph of this section. For these tests, dry sand was used as a backfill material. The surface of the backfill was kept horizontal (that is, $i = 0$; Figure 8.2). The properties of the sand backfill were:

Dry unit weight of compaction of the backfill: $15.94 - 16.11\ \text{kN/m}^3$

Copyright 2017 Cengage Learning. All Rights Reserved. May not be copied, scanned, or duplicated, in whole or in part. Due to electronic rights, some third party content may be suppressed from the eBook and/or eChapter(s). Editorial review has deemed that any suppressed content does not materially affect the overall learning experience. Cengage Learning reserves the right to remove additional content at any time if subsequent rights restrictions require it.

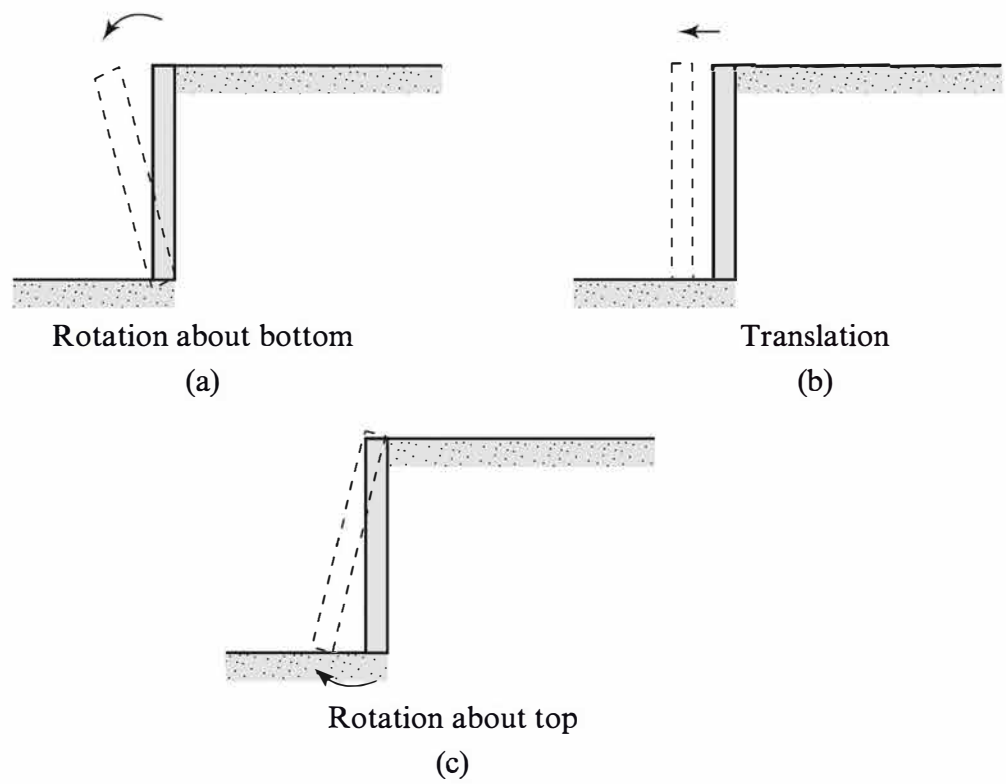

Figure 8.10 Modes of wall rotation for active pressure

Relative density of the backfill: 49.5 – 57.6%

Angle of friction of the soil: 38.5 – 40.1°

For these tests, the model retaining wall was rotated about its bottom. The magnitude of k_h was varied from 0 to about 0.6, and k_v was equal to 0. From Eq. (8.4) with $k_v = 0$,

$$K_{AE} = \frac{P_{AE}}{\frac{1}{2}\gamma H^2} \tag{8.21}$$

Figure 8.11 shows the variation of the experimental values of $K_{AE}\cos\delta$ obtained from the tests of Ishibashi and Fang (1987). Also plotted in Figure 8.11 is the theoretical variation of $K_{AE}\cos\delta$ obtained from Eq. (8.5) with $k_v = 0$, $\beta = 0°$, and $i = 0°$. In plotting this theoretical variation, it has been assumed that $\phi = 39.2°$ and $\delta = \phi/2$. The comparison between the Mononobe-Okabe theoretical curve and the experimental curve shows that

$$P_{AE(\text{measured})} \approx 1.23 \text{ to } 1.43 P_{AE(\text{theory})}$$

B. Translation of the Wall

Dynamic active earth pressure measurement behind a vertical rigid model retaining wall undergoing translation was reported by Sherif, Ishibashi, and Lee (1982). The details of the test conditions are as follows:

Retaining wall:

Height = 1 m

$\beta = 0°$

Copyright 2017 Cengage Learning. All Rights Reserved. May not be copied, scanned, or duplicated, in whole or in part. Due to electronic rights, some third party content may be suppressed from the eBook and/or eChapter(s). Editorial review has deemed that any suppressed content does not materially affect the overall learning experience. Cengage Learning reserves the right to remove additional content at any time if subsequent rights restrictions require it.

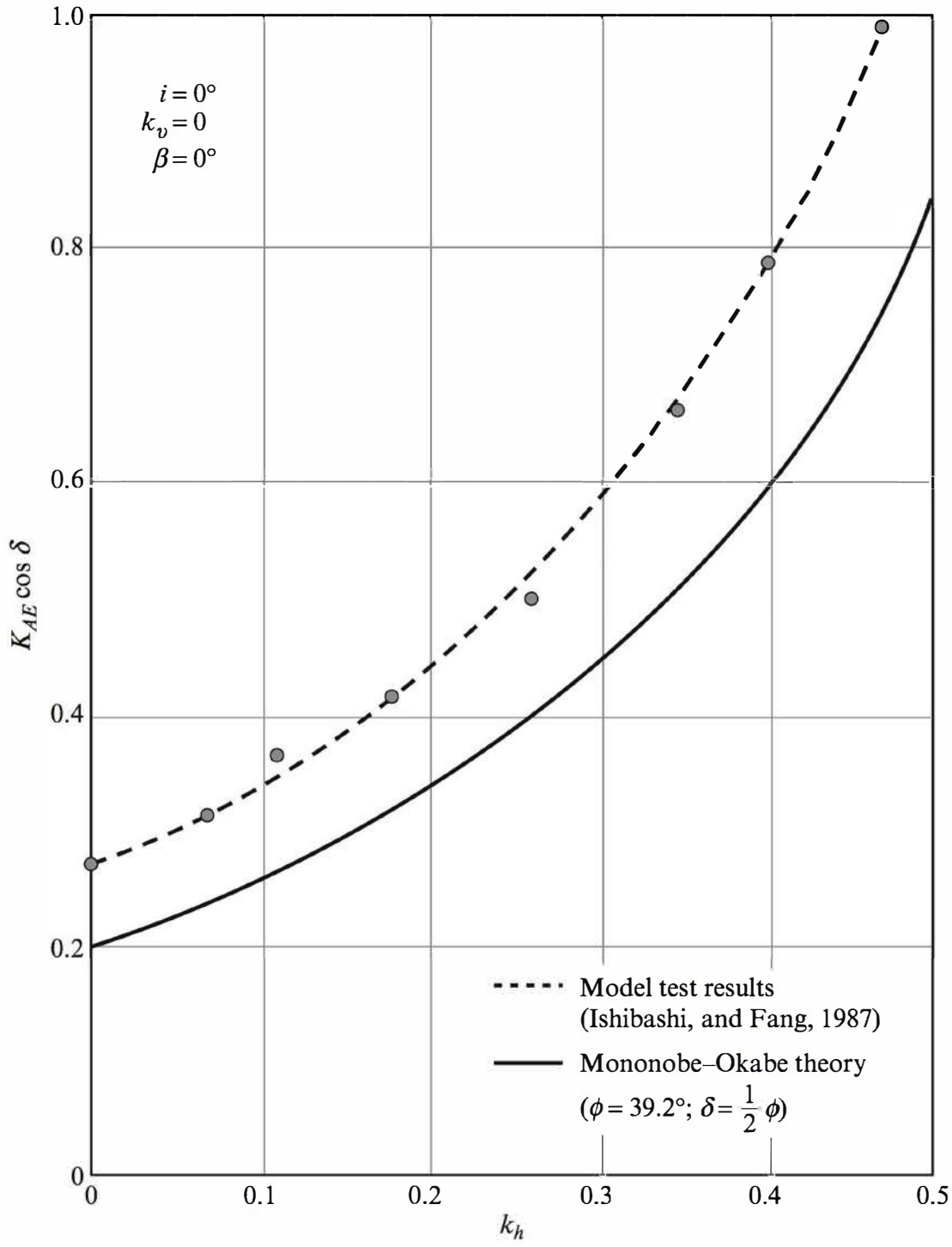

Figure 8.11 Wall rotation about the bottom for active pressure—comparison of theory with model test results

Average properties of backfill (sand):

$$\text{Unit weight} = 16.28 \text{ kN/m}^3$$

$$\text{Angle of friction, } \phi = 40.9°$$

$$\text{Angle of wall friction, } \delta = 23.9°$$

$$\text{Slope of the backfill, } i = 0°$$

For these tests the magnitude of $K_{AE} \cos\delta$ was varied from 0 to 0.5 and k_v was 0. Figure 8.12 shows the experimental variation of $K_{AE} \cos\delta$ obtained from these model tests. Also shown in this figure is the variation of $K_{AE} \cos\delta$ obtained from

Copyright 2017 Cengage Learning. All Rights Reserved. May not be copied, scanned, or duplicated, in whole or in part. Due to electronic rights, some third party content may be suppressed from the eBook and/or eChapter(s). Editorial review has deemed that any suppressed content does not materially affect the overall learning experience. Cengage Learning reserves the right to remove additional content at any time if subsequent rights restrictions require it.

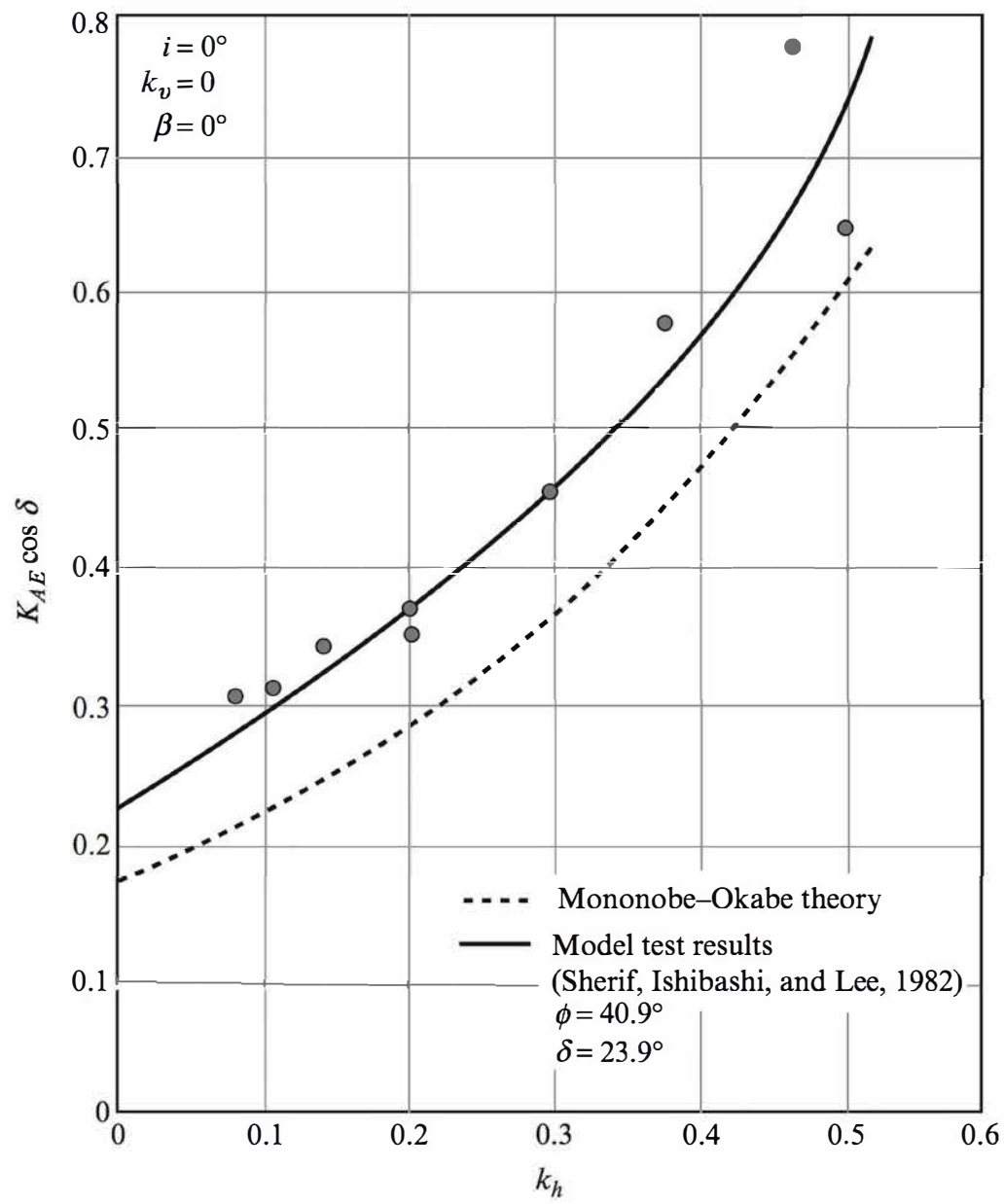

Figure 8.12 Translation of wall for active pressure—comparison of theory with model test results

the Mononobe-Okabe theory [Eq. (8.5)]. Based on this plot it appears that the experimental values P_{AE} are about 30% higher than those obtained from Eqs. (8.4) and (8.5).

Sherif, Ishibashi, and Lee (1982) also developed an empirical relationship for the magnitude of wall translation for development of the active state, which can be given as

$$\Delta = H(7 - 0.13\phi)10^{-4} \tag{8.22}$$

where

Δ = lateral translation of the wall

H = height of the wall

In Eq. (8.22), the value of ϕ is in degrees.

Copyright 2017 Cengage Learning. All Rights Reserved. May not be copied, scanned, or duplicated, in whole or in part. Due to electronic rights, some third party content may be suppressed from the eBook and/or eChapter(s). Editorial review has deemed that any suppressed content does not materially affect the overall learning experience. Cengage Learning reserves the right to remove additional content at any time if subsequent rights restrictions require it.

C. Rotation of the Wall about the Top

Sherif and Fang (1984) reported the dynamic earth pressure distribution behind a 1 m high rigid vertical retaining wall ($\beta = 0°$) undergoing rotation about its top. A sand with an average unit weight of 15.99 kN/m³ was used as a backfill. The surface of the backfill was horizontal (that is, $i = 0°$). The nature of variation of the maximum active horizontal earth pressure distribution ($p_{AE} \cos \delta$, where p = active earth pressure at a given depth) obtained from these tests is shown in Figure 8.13. Also plotted in this figure are the theoretical variations of $p_{AE} \cos \delta$ obtained from the Mononobe-Okabe solution (with $\beta = 0°$, $i = 0$, and $k_v = 0$) for various values of k_h. From the comparison of the theoretical and experimental plots, the following general conclusions can be drawn.

1. The nature of variation of dynamic earth pressure for wall rotation about the top is very much different than that predicted by the Mononobe-Okabe theory.
2. For a given value of k_h,

$$P_{AE} \cos \delta = \int (p_{AE} \cos \delta) dy \tag{8.23}$$

   where y = depth measured from the top of the wall.
3. For a given value of k_h, the horizontal component of the lateral force, $P_{AE} \cos \delta$, calculated from the experimental curves by using Eq. (8.23), is about 15% to 20% higher than the predicted by the Mononobe-Okabe theory.

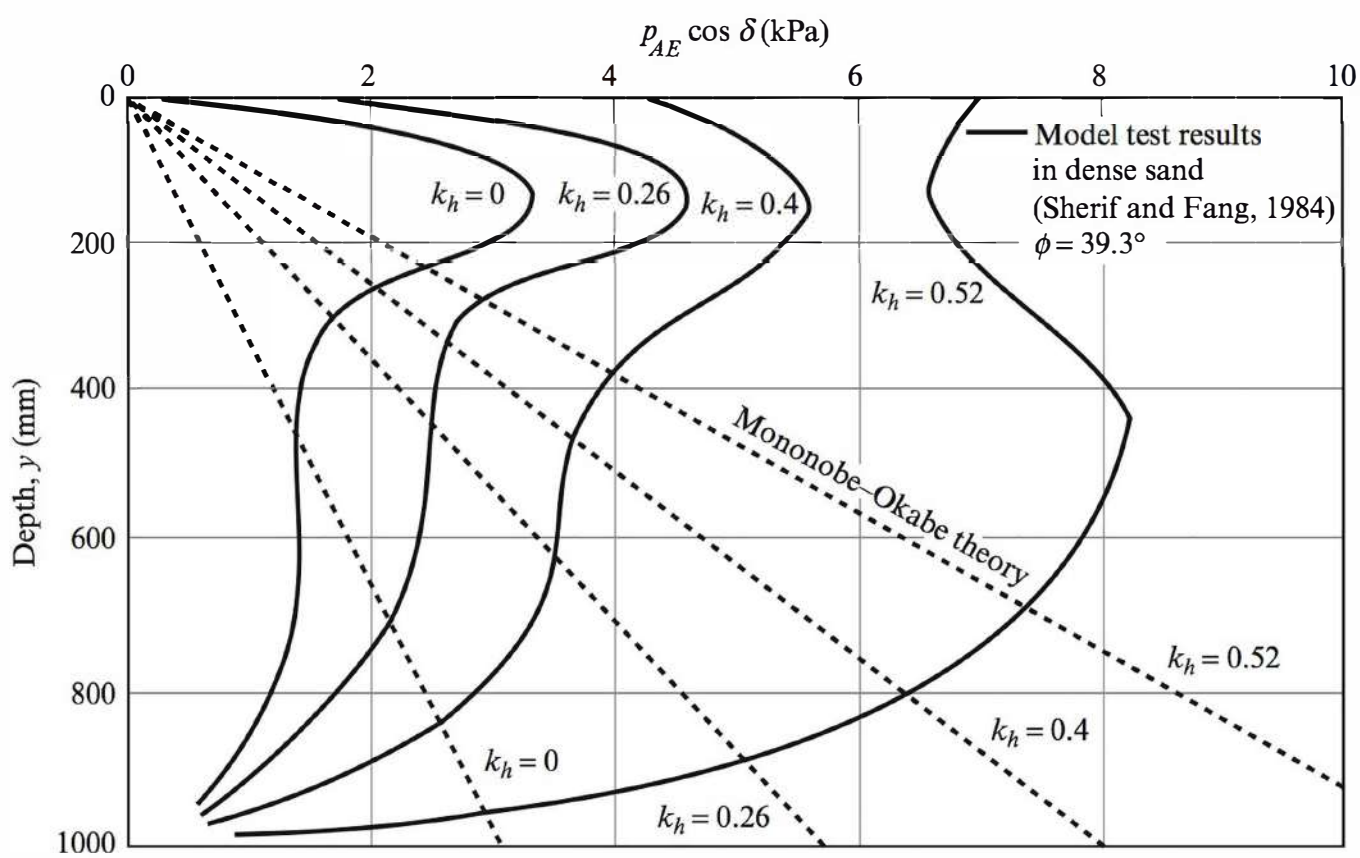

Figure 8.13 Rotation of wall about the top for active pressure—comparison of theory with model test results ($i = 0°$, $\beta = 0°$, $k_v = 0$)

Copyright 2017 Cengage Learning. All Rights Reserved. May not be copied, scanned, or duplicated, in whole or in part. Due to electronic rights, some third party content may be suppressed from the eBook and/or eChapter(s). Editorial review has deemed that any suppressed content does not materially affect the overall learning experience. Cengage Learning reserves the right to remove additional content at any time if subsequent rights restrictions require it.

8.8 POINT OF APPLICATION OF THE RESULTANT ACTIVE FORCE, P_{AE}

A. Rotation about the Bottom of the Wall

The original Mononobe-Okabe solution for the active force on retaining structures implied that the resultant force will act at a distance of $\frac{1}{3}H$ measured from the bottom of the wall (H =height of the wall) similar to that in the static case ($k_h = k_v = 0$). However, all the laboratory tests that have been conducted so far indicate that the resultant pressure P_{AE} acts at a distance $\bar{H}$, which is somewhat greater than $\frac{1}{3}H$ measured from the bottom of the wall. This is shown in Figure 8.14.

Prakash and Basavanna (1969) have made a theoretical evaluation for determination of $\bar{H}$. Based on the force-equilibrium analysis, their study shows that $\bar{H}$ increases from $\frac{1}{3}H$ for $k_h = 0$ to about $\frac{1}{2}H$ for $k_h = 0.3$ (for $\phi = 30°$, $\delta = 7.5°$, $k_v = 0$, $i = \beta = 0$). For similar conditions, the moment-equilibrium analysis gave a value of $\bar{H} = \frac{1}{3}H$ and $k_h = 0$, which increases to a value of $\bar{H} \approx H/1.9$ at $k_h = 0.3$.

For practical design considerations, Seed and Whitman (1969) have proposed the following procedure for determination of the line of action of P_{AE}.

1. Calculate P_A [Eq. (8.1)];
2. Calculate P_{AE} [Eq. (8.4)];
3. Calculate $\Delta P_{AE} = P_{AE} - P_A$. The term ΔP_{AE} is the incremental force due to earthquake condition;

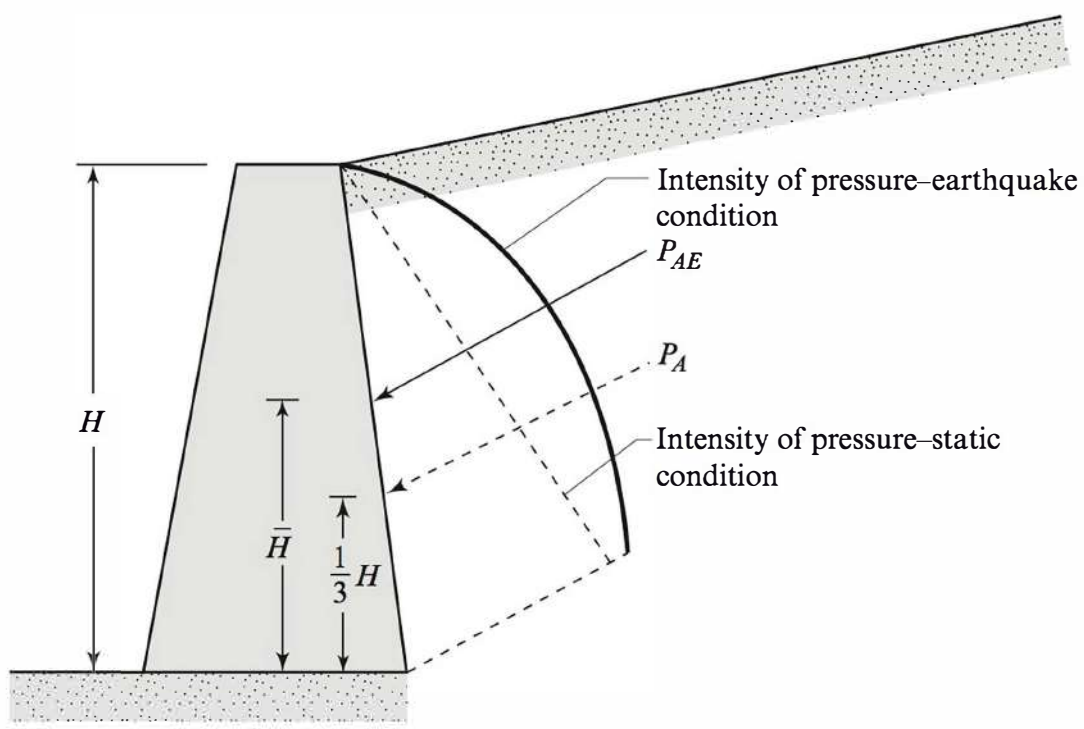

Figure 8.14 Point of application of resultant active earth pressure

Copyright 2017 Cengage Learning. All Rights Reserved. May not be copied, scanned, or duplicated, in whole or in part. Due to electronic rights, some third party content may be suppressed from the eBook and/or eChapter(s). Editorial review has deemed that any suppressed content does not materially affect the overall learning experience. Cengage Learning reserves the right to remove additional content at any time if subsequent rights restrictions require it.

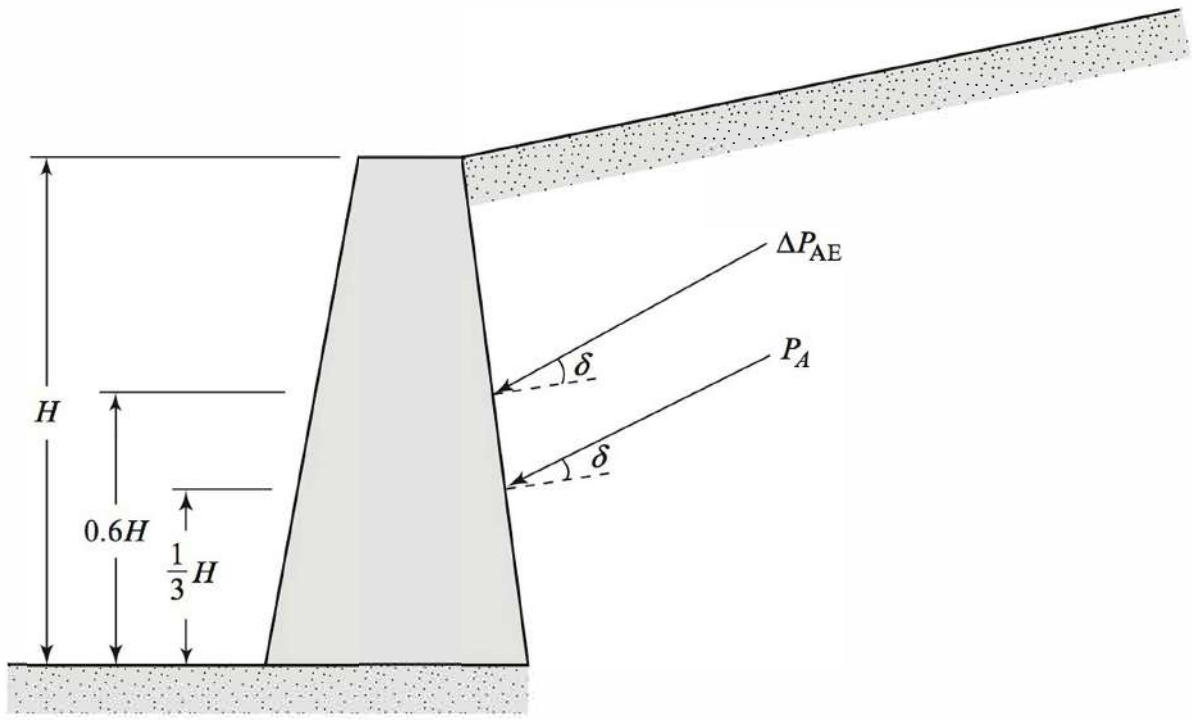

Figure 8.15

4. Assume that P_A acts at a distance of $\frac{1}{3}H$ from the bottom of the wall (Figure 8.15);
5. Assume that ΔP_{AE} acts at a distance of $0.6H$ from the bottom of the wall (Figure 8.15); then

$$\bar{H} = \frac{(P_A)\left(\frac{1}{3}H\right) + (\Delta P_{AE})(0.6H)}{P_{AE}}$$

B. Translation of the Wall

Sherif, Ishibashi, and Lee (1982) suggested that, for wall translation, the following procedure can be used to estimate the location of the line of action of the active force, P_{AE}.

1. Calculate P_A [Eq. (8.1)];
2. Calculate P_{AE} [Eq. (8.4)];
3. Calculate $\Delta P_{AE} = P_{AE} - P_A$; and
4. Referring to Figure 8.16, calculate

$$\bar{H} = \frac{(P_A)(0.42H) + (\Delta P_{AE})(0.48H)}{P_{AE}}$$

C. Rotation about the Top of the Wall

For rotation of the wall about its top (Figure 8.17), $\bar{H}$ is about $0.55H$ (Sherif and Fang, 1984).

Copyright 2017 Cengage Learning. All Rights Reserved. May not be copied, scanned, or duplicated, in whole or in part. Due to electronic rights, some third party content may be suppressed from the eBook and/or eChapter(s). Editorial review has deemed that any suppressed content does not materially affect the overall learning experience. Cengage Learning reserves the right to remove additional content at any time if subsequent rights restrictions require it.

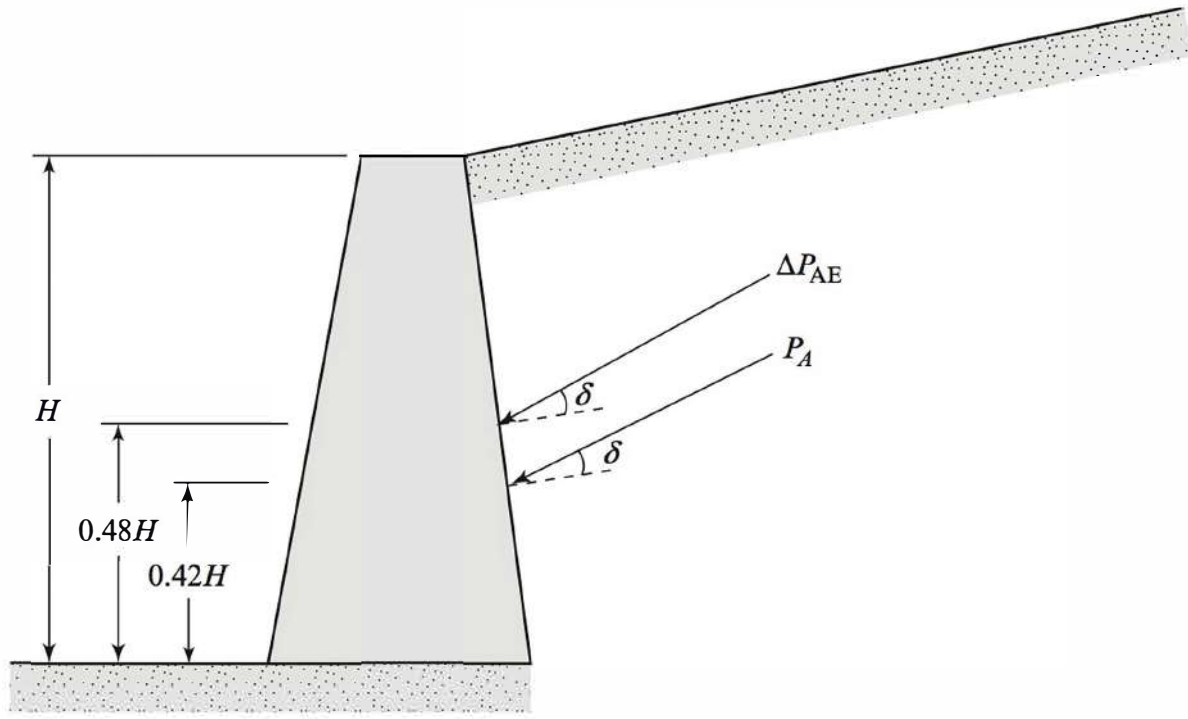

Figure 8.16

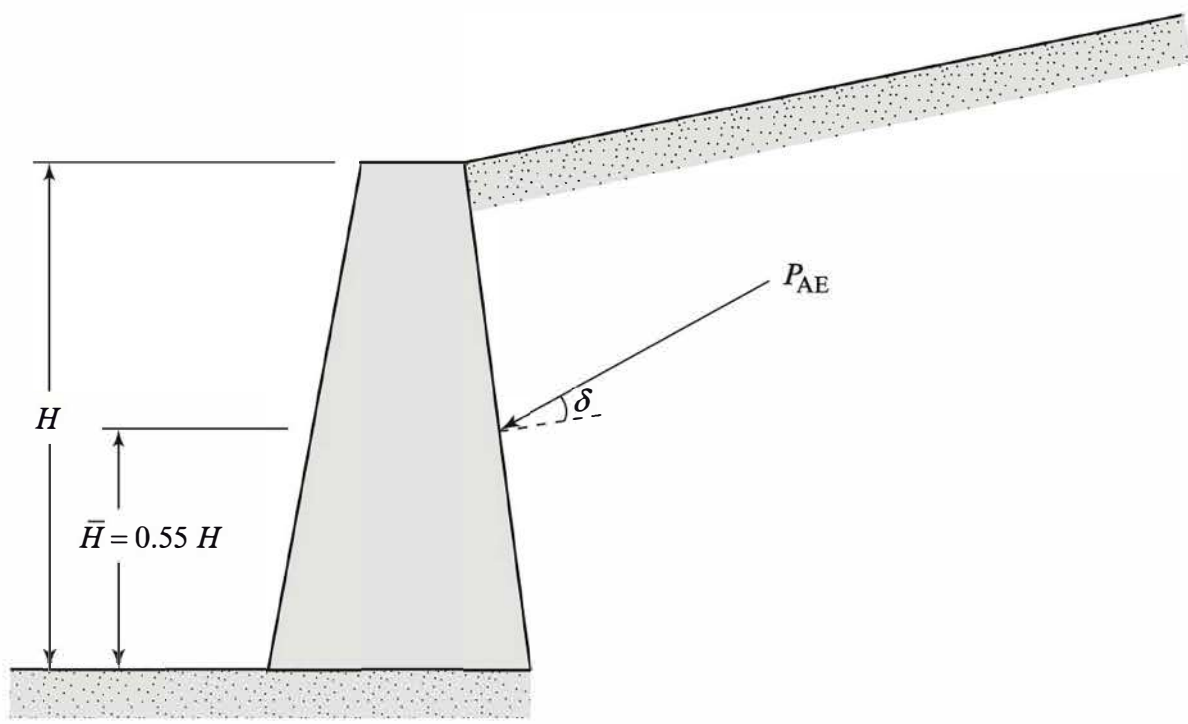

Figure 8.17

EXAMPLE 8.2

Referring to Example 8.1, determine the location of the line of action for P_{AE}. Assume rotation of the wall about its bottom.

SOLUTION:

The value of P_{AE} in Example 8.1 has been determined to be 77.81 kN/m.

$$P_A = \frac{1}{2}\gamma H^2 K_A$$

Copyright 2017 Cengage Learning. All Rights Reserved. May not be copied, scanned, or duplicated, in whole or in part. Due to electronic rights, some third party content may be suppressed from the eBook and/or eChapter(s). Editorial review has deemed that any suppressed content does not materially affect the overall learning experience. Cengage Learning reserves the right to remove additional content at any time if subsequent rights restrictions require it.

For $\phi = 36°$, $\delta = 18°$, $K_A = 0.236$ [Eq. (8.2)]. Thus,

$$P_A = \frac{1}{2}(17.6)(4.5)^2(0.236) = 42.06 \text{ kN/m}$$

This acts at a distance equal to $\frac{4.5}{3} = 1.5$ m from the bottom of the wall. Again,

$$\Delta P_{AE} = 77.81 - 42.06 = 35.75 \text{ kN/m}$$

The line of action of ΔP_{AE} intersects the wall at a distance of $0.6H = 2.7$ m measured from the bottom, so

$$\bar{H} = \frac{(1.5)(42.06) + (2.7)(35.75)}{77.81} = \mathbf{2.05\ m}$$

8.9 DESIGN OF GRAVITY RETAINING WALLS BASED ON LIMITED DISPLACEMENT

Richards and Elms (1979) have proposed a procedure for design of gravity retaining walls based on limited displacement. In this study, they have taken into consideration the wall inertia effect and concluded that there is some lateral movement of the wall even for mild earthquakes. In order to develop this procedure, consider a gravity retaining wall as shown in Figure 8.18, along with the forces acting on it during an earthquake. For stability, summing the forces in the vertical direction,

$$N = W_w - k_v W_w - P_{AE}\sin(\delta + \beta) \tag{8.24}$$

where N is the vertical component of the reaction at the base of the wall and W_w is the weight of the wall.

Similarly, summing the forces in the horizontal direction,

$$S = k_h W_w + P_{AE}\cos(\delta + \beta) \tag{8.25}$$

where S is the horizontal component of the reaction at the base of the wall. At sliding,

$$S = N\tan\phi_b \tag{8.26}$$

where ϕ_b is the soil-wall friction angle at the base of the wall.

Substituting Eqs. (8.24) and (8.25) into Eq. (8.26), one obtains

$$k_h W_w + P_{AE}\cos(\delta + \beta) = [W_w(1 - k_v) + P_{AE}\sin(\delta + \beta)]\tan\phi_b$$

or

$$W_w[(1 - k_v)\tan\phi_b - k_h] = P_{AE}[\cos(\delta + \beta) - \sin(\delta + \beta)\tan\phi_b]$$

$$W_w = \frac{P_{AE}\left[\cos(\delta + \beta) - \sin(\delta + \beta)\tan\phi_b\right]}{(1 - k_v)\tan\phi_b - k_h} \tag{8.27}$$

Copyright 2017 Cengage Learning. All Rights Reserved. May not be copied, scanned, or duplicated, in whole or in part. Due to electronic rights, some third party content may be suppressed from the eBook and/or eChapter(s). Editorial review has deemed that any suppressed content does not materially affect the overall learning experience. Cengage Learning reserves the right to remove additional content at any time if subsequent rights restrictions require it.

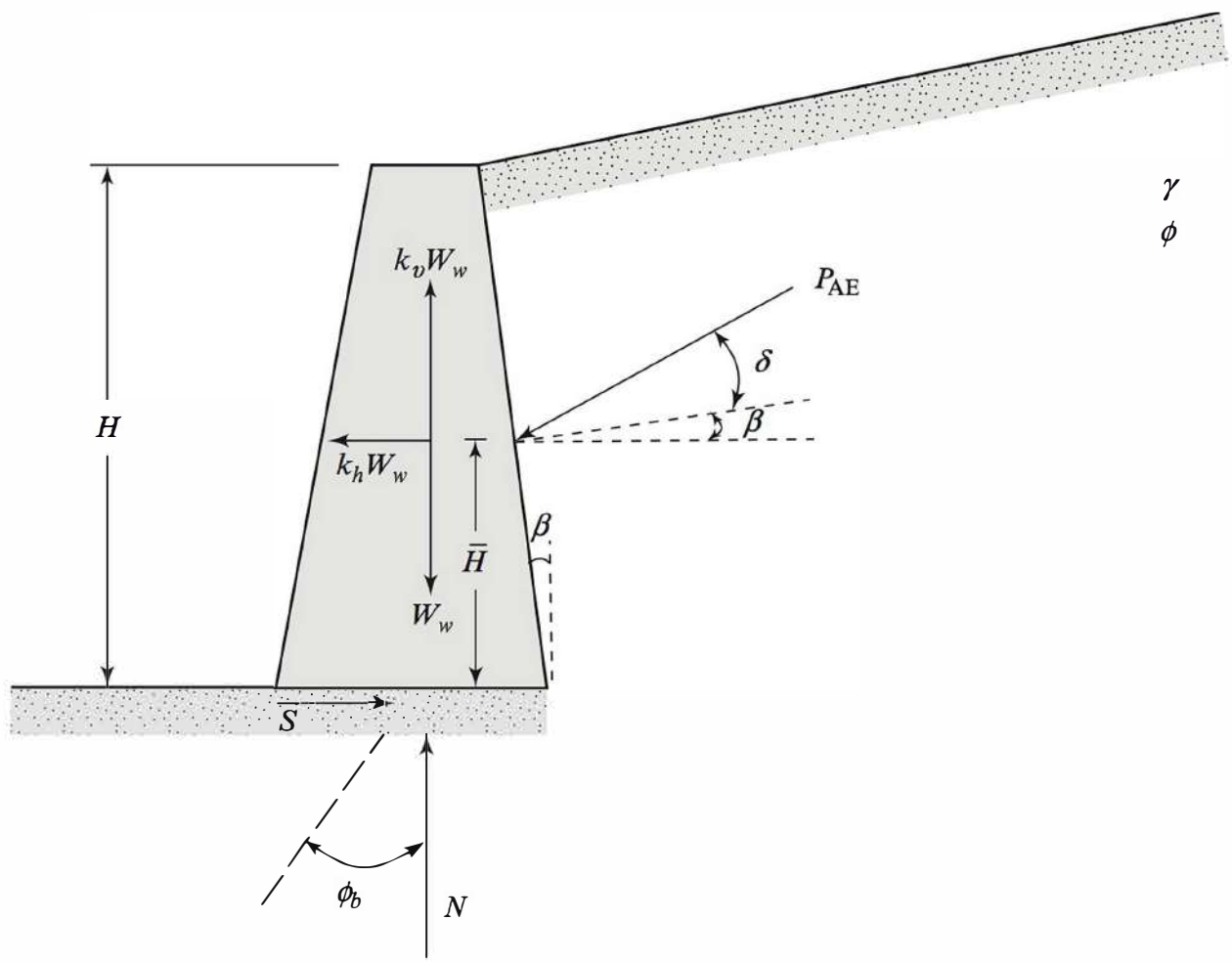

Figure 8.18 Derivation of Eq. (8.28)

From Eq. (8.4), $P_{AE} = \frac{1}{2}\gamma H^2(1-k_v)K_{AE}$. Substitution of this equation into Eq. (8.27) yields

$$W_w = \frac{\frac{1}{2}\gamma H^2 K_{AE}\left[\cos(\delta+\beta) - \sin(\delta+\beta)\tan\phi_b\right]}{(\tan\phi_b - \tan\theta)} \tag{8.28}$$

where $\tan\theta = k_h/(1-k_v)$.

It may be noted that, in Eq. (8.28), W_w is equal to infinity if

$$\tan\phi_b = \tan\theta \tag{8.29}$$

This implies that infinite mass of the wall is required to prevent motion. The critical value of $k_h = k_{h(\mathrm{cr})}$ can thus be given by relation

$$\tan\theta = \frac{k_{h(\mathrm{cr})}}{1-k_v} = \tan\phi_b$$

or

$$k_{h(\mathrm{cr})} = (1-k_v)\tan\phi_b \tag{8.30}$$

Equation (8.28) can also be written in the form

Copyright 2017 Cengage Learning. All Rights Reserved. May not be copied, scanned, or duplicated, in whole or in part. Due to electronic rights, some third party content may be suppressed from the eBook and/or eChapter(s). Editorial review has deemed that any suppressed content does not materially affect the overall learning experience. Cengage Learning reserves the right to remove additional content at any time if subsequent rights restrictions require it.

$$W_w = \left[\frac{1}{2}\gamma H^2 (1 - k_v) K_{AE}\right] C_{IE} \tag{8.31}$$

where

$$C_{IE} = \frac{\cos(\delta + \beta) - \sin(\delta + \beta)\tan\phi_b}{(1 - k_v)(\tan\phi_b - \tan\phi)} \tag{8.32}$$

Figure 8.19 shows the variation of C_{IE} with k_h for various values of $k_v (\phi = \phi_b = 35°, \delta = \frac{1}{2}\phi, i = \beta = 0)$. Also, Figure 8.20 shows the variation of C_{IE} with k_h for various values of wall friction angle, δ $(\phi = \phi_b = 35°, i = \beta = 0, k_v = 0)$.

Note that Eq. (8.31) is for the limiting equilibrium condition for sliding with earthquake effects takes into consideration. For the static condition (i.e., $k_h = k_v = 0$), Eq. (8.31) becomes

$$W = \frac{1}{2}\gamma H^2 K_A C_I \tag{8.33}$$

where $W = W_w$ (for static condition) and

$$C_I = \frac{\cos(\delta + \beta) - \sin(\delta + \beta)\tan\phi_b}{\tan\phi_b} \tag{8.34}$$

Thus, comparing Eqs. (8.31) and (8.33), we can write that

$$\frac{W_w}{W} = F_T F_I = F_W \tag{8.35}$$

where

$$F_T = \frac{K_{AE}(1 - k_v)}{K_A} = \text{soil thrust factor}$$

$$F_I = \frac{C_{IE}}{C_I} = \text{wall inertia factor}$$

and F_W is a factor of safety applied to the weight of the wall to take into account the effect of soil pressure and wall inertia. Figure 8.21 shows a plot of F_T, F_I, and F_W for various values of k_h $(\phi = \phi_b = 35°, \delta = \frac{1}{2}\phi, k_v = 0, \beta = i = 0)$.

Richards and Elms (1979) have explained the importance of inertia factors given in Eq. (8.35). Referring to Figure 8.21, suppose that one neglects the wall inertia factor (which is not considered in the design procedure outlined in Sections 8.2 and 8.3; i.e., $F_I = 1$). In such a case,

$$F_W = F_T = \frac{W_w}{W}$$

Copyright 2017 Cengage Learning. All Rights Reserved. May not be copied, scanned, or duplicated, in whole or in part. Due to electronic rights, some third party content may be suppressed from the eBook and/or eChapter(s). Editorial review has deemed that any suppressed content does not materially affect the overall learning experience. Cengage Learning reserves the right to remove additional content at any time if subsequent rights restrictions require it.

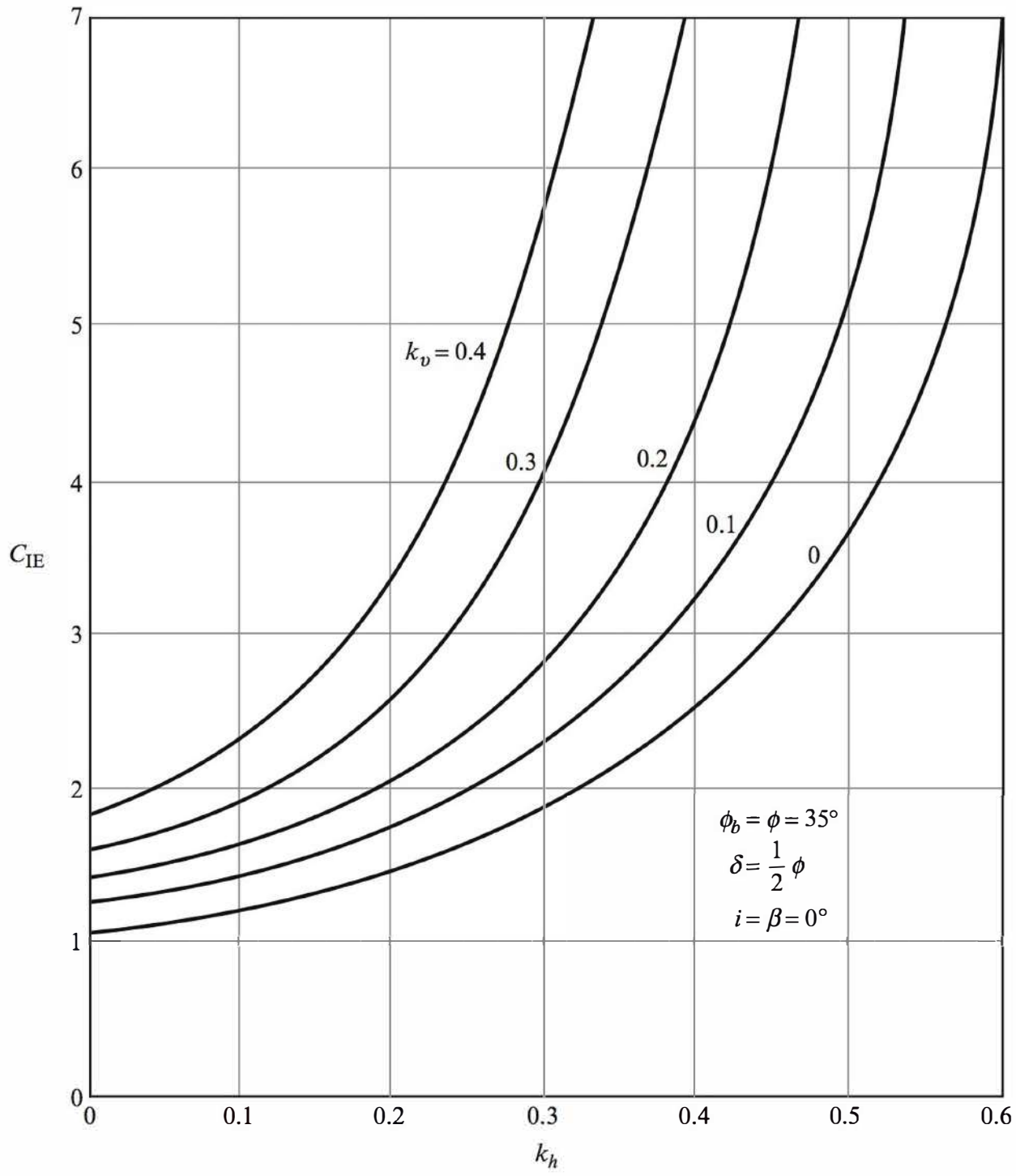

Figure 8.19 Effect of k_v on the value of C_{IE} (from Richards and Elms, 1979)

Source: Richards, R. and and Elms, D.G. (1979). "Seismic Behavior of Gravity Retaining Walls," *Journal of the Geotechnical Engineering Division*, ASCE, Vol. 105, No. GT4, pp. 449–464. With permission from ASCE.

For a value of $F_W = 1.5$, the critical horizontal acceleration is equal to 0.18. However, if the wall inertia factor is considered, the critical horizontal acceleration corresponding to $F_W = 1.5$ is equal to 0.105. In other words, if a gravity retaining wall is designed such that $W_w = 1.5W$, the wall will start to move laterally at a value of $k_h = 0.105$. Based on the procedure described in Section 8.2, if $W_w = 1.5\,W$, it is assumed that the wall will not move laterally until a value of $k_h = 0.18$ is reached.

These considerations show that, for no lateral movement, the weight of the wall has to be increased by a considerable amount over the static condition, which may prove to be very expensive. Thus, for actual design with reasonable

Copyright 2017 Cengage Learning. All Rights Reserved. May not be copied, scanned, or duplicated, in whole or in part. Due to electronic rights, some third party content may be suppressed from the eBook and/or eChapter(s). Editorial review has deemed that any suppressed content does not materially affect the overall learning experience. Cengage Learning reserves the right to remove additional content at any time if subsequent rights restrictions require it.

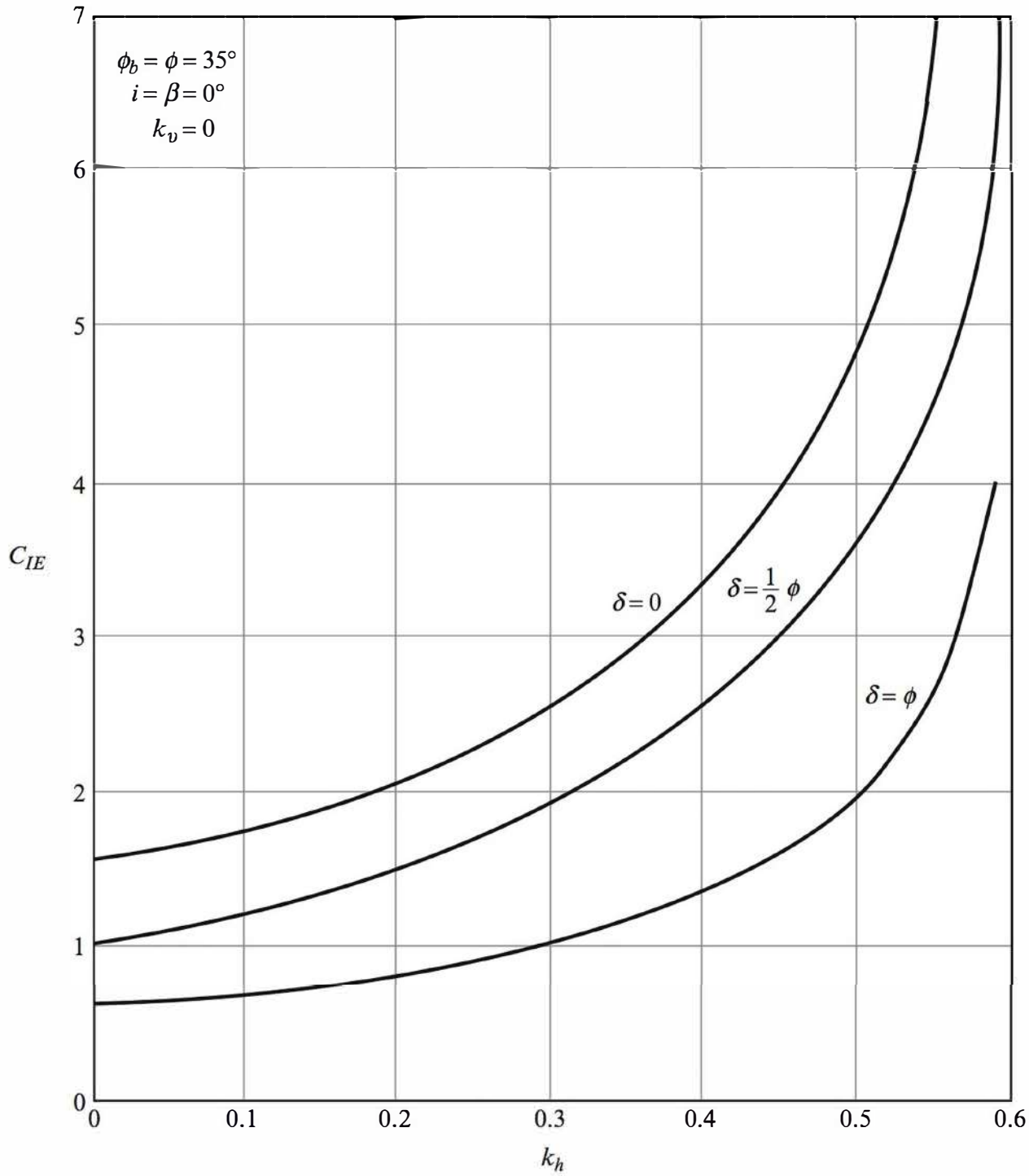

Figure 8.20 Effect of wall friction on C_{IE} (from Richards and Elms, 1979)

Source: Richards, R. and and Elms, D.G. (1979). "Seismic Behavior of Gravity Retaining Walls," *Journal of the Geotechnical Engineering Division*, ASCE, Vol. 105, No. GT4, pp. 449–464. With permission from ASCE.

cost, one has to assume some lateral displacement of the wall will take place during an earthquake; the procedure for determination of the wall weight (W_w) is then as follows:

1. Determine an acceptable displacement d of the wall.
2. Determine a design value of k_h from the equation

$$k_h = A_a \left(\frac{5.08 A_v^2}{A_a d} \right)^{1/4} \tag{8.36}$$

Copyright 2017 Cengage Learning. All Rights Reserved. May not be copied, scanned, or duplicated, in whole or in part. Due to electronic rights, some third party content may be suppressed from the eBook and/or eChapter(s). Editorial review has deemed that any suppressed content does not materially affect the overall learning experience. Cengage Learning reserves the right to remove additional content at any time if subsequent rights restrictions require it.

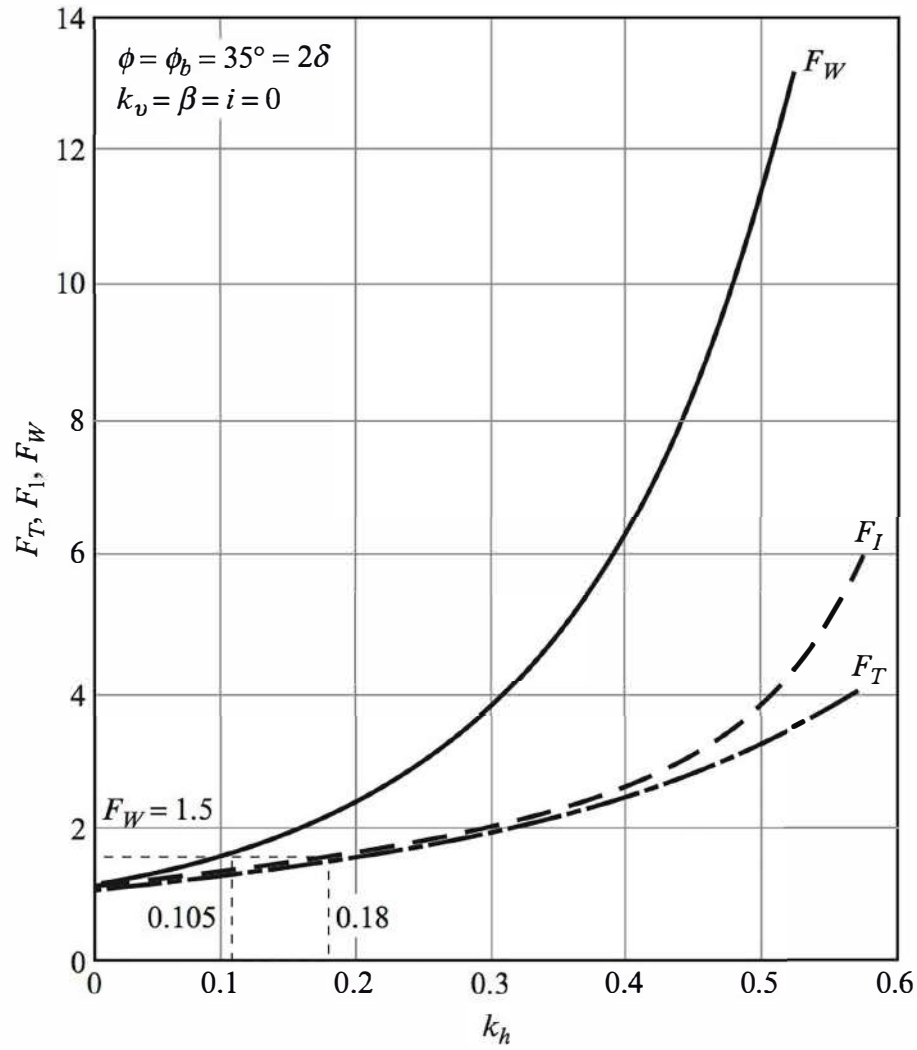

Figure 8.21 Variation of F_T, F_I, and F_W (from Richards and Elms, 1979)

Source: Richards, R. and and Elms, D.G. (1979). "Seismic Behavior of Gravity Retaining Walls," *Journal of the Geotechnical Engineering Division*, ASCE, Vol. 105, No. GT4, pp. 449–464. With permission from ASCE.

where A_a and A_v are effective acceleration coefficient and displacement d is in mm. The values of A_a and A_v for a given region in the United States are given by the Applied Technology Council (1978).

Equation (8.36) has been suggested by Richards and Elms (1979) and is based on study of Newmark (1965) and Franklin and Chang (1977).

3. Using the above value of k_h, and assuming $k_v = 0$, determine the value of K_{AE}.
4. Determine the weight of the wall W_w from Eq. (8.31).
5. Apply a factor of safety to W_w obtained in Step 4.

A slight modification of this design procedure was proposed by Nadim and Whitman 1983). This modification is intended primarily to account for the amplification of the ground motion in the backfill.

EXAMPLE 8.3

Determine the weight of a retaining wall 4 m high (given $\beta = 0, i = 0$, $\gamma = 17.29$ kN/m^3, $\phi_b = \phi = 34°$, $\delta = \frac{1}{2}\phi$, $A_v = 0.2$, $A_a = 0.2$, factor of safety = 1.5)

Copyright 2017 Cengage Learning. All Rights Reserved. May not be copied, scanned, or duplicated, in whole or in part. Due to electronic rights, some third party content may be suppressed from the eBook and/or eChapter(s). Editorial review has deemed that any suppressed content does not materially affect the overall learning experience. Cengage Learning reserves the right to remove additional content at any time if subsequent rights restrictions require it.

a. for static condition;
b. for zero displacement condition under earthquake loading; and
c. for a displacement of 50.8 mm under earthquake loading.

SOLUTION:

a. From Eq. (8.33),

$$W = \frac{1}{2}\gamma H^2 K_A C_I$$

From Table 8.2, $K_A = 0.256$ (for $\phi = 34°, \delta = 1.7°, i = 0, \beta = 0$).

$$C_I = \frac{\cos(\delta+\beta) - \sin(\delta+\beta)\tan\phi_b}{\tan\phi_b} = \frac{\cos 17 - \sin 17(\tan 34)}{\tan 34}$$

$$= 1.125$$

Thus

$$W = \frac{1}{2}(17.29)(4)^2(0.256)(1.125) = 39.84 \text{ kN/m}$$

With a factor of safety of 1.5,

the weight of the wall is equal to $(1.5)(39.84) =$ **59.76 kN/m**.

b. From Eq. (8.31),

$$W_w = \left[\frac{1}{2}\gamma H^2(1-k_v)K_{AE}\right]C_{IE}$$

Assume $k_v = 0$.

$$C_{IE} = \frac{\cos(\delta+\beta) - \sin(\delta+\beta)\tan\phi_b}{(1-k_v)(\tan\phi_b - \tan\phi)}$$

$$\tan\theta = \frac{k_h}{1-k_v} = \frac{0.2}{1} = 0.2; \theta = 11.31°$$

$$C_{IE} = \frac{\cos 17 - \sin 17(\tan 34)}{\tan 34 - 0.2} = 1.6$$

Again, from Eq. (8.5),

$$K_{AE} = \frac{\cos^2(34-11.31)}{\cos(11.31)[\cos(17+11.31)]\left[1+\sqrt{\frac{\sin(34+17)\sin(34-11.31)}{\cos(17+11.31)}}\right]^2}$$

$$= 0.393$$

$$W_w = \frac{1}{2}(17.29)(4)^2(1-0)(0.393)(1.6) = 86.98 \text{ kN/m}$$

With a safety factor of 1.5, the weight of wall $= (86.98)(1.5) =$ **130.47kN/m**.

Copyright 2017 Cengage Learning. All Rights Reserved. May not be copied, scanned, or duplicated, in whole or in part. Due to electronic rights, some third party content may be suppressed from the eBook and/or eChapter(s). Editorial review has deemed that any suppressed content does not materially affect the overall learning experience. Cengage Learning reserves the right to remove additional content at any time if subsequent rights restrictions require it.

c. From Eq. (8.36),

$$k_h = A_a\left[\frac{5.08A_v^2}{A_a d}\right]^{1/4} = 0.2\left[\frac{(5.08)(0.2)^2}{(0.2)(50.8)}\right]^{1/4} = 0.075$$

$$\tan\theta = \frac{k_h}{1-k_v} = \frac{0.075}{1-0} = 0.075$$

or

$$\theta = 4.29°$$

$$C_{IE} = \frac{\cos 17 - \sin 17(\tan 34)}{\tan 34 - 0.075} = \frac{0.7591}{0.5995} = 1.27$$

Using Eq. (8.5)

$$K_{AE} = \frac{\cos^2(34-4.29)}{\cos(4.29)\left[\cos(17+4.29)\right]\left[1+\sqrt{\frac{\sin(34+17)\sin(34-4.29)}{\cos(17+4.29)}}\right]^2}$$

$$= 0.3$$

Thus, with a factor of safety of 1.5,

$$W_w = (1.5)\left(\frac{1}{2}\right)(17.29)(4)^2(0.3)(1.27) = \mathbf{79.05\ kN/m}$$

8.10 HYDRODYNAMIC EFFECTS OF PORE WATER

The lateral earth pressure theory developed in the preceding sections of this chapter has been for retaining walls with dry soil backfills. However, for quay walls (Figure 8.22), the hydrodynamic effect of the water also has to be taken into consideration. This is usually done according to the Westergaard theory (1933) that was derived to obtain the dynamic water pressure on the face of a concrete dam. Based on this theory, the water pressure due to an earthquake at a depth y (Figure 8.22) may be expressed as

$$p_1 = \frac{7}{8}k_h\gamma_w h^{1/2}y^{1/2} \tag{8.37}$$

where p_1 is the intensity of pressure on the seaward side, γ_w is the unit weight of water, and h is the total depth of water. Hence, the total dynamic water force on the seaward side per unit length of the wall $[P_{1(w)}]$ can be obtained by integration as

$$P_{1(w)} = \int p_1 dy = \int_0^h \frac{7}{8}k_h\gamma_w h^{1/2}y^{1/2}dy = \frac{7}{12}k_h\gamma_w h^2 \tag{8.38}$$

Copyright 2017 Cengage Learning. All Rights Reserved. May not be copied, scanned, or duplicated, in whole or in part. Due to electronic rights, some third party content may be suppressed from the eBook and/or eChapter(s). Editorial review has deemed that any suppressed content does not materially affect the overall learning experience. Cengage Learning reserves the right to remove additional content at any time if subsequent rights restrictions require it.

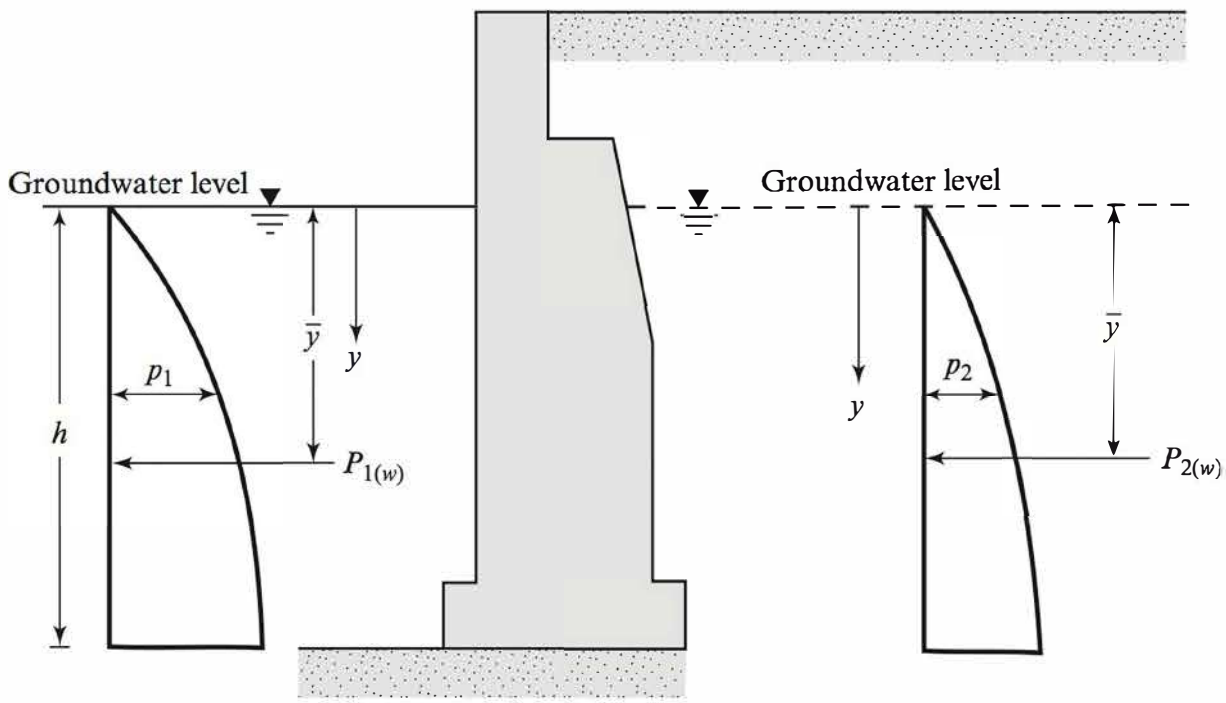

Figure 8.22 Hydrodynamic effects on a quay wall

The location of the resultant water pressure is

$$\bar{y} = \frac{1}{P_{1(w)}}\int_0^h (p_1\,dy)y = \frac{1}{P_{1(w)}}\left(\frac{7}{8}k_h\gamma_w h^{1/2}\right)\int_0^h (y^{1/2})(y)dy$$

$$= \frac{1}{P_{1(w)}}\left(\frac{7}{8}k_h\gamma_w h^{1/2}\right)(h^{5/2})\frac{2}{5} = \frac{1}{P_{1(w)}}\left(\frac{7}{20}k_h\gamma_w h^3\right)$$

or

$$\bar{y} = \left(\frac{7}{12}k_h\gamma_w h^2\right)^{-1}\left(\frac{7}{20}k_h\gamma_w h^3\right) = 0.6h \tag{8.39}$$

Matsuo and O'Hara (1960) have suggested that the increase of the pore water pressure on the landward side is approximately 70% of that on the seaward side. Thus,

$$p_2 = 0.7\left(\frac{7}{8}k_h\gamma_w h^{1/2}y^{1/2}\right) = 0.6125k_h\gamma_w h^{1/2}y^{1/2} \tag{8.40}$$

where p_2 is the dynamic pore water pressure on the landward side at a depth y. The total dynamic pore water force increase $[P_{2(w)}]$ per unit length of the wall is

$$P_{2(w)} = 0.7\left(\frac{7}{12}k_h\gamma_w h^2\right) = 0.4083k_h\gamma_w h^2 \tag{8.41}$$

Copyright 2017 Cengage Learning. All Rights Reserved. May not be copied, scanned, or duplicated, in whole or in part. Due to electronic rights, some third party content may be suppressed from the eBook and/or eChapter(s). Editorial review has deemed that any suppressed content does not materially affect the overall learning experience. Cengage Learning reserves the right to remove additional content at any time if subsequent rights restrictions require it.

During an earthquake, the force on the wall per unit length on the seaward side will be reduced by $P_{1(w)}$ and that on the landward side will be increased by $P_{2(w)}$. Thus, the total increase of the force per unit length of the wall is equal to

$$P_w = P_{1(w)} + P_{2(w)} = 1.7\left(\frac{7}{12}k_h\gamma_w h^2\right) = 0.9917k_h\gamma_w h^2 \tag{8.42}$$

EXAMPLE 8.4

Refer to Figure 8.22. For the quay wall, $h = 10$ m. Determine the total dynamic force increase due to water for $k_h = 0.2$.

SOLUTION:

From Eq. (8.42)

$$P_w = 0.9917k_h\gamma_w h^2$$
$$= 0.9917(0.2)(9.81)(10)^2 = \mathbf{194.6\ kN/m}$$

8.11 ACTIVE EARTH PRESSURE THEORY FOR c - ϕ BACKFILL

A. Analysis of Prakash and Saran (1966), and Saran and Prakash (1968)

The Mononobe-Okabe equation for estimating P_{AE} for cohessionless backfill also can be extended to c-ϕ soil (Prakash and Saran, 1966; Saran and Prakash, 1968). Figure 8.23 shows a retaining wall of height H with a horizontal c-ϕ soil as backfill. The depth of tensile crack that may develop in a c-ϕ soil is given as

$$z_0 = \frac{2c}{\gamma\sqrt{K_a}} \tag{8.43}$$

where

$$K_a = \tan^2\left(45 - \frac{\phi}{2}\right) \tag{8.44}$$

Referring to Figure 8.23, the forces acting on the soil wedge (per unit length of the wall) are as follows:

a. The weight of the wedge $ABCDE, W$
b. Resultant of the shear and normal forces on the failure surface CD, F
c. Active force, P_{AE}
d. Horizontal inertia force, k_hW

Copyright 2017 Cengage Learning. All Rights Reserved. May not be copied, scanned, or duplicated, in whole or in part. Due to electronic rights, some third party content may be suppressed from the eBook and/or eChapter(s). Editorial review has deemed that any suppressed content does not materially affect the overall learning experience. Cengage Learning reserves the right to remove additional content at any time if subsequent rights restrictions require it.

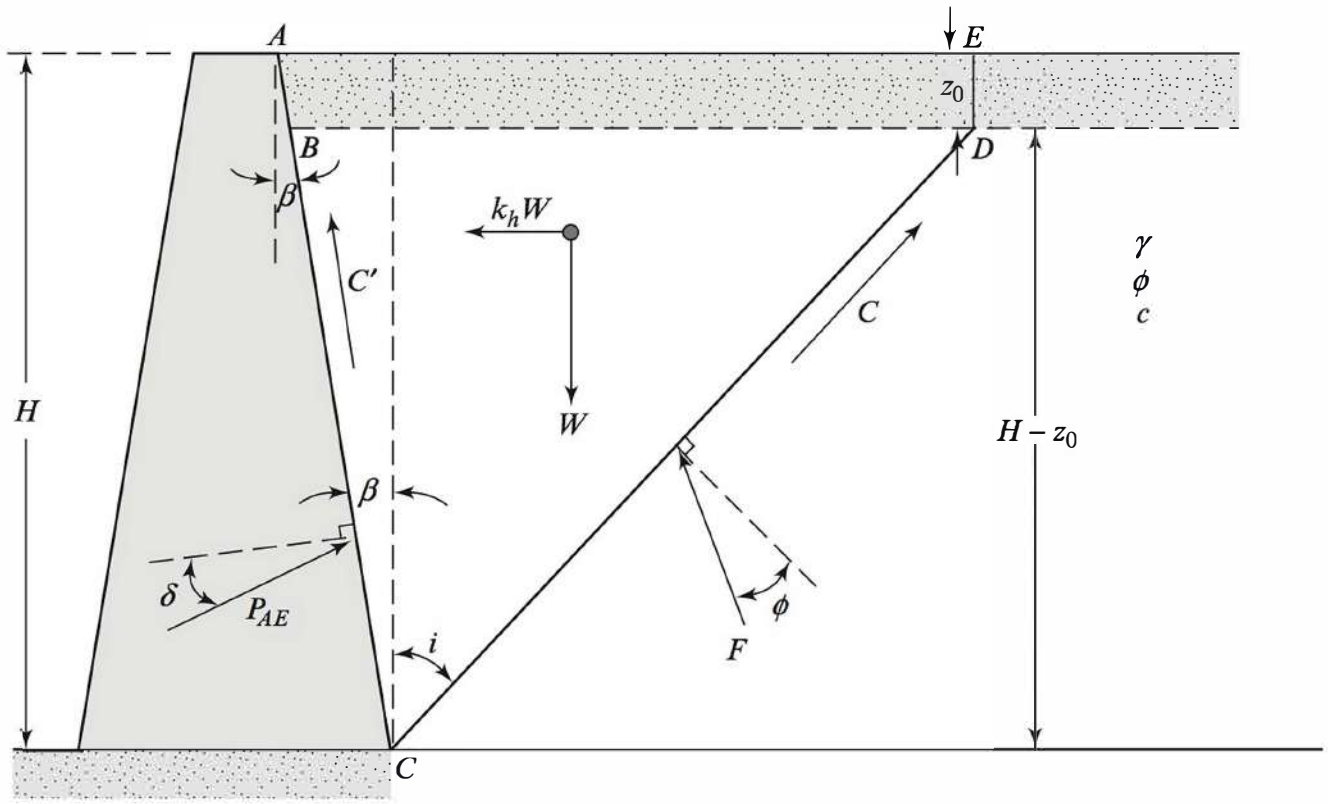

Figure 8.23 Trial failure wedge behind a retaining wall with C-ϕ backfill

e. Cohesive force along CD, $C = c(\overline{CD})$
f. Adhesive force along BC, $C' = c(\overline{BC})$

It is important to realize that the following two assumptions have been made:

1. The vertical inertia force ($k_v W$) has been taken to be zero.
2. The *unit adhesion* along the soil-wall interface (BC) has been taken to be equal to the cohesion (c) of the soil.

Considering these forces, we can show that

$$P_{AE} = \gamma(H - z_0)^2 N'_{a\gamma} - c(H - z_0) N'_{ac} \tag{8.45}$$

where

$$N'_{ac} = \frac{\cos\eta' \sec\beta + \cos\phi \sec i}{\sin(\eta' + \delta)} \tag{8.46}$$

$$N'_{a\gamma} = \frac{\left[(n + 0.5)(\tan\beta + \tan i) + n^2 \tan\beta\right]\left[\cos(i + \phi) + k_h \sin(i + \phi)\right]}{\sin(\eta' + \delta)} \tag{8.47}$$

in which

$$\eta' = \beta + i + \phi \tag{8.48}$$

$$n = \frac{z_0}{H - z_0} \tag{8.49}$$

Copyright 2017 Cengage Learning. All Rights Reserved. May not be copied, scanned, or duplicated, in whole or in part. Due to electronic rights, some third party content may be suppressed from the eBook and/or eChapter(s). Editorial review has deemed that any suppressed content does not materially affect the overall learning experience. Cengage Learning reserves the right to remove additional content at any time if subsequent rights restrictions require it.

The values of N'_{ac} and $N'_{a\gamma}$ can be determined by optimizing each coefficient separately. Thus, Eq. (8.45) gives the upper bound of P_{AE}.

For the static condition, $k_h = 0$. Thus,

$$P_{AE} = \gamma(H - z_0)^2 N_{a\gamma} - c\left(H - z_0\right) N_{ac} \tag{8.50}$$

The relationships for N_{ac} and $N_{a\gamma}$ can be determined by substituting $k_h = 0$ into Eqs. (8.46) and (8.47). Hence,

$$N_{ac} = N'_{ac} = \frac{\cos\eta' \sec\beta + \cos\phi \sec i}{\sin\left(\eta' + \delta\right)} \tag{8.51}$$

$$N_{a\gamma} = \frac{N'_{a\gamma}}{\lambda} = \frac{\left[\left(n + 0.5\right)\left(\tan\beta + \tan i\right) + n^2 \tan\beta\right]\left[\cos\left(i + \phi\right)\right]}{\sin\left(\eta' + \delta\right)} \tag{8.52}$$

The variations of $N_{ac}, N_{a\gamma}$ and λ with ϕ and θ are shown in Figures 8.24 through 8.27.

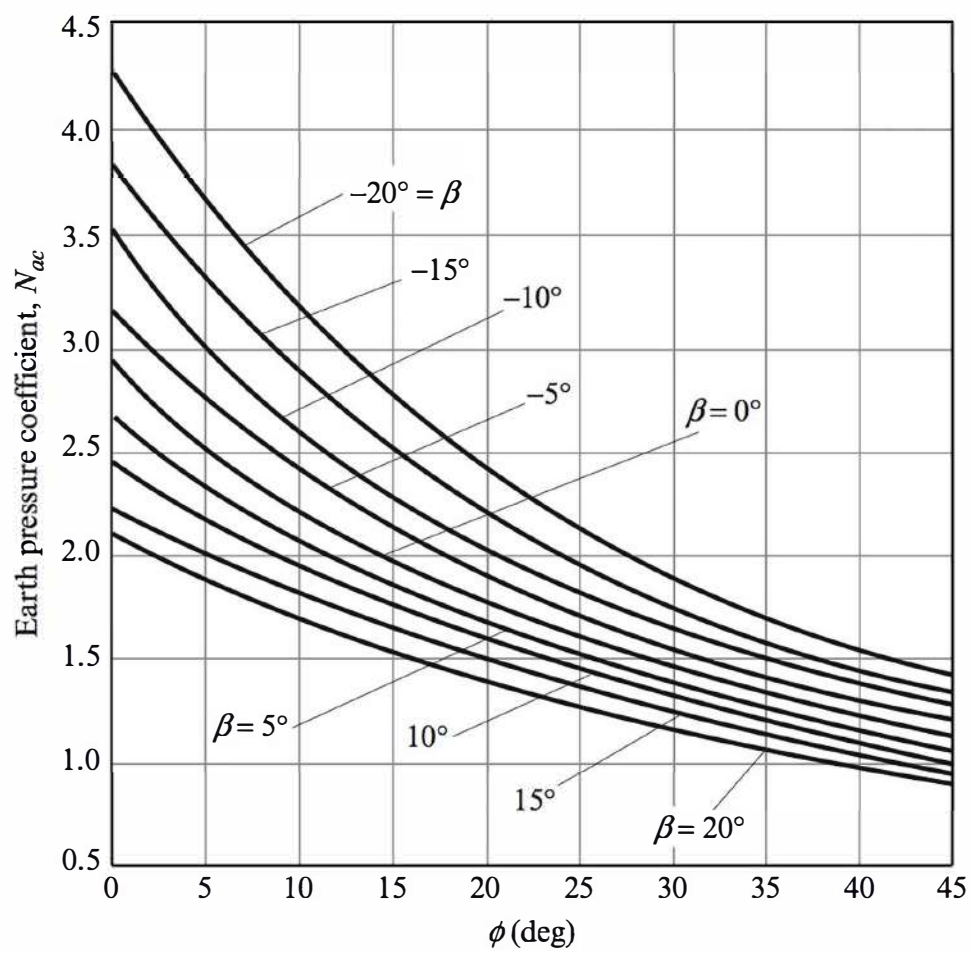

Figure 8.24 Variation of $N_{ac} = N'_{ac}$ with ϕ and β (Based on Prakash and Saran, 1966, and Saran and Prakash, 1968)

Source: Based on Prakash, S., and Saran, S. (1966). "Static and Dynamic Earth Pressure Behind Retaining Walls," *Proceedings, 3rd Symposium on Earthquake Engineering, Roorkee, India*, Vol. 1, pp. 277–288. Saran, S., and Prakash, S. (1968). "Dimensionless Parameters for Static and Dynamic Earth Pressure for Retaining Walls," *Indian Geotechnical Journal*, Vol. 7, No. 3, pp. 295–310.

Copyright 2017 Cengage Learning. All Rights Reserved. May not be copied, scanned, or duplicated, in whole or in part. Due to electronic rights, some third party content may be suppressed from the eBook and/or eChapter(s). Editorial review has deemed that any suppressed content does not materially affect the overall learning experience. Cengage Learning reserves the right to remove additional content at any time if subsequent rights restrictions require it.

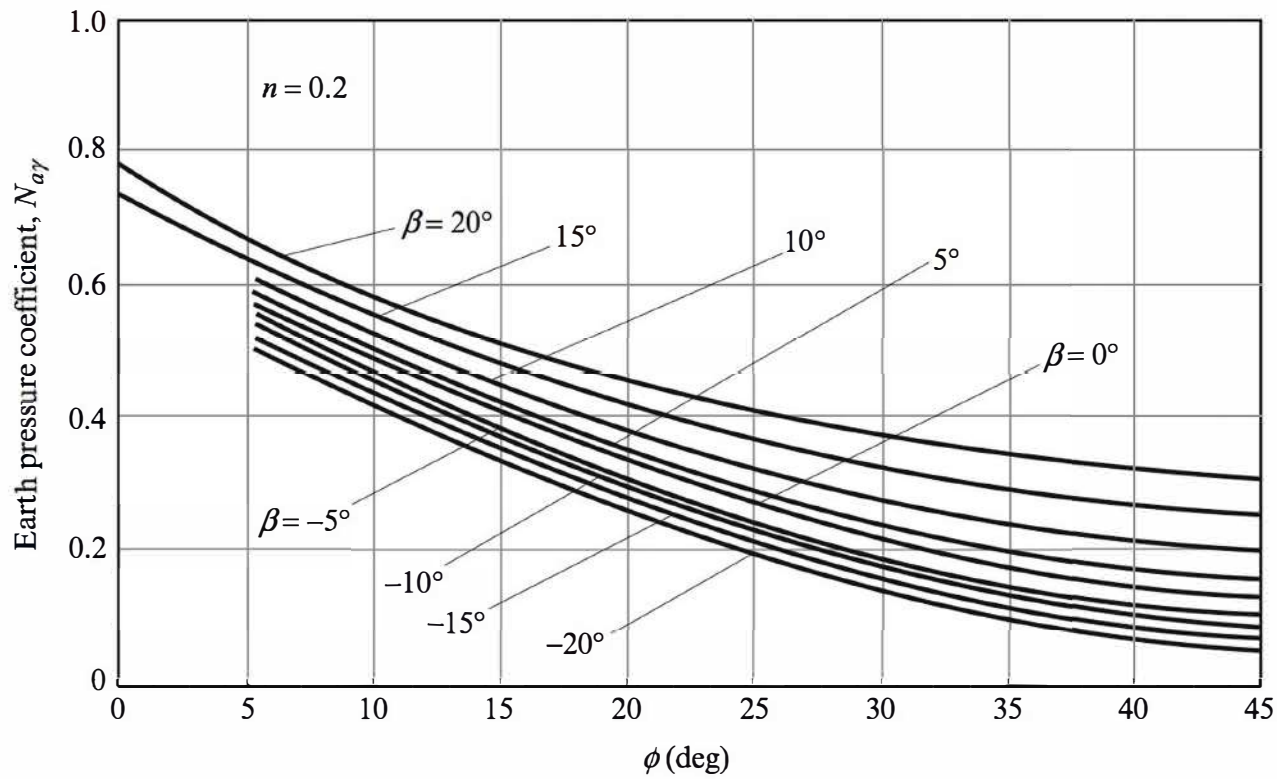

Figure 8.25 Variation of $N_{a\gamma}$ with ϕ and β ($n = 0.2$) (Based on Prakash and Saran, 1966, and Saran and Prakash, 1968)

Source: Based on Prakash, S., and Saran, S. (1966). "Static and Dynamic Earth Pressure Behind Retaining Walls," Proceedings, 3rd Symposium on Earthquake Engineering, Roorkee, India, Vol. 1, pp. 277–288. Saran, S., and Prakash, S. (1968). "Dimensionless Parameters for Static and Dynamic Earth Pressure for Retaining Walls," *Indian Geotechnical Journal*, Vol. 7, No. 3, pp. 295–310.

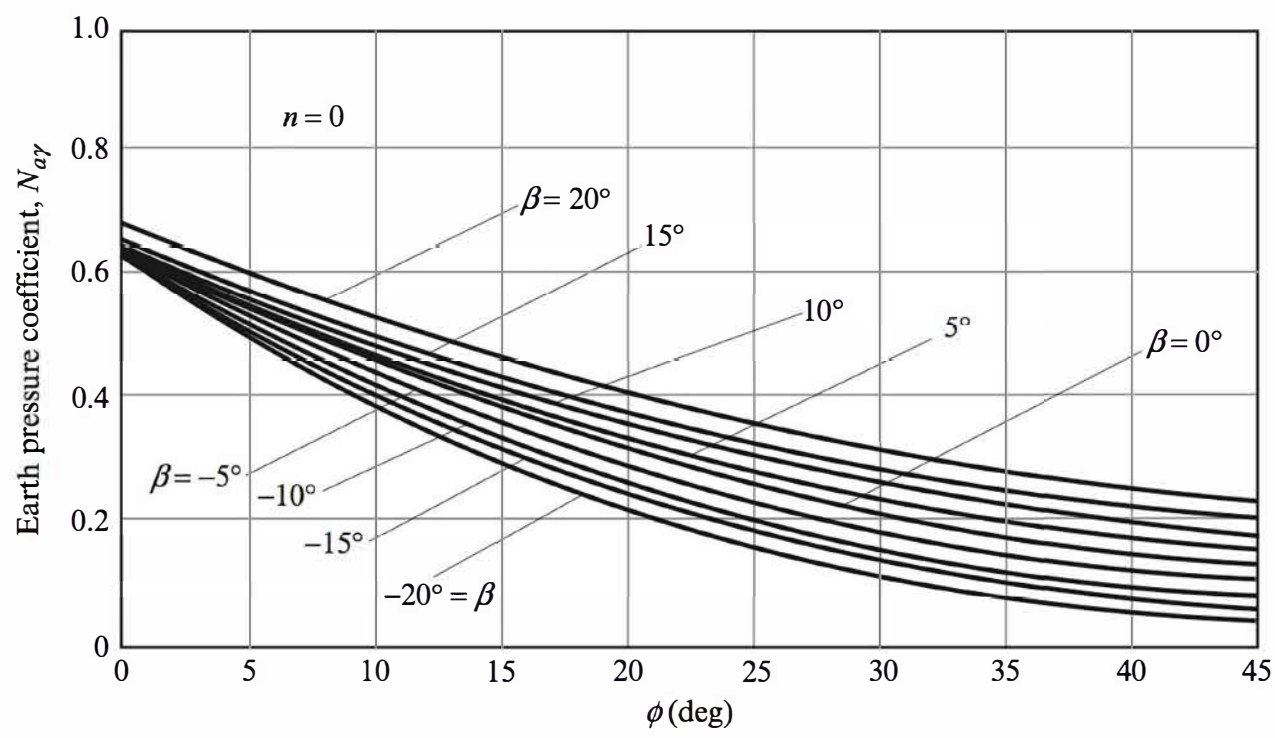

Figure 8.26 Variation of $N_{a\gamma}$ with ϕ and β ($n = 0$) (Based on Prakash and Saran, 1966, and Saran and Prakash, 1968)

Source: Based on Prakash, S., and Saran, S. (1966). "Static and Dynamic Earth Pressure Behind Retaining Walls," *Proceedings, 3rd Symposium on Earthquake Engineering, Roorkee, India*, Vol. 1, pp. 277–288. Saran, S., and Prakash, S. (1968). "Dimensionless Parameters for Static and Dynamic Earth Pressure for Retaining Walls," *Indian Geotechnical Journal*, Vol. 7, No. 3, pp. 295–310.

Copyright 2017 Cengage Learning. All Rights Reserved. May not be copied, scanned, or duplicated, in whole or in part. Due to electronic rights, some third party content may be suppressed from the eBook and/or eChapter(s). Editorial review has deemed that any suppressed content does not materially affect the overall learning experience. Cengage Learning reserves the right to remove additional content at any time if subsequent rights restrictions require it.

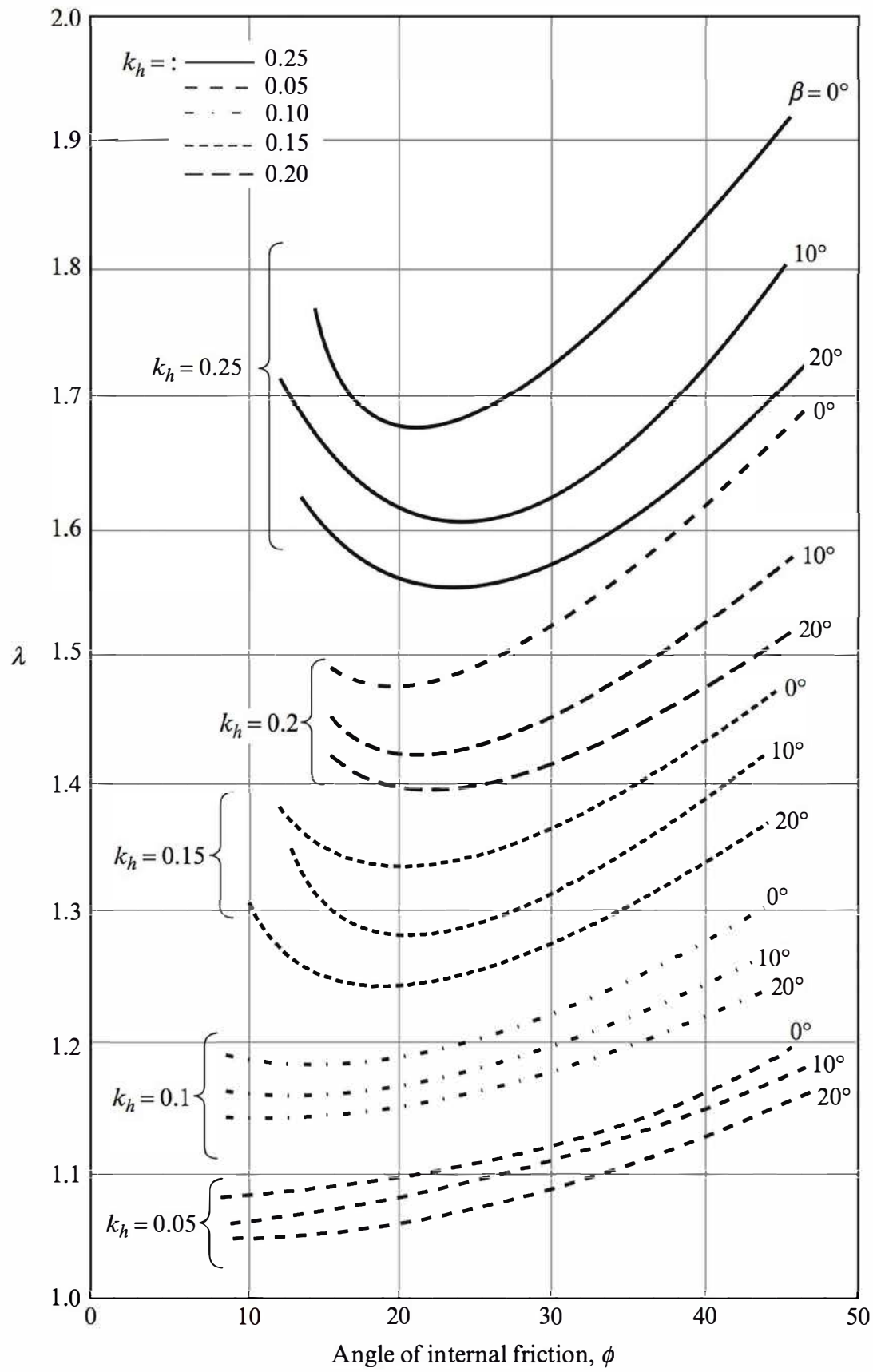

Figure 8.27 Variation of λ with k_h, ϕ and β (Based on Prakash and Saran, 1966, and Saran and Prakash, 1968)

Source: Based on Prakash, S., and Saran, S. (1966). "Static and Dynamic Earth Pressure Behind Retaining Walls," *Proceedings, 3rd Symposium on Earthquake Engineering, Roorkee, India*, Vol. 1, pp. 277–288. Saran, S., and Prakash, S. (1968). "Dimensionless Parameters for Static and Dynamic Earth Pressure for Retaining Walls," *Indian Geotechnical Journal*, Vol. 7, No. 3, pp. 295–310.

Copyright 2017 Cengage Learning. All Rights Reserved. May not be copied, scanned, or duplicated, in whole or in part. Due to electronic rights, some third party content may be suppressed from the eBook and/or eChapter(s). Editorial review has deemed that any suppressed content does not materially affect the overall learning experience. Cengage Learning reserves the right to remove additional content at any time if subsequent rights restrictions require it.

EXAMPLE 8.4

For a retaining wall, the following are given.

- $H = 8.54$ m
- $\beta = +10°$
- $\phi = 20°$
- $c = 10.06$ kN/m^2
- $\gamma = 18.55$ kN/m^3
- $k_h = 0.1$ and $k_v = 0$

Determine the magnitude of the active force, P_{AE}.

SOLUTION:

From Eq. (8.43),

$$z_0 = \frac{2c}{\gamma\sqrt{K_a}} = \frac{2c}{\gamma \tan\left(45 - \frac{\phi'}{2}\right)} = \frac{(2)(10.06)}{(18.55)\tan\left(45 - \frac{20}{2}\right)} = 1.55 \text{ m}$$

From Eq. [8.49]

$$n = \frac{z_0}{H - z_0} = \frac{1.55}{8.54 - 1.55} = 0.22 \approx 0.2$$

From Eqs. (8.45), (8.51), and (8.52).

$$P_{AE} = \gamma(H - z_0)^2(\lambda N_{a\gamma}) - c(H - z_0)N_{ac}$$

For $\beta = 10°$, $\phi = 20°$, $k_h = 0.1$, and $n \approx 0.2$,

$$N_{ac} = 1.60 \quad \text{(Figure 8.24)}$$
$$N_{a\gamma} = 0.375 \quad \text{(Figure 8.25)}$$
$$\lambda = 1.17 \quad \text{(Figure 8.27)}$$

Thus,

$$P_{AE} = (18.55)(8.54 - 1.55)^2(1.17 \times 0.375) - (10.06)(8.54 - 1.55)(1.60)$$
$$= \mathbf{285.15\ kN/m}$$

B. Analysis of Shukla, Gupta, and Sivakugan (2009)

Shukla et al. (2009) developed a procedure for estimation of P_{AE} for a retaining wall with a vertical back face and horizontal backfill with a $c - \phi$ (Figure 8.28a). In Figure 8.28a, ABC is the trial failure wedge. The following assumptions have been made in the analysis:

1. The effect of tensile crack is not taken into account.
2. The friction and adhesion between the back face of the wall and the backfill are neglected.

Copyright 2017 Cengage Learning. All Rights Reserved. May not be copied, scanned, or duplicated, in whole or in part. Due to electronic rights, some third party content may be suppressed from the eBook and/or eChapter(s). Editorial review has deemed that any suppressed content does not materially affect the overall learning experience. Cengage Learning reserves the right to remove additional content at any time if subsequent rights restrictions require it.

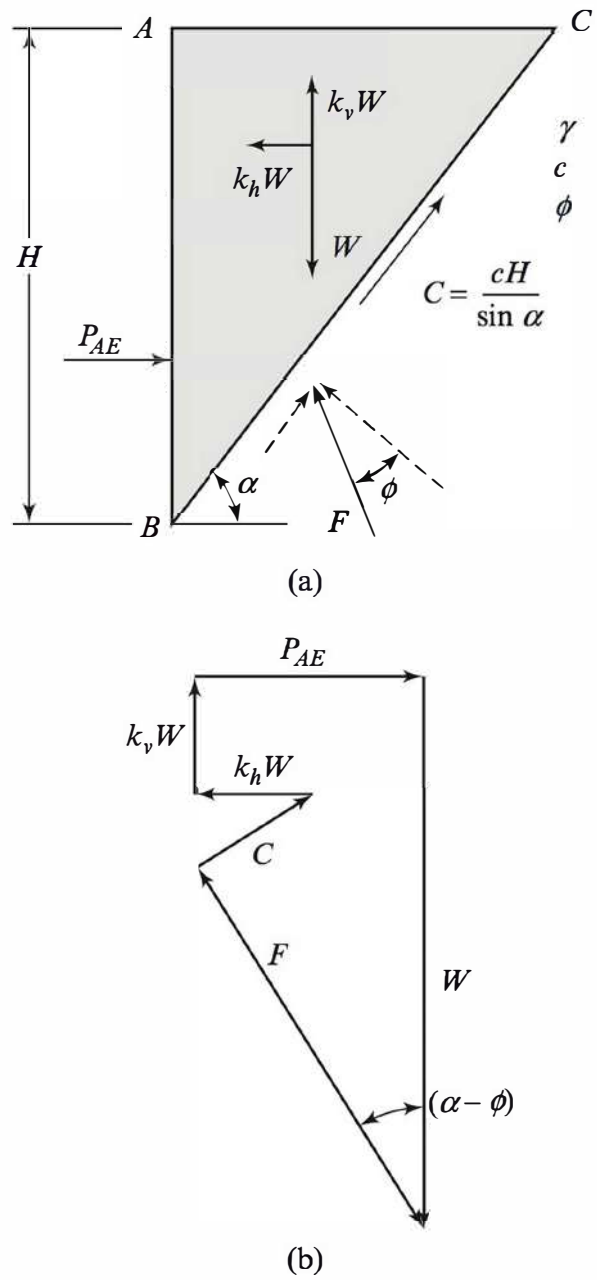

Figure 8.28 Estimation of P_{AE} with $c - \phi$ backfill: (a) trial failure wedge, (b) force polygon

Figure 8.28b shows the polygon for all the forces acting on the wedge ABC. The notations are similar to those shown in Figure 8.23. According to this analysis, the critical wedge angle $\alpha = \alpha_c$ for maximum value of P_{AE} can be given as

$$\tan\alpha_c = \frac{\sin\phi\sin(\phi-\theta) + m\sin 2\phi + \left[\begin{array}{l}\sin\phi\sin(\phi-\theta)\cos\theta \\ +4m^2\cos^2\phi + 2m\cos\phi \\ \{\sin\phi\cos\theta + \sin(\phi-\theta)\}\end{array}\right]^{0.5}}{\sin\phi\cos(\phi-\bar{\beta}) + 2m\cos^2\phi} \tag{8.53}$$

where

$$m = \frac{c'\cos\theta}{\gamma H(1-k_v)} \tag{8.54}$$

Copyright 2017 Cengage Learning. All Rights Reserved. May not be copied, scanned, or duplicated, in whole or in part. Due to electronic rights, some third party content may be suppressed from the eBook and/or eChapter(s). Editorial review has deemed that any suppressed content does not materially affect the overall learning experience. Cengage Learning reserves the right to remove additional content at any time if subsequent rights restrictions require it.

For definition of θ, see Eq. (8.6).

Thus, the magnitude of P_{AE} can be expressed as

$$\frac{P_{AE}}{\gamma H^2} = P_{AE}^* = \frac{1}{2}(1 - k_v)K_{AE\gamma} - c^* K_{AEc} \tag{8.55}$$

where

$$c^* = \frac{c}{\gamma H} \tag{8.56}$$

$$K_{AE\gamma} = \frac{\cos(\phi - \theta) - \dfrac{\sin(\phi - \theta)}{\tan \alpha_c}}{\cos \theta(\cos \phi + \tan \alpha_c \sin \phi)} \tag{8.57}$$

$$K_{AEc} = \frac{\cos \phi\,(1 + \tan^2 \alpha_c)}{\tan \alpha_c(\cos \phi + \tan \alpha_c \sin \phi)} \tag{8.58}$$

Figure 8.29 gives plots of P_{AE}^* against ϕ for various values of c^* and k_h ($k_v = 0$).

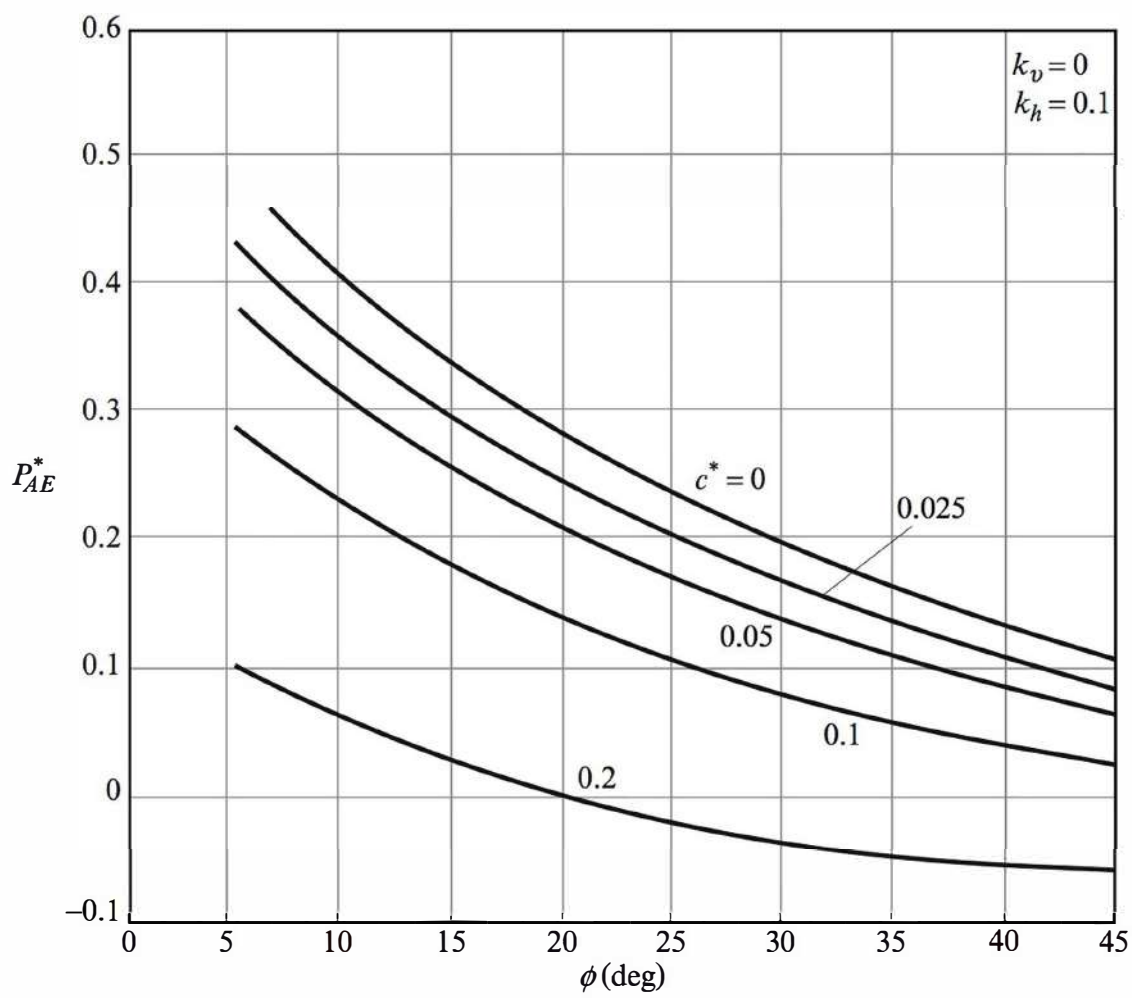

(a)

Figure 8.29 Plot of P_{AE}^* vs. ϕ for various values of c^*: (a) $k_h = 0.1$, (b) $k_h = 0.2$, (c) $k_h = 0.3$, (d) $k_h = 0.4$ (Note: $k_v = 0$)

Copyright 2017 Cengage Learning. All Rights Reserved. May not be copied, scanned, or duplicated, in whole or in part. Due to electronic rights, some third party content may be suppressed from the eBook and/or eChapter(s). Editorial review has deemed that any suppressed content does not materially affect the overall learning experience. Cengage Learning reserves the right to remove additional content at any time if subsequent rights restrictions require it.

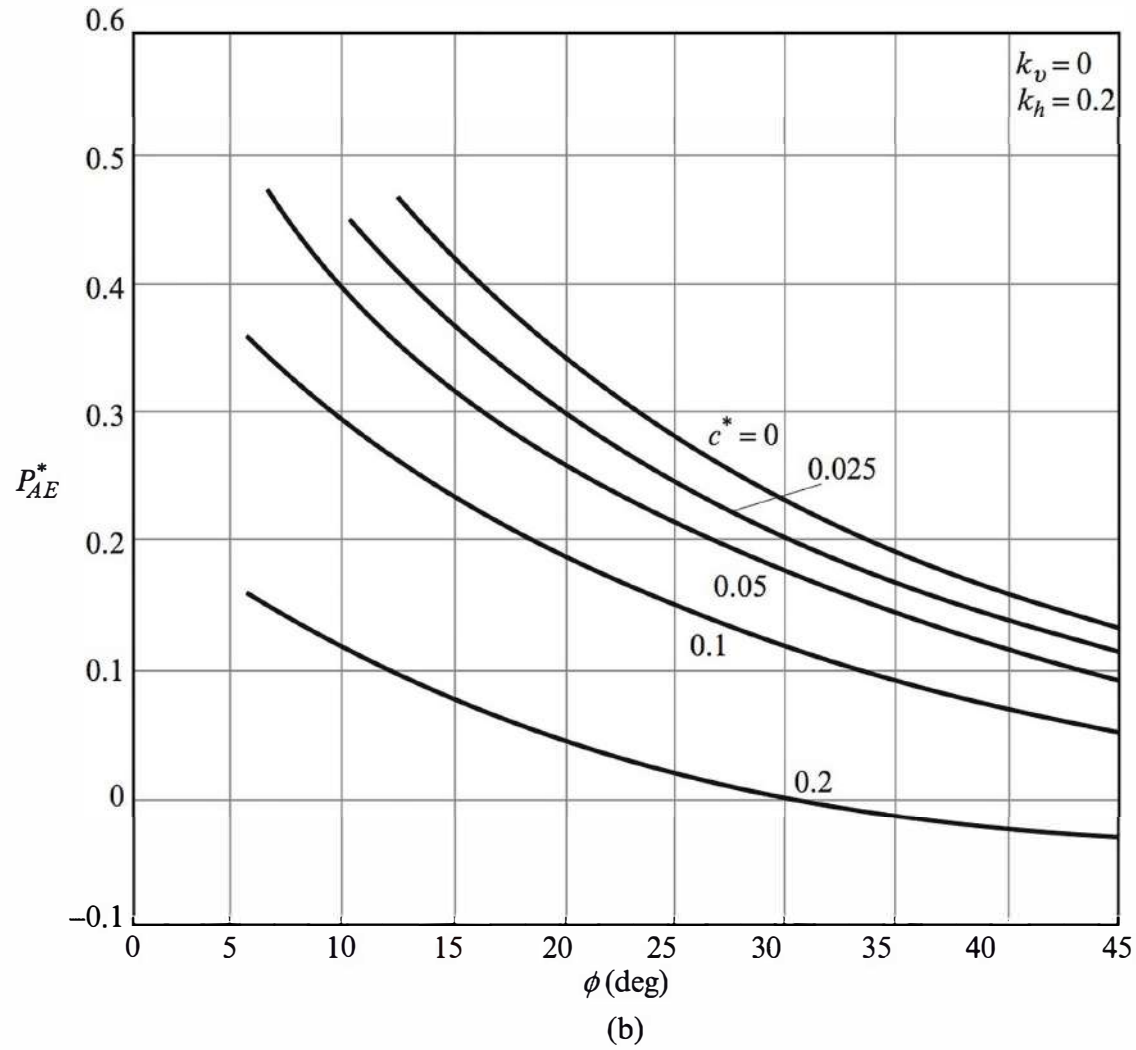

(b)

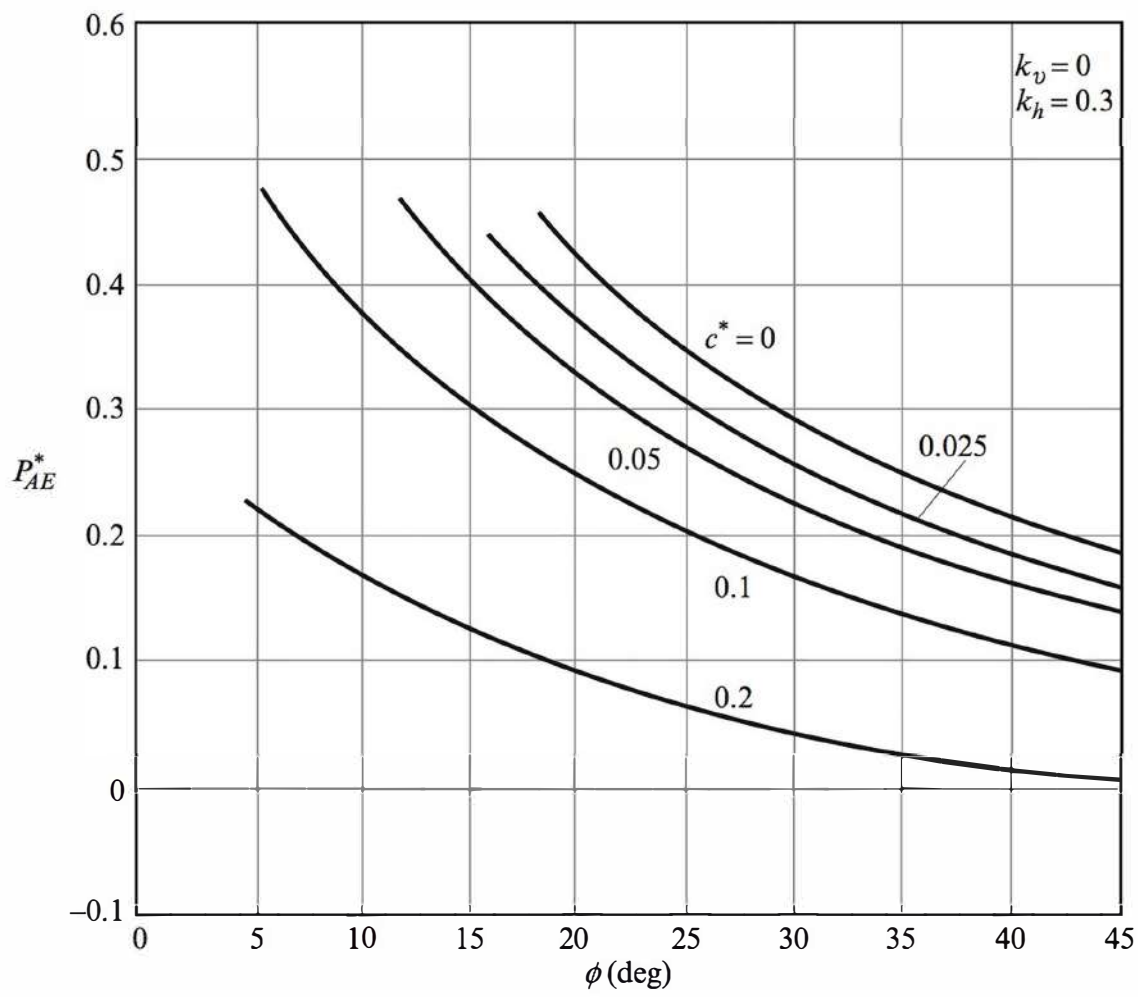

(c)

Figure 8.29 (*Continued*)

Copyright 2017 Cengage Learning. All Rights Reserved. May not be copied, scanned, or duplicated, in whole or in part. Due to electronic rights, some third party content may be suppressed from the eBook and/or eChapter(s). Editorial review has deemed that any suppressed content does not materially affect the overall learning experience. Cengage Learning reserves the right to remove additional content at any time if subsequent rights restrictions require it.

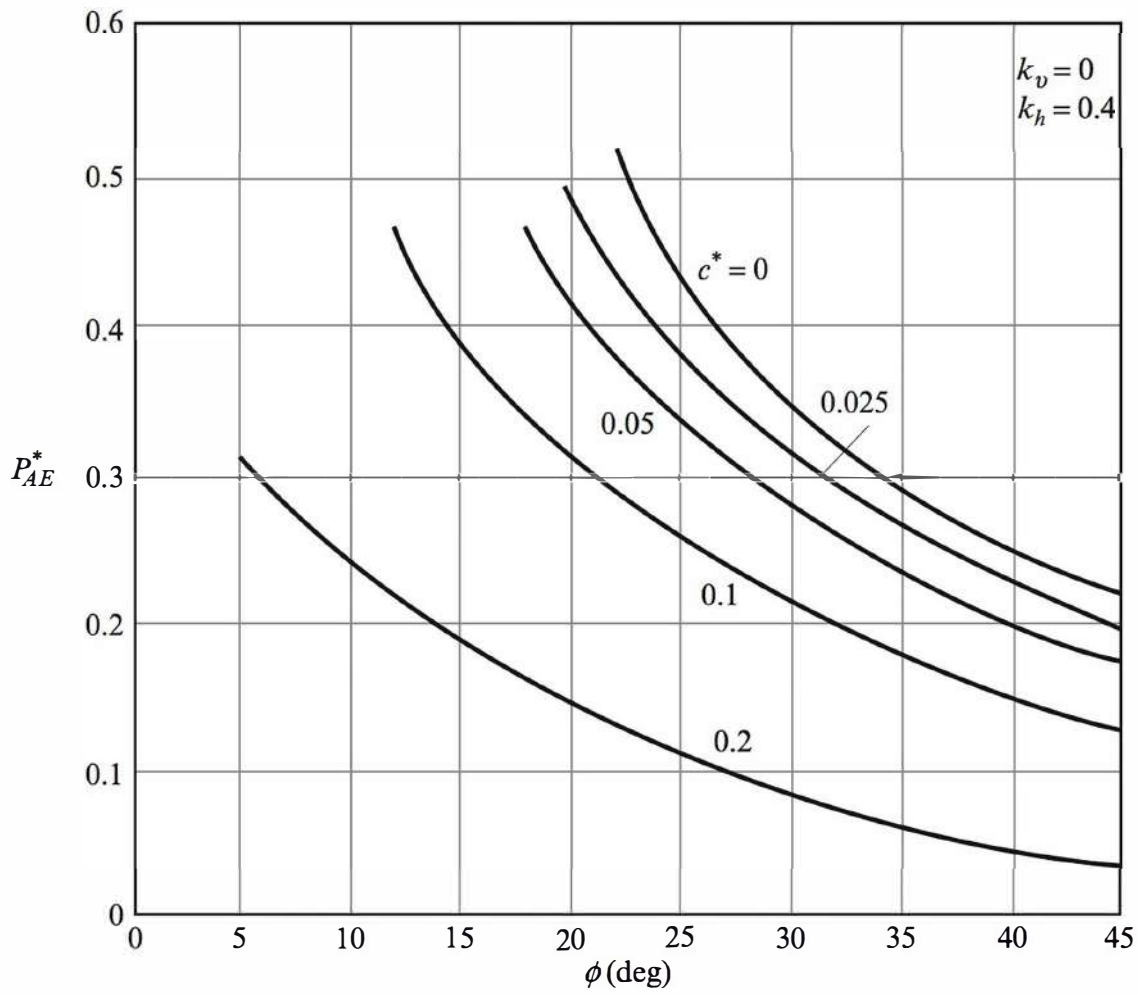

(d)

Figure 8.29 (*Continued*)

EXAMPLE 8.5

For a retaining wall with a vertical backfill, the following are given.

- $H = 8.54$ m
- $\phi = 20°$
- $c = 7.9$ kN/m^2
- $\gamma = 18.55$ kN/m^3
- $k_h = 0.1$, $k_v = 0$

Determine the magnitude of the active force, P_{AE}

SOLUTION:

From Eq. (8.56),

$$c^* = \frac{c}{\gamma H} = \frac{7.9}{(18.55)(8.54)} = 0.0499 \approx 0.05$$

$$\phi = 20°$$

From Figure 8.29a, for $\phi = 20°$ and $c^* = 0.05$, the value of $P^*_{AE} \approx 0.21$. Hence

$$P_{AE} = P^*_{AE}\gamma H^2 = (0.21)(18.55)(8.54)^2 = \mathbf{284.1\ kN/m}$$

Copyright 2017 Cengage Learning. All Rights Reserved. May not be copied, scanned, or duplicated, in whole or in part. Due to electronic rights, some third party content may be suppressed from the eBook and/or eChapter(s). Editorial review has deemed that any suppressed content does not materially affect the overall learning experience. Cengage Learning reserves the right to remove additional content at any time if subsequent rights restrictions require it.

8.12 DYNAMIC PASSIVE FORCE ON RETAINING WALL (GRANULAR SOIL)

Figure 8.30 shows a retaining wall having a granular soil as the backfill material. If the wall is pushed toward the soil mass, at a certain stage failure in the soil will occur along a plane BC. At failure the force, P_{PE}, per unit length of the retaining wall is the dynamic passive force. The force per unit length of the wall that needs to be considered for equilibrium of the soil wedge is shown in Figure 8.30. The notations W, ϕ, δ, γ, k_h, and k_v have the same meaning as described in Figure 8.2 (Section 8.2). Using the basic assumptions for the soil given in Section 8.2, the passive force (P_{PE}) may also be derived as (Kapila, 1962)

$$P_{PE} = \frac{1}{2}\gamma H^2(1-k_v)K_{PE} \tag{8.59}$$

where

$$K_{PE} = \frac{\cos^2(\phi+\beta-\theta)}{\cos\theta\cos^2\beta\cos(\delta-\beta+\theta)\left[1-\left\{\frac{\sin(\phi+\delta)\sin(\phi+i-\theta)}{\cos(i-\beta)\cos(\delta-\beta+\theta)}\right\}^{1/2}\right]^2} \tag{8.60}$$

and

$$\theta = \tan^{-1}[k_h/(1-k_v)]$$

Note that Eq. (8.59) has been derived for dry cohesionless backfill. Kapila has also developed a graphical procedure for determination of P_{PE}.

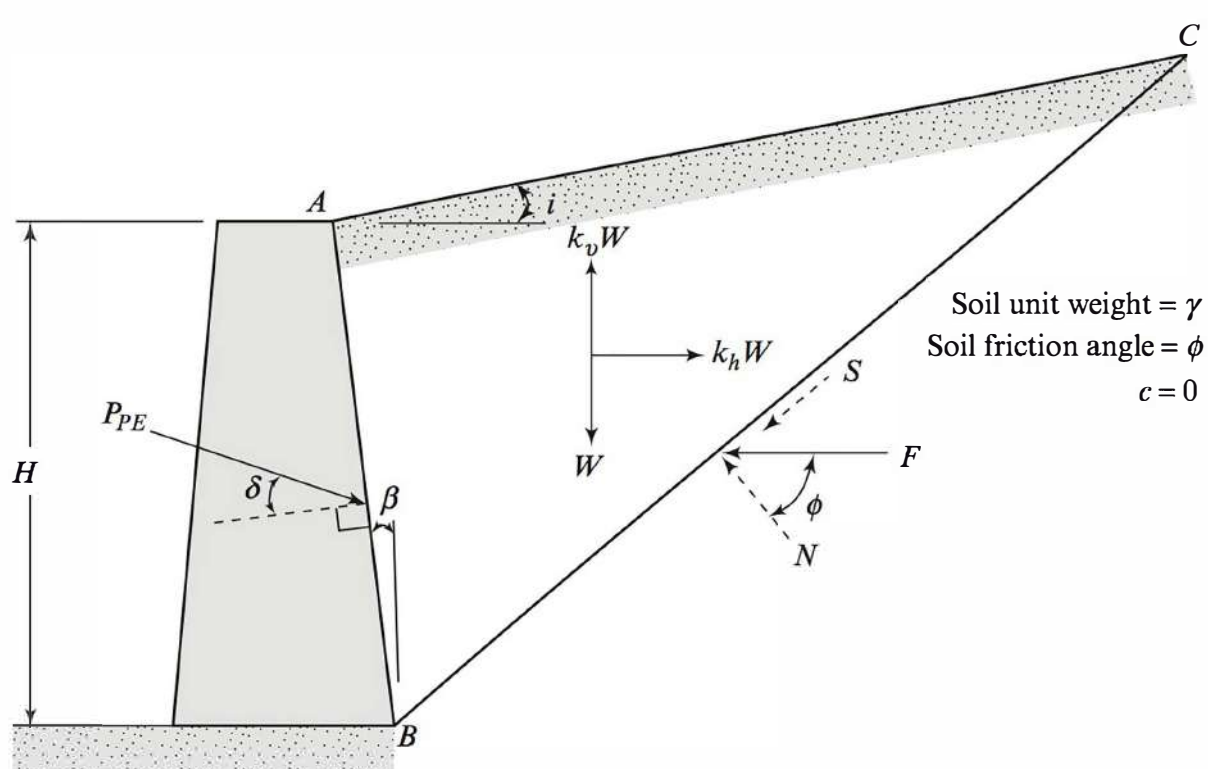

Figure 8.30 Passive force, P_{PE}, on a retaining wall

Copyright 2017 Cengage Learning. All Rights Reserved. May not be copied, scanned, or duplicated, in whole or in part. Due to electronic rights, some third party content may be suppressed from the eBook and/or eChapter(s). Editorial review has deemed that any suppressed content does not materially affect the overall learning experience. Cengage Learning reserves the right to remove additional content at any time if subsequent rights restrictions require it.

Figure 8.31 shows the variation of K_{PE} for various values of soil friction angle ϕ and k_h (with $k_v = i = \beta = \delta = 0$). From the figure it can be seen that, with other parameters remaining the same, the magnitude of K_{PE} increases with the increase of soil friction angle ϕ.

Figure 8.32 shows the influence of the backfill slope angle of K_{PE}. Other factors remaining constant, the magnitude of K_{PE} increases with increase of i.

A more advanced analysis based on kinematical method of limit analysis on seismic passive earth pressure coefficients can be found in Soubra (2000). According to this solution, the passive force can be expressed [Eq. (8.59)]. The variation of K_{PE} for $i = 0$, $\beta = 0$, $k_v = 0$, and $c = 0$ obtained by Soubra (2000) has been compiled and given in Table 8.9.

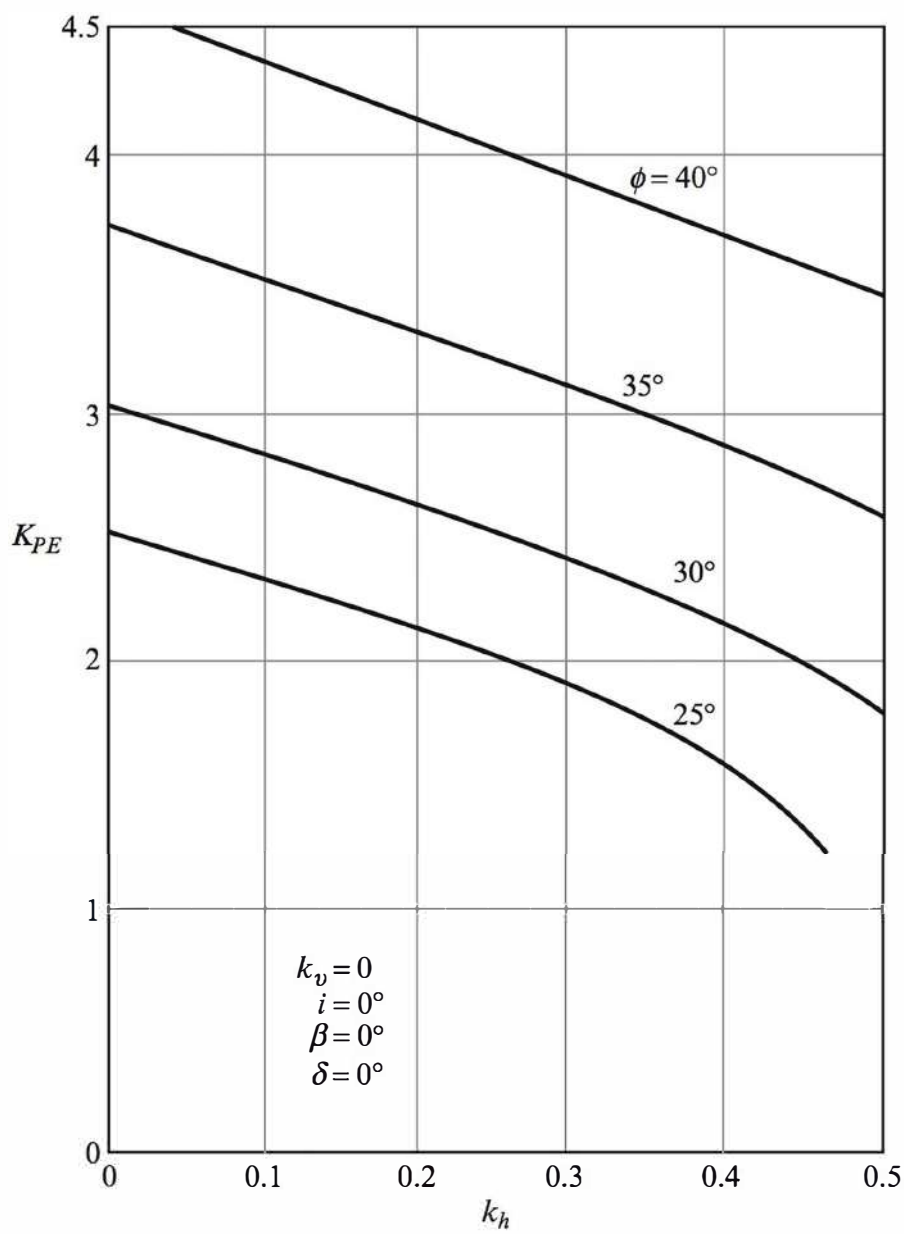

Figure 8.31 Variation of K_{PE} with soil friction angle and k_h (from Davies, Richards, and Chen, 1986)

Source: Davies, T.G., Richards, R., and Chen, K.H. (1986). "Passive Pressure during Seismic Loading," *Journal of Geotechnical Engineering*, ASCE, Vol. 112, No. GT4, pp. 479–484. With permission from ASCE.

Copyright 2017 Cengage Learning. All Rights Reserved. May not be copied, scanned, or duplicated, in whole or in part. Due to electronic rights, some third party content may be suppressed from the eBook and/or eChapter(s). Editorial review has deemed that any suppressed content does not materially affect the overall learning experience. Cengage Learning reserves the right to remove additional content at any time if subsequent rights restrictions require it.

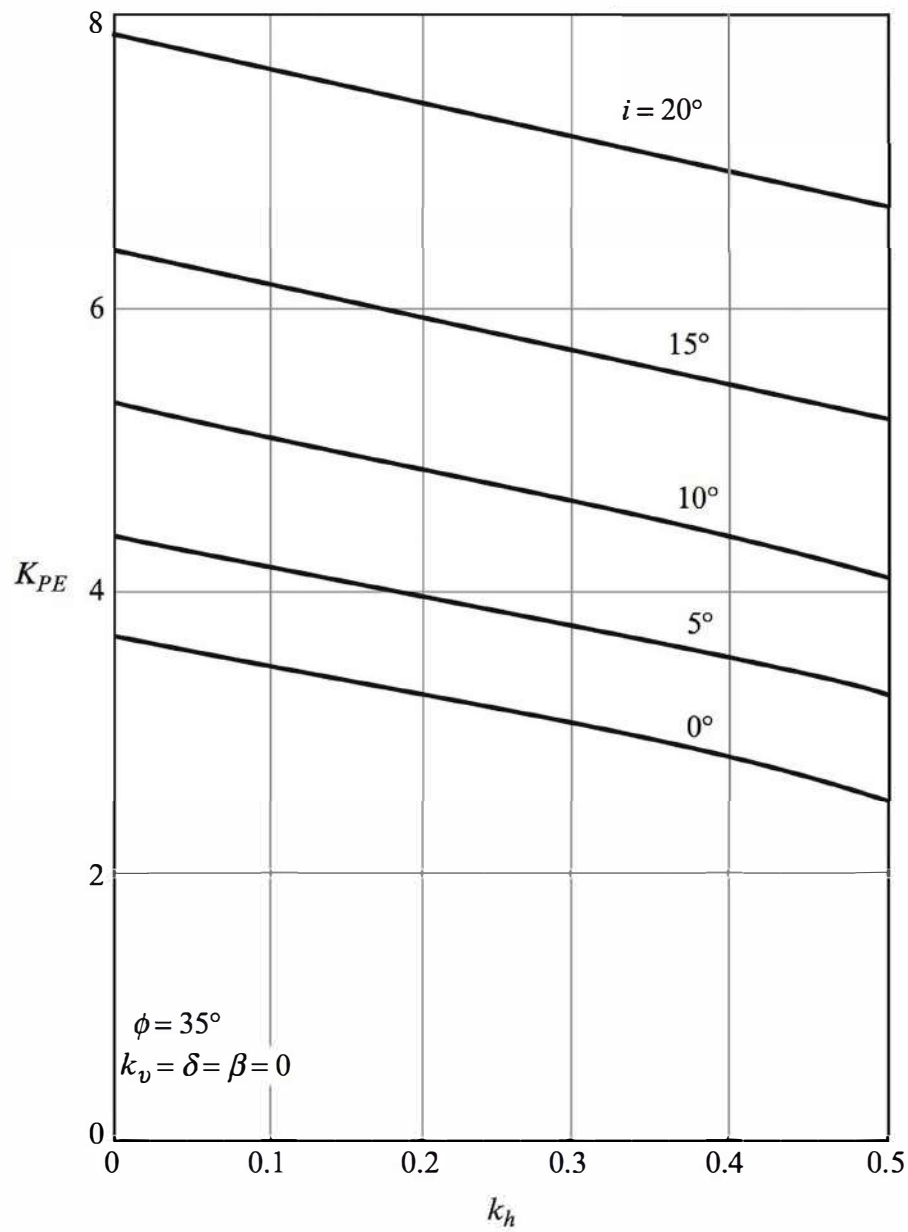

Figure 8.32 Influence of backfill slope on K_{PE} (from Davies, Richards, and Chen, 1986)

Source: Davies, T.G., Richards, R., and Chen, K.H. (1986). "Passive Pressure during Seismic Loading," *Journal of Geotechnical Engineering*, ASCE, Vol. 112, No. GT4, pp. 479–484. With permission from ASCE.

Table 8.9 Variation of K_{PE} for $i = 0$, $\beta = 0$, and $k_v = 0$ (compiled from Soubra, 2000)

		ϕ(deg)				
δ/ϕ	k_h	25	30	35	40	45
0	0	2.46	3.0	3.69	4.6	5.83
	0.1	2.30	3.82	3.49	4.38	5.58
	0.2	2.12	2.63	3.29	4.15	5.33
	0.3	1.91	2.42	3.06	3.91	5.07
1/3	0	3.08	4.05	5.48	7.70	11.35
	0.1	2.84	3.77	5.14	7.27	10.78
	0.2	2.58	3.47	4.78	6.81	10.19

Copyright 2017 Cengage Learning. All Rights Reserved. May not be copied, scanned, or duplicated, in whole or in part. Due to electronic rights, some third party content may be suppressed from the eBook and/or eChapter(s). Editorial review has deemed that any suppressed content does not materially affect the overall learning experience. Cengage Learning reserves the right to remove additional content at any time if subsequent rights restrictions require it.

		ϕ(deg)				
δ/ϕ	k_h	25	30	35	40	45
	0.3	2.28	3.13	4.39	6.33	9.57
1/2	0	3.43	4.69	6.67	9.99	15.98
	0.1	3.15	4.35	6.24	9.40	15.15
	0.2	2.85	3.99	5.78	8.79	14.29
	0.3	2.5	3.59	5.19	8.15	13.40
2/3	0	3.79	5.40	8.06	12.83	22.22
	0.1	3.48	5.00	7.53	12.08	21.06
	0.2	3.14	4.57	6.96	11.28	19.86
	0.3	2.74	4.10	6.35	10.44	18.61

Source: Based on data from Soubra, A.-H. (2000). "Static and Seismic Passive Earth Pressure Coefficients on Rigid Retaining Structures," *Canadian Geotechnical Journal*, Vol. 37, pp. 463–478.

EXAMPLE 8.6

Consider a retaining wall with the following:

$H = 4$ m $\quad \gamma = 17$ kN/m^3

$\beta = 0 \quad \delta/\phi = 2/3$

$i = 0 \quad k_h = 0.2$

$\phi = 30° \quad k_v = 0$

Estimate the passive force P_{PE}

a. Using Eqs. (8.59) and (8.60)
b. Using Eq. (8.59) and Table 8.9

SOLUTION:

a. $$\theta = \tan^{-1}\left(\frac{k_h}{1-k_v}\right) = \tan^{-1}\left(\frac{0.2}{1-0}\right) = 11.3°$$

$\delta/\phi = 2/3; \delta = 2/3(30) = 20°.$

Substituting $i = 0$, $\beta = 0$, $\phi = 30°$, and $\delta = 20°$ in Eq. (8.60), we obtain $K_{PE} = 4.975$. Eq. (8.59):

$$P_{AE} = \frac{1}{2}\gamma H^2(1-k_v)K_{PE} = \frac{1}{2}(17)(4)^2(1-0)(4.975) = \mathbf{676.6\ kN/m}$$

b. From Table 8.9, for $k_h = 0.2$, $\delta/\phi = 2/3$, and $\phi = 30°$, the value of $K_{PE} = 4.75$.

$$P_{PE} = \frac{1}{2}(17)(4)^2(1-0)(4.57) = \mathbf{621.52\ kN/m}$$

Copyright 2017 Cengage Learning. All Rights Reserved. May not be copied, scanned, or duplicated, in whole or in part. Due to electronic rights, some third party content may be suppressed from the eBook and/or eChapter(s). Editorial review has deemed that any suppressed content does not materially affect the overall learning experience. Cengage Learning reserves the right to remove additional content at any time if subsequent rights restrictions require it.

8.13 DYNAMIC PASSIVE FORCE WITH C–ϕ SOIL BACKFILL

Shukla, Sivakugan, and Das (2011) developed an expression for passive force on a retaining wall (A_1A_2) of height H with a vertical back face and horizontal backfill with c–ϕ soil with a surcharge of q/unit area as shown in Figure 8.33a. In this analysis, the friction and adhesion between the back face of the wall and the backfill were neglected. Figures 8.33b and 8.33c show the force polygons

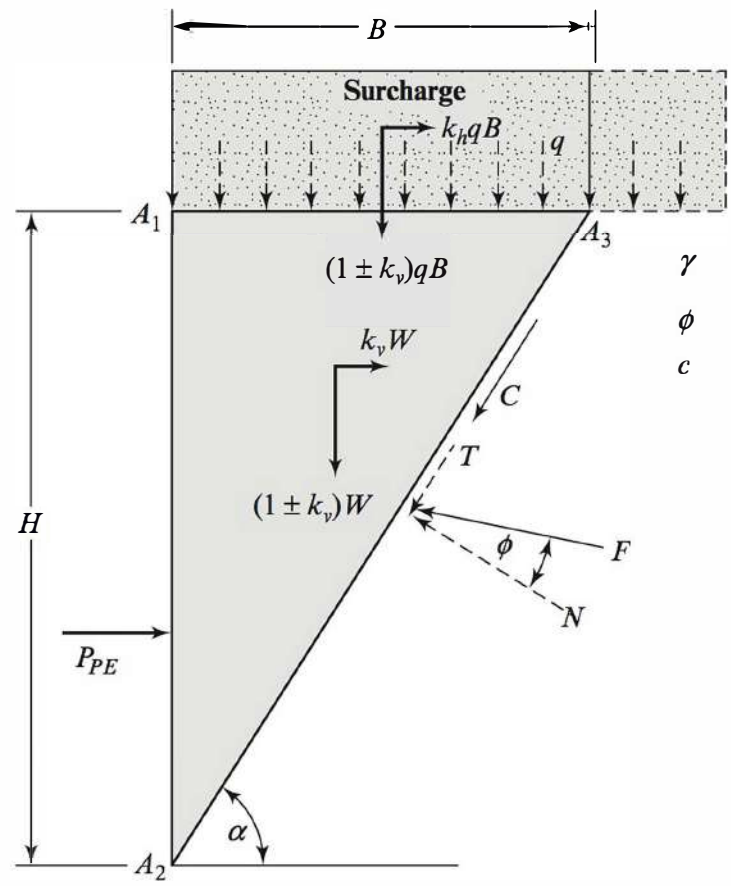

(a)

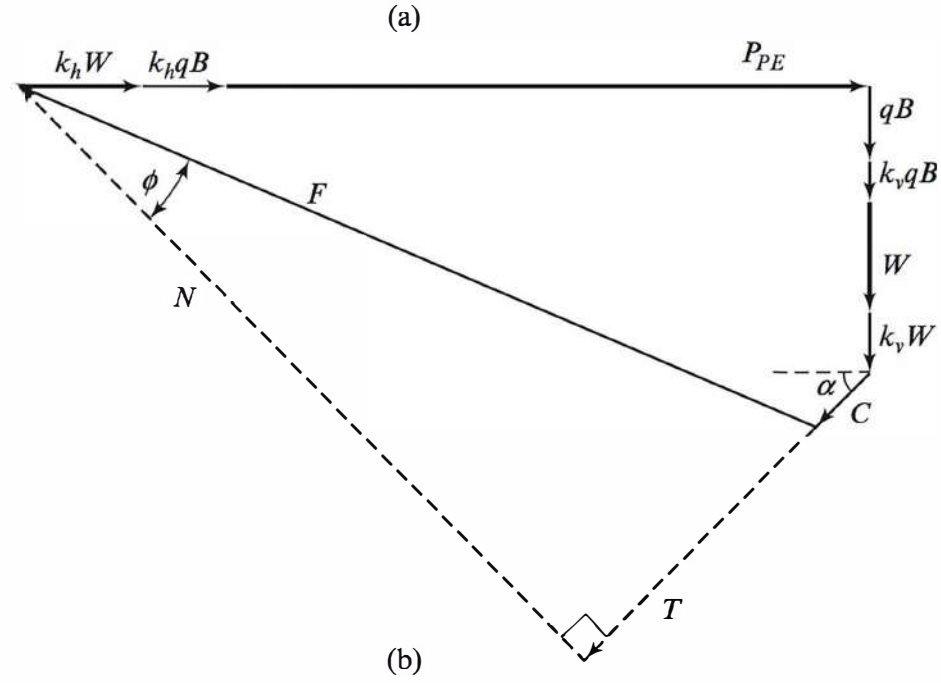

(b)

Figure 8.33 (a) Trial failure wedge; (b) force polygon when the vertical seismic inertial force acts downward; and (c) force polygon when the vertical seismic inertial force acts vertically upward

Copyright 2017 Cengage Learning. All Rights Reserved. May not be copied, scanned, or duplicated, in whole or in part. Due to electronic rights, some third party content may be suppressed from the eBook and/or eChapter(s). Editorial review has deemed that any suppressed content does not materially affect the overall learning experience. Cengage Learning reserves the right to remove additional content at any time if subsequent rights restrictions require it.

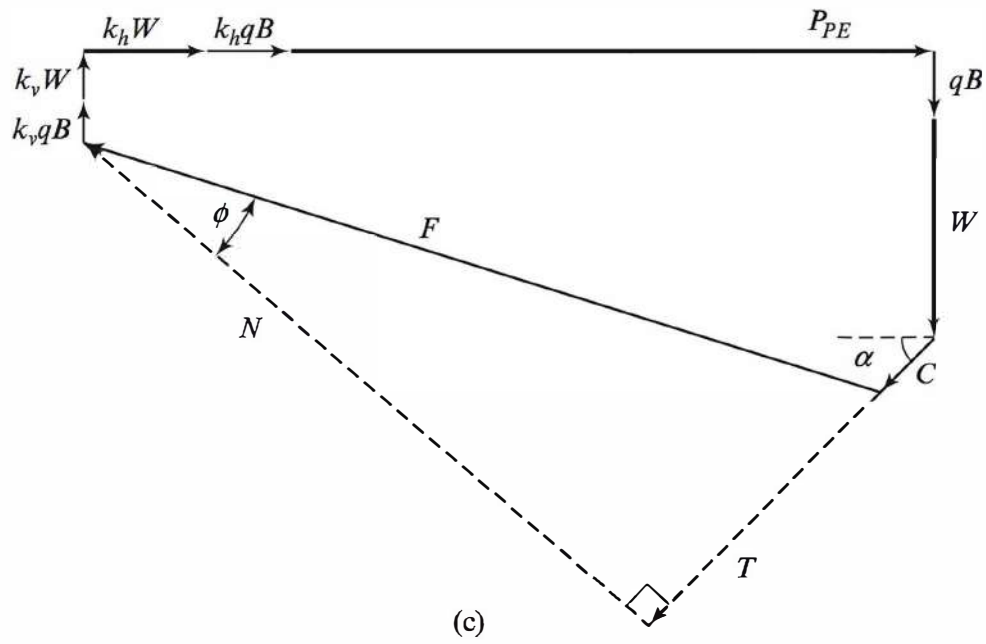

Figure 8.33 (*Continued*)

when the seismic inertial force acts vertically downwards and upwards, respectively. Note that N and T are the normal and tangential component forces due to friction along the trial failure surface A_2A_3 which makes an angle α with the horizontal, and F is the resultant of N and T. Also, $C = (c)(\overline{A_2A_3})$ and W = weight of the trial wedge per unit length of the wall $= \frac{1}{2}\gamma HB$.

According to this solution,

$$P_{PE} = (1 \pm k_v)\left(q + \tfrac{1}{2}\gamma H\right)HK_{PE\gamma} + cHK_{PEC} \tag{8.61}$$

where

$$K_{PE\gamma} = \frac{\dfrac{(\cos\phi - \theta) + \sin(\phi - \theta)}{\tan\alpha_c}}{(\cos\phi - \sin\phi\tan\alpha_c)\cos\theta} \tag{8.62}$$

$$K_{PEC} = \frac{(1 + \tan^2\alpha_c)\cos\phi}{(\cos\phi - \sin\phi\tan\alpha_c)\tan\alpha_c} \tag{8.63}$$

α_c = critical value of wedge inclination, α

$$= \tan^{-1}\left\{\frac{-[\sin\phi\sin(\phi - \theta) + m\sin 2\phi] + \sqrt{\sin\phi\sin(\phi - \theta)\cos\theta + 4m^2\cos^2\phi + 2m\cos\phi[\sin\phi\cos\theta + \sin(\phi - \theta)]}}{\sin\phi\cos(\phi - \theta) + 2m\cos^2\phi}\right\} \tag{8.64}$$

$$m = \frac{c\cos\theta}{(1 \pm k_v)(2q + \gamma H)} \tag{8.65}$$

Copyright 2017 Cengage Learning. All Rights Reserved. May not be copied, scanned, or duplicated, in whole or in part. Due to electronic rights, some third party content may be suppressed from the eBook and/or eChapter(s). Editorial review has deemed that any suppressed content does not materially affect the overall learning experience. Cengage Learning reserves the right to remove additional content at any time if subsequent rights restrictions require it.

and

$$\theta = \tan^{-1}\left(\frac{k_h}{1-k_v}\right) \tag{8.66}$$

Figures 8.34 and 8.35, respectively, show the variation of i_c and P_{PE} for a specific case ($H = 4$ m, $\phi = 26°$, $c = 10$ kPa, $\gamma = 15$ kN/m^3, $k_h = 0.3$).

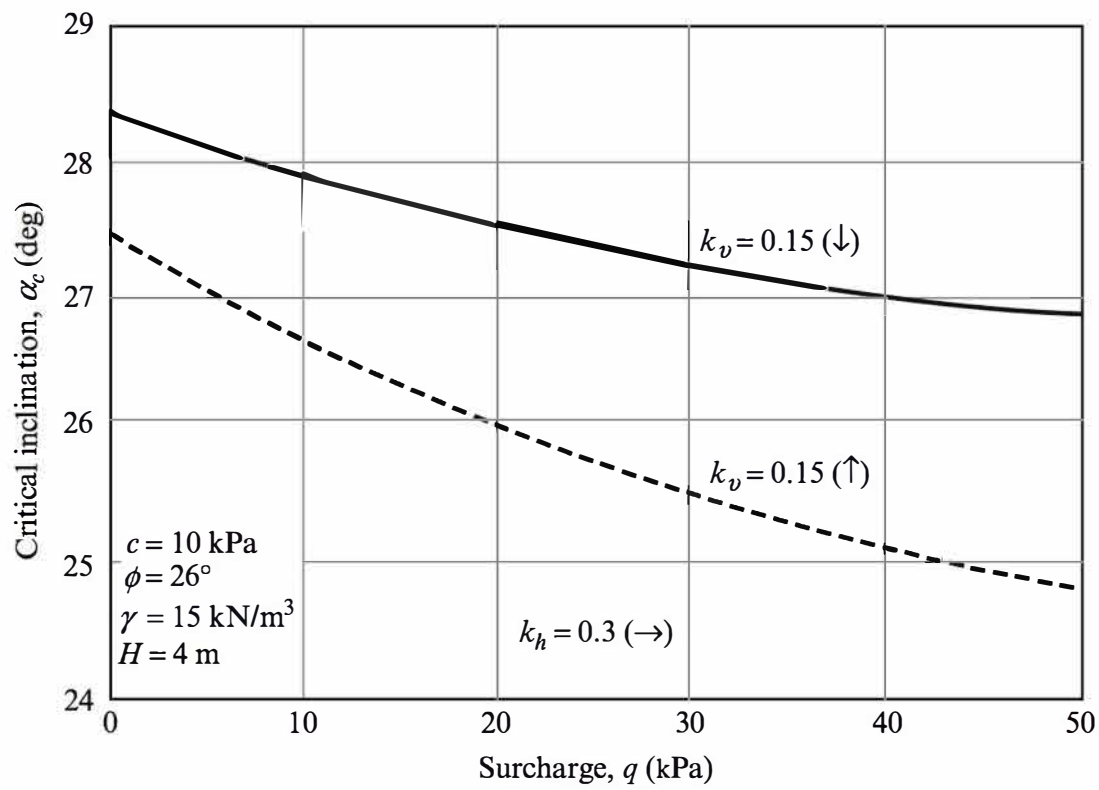

Figure 8.34 Variation of $\alpha = \alpha_c$ with surcharge q [Eq. (8.64)]

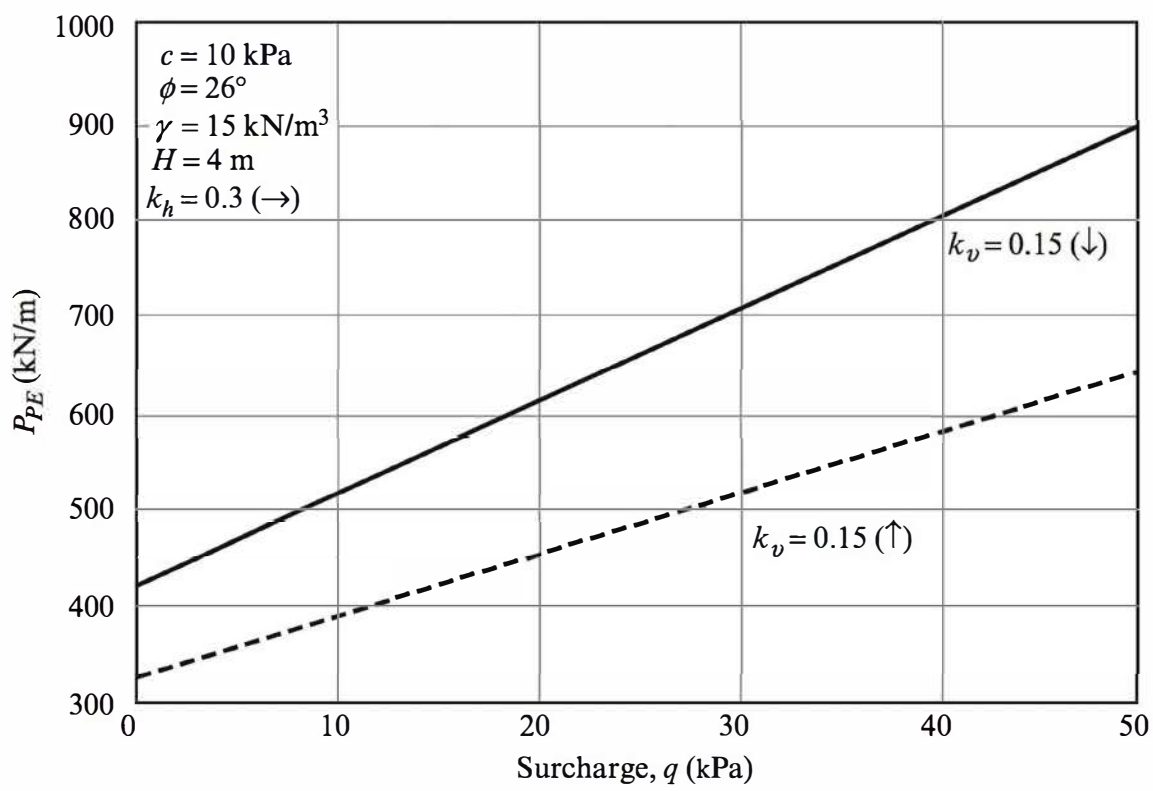

Figure 8.35 Variation of P_{PE} with q [Eq. (8.61)]

Copyright 2017 Cengage Learning. All Rights Reserved. May not be copied, scanned, or duplicated, in whole or in part. Due to electronic rights, some third party content may be suppressed from the eBook and/or eChapter(s). Editorial review has deemed that any suppressed content does not materially affect the overall learning experience. Cengage Learning reserves the right to remove additional content at any time if subsequent rights restrictions require it.

PROBLEMS

8.1 A retaining wall is 5.5 m high with a vertical back ($\beta = 0°$). It has a horizontal cohesionless soil (dry) as backfill. Given:

Unit weight of soil = 15 kN/m^3

Angle of friction $\phi = 30°$

$k_h = 0.35$ $\quad k_v = 0$ $\quad \delta = 15°$

Determine the active force P_{AE} per unit length of the retaining wall.

8.2 Refer to Problem 8.1. Determine the location of the point of intersection of the resultant force P_{AE} with the back face of the retaining wall. Assume the wall (a) rotates about the bottom, and (b) translates.

8.3 Refer to Figure 8.2. Given:

$H = 3$ m	$\phi = 40°$	$k_h = 0.3$
$\beta = 10°$	$\delta = 13°$	$k_v = 0.1$
$i = 10°$	$\gamma = 15.72$ kN/m^3	

Determine the active forcer per unit length P_{AE} and the location of the resultant. Assume that the wall is rotating about its bottom.

8.4 Refer to Problem 8.3. Where would be the location of the resultant if the wall is rotating about its top?

8.5 Redo Problem 8.1 using the modified Culmann graphical solution procedure.

8.6 For a retaining wall with vertical back face and horizontal backfill, the following are given; $H = 6$ m, $c = 12$ kPa, $\phi = 25°$, $\gamma = 17.8$ kN/m^3, $k_h = 0.2$, and $k_v = 0$. Estimate the active force P_{AE} per unit length of the wall. Use Eq. (8.45) and ignore the tensile crack.

8.7 Solve Problem 8.6 using Eq. (8.55).

8.8 For the retaining wall and the backfill given in Problem 8.1, determine the passive force P_{PE} per unit length of the wall. Use Eqs. (8.59) and (8.60).

8.9 Solve Problem 8.8 using Eq. (8.59) and Table 8.9.

8.10 For a retaining wall and the backfill given in Problem 8.3, determine the passive force P_{PE} per unit length. Use Egs. (8.59) and (8.60).

8.11 Consider a 3.6 m high gravity vertical retaining wall ($\beta = 0°$) with a horizontal backfill ($i = 0°$).

Copyright 2017 Cengage Learning. All Rights Reserved. May not be copied, scanned, or duplicated, in whole or in part. Due to electronic rights, some third party content may be suppressed from the eBook and/or eChapter(s). Editorial review has deemed that any suppressed content does not materially affect the overall learning experience. Cengage Learning reserves the right to remove additional content at any time if subsequent rights restrictions require it.

Given for the soil are $\phi = 32°$, $\gamma = 19.5$ kN/m^3 and $\delta = 0$.

a. Calculate P_{AE} and the location of resultant with $k_v = 0.1$ and $k_h = 0.15$.

b. For the results of (a), what should be the weight of the wall per meter length for no lateral movement? The factor of safety against sliding is 1.4.

c. What should be the weight of the wall for an allowable lateral displacement of 25 mm? Given $A_v = A_a = 0.15$; the factor of safety against sliding is 1.4.

References

Amano, R., Azuma, H., and Ishii, Y. (1956). "Aseismic Design of Quay Walls in Japan," *Proceedings*, 1st World Conference on Earthquake Engineering, Berkeley, California.

Applied Technology Council (1978). "Tentative Provisions for the Development of Seismic Regulations for Buildings," *Publication ATC 3–06*, Palo Alto, California.

Arango, I. (1969). Personal communication with Seed, H. B. and Whitman, R. V. (1970).

Coulomb, C. A. (1776). "Essai sur une Application des Regles de Maximis et Minimis a quelques Problemes de Statique, relatifs a 1'Architecture,' *Mem. Roy. des Sciences*, Paris, Vol 3. p. 38.

Culmann, C. (1875). *Die graphische Statik*, Meyer and Zeller, Zurich.

Davies, T. G., Richards, R., and Chen, K. H. (1986). "Passive Pressure during Seismic Loading." *Journal of Geotechnical Engineering,* ASCE, Vol. 112, No. GT4, pp. 479–484.

Duke, C. M., and Leeds, D. J. (1963). "Response of Soils, Foundations, and Earth Structures to the Chilean Earthquake of 1960," *Bulletin of the Seismological Society of America*, Vol. 53, No. 2, pp. 309–357.

Franklin, A. G., and Chang, F. K. (1977). "Earthquake Resistance of Earth and Rockfill Dams," *Report 5, Miscellaneous Paper S71 – 17*, Soils and Pavement Laboratory, US Army Engineer Waterways Experiment Station, Vicksburg, Mississippi.

Hayashi, S., Kubo, K., and Nakase, A. (1966). "Damage to Harbor Structures in the Nigata Earthquake," *Soils and Foundations*, Vol. 6, No. 1, pp. 26–32.

Ishibashi, I., and Fang, Y. S. (1987). "Dynamic Earth Pressures with Different Wall Movement Modes," *Soils and Foundations*, Vol. 27, No. 4, pp. 11–12.

Jacobsen, L. S. (1939). Described in Appendix D of "The Kentucky Project," *Technical Report No. 13*, Tennessee Valley Authority, 1951.

Kapila, J. P. (1962). "Earthquake Resistant Design of Retaining Walls," *Proceedings*, 2nd Earthquake Symposium, University of Roorkee, Roorkee, India.

Matsuo, H., and O'Hara S. (1960). "Lateral Earth Pressures and Stability of Quay Walls During Earthquakes," *Proceedings*, 2nd World Conference on Earthquake Engineering, Japan, Vol.1.

Mononobe, N. (1929). "Earthquake-Proof Construction of Masonry Dams," *Proceedings*, World Engineering Conference, Vol. 9, pp. 274–280.

Mononobe, N.,and Matsuo, H. (1929). "On the Determination of Earth Pressures During Earthquakes," *Proceedings*, World Engineering Conference, Vol. 9, pp. 176–182.

Nadim, F., and Whitman, R. V. (1983). "Seismically Induced Movement of Retaining Walls," *Journal of Geotechnical Engineering*, ASCE, Vol. 109, No. GT7, pp. 915–931.

Nazarian, H. N., and Hadjan, A. H. (1979). "Earthquake-Induced Lateral Soil Pressure on Structures," *Journal of the Geotechnical Engineering* Division, ASCE, Vol. 105, No. GT9, pp. 1049–1066.

Newmark, N. M. (1965). "Effect of Earthquakes on Dams and Embankments," *Geotechnique*, Vol. 15, No. 2, pp. 139–160.

Copyright 2017 Cengage Learning. All Rights Reserved. May not be copied, scanned, or duplicated, in whole or in part. Due to electronic rights, some third party content may be suppressed from the eBook and/or eChapter(s). Editorial review has deemed that any suppressed content does not materially affect the overall learning experience. Cengage Learning reserves the right to remove additional content at any time if subsequent rights restrictions require it.

Okabe, S. (1926), "General Theory of Earth Pressure," *Journal of the Japanese Society of Civil Engineers*, Vol. 12, No. 1, pp. 123–134.

Prakash, S., and Basavanna, B. M. (1969). "Earth Pressure Distribution Behind Retaining Wall During Earthquake," *Proceedings*, 4th World Conference on Earthquake Engineering, Santiago, Chile.

Prakash, S., and Saran, S. (1966). "Static and Dynamic Earth Pressure Behind Retaining Walls," *Proceedings*, 3rd Symposium on Earthquake Engineering, Roorkee, India, Vol. 1, pp. 277–288.

Richards, R., and Elms, D. G. (1979). "Seismic Behavior of Gravity Retaining Walls," *Journal of the Geotechnical Engineering Division*, ASCE, Vol. 105, No. GT4, pp. 449–464.

Saran, S., and Prakash, S. (1968). "Dimensionless Parameters for Static and Dynamic Earth Pressure for Retaining Walls," *Indian Geotechnical Journal*, Vol. 7, No. 3, pp. 295–310.

Seed, H. B., and Whitman, R. V. (1970). "Design of Earth Retaining Structures of Dynamic Loads," *Proceedings*, Speciality Conference on Lateral Stresses in the Ground and Design of Earth Retaining Structures, ASCE, pp. 103–147.

Sherif, M. A., and Fang, Y. S. (1984). "Dynamic Earth Pressures on Walls Rotating About the Top," *Soils and Foundations*, Vol. 24, No. 4, pp. 109–117.

Sherif, M. A., Ishibashi, I., and Lee, C. D. (1982). "Earth Pressure Against Rigid Retaining Walls," *Journal of the Geotechnical Engineering Division*, ASCE, Vol. 108, No. GT5, pp. 679–696.

Shukla, S. K., Gupta, S. K., and Sivakugan, N. (2009). "Active Earth Pressure on Retaining Wall for $c - \phi$ Soil Backfill under Seismic Loading Condition," *Journal of Geotechnical and Geoenvironmental Engineering*, ASCE, Vol. 135, No. 5, pp. 690–696.

Shukla, S. K., Sivakugan, N., and Das, B. (2011). "Analytical Expression for Dyamic Passive Pressure from $c - \phi$ Soil Backfill with Surcharge," *International Journal of Geotechnical Engineering,* J. Ross Publishing, Vol. 5, No. 3, pp. 357–362.

Soubra, A. H. (2000). "Static and Seismic Passive Earth Pressure Coefficients on Rigid Retaining Structures," *Canadian Geotechnical Journal*, Vol. 37, pp. 463–478.

Westergaard, H. M. (1933). "Water Pressures on Dams During Earthquakes," *Transactions*, ASCE, Vol. 98, pp. 418–433.

Copyright 2017 Cengage Learning. All Rights Reserved. May not be copied, scanned, or duplicated, in whole or in part. Due to electronic rights, some third party content may be suppressed from the eBook and/or eChapter(s). Editorial review has deemed that any suppressed content does not materially affect the overall learning experience. Cengage Learning reserves the right to remove additional content at any time if subsequent rights restrictions require it.

Compressibility of Soils under Dynamic Loads

9

9.1 INTRODUCTION

Permanent settlements under vibratory machine foundations can generally be placed under two categories:

1. Elastic and consolidation settlement due to the static weight
2. Settlement due to vibratory compaction of the foundation soil

Permanent settlement in soils can also be induced due to the vibration caused by an earthquake. The elastic and consolidation settlement due to static loads is not discussed here since the conventional methods of calculation can be found in most standard soil mechanics texts. In this chapter, the present available methods to evaluate permanent settlement due to dynamic loading conditions are presented.

9.2 COMPACTION OF GRANULAR SOILS: EFFECT OF VERTICAL STRESS AND VERTICAL ACCELERATION

The fact that granular soils can be compacted by vibration is well known. Dry granular soils are likely to exhibit more compaction due to vibration as compared to moist soils. This is because of the surface tension effect in moist soils, which offers a resistance for the soil particles to roll and slide and arrange themselves into a denser state.

Laboratory studies have been made in the past to evaluate the effect of cyclic *controlled vertical stress* at low frequencies, i.e., at low acceleration levels on confined granular soils (D'Appolonia, 1970). Such laboratory tests can be performed by taking a granular soil specimen in a mold, as shown in Figure 9.1a. A confining vertical air pressure σ_z is first applied to the specimen, after which a vertical dynamic stress of amplitude σ_d is applied repeatedly.

The permanent compressions of the specimen are recorded after the elapse of several cycles of dynamic stress application. Also, several investigations on

Copyright 2017 Cengage Learning. All Rights Reserved. May not be copied, scanned, or duplicated, in whole or in part. Due to electronic rights, some third party content may be suppressed from the eBook and/or eChapter(s). Editorial review has deemed that any suppressed content does not materially affect the overall learning experience. Cengage Learning reserves the right to remove additional content at any time if subsequent rights restrictions require it.

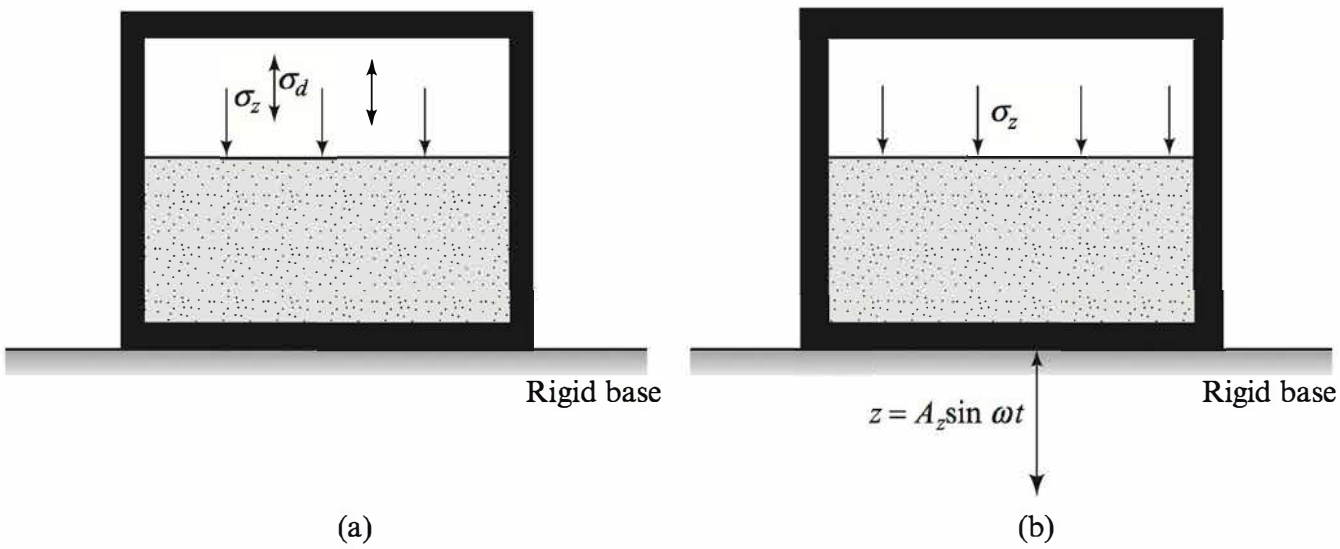

Figure 9.1 Compaction of granular soil by (a) controlled vertical stress; and (b) controlled vertical acceleration

confined dry granular soils have been conducted (e.g., see D'Appolonia and D'Appolonia, 1967; Ortigosa and Whitman, 1968) in which a *controlled vertical acceleration* is imposed on the specimen, which produces small dynamic stress changes. For these tests, the specimen is placed in a mold fixed to a vibrating table (Figure 9.1b). Then vertical confining air pressure σ_z is applied to the specimen. After that, the specimen is subjected to vertical vibration for a period of time.

Note that, for vertical vibration,

$$z = A_z \sin \omega t$$

where A_z is the amplitude of the vertical vibration. The magnitude of the *peak acceleration* is equal to $A_z\omega^2 = A_z(2\pi f)^2$. Thus, the peak acceleration is controlled by the *amplitude of displacement* and the *frequency of vibration*. For *constant peak acceleration* of vibration, the drive mechanism has to be adjusted for A_z and f. The vertical compression of the specimen can be determined at the end of a test.

Thus the first type of test described above is run with repeated stresses with *negligible acceleration*; the second type is for repeated acceleration with *small dynamic stress on soils*.

Figure 9.2 shows the results of a number of tests conducted on a dune sand for controlled vertical stress condition. For all tests, the sand specimens were compacted to an initial relative density of about 60%.

The frequencies of load application were in a range of 1.8-6 Hz. Along the ordinate are plotted the vertical strain, which is equal to $\Delta H/H$ (where H is the initial height of the specimen and ΔH is the vertical compression of the specimen after a given number of load cycles). It may be seen that, for a given value of σ_d/σ_z,

$$\frac{\Delta H}{H} \propto \log N$$

Copyright 2017 Cengage Learning. All Rights Reserved. May not be copied, scanned, or duplicated, in whole or in part. Due to electronic rights, some third party content may be suppressed from the eBook and/or eChapter(s). Editorial review has deemed that any suppressed content does not materially affect the overall learning experience. Cengage Learning reserves the right to remove additional content at any time if subsequent rights restrictions require it.

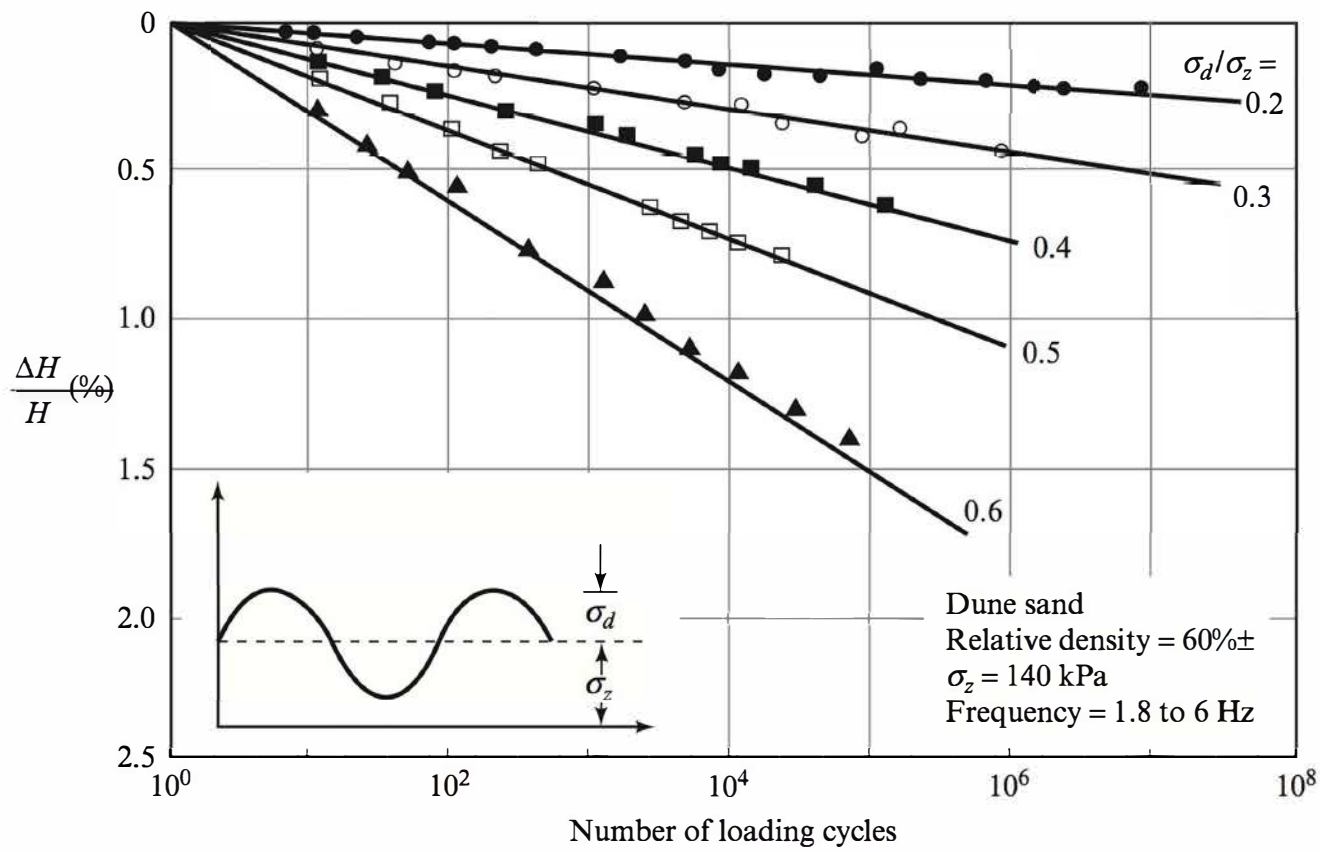

Figure 9.2 Compression of a dune sand under controlled vertical stress condition (from D'Appolonia, 1970)

Source: D'Appolonia, E. (1970). "Dynamic Loadings," *Journal of the Soil Mechanics and Foundations Division*, ASCE, Vol. 96, No. SM1, pp. 49–72. With permission from ASCE.

where N is the number of load cycle applications. Also note that, for a given number of load cycles, the vertical strain increases with increasing values of σ_d/σ_z.

Figure 9.3 shows the nature of the results obtained from controlled vertical acceleration tests on dry sand by Ortigosa and Whitman (1968). Note that, even at zero confining pressure, no vertical strain is induced up to a peak acceleration of about $1g$ ($1\times$ acceleration due to gravity). Similar test results of D'Appolonia (1970) are shown in Figure 9.4, for which $\sigma_z = 0$. The terminal dry unit weight shown in Figure 9.4 is the unit weight of sand at the end of the test.

Krizek and Fernandez (1971) also conducted several laboratory tests with controlled vertical acceleration to study the densification of damp clayey sand. Tests were conducted with air-dry and damp specimens of Ottawa sand, grundite, and three mixtures of Ottawa sand and grundite: 90%–10%, 80%–20%, 70%–30%. Table 9.1 gives the details of the specimens used for the tests.

For conducting the tests, approximately 0.017 m^3 of soil samples—air dry and moist—were placed in a loose condition in a cylindrical mold 457 mm high and 305 mm in diameter. They were subjected to vertical vibrations for a period of time under various vertical pressures (σ_z). The range of time for vibratory compaction for the specimens was varied. Maximum vertical accelerations up to a value of about 6 g were used.

Copyright 2017 Cengage Learning. All Rights Reserved. May not be copied, scanned, or duplicated, in whole or in part. Due to electronic rights, some third party content may be suppressed from the eBook and/or eChapter(s). Editorial review has deemed that any suppressed content does not materially affect the overall learning experience. Cengage Learning reserves the right to remove additional content at any time if subsequent rights restrictions require it.

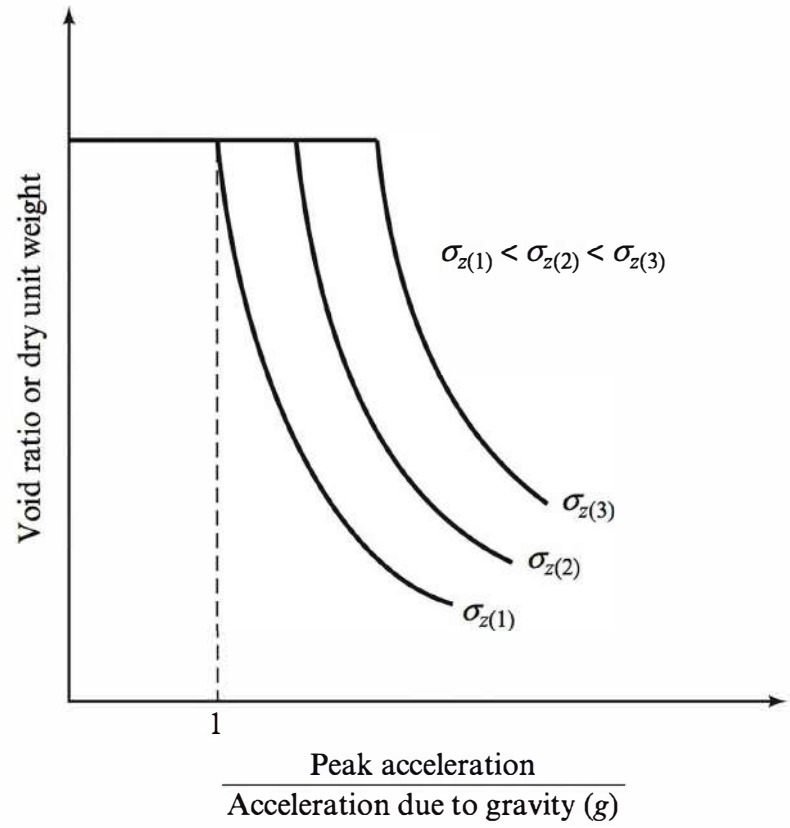

Figure 9.3 Nature of variation of void ratio or dry unit weight of dry sand in controlled vertical acceleration tests

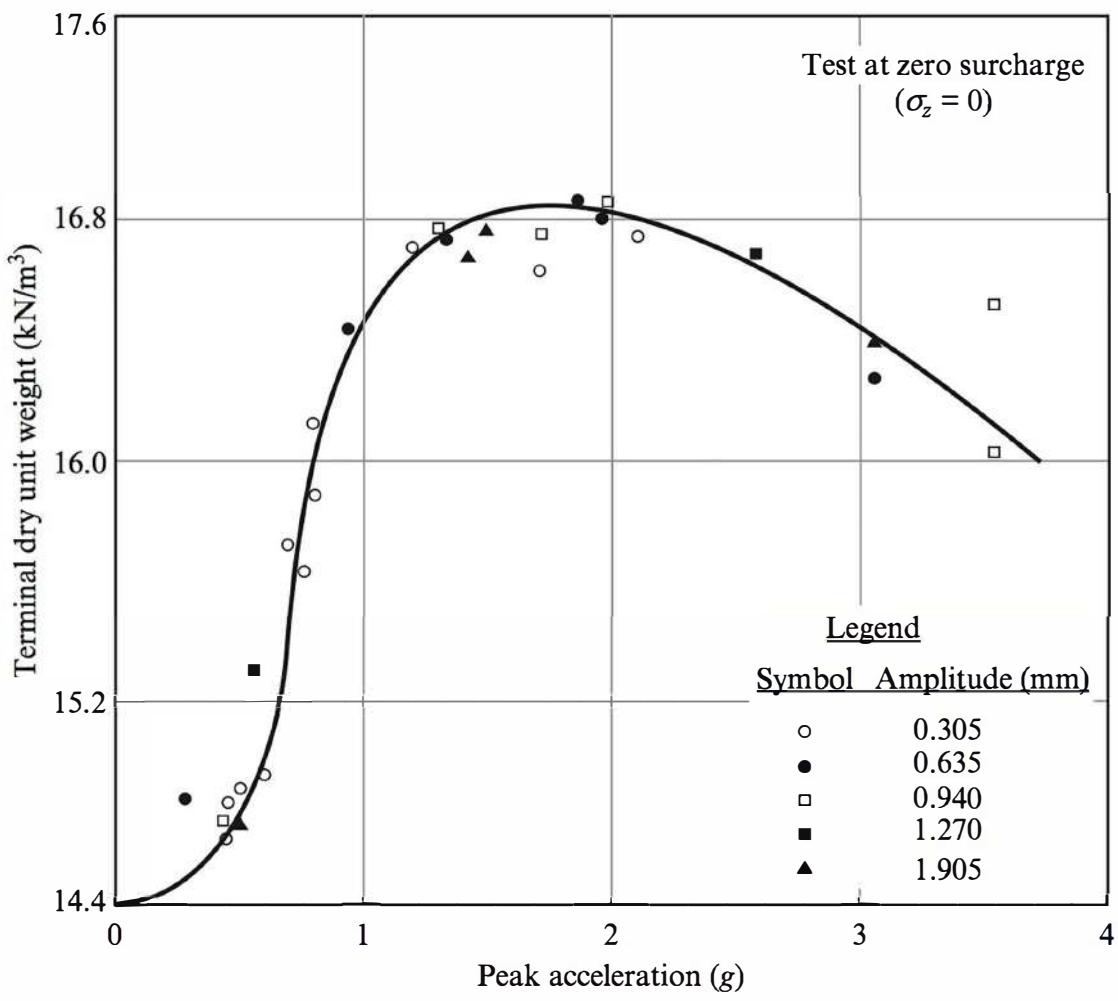

Figure 9.4 Correlation between terminal unit weight and peak vertical acceleration for a dune sand (redrawn from D'Appolonia, 1970)

Source: D'Appolonia, E. (1970). "Dynamic Loadings," *Journal of the Soil Mechanics and Foundations Division*, ASCE, Vol. 96, No. SM1, pp. 49–72. With permission from ASCE.

Copyright 2017 Cengage Learning. All Rights Reserved. May not be copied, scanned, or duplicated, in whole or in part. Due to electronic rights, some third party content may be suppressed from the eBook and/or eChapter(s). Editorial review has deemed that any suppressed content does not materially affect the overall learning experience. Cengage Learning reserves the right to remove additional content at any time if subsequent rights restrictions require it.

Table 9.1 Details of the Specimens Used in the Tests by Krizek and Fernandez (1971)

Soil	Percent of mix	Moisture content: Air dry (%)	Moisture content: Damp (%)	Modified Proctor dry unit weight (kN/m^3)	Optimum moisture content, modified Proctor test (%)
Ottawa sand	-	0.6	4.4 ± 0.5	16.92	11.0
Grundite	-	2.42	Not tested	16.00	18.5
Mix-10	90% Ottawa sand + 10% grundite	0.26	5 ± 0.5	17.99	8.0
Mix-20	80% Ottawa sand + 20% grundite	0.51	4.5 ± 0.5	18.96	9.0
Mix-30	70% Ottawa sand + 30% grundite	0.72	5 ± 0.3	19.49	9.5

Source: Based on Krizek, R. J., and Fernandez, J. J. (1971). "Vibratory Densification of Damp Clayey Sands," *Journal of the Soil Mechanics and Foundations Division*, ASCE, Vol. 98, No. SM8, pp. 1069–1079.

Figure 9.5 shows the time rate of vibratory compaction of air-dry and moist sand-grundite mixtures. It needs to be pointed out that very few tests were conducted for $a_{max}/g < 1$ (a_{max} = peak acceleration). However, from this study the following general conclusions may be drawn:

1. Significant vibratory densification does not occur with peak acceleration levels of less than 1 g.
2. The terminal vibratory dry unit weight of *air-dry* soils slightly decreases for $a_{max}/g > 2$. This is true only for zero confining pressure ($\sigma_z = 0$).
3. An increase of the clay percentage in soils has a tendency to reduce $\gamma_{d(\text{termin}-\text{vibrat})}/\gamma_{d(\text{modif max Proctor})}$.
4. Increase of moisture content has a significant influence in reducing $\gamma_{d(\text{termin}-\text{vibrat})}/\gamma_{d(\text{modif max Proctor})}$.

9.3 SETTLEMENT OF STRIP FOUNDATION ON GRANULAR SOIL UNDER THE EFFECT OF CONTROLLED CYCLIC VERTICAL STRESS

In Section 9.2, some laboratory experimental observations of settlement of *laterally confined* sand specimens were presented. In these cases, the loads have been applied over the full surface area. However, in the field, the load covers only a small area, and settlement in these cases includes those caused by the induced shear strains. In the case of foundations, the shear strain increase with the increase of σ_d/q_u (where σ_d is the amplitude of dynamic load and q_u is the ultimate bearing capacity). In this section, some developments on settlement of strip footings under the effect of controlled cycling vertical stress applied at *low frequencies* (i.e., negligible acceleration) are discussed.

Copyright 2017 Cengage Learning. All Rights Reserved. May not be copied, scanned, or duplicated, in whole or in part. Due to electronic rights, some third party content may be suppressed from the eBook and/or eChapter(s). Editorial review has deemed that any suppressed content does not materially affect the overall learning experience. Cengage Learning reserves the right to remove additional content at any time if subsequent rights restrictions require it.

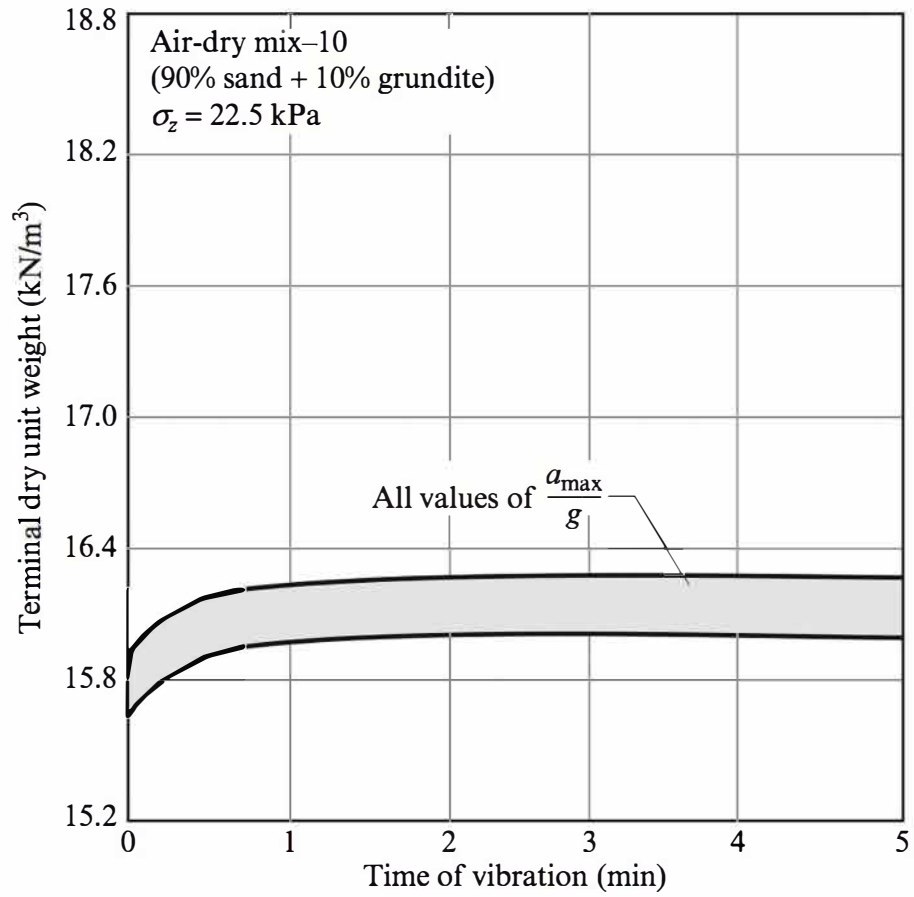

(a)

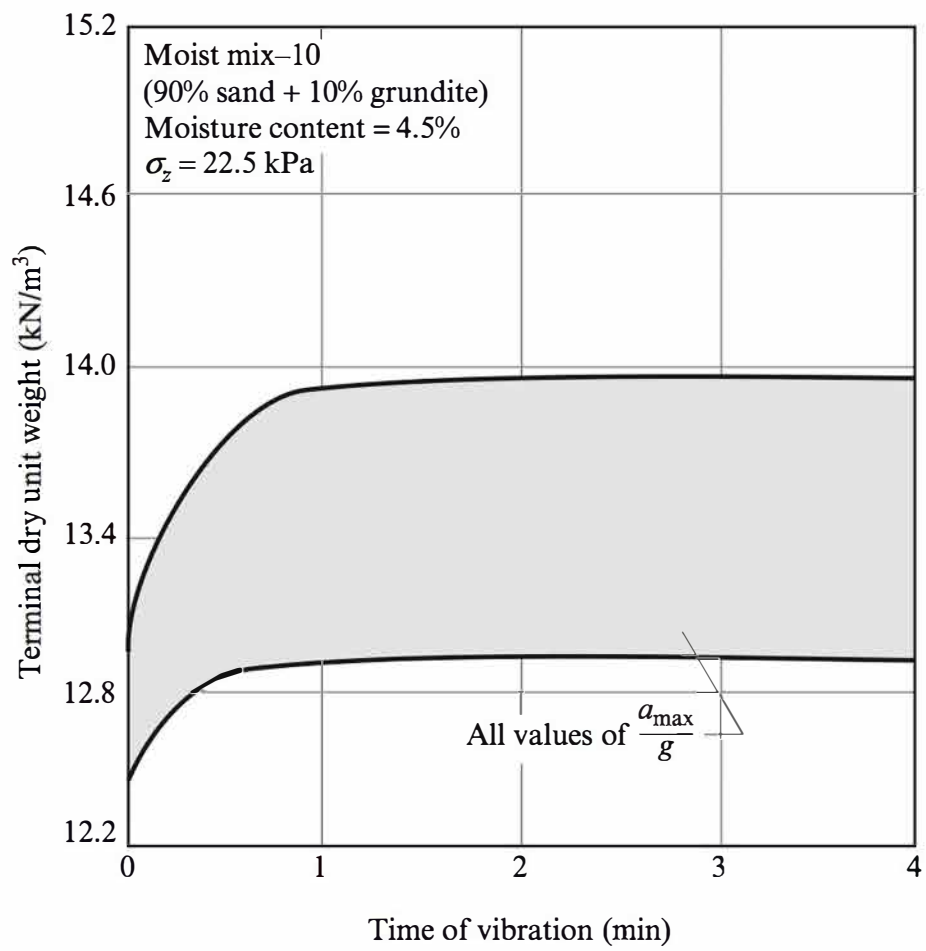

(b)

Figure 9.5 Time rate of vibratory compaction for air-dry and moist sand-grundite mixtures (redrawn from Krizek and Fernandez, 1971)

Source: Krizek, R.J· and Fernandez, J.J· (1971). "Vibratory Densification of Damp Clayey Sands," *Journal of the Soil Mechanics and Foundations Division*, ASCE, Vol. 98, No. SM8, pp. 1069–1079. With permission from ASCE.

Copyright 2017 Cengage Learning. All Rights Reserved. May not be copied, scanned, or duplicated, in whole or in part. Due to electronic rights, some third party content may be suppressed from the eBook and/or eChapter(s). Editorial review has deemed that any suppressed content does not materially affect the overall learning experience. Cengage Learning reserves the right to remove additional content at any time if subsequent rights restrictions require it.

Raymond and Komos (1978) conducted laboratory model tests with strip foundations with widths of 75 mm and 228 mm resting on 20–30 Ottawa sand in a large box. The cyclic loads on model strip foundations were applied by a Bellofram loading piston activated by an air pressure system. The loadings approximated a rectangular wave from as shown in Figure 9.6a with a frequency of 1 Hz. The settlement of the foundations was measured by a dial gauge together with a DVDT activating a strip chart recorder. For conducting the tests, the ultimate static bearing capacities (q_u) were first experimentally determined. The foundations were then subjected to various magnitudes of cyclic load ($\sigma_d/q_u = 13.5\% - 90\%$, where $\sigma_d = Q_0/A$, and A is the area of the model footing). The load settlement relationships obtained from the tests for the 228 mm foundations are shown in Figure 9.6b. In this figure, S_N is the permanent settlement of the foundation and N is the number of cycles of load application. Such plots may be given by an empirical relation as

$$\frac{S_N}{\log N} = a + bS_N \tag{9.1}$$

where a and b are two constants.

The experimental values of a and b for these two foundations may be approximated by the following equations.

For 75 mm wide foundation:

$$a = -0.0811 + 0.0115F \tag{9.2}$$

$$b = 0.12420 + 0.00127F \tag{9.3}$$

For 228 mm wide foundation:

$$a = -0.1053 + 0.0421F \tag{9.4}$$

$$b = 0.0812 + 0.0031F \tag{9.5}$$

where $F = \sigma_d/q_u$ and S_N is measured in millimeters. Equations (9.1)–(9.5) are valid up to a load cycle $N = 10^5$.

Figure 9.7 shows the experimental results of the variation of σ_d with $\log N$ for various values of S_N. For a given value of S_N, the plot of σ_d versus $\log N$ is approximately linear up to a value of $\sigma_d \approx (1/4)q_u$. For $\sigma_d < (1/4)q_u$, the slope of σ_d versus $\log N$ becomes smaller and the response tends toward elastic conditions.

From Eqs. (9.2)–(9.5), it may be seen that, *for a given soil*, the parameters a and b are functions of the width of the foundation B. Thus, Eqs. (9.2) and (9.4) have been combined by Raymond and Komos to the form

$$a = -0.15125 + 0.0000693B^{1.18}(F + 6.09) \tag{9.6}$$

Copyright 2017 Cengage Learning. All Rights Reserved. May not be copied, scanned, or duplicated, in whole or in part. Due to electronic rights, some third party content may be suppressed from the eBook and/or eChapter(s). Editorial review has deemed that any suppressed content does not materially affect the overall learning experience. Cengage Learning reserves the right to remove additional content at any time if subsequent rights restrictions require it.

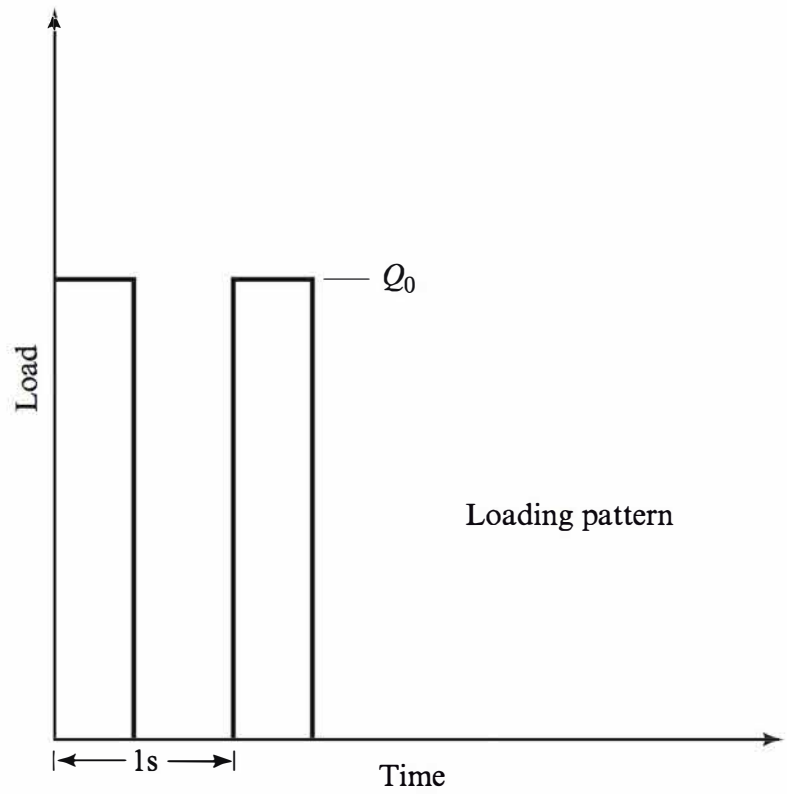

(a)

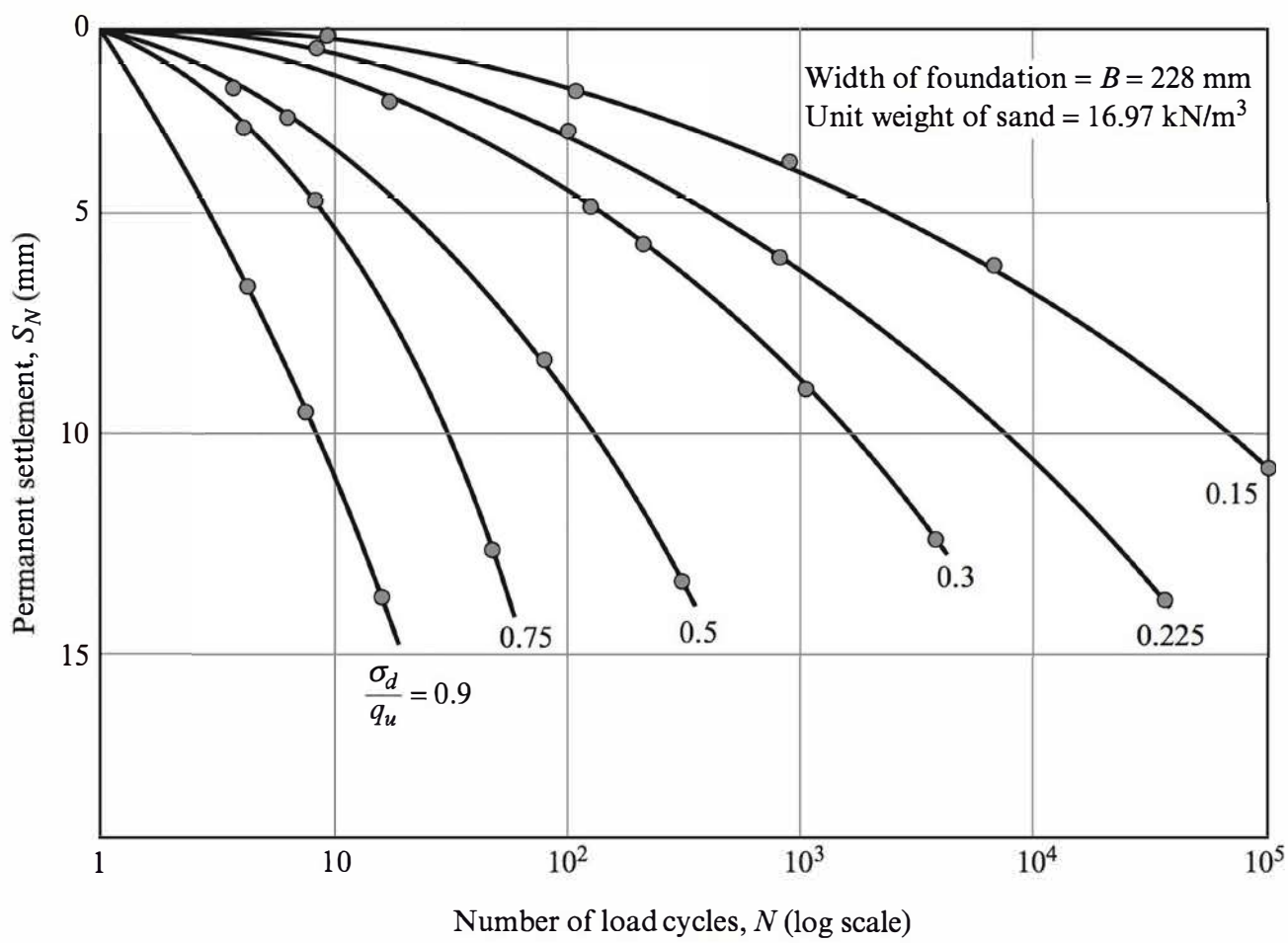

(b)

Figure 9.6 Plastic deformation due to repeated loading in plane strain case (redrawn from Raymond and Komos, 1978)

Source: Raymond, G.P. and Komos, F.E. (1978). "Repeated Loading test of a Model Plane Strain Footing," *Canadian Geotechnical Journal*, Vol. 15, No. 2, pp. 190–201.

Copyright 2017 Cengage Learning. All Rights Reserved. May not be copied, scanned, or duplicated, in whole or in part. Due to electronic rights, some third party content may be suppressed from the eBook and/or eChapter(s). Editorial review has deemed that any suppressed content does not materially affect the overall learning experience. Cengage Learning reserves the right to remove additional content at any time if subsequent rights restrictions require it.

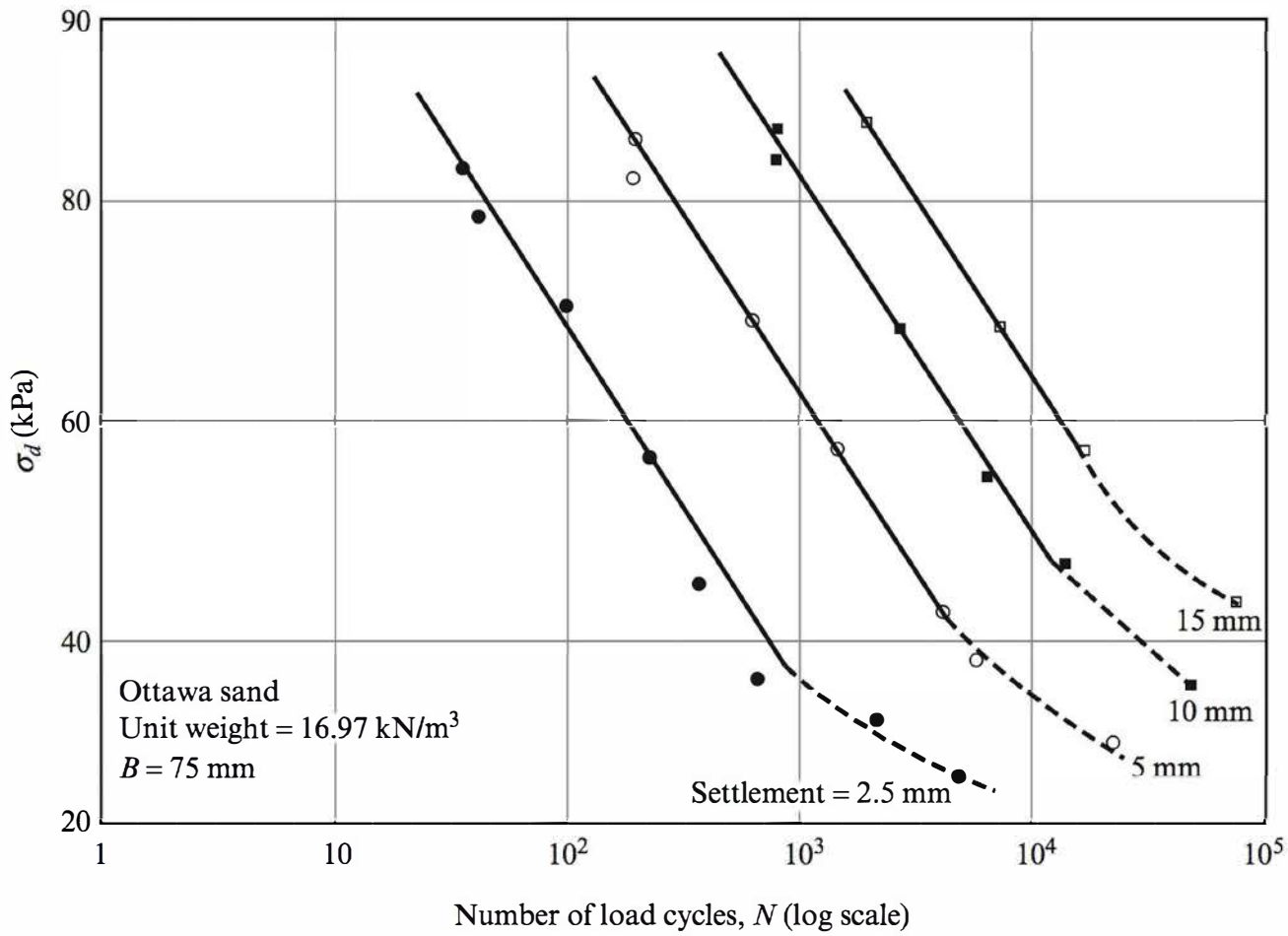

Figure 9.7 Variation of σ_d with $\log N$ for various values of permanent settlement (redrawn from Raymond and Komos, 1978)

Source: Raymond, G.P. and Komos, F.E. (1978). "Repeated Loading test of a Model Plane Strain Footing," *Canadian Geotechnical Journal*, Vol. 15, No. 2, pp. 190–201.

where B is the width of the foundations. Similarly, Eqs. (9.3) and (9.5) can be combined as

$$b = 0.153579 + 0.0000363B^{0.821}(F - 23.1) \tag{9.7}$$

Equations (9.6) and (9.7) are valid for only two different sizes of foundation and for one soil. The general form of the equations for all sizes of foundations and all soils can be written as

$$a = a_1 + a_2B^{1.18}F + a_3B^{1.18} \tag{9.8}$$

and

$$b = b_1 + b_2B^{0.821}F - b_3B^{0.821} \tag{9.9}$$

where a_1, a_2, a_3, b_1, b_2, b_3 are parameters for a given soil. However,

$$F = \frac{\sigma_d}{q_u}$$

and

$$q_u = \frac{1}{2}\gamma BN_\gamma \text{ (for surface foundation)} \tag{9.10}$$

Copyright 2017 Cengage Learning. All Rights Reserved. May not be copied, scanned, or duplicated, in whole or in part. Due to electronic rights, some third party content may be suppressed from the eBook and/or eChapter(s). Editorial review has deemed that any suppressed content does not materially affect the overall learning experience. Cengage Learning reserves the right to remove additional content at any time if subsequent rights restrictions require it.

where N_γ is the static bearing capacity factor (Chapter 6) and γ is the unit weight of soil.
Thus,

$$F = \frac{\sigma_d}{(1/2)\gamma B N_\gamma} \tag{9.11}$$

Substitution of Eq. (9.11) into Eqs. (9.8) and (9.9) yields

$$a = a_1 + a_4 \sigma_d B^{0.18} + a_3 B^{1.18} \tag{9.12}$$

and

$$b = b_1 + b_4 \sigma_d B^{-0.18} - b_3 B^{0.82} \tag{9.13}$$

where

$$a_4 = \frac{a_2}{(1/2)\gamma N_\gamma} \tag{9.14}$$

$$b_4 = \frac{b_2}{(1/2)\gamma N_\gamma} \tag{9.15}$$

and B is in millimeters.

If the values of a_1, a_3, a_4, b_1, b_3, b_4, which are the plastic properties of given soil at a given density of compaction, can be determined by laboratory testing, the settlement of a given strip foundation can be determined by combining Eqs. (9.1), (9.12), and (9.13). It needs to be pointed out that, for given values of σ_d and N, the value of S_N *decreases* with the increase of the width of the foundation. This fact is demonstrated in Figure 9.8 for five different foundations.

Analysis of this type may be used in the estimation of the settlement of railroad ties subjected to dynamic loads due to the movement of trains.

9.4 SETTLEMENT OF MACHINE FOUNDATION ON GRANULAR SOILS SUBJECTED TO VERTICAL VIBRATION

For machine foundation subjected to vertical vibrations, many investigators believe that the *peak acceleration* is the main controlling parameter for the settlement of the foundation. Depending on the relative density of granular soils, the solid particles come to an equilibrium condition under a given peak acceleration level. This *threshold acceleration* level must be exceeded before additional densification can take place.

The general nature of the settlement-time relationship for a foundation is shown in Figure 9.9. Note that in Figure 9.9, A_z is the amplitude of the foundation vibration and W is the weight of the foundation. The foundation settlement gradually increases with time and reaches a maximum value, beyond which it remains constant.

Copyright 2017 Cengage Learning. All Rights Reserved. May not be copied, scanned, or duplicated, in whole or in part. Due to electronic rights, some third party content may be suppressed from the eBook and/or eChapter(s). Editorial review has deemed that any suppressed content does not materially affect the overall learning experience. Cengage Learning reserves the right to remove additional content at any time if subsequent rights restrictions require it.

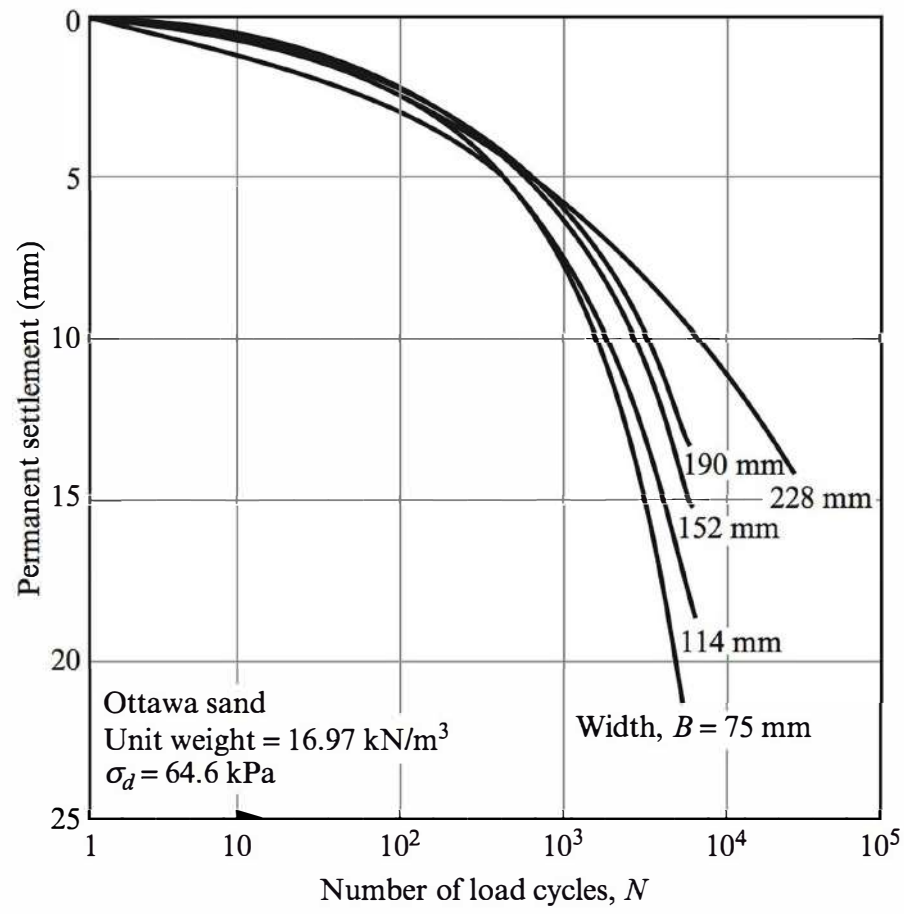

Figure 9.8 Plot of settlement versus number of load cycles for a constant value of σ_d (redrawn from Raymond and Komos, 1978)

Source: Raymond, G.P. and Komos, F.E. (1978). "Repeated Loading test of a Model Plane Strain Footing," *Canadian Geotechnical Journal*, Vol. 15, No. 2, pp. 190–201.

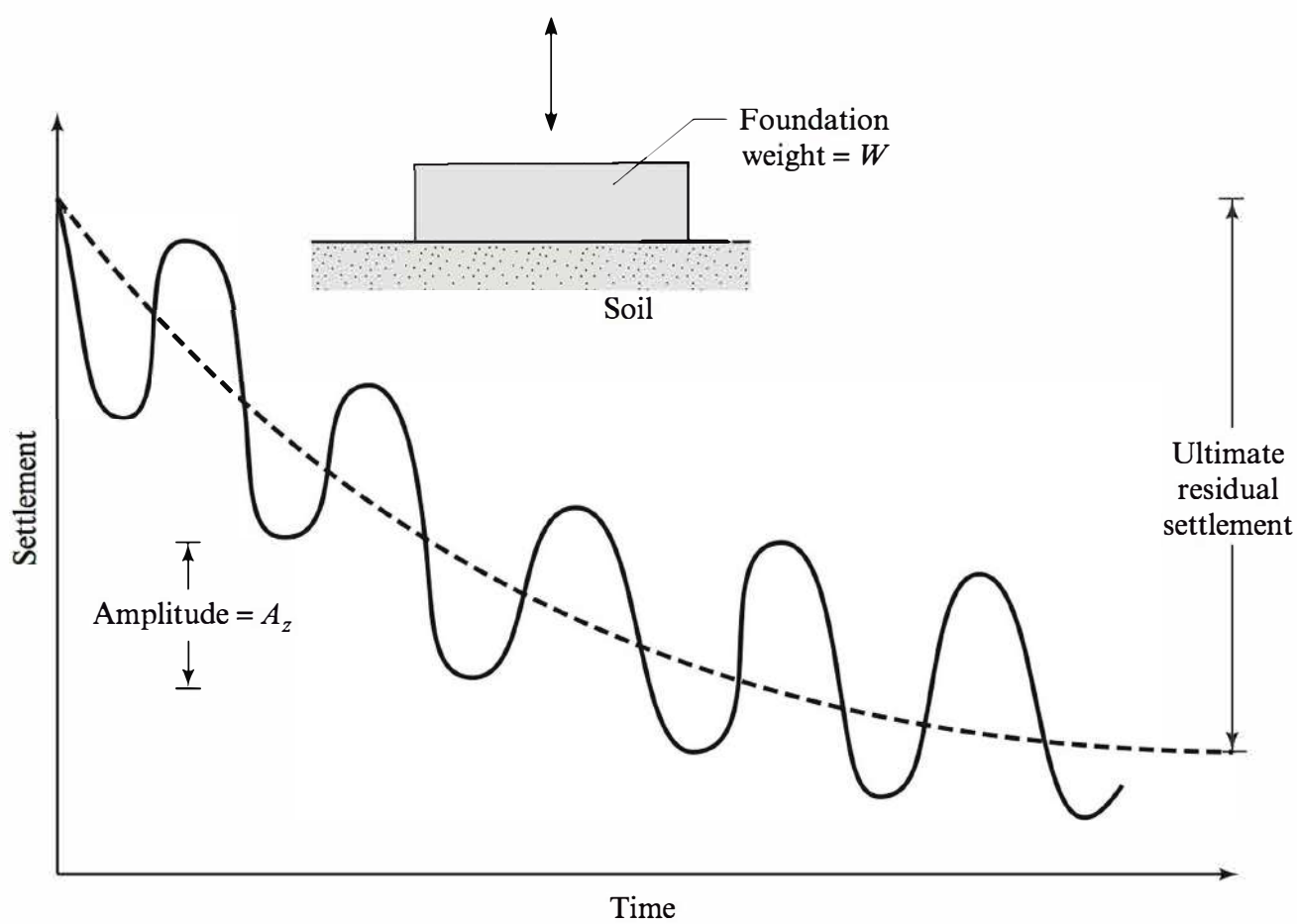

Figure 9.9 Settlement-time relationship for a machine foundation subjected to vertical vibration

Copyright 2017 Cengage Learning. All Rights Reserved. May not be copied, scanned, or duplicated, in whole or in part. Due to electronic rights, some third party content may be suppressed from the eBook and/or eChapter(s). Editorial review has deemed that any suppressed content does not materially affect the overall learning experience. Cengage Learning reserves the right to remove additional content at any time if subsequent rights restrictions require it.

Brumund and Leonards (1972) have studied the settlement of circular foundations resting on sand subjected to vertical excitation by means of laboratory model tests. According to them, the *energy per cycle of vibration* imparted to the soil by the foundation can be used as the parameter for determination of settlement of foundations.

The model tests of Brumund and Leonards were conducted in a 0.057 m^3 container. They used 20–30 Ottawa sand, compacted to a relative density of 70%. The model foundation used for the tests was 101.6 mm in diameter. The static ultimate bearing capacity was first experimentally determined before beginning the dynamic tests. The duration of vibration of the model foundation was chosen to be 20 min for all tests. Figure 9.10 shows the plot of the experimental results of settlement S against the peak acceleration for a constant frequency of vibration. For a given foundation weight W, the settlement increases linearly with the peak acceleration level. However, for a given frequency of vibration and peak acceleration level, the settlement increases with the increase of W.

Figure 9.11 shows a plot of settlement S against the energy transmitted per cycle to the soil by the foundation.

The data include the following:

1. A frequency range of 14–59.3 Hz (both above and below the resonant frequency)
2. A range in static pressure of $0.27–0.55 \times$ static ultimate bearing capacity q_u. The static pressure q can be defined as

$$q = \frac{W}{A} \tag{9.16}$$

   where A is the area of the foundation.

3. A range in maximum downward dynamic force of $0.3W - W$. The maximum downward dynamic force may theoretically be obtained from Eq. (2.90) as

$$F_{\text{dynam(max)}} = A_z \sqrt{k^2 + (c\omega)^2}$$

where A_z = amplitude of foundation vibration

$$k = \text{spring constant} = \frac{4Gr_0}{1-\mu} \quad \text{(see Chapter 5)}$$

$$c = \left(\frac{3.4}{1-\mu}\right) r_0^2 \sqrt{G\rho} \quad \text{(see chapter 5)}$$

G = shear modulus of soil

r_0 = radius of foundation

Copyright 2017 Cengage Learning. All Rights Reserved. May not be copied, scanned, or duplicated, in whole or in part. Due to electronic rights, some third party content may be suppressed from the eBook and/or eChapter(s). Editorial review has deemed that any suppressed content does not materially affect the overall learning experience. Cengage Learning reserves the right to remove additional content at any time if subsequent rights restrictions require it.

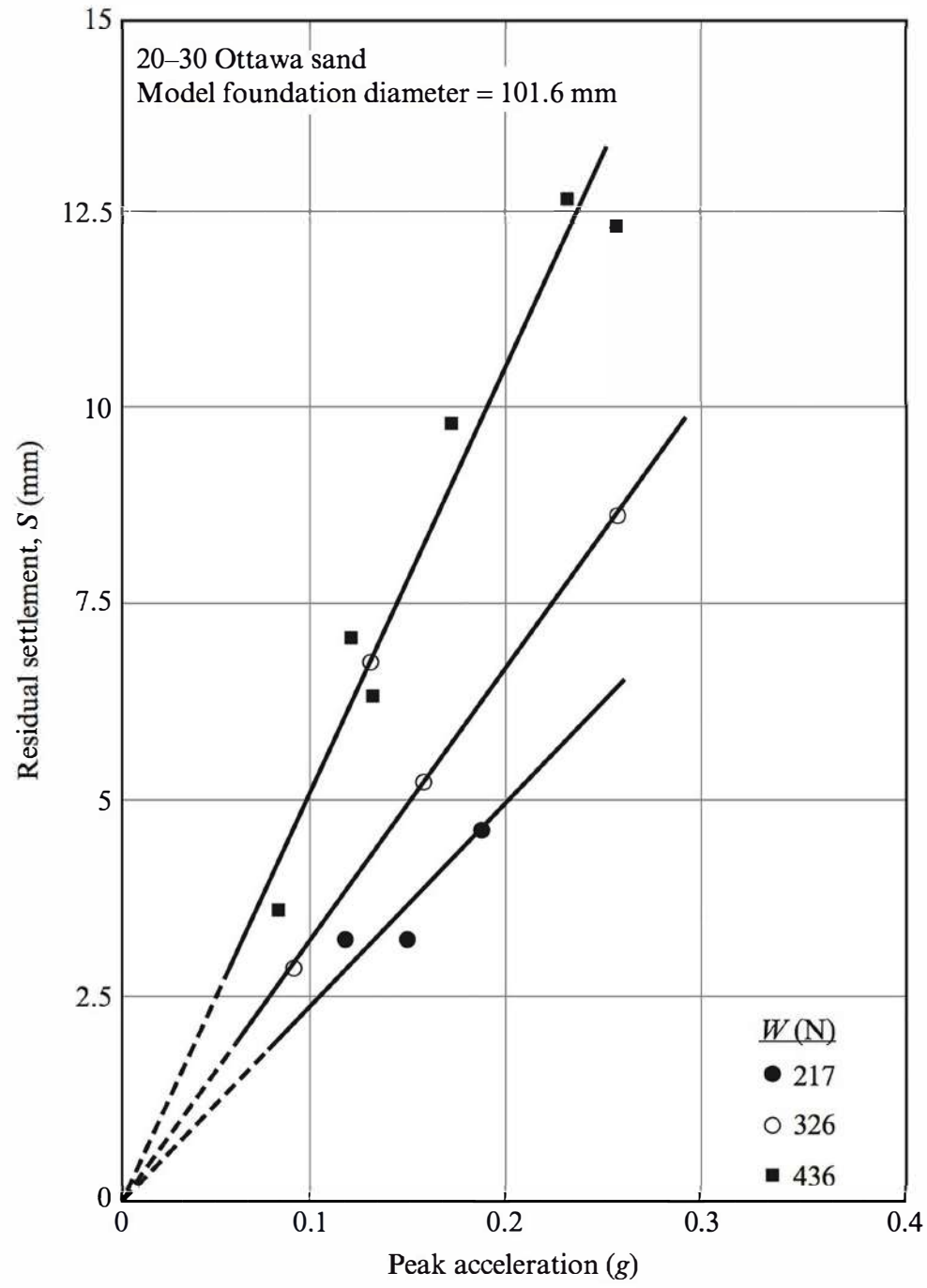

Figure 9.10 Plot of settlement versus peak acceleration for model foundation at a frequency of 20 Hz (from Brumund and Leonards, 1972)

Source: Brumund, W.F., and Leonards, G.A. (1972). "Subsidence of Sand Due to Surface Vibration," *Journal of the Soil Mechanics and Foundations*, ASCE, Vol. 98, No. SM1, pp. 27–42. With permission from ASCE.

$\mu =$ Poisson's ratio of soil

$\rho =$ density of soil

$\omega = 2\pi f \quad (f =$ frequency of vibration)

The equation for the determination of *energy transmitted* to the soil per cycle (E_{Tr}) may be obtained as follows:

$$E_{Tr} = \int F dz = F_{av} A_z \tag{9.17}$$

Copyright 2017 Cengage Learning. All Rights Reserved. May not be copied, scanned, or duplicated, in whole or in part. Due to electronic rights, some third party content may be suppressed from the eBook and/or eChapter(s). Editorial review has deemed that any suppressed content does not materially affect the overall learning experience. Cengage Learning reserves the right to remove additional content at any time if subsequent rights restrictions require it.

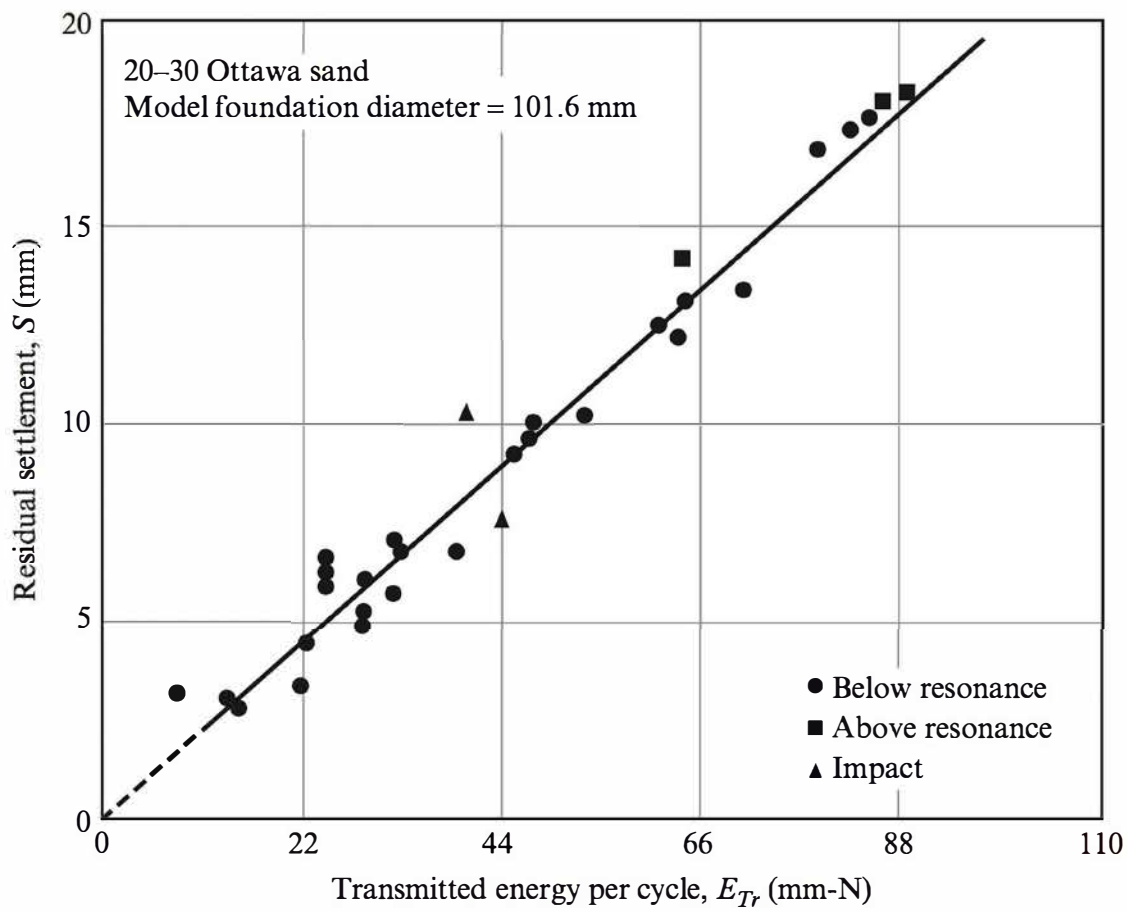

Figure 9.11 Plot of settlement versus transmitted energy per cycle (from Brumund and Leonards, 1972)

Source: Brumund, W.F., and Leonards, G.A. (1972). "Subsidence of Sand Due to Surface Vibration," *Journal of the Soil Mechanics and Foundations*, ASCE, Vol. 98, No. SM1, pp. 27–42. With permission from ASCE.

where F is the total contact force on the soil and F_{av} is the average contact force on the soil per cycle; however,

$$F_{av} = \frac{1}{2}(F_{\max} + F_{\min}) \tag{9.18}$$

$$F_{\max} = W + F_{\text{dyman(max)}} \tag{9.19}$$

and

$$F_{\max} = W - F_{\text{dynam(max)}} \tag{9.20}$$

Substituting Eqs. (9.19) and (9.20) into Eq. (9.18),

$$F_{av} = W \tag{9.21}$$

Thus, from Eqs. (9.17) and (9.21),

$$E_{Tr} = WA_z \tag{9.22}$$

Figure 9.11 shows that the transmitted energy per cycle of oscillation E_{Tr} varies linearly with the settlement. A plot of the experimental results of settlement against peak acceleration for different ranges of E_{Tr} is plotted in Figure 9.12. This

Copyright 2017 Cengage Learning. All Rights Reserved. May not be copied, scanned, or duplicated, in whole or in part. Due to electronic rights, some third party content may be suppressed from the eBook and/or eChapter(s). Editorial review has deemed that any suppressed content does not materially affect the overall learning experience. Cengage Learning reserves the right to remove additional content at any time if subsequent rights restrictions require it.

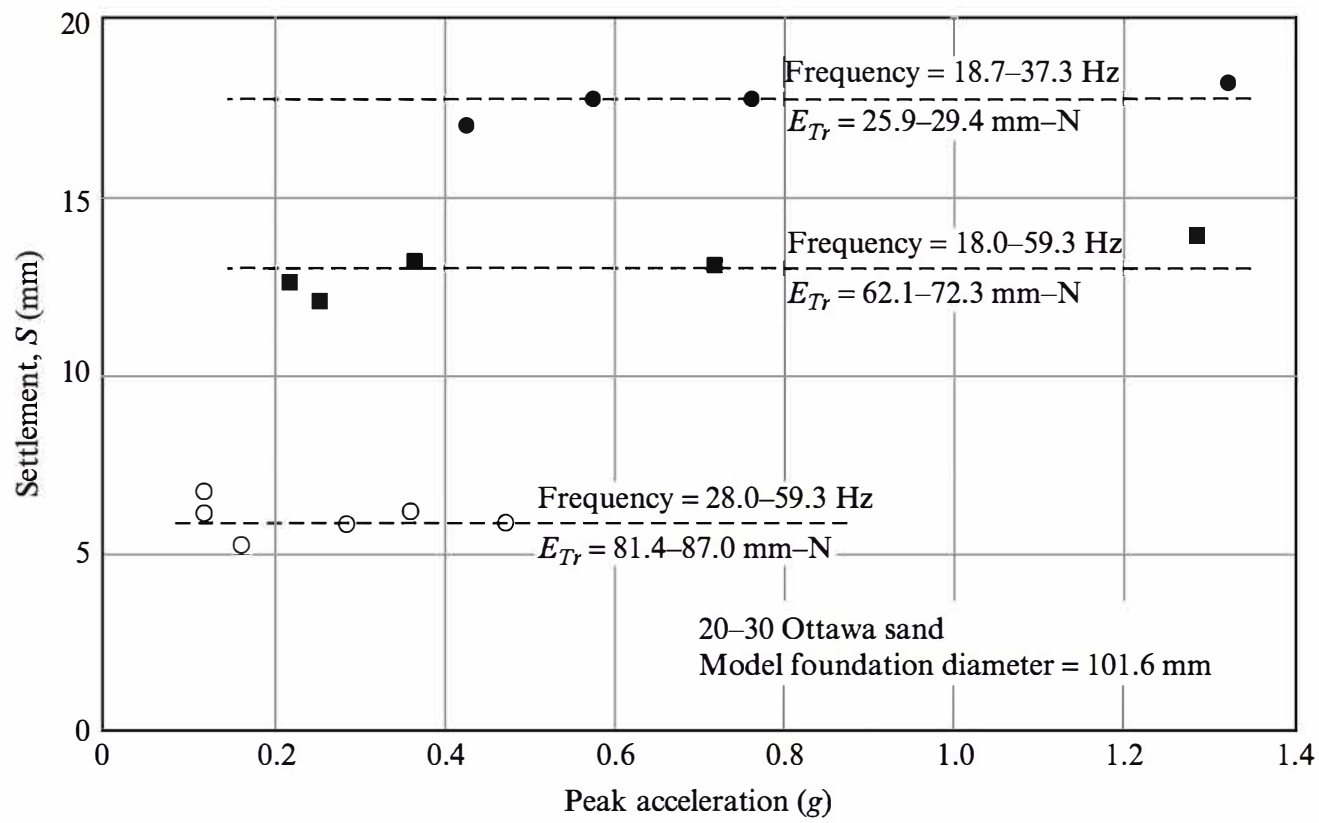

Figure 9.12 Settlement versus peak acceleration for three levels of transmitted energy (from Brumund and Leonards, 1972)

Source: Brumund, W.F., and Leonards, G.A. (1972). "Subsidence of Sand Due to Surface Vibration," *Journal of the Soil Mechanics and Foundations*, ASCE, Vol. 98, No. SM1, pp. 27–42. With permission from ASCE.

clearly demonstrates that, if the value of the transmitted energy is constant, the residual settlement remains constant irrespective of the level of peak acceleration.

The preceding concept is very important for the analysis of settlement of foundation of machineries subjected to vertical vibration. However, at this time, techniques of extrapolation of settlement of prototype foundations from laboratory model tests are not available. In any case, if the foundation soil is granular and loose, it is always advisable to take precautions to avoid possible problem in settlement. A specification of at least 70% relative density of compaction is often cited.

On similar lines, the settlement of structures such as tall buildings, due to vibratory load, is often a result of structure rocking back and forth. This type of settlement is caused by dynamic structural loads that momentarily increase the foundation pressure acting on the soil. Lightly loaded structures are least vulnerable to this type of settlement.

9.5 SETTLEMENT OF SAND DUE TO CYCLIC SHEAR STRAIN

The experimental laboratory observations described in Section 9.2 have shown that when a sand layer is subjected to controlled vertical acceleration, considerable settlement does not occur up to a peak acceleration level of $a_{max} = g$.

Copyright 2017 Cengage Learning. All Rights Reserved. May not be copied, scanned, or duplicated, in whole or in part. Due to electronic rights, some third party content may be suppressed from the eBook and/or eChapter(s). Editorial review has deemed that any suppressed content does not materially affect the overall learning experience. Cengage Learning reserves the right to remove additional content at any time if subsequent rights restrictions require it.

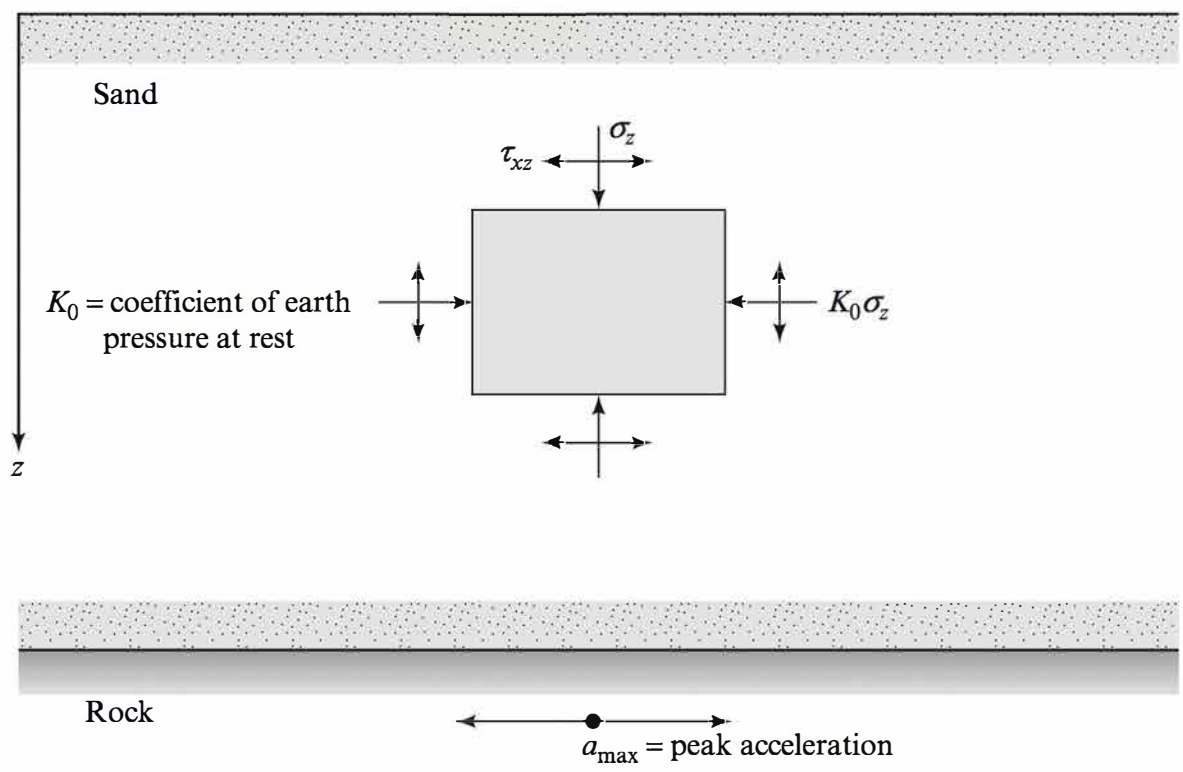

Figure 9.13 Settlement of sand due to cyclic shear strain

However, in several instances, the cyclic shear strains induced in the soil layers due to ground-shaking seismic events have caused considerable damage (Figure 9.13). The controlling parameters for settlement in granular soils due to cyclic shear strain have been studied in detail by Silver and Seed (1971). It was stated that relative density, maximum shear strain induced in the soil, and number of shear strain cycles are the main factors that control the amount of volumetric compression occurring in dry sands. These three factors are related to peak ground acceleration and the magnitude of the earthquake. Some of the results of this study are presented in this section.

The laboratory work of Silver and Seed was conducted on sand by using simple shear equipment developed by the Norwegian Geotechnical Institute. The frequency of the shear stress application to the sand specimens was 1 Hz. Dry sand specimens were tested at various relative densities of compaction being subjected to varying normal stresses σ_z and amplitudes of shear strain γ'_{xz}.

An example of the nature of variation of the vertical strain $\varepsilon_z = \Delta H/H$ (H = initial height of the specimen, ΔH = settlement) with number of cycles of shear strain application for a medium dense sand is shown in Figure 9.14. For these tests, the initial relative density (R_D) of compaction was 60%. Based on Figure 9.14, the following observations can be made.

a. For a given normal stress σ_z and amplitude of shear strain γ'_{xz}, the vertical strain increases with the number of strain cycles. However, a large portion of the vertical strain occurs in the first few cycles. For example, in Figure 9.14,

Copyright 2017 Cengage Learning. All Rights Reserved. May not be copied, scanned, or duplicated, in whole or in part. Due to electronic rights, some third party content may be suppressed from the eBook and/or eChapter(s). Editorial review has deemed that any suppressed content does not materially affect the overall learning experience. Cengage Learning reserves the right to remove additional content at any time if subsequent rights restrictions require it.

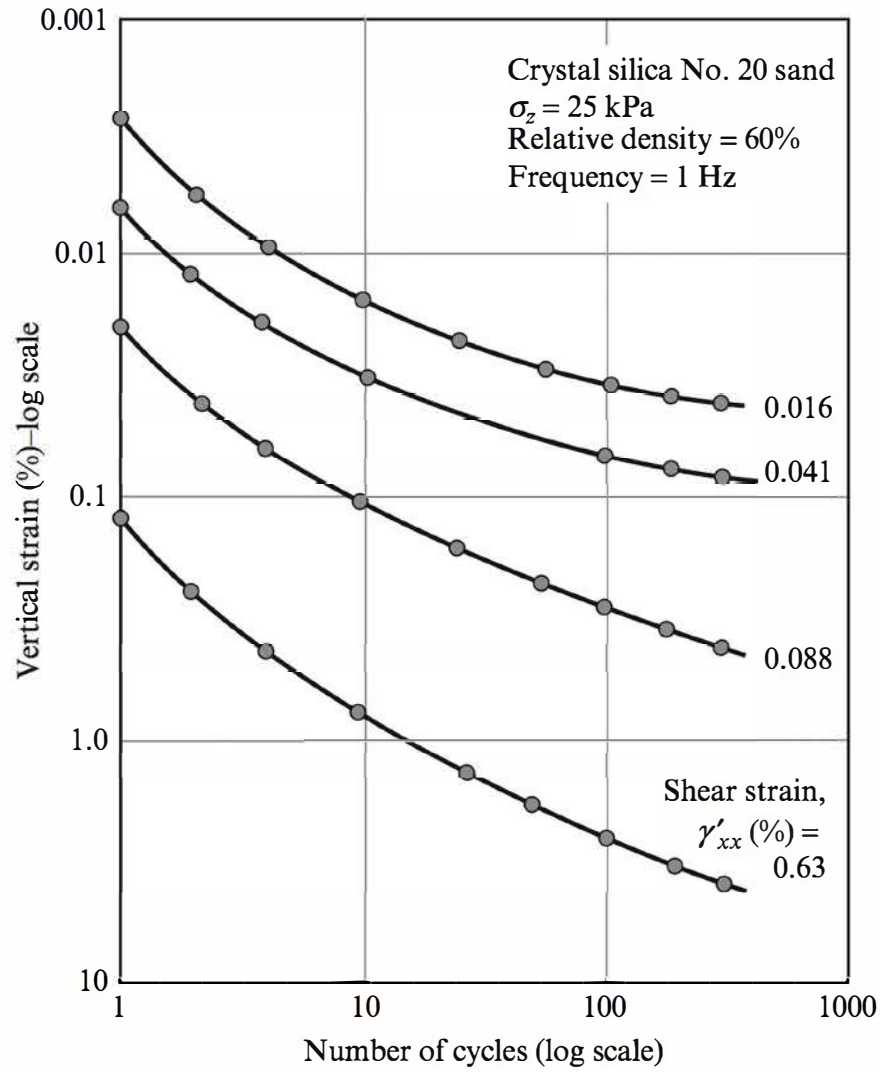

Figure 9.14 Variation of vertical strain with number of cycles (from Silver and Seed, 1971)

Source: Silver, M.L., and Seed, H.B. (1971). "Volume Changes in Sands During Cyclic Loading," *Journal of the Soil Mechanics and Foundations Division*, ASCE, Vol. 97, No. SM9, pp. 1171–1182. With permission from ASCE.

the vertical strain occurring in the first 10 cycles is approximately equal to or more than that occurring in the next 40–50 cycles.

b. For a given value of the vertical stress and number of cycles N, the vertical strain increases with the increase of the shear strain amplitude.

However, one has to keep in mind that a small amount of compaction (i.e., increase in the relative density) could markedly reduce the settlement of a given soil. Silver and Seed (1971) also observed that, at higher amplitudes of cyclic shear strain $\gamma'_{xz} > 0.05\%$ for a given value of N, the vertical strain is not significantly affected by the magnitude of the vertical stress. This may not be true where the shear strain is less than 0.05%.

The basic understanding of the laboratory test results for the settlement due to cyclic shear strain application may now be used for calculation of settlement of sand layers due to seismic effect. This is presented in the following section.

Copyright 2017 Cengage Learning. All Rights Reserved. May not be copied, scanned, or duplicated, in whole or in part. Due to electronic rights, some third party content may be suppressed from the eBook and/or eChapter(s). Editorial review has deemed that any suppressed content does not materially affect the overall learning experience. Cengage Learning reserves the right to remove additional content at any time if subsequent rights restrictions require it.

9.6 CALCULATION OF SETTLEMENT OF DRY SAND LAYERS SUBJECTED TO SEISMIC EFFECT

Seed and Silver (1972) have suggested a procedure to calculate the settlement of a sand layer subjected to seismic effect. This procedure is outlined in a step-by-step manner.

1. Since the primary source of ground motion in a soil deposit during an earthquake is due to the upward propagation of motion from the underlying rock formation, adopt a representative history of horizontal acceleration for the base.
2. Divide the soil layer into n layers. They need not be of equal thickness.
3. Calculate the average value of the vertical effective stress $\bar{\sigma}_z$ for each layer. (Note: In dry sand, total stress is equal to effective stress.)
4. Determine the representative relative densities for each layer.
5. Using the damping ratio and the shear moduli characteristics given in Section 4.19, calculate the history of shear strains at the middle of all n layers.
6. Convert the irregular strain histories obtained for each layer (Step 5) into average shear strains and equivalent number of uniform cycles (see Chapter 7).
7. Conduct laboratory tests with simple shear equipment on representative soil specimens from each layer to obtain the vertical strains for the equivalent number of strain cycles calculated in Step 6. This has to be done for the average effective vertical stress levels $\bar{\sigma}_z$ calculated in Step 3 and the corresponding average shear strain levels calculated in Step 6.
8. Calculate the total settlement as

$$\Delta H = \varepsilon_{z(1)}H_1 + \varepsilon_{z(2)}H_2 + \cdots + \varepsilon_{z(n)}H_n \tag{9.23}$$

where $\varepsilon_{z(1)}, \varepsilon_{z(2)}, \ldots$ are average vertical strains determined in Step 7 for layers $1, 2, \ldots$ and $H_1, H_2, \ldots$ are layer thicknesses.

The applicability of this procedure is explained in Example 9.1.

EXAMPLE 9.1

A 20 m-thick sand layer is shown in Figure 9.15a. The unit weight of soil is 16.1 kN/m^3. Using a design earthquake record, the average shear strain in the soil layer has been evaluated and plotted in Figure 9.15a. (Note: It was assumed that $\gamma'_{av} \approx 0.65\gamma'_{max}$. In this evaluation, the procedure outlined in Section 4.19 was followed with $G_{max} = 218.82K_{2(max)}\bar{\sigma}^{1/2}$ kPa and damping = 20%. The number of equivalent cycles of shear strain application was estimated to be 10. Cyclic simple shear tests on representative specimens of this sand were conducted with their *corresponding vertical stresses* as in the field. The results of these tests are shown in Figure 9.15b. Estimate the probable settlement of the sand layer.

Copyright 2017 Cengage Learning. All Rights Reserved. May not be copied, scanned, or duplicated, in whole or in part. Due to electronic rights, some third party content may be suppressed from the eBook and/or eChapter(s). Editorial review has deemed that any suppressed content does not materially affect the overall learning experience. Cengage Learning reserves the right to remove additional content at any time if subsequent rights restrictions require it.

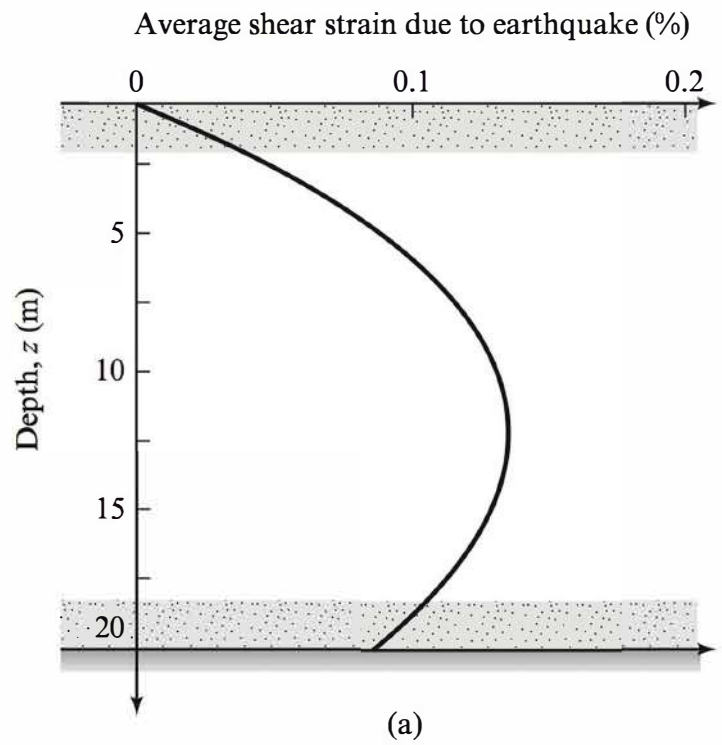

(a)

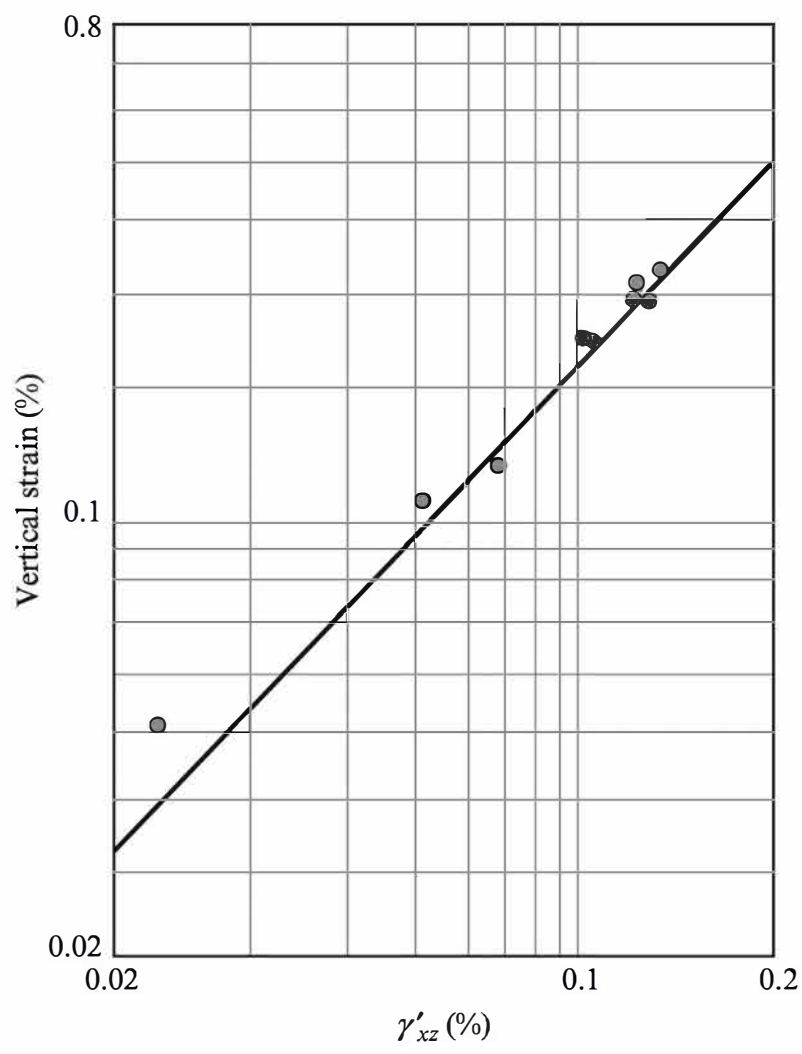

(b)

Figure 9.15 (a) Plot of average shear strain induced due to earthquake (sand unit weight = 16.1 kN/m^3; relative density = 50%); (b) laboratory simple shear test results (number of cycles = 10)

Copyright 2017 Cengage Learning. All Rights Reserved. May not be copied, scanned, or duplicated, in whole or in part. Due to electronic rights, some third party content may be suppressed from the eBook and/or eChapter(s). Editorial review has deemed that any suppressed content does not materially affect the overall learning experience. Cengage Learning reserves the right to remove additional content at any time if subsequent rights restrictions require it.

SOLUTION:

From Figure 9.15b, it can be seen that, even though tests were conducted with different values of $\bar{\sigma}_z$, the results of ε_z versus γ'_{xz} are almost linear in a log-log plot. This shows that the magnitude of the effective overburden pressure has practically no influence on the vertical strain. Thus, for this calculation, the average line of the experimental results is used. For calculation of settlement, the following table can be prepared.

Depth (m)	H (m)	Shear strain at the middle of layer, γ'_{xz} (%)	ε_z (%)	$H\varepsilon_z \times 10^{-2}$ (m)
0–2.5	2.5	0.025	0.043	0.1075
2.5–5.0	2.5	0.065	0.13	0.325
5.0–7.5	2.5	0.100	0.22	0.550
7.5–10.0	2.5	0.125	0.28	0.700
10.0–12.5	2.5	0.140	0.31	0.775
12.5–15.0	2.5	0.135	0.30	0.750
15.0–17.5	2.5	0.125	0.28	0.700
17.5–20.0	2.5	0.105	0.23	0.575

$$\begin{aligned}\Delta H &= \sum H\varepsilon_z \\ &= 4.4825 \times 10^{-2}\,\text{m} \\ &\approx \mathbf{44.8\ mm}\end{aligned}$$

9.7 SETTLEMENT OF A DRY SAND LAYER DUE TO MULTIDIRECTIONAL SHAKING

Pyke, Seed, and Chan (1975) have made studies to calculate the settlement of a dry sand layer subjected to multidirectional shaking; i.e., shaking with accelerations in the x, y, and z directions as shown in Figure 9.16. The conclusions of this study show that the settlements caused by combined *horizontal motions* are approximately equal to the sum of the settlement caused by the components acting separately. The effect of the vertical acceleration is again to increase the settlement.

Figure 9.17 shows the effect of the vertical acceleration on settlement on Monterey No. 0 sand with an initial relative density of 60%. As an example, let us consider the problem of settlement given in Example 9.1. If the same sand layer is subjected to similar base accelerations in the x and y directions, and if the

Copyright 2017 Cengage Learning. All Rights Reserved. May not be copied, scanned, or duplicated, in whole or in part. Due to electronic rights, some third party content may be suppressed from the eBook and/or eChapter(s). Editorial review has deemed that any suppressed content does not materially affect the overall learning experience. Cengage Learning reserves the right to remove additional content at any time if subsequent rights restrictions require it.

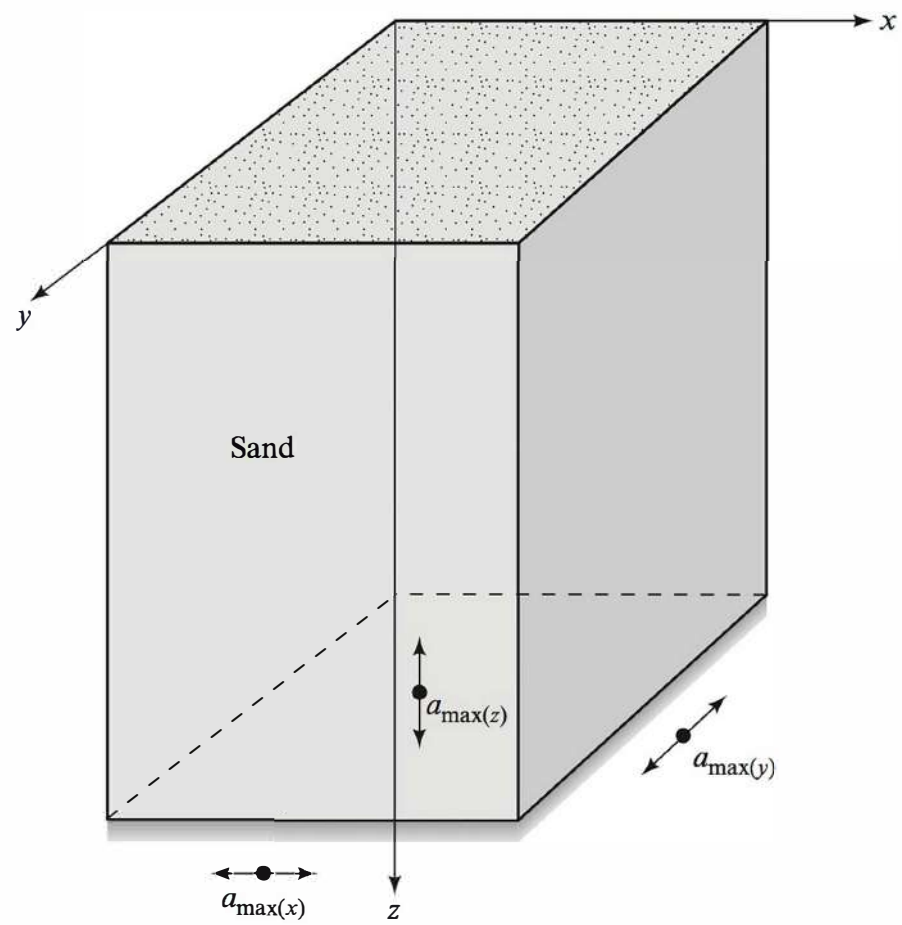

Figure 9.16 Multidirectional shaking—definition

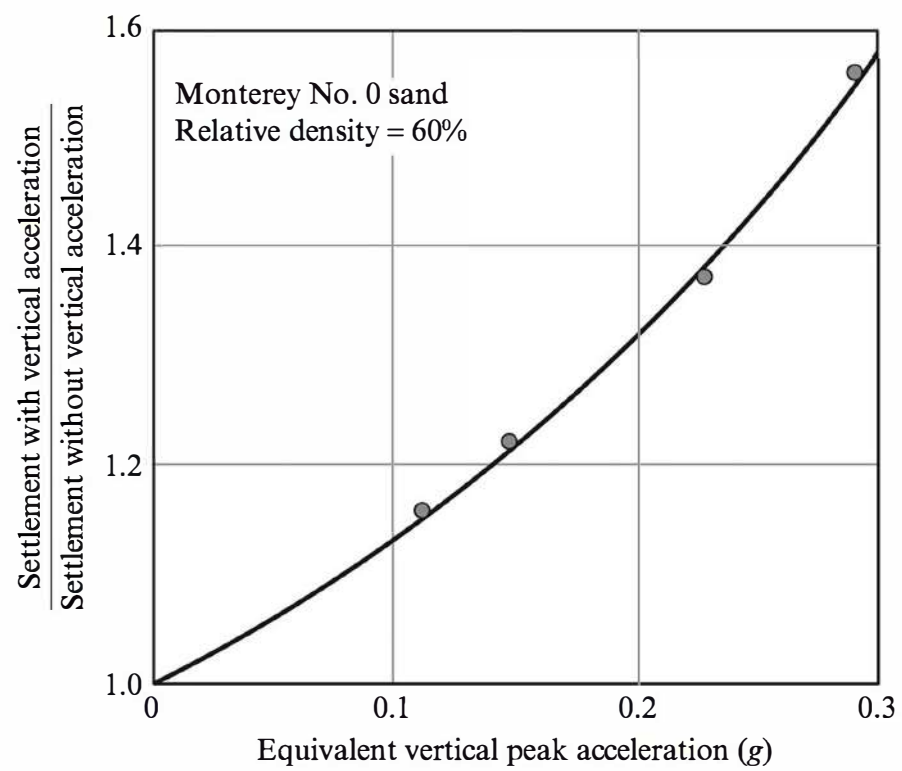

Figure 9.17 Effect of vertical motion superimposed on horizontal motion (from Pyke, Seed, and Chan, 1975)

Source: Pyke, R., Seed, H.B., and Chan, C.K. (1975). "Settlement of Sands Under Multidirectional Shaking," *Journal of the Geotechnical Engineering Division*, ASCE, Vol. 101, No. GT4, pp. 379–398. With permission from ASCE.

Copyright 2017 Cengage Learning. All Rights Reserved. May not be copied, scanned, or duplicated, in whole or in part. Due to electronic rights, some third party content may be suppressed from the eBook and/or eChapter(s). Editorial review has deemed that any suppressed content does not materially affect the overall learning experience. Cengage Learning reserves the right to remove additional content at any time if subsequent rights restrictions require it.

average vertical acceleration in the layer is about $0.2g$, the total settlement can be estimated as follows:

Settlement due to the component in the x direction = 44.8 mm

Settlement due to the component in the y direction = 44.8 mm

Total settlement due to horizontal motions = 89.6 mm

For $a_{z(\max)} = 0.2\ g$, from Figure 9.17, the ratio of settlement is about 1.3. Thus, the total settlement due to all three components is equal to 1.3(89.6) = 116.48 mm. It needs to be pointed out that vertical acceleration acting alone without horizontal motion has practically no effect on settlement up to about $1g$. However, when it acts in combination with the horizontal motion, it produces a marked increase of total settlement.

PROBLEMS

9.1 The results of a set of laboratory simple shear tests on a dry sand are given below (vertical stress $\bar{\sigma}_z = 20$ kPa; number of cycles = 12; frequency = 1 Hz; initial relative density of specimens = 65%).

Peak shear strain γ'_{xz} (%)	Vertical strain (%)	Peak shear strain γ'_{xz} (%)	Vertical strain (%)
0.02	0.035	0.10	0.095
0.04	0.060	0.15	0.200
0.06	0.075	0.20	0.280
0.08	0.090		

Plot the results on log-log graph paper. Approximate the results in the form of an equation

$$\gamma'_{xz} = m\varepsilon_z^n$$

9.2 A dry sand deposit is 12 m thick, and its relative density is 65%. This layer of sand may be subjected to an earthquake. The number of equivalent cycles of shear stress application due to an earthquake is estimated to be 12. Following is the variation of the *average* expected shear strain with depth.

Copyright 2017 Cengage Learning. All Rights Reserved. May not be copied, scanned, or duplicated, in whole or in part. Due to electronic rights, some third party content may be suppressed from the eBook and/or eChapter(s). Editorial review has deemed that any suppressed content does not materially affect the overall learning experience. Cengage Learning reserves the right to remove additional content at any time if subsequent rights restrictions require it.

Depth (m)	Average shear strain (%)	Depth (m)	Average shear strain (%)
0	0	7.5	0.186
1.5	0.080	9.0	0.170
3.0	0.135	10.5	0.160
4.5	0.155	12.0	0.140
6.0	0.175		

Estimate the probable settlement of the sand layer using the laboratory test results given in Problem 9.1.

9.3 Repeat Problem 9.2 for the following (depth of sand layer = 10 m):

Depth (m)	Average shear strain (%)
0	0
2.5	0.100
5.0	0.140
7.5	0.135
10.0	0.117

References

Brumund, W. F., and Leonards, G. A. (1972). "Subsidence of Sand Due to Surface Vibration," *Journal of the Soil Mechanics and Foundations,* ASCE, Vol. 98, No. SM1, pp. 27–42.

D'Appolonia, D. J., and D'Appolonia, E. (1967). "Determination of the Maximum Density of Cohensionless Soils," *Proceedings*, 3rd Asian Regional Conference on Soil Mechanics and Foundation Engineering, Haifa, Israel, Vol. 1, p. 266.

D'Appolonia, E. (1970). "Dynamic Loadings," *Journal of the Soil Mechanics and Foundations Division*, ASCE, Vol. 96, No. SM1, pp. 49–72.

Krizek, R. J·, and Fernandez, J. J· (1971). "Vibratory Densification of Damp Clayey Sands," *Journal of the Soil Mechanics and Foundations Division*, ASCE, Vol. 97, No. SM8, pp. 1069–1079.

Ortigosa, P., and Whitman, R. V. (1968). "Densification of Sand by Vertical Vibrations with Almost Constant Stress," *Publication No. 206*, Department of Civil Engineering, Massachusetts Institute of Technology, Cambridge.

Pyke, R., Seed, H. B., and Chan, C. K. (1975). "Settlement of Sands Under Multidirectional Shaking," *Journal of the Geotechnical Engineering Division*, ASCE, Vol. 101, No. GT4, pp. 379–398.

Raymond, G. P., and Komos, F. E. (1978). "Repeated Load Testing of a Model Plane Strain Footings," *Canadian Geotechnical Journal*, Vol. 15, No. 2, pp. 190–201.

Seed, H. B., and Silver, M. L. (1972). "Settlement of Dry Sands During Earthquakes," *Journal of the Soil Mechanics and Foundations Division*, ASCE, Vol. 98, No. SM4, pp. 381–397.

Silver, M. L., and Seed, H. B. (1971). "Volume Changes in Sands During Cyclic Loading," *Journal of the Soil Mechanics and Foundations Division*, ASCE, Vol. 97, No. SM9, pp. 1171–1182.

Copyright 2017 Cengage Learning. All Rights Reserved. May not be copied, scanned, or duplicated, in whole or in part. Due to electronic rights, some third party content may be suppressed from the eBook and/or eChapter(s). Editorial review has deemed that any suppressed content does not materially affect the overall learning experience. Cengage Learning reserves the right to remove additional content at any time if subsequent rights restrictions require it.

Liquefaction of Soil

10

10.1 INTRODUCTION

During earthquakes, major destruction of various types of structures occurs due to the creation of fissures, abnormal and/or unequal movement, and loss of strength or stiffness of the ground. The loss of strength or stiffness of the ground results in the settlement of buildings, failure of earth dams, landslides, and other hazards. The process by which loss of strength occurs in soil is called *soil liquefaction*. The phenomenon of soil liquefaction is primarily associated with medium- to fine-grained *saturated cohesionless soils*. Examples of soil liquefaction-related damage are the June 16, 1964, earthquake at Niigata, Japan, the 1964 Alaskan earthquake, and also the 2001 *Republic Day* earthquake at Bhuj, India. Most of the destruction at port and harbor facilities during earthquakes is attributable to liquefaction. Classical examples are Kobe Port, Japan (1995 earthquake) and at Kandla Port, India (2001 earthquake).

One of the first attempts to explain the liquefaction phenomenon in sandy soils was made by Casagrande (1936) and is based on the concept of *critical void ratio*. Dense sand, when subjected to shear, tends to dilate; loose sand, under similar conditions, tends to decrease in volume. The void ratio at which sand does not change in volume when subjected to shear is referred to as the *critical void ratio*. Casagrande explained that deposits of sand that have a void ratio larger than the critical void ratio tend to decrease in volume when subjected to vibration by a *seismic effect*. If drainage is unable to occur, the pore water pressure increases. Based on the effective stress principles, at any depth of a soil deposit

$$\sigma' = \sigma - u \tag{10.1}$$

where σ' = effective stress
σ = total stress
u = pore water pressure

Copyright 2017 Cengage Learning. All Rights Reserved. May not be copied, scanned, or duplicated, in whole or in part. Due to electronic rights, some third party content may be suppressed from the eBook and/or eChapter(s). Editorial review has deemed that any suppressed content does not materially affect the overall learning experience. Cengage Learning reserves the right to remove additional content at any time if subsequent rights restrictions require it.

If the magnitude of σ remains practically constant, and the pore water pressure gradually increases, a time may come when σ will be equal to u. At that time, σ' will be equal to zero. Under this condition, the sand does not possess any shear strength, and it transforms into a liquefied state. However, one must keep in mind the following facts, which show that the critical void ratio concept may not be sufficient for a quantitative evaluation of soil liquefaction potential of sand deposits:

1. Critical void ratio is not a constant value but changes with confining pressure.
2. Volume changes due to dynamic loading conditions are different than the one-directional static load conditions realized in the laboratory by direct shear and triaxial shear tests.

For that reason, since the mid-1960s intensive investigations have been carried out around the world to determine the soil parameters that control liquefaction. In this chapter, the findings of some of these studies are discussed.

10.2 FUNDAMENTAL CONCEPT OF LIQUEFACTION

Figure 10.1 shows the gradual densification of sand by repeated back-and-forth straining in a simple shear test. For this case drainage from the soil occurs freely. Each cycle of straining reduces the void ratio of the soil by a certain amount, although at a decreasing rate. It is important to note that there exists a threshold shear strain, below which no soil densification can take place, irrespective of the number of cycles. Decrease in volume of the sand, as shown in Figure 10.1, can take place only if drainage occurs freely. However, under earthquake conditions, due to rapid cyclic straining this will not be the condition. Thus, during straining gravity loadings is transferred from soil solids to the pore water. The result will be an increase of pore water pressure with a reduction in the capacity of the soil to resist loading.

This is schematically shown in Figure 10.2. In this figure, let A be the point on the compression curve that represents the void ratio (e_0) and effective state of stress (σ'_A) at a certain depth in a saturated sand deposit. Due to a certain number of earthquake-related cyclic straining, let $AB = \Delta e$ be the equivalent change of void ratio of the soil at that depth if full drainage is allowed. However, if drainage is prevented, the void ratio will remain as e_0 and the effective stress will be reduced to the level of σ'_C, with an increase of pore water pressure of magnitude Δu. So the state of the soil can be represented by point C. If the number of cyclic straining is large enough, the magnitude of Δu may become equal to σ'_A, and the soil will liquefy.

Copyright 2017 Cengage Learning. All Rights Reserved. May not be copied, scanned, or duplicated, in whole or in part. Due to electronic rights, some third party content may be suppressed from the eBook and/or eChapter(s). Editorial review has deemed that any suppressed content does not materially affect the overall learning experience. Cengage Learning reserves the right to remove additional content at any time if subsequent rights restrictions require it.

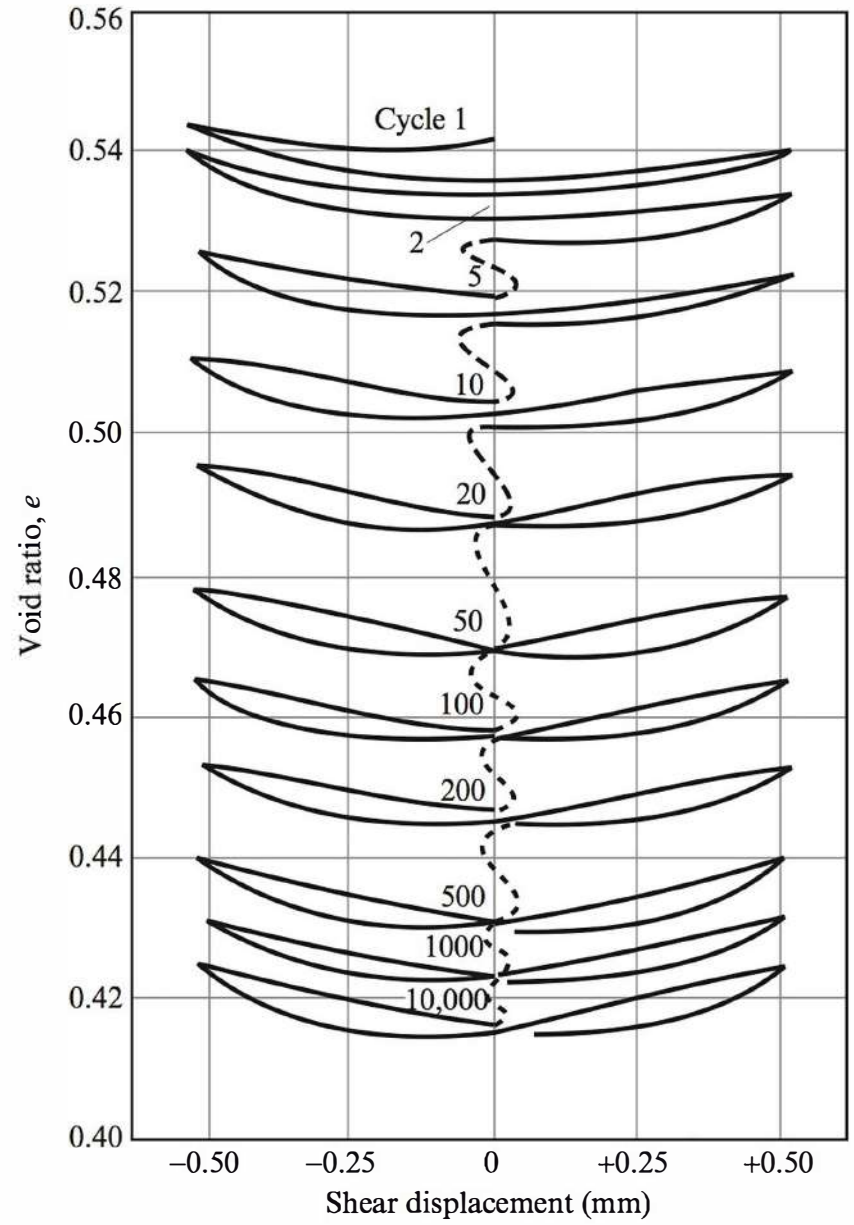

Figure 10.1 Void ratio versus cyclic shear displacement for densification of a sand with successive cycles of shear (from Youd, 1972)

Source: Youd, T.L. (1972). "Compaction of Sands by Repeated Straining," *Journal of the Soil Mechanics and Foundations Division*, ASCE, Vol. 98, No. SM7, pp. 709–725. With permission from ASCE.

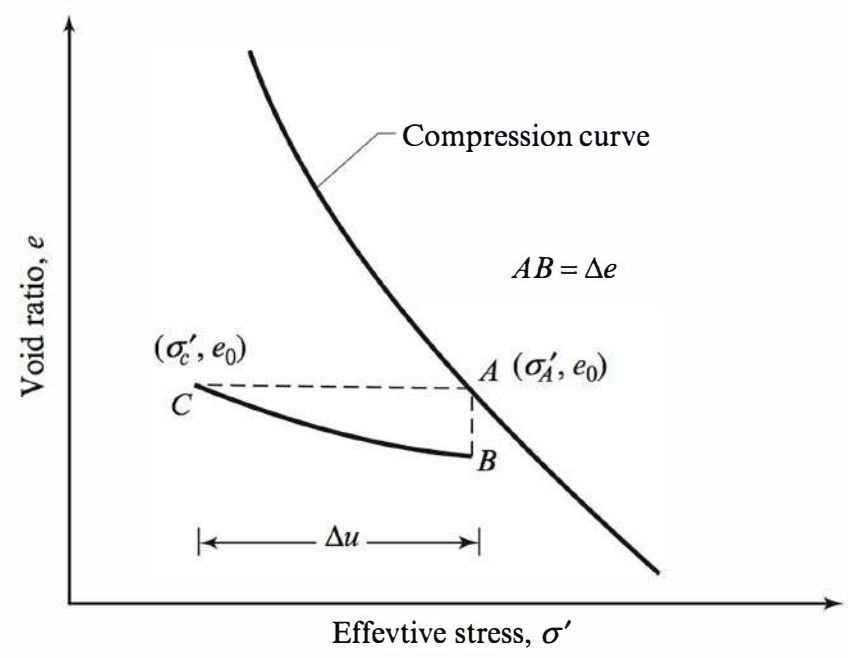

Figure 10.2 Mechanism of pore water pressure generation due to cyclic loading in undrained conditions

Copyright 2017 Cengage Learning. All Rights Reserved. May not be copied, scanned, or duplicated, in whole or in part. Due to electronic rights, some third party content may be suppressed from the eBook and/or eChapter(s). Editorial review has deemed that any suppressed content does not materially affect the overall learning experience. Cengage Learning reserves the right to remove additional content at any time if subsequent rights restrictions require it.

10.3 LABORATORY STUDIES TO SIMULATE FIELD CONDITIONS FOR SOIL LIQUEFACTION

If one considers a soil element in the field, as shown in Figure 10.3a, when earthquake effects are not present, the vertical effective stress on the element is equal to σ', which is equal to σ_v, and the horizontal effective stress on the element equals $K_0\sigma_v$, where K_0 is the at-rest earth pressure coefficient. Due to ground-shaking during an earthquake, a cyclic shear stress τ_h will be imposed on the soil element. This is shown in Figure 10.3b. Hence, any laboratory test to study the liquefaction problem must be designed in a manner so as to simulate the condition of a constant normal stress and a cyclic shear stress on a plane of the soil specimen. Various types of laboratory test procedure have been adopted in the past, such as the dynamic triaxial test (Seed and Lee, 1966; Lee and Seed, 1967), cyclic simple shear test (Peacock and Seed, 1968; Finn, Bransby, and Pickering, 1970; Seed and Peacock, 1971), cyclic torsional shear test (Yoshimi and Oh-oka, 1973; Ishibashi and Sherif, 1974), and shaking table test (Prakash and Mathur, 1965). However, the most commonly used laboratory test procedures are the dynamic triaxial tests and the simple shear tests. These are discussed in detail in the following sections.

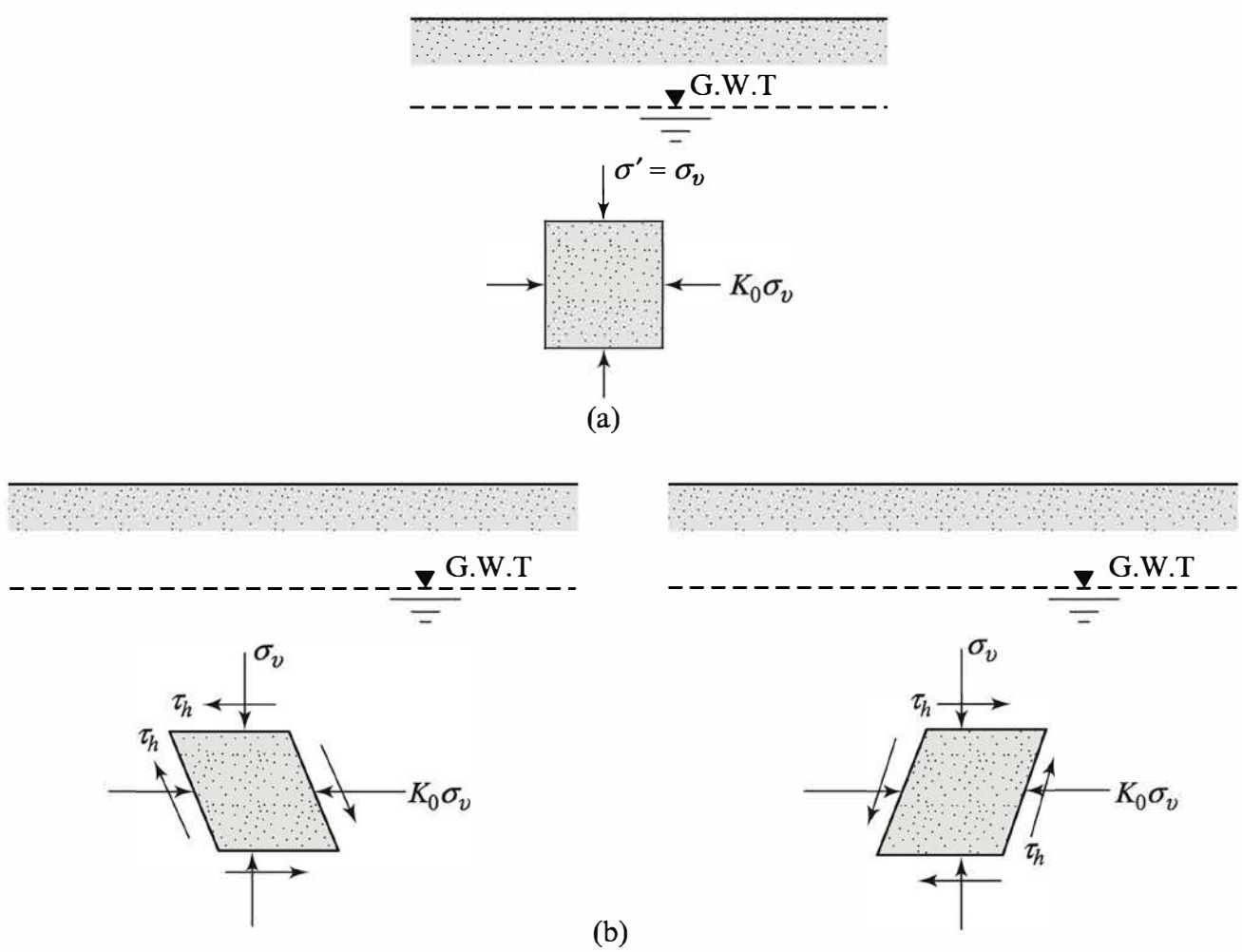

Figure 10.3 Application of cyclic shear stress on a soil element due to an earthquake

Copyright 2017 Cengage Learning. All Rights Reserved. May not be copied, scanned, or duplicated, in whole or in part. Due to electronic rights, some third party content may be suppressed from the eBook and/or eChapter(s). Editorial review has deemed that any suppressed content does not materially affect the overall learning experience. Cengage Learning reserves the right to remove additional content at any time if subsequent rights restrictions require it.

Dynamic Triaxial Test

10.4 GENERAL CONCEPTS AND TEST PROCEDURES

Consider a saturated soil specimen in a triaxial test, as shown in Figure 10.4a, which is consolidated under an all-around pressure of σ_3. The corresponding Mohr's circle is shown in Figure 10.4b. If the stresses on the specimen are changed such that the axial stress is equal to $\sigma_3 + (1/2)\sigma_d$ and the radial stress is $\sigma_3 - (1/2)\sigma_d$ (Figure10.4c), and drainage into or out of the specimen is not allowed, then the corresponding total stress Mohr's circle is of the nature shown in Figure 10.4d. Note that the stresses on the plane $X-X$ are

$$\text{Total normal stress} = \sigma_3, \text{ shear stress} = +\frac{1}{2}\sigma_d$$

and the stresses on the plane $Y-Y$ are

$$\text{Total normal stress} = \sigma_3, \text{ shear stress} = -\frac{1}{2}\sigma_d$$

Similarly, if the specimen is subjected to a stress condition as shown in Figure 10.4e, the corresponding total stress Mohr's circle will be as shown in Figure 10.4f. The stresses on the plane $X - X$ are

$$\text{Total normal stress} = \sigma_3, \text{ shear stress} = -\frac{1}{2}\sigma_d$$

The stresses on the plane $Y - Y$ are

$$\text{Total normal stress} = \sigma_3, \text{ shear stress} = +\frac{1}{2}\sigma_d$$

It can be seen that, if cyclic normal stresses of magnitude $(1/2)\,\sigma_d$ are applied simultaneously in the horizontal and vertical directions, one can achieve a stress condition along planes $X - X$ and $Y - Y$ that will be similar to the cyclic shear stress application shown in Figure 10.3b.

However, for saturated sands, actual laboratory tests can be conducted by applying an all-around consolidation pressure of σ_3 and then applying a cyclic load having an amplitude of σ_d in the axial direction only without allowing drainage as shown in Figure 10.5a. The axial strain and the excess pore water pressure can be measured along with the number of cycles of load (σ_d) application.

The question may now arise as to how the loading system shown in Figure 10.5a would produce stress conditions shown in Figure 10.4c and e. This can be explained as follows. The stress condition shown in Figure 10.5b is the sum of the stress conditions shown in Figure 10.5c and d. The effect of the stress

Copyright 2017 Cengage Learning. All Rights Reserved. May not be copied, scanned, or duplicated, in whole or in part. Due to electronic rights, some third party content may be suppressed from the eBook and/or eChapter(s). Editorial review has deemed that any suppressed content does not materially affect the overall learning experience. Cengage Learning reserves the right to remove additional content at any time if subsequent rights restrictions require it.

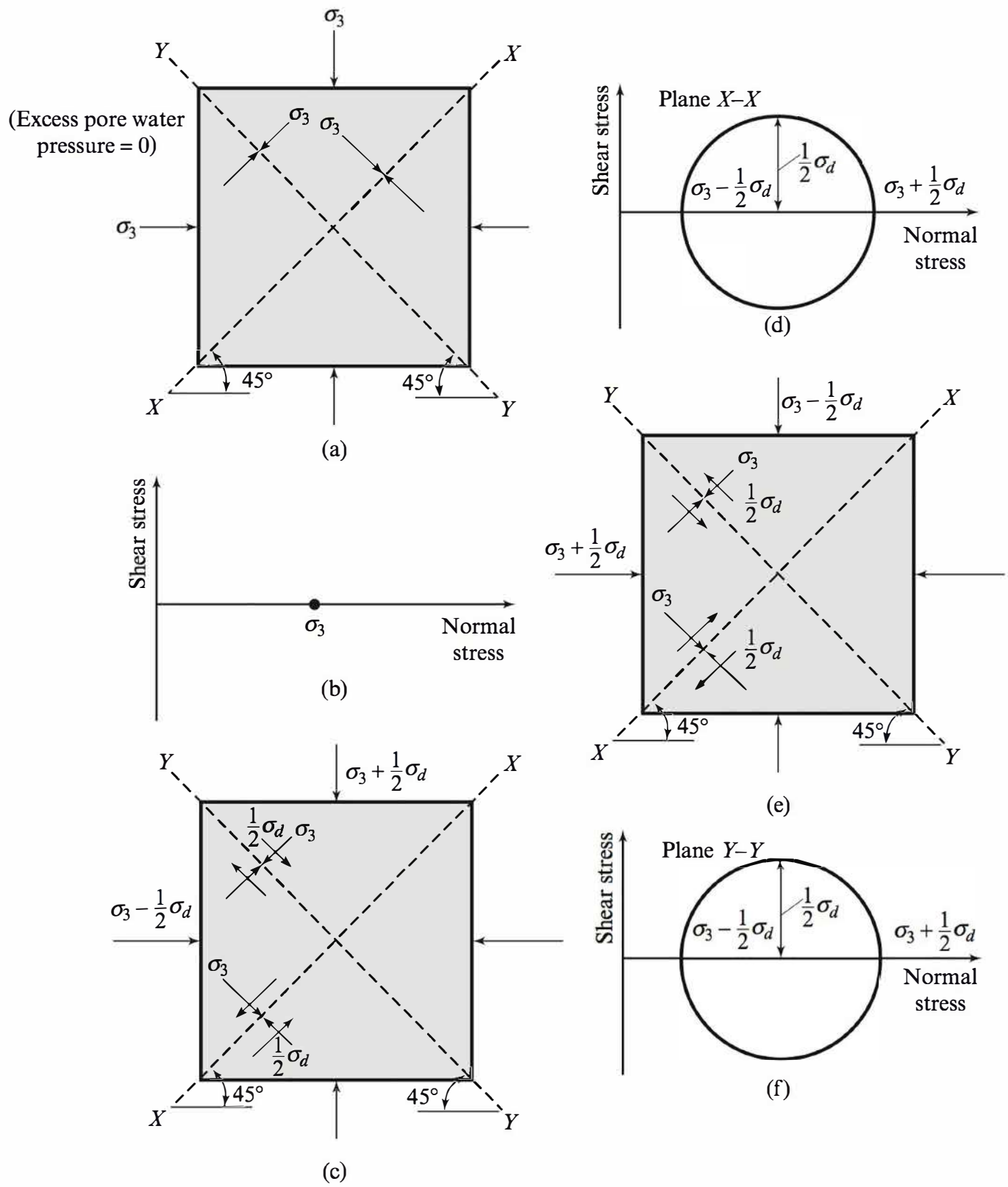

Figure 10.4 Simulation of cyclic shear stress on a plane for a triaxial test specimen

condition shown in Figure 10.5d is to reduce the excess pore water pressure of the specimen by an amount equal to $(1/2)\,\sigma_d$ without causing any change in the axial strain. Thus, the effect of the stress conditions shown in Figure 10.5b (which is the same as Figure 10.4c) can be achieved by only subtracting a pore water pressure $u = (1/2)\,\sigma_d$ from that observed from the loading condition shown in Figure 10.5c. Similarly, the loading condition shown in Figure 10.5e is the

Copyright 2017 Cengage Learning. All Rights Reserved. May not be copied, scanned, or duplicated, in whole or in part. Due to electronic rights, some third party content may be suppressed from the eBook and/or eChapter(s). Editorial review has deemed that any suppressed content does not materially affect the overall learning experience. Cengage Learning reserves the right to remove additional content at any time if subsequent rights restrictions require it.

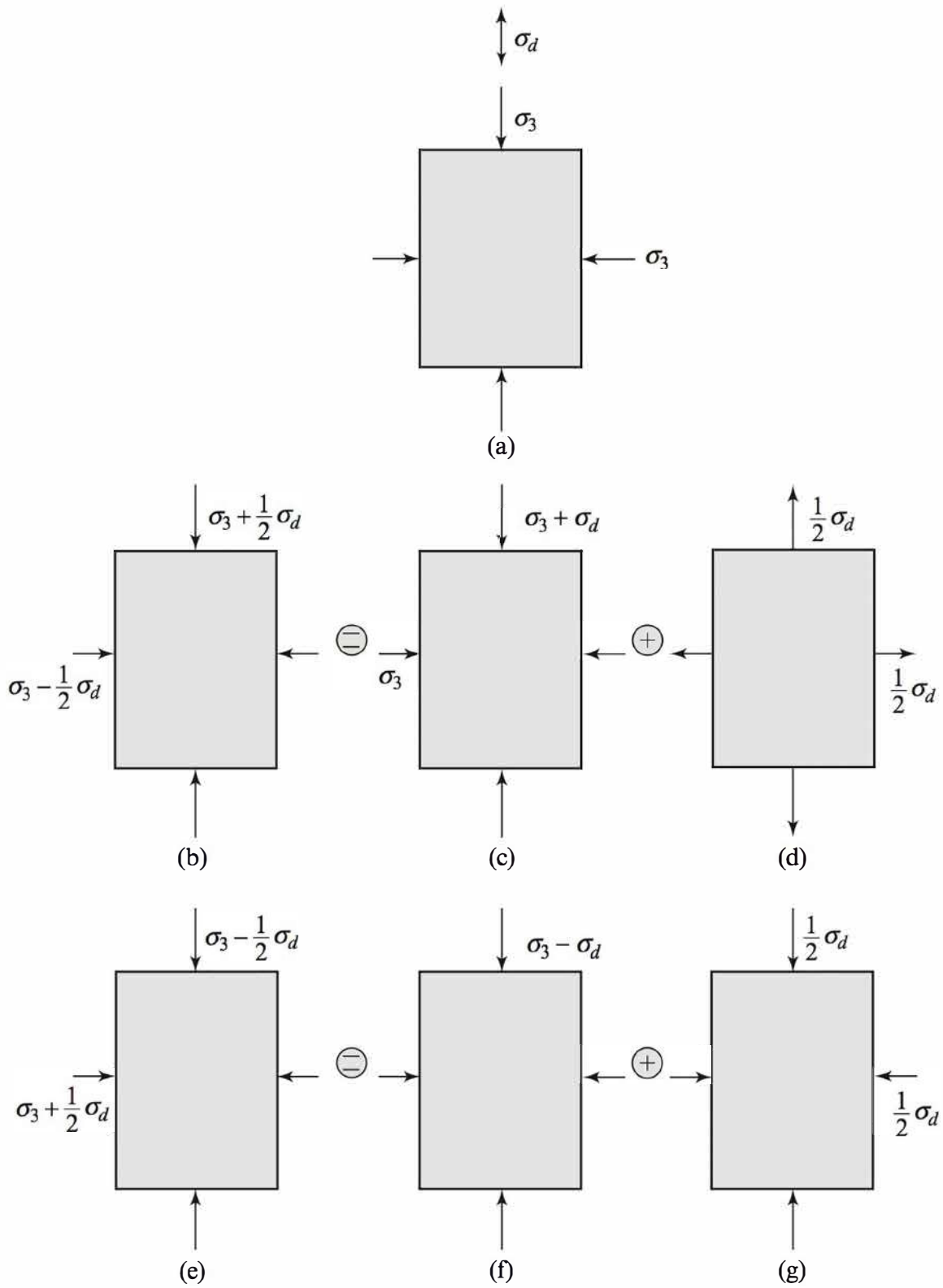

Figure 10.5

loading condition in Figure 10.5f plus the loading condition in Figure 10.5g. The effect of the stress condition shown in Figure 10.5g is only to increase the pore water pressure by an amount $(1/2)\,\sigma_d$. Thus the effect of the stress conditions shown in Figure 10.5e (which is the same as in Figure 10.4e) can be achieved by only adding $(1/2)\,\sigma_d$ to the pore water pressure observed from the loading condition in Figure 10.5f.

Copyright 2017 Cengage Learning. All Rights Reserved. May not be copied, scanned, or duplicated, in whole or in part. Due to electronic rights, some third party content may be suppressed from the eBook and/or eChapter(s). Editorial review has deemed that any suppressed content does not materially affect the overall learning experience. Cengage Learning reserves the right to remove additional content at any time if subsequent rights restrictions require it.

10.5 TYPICAL RESULTS FROM CYCLIC TRIAXIAL TEST

Several cyclic undrained triaxial tests on saturated soil specimens have been conducted by Seed and Lee (1966) on Sacramento River sand retained between No. 50 and No. 100 U.S sieves. The results of a typical test in *loose sand* (void ratio, $e = 0.87$) is shown in Figure 10.6. For this test, the initial all around pressure and initial pore water pressure were 200 kPa and 100 kPa, respectively. Thus the all around consolidation pressure σ_3 is equal to 100 kPa. The cyclic deviator stress σ_d was applied with a frequency of 2 Hz. Figure 10.7 is a plot of the

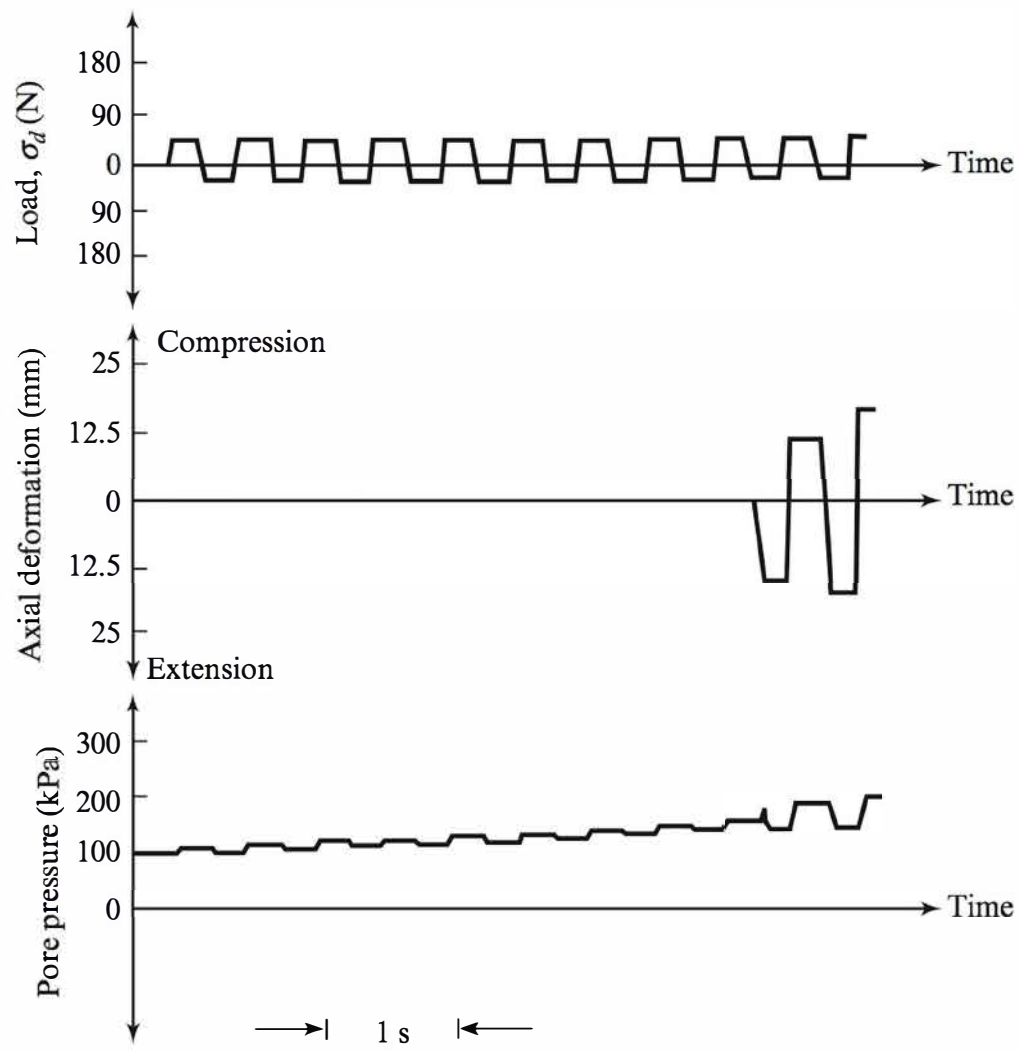

Test No. 114
Relative density = 38%
Initial void ratio = 0.87
Initial pore water pressure = 100 kPa
Initial confining pressure = 200 kPa
$\sigma_d = 40$ kPa

Figure 10.6 Typical pulsating load test on loose saturated Sacramento River sand (redrawn from Seed and Lee, 1966)

Source: Seed, H.B., and Lee, K.L. (1966). "Liquefaction of Saturated Sands During Cyclic Loading," *Journal of the Soil Mechanics and Foundations Division*, ASCE, Vol.92, No. SM6, pp. 105–134. With permission from ASCE.

Copyright 2017 Cengage Learning. All Rights Reserved. May not be copied, scanned, or duplicated, in whole or in part. Due to electronic rights, some third party content may be suppressed from the eBook and/or eChapter(s). Editorial review has deemed that any suppressed content does not materially affect the overall learning experience. Cengage Learning reserves the right to remove additional content at any time if subsequent rights restrictions require it.

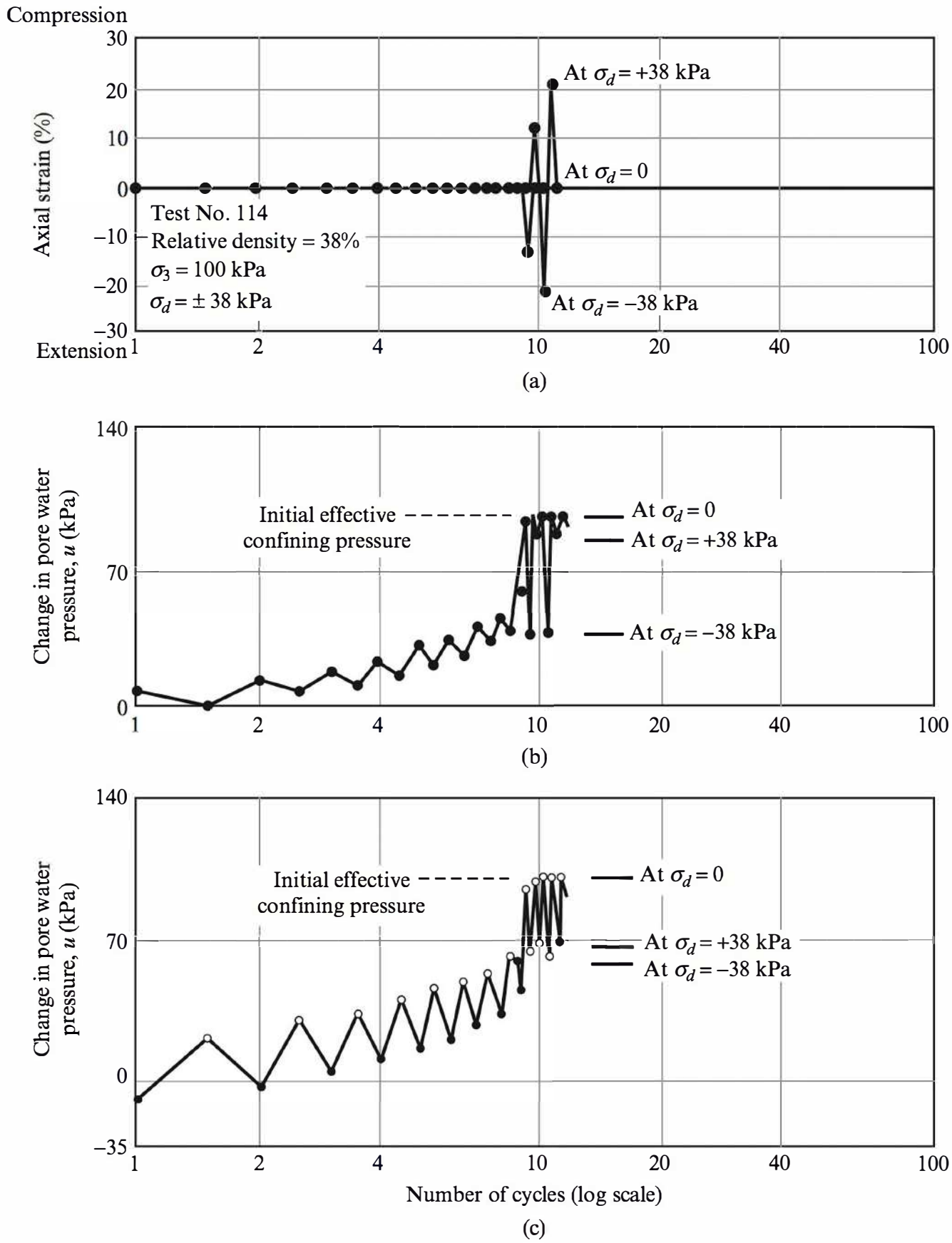

Figure 10.7 Typical pulsating load test on loose Sacramento River sand: (a) plot of axial strain versus number of cycle of load application; (b) observed change in pore water pressure versus number of cycles of load application; (c) change in pore water pressure (corrected to mean principal stress condition) versus number of cycles of load application (from Seed and Lee, 1966)

Source: Seed, H.B., and Lee, K.L. (1966). "Liquefaction of Saturated Sands During Cyclic Loading," *Journal of the Soil Mechanics and Foundations Division*, ASCE, Vol.92, No. SM6, pp. 105–134. With permission from ASCE.

Copyright 2017 Cengage Learning. All Rights Reserved. May not be copied, scanned, or duplicated, in whole or in part. Due to electronic rights, some third party content may be suppressed from the eBook and/or eChapter(s). Editorial review has deemed that any suppressed content does not materially affect the overall learning experience. Cengage Learning reserves the right to remove additional content at any time if subsequent rights restrictions require it.

axial strain, change in pore water pressure u, and the change in pore water pressure corrected to mean extreme principal stress conditions (i.e., subtracting or adding (1/2) σ_d from or to the observed pore water pressure) against the number of cycles of load application. Figure 10.7c shows that the change in pore water pressure becomes equal to σ_3 during the ninth cycle, indicating that the effective confining pressure is equal to zero. During the tenth cycle, the axial strain exceeded 20% and the soil liquefied.

The relationship between the magnitude of σ_d against the number of cycles of pulsating stress applications for the liquefaction of the same loose sand [$e = 0.87$, $\sigma_3 = 100$ kPa is shown in Figure 10.8. Note that the number of cycles of pulsating stress application increases with the decrease of the value of σ_d.

The nature of variation of the axial strain and the corrected pore water pressure for a pulsating load test in a dense Sacramento River sand is shown in Figure 10.9. After about 13 cycles, the change in pore water pressure becomes equal to σ_3; however, the axial strain amplitude did not exceed 10% after even 30 cycles of load application. This is a condition with a peak cyclic pore pressure ratio 100%, with limited strain potential due to the remaining resistance of the soil to deformation, or due to the fact that the soil dilates. Dilation of the soil reduces the pore water pressure and helps stabilization of soil under load. This may be referred to as cyclic mobility (Seed, 1979). More discussion on this subject is given in Section 10.11.

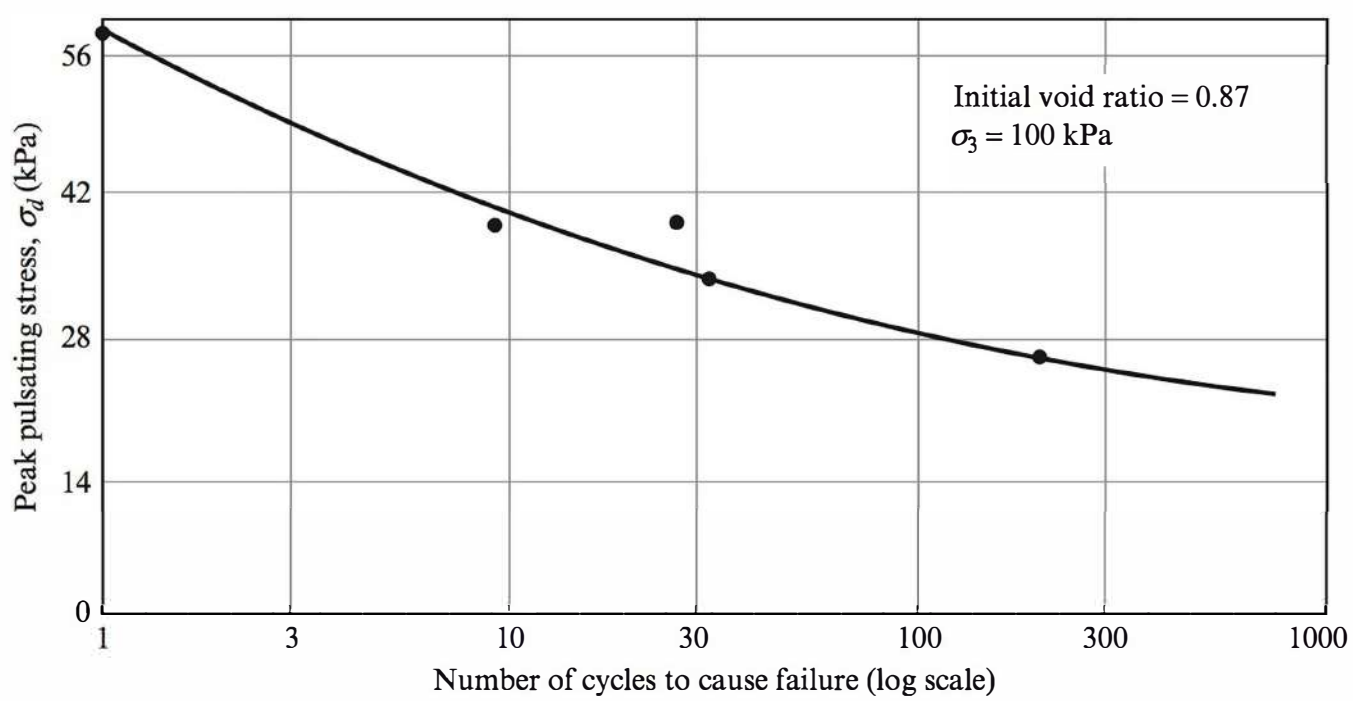

Figure 10.8 Relationship between pulsating deviator stress and number of cycles required to cause failure in Sacramento River sand (redrawn from Seed and Lee, 1966)

Source: Seed, H.B., and Lee, K.L. (1966). "Liquefaction of Saturated Sands During Cyclic Loading," *Journal of the Soil Mechanics and Foundations Division*, ASCE, Vol.92, No. SM6, pp. 105–134. With permission from ASCE.

Copyright 2017 Cengage Learning. All Rights Reserved. May not be copied, scanned, or duplicated, in whole or in part. Due to electronic rights, some third party content may be suppressed from the eBook and/or eChapter(s). Editorial review has deemed that any suppressed content does not materially affect the overall learning experience. Cengage Learning reserves the right to remove additional content at any time if subsequent rights restrictions require it.

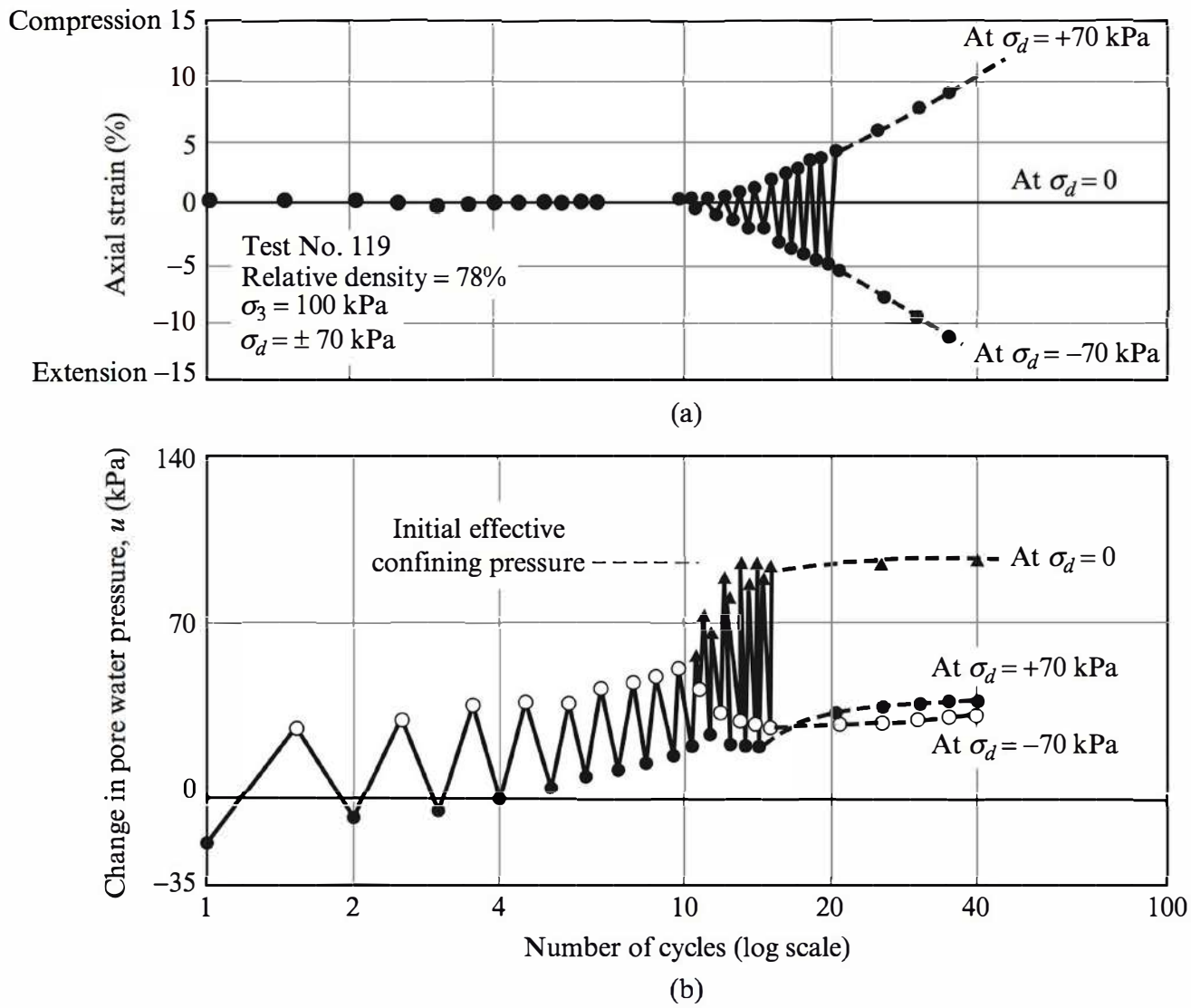

Figure 10.9 Typical pulsating load test on dense Sacramento River sand: (a) plot of axial strain versus number of cycles of load application; (b) corrected change of pore water pressure versus number of cycles of load application (from Seed and Lee, 1966)

Source: Seed, H.B., and Lee, K.L. (1966). "Liquefaction of Saturated Sands During Cyclic Loading," *Journal of the Soil Mechanics and Foundations Division*, ASCE, Vol.92, No. SM6, pp. 105–134. With permission from ASCE.

A summary of axial strain, number of cycles for liquefaction, and the relative density for Sacramento River sand are given in Figure 10.10 [for $\sigma_3 = 100$ kPa]. However, a different relationship may be obtained if the confining pressure σ_3 is changed.

It has been mentioned earlier that the critical void ratio of sand cannot be used as a unique criterion for a quantitative evaluation of the liquefaction potential. This can now be seen from Figure 10.11, which shows the critical void ratio line for Sacramento River sand. Based on the initial concept of critical void ratio, one would assume that a soil specimen represented by a point to the left of the critical void ratio line would *not* be susceptible to liquefaction; likewise, a

Copyright 2017 Cengage Learning. All Rights Reserved. May not be copied, scanned, or duplicated, in whole or in part. Due to electronic rights, some third party content may be suppressed from the eBook and/or eChapter(s). Editorial review has deemed that any suppressed content does not materially affect the overall learning experience. Cengage Learning reserves the right to remove additional content at any time if subsequent rights restrictions require it.

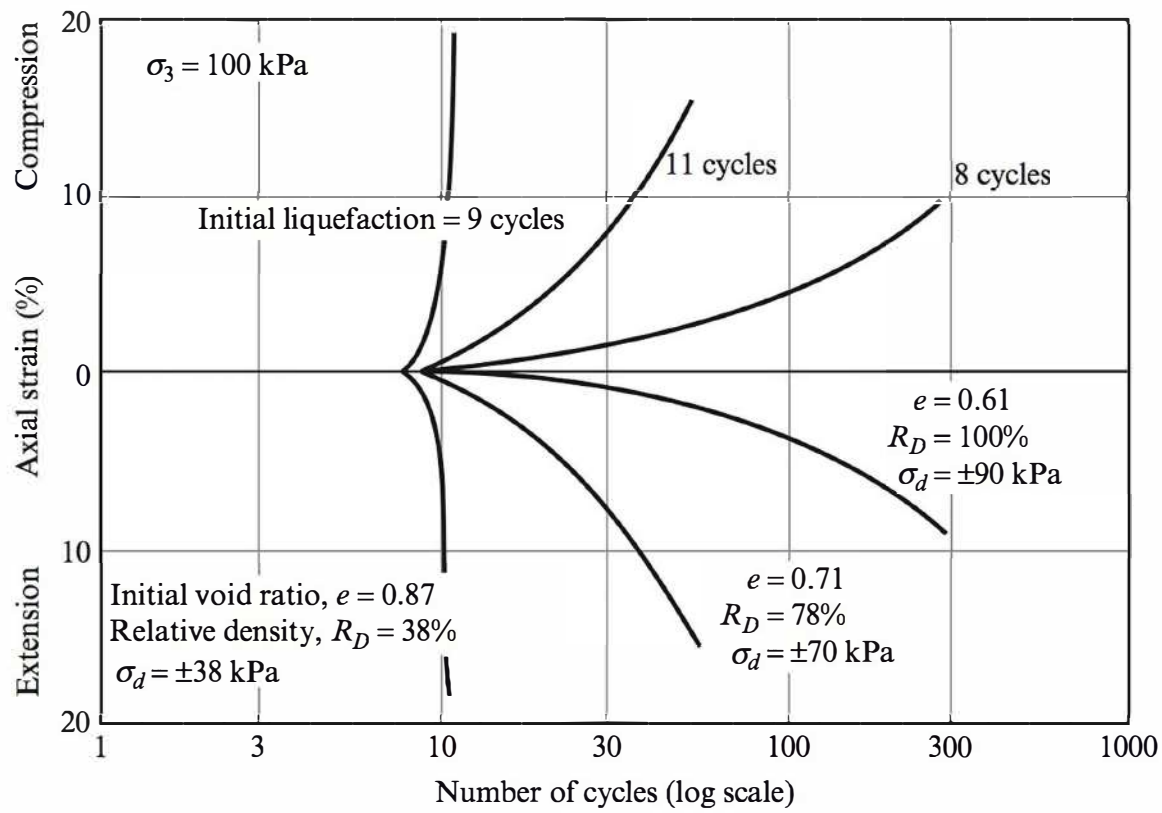

Figure 10.10 Axial strain from initial liquefaction for pulsating load tests at three densities for Sacramento River sand (from Seed and Lee, 1966)

Source: Seed, H.B., and Lee, K.L. (1966). "Liquefaction of Saturated Sands During Cyclic Loading," *Journal of the Soil Mechanics and Foundations Division*, ASCE, Vol.92, No. SM6, pp. 105–134. With permission from ASCE.

specimen that plots to the right of the critical void ratio line *would* be vulnerable to liquefaction. In order to test this concept, the cyclic load test results on two specimens are shown as *A* and *B* in Figure 10.11. Under a similar pulsating stress $\sigma_d = \pm 120$ kPa, specimen *A* liquefied in 57 cycles, whereas specimen *B* did not fail even in 10,000 cycles. This is contrary to the aforementioned assumptions.

Thus, the liquefaction potential depends on five important factors:

1. Relative density R_D
2. Confining pressure σ_3
3. Peak pulsating stress σ_d
4. Number of cycles of pulsating stress application
5. Overconsolidation ratio

The importance of the first four factors is discussed in the following section. The overconsolidation ratio is discussed in Section 10.9. Soil grain size characteristics, particle shape, aging and cementation, depositional environment, drainage conditions, and construction-induced loads are also known to have some effects on the liquefaction potential.

Copyright 2017 Cengage Learning. All Rights Reserved. May not be copied, scanned, or duplicated, in whole or in part. Due to electronic rights, some third party content may be suppressed from the eBook and/or eChapter(s). Editorial review has deemed that any suppressed content does not materially affect the overall learning experience. Cengage Learning reserves the right to remove additional content at any time if subsequent rights restrictions require it.

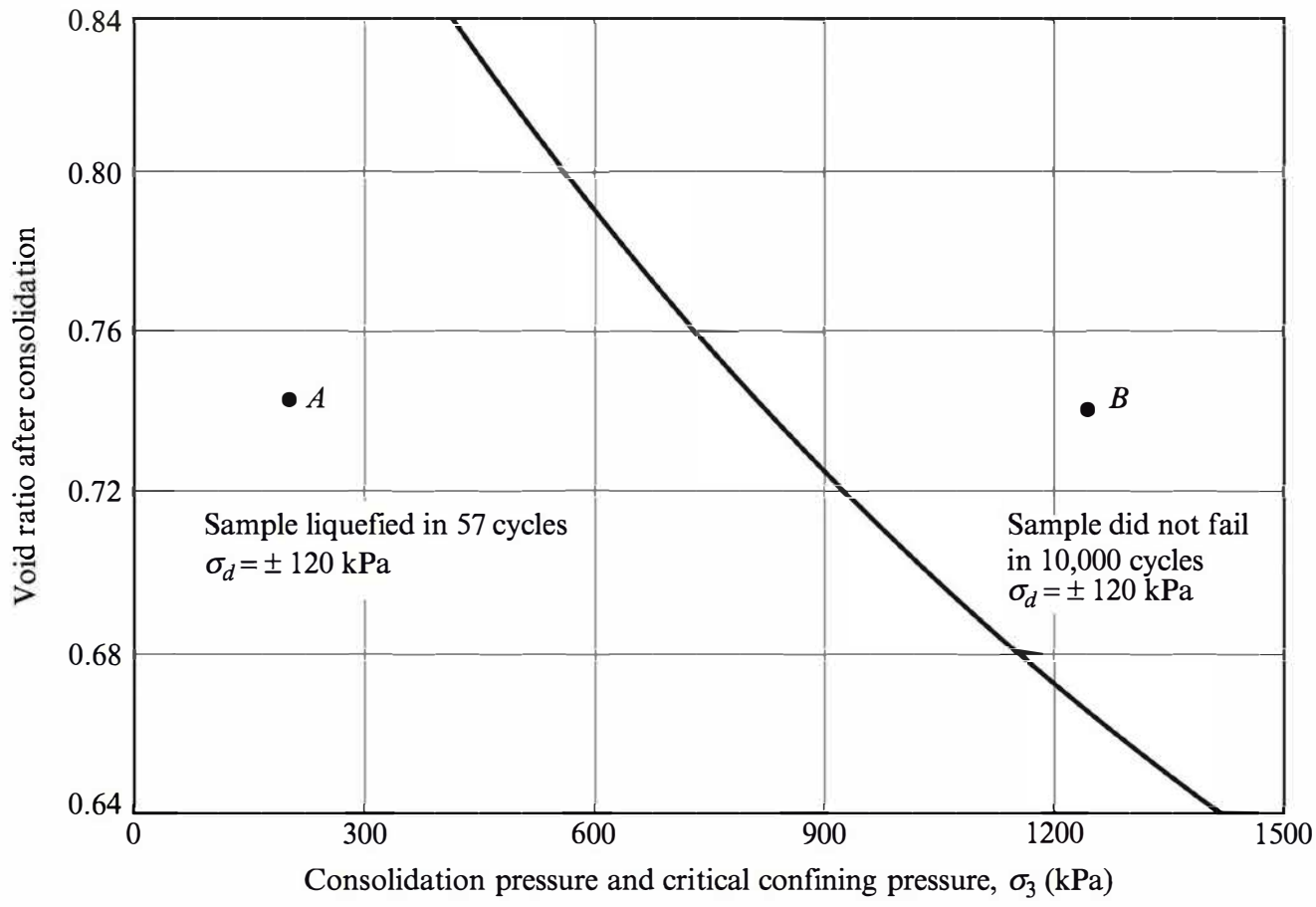

Figure 10.11 Critical confining pressure-void ratio relationship for Sacramento River sand (redrawn from Seed and Lee, 1966)

Source: Seed, H.B., and Lee, K.L. (1966). "Liquefaction of Saturated Sands During Cyclic Loading," *Journal of the Soil Mechanics and Foundations Division*, ASCE, Vol.92, No. SM6, pp. 105–134. With permission from ASCE.

10.6 INFLUENCE OF VARIOUS PARAMETERS ON SOIL LIQUEFACTION POTENTIAL

Influence of the Initial Relative Density

The effect of the initial relative density of a soil on liquefaction is shown in Figure 10.12. All tests shown in Figure 10.12 are for $\sigma_3 = 100$ kPa.

The initial liquefaction corresponds to the condition when the pore water pressure becomes equal to the confining pressure σ_3. In most cases, 20% double amplitude strain is considered as failure. It may be seen that, for a given value of σ_d, the initial liquefaction and the failure occur simultaneously for loose sand (Figure 10.12a). However, as the relative density increases, the difference between the number of cycle to cause 20% double amplitude strain and to cause initial liquefaction increases.

Influence of Confining Pressure

The influence of the confining pressure σ_3 on initial liquefaction and 20% double amplitude strain condition is shown in Figure 10.13. For a given initial relative

Copyright 2017 Cengage Learning. All Rights Reserved. May not be copied, scanned, or duplicated, in whole or in part. Due to electronic rights, some third party content may be suppressed from the eBook and/or eChapter(s). Editorial review has deemed that any suppressed content does not materially affect the overall learning experience. Cengage Learning reserves the right to remove additional content at any time if subsequent rights restrictions require it.

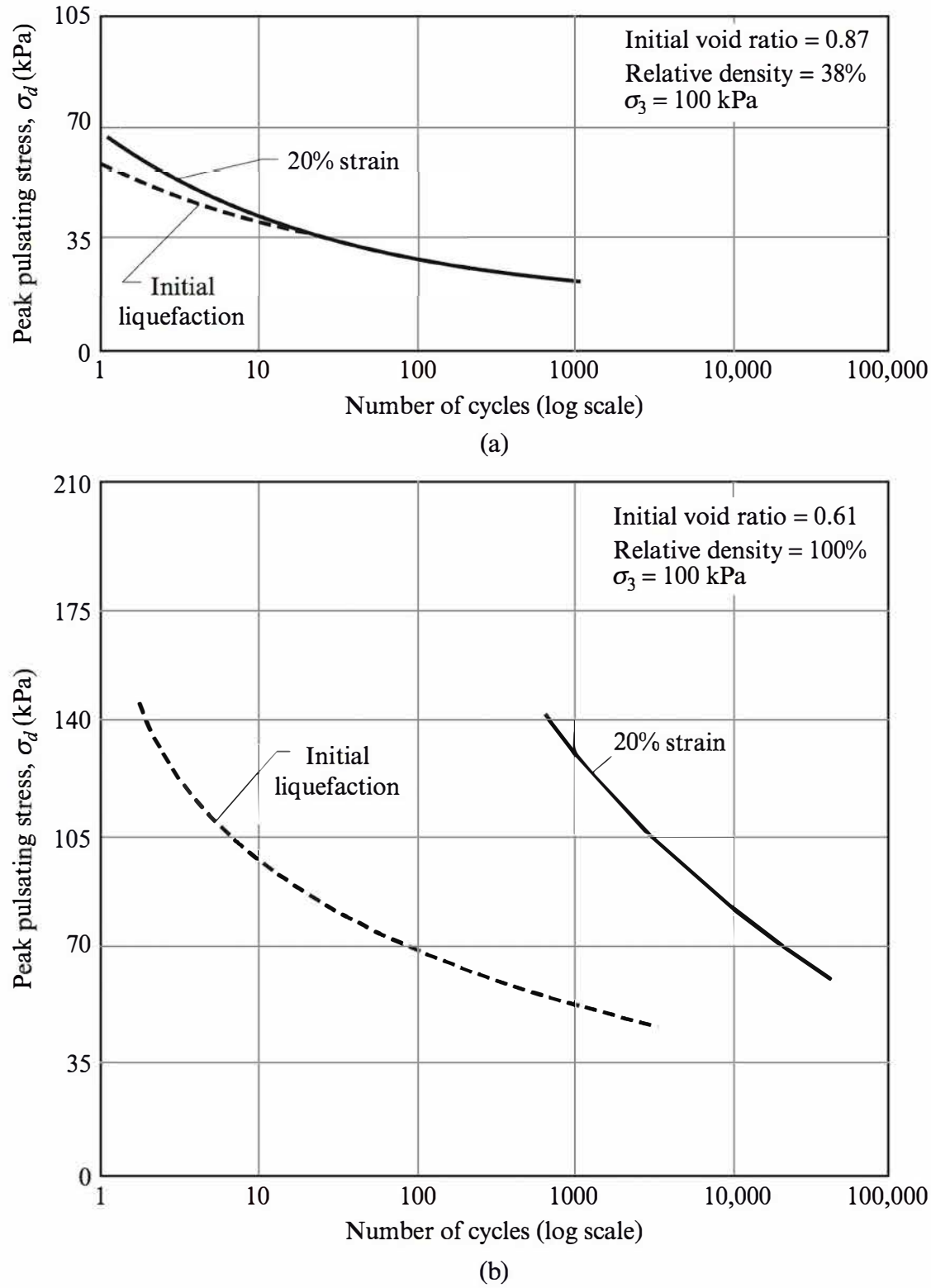

Figure 10.12 Influence of initial relative density on liquefaction for Sacramento River sand (redrawn from Lee and Seed, 1967)

Source: Lee, K.L., and Seed, H.B. (1967). "Cyclic Stress Condition Causing Liquefaction of Sand," *Journal of the Soil Mechanics and Foundations Division*, ASCE, Vol.93, No. SM1, pp. 47–70. With permission from ASCE.

density and peak pulsating stress, the number of cycles to cause initial liquefaction or 20% strain increases with the increase of the confining pressure. This is true for all relative densities of compaction. Conditions that can create greater confining pressure are deeper ground water table, soil located at a deeper depth and addition of surcharge on the ground surface.

Copyright 2017 Cengage Learning. All Rights Reserved. May not be copied, scanned, or duplicated, in whole or in part. Due to electronic rights, some third party content may be suppressed from the eBook and/or eChapter(s). Editorial review has deemed that any suppressed content does not materially affect the overall learning experience. Cengage Learning reserves the right to remove additional content at any time if subsequent rights restrictions require it.

Influence of the Peak Pulsating Stress

Figure 10.14 shows the variation of the peak pulsating stress σ_d with the confining pressure for initial liquefaction in 100 cycles (Figure 10.14a) and for 20% axial strain in 100 cycles (Figure 10.14b). Note that for a given initial void ratio (i.e., relative density R_D) and number of cycles of load application, the variation of σ_d for initial liquefaction with σ_3 is practically linear. A similar relation also exists for loose sand with a 20% axial strain condition. It is worth noting that the peak pulsating stress is a function of *peak ground acceleration* expected at the site.

It is also observed that, for sand having the same initial void ratio and same effective confining pressure, the higher the pulsating stress, the lower the number of cycles of deviatoric stress required to cause liquefaction.

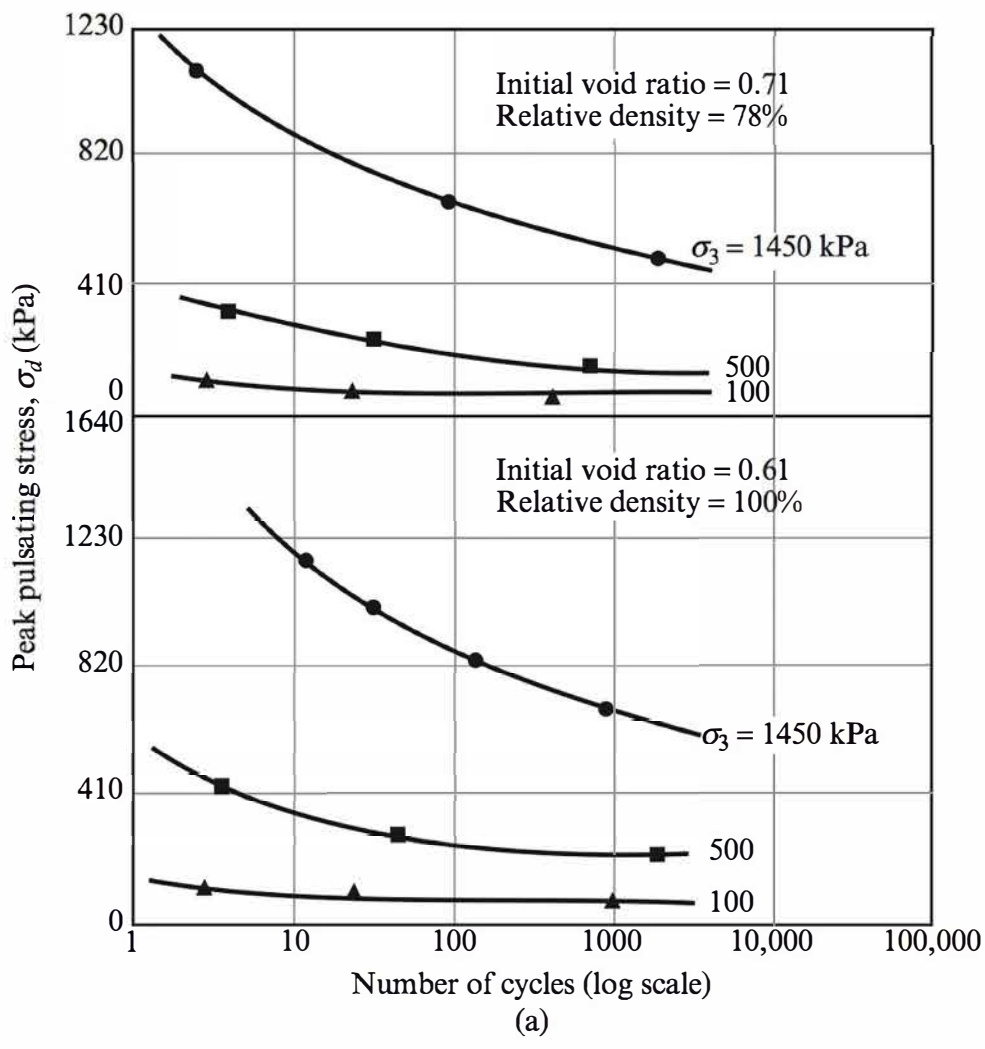

Figure 10.13 Influence of confining pressure on liquefaction of Sacramento River sand: (a) initial liquefaction; (b) 20% strain (redrawn from Lee and Seed, 1967)

Source: Lee, K.L., and Seed, H.B. (1967). "Cyclic Stress Condition Causing Liquefaction of Sand," *Journal of the Soil Mechanics and Foundations Division*, ASCE, Vol.93, No. SM1, pp. 47–70. With permission from ASCE.

Copyright 2017 Cengage Learning. All Rights Reserved. May not be copied, scanned, or duplicated, in whole or in part. Due to electronic rights, some third party content may be suppressed from the eBook and/or eChapter(s). Editorial review has deemed that any suppressed content does not materially affect the overall learning experience. Cengage Learning reserves the right to remove additional content at any time if subsequent rights restrictions require it.

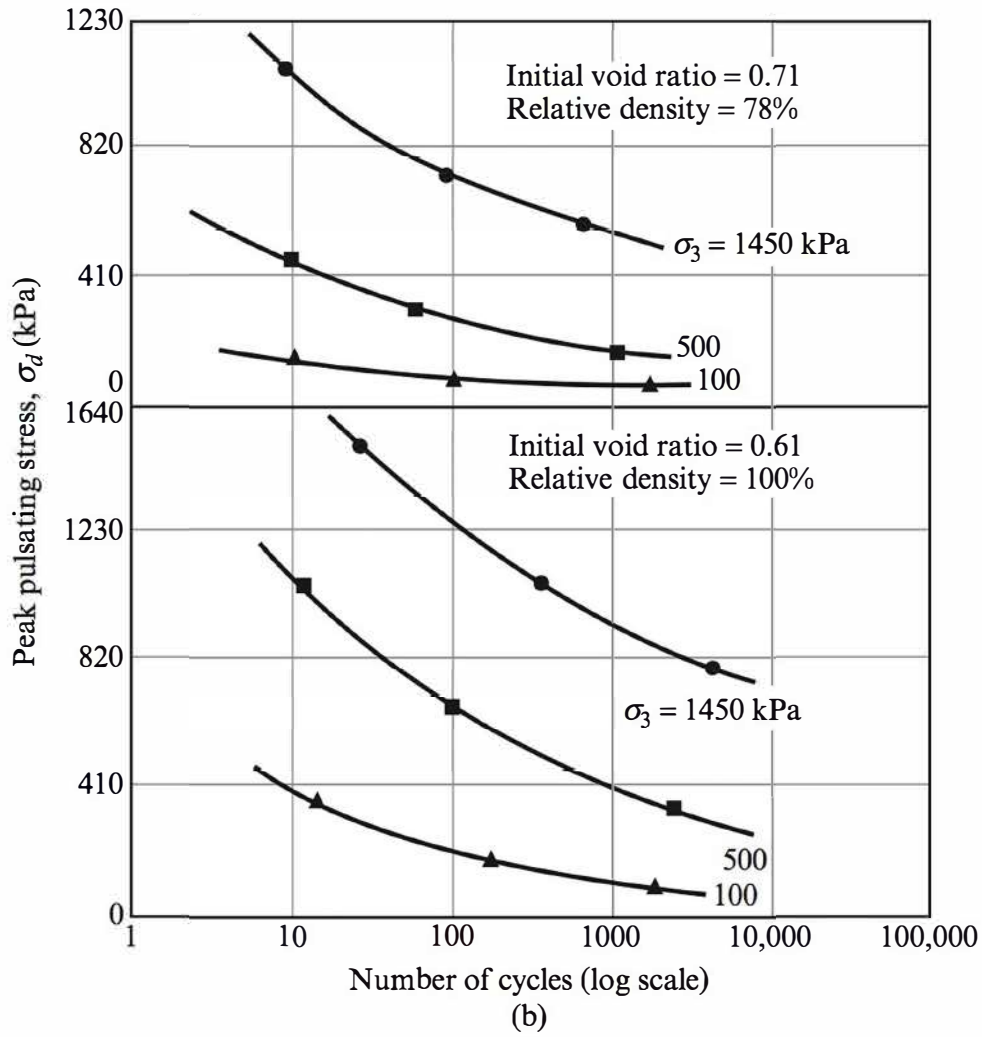

Figure 10.13 (*Continued*)

10.7 DEVELOPMENT OF STANDARD CURVES FOR INITIAL LIQUEFACTION

By compiling the results of liquefaction tests conducted by several investigators on various types of sand, average standard curves for initial liquefaction for a given number of load cycle applications can be developed. These curves can then be used for evaluation of liquefaction potential in the field. Some of these plots developed by Seed and Idriss (1971) are given in Figure 10.15.

Figure 10.15 is a plot of $(1/2)(\sigma_d/\sigma_3)$ versus D_{50} to cause initial liquefaction in 10 cycles of stress application. The plot is for an initial relative density of compaction of 50%. Note that D_{50} in Figure 10.15 is the median grain size, i.e., the size through which 50% of the soil will pass. It should be kept in mind that $(1/2)\sigma_d$ is the magnitude of the maximum cyclic shear stress imposed on a soil specimen (see planes $X-X$ and $Y-Y$ of Figure 10.4d, f). Another plot for initial liquefaction in 30 cycles of stress application is also given in Figure 10.15. These curves are used in Section 10.15 for evaluation of liquefaction potential.

Copyright 2017 Cengage Learning. All Rights Reserved. May not be copied, scanned, or duplicated, in whole or in part. Due to electronic rights, some third party content may be suppressed from the eBook and/or eChapter(s). Editorial review has deemed that any suppressed content does not materially affect the overall learning experience. Cengage Learning reserves the right to remove additional content at any time if subsequent rights restrictions require it.

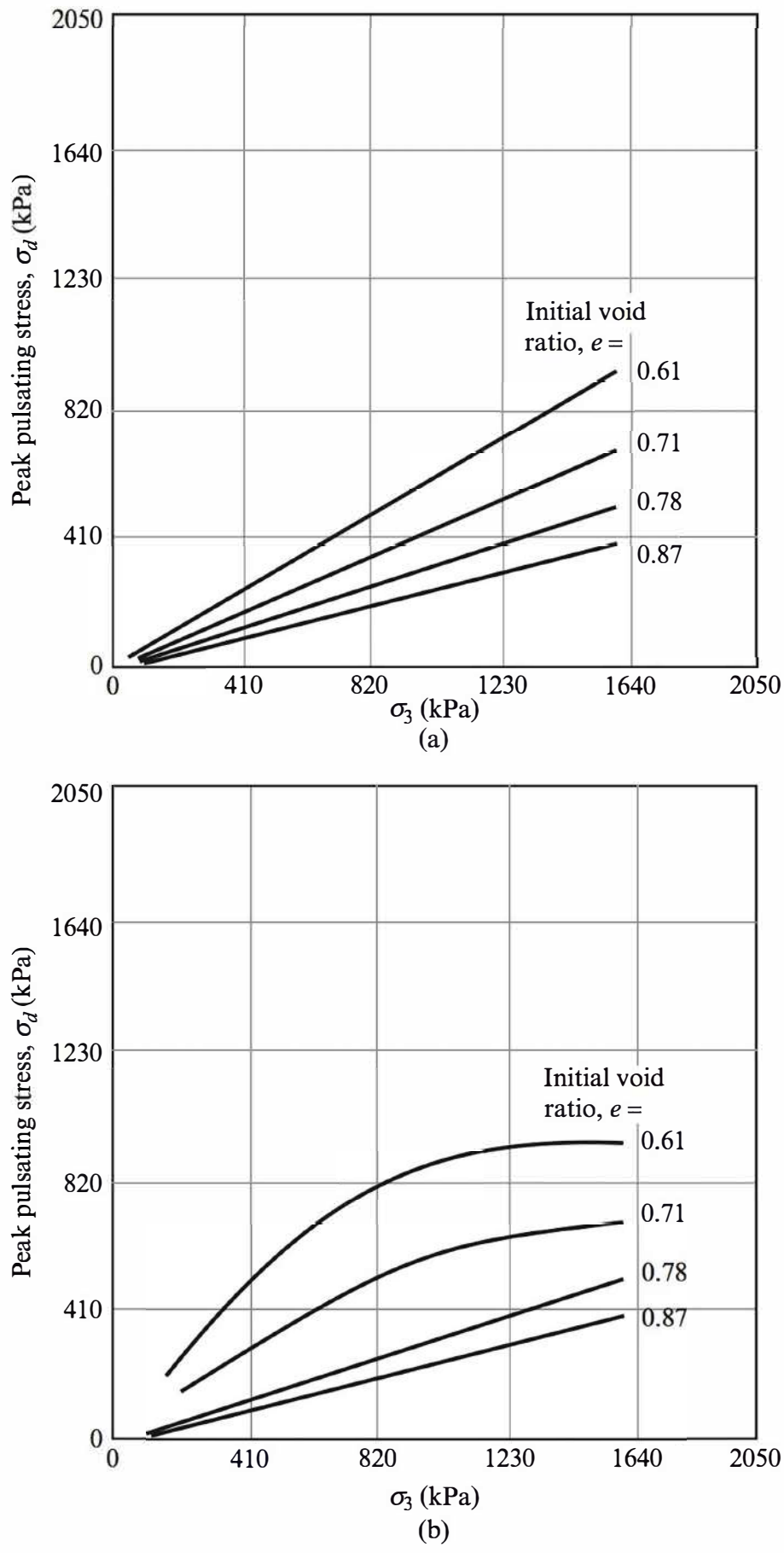

Figure 10.14 Influence of pulsating stress on the liquefaction of Sacramento River sand (a) initial liquefaction in 100 cycles; (b) 20% strain in 100 cycles (redrawn from Lee and Seed, 1967)

Source: Lee, K.L., and Seed, H.B. (1967). "Cyclic Stress Condition Causing Liquefaction of Sand," *Journal of the Soil Mechanics and Foundations Division*, ASCE, Vol.93, No. SM1, pp. 47–70. With permission from ASCE.

Copyright 2017 Cengage Learning. All Rights Reserved. May not be copied, scanned, or duplicated, in whole or in part. Due to electronic rights, some third party content may be suppressed from the eBook and/or eChapter(s). Editorial review has deemed that any suppressed content does not materially affect the overall learning experience. Cengage Learning reserves the right to remove additional content at any time if subsequent rights restrictions require it.

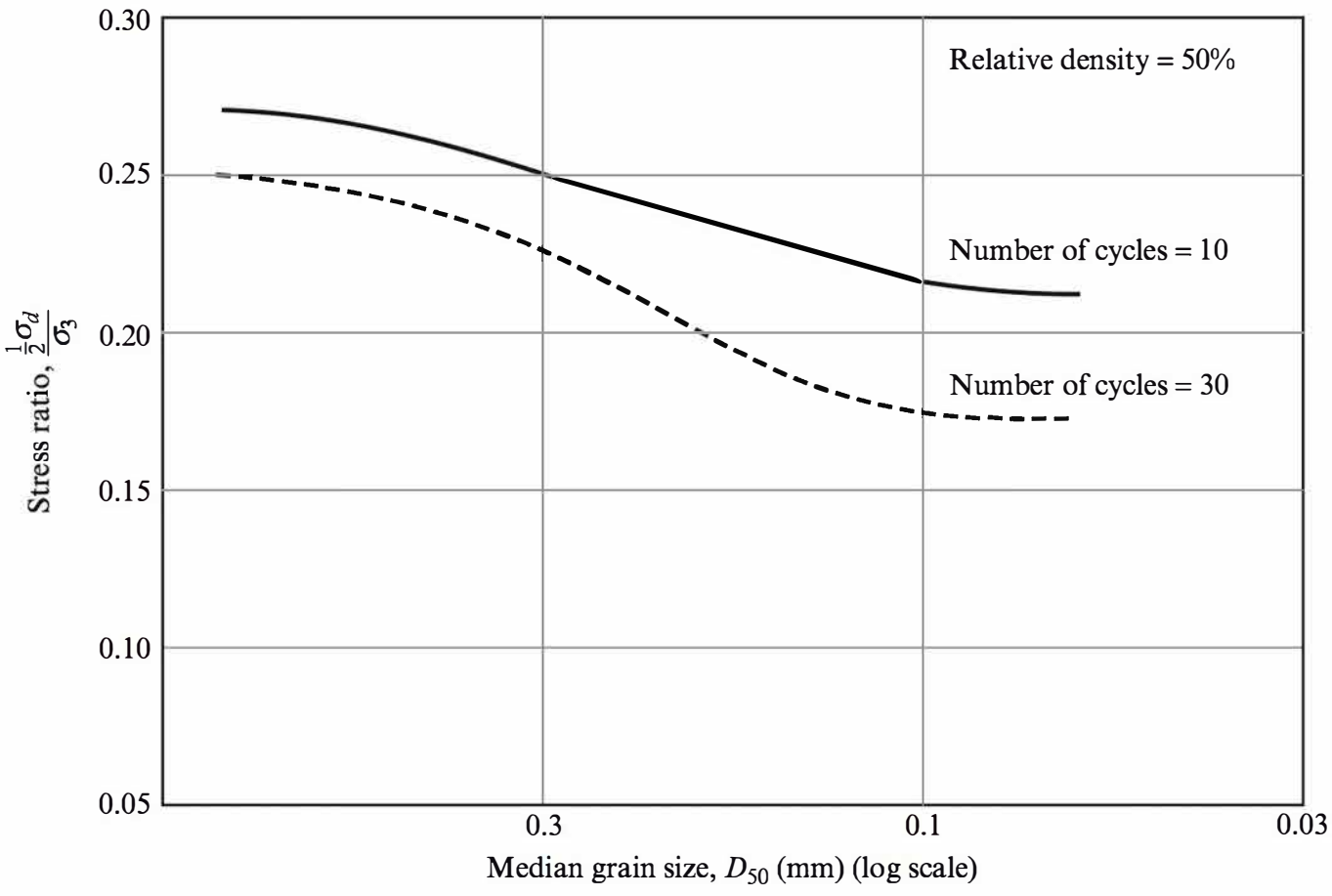

Figure 10.15 Stress ratio causing initial liquefaction of sands in 10 and 30 cycles (from Seed and Idriss, 1971)

Source: Seed, H. B. and Idriss, I. M. (1971). "Simplified Procedure for Evaluating Soil Liquefaction Potential," *Journal of the Soil Mechanics and Foundations Division*, ASCE, Vol. 97, No. SM9, pp. 1249–1273. With permission from ASCE.

Cyclic Simple Shear Test

10.8 GENERAL CONCEPTS

Cyclic simple shear tests can be used to study liquefaction of saturated sand by using the simple shear apparatus (also see Chapter 4). In this type of test, the soil specimen is consolidated by a vertical stress σ_v. At this time, lateral stress is equal to $K_0\sigma_v$ (K_0 = coefficient of earth pressure at rest). The initial stress conditions of a specimen in a simple shear device are shown in Figure 10.16a; the corresponding Mohr's circle is shown in Figure 10.16b. After that, a cyclic horizontal shear stress of peak magnitude τ_h is applied (undrained condition) to the specimen as shown in Figure 10.16c. The pore water pressure and the strain are observed with the number of cycles of horizontal shear stress application.

Using the stress conditions on the soil specimen at a certain time during the cyclic shear test, a Mohr's circle is plotted in Figure 10.16d. Note that the maximum shear stress on the specimen in simple shear is not τ_h, but

Copyright 2017 Cengage Learning. All Rights Reserved. May not be copied, scanned, or duplicated, in whole or in part. Due to electronic rights, some third party content may be suppressed from the eBook and/or eChapter(s). Editorial review has deemed that any suppressed content does not materially affect the overall learning experience. Cengage Learning reserves the right to remove additional content at any time if subsequent rights restrictions require it.

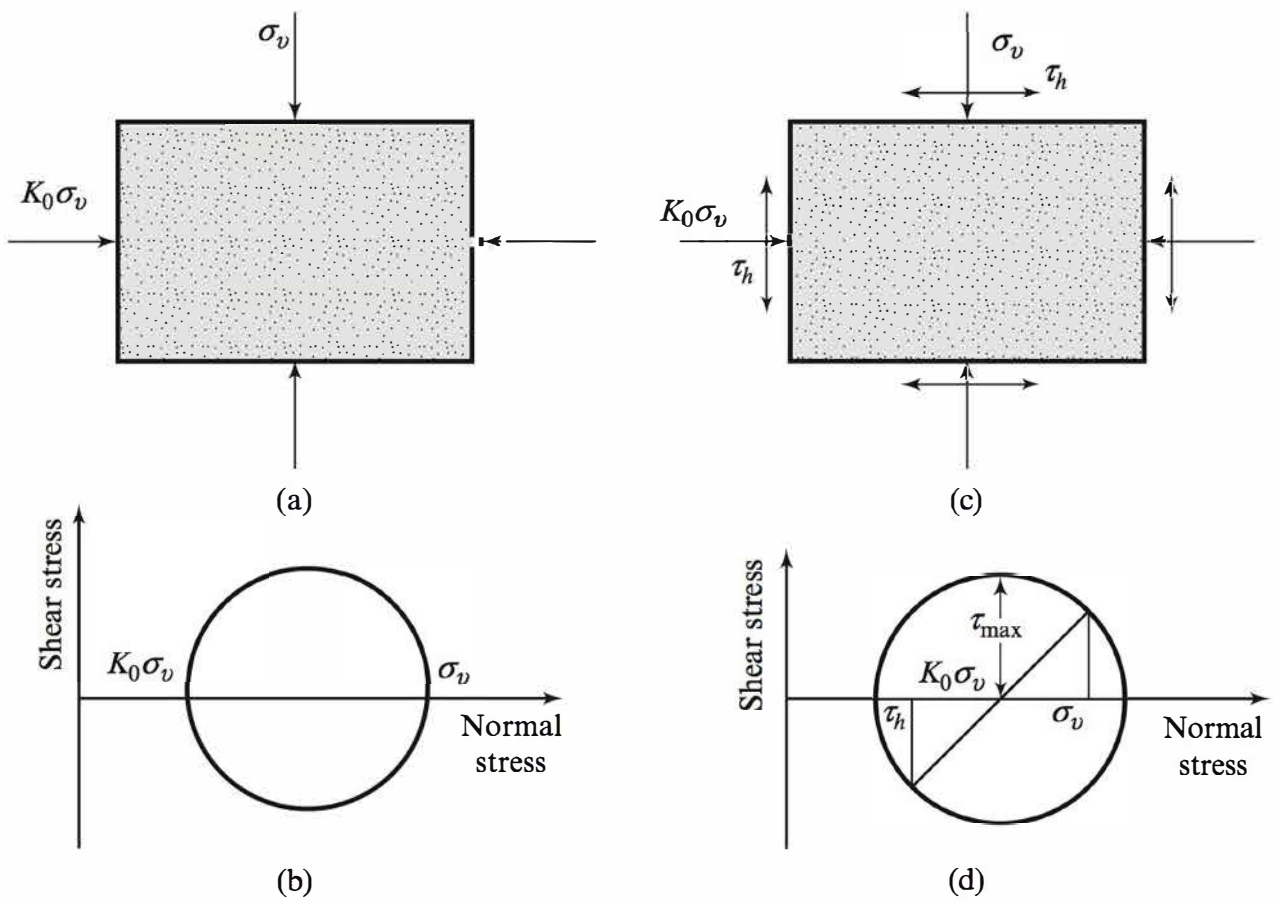

Figure 10.16 Maximum shear stress for cyclic simple shear test

$$\tau_{max} = \sqrt{\tau_h^2 + \left[\frac{1}{2}\sigma_v\left(1 - K_0\right)\right]^2} \tag{10.2}$$

10.9 TYPICAL TEST RESULTS

Typical results of some soil liquefaction tests on Monterey sand using simple shear apparatus are shown in Figure 10.17. Note that these are for the initial liquefaction condition. From the figure the following facts may be observed:

1. For a given value of σ_v and relative density R_D, a decrease of τ_h requires an increase of the number of cycles to cause liquefaction.
2. For a given value of R_D and number of cycles of stress application, a decrease of σ_v requires a decrease of the peak value of τ_h for causing liquefaction.
3. For a given value of σ_v and number of cycles of stress application, τ_h for causing liquefaction increases with the increase of the relative density.

Another important factor—the variation of the peak value of τ_h for causing initial liquefaction with the initial relative density of compaction (for a given value of σ_v and number of stress cycle application)—is shown in Figure 10.18.

For a relative density up to about 80%, the peak value of τ_h for initial liquefaction increases linearly with R_D. At higher relative densities (which may not be practical to achieve in the field, particularly if fines are present), the relationship is nonlinear.

Copyright 2017 Cengage Learning. All Rights Reserved. May not be copied, scanned, or duplicated, in whole or in part. Due to electronic rights, some third party content may be suppressed from the eBook and/or eChapter(s). Editorial review has deemed that any suppressed content does not materially affect the overall learning experience. Cengage Learning reserves the right to remove additional content at any time if subsequent rights restrictions require it.

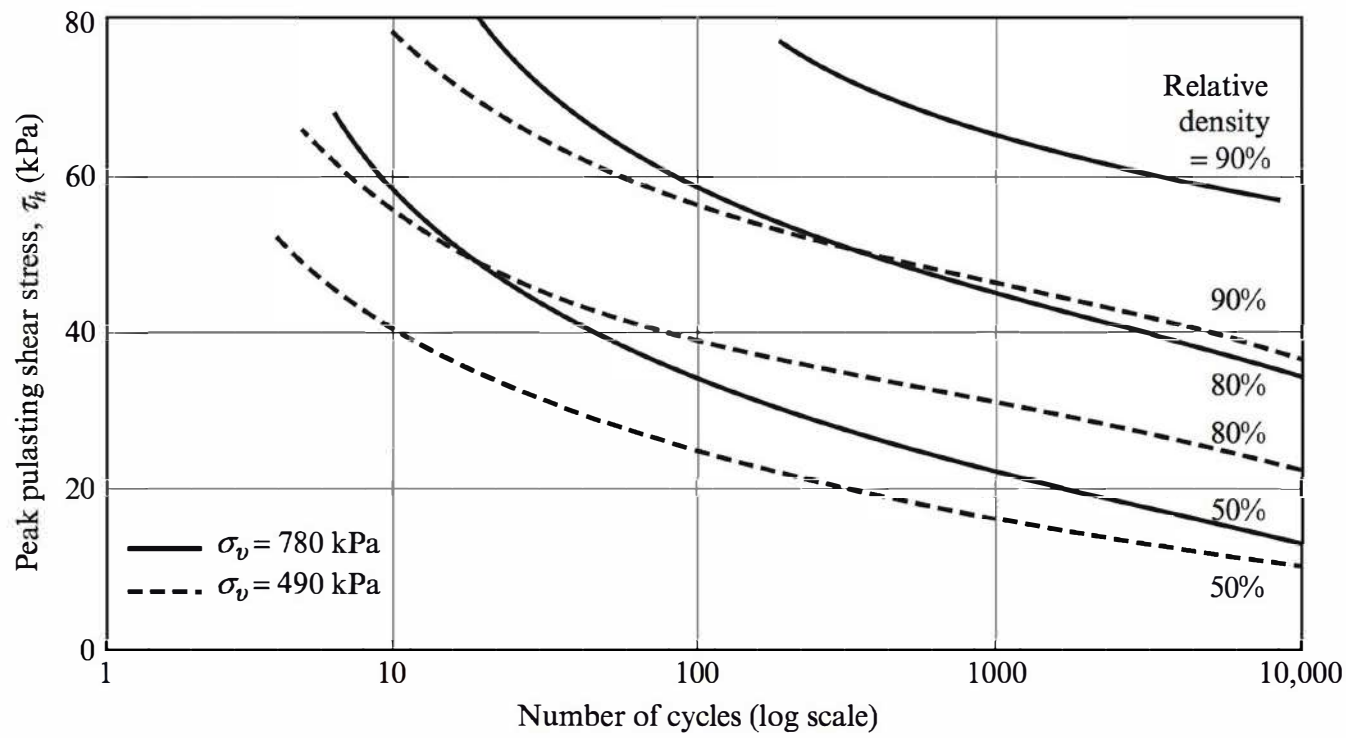

Figure 10.17 Initial liquefaction in cyclic simple shear test on Monterey sand (redrawn from Peacock and Seed, 1968)

Source: Peacock, W.H., and Seed, H. B. (1968), "Sand Liquefaction Under Cyclic Loading Simple Shear Conditions," *Journal of the Soil Mechanics and Foundations Division*, ASCE, Vol. 94, No. SM3, pp. 689–708. With permission from ASCE.

Influence of Test Conditions

In simple shear test equipment, there is always some nonuniformity of stress conditions. This causes specimens to develop liquefaction under lower applied horizontal cyclic stresses as compared to that in the field. This happens even though care is taken to improve the preparation of the specimens and rough platens are used at the top and bottom of the specimens to be tested. For that reason, for a given value of σ_v, R_D, and number of cyclic shear stress application, the peak value of τ_h in the field is about 15%–50% higher than that obtained from the cyclic simple shear test. This fact has been demonstrated by Seed and Peacock (1971) for a uniform medium sand ($R_D \approx 50\%$) in which the field values are about 20% higher than the laboratory values.

Influence of Overconsolidation Ratio on the Peak Value of τ_h Causing Liquefaction

For the cyclic simple shear test, the value of τ_h is highly dependent on the value of the initial lateral earth pressure coefficient at rest (K_0). The value of K_0, is in turn, dependent on the over consolidation ratio (OCR). The variation of τ_h/σ_v for initial liquefaction with the overconsolidation ratio as determined by the cyclic simple shear test is shown in Figure 10.19. For a given relative density and number of cycles causing initial liquefaction, the value of τ_h/σ_v decreases with the decrease of K_0. It needs to be mentioned at this point that all the cyclic triaxial studies for liquefaction are conducted for the initial value of $K_0 = 1$.

Copyright 2017 Cengage Learning. All Rights Reserved. May not be copied, scanned, or duplicated, in whole or in part. Due to electronic rights, some third party content may be suppressed from the eBook and/or eChapter(s). Editorial review has deemed that any suppressed content does not materially affect the overall learning experience. Cengage Learning reserves the right to remove additional content at any time if subsequent rights restrictions require it.

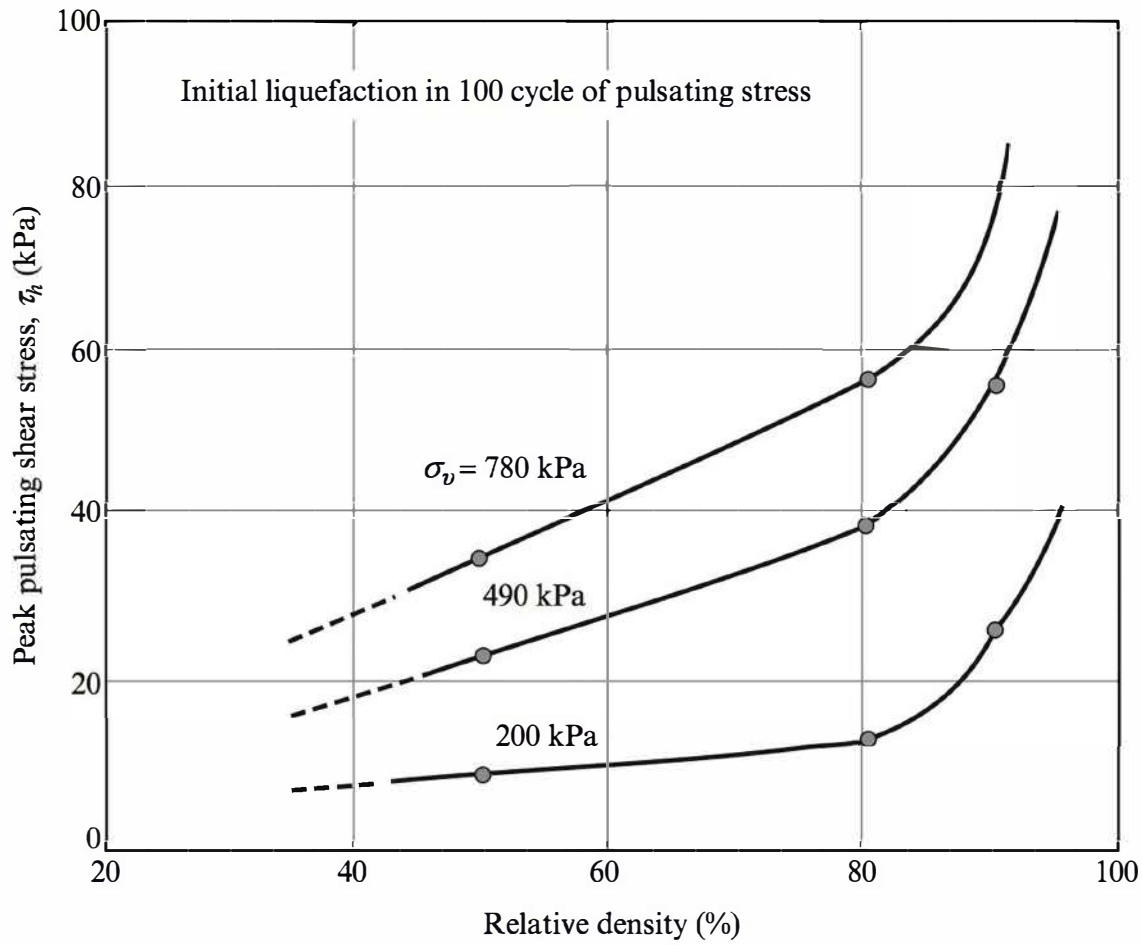

Figure 10.18 Effect of relative density on cyclic shear stress causing initial liquefaction of Monterey sand (redrawn from Peacock and Seed, 1968)

Source: Peacock, W.H., and Seed, H. B. (1968), "Sand Liquefaction Under Cyclic Loading Simple Shear Conditions," *Journal of the Soil Mechanics and Foundations Division*, ASCE, Vol. 94, No. SM3, pp. 689–708. With permission from ASCE.

10.10 RATE OF EXCESS PORE WATER PRESSURE INCREASE

Seed and Booker (1977) and DeAlba, Chan, and Seed (1975) measured the rate of excess pore water pressure increase in saturated sands during liquefaction using cyclic simple shear tests. The range of the variation of pore water pressure generation u_g during cyclic loading is shown in Figure 10.20. The average value of the variation of u_g can be expressed in a nondimensional form as (Seed, Martin, and Lysmer, 1975)

$$\boxed{\frac{u_g}{\sigma_v} = \left(\frac{2}{\pi}\right) \arcsin \left(\frac{N}{N_i}\right)^{1/2\alpha}} \tag{10.3}$$

where u_g = excess pore water pressure generated
σ_v = initial consolidation pressure
N = number of cycles of shear stress application

Copyright 2017 Cengage Learning. All Rights Reserved. May not be copied, scanned, or duplicated, in whole or in part. Due to electronic rights, some third party content may be suppressed from the eBook and/or eChapter(s). Editorial review has deemed that any suppressed content does not materially affect the overall learning experience. Cengage Learning reserves the right to remove additional content at any time if subsequent rights restrictions require it.

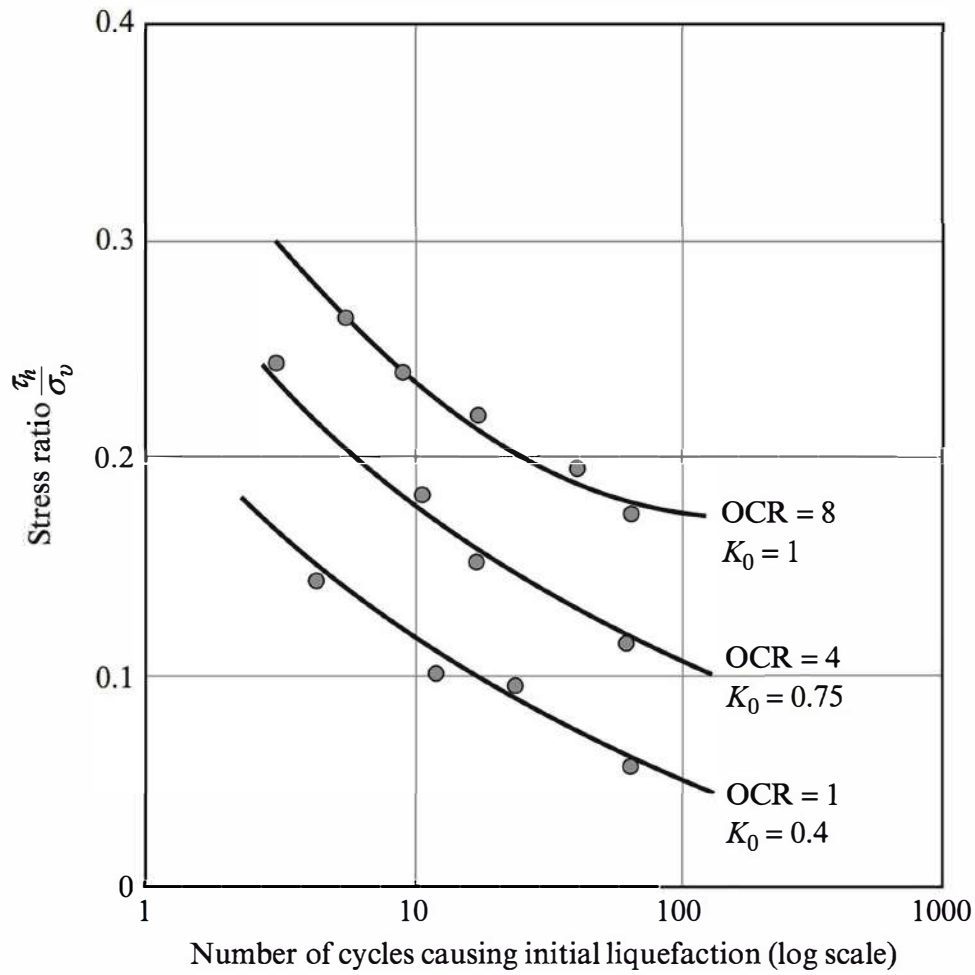

Figure 10.19 Influence of overconsolidation ratio on stresses causing liquefaction in simple shear tests (redrawn from Seed and Peacock, 1971)

Source: Seed, H. B., and Peacock, W. H. (1971). "Test Procedures for Measuring Soil Liquefaction Characteristics," *Journal of the Soil Mechanics and Foundations Division*, ASCE, Vol. 97, No. SM8, pp. 1099–1119. With permission from ASCE.

N_i = number of cycles of shear stress needed for initial liquefaction
α = constant (≈ 0.7)

Hence, the rate of change of u_g with N can be given as

$$\frac{\partial u_g}{\partial N} = \left(\frac{2\sigma_v}{\alpha\,\pi N_i}\right)\left[\frac{1}{\sin^{2\alpha-1}\left(\frac{\pi}{2}r_u\right)\cos\left(\frac{\pi}{2}r_u\right)}\right] \tag{10.4}$$

where

$$r_u = \frac{u_g}{\sigma_v} \tag{10.5}$$

The preceding relationship is very useful in the study of the stabilization of potentially liquefiable sand deposits.

Copyright 2017 Cengage Learning. All Rights Reserved. May not be copied, scanned, or duplicated, in whole or in part. Due to electronic rights, some third party content may be suppressed from the eBook and/or eChapter(s). Editorial review has deemed that any suppressed content does not materially affect the overall learning experience. Cengage Learning reserves the right to remove additional content at any time if subsequent rights restrictions require it.

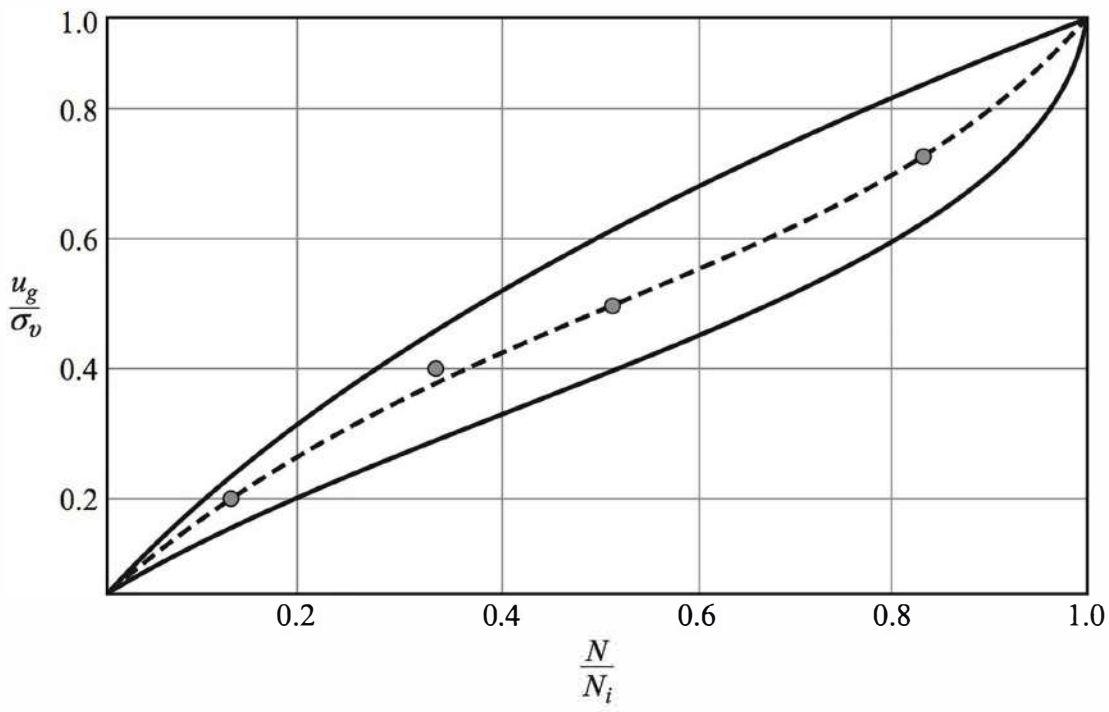

Figure 10.20 Rate of pore water pressure buildup in cyclic simple shear test (from Seed and Booker, 1977)

Source: Seed, H. B., and Booker, J. R. (1977). "Stabilization of Potentially Liquefiable Sand Deposits," Journal of the Geotechnical Engineering Division, ASCE, Vo. 103, No. GT7, pp. 757–768. With permission from ASCE.

10.11 LARGE-SCALE SIMPLE SHEAR TESTS

In the study of soil liquefaction of granular soils, certain aspects of the test procedures have remained a matter for concern. Some of those concerns are as follows:

a. Stress concentration in small-scale simple shear tests leads to some inaccuracy in the results (Castro, 1969).
b. Stress concentration at the base and cap of cyclic triaxial test specimens and the possibility of necking leads to nonuniformity of strain and redistribution of water content (Castro, 1975).
c. Attempts to study liquefaction by using shaking table tests (e.g., Emery, Finn, and Lee, 1972; Finn, Emery, and Gupta, 1970; OHara, 1972; Ortigosa, 1972; Tanimoto, 1967l; Whitman, 1970; Yoshimi, 1967) have also raised some questions, since the results, in some cases, have been influenced by the confining effects of the sides of the box.

For that reason, DeAlba, Seed, and Chan (1976) conducted large-scale simple shear tests with one-directional cyclic stress application. The specimens of sand used for testing had dimensions of 2300 mm × 1100 mm × 100 mm (depth). Each specimen was constructed over a shaking table. A rubber membrane was placed over the sand to prevent drainage. An inertia mass was also placed on top

Copyright 2017 Cengage Learning. All Rights Reserved. May not be copied, scanned, or duplicated, in whole or in part. Due to electronic rights, some third party content may be suppressed from the eBook and/or eChapter(s). Editorial review has deemed that any suppressed content does not materially affect the overall learning experience. Cengage Learning reserves the right to remove additional content at any time if subsequent rights restrictions require it.

of the sand. Movement of the shaking table produced cyclic stress conditions in the sand. The cyclic shear stress was determines as

$$\tau_h = \frac{W}{g} a_m \tag{10.6}$$

where W = total pressure exerted at the base by the specimen and the inertia mass
a_m = peak acceleration of the uniform cyclic motion
g = acceleration due to gravity

From the measured displacement (Δ) of the inertia mass during shaking, the average single-amplitude cyclic shear strain could be obtained as

$$\gamma' = \pm \frac{\Delta}{2h} \tag{10.7}$$

where γ' = average single amplitude cyclic shear strain
h = specimen height

Figure 10.21 shows the variation of τ_h/σ_v against the number of cycles of initial liquefaction ($N = N_i$) for various values of the relative density of sand (R_D). Note that this has been corrected for the compliance effects of the specimens and the pore water pressure-measuring system and the effects of membrane penetration. The nature of these plots is similar to those shown in Figure 10.17.

Figure 10.22 shows a comparison of the variation of τ_h/σ_v versus N_i (for $R_D = 50\%$) obtained from the reported results of Ortigosa (1972), OHara (1972), Finn, Emery, and Gupta (1971), and the large-scale simple shear test results of

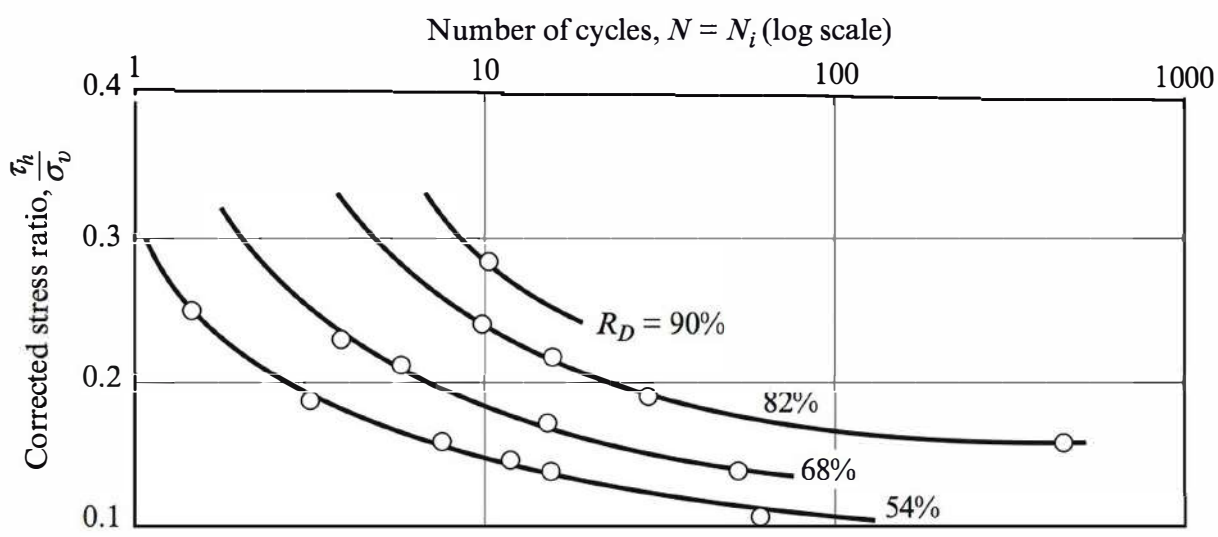

Figure 10.21 Corrected τ_h/σ_v versus N_i for initial liquefaction from large-scale simple shear tests (from DeAlba, Seed, and Chan, 1976)

Source: DeAlba, P., Seed, H. B., and Chan, C. K. (1976). "Sand Liquefaction in Large-Scale Simple Shear Tests," *Journal of Geotechnical Engineering Division*, ASCE, Vol. 102, NO. GT9, pp. 909–927. With permission from ASCE.

Copyright 2017 Cengage Learning. All Rights Reserved. May not be copied, scanned, or duplicated, in whole or in part. Due to electronic rights, some third party content may be suppressed from the eBook and/or eChapter(s). Editorial review has deemed that any suppressed content does not materially affect the overall learning experience. Cengage Learning reserves the right to remove additional content at any time if subsequent rights restrictions require it.

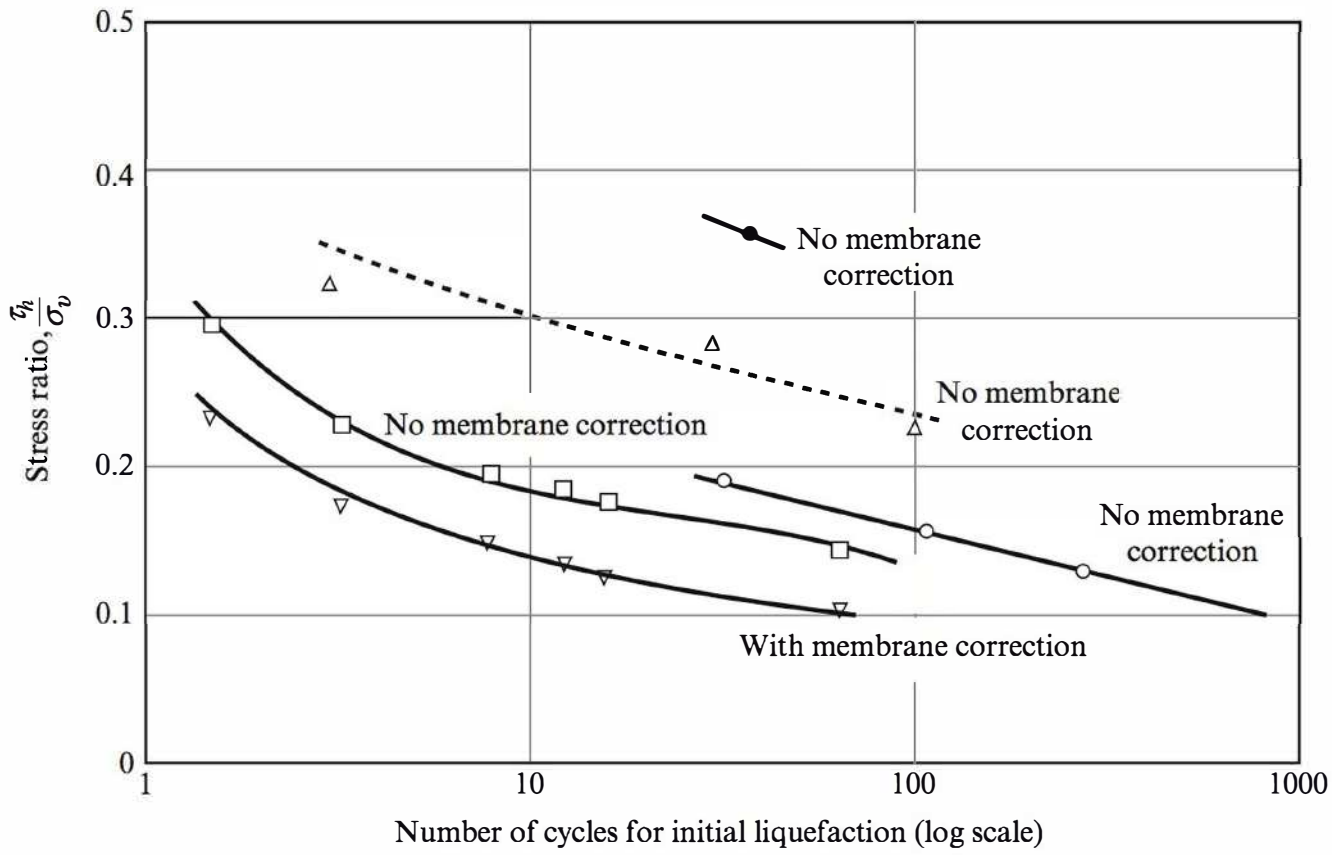

LEGEND

	Author	Length/height ratio	Material	Sample preparation
•	Ortigosa (1972)	2.3:1	Medium sand	Poured dry, compacted
Δ	OHara (1972)	3.4:1	Fine sand	
O	Finn et al. (1971) (extrapolated)	10.3:1	Medium sand	Pluviated through water
□	DeAlba et al. (1976)	22.5:1	Medium sand	Pluviated through air
∇	DeAlba et al. (1976)	22.5:1	Medium sand	Pluviated through air

Figure 10.22 Comparison of shaking table test results—$R_D = 50\%$ (from DeAlba, Seed, and Chan, 1976)

Source: DeAlba, P., Seed, H. B., and Chan, C. K. (1976). "Sand Liquefaction in Large-Scale Simple Shear Tests," *Journal of Geotechnical Engineering Division*, ASCE, Vol. 102, NO. GT9, pp. 909–927. With permission from ASCE.

DeAlba, Chan, and Seed (1976). The differences between the results are primarily due to (1) the effect of membrane penetration and compliance effects, (2) the length-to-height ratio of the specimens and hence the boundary conditions, and (3) the nature of sample preparation. It is thus evident from Figure 10.22 that care should be taken to provide proper boundary conditions if meaningful data are to be obtained from shaking table tests.

Figure 10.23 shows the comparison of τ_h/σ_v versus number of cycles for initial liquefaction of saturated sand at $R_D = 50\%$ obtained from various studies using small-scale and large-scale simple shear devices. The sample preparation

Copyright 2017 Cengage Learning. All Rights Reserved. May not be copied, scanned, or duplicated, in whole or in part. Due to electronic rights, some third party content may be suppressed from the eBook and/or eChapter(s). Editorial review has deemed that any suppressed content does not materially affect the overall learning experience. Cengage Learning reserves the right to remove additional content at any time if subsequent rights restrictions require it.

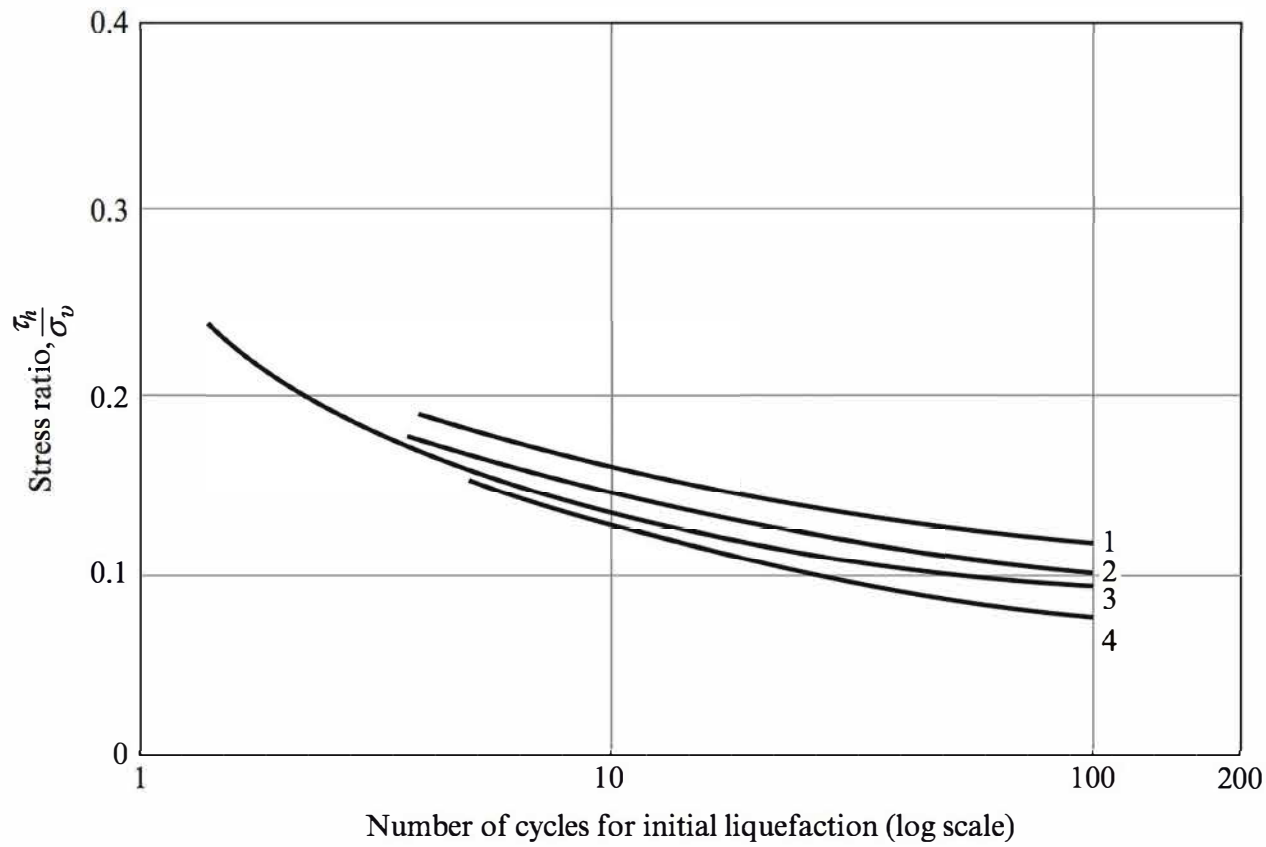

Curve No.	Reference	Type of Test
1	Yoshimi and Oh-oka (1973)	Ring torsion
2	Finn (1972)	Simple shear
3	DeAlba et al (1976)	Shaking table (corrected)
4	Seed and Peacock (1971)	Simple shear

Figure 10.23 Comparison of shaking table and simple shear liquefaction test results—$R_D = 50\%$ (from DeAlba, Seed, and Chan, 1976)

Source: DeAlba, P., Seed, H. B., and Chan, C. K. (1976). "Sand Liquefaction in Large-Scale Simple Shear Tests," *Journal of Geotechnical Engineering Division*, ASCE, Vol. 102, NO. GT9, pp. 909–927. With permission from ASCE.

techniques in all the studies were similar. Based on Figure 10.23, it can be concluded that the results are in good agreement and the errors due to stress concentration in small-scale simple shear tests are not very large.

The variation of single-amplitude cyclic shear strain [Eq. (10.7)] with N for dense sands obtained from large-scale simple shear tests is shown in Figure 10.24. Note that the magnitude of γ' increased gradually with N after initial liquefaction up to a maximum limiting value and remained constant thereafter.

Figure 10.25 shows the relationships between cyclic stress ratio and number of stress cycles producing average shear strains of 5%, 10%, 15%, and 20% calculated from displacements measured from the large-scale simple shear tests. The results of Figure 10.25 have been replotted as values of cyclic stress ratio causing initial liquefaction, or different levels of shear (for $N = 10$), versus relative densities in

Copyright 2017 Cengage Learning. All Rights Reserved. May not be copied, scanned, or duplicated, in whole or in part. Due to electronic rights, some third party content may be suppressed from the eBook and/or eChapter(s). Editorial review has deemed that any suppressed content does not materially affect the overall learning experience. Cengage Learning reserves the right to remove additional content at any time if subsequent rights restrictions require it.

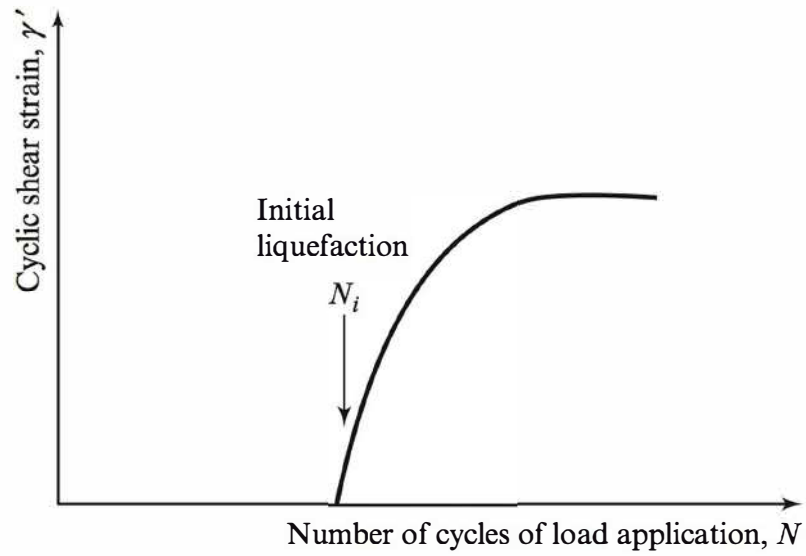

Figure 10.24 Nature of variation of γ' with number of cycles of load application

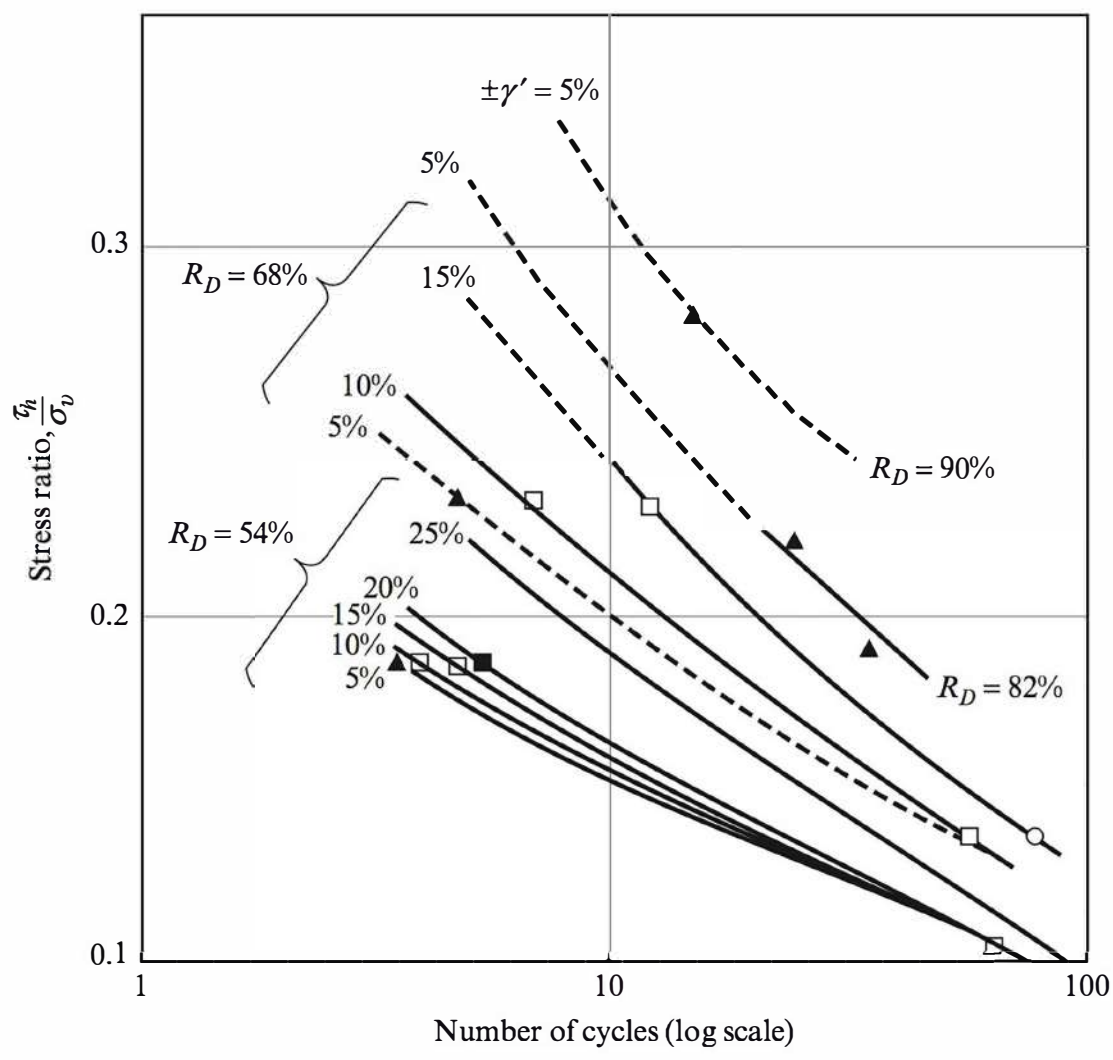

Figure 10.25 Relationship between τ_h/σ_v and number of cycles causing different levels of strain (from DeAlba, Seed, and Chan, 1976)

Source: DeAlba, P., Seed, H. B., and Chan, C. K. (1976). "Sand Liquefaction in Large-Scale Simple Shear Tests," *Journal of Geotechnical Engineering Division*, ASCE, Vol. 102, NO. GT9, pp. 909–927. With permission from ASCE.

Copyright 2017 Cengage Learning. All Rights Reserved. May not be copied, scanned, or duplicated, in whole or in part. Due to electronic rights, some third party content may be suppressed from the eBook and/or eChapter(s). Editorial review has deemed that any suppressed content does not materially affect the overall learning experience. Cengage Learning reserves the right to remove additional content at any time if subsequent rights restrictions require it.

Figure 10.26a. The results show that each curve is asymptotic to a certain value of R_D. Hence a curve of limiting shear strain versus R_D can be obtained as shown in Figure 10.26b.

Based on Figure 10.26, the following conclusions can be drawn.

1. For initial $R_D \leq 45\%$, the application of cyclic stress ratio high enough to cause initial liquefaction also causes unlimited shear strain. This corresponds to a condition of liquefaction.

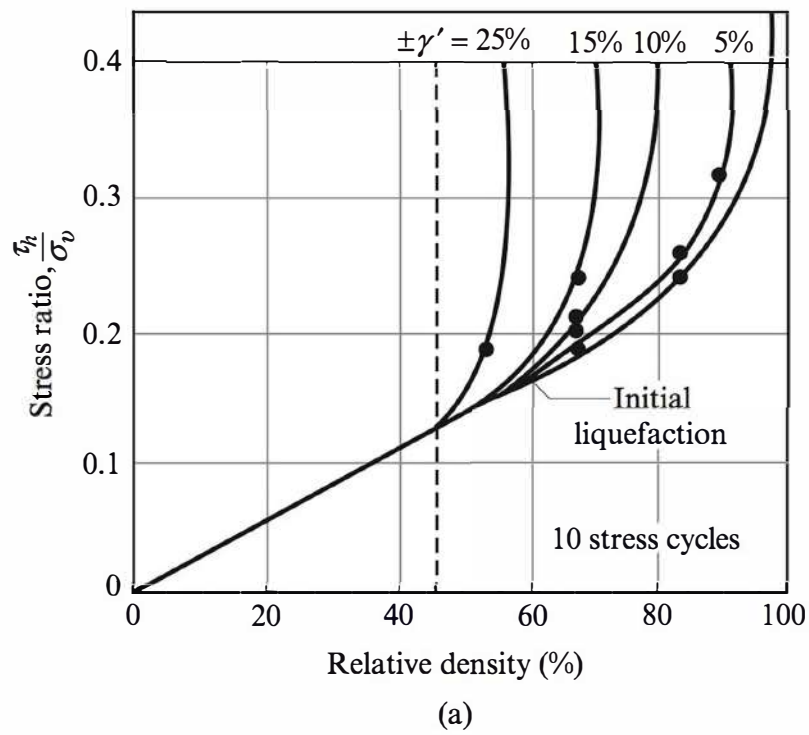

(a)

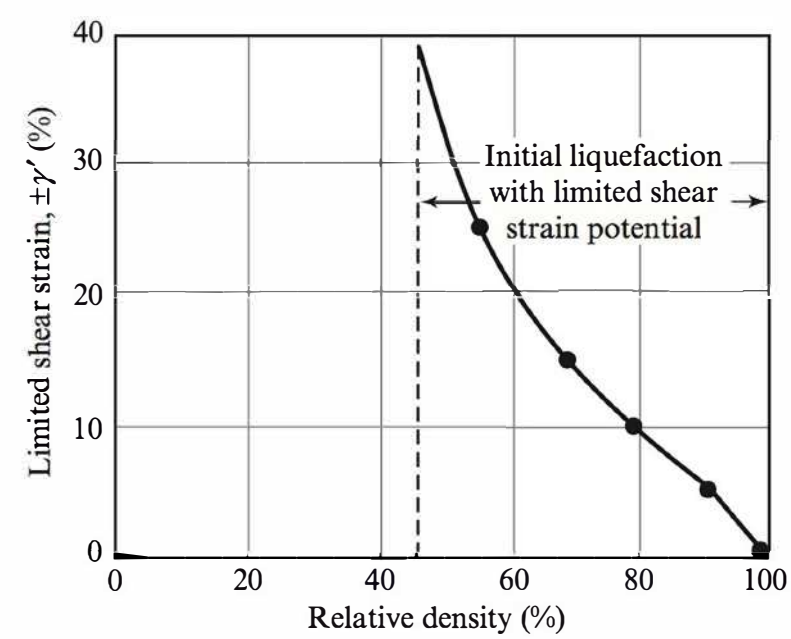

(b)

Figure 10.26 Limiting shear strains—10 cycles of stress (from DeAlba, Seed, and Chan, 1976)

Source: DeAlba, P., Seed, H. B., and Chan, C. K. (1976). "Sand Liquefaction in Large-Scale Simple Shear Tests," *Journal of Geotechnical Engineering Division*, ASCE, Vol. 102, NO. GT9, pp. 909–927. With permission from ASCE.

Copyright 2017 Cengage Learning. All Rights Reserved. May not be copied, scanned, or duplicated, in whole or in part. Due to electronic rights, some third party content may be suppressed from the eBook and/or eChapter(s). Editorial review has deemed that any suppressed content does not materially affect the overall learning experience. Cengage Learning reserves the right to remove additional content at any time if subsequent rights restrictions require it.

2. For initial $R_D > 45\%$, the application of cyclic stress ratio high enough to cause initial liquefaction will result in a limited amount of shear strain. This is the case of soil with limited strain potential or the condition of cyclic mobility.
3. The limiting strain potential decreases with the increase of the initial relative density of soil.

Before moving on to establish procedures for determination of liquefaction in the field, the results from the laboratory tests can be summarized as follows:

1. Liquefaction is a phenomenon in which the strength and stiffness of a soil is reduced by earthquake shaking or other rapid loading. Liquefaction and related phenomena have been responsible for tremendous amounts of damage in historical earthquakes around the world.
2. Flow liquefaction is a phenomenon in which the static equilibrium is destroyed by static or dynamic loads in a soil deposit with low residual strength. Residual strength is the strength of a liquefied soil.
3. Cyclic mobility is a liquefaction phenomenon, triggered by cyclic loading, occuring in soil deposits with static shear stresses lower than the soil strength. Deformations due to cyclic mobility develop incrementally because of static and dynamic stresses that exist during an earthquake.
4. To understand liquefaction, it is important to recognize the conditions that exist in a soil deposit before an earthquake.

Development of a Procedure for Determination of Field Liquefaction

10.12 CORRELATION OF LIQUEFACTION RESULTS FROM SIMPLE SHEAR AND TRIAXIAL TESTS

The conditions for determination of field liquefaction problems are related to the ratio of τ_h/σ_v; this is also true for the case of cyclic simple shear stress tests. However, in the case of triaxial tests, the results are related to the ratio of $(1/2)(\sigma_d/\sigma_3)$. It appears that a correlation between τ_h/σ_v and $(1/2)(\sigma_d/\sigma_3)$ needs to be developed (for a given number of cyclic stress application to cause liquefaction). Seed and Peacock (1971) considered the following alternative criteria for correlation for the onset of soil liquefaction.

1. The maximum ratio of the shear stress developed during cyclic loading to the normal stress during consolidation on any plane of the specimen can be a controlling factor. For triaxial specimens, this is equal to $(1/2)(\sigma_d/\sigma_3)$, and for simple shear specimens it is about $\tau_h/(K_0\sigma_v)$. Thus,

Copyright 2017 Cengage Learning. All Rights Reserved. May not be copied, scanned, or duplicated, in whole or in part. Due to electronic rights, some third party content may be suppressed from the eBook and/or eChapter(s). Editorial review has deemed that any suppressed content does not materially affect the overall learning experience. Cengage Learning reserves the right to remove additional content at any time if subsequent rights restrictions require it.

$$\frac{\tau_h}{K_0\sigma_v} = \frac{\frac{1}{2}\sigma_d}{\sigma_3}$$

or

$$\left[\frac{\tau_h}{\sigma_v}\right]_{\text{simple shear}} = K_0\left[\frac{\frac{1}{2}\sigma_d}{\sigma_3}\right] \tag{10.8}$$

2. Another possible condition for the onset of liquefaction can be the maximum ratio of change in shear stress during cyclic loading to the normal stress during consolidation on any plane. For simple shear specimens this is about $\tau_h/(K_0\sigma_v)$, and for triaxial specimens it is $(1/2)(\sigma_d/\sigma_3)$. This leads to the same equation as Eq. (10.8)
3. The third possible alternative can be given by the *ratio of the maximum shear stress* induced in a specimen during cyclic loading to the mean principal stress on the specimen during consolidation. For simple shear specimens:

$$\text{Maximum shear stress during cyclic loading} = \sqrt{\tau_h^2 + \left[\frac{1}{2}\sigma_v\left(1-K_0\right)^2\right]} \tag{10.2}$$

Mean principal stress during consolidation (Figure 10.16a)

$$= \frac{1}{3}(\sigma_v + K_0\sigma_v + K_0\sigma_v) = \frac{1}{3}\sigma_v(1+2K_0) \tag{10.9}$$

For triaxial specimens, maximum shear stress during cyclic loading $= 1/2\sigma_d$ and mean principal stress during consolidation $= \sigma_3$; so

$$\frac{\sqrt{\tau_h^2 + \left[\frac{1}{2}\sigma_v\left(1-K_0\right)^2\right]}}{\frac{1}{3}\sigma_v\left(1+2K_0\right)} = \frac{\frac{1}{2}\sigma_d}{\sigma_3}$$

$$\frac{\sqrt{\left(\tau_h/\sigma_v\right)^2 + \left[\frac{1}{2}\left(1-K_0\right)^2\right]}}{\frac{1}{3}\left(1+2K_0\right)} = \frac{\frac{1}{2}\sigma_d}{\sigma_3}$$

$$\left[\frac{\tau_h}{\sigma_v}\right]_{\text{simple shear}} = \sqrt{\left(\frac{\frac{1}{2}\sigma_d}{\sigma_3}\right)^2\left[\frac{1}{3}\left(1+2K_0\right)\right]^2 - \left[\frac{1}{2}\left(1-K_0\right)\right]^2}$$

Copyright 2017 Cengage Learning. All Rights Reserved. May not be copied, scanned, or duplicated, in whole or in part. Due to electronic rights, some third party content may be suppressed from the eBook and/or eChapter(s). Editorial review has deemed that any suppressed content does not materially affect the overall learning experience. Cengage Learning reserves the right to remove additional content at any time if subsequent rights restrictions require it.

or

$$\left[\frac{\tau_h}{\sigma_v}\right]=\left(\frac{\frac{1}{2}\sigma_d}{\sigma_3}\right)\sqrt{\frac{1}{9}(1+2K_0)^2-\frac{\frac{1}{4}(1-K_0)^2}{\left(\frac{1}{2}\sigma_d/\sigma_3\right)^2}} \tag{10.10}$$

4. The fourth possible alternative may be the *ratio of maximum change in shear stress* on any plane during cyclic loading *to the mean principal stress* during consolidation. Thus, for simple shear specimens, it is equal to $3\tau_h/[\sigma_v(1+2K_0)]$, and for triaxial specimens it is $(1/2)(\sigma_d/\sigma_3)$; so

$$\left[\frac{\tau_h}{\sigma_v}\right]_{\text{simple shear}}=\frac{1}{3}(1+2K_0)\left(\frac{\frac{1}{2}\sigma_d}{\sigma_3}\right) \tag{10.11}$$

Thus, in general, it can be written as

$$\left(\frac{\tau_h}{\sigma_v}\right)_{\text{simple shear}}=\alpha'\left(\frac{\frac{1}{2}\sigma_d}{\sigma_3}\right)_{\text{triax}} \tag{10.12}$$

where $\alpha' = K_0$ for Cases 1 and 2,

$$\alpha'=\sqrt{\frac{1}{9}(1+2K_0)^2-\frac{\frac{1}{4}(1-K_0)^2}{\left(\frac{1}{2}\sigma_d/\sigma_3\right)^2}} \qquad \text{for Case 3}$$

and

$$\alpha'=\frac{1}{3}(1+2K_0) \qquad \text{for Case 4}$$

The values of α' for the four cases considered here are given in Table 10.1.

From Table 10.1 it may be seen that for normally consolidated sands, the value of α' is generally in the range 45%–50%, with an average of about 47%.

Finn, Emery, and Gupta (1971) have shown that, for initial liquefaction of normally consolidated sands, α' is equal to $(1/2)(1+K_0)$. The value of K_0 can be given by the relation (Jaky, 1944)

$$K_0 = 1-\sin\phi \tag{10.13}$$

Copyright 2017 Cengage Learning. All Rights Reserved. May not be copied, scanned, or duplicated, in whole or in part. Due to electronic rights, some third party content may be suppressed from the eBook and/or eChapter(s). Editorial review has deemed that any suppressed content does not materially affect the overall learning experience. Cengage Learning reserves the right to remove additional content at any time if subsequent rights restrictions require it.

Table 10.1 Values of α' [Eq. (10.12)][a]

K_0	Case 1	Case 2	Case 3	Case 4
0.4	0.4	0.4	-	0.60
0.5	0.5	0.5	0.25	0.67
0.6	0.6	0.6	0.54	0.73
0.7	0.7	0.7		0.80
0.8	0.8	0.8	0.83	0.87
0.9	0.9	0.9		0.93
1.0	1.0	1.0	1.00	1.00

[a]After Seed and Peacock (1971).

Source: Seed, H. B., and Peacock, W. H. (1971). "Test Procedures for Measuring Soil Liquefaction Characteristics," *Journal of the Soil Mechanics and Foundations Division*, ASCE, Vol. 97, No. SM8, pp. 1099–1119. With permission from ASCE.

Castro (1975) has proposed that the initial liquefaction may be controlled by the criteria of the *ratio of the octahedral shear stress* during cycle loading *to the effective octahedral normal stress during consolidation*. The effective octahedral normal stress during consolidation σ'_{oct} is given by relation

$$\sigma'_{oct} = \frac{1}{3}\left(\sigma'_1 + \sigma'_2 + \sigma'_3\right) \tag{10.14}$$

where σ'_1, σ'_2, σ'_3 are, respectively, the major, intermediate, and minor effective principal stresses.

The octahedral shear stress τ_{oct} during cyclic loading is

$$\tau_{oct} = \frac{1}{3}[(\sigma_1 - \sigma_3)^2 + (\sigma_1 - \sigma_2)^2 + (\sigma_2 - \sigma_3)^2]^{1/2} \tag{10.15}$$

where σ_1, σ_2, σ_3 are, respectively, the major, intermediate, and minor principal stresses during cyclic loading.

For cyclic triaxial tests,

$$\left(\frac{\tau_{oct}}{\sigma'_{oct}}\right)_{triax} = \frac{2}{3}\sqrt{2}\left(\frac{\frac{1}{2}\sigma_d}{\sigma_3}\right)_{triax} \tag{10.16}$$

For cyclic simple shear tests,

$$\left(\frac{\tau_{oct}}{\sigma'_{oct}}\right)_{simple\ shear} = \left(\frac{\sqrt{6}}{1+2K_0}\right)\left(\frac{\tau_h}{\sigma_v}\right)_{simple\ shear} \tag{10.17}$$

Copyright 2017 Cengage Learning. All Rights Reserved. May not be copied, scanned, or duplicated, in whole or in part. Due to electronic rights, some third party content may be suppressed from the eBook and/or eChapter(s). Editorial review has deemed that any suppressed content does not materially affect the overall learning experience. Cengage Learning reserves the right to remove additional content at any time if subsequent rights restrictions require it.

Thus,

$$\left(\frac{\tau_{oct}}{\sigma'_{oct}}\right)_{\text{simple shear}} = \left(\frac{\tau_{oct}}{\sigma'_{oct}}\right)_{\text{triax}}$$

or

$$\left(\frac{\sqrt{6}}{1+2K_0}\right)\left(\frac{\tau_h}{\sigma_v}\right)_{\text{simple shear}} = \frac{2}{3}\sqrt{2}\left(\frac{\frac{1}{2}\sigma_d}{\sigma_3}\right)_{\text{triax}}$$

or

$$\left(\frac{\tau_{oct}}{\sigma'_{oct}}\right)_{\text{simple shear}} = \frac{2}{3}\sqrt{2}\left(\frac{1+2K_0}{\sqrt{6}}\right)\left(\frac{\frac{1}{2}\sigma_d}{\sigma_3}\right)_{\text{triax}}$$

$$= \frac{\frac{2}{3}(1+2K_0)}{\sqrt{3}}\left(\frac{\frac{1}{2}\sigma_d}{\sigma_3}\right)_{\text{triax}} \tag{10.18}$$

Comparing Eqs. (10.12) and (10.18),

$$\alpha' = \frac{\frac{2}{3}(1+2K_0)}{\sqrt{3}} \tag{10.19}$$

10.13 CORRELATION OF THE LIQUEFACTION RESULTS FROM TRIAXIAL TESTS TO FIELD CONDITIONS

Section 10.9 explained that the field value of (τ_h/σ_v) for initial liquefaction is about 15%–50% higher than that obtained from simple shear tests. Thus,

$$\left(\frac{\tau_h}{\sigma_v}\right)_{\text{field}} = \beta\left(\frac{\tau_h}{\sigma_v}\right)_{\text{simple shear}} \tag{10.20}$$

The approximate variation of β with relative density of sand is given in Figure 10.27. Combining Eqs (10.12) and (10.20), one obtains

$$\left(\frac{\tau_h}{\sigma_v}\right)_{\text{field}} = \beta\left(\frac{\tau_h}{\sigma_v}\right)_{\text{simple shear}} = \alpha'\beta\left(\frac{\frac{1}{2}\sigma_d}{\sigma_3}\right)_{\text{triax}} = C_r\left(\frac{\frac{1}{2}\sigma_d}{\sigma_3}\right) \tag{10.21}$$

where $C_r = \alpha'\beta$

Copyright 2017 Cengage Learning. All Rights Reserved. May not be copied, scanned, or duplicated, in whole or in part. Due to electronic rights, some third party content may be suppressed from the eBook and/or eChapter(s). Editorial review has deemed that any suppressed content does not materially affect the overall learning experience. Cengage Learning reserves the right to remove additional content at any time if subsequent rights restrictions require it.

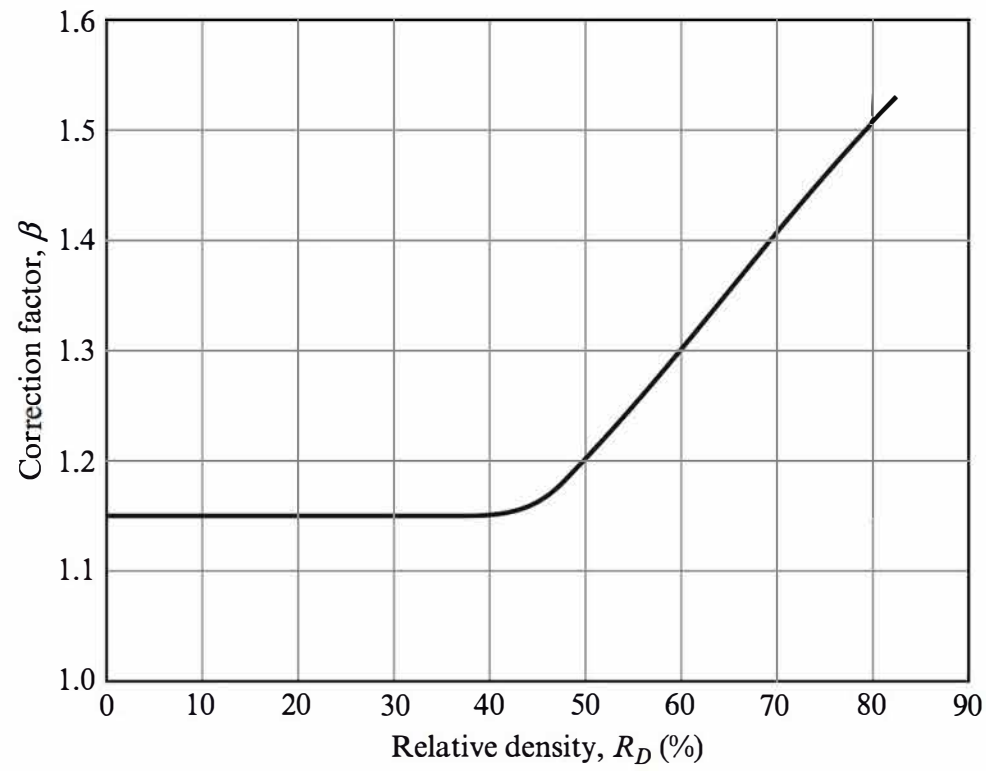

Figure 10.27 Variation of correction factor β with relative density [Eq. (10.20)]

Using an average value of $\alpha' = 0.47$ and the values of β given in Figure 10.27, the variation of C_r with relative density can be obtained. This is shown in Figure 10.28.

Equation (10.21) presents the correlations for initial liquefaction between the stress ratios in the field, cyclic simple shear tests, and cyclic triaxial tests for a

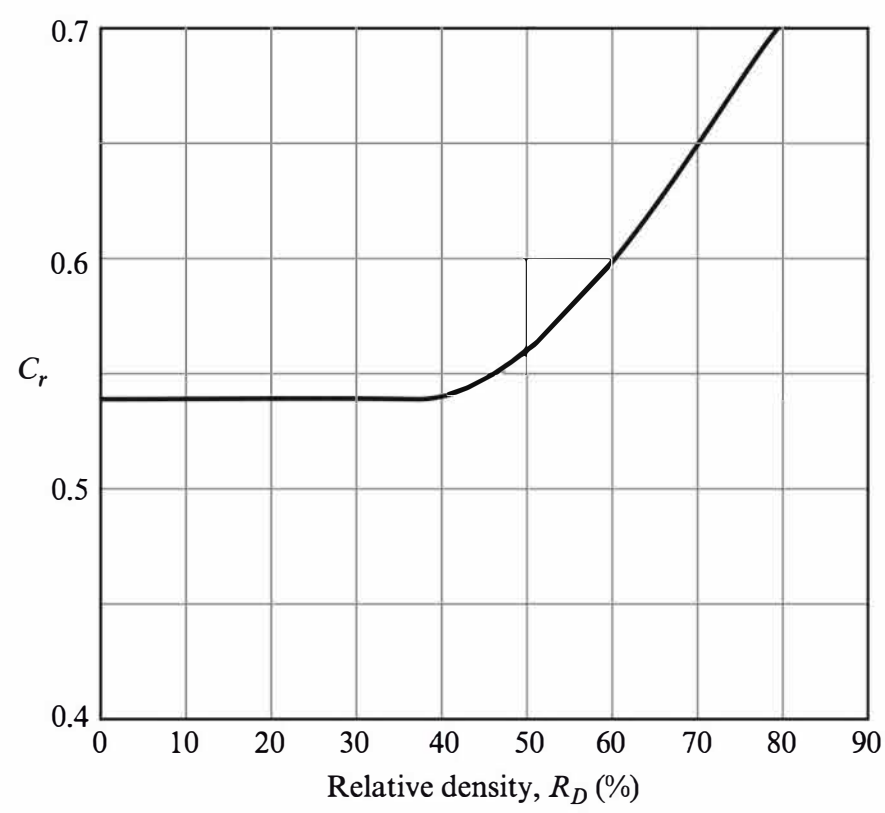

Figure 10.28 Variation of C_r with relative density [Eq. (10.21)]

Copyright 2017 Cengage Learning. All Rights Reserved. May not be copied, scanned, or duplicated, in whole or in part. Due to electronic rights, some third party content may be suppressed from the eBook and/or eChapter(s). Editorial review has deemed that any suppressed content does not materially affect the overall learning experience. Cengage Learning reserves the right to remove additional content at any time if subsequent rights restrictions require it.

given sand at the same relative density. However, when laboratory tests are conducted at relative density, say, $R_{D(1)}$, whereas the fields conditions show the sand deposit to be a relative density of $R_{D(2)}$, one has to convert the laboratory test results to correspond to a relative density of $R_{D(2)}$. It has been shown in Figure 10.18 that τ_h for initial liquefaction in the laboratory in a given number of cycles is approximately proportional to the relative density (for $R_D \leq 80\%$).

Thus,

$$\tau_{h[R_{D(2)}]} = \tau_{h[R_{D(1)}]}\left[\frac{R_{D(2)}}{R_{D(1)}}\right] \tag{10.22}$$

where $\tau_{h[R_{D(1)}]}$ is the cyclic peak shear stress required to cause initial liquefaction in the laboratory for a given value of σ_v and number of cycles, by simple shear test $(R_D = R_{D(1)})$; and $\tau_{h[R_{D(2)}]}$ is the cyclic peak stress required to cause initial liquefaction in the field for the same value of σ_v and *number of cycles*, by simple shear test $(R_D = R_{D(2)})$. Combining Eqs. (10.21) and (10.22)

$$\boxed{\left(\frac{\tau_h}{\sigma_v}\right)_{\text{field}[R_{D(2)}]} = C_r\left(\frac{\frac{1}{2}\sigma_d}{\sigma_3}\right)_{\text{triax}[R_{D(1)}]} \cdot \frac{R_{D(2)}}{R_{D(1)}}} \tag{10.23}$$

10.14 ZONE OF INITIAL LIQUEFACTION IN THE FIELD

There are five general steps for determining the zone in the field where soil liquefaction due to an earthquake can be initiated:

1. Establish a design earthquake.
2. Determine the time history of shear stresses induced by the earthquake at various depths of sand layer.
3. Convert the shear stress–time histories into N number of equivalent stress cycles (see Section 7.8). These can be plotted against depth, as shown in Figure 10.29.
4. Using the laboratory test results, determine the magnitude of the cyclic stresses required to cause initial liquefaction in the field in N cycles (determined from Step 3) at various depths. Note that the cyclic shear stress levels change with depth due to change of σ_v. These can be plotted with depth as shown in Figure 10.29.
5. The zone in which the cyclic shear stress levels required to cause initial liquefaction (Step 4) are equal to or less than the equivalent cyclic shear stresses induced by an earthquake is the zone of possible liquefaction. This is shown in Figure 10.29.

Copyright 2017 Cengage Learning. All Rights Reserved. May not be copied, scanned, or duplicated, in whole or in part. Due to electronic rights, some third party content may be suppressed from the eBook and/or eChapter(s). Editorial review has deemed that any suppressed content does not materially affect the overall learning experience. Cengage Learning reserves the right to remove additional content at any time if subsequent rights restrictions require it.

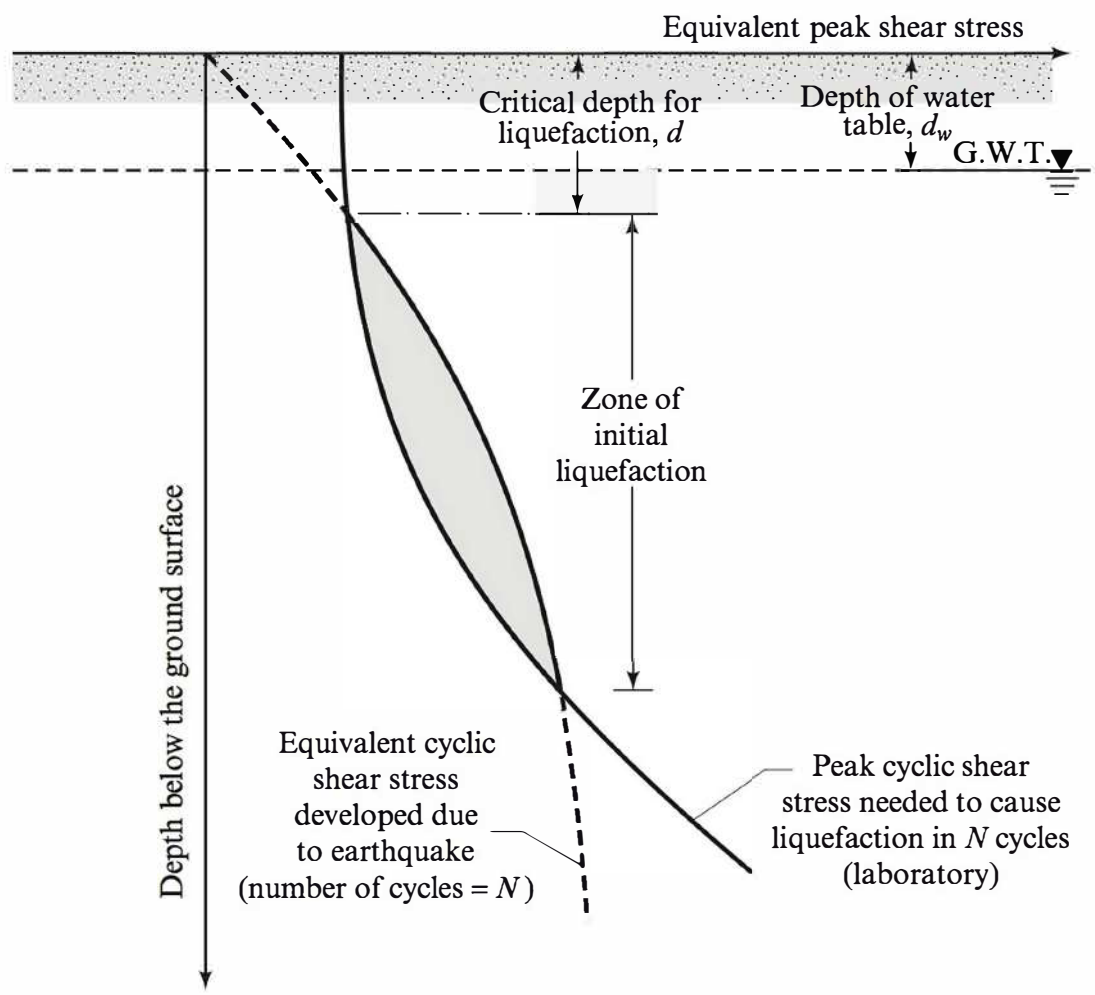

Figure 10.29 Zone of initial liquefaction in the field

10.15 RELATION BETWEEN MAXIMUM GROUND ACCELERATION AND THE RELATIVE DENSITY OF SAND FOR SOIL LIQUEFACTION

This section discusses a simplified procedure developed by Seed and Idriss (1971) to determine the relation between the maximum ground acceleration due to an earthquake and the relative density of a sand deposit in the field for the initial liquefaction condition. Figure 10.30a shows a layer of sand deposit in which we consider a column of soil of height h and unit area of cross section. Assuming the soil column to behave as a *rigid body*, the maximum shear stress at a depth h due to a maximum ground surface acceleration of a_{max} can be given by

$$\tau_{max} = \left(\frac{\gamma h}{g}\right) a_{max} \tag{10.24}$$

where τ_{max} = the maximum shear stress
γ = the unit weight of soil
g = acceleration due to gravity.

Copyright 2017 Cengage Learning. All Rights Reserved. May not be copied, scanned, or duplicated, in whole or in part. Due to electronic rights, some third party content may be suppressed from the eBook and/or eChapter(s). Editorial review has deemed that any suppressed content does not materially affect the overall learning experience. Cengage Learning reserves the right to remove additional content at any time if subsequent rights restrictions require it.

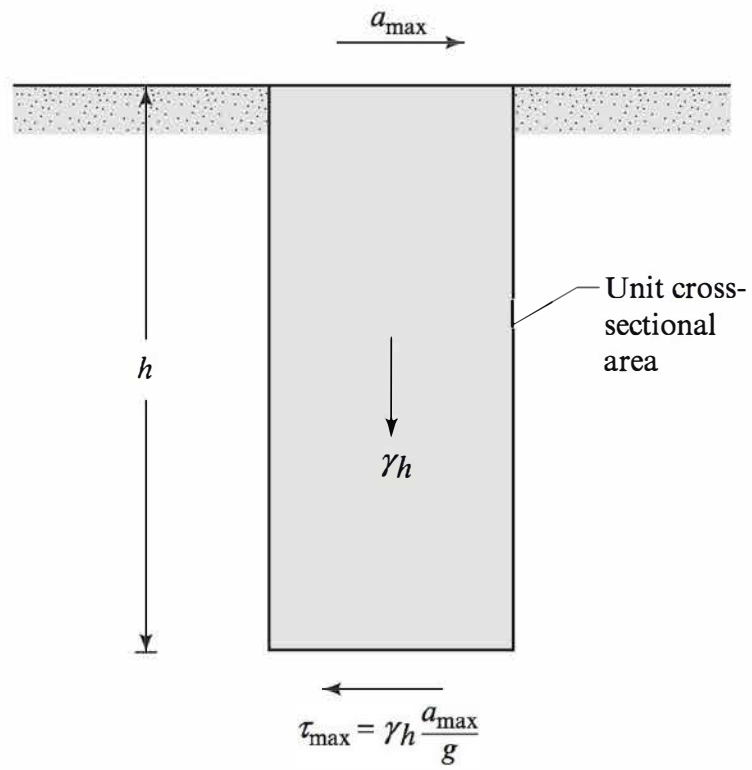

(a)

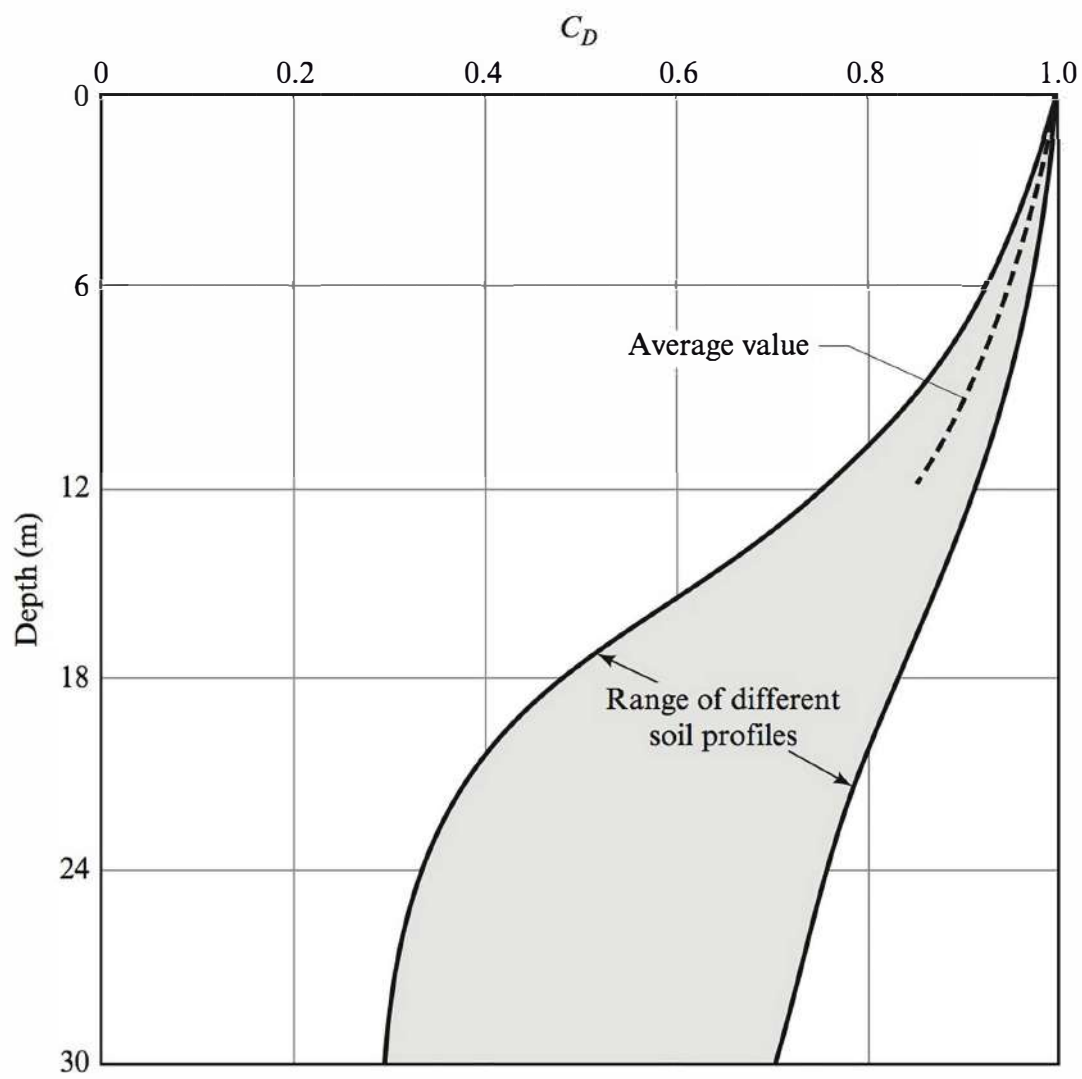

(b)

Figure 10.30 (a) Maximum shear stress at a depth for a rigid soil column; (b) range of the shear stress reduction factor C_D for the deformable nature of soil (from Seed and Idriss, 1971)

Source: Seed, H. B. and Idriss, I. M. (1971). "Simplified Procedure for Evaluating Soil Liquefaction Potential," *Journal of the Soil Mechanics and Foundations Division*, ASCE, Vol. 97, No. SM9, pp. 1249–1273. With permission from ASCE.

Copyright 2017 Cengage Learning. All Rights Reserved. May not be copied, scanned, or duplicated, in whole or in part. Due to electronic rights, some third party content may be suppressed from the eBook and/or eChapter(s). Editorial review has deemed that any suppressed content does not materially affect the overall learning experience. Cengage Learning reserves the right to remove additional content at any time if subsequent rights restrictions require it.

However, the soil column is not a rigid body. For the deformable nature of the soil, the maximum shear stress at a depth h, determined by Eq. (10.24), needs to be modified as

$$\tau_{\max(\text{modif})} = C_D\left[\left(\frac{\gamma h}{g}\right)a_{\max}\right] \tag{10.25}$$

where C_D is a stress reduction factor. The range of C_D for different soil profiles is shown in Figure 10.30b, along with the average value up to a depth of 12.0 m.

It has been shown that the maximum shear stress determined from the shear stress–time history during an earthquake can be converted into an equivalent number of significant stress cycles. According to Seed and Idriss, one can take

$$\boxed{\tau_{av} = 0.65\tau_{\max(\text{modif})} = 0.65C_D\left[\left(\frac{\gamma h}{g}\right)a_{\max}\right]} \tag{10.26}$$

The corresponding number of significant cycles N for τ_{av} is given in Table 10.2.

Note that although the values of N given in the table are somewhat different from those given in Figure 7.15, it does not make a considerable difference in the calculations. One can now combine Eq. (10.23), which gives the correlation of laboratory results of cyclic triaxial test to the field conditions, and Eq. (10.26) to determine the relationships between $a_{\max}$ and R_D. This can be better shown with the aid of a numerical example.

In general, the critical depth of liquefaction (see Figure 10.29) occurs at a depth of about 6.0 m) when the depth of water table d_w is 0–3.0 m; similarly, the critical depth is about 9.0 m when the depth of water table is about 4.5 m.

Liquefaction occurs in sands having a median size D_{50} of 0.075–0.2 mm.

Consider a case where

$$\begin{aligned}
D_{50} &= 0.075 \text{ mm}\\
d_w &= 4.5 \text{ m}\\
\gamma &= \text{unit weight of soil above the ground water table (GWT)}\\
&= 18.5 \text{ kN/m}^3\\
\gamma_{\text{sat}} &= \text{unit weight of soil below GWT} = 19.6 \text{ kN/m}^3\\
\gamma' &= \text{effective unit weight of soil below GWT}\\
&= (19.6 - 9.81) = 9.79 \text{ kN/m}^3\\
&\text{significant number of stress cycles} = 10\\
&\qquad\qquad (\text{earthquake magnitude} = 7)
\end{aligned}$$

Copyright 2017 Cengage Learning. All Rights Reserved. May not be copied, scanned, or duplicated, in whole or in part. Due to electronic rights, some third party content may be suppressed from the eBook and/or eChapter(s). Editorial review has deemed that any suppressed content does not materially affect the overall learning experience. Cengage Learning reserves the right to remove additional content at any time if subsequent rights restrictions require it.

Table 10.2 Significant Number of Stress Cycles N Corresponding to τ_{av}

Earthquake magnitude	N
7	10
7.5	20
8	30

The critical depth of liquefaction d is about 9 m. At that depth the total normal stress is equal to

$$4.5\,(\gamma) + 4.5\,\gamma_{\text{sat}} = 4.5(18.5) + 4.5(19.6) = 171.45\text{ kPa}$$

From Eq. (10.26)

$$\tau_{av} = 0.65C_D\left[\left(\frac{\gamma h}{g}\right)a_{\max}\right]$$

The value of C_D for $d = 9$ m is 0.925 (Fig. 10.30). Thus,

$$\tau_{av} = \frac{(0.65)(0.925)(171.45)a_{\max}}{g} = \frac{103.08\,a_{\max}}{g} \tag{10.27}$$

Again, from Eq. (10.23)

$$\tau_{h(\text{field})[R_{D(2)}]} = \sigma_v C_r\left(\frac{(1/2)\sigma_d}{\sigma_3}\right)_{\text{triax}[R_{D(1)}]}\cdot\frac{R_{D(2)}}{R_{D(1)}}$$

At a depth 9 m below the ground surface, the initial *effective* stress σ_v is equal to $4.5(\gamma) + 4.5(\gamma') = 4.5(18.5) + 4.5(9.79) = 127.31$ kPa.

From Figure 10.15, for $D_{50} = 0.075$ mm, $\left(\frac{(1/2)\sigma_d}{\sigma_3}\right)_{\text{triaxial } R_{D(1)} = 50\%} \approx 0.215.$

Hence

$$\tau_{h(\text{field})[R_{D(2)}]} = \frac{127.31\left[C_r(0.215)\right]R_{D(2)}}{50} = 0.547\,C_r R_{D(2)} \tag{10.28}$$

For liquefaction, τ_{av} of Eq. (10.27) should be equal to $\tau_{h(\text{field})[R_{D(2)}]}$.

Hence,

$$\frac{103.08\,a_{\max}}{g} = 0.547C_r R_{D(2)}$$

Copyright 2017 Cengage Learning. All Rights Reserved. May not be copied, scanned, or duplicated, in whole or in part. Due to electronic rights, some third party content may be suppressed from the eBook and/or eChapter(s). Editorial review has deemed that any suppressed content does not materially affect the overall learning experience. Cengage Learning reserves the right to remove additional content at any time if subsequent rights restrictions require it.

Table 10.3 Relation Between a_{max}/g versus $R_{D(2)}$ [Eq. (10.29)]

$R_{D(2)}$ (%)	C_r^a	$\frac{a_{max}}{g}$
20	0.54	0.0572
30	0.54	0.0859
40	0.54	0.1144
50	0.56	0.1484
60	0.61	0.1940
70	0.66	0.2449
80	0.71	0.3010

[a]From Figure 10.28.

or

$$\frac{a_{max}}{g} = 0.0053 C_r R_{D(2)} \tag{10.29}$$

It is now possible to prepare Table 10.3 to determine the variation of a_{max}/g with $R_{D(2)}$. Note that $R_{D(2)}$ is the relative density in the field.

Figure 10.31 shows a plot of a_{max}/g versus the relative density as determined from Table 10.3. For this given soil (i.e., given D_{50}, d_w, and number of significant stress cycles N), if the relative density in the field and a_{max}/g are such that they plot as point A in Figure 10.31 (i.e., above the curve showing the relationship of Eq. (10.29)], then liquefaction would occur. On the other hand, if the relative density and a_{max}/g plot as point B [i.e., below the curve showing the relationship of Eq. (10.29)], then liquefaction would not occur.

Diagrams of the type shown in Figure 10.31 could be prepared for various combinations of D_{50}, d_w, and N. Since, in the field, for liquefaction the range of D_{50} is 0.075–0.2 mm and the range of N is about 10–20, one can take the critical combinations (i.e., $D_{50} = 0.075$ mm, $N = 20$; $D_{50} = 0.2$ mm, $N = 10$) and plot graphs as shown in Figure 10.32. These graphs provide a useful guide in the evaluation of liquefaction potential in the field.

These graphs are also useful, particularly when implementing a possible ground improvement technique in the field to reduce the liquefaction susceptibility. Using this, one can find how much increase in relative density or in other words, how much compaction is required to be achieved in the field (using principles of basic soil mechanics), once the in situ conditions of the soil and the possible maximum ground acceleration the site likely to experience are known.

Copyright 2017 Cengage Learning. All Rights Reserved. May not be copied, scanned, or duplicated, in whole or in part. Due to electronic rights, some third party content may be suppressed from the eBook and/or eChapter(s). Editorial review has deemed that any suppressed content does not materially affect the overall learning experience. Cengage Learning reserves the right to remove additional content at any time if subsequent rights restrictions require it.

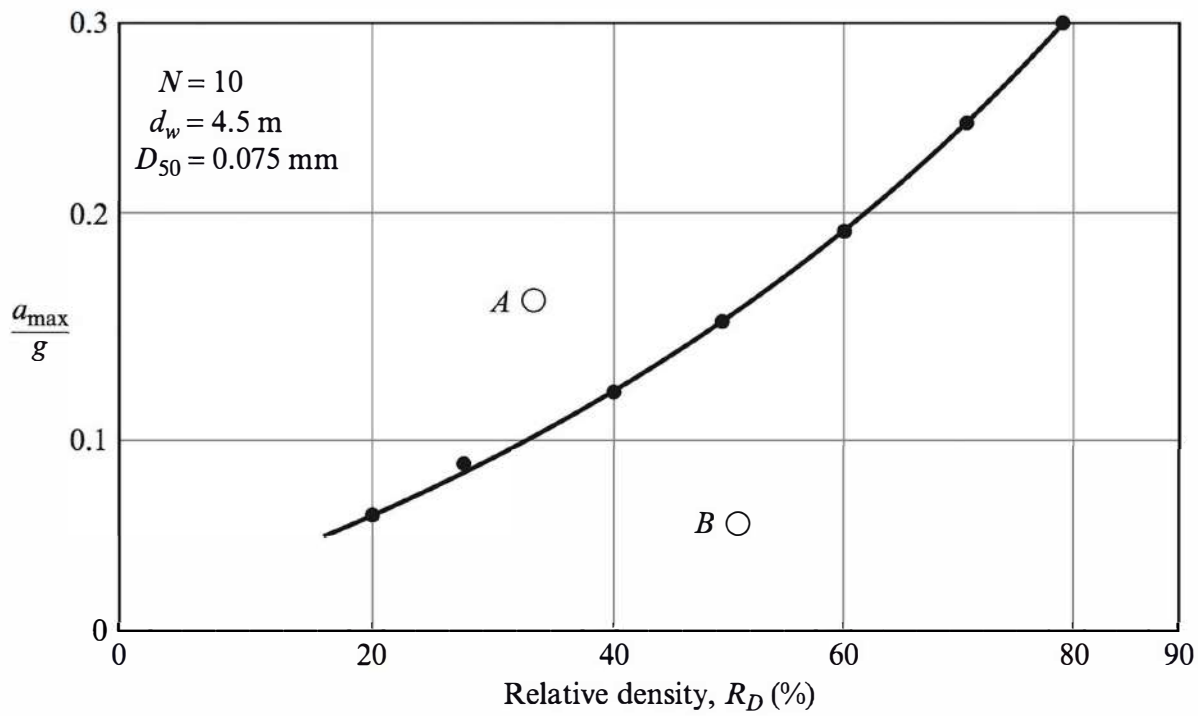

Figure 10.31 Plot of a_{max}/g versus relative density from Table 10.3

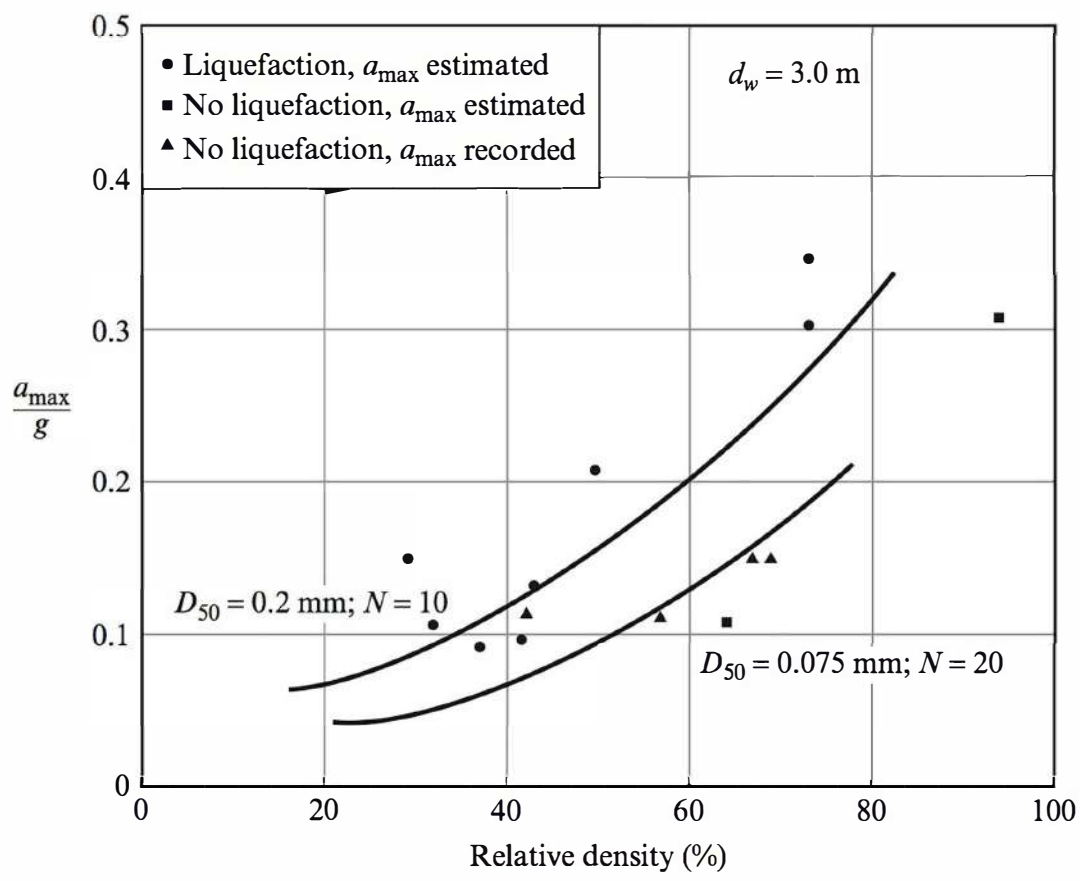

Figure 10.32 Evaluation of liquefaction potential for sand below the ground surface (redrawn from Seed and Idriss, 1971)

Source: Seed, H. B. and Idriss, I. M. (1971). "Simplified Procedure for Evaluating Soil Liquefaction Potential," *Journal of the Soil Mechanics and Foundations Division*, ASCE, Vol. 97, No. SM9, pp. 1249–1273. With permission from ASCE.

Copyright 2017 Cengage Learning. All Rights Reserved. May not be copied, scanned, or duplicated, in whole or in part. Due to electronic rights, some third party content may be suppressed from the eBook and/or eChapter(s). Editorial review has deemed that any suppressed content does not materially affect the overall learning experience. Cengage Learning reserves the right to remove additional content at any time if subsequent rights restrictions require it.

10.16 LIQUEFACTION ANALYSIS FROM STANDARD PENETRATION RESISTANCE

Another way of evaluating the soil liquefaction potential is to prepare correlation charts with the standard penetration resistance. After the occurrence of the Niigata earthquake of 1964, Kishida (1966), Kuizumi (1966), and Ohasaki (1966) studied the areas in Niigata where liquefaction had and had not occurred. They developed criteria, based primarily on standard penetration resistance of sand deposits, to differentiate between liquefiable and nonliquefiable conditions. Subsequently, a more detailed collection of field data for liquefaction potential was made by Seed and Peacock (1971). These results and some others were presented by Seed, Mori, and Chan (1971) in a graphical form, which is a plot of τ_h/σ_v versus $(N_1)_{60}$. This is shown in Figure 10.33. In this figure note that $(N_1)_{60}$ is the corrected standard penetration resistance for an effective overburden pressure

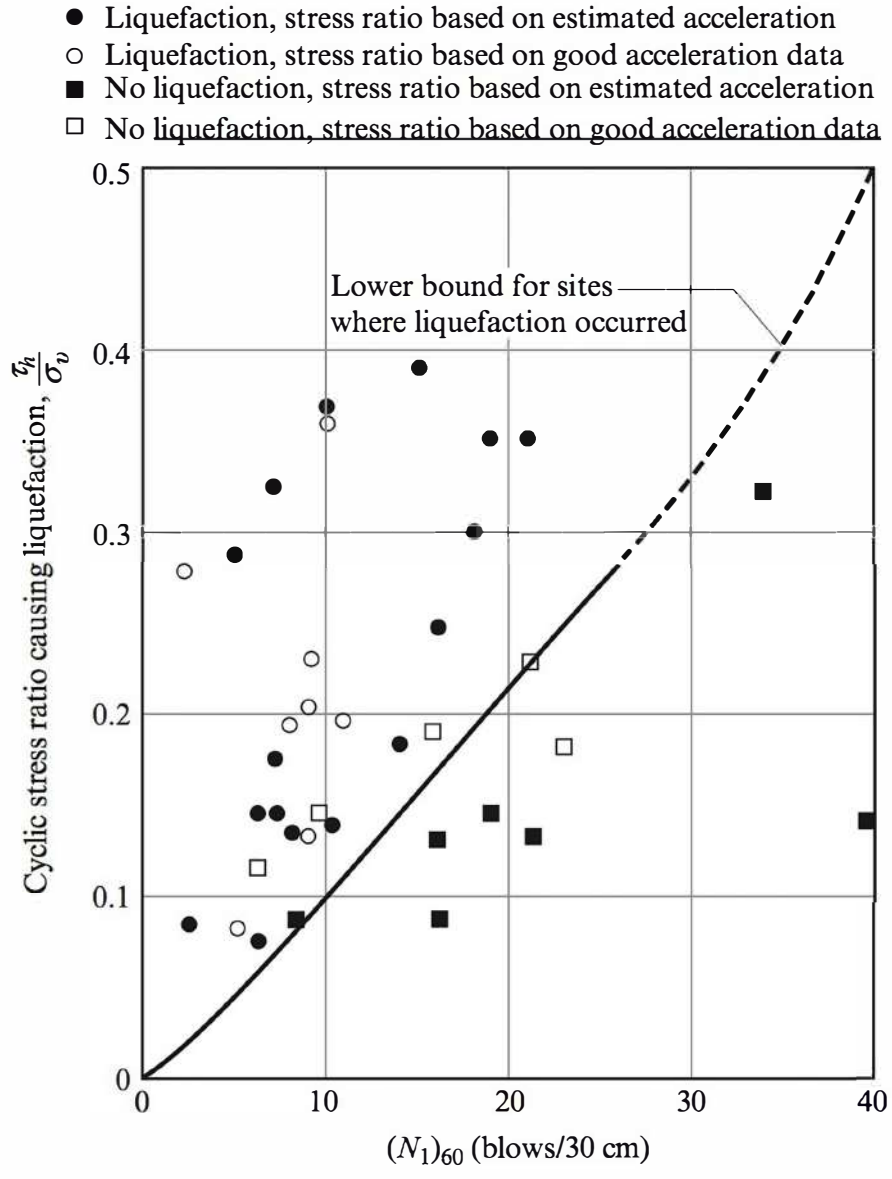

Figure 10.33 Correlation between τ_h/σ_v and $(N_1)_{60}$ (from Seed, 1979)

Source: Seed, H. B. (1979). "Soil Liquefaction and Cyclic Mobility Evaluation for Level Ground During Earthquakes," *Journal of the Geotechnical Engineering Division*, ASCE, Vol. 105, No. GT2, pp. 201–255. With permission from ASCE.

Copyright 2017 Cengage Learning. All Rights Reserved. May not be copied, scanned, or duplicated, in whole or in part. Due to electronic rights, some third party content may be suppressed from the eBook and/or eChapter(s). Editorial review has deemed that any suppressed content does not materially affect the overall learning experience. Cengage Learning reserves the right to remove additional content at any time if subsequent rights restrictions require it.

of 100 kPa (i.e., N_{60}, which is the standard penetration resistance for an average energy ratio of 60% corrected to an effective overburden pressure of 100 kPa). Figure 10.33 shows the lower bounds of the correlation curve causing liquefaction in the field. However, correlation charts such as this cannot be used with confidence in the field, primarily because they do not take into consideration the magnitude of the earthquake and the duration of shaking.

In order to develop a better correlation chart, Seed (1979) considered the results of the large-scale simple shear test conducted by DeAlba, Chan, and Seed (1976), which were discussed in Section 10.11. These results were corrected to take into account the significant factors that effect the field condition, and they are shown in Table 10.4. It is important to realize that the $(\tau_h/\sigma_v)_{\text{test}}$ values listed in Table 10.4 are those required for a peak cyclic pore pressure ratio of 100% and cyclic shear strain of ±5%. Also, the correlation between R_D and $(N_1)_{60}$ shown in columns 1 and 2 are via the relationship established by Bieganousky and Marcuson (1977).

Excellent agreement is observed when the values of $(N_1)_{60}$ and the corresponding $(\tau_h/\sigma_v)_{\text{field}}$ values (columns 2 and 6) shown in Table 10.4 are superimposed on the lower-bound correlation curve shown in Figure 10.33. Hence the lower-bound curve of Figure 10.33 is for an earthquake magnitude $M = 7.5$. Proceeding in a similar manner and utilizing the results shown in Table 10.4, lower-bound curves for $M = 6$, 7.5, and 8.25 can be obtained as shown in Figure 10.34. Also shown in this figure is the variation of the limited strain potential in percent (for effective overburden pressure of 100 kPa). Figure 10.34 can be used for determination of the liquefaction potential in the field. In doing so, it is important to remember that

$$(N_1)_{60} = C_N N_{60} \tag{10.30}$$

Table 10.4 Data from Large-scale Simple Shear Tests on Freshly Deposited Sand[a]

		$M = 5-6$ 5 cycles		$M = 7-7.5$ 15 cycles		$M = 8-8.25$ 25 cycles	
Relative density, R_D	**$(N_1)_{60}$ (blows/30 cm)**	$\left(\frac{\tau_h}{\sigma_v}\right)_{\text{test}}$	$\left(\frac{\tau_h}{\sigma_v}\right)_{\text{field}}$	$\left(\frac{\tau_h}{\sigma_v}\right)_{\text{test}}$	$\left(\frac{\tau_h}{\sigma_v}\right)_{\text{field}}$	$\left(\frac{\tau_h}{\sigma_v}\right)_{\text{test}}$	$\left(\frac{\tau_h}{\sigma_v}\right)_{\text{field}}$
(1)	**(2)**	**(3)**	**(4)**	**(5)**	**(6)**	**(7)**	**(8)**
54	13.5	0.22	0.25	0.17	0.19	0.155	0.175
68	23	0.30	0.34	0.24	0.27	0.210	0.235
82	33	0.44	0.49	0.32	0.37	0.280	0.315
90	39	0.59	0.66	0.41	0.46	0.360	0.405

Note: $(N_1)_{60}$ = standard penetration resistance (N_{60}), corrected to an effective overburden pressure of 100 kPa; M = magnitude of earthquake.

[a]After Seed (1979).

Source: Seed, H. B. (1979). "Soil Liquefaction and Cyclic Mobility Evaluation for Level Ground During Earthquakes," *Journal of the Geotechnical Engineering Division*, ASCE, Vol. 105, No. GT2, pp. 201–255. With permission from ASCE.

Copyright 2017 Cengage Learning. All Rights Reserved. May not be copied, scanned, or duplicated, in whole or in part. Due to electronic rights, some third party content may be suppressed from the eBook and/or eChapter(s). Editorial review has deemed that any suppressed content does not materially affect the overall learning experience. Cengage Learning reserves the right to remove additional content at any time if subsequent rights restrictions require it.

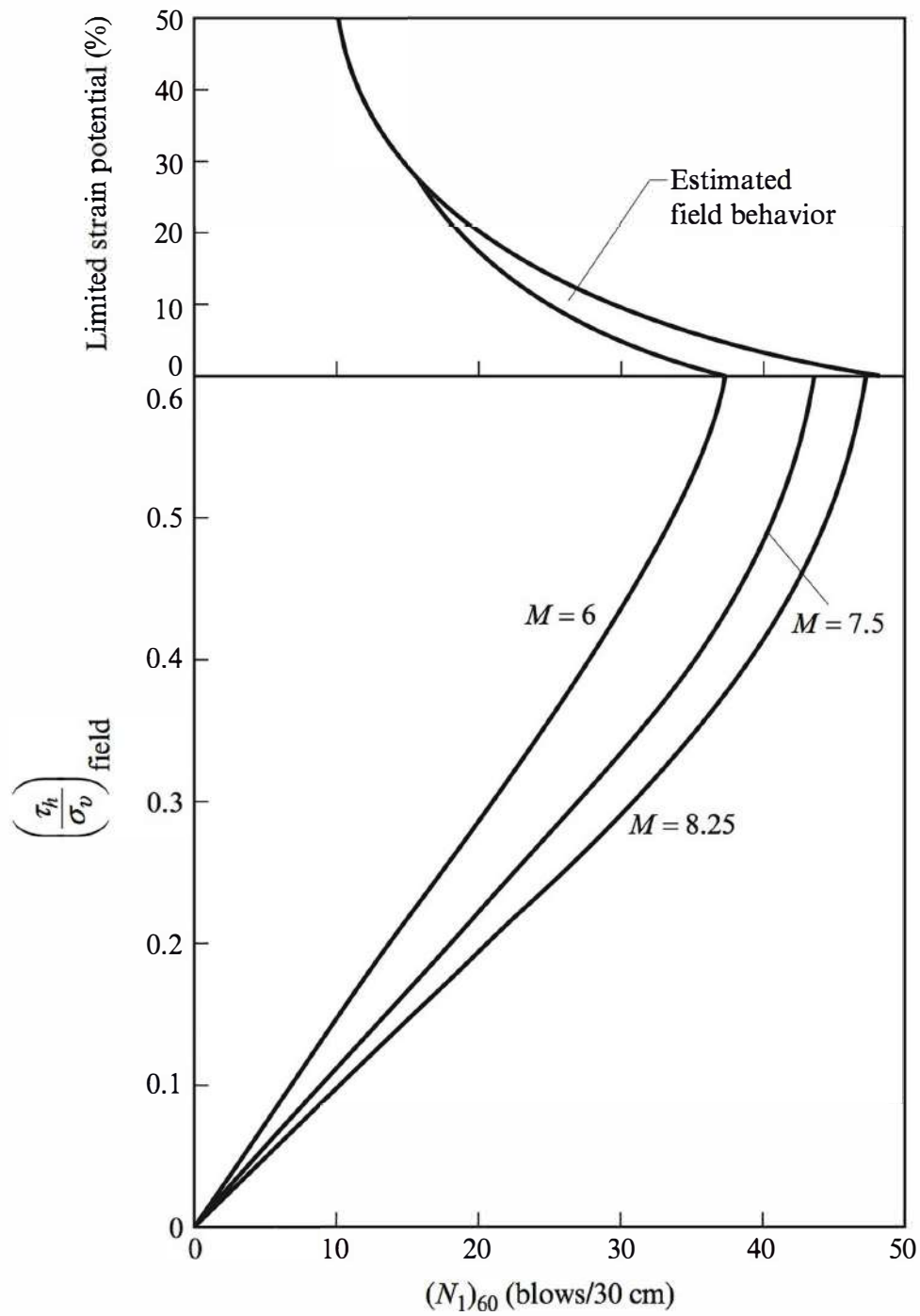

Figure 10.34 Variation of $(\tau_h/\sigma_v)_{\text{field}}$ with $(N_1)_{60}$ and M (from Seed, 1979)

Source: Seed, H. B. (1979). "Soil Liquefaction and Cyclic Mobility Evaluation for Level Ground During Earthquakes," *Journal of the Geotechnical Engineering Division*, ASCE, Vol. 105, No. GT2, pp. 201–255. With permission from ASCE.

where

N_{60} = field standard penetration test values for an average energy ratio of 60%

C_N = correction factor to convert to an effective overburden pressure (σ'_v) of 100 kPa

The correction factor can be expressed as (Liao and Whitman, 1986)

$$C_N = 9.78\sqrt{\frac{1}{\sigma'_v}} \tag{10.31}$$

where σ'_v is in kPa.

Copyright 2017 Cengage Learning. All Rights Reserved. May not be copied, scanned, or duplicated, in whole or in part. Due to electronic rights, some third party content may be suppressed from the eBook and/or eChapter(s). Editorial review has deemed that any suppressed content does not materially affect the overall learning experience. Cengage Learning reserves the right to remove additional content at any time if subsequent rights restrictions require it.

A slight variation of Figure 10.34 is given by Seed, Idriss, and Arango (1983) and Seed and Idriss (1982). It can be seen from this figure that, if $(N_1)_{60}$ is more than 30, liquefaction is unlikely to occur, in general.

Discussion regarding soil liquefaction has so far been limited to the case of clean sands; however, liquefaction can, and has been, observed in silty sands, mine tailings and silts. It is generally reported that mine tailings behave similar to clean sands under seismic loading. Information regarding the liquefaction of silty sand is somewhat limited, and there is no consensus among the researchers as of date. In general, it is observed that liquefaction resistance of silty sands, up to certain silt content, is more than that of clean sands. It may be due to the fact that voids in clean sands are occupied by silt particles and thus these may inhibit a quick volume change behavior. Seed et al. (1984) presented limited correlations between $(\tau_h/\sigma_v)_{\text{field}}$, $(N_1)_{60}$ and percent fines (F) for an earthquake magnitude $M = 7.5$, which can be summarized as follows:

Percent of fines, F	$(N_1)_{60}$	**Lower bound of $(\tau_h/\sigma_v)_{\text{field}}$ for which liquefaction is likely ($M = 7.5$)**
≤ 5	5	0.055
	10	0.115
	15	0.170
	20	0.220
	25	0.295
	30	0.500
10	5	0.098
	10	0.160
	15	0.225
	20	0.295
	25	0.500
35	5	0.130
	10	0.185
	15	0.260
	20	0.400

EXAMPLE 10.1

Geotechnical investigations carried out in a deposit of sand provided the field standard penetration numbers N_{60} as given in the table below. During the geotechnical investigations, it is also observed that groundwater table is

Copyright 2017 Cengage Learning. All Rights Reserved. May not be copied, scanned, or duplicated, in whole or in part. Due to electronic rights, some third party content may be suppressed from the eBook and/or eChapter(s). Editorial review has deemed that any suppressed content does not materially affect the overall learning experience. Cengage Learning reserves the right to remove additional content at any time if subsequent rights restrictions require it.

encountered at a depth of 3.0 m measured from the ground surface. Given for the sand:

$$\text{Dry unit weight} = 17.6\ \text{kN/m}^3$$

$$\text{Saturated unit weight} = 19.6\ \text{kN/m}^3$$

Determine, for an earthquake magnitude of 7.5, if liquefaction will occur at the site. Assume that the maximum peak ground acceleration at the site is $a_{max} = 0.15\,g$.

Depth (m)	N_{60} (blows/30cm)
1.5	6
3.0	8
4.5	10
6.0	14
7.5	16
9.0	20
10.5	20

SOLUTION:

Step 1. The following table can now be prepared for calculating the shear resistance available in the sand deposit at different depths.

Depth (m)	Vertical effective stress (kPa)	C_N [Eq. (10.31)]	$(N_1)_{60}$[a] (blows/30 cm)	$\left(\frac{\tau_h}{\sigma_v}\right)_{field}$[b]	τ_h (kPa)
1.5	26.4	1.90	11	0.128	3.38
3.0	52.8	1.35	11	0.128	6.76
4.5	67.4	1.19	12	0.140	9.45
6.0	82.1	1.08	15	0.168	13.80
7.5	96.8	0.99	16	0.184	17.82
9.0	111.5	0.93	19	0.210	23.42
10.5	126.2	0.87	17	0.195	24.61

[a] $(N_1)_{60} = C_N N_{60}$ (rounded off).

[b] From Figure 10.34.

Step 2. The following table can now be prepared for calculation of the shear stresses induced in the sand deposit at different depths [τ_{av} using Equation (10.26)].

Copyright 2017 Cengage Learning. All Rights Reserved. May not be copied, scanned, or duplicated, in whole or in part. Due to electronic rights, some third party content may be suppressed from the eBook and/or eChapter(s). Editorial review has deemed that any suppressed content does not materially affect the overall learning experience. Cengage Learning reserves the right to remove additional content at any time if subsequent rights restrictions require it.

Depth (m)	Total vertical stress (kPa)	$\frac{a_{max}}{g}$	C_D[a]	τ_{av}[b] (kPa)
3.0	52.8	0.15	0.98	5.04
4.5	82.2	0.15	0.97	11.97
6.0	111.6	0.15	0.96	15.99
7.5	141.0	0.15	0.95	20.02
9.0	170.4	0.15	0.94	23.94
10.5	199.8	0.15	0.90	26.91

[a]Figure 10.30 (b)

[b]$\tau_{av} = 0.65\, C_D[(\gamma h/g)a_{max}]$

Step 3. Check to see if $\tau_{av} \geq \tau_h$ at any depth in the sand deposit. In that case, liquefaction would occur. From the preceding two tables, it can be seen that between depths of 3.0 m and 10.5 m, τ_{av} is greater than τ_h, **so liquefaction occurs between these depths**.

10.17 OTHER CORRELATIONS FOR FIELD LIQUEFACTION ANALYSIS

Correlation with Cone Penetration Resistance

In many cases during field exploration, the variation of the cone penetration resistance is measured with depth. Similar to the standard penetration number N_{60}, the field cone penetration resistance needs to be corrected to a standard effective overburden pressure. Thus, for clean sand (Ishihara, 1985)

$$q_c' = C_N\, q_c \tag{10.32}$$

where q_c = field cone penetration resistance (kg/cm²)
C_N = correction factor
q_c' = corrected cone penetration resistance (kg/cm²) (corrected to $\sigma_v' = 100$ kPa)

If the value of q_c' for $\sigma_v' = 100$ kPa is needed, then Eq. (10.31) may be used. It has been noted from several field tests that

$$q'_{c(\sigma_v' = 100\text{ kPa})} = A(N_1)_{60} \tag{10.33}$$

where $A = 4$ to 5 for clean sands.

Assuming the value of A to be about 4,

$$q'_{c(\sigma_v' = 100\text{ kPa})} \approx 4(N_1)_{60}$$

Copyright 2017 Cengage Learning. All Rights Reserved. May not be copied, scanned, or duplicated, in whole or in part. Due to electronic rights, some third party content may be suppressed from the eBook and/or eChapter(s). Editorial review has deemed that any suppressed content does not materially affect the overall learning experience. Cengage Learning reserves the right to remove additional content at any time if subsequent rights restrictions require it.

Thus,

$$(N_1)_{60} \approx \frac{q'_{c(\sigma'_v = 100\text{ kPa})}}{4} \tag{10.34}$$

Once the estimated values for $(N_1)_{60}$ are known, Figure 10.34 can be used to check the possibility for liquefaction in the field.

Use of Threshold Strain

It was discussed in Section 10.2 that for densification of sand under drained condition, a threshold shear strain level must be exceeded. Similarly, under undrained conditions, a threshold cyclic shear strain level needs to be exceeded to cause build up of excess pore water pressure and thus possible liquefaction. So if it can be shown that a cyclic shear strain in soil as a result of an earthquake does not exceed a certain threshold level, liquefaction cannot occur. This would provide a conservative evaluation due to the fact that liquefaction may not always occur even if the strains do exceed the threshold level (Committee on Earthquake Engineering, Commission of Engineering and Technical Systems, 1985).

The peak shear strain caused by earthquake ground motion can be estimated from Eq. (10.25) as

$$\gamma' = \frac{\tau_{\max(\text{modif})}}{G} = \frac{C_D\left[(\gamma h/g)a_{\max}\right]}{G} \tag{10.35}$$

where γ' = peak shear strain
G = shear modulus

or

$$\gamma' = \frac{C_D \rho h a_{\max}}{G} = \frac{C_D h a_{\max}}{(G/\rho)(G_{\max}/G_{\max})} = \frac{C_D h a_{\max}}{(G/G_{\max})\upsilon_s^2} \tag{10.36}$$

where υ_s = shear wave velocity in soil
$G_{\max}$ = maximum shear modulus (see Chapter 4)

The magnitude of $G/G_{\max}$ can be assumed to be about 0.8. Substituting into Eq. (10.36) and combining with an average value of C_D,

$$\gamma' = \frac{1.2 a_{\max} h}{\upsilon_s^2} \tag{10.37}$$

By measuring υ_s with depth h, the variation of γ' can be calculated. The typical value of the threshold strain is about 0.01% (Dobry et al., 1981). If the magnitude of the calculated γ' does not exceed this threshold limit, then there is safety against liquefaction.

Copyright 2017 Cengage Learning. All Rights Reserved. May not be copied, scanned, or duplicated, in whole or in part. Due to electronic rights, some third party content may be suppressed from the eBook and/or eChapter(s). Editorial review has deemed that any suppressed content does not materially affect the overall learning experience. Cengage Learning reserves the right to remove additional content at any time if subsequent rights restrictions require it.

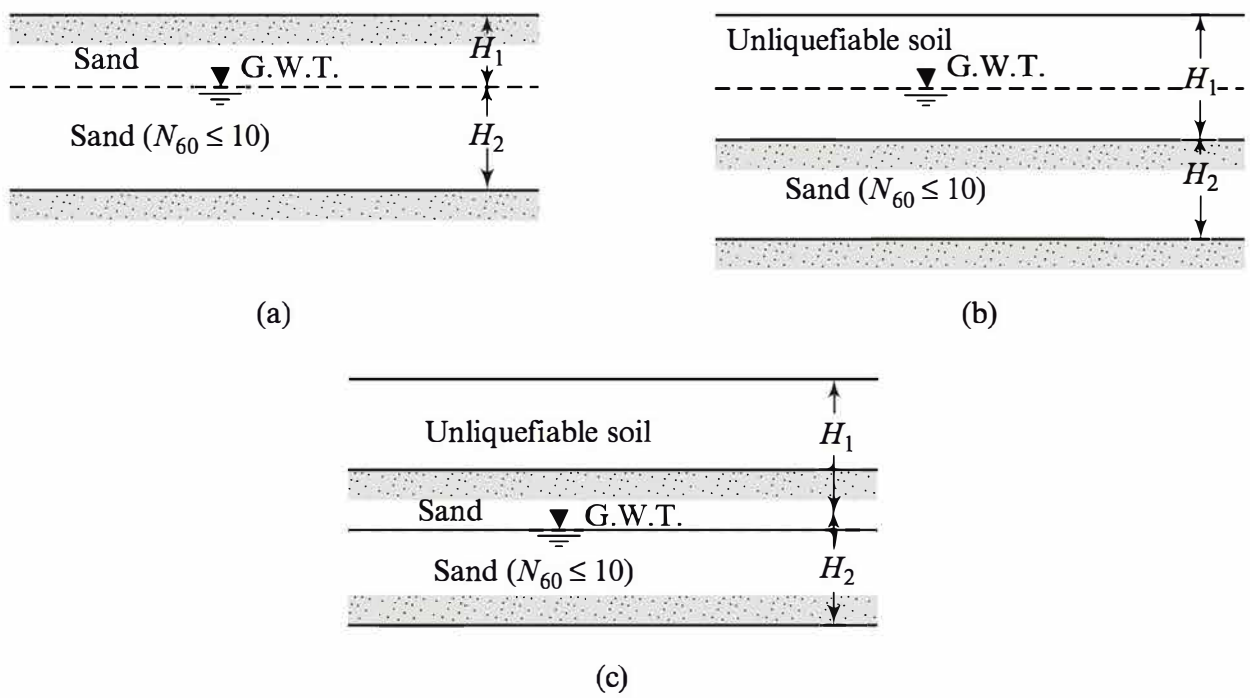

Figure 10.35 Definition of liquefaction-resistance stratum (H_1) and liquefiable stratum (H_2)

Correlation with Overlying Liquefaction-Resistant Stratum

The earthquake of magnitude 7.7 that occurred on May 26, 1983, in the northern part of Japan has provided enough data to study the effect of an overlying liquefaction-resistant stratum on the liquefaction potential of sand *with standard penetration resistance* $N_{60} \leq 10$. Figure 10.35 defines the terms H_1 and H_2 which are, respectively, the liquefaction resistant stratum and the liquefiable stratum. Based on field observations, Ishihara (1985) developed a correlation chart between H_1, H_2, and maximum acceleration a_{max}. This correlation chart is shown in Figure 10.36.

10.18 SIMPLIFIED PROCEDURES FOR DETERMINING SOIL LIQUEFACTION USING IN SITU INDEX

The simplified procedures pioneered by Seed and Idriss (1971) following the disastrous earthquakes in Alaska, USA and in Niigata, Japan in 1964 are the most widely used methods for liquefaction potential evaluation in North America and throughout much of the world. The Seed and Idriss procedure (1971) has been modified and improved periodically by several researchers with various field and test data. The simplified procedures described in this section require two terms to assess the liquefaction resistance of soils: (1) the seismic loading on a soil element, expressed in terms of cyclic stress ratio (CSR); and (2) the capacity of the soil to resist liquefaction, expressed in terms of cyclic resistance ratio (CRR). Using these procedures, the factor of safety (F_s) against liquefaction is defined as the ratio of CRR over CSR:

$$F_s = \frac{\text{CRR}}{\text{CSR}} \tag{10.38}$$

Copyright 2017 Cengage Learning. All Rights Reserved. May not be copied, scanned, or duplicated, in whole or in part. Due to electronic rights, some third party content may be suppressed from the eBook and/or eChapter(s). Editorial review has deemed that any suppressed content does not materially affect the overall learning experience. Cengage Learning reserves the right to remove additional content at any time if subsequent rights restrictions require it.

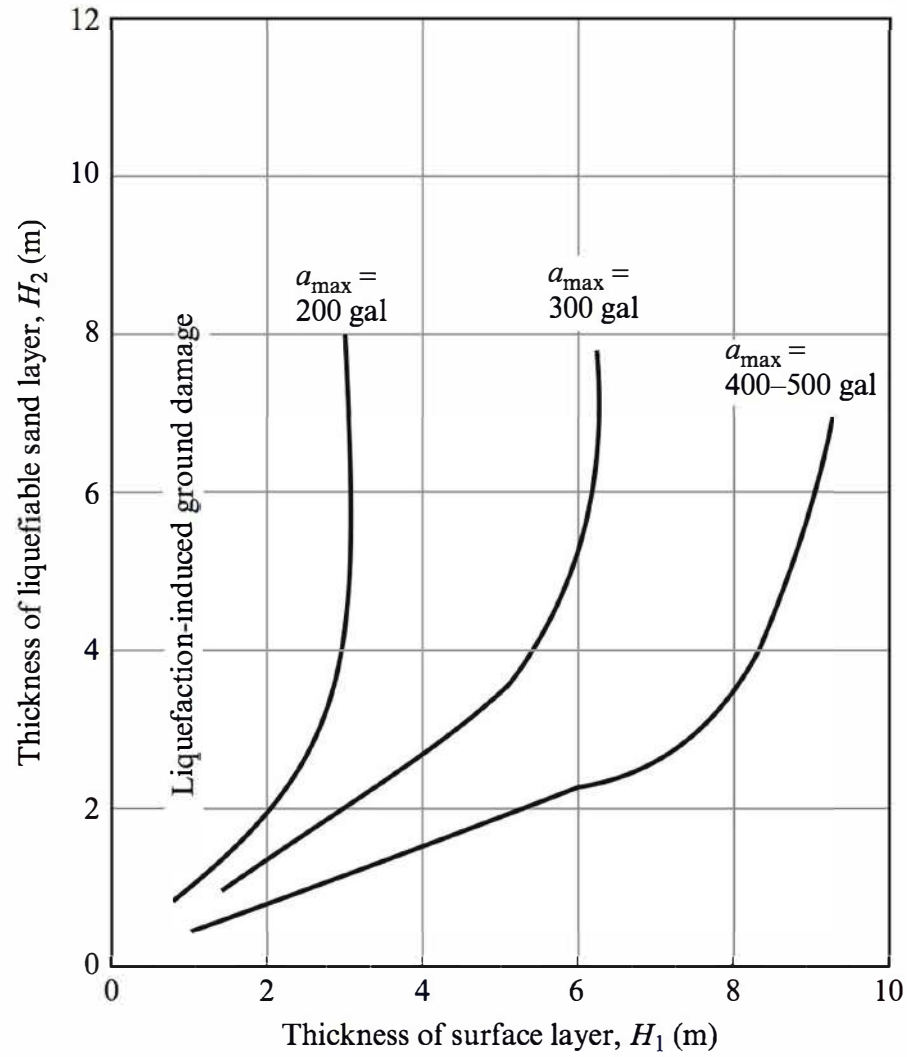

Figure 10.36 Ishihara's proposed boundary curves for site identification of liquefaction-induced damage

In deterministic analysis, the liquefaction is likely to occur if $F_s \leq 1.0$. The simplified procedures necessitate the use of in situ index testing in common practice. Four in situ test methods are widely used in the simplified procedures to determine the liquefaction potential: (1) the standard penetration test (SPT); (2) the cone penetration test (CPT); (3) measurement of in situ shear wave velocity (υ_s); and (4) the Becker penetration test (BPT). Table 10.5 summarizes the advantages and disadvantages of each test.

Cyclic Stress Ratio

Based on the formulation of Eq. (10.26) by Seed and Idriss (1971), the adjusted cyclic stress ratio (CSR) is expressed as (Idriss and Boulanger, 2010):

$$\text{CSR} = \frac{0.65\left(\dfrac{a_{\max}}{g}\right)\left(\dfrac{\sigma_v}{\sigma'_v}\right)\gamma_d}{(MSF)(K_\sigma)} \tag{10.39}$$

where a_{max} = peak horizontal acceleration at ground surface (g)
g = acceleration due to gravity
σ_υ = total stress of the soil at the required depth (kPa)

Copyright 2017 Cengage Learning. All Rights Reserved. May not be copied, scanned, or duplicated, in whole or in part. Due to electronic rights, some third party content may be suppressed from the eBook and/or eChapter(s). Editorial review has deemed that any suppressed content does not materially affect the overall learning experience. Cengage Learning reserves the right to remove additional content at any time if subsequent rights restrictions require it.

Table 10.5 Comparison of Advantages and Disadvantages of Various Field Tests for Evaluating Liquefaction Resistance (Summarized from Youd et al., 2001)

Test type (1)	Data available from liquefaction sites (2)	Stress-strain behavior (3)	Repeatability (4)	Soil type (5)
SPT	Abundant	Partially drained, large strain	Poor to good	Nongravel
CPT	Abundant	Drained, large strain	Very good	Nongravel
v_s	Limited	Small strain	Good	All
BPT	Sparse	Partially drained	Poor	Mostly gravel

Source: Based on data from Youd, T. L., Idriss, I. M., Andrus, R.D., Arango, I., Castro, G., Christian, J.T., Dobry, R., Liam Finn, W.D., Harder, L.F., Jr., Hynes, M.E., Ishihara, K., Koester, J.P., Liao, S.S.C., Marcuson, W.F., III, Martin, G.R., Mitchell, J.K., Moriwaki, Y., Power, M.S., Robertson, P.K., Seed, R.B., and Stokoe, K.H., II. (2001). "Liquefaction resistance of soils: summary report from the 1996 NCEER and 1998 NCEER/NSF workshops on evaluation of liequefaction resistance of soils." *Journal of Geotechnical and Geoenvironmental Engineering*, ASCE, Vol. 127, No. 10, pp. 817–833.

σ'_v = effective stress of the soil at the required depth (kPa)
γ_d = depth-dependent shear stress reduction factor;
MSF = magnitude scaling factor
K_σ = overburden correction factor for cyclic stress ratio

For practical interest, the parameter γ_d can be estimated as a function of depth and earthquake moment magnitude (M_w). [For the definition of M_w, see Eq. (7.2).] The following correlations are suggested by Idriss and Boulanger (2010):

$$\ln(\gamma_d) = \alpha + \beta M_w \tag{10.40}$$

where

$$\alpha = -1.012 - 1.126 \sin\left(\underbrace{5.133 + \frac{z}{11.73}}_{\text{radians}}\right) \tag{10.41}$$

$$\beta = 0.106 + 0.118 \sin\left(\underbrace{5.142 + \frac{z}{11.28}}_{\text{radians}}\right) \tag{11.42}$$

where z is depth of interest (m) and M_w is moment magnitude (dimensionless). These equations are applicable to a depth $z \leq 34$ m. For $z > 34$ m, the following expression is applicable:

$$\gamma_d = 0.12 \exp(0.22 M_w) \tag{10.43}$$

Copyright 2017 Cengage Learning. All Rights Reserved. May not be copied, scanned, or duplicated, in whole or in part. Due to electronic rights, some third party content may be suppressed from the eBook and/or eChapter(s). Editorial review has deemed that any suppressed content does not materially affect the overall learning experience. Cengage Learning reserves the right to remove additional content at any time if subsequent rights restrictions require it.

The magnitude scaling factor (MSF) is given as follows:

$$MSF = -0.058 + 6.9\exp(-0.25M_w) \leq 1.8 \tag{10.44}$$

Overburden Correction Factor for CSR, K_σ

The following equations are suggested by Idriss and Boulanger (2010) to evaluate overburden correction factor K_σ using SPT blow count:

$$K_\sigma = 1 - C_\sigma \ln\left(\frac{\sigma'_v}{p_a}\right) \leq 1.1 \tag{10.45}$$

where p_a = atmospheric pressure ($\approx$ 100 kPa)

$$C_\sigma = \frac{1}{18.9 - 2.55\sqrt{(N_1)_{60,cs}}} \leq 0.3 \tag{10.46}$$

The term $(N_1)_{60,cs}$ is the equivalent clean-sand corrected blow count, computed as:

$$(N_1)_{60,cs} = (N_1)_{60} + \Delta(N_1)_{60} \tag{10.47}$$

The adjustment $\Delta(N_1)_{60}$ is a function of fines content (FC in %) and can be computed as:

$$\Delta(N_1)_{60} = \exp\left[1.63 + \frac{9.7}{FC + 0.01} - \left(\frac{15.7}{FC + 0.01}\right)^2\right] \tag{10.48}$$

The term $(N_1)_{60}$ is the overburden corrected blow count, defined as:

$$(N_1)_{60} = C_N(N_{60}) \tag{10.49}$$

where N_{60} is the SPT blow count measured with an energy ratio of 60%, and C_N is defined as:

$$C_N = \left(\frac{p_a}{\sigma'_v}\right)^m \leq 1.7 \tag{10.50}$$

where

$$m = 0.784 - 0.0768\sqrt{(N_1)_{60,cs}} \tag{10.51}$$

K_σ can also be estimated using CPT data as follows:

$$K_\sigma = 1 - C_\sigma \ln\left(\frac{\sigma'_v}{p_a}\right) \leq 1.0 \tag{10.52}$$

Copyright 2017 Cengage Learning. All Rights Reserved. May not be copied, scanned, or duplicated, in whole or in part. Due to electronic rights, some third party content may be suppressed from the eBook and/or eChapter(s). Editorial review has deemed that any suppressed content does not materially affect the overall learning experience. Cengage Learning reserves the right to remove additional content at any time if subsequent rights restrictions require it.

where

$$C_\sigma = \frac{1}{37.3 - 8.27(q_{c1N})^{0.264}} \leq 0.3 \tag{10.53}$$

where q_{c1N} is the normalized cone penetration resistance (Robertson and Wride, 1998):

$$q_{c1N} = \left(\frac{q_c}{p_a}\right)\left(\frac{p_a}{\sigma'_v}\right)^n \tag{10.54}$$

where q_c = the cone tip resistance (MPa)
p_a = the atmospheric pressure ($\approx$100 kPa)
σ'_v = the effective stress of the soil at the required depth (kPa)
n = the exponent that varies with soil type and is typically equal to 0.5.

Liquefaction Analysis from Standard Penetration Resistance

The cyclic resistance ratio (CRR) corrected to $M_w = 7.5$ can be expressed in terms of the overburden corrected blow count (Youd et al., 2001):

$$\text{CRR} = \frac{1}{34 - (N_1)_{60}} + \frac{(N_1)_{60}}{135} + \frac{50}{[(10)(N_1)_{60} + 45]^2} - \frac{1}{200} \tag{10.55}$$

The CRR adjusted to $M_w = 7.5$ and $\sigma'_v = 100$ kPa expressed in terms of equivalent clean-sand corrected blow count can be given as (Idriss and Boulanger, 2010):

$$\text{CRR} = \exp\left\{\frac{(N_1)_{60.cs}}{14.1} + \left[\frac{(N_1)_{60.cs}}{126}\right]^2 - \left[\frac{(N_1)_{60.cs}}{23.6}\right]^3 - \left[\frac{(N_1)_{60.cs}}{25.4}\right]^4 - 2.8\right\} \tag{10.56}$$

Figure 10.37 shows the SPT boundary curve defined by Eq. (10.56) which distinguishes the liquefied cases and non-liquefied cases.

Liquefaction Analysis from Cone Penetration Resistance

The CRR corrected for $M_w = 7.5$ can be estimated using the simplified equation proposed by Robertson and Wride (1998):

$$\text{CRR} = 93\left[\frac{(q_{c1N})_{cs}}{1000}\right]^3 + 0.08 \qquad [\text{for } 50 \leq (q_{c1N})_{cs} < 160] \tag{10.57}$$

$$\text{CRR} = 0.833\left[\frac{(q_{c1N})_{cs}}{1000}\right] + 0.05 \quad [\text{for } (q_{c1N})_{cs} < 50] \tag{10.58}$$

Copyright 2017 Cengage Learning. All Rights Reserved. May not be copied, scanned, or duplicated, in whole or in part. Due to electronic rights, some third party content may be suppressed from the eBook and/or eChapter(s). Editorial review has deemed that any suppressed content does not materially affect the overall learning experience. Cengage Learning reserves the right to remove additional content at any time if subsequent rights restrictions require it.

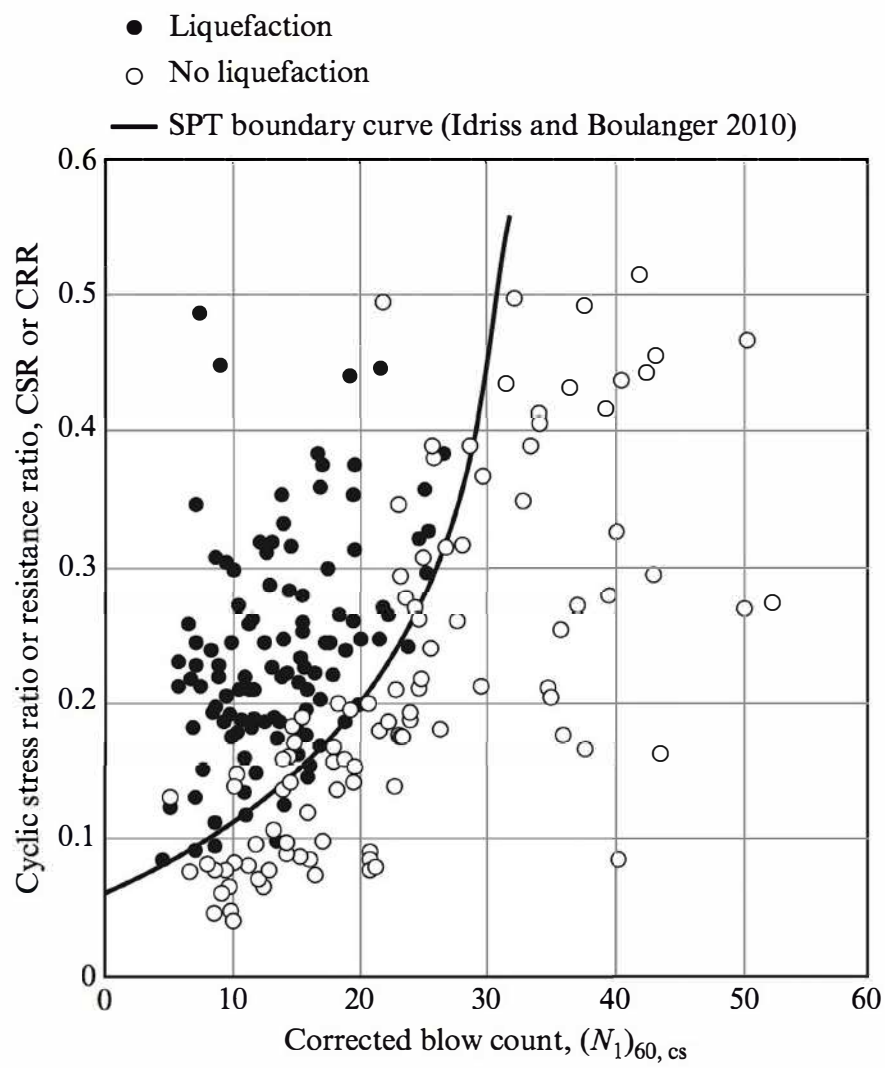

Figure 10.37 SPT clean sand boundary curve for magnitude 7.5 earthquakes with data from liquefaction case histories

where $(q_{c1N})_{cs}$ is the equivalent clean sand normalized CPT penetration resistance and can be estimated as:

$$(q_{c1N})_{cs} = K_c q_{c1N} \tag{10.59}$$

where q_{c1N} is the normalized cone penetration resistance computed with Eq. (10.54) and K_c is a correction factor which is a function of soil behavior index I_c. The soil behavior index I_c can be estimated as:

$$I_c = [(3.47 - Q)^2 + (\log_{10} F + 1.22)^2]^{0.5} \tag{10.60}$$

where $F = [f_s/(q_c - \sigma_v)](100)$ is the normalized friction ratio (%)
f_s = the CPT sleeve friction (kPa)
Q = normalized CPT penetration resistance (dimensionless) and can be computed as:

$$Q = \left(\frac{q_c - \sigma_v}{p_{a2}}\right)\left(\frac{p_a}{\sigma'_v}\right)^n \tag{10.61}$$

Copyright 2017 Cengage Learning. All Rights Reserved. May not be copied, scanned, or duplicated, in whole or in part. Due to electronic rights, some third party content may be suppressed from the eBook and/or eChapter(s). Editorial review has deemed that any suppressed content does not materially affect the overall learning experience. Cengage Learning reserves the right to remove additional content at any time if subsequent rights restrictions require it.

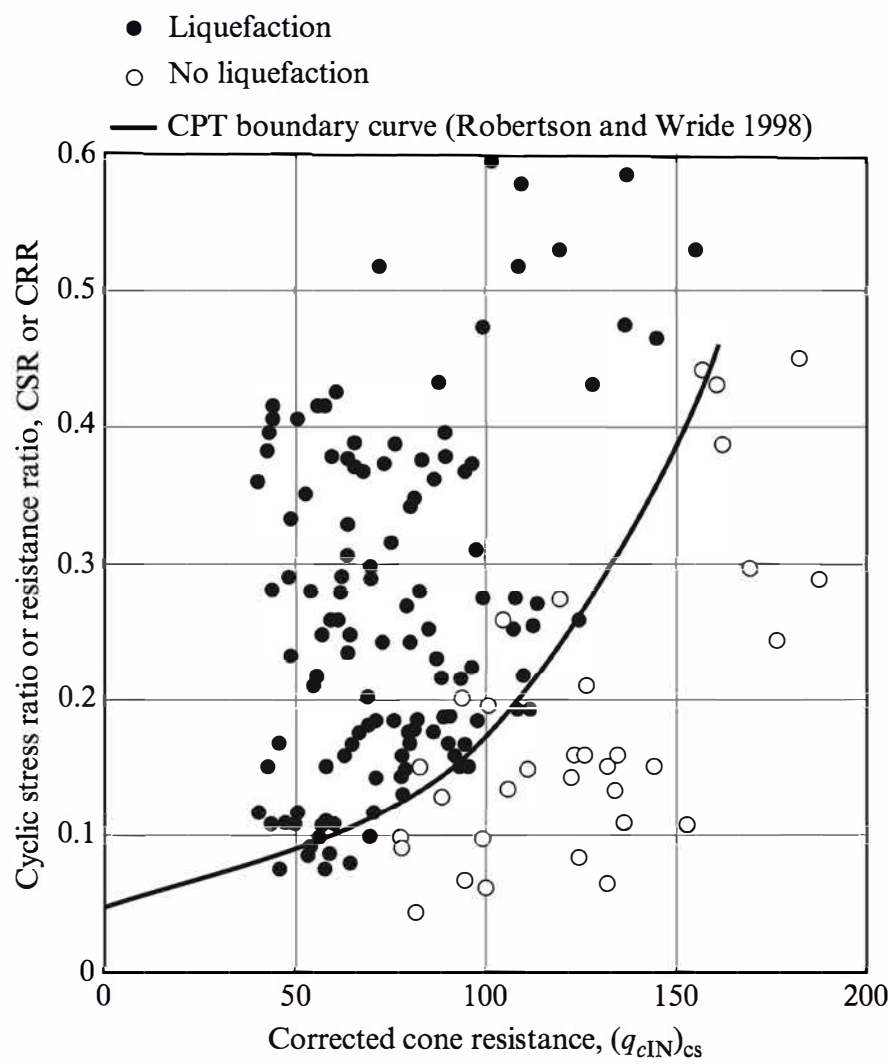

Figure 10.38 CPT clean sand boundary curve for magnitude 7.5 earthquakes with data from liquefaction case histories

where the exponent n is typically equal to 1.0; p_{a2} is a reference pressure in the same units as q_c and σ_v (i.e., $p_{a2} = 0.1$ MPa if q_c and σ_v are in MPa). Thus K_c is expressed as:

$$K_c = 1 \quad (\text{for } I_c \leq 1.64) \tag{10.62}$$

$$K_c = -0.403I_c^4 + 5.581I_c^3 - 21.63I_c^2 + 33.75I_c - 17.88 \quad (\text{for } I_c > 1.64) \tag{10.63}$$

Figure 10.38 shows the CPT boundary curve which distinguishes the liquefied cases and non-liquefied cases [defined by Eqs. (10.57) and (10.58)].

Liquefaction Analysis from Shear Wave Velocity

In the v_s-based method, the CRR corrected to an earthquake magnitude 7.5 is calculated as (Andrus and Stokoe, 2000):

$$\text{CRR} = 0.22\left[\frac{(v_{s1})_{cs}}{100}\right]^2 + 2.8\left[\frac{1}{215 - (v_{s1})_{cs}} - \frac{1}{215}\right] \tag{10.64}$$

Copyright 2017 Cengage Learning. All Rights Reserved. May not be copied, scanned, or duplicated, in whole or in part. Due to electronic rights, some third party content may be suppressed from the eBook and/or eChapter(s). Editorial review has deemed that any suppressed content does not materially affect the overall learning experience. Cengage Learning reserves the right to remove additional content at any time if subsequent rights restrictions require it.

where $(\upsilon_{s1})_{cs}$ is the clean soil equivalence of the stress-corrected shear wave velocity (m/s), which is calculated using a fines content adjustment factor K_{cs}:

$$(\upsilon_{s1})_{cs} = K_{cs}\upsilon_{s1} = K_{cs}\upsilon_s\left(\frac{p_a}{\sigma'_v}\right)^{0.25} \tag{10.65}$$

where υ_{s1} is the overburden stress-corrected shear wave velocity (m/s); υ_s is the in situ measurement of small-strain shear wave velocity (m/s) and K_{cs} is the fines content adjustment factor, estimated as follows:

$$K_{cs} = 1 \quad (\text{for } FC \leq 5\%) \tag{10.66}$$

$$K_{cs} = 1 + T(FC - 5) \quad (\text{for } 5\% < FC < 35\%) \tag{10.67}$$

$$K_{cs} = 1 + 30T \qquad (\text{for } FC \geq 35\%) \tag{10.68}$$

where $$T = 0.009 - 0.0109\left(\frac{\upsilon_{s1}}{100}\right) + 0.0038\left(\frac{\upsilon_{s1}}{100}\right)^2$$

Liquefaction Analysis from Becker penetration test

The aforementioned SPT, CPT and υ_s-based methods are more suitable for evaluating liquefaction resistance of non-gravelly soils. For gravelly soils, the Becker penetration test (BPT) through correlations with SPT is widely used for foundation design and liquefaction analysis, particularly in western North America. Typically, the BPT facility consists of a double-walled casing with 168 mm in diameter and 3 m in length driven into the ground with a double acting diesel-driven pile hammer. The Becker penetration resistance is determined to be the number of blow count needed for the casing to penetrate an increment of 300 mm. The measured BPT blow count normalized to the 30% reference energy level is (Sy and Campanella, 1994):

$$N_{b30} = N_b\left(\frac{E}{30}\right) \tag{10.69}$$

where N_b is the measured blow count, and E is the measured maximum transferred energy expressed as a percentage of the rated hammer energy of 11.0 kJ.

Very few liquefaction case histories with BPT data have been reported. Hence BPT is generally used to estimate the equivalent SPT-N values, and the liquefaction resistance is evaluated using simplified procedures based on SPT. Figure 10.39 shows the BPT-SPT correlation considering various levels of shaft resistance (R_s).

In simplified procedures, a factor of safety of 1.2–1.5 is recommended by the Building Seismic Safety Council (1997) to account for the possible uncertainties.

Copyright 2017 Cengage Learning. All Rights Reserved. May not be copied, scanned, or duplicated, in whole or in part. Due to electronic rights, some third party content may be suppressed from the eBook and/or eChapter(s). Editorial review has deemed that any suppressed content does not materially affect the overall learning experience. Cengage Learning reserves the right to remove additional content at any time if subsequent rights restrictions require it.

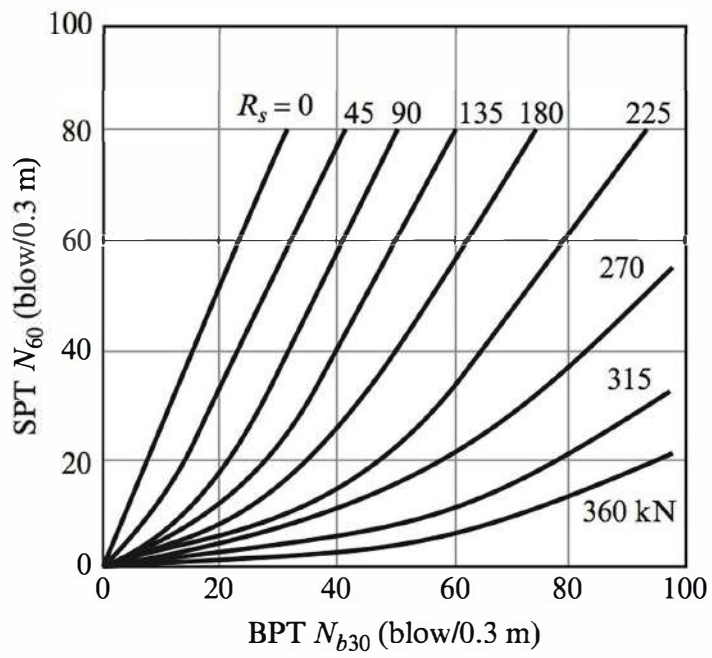

Figure 10.39 BPT-SPT correlations for different BPT resistances (R_s, in kN) (from Sy and Campanella, 1994)

Source: Sy, A., and Campanella, R. G. (1994). "Becker and Standard Penetration Tests (BPT-CPT) Correlations and Considerations of Casing Friction." *Canadian Geotechnical Journal*, Vol. 31(3), pp. 343–356. Copyright © 2008 Canadian Science Publishing or its licensors. Reproduced with permission.

EXAMPLE 10.2

Determine the factor of safety (F_s) against liquefaction for a site with the following seismic and soil parameters at the critical depth $z = 8.2$ m and ground water table depth at 1.5 m: $a_{\max} = 0.20$ g, $M_w = 7.0$, $(N_1)_{60} = 7.6$, $FC = 67\%$, $\sigma_v = 155$ kPa, $\sigma'_v = 89$ kPa.

SOLUTION:

Step 1: Determination of cyclic resistance ratio (CRR):
From Eq. (10.48),

$$\Delta(N_1)_{60} = \exp\left[1.63 + \frac{9.7}{FC + 0.01}\left(\frac{15.7}{FC + 0.01}\right)^2\right]$$

$$= \exp\left[1.63 + \frac{9.7}{67 + 0.01} - \left(\frac{15.7}{67 + 0.01}\right)^2\right] = 5.6$$

From Eq. (10.47),

$$(N_1)_{60,cs} = (N_1)_{60} + \Delta(N_1)_{60} = 7.6 + 5.6 = 13.2$$

From Eq. (10.56),

Copyright 2017 Cengage Learning. All Rights Reserved. May not be copied, scanned, or duplicated, in whole or in part. Due to electronic rights, some third party content may be suppressed from the eBook and/or eChapter(s). Editorial review has deemed that any suppressed content does not materially affect the overall learning experience. Cengage Learning reserves the right to remove additional content at any time if subsequent rights restrictions require it.

$$\text{CRR} = \exp\left\{\frac{(N_1)_{60,cs}}{14.1} + \left[\frac{(N_1)_{60,cs}}{126}\right]^2 - \left[\frac{(N_1)_{60,cs}}{23.6}\right]^3 - \left[\frac{(N_1)_{60,cs}}{25.4}\right]^4 - 2.8\right\}$$

$$= \exp\left[\frac{13.2}{14.1} + \left(\frac{13.2}{126}\right)^2 - \left(\frac{13.2}{23.6}\right)^3 - \left(\frac{13.2}{25.4}\right)^4 - 2.8\right] = 0.142$$

Step 2: Determination of cyclic stress ratio (CSR):

From Eq. (10.39),

$$\text{CSR} = \frac{0.65\left(\frac{a_{\max}}{g}\right)\left(\frac{\sigma_v}{\sigma'_v}\right)\gamma_d}{(MSF)(K_\sigma)}$$

Stress reduction factor [Eqs. (10.40), (10.41), and (10.42)]:

$$\alpha = -1.012 - 1.126\sin\left(5.133 + \frac{z}{11.73}\right)$$

$$= -1.012 - 1.126\sin\left(5.133 + \frac{8.2}{11.73}\right) = -0.5249$$

$$\beta = 0.106 + 0.118\sin\left(5.142 + \frac{z}{11.28}\right)$$

$$= 0.106 + 0.118\sin\left(5.142 + \frac{8.2}{11.28}\right) = 0.0589$$

$$\gamma_d = \exp(\alpha + \beta M_w) = \exp[-0.5249 + (0.0589)(7.0)] = 0.89$$

Magnitude scaling factor [Eq. (10.44)]:

$$MSF = -0.058 + 6.9\exp(-0.25M_w) = -0.058 + 6.9\exp[(0.25)(-7)] = 1.14 \le 1.8$$

Overburden correction factor for CSR [Eq. (10.46)]:

$$C_\sigma = \frac{1}{18.9 - 2.55\sqrt{(N_1)_{60,cs}}} \le 0.3 = \frac{1}{18.9 - 2.55\sqrt{13.2}} = 0.1 \le 0.3$$

From Eq. (10.45),

$$K_\sigma = 1 - C_\sigma \ln\left(\frac{\sigma'_v}{p_a}\right) \le 1.0 = 1 - (0.1)\ln\left(\frac{89}{100}\right) = 1.01 \le 1.1$$

From Eq. (10.39),

$$\text{CSR} = \frac{0.65\left(\frac{a_{\max}}{g}\right)\left(\frac{\sigma_v}{\sigma'_v}\right)\gamma_d}{(MSF)(K_\sigma)} = \frac{(0.65)(0.20)\left(\frac{155}{89}\right)(0.89)}{(1.14)(1.01)} = 0.175$$

Copyright 2017 Cengage Learning. All Rights Reserved. May not be copied, scanned, or duplicated, in whole or in part. Due to electronic rights, some third party content may be suppressed from the eBook and/or eChapter(s). Editorial review has deemed that any suppressed content does not materially affect the overall learning experience. Cengage Learning reserves the right to remove additional content at any time if subsequent rights restrictions require it.

Step 3: Determination of factor of safety (F_S):

$$F_s = \frac{CRR}{CSR} = \frac{0.142}{0.175} = \mathbf{0.81}$$

EXAMPLE 10.3

Determine the factor of safety (F_s) against liquefaction for a site with the following seismic and soil parameters at depth $z = 4.6$ m and ground water table depth at 2.7 m: $a_{\max} = 0.25$ g, $M_w = 7.6$, $\sigma_v = 81.2$ kPa, $\sigma'_v = 62.6$ kPa, $q_c = 8.5$ MPa, $I_c = 1.93$.

SOLUTION:

Step 1: Determination of cyclic resistance ratio (CRR):

From Eq. (10.54),

$$q_{c1N} = \left(\frac{q_c}{p_a}\right)\left(\frac{p_a}{\sigma'_v}\right)^n = \left(\frac{8500}{100}\right)\left(\frac{100}{62.6}\right)^{0.5} = 107.43$$

From Eq. (10.63),

$$K_c = -0.403I_c^4 + 5.581I_c^3 - 21.63I_c^2 + 33.75I_c - 17.88$$
$$= -0.403(1.93)^4 + 5.581(1.93)^3 - 21.63(1.93)^2 + 33.75(1.93) - 17.88 = 1.22$$

From Eq. (10.59),

$$(q_{c1N})_{cs} = (1.22)(107.43) = 131.06$$

From Eq. (10.57), for $50 \le (q_{c1N})_{cs} < 160$,

$$\text{CRR} = 93\left[\frac{(q_{c1N})_{cs}}{1000}\right]^3 + 0.08 = 93\left(\frac{131.06}{1000}\right)^3 + 0.8 = 0.289$$

Step 2: Determination of cyclic stress ratio (CSR):

From Eq. (10.39),

$$\text{CSR} = \frac{0.65\left(\frac{a_{\max}}{g}\right)\left(\frac{\sigma_v}{\sigma'_v}\right)\gamma_d}{(MSF)(K_\sigma)}$$

Stress reduction factor [Eqs. (10.40), (10.41), and (10.42)]:

$$\alpha = -1.012 - 1.126\sin\left(5.133 + \frac{z}{11.73}\right)$$
$$= -1.012 - 1.126\sin\left(5.133 + \frac{4.6}{11.73}\right) = -0.2379$$

Copyright 2017 Cengage Learning. All Rights Reserved. May not be copied, scanned, or duplicated, in whole or in part. Due to electronic rights, some third party content may be suppressed from the eBook and/or eChapter(s). Editorial review has deemed that any suppressed content does not materially affect the overall learning experience. Cengage Learning reserves the right to remove additional content at any time if subsequent rights restrictions require it.

$$\beta = 0.106 + 0.118\sin\left(5.142 + \frac{z}{11.28}\right)$$
$$= 0.106 + 0.118\sin\left(5.142 + \frac{4.6}{11.28}\right) = 0.0270$$

$$\gamma_d = \exp(\alpha + \beta M_w) = \exp[-0.2379 + (0.0270)(7.6)] = 0.97$$

Magnitude scaling factor [Eq. (10.44)]:

$$MSF = -0.058 + 6.9\exp(-0.25M_w) = -0.058 + 6.9\exp[-(0.25)(7.6)] = 0.97 \leq 1.8$$

Overburden correction factor for CSR [Eq. (10.53)]:

$$C_\sigma = \frac{1}{3.73 - 8.27(q_{c1N})^{0.264}} \leq 0.3 = \frac{1}{3.73 - 8.27(107.43)^{0.264}} = 0.11 \leq 0.3$$

From Eq. (10.52),

$$K_\sigma = 1 - C_\sigma \ln\left(\frac{\sigma'_v}{p_a}\right) \leq 1.0 = 1 - (0.11)\ln\left(\frac{62.6}{100}\right) = 1.05 \leq 1.0$$

From Eq. (10.39),

$$\text{CSR} = \frac{0.65\left(\frac{a_{\max}}{g}\right)\left(\frac{\sigma_v}{\sigma'_v}\right)\gamma_d}{(MSF)(K_\sigma)} = \frac{(0.65)(0.25)\left(\frac{81.2}{62.6}\right)(0.97)}{(0.97)(1)} = 0.211$$

Step 3: Determination of factor of safety (F_S):

$$F_s = \frac{CRR}{CSR} = \frac{0.289}{0.211} = \mathbf{1.37}$$

10.19 REMEDIAL ACTION TO MITIGATE LIQUEFACTION

In order to ensure the functionality and safety of engineering projects that are likely to be subjected to damage due to possible liquefaction of the subsoil, several actions can be taken:

1. Removal or replacement of undesirable soil. If liquefaction of a soil layer under a structure is a possibility, then it may be excavated and recompacted with or without additives. Otherwise the potentially liquefiable soil may be replaced with nonliquefiable soil.
2. Densification of the in situ material. This can be achieved by using several techniques such as vibroflotation, dynamic compaction, and compaction piles.

Copyright 2017 Cengage Learning. All Rights Reserved. May not be copied, scanned, or duplicated, in whole or in part. Due to electronic rights, some third party content may be suppressed from the eBook and/or eChapter(s). Editorial review has deemed that any suppressed content does not materially affect the overall learning experience. Cengage Learning reserves the right to remove additional content at any time if subsequent rights restrictions require it.

3. In situ soil improvement by grouting and chemical stabilization.
4. Use of relief wells such as gravel or rock drains for the control of undesirable pore water pressure. Figure 10.40 is a schematic diagram of gravel or rock drains. The purpose of the installation of gravel or rock drains is to dissipate the excess pore water pressure almost as fast as it is generated in the

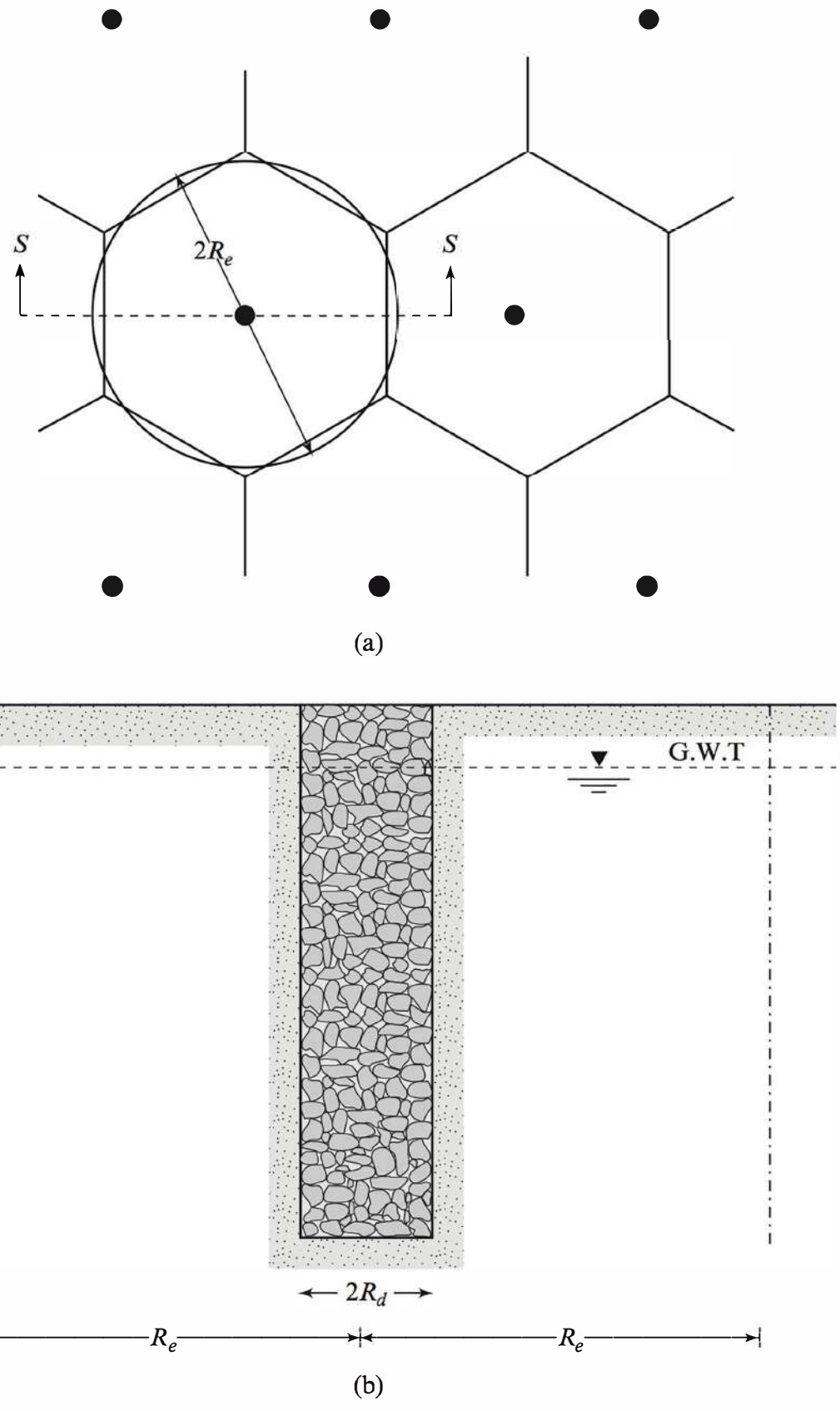

Figure 10.40 Gravel drains: (a) plan; (b) section at $S-S$

Copyright 2017 Cengage Learning. All Rights Reserved. May not be copied, scanned, or duplicated, in whole or in part. Due to electronic rights, some third party content may be suppressed from the eBook and/or eChapter(s). Editorial review has deemed that any suppressed content does not materially affect the overall learning experience. Cengage Learning reserves the right to remove additional content at any time if subsequent rights restrictions require it.

same deposit due to cyclic loading. The design principles of gravel and rock drains have been developed by Seed and Booker (1977) and are described here. Assuming that Darcy's law is valid, the continuity of flow equation in the sand layer may be written as

$$\frac{\partial}{\partial x}\left(\frac{k_h}{\gamma_w}\frac{\partial u}{\partial x}\right)+\frac{\partial}{\partial y}\left(\frac{k_h}{\gamma_w}\frac{\partial u}{\partial y}\right)+\frac{\partial}{\partial z}\left(\frac{k_v}{\gamma_w}\frac{\partial u}{\partial z}\right)=\frac{\partial \varepsilon}{\partial t} \tag{10.70}$$

where k_h = coefficient of permeability of the sand in the horizontal direction
k_v = coefficient of permeability of the sand in the vertical direction
u = excess pore water pressure
γ_w = unit weight of water
ε = volumetric strain (compression positive)

During a time interval dt, the pore water pressure in a soil element changes by du. However, if a cyclic shear stress is applied on a soil element, there is an increase of pore water pressure. In a time dt, there are dN number of cyclic shear stresses; the corresponding increase of pore water pressure is $(\partial u_g/\partial N)dN$ (where u_g is the excess pore water pressure generated by cyclic shear stress—see also Section 10.10). Thus, the net change in pore water pressure in time dt is equal to $[du-(\partial u_g/\partial N)dN]$, and

$$\partial \varepsilon = m_{v_3}[\partial u-(\partial u_g/\partial N)dN]$$

or

$$\frac{\partial \varepsilon}{\partial t}=m_{v_3}\left(\frac{\partial u}{\partial t}-\frac{\partial u_g}{\partial N}\frac{\partial N}{\partial t}\right) \tag{10.71}$$

where m_{v_3} = coefficient of volume compressibility.

Combining Eqs. (10.70) and (10.71),

$$\frac{\partial}{\partial x}\left(\frac{k_h}{\gamma_w}\frac{\partial u}{\partial x}\right)+\frac{\partial}{\partial y}\left(\frac{k_h}{\gamma_w}\frac{\partial u}{\partial y}\right)\frac{\partial}{\partial z}\left(\frac{k_v}{\gamma_w}\frac{\partial u}{\partial z}\right)=m_{v_3}\left(\frac{\partial u}{\partial t}-\frac{\partial u_g}{\partial N}\frac{\partial N}{\partial t}\right) \tag{10.72}$$

If m_{v_3} is a constant and radial symmetry exists, then Eq. (10.72) can be written in cylindrical coordinates as

$$\frac{k_h}{\gamma_w m_{v_3}}\left(\frac{\partial^2 u}{\partial^2 r}+\frac{1}{r}\frac{\partial u}{\partial r}\right)+\frac{k_v}{\gamma_w m_{v_3}}\frac{\partial^2 u}{\partial z^2}=\frac{\partial u}{\partial t}-\frac{\partial u_g}{\partial N}\frac{\partial N}{\partial t} \tag{10.73}$$

Copyright 2017 Cengage Learning. All Rights Reserved. May not be copied, scanned, or duplicated, in whole or in part. Due to electronic rights, some third party content may be suppressed from the eBook and/or eChapter(s). Editorial review has deemed that any suppressed content does not materially affect the overall learning experience. Cengage Learning reserves the right to remove additional content at any time if subsequent rights restrictions require it.

For the condition of purely radial flow, Eq. (10.73) takes the form

$$\frac{k_h}{\gamma_w m_{v_3}}\left(\frac{\partial^2 u}{\partial^2 r}+\frac{1}{r}\frac{\partial u}{\partial r}\right)=\frac{\partial u}{\partial t}-\frac{\partial u_g}{\partial N}\frac{\partial N}{\partial t} \tag{10.74}$$

In order to solve Eq. (10.74), it is necessary to evaluate the terms k_h, m_{v_3}, $\partial N/\partial t$, and $\partial u_g/\partial N$. The value of k_h can be easily determined from field pumping tests. The coefficient of volume compressibility can be determined from cyclic triaxial tests (Lee and Albaisa, 1974). The term $\partial N/\partial t$ can be expressed as

$$\frac{\partial N}{\partial t}=\frac{N_s}{t_d} \tag{10.75}$$

where N_s = significant number of uniform stress cycles due to an earthquake
t_d = duration of an earthquake.

The rate of excess pore water pressure build up, $\partial u_g/\partial N$, in a saturated undrained cyclic simple shear test is given by Eq. (10.4) (Section 10.10). For radial flow conditions, the relation given by Eq. (10.74) has been solved by Seed and Booker (1977). It has been shown that the ratio u/σ_v is a function of the following parameters:

$$\frac{R_d}{R_e}=\frac{\text{radius of rock or gravel drains}}{\text{effective radius of the rock or gravel drains}} \tag{10.76}$$

N_s/N_i, and

$$\boxed{T_{ad}=\frac{k_h}{\gamma_w}\left(\frac{t_d}{m_{v_3}R_d^2}\right)} \tag{10.77}$$

Using these parameters, the solution to Eq. (10.74) is given in a nondimensional form in Figure 10.41 for design of rock or gravel drains. In Figure 10.41, the term r_g is defined as

$$r_g=\frac{\text{greatest limiting value of } u_g \text{ chosen for design}}{\sigma_v} \tag{10.78}$$

In obtaining the solutions given in Figure 10.41, it was assumed that the coefficient of permeability of the material used in the gravel or rock drains is infinity. However, in practical cases, it would be sufficient to have a value of

$$\frac{k_{h(\text{rock or gravel})}}{k_{(\text{sand})}}\approx 200$$

Copyright 2017 Cengage Learning. All Rights Reserved. May not be copied, scanned, or duplicated, in whole or in part. Due to electronic rights, some third party content may be suppressed from the eBook and/or eChapter(s). Editorial review has deemed that any suppressed content does not materially affect the overall learning experience. Cengage Learning reserves the right to remove additional content at any time if subsequent rights restrictions require it.

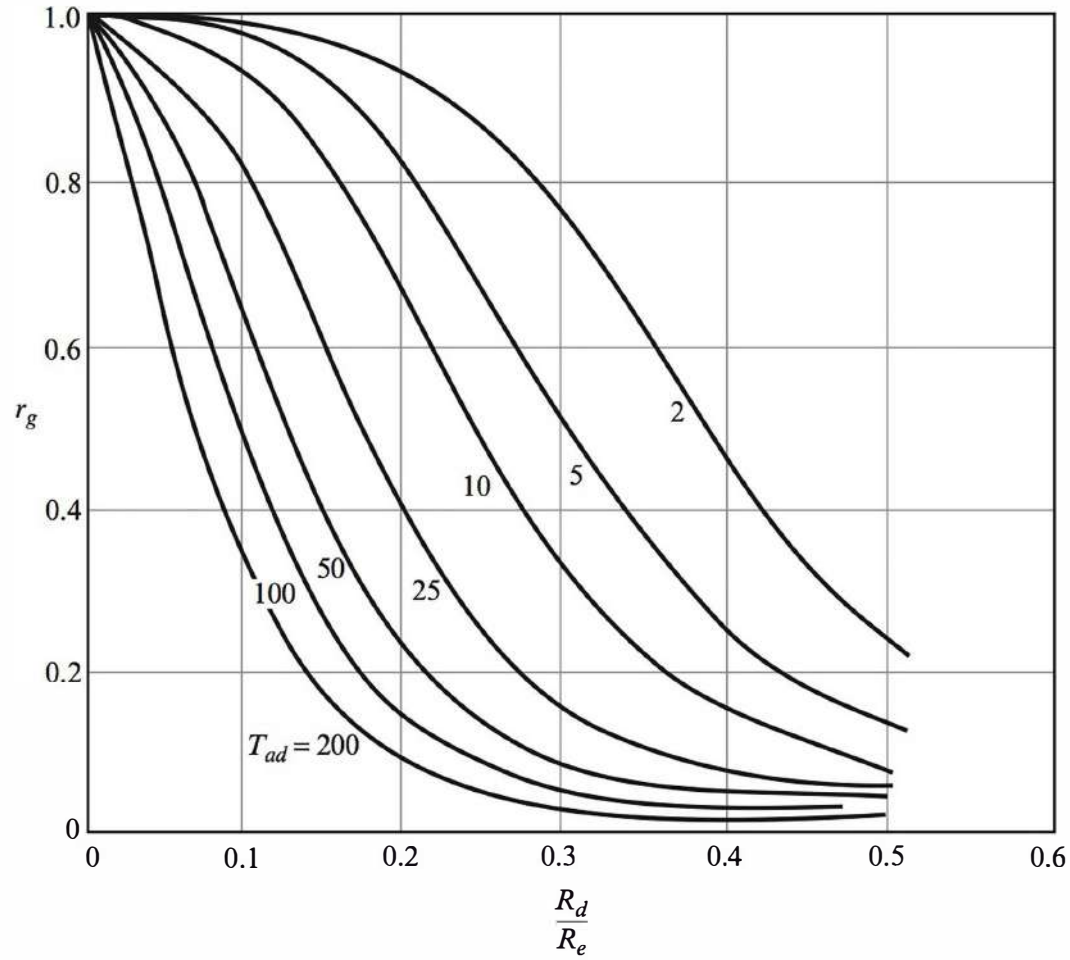

(a)

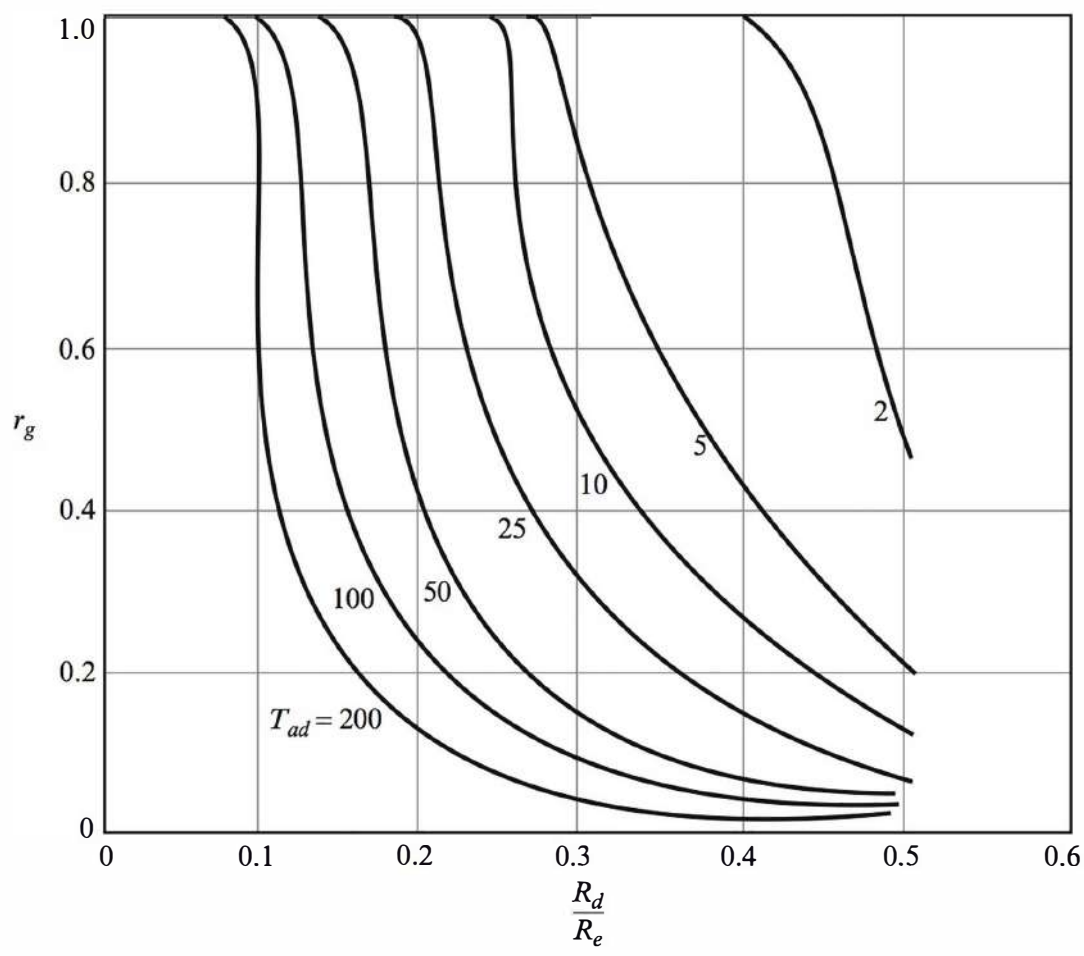

(b)

Figure 10.41 Relation between greatest pore water pressure ratio and drain system parameters: (a) $N_s/N_i = 1$; (b) $N_s/N_i = 2$; (c) $N_s/N_i = 3$; (d) $N_s/N_i = 4$ (from Seed and Booker, 1977)

Source: Seed, H. B., and Booker, J. R. (1977). "Stabilization of Potentially Liquefiable Sand Deposits," *Journal of the Geotechnical Engineering Division*, ASCE, Vo. 103, No. GT7, pp. 757–768. With permission from ASCE.

Copyright 2017 Cengage Learning. All Rights Reserved. May not be copied, scanned, or duplicated, in whole or in part. Due to electronic rights, some third party content may be suppressed from the eBook and/or eChapter(s). Editorial review has deemed that any suppressed content does not materially affect the overall learning experience. Cengage Learning reserves the right to remove additional content at any time if subsequent rights restrictions require it.

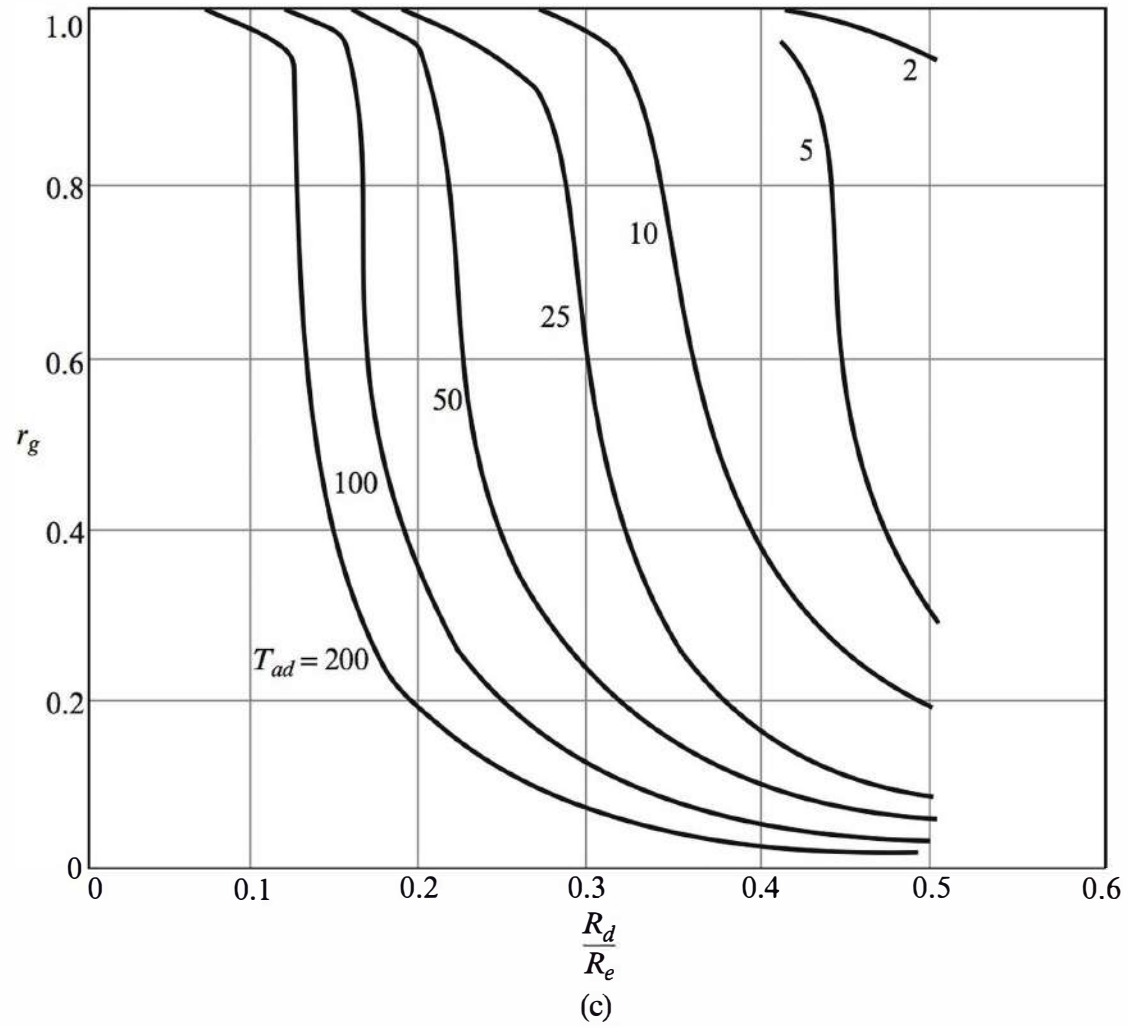

(c)

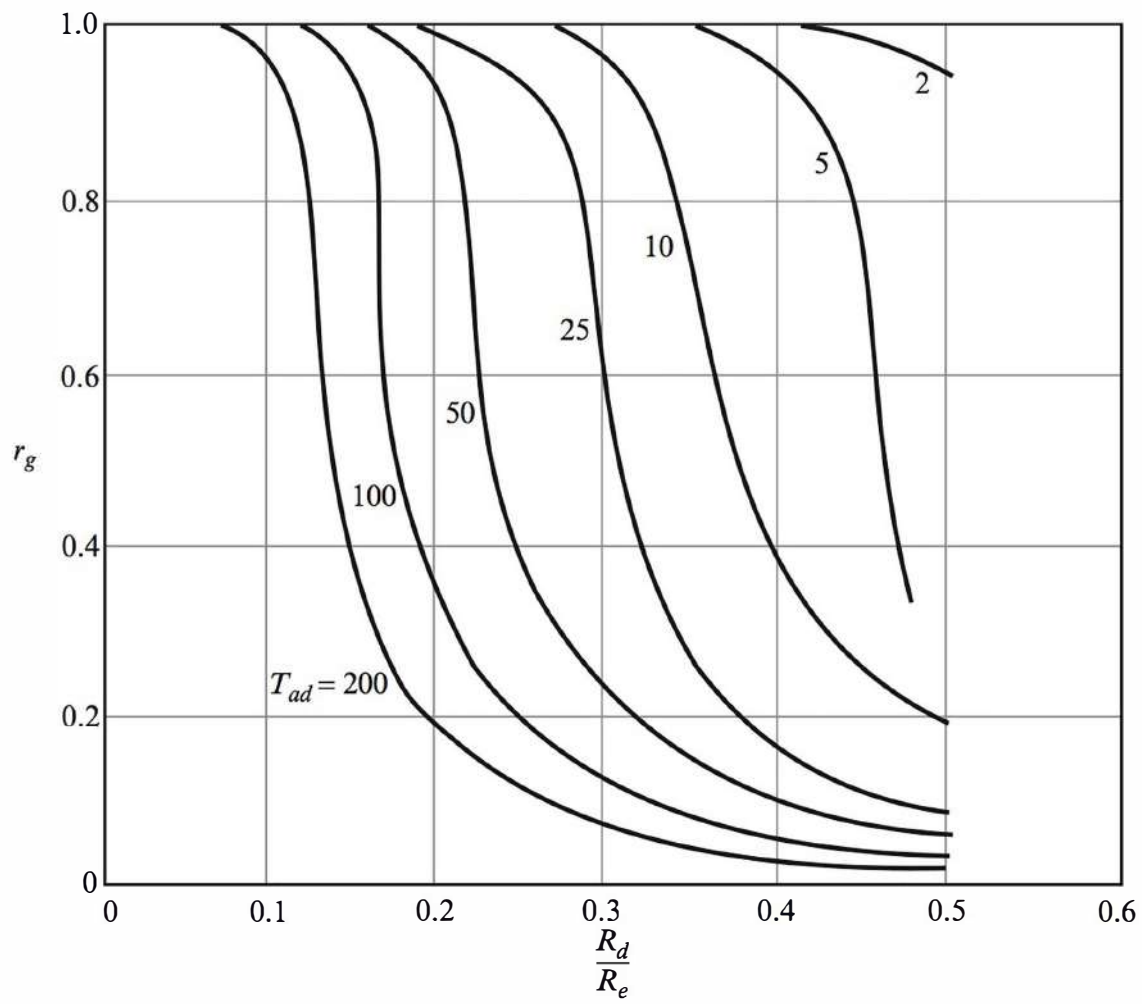

(d)

Figure 10.41 (*Continued*)

Copyright 2017 Cengage Learning. All Rights Reserved. May not be copied, scanned, or duplicated, in whole or in part. Due to electronic rights, some third party content may be suppressed from the eBook and/or eChapter(s). Editorial review has deemed that any suppressed content does not materially affect the overall learning experience. Cengage Learning reserves the right to remove additional content at any time if subsequent rights restrictions require it.

EXAMPLE 10.4

For a sand deposit, it is given that

$$m_{v_3} = 2.8 \times 10^{-5} \text{m}^2/\text{kN}$$
$$k_h = 0.02 \text{ mm/s} = 2 \times 10^{-5} \text{ m/s}$$

For a design earthquake, the equivalent number of uniform stress cycles (for uniform stress $= \tau_{av}$) was determined to be 30. The duration of the earthquake is about 65 s.

From laboratory tests, it was determined that 12 cycles of cyclic stress application (the peak magnitude of the cyclic stress is equal to τ_{av}) would be enough to cause initial liquefaction in the sand.

Assuming that the radius of the gravel drains to be used is 0.25 m, and $r_g = 0.6$, determine the spacing of gravel drains.

SOLUTION:

From Eq. (10.77),

$$T_{ad} = \frac{k_h}{\gamma_w}\left(\frac{t_d}{m_{v_3} R_d^2}\right) = \frac{2 \times 10^{-5}}{9.81}\left[\frac{65}{2.8 \times 10^{-5}(0.25)^2}\right] = 75.72$$

$$\frac{N_s}{N_i} = 30/12 = 2.5, \qquad r_g = 0.6$$

Referring to Figure 10.41b, for $T_{ad} = 75.72$, $N_s/N_i = 2$, $r_g = 0.6$,

$$\frac{R_d}{R_e} \approx 0.17$$

From Figure 10.41c, for $T_{ad} = 75.72$, $N_s/N_1 = 3$, $r_g = 0.6$,

$$\frac{R_d}{R_e} \approx 0.2$$

Thus, for $N_s/N_i = 2.5$, $R_d/R_e \approx \frac{1}{2}(0.17 + 0.2) = 0.185$. Hence,

$$R_e = \frac{R_d}{0.185} = \frac{0.25}{0.185} = \mathbf{1.35\ m}$$

PROBLEMS

10.1 Explain the terms *initial liquefaction* and *cyclic mobility*.

10.2 For a sand deposit the following is given:

Copyright 2017 Cengage Learning. All Rights Reserved. May not be copied, scanned, or duplicated, in whole or in part. Due to electronic rights, some third party content may be suppressed from the eBook and/or eChapter(s). Editorial review has deemed that any suppressed content does not materially affect the overall learning experience. Cengage Learning reserves the right to remove additional content at any time if subsequent rights restrictions require it.

Median grain size (D_{50}) = 0.2 mm

Depth of water table = 3 m

Unit weight of soil above GWT = 17 kN/m^3

Unit weight of soil below GWT = 19.5 kN/m^3

Expected earthquake magnitude = 7.5

Make all calculations and prepare a graph showing the variation of a_{max}/g and the relative density in the field for liquefaction to occur.

10.3 Repeat Problem 10.2 for a median grain size of 0.075 mm.

10.4 Repeat Problem 10.2 for the following conditions:

Mean grain size (D_{50}) = 0.075 mm

Depth of water table = 4.6 m

Unit weight of soil above GWT = 15 kN/m^3

Unit weight of soil below GWT = 18 kN/m^3

Expected earthquake magnitude = 8

10.5 Repeat Problem 10.4 for a mean grain size of 0.2 mm.

10.6 Consider the soil and the groundwater table conditions given in Problem 10.2. Assume that the relative density in the field is 60%. The maximum expected intensity of ground shaking (a_{max}/g) is 0.2 and the magnitude of earthquake is 7.5.

a. Calculate and plot the variation of the shear stress τ_{av} induced in the sand deposit with depth 0–21 m. Use Eq. (10.26).

b. Calculate the variation of the shear stress required to cause liquefaction with depth. Plot the shear stress determined in the same graph as used in (a). Use Eq. (10.23).

c. From the plotted graph, determine the depth at which liquefaction is initiated.

10.7 Repeat Problem 10.6(a)–(c) for the data given in Problem 10.4. Assume the relative density of the sand to be 60% and the maximum expected intensity of ground shaking to be 0.15g.

10.8 The standard penetration test results (N_{60}) of a sand deposit at a certain site are given below in tabular form. The groundwater table in located at a depth of 2 m below the ground surface. The dry and saturated unit weights of sand are 17 kN/m^3 and 19.0 kN/m^3, respectively. For an expected earthquake magnitude $M = 6$ and maximum acceleration $a_{max} = 0.1\,g$, will liquefaction occur?

Copyright 2017 Cengage Learning. All Rights Reserved. May not be copied, scanned, or duplicated, in whole or in part. Due to electronic rights, some third party content may be suppressed from the eBook and/or eChapter(s). Editorial review has deemed that any suppressed content does not materially affect the overall learning experience. Cengage Learning reserves the right to remove additional content at any time if subsequent rights restrictions require it.

Depth (m)	N_{60} (blows/30 cm)
1.5	8
3.0	7
4.5	12
6.0	15
7.5	17
9.0	17

10.9 In a sand deposit, the groundwater table is located at a depth of 2 m measured from the ground surface. Following are the shear wave velocities in the sand deposit.

Depth (m)	Shear wave velocity, v_s (m/s)
2 – 4	450
4 – 6	600
6 – 10	675

For a maximum ground acceleration $a_{max} = 0.16\ g$, determine whether liquefaction is likely to occur.

10.10 Determine the factor of safety (F_s) against liquefaction for a site with the following seismic and soil parameters at the critical depth $z = 2.8$ m and ground water table depth at 0.5 m: $a_{max} = 0.12$ g, $M_w = 6.5$, $(N_1)_{60} = 6.9$, $FC = 5\%$, $\sigma_v = 53$ kPa, and $\sigma'_v = 30$ kPa.

10.11 Determine the factor of safety (F_s) against liquefaction for a site with the following seismic and soil parameters at depth $z = 5.5$ m and ground water table depth at 2.0 m: $a_{max} = 0.18$ g, $M_w = 6.5$, $\sigma_v = 102.0$ kPa, $\sigma'_v = 67.7$ kPa , $q_c = 2.5$ MPa, and $I_c = 2.10$.

10.12 Solve the gravel drain problem given Example 10.4 for $r_g = 0.7$.

10.13 Repeat Example 10.4 of the gravel drain with the following data:

$$m_{v_3} = 3.5 \times 10^{-5}\ \text{m}^2/\text{kN}$$

$$k_h = 1.4 \times 10^{-5}\ \text{m/s}$$

Equivalent number of uniform stress cycles due to earthquakes = 20

Duration of earthquake = 50 s

Number of uniform stress cycles for liquefaction = 12

Radius of gravel drains = 0.3 m

$r_g = 0.7$

Copyright 2017 Cengage Learning. All Rights Reserved. May not be copied, scanned, or duplicated, in whole or in part. Due to electronic rights, some third party content may be suppressed from the eBook and/or eChapter(s). Editorial review has deemed that any suppressed content does not materially affect the overall learning experience. Cengage Learning reserves the right to remove additional content at any time if subsequent rights restrictions require it.

References

Andrus, R.D. and Stokoe, K.H. (2000). "Liquefaction Resistance of Soils from Shear Wave Velocity." *Journal of Geotechnical and Geoenvironmental Engineering*, ASCE, Vol. 126, No. 11, pp. 1015–1025.

Bieganousky, W. A., and Marcuson, W. F., III (1977). "Liquefaction Potential of Dams and Foundations, Report 2. Laboratory Standard Penetration Test on Platte River Sand and Standard Concrete Sand," *WES Report No. 76-2*, US Army Waterways Experiment Station, Vicksburg, Mississippi.

Building Seismic Safety Council (1997) *NEHRP Recommended Provisions For Seismic Regulations for New Buildings and Other Structures, Part 2: Commentary*, Foundation Design Requirements, Washington, D.C.

Casagrande, A. (1936). Characteristics of Cohesionless Soils Affecting the Stability of Slopes and Earthfills," *Journal of the Boston Society of Civil Engineers*, January, Vol. 23 pp. 257–276.

Castro, G. (1969). "Liquefaction of Sands," *Harvard Soil Mechanics Series No. 81*, Cambridge, Massachusetts.

Castro, G. (1975). "Liquefaction and Cyclic Mobility of Saturated Sands," *Journal of the Geotechnical Engineering Division,* ASCE, Vol. 101, No. GT6, pp. 551–569.

Commission on Engineering and Technical Systems—Committee on Earthquake Engineering (1985). "Liquefaction of Soils During Earthquakes," National Academy Press, Washington, D.C.

DeAlba, P., Chan, C. K., and Seed, H. B. (1975), "Determination of Soil Liquefaction Characteristics by Large Scale Laboratory Tests," *Report No. EERC 75-14*, Earthquake Engineering Research Center, University of California, Berkeley, California.

DeAlba, P., Seed, H. B., and Chan, C. K. (1976). "Sand Liquefaction in Large-Scale Simple Shear Tests," *Journal of Geotechnical Engineering Division*, ASCE, Vol. 102, NO. GT9, pp. 909–927.

Dobry, R., Stokoe, K. H., Land R. S., and Youd, T. L. (1981). "Liquefaction for S-wave Velocity," *Preprint 81-544*, ASCE National Convention, St. Louis, Missouri.

Emery, J. J., Finn, W. D. L., and Lee, K. W. (1972). "Uniformity of Saturated Sand Samples," *Soil Mechanics Series,* University of British Columbia, Vancouver, British Columbia, Canada.

Finn, W. D. L. (1972). "Soil Dynamic—Liquefaction of Sands," *Proceedings*, International Conference on Microzonation for Safer Construction Research and Application, Seattle, Washington, Vol. 1.

Finn, W. D. L., Bransby, P. L., and Pickering D. J. (1970). "Effect of Strain History on Liquefaction of Sands," *Journal of the Soil Mechanics and Foundations Division*, ASCE, Vol. 96. No. SM6, pp. 1917–1934.

Finn, W. D. L., Emery, J. J., and Gupta, Y. P. (1970). "A Shaking Table Study of the Liquefaction of Saturated Sands during Earthquake Engineering," *Proceedings*, 3rd European Symposium on Earthquake Engineering, Sofia, Bulgaria.

Finn, W. D. L., Emery. J. J., and Gupta, Y. P. (1971). "Soil Liquefaction Studies Using a Shaking Table," *Closed Loop Magazine*, Fall/Winter, MTS Systems Corporation, Minneapolis, Minnesota.

Finn, W. D. L., Pickering, D. J., and Bransby, P. L. (1971). "Sand Liquefaction in Triaxial and Simple Shear Tests," *Journal of the Soil Mechanics and Foundations Division*, ASCE, Vol. 97, No. SM4, pp. 639–659.

Idriss, I.M. and Boulanger, R.W. (2010). *SPT-based Liquefaction Triggering Procedures*, Report No. UCD/CGM-10/02, Center for Geotechnical Modeling, Department of Civil and Environmental Engineering, University of California at Davis.

Ishibashi, I., and Sherif, M. A. (1974), "Soil Liquefaction by Torsional Simple Shear Device," *Journal of the Geotechnical Engineering Division*, ASCE, Vol. 100, No. GT8, pp. 871–888.

Ishihara, K. (1985). "Stability of Natural Deposits During Earthquakes," *Proceedings*, 11th International Conference on Soil Mechanics and Foundation Engineering, Vol. 1, pp. 321–376, San Francisco, California.

Copyright 2017 Cengage Learning. All Rights Reserved. May not be copied, scanned, or duplicated, in whole or in part. Due to electronic rights, some third party content may be suppressed from the eBook and/or eChapter(s). Editorial review has deemed that any suppressed content does not materially affect the overall learning experience. Cengage Learning reserves the right to remove additional content at any time if subsequent rights restrictions require it.

Jaky, J. (1944). "The Coefficient of Earth Pressure at Rest," *Journal of the Society of the Hungarian Architectural Engineers*, Vol. 21, pp. 355–358.

Kishida, H. (1966), "Damage to Reinforced Concrete Buildings in Niigata City with Special Reference to Foundation Engineering," *Soils and Foundations*, Tokyo, Japan, Vol. 7, No. 1, pp. 75–92.

Kuizumi, Y. (1966). "Changes in Density of Sand Subsoil Caused by the Niigata Earthquake," *Soils and Foundations*, Tokyo, Japan, Vol. 8, No. 2, pp. 38–44.

Lee, K. L., and Albaisa, A. (1974). "Earthquake Induced Settlements in Saturated Sands," *Journal of the Geotechnical Engineering Division*, ASCE, Vol. 100, No. GT4, pp. 387–404.

Lee, K. L., and Seed, H. B. (1967). "Cyclic Stress Conditions Causing Liquefaction of Sand," *Journal of the Soil Mechanics and Foundations Division*, ASCE, Vol. 93, No. SM1, pp. 47–70.

Liao, S. and Whitman, R. V. (1986). "Overburden Correction Factors for SPT in Sand," *Journal of Geotechnical Engineering*, ASCE, Vol. 112, No. GT3, pp. 373–377.

OHara, S. (1972). "The Results of Experiment on the Liquefaction of Saturated Sands with a Shaking Box: Comparison with Other Methods," *Technology Report of the Yamaguchi University*, Vol. 1, No. 1, Yamaguchi, Japan.

Ohasaki, Y. (1966). "Niigata Earthquake 1964, Building Damage and Soil Conditions," *Soils and Foundations*, Tokyo, Japan, Vol. 6, No.2, pp. 14–37.

Ortigosa, P. (1972). "Licuacion de Arenas Sometidas a Vibraciones Horizontales," *Revista del Instituto de Investigaciones de Ensoyes de Materials*, Vol. II, No. 3.

Peacock, W.H., and Seed, H. B. (1968), "Sand Liquefaction Under Cyclic Loading Simple Shear Conditions," *Journal of the Soil Mechanics and Foundations Division*, ASCE, Vol. 94, No. SM3, pp. 689–708.

Prakash, S., and Mathur, J. N. (1965). "Liquefaction of Fine Sand Under Dynamic Loading," *Proceedings*, 5th Symposium of the Civil and Hydraulic Engineering Departments, Indian Institute of Science, Bangalore, India.

Robertson, P.K., and Wride, C.E. (1998). "Evaluating Cyclic Liquefaction Potential Using the Cone Penetration Test." *Canadian Geotechnical Journal*, Vol. 35, No. 3, pp. 442–459.

Seed, H. B. (1979). "Soil Liquefaction and Cyclic Mobility Evaluation for Level Ground During Earthquakes," *Journal of the Geotechnical Engineering Division*, ASCE, Vol. 105, No. GT2, pp. 201–255.

Seed, H. B., and Booker, J. R. (1977). "Stabilization of Potential Liquefiable Sand Deposits Using Gravel Drains," *Journal of the Geotechnical Engineering Division*, ASCE, Vo. 103, No. GT7, pp. 757–768.

Seed, H. B. and Idriss, I. M. (1971). "Simplified Procedure for Evaluating Soil Liquefaction Potential," *Journal of the Soil Mechanics and Foundations Division*, ASCE, Vol. 97, No. SM9, pp. 1249–1273.

Seed, H. B., and Idriss, I. M. (1982). "Ground Motion and Soil Liquefaction During Earthquakes," *Monograph Series*, Earthquake Engineering Research Institute, University of California, Berkeley, California.

Seed, H. B., Idriss, I. M., and Arango, I. (1983), "Evaluation of Liquefaction Potential Using Field Performance Data," *Journal of Geotechnical Engineering*, ASCE, Vol. 109, NO. GT3, pp. 458–482.

Seed, H. B., and Lee, K. L. (1966). "Liquefaction of Saturated Sands During Cyclic Loading," *Journal of the Soil Mechanics and Foundations Division*, ASCE, Vol. 92, No. SM6, pp. 105–134.

Seed, H. B., Martin, P. O., and Lysmer, J. (1975). "The Generation and Dissipation of Pore Water Pressure During Soil Liquefaction," *Report No. EERC 75–26*, Earthquake Engineering Research Institute, University of California, Berkeley, California.

Seed, H. B., Mori, K., and Chan, C. K. (1977). "Influence of Seismic History on Liquefaction of Sands," *Journal of the Geotechnical Engineering Division*, ASCE, Vol. 103, No. GT4, pp. 246–270.

Copyright 2017 Cengage Learning. All Rights Reserved. May not be copied, scanned, or duplicated, in whole or in part. Due to electronic rights, some third party content may be suppressed from the eBook and/or eChapter(s). Editorial review has deemed that any suppressed content does not materially affect the overall learning experience. Cengage Learning reserves the right to remove additional content at any time if subsequent rights restrictions require it.

Seed, H. B., and Peacock, W. H. (1971). "The Procedure for Measuring Soil Liquefaction Characteristics," *Journal of the Soil Mechanics and Foundations Division*, ASCE, Vol. 97, No. SM8, pp. 1099–1119.

Seed, H. B., Tokimatsu, K., Harder, L. F., and Chung, R. M. (1984). "The Influence of SPT Procedures in Soil Liquefaction Resistance Evaluation," *Report NO. EERC-84/15*, Earthquake Engineering Research Institute, University of California, Berkeley, California.

Sy, A. and Campanella, R.G. (1994). "Becker and Standard Penetration Tests (BPT-CPT) Correlations with Consideration of Casing Friction." *Canadian Geotechnical Journal*, Vol. 31, pp. 343–356.

Tanimoto, K. (1967). "Liquefaction of a Sand Layer Subjected to Shock and Vibratory Loads," *Proceedings*, 3rd Asian Regional Conference on Soil Mechanics and Foundation Engineering, Haifa, Israel, Vol. 1.

Whitman, R. V. (1970). "Summary of Results from Shaking Table Tests at University of Chile Using a Medium Sand," Progress Report No. 9, Effect of Local Soil Conditions upon Earthquake Damage, *Research Report R70-25*, *Soils Publication No. 258*, Massachusetts Institute of Technology, Cambridge, Massachusetts.

Yoshimi, Y. (1967). "An Experimental Study of Liquefaction of Saturated Sands," *Soils and Foundations*, Tokyo, Japan, Vol. 7, No. 2.

Yoshimi, Y. (1970). "Liquefaction of Saturated Sand During Vibration Under Quasi-plane-Strain Conditions," *Proceedings*, 3rd Japan Earthquakes Engineering Symposium, Tokyo, Japan.

Yoshimi, Y., and Oh-oka, H. (1973). "A Ring Torsion Apparatus for Simple Shear Tests," *Proceedings*, 8th International Conference on Soil Mechanics and Foundation Engineering, Vol. 1.2, Moscow, USSR.

Youd, T. L. (1972). "Compaction of Sand by Repeated Straining," *Journal of the Soil Mechanics and Foundations Division*, ASCE, Vol. 98, No. SM7, pp. 709–725.

Youd, T. L., Idriss, I. M., Andrus, R.D., Arango, I., Castro, G., Christian, J.T., Dobry, R., Liam Finn, W.D., Harder, L.F., Jr., Hynes, M.E., Ishihara, K., Koester, J.P., Liao, S.S.C., Marcuson, W.F., III, Martin, G.R., Mitchell, J.K., Moriwaki, Y., Power, M.S., Robertson, P.K., Seed, R.B., and Stokoe, K.H., II. (2001). "Liquefaction resistance of soils: summary report from the 1996 NCEER and 1998 NCEER/NSF workshops on evaluation of liquefaction resistance of soils." *Journal of Geotechnical and Geoenvironmental Engineering*, ASCE, Vol. 127, No. 10, pp. 817–833.

Copyright 2017 Cengage Learning. All Rights Reserved. May not be copied, scanned, or duplicated, in whole or in part. Due to electronic rights, some third party content may be suppressed from the eBook and/or eChapter(s). Editorial review has deemed that any suppressed content does not materially affect the overall learning experience. Cengage Learning reserves the right to remove additional content at any time if subsequent rights restrictions require it.

Machine Foundations on Piles

11

11.1 INTRODUCTION

It was mentioned in Section 5.4 that, for low-speed machines subjected to vertical vibration, the natural frequency of the foundation-soil system should be at least twice the operating frequency. In the design of these types of foundations, if changes in size and mass of the foundation (more popularly known as *tuning* of a foundation) do not lead to a satisfactory design, a pile foundation may be considered. It is also possible that the subsoil conditions are such that the vibration of a shallow machine foundation may lead to undesirable settlement. In many circumstances the load-bearing capacity of the soil may be low compared to the static and dynamic load imposed by the machine and the shallow foundation. In that case the design will then dictate consideration of the use of piles. It should be kept in mind that the use of piles will, in general, increase the natural frequency of the soil–pile system and may also increase the amplitude of vibration at resonance.

The soil–structure interaction of the deep foundations is not well understood and although rigorous theoretical solutions exist, they are mostly confined to researchers. The practice in design offices is usually based on ignoring the stiffness of the soil and only the stiffness of the pile is taken into account.

In this chapter, the fundamental concepts of pile foundations of vibrating machines will be considered. It should also be kept in mind that the piles supporting machine foundations are for cases of *low amplitudes of vibration* (because allowable motion is small and dynamic loads are small compared to static loads) in contrast to those encountered under earthquake-type loading (large strain conditions). For that reason, when encountered with the selection of proper parameters for soil such as the shear modulus G, the value that correspond to low amplitudes of strain should be used. Elastic theory thus is the basis of design methods described in this chapter.

Copyright 2017 Cengage Learning. All Rights Reserved. May not be copied, scanned, or duplicated, in whole or in part. Due to electronic rights, some third party content may be suppressed from the eBook and/or eChapter(s).
Editorial review has deemed that any suppressed content does not materially affect the overall learning experience. Cengage Learning reserves the right to remove additional content at any time if subsequent rights restrictions require it.

Piles Subjected to Vertical Vibration

In general, piles can be grouped into two broad categories:

1. *End-bearing piles.* These piles penetrate through soft soil layers up to a hard stratum or rock. The hard stratum or rock can be considered as rigid.
2. *Friction piles or floating piles.* The tips of these piles do not rest on hard stratum. The piles resist the applied load by means of frictional resistance developed at the soil-pile interface.

11.2 END-BEARING PILES

Figure 11.1 shows a pile driven up to a rock layer. The length of the pile is equal to L, and the load on the pile coming from the foundations is W. This problem can be approximately treated as a vertical rod *fixed at the base* (that is, at the rock layer) and free on top. For determining the natural frequency of the piles, three possible cases may arise.

Case 1. If W is very small (≈ 0), the natural frequency of vibration can be given by following Eq. (3.57) as

$$\boxed{f_n = \frac{\omega_n}{2\pi} = \frac{1}{4L}\sqrt{\frac{E_P}{\rho_P}}} \tag{11.1}$$

where f_n = natural frequency of vibration
ω_n = natural circular frequency
E_P = modulus of elasticity of the pile material
ρ_P = density of the pile material

Case 2. If W is of the same order of magnitude as the weight of the pile, the natural frequency of vibration can be given by Eq. (4.20). (Note similar end conditions between Figure 4.13 and Figure 11.1.) Thus,

$$\frac{AL\gamma_P}{W} = \left[\frac{\omega_n L}{\upsilon_{c(P)}}\right]\tan\left[\frac{\omega_n L}{\upsilon_{c(P)}}\right] \tag{11.2}$$

or

$$\boxed{\frac{L\gamma_P}{\sigma_0} = \left[\frac{\omega_n L}{\upsilon_{c(P)}}\right]\tan\left[\frac{\omega_n L}{\upsilon_{c(P)}}\right]} \tag{11.3}$$

where A = area of the cross section of the pile
γ_P = unit weight of the pile material
ω_n = natural circular frequency
$\upsilon_{c(P)}$ = longitudinal wave propagation velocity in the pile
$\sigma_0 = \dfrac{W}{A}$

Copyright 2017 Cengage Learning. All Rights Reserved. May not be copied, scanned, or duplicated, in whole or in part. Due to electronic rights, some third party content may be suppressed from the eBook and/or eChapter(s). Editorial review has deemed that any suppressed content does not materially affect the overall learning experience. Cengage Learning reserves the right to remove additional content at any time if subsequent rights restrictions require it.

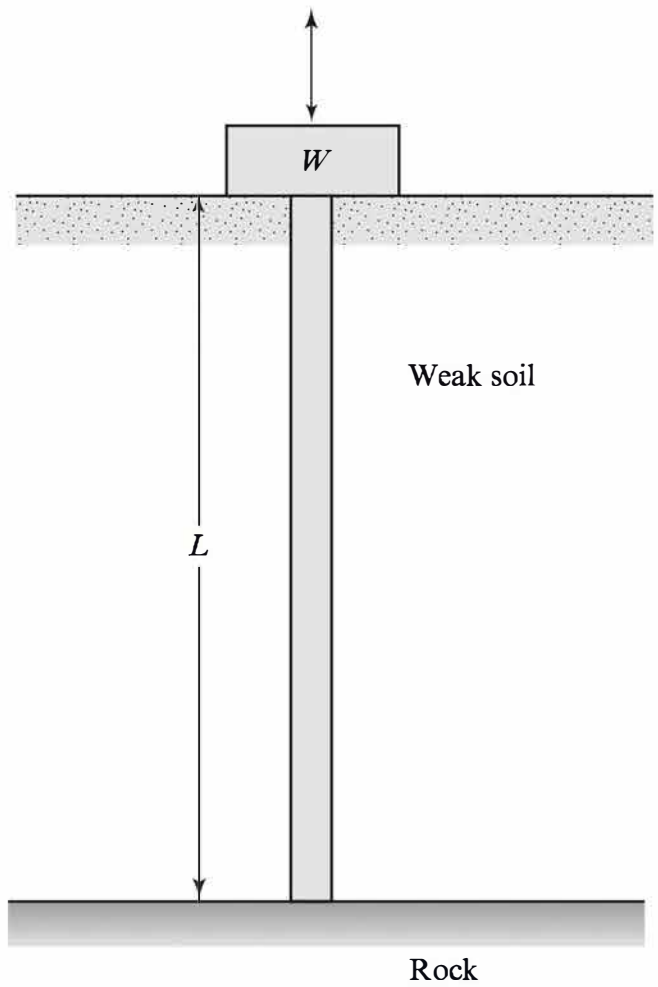

Figure 11.1 End-bearing pile

Figure 11.2 shows a plot of $\omega_n L/\upsilon_{c(P)}$ against $L\gamma_P/\sigma_0$ that can be used to determine ω_n and f_n. Note that

$$f_n = \frac{\omega_n}{2\pi} \tag{11.4}$$

Case 3. If W is larger and the weight of the pile is negligible in comparison, then from Eq. (11.2)

$$\frac{AL\gamma_P}{W} \approx \left[\frac{\omega_n L}{\upsilon_{c(P)}}\right]^2$$

However,

$$\upsilon_{c(P)} = \sqrt{\frac{E_P}{\rho_P}} = \sqrt{\frac{E_P g}{\gamma_P}}$$

where g = acceleration due to gravity.
So,

$$\omega_n = \sqrt{\frac{AE_P g}{LW}}$$

Copyright 2017 Cengage Learning. All Rights Reserved. May not be copied, scanned, or duplicated, in whole or in part. Due to electronic rights, some third party content may be suppressed from the eBook and/or eChapter(s). Editorial review has deemed that any suppressed content does not materially affect the overall learning experience. Cengage Learning reserves the right to remove additional content at any time if subsequent rights restrictions require it.

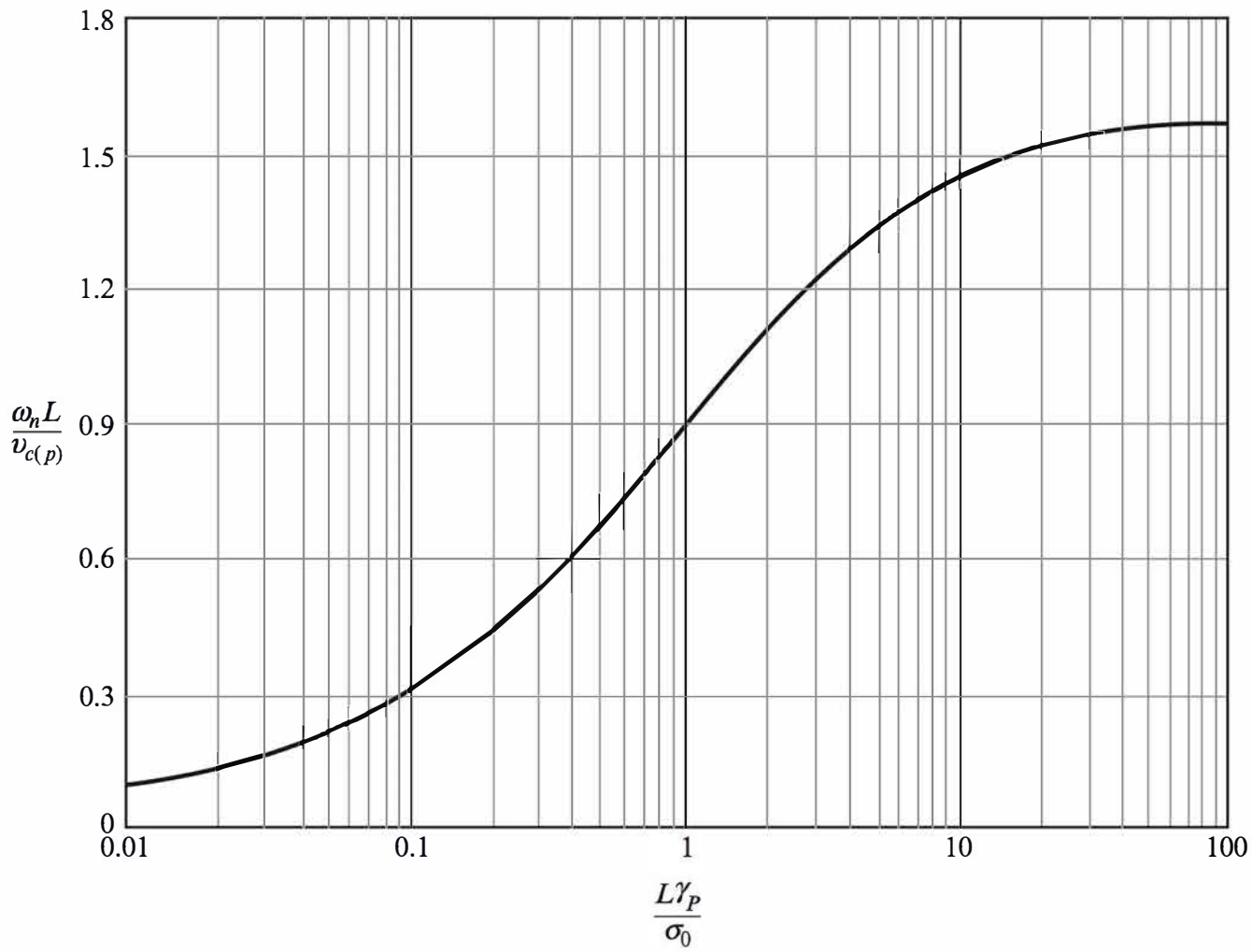

Figure 11.2 Plot of Eq. (11.3)

or

$$\boxed{f_n = \frac{1}{2\pi}\sqrt{\frac{E_P g}{\sigma_0 L}}} \tag{11.5}$$

where σ_0 = axial stress = W/A.

Richart (1962) prepared a graph for f_n with various values of pile length L and σ_0, and this is shown in Figure 11.3. In preparing Figure 11.3, the following material properties have been used.

Material	E_P (kPa)	γ_P (kN/m³)
Steel	200×10^6	75.5
Concrete	21×10^6	23.6
Wood	8.25×10^6	6.3

EXAMPLE 11.1

A machine foundation is supported by four prestressed concrete plies driven to bedrock. The length of each pile is 24 m, and they are 0.3 m × 0.3 m in cross section. The weight of the machine and the foundation is 1360 kN.

Copyright 2017 Cengage Learning. All Rights Reserved. May not be copied, scanned, or duplicated, in whole or in part. Due to electronic rights, some third party content may be suppressed from the eBook and/or eChapter(s). Editorial review has deemed that any suppressed content does not materially affect the overall learning experience. Cengage Learning reserves the right to remove additional content at any time if subsequent rights restrictions require it.

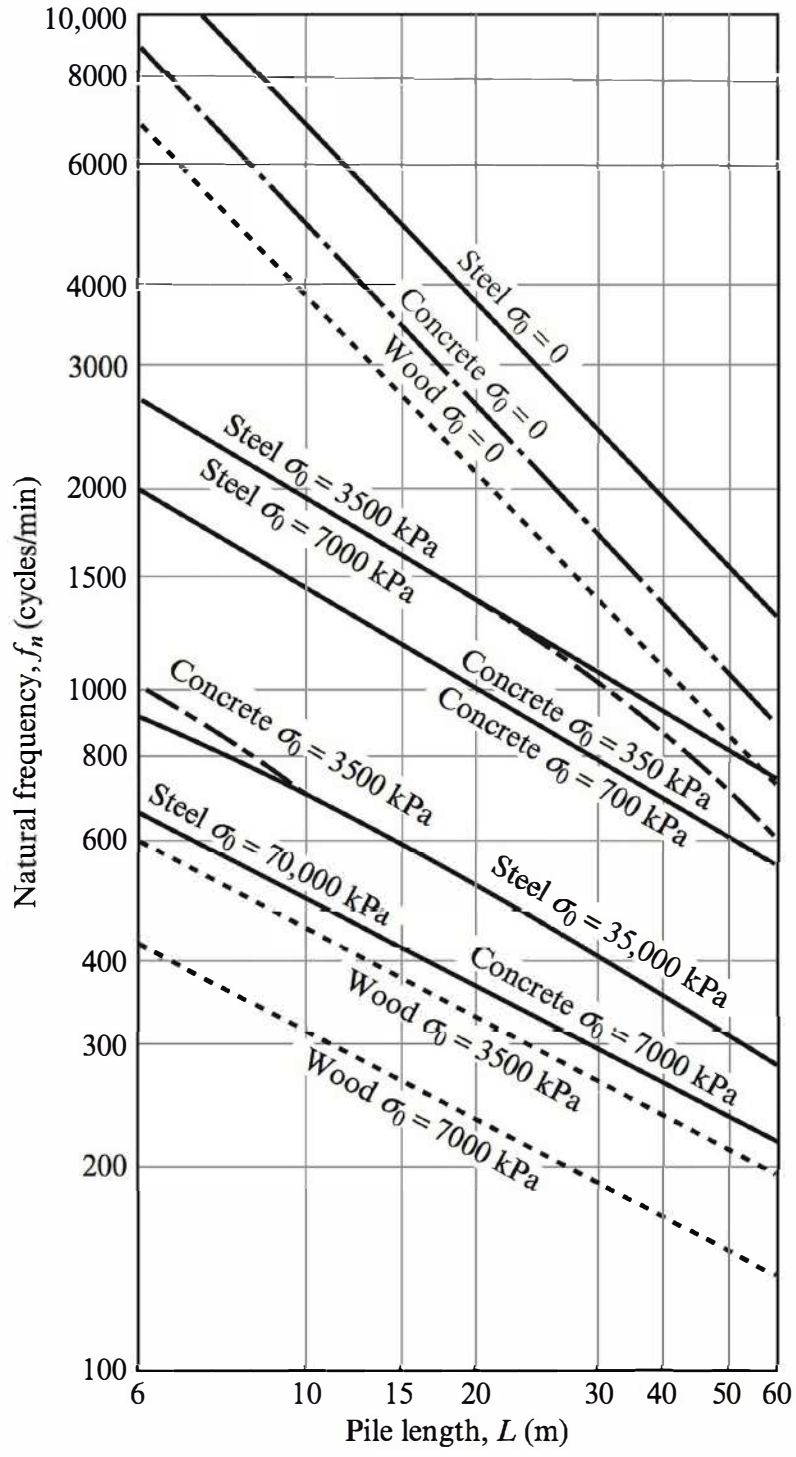

Figure 11.3 Resonant frequency for vertical vibration of a point bearing pile (from Richart, 1962)

Source: Richart, F.E., Jr. (1962). "Foundation Vibrations," *Transactions*, ASCE, Vol. 27, Part 1, pp. 863–898. With permission from ASCE.

Given: unit weight of concrete = 24 kN/m^3 and the modulus of elasticity of the concrete used for the piles = 24.5×10^6 kPa. Determine the natural frequency of the pile-foundation system.

SOLUTION:

There are four piles. The weight carried by each pile is

$$W = \frac{1360 \text{ kN}}{4} = 340 \text{ kN}$$

Copyright 2017 Cengage Learning. All Rights Reserved. May not be copied, scanned, or duplicated, in whole or in part. Due to electronic rights, some third party content may be suppressed from the eBook and/or eChapter(s). Editorial review has deemed that any suppressed content does not materially affect the overall learning experience. Cengage Learning reserves the right to remove additional content at any time if subsequent rights restrictions require it.

The weight of each pile is

$$AL\gamma_P = \underbrace{0.3 \times 0.3}_{\substack{\uparrow \\ \text{Area of} \\ \text{cross section}}} \underbrace{\times 24 \times}_{\substack{\uparrow \\ \text{Length}}} (24) = 51.84 \text{ kN}$$

$$\upsilon_{c(P)} = \sqrt{\frac{E_P}{\rho_P}} = \sqrt{\frac{(24.5 \times 10^6)}{(24/9.81)}} = 3164.6 \text{ m/s}$$

From Eq. (11.2),

$$\frac{AL\gamma_P}{W} = \left[\frac{\omega_n L}{\upsilon_{c(P)}}\right] \tan\left[\frac{(\omega_n)L}{\upsilon_{c(P)}}\right]$$

So

$$\frac{51.84}{340} = \left[\frac{(\omega_n)(24)}{(3164.6)}\right] \tan\left[\frac{(\omega_n)(24)}{(3164.6)}\right]$$

or

$$0.1525 = [(\omega_n)(0.00758)]\tan[(\omega_n)(0.00758)]$$

From Figure 11.2, for $\frac{L\gamma_P}{\sigma_0} = 0.1525$

$$\frac{\omega_n L}{\upsilon_{c(P)}} \approx 0.36$$

$$\omega_n = \frac{(0.36)(3164.6)}{24} \approx 47.5 \text{ rad/s}$$

$$f_n = \mathbf{7.56\ Hz}$$

11.3 FRICTION PILES

Figure 11.4a shows a pile having a length of embedment equal to L and a radius of R. The pile is subjected to a dynamic load

$$Q = Q_0 e^{i\omega t} \tag{11.6}$$

It is possible to idealize the pile to a mass-spring-dashpot system, as shown in Figure 11.4b. The mass m shown in Figure 11.4b can be assumed to be the mass of the cap and machinery. The mathematical formulation for obtaining the stiffness (k_z) and the damping (c_z) parameters has been given by Novak (1977). In developing the theory, the following assumptions were made:

1. The pile is vertical, elastic, and circular in cross section.
2. The pile is floating.

Copyright 2017 Cengage Learning. All Rights Reserved. May not be copied, scanned, or duplicated, in whole or in part. Due to electronic rights, some third party content may be suppressed from the eBook and/or eChapter(s). Editorial review has deemed that any suppressed content does not materially affect the overall learning experience. Cengage Learning reserves the right to remove additional content at any time if subsequent rights restrictions require it.

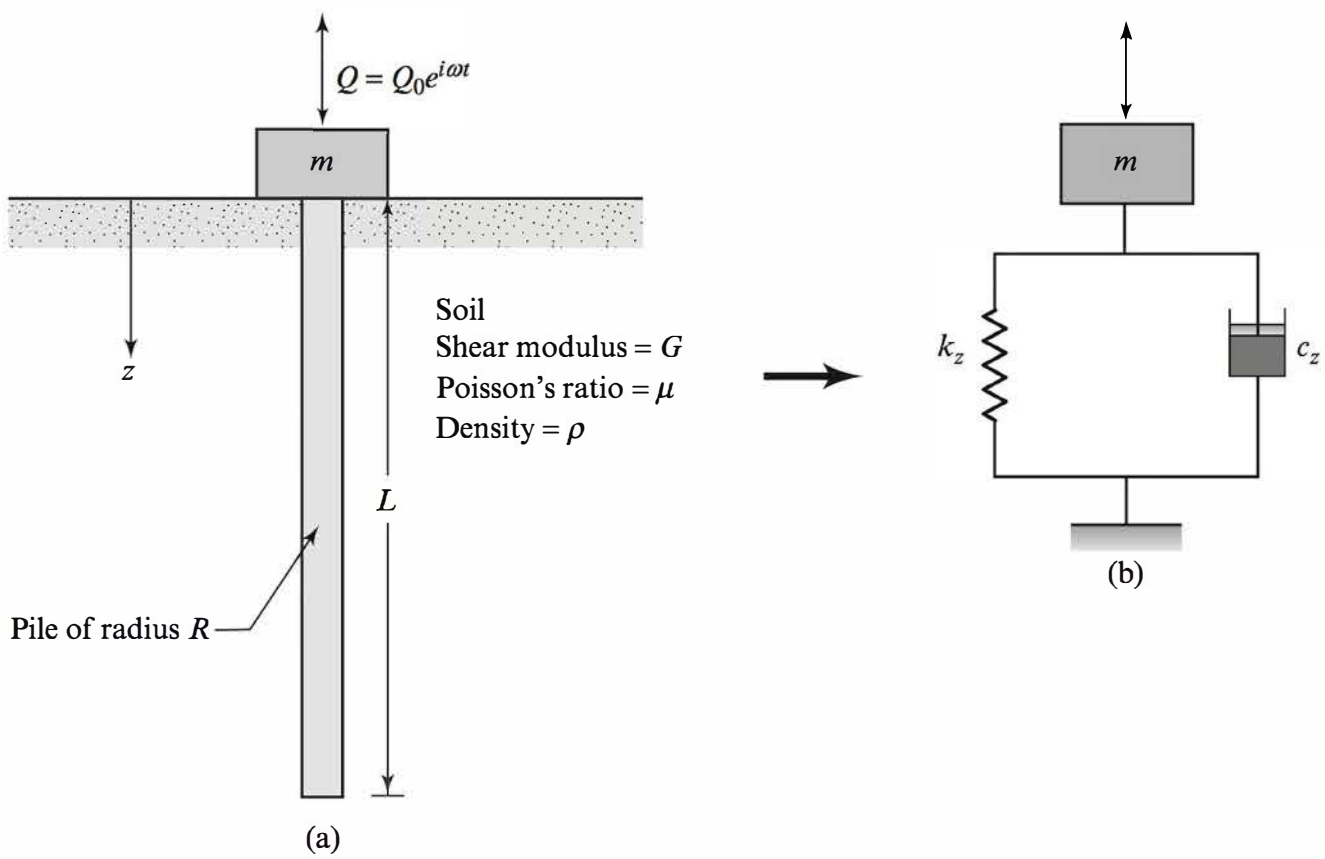

Figure 11.4 Friction pile-vertical vibration

3. The pile is perfectly connected to the soil.
4. The soil above the pile tip behaves as infinitesimal, thin, independent linearly elastic layers.

The last assumption leads to the assumption of plane strain condition. Referring to Figure 11.5, the dynamic stiffness and damping of the pile can then be described in terms of complex stiffness (Novak and El-Sharnouby, 1983) as

$$K = K_1 + iK_2 \tag{11.7}$$

The applied force Q and displacement z are related to K in the following manner:

$$Q = Kz = (K_1 + iK_2)z \tag{11.8}$$

where $i = \sqrt{-1}$
K_1 = real part of K = Re K
K_2 = imaginary part of K = Im K

Hence, the spring constant is

$$k_z = K_1 = \text{Re}\, K \tag{11.9}$$

and the equivalent viscous damping is

$$c_z = \frac{K_2}{\omega} = \frac{\text{Im}\, K}{\omega} \tag{11.10}$$

Copyright 2017 Cengage Learning. All Rights Reserved. May not be copied, scanned, or duplicated, in whole or in part. Due to electronic rights, some third party content may be suppressed from the eBook and/or eChapter(s). Editorial review has deemed that any suppressed content does not materially affect the overall learning experience. Cengage Learning reserves the right to remove additional content at any time if subsequent rights restrictions require it.

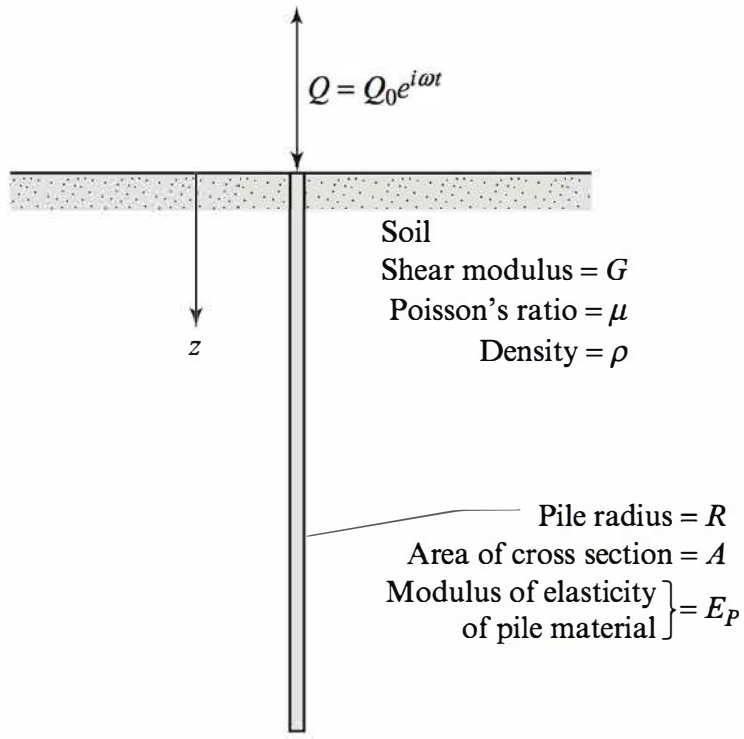

Figure 11.5 Dynamic stiffness and damping constant for a single pile–vertical mode of vibration

Combining Eqs. (11.7), (11.9), and (11.10),

$$K = k_z + i\omega c_z \tag{11.11}$$

So, the force-displacement relation can be expressed as

$$Q = (k_z + i\omega c_z)z$$

or

$$Q = k_z z + c_z \dot{z} \tag{11.12}$$

where $\dot{z} = dz/dt$

The relationships for k_z and c_z have been given by Novak and El-Sharnouby (1983) as

$$\boxed{k_z = \left(\frac{E_P A}{R}\right) f_{z1}} \tag{11.13}$$

and

$$\boxed{c_z = \left(\frac{E_P A}{\sqrt{G/\rho}}\right) f_{z2}} \tag{11.14}$$

where E_P = modulus of elasticity of the pile material
A = area of pile cross section
G = shear modulus of soil
ρ = density of soil
f_{z1}, f_{z2} = nondimensional parameters

Copyright 2017 Cengage Learning. All Rights Reserved. May not be copied, scanned, or duplicated, in whole or in part. Due to electronic rights, some third party content may be suppressed from the eBook and/or eChapter(s). Editorial review has deemed that any suppressed content does not materially affect the overall learning experience. Cengage Learning reserves the right to remove additional content at any time if subsequent rights restrictions require it.

The variations of f_{z1}, and f_{z2} for end-bearing piles are shown in Figures 11.6 and 11.7. Similarly, the f_{z1} and f_{z2} variations for floating piles are shown in Figures 11.8 and 11.9.

Pile foundations are generally constructed in groups. The stiffness and damping constants of a pile group are not simple summations of the stiffness and damping constant of individual piles. Novak (1977) suggested that when piles are closely spaced, the displacement of one pile is increased due to the displacement of all other piles and conversely, the stiffness and damping of the group are reduced. Hence, the stiffness of the pile group can be obtained as

$$\boxed{k_{z(g)} = \frac{\sum_{1}^{n} k_z}{\sum_{r=1}^{n} \alpha_r}} \tag{11.15}$$

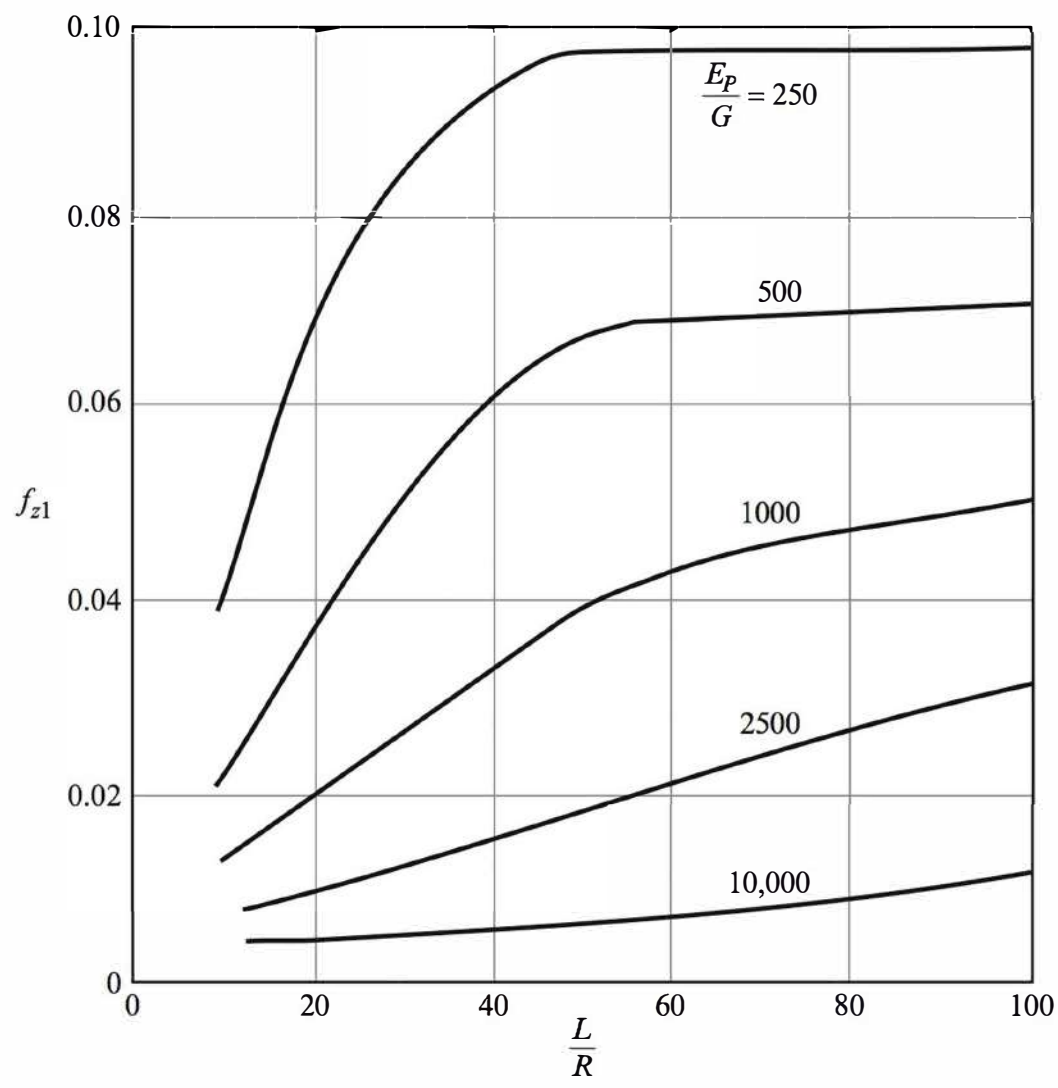

Figure 11.6 Variation of f_{z1} with L/R and E_P/G for end-bearing piles (from Novak and El-Sharnouby, 1983)

Source: Novak, M. and El-Sharnouby, B. (1983). "Stiffness Constants of Single Piles," *Journal of the Geotechnical Engineering Division*, ASCE, Vol. 109, No. GT7, pp. 961–974. With permission from ASCE.

Copyright 2017 Cengage Learning. All Rights Reserved. May not be copied, scanned, or duplicated, in whole or in part. Due to electronic rights, some third party content may be suppressed from the eBook and/or eChapter(s). Editorial review has deemed that any suppressed content does not materially affect the overall learning experience. Cengage Learning reserves the right to remove additional content at any time if subsequent rights restrictions require it.

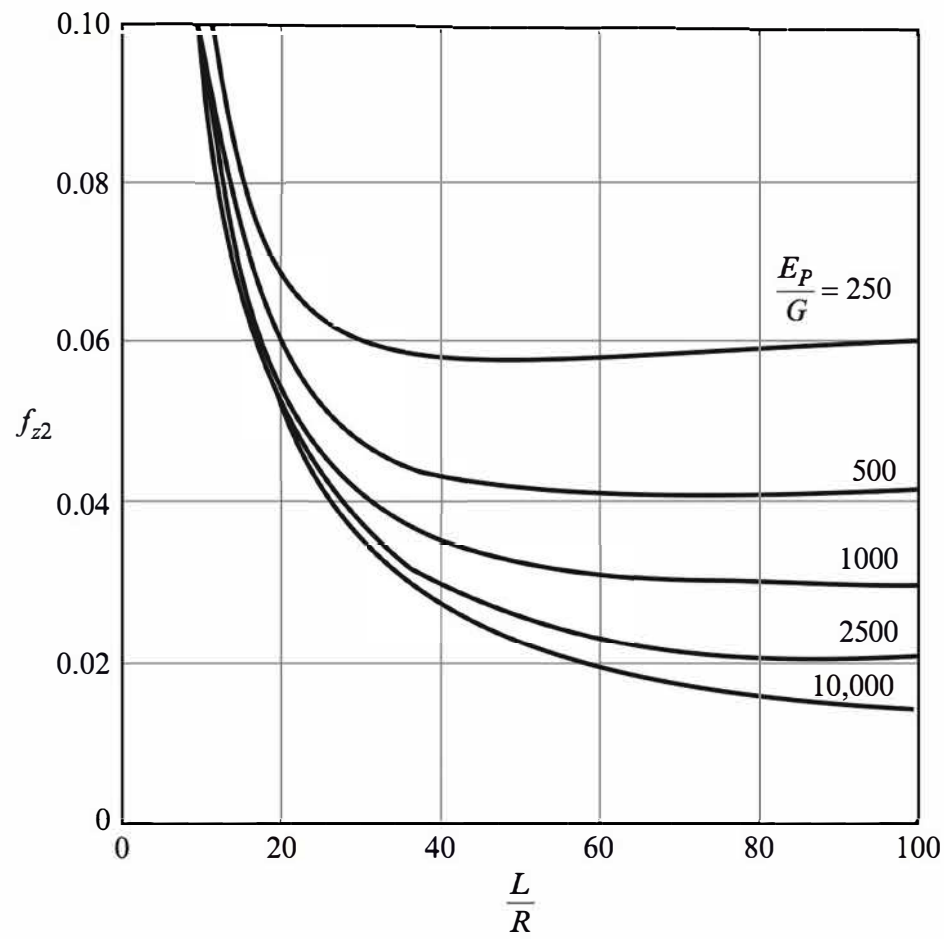

Figure 11.7 Variation of f_{z2} with L/R and E_P/G for end-bearing piles (from Novak and El-Sharnouby, 1983)

Source: Novak, M. and El-Sharnouby, B. (1983). "Stiffness Constants of Single Piles," *Journal of the Geotechnical Engineering Division*, ASCE, Vol. 109, No. GT7, pp. 961–974. With permission from ASCE.

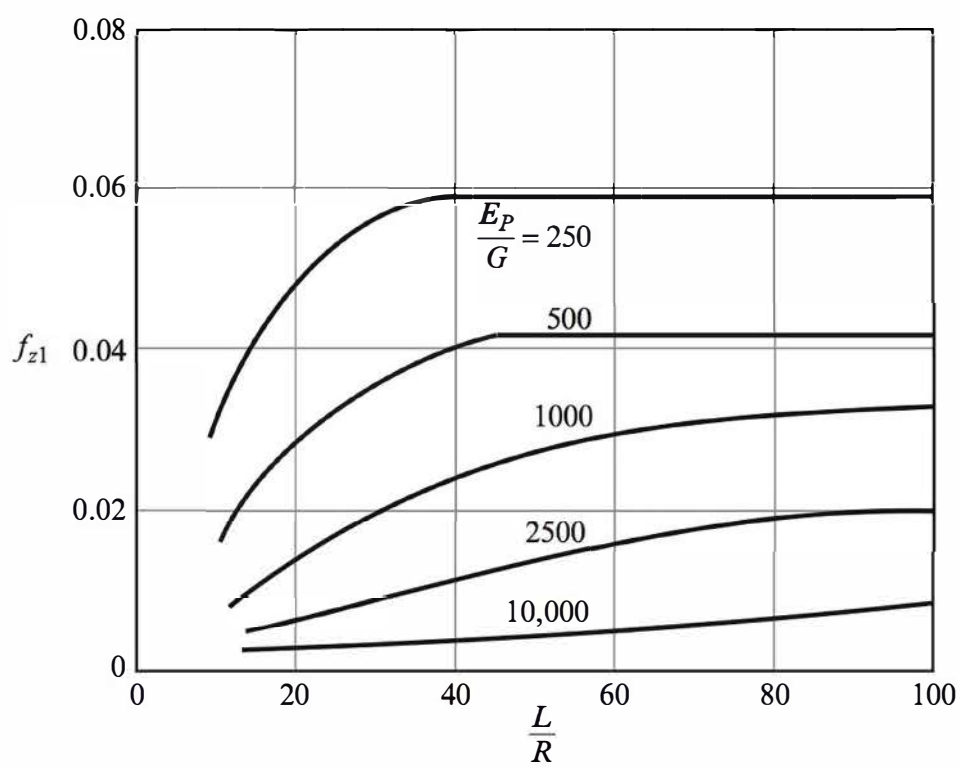

Figure 11.8 Variation of f_{z1} with L/R and E_P/G for floating piles (from Novak and El-Sharnouby, 1983)

Source: Novak, M. and El-Sharnouby, B. (1983). "Stiffness Constants of Single Piles," *Journal of the Geotechnical Engineering Division*, ASCE, Vol. 109, No. GT7, pp. 961–974. With permission from ASCE.

Copyright 2017 Cengage Learning. All Rights Reserved. May not be copied, scanned, or duplicated, in whole or in part. Due to electronic rights, some third party content may be suppressed from the eBook and/or eChapter(s). Editorial review has deemed that any suppressed content does not materially affect the overall learning experience. Cengage Learning reserves the right to remove additional content at any time if subsequent rights restrictions require it.

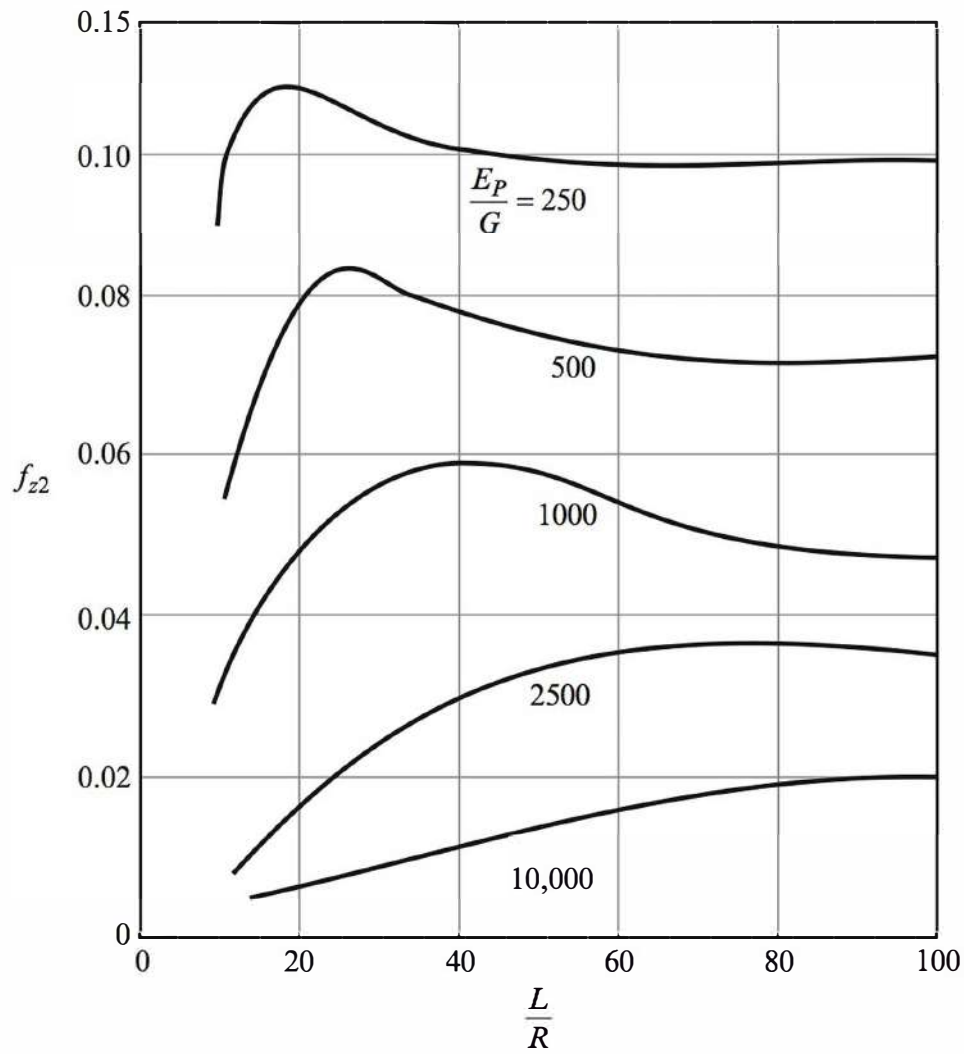

Figure 11.9 Variation of f_{z2} with L/R and E_P/G for floating piles (from Novak and El-Sharnouby, 1983)

Source: Novak, M. and El-Sharnouby, B. (1983). "Stiffness Constants of Single Piles," *Journal of the Geotechnical Engineering Division*, ASCE, Vol. 109, No. GT7, pp. 961–974. With permission from ASCE.

and

$$c_{z(g)} = \frac{\sum_{1}^{n} c_z}{\sum_{r=1}^{n} \alpha_r} \tag{11.16}$$

where $k_{z(g)}$ = spring constant for the pile group
$c_{z(g)}$ = dashpot constant for the pile group
n = number of piles in the group
α_r = the interaction factor describing the contribution of the rth pile to the displacement of the reference pile (that is, $\alpha_1 = 1$)

Since no analytical solutions for the dynamic interaction of piles are available at the present time, an estimate of α_r can be obtained from the static solution of Poulos (1968). This is shown in Figure 11.10.

Copyright 2017 Cengage Learning. All Rights Reserved. May not be copied, scanned, or duplicated, in whole or in part. Due to electronic rights, some third party content may be suppressed from the eBook and/or eChapter(s). Editorial review has deemed that any suppressed content does not materially affect the overall learning experience. Cengage Learning reserves the right to remove additional content at any time if subsequent rights restrictions require it.

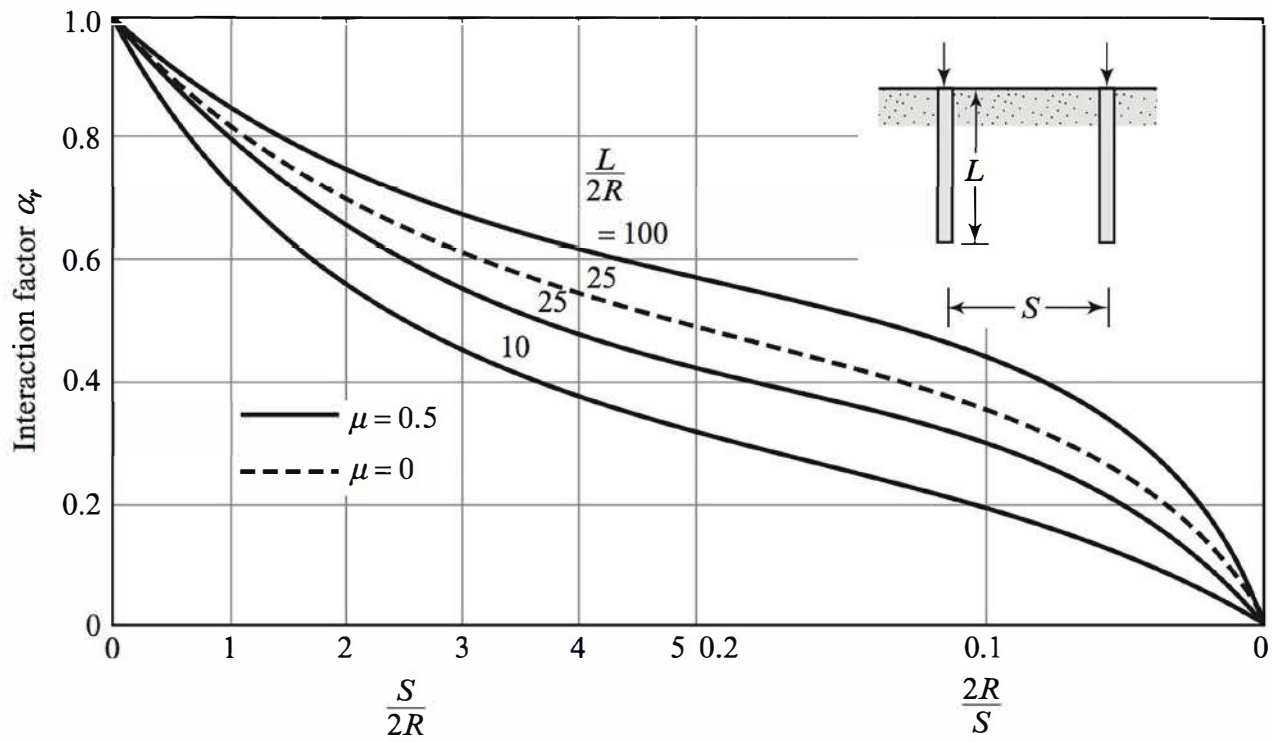

Figure 11.10 Variation of interaction factor α_r (from Poulos, 1968)

Source: Poulos, H.G. (1968). "Analysis of the Settlement of Pile Groups," *Geotechnique, Institution of Civil Engineers*, London, Vol. 18, No. 4, pp. 449–471.

For group piles, a cap is constructed over the piles (Figure 11.11). In the estimation of stiffness and damping constants, the contribution of the pile cap should be taken into account. The relationships describing the stiffness and geometric damping of embedment foundations are given in Chapter 5 as

$$k_{z(\text{cap})} = Gr_0\left[\bar{C}_1 + \frac{G_s}{G}\frac{D_f}{r_0}\bar{S}_1\right] \tag{5.119}$$

and

$$c_{z(\text{cap})} = r_0^2\sqrt{\rho G}\left[\bar{C}_2 + \bar{S}_2\frac{D_f}{r_0}\sqrt{\frac{G_s\rho_s}{G\rho}}\right] \tag{5.120}$$

Since the soil located below the pile cap may be of poor quality and it may shrink away with time, it would be on the safe side to ignore the effect of the cap base—that is, $\bar{C}_1 = 0$ and $\bar{C}_2 = 0$. So

$$k_{z(\text{cap})} = G_s D_f \bar{S}_1 \tag{11.17}$$

and

$$c_{z(\text{cap})} = D_f r_0 \bar{S}_2 \sqrt{G_s \rho_s} \tag{11.18}$$

Thus, for the group pile and cap,

$$\boxed{k_{z(T)} = \frac{\sum_{1}^{n} k_z}{\sum_{r=1}^{n} \alpha_r} + G_s D_f \bar{S}_1} \tag{11.19}$$

Copyright 2017 Cengage Learning. All Rights Reserved. May not be copied, scanned, or duplicated, in whole or in part. Due to electronic rights, some third party content may be suppressed from the eBook and/or eChapter(s). Editorial review has deemed that any suppressed content does not materially affect the overall learning experience. Cengage Learning reserves the right to remove additional content at any time if subsequent rights restrictions require it.

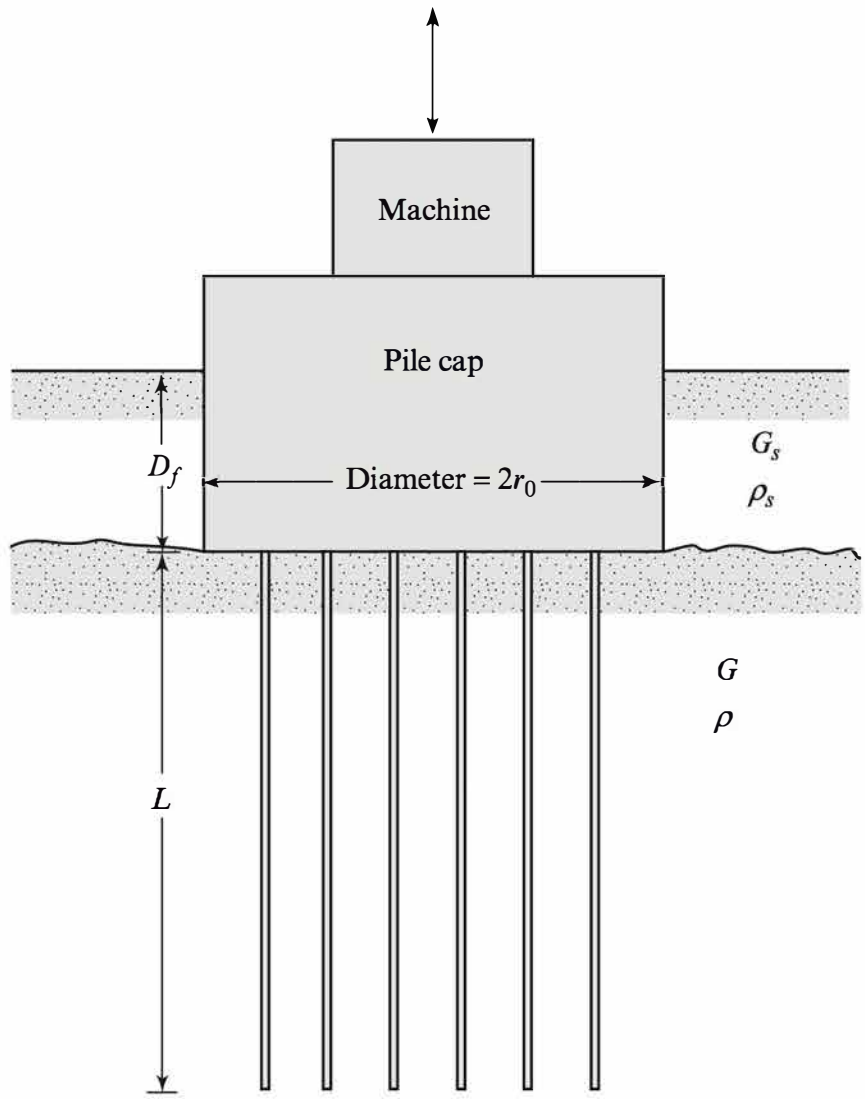

Figure 11.11 Group pile with pile cap

and

$$c_{z(T)} = \frac{\sum_{1}^{n} c_z}{\sum_{r=1}^{n} \alpha_r} + D_f r_0 \bar{S}_2 \sqrt{G_s \rho_s} \tag{11.20}$$

where $k_{z(T)}$ and $c_{z(T)}$ are the stiffness and damping constants for the pile group and cap, respectively.

The variations for $\bar{S}_1$ and $\bar{S}_2$ are given in Table 5.6. Once the values of $k_{z(T)}$ and $c_{z(T)}$ are determined, the response of the system can be calculated using the principles described in Chapter 2, as briefly outlined here.

a. Damping ratio:

$$D_z = \frac{c_{z(T)}}{2\sqrt{k_{z(T)} m}} \tag{11.21}$$

where $m =$ mass of the pile cap and the machine supported by it.

Copyright 2017 Cengage Learning. All Rights Reserved. May not be copied, scanned, or duplicated, in whole or in part. Due to electronic rights, some third party content may be suppressed from the eBook and/or eChapter(s). Editorial review has deemed that any suppressed content does not materially affect the overall learning experience. Cengage Learning reserves the right to remove additional content at any time if subsequent rights restrictions require it.

b. Undamped natural frequency:

$$\omega_n = \sqrt{\frac{k_{z(T)}}{m}} \tag{11.22}$$

$$f_n = \frac{1}{2\pi}\sqrt{\frac{k_{z(T)}}{m}} \tag{11.23}$$

c. Damped natural frequency:

$$f_m = f_n\sqrt{1 - 2D_z^2} \quad \text{(for constant force excitation)} \tag{11.24}$$

$$f_m = \frac{f_n}{\sqrt{1 - 2D_z^2}} \quad \text{(for rotating mass–type excitation)} \tag{11.25}$$

d. Amplitude of vibration at resonance:

$$A_z = \frac{Q_0}{k_{z(T)}}\frac{1}{2D_z\sqrt{1 - D_z^2}} \quad \text{(for constant force excitation)} \tag{11.26}$$

$$A_z = \frac{m_1 e}{m}\frac{1}{2D_z\sqrt{1 - D_z^2}} = \text{(for rating mass–type excitation)} \tag{11.27}$$

e. Amplitude of vibration at frequency other than resonance:

$$A_z = \frac{\dfrac{Q_0}{k_{z(T)}}}{\sqrt{\left(1 - \dfrac{\omega^2}{\omega_n^2}\right)^2 + 4D_z^2\dfrac{\omega^2}{\omega_n^2}}} \quad \text{(for constant force excitation)} \tag{11.28}$$

$$A_z = \frac{\dfrac{m_1 e}{m}\left(\dfrac{\omega}{\omega_n}\right)^2}{\sqrt{\left(1 - \dfrac{\omega^2}{\omega_n^2}\right)^2 + 4D_z^2\dfrac{\omega^2}{\omega_n^2}}} \quad \text{(for rotating mass–type excitation)} \tag{11.29}$$

The nature of variation of A_z with ω for floating piles and point-bearing piles is shown in Figure 11.12. From this figure, it can be seen that the relaxation of the pile tips reduces both the resonant frequency and amplitude of vibration.

Copyright 2017 Cengage Learning. All Rights Reserved. May not be copied, scanned, or duplicated, in whole or in part. Due to electronic rights, some third party content may be suppressed from the eBook and/or eChapter(s). Editorial review has deemed that any suppressed content does not materially affect the overall learning experience. Cengage Learning reserves the right to remove additional content at any time if subsequent rights restrictions require it.

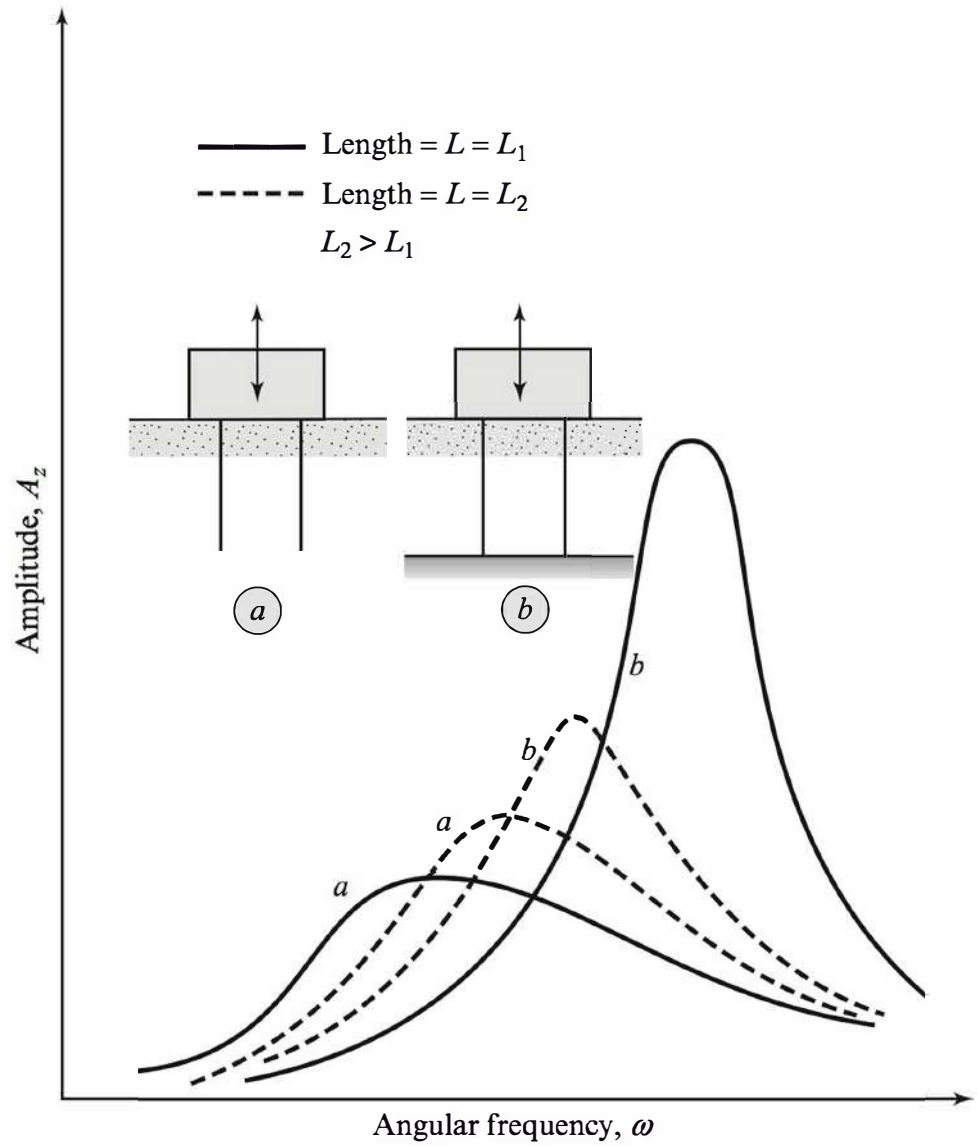

Figure 11.12 Nature of variation of A_z with ω for floating and point-bearing piles

EXAMPLE 11.2

A group of four piles is supporting a machine foundation, as shown in Figure 11.13. Determine $k_{z(T)}$ and $c_{z(T)}$. Given: $E_P = 21 \times 10^6$ kPa, $G = G_s =$ 28,000 kPa, $\gamma = \gamma_s = 19$ kN/m^3. Assume Poisson's ratio of soil, $\mu = 0.5$.

SOLUTION:

Equivalent radius of pile cross section:

$$R = \left(\frac{0.3 \times 0.3}{\pi}\right)^{1/2} = 0.17 \text{ m}$$

Length of piles = $L = 12$ m:

$$\frac{L}{R} = \frac{12}{0.17} = 70.6$$

Given $E_P = 21 \times 10^6$ kPa; $G_s = G = 28{,}000$ kPa.

Copyright 2017 Cengage Learning. All Rights Reserved. May not be copied, scanned, or duplicated, in whole or in part. Due to electronic rights, some third party content may be suppressed from the eBook and/or eChapter(s). Editorial review has deemed that any suppressed content does not materially affect the overall learning experience. Cengage Learning reserves the right to remove additional content at any time if subsequent rights restrictions require it.

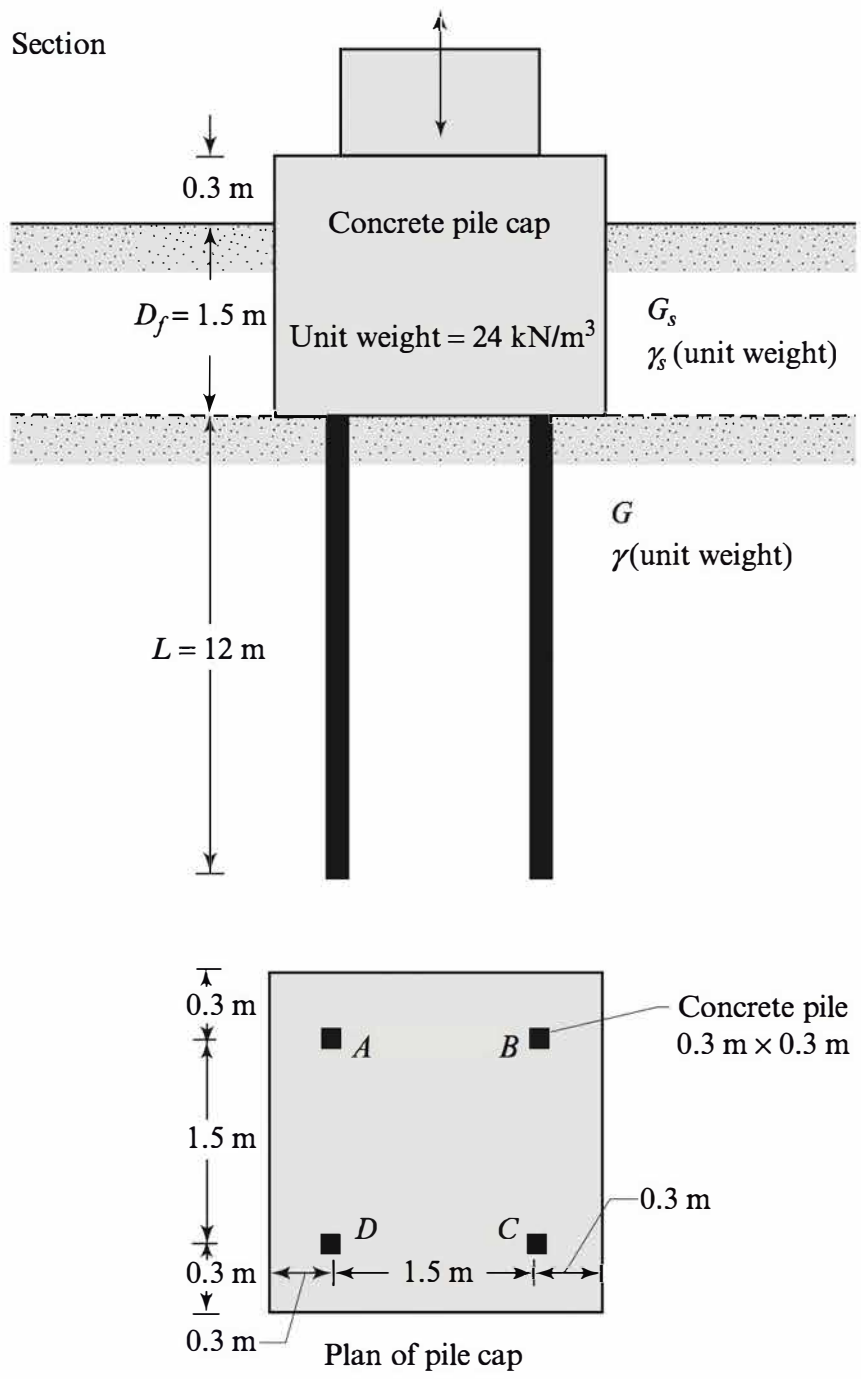

Figure 11.13

So

$$\frac{E_P}{G} = \frac{21 \times 10^6}{28000} = 750$$

Referring to Figures 11.8 and 11.9, for $E_P/G = 750$ and $L/R = 70.6$, the magnitudes of f_{z1} and f_{z2} are

$$f_{z1} \approx 0.034 \quad \text{and} \quad f_{z2} \approx 0.06$$

Hence, from Eqs. (11.13) and (11.14)

Copyright 2017 Cengage Learning. All Rights Reserved. May not be copied, scanned, or duplicated, in whole or in part. Due to electronic rights, some third party content may be suppressed from the eBook and/or eChapter(s). Editorial review has deemed that any suppressed content does not materially affect the overall learning experience. Cengage Learning reserves the right to remove additional content at any time if subsequent rights restrictions require it.

$$k_z = \left(\frac{E_P A}{R}\right) f_{z1} = \left[\frac{(21 \times 10^9)(0.3 \times 0.3)}{0.17}\right](0.034)$$
$$= 378 \times 10^6 \text{ N/m}$$

$$c_z = \left(\frac{E_P A}{\sqrt{G/\rho}}\right) f_{z2}$$

However,

$$\sqrt{\frac{G}{\rho}} = \sqrt{\frac{28000 \times 9.81}{19}} = 120.24 \text{ m/s}$$

So

$$c_z = \left[\frac{(21 \times 10^9)(0.3 \times 0.3)}{120.24}\right](0.06)$$
$$= 94.311 \times 10^4 \text{ N-s/m}$$

In order to determine the stiffness and damping constants for group piles, Eqs. (11.15) and (11.16) can be used. However, $\sum_{r=1}^{n} \alpha_r$ needs to be considered first. This can be done by using Figure 11.10 and preparing the following table.

Reference pile → / Interacting pile	A[a]	B	C	D
A	1.00	0.54	0.48	0.54
B	0.54	1.00	0.54	0.48
C	0.48	0.54	1.00	0.54
D	0.54	0.48	0.54	1.00
	2.56	2.56	2.56	2.56

[a] *Note:* Reference pile A.

For interaction between piles A and A, $S = 0$ and $S/2R = 0$. So $\alpha_r = 1$. For interaction between piles A and B, $S = 1.5$ m, $2R = (2)(0.17) = 0.34$ m, and $S/2R = 1.5/0.34 = 4.412$. So $\alpha_r \approx 0.54$. Similarly, for interaction between piles A and D, $\alpha_r \approx 0.54$. Between piles A and C,

$$\frac{S}{2R} = \frac{\sqrt{(1.5)^2 + (1.5)^2}}{0.34} = 6.23$$

or

$$\frac{2R}{S} = 0.16 \quad \alpha_r \approx 0.48$$

The average value of $\sum_{r=1}^{n} \alpha_r = 2.56$. Hence, using Eq. (11.15),

Copyright 2017 Cengage Learning. All Rights Reserved. May not be copied, scanned, or duplicated, in whole or in part. Due to electronic rights, some third party content may be suppressed from the eBook and/or eChapter(s). Editorial review has deemed that any suppressed content does not materially affect the overall learning experience. Cengage Learning reserves the right to remove additional content at any time if subsequent rights restrictions require it.

$$k_{z(g)} = \frac{(4)(378 \times 10^6)}{2.56} = 590.63 \times 10^6 \text{ N/m}$$

$$c_{z(g)} = \frac{(4)(943.11 \times 10^3)}{2.56} = 147.36 \times 10^4 \text{ N·s/m}$$

Again, for the contributions of the pile cap, $k_{z(\text{cap})}$ [Eq. (11.17)] and $c_{z(\text{cap})}$ [Eq. (11.18)] need to be determined. Given:

$$D_f = 1.5 \text{ m}; \qquad G = 28{,}000 \text{ kPa}$$

$$\bar{S}_1 = 2.7 \text{ (Table 5.6)}; \qquad \bar{S}_2 = 6.7 \text{(Table 5.6)}$$

$$r_0 = \sqrt{\frac{2.1 \times 2.1}{\pi}} = 1.185 \text{ m}$$

From Eq. (11.17),

$$k_{z(\text{cap})} = G_s D_f \bar{S}_1 = (28000 \times 10^3) \times (1.5) \times (2.7)$$
$$= 113.4 \times 10^6 \text{ N/m}$$

Similarly, from Eq. (11.18),

$$c_{z(\text{cap})} = D_f r_0 \bar{S}_2 \sqrt{G_s \rho_s}$$
$$= (1.5) \times (1.185) \times (6.7) \sqrt{\frac{(28000 \times 10^3)(19 \times 10^3)}{9.81}}$$
$$= 277.33 \times 10^4 \text{ N·s/m}$$

So

$$k_{z(T)} = k_{z(g)} + k_{z(\text{cap})} = 590.63 \times 10^6 + 113.4 \times 10^6$$
$$= \mathbf{704.03 \times 10^6 \text{ N/m} = 704.03 \times 10^3 \text{ kN/m}}$$

$$c_{z(T)} = c_{z(g)} + c_{z(\text{cap})} = 147.36 \times 10^4 + 277.33 \times 10^4$$
$$= \mathbf{424.69 \times 10^4 \text{ N·s/m}}$$

EXAMPLE 11.3

Refer to Example 11.2. If the weight of the machine being supported is 70 kN, determine the damping ratio.

SOLUTION:

Weight of the pile cap:

$$(2.1)(2.1)(1.8)(24) = 190.512 \text{ kN} = 190512 \text{ N}$$

Copyright 2017 Cengage Learning. All Rights Reserved. May not be copied, scanned, or duplicated, in whole or in part. Due to electronic rights, some third party content may be suppressed from the eBook and/or eChapter(s). Editorial review has deemed that any suppressed content does not materially affect the overall learning experience. Cengage Learning reserves the right to remove additional content at any time if subsequent rights restrictions require it.

Total weight of pile cap and machine:

$$190.512 + 70 = 260.512 \text{ kN} = 260512 \text{ N}$$

From Eq. (11.21),

$$D_z = \frac{c_{z(T)}}{2\sqrt{k_{z(T)}m}} = \frac{424.69 \times 10^4}{2\sqrt{(704.03 \times 10^6)[260512/9.81]}} = \mathbf{0.491}$$

Sliding, Rocking, and Torsional Vibration

11.4 SLIDING AND ROCKING VIBRATION

Novak (1974) and Novak and El-Sharnouby (1983) derived the stiffness and damping constants for a single pile in a similar manner as described for the case of vertical vibration in Section 11.3. Following are the relationships for the spring and dashpot coefficients for single piles

Sliding Vibration of Single Pile

$$\boxed{k_x = \frac{E_P I_P}{R^3} f_{x1}} \tag{11.30}$$

$$\boxed{c_x = \frac{E_P I_P}{R^2 v_s} f_{x2}} \tag{11.31}$$

Table 11.1 Stiffness and Damping Parameters for Sliding Vibration ($L/R > 25$)

Poisson's ratio of soil, μ	(E_P/G)	f_{x1}	f_{x2}
0.25	10,000	0.0042	0.0107
	2,500	0.0119	0.0297
	1,000	0.0236	0.0579
	500	0.0395	0.0953
	250	0.0659	0.1556
0.40	10,000	0.0047	0.0119
	2,500	0.0132	0.0329
	1,000	0.0261	0.0641
	500	0.0436	0.1054
	250	0.0726	0.1717

Note: G = shear modulus of soil.

Copyright 2017 Cengage Learning. All Rights Reserved. May not be copied, scanned, or duplicated, in whole or in part. Due to electronic rights, some third party content may be suppressed from the eBook and/or eChapter(s). Editorial review has deemed that any suppressed content does not materially affect the overall learning experience. Cengage Learning reserves the right to remove additional content at any time if subsequent rights restrictions require it.

where E_P = modulus of elasticity of the pile material
I_P = moment of inertia of the pile cross section
υ_s = shear wave velocity in soil
R = radius of the pile

The variations of f_{x1} and f_{x2} are given in Table 11.1, which is based on the analysis on Novak (1974) and Novak and El-Sharnouby (1983).

When piles are installed in groups and subjected to sliding vibration, the spring constant and the damping coefficient of the group can be given as

$$\boxed{k_{x(g)} = \frac{\sum_{1}^{n} k_x}{\sum_{r=1}^{n} \alpha_{L(r)}}} \tag{11.32}$$

and

$$\boxed{c_{x(g)} = \frac{\sum_{1}^{n} c_x}{\sum_{r=1}^{n} \alpha_{L(r)}}} \tag{11.33}$$

where $\alpha_{L(r)}$ = interaction factor (Poulos, 1971)
$k_{x(g)}$ = spring constant for the pile group
$c_{x(g)}$ = damping coefficient for the pile group
n = number of piles in the group.

The variation of $\alpha_{L(r)}$ is given in Figure 11.14.

As in the case of vertical vibration, the effect of the pile cap (Figure 11.15) needs to be taken into account in the determination of total stiffness and damping constant. In Eqs. (5.122) and (5.123), the relationships for k_x and c_x for embedded foundations have been described as

$$\boxed{k_x = Gr_0\left[\bar{C}_{x1} + \frac{G_s}{G}\frac{D_f}{r_0}\bar{S}_{x1}\right]} \tag{5.122}$$

$$\boxed{c_x = r_0^2\sqrt{\rho G}\left[\bar{C}_{x2} + \bar{S}_{x2}\frac{D_f}{r_0}\sqrt{\frac{G_s\rho_s}{G\rho}}\right]} \tag{5.123}$$

Assuming $\bar{C}_{x1} = 0$ and $\bar{C}_{x2} = 0$

$$k_{x(\text{cap})} = G_s D_f \bar{S}_{x1} \tag{11.34}$$

and

$$c_{x(\text{cap})} = D_f r_0 \bar{S}_{x2}\sqrt{G_s\rho_s} \tag{11.35}$$

Copyright 2017 Cengage Learning. All Rights Reserved. May not be copied, scanned, or duplicated, in whole or in part. Due to electronic rights, some third party content may be suppressed from the eBook and/or eChapter(s). Editorial review has deemed that any suppressed content does not materially affect the overall learning experience. Cengage Learning reserves the right to remove additional content at any time if subsequent rights restrictions require it.

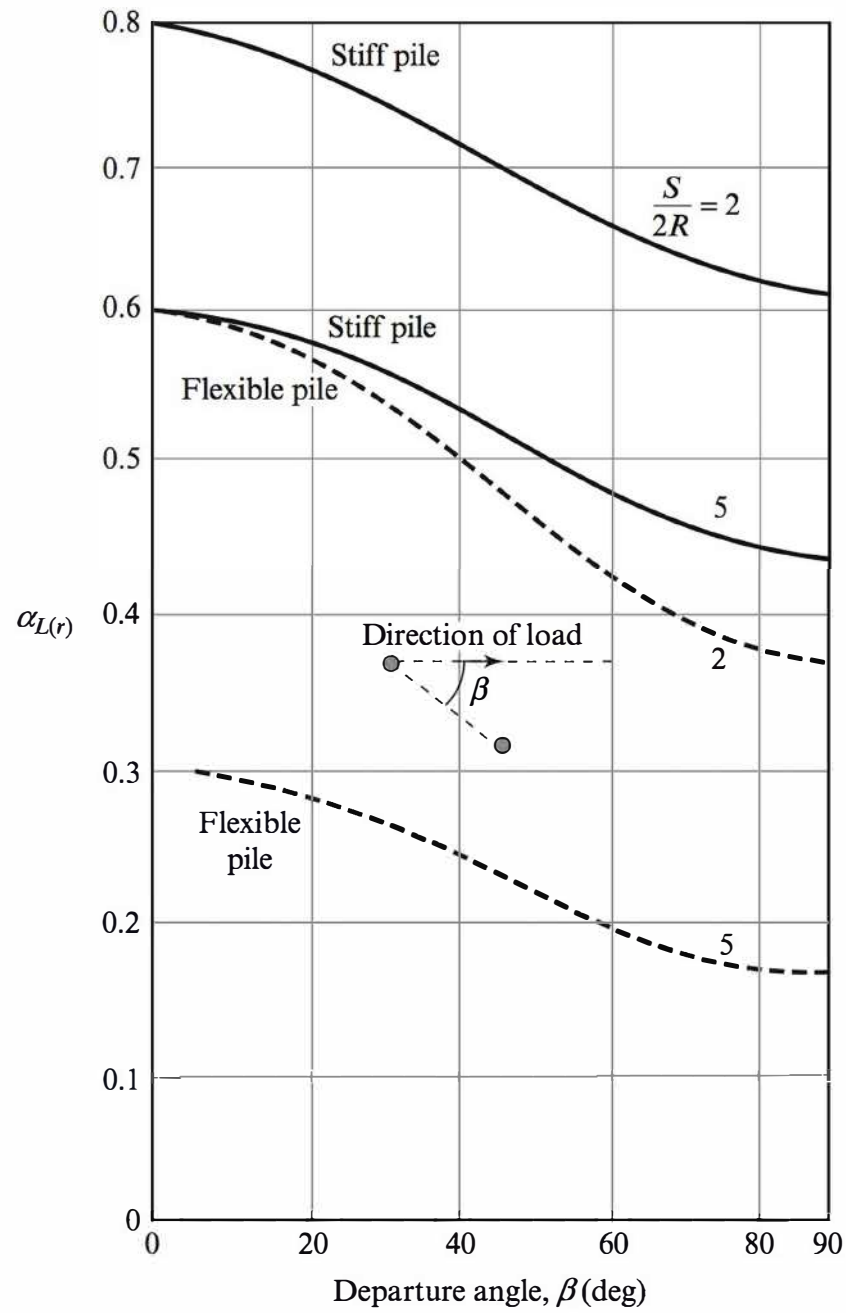

Figure 11.14 Variation of $\alpha_{L(r)}$ (from Poulos, 1971)

Source: Poulos, H.G. (1971). "Behavior of Laterally Loaded Piles: II. Pile Groups," *Journal of the Soil Mechanics and Foundations Division*, ASCE, Vol. 97, No. SM5, pp. 733–751. With permission from ASCE.

Hence, for the group pile and cap,

$$k_{x(T)} = \frac{\sum_{1}^{n} k_x}{\sum_{r=1}^{n} \alpha_{L(r)}} + G_s D_f \bar{S}_{x1} \tag{11.36}$$

and

$$c_{x(T)} = \frac{\sum_{1}^{n} c_x}{\sum_{r=1}^{n} \alpha_{L(r)}} + D_f r_0 \bar{S}_{x2} \sqrt{G_s \rho_s} \tag{11.37}$$

Copyright 2017 Cengage Learning. All Rights Reserved. May not be copied, scanned, or duplicated, in whole or in part. Due to electronic rights, some third party content may be suppressed from the eBook and/or eChapter(s). Editorial review has deemed that any suppressed content does not materially affect the overall learning experience. Cengage Learning reserves the right to remove additional content at any time if subsequent rights restrictions require it.

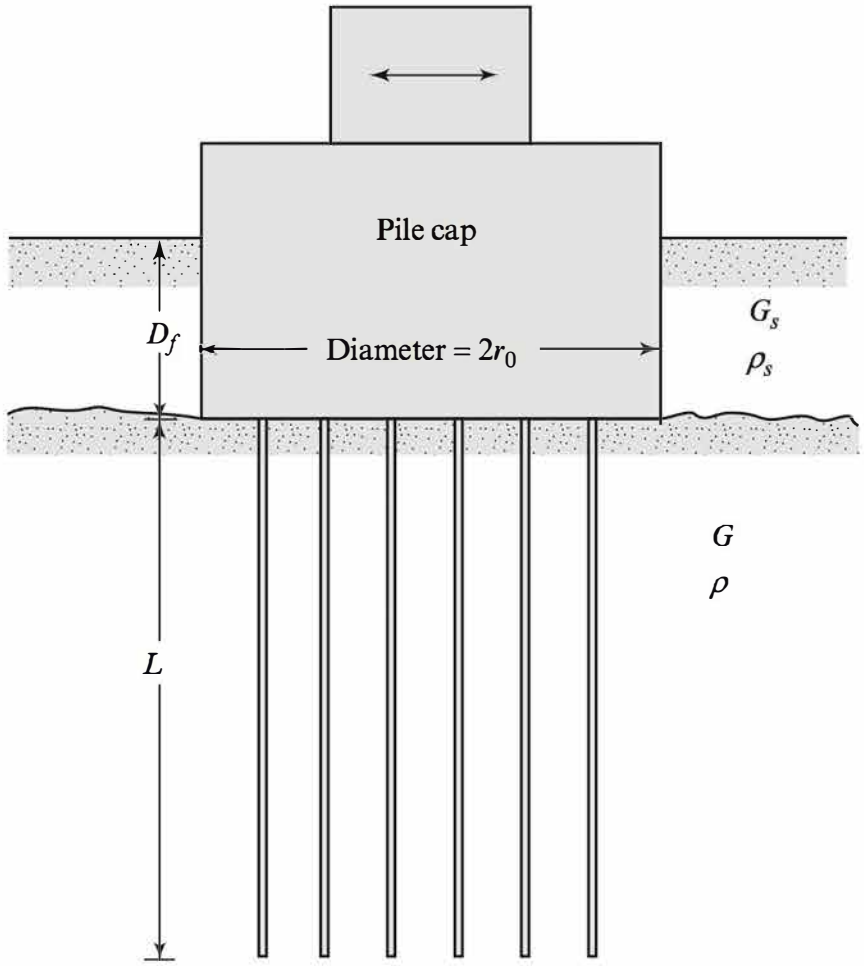

Figure 11.15 Effect of pile cap on stiffness and damping constants—sliding vibration

The damping ratio D_x for the system can then be determined as

$$\boxed{D_x = \frac{c_{x(T)}}{2\sqrt{k_{x(T)}m}}} \tag{11.38}$$

where m = mass of the pile cap and the machine supported. The damped natural frequency f_m is given as

$$f_m = \frac{1}{2\pi}\left[\sqrt{\frac{k_{z(T)}}{m}}\right]\left[\sqrt{1-2D_x^2}\right] \quad \text{(for constant force excitation)} \tag{11.39}$$

and

$$f_n = \frac{1}{2\pi}\frac{\sqrt{k_{x(T)}/m}}{\sqrt{1-2D_x^2}} \tag{11.40}$$

The amplitudes of vibration can be calculated using Eqs. (5.58), (5.59), (5.60), and (5.61). While using these equations, k_x needs to be replaced by $k_{x(T)}$.

Rocking Vibration for Single Pile

$$k_\theta = \frac{E_P I_P}{R} f_{\theta 1} \tag{11.41}$$

Copyright 2017 Cengage Learning. All Rights Reserved. May not be copied, scanned, or duplicated, in whole or in part. Due to electronic rights, some third party content may be suppressed from the eBook and/or eChapter(s). Editorial review has deemed that any suppressed content does not materially affect the overall learning experience. Cengage Learning reserves the right to remove additional content at any time if subsequent rights restrictions require it.

$$c_\theta = \frac{E_P I_P}{\upsilon_s} f_{\theta 2} \tag{11.42}$$

The terms E_P, I_P, υ_s and R have been defined in relation to Eqs. (11.30) and (11.31). The numerical values of $f_{\theta 1}$ and $f_{\theta 2}$ obtained by Novak (1974) and Novak and El-Sharnouby (1987) are given in Table 11.2.

Table 11.2 The Stiffness and Damping Parameters for Rocking Vibration ($L/R > 25$)

Poisson's ratio of soil, μ	(E_P/G)	$f_{\theta 1}$	$f_{\theta 2}$
0.25	10,000	0.2135	0.1577
	2,500	0.2998	0.2152
	1,000	0.3741	0.2598
	500	0.4411	0.2953
	250	0.5186	0.3299
0.4	10,000	0.2207	0.1634
	2,500	0.3097	0.2224
	1,000	0.3860	0.2677
	500	0.4547	0.3034
	250	0.5336	0.3377

Note: G = shear modulus of soil.

For coupling between horizontal translation and rocking, the cross stiffness and damping constants are as follows:

$$\boxed{k_{x\theta} = \frac{E_P I_P}{R} f_{x\theta 1}} \tag{11.43}$$

$$\boxed{c_{x\theta} = \frac{E_P I_P}{R \upsilon_s} f_{x\theta 2}} \tag{11.44}$$

The numerical values for $f_{x\theta 1}$ and $f_{x\theta 2}$ are given in Table 11.3, which is based on the works of Novak (1974) and Novak and El-Sharnouby (1983).

Table 11.3 Values of $f_{x\theta 1}$ and $f_{x\theta 2}$

Poisson's ratio of soil, μ	(E_P/G)	$f_{x\theta 1}$	$f_{x\theta 2}$
0.25	10,000	−0.0217	−0.0333
	2,500	−0.0429	−0.0646
	1,000	−0.0668	−0.0985
	500	−0.0929	−0.1337
	250	−0.1281	−0.1786

Copyright 2017 Cengage Learning. All Rights Reserved. May not be copied, scanned, or duplicated, in whole or in part. Due to electronic rights, some third party content may be suppressed from the eBook and/or eChapter(s). Editorial review has deemed that any suppressed content does not materially affect the overall learning experience. Cengage Learning reserves the right to remove additional content at any time if subsequent rights restrictions require it.

Poisson's ratio of soil, μ	(E_P/G)	$f_{x\theta 1}$	$f_{x\theta 2}$
0.4	10,000	−0.0232	−0.0358
	2,500	−0.0459	−0.0692
	1,000	−0.0714	−0.1052
	500	−0.0991	−0.1425
	250	−0.1365	−0.1896

Note: G = shear modulus of soil.

For group piles the stiffness $k_{\theta(g)}$ and damping $c_{\theta(g)}$ constants can be written as

$$\boxed{k_{\theta(g)} = \sum_{1}^{n}\left[k_\theta + k_z x_r^2 + k_x Z_c^2 - 2Z_c k_{x\theta}\right]} \tag{11.45}$$

The terms x_r and Z_c are defined in Figure 11.16. Similarly,

$$\boxed{c_{\theta(g)} = \sum_{1}^{n}\left[c_\theta + c_z x_r^2 + c_x Z_c^2 - 2Z_c c_{x\theta}\right]} \tag{11.46}$$

The stiffness $k_{\theta(\text{cap})}$ and damping $c_{\theta(\text{cap})}$ for the pile cap can be obtained from the following equations (Prakash and Puri, 1988):

$$k_{\theta(\text{cap})} = G_s r_0^2 D_f \bar{S}_{\theta 1} + G_s r_0^2 D_f \left[\frac{\delta^2}{3} + \left(\frac{Z_c}{r_0}\right)^2 - \delta\left(\frac{Z_c}{r_0}\right)\right]\bar{S}_{x1} \tag{11.47}$$

and

$$c_{\theta(\text{cap})} = \delta r_0^4 \sqrt{G_s \rho_s}\left\{\bar{S}_{\theta 2} + \left[\frac{\delta^2}{3} + \left(\frac{Z_c}{r_0}\right)^2 - \delta\left(\frac{Z_c}{r_0}\right)\right]\bar{S}_{x2}\right\} \tag{11.48}$$

where r_0 = equivalent radius of the pile cap

$$\delta = \frac{D_f}{r_0} \tag{11.49}$$

Thus, the total stiffness $k_{\theta(T)}$ and damping $c_{\theta(T)}$ constants are

$$k_{\theta(T)} = k_{\theta(g)} + k_{\theta(\text{cap})} \tag{11.50}$$

and

$$c_{\theta(T)} = c_{\theta(g)} + c_{\theta(\text{cap})} \tag{11.51}$$

Once the magnitudes of $k_{\theta(T)}$ and $c_{\theta(T)}$ are determined, the response of the system can be calculated in the same manner as outlined in Chapter 2 and Section 5.5.

Copyright 2017 Cengage Learning. All Rights Reserved. May not be copied, scanned, or duplicated, in whole or in part. Due to electronic rights, some third party content may be suppressed from the eBook and/or eChapter(s). Editorial review has deemed that any suppressed content does not materially affect the overall learning experience. Cengage Learning reserves the right to remove additional content at any time if subsequent rights restrictions require it.

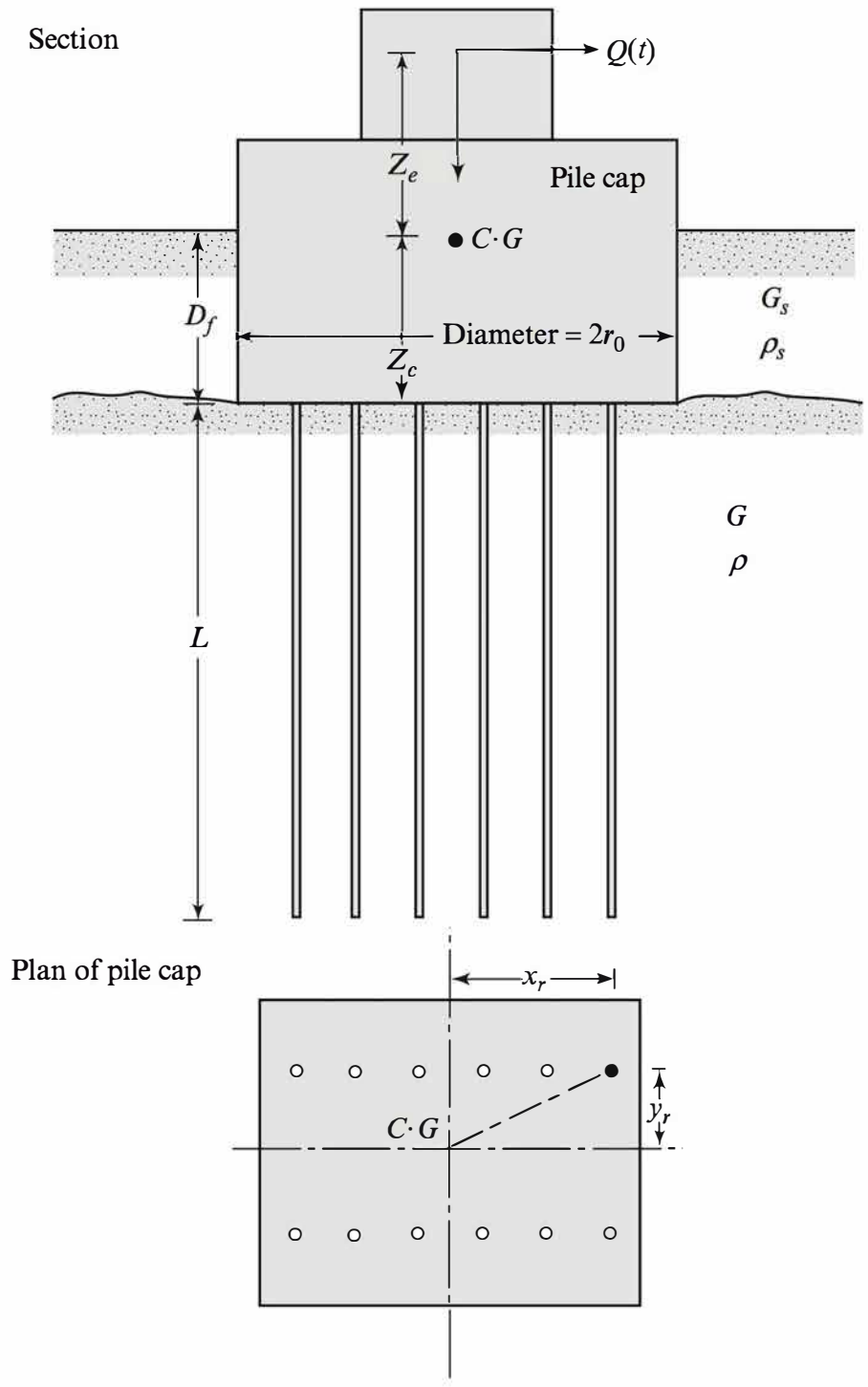

Figure 11.16 Definition of parameters in Eqs. (11.45) and (11.46)

For convenience, this is outlined here as well.

a. Damping ratio:

$$D_\theta = \frac{c_{\theta(T)}}{2\sqrt{k_{\theta(T)} I_g}} \tag{11.52}$$

where I_g = mass moment of inertia for the pile cap and the machinery about the centroid of the block. Referring to Figure 11.17a,

$$\begin{aligned} I_g &= \text{mass moment of inertia about the } y \text{ axis} \\ &= \frac{m}{12}(L^2 + h^2) \end{aligned} \tag{11.53a}$$

and, similarly, referring to Figure 11.17b,

Copyright 2017 Cengage Learning. All Rights Reserved. May not be copied, scanned, or duplicated, in whole or in part. Due to electronic rights, some third party content may be suppressed from the eBook and/or eChapter(s). Editorial review has deemed that any suppressed content does not materially affect the overall learning experience. Cengage Learning reserves the right to remove additional content at any time if subsequent rights restrictions require it.

$$I_g = \text{mass moment of inertia about the } y \text{ axis}$$
$$= \frac{m}{12}(3r_0^2 + h^2) \tag{11.53b}$$

b. *Undamped natural frequency:*

$$\omega_n = \sqrt{\frac{k_{\theta(T)}}{I_g}} \tag{11.54}$$

$$f_n = \frac{1}{2\pi}\sqrt{\frac{k_{\theta(T)}}{I_g}} \tag{11.55}$$

c. *Damped natural frequency:*

$$f_m = f_n\sqrt{1 - 2D_\theta^2} \text{ (for constant force excitation)} \tag{11.56}$$

$$f_m = \frac{f_n}{\sqrt{1 - 2D_\theta^2}} \text{ (for rotating mass-type excitation)} \tag{11.57}$$

The amplitude of vibration can be determined by using Eqs. (5.46), (5.47), (5.48), and (5.49).

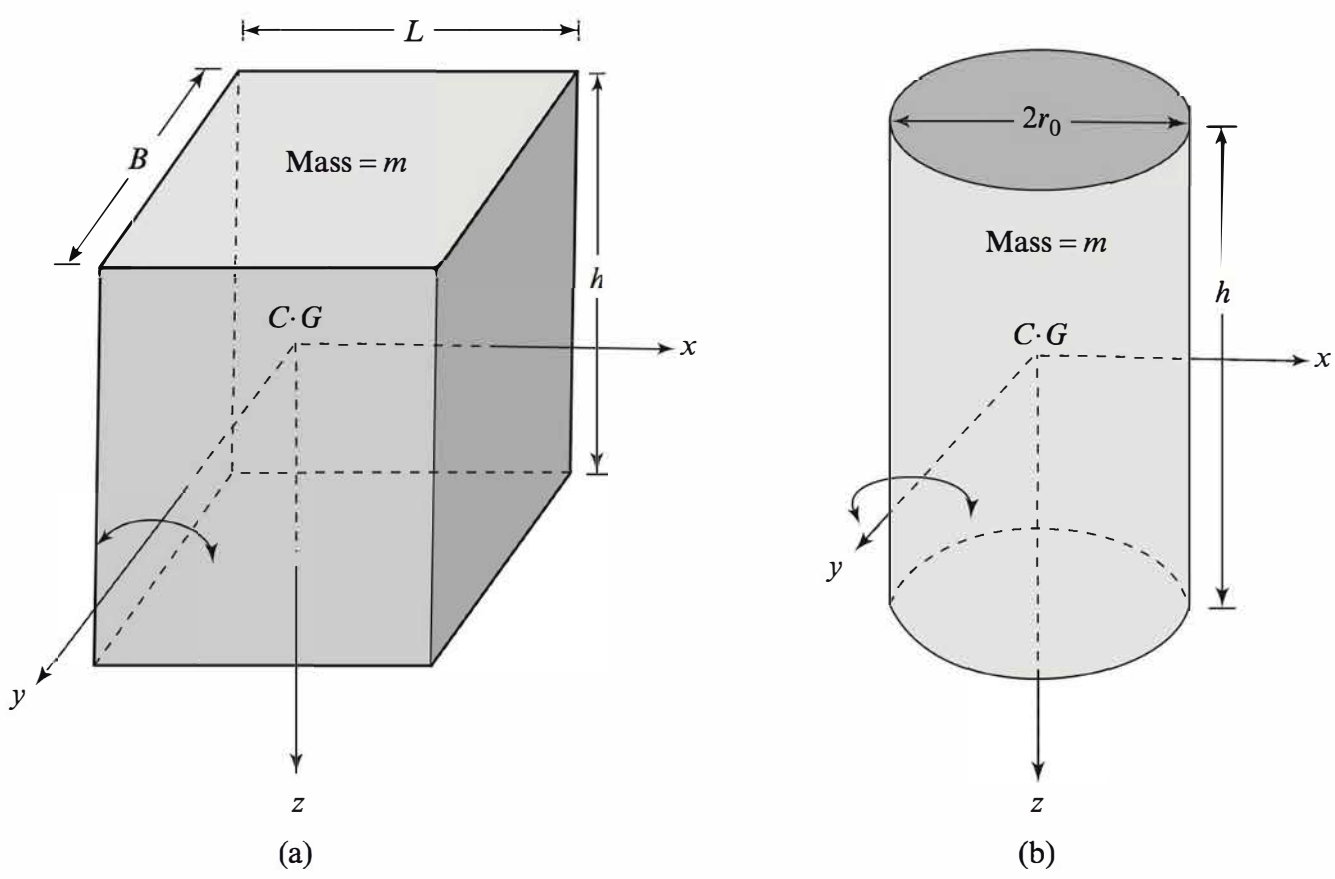

Figure 11.17 Mass moment of inertia I_g

Copyright 2017 Cengage Learning. All Rights Reserved. May not be copied, scanned, or duplicated, in whole or in part. Due to electronic rights, some third party content may be suppressed from the eBook and/or eChapter(s). Editorial review has deemed that any suppressed content does not materially affect the overall learning experience. Cengage Learning reserves the right to remove additional content at any time if subsequent rights restrictions require it.

EXAMPLE 11.4

Refer to Example 11.2. Determine $k_{x(T)}$ and $c_{x(T)}$ for the sliding mode of vibration. Assume Poisson's ratio of soil, $\mu = 0.25$.

SOLUTION:

Stiffness and damping constants for single pile: From Eqs. (11.30) and (11.31),

$$k_x = \frac{E_P I_P}{R^3} f_{x1}$$

and

$$c_x = \frac{E_P I_P}{R^2 v_s} f_{x2}$$

Given $E_P = 21 \times 10^6 \text{kPa}$; $R = 0.17$ m.

$$I_P = \frac{\pi}{4} R^4 = \frac{\pi}{4}(0.17)^4 = 6.54 \times 10^{-4} \text{m}^4$$

$$v_s = \sqrt{\frac{G}{\rho}} = \sqrt{\frac{28000 \times 9.81}{19}} = 120.24 \text{ m/s}$$

$$\frac{E_P}{G} = \frac{21 \times 10^6}{28,000} = 750$$

From Table 11.1, for $\mu = 0.25$ and $E_P/G = 750$, $f_{x1} = 0.027$ and $f_{x2} = 0.068$. So

$$k_x = \frac{E_P I_P}{R^3} f_{x1} = \frac{(21 \times 10^6 \times 10^3)(6.54 \times 10^{-4})}{(0.17)^3}(0.027)$$
$$= 75.48 \times 10^6 \text{ N/m}$$

$$c_x = \frac{E_P I_P}{R^3 v_s} f_{x2} = \frac{(21 \times 10^6 \times 10^3)(6.54 \times 10^{-4})}{(0.17)^2 (120.24)}(0.068)$$
$$= 268.76 \times 10^3 \text{ N·s/m}$$

Stiffness and damping constants for group pile: From Eqs. (11.32) and (11.33),

$$k_{x(g)} = \frac{\sum_1^n k_x}{\sum_{r=1}^n \alpha_{L(r)}}$$

Copyright 2017 Cengage Learning. All Rights Reserved. May not be copied, scanned, or duplicated, in whole or in part. Due to electronic rights, some third party content may be suppressed from the eBook and/or eChapter(s). Editorial review has deemed that any suppressed content does not materially affect the overall learning experience. Cengage Learning reserves the right to remove additional content at any time if subsequent rights restrictions require it.

and

$$c_{x(g)} = \frac{\sum_{1}^{n} c_x}{\sum_{r=1}^{n} \alpha_{L(r)}}$$

To find $\alpha_{L(r)}$ with A as the *reference pile*, the following table can be prepared using Figure 11.14. Assume piles to be flexible.

Reference pile →		A	
Interacting pile ↓	β**(deg)**	$\frac{S}{2R}$	$\alpha_{L(r)}$
A	0	0.00	1.00
B	0	4.41	0.32
C	45	6.24	0.27
D	90	4.41	0.18
			1.77

Similarly, for the other reference piles, $\sum \alpha_{L(r)}$ will be 1.77. So, the average value of $\sum_{r=1}^{n} \alpha_{L(r)} = 1.77$. Thus,

$$k_{x(g)} = \frac{(4)(75.48 \times 10^6)}{1.77} = 170.58 \times 10^6 \text{ N/m}$$

$$c_{x(g)} = \frac{(4)(268.76 \times 10^3)}{1.77} = 607.37 \times 10^3 \text{ N·s/m}$$

Stiffness and damping for pile cap: From Eqs. (11.34) and (11.35),

$$k_{x(\text{cap})} = G_s D_f \bar{S}_{x1}$$

and

$$c_{x(\text{cap})} = D_f r_0 \bar{S}_{x2} \sqrt{G_s \rho_s}$$

From Chapter 5 with $\mu = 0.25$, $\bar{S}_{x1} = 4.0$ and $\bar{S}_{x2} = 9.10$. So

$$\begin{aligned} k_{x(\text{cap})} &= (28000 \times 10^3) \times (1.5) \times (4.0) \\ &= 168 \times 10^6 \text{ N/m} \end{aligned}$$

$$\begin{aligned} c_{x(\text{cap})} &= (1.5) \times (1.185) \times (9.1) \sqrt{\frac{(28000 \times 10^3) \times (19 \times 10^3)}{9.81}} \\ &= 3.77 \times 10^6 \text{ N·s/m} \end{aligned}$$

Copyright 2017 Cengage Learning. All Rights Reserved. May not be copied, scanned, or duplicated, in whole or in part. Due to electronic rights, some third party content may be suppressed from the eBook and/or eChapter(s). Editorial review has deemed that any suppressed content does not materially affect the overall learning experience. Cengage Learning reserves the right to remove additional content at any time if subsequent rights restrictions require it.

Total stiffness and damping:

$$k_{x(T)} = k_{x(g)} + k_{x(\text{cap})} = 170.58 \times 10^6 + 168 \times 10^6$$
$$= \mathbf{338.58 \times 10^6\ N/m}$$
$$c_{x(T)} = c_{x(g)} + c_{x(\text{cap})} = 607.37 \times 10^3 + 3.77 \times 10^6$$
$$= \mathbf{4.38 \times 10^6\ N \cdot s/m}$$

EXAMPLE 11.5

In Example 11.4, if the weight of the machine being supported is 90 kN, determine the damping ratio.

SOLUTION:

Weight of the pile cap: 190.512 kN

Total weight of the pile cap and machine:

$$190.512 + 90 = 280.512 \text{ kN} = 280512 \text{ N}$$

From Eq. (11.38),

$$D_x = \frac{c_{x(T)}}{2\sqrt{k_{x(T)}m}} = \frac{4.38 \times 10^6}{2\sqrt{(338.58 \times 10^6)[280512/(9.81)]}} = \mathbf{0.705}$$

EXAMPLE 11.6

Refer to Example 11.2. Determine $k_{\theta(T)}$ and $c_{\theta(T)}$ for the rocking mode of vibration. Assume Poisson's ratio of soil to be 0.25.

SOLUTION:

Stiffness and damping constants for single pile: From Eqs. (11.41) and (11.42),

$$k_\theta = \frac{E_P I_P}{R} f_{\theta 1}$$

and

$$c_\theta = \frac{E_P I_P}{v_s} f_{\theta 2}$$

$$\frac{E_P}{G} = \frac{21 \times 10^6}{28{,}000} = 750$$

Copyright 2017 Cengage Learning. All Rights Reserved. May not be copied, scanned, or duplicated, in whole or in part. Due to electronic rights, some third party content may be suppressed from the eBook and/or eChapter(s). Editorial review has deemed that any suppressed content does not materially affect the overall learning experience. Cengage Learning reserves the right to remove additional content at any time if subsequent rights restrictions require it.

From Table 11.2, for $\mu = 0.25$ and $E_P/G = 750$, the values of $f_{\theta 1}$ and $f_{\theta 2}$ are 0.39 and 0.275, respectively.

$$k_\theta = \frac{(21 \times 10^6 \times 10^3) \times (6.56 \times 10^{-4})}{0.17}(0.39)$$
$$= 31.60 \times 10^6 \text{ N·m/rad}$$
$$c_\theta = \frac{(21 \times 10^6 \times 10^3) \times (6.56 \times 10^{-4})}{120.24}(0.275)$$
$$= 31.51 \times 10^3 \text{ N·m·s/rad}$$

Cross-stiffness and cross-damping constants: From Eqs. (11.43) and (11.44),

$$k_{x\theta} = \frac{E_P I_P}{R^2} f_{x\theta 1}$$
$$c_{x\theta} = \frac{E_P I_P}{R v_s} f_{x\theta 2}$$

From Table 11.3, $f_{x\theta 1} = -0.076$ and $f_{x\theta 2} = -0.115$. Thus,

$$k_{x\theta} = \frac{(21 \times 10^6 \times 10^3) \times (6.54 \times 10^{-4})}{(0.17)^2}(-0.076)$$
$$= -36.23 \times 10^6 \text{ N/rad}$$
$$c_{x\theta} = \frac{(21 \times 10^6 \times 10^3)(6.54 \times 10^{-4})}{(0.17)(120.24)}(-0.115)$$
$$= -77.50 \times 10^3 \text{ N·s/rad}$$

Stiffness and damping constants for pile group: From Eqs. (11.45) and (11.46),

$$k_{\theta(g)} = \sum_1^n [k_\theta + k_z x_r^2 + k_x Z_c^2 - 2Z_c k_{x\theta}]$$

and

$$c_{\theta(g)} = \sum_1^n [c_\theta + c_z x_r^2 + c_x Z_c^2 - 2Z_c c_{x\theta}]$$

From this problem,

$$n = 4$$
$$k_\theta = 31.60 \times 10^6 \text{ N·m/rad}$$
$$k_z = 378 \times 10^6 \text{ N/m} \qquad \text{(from problem 11.2)}$$
$$x_r = (1.5/2) = 0.75 \text{ m}$$
$$k_x = 75.58 \times 10^6 \text{ N/m} \qquad \text{(from Problem 11.4)}$$
$$k_{x\theta} = -36.23 \times 10^6 \text{ N/m}$$
$$Z_c = 0.9 \text{ m}$$

Copyright 2017 Cengage Learning. All Rights Reserved. May not be copied, scanned, or duplicated, in whole or in part. Due to electronic rights, some third party content may be suppressed from the eBook and/or eChapter(s). Editorial review has deemed that any suppressed content does not materially affect the overall learning experience. Cengage Learning reserves the right to remove additional content at any time if subsequent rights restrictions require it.

So

$$k_{\theta(g)} = 4[31.6 \times 10^6 + (378 \times 10^6)(0.75)^2 + (75.58 \times 10^6)(0.9)^2 - (2)(0.9)(-36.33 \times 10^6)$$
$$= 1.48 \times 10^9 \text{ N·m/rad}$$

Similarly, with

$$n = 4$$
$$c_\theta = 31.51 \times 10^3 \text{ N·m·s/rad}$$
$$c_z = 943.11 \times 10^3 \text{ N·s/m} \quad \text{(from problem 11.2)}$$
$$x_r = 0.75 \text{ m}$$
$$c_x = 268.76 \times 10^3 \text{ N·s/m} \quad \text{(from problem 11.4)}$$
$$c_{x\theta} = -77.50 \times 10^3 \text{ N·s/rad}$$
$$Z_c = 0.9 \text{ m}$$

the result is

$$c_{\theta(g)} = 4[(31.51 \times 10^3) + (943.11 \times 10^3)(0.75)^2 + (268.76 \times 10^3)(0.9)^2 - (2)(0.9)(-77.5 \times 10^3)]$$
$$= 3.68 \times 10^6 \text{ N·m·s/rad}$$

Stiffness and damping of pile cap: From Eq. (11.47),

$$k_{\theta(\text{cap})} = G_s r_0^2 D_f \bar{S}_{\theta 1} + G_s r_0^2 D_f \left[\frac{\delta^2}{3} + \left(\frac{Z_c}{r_0}\right)^2 - \delta\left(\frac{Z_c}{r_0}\right)\right]\bar{S}_{x1}$$

where

$$\delta = \frac{D_f}{r_0} = \frac{1.5}{1.185} = 1.266$$

So

$$k_{\theta(\text{cap})} = (28000 \times 10^3)(1.185)^2(1.5)(2.5) + (28000 \times 10^3)(1.185)^2(1.5) \times \left[\frac{(1.266)^2}{3} + \left(\frac{0.9}{1.185}\right)^2 - (1.266)\left(\frac{0.9}{1.185}\right)\right](4)$$
$$= 182.73 \times 10^6 \text{ N·m/rad}$$

Again, from Eq. (11.48)

$$c_{\theta(\text{cap})} = \delta r_0^4 \sqrt{G_s \rho_s}\left\{\bar{S}_{\theta 2} + \left[\frac{\delta^2}{3} + \left(\frac{Z_c}{r_0}\right)^2 - \delta\left(\frac{Z_c}{r_0}\right)\right]\bar{S}_{x2}\right\}$$

Copyright 2017 Cengage Learning. All Rights Reserved. May not be copied, scanned, or duplicated, in whole or in part. Due to electronic rights, some third party content may be suppressed from the eBook and/or eChapter(s). Editorial review has deemed that any suppressed content does not materially affect the overall learning experience. Cengage Learning reserves the right to remove additional content at any time if subsequent rights restrictions require it.

or

$$c_{\theta(\text{cap})} = (1.266)(1.185)^4\sqrt{(28000 \times 10^3)(19 \times 10^3)/9.81}$$
$$\left\{1.8 + \left[\frac{(1.266)^2}{3} + \left(\frac{0.9}{1.185}\right)^2 - (1.266)\left(\frac{0.9}{1.185}\right)\right](9.1)\right\}$$
$$= 1.84 \times 10^6\,\text{N·m·s/rad}$$

Total stiffness and damping:

$$k_{\theta(T)} = k_{\theta(g)} + k_{\theta(\text{cap})} = 1.48 \times 10^9 + 182.73 \times 10^6$$
$$= \mathbf{1.66 \times 10^9\,N{\cdot}m/rad}$$
$$c_{\theta(T)} = c_{\theta(g)} + c_{\theta(\text{cap})} = 3.68 \times 10^6 + 1.84 \times 10^6$$
$$= \mathbf{5.52 \times 10^6\,N{\cdot}m{\cdot}s/rad}$$

11.5 TORSIONAL VIBRATION OF EMBEDDED PILES

Torsional vibration of an embedded pile was analyzed by Novak and Howell (1977) and Novak and El-Sharnouby (1983). According to these analyses, the pile (Figure 11.18) is assumed to be vertical, circular in cross section (radius = R), elastic, end-bearing, and perfectly connected to the soil. The soil is considered to be a linear, viscoelastic medium with frequency-independent material damping of the hysteretic type. Referring to Figure 11.18, the pile is undergoing a complex harmonic rotation around the vertical axis, which can be described as

$$\alpha(z,t) = \alpha(z)e^{i\omega t} \tag{11.58}$$

where $\alpha(z)$ = complex amplitude of pile rotation at a depth z
$i = \sqrt{-1}$

The motion of the pile is resisted by a torsional soil reaction. The elastic soil reaction setting on a pile element dz can then be given as

$$GR^2(S_{\alpha 1} + iS_{\alpha 2})[\alpha(z,t)]dz \tag{11.59}$$

where

$$S_{\alpha 1}(a_0) = \text{stiffness parameter}$$
$$= 2\pi\left(2 - a_0\frac{J_0J_1 + Y_0Y_1}{J_1^2 + Y_1^2}\right) \tag{11.60}$$

$$S_{\alpha 2}(a_0) = \text{damping parameter}$$
$$= \frac{4}{J_1^2 + Y_1^2} \tag{11.61}$$

Copyright 2017 Cengage Learning. All Rights Reserved. May not be copied, scanned, or duplicated, in whole or in part. Due to electronic rights, some third party content may be suppressed from the eBook and/or eChapter(s). Editorial review has deemed that any suppressed content does not materially affect the overall learning experience. Cengage Learning reserves the right to remove additional content at any time if subsequent rights restrictions require it.

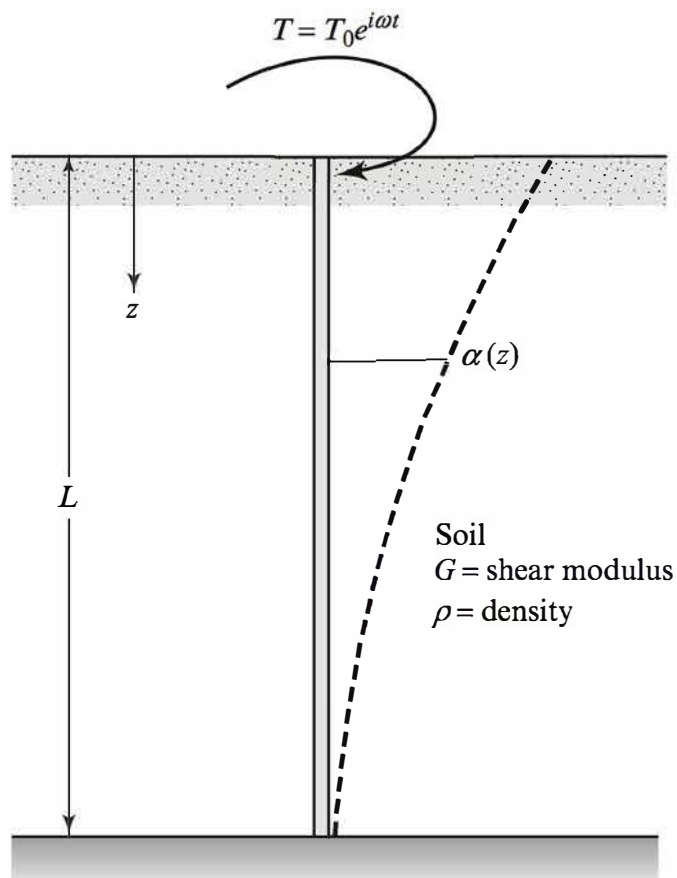

Figure 11.18 Torsional vibration of embedded pile

$$a_0 = \text{dimensionless frequency} = \omega R\sqrt{\frac{\rho}{G}}$$

R = pile radius

G = shear modulus of soil

ρ = density of soil

$J_0(a_0), J_1(a_0)$ = Bessel functions of the first kind and of order 0 and 1, respectively

$Y_0(a_0), Y_1(a_0)$ = Bessel functions of the second kind and of order 0, and 1, respectively

The parameters $S_{\alpha 1}$ and $S_{\alpha 2}$ also depend on the material damping of the soil. It was mentioned in Chapter 5 that the material damping is more important for torsional mode of vibration than any other. This damping can be included by addition of an out-of-phase complement to the soil shear modulus, or

$$G^* = G_1 + iG_2 = G_1(1 + i\tan\delta) \tag{11.62}$$

where $\tan\delta = \dfrac{G_2}{G_1}$

G_1, G_2 = real and imaginary parts, respectively, of the complex shear modulus

δ = loss angle

Copyright 2017 Cengage Learning. All Rights Reserved. May not be copied, scanned, or duplicated, in whole or in part. Due to electronic rights, some third party content may be suppressed from the eBook and/or eChapter(s). Editorial review has deemed that any suppressed content does not materially affect the overall learning experience. Cengage Learning reserves the right to remove additional content at any time if subsequent rights restrictions require it.

Thus, the term G in Eq. (11.59) can be replaced by G^*. Also G^* enters Eqs. (11.60) and (11.61) through the dimensionless frequency α_0. Using this method of analysis, Novak and Howell (1977) showed that the stiffness and damping constants of fixed-tip single piles can be given as

$$\boxed{k_\alpha = \frac{G_P J}{R} f_{\alpha 1}} \tag{11.63}$$

and

$$\boxed{c_\alpha = \frac{G_P J}{\sqrt{G/\rho}} f_{\alpha 2}} \tag{11.64}$$

where G_p = shear modulus of the pile material
J = polar moment of inertia of the pile cross section
f_{a1}, f_{a2} = nondimensional parameters

The variations of $f_{\alpha 1}$ and $f_{\alpha 2}$ for timber piles ($\rho/\rho_P = 2$) are shown in Figures 11.19 and 11.20. Figures 11.21 and 11.22 show similar variations for concrete piles ($\rho/\rho_P = 0.7$). It is important to note the following:

1. For a given type of pile, the nondimensional parameter $f_{\alpha 2}$ is relatively more frequency dependent than $f_{\alpha 1}$.
2. Novak and Howell (1977) showed that the displacement of slender piles rapidly diminishes with increasing depth and varies to a lesser degree with frequency. So the effect of the tip condition is less important for slender piles in which the tip is fixed by the soil.
3. The pronounced effect of material damping may be seen in Figures 11.20 and 11.22. The value of $\tan\delta = 0.1$ is of typical order in soil. At low frequencies the material damping significantly increases the torsional damping of the pile. (Compare $f_{\alpha 2}$ values for $\tan\delta = 0.1$ to those for $\tan\delta = 0$ for a given value of a_0).

Group Piles Subjected to Torsional Vibration

If a group pile is subjected to torsional vibration as shown in Figure 11.23, the torsional stiffness $[k_{\alpha(g)}]$ and damping $[c_{\alpha(g)}]$ constants can be expressed as

$$k_{\alpha(g)} = \sum_1^n \left[k_\alpha + k_x\left(x_r^2 + y_r^2\right)\right] \tag{11.65}$$

and

$$c_{\alpha(g)} = \sum_1^n \left[c_\alpha + c_x\left(x_r^2 + y_r^2\right)\right] \tag{11.66}$$

Copyright 2017 Cengage Learning. All Rights Reserved. May not be copied, scanned, or duplicated, in whole or in part. Due to electronic rights, some third party content may be suppressed from the eBook and/or eChapter(s). Editorial review has deemed that any suppressed content does not materially affect the overall learning experience. Cengage Learning reserves the right to remove additional content at any time if subsequent rights restrictions require it.

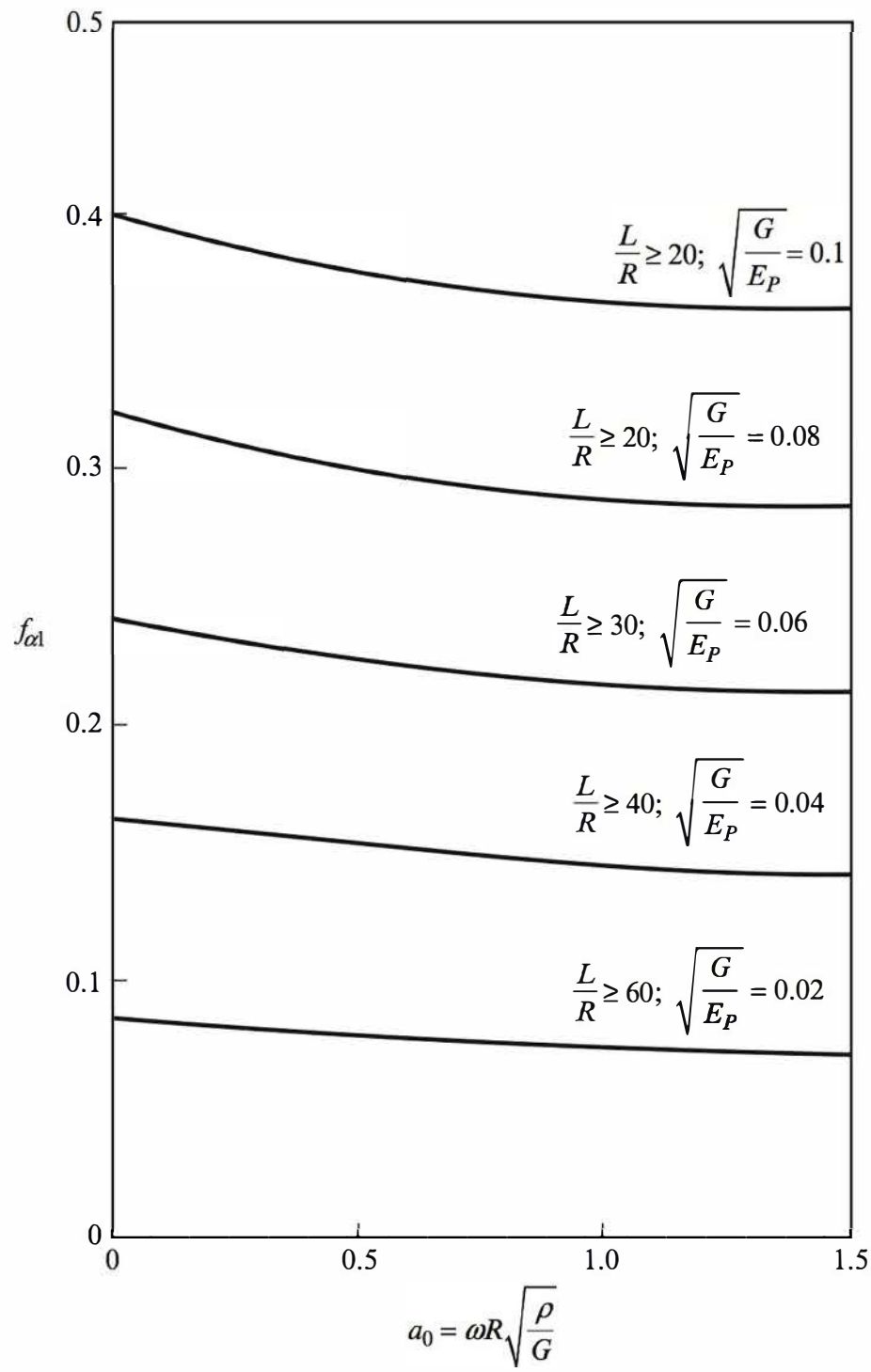

Figure 11.19 Variation of $f_{\alpha 1}$ for timber pile $\rho/\rho_P = 2$; ρ_P = density of pile material (from Novak and Howell, 1977)

Source: Novak, M. and Howell, J.F. (1977). "Torsional Vibrations of Pile Foundations," *Journal of the Geotechnical Engineering Division*, ASCE, Vol. 103, No. GT4, pp. 271–285. With permission from ASCE.

The expressions for k_α and c_α are given in Equations (11.63) and (11.64), and k_x and c_x are the stiffness and damping constants for sliding vibration [Eqs. (11.30) and (11.31)]. Note that the contribution of the sliding component for a pile in the group increases with the square of the distance ($R_r = \sqrt{x_r^2 + y_r^2}$) from the reference point. So the torsion of piles in a group is more important for a small number of large-diameter piles than a larger number of small-diameter piles.

Copyright 2017 Cengage Learning. All Rights Reserved. May not be copied, scanned, or duplicated, in whole or in part. Due to electronic rights, some third party content may be suppressed from the eBook and/or eChapter(s). Editorial review has deemed that any suppressed content does not materially affect the overall learning experience. Cengage Learning reserves the right to remove additional content at any time if subsequent rights restrictions require it.

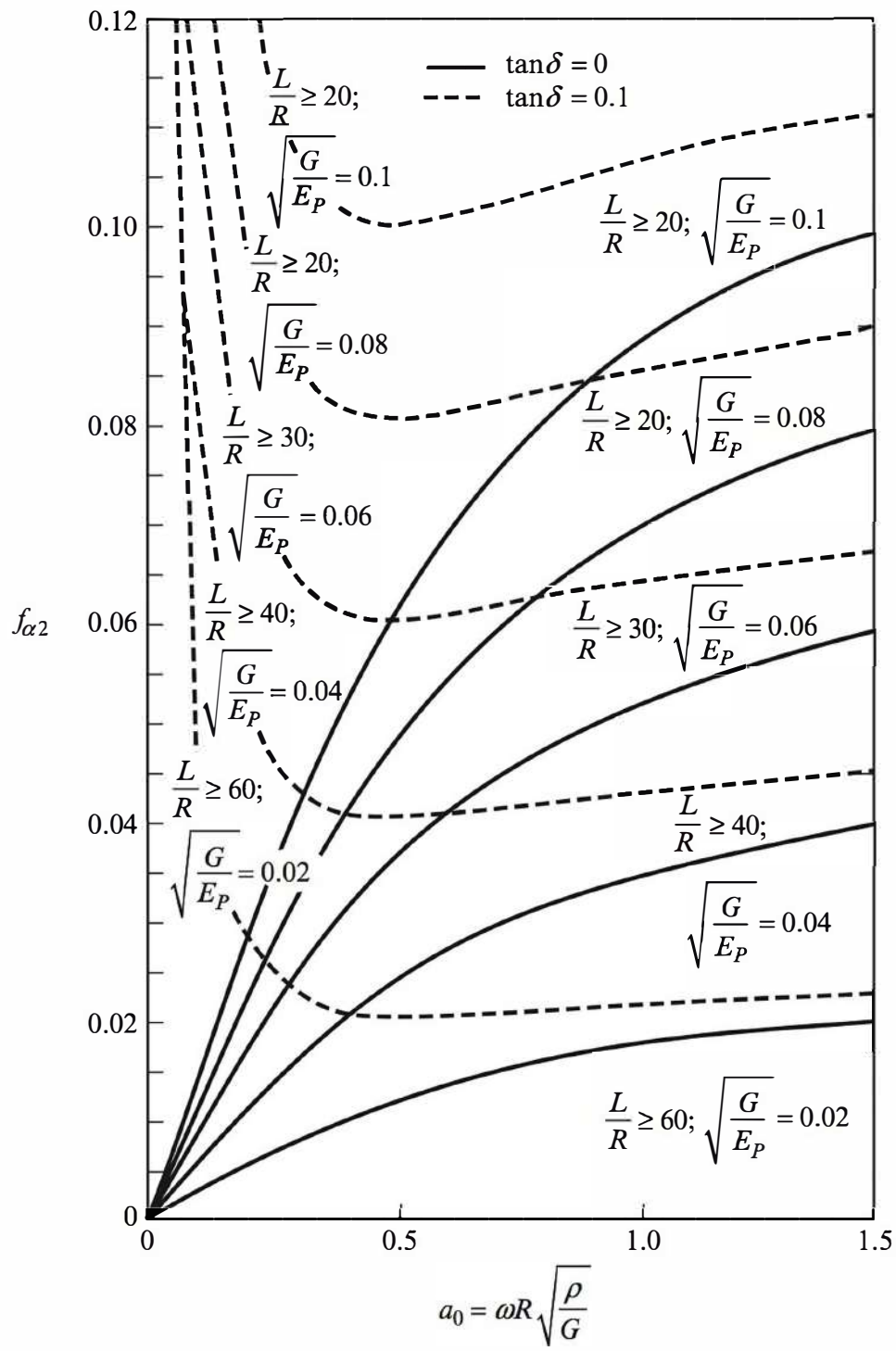

Figure 11.20 Variation of $f_{\alpha 2}$ for timber pile $\rho/\rho_P = 2$; ρ_P = density of pile material (from Novak and Howell, 1977)

Source: Novak, M. and Howell, J.F. (1977). "Torsional Vibrations of Pile Foundations," *Journal of the Geotechnical Engineering Division*, ASCE, Vol. 103, No. GT4, pp. 271–285. With permission from ASCE.

The contribution of the pile cap to the stiffness and damping constants can be obtained from Eqs. (5.126a) and (5.126b). Assuming $\bar{C}_{\alpha 1}$ and $\bar{C}_{\alpha 2}$ in those equations to be equal to zero

$$k_{\alpha(\text{cap})} = D_f G_s r_0^2 \bar{S}_{\alpha 1} \tag{11.67}$$

and

$$c_{\alpha(\text{cap})} = D_f r_0^3 \bar{S}_{\alpha 2} \sqrt{G_s \rho_s} \tag{11.68}$$

Copyright 2017 Cengage Learning. All Rights Reserved. May not be copied, scanned, or duplicated, in whole or in part. Due to electronic rights, some third party content may be suppressed from the eBook and/or eChapter(s). Editorial review has deemed that any suppressed content does not materially affect the overall learning experience. Cengage Learning reserves the right to remove additional content at any time if subsequent rights restrictions require it.

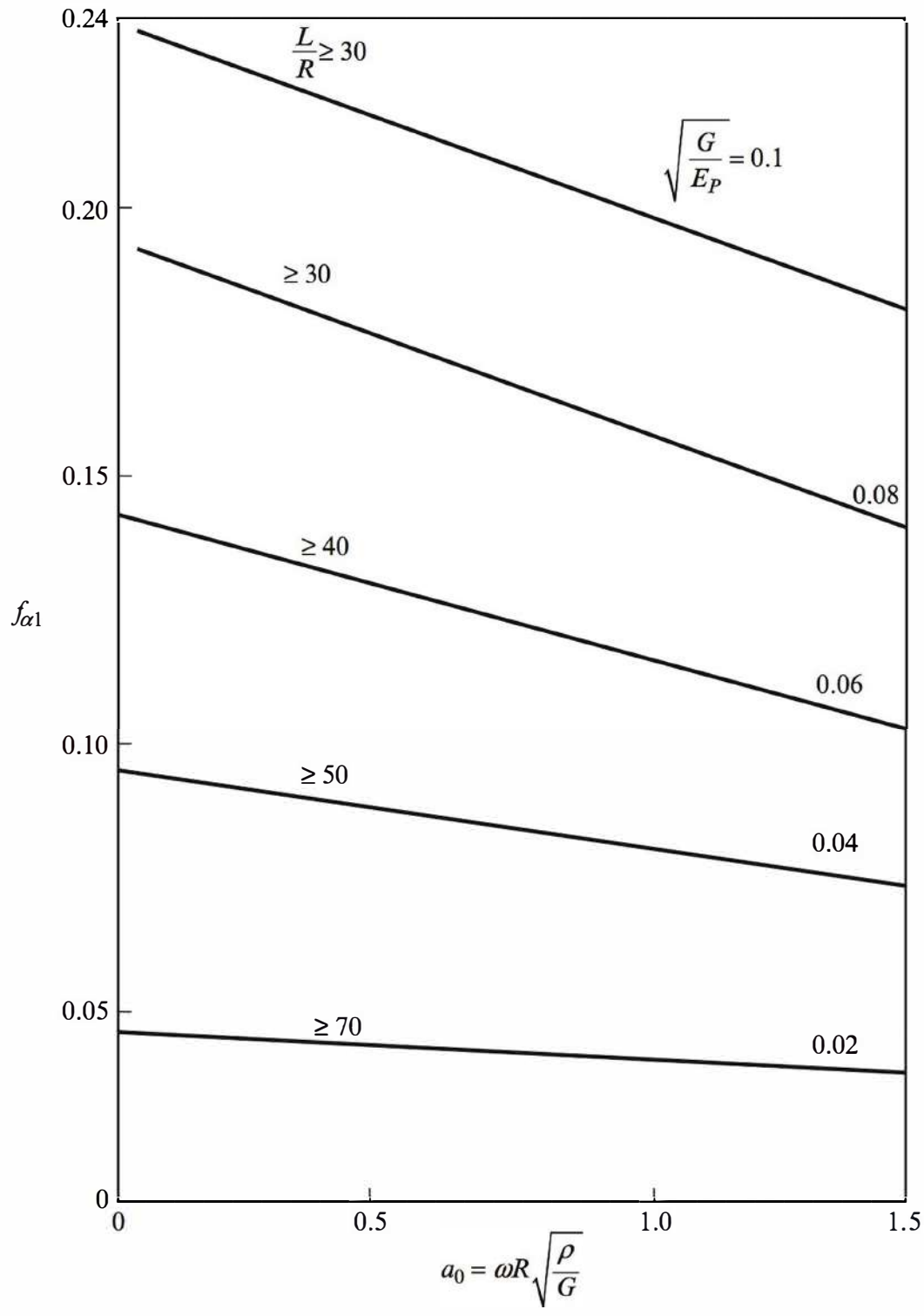

Figure 11.21 Variation of $f_{\alpha 1}$ for concrete pile $\rho/\rho_p = 2$; ρ_p = density of pile material (from Novak and Howell, 1977)

Source: Novak, M. and Howell, J.F. (1977). "Torsional Vibrations of Pile Foundations," *Journal of the Geotechnical Engineering Division*, ASCE, Vol. 103, No. GT4, pp. 271–285. With permission from ASCE.

Thus, the total stiffness $[k_{\alpha(T)}]$ and damping $[c_{\alpha(T)}]$ constants are as follows.

$$\boxed{\begin{aligned} k_{\alpha(T)} &= k_{\alpha(g)} + k_{\alpha(\text{cap})} \\ &= \sum_{1}^{n}\left[k_\alpha + k_x\left(x_r^2 + y_r^2\right)\right] + D_f G_s r_0^2 \bar{S}_{\alpha 1} \end{aligned}} \tag{11.69}$$

Copyright 2017 Cengage Learning. All Rights Reserved. May not be copied, scanned, or duplicated, in whole or in part. Due to electronic rights, some third party content may be suppressed from the eBook and/or eChapter(s). Editorial review has deemed that any suppressed content does not materially affect the overall learning experience. Cengage Learning reserves the right to remove additional content at any time if subsequent rights restrictions require it.

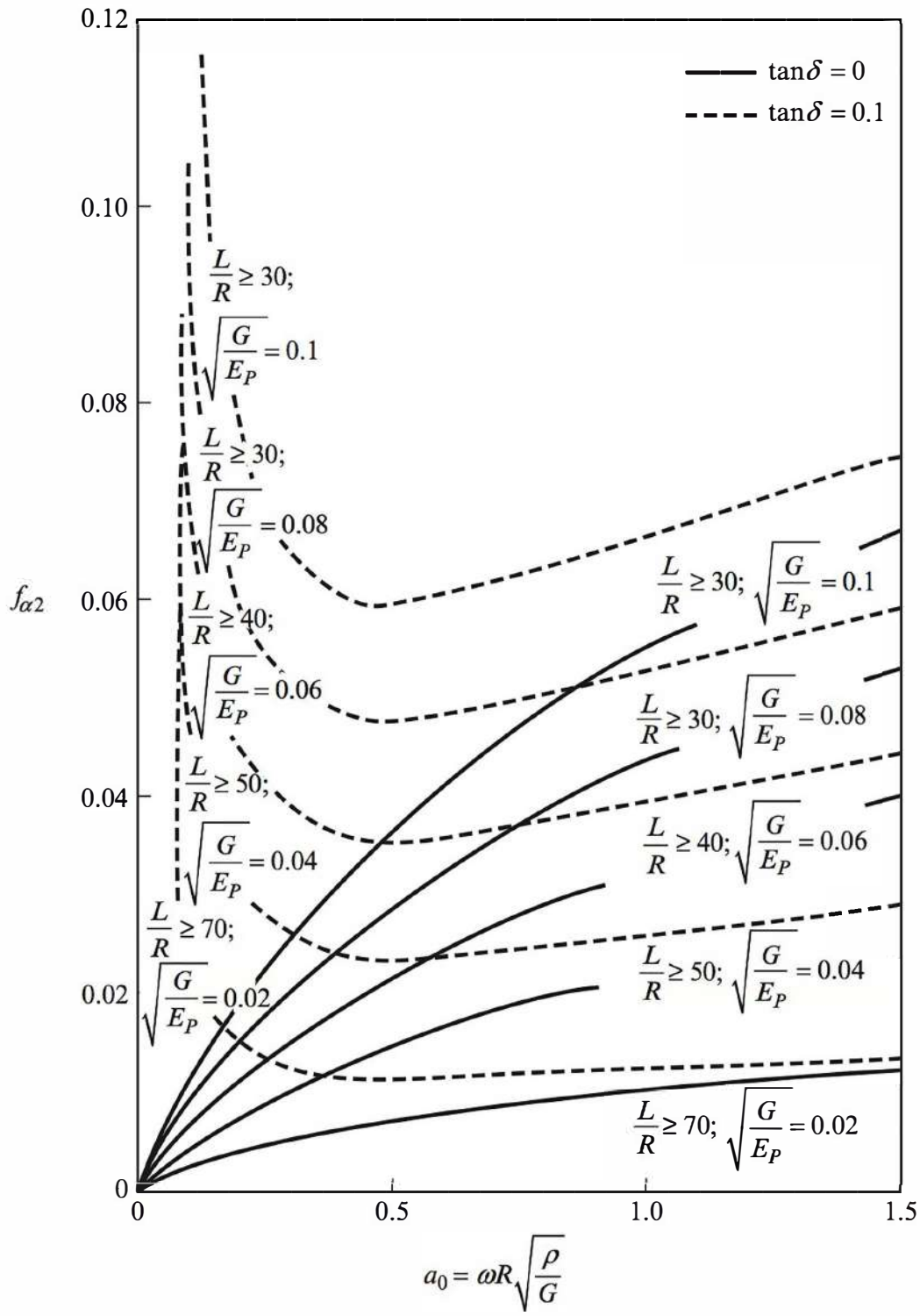

Figure 11.22 Variation of $f_{\alpha 2}$ for concrete pile $\rho/\rho_P = 0.7$; ρ_P = density of pile material (from Novak and Howell, 1977)

Source: Novak, M. and Howell, J.F. (1977). "Torsional Vibrations of Pile Foundations," *Journal of the Geotechnical Engineering Division*, ASCE, Vol. 103, No. GT4, pp. 271–285. With permission from ASCE.

$$\boxed{\begin{aligned} c_{\alpha(T)} &= c_{\alpha(g)} + c_{\alpha(\text{cap})} \\ &= \sum_{1}^{n}\left[c_\alpha + c_x\left(x_r^2 + y_r^2\right)\right] + D_f r_0^3 \bar{S}_{\alpha 2}\sqrt{G_s \rho_s} \end{aligned}} \tag{11.70}$$

Following are the relationships for calculation of response of the system.

Copyright 2017 Cengage Learning. All Rights Reserved. May not be copied, scanned, or duplicated, in whole or in part. Due to electronic rights, some third party content may be suppressed from the eBook and/or eChapter(s). Editorial review has deemed that any suppressed content does not materially affect the overall learning experience. Cengage Learning reserves the right to remove additional content at any time if subsequent rights restrictions require it.

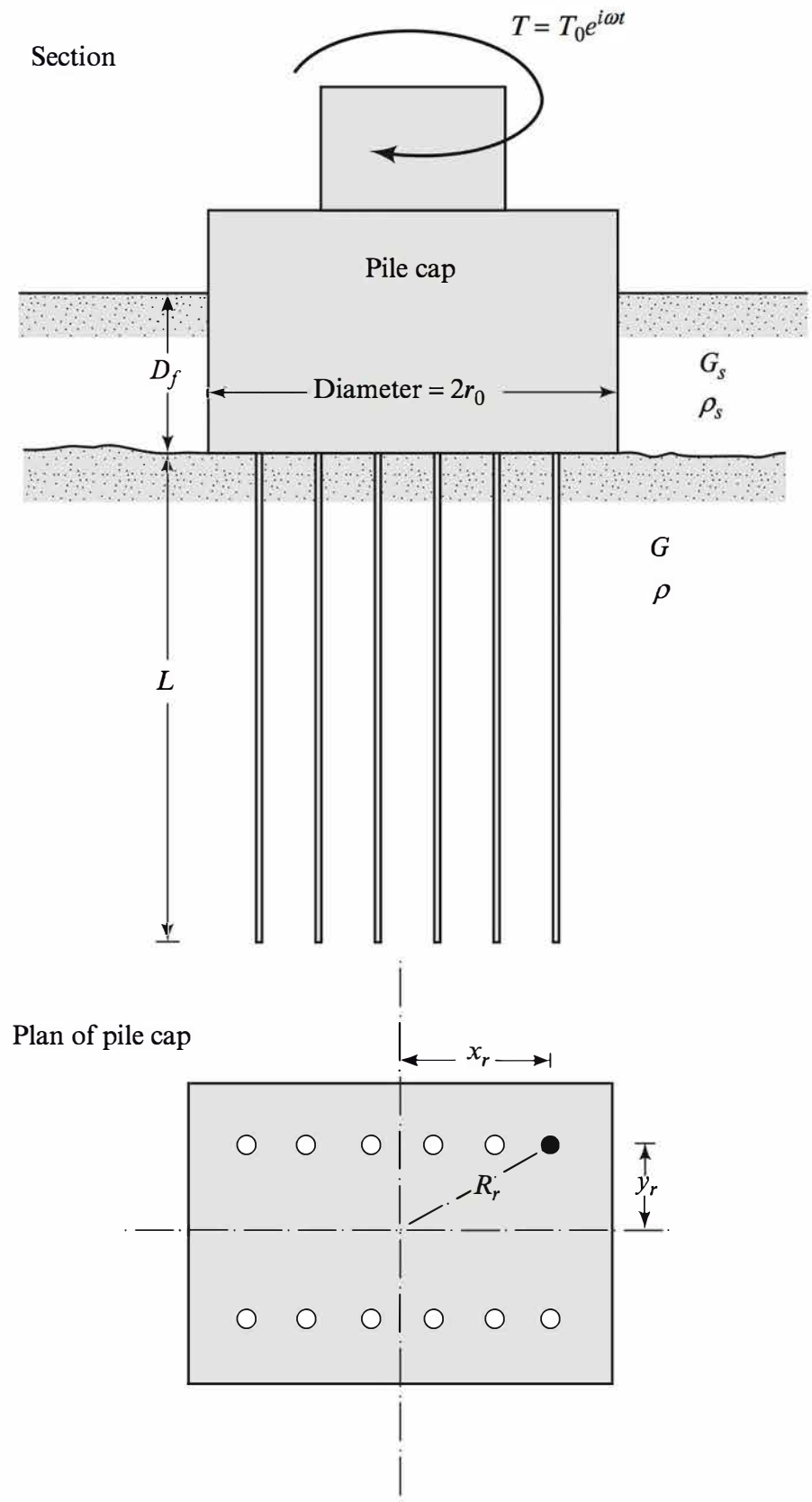

Figure 11.23 Group pile subjected to torsional vibration

a. Damping ratio:

$$D_\alpha = \frac{c_{\alpha(T)}}{2\sqrt{k_{\alpha(T)} J_{zz}}} \tag{11.71}$$

where J_{zz} = mass moment of inertia of the pile cap and machinery about a vertical axis passing through the centroid. Referring to Figure 11.24a,

Copyright 2017 Cengage Learning. All Rights Reserved. May not be copied, scanned, or duplicated, in whole or in part. Due to electronic rights, some third party content may be suppressed from the eBook and/or eChapter(s). Editorial review has deemed that any suppressed content does not materially affect the overall learning experience. Cengage Learning reserves the right to remove additional content at any time if subsequent rights restrictions require it.

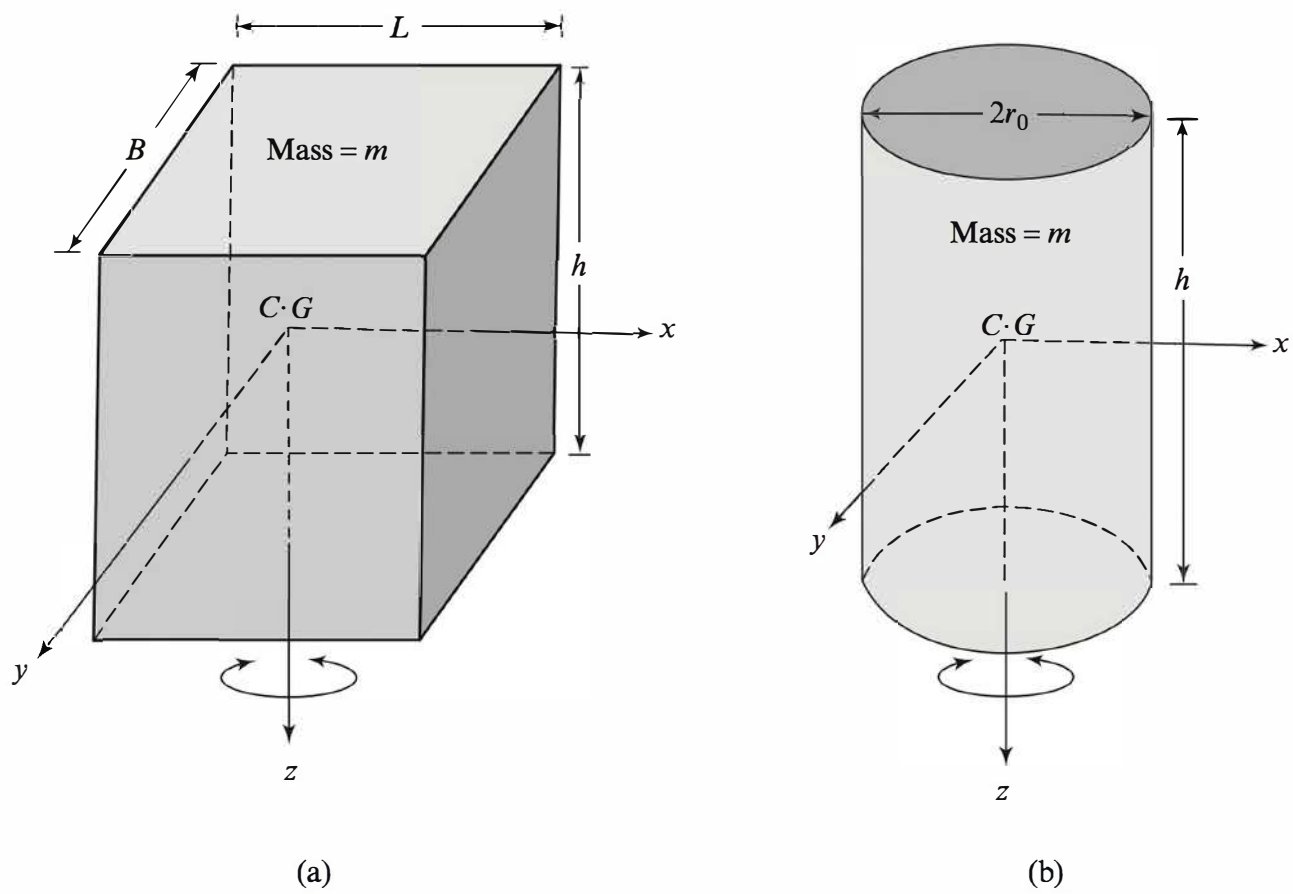

Figure 11.24 Mass moment of inertia J_{zz}

$$J_{zz} = \text{mass moment of inertia about the } z \text{ axis} = \frac{m}{12}(L^2 + B^2) \tag{11.72}$$

Referring to Figure 11.24b,

$$J_{zz} = \text{mass moment of inertia about the } z \text{ axis} = \frac{mr_0^2}{2} \tag{11.73}$$

b. Undamped natural frequency:

$$\omega_n = \sqrt{\frac{k_{\alpha(T)}}{J_{zz}}} \tag{11.74}$$

$$f_n = \frac{1}{2\pi}\sqrt{\frac{k_{\alpha(T)}}{J_{zz}}} \tag{11.75}$$

c. Damped natural frequency:

$$f_m = f_n\sqrt{1 - 2D_\alpha^2} \quad \text{(for constant force excitation)} \tag{11.76}$$

$$f_m = \frac{f_n}{\sqrt{1 - 2D_\alpha^2}} \quad \text{(for rotating mass-type excitation)} \tag{11.77}$$

d. *Amplitude of vibration at resonance:* Equations (5.68) and (5.69) can be used to calculate the amplitude of vibration. [Replace k_α in Eq. (5.68) by $k_{\alpha(T)}$.]

Copyright 2017 Cengage Learning. All Rights Reserved. May not be copied, scanned, or duplicated, in whole or in part. Due to electronic rights, some third party content may be suppressed from the eBook and/or eChapter(s). Editorial review has deemed that any suppressed content does not materially affect the overall learning experience. Cengage Learning reserves the right to remove additional content at any time if subsequent rights restrictions require it.

PROBLEMS

11.1 A machine foundation is supported by six piles, as shown in Figure P11.1. Given:

Type: concrete

Size: 405 mm × 405 mm in cross section

Length: 30 m

Unit weight of concrete = 23 kN/m^3

Modulus of elasticity = 21×10^6 kPa

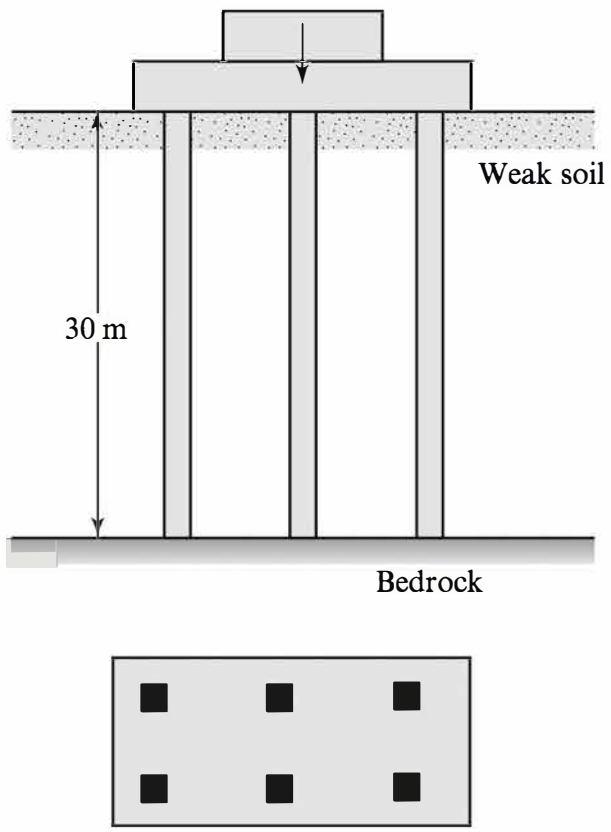

Figure P11.1

Machine and foundation

Weight = 2030 kN

Determine the natural frequency of the pile-foundation system for vertical vibration. Use the procedure outlined in Section 11.2.

11.2 A wooden pile is shown in Figure P11.2. The pile has a diameter of 230 mm. Given: $E_P = 8.5 \times 10^6$ kPa. Determine its stiffness and damping constants for

a. vertical vibration,
b. sliding, and
c. rocking vibration.

Copyright 2017 Cengage Learning. All Rights Reserved. May not be copied, scanned, or duplicated, in whole or in part. Due to electronic rights, some third party content may be suppressed from the eBook and/or eChapter(s). Editorial review has deemed that any suppressed content does not materially affect the overall learning experience. Cengage Learning reserves the right to remove additional content at any time if subsequent rights restrictions require it.

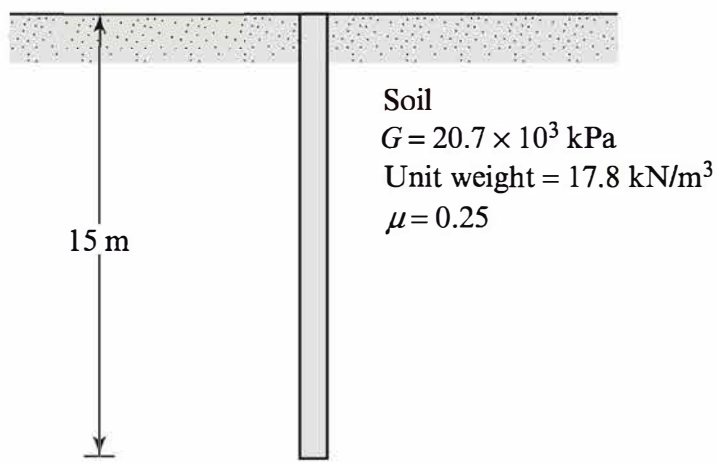

Figure P11.2

11.3 Refer to Problem 11.2. Assume that the Poisson's ratio for wooden piles is 0.35. Determine the approximate stiffness and damping constants for the pile for torsional vibration.

11.4 Solve Problem 11.2 assuming that the piles are made of concrete with $E_P = 21 \times 10^6$ kPa.

11.5 Refer to Problem 11.4. Assume that the Poisson's ratio for concrete piles is 0.33. Determine the approximate stiffness and damping constants for the pile for torsional vibration.

11.6 – 11.11 For Problems 11.6–11.11, refer to the accompanying figure. Given:

Pile

$$L = 25 \text{ m}$$
$$\text{Size} = 380 \text{ mm} \times 380 \text{ mm in cross section}$$
$$E_p = 21 \times 10^6 \text{ kPa}$$
$$\text{Poisson's ratio, } \mu_{\text{pile}} = 0.35$$

Pile cap

$$B = 3.4 \text{ m}$$
$$x' = 0.5 \text{ m}$$
$$D_f = 2 \text{ m}$$
$$h = 3 \text{ m}$$

The pile cap is made of concrete. Unit weight of concrete is 23 kN/m^3.

Soil

$$G = G_s = 24{,}500 \text{ kPa}$$
$$\text{Unit weight, } \gamma = \gamma_s = 18.5 \text{ kN/m}^3$$
$$\text{Poisson's ratio, } \mu = 0.25$$

Copyright 2017 Cengage Learning. All Rights Reserved. May not be copied, scanned, or duplicated, in whole or in part. Due to electronic rights, some third party content may be suppressed from the eBook and/or eChapter(s). Editorial review has deemed that any suppressed content does not materially affect the overall learning experience. Cengage Learning reserves the right to remove additional content at any time if subsequent rights restrictions require it.

11.6 Determine $k_{z(g)}$ and $c_{z(g)}$ for the pile group for the vertical mode of vibration.

11.7 Determine the total stiffness and damping constants $k_{z(T)}$ and $c_{z(T)}$ for the vertical mode of vibration.

11.8 Determine $k_{x(g)}$ and $c_{x(g)}$ for the pile group for the horizontal mode of vibration.

11.9 Determine the total stiffness and damping constants $k_{x(T)}$ and $c_{x(T)}$ for the horizontal mode of vibration.

11.10 Determine $k_{\theta(g)}$ and $c_{\theta(g)}$ for the pile group for the rocking mode of vibration.

11.11 Determine the total stiffness and damping constants $k_{\theta(T)}$ and $c_{\theta(T)}$ for the rocking mode of vibration.

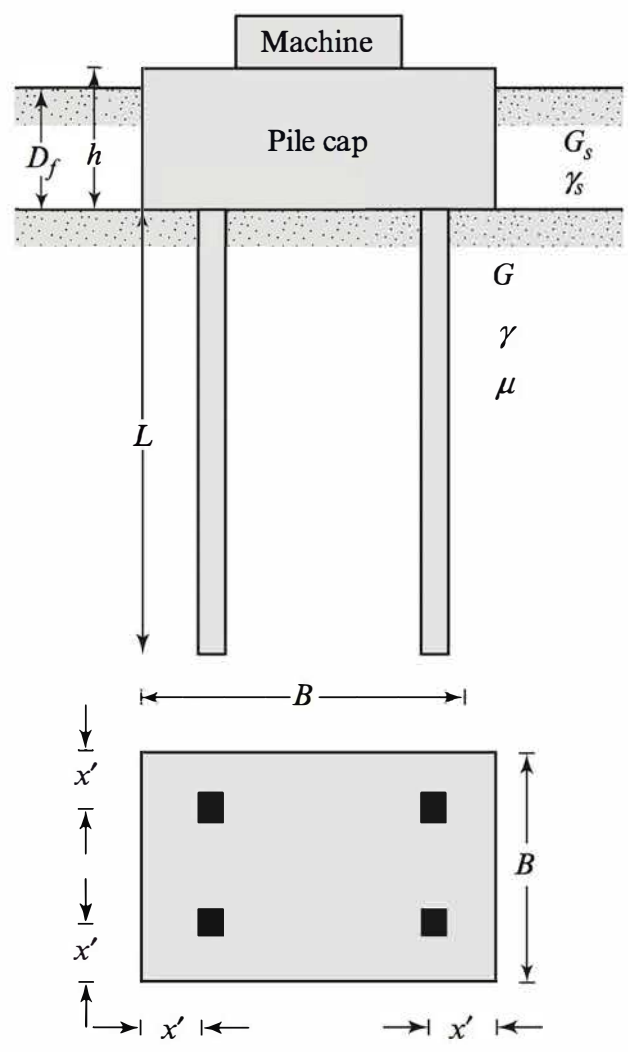

Figure P11.6–P11.11

Copyright 2017 Cengage Learning. All Rights Reserved. May not be copied, scanned, or duplicated, in whole or in part. Due to electronic rights, some third party content may be suppressed from the eBook and/or eChapter(s). Editorial review has deemed that any suppressed content does not materially affect the overall learning experience. Cengage Learning reserves the right to remove additional content at any time if subsequent rights restrictions require it.

References

Novak, M. (1974). "Dynamic Stiffness and Damping of Piles," *Canadian Geotechnical Journal*, Vol. 11, No. 4, pp. 574–598.

Novak, M. (1977). "Vertical Vibration of Floating Piles," *Journal of the Engineering Mechanics Division*, ASCE, Vol. 103, No. EM1, pp. 153–168.

Novak, M., and El-Sharnouby, B. (1983). "Stiffness and Damping Constants of Single Piles," *Journal of the Geotechnical Engineering Division*, ASCE, Vol. 109, No. GT7, pp. 961–974.

Novak, M., and Howell, J. F. (1977). "Torsional Vibrations of Pile Foundations," *Journal of the Geotechnical Engineering Division*, ASCE, Vol. 103, No. GT4, pp. 271–285.

Poulos, H. G. (1968). "Analysis of Settlement of Pile Groups," *Geotechnique*, Vol. 18, No. 4, pp. 449–471.

Poulos, H. G. (1971). "Behavior of Laterally Loaded Piles: II. Pile Groups," *Journal of the Soil Mechanics and Foundation Division*, ASCE, Vol. 97, No. SM5, pp. 733–751.

Prakash, S. and Puri, V. K. (1988). *Foundation for Machines: Analysis and Design*, John Wiley and Sons, Inc., New York.

Richart, F. E., Jr. (1962). "Foundation Vibrations," *Transactions*, ASCE, Vol. 127, Part I, pp. 863–898.

Copyright 2017 Cengage Learning. All Rights Reserved. May not be copied, scanned, or duplicated, in whole or in part. Due to electronic rights, some third party content may be suppressed from the eBook and/or eChapter(s). Editorial review has deemed that any suppressed content does not materially affect the overall learning experience. Cengage Learning reserves the right to remove additional content at any time if subsequent rights restrictions require it.

Seismic Stability of Earth Embankments

12

12.1 INTRODUCTION

Sudden ground displacement during earthquakes induces large inertial forces in embankments. As a result, the slope of an embankment is subjected to several cycles of alternating inertia force. There are several recorded cases in the past that show severe damage or collapse of earth embankment slopes due to earthquakes-induced vibration (e.g., Ambraseys, 1960; Seed, Makdisi, and DeAlba, 1978). These damages include flow slides of saturated cohesionless soil slopes and slopes of cohesive soil with thin lenses of saturated sand inside them. Such flow slides are due to liquefaction of saturated sand deposits. Fundamental concepts of liquefaction were presented in Chapter 10. Other types of damages include collapse or deformation of dry or dense slopes in sand and also in cohesive soils. In the following sections, the analysis for the stability of earth embankments for these types of slopes under earthquake loading conditions will be treated. It will be assumed that these soils experience very little reduction in strength due to cyclic loading. This is what is generally known as *inertial stability analysis*.

In general, deformations suffered by an earth embankment during a strong earthquake may take several forms, such as those shown in Figure 12.1a, b, and c. Figure 12.1a shows a type of deformation pattern that may be concentrated in a narrow zone with a definite slip surface. However, substantial deformation may occur without the development of a slip surface, as shown in Figure 12.1b. In cohesionless slopes, the slip surface is usually a plane, as shown in Figure 12.1c (Seed and Goodman, 1964).

12.2 FREE VIBRATION OF EARTH EMBANKMENTS

For a proper evaluation of the seismic stability of earth embankments, it is necessary to have some knowledge of the vibration of embankments due to earthquakes, with some simplifying assumptions. This can be done by the use of one-dimensional *shear slice theory* (Mononobe, Takata, and Matumura, 1963; Seed and Martin, 1966). Figure 12.2 shows an earth embankment in the form of

Copyright 2017 Cengage Learning. All Rights Reserved. May not be copied, scanned, or duplicated, in whole or in part. Due to electronic rights, some third party content may be suppressed from the eBook and/or eChapter(s).
Editorial review has deemed that any suppressed content does not materially affect the overall learning experience. Cengage Learning reserves the right to remove additional content at any time if subsequent rights restrictions require it.

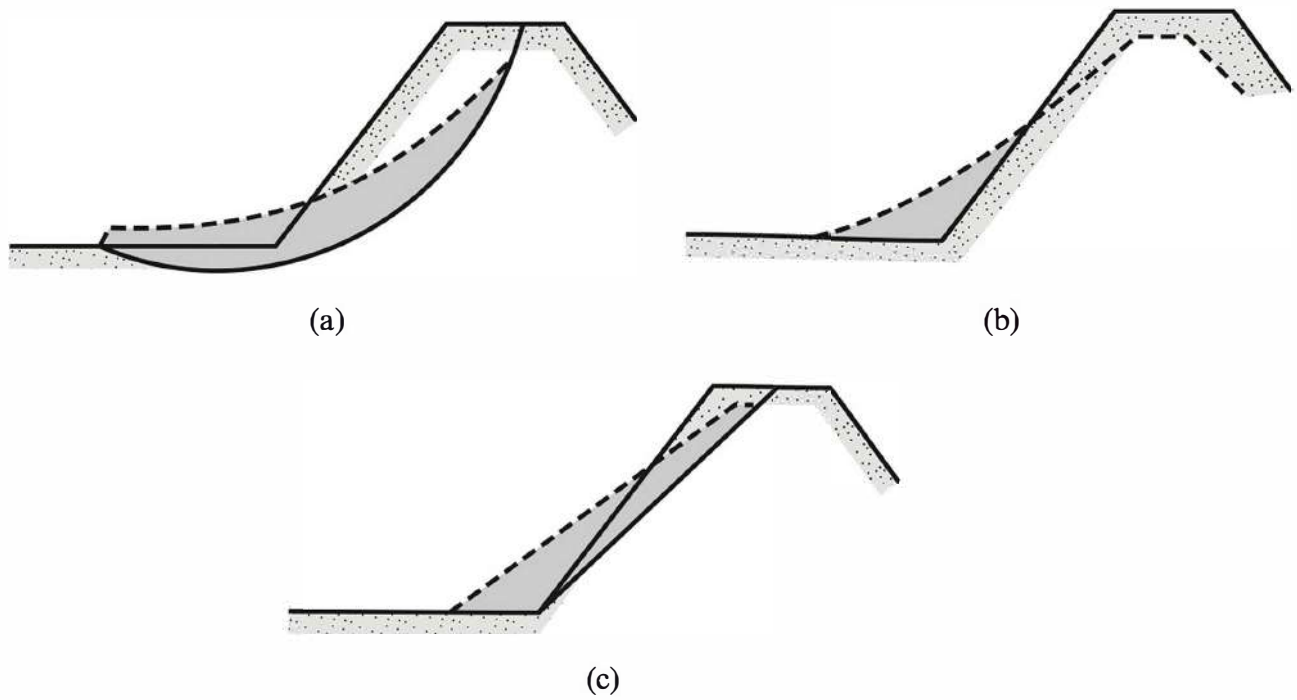

Figure 12.1 Deformation of earth embankments

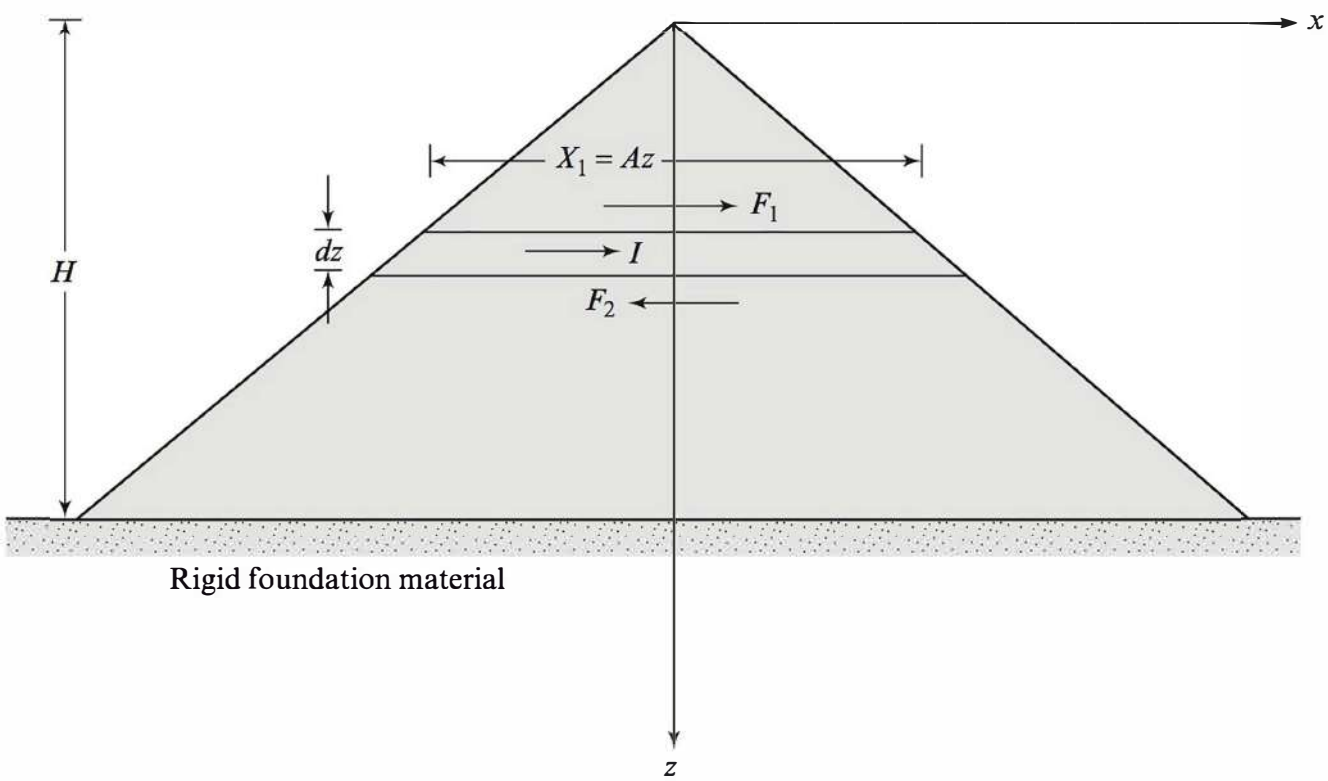

Figure 12.2 Free vibration of an earth embankment

a triangular wedge. The height of the wedge is H. Now, the following assumptions will be made:

1. The earth embankment is infinitely long;
2. The foundation material is rigid;
3. The width-to-height ratio of the embankment is large. This means that the deformation of the embankment is due only to shear; and
4. The shear stress on any horizontal plane is uniform.

Copyright 2017 Cengage Learning. All Rights Reserved. May not be copied, scanned, or duplicated, in whole or in part. Due to electronic rights, some third party content may be suppressed from the eBook and/or eChapter(s). Editorial review has deemed that any suppressed content does not materially affect the overall learning experience. Cengage Learning reserves the right to remove additional content at any time if subsequent rights restrictions require it.

Regarding the first assumption made, it can be shown that when the length-to-height ratio of an embankment is four or greater, then effect of end restraints on the natural frequencies of vibration is negligible. So, for all practical purposes most of the embankments can be assumed to be infinitely long.

Consider an elementary strip of thickness dz, as shown in Figure 12.2. The forces acting on this elementary strip (per unit length at right angles to the section shown) are

a. Shear force:

$$F_1 = G\frac{\partial u}{\partial z}X_1$$

b. Shear force:

$$F_2 = F_1 + \frac{\partial F_1}{\partial z}dz$$

c. Inertia force:

$$\begin{aligned} I &= (\text{mass})(\text{acceleration}) \\ &= \left(\frac{\gamma}{g}.X_1.dz\right)\frac{\partial^2 u}{\partial t^2} = \rho A z\frac{\partial^2 u}{\partial t^2}dz \end{aligned}$$

where G = shear modulus of the embankment material
u = displacement in the x direction
g = unit weight of embankment material
A = a constant of proportionality
$\rho = \gamma/g$ = density of the embankment material

Note that

$$F_2 - F_1 = I$$

So

$$\left[AG\frac{\partial u}{\partial z}z + AG\frac{\partial}{\partial z}\left(z\frac{\partial u}{\partial z}\right)\partial z\right] - \left[AG\frac{\partial u}{\partial z}z\right] = \rho A z\frac{\partial^2 u}{\partial t^2}dz$$

or

$$\frac{\partial^2 u}{\partial t^2} = \frac{G}{\rho}\left(\frac{\partial^2 u}{\partial z^2} + \frac{1}{z}\frac{\partial u}{\partial z}\right) \tag{12.1}$$

In the preceding equation, the viscous damping force has been neglected, and the boundary conditions for solving it are as follows:

a. $\partial u/\partial z = 0$ at $z = 0$ for all values of t; and
b. $u = 0$ at $z = H$ for all values of t.

Copyright 2017 Cengage Learning. All Rights Reserved. May not be copied, scanned, or duplicated, in whole or in part. Due to electronic rights, some third party content may be suppressed from the eBook and/or eChapter(s). Editorial review has deemed that any suppressed content does not materially affect the overall learning experience. Cengage Learning reserves the right to remove additional content at any time if subsequent rights restrictions require it.

The solution to Eq. (12.1) is

$$\boxed{u(z,t) = \sum_{n=1}^{n=\infty} [A_n \sin\omega_n t + B_n \cos\omega_n t] J_0\left(\beta_n \frac{z}{H}\right)} \tag{12.2}$$

where

A_n, B_n = constants

J_0 = Bessel function of first kind and order 0

β_n = the zero value of the frequency equation $J_0\left(\omega_n H \times \sqrt{\frac{\rho}{G}}\right) = 0$

(So $\beta_1 = 2.404, \beta_2 = 5.22, \beta_3 = 8.65, \ldots$)

ω_n = undamped natural circular frequency of embankment in the nth mode of vibration $= \frac{\beta_n}{H}\sqrt{\frac{G}{\rho}}$

Thus,

$$\boxed{\begin{aligned} \omega_1 &= \frac{\beta_1}{H}\sqrt{\frac{G}{\rho}} = \frac{2.404}{H}\sqrt{\frac{G}{\rho}} \\ \omega_2 &= \frac{5.52}{H}\sqrt{\frac{G}{\rho}} \\ \omega_3 &= \frac{8.65}{H}\sqrt{\frac{G}{\rho}} \end{aligned}} \tag{12.3}$$

Here it is worth noting that implicitly the shear modulus is assumed to be constant throughout the height of the embankment, which is not true. However, for an accurate estimation of ω_1, this is a good assumption.

12.3 FORCED VIBRATION OF AN EARTH EMBANKMENT

Figure 12.3 shows a triangular earth embankment being subjected to a horizontal ground motion, $u_g(t)$. The equation of motion for the analysis of the vibration of an embankment for such a case can be given as (Seed and Martin, 1966)

$$\frac{\partial^2 u}{\partial t^2} - \frac{G}{\rho}\left[\frac{\partial^2 u}{\partial t^2} + \frac{1}{z}\frac{\partial u}{\partial t}\right] = -\frac{\partial^2 u_g}{\partial t^2} \tag{12.4}$$

The solution to Eq. (12.4) can be given as

$$\boxed{u(z,t) = \sum_{n=1}^{n=\infty} \frac{2J_0[\beta_n(z/H)]}{\omega_n \beta_n J_1(\beta_n)} \int_0^t \ddot{u}_g \sin[\omega_n(t-t')]dt'} \tag{12.5}$$

Copyright 2017 Cengage Learning. All Rights Reserved. May not be copied, scanned, or duplicated, in whole or in part. Due to electronic rights, some third party content may be suppressed from the eBook and/or eChapter(s). Editorial review has deemed that any suppressed content does not materially affect the overall learning experience. Cengage Learning reserves the right to remove additional content at any time if subsequent rights restrictions require it.

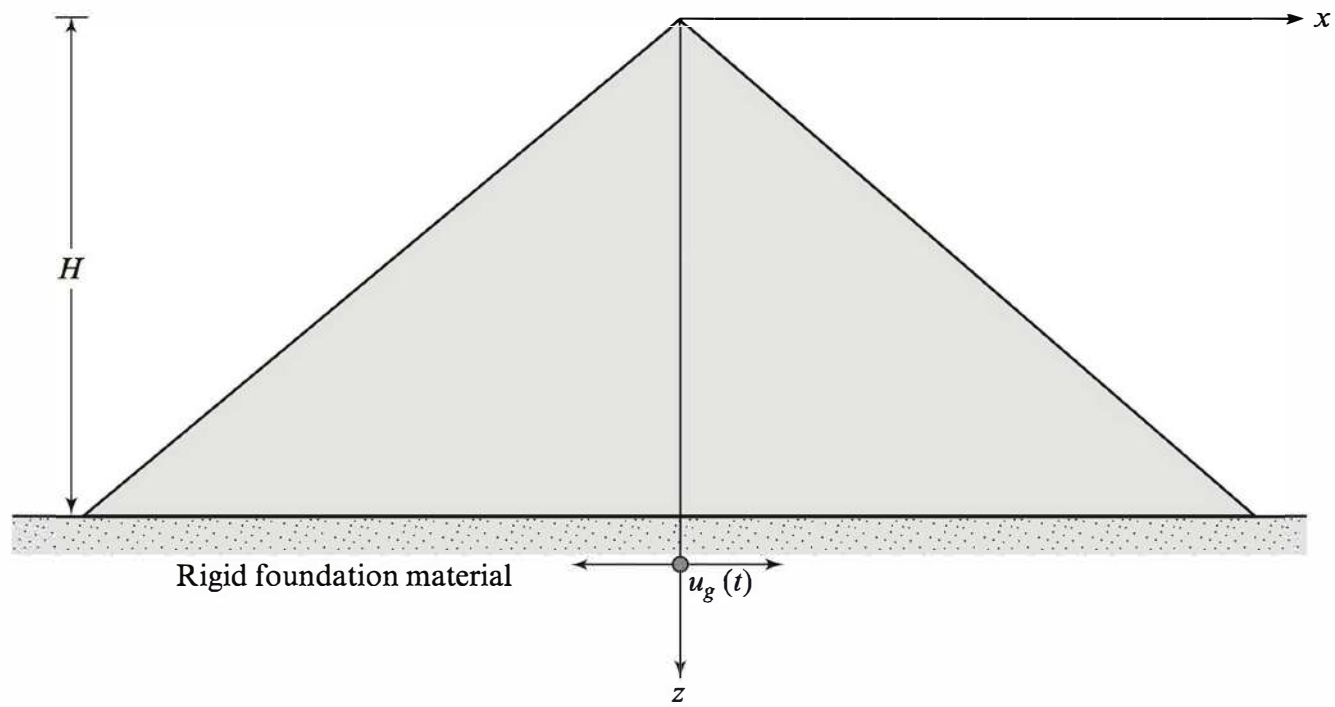

Figure 12.3 Forced vibration of an earth embankment

where J_1 = Bessel function of the first order.

Like all materials, soil possesses the property of damping out vibrations. The viscous damping factor of soil in the embankment has not been included in Eqs. (12.4) and (12.5). If viscous damping (see Chapter 2) is included, then Eq. (12.5) will be modified to the form

$$u(z,t) = \sum_{n=1}^{n=\infty} \frac{2J_0[\beta_n(z/H)]}{\omega_n \beta_n J_1(\beta_n)} \int_0^t \ddot{u}_g e^{-D_n\omega_n(t-t')} \sin[\omega_d(t-t')]dt' \tag{12.6}$$

where D_n = damping factor in the nth mode

$\omega_d = \omega_n\sqrt{1-D_n^2}$ = damped natural angular frequency in the nth mode

The relative velocity, $\dot{u}(z,t)$, and acceleration, $\ddot{u}(z,t)$, at any depth z and time t can be obtained by proper differentiation of Eq. (12.6). The absolute acceleration can be given by

$$\ddot{u}_a(z,t) = \ddot{u}(z,t) + \ddot{u}_g(t) \tag{12.7}$$

where $\ddot{u}_a(z,t)$ = absolute acceleration. For the case of zero damping ($D_n = 0$), it can be shown from Eq. (12.4) that the modal contribution to the absolute acceleration can be given by

$$\ddot{u}_{an}(z,t) = \omega_n^2 u_n(z,t) \tag{12.8}$$

For small values of damping (that is, $D_n \approx 0$), $\omega_d \approx \omega_n$. Thus, from Eq. (12.6),

Copyright 2017 Cengage Learning. All Rights Reserved. May not be copied, scanned, or duplicated, in whole or in part. Due to electronic rights, some third party content may be suppressed from the eBook and/or eChapter(s). Editorial review has deemed that any suppressed content does not materially affect the overall learning experience. Cengage Learning reserves the right to remove additional content at any time if subsequent rights restrictions require it.

$$\boxed{\ddot{u}_a(z,t) = \sum_{n=1}^{n=\infty} 2\omega_n \left[\frac{1}{\beta_n J_1(\beta_n)}\right]\left[J_0\left(\beta_n \frac{z}{H}\right)\int_0^t \ddot{u}_g e^{-D_n\omega_n(t-t')} \times \sin[\omega_n(t-t')]dt'\right]} \tag{12.9a}$$

The preceding equation can be rewritten as

$$\ddot{u}_a(z,t) = \sum_{n=1}^{n=\infty} \ddot{u}_{an}(z,t) \tag{12.9b}$$

where

$$\ddot{u}_{an}(z,t) = \omega_n \eta_n(z) V_n(t) \tag{12.10}$$

$$\omega_n = \frac{\beta_n}{H}\sqrt{\frac{G}{\rho}} \tag{12.11}$$

$$\eta_n(z) = \frac{2J_0[\beta_n(z/H)]}{\beta_n J_1(\beta_n)} \tag{12.12}$$

$$\boxed{V_n(t) = \int_0^t \ddot{u}_g e^{-D_n\omega_n(t-t')} \sin[\omega_n(t-t')]dt'} \tag{12.13}$$

For a given ground acceleration record $[\ddot{u}_g(t)]$ and embankment, Eq. (12.9) can be programmed in a computer and the variation of the absolute acceleration with depth can be obtained. An example for such a case is shown in Figure 12.4. Figure 12.4b shows the variation of acceleration of a 30 m high embankment with time that has been subjected to a ground acceleration, as shown in Figure 12.4a.

12.4 VELOCITY AND ACCELERATION SPECTRA

The term $V_n(t)$ given by Eq. (12.13) is a function of the ground acceleration ($\ddot{u}_g$), damping (D_n), natural frequency (ω_n) and the time (t). For a given earthquake record, the maximum value of $V_n(t)$ that will correspond to a given value of ω_n can easily be determined. This is referred to as the spectral velocity, S_{Vn}, where

$$\boxed{S_{Vn} = \left\{\int_0^t \ddot{u}_g e^{-D_n\omega_n(t-t')} \sin[\omega_n(t-t')]dt'\right\}_{\max}} \tag{12.14}$$

The spectral velocities, S_{Vn}, corresponding to various values of ω_n can be calculated and plotted in a graphical form (for a given value of D_n). This is called a *velocity spectrum*. Note that S_{Vn} has the units of velocity. Similar plots can be

Copyright 2017 Cengage Learning. All Rights Reserved. May not be copied, scanned, or duplicated, in whole or in part. Due to electronic rights, some third party content may be suppressed from the eBook and/or eChapter(s). Editorial review has deemed that any suppressed content does not materially affect the overall learning experience. Cengage Learning reserves the right to remove additional content at any time if subsequent rights restrictions require it.

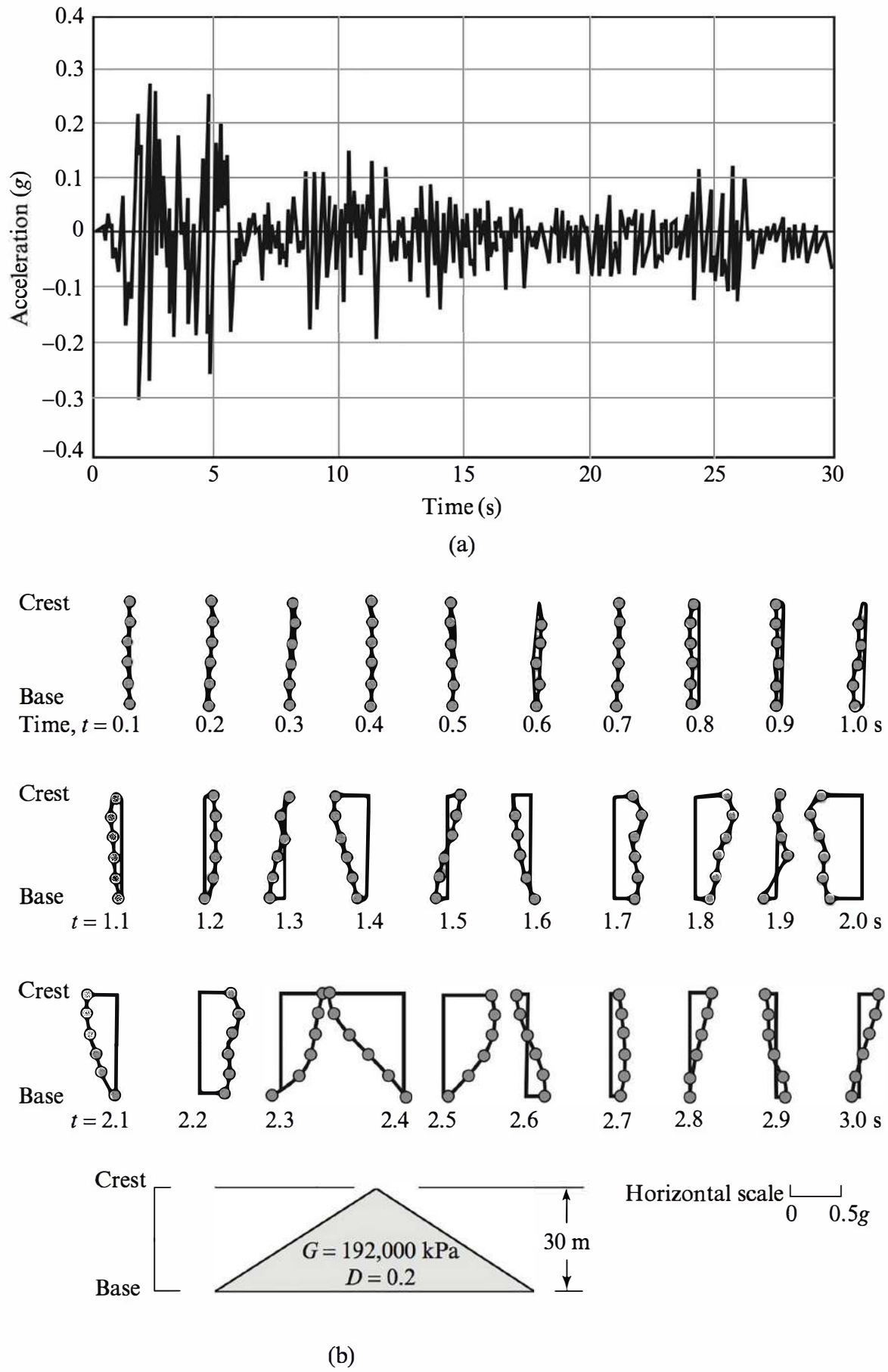

Figure 12.4 (a) Accelerogram of el Centro, California, earthquake, May 18, 1940—N-S component; (b) Acceleration distribution at 0.1-s intervals for 30-m-high dam subjected to El Centro earthquake (from Seed and Martin, 1966)

Source: Seed, H.B., and Martin, G.R. (1966). "The Seismic Coefficient in Earth Dam Designs," *Journal of the Soil Mechanics and Foundations Division*, ASCE, Vol. 92, No. SM3, pp. 25–58. With permission from ASCE.

Copyright 2017 Cengage Learning. All Rights Reserved. May not be copied, scanned, or duplicated, in whole or in part. Due to electronic rights, some third party content may be suppressed from the eBook and/or eChapter(s). Editorial review has deemed that any suppressed content does not materially affect the overall learning experience. Cengage Learning reserves the right to remove additional content at any time if subsequent rights restrictions require it.

made for a number of values of the damping ratio. Figure 12.5 shows the nature of the plot of S_{Vn} with the natural period. Note that

$$T_n = \frac{2\pi}{\omega_n} \tag{12.15}$$

where T_n = natural period.

For a given mode of vibration of an embankment, the maximum value of the acceleration can be given as

$$[\ddot{u}_{an}(z)]_{\max} = \omega_n \eta_n(z) S_{Vn} \tag{12.16}$$

Again, keeping in mind that acceleration is equal to natural frequency times the velocity, Eq. (12.16) can be rewritten as

$$[\ddot{u}_{an}(z)]_{\max} = \eta_n(z) S_{an} \tag{12.17}$$

where S_{an} = spectral acceleration = $\omega_n S_{Vn}$

The expression for $\eta_n(z)$ is given by Eq. (12.12). Since the values of β_n (for $n = 1,2,3,\ldots$) are known, $\eta_n(z)$ can easily be calculated. The variation of $\eta_n(z)$ for $n = 1, 2, 3$ is shown in Figure 12.6. Thus, the spectral acceleration for a given value of D_n and ω_n (or T_n) can be calculated. A plot of S_{an} versus T_n is referred to as the *acceleration spectrum*. Figure 12.7 shows an example of an acceleration response spectra.

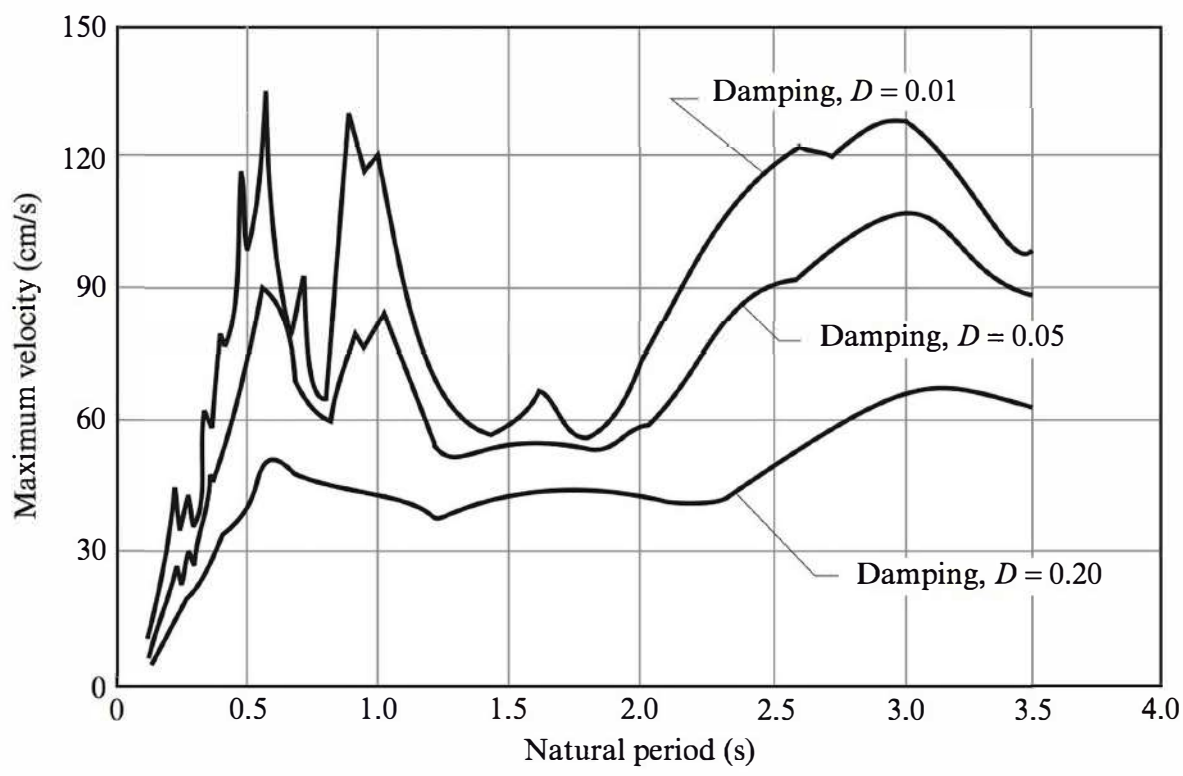

Figure 12.5 Velocity response spectra for El Centro (1940) earthquake (from Seed, 1975)

Source: Copyright 1975. From Seed, H.B. (1975). "Earthquake Effects on Soil-Foundation System," in *Foundation Engineering Handbook*, eds. H.F. Winterkorn and H.Y. Fang. Reproduced by permission of Taylor and Francis Group, LLC, a division of Informa plc.

Copyright 2017 Cengage Learning. All Rights Reserved. May not be copied, scanned, or duplicated, in whole or in part. Due to electronic rights, some third party content may be suppressed from the eBook and/or eChapter(s). Editorial review has deemed that any suppressed content does not materially affect the overall learning experience. Cengage Learning reserves the right to remove additional content at any time if subsequent rights restrictions require it.

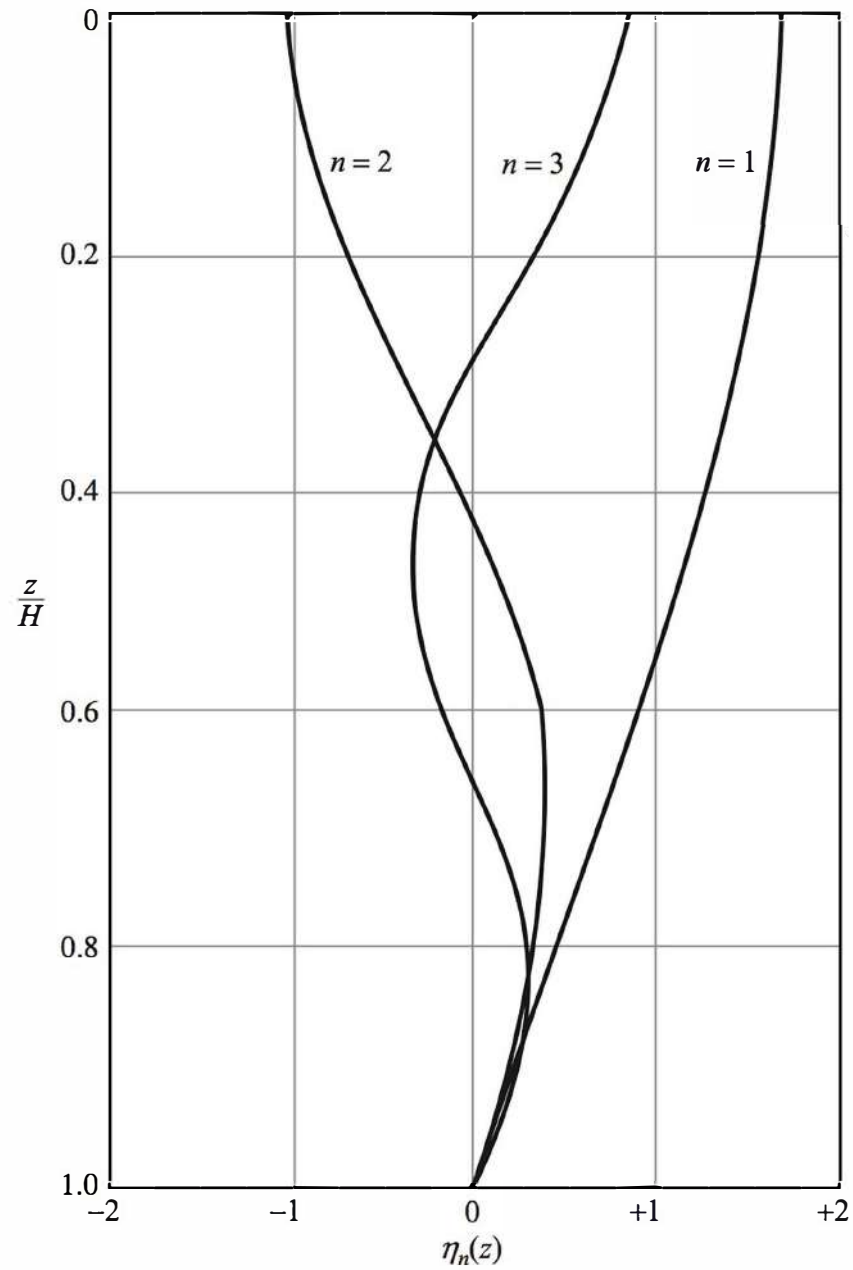

Figure 12.6 Variation $\eta_n(z)$ with z/H [Eq. (12.12)] (from Seed and Martin, 1966)

Source: Seed, H.B., and Martin, G.R. (1966). "The Seismic Coefficient in Earth Dam Designs," *Journal of the Soil Mechanics and Foundations Division*, ASCE, Vol. 92, No. SM3, pp. 25–58. With permission from ASCE.

12.5 APPROXIMATE METHOD FOR EVALUATION OF MAXIMUM CREST ACCELERATION AND NATURAL PERIOD OF EMBANKMENTS

Based on the theory presented in Section 12.3, Makdisi and Seed (1979) have presented a simplified method for estimating the maximum crest acceleration [$\ddot{u}_{a(\max)}$ at $z = 0$] and the natural period of embankment (Figure 12.8). According to this theory, the maximum crest acceleration can be given approximately by the square root of the sum of the square of maximum acceleration at the crest for the first three modes, or

Copyright 2017 Cengage Learning. All Rights Reserved. May not be copied, scanned, or duplicated, in whole or in part. Due to electronic rights, some third party content may be suppressed from the eBook and/or eChapter(s). Editorial review has deemed that any suppressed content does not materially affect the overall learning experience. Cengage Learning reserves the right to remove additional content at any time if subsequent rights restrictions require it.

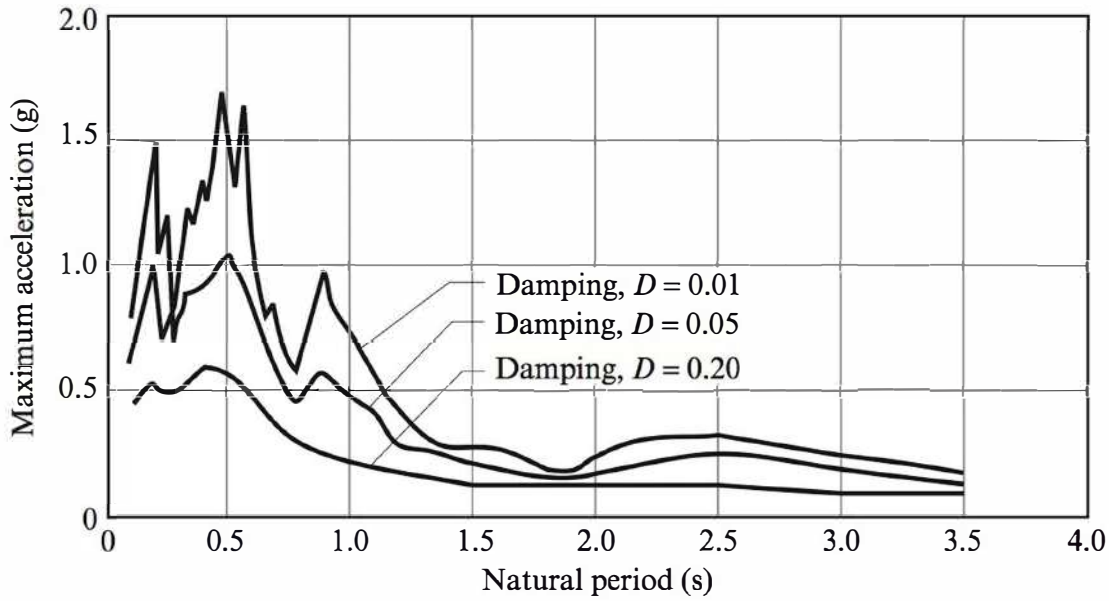

Figure 12.7 Acceleration response spectra for El Centro (1940) earthquake (from Seed, 1975)

Source: Copyright 1975. From Seed, H.B. (1975). "Earthquake Effects on Soil-Foundation System," in *Foundation Engineering Handbook*, eds. H.F. Winterkorn and H.Y. Fang. Reproduced by permission of Taylor and Francis Group, LLC, a division of Informa plc.

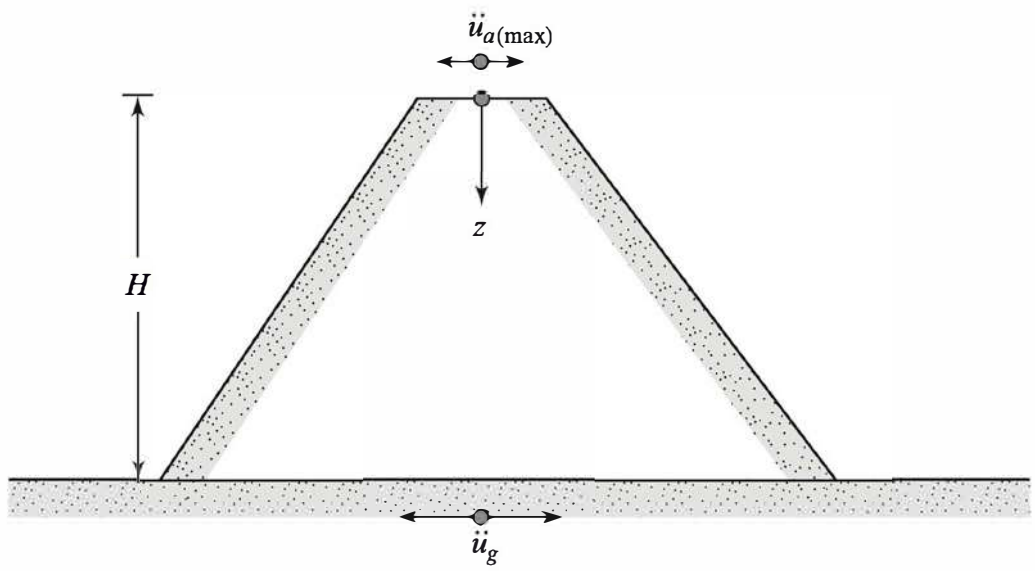

Figure 12.8 Approximate method for evaluation of maximum crest acceleration

$$\ddot{u}_{a(\max)}(\text{at } z = 0) = \sqrt{\sum_{n=1}^{3} [\ddot{u}_{an}(0)]^2_{\max}} \tag{12.18}$$

From Eq. (12.17)

$$[\ddot{u}_{a1}(0)]^2_{\max} = \eta_1(0) S_{a1}$$

But $\eta_1(0) = 1.6$ (Figure 12.6). So

$$[\ddot{u}_{a1}(0)]_{\max} = 1.6 S_{a1} \tag{12.19}$$

Similarly, for the second and third modes,

Copyright 2017 Cengage Learning. All Rights Reserved. May not be copied, scanned, or duplicated, in whole or in part. Due to electronic rights, some third party content may be suppressed from the eBook and/or eChapter(s). Editorial review has deemed that any suppressed content does not materially affect the overall learning experience. Cengage Learning reserves the right to remove additional content at any time if subsequent rights restrictions require it.

$$[\ddot{u}_{a2}(0)]_{\max} = 1.06S_{a2} \tag{12.20}$$

$$[\ddot{u}_{a3}(0)]_{\max} = 0.86S_{a3} \tag{12.21}$$

Now, combining Eqs. (12.18) through (12.21),

$$\boxed{[\ddot{u}_a(0)]_{\max} = \sqrt{(1.6S_{a1})^2 + (1.06S_{a2})^2 + (0.86S_{a3})^2}} \tag{12.22}$$

The step-by-step procedure for obtaining the maximum crest acceleration is given next.

1. Plot graphs of the variations of $G/G_{\max}$ versus shear strain (γ') and D versus shear strain (γ') for the soil present in the embankment as shown in Figure 12.9 (*Note*: G = shear modulus, $G_{\max}$ = maximum shear modulus, D = damping ratio.) This can be done by using the principles outlined in Chapter 4.
2. Obtain an acceleration spectra for the design earthquake.
3. Assume a value of the shear modulus G and calculate $G/G_{\max}$
4. For the assumed value of $G/G_{\max}$(Step 3), determine the shear strain γ' (Figure 12.9).
5. Corresponding to the shear strain obtained in Step 4, obtain the damping ratio D (Figure 12.9).
6. Calculate $\omega_n\left(n = 1, 2, \text{ and } 3\right)$ using Eq. (12.3). The value of the shear modulus to be used is from Step 3.
7. Using the damping ratio obtained in Step 5 and ω_1, ω_2, and ω_3 obtained in Step 6, obtain spectral accelerations S_{a1}, S_{a2}, and S_{a3}. (This is from the acceleration spectra obtained in Step 2.)

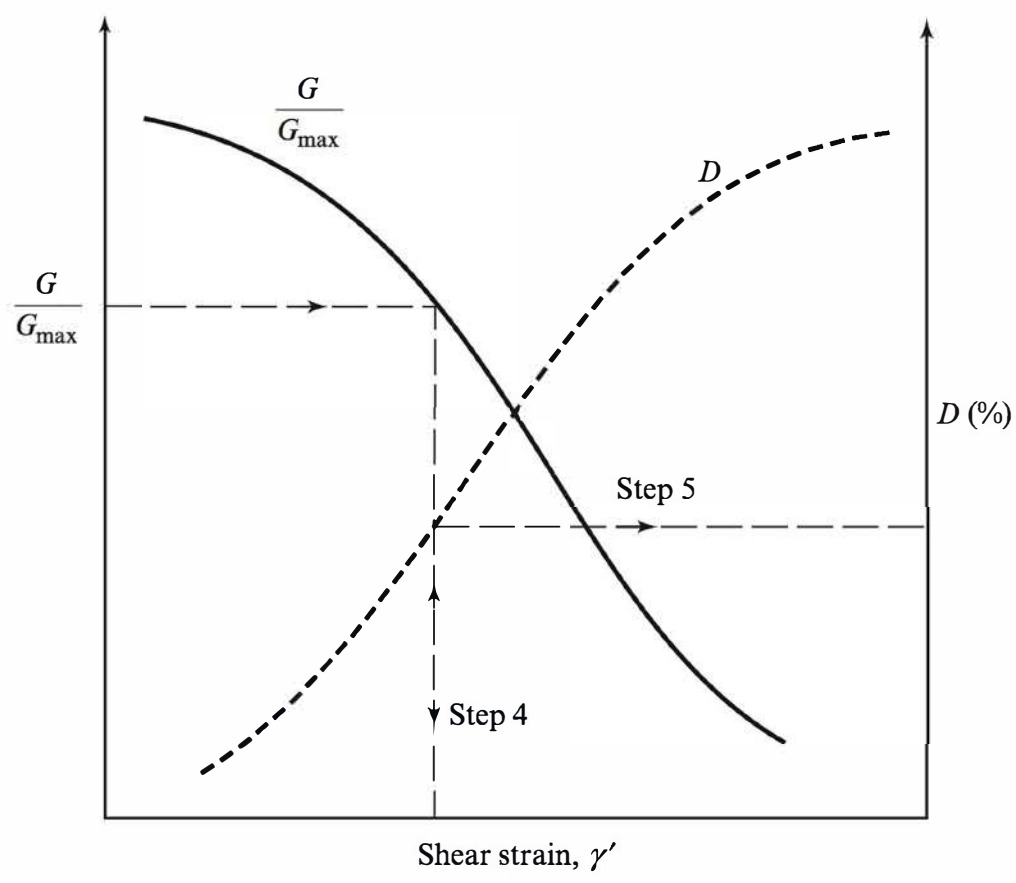

Figure 12.9 Nature of variation of $G/G_{\max}$ and D with shear strain

Copyright 2017 Cengage Learning. All Rights Reserved. May not be copied, scanned, or duplicated, in whole or in part. Due to electronic rights, some third party content may be suppressed from the eBook and/or eChapter(s). Editorial review has deemed that any suppressed content does not materially affect the overall learning experience. Cengage Learning reserves the right to remove additional content at any time if subsequent rights restrictions require it.

8. Calculate the maximum crest acceleration using Eq. (12.22).
9. Calculate the average equivalent shear strain in the embankment as follows. The shear strain, $\gamma'(z,t)$, can be given by (Figure 12.8)

$$\gamma'(z,t) = \sum_{n=1}^{\infty} \frac{2J_1\left[\beta_n\left(z/H\right)\right]}{H\omega_n J_1(\beta_n)} V_n(t) \tag{12.23}$$

The terms in the right-hand side of Eq. (12.23) have all been defined in Sections 12.2 and 12.3. In Section 12.2, we have defined ω_n as

$$\omega_n = \frac{\beta_n}{H}\sqrt{\frac{G}{\rho}}$$

or

$$\omega_n^2 = \frac{\beta_n^2}{H^2} \times \frac{G}{\rho} \tag{12.24}$$

Substituting Eq. (12.24) into Eq. (12.23), we obtain

$$\gamma'(z,t) = H\frac{\rho}{G}\left[\sum_{n=1}^{\infty} \frac{2J_1\left(\beta_n\left(z/H\right)\right)}{\beta_n^2 J_1(\beta_n)} \omega_n V_n(t)\right] \tag{12.25}$$

$$= H\frac{\rho}{G}\left[\sum_{n=1}^{\infty} \phi_n'(z)\omega_n V_n(t)\right] \tag{12.26}$$

where

$$\phi_n'(z) = \frac{2J_1\left[\beta_n(z/H)\right]}{\beta_n^2 J_1(\beta_n)} \tag{12.27}$$

The variations of ϕ_n' with depth (z) for $n = 1$, 2, and 3 are given in Figure 12.10. The maximum shear strain at any depth z of embankment can be approximated by considering the contribution of the first mode only. Thus,

$$\gamma'_{\max}(z) = H\frac{\rho}{G}\phi_1'(z)S_{a1} \tag{12.28}$$

The average value of the maximum shear strain can be given as

$$\left(\gamma'_{av}\right)_{\max} = H\frac{\rho}{G}\left(\phi_1'\right)_{av} S_{a1} \tag{12.29}$$

$\left(\phi_1'\right)_{av}$ can be obtained from Figure 12.10 as 0.3. So

$$\left(\gamma'_{av}\right)_{\max} = 0.3H\frac{\rho}{G}S_{a1} \tag{12.30}$$

The average equivalent maximum cyclic shear strain can be about 65% of $\left(\gamma'_{av}\right)_{\max}$. Thus

Copyright 2017 Cengage Learning. All Rights Reserved. May not be copied, scanned, or duplicated, in whole or in part. Due to electronic rights, some third party content may be suppressed from the eBook and/or eChapter(s). Editorial review has deemed that any suppressed content does not materially affect the overall learning experience. Cengage Learning reserves the right to remove additional content at any time if subsequent rights restrictions require it.

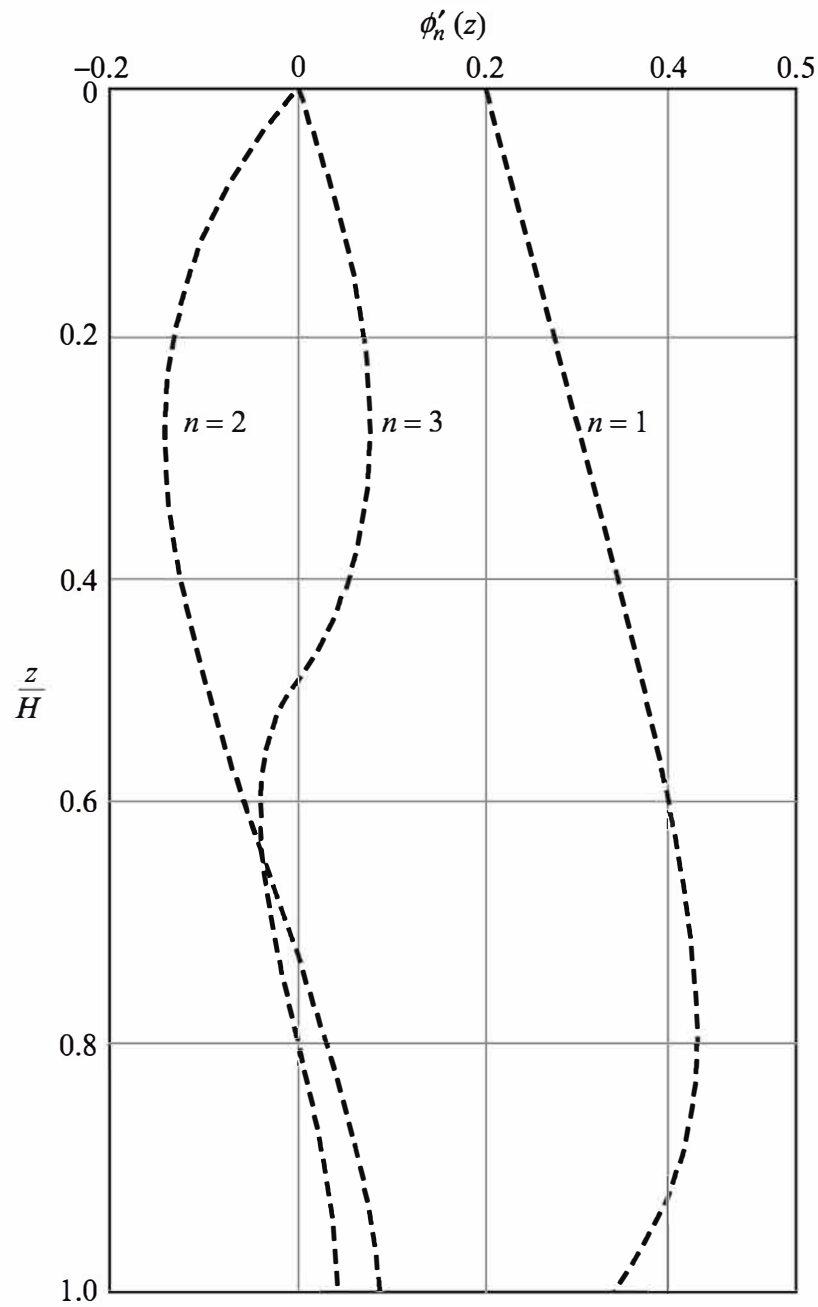

Figure 12.10 Variation of $\phi_n'(z)$ with z/H (from Makdisi and Seed, 1979)

Source: Makdisi, F.I., and Seed, H.B. (1979). "Simplified Procedure for Evaluating Embankment Response," *Journal of the Geotechnical Engineering Division*, ASCE, Vol. 105, No. GT12, pp. 1427–1434. With permission from ASCE.

$$\boxed{(\gamma'_{av})_{eq} = (0.3)(0.65)H\frac{\rho}{G}S_{a1} = 0.195H\frac{\rho}{G}S_{a1}} \tag{12.31}$$

10. Compare $(\gamma'_{av})_{eq}$ to the shear strain obtained in Step 4. If they are the same, then the maximum crest acceleration obtained in Step 8 is correct. The natural period of the embankment can be calculated at $2\pi/\omega_1$.

11. If $(\gamma'_{av})_{eq}$ from Step 9 is different than the strain obtained in Step 4, then obtain new values for G and D corresponding to the strain level $(\gamma'_{av})_{eq}$ obtained in Step 9. Repeat Steps 6 through 10. A few iterations of this type will give the correct values of $[\ddot{u}_a(0)]_{max}, G, D$, and the natural period.

Copyright 2017 Cengage Learning. All Rights Reserved. May not be copied, scanned, or duplicated, in whole or in part. Due to electronic rights, some third party content may be suppressed from the eBook and/or eChapter(s). Editorial review has deemed that any suppressed content does not materially affect the overall learning experience. Cengage Learning reserves the right to remove additional content at any time if subsequent rights restrictions require it.

EXAMPLE 12.1

An earth embankment is 30 m high. For the embankment soil, given:

$$\text{Unit weight}, \gamma = 19.65 \text{ kN/m}^3$$

$$\text{Maximum shear modulus} = 160{,}000 \text{ kPa}$$

Figure 12.11 shows the nature of variation of G/G_{max} and D with shear strain. Figure 12.12 shows a normalized acceleration spectra (maximum ground acceleration is 0.25 g). Determine the maximum crest acceleration.

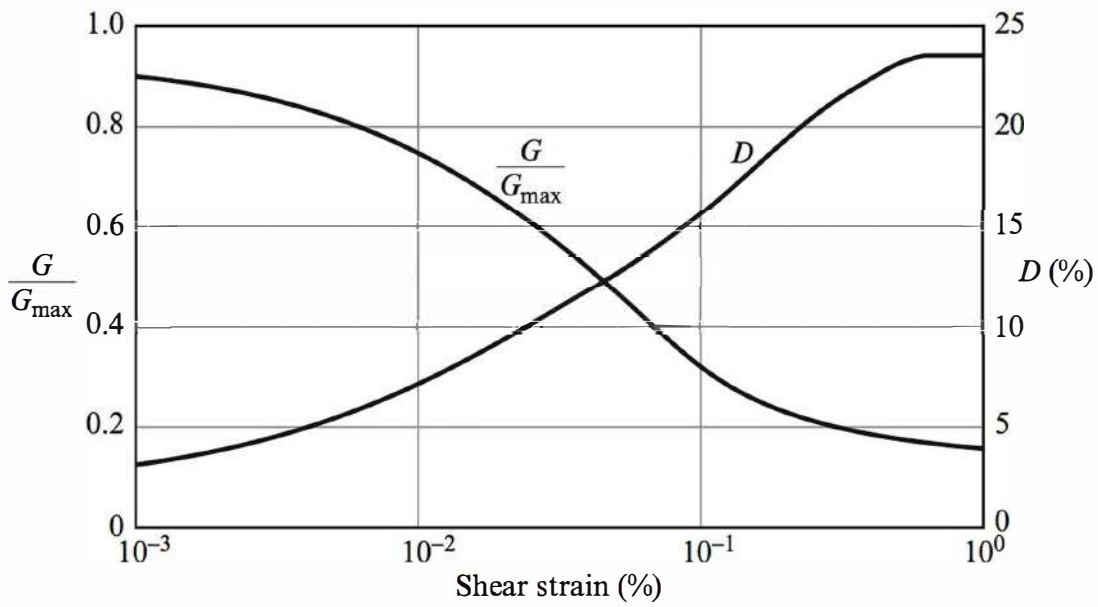

Figure 12.11

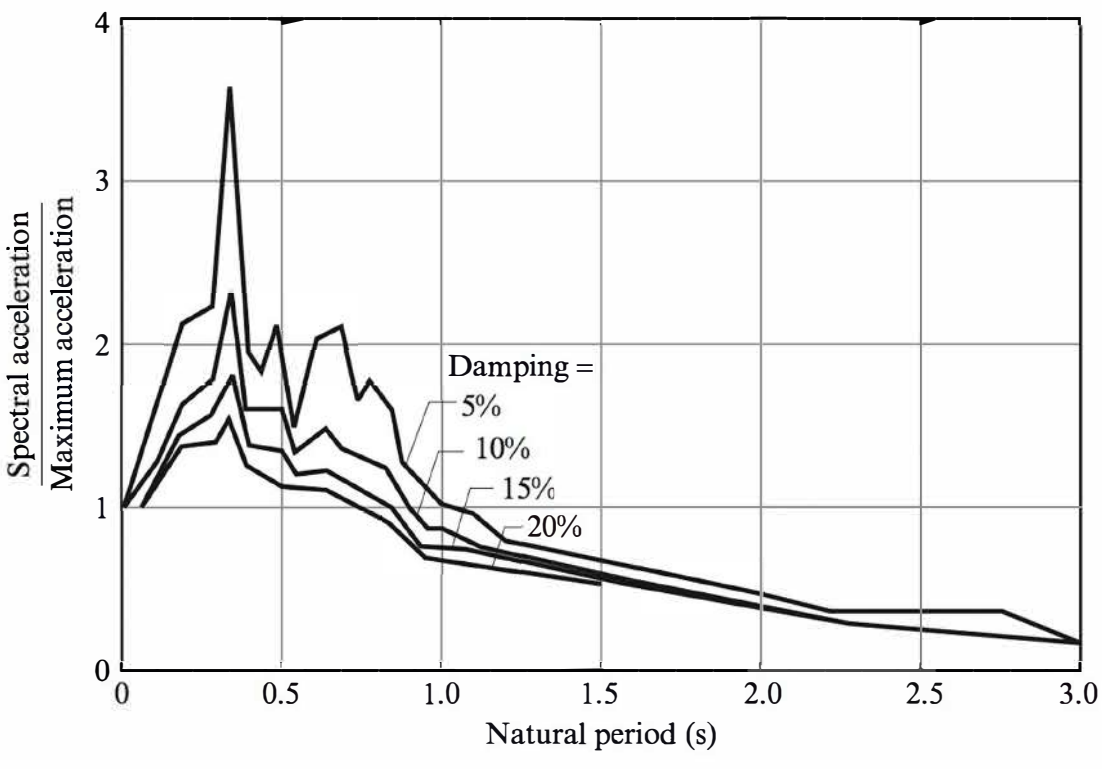

Figure 12.12 Normalized acceleration response spectra—Taft Record, N – S component (from Makdisi and Seed, 1979)

Copyright 2017 Cengage Learning. All Rights Reserved. May not be copied, scanned, or duplicated, in whole or in part. Due to electronic rights, some third party content may be suppressed from the eBook and/or eChapter(s). Editorial review has deemed that any suppressed content does not materially affect the overall learning experience. Cengage Learning reserves the right to remove additional content at any time if subsequent rights restrictions require it.

SOLUTION:

Iteration 1

Let G/G_{max} be equal to 0.4. From Figure 12.11, for $G/G_{max} = 0.4$, the magnitude of shear strain is 0.07% and $D \approx 14\%$. If $G/G_{max} = 0.4$,

$$G = (0.4)(160{,}000) = 64{,}000 \text{ kPa}$$

From Eq. (12.3),

$$\omega_1 = \frac{2.404}{H}\sqrt{\frac{G}{\rho}} = \frac{2.404}{30}\sqrt{\frac{64{,}000}{(19.65/9.81)}} = 14.32 \text{ rad/s}$$

So

$$\text{Period } T_1 = \frac{2\pi}{\omega_1} = 0.435 \text{ s}$$

$$\omega_2 = \frac{5.52}{H}\sqrt{\frac{G}{\rho}} = \frac{5.52}{H}\sqrt{\frac{64{,}000}{(19.65/9.81)}} = 32.89 \text{ rad/s}$$

$$\text{Period } T_2 = \frac{2\pi}{\omega_2} = 0.191 \text{ s}$$

$$\omega_3 = \frac{8.65}{H}\sqrt{\frac{G}{\rho}} = \frac{8.65}{30}\sqrt{\frac{64{,}000}{(19.65/9.81)}} = 51.54 \text{ rad/s}$$

$$\text{Period } T_3 = \frac{2\pi}{\omega_3} = 0.122 \text{ s}$$

From Figure 12.12, for these values of T_1, T_2, and T_3 and $D \approx 14\%$, the spectral accelerations are as follows:

$$S_{a1} = (1.35)(0.25\,g) = 0.3375\,g$$
$$S_{a2} = (1.41)(0.25\,g) = 0.3525\,g$$
$$S_{a3} = (1.18)(0.25\,g) = 0.29\,g$$

From Eq. (12.22)

$$\begin{aligned}[\ddot{u}_a(0)]_{max} &= \sqrt{(1.6S_{a1})^2 + (1.06S_{a2})^2 + (0.86S_{a3})^2} \\ &= \sqrt{(1.6 \times 0.3375\,g)^2 + (1.06 \times 0.3525\,g)^2 + (0.86 \times 0.295\,g)^2} \\ &= 0.704\,g\end{aligned}$$

Using Eq. (12.31),

$$\begin{aligned}(\gamma'_{av})_{eq} &= 0.195H\frac{\rho}{G}S_{a1} \\ &= (0.195)(30)\left(\frac{19.65/9.81}{64{,}000}\right)(0.3375 \times 9.81) = 0.061\%\end{aligned}$$

Copyright 2017 Cengage Learning. All Rights Reserved. May not be copied, scanned, or duplicated, in whole or in part. Due to electronic rights, some third party content may be suppressed from the eBook and/or eChapter(s). Editorial review has deemed that any suppressed content does not materially affect the overall learning experience. Cengage Learning reserves the right to remove additional content at any time if subsequent rights restrictions require it.

The above value of $(\gamma'_{av})_{eq}$ is approximately the same as the assumed value. So

$$[\ddot{u}_a(0)]_{max} \approx \mathbf{0.70\,g}$$

12.6 FUNDAMENTAL CONCEPTS OF STABILITY ANALYSIS

Until the mid-1960s, most of the earth embankment slopes were analyzed by the so-called pseudostatic method. According to this method, a trial failure surface ABC, as shown in Figure 12.13 is chosen. ABC is an arc of a circle with its center at O. Considering the unit length of the embankment at a right angle to the cross section shown, the forces acting on trail failure surface are as follows:

a. Weight of the wedge, W.
b. Inertia force on the wedge, k_hW, which accounts for the effect of an earthquake on the trial wedge. The factor k_h is the average coefficient of horizontal acceleration.
c. Resisting force per unit area, s, which is the shear strength of the soil acting along the trial failure surface, ABC.

The factor of safety with respect to strength, F_s, is calculated as

$$F_s = \frac{\text{resisting moment about } O}{\text{overturning moment about } O} = \frac{s(ABC)R}{WL_1 + k_hWL_2}$$

This procedure is repeated with several trial failure surfaces to determine the minimum values of F_s. It is assumed that if the minimum value of F_s is equal to or greater than 1, the slope is stable.

The magnitude of k_h used for the design of many dams in the past ranged from 0.05 to 0.15 in the United States. In Japan, this value has been less than 0.2. Following are some examples of this type of assumption in the design of earth dams (Seed, 1981).

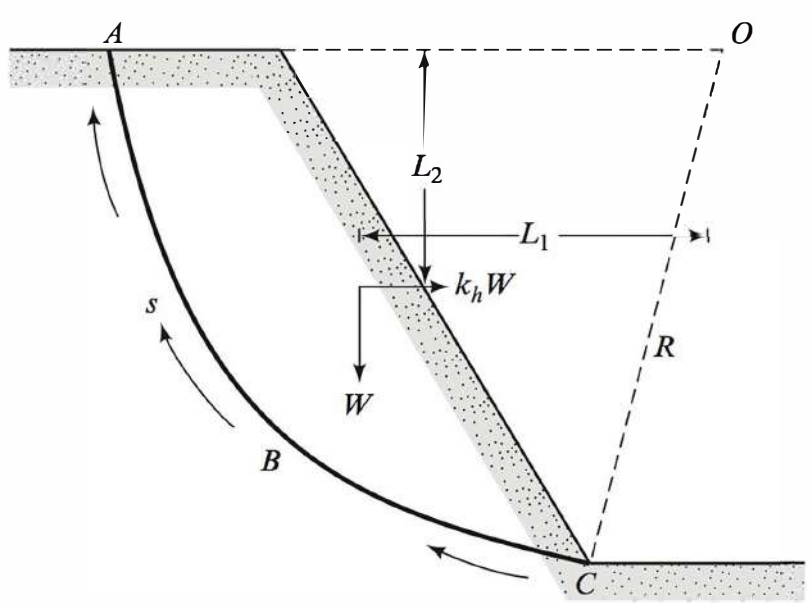

Figure 12.13 Stability analysis for slope

Copyright 2017 Cengage Learning. All Rights Reserved. May not be copied, scanned, or duplicated, in whole or in part. Due to electronic rights, some third party content may be suppressed from the eBook and/or eChapter(s). Editorial review has deemed that any suppressed content does not materially affect the overall learning experience. Cengage Learning reserves the right to remove additional content at any time if subsequent rights restrictions require it.

Dam	Country	Horizontal seismic coefficient, k_h	Minimum factor of safety, F_s
Aviemore	New Zealand	0.1	1.5
Bersemisnoi	Canada	0.1	1.25
Digma	Chile	0.1	1.15
Globocica	Yugoslavia	0.01	1.0
Karamauri	Turkey	0.1	1.2
Kisenyama	Japan	0.12	1.15
Mica	Canada	0.1	1.25
Misakubo	Japan	0.12	—
Nezahualcoyotl	Mexico	0.15	1.35
Oroville	United States	0.1	1.2
Paloma	Chile	0.12 to 0.2	1.25 to 1.2
Ramganga	India	0.12	1.2
Tercan	Turkey	0.15	1.2
Yeso	Chile	0.12	1.5

A second method that has gained acceptance more recently is the determination of the displacement of slopes due to earthquakes. This method is primarily based on the original concept proposed by Newmark (1965) and can be explained in the following manner.

Consider a slope as shown in Figure 12.14. When this slope is subjected to an earthquake, the stability of the slope will depend on the shear strength of the soil and the average coefficient of horizontal acceleration. The factor of safety of the soil mass located above the most critical surface $ABCD$ will become equal to 1 when k_h becomes equal to k_y. This value of $k_h = k_y$ may be defined

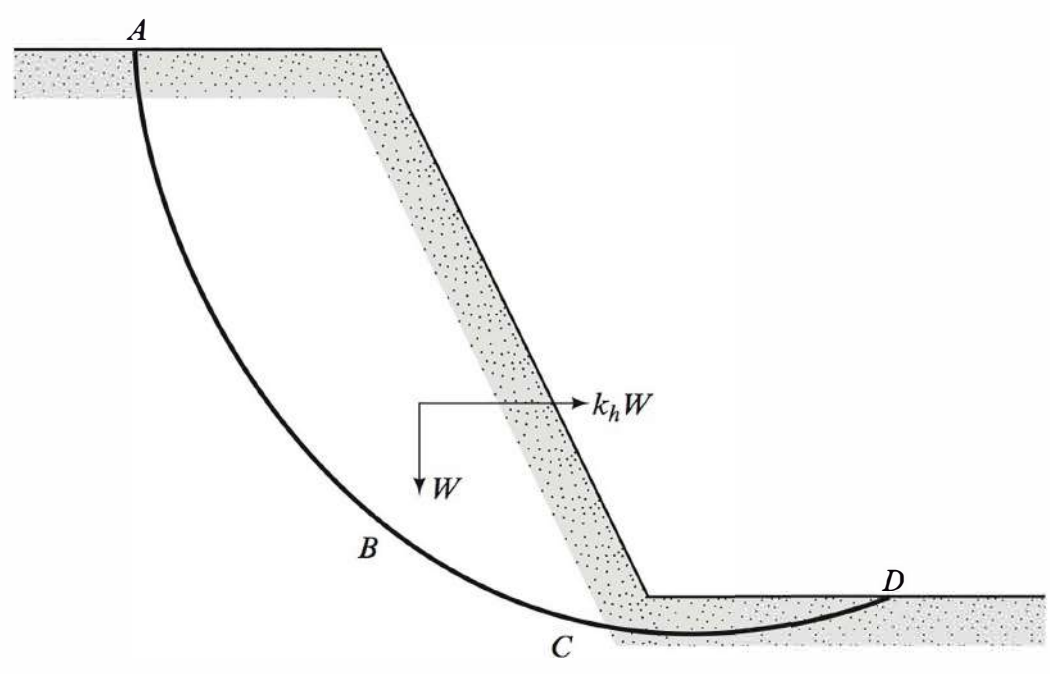

Figure 12.14 Soil slope

Copyright 2017 Cengage Learning. All Rights Reserved. May not be copied, scanned, or duplicated, in whole or in part. Due to electronic rights, some third party content may be suppressed from the eBook and/or eChapter(s). Editorial review has deemed that any suppressed content does not materially affect the overall learning experience. Cengage Learning reserves the right to remove additional content at any time if subsequent rights restrictions require it.

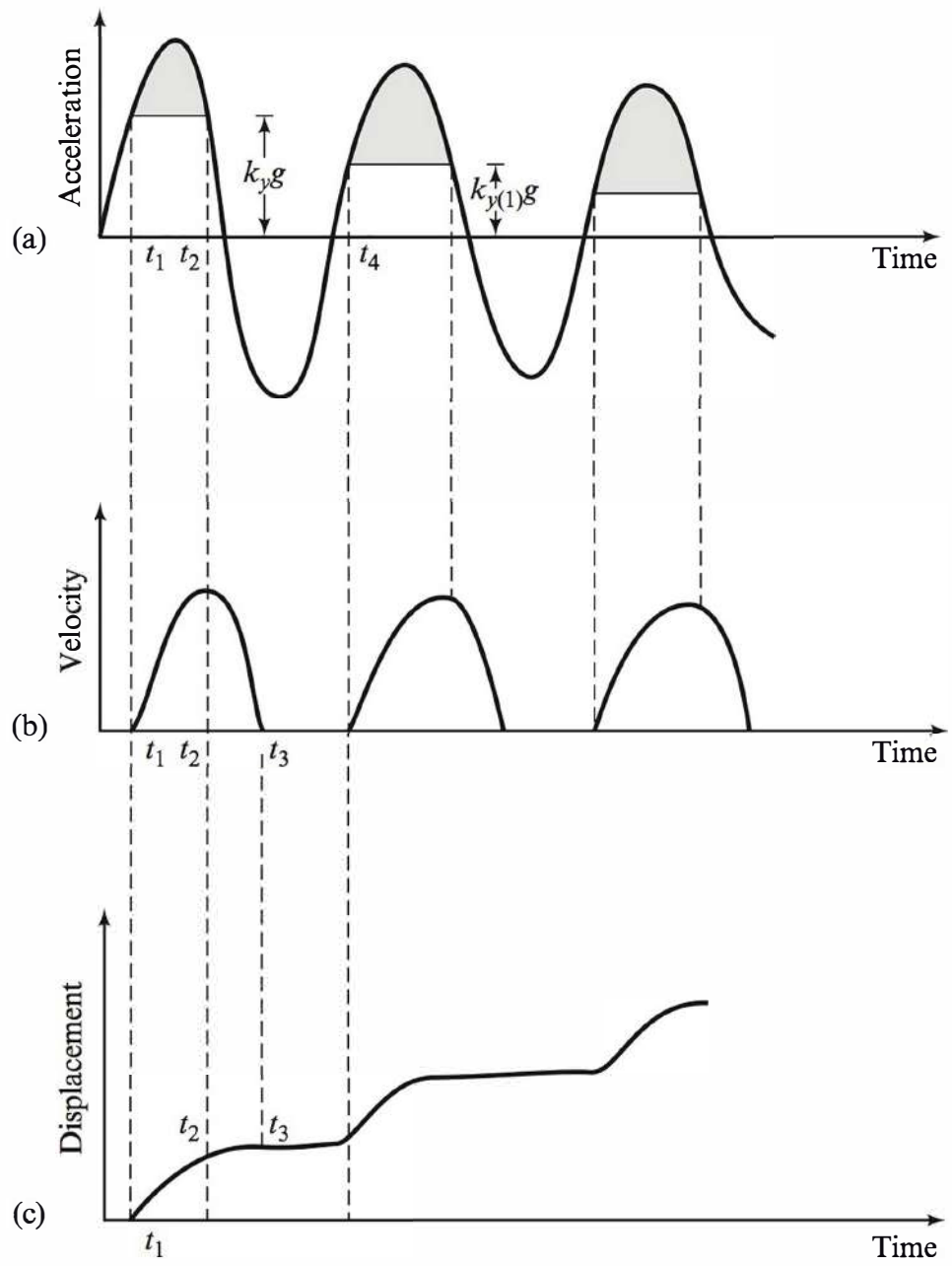

Figure 12.15 Integration method to determine down-slope displacement

as the *coefficient of yield acceleration*. Now refer to Figure 12.15a, which shows a plot of the horizontal acceleration with time to which the soil wedge *ABCD* is being subjected (Figure 12.14). At time $t = t_1$, the horizontal acceleration is $k_y g$ (g = acceleration due to gravity). Between time $t = t_1$ to $t = t_2$, the velocity of the sliding wedge will increase. This velocity can be determined by integration of the shaded area. The velocity will gradually decrease and become equal to zero at $t = t_3$ (Figure 12.15b). The displacement of the soil wedge can now be determined by integration of the area under the velocity versus time plot between $t = t_1$ and $t = t_3$ (Figure 12.15c).

It is important to note that the peak shear strength of the soil along the critical surface *ABCD* has now been mobilized. Hence, when the horizontal acceleration reaches $k_{y(1)}g$ (which is less than $k_y g$) at time $t = t_4$, the velocity of the sliding wedge will again increase, since the post-peak strength will be mobilized. As before, we can determine the velocity and the displacement of the sliding wedge by using the integration method. Hence, with time, the displacement of the

Copyright 2017 Cengage Learning. All Rights Reserved. May not be copied, scanned, or duplicated, in whole or in part. Due to electronic rights, some third party content may be suppressed from the eBook and/or eChapter(s). Editorial review has deemed that any suppressed content does not materially affect the overall learning experience. Cengage Learning reserves the right to remove additional content at any time if subsequent rights restrictions require it.

wedge gradually increases. In most cases of embankment stability consideration, it can be shown (Seed, 1981) that where the crest acceleration does not exceed 0.75 g, deformation of such embankments will usually be acceptably small if the embankment has $F_s = 1.15$ as determined by the pseudostatic analysis.

Average Value of k_h

In reference to Figure 12.13, it has been mentioned in this section that an average value of k_h is usually assumed for the pseudostatic method of analysis of slopes. It is now essential to have a general theoretical background as to what this average value of k_h is. The following theoretical derivation has been recommended by Seed and Martin (1966).

Figure 12.16 shows a hypothetical earth embankment, which is triangular in cross section. Let us consider the inertia force on an arbitrary soil wedge Oac. The displacement of the embankment at a depth z can be given as [Eqs. (12.6) and (12.13)]

$$u(z,t) = \sum_{n=1}^{n=\infty} \frac{2J_0[\beta_n(z/H)]}{\omega_n \beta_n J_0(\beta_n)} . V_n(t) \tag{12.32}$$

So, the distribution of shear strain can be obtained as

$$\frac{\partial u}{\partial z}(z,t) = \sum_{n=1}^{n=\infty} \frac{2J_1[\beta_n(z/H)]}{H\omega_n J_1(\beta_n)} . V_n(t) \tag{12.33}$$

Hence, the distribution shear stress, $\tau(z,t)$ is

$$\tau(z,t) = G\frac{\partial u}{\partial z}(z,t) = \sum_{n=1}^{n=\infty} \frac{2GJ_1[\beta_n(z/H)]}{H\omega_n J_1(\beta_n)} V_n(t) \tag{12.34}$$

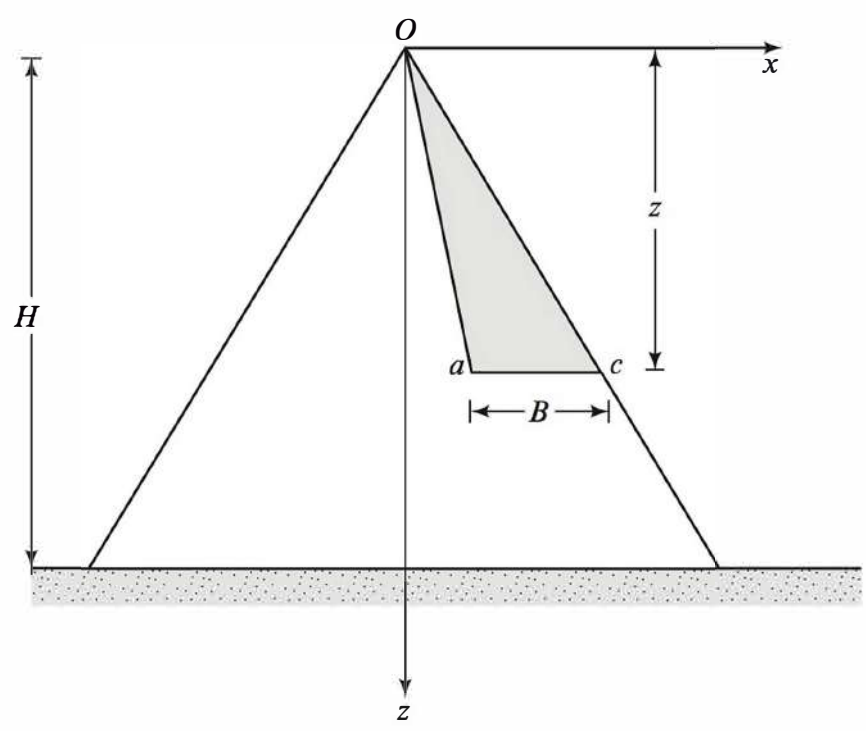

Figure 12.16 Analysis for average value of k_h

Copyright 2017 Cengage Learning. All Rights Reserved. May not be copied, scanned, or duplicated, in whole or in part. Due to electronic rights, some third party content may be suppressed from the eBook and/or eChapter(s). Editorial review has deemed that any suppressed content does not materially affect the overall learning experience. Cengage Learning reserves the right to remove additional content at any time if subsequent rights restrictions require it.

The shear force, $F(z,t)$, acting on the base of the wedge Oac is

$$F(z,t) = \tau(z,t)B \tag{12.35}$$

However,

$F(z,t) = (\text{mass of the wedge } Oac)\ \ddot{u}_a(t)_{av}$

$$= \left(\frac{1}{2}\rho Bz\right)\ddot{u}_a(t)_{av} \tag{12.36}$$

where $\ddot{u}_a(t)_{av}$ = average lateral acceleration
ρ = density of the soil in the wedge

So

$$\ddot{u}_a(t)_{av} = \frac{2F(z,t)}{\rho Bz} = \frac{2\tau(z,t)B}{\rho Bz} = \frac{2\tau(z,t)}{\rho z} \tag{12.37}$$

Combining Eqs. (12.34) and (12.37),

$$\ddot{u}_a(t)_{av} = \sum_{n=1}^{n=\infty} \frac{4GJ_1[\beta_n(z/H)]}{\rho H\omega_n z J_1(\beta_n)} V_n(t) \tag{12.38}$$

So

$$\boxed{k_h = \frac{1}{g}\ddot{u}_a(t)_{av} = \sum_{n=1}^{n=\infty} \frac{4GJ_1[\beta_n(z/H)]}{g\rho H\omega_n z J_1(\beta_n)} . V_n(t)} \tag{12.39}$$

The value of k_h is a function of time. Since the average acceleration varies with the depth z, the magnitude of k_h also varies with time. Figure 12.17 shows the results of a calculation for k_h for a model embankment at four different levels.

Yield Strength

In the analysis of stability for earth embankments, it is important to make proper selection of the yield strength of soil to determine the shear strength parameters. The yield strength is defined as the maximum stress level below which the material exhibits a near-elastic behavior when subjected to cyclic stresses of numbers and frequencies similar to those induced by earthquake shaking.

Figure 12.18 shows the concept of cyclic yield strength of a clayey soil (Makdisi and Seed, 1978). The material in this case has an yield strength of about 90% of its static undrained strength. In Figure 12.18, it can be seen that under 100 cycles of stress, which amounts 80% of static undrained strength, the material behaves in a near-elastic manner. However, when 10 cycles of stress, which amounts to 95% of static undrained strength, is applied, substantially large permanent deformation is observed (Figure 12.18). Hence, the yield strength is about 90% of its static undrained strength.

Copyright 2017 Cengage Learning. All Rights Reserved. May not be copied, scanned, or duplicated, in whole or in part. Due to electronic rights, some third party content may be suppressed from the eBook and/or eChapter(s). Editorial review has deemed that any suppressed content does not materially affect the overall learning experience. Cengage Learning reserves the right to remove additional content at any time if subsequent rights restrictions require it.

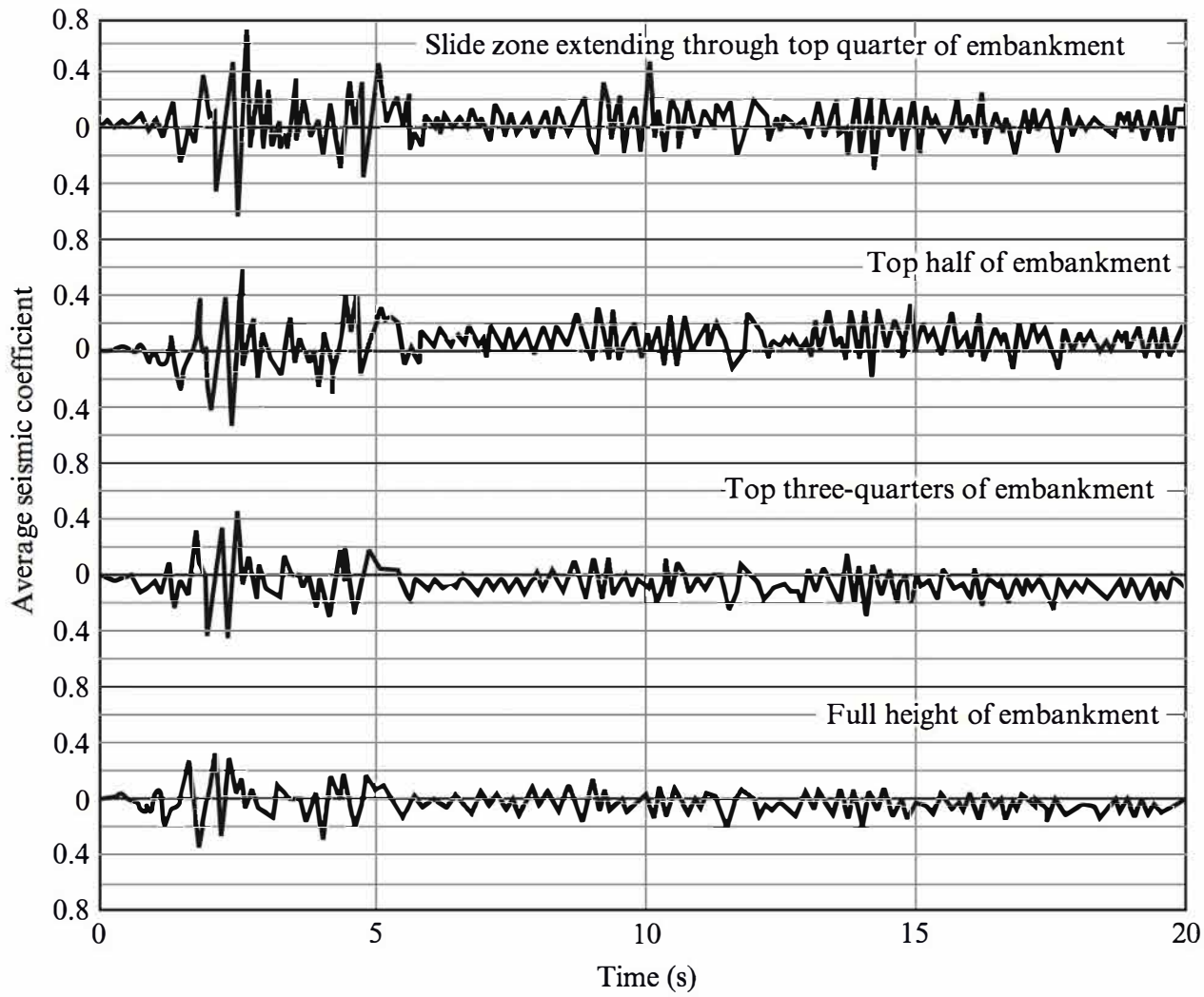

Figure 12.17 Values of average seismic coefficient for 30-m-high embankment subjected to El Centro earthquakes (shear wave velocity, v_s = 300 m/s, 20% critical damping) (from Seed and Martin, 1966)

Source: Based on Seed, H.B., and Martin, G.R. (1966). "The Seismic Coefficient in Earth Dam Designs," *Journal of the Soil Mechanics and Foundations Division*, ASCE, Vol. 92, No. SM3, pp. 25–58.

Stability Analysis

The remainder of this chapter is divided into two parts. The first part is devoted to the pseudostatic methods of stability analysis and the second part to the determination of the deformation of slopes.

Pseudostatic Analysis

12.7 CLAY SLOPES (ϕ = 0 CONDITION)—KOPPULA'S ANALYSIS

A clay ($\phi = 0$ condition) slope of height H is shown in Figure 12.19a. In order to determine the minimum factor of safety of the slope with respect to strength, we consider a trial failure surface ABC, which is an arc of a circle

Copyright 2017 Cengage Learning. All Rights Reserved. May not be copied, scanned, or duplicated, in whole or in part. Due to electronic rights, some third party content may be suppressed from the eBook and/or eChapter(s). Editorial review has deemed that any suppressed content does not materially affect the overall learning experience. Cengage Learning reserves the right to remove additional content at any time if subsequent rights restrictions require it.

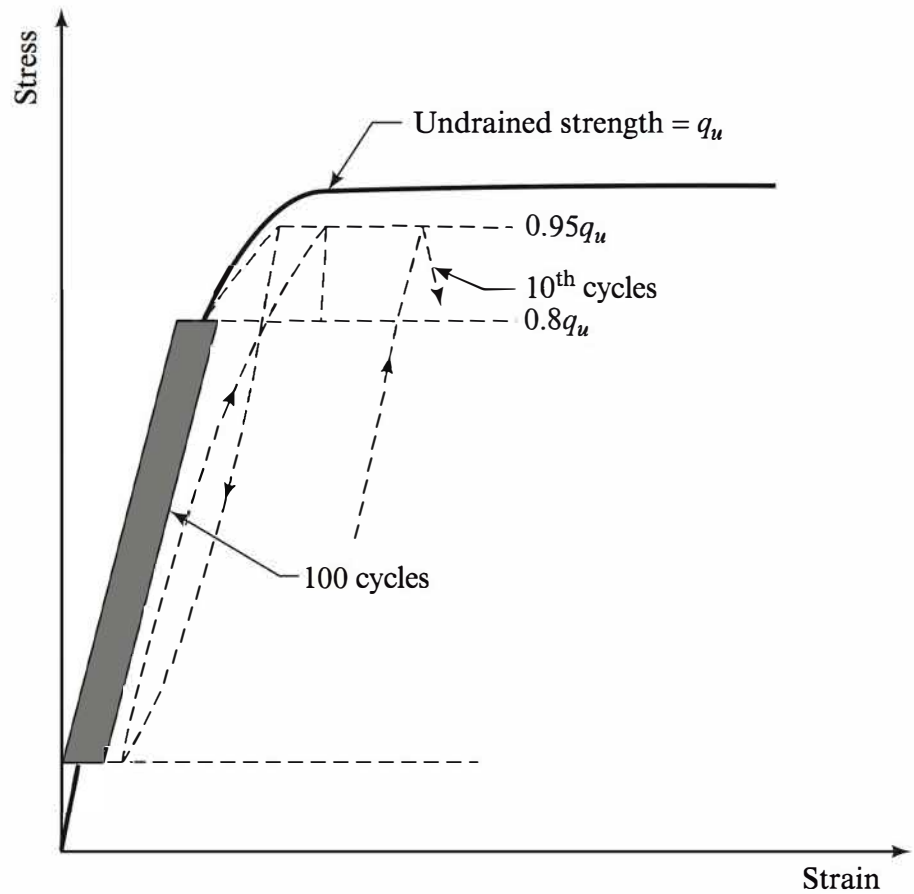

Figure 12.18 Concept of cyclic yield strength

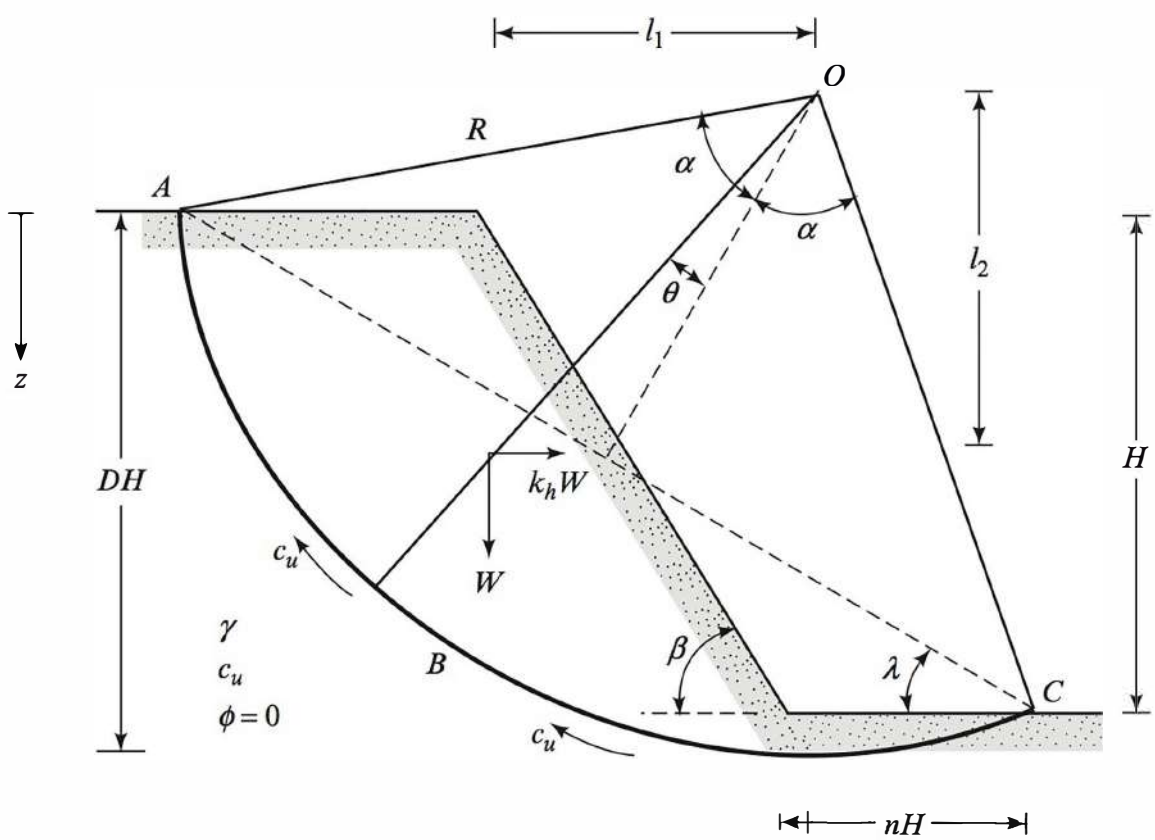

Figure 12.19 Koppula's analysis for clay slopes (ϕ = 0 condition)

with its center located at O. Let the saturated unit weight and the undrained cohesion of the clay soil be equal to γ and c_u, respectively. The undrained cohesion c_u may increase with depth z measured from the top of the slope and can be expressed as

Copyright 2017 Cengage Learning. All Rights Reserved. May not be copied, scanned, or duplicated, in whole or in part. Due to electronic rights, some third party content may be suppressed from the eBook and/or eChapter(s). Editorial review has deemed that any suppressed content does not materially affect the overall learning experience. Cengage Learning reserves the right to remove additional content at any time if subsequent rights restrictions require it.

$$c_u = c_0 + a_0 z \tag{12.40}$$

where a_0 = constant.

Per unit length of the slope, for consideration of the stability of the soil mass located above the trial failure surface, the following forces need to be considered:

a. Weight of the soil mass, W;
b. Undrained cohesion, c_u, per unit area along the trial failure surface ABC; and
c. Inertia force on the soil mass, $k_h W$ (where k_h = average horizontal acceleration of the mass)

The overturning moment, M_D, about O can be given as

$$M_D = \underbrace{Wl_1}_{M_W} + \underbrace{k_h W l_2}_{M_E} \tag{12.41}$$

Koppula (1984) has expressed M_W and M_E in the following forms:

$$M_W = \frac{\gamma H^3}{12}(1 - 2\cot^2\beta - 3\cot\alpha\cot\beta + 3\cot\beta\cot\lambda + 3\cot\lambda\cot\alpha - 6n\cot\beta - 6n^2 - 6n\cot\alpha + 6n\cot\lambda) \tag{12.42}$$

$$M_E = \frac{k_h\gamma H^3}{12}(\cot\beta + \cot^3\lambda + 3\cot\alpha\cot^2\lambda - 3\cot\alpha\cot\beta\cot\lambda - 6n\cot\alpha\cot\lambda) \tag{12.43}$$

The restoring moment M_R about O is

$$M_R = R\int_{-\alpha}^{+\alpha} c_u R\, d\theta \tag{12.44}$$

where R = radius of the circular arc

$$c_u = c_0 + a_0[R\cos(\lambda + \theta) - R\cos(\alpha - \lambda) + H] \tag{12.45}$$

Combining Eqs. (12.44) and (12.45)

$$M_R = \frac{a_0 H^3}{4\sin^2\alpha\sin^2\lambda}\left[\alpha(1 - \cot\alpha\cos\lambda) + \cot\lambda\right] + \frac{c_0 H^2\alpha}{2\sin^2\alpha\sin^2\lambda} \tag{12.46}$$

The factor of safety F_s against sliding can be given as

$$\boxed{F_s = \frac{M_R}{M_W + M_E}} \tag{12.47}$$

The minimum value of F_s has to be determined by considering several trial failure surfaces. Koppula (1984) has expressed a minimum factor of safety in the form

$$\boxed{F_s = \frac{a_0}{\gamma}N_1 + \frac{c_0}{\gamma H}N_2} \tag{12.48}$$

Copyright 2017 Cengage Learning. All Rights Reserved. May not be copied, scanned, or duplicated, in whole or in part. Due to electronic rights, some third party content may be suppressed from the eBook and/or eChapter(s). Editorial review has deemed that any suppressed content does not materially affect the overall learning experience. Cengage Learning reserves the right to remove additional content at any time if subsequent rights restrictions require it.

where N_1 and N_2 = stability numbers. Stability numbers are functions of k_h, the slope angle β, and also the depth factor, D (for the definition of depth factor, see Figure 12.19). Figure 12.20 shows the variation of N_1 and k_h varying from 0 to 0.4 and β varying from 0° to 90°. In a similar manner, the variation of N_2 with k_h and D for $\beta \leq 50°$ is shown in Figure 12.21. For $\beta \geq 55°$, the variation of N_2 with k_h is given in Figure 12.22. In order to use Eq. (12.48) and Figures 12.20, 12.21, and 12.22, the following points needs to be kept in mind.

1. If the undrained shear strength of the soil increases linearly from zero at the top, then

$$c_u = a_0 z \tag{12.49}$$

For this case, the critical slip surface associated with minimum F_s passes through the toe of the slope and lies within the slope. So

$$\left.\begin{aligned} n &= 0 \\ D &= 0 \end{aligned}\right\} \tag{12.50}$$

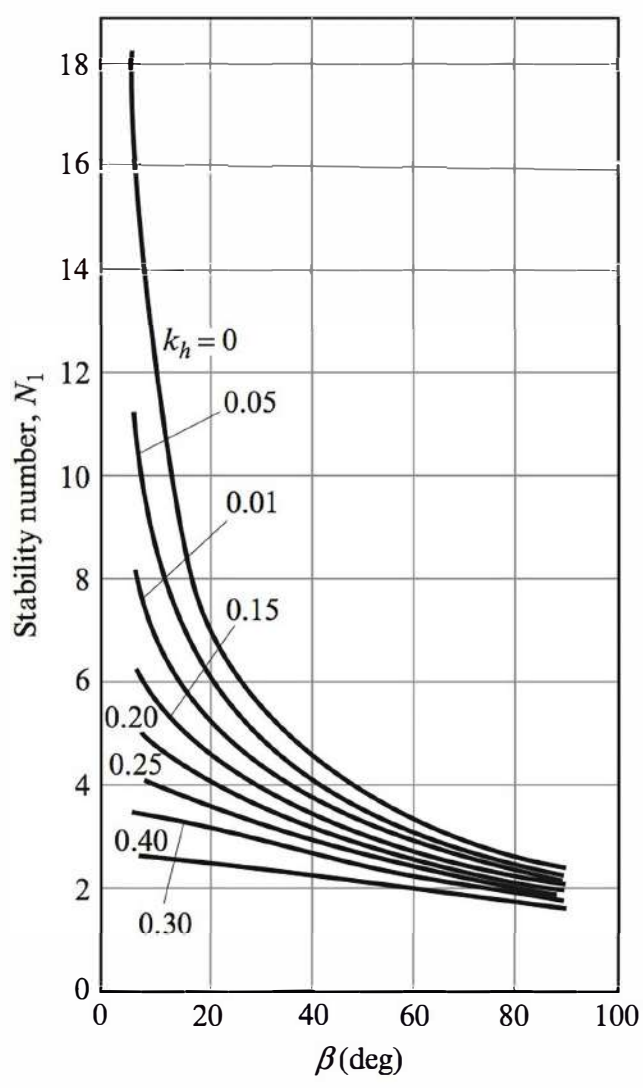

Figure 12.20 Variation of N_1 with slope angle β (from Koppula, 1984)

Source: Koppula, S.D. (1984). "Pseudo-Static Analysis of Clay Slopes Subjected to Earthquakes," *Geotechnique*, Institution of Civil Engineers, London, Vol. 34, No. 1, pp. 71–79.

Copyright 2017 Cengage Learning. All Rights Reserved. May not be copied, scanned, or duplicated, in whole or in part. Due to electronic rights, some third party content may be suppressed from the eBook and/or eChapter(s). Editorial review has deemed that any suppressed content does not materially affect the overall learning experience. Cengage Learning reserves the right to remove additional content at any time if subsequent rights restrictions require it.

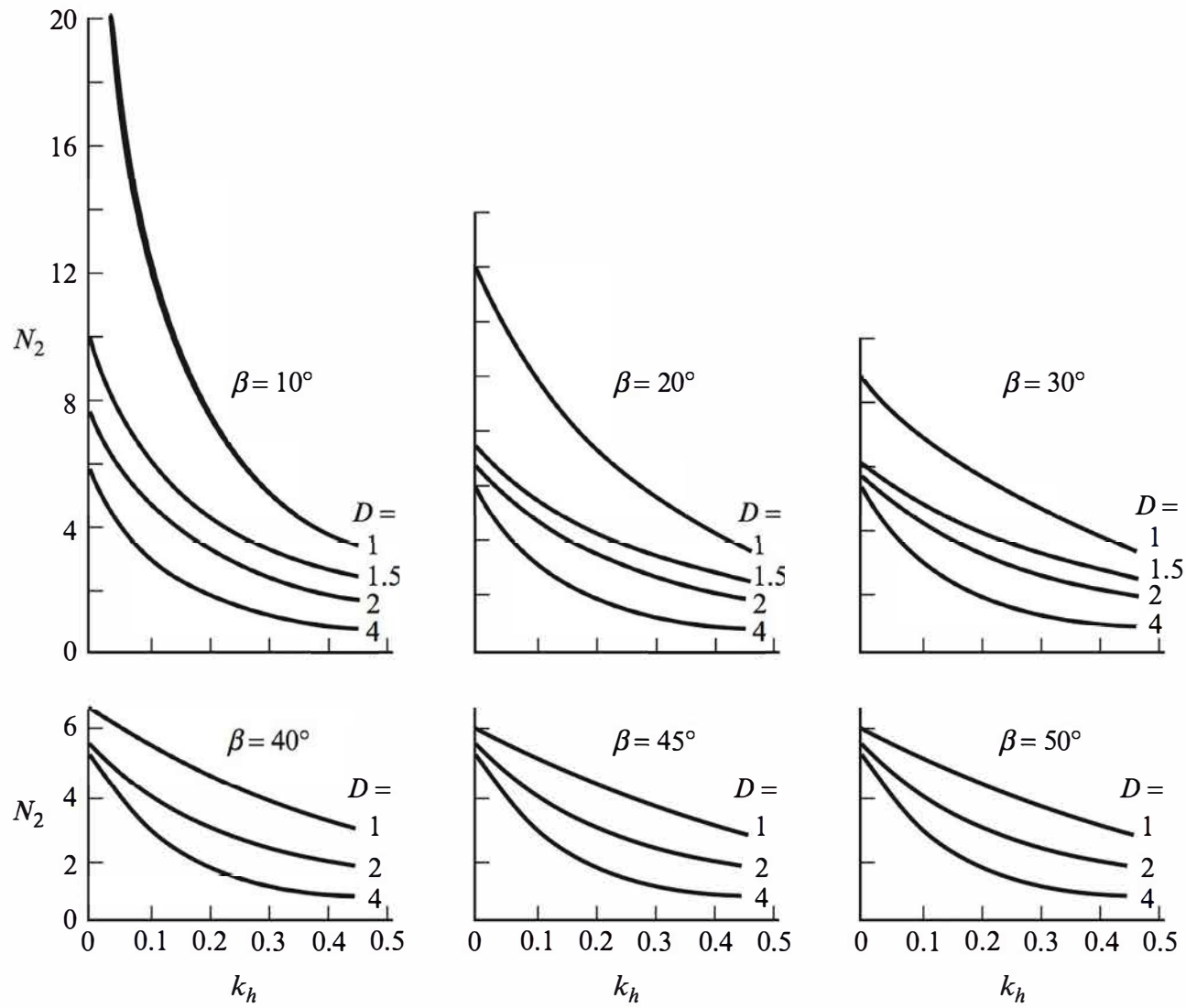

Figure 12.21 Variation of N_2 with k_h and β (from Koppula, 1984)

Source: Koppula, S.D. (1984). "Pseudo-Static Analysis of Clay Slopes Subjected to Earthquakes," *Geotechnique*, Institution of Civil Engineers, London, Vol. 34, No. 1, pp. 71–79.

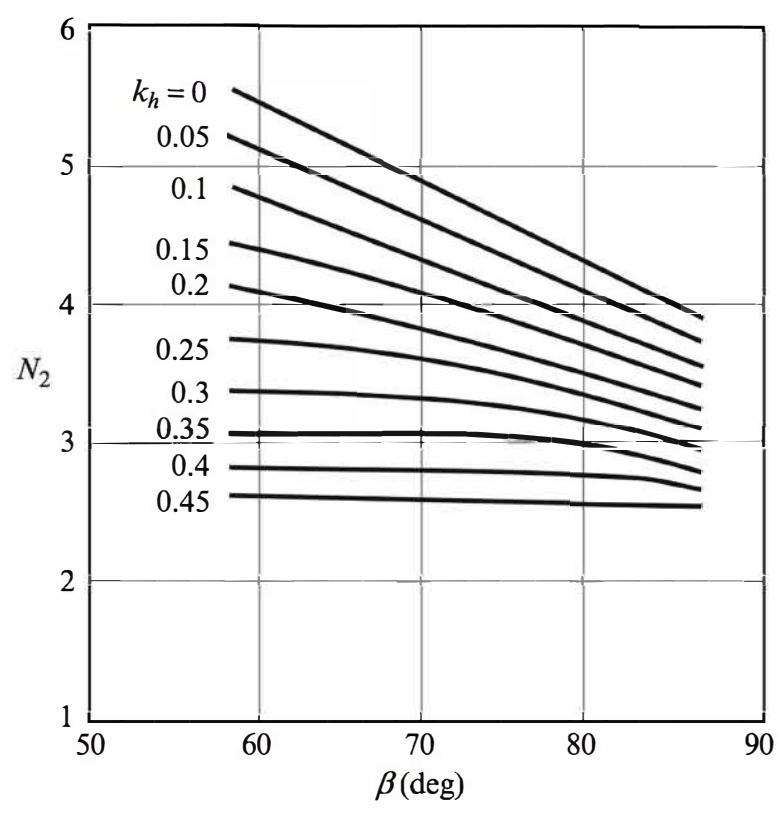

Figure 12.22 Variation of N_2 with $\beta \geq 55°$ and k_h (from Koppula, 1984)

Source: Koppula, S.D. (1984). "Pseudo-Static Analysis of Clay Slopes Subjected to Earthquakes," *Geotechnique*, Institution of Civil Engineers, London, Vol. 34, No. 1, pp. 71–79.

Copyright 2017 Cengage Learning. All Rights Reserved. May not be copied, scanned, or duplicated, in whole or in part. Due to electronic rights, some third party content may be suppressed from the eBook and/or eChapter(s). Editorial review has deemed that any suppressed content does not materially affect the overall learning experience. Cengage Learning reserves the right to remove additional content at any time if subsequent rights restrictions require it.

Also

$$F_s = \frac{a_0}{\gamma} N_1 \tag{12.51}$$

2. If the magnitude of c_u is constant with depth, then

$$\left.\begin{aligned} a_0 &= 0 \\ c_u &= c_0 \end{aligned}\right\} \tag{12.52}$$

For this case

$$F_s = \frac{c_0}{\gamma H} N_2 \tag{12.53}$$

The stability number N_2 is a function of β, D, and k_h if $\beta \leq 53°$. However, if $\beta \geq 53°$, then N_2 is a function of β and k_h only (that is, $n = 0$ and $D = 0$).

EXAMPLE 12.2

Refer to the slope shown in Figure 12.19. Given:

$$H = 15\text{ m} \qquad \gamma = 18\text{ kN/m}^3$$
$$\beta = 60° \qquad c_u = 48 + 3z\text{ (kPa)}$$

Determine the factor of safety F_s for $k_h = 0.3$.

SOLUTION:

From Eq. (12.48)

$$F_s = \frac{a_0}{\gamma} N_1 + \frac{c_0}{\gamma H} N_2$$

From Figure 12.20, for $\beta = 60°$ and $k_h = 0.3$, the magnitude of $N_1 \approx 2.38$. Again, from Figure 12.22, for $\beta = 60°$ and $k_h = 0.3$, the magnitude of N_2 is about 3.28. So

$$F_s = \left(\frac{3}{18}\right)(2.38) + \frac{48}{(18)(15)}(3.28) = 0.397 + 0.583 = \mathbf{0.98}$$

Copyright 2017 Cengage Learning. All Rights Reserved. May not be copied, scanned, or duplicated, in whole or in part. Due to electronic rights, some third party content may be suppressed from the eBook and/or eChapter(s). Editorial review has deemed that any suppressed content does not materially affect the overall learning experience. Cengage Learning reserves the right to remove additional content at any time if subsequent rights restrictions require it.

12.8 SLOPES WITH c-ϕ SOIL—MAJUMDAR'S ANALYSIS

Taylor (1937) proposed the friction circle method of analyzing the stability of slopes with c-ϕ soils. In this analysis, the effect of earthquakes was not taken into consideration. The details of this slope stability analysis can be found in most soil mechanics textbooks (for example, Das, 2010). However, it can be summarized as follows.

Figure 12.23 shows a slope made of a soil having a shear strength that can be given as

$$\tau_f = c + \sigma' \tan\phi \tag{12.54}$$

where τ_f = shear strength
c = cohesion
σ' = effective normal stress
ϕ = drained friction angle

For ϕ greater than about 3°, the *critical circle* for stability analysis always passes through the toe, as shown in Figure 12.23.

For stability analysis, one can define three different factors of safety for the soil at any point along the critical surface:

1. Factor of safety with respect to friction:

$$F_\phi = \frac{\tan\phi}{\tan\phi_d}$$

where ϕ_d = developed friction angle ($\leq \phi$).

2. Factor of safety with respect to cohesion:

$$F_c = \frac{c}{c_d}$$

where c_d = developed cohesion ($\leq c$).

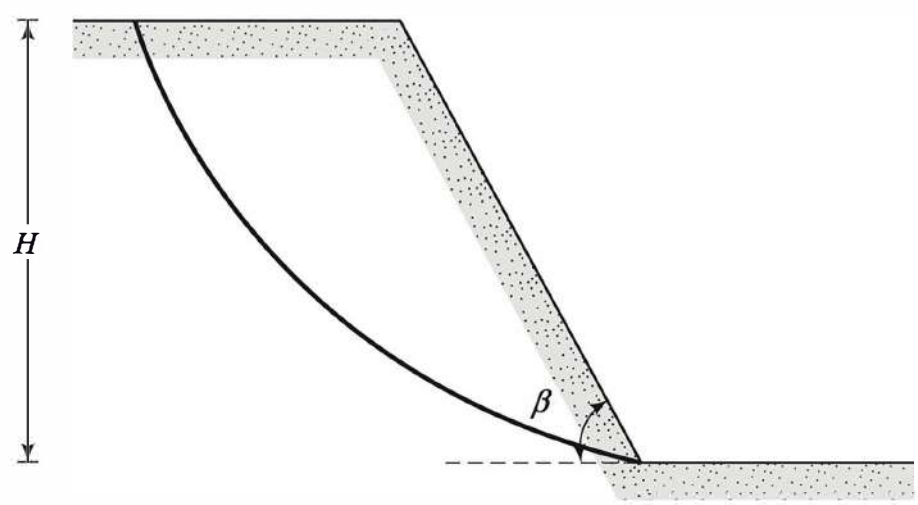

Figure 12.23 Slopes with c-ϕ soil

Copyright 2017 Cengage Learning. All Rights Reserved. May not be copied, scanned, or duplicated, in whole or in part. Due to electronic rights, some third party content may be suppressed from the eBook and/or eChapter(s). Editorial review has deemed that any suppressed content does not materially affect the overall learning experience. Cengage Learning reserves the right to remove additional content at any time if subsequent rights restrictions require it.

3. Factor of safety with respect to strength:

$$\boxed{F_s = \frac{c + \sigma' \tan\phi}{c_d + \sigma' \tan\phi_d}} \tag{12.55}$$

It is obvious from the preceding definitions that if

$$\frac{c}{c_d} = \frac{\tan\phi}{\tan\phi_d}$$

then

$$F_c = F_\phi = F_s \tag{12.56}$$

It is important to note that the relationship for the factor of safety developed in Section 12.7 is the factor of safety with respect to strength.

Using the preceding concepts for factor of safety, Taylor's analysis (1937) for the stability of slopes by the friction circles method can be given in a graphical form, the nature of which is shown in Figure 12.24. Note that in Figure 12.24 the term m is defined as

$$m = \frac{c_d}{\gamma H}$$

Majumdar (1971) expanded Taylor's analysis of slope by taking into consideration the horizontal earthquake forces as shown in Figure 12.25. By simple mathematical manipulations, Majumdar showed that if the actual effective friction angle ϕ of the soil can be modified to ϕ_m, it can then be used in Taylor's analysis to determine the factor of safety with respect to strength (F_s) for the critical surface of a slope.

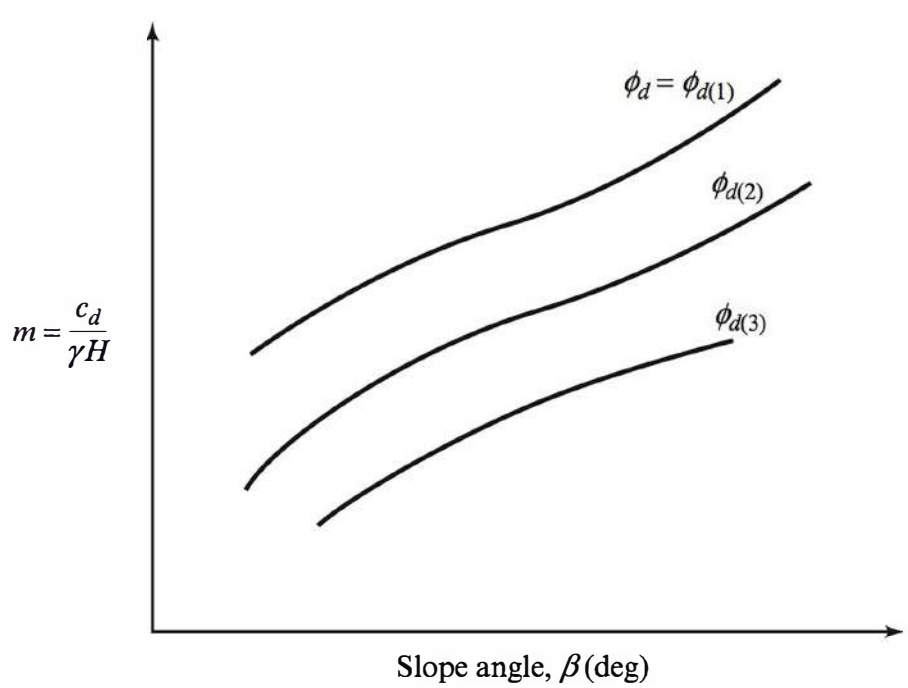

Figure 12.24 Nature of variation of m with β and ϕ_d

Copyright 2017 Cengage Learning. All Rights Reserved. May not be copied, scanned, or duplicated, in whole or in part. Due to electronic rights, some third party content may be suppressed from the eBook and/or eChapter(s). Editorial review has deemed that any suppressed content does not materially affect the overall learning experience. Cengage Learning reserves the right to remove additional content at any time if subsequent rights restrictions require it.

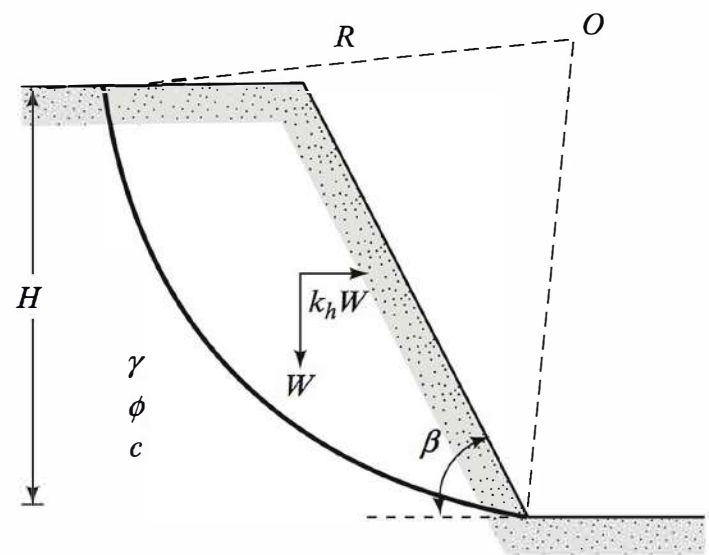

Figure 12.25 Analysis of slopes with c-ϕ soil

The relationship between ϕ and ϕ_m can be expressed as

$$\phi_m = \tan^{-1}(M \tan\phi) \tag{12.57}$$

The term M in Eq. (12.57) is a function of the slope angle (β) and the horizontal coefficient of acceleration (k_h). Figure 12.26 shows the variation of M with k_h for $\beta = 15°, 30°, 45°, 60°$, and $75°$.

Figure 12.27 shows the modified plot of Taylor's chart (that is, m versus β) for use of stability analysis. It is important to note that ϕ_d for a given soil is always less than or equal to ϕ_m.

In order to determine the factor of safety for a given slope, the following step-by-step procedure can be applied.

1. Determine the soil parameters ϕ and c and the unit weight γ.
2. Determine the parameters for the slope, that is, β and H.
3. For given values of ϕ, β, and k_h, determine the factor M from Figure 12.26.
4. Assume several values for the developed friction angle ϕ_d (such as $\phi_{d(1)}$, $\phi_{d(2)}$, $\phi_{d(3)}$,...). Note that $\phi_d \leq \phi_m$.
5. For each assumed value of ϕ_d, determine the factor of safety with respect to friction, or

$$F_{\phi(1)} = \frac{\tan\phi_m}{\tan\phi_{d(1)}}$$

$$F_{\phi(2)} = \frac{\tan\phi_m}{\tan\phi_{d(2)}}$$

$$F_{\phi(3)} = \frac{\tan\phi_m}{\tan\phi_{d(3)}}$$

6. With each assumed value of ϕ_d and the slope angle β, go to Figure 12.27 and determine the stability number m.

Copyright 2017 Cengage Learning. All Rights Reserved. May not be copied, scanned, or duplicated, in whole or in part. Due to electronic rights, some third party content may be suppressed from the eBook and/or eChapter(s). Editorial review has deemed that any suppressed content does not materially affect the overall learning experience. Cengage Learning reserves the right to remove additional content at any time if subsequent rights restrictions require it.

7. From the values of m calculated in Step 6, calculate c_d and the factor of safety with respect to cohesion (F_c) as

$$c_{d(1)} = m_1 \gamma H; \qquad F_{c(1)} = \frac{c}{c_{d(1)}}$$

$$c_{d(2)} = m_2 \gamma H; \qquad F_{c(2)} = \frac{c}{c_{d(2)}}$$

8. Plot a graph of F_ϕ versus F_c as determined from Steps 5 and 7 (Figure 12.28) and determine $F_s = F_c = F_\phi$.

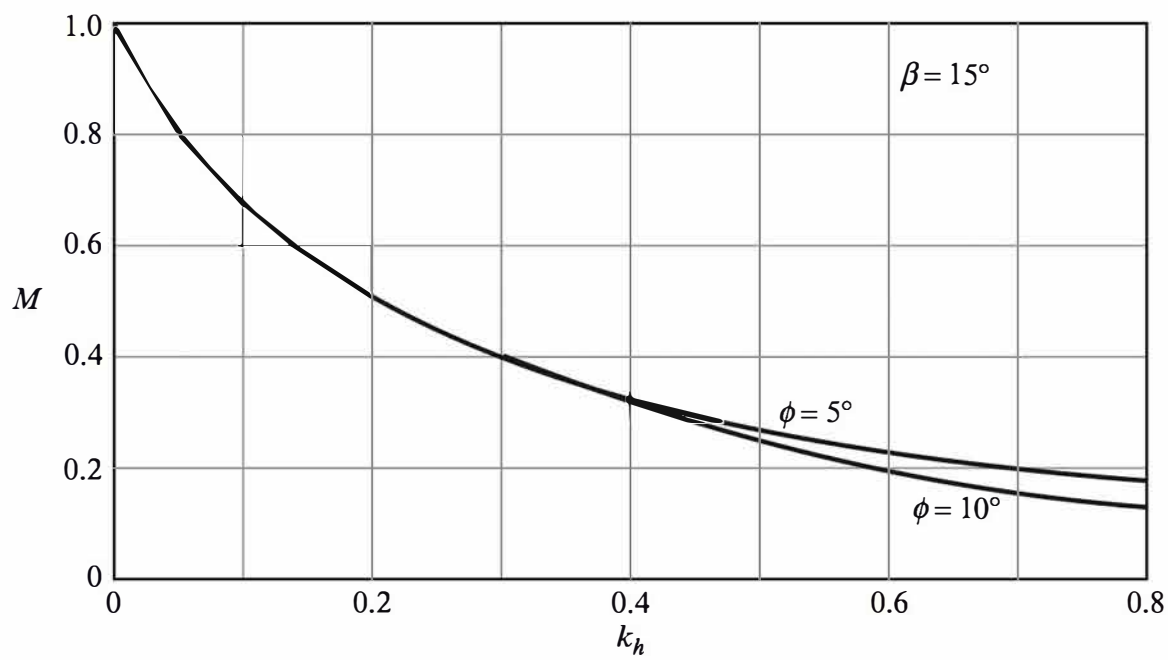

(a)

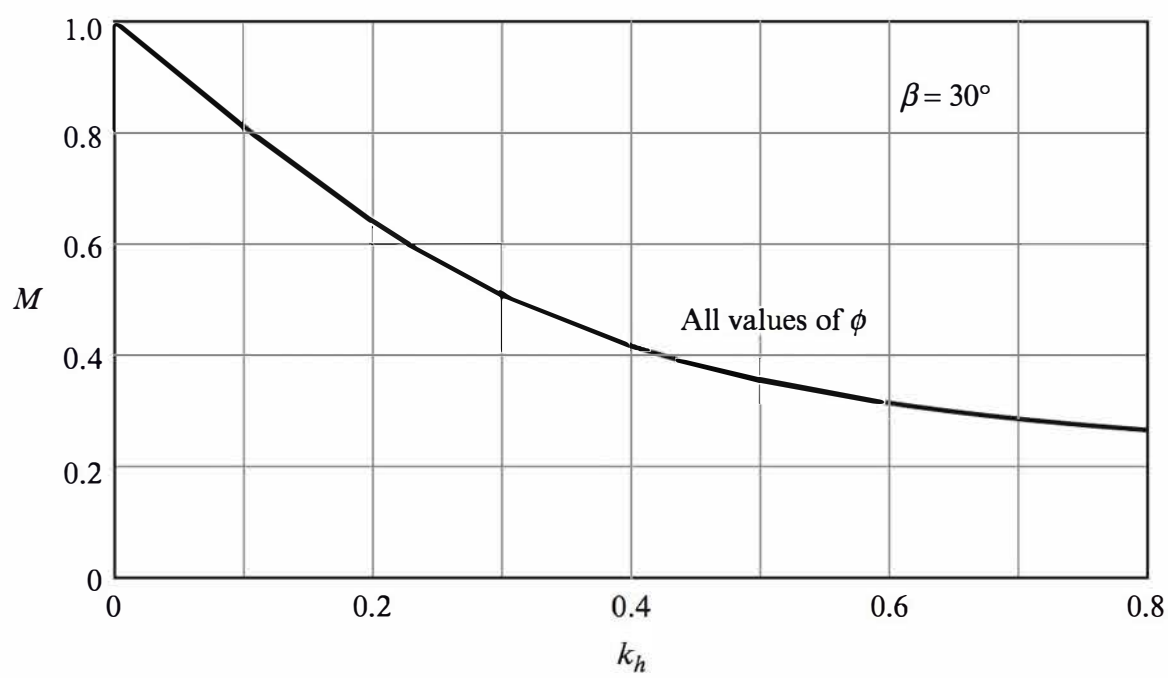

(b)

Figure 12.26 Variation of M with k_h (from Majumdar, 1971)

Source: Majumdar, D.K. (1971). "Stability of Soill Slopes Under Horizontal Earthquake Force," *Geotechnique, Institution of Civil Engineers*, London, Vol. 21, No. 1, pp. 372–378.

Copyright 2017 Cengage Learning. All Rights Reserved. May not be copied, scanned, or duplicated, in whole or in part. Due to electronic rights, some third party content may be suppressed from the eBook and/or eChapter(s). Editorial review has deemed that any suppressed content does not materially affect the overall learning experience. Cengage Learning reserves the right to remove additional content at any time if subsequent rights restrictions require it.

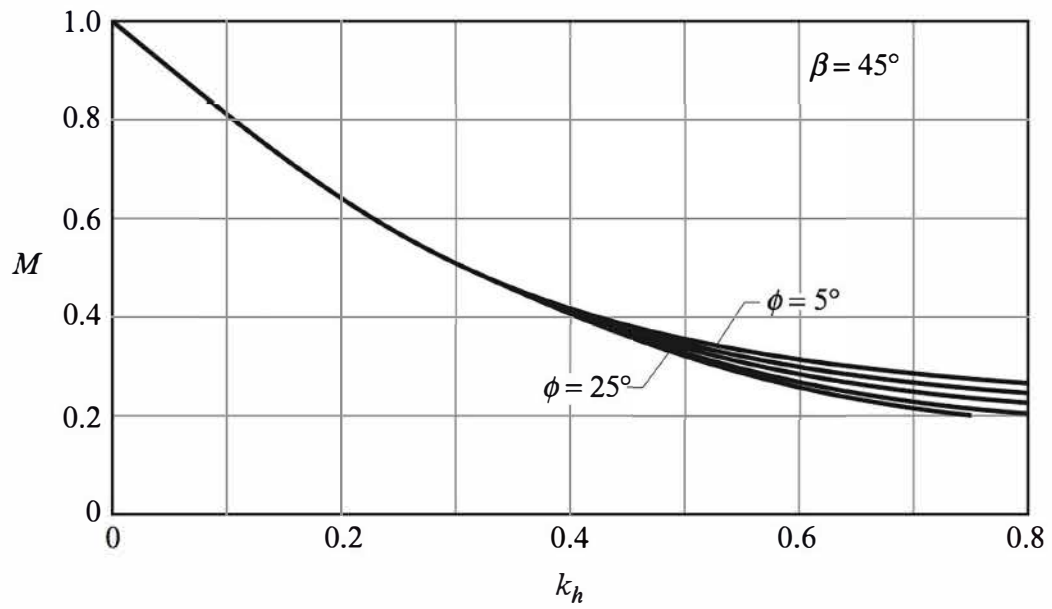

(c)

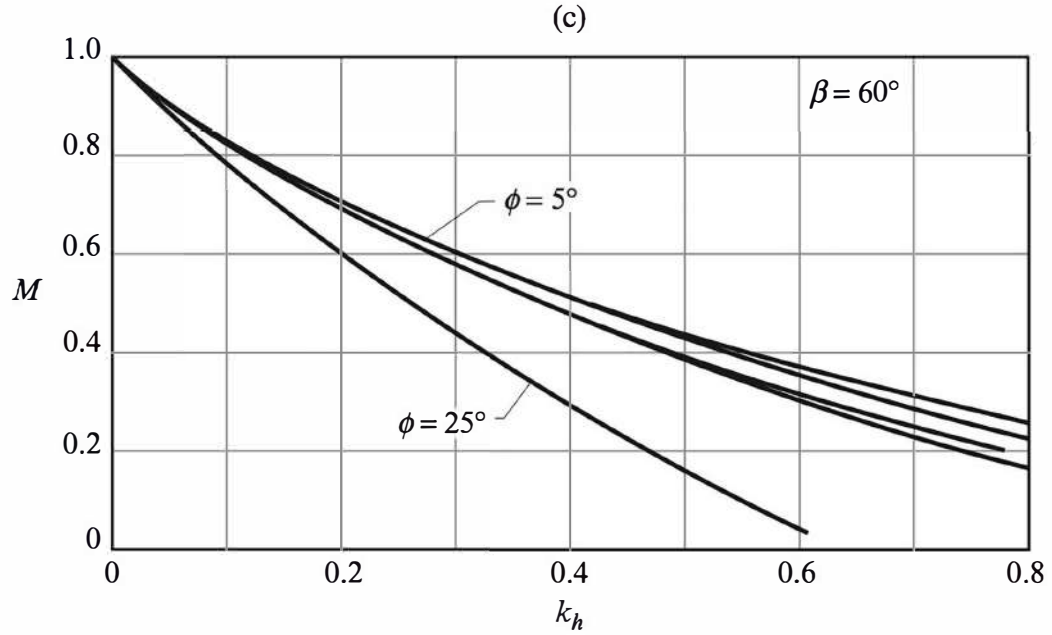

(d)

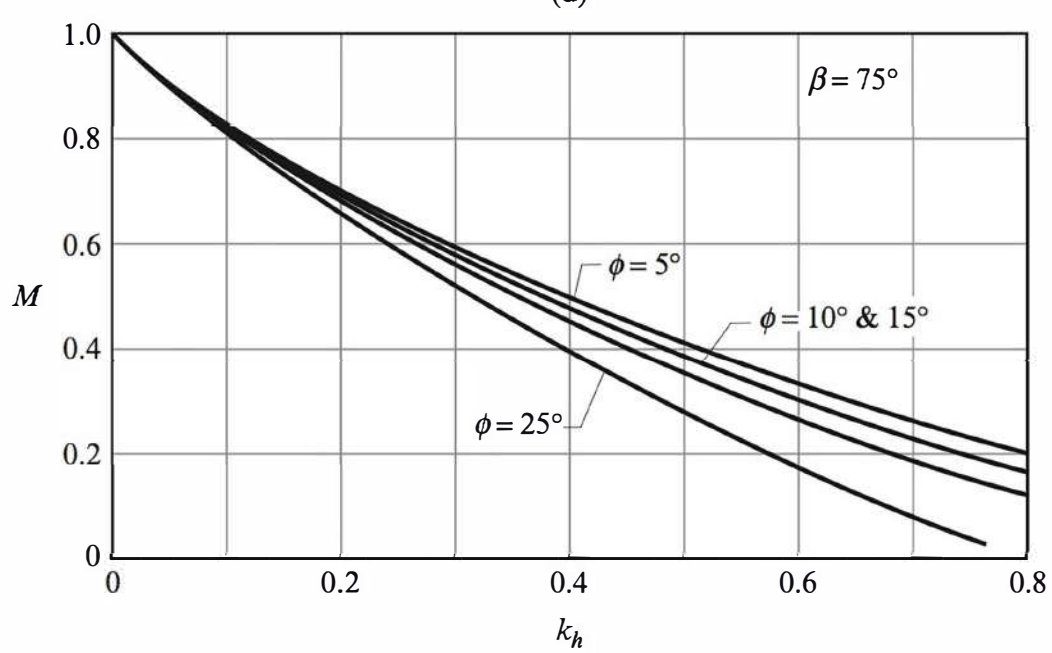

(e)

Figure 12.26 (*Continued*)

Copyright 2017 Cengage Learning. All Rights Reserved. May not be copied, scanned, or duplicated, in whole or in part. Due to electronic rights, some third party content may be suppressed from the eBook and/or eChapter(s). Editorial review has deemed that any suppressed content does not materially affect the overall learning experience. Cengage Learning reserves the right to remove additional content at any time if subsequent rights restrictions require it.

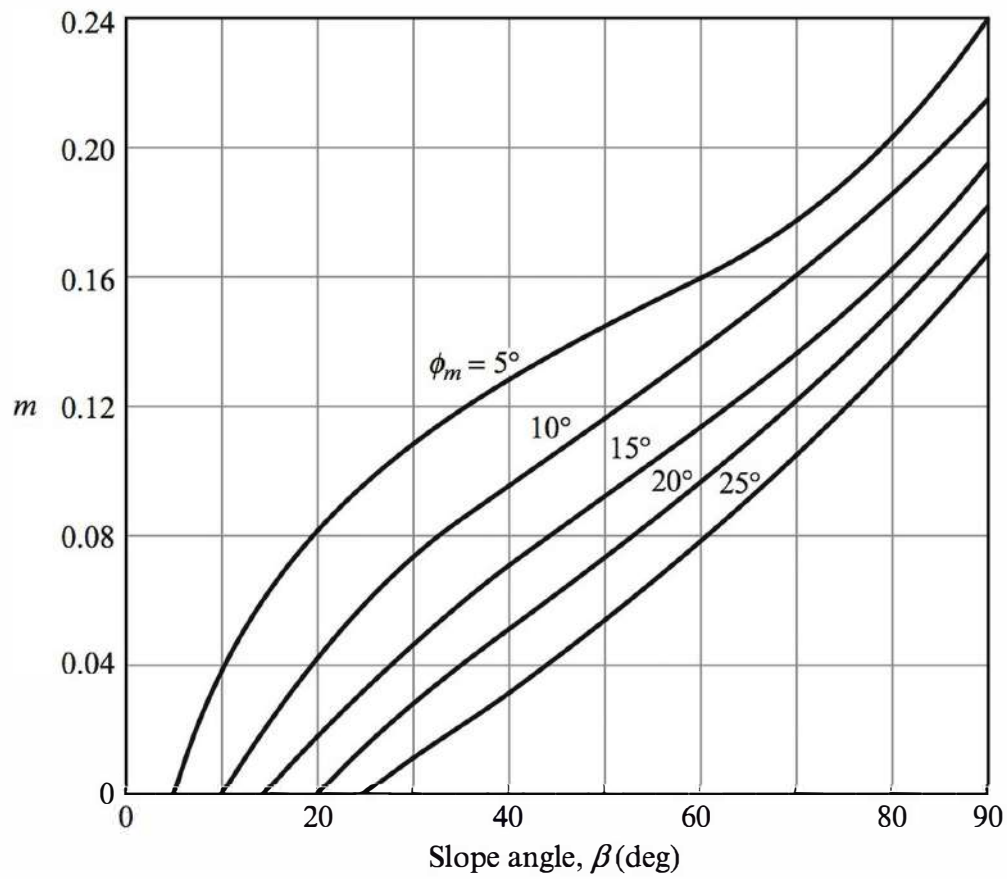

Figure 12.27 Modified Taylor's chart

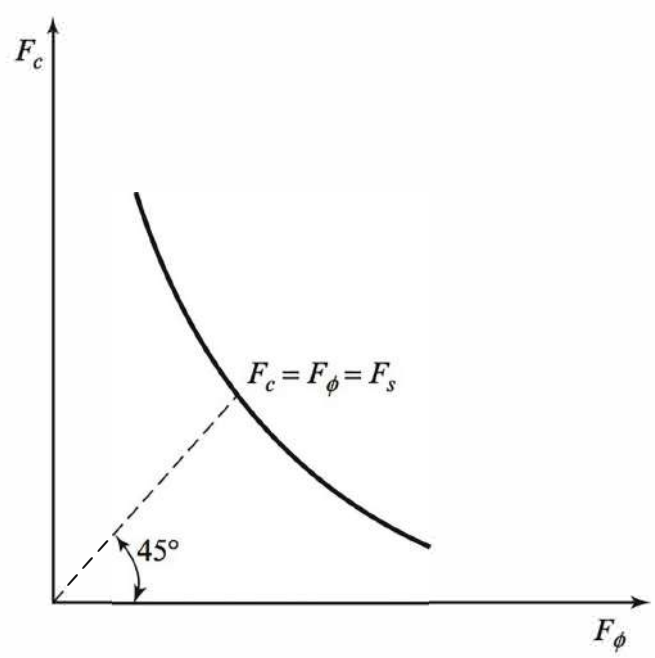

Figure 12.28 Calculation of F_s

EXAMPLE 12.3

A homogenous slope is shown in Figure 12.29a. Using the procedure described in this section, determine the factor of safety with respect to strength. Use $k_h = 0.3$.

Copyright 2017 Cengage Learning. All Rights Reserved. May not be copied, scanned, or duplicated, in whole or in part. Due to electronic rights, some third party content may be suppressed from the eBook and/or eChapter(s). Editorial review has deemed that any suppressed content does not materially affect the overall learning experience. Cengage Learning reserves the right to remove additional content at any time if subsequent rights restrictions require it.

SOLUTION:

Given $H = 12$ m, $\beta = 30°$, $\gamma = 16$ kN/m^3, $c = 20$ kPa, and $\phi = 34°$. Now, referring to Figure 12.26b, for $k_h = 0.3$, $M \approx 0.54$. So

$\phi_m = \tan^{-1}(M \tan\phi) = \tan^{-1}[(0.54)(\tan 34)] = 20°$

The following table can be prepared.

Assumed developed friction angle, ϕ_d (deg)	$\tan\phi_d$	$F_\phi = \dfrac{\tan\phi_m}{\tan\phi_d}$	m (Figure 12.27)	$F_c \dfrac{c}{c_d} = \dfrac{c}{m\gamma H}$
5	0.0875	4.16	0.110	0.95
10	0.1760	2.07	0.075	1.39
15	0.2680	1.36	0.046	2.26
20	0.3640	1.00	0.025	4.17

A plot of F_ϕ versus F_c is shown in Figure 12.29b, from which $F_s = F_c = F_\phi = \mathbf{1.73}$.

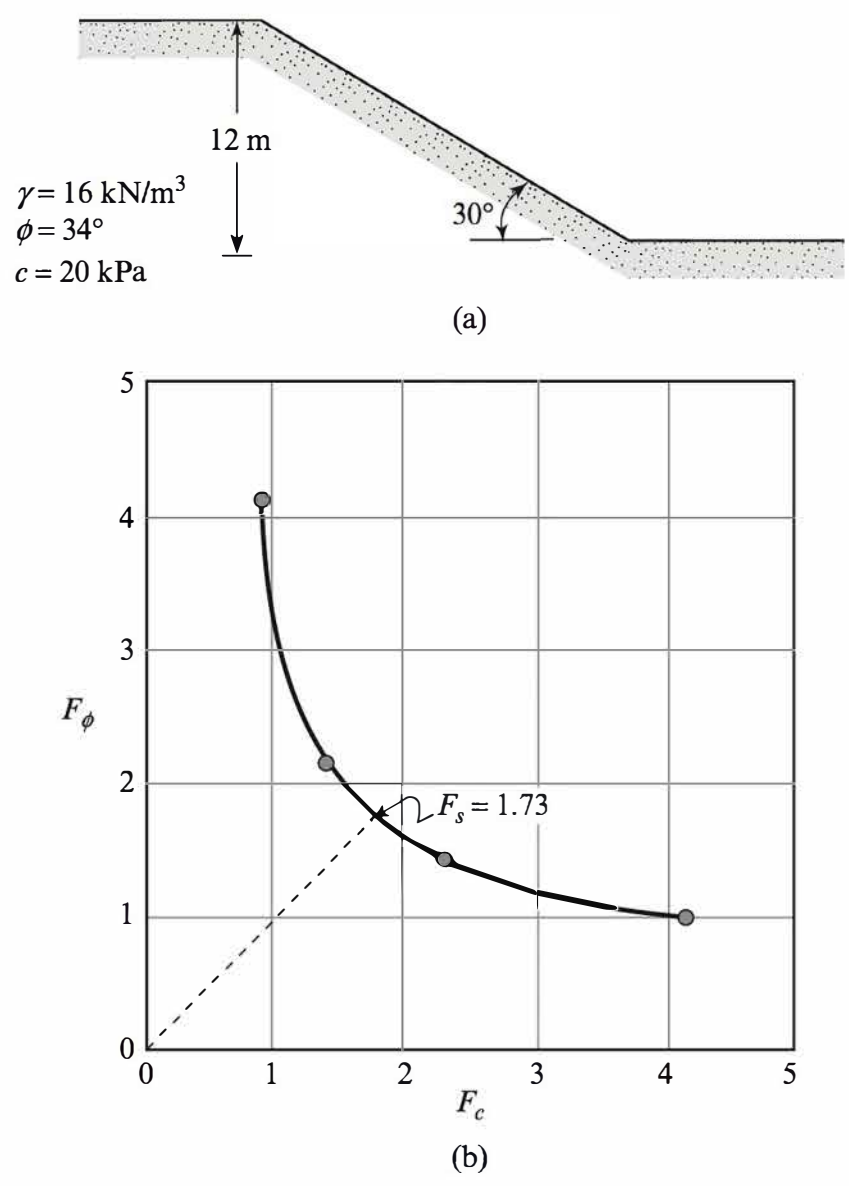

Figure 12.29

Copyright 2017 Cengage Learning. All Rights Reserved. May not be copied, scanned, or duplicated, in whole or in part. Due to electronic rights, some third party content may be suppressed from the eBook and/or eChapter(s). Editorial review has deemed that any suppressed content does not materially affect the overall learning experience. Cengage Learning reserves the right to remove additional content at any time if subsequent rights restrictions require it.

12.9 SLOPES WITH c-ϕ SOIL—PRATER'S ANALYSIS

It was mentioned in Section 12.6 that, due to earthquakes, slopes may undergo permanent deformation. Prater (1979) has analyzed slopes with $c-\phi$ soils to determine the *yield horizontal acceleration*, which is defined as the *threshold horizontal acceleration*, $k_h = k_y$, acting upon a sliding mass, above which permanent deformation occurs. It corresponds to a factor of safety with respect to strength (F_s) of unity. In this analysis the failure surface was assumed to be an arc of a logarithmic spiral defined by the equation (Figure 12.30)

$$r = r_0 e^{\theta \tan\theta} \tag{12.58}$$

where ϕ = soil friction angle. Prater's analysis for determination of the yield acceleration is summarized next.

Figure 12.31 shows a homogenous slope. The unit weight, cohesion, and angle of friction of the soil are, respectively, γ, c, and ϕ. ABC is a trial failure surface that is the arc of a logarithmic spiral. Referring to Figure 12.31,

$$m = e^{p \tan\phi} \tag{12.59}$$

$$d = \frac{r_0}{H} = \left[\sin t \sqrt{1 + m^2 - 2m\cos p}\right]^{-1} \tag{12.60}$$

$$j = t + \sin^{-1}\left(\frac{\sin p}{\sqrt{1 + m^2 - 2m\cos p}}\right) \tag{12.61}$$

$$q = \pi - p - j \tag{12.62}$$

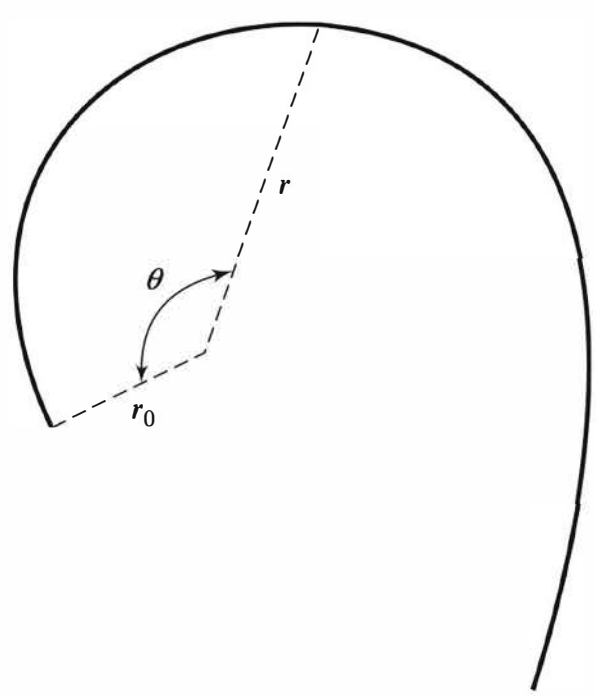

Figure 12.30 Log spiral

Copyright 2017 Cengage Learning. All Rights Reserved. May not be copied, scanned, or duplicated, in whole or in part. Due to electronic rights, some third party content may be suppressed from the eBook and/or eChapter(s). Editorial review has deemed that any suppressed content does not materially affect the overall learning experience. Cengage Learning reserves the right to remove additional content at any time if subsequent rights restrictions require it.

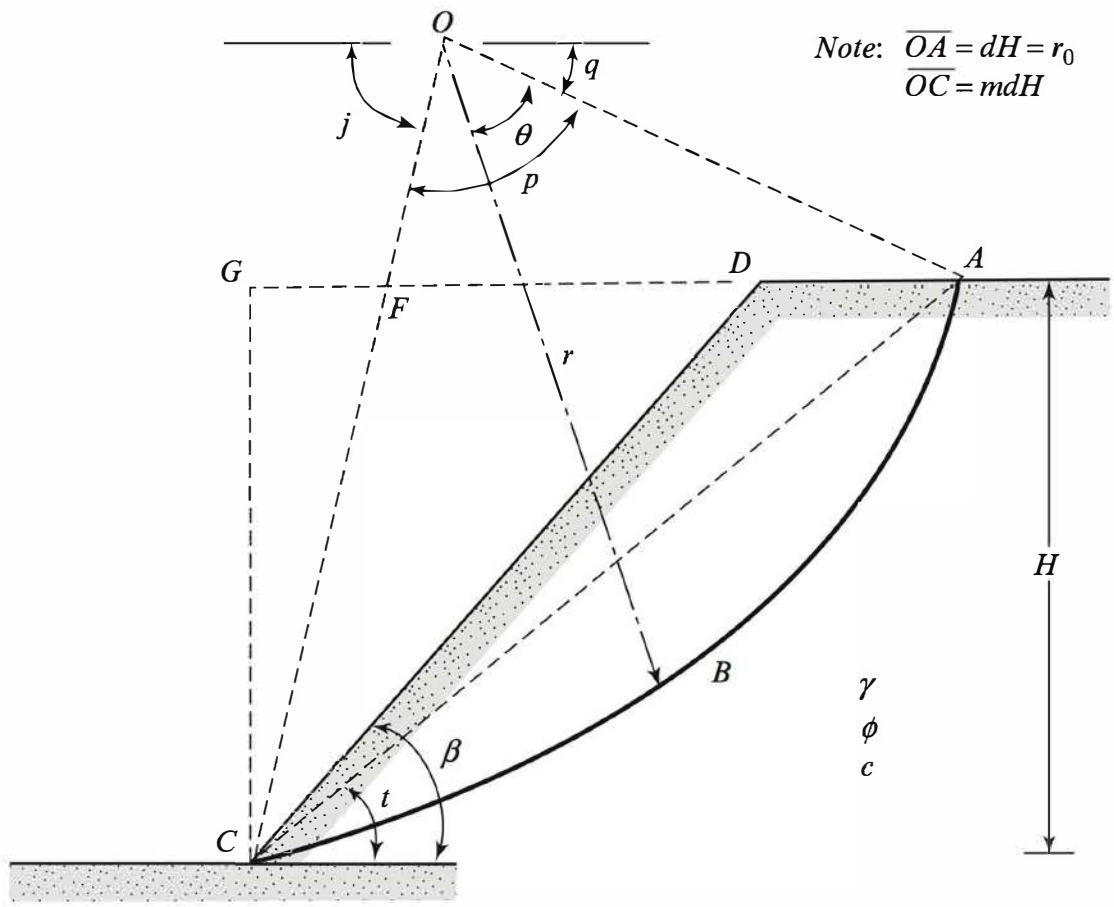

Figure 12.31 Prater's analysis for determination of yield acceleration

Considering a unit length of the embankment at right angles to the cross section shown, the overturning moment about O can be given as

$$M_D = M_W + M_E = (1 \mp k_v)M_g + M_E \tag{12.63}$$

where

$$M_g = \text{moment due to gravity force} = (M_1 - M_2 - M_3) \tag{12.64}$$

$$M_1 = \text{moment of the soil weight in the area } OABC \text{ about } O = \frac{\gamma d^3 H^3}{3(9\tan^2\phi + 1)}[m^3 \sin j - \sin q) - 3\tan\phi(m^3 \cos j + \cos q)] \tag{12.65}$$

$$M_2 = \text{moment of the soil weight in the area } OAF \text{ about } O = \frac{\gamma d^3 H^3}{6}[\sin^3 q(\cot^2 q - \cot^2 j)] \tag{12.66}$$

$$M_3 = \text{moment of the soil weight in the area } CDF \text{ about } O = \frac{\gamma H^3}{6}[\cot^2 \beta - \cot^2 j - 3md \cos j(\cot\beta - \cot j)] \tag{12.67}$$

Copyright 2017 Cengage Learning. All Rights Reserved. May not be copied, scanned, or duplicated, in whole or in part. Due to electronic rights, some third party content may be suppressed from the eBook and/or eChapter(s). Editorial review has deemed that any suppressed content does not materially affect the overall learning experience. Cengage Learning reserves the right to remove additional content at any time if subsequent rights restrictions require it.

k_v = average vertical acceleration

M_E = moment due to horizontal inertia force

$$= M_e k_h = (M_4 - M_5 - M_6)k_h \tag{12.68}$$

$$M_4 = \frac{\gamma d^3 H^3}{3(9\tan^2\phi + 1)}[(m^3\cos j + \cos q) + 3\tan\phi(m^3\sin j - \sin q)] \tag{12.69}$$

$$M_5 = \frac{\gamma d^3 H^3}{3}[\sin^3 q(\cos q + \cos j)] \tag{12.70}$$

$$M_6 = \frac{\gamma H^3}{6}(3d\sin q + 1)(\cot\beta - \cot j) \tag{12.71}$$

k_h = average horizontal acceleration

Hence, combining Eqs. (12.63) through (12.71), an expression for the overturning moment, M_D, can be obtained.

The restoring moment, M_R, can now be expressed as

$$M_R = \begin{bmatrix} \text{moment of the cohensive} \\ \text{force developed along} \\ \text{the trial failure} \\ \text{surrace } ABC, M_c \end{bmatrix} + \begin{bmatrix} \text{moment of the frictional} \\ \text{force developed along} \\ \text{the trial failure} \\ \text{surface } ABC, M_f \end{bmatrix}$$

However, based on the property of logarithmic spiral, the line of action of the resultant frictional force at any given point along the trial failure surface will pass through the origin O. Hence

$$M_f = 0$$

$$M_c = \frac{cd^2H^2(m^2 - 1)}{2\tan\phi} \tag{12.72}$$

So, for equilibrium of the soil mass located above the trial failure surface

$$M_D - M_c = 0$$

$$M_g(1 \mp k_v) + M_e k_h - M_c = 0$$

$$M_g \mp M_g k_v + M_e k_h - M_c = 0$$

or

$$\boxed{k_h = \frac{M_c - M_g}{M_e \mp bM_g}} \tag{12.73}$$

Copyright 2017 Cengage Learning. All Rights Reserved. May not be copied, scanned, or duplicated, in whole or in part. Due to electronic rights, some third party content may be suppressed from the eBook and/or eChapter(s). Editorial review has deemed that any suppressed content does not materially affect the overall learning experience. Cengage Learning reserves the right to remove additional content at any time if subsequent rights restrictions require it.

where

$$b = \frac{k_v}{k_h} \tag{12.74}$$

Prater (1979) has suggested that a realistic value of b would be 0.3. The yield acceleration k_h for the most critical surface can be determined by trial and error. Table 12.1 shows the magnitudes of the yield acceleration determined in this manner with $b = 0$.

12.10 SLOPES WITH c-ϕ SOIL—CONVENTIONAL METHOD OF SLICES

In the analysis for the stability of slopes provided in Section 12.7, 12.8, and 12.9, it is assumed that the soil is homogeneous. However, in a given slope, layered soil can be encountered. The method of slices is a general method that can easily account for the change of γ, c, and ϕ in the soil layers.

In order to explain this method, let us consider a slope as shown in Figure 12.32. Let ABC be a trial failure surface. Note that ABC is an arc of a circle with its center at O.

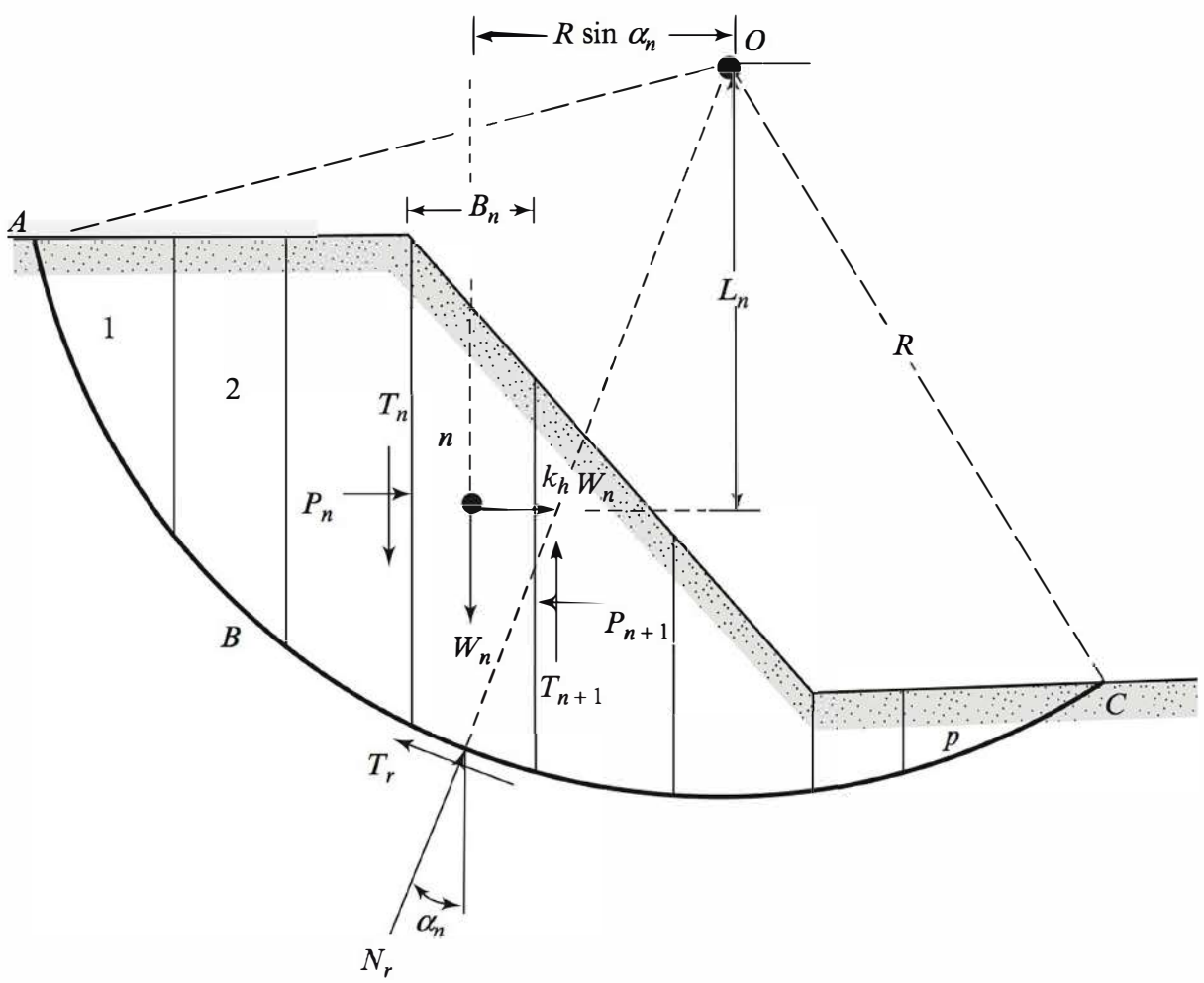

Figure 12.32 Conventional method of slices

Copyright 2017 Cengage Learning. All Rights Reserved. May not be copied, scanned, or duplicated, in whole or in part. Due to electronic rights, some third party content may be suppressed from the eBook and/or eChapter(s). Editorial review has deemed that any suppressed content does not materially affect the overall learning experience. Cengage Learning reserves the right to remove additional content at any time if subsequent rights restrictions require it.

Table 12.1 Yield acceleration, $k_h = k_y$

		$c/\gamma H$			
β(deg)	$\tan\phi$	0.05	0.10	0.15	0.20
15	0.1	0.00	0.08	0.15	0.20
	0.2	0.10	0.20	0.27	0.33
	0.3	0.20	0.31	0.39	0.44
	0.4	0.30	0.41	0.50	0.55
	0.5	0.40	0.51	0.60	0.66
	0.6	0.49	0.61	0.70	0.76
	0.7	0.58	0.70	0.80	0.87
	0.8	0.66	0.79	0.89	0.97
	0.9	0.74	0.87	0.98	1.07
30	0.1	—	0.00	0.13	0.20
	0.2	0.00	0.11	0.25	0.35
	0.3	0.05	0.22	0.37	0.46
	0.4	0.14	0.32	0.46	0.56
	0.5	0.24	0.41	0.55	0.66
	0.6	0.32	0.50	0.63	0.75
	0.7	0.40	0.57	0.72	0.83
	0.8	0.47	0.65	0.79	0.91
	0.9	0.53	0.71	0.86	0.98
45	0.1	—	—	0.07	0.22
	0.2	—	0.00	0.18	0.33
	0.3	—	0.11	0.28	0.42
	0.4	0.00	0.20	0.37	0.51
	0.5	0.06	0.29	0.46	0.59
	0.6	0.14	0.36	0.53	0.67
	0.7	0.21	0.43	0.59	0.74
	0.8	0.27	0.49	0.66	0.80
	0.9	0.33	0.54	0.71	0.84
60	0.1	—	—	0.00	0.16
	0.2	—	—	0.08	0.26
	0.3	—	0.00	0.18	0.34
	0.4	—	0.05	0.26	0.42
	0.5	—	0.13	0.33	0.49
	0.6	0.00	0.20	0.39	0.55
	0.7	0.01	0.26	0.45	0.60

(*Continued*)

Copyright 2017 Cengage Learning. All Rights Reserved. May not be copied, scanned, or duplicated, in whole or in part. Due to electronic rights, some third party content may be suppressed from the eBook and/or eChapter(s). Editorial review has deemed that any suppressed content does not materially affect the overall learning experience. Cengage Learning reserves the right to remove additional content at any time if subsequent rights restrictions require it.

		$c/\gamma H$			
β(deg)	$\tan\phi$	0.05	0.10	0.15	0.20
	0.8	0.07	0.32	0.50	0.65
	0.9	0.13	0.36	0.54	0.69
75	0.1	—	—	—	0.04
	0.2	—	—	0.00	0.14
	0.3	—	—	0.02	0.22
	0.4	—	—	0.10	0.29
	0.5	—	0.00	0.17	0.35
	0.6	—	0.01	0.23	0.40
	0.7	—	0.07	0.28	0.44
	0.8	—	0.12	0.32	0.38
	0.9	—	0.16	0.35	0.51

Note: $b = 0$.

The soil above the trial failure surface is divided into several slices. The length of each slice need not be the same. For the nth slice, consider a unit thickness at right angles to the cross section shown. The weight and the inertia forces are, respectively, W_n and k_hW_n. The forces P_n and P_{n+1} are the normal forces acting on the sides of the slice. Similarly, the shearing forces acting on the sides of the slice are T_n and T_{n+1}. The forces P_n, P_{n+1}, T_n and T_{n+1} are difficult to determine. However, we can make an approximate assumption that the resultant of P_n and T_n are equal in magnitude to the resultants of P_{n+1} and T_{n+1} and also their lines of action coincide. The normal reaction at the base of the slice is $N_r = W_n\cos\alpha_n$. It is assumed that the inertia force k_hW_n has no effect on the magnitude of N_r. So the resisting tangential force T_r can be given as

$$T_r = \frac{1}{F_s}(cB_n\sec\alpha_n + N_r\tan\phi)$$
$$= \frac{1}{F_s}(cB_n\sec\alpha_n + W_n\cos\alpha_n\tan\phi) \tag{12.75}$$

Now, taking the moment about O for all the slices,

$$\sum_{n=1}^{p}(W_nR\sin\alpha_n + k_hW_nL_n) = \sum_{n=1}^{p}\frac{R}{F_s}(cB_n\sec\alpha_n + W_n\cos\alpha_n\tan\phi) \tag{12.76}$$

or

$$\boxed{F_s = \frac{\sum_{n=1}^{p}(cB_n\sec\alpha_n + W_n\cos\alpha_n\tan\phi)}{\sum_{n=1}^{p}[W_n\sin\alpha_n + k_hW_n(L_n/R)]}} \tag{12.77}$$

Copyright 2017 Cengage Learning. All Rights Reserved. May not be copied, scanned, or duplicated, in whole or in part. Due to electronic rights, some third party content may be suppressed from the eBook and/or eChapter(s). Editorial review has deemed that any suppressed content does not materially affect the overall learning experience. Cengage Learning reserves the right to remove additional content at any time if subsequent rights restrictions require it.

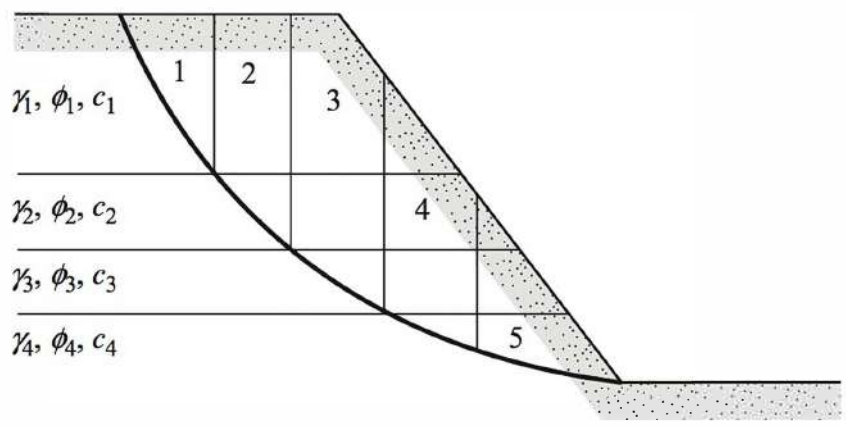

Figure 12.33 Method of slices for slopes in layered soil

Note that the value of α_n may be either positive or negative. The value of α_n is positive when the slope of the arc is in the same quadrant as the ground slope. To find the minimum factor of safety—that is, the factor of safety with reference to the critical circle—several trials have to be made, each time changing the center of the trial circle.

For convenience, a slope in homogeneous soil is shown in Figure 12.32. However, the method of slices can be extended to slopes of layered soil, as shown in Figure 12.33. The general procedure of stability analysis is the same; however, some minor points need to be kept in mind. While using Eq. (12.77), the values of ϕ and c will not be the same for all slices. For example, for slice 2, one has to use $\phi = \phi_2$ and $c = c_2$; similarly, for slice 3, $\phi = \phi_3$ and $c = c_3$ will need to be used.

Deformation of Slopes

12.11 SIMPLIFIED PROCEDURE FOR ESTIMATION OF EARTHQUAKE-INDUCED DEFORMATION

The concept relating to the deformation of embankment slopes due to earthquake-induced vibration was briefly described in Section 12.6. Following is a simplified step-by-step procedure developed by Makdisi and Seed (1978) for estimation of the deformation. When this procedure is applied, it is assumed that the shear strength of the soil does not change during shaking. Hence this method cannot be used in cases where there is pore pressure buildup.

1. Determine the height of the embankment (H) and the shear strength parameters of the soil (c and ϕ).
2. Determine the maximum crest acceleration $[\ddot{u}_a(0)]_{\max}$ and the first natural period ($T_1 = 2\pi/\omega$) by using the method described in Section 12.5.

Copyright 2017 Cengage Learning. All Rights Reserved. May not be copied, scanned, or duplicated, in whole or in part. Due to electronic rights, some third party content may be suppressed from the eBook and/or eChapter(s). Editorial review has deemed that any suppressed content does not materially affect the overall learning experience. Cengage Learning reserves the right to remove additional content at any time if subsequent rights restrictions require it.

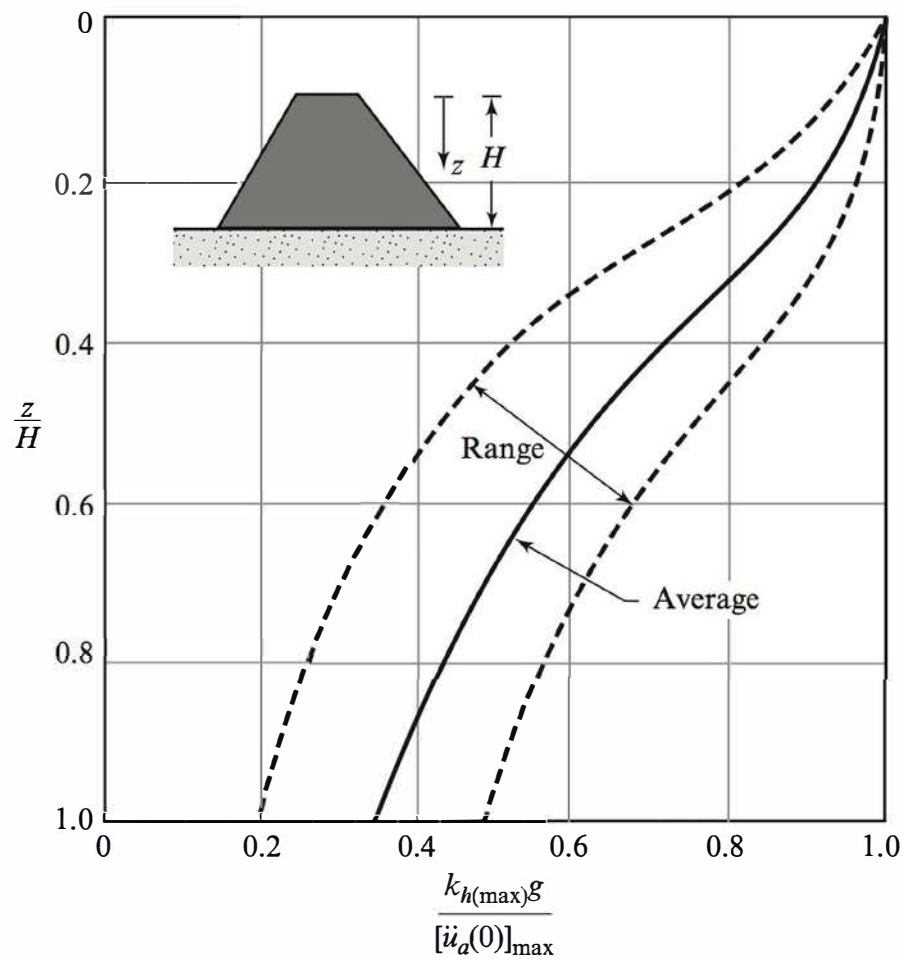

Figure 12.34 Variation of maximum acceleration ratio with depth of sliding mass (from Makdisi and Seed, 1978)

Source: Makdisi, F.I., and Seed, H.B. (1978). "Simplified Procedure for Estimating Dam and Embankment Earthquake-Induced deformations," *Journal of the Geotechnical Engineering Division*, ASCE, Vol. 104, No. GT7, pp. 849–859. With permission from ASCE.

3. With reference to Figure 12.34, choose the critical section likely to deform and determine the magnitude of $k_{h(\max)}g/[\ddot{u}_a(0)]_{\max}$ from Figure 12.34. Note that $k_{h(\max)}$ is the coefficient of the maximum average horizontal acceleration for a given value of z/H. The concept of the coefficient of average acceleration was explained in Section 12.6. Now determine the magnitude of $k_{h(\max)}g$.
4. Determine the yield acceleration—that is, the acceleration $k_y g$ (see Section 12.9) for which the sliding mass has $F_s = 1$.
5. Determine $[k_y/k_{h(\max)}]$ and the magnitude of the earthquake (M). With these values, go to Figure 12.35 to obtain $[U/k_{h(\max)}gT_1]$ (in seconds). With the known values of $k_{h(\max)}g$ (Step 3) and T_1 (Step 2), the magnitude U can be determined. Note that U is the deformation in the horizontal direction.

EXAMPLE 12.4

Refer to the soil embankment in Example 12.1 (Figure 12.36).

a. Calculate the yield acceleration $k_y g$ by using the concept described in Section 12.9. Use Table 12.1 with $b = 0$.

Copyright 2017 Cengage Learning. All Rights Reserved. May not be copied, scanned, or duplicated, in whole or in part. Due to electronic rights, some third party content may be suppressed from the eBook and/or eChapter(s). Editorial review has deemed that any suppressed content does not materially affect the overall learning experience. Cengage Learning reserves the right to remove additional content at any time if subsequent rights restrictions require it.

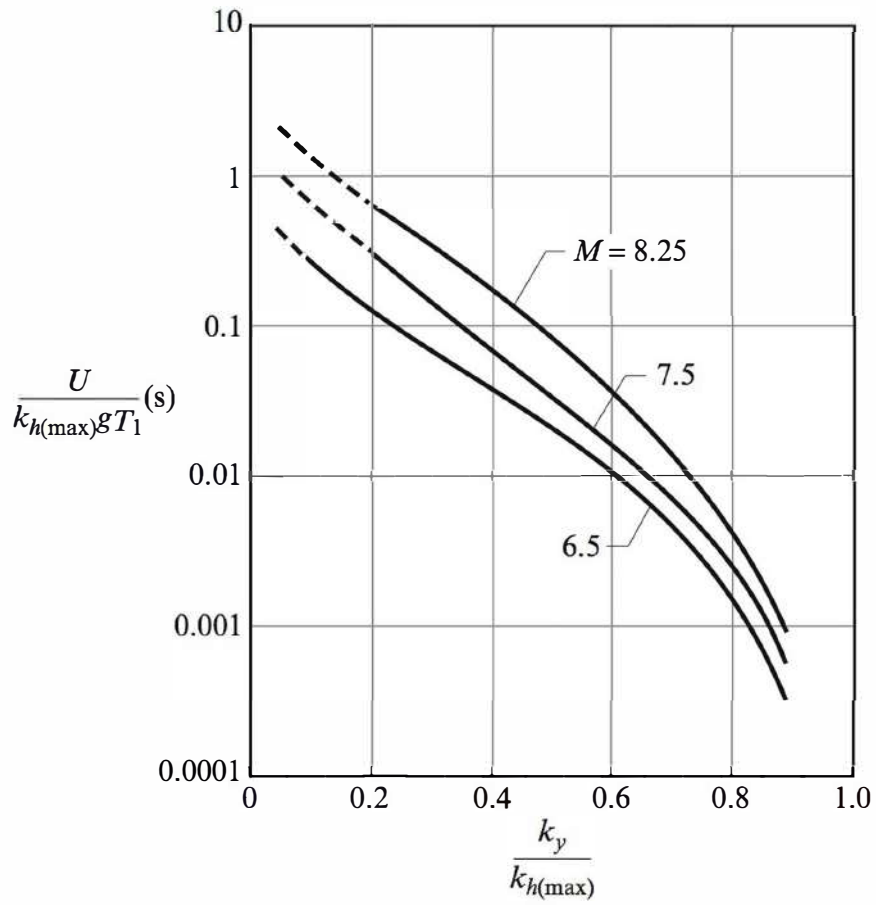

Figure 12.35 Variation of $[U/k_{h(\max)}gT_1]$ with $k_y/k_{h(\max)}$ (from Makdisi and Seed, 1978)

Source: Makdisi, F.I., and Seed, H.B. (1978). "Simplified Procedure for Estimating Dam and Embankment Earthquake-Induced deformations," *Journal of the Geotechnical Engineering Division*, ASCE, Vol. 104, No. GT7, pp. 849–859. With permission from ASCE.

b. For the critical failure surface passing through the toe of the embankment, calculate the slope deformation using the procedure described in Section 12.11. Use the magnitude of earthquake $M = 7.0$. Also use the results of Example 12.1 for maximum crest acceleration.

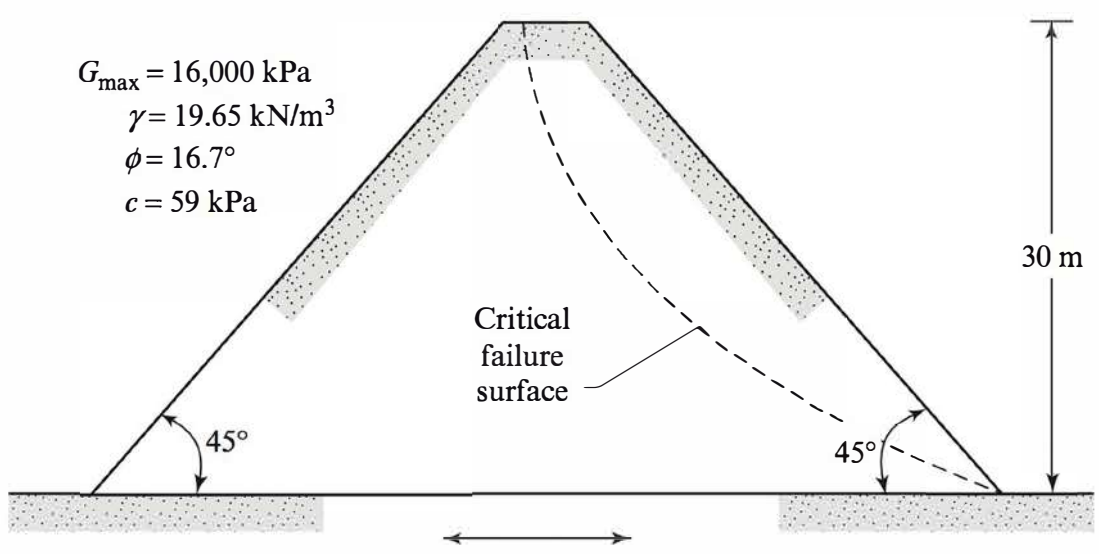

Figure 12.36

Copyright 2017 Cengage Learning. All Rights Reserved. May not be copied, scanned, or duplicated, in whole or in part. Due to electronic rights, some third party content may be suppressed from the eBook and/or eChapter(s). Editorial review has deemed that any suppressed content does not materially affect the overall learning experience. Cengage Learning reserves the right to remove additional content at any time if subsequent rights restrictions require it.

SOLUTION:

a. Referring to Table 12.1, for $\beta = 45°$, $\tan\phi = \tan 16.7 = 0.3$, and $c/\gamma H = 59/[(19.65)(30)] = 0.1$, the magnitude of k_y is 0.11.

So, the yield acceleration is **0.11*g***.

b. Referring to Figure 12.34, for $z/H = 1$, the average value of $[k_{h(\max)}g]/[\ddot{u}_a(0)]_{\max}$ is about 0.34. From Example 12.1, $[\ddot{u}_a(0)]_{\max} = 0.70\ g$. So

$$\frac{k_{h(\max)}g}{\left[\ddot{u}_a(0)_{\max}\right]} = 0.34$$

$$k_{h(\max)} = \frac{(0.34)(0.70\ g)}{g} = 0.238$$

Thus,

$$\frac{k_y}{k_{h(\max)}} = \frac{0.11}{0.238} = 0.462$$

Also, from Example 12.1, $T_1 = 0.435$ sec. For earthquake magnitude $M = 7.0$, referring to Figure 12.35,

$$\frac{U}{k_{h(\max)}gT_1} \approx 0.036$$

So

$$U = (0.036)(0.238)(9.81)(0.435) = 0.0366 \text{ m} = \mathbf{36.6\ mm}$$

PROBLEMS

12.1 An earth embankment is 25 m high. For the embankment soil,

Unit weight = 18 kN/m^3

At a certain shear strain level

$G = 50{,}000$ kPa and $D = 15\%$

Using the acceleration spectra given in Figure 12.12 (maximum ground acceleration is 0.23 g), estimate the maximum crest acceleration of the embankment.

Copyright 2017 Cengage Learning. All Rights Reserved. May not be copied, scanned, or duplicated, in whole or in part. Due to electronic rights, some third party content may be suppressed from the eBook and/or eChapter(s). Editorial review has deemed that any suppressed content does not materially affect the overall learning experience. Cengage Learning reserves the right to remove additional content at any time if subsequent rights restrictions require it.

12.2 An earth embankment is 18 m high. For the embankment soil,

$$\text{Unit weight} = 18.5\ \text{kN/m}^3$$
$$\text{Maximum shear modulus} = 165{,}000\ \text{kPa}$$

Using the variation of G/G_{max} and D with shear strain as given in Figure 12.11 and the acceleration spectra given in Figure 12.12 (maximum ground acceleration = 0.2 g), determine the maximum crest acceleration.

12.3 A clay ($\phi = 0°$) is built over a layer of rock. For the slope,

$$\text{Height} = 20\text{m}$$
$$\text{Slope angle}, \beta = 30°$$
$$\text{Saturated unit weight of soil} = 17.8\ \text{kN/m}^3$$
$$\text{Undrained shear strength}, c_u = 5z\ \text{kPa}$$
$$(z = \text{depth measured from the top of the slope})$$

Determine the factor of safety F_s if $k_h = 0.4$. Use the procedure outlined in Section 12.7.

12.4 Redo Problem 12.3 assuming $c_u = 40 + 5z$ kPa and other parameters remain the same.

12.5 Refer to Problem 12.3. Other parameters remaining the same, let the slope angle β be changed from 30° to 75°. Calculate and plot the variation of the factor of safety (F_s) with β. Use the procedure outlined in Section 12.7.

12.6 For a homogenous soil,

$$\text{Slope angle}, \beta = 30°$$
$$\text{Height}, H = 15\ \text{m}$$
$$\text{Soil cohesion} = 60\ \text{kPa}$$
$$\text{Soil friction angle}, \phi = 25°$$
$$\text{Unit weight of soil} = 19.5\ \text{kN/m}^3$$
$$k_h = 0.25$$

Determine the factor of safety with respect to strength. Use the procedure described in Section 12.8.

Copyright 2017 Cengage Learning. All Rights Reserved. May not be copied, scanned, or duplicated, in whole or in part. Due to electronic rights, some third party content may be suppressed from the eBook and/or eChapter(s). Editorial review has deemed that any suppressed content does not materially affect the overall learning experience. Cengage Learning reserves the right to remove additional content at any time if subsequent rights restrictions require it.

12.7 Repeat Problem 12.6 with the following:

$$\begin{aligned} \text{Slope angle, } \beta &= 45° \\ \text{Height, } H &= 25 \text{ m} \\ \text{Soil cohesion} &= 60 \text{ kPa} \\ \text{Soil friction angle, } \phi &= 20° \\ \text{Unit weight of soil} &= 19 \text{ kN/m}^3 \\ k_h &= 0.25 \end{aligned}$$

12.8 For the slope described in Problem 12.6, what would be the yield acceleration (that is, $k_h g$)? Use the procedure described in Section 12.9. Use $b = 0$.

12.9 The properties of the soil of a given slope 15.3 m high are as follows:

$$\begin{aligned} \text{Unit weight, } \gamma &= 18.5 \text{ kN/m}^3 \\ \text{Cohesion, } c &= 42.5 \text{ kPa} \\ \text{Angle of friction, } \phi &= 20° \end{aligned}$$

The yield acceleration for the slope was estimated to be 0.36. This was done using the procedure described in Section 12.9 with $b = 0$. Estimate the slope angle β.

12.10 A homogeneous slope is shown in Figure P12.10. For the trial failure surface shown, determine the factor of safety with respect to strength. Use the method of slices. (*Note:* The slope angle is $\beta = 30°$.)

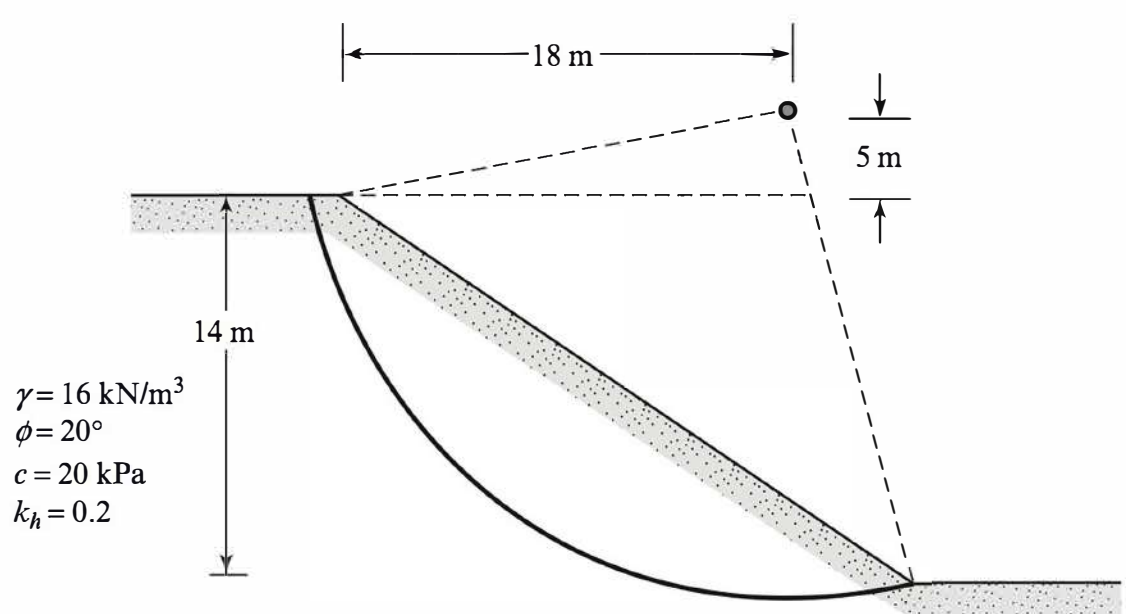

Figure P12.10

Copyright 2017 Cengage Learning. All Rights Reserved. May not be copied, scanned, or duplicated, in whole or in part. Due to electronic rights, some third party content may be suppressed from the eBook and/or eChapter(s). Editorial review has deemed that any suppressed content does not materially affect the overall learning experience. Cengage Learning reserves the right to remove additional content at any time if subsequent rights restrictions require it.

12.11 A 25 m high embankment (c-ϕ soil) is constructed over a hard stratum, The critical failure circle passes through the toe of the slope and the average yield acceleration of the slope is 0.15 g. The maximum crest acceleration due to an earthquake of magnitude $M = 7.5$ has been estimated to be 0.6 g. The first natural period is 0.8 s. Estimate the slope deformation. Use the procedure described in Section 12.11.

12.12 Refer to Example 12.4. Other quantities remaining the same, if the soil friction angle ϕ is changed to 21.8°, estimate the slope deformation.

References

Ambraseys, N. N. (1960). "On the Seismic Behavior of Earth Dams," *Proceedings*, 2nd World Conference on Earthquake Engineering, Tokyo, Vol. I, pp. 331–345.

Das, B. M. (2010). *Principles of Geotechnical Engineering*, 7th ed., Cengage, Boston MA.

Koppula, S. D. (1984). "Pseudo-Static Analysis of Clay Slopes Subjected to Earthquakes," *Geotechnique*, Institute of Civil Engineers, London, Vol. 34, No. 1, pp. 71–79.

Majumdar, D. K. (1971). "Stability of Soil Slopes under Horizontal Earthquake Force," *Geotechnique*, Institute of Civil Engineers, London, Vol. 21, No. 1, pp. 372–378.

Makdisi, F. I., and Seed, H. B. (1978). "Simplified Procedure for Estimating Dam and Embankment Earthquake-Induced Deformations," *Journal of the Geotechnical Engineering Division*, ASCE, Vol. 104, No. GT7, pp. 849–859.

Makdisi, F. I., and Seed, H. B. (1979). "Simplified Procedure for Evaluating Embankment Response," *Journal of the Geotechnical Engineering Division*, ASCE, Vol. 105, No. GT12, pp. 1427–1434.

Mononobe, N., Takata, A., and Matumura, M. (1936). "Seismic Stability of Earth Dams," *Proceedings*, 2nd Congress of Large Dams, Vol. 4, Washington, D. C.

Newmark, N. M. (1965). "Effect of Earthquakes on Dams and Embankments," *Geotechnique*, Institute of Civil Engineers, London, Vol. 15, No. 2, p. 139.

Prater, E. G (1979). "Yield Acceleration for Seismic Stability of Slopes," Journal of the *Geotechnical Engineering Division*, ASCE, Vol. 105, No. GT5, pp. 682–687.

Seed, H. B. (1975). "Earthquake Effects on Soil-Foundation System" in *Foundation Engineering Handbook* (H. F. Winterkorn and H. Y. Faud, eds.), Van Nostrand Reinhold, New York.

Seed, H. B. (1981). "Earthquake-Resistant Design of Earth Dams," *Proceedings*, International Conference on Recent Advances in Geotechnical Earthquake Engineering and Soil Dynamics, University of Missouri-Rolla, Vol. III, pp. 1157–1177.

Seed, H. B., and Goodman, R. E. (1964). "Earthquake Stability of Slopes of Cohesionless Soils," *Journal of the Soil Mechanics and Foundations Division,* ASCE, Vol. 90, No. SM6, pp. 43–56.

Seed, H. B., and Martin, G. R. (1966). "The Seismic Coefficient of Earth Dam Designs," *Journal of the Soil Mechanics and Foundations Division*, ASCE, Vol. 92, No. SM3, pp. 25–58.

Seed, H. B., Makdisi, F. I., and DeAlba, P. (1978). "Performance of Earth Dams During Earthquakes," *Journal of the Geotechnical Engineering Division*, ASCE, Vol. 104, No. GT7, pp. 967–944.

Taylor, D. W. (1937). "Stability of Earth Slopes," *Journal of the Boston Society of Civil Engineers*, Vol. 24, No. 3, pp. 197–246.

Copyright 2017 Cengage Learning. All Rights Reserved. May not be copied, scanned, or duplicated, in whole or in part. Due to electronic rights, some third party content may be suppressed from the eBook and/or eChapter(s). Editorial review has deemed that any suppressed content does not materially affect the overall learning experience. Cengage Learning reserves the right to remove additional content at any time if subsequent rights restrictions require it.

APPENDIX A

Primary and Secondary Forces of Single-Cylinder Engines

Machinery involving a crank mechanism produces a reciprocating force. This mechanism is shown in Figure A.1a, in which

$$OA = \text{crank length} = r_1$$

$$AB = \text{length of the connecting rod} = r_2$$

Let the crank rotate at a constant angular velocity ω. At time $t = 0$, the vertical distance between O and B (Figure A.1b) is equal to $r_1 + r_2$. At time t, the vertical distance between O and B is equal to $r_1 + r_2 - z$, or

$$z = (r_1 + r_2) - (r_2 \cos\alpha + r_1 \cos\omega t) \tag{A.1}$$

But,

$$r_2 \sin\alpha = r_1 \sin\omega t \tag{A.2}$$

Now,

$$\cos\alpha = \sqrt{1 - \sin^2\alpha} = \sqrt{1 - \left(\frac{r_1}{r_2}\right)^2 \sin^2\omega t}$$

$$\approx 1 - \frac{1}{2}\left(\frac{r_1}{r_2}\right)^2 \sin^2\omega t \tag{A.3}$$

Substituting Eq. (A.3) into Eq. (A.1),

$$\begin{aligned} z &= (r_1 + r_2) - (r_2 \cos\alpha + r_1 \cos\omega t) \\ &= r_2(1 - \cos\alpha) + r_1(1 - \cos\omega t) \\ &= r_2\left[1 - 1 + \frac{1}{2}\left(\frac{r_1}{r_2}\right)^2 \sin^2\omega t\right] + r_1(1 - \cos\omega t) \end{aligned}$$

Copyright 2017 Cengage Learning. All Rights Reserved. May not be copied, scanned, or duplicated, in whole or in part. Due to electronic rights, some third party content may be suppressed from the eBook and/or eChapter(s). Editorial review has deemed that any suppressed content does not materially affect the overall learning experience. Cengage Learning reserves the right to remove additional content at any time if subsequent rights restrictions require it.

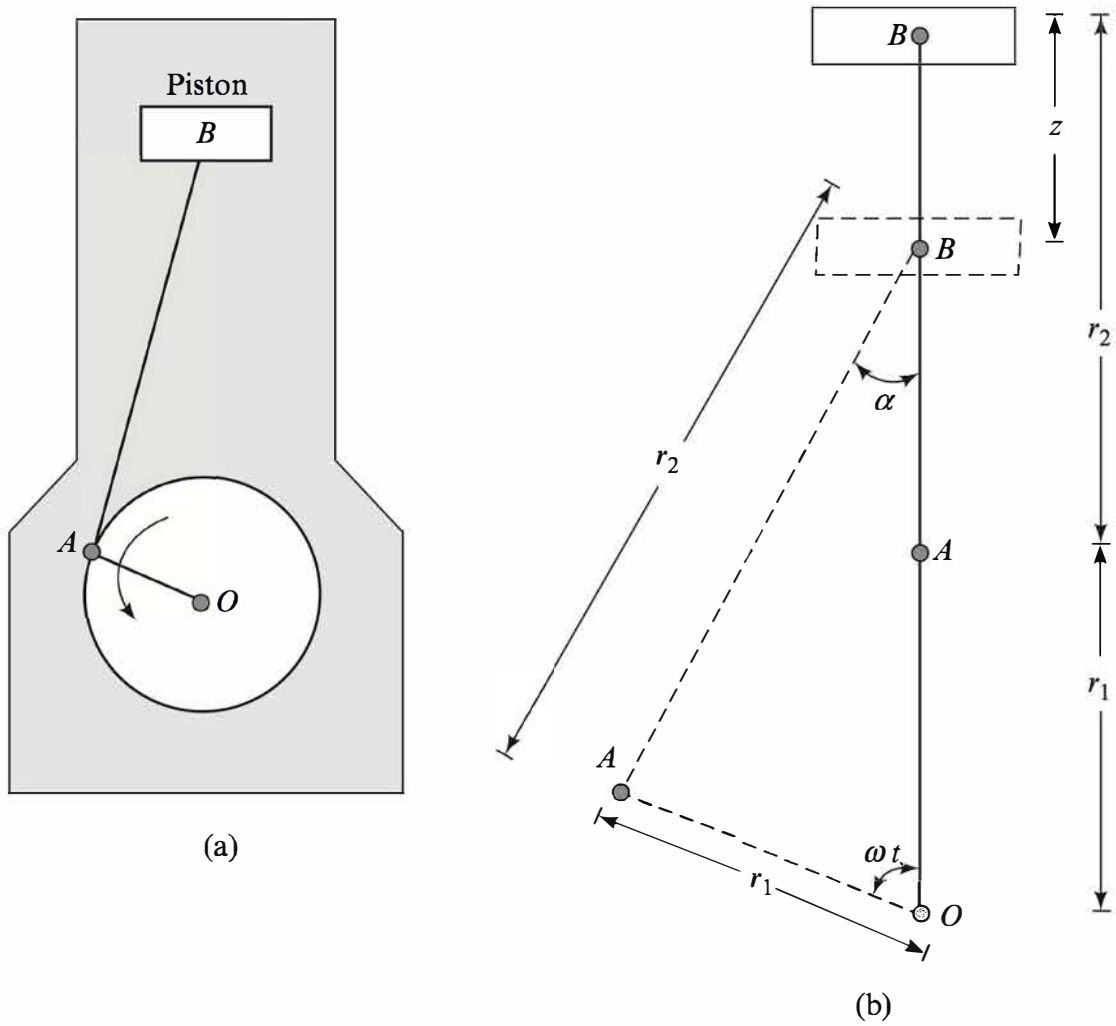

Figure A.1

$$= \left(\frac{\frac{1}{2} r_1^2}{r_2} \right) \sin^2 \omega t + r_1 (1 - \cos \omega t) \tag{A.4}$$

However,

$$\sin^2 \omega t = \frac{1}{2}(1 - \cos 2\omega t) \tag{A.5}$$

Substituting Eq. (A.5) into Eq. (A.4), one obtains

$$z = \left(\frac{\frac{1}{4} r_1^2}{r_2} \right) (1 - \cos 2\omega t) + r_1 (1 - \cos \omega t)$$

Copyright 2017 Cengage Learning. All Rights Reserved. May not be copied, scanned, or duplicated, in whole or in part. Due to electronic rights, some third party content may be suppressed from the eBook and/or eChapter(s). Editorial review has deemed that any suppressed content does not materially affect the overall learning experience. Cengage Learning reserves the right to remove additional content at any time if subsequent rights restrictions require it.

$$= \left(r_1 + \frac{\frac{1}{4} r_1^2}{r_2} \right) - \left[r_1 \cos \omega t + \left(\frac{\frac{1}{4} r_1^2}{r_2} \right) \cos 2\omega t \right] \tag{A.6}$$

The acceleration of the piston can be given by

$$\ddot{z} = r_1 \omega^2 \left[\cos \omega t + \left(\frac{r_1}{r_2} \right) \cos 2\omega t \right] \tag{A.7}$$

If the mass of the piston is m, the force can be obtained as

$$F = m\ddot{z} = m r_1 \omega^2 \cos \omega t + m \left(\frac{r_1^2}{r_2} \right) \omega^2 \cos 2\omega t \tag{A.8}$$

The first term of Eq. (A.8) is the primary force, and the maximum primary force

$$F_{\max(\text{prim})} = m r_1 \omega^2 \tag{A.9}$$

Similarly, the second term of Eq. (A.8) is generally referred to as the secondary force, and

$$F_{\max(\text{sec})} = m \left(\frac{r_1^2}{r_2} \right) \omega^2 \tag{A.10}$$

Copyright 2017 Cengage Learning. All Rights Reserved. May not be copied, scanned, or duplicated, in whole or in part. Due to electronic rights, some third party content may be suppressed from the eBook and/or eChapter(s). Editorial review has deemed that any suppressed content does not materially affect the overall learning experience. Cengage Learning reserves the right to remove additional content at any time if subsequent rights restrictions require it.

INDEX

Copyright 2017 Cengage Learning. All Rights Reserved. May not be copied, scanned, or duplicated, in whole or in part. Due to electronic rights, some third party content may be suppressed from the eBook and/or eChapter(s). Editorial review has deemed that any suppressed content does not materially affect the overall learning experience. Cengage Learning reserves the right to remove additional content at any time if subsequent rights restrictions require it.

Copyright 2017 Cengage Learning. All Rights Reserved. May not be copied, scanned, or duplicated, in whole or in part. Due to electronic rights, some third party content may be suppressed from the eBook and/or eChapter(s). Editorial review has deemed that any suppressed content does not materially affect the overall learning experience. Cengage Learning reserves the right to remove additional content at any time if subsequent rights restrictions require it.

Copyright 2017 Cengage Learning. All Rights Reserved. May not be copied, scanned, or duplicated, in whole or in part. Due to electronic rights, some third party content may be suppressed from the eBook and/or eChapter(s). Editorial review has deemed that any suppressed content does not materially affect the overall learning experience. Cengage Learning reserves the right to remove additional content at any time if subsequent rights restrictions require it.

Copyright 2017 Cengage Learning. All Rights Reserved. May not be copied, scanned, or duplicated, in whole or in part. Due to electronic rights, some third party content may be suppressed from the eBook and/or eChapter(s). Editorial review has deemed that any suppressed content does not materially affect the overall learning experience. Cengage Learning reserves the right to remove additional content at any time if subsequent rights restrictions require it.